सत्यमेव जयते

INDIAN AGRICULTURAL
RESEARCH INSTITUTE, NEW DELHI

48564

I.A.R.I.6.
GIP NLK—H-3 I.A.R.I.—10-5 55—15,000

PROCEEDINGS

OF THE

ROYAL SOCIETY OF LONDON

SERIES A. MATHEMATICAL AND PHYSICAL SCIENCES

VOL 200

48564
IARI

LONDON
Published for the Royal Society by the
Cambridge University Press
Bentley House, N.W.1

22 February 1950

Printed in Great Britain at the University Press, Cambridge
(Brooke Crutchley, University Printer)
and published by the Cambridge University Press
Cambridge, and Bentley House, London
Agents for Canada, India, and Pakistan: Macmillan

CONTENTS

SERIES A VOLUME 200

No. A 1060. 22 December 1949

PAGE

Vibration-rotation bands of allene. By C. H. Miller and H. W. Thompson, F.R.S. 1

Vibration-rotation bands of some polyatomic molecules. By A. R. H. Cole and H. W. Thompson, F.R.S. 10

On Heisenberg's elementary theory of turbulence. By S. Chandrasekhar, F.R.S. 20

Some theorems on perturbation theory. By E. C. Titchmarsh, F.R.S. . . 34

Plastic deformation of silver chloride. II. Photoelastic study of the internal stresses in glide packets. By J. F. Nye. (Plates 1 to 4) 47

Experiments on the superconductive transition. By D. K. C. MacDonald and K. Mendelssohn 66

Correlated incompressible and compressible boundary layers. By K. Stewartson 84

The sedimentation and diffusion of small particles. By C. N. Davies . . . 100

The inflammation of alkyl nitrate vapours and the effect of inert diluents. By P. Gray and A. D. Yoffe 114

One-dimensional dislocations. III. Influence of the second harmonic term in the potential representation, on the properties of the model. By F. C. Frank and J. H. van der Merwe 125

No. A 1061. 6 January 1950

A discussion on the physics and chemistry of hydrocarbon gels. By E. K. Rideal, F.R.S. and others. (Plate 5) 135

The tides in oceans on a rotating globe. V. By G. R. Goldsbrough, F.R.S. . 191

A comparison of the compressibilities of some gases with that of nitrogen at pressures below one atmosphere. By G. A. Bottomley, Doreen S. Massie and R. Whytlaw-Gray, F.R.S. 201

The relativity of Galilean frames. By E. A. Milne, F.R.S. 219

The dynamics of the combustion products behind plane and spherical detonation fronts in explosives. By Sir Geoffrey Taylor, F.R.S. 235

The velocity of sound in general relativity, with a discussion of the problem of the fluid sphere with constant velocity of sound. By A. R. Curtis 248

Thermal conductivities of organic vapours. By J. D. Lambert, E. N. Staines and S. D. Woods 262

Polar structures in the theory of conjugated molecules. I. Identification of the ethylene π-electron states. By D. P. Craig 272

Flash photolysis and spectroscopy. A new method for the study of free radical reactions. By G. Porter. (Plates 6 to 8) 284

No. A 1062. 7 February 1950

PAGE

The mechanism and kinetics of the heterogeneous polymerization of vinyl monomers. I. The benzoyl peroxide catalyzed polymerization of vinyl chloride. By W. I. Bengough and R. G. W. Norrish, F.R.S. 301

The characters of a collineation group in five dimensions. By J. A. Todd, F.R.S. 320

Studies in copolymerization. I. The evaluation of the kinetic coefficients for the copolymerization of styrene and methyl methacrylate. By H. W. Melville, F.R.S. and L. Valentine 337

Studies in copolymerization. II. A discussion of the validity of the results and some theoretical implications. By H. W. Melville, F.R.S. and L. Valentine 358

The mechanics of large bubbles rising through extended liquids and through liquids in tubes. By R. M. Davies and Sir Geoffrey Taylor, F.R.S. 375

Polar structures in the theory of conjugated molecules. II. Symmetry properties and matrix elements for polar structures. By D. P. Craig 390

Polar structures in the theory of conjugated molecules. III. The energy levels of benzene. By D. P. Craig 401

The nature of the sulphur-oxygen bond. By W. Moffitt 409

New terms of the $5d^8 6s^2$ and $5d^8 6s 6p$ configurations of the spectrum of Hg III. By E. W. Foster 429

A class of enumerations of importance in genetics. By R. A. Fisher, F.R.S. (Abstract) 438

The utilization of carbon sources by *Bact. lactis aerogenes*. I. General survey. By A. C. Baskett and Sir Cyril Hinshelwood, F.R.S. (Abstract) . . . 438

The utilization of carbon sources by *Bact. lactis aerogenes*. II. The significance of the tricarboxylic acid cycle. By A. C. Baskett and Sir Cyril Hinshelwood, F.R.S. (Abstract) 439

The utilization of potassium by *Bact. lactis aerogenes*. By A. A. Eddy and Sir Cyril Hinshelwood, F.R.S. With an Appendix by C. J. Danby, A. A. Eddy and Sir Cyril Hinshelwood, F.R.S. (Abstract) 439

No. A 1063. 22 February 1950

The effect of thermal cycles on the structure of alloys: diffusion effects in two phase alloys. By R. J. Davis and W. Hume-Rothery, F.R.S. 441

The kinetics of the thermal decomposition of normal paraffin hydrocarbons. I. The inhibition of chains and the nature of the residual reaction. By F. J. Stubbs and Sir Cyril Hinshelwood, F.R.S. 458

Configurational interaction in molecular orbital theory. A higher approximation in the non-empirical method. By D. P. Craig 474

Ionospheric cross-modulation at oblique incidence. By L. G. H. Huxley . . 486

The supersonic flow of compressible fluid through axially symmetric tubes of uniform and varying section. By R. K. Tempest 511

On the formulation of rheological equations of state. By J. G. Oldroyd . . 523

Electronic wave functions. I. A general method of calculation for the stationary states of any molecular system. By S. F. Boys 542

The diffraction of blast. II. By M. J. Lighthill 554

The dimerization of ammonia and amines. By J. D. Lambert and E. D. T. Strong 566

On the asymptotic distribution of eigenvalues. By J. S. de Wet and F. Mandl . 572

Index 581

Vibration-rotation bands of allene

BY C. H. MILLER AND H. W. THOMPSON, F.R.S
The Physical Chemistry Laboratory, Oxford

(*Received* 30 *June* 1949)

The vibrational absorption spectrum of allene has been reinvestigated using a new grating spectrometer of high resolving power. The rotational structure of many of the bands has been measured and discussed in relation to the geometrical structure of the molecule. The perpendicular-type bands associated with absorption of the fundamental frequencies of degenerate oscillations show features of particular interest. Two of these bands provide an elegant example of a type of Coriolis perturbation originally predicated by Nielsen, and which results in an unusual arrangement of the Q branches in each band.

Measurement of the vibration-rotation spectra of some of the simpler polyatomic molecules has shown that the arrangement of energy levels predicted by simple theory is often disturbed by special interactions. Among the most important of these are the Coriolis perturbations, which lead to irregular spacings of the rotation lines in the perpendicular-type bands of linear molecules or symmetrical rotators. This phenomenon has been discussed in detail by Nielsen (1944) and by Herzberg (1945). Nielsen (1937) has also drawn attention to one peculiar effect of such a vibrational-rotational interaction which may occur when a molecule has two degenerate oscillations of about the same frequency. This manifests itself by a convergence of the Q branches in the fundamental absorption bands towards the sides of the bands which are adjacent to each other, and a divergence of the Q branches towards the outer sides. The effect has been noticed with formaldehyde (Ebers & Nielsen 1937) and with several other molecules, but in most cases the small degree of molecular asymmetry and other factors seem to cause additional irregularities.

A very good example of this phenomenon was discovered some time ago in the spectrum of allene (Thompson & Harris 1944), but owing to inadequate resolving power of the prism spectrometer used, it could not be investigated fully. The bands have now been re-examined using the higher resolving power of a grating spectrometer. Other bands have also been remeasured, one of which—a perpendicular-type band near 3μ—provides a sharp contrast from those just mentioned by having an essentially regular spacing of the Q branches.

EXPERIMENTAL METHOD

Allene ($CH_2:C:CH_2$) was prepared by a modification of the method of Tapley & Giesey (1926). Allyl bromide was converted into 1.2.3-tribromopropane, and 2.3-dibromopropene was then obtained by the action of alkali. The product was treated with zinc dust suspended in 80 % ethyl alcohol. The allene evolved was condensed in a liquid air trap and purified by fractionation *in vacuo*. No impurities likely to be present could be detected by their infra-red absorption bands.

The spectrum was measured under medium dispersion using a recording rock-salt prism spectrometer of the usual kind.

The grating spectrometer was built in this laboratory, and since it will be used for many measurements of this kind, a brief description is given now. The optical arrangement is of the Pfund-Hardy type shown in figure 1.

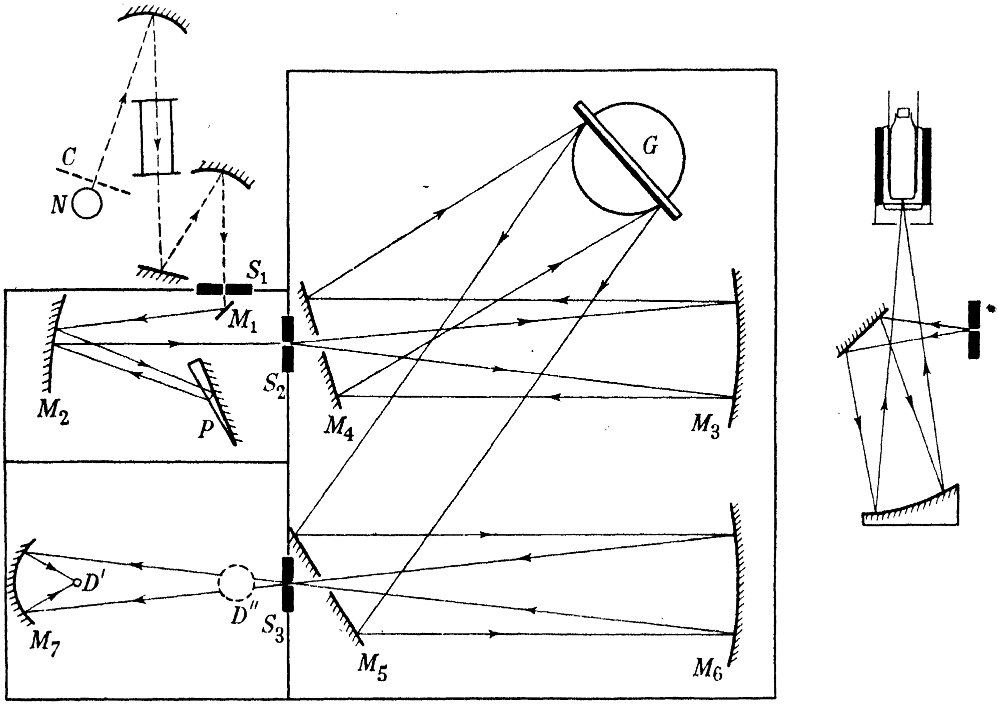

Figure 1

The large paraboloidal mirros M_3, M_6 are 25 cm. in diameter and of about 60 cm. focal length. The effective area of the echelette gratings is about 12·5 × 10 cm. Two ruled gratings obtained from the University of Michigan, and with 2400 and 1200 lines per inch respectively, were used between 6 and 14μ. A third grating with 7200 lines per inch was an aluminized replica from a Wood master, and used around 3μ. The grating turn-table can be caused to rotate continuously at any desired speed by a synchronous motor with suitable gears; alternatively, it can be rotated by a manual drive, readings being taken on a calibrated revolution counter geared to the motion. For the foreprism P, either a 20°-angled rock-salt prism or a 12°-angled potassium bromide prism is used, the latter at wave-lengths greater than about 11μ; each prism has a plane mirror on its back face. The whole instrument is enclosed in a plastic box, all controls for the slits and foreprism table being on the outside. The calibration of the spectrometer was carried out using known absorption lines of water vapour, ammonia, methane and carbon dioxide. The absorption cells were glass or metal tubes 5 cm. in diameter and 5 to 20 cm. in length with flanged ends upon which rock-salt plates were fixed with soft Apiezon wax.

Two detectors (D', D'') were used. One is an evacuated Schwarz thermocouple of about 100 Ω resistance and response time rather less than 0·2 sec. The image at the back slit S_3 is reduced fivefold by the ellipsoidal mirror M_7 before falling on the receiver of the couple. This thermocouple was used for all spectral regions. Between 2 and 5μ, however, photoconductive cells of lead sulphide and lead telluride, cooled by solid carbon dioxide or liquid air respectively, were used to obtain higher sensitivity and correspondingly greater resolving power. With the thermocouple it is usually possible to resolve lines about 1 cm.$^{-1}$ apart, and with the photoconductive cells at 3μ sharp lines more than 0·3 cm.$^{-1}$ apart can be separated in the most favourable circumstances. In the latter case the limiting factor at present is the quality of the optical system rather than lack of detector sensitivity. When using the photoconductive cells, the image is condensed on to the active surface of the detector by the system of mirrors shown at the side of figure 1.

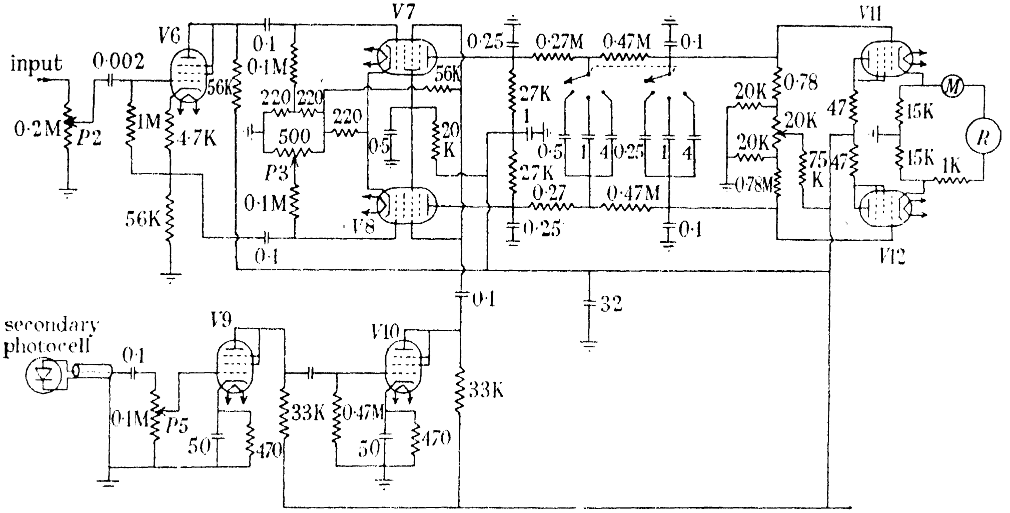

Figure 2

The spectra were generally recorded continuously on a milliammeter pen recorder. The system of amplification necessary for this differed for the two detectors. In each case the beam of radiation entering the instrument was interrupted at a constant frequency by a shutter placed just in front of the source. With the relatively slow thermocouple, low frequency was necessary and 4 c./sec. proved most suitable. The electronic amplifier has been described in detail elsewhere (Miller, Richards & Thompson 1947). The output from the couple was fed into a transformer with step-up ratio of 200, and the resulting a.c. voltage then amplified by a carefully tuned valve amplifier with a band pass of about one cycle.

When the photoconductive cells were being used, the entrant beam was chopped at higher frequency, 800 c./sec. for the lead sulphide cell and about 400 c./sec. for the telluride cell. The d.c. voltage applied across the cell could be varied between 50 and 200 V. The output signal was then fed across a load resistance (variable between 10^5 and $1{\cdot}8\times10^6\,\Omega$) into a valve amplifier, tuned with resistance-capacity filters, so as to have a flat response for frequencies between 120 and 1200 c./sec. The resultant output voltage was then introduced into a homodyne (phase sensitive) rectifier shown in figure 2.

The phase-splitting valve V_6 (type VR 91) produces a push-pull signal voltage required for the rectifier stage V_7/V_8 (type 6 L 7). The second pair of control grids in this stage are connected in parallel and are supplied with a reference voltage of the same frequency as the signal, the phase of which is adjusted with respect to the signal so that a d.c. voltage results which is proportional to the size of the signal voltage. Noise accompanying the signal, but differing from it in frequency, passes through as small a.c. voltages which can be filtered out. The reference voltage is obtained from a rectifier-type photocell illuminated periodically from a small filament bulb placed behind the interrupter sector used for chopping the main beam of radiation, amplification being effected by two resistance-capacity coupled stages V_9/V_{10} (type VR 91).

The push-pull output from V_7/V_8 is led into a two-stage resistance-capacity filter, the time constant of which can be varied by switches, the overall time of response being variable between 0·2 and 20 sec. The output from the filter is fed to a cathode follower stage V_{11}/V_{12} (type VR 91) and thence to the pen recorder.

The power supplies are obtained from conventional valve-regulated smoothed circuits, and the entire system of homodyne rectification has been found better than a conventional tuned amplifier for the elimination of noise and for obtaining the best operating conditions.

The region 8 *to* 14μ

The most striking feature of the whole spectrum is the pair of perpendicular-type bands between 8 and 14μ. Each band contains, as found previously, a succession of intense Q branches above the general background absorption, corresponding to rotational transitions $\Delta J = 0$, $\Delta K = \pm 1$. Between these Q branches, however, other absorption maxima are now seen. They are probably due in general to accumulations of intensity resulting from overlapping lines in the subsidiary P and R branches ($\Delta J = \pm 1$) associated with each change of ΔK, but some of the peaks appear to be satellites of the main Q branches. This is particularly noticeable in band A between 840 and 900 cm.$^{-1}$, and the satellites increase steadily in intensity towards lower frequencies so that the main Q branch at 845·5 cm.$^{-1}$ has an almost equally strong neighbour at 847·5 cm.$^{-1}$.

The bands are shown in figure 3 and the positions (cm.$^{-1}$) of the submaxima are given in table 1. For convenience in reference the Q branches have been numbered arbitrarily. The blunt nature of most of the peaks made it impossible to fix the positions to within 0·1 cm.$^{-1}$.

It is also seen that there is a well-marked alternation of intensity among the Q branches, as would be expected with a molecule of this symmetry type with identical hydrogen nuclei.

The region 3·1 *to* 3·4μ

The previous measurement showed two bands in this region connected with stretching vibrations of C—H bonds. Each of these bands is now resolved into rotational structure, shown in figure 4. One has the three-branch contour typical of a parallel-type band, with Q branch at 3006 cm.$^{-1}$ and P/R maxima at 2996/3020 cm.$^{-1}$. It is possible that using lower pressures the individual P and R lines in the two side

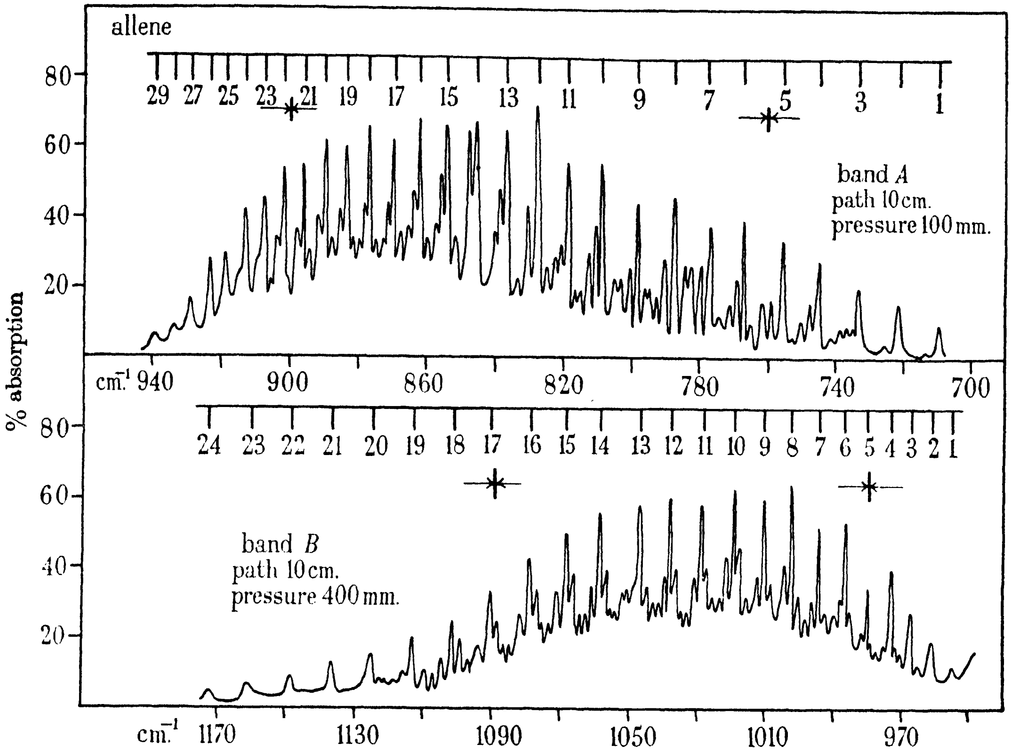

FIGURE 3

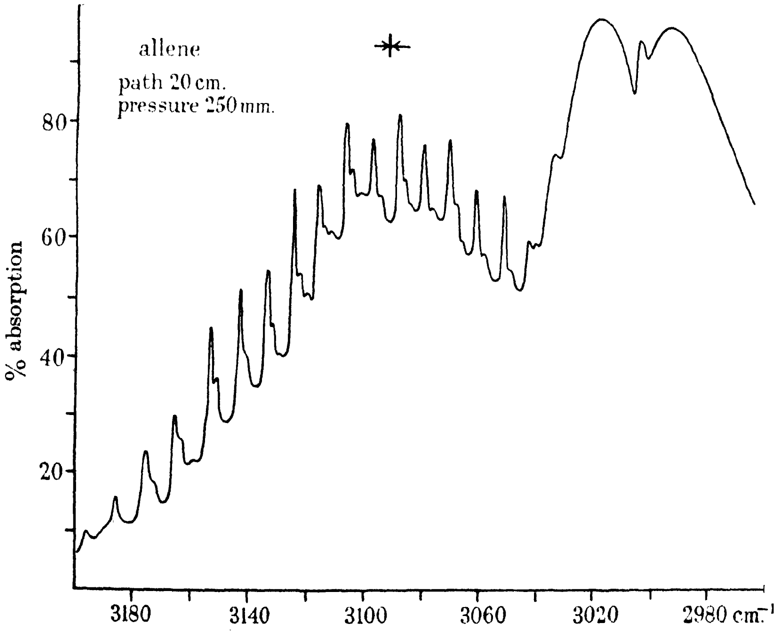

FIGURE 4

TABLE 1

s = strong, w = weak

Q	ν (cm.$^{-1}$, *vacuo*)	Q	ν (cm.$^{-1}$, *vacuo*)	Q	ν (cm.$^{-1}$, *vacuo*)
			band A		
1	709·9	9	798·1 *w*	17	869·5 *w*
	713·3		800·5		871·2
2	721·7		802·7		872·0
	724·9		804·9		874·5
3	733·2	10	808·2 *s*	18	876·5 *s*
	734·7		810·2		877·9
	736·4		812·7		879·8
	737·7		814·6		881·7
	740·8		816·0	19	883·5 *w*
4	744·6	11	818·3 *w*		884·7
	747·0		820·2		887·6
	749·7		822·0	20	889·6 *s*
	752·5		824·6		891·7
5	755·5	12	827·6 *s*		894·2
	758·2		830·5	21	895·8 *w*
	761·2		833·4		897·5
	765·0	13	836·5 *w*		(900·0)
6	766·6		838·1	22	901·8 *s*
	769·0		839·5		903·8
	771·6	14	845·5 *s*		905·5
	774·6		847·5	23	907·3 *w*
7	777·1 *w*		851·8	24	912·7 *s*
	779·5	15	854·0 *w*	25	918·2 *w*
	782·4		855·6	26	923·1 *s*
	784·0		856·5	27	(928·4)
8	787·7 *s*		860·0	28	(933·5)
	790·1	16	862·0 *s*	29	(938·6)
	792·6		863·6		
	794·7		864·9		
	795·5		867·9		
			band B		
1	955·2	10	1019·4 *s*	15	1068·5
2	961·0		1021·6		1071·1
	965·0		1023·6		1073·9
3	967·2		1025·5		1075·9
	970·4		1027·3		1077·1
	972·1	11	1028·5 *w*	16	1079·1
4	973·3 *s*		1030·8		1082·0
	974·4		1033·1		1085·0
	977·5		1035·0		1086·5
	979·0		1036·5		1088·4
5	980·0 *w*	12	1038·0 *s*	17	1090·2
	981·6		1039·7		1092·8
	985·9		1041·2		1096·8
6	986·8 *s*		1042·8		1099·4
	987·5		1044·7	18	1101·6
	989·5	13	1047·1 *w*		1104·6
	993·1		1050·6		1107·0
7	994·2 *w*		1052·0		1109·6
	996·1		1054·0	19	1113·3
	998·5		1055·5		1116·1
	1000·0		1056·9		1119·0
8	1002·4 *s*	14	1058·3 *s*		1121·7
	1004·3		1061·1		1123·0
	1009·4		1062·9	20	1125·1
9	1010·5 *w*		1063·9	21	1136·8
	1012·5		1066·8	22	(1148·6)
	1016·1			23	(1160·6)
	1018·0			24	(1172·6)

branches might be resolvable, but these lines appear to be heavily broadened and have not yet been separated.

The other band at higher frequency has a perpendicular-type structure, with a series of intense Q branches standing out above the general background absorption. These Q branches show an alternation of intensity, and their positions are given in table 2.

TABLE 2

s = strong; w = weak

ν (cm.$^{-1}$, *vacuo*)		$\Delta\nu$
3035·2		8·9
3044·1		8·8
3052·9	*s*	9·2
3062·1	*w*	9·0
3070·1	*s*	9·1
3080·2	*w*	8·9
3089·1	*s*	8·9
3098·0	*w*	9·2
3107·2	*s*	9·4
3116·6	*w*	8·4
3125·0	*s*	9·1
3134·1	*w*	9·4
3143·5	*s*	10·0
3153·5	*w*	12·0
3165·5		9·9
3175·4		9·8
3185·2		10·4
3195·6		

Bands in other regions

The band previously found near 5μ has been re-examined and found to have three submaxima at 1964, 1952, 1940 cm.$^{-1}$, typical of the parallel-type contour. The two bands near 1390 and 1695 cm.$^{-1}$ appear also to be of this type, but have not been measured in detail.

GENERAL DISCUSSION

The most interesting points for discussion concern the perpendicular-type bands which arise from the absorption of the fundamental frequencies of degenerate vibrations. Assuming that in allene the bond lengths are $\nu_{\mathrm{C—C}} = 1{\cdot}33$ Å, $\nu_{\mathrm{C—H}} = 1{\cdot}07$ Å, and the H—C—H angle is 120°, the moment of inertia (I_C) about the twofold axis of rotation is $5{\cdot}8 \times 10^{-40}$ g.cm.^{2} and the other two equal moments of inertia are about 96×10^{-40}. In the simplest case, therefore, the spacing of Q branches in a perpendicular band should be given by $2(A - C)$, in which $C = h/8\pi^2 I_C$ and $A = 8/h\pi^2 I_A$. This gives a value close to 9 cm.$^{-1}$. The effect of Coriolis interaction is usually to modify this spacing to a value $2\{(1+\zeta)A - C\}$, ζ being the Coriolis coupling coefficient. The band around 3100 cm.$^{-1}$ is seen to consist essentially of Q branches with spacing close to 9 cm.$^{-1}$, and the Coriolis coefficient in this case must be very small. A similar result was found by Eyster (1938) for a harmonic band of allene at 9100 cm.$^{-1}$. In both bands, however, the regular spacing is disturbed, and the reason for the irregularities is not obvious. It is perhaps worth noting that there are signs of a slight divergence of the rQ branches in the direction of higher frequencies, a peculiarity also found by Eyster for the harmonic band. The band now measured around 3100 cm.$^{-1}$ shows the alternation of intensity in the Q branches which is to be expected. It is not at present possible to assign K values to these Q branches but it seems probable that the band origin lies near 3100 cm.$^{-1}$.

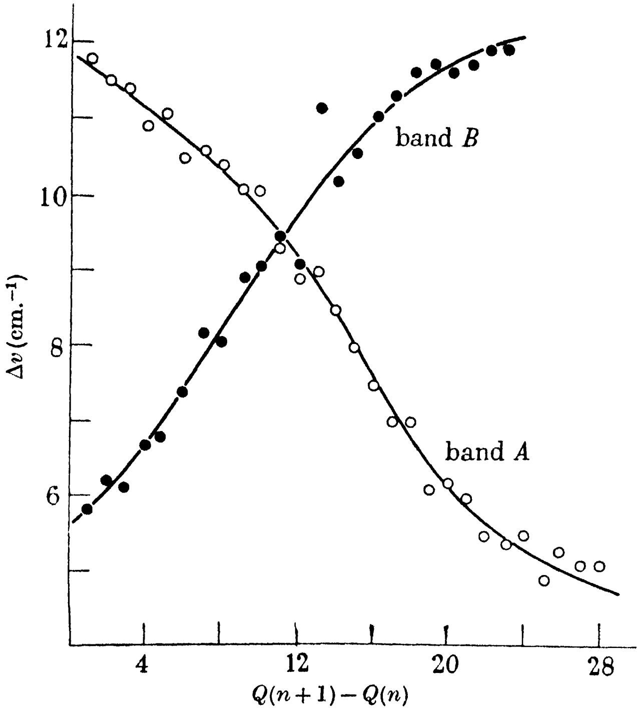

Figure 5

The structure of the pair of perpendicular bands between 8 and 14μ provides a sharp contrast with the above. These bands illustrate lucidly the type of Coriolis perturbation first discussed by Nielsen (1937) which may arise when two degenerate vibrations have approximately the same frequency. Near the centre of each band the spacing of Q branches is close to the above value of 9 cm.$^{-1}$, but it falls on the sides of the bands adjacent to each other, and rises on the outer sides of the bands. This effect is shown in figure 5, and there can be no doubt about its dominating influence upon the arrangement of the Q branches. In both bands, however, there are anomalies and finer details which cannot be properly accounted for. In one band the 'limiting' spacings are at approximately 12 and 5 cm.$^{-1}$, and in the other 12 and 6 cm.$^{-1}$. Making reasonable approximations, and disregarding the small change in the mean values of the moments of inertia in the lower and upper states, the arrangement of the Q branches in the two bands was found by Nielsen (1944) to be given by

$$\nu = \left(\frac{\nu_1+\nu_2}{2}\right) - \{A - C\} \pm \sqrt{\left\{\left(\frac{\nu_1-\nu_2}{2}\right)^2 + 4K^2\zeta A^2 \pm 2K(A - C)\right\}},$$

in which $K = 0, \pm 1, \pm 2, \ldots$. This formula implies limiting spacings of

$$2\{(1 \pm \zeta)A - C\}.$$

The assignment of K values to the Q lines in the two bands and the location of their centres is not immediately obvious. The most satisfactory fit with the experimental results which we have been able to obtain is given by the formula

$$\nu = 932{\cdot}5 \pm 9{\cdot}0K \pm \surd(9220+34K^2).$$

According to this, the $K = 0$ lines are respectively 836·5 and 1028·5, these being the first lines of the rQ branches and being 'weak' in the scheme of alternating intensities. The above expression gives a reasonably satisfactory fit with the Q lines for values of K up to about 8 on each side of each band, and the parameters are consistent with those to be expected if the moments of inertia have the values estimated above. The expression implies a value of about 0·6 for the Coriolis coupling coefficient ζ. We have explored the introduction of a term in K^2 to allow for the slight alteration of moments of inertia in the excited levels, but this does not seem to eliminate the discrepancies. The band origins would appear to be near to 832 and 1025 cm.$^{-1}$. The apparent doubling of Q branches already mentioned also required explanation, and may be connected in some way with the removal of vibrational degeneracy.

The parallel-type bands of allene have the expected structure, the separation between R and P maxima in the contour agreeing well with the value calculated from the formula of Dennison & Gerhard (1933).

The present results confirm in all essentials the assignment of frequencies previously made, but a minor alteration may be needed in the values for the C—H stretching modes. Raman intervals measured by Linnett & Avery (1938) were 2858, 2992 and 3062 cm.$^{-1}$, of which the first is the harmonic of the C—H deformation at 1430 cm.$^{-1}$. The present work gives a parallel band at 3006 cm.$^{-1}$, and a perpendicular band near 3100 cm.$^{-1}$. It may therefore be best to assign 3062 (Raman) to the A_1 class vibration which is not permitted in the infra-red 3006 (Raman 2992) to the B_2 class vibration, and 3100 to the E (degenerate) class. This value for the degenerate vibration is parallel to that found for the analogous mode in the isoelectronic molecule keten, namely about 3160 cm.$^{-1}$ (Halverson & Williams 1947).

We are grateful to the Government Grant Committee of the Royal Society and to the Hydrocarbon Research Group of the Institute of Petroleum for grants in aid of equipment, and to the Telecommunications Research Establishment, Malvern, for photoconductive cells. We also thank the Rhodes Trustees for a Scholarship to one of us (C. H. M.).

REFERENCES

Dennison, D. M. & Gerhard, S. L. 1933 *Phys. Rev.* **43**, 197.
Ebers, E. S. & Nielsen, H. H. 1937 *J. Chem. Phys.* **5**, 822.
Eyster, E. H. 1938 *J. Chem. Phys.* **6**, 580.
Halverson, F. & Williams, V. Z. 1947 *J. Chem. Phys.* **15**, 552.
Herzberg, G. 1945 *Infra-red and Raman spectra.* New York: van Nostrand.
Linnett, J. W. & Avery, W. H. 1938 *J. Chem. Phys.* **6**, 686.
Miller, C. H., Richards, R. E. & Thompson, H. W. 1947 *Rep. Inst. Pretoleum Hydr. Res. Group*, no. 23.
Nielsen, H. H. 1937 *J. Chem. Phys.* **5**, 818.
Nielsen, H. H. 1944 *J. Opt. Soc. Amer.* **34**, 521.
Tapley, M. W. & Giesey, P. M. 1926 *J. Amer. Pharm. Ass.* p. 173.
Thompson, H. W. & Harris, G. P. 1944 *Trans. Faraday Soc.* **40**, 295.

Vibration-rotation bands of some polyatomic molecules

By A. R. H. Cole and H. W. Thompson, F.R.S.
The Physical Chemistry Laboratory, Oxford

(*Received* 30 *June* 1949)

The rotational structures of some vibrational absorption bands of vinyl chloride, vinyl fluoride, vinylidene fluoride and glyoxal have been measured with high dispersion. An analysis of bands of different types has been carried out in order to test vibrational assignments and to correlate the observed rotational structure with the molecular geometry. An ambiguity in the allocation of vibration frequencies of vinyl fluoride has been removed, and the frequencies for the different vinyl halides have been correlated with each other. Glyoxal has been shown to possess the *trans* structure, in agreement with conclusions based on other physical measurements.

Perhaps the most important reasons for measuring the rotational fine structure of vibration bands of polyatomic molecules are (*a*) the derivation of the moments of inertia, and (*b*) the assignment of the vibration frequencies to particular normal modes. In either case, complete success is limited by the degree of molecular symmetry, but even with asymmetrical rotators it is sometimes possible to carry out an approximate analysis which is sufficient for the purposes involved. We have recently remeasured some of the vibration bands of certain asymmetrical molecules, for which either the vibrational assignment made previously on the basis of low-dispersion measurements was in question, or the molecular geometry was undecided. In this paper we describe the results for some of these molecules.

The spectra were measured with the high dispersion of a recording grating spectrometer, described in the preceding paper (Miller & Thompson 1949), and the other experimental arrangements were similar. The wave numbers given below have been referred to vac. units.

(1) Vinyl fluoride (CH_2:CHF)

The spectrum was measured previously with medium dispersion (Torkington & Thompson 1945*a*), and an assignment of frequencies was made on the basis of the band contours, general magnitudes, and in relation to the other vinyl halides (Thompson & Torkington 1944, 1945*b*). More recently Pitzer & Freeman (1946) have suggested a modified assignment, but Torkington (1949) has proposed a further re-allocation of the frequencies which leads to a more satisfactory treatment of the force constants in the whole series of the vinyl halides. It was therefore hoped to obtain more experimental evidence about the assignment of frequencies from the details of the rotational fine structure of the bands concerned.

The sample of vinyl fluoride was a purified specimen supplied by Imperial Chemical Industries Ltd. (General Chemicals Division). It had been prepared from vinyl bromide by conversion to 1.2.2-tribromoethane, the latter being treated with antimony fluoride and antimony pentachloride to obtain 1.2-dibromo-2-fluoro-ethane, and this being treated with zinc dust in alcohol. The product was fractionated at low temperatures.

The bands in the region 8 to 15μ were measured and are shown in figures 1 and 2. The molecule falls in the symmetry class C_s. The twelve normal modes will include nine planar and three out-of-plane vibrations, all of which may appear as fundamentals in the infra-red. To a first approximation these vibrations will be of the following kinds, as discussed in the earlier papers:

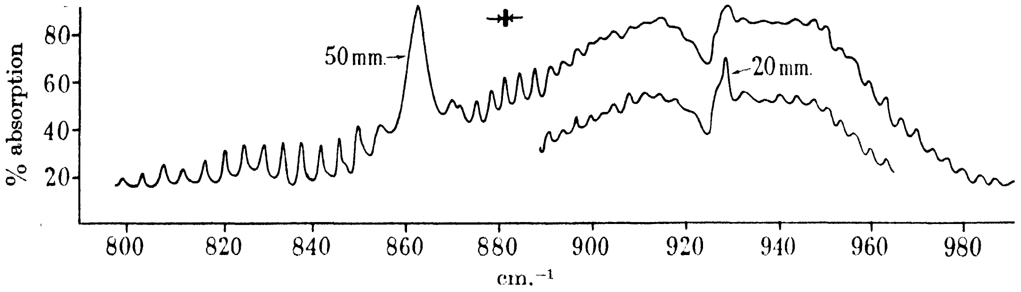

FIGURE 1. Vinyl fluoride. Path length 10 cm., pressures 50 and 20 mm.

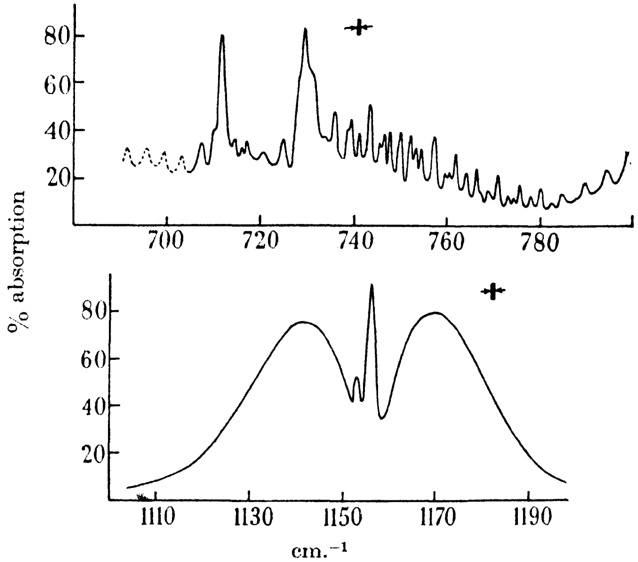

FIGURE 2. Vinyl fluoride. Path length 10 cm., pressure 200 mm.

3 C—H stretching ν_{10}, ν_{11}, ν_{12},
1 C—F stretching ν_3,
1 C=C stretching ν_9,
1 symmetrical CH_2 planar deformation ν_8,
1 CH_2 planar rocking ν_6,
1 CH planar deformation ν_7,
1 CH_2 out-of-plane deformation ν_4,
1 CH out-of-plane deformation ν_5,
1 torsional oscillation ν_2,
1 planar C—C—F deformation ν_1

The main ambiguity in the previous assignments involves the out-of-plane vibrations. The assignments are given in table 1. From known dimensions in related molecules based on electron-diffraction measurements, we may assume that in vinyl fluoride $r_{C=C} = 1{\cdot}35\,\text{Å}$, $r_{C-H} = 1{\cdot}08\,\text{Å}$, $r_{C-F} = 1{\cdot}36\,\text{Å}$, and angles of 120°. The principal moments of inertia are then 12·9, 80·2 and $93{\cdot}1 \times 10^{-40}$ g.cm.^{2}. The least axis (A) is in the plane of the molecule, inclined at 29° to the C=C bond, as shown in figure 3, and the major axis (C) is perpendicular to the molecular plane. The molecule will behave very nearly like a symmetrical top with $I_B = I_C = 86{\cdot}7 \times 10^{-40}$, but there will be slight deviations arising from the asymmetry and also from the hybrid character of the bands due to planar modes. The out-of-plane vibrations will give rise to pure C type perpendicular bands, with a spacing of Q branches about $2(A-B)$ in which $A = h/8\pi^2cI_A$, $B = h/8\pi^2cI_B$. Using the above values, this spacing is 3·7 cm.$^{-1}$. There will also be an accumulation of intensity near the band centre. The A type bands will have P, Q, R contour, in which the P-R spacing calculated from the formula of Gerhard & Dennison (1933) is about 26 cm.$^{-1}$. B type bands will have an essentially perpendicular type structure, but a loss of intensity near the centre. The planar modes will give rise to A/B hybrids.

TABLE 1

mode	Thompson & Torkington	Pitzer & Freeman	Torkington
ν_2	715	715	715
ν_4	732	860	860
ν_5	860	924	732
ν_6	924	—	924
ν_3	1153	—	1153

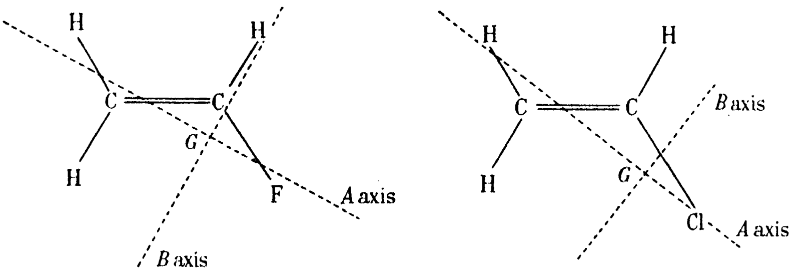

FIGURE 3

The rotational structure of the bands now measured provides us with a clear allocation of the frequencies. Figure 1 shows two bands at 862·7 and 928 cm.$^{-1}$. The former is a simple C type band with well resolved Q branches, which have been fitted to the formula (1),

$$\nu = \nu_0 + 1{\cdot}78 + 3{\cdot}56K - 0{\cdot}035K^2, \tag{1}$$

in which $K = 0, 1, 2, \ldots$ for the rQ branches, and $-1, -2, \ldots$ for the pQ branches. The actual positions of the Q branches observed and calculated are given in table 2. In this band, the central peak at 862·7 cm.$^{-1}$ occurs between the first lines of the pQ

and *rQ* branches, and corresponds to the transition $\Delta v = 1$, $\Delta J = 0$, $\Delta K = 0$; in the case of the symmetric top this transition would not occur. The above formula (1) leads to the results

$$(A''-B'') = 1{\cdot}816\,\text{cm.}^{-1}, \quad (A'-B') = 1{\cdot}781\,\text{cm.}^{-1}.$$

The value of $(A''-B'')$ calculated from the moments of inertia assumed above is 1·85 cm.$^{-1}$. It is therefore concluded that either the assumed molecular dimensions are slightly in error, or there is some slight disturbance due to the asymmetry, and the former of these is perhaps the more likely.

TABLE 2. $\nu_0 = 862{\cdot}7$ CM.$^{-1}$

	pQ branches				*rQ* branches		
K''	$\nu_{\text{obs.}}$	$\nu_{\text{calc.}}$	Δ	K''	$\nu_{\text{obs.}}$	$\nu_{\text{calc.}}$	Δ
1	—	860·9	—	0	—	864·5	—
2	—	857·2	—	1	—	868·0	—
3	—	853·5	—	2	—	871·5	—
4	849·7	849·7	0	3	875·0	874·8	−0·2
5	845·8	845·8	0	4	878·2	878·2	0
6	841·9	841·9	0	5	881·3	881·4	0·1
7	837·8	837·8	0	6	884·5	884·6	0·1
8	833·7	833·8	0·1	7	887·8	887·7	−0·1
9	829·6	829·6	0	8	890·9	890·7	−0·2
10	825·4	825·4	0	9	893·8	893·7	−0·1
11	821·2	821·1	−0·1	10	896·3	896·6	0·3
12	816·9	816·7	−0·2	11	899·5	899·4	−0·1
13	812·4	812·3	−0·1				
14	807·8	807·8	0				
15	803·4	803·2	−0·2				

The band centred at 928 cm.$^{-1}$ is clearly a *B*/*A* hybrid. The *Q* branches of the perpendicular (*B*) component have been partially separated, more clearly on the higher frequency side, where the spacing of about 3·5 cm.$^{-1}$ is close to that expected. This *B* type structure will have a central minimum, which is clearly present, but the contribution from *A* type structure introduces a central peak and adds a background to the *pQ* and *rQ* branches which makes the latter less prominent.

Vinyl fluoride also shows two perpendicular type bands at 711·7 and 729·6 cm.$^{-1}$, shown in figure 2. The *Q* branches in these bands overlap badly, and it is impossible to separate them into clearly defined series. Also, at the lower frequency side, accurate measurement was difficult because of the absorption by atmospheric carbon dioxide. However, the mean spacings in each case are obviously close to 3 cm.$^{-1}$, and the slightly low value may arise partly because it is obtained from the *rQ* branches where slight convergence may be occurring. It is certain that both these bands involve purely out-of-plane vibrations.

Another band of vinyl fluoride at 1156 cm.$^{-1}$, shown in figure 2, has *A* type contour, with slight superposition of *B* type character. The spacing of *P*/*R* maxima is 28 cm.$^{-1}$, agreeing closely with the expected value. This band is due to the C—F stretching mode.

The rotational structure of the bands just described shows unequivocally that the vibrational assignment suggested by Torkington is correct. The band at 928 cm.$^{-1}$

cannot be due to an out-of-plane vibration, as suggested by Pitzer & Freeman, and is more fittingly assigned to the planar rocking mode. The rotational structure alone does not allow us to decide which of 729·6 and 862·7 cm.$^{-1}$ should be ν_4 and which ν_5, but the assignment selected by Torkington gives complete uniformity and confirms in the values of the force constants the peculiar effects brought about by introduction of fluorine.

(2) VINYL CHLORIDE (CH_2:CHCl)

The spectrum was measured previously by Thompson & Torkington (1944, 1945*b*), and a satisfactory assignment of frequencies was made. The sample now used was from a cylinder of a commercial product, repurified by fractionation *in vacuo*.

The bands between 9 and 12μ have been remeasured and are shown in figure 4. Two of the bands are seen clearly to show a perpendicular *C* type structure associated with out-of-plane vibrations of value 896·8 and 942·5 cm.$^{-1}$. The other band at 1030 cm.$^{-1}$ is a *B*/*A* hybrid associated with the planar rocking of the CH_2 group.

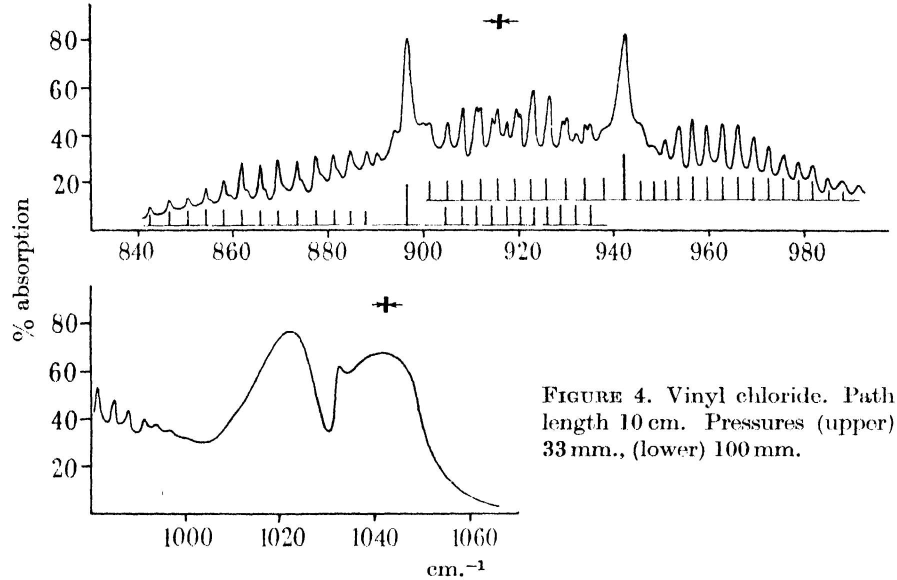

FIGURE 4. Vinyl chloride. Path length 10 cm. Pressures (upper) 33 mm., (lower) 100 mm.

Assuming that in vinyl chloride $r_{C=C} = 1{\cdot}35$ Å, $r_{C—H} = 1{\cdot}08$ Å, $r_{C—Cl} - 1{\cdot}69$ Å’ and with angles 120°, the moments of inertia are 15·4, 133·9 and 149·3 × 10^{-40} g.cm.^{2}. The least axis is inclined at 38° to the C=C bond as shown in figure 3. Similar considerations about the rotational structure apply here as for vinyl fluoride discussed above, except that the proportion of different types in the hybrid bands is altered, and in the present case *A* and *B* contribute about equally.

The location of the *Q* branches in the bands at 896·8 and 942·5 cm.$^{-1}$ is given in tables 3 and 4. In the former case the positions can be adequately reproduced by the formula

$$\nu = \nu_0 + 1{\cdot}67 + 3{\cdot}344K - 0{\cdot}027K^2, \tag{2}$$

in which $K = 0, 1, 2, \ldots$ for the rQ branches, and $K = -1, -2, \ldots$ for the pQ branches. In the same way the position of the *Q* branches in the other band can be fitted roughly to the formula

$$\nu = \nu_0 + 1{\cdot}67 + 3{\cdot}334K - 0{\cdot}022K^2, \tag{3}$$

but in this case the agreement over the whole band is not so good. It seems that here the rQ branches are linearly spaced out to about $K'' = 15$, which would mean that this band requires no term in K^2, but, on the other hand, the pQ branches show a slight divergence towards lower frequencies. The values of $(A''-B'')$ thus determined are 1·70 and 1·69 cm.$^{-1}$ which are to be compared with the value 1·62 cm.$^{-1}$ calculated from the moment of inertia assumed above.

The rotational structure of these bands confirms their assignment made previously.

TABLE 3. $\nu_0 = 896{\cdot}8$ CM.$^{-1}$

pQ branches				rQ branches			
K''	$\nu_{\text{obs.}}$	$\nu_{\text{calc.}}$	Δ	K''	$\nu_{\text{obs.}}$	$\nu_{\text{calc.}}$	Δ
1	—	895·1	—	0	—	898·5	—
2	—	891·7	—	1	—	901·8	—
3	888·2	888·2	0	2	905·1	905·1	0
4	884·7	884·6	−0·1	3	908·3	908·3	0
5	881·1	881·1	0	4	911·5	911·4	−0·1
6	877·6	877·4	−0·2	5	914·5	914·5	0
7	873·7	873·7	0	6	917·6	917·6	0
8	869·7	870·0	0·3	7	920·4	920·6	0·2
9	866·0	866·2	0·2	8	923·3	923·5	0·2
10	862·1	862·3	0·2	9	926·5	926·4	−0·1
11	858·3	858·4	0·1	10	929·5	929·2	−0·3
12	854·6	854·5	−0·1	11	932·3	932·0	−0·3
13	850·7	850·4	−0·3	12	935·0	934·7	−0·3
14	846·9	846·4	−0·5				
15	842·8	842·2	−0·6				

TABLE 4. $\nu_0 = 942{\cdot}5$ CM.$^{-1}$

pQ branches				rQ branches			
K''	$\nu_{\text{obs.}}$	$\nu_{\text{calc.}}$	Δ	K''	$\nu_{\text{obs.}}$	$\nu_{\text{calc.}}$	Δ
1	—	940·8	—	0	—	944·2	—
2	—	937·4	—	1	—	947·5	—
3	933·9	934·0	0·1	2	950·7	950·8	0·1
4	930·4	930·5	0·1	3	953·8	954·0	0·2
5	926·8	927·0	0·2	4	956·7	957·2	0·5
6	923·1	923·4	0·3	5	959·9	960·3	0·4
7	919·5	919·7	0·2	6	962·9	963·4	0·5
8	915·7	916·1	0·4	7	966·1	966·4	0·3
9	912·1	912·4	0·3	8	969·4	969·4	0
10	908·6	908·6	0	9	972·7	972·4	−0·3
11	905·1	904·8	−0·3	10	975·8	975·3	−0·5
12	901·2	901·0	−0·2	11	979·0	978·2	−0·8
				12	981·9	981·0	−0·9
				13	985·1	983·8	−1·3
				14	988·2	986·5	−1·7
				15	991·3	989·2	−2·1

(3) VINYLIDENE FLUORIDE ($CH_2{:}CF_2$)

The sample, also supplied by Imperial Chemical Industries Ltd., had been prepared as given in the previous paper by Torkington & Thompson (1945*a*), who measured the spectrum and made a tentative assignment of some frequencies. Several bands have been remeasured (figure 5), and the detailed contour is made more evident than in the earlier work. The band at 803 cm.$^{-1}$ is certainly of the type C predicted by Badger & Zumwalt (1938) but the splitting of the submaxima cannot at present be explained. This frequency must be attributed to an out-of-plane deformation mode, and almost certainly that which involves a bending of the CH_2 group. The band at 955 cm.$^{-1}$, previously detected as a shoulder, is now seen to have a B type contour with central minimum. The previous allocation of the band at 926 cm.$^{-1}$ to the symmetrical CF_2 stretching mode seems correct. This vibration would involve a change of electric moment parallel to the C=C axis. As pointed out in the earlier paper, this axis will be the intermediate axis of inertia if we assume conventional bond lengths and angles, namely, $r_{\mathrm{C=C}} = 1{\cdot}35$ Å, $r_{\mathrm{C-H}} = 1{\cdot}08$ Å, $r_{\mathrm{C-F}} = 1{\cdot}36$ Å and angles of 120°, and the band due to the CF_2 stretching mode should then have a B type contour. This is certainly not the case, for the band has the appearance of an essentially A type structure, and in order to meet the case it is necessary to interchange the A and B axes of inertia by assuming shorter C—F bond lengths. At the same time, the band at 926 cm.$^{-1}$ has a small submaximum at 922·5 cm.$^{-1}$, the cause of which is not clear, for hybrid structure should not occur in this case.

A weak absorption peak occurs at 897 cm.$^{-1}$, not previously found.

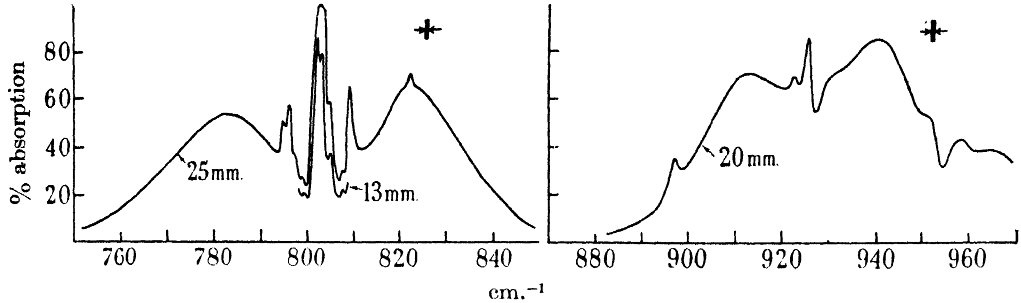

Figure 5. Vinylidene fluoride. Path length 10 cm. Pressures (left) 25 and 13 mm., (right) 20 mm.

(4) Glyoxal (CHO:CHO)

The ultra-violet, fluorescence and infra-red spectra of this molecule have been studied previously by Thompson (1940) and more recently by Gaydon (1947). There still remains some doubt about the vibrational assignment, and although the geometrical form of the molecule suggested by electron diffraction (LuValle & Schomaker 1939) would be the *trans* structure, the spectroscopic evidence is still uncertain.

Glyoxal was prepared by heating the polymer with phosphorus pentoxide *in vacuo*, the product being refractionated *in vacuo* several times before being allowed to evaporate into the absorption cell. The tendency of the vapour to polymerize was reduced by using fairly low pressures (*c.* 100 mm.). The spectrum was measured with medium dispersion for comparison with the earlier data, and certain differences were noticed in the region 1000 to 1100 cm.$^{-1}$. It was also found that a broad absorption in this range remained in the cell after evacuation, and a waxy film often appeared on the windows. Further examination confirmed that these spurious bands were due to the polymer, and the bands given earlier at 985, 1098 and 1379 cm.$^{-1}$ were due to some impurity of this kind. The spectrum of pure glyoxal is shown in figure 6. The bands around 800, 1310 and 2836 cm.$^{-1}$ were then measured with high dispersion, with the results shown in figure 7. Lines between 1340 and 1360 were obscured by the absorption of atmospheric water vapour.

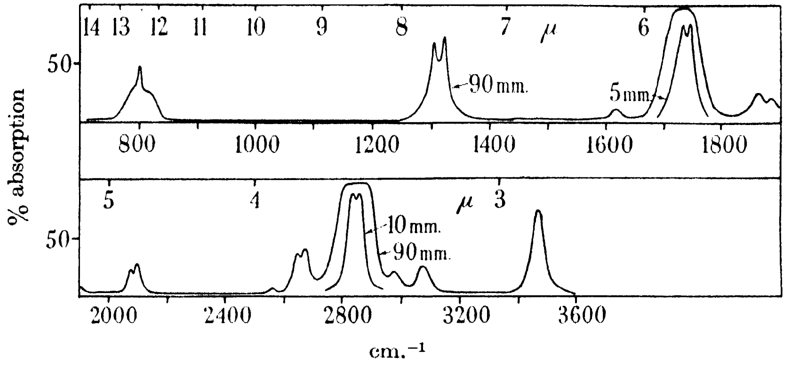

FIGURE 6. Glyoxal. Path length 27 cm.

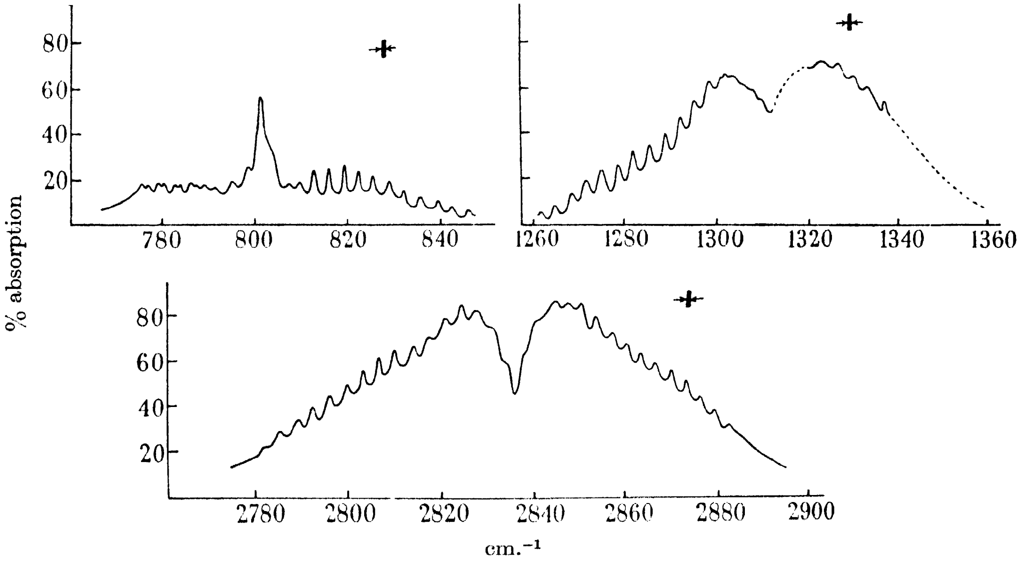

FIGURE 7. Glyoxal. Upper figures: path length 20 cm., pressure 100 mm. Lower figure: path length 10 cm., pressure 20 mm.

Three geometrical forms are possible for this molecule, namely, the *cis*, *trans* and non-planar structures. Molecules such as this, involving pronounced resonance stabilization, may be expected to have a planar form, and on other grounds, too, the non-planar structure can be discarded. The principal moments of inertia and the directions of the axes will be different for the *cis* and *trans* structures. Assuming values suggested by LuValle & Schomaker, $r_{\text{C—H}} = 1{\cdot}09$ Å, $r_{\text{C=O}} = 1{\cdot}20$ Å, $r_{\text{C—C}} = 1{\cdot}47$ Å and $\text{C—}\hat{\text{C}}\text{—O} = 123^\circ$, $\text{C—}\hat{\text{C}}\text{—H} = 120^\circ$, we obtain for the moments of inertia of the *trans* form 14·3, 171·3 and 185·6 × 10^{-40} g.cm.², and for the *cis* form 23·6, 128·4 and 152·0 × 10^{-40} g.cm.². The *trans* form will behave approximately like a symmetric top, and the *cis* structure also, but to a less extent. The principal axes of inertia lie with respect to the bands as shown in figure 8. In the *trans* form, which has a centre of symmetry at *G*, the least (*A*) axis is inclined at 32° to the C—C bond.

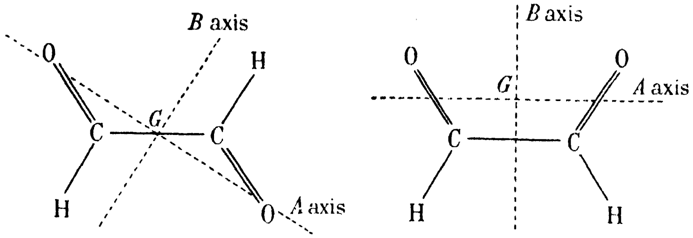

FIGURE 8

For the *trans* form C_{2h}, six fundamentals will be permitted in the infra-red, and the other six in the Raman spectrum. Of the six infra-red active frequencies, at least one, the torsional mode, will lie too low to be measured here. The *cis* structure C_{2v} will permit ten fundamentals in the infra-red.

TABLE 5. *rQ* BRANCHES

K''	ν	$\Delta\nu$
central peak	801·5	
0	—	
1	807·2	
		2·8
2	810·0	
		3·0
3	813·0	
		3·2
4	816·2	
		3·3
5	819·5	
		3·1
6	822·6	
		3·2
7	825·8	
		3·4
8	829·2	
		3·2
9	832·4	
		3·6
10	836·0	
		3·4
11	839·4	
		3·4
12	842·8	
		3·2
13	846·0	

The spectrum actually observed is remarkably free from absorption bands, and this may in itself suggest a preference for the *trans* structure. The removal of the spurious bands due to the polymer avoids the difficulty of having to interpret several strong bands as combination tones, as mentioned in the earlier work.

The band at 801·5 cm.⁻¹ is clearly a *C* type band, with change of electric moment perpendicular to the molecular plane. The spacing between *Q* branches in such a band will be different for the *cis* and *trans* structure owing to the big difference in the least moment of inertia. Although the *pQ* branches on the lower frequency side appear to be complicated and split by some effect, the *rQ* branches are well marked at positions given in table 5, with a mean spacing close to 3·3 cm.⁻¹. If the *trans* structure is assumed and the molecule is regarded as a symmetric top with moments

14·3 and 178·5 × 10^{-40} g.cm.^{2}, the calculated spacing of these Q branches will be 3·6 cm.$^{-1}$. For the *cis* structure, the spacing would be about 2 cm.$^{-1}$, which is far below that observed. This result provides a strong argument for the *trans* structure. The band at 2836 cm.$^{-1}$ is seen to have a B type structure with Q branches on each side of the central gap. The positions are given in table 6, and are fairly well reproduced by an equation

$$\nu = \nu_0 + 1{\cdot}67 + 3{\cdot}34K - 0{\cdot}012K^2,$$

in which $\nu_0 = 2836{\cdot}2$ cm.$^{-1}$, and $K = 0, +1, +2, \ldots$ for the rQ branches, and $K = -1, -2, \ldots$ for the pQ branches. This band is assigned to the C—H stretching vibration (ν_9) which will involve a change of electric moment almost parallel to the intermediate (B) axis of inertia. The spacing between Q branches agrees closely with that in the previous band, and the same conclusions follow (table 6). The band at 1311·5 cm.$^{-1}$ is also a B type band, and the pQ branches have been well resolved. Table 7 gives the positions of these lines, and the spacing is again found to be about 3·4 cm.$^{-1}$, which agrees with the results just given. This band is assigned to a planar deformation of the CHO groups (table 7).

TABLE 6. $\nu_0 = 2836{\cdot}2$ CM.$^{-1}$

pQ branches				*rQ* branches			
K''	$\nu_{\text{obs.}}$	$\nu_{\text{calc.}}$	Δ	K''	$\nu_{\text{obs.}}$	$\nu_{\text{calc.}}$	Δ
1	2834·1	2834·5	0·4	0	2838·1	2837·9	0·2
2	31·1	31·1	0	1	40·8	41·2	0·4
3	27·7	27·8	0·1	2	44·7	44·5	0·2
4	24·4	24·3	−0·1	3	47·5	47·8	0·3
5	21·0	20·9	−0·1	4	50·5	51·0	0·5
6	17·4	17·4	0	5	53·9	54·3	0·4
7	14·0	13·9	−0·1	6	57·3	57·5	0·2
8	10·0	10·4	0·4	7	60·3	60·3	0
9	2806·6	2806·8	0·2	8	63·4	63·8	0·4
10	2803·4	2803·3	−0·1	9	66·7	67·0	0·3
11	2799·6	2799·7	0·1	10	70·3	70·1	−0·2
12	96·0	96·1	0·1	11	73·6	73·2	0·4
13	92·6	92·4	−0·2	12	76·5	76·2	−0·3
14	89·1	88·8	−0·3	13	79·5	79·3	−0·2
15	85·3	85·1	−0·2	14	82·6	82·3	−0·3

TABLE 7. BAND AT 1311·5 CM.$^{-1}$

pQ branches			*rQ* branches		
K''	$\nu_{\text{obs.}}$	$\Delta\nu$	K''	$\nu_{\text{obs.}}$	$\Delta\nu$
3	1302·0	3·4	3	1323·0	3·9
4	1298·6	3·2	4	1326·9	3·1
5	1295·4	3·4	5	1330·0	3·2
6	1292·0	3·1	6	1333·2	3·7
7	1288·9	3·5	7	1336·9	
8	1285·4	3·5			
9	1281·9	3·4			
10	1278·5	3·5			
11	1275·0	3·2			
12	1271·8	3·4			
13	1268·4	3·4			
14	1265·0	3·1			
15	1261·9				

As regards the general problem of assignment of frequencies to the normal modes, the present results strengthen previous suggestions, except for the value 985 cm.$^{-1}$ which was attributed to a fundamental, but is now known to be spurious.

We are grateful to the Government Grant Committee of the Royal Society for financial help. One of us (A. R. H. C.) also thanks the University of Western Australia for a Hackett Research Studentship, and the Trustees of the Carnegie Grants Committee for a grant.

REFERENCES

Badger, R. M. & Zumwalt, L. 1938 *J. Chem. Phys.* **6**, 711.
Gaydon, A. G. 1947 *Trans. Faraday Soc.* **43**, 36.
Gerhard, S. L. & Dennison, D. M. 1933 *Phys. Rev.* **43**, 197.
LuValle, J. E. & Schomaker, V. 1939 *J. Amer. Chem. Soc.* **61**, 3520.
Miller, C. H. & Thompson, H. W. 1949 *Proc. Roy. Soc.* A, **200**, 1.
Pitzer, K. & Freeman, N. K. 1946 *J. Chem. Phys.* **20**, 586.
Thompson, H. W. 1940 *Trans. Faraday Soc.* **36**, 988.
Torkington, P. 1949 *Proc. Roy. Soc.* A (in the Press).
Torkington, P. & Thompson, H. W. 1944 *J. Chem. Soc.* p. 303.
Torkington, P. & Thompson, H. W. 1945*a* *Trans. Faraday Soc.* **41**, 236.
Torkington, P. & Thompson, H. W. 1945*b* *Proc. Roy. Soc.* **A, 184**, 21.

On Heisenberg's elementary theory of turbulence

BY S. CHANDRASEKHAR, F.R.S., *Yerkes Observatory*

(*Received* 22 *July* 1949)

In this paper the spectrum of turbulence is considered on the basis of an elementary theory recently developed by Heisenberg. Explicit solutions for the spectrum have been obtained both when the conditions are stationary and an equilibrium spectrum obtains and when the conditions are non-stationary and the turbulence is decaying. In the former case the problem admits of an explicit solution. In the latter case the problem reduces to determining a one-parametric family of solutions of a certain second-order differential equation. The decay spectra for various values of the Reynolds number (which remains constant during the decay) are illustrated.

1. INTRODUCTION

In two recent papers Heisenberg (1948*a*, *b*) has developed an elementary theory for determining the spectrum of turbulence on an easily visualizable picture of what is taking place in a turbulent medium. The physical ideas underlying Heisenberg's theory are stated very simply:

Considering the rate of dissipation of energy by eddies with wave numbers less than a particular k, Heisenberg distinguishes between the energy directly dissipated in the form of molecular motion and thermal energy and the energy communicated in the form of kinetic energy to all eddies with wave numbers exceeding the specified k. According to the equations of hydrodynamics we can write for the dissipation into thermal energy, per unit volume, the expression

$$\epsilon_k(\text{thermal}) = 2\rho\nu\int_0^k F(k)\,k^2\,dk, \tag{1}$$

where $F(k)$ denotes the spectrum of turbulence, ν the kinematic viscosity (i.e. the coefficient of viscosity as ordinarily defined divided by the density ρ). Equation (1) follows from the usual expression for the total dissipation of energy by viscosity in an isotropically turbulent medium, namely

$$\epsilon = \rho\nu\,\overline{|\operatorname{curl}\mathbf{v}|^2} = 2\rho\nu\int_0^\infty F(k)\,k^2dk. \tag{2}$$

In analogy with (1) Heisenberg writes for the energy transferred to all eddies with wave numbers exceeding a given k by eddies with wave numbers less than this k, the expression

$$\epsilon_k(\text{mechanical}) = 2\rho\nu_k\int_0^k F(k)\,k^2dk. \tag{3}$$

In writing this expression, the assumption is made that the process of energy transfer between the sets of eddies considered can be visualized in terms of a suitably defined coefficient of '*eddy viscosity*' ν_k. Heisenberg further assumes that ν_k can be expressed as an integral over the spectrum in the form

$$\nu_k = \kappa\int_k^\infty \frac{dk}{k^{\frac{3}{2}}}\sqrt{F(k)}, \tag{4}$$

where κ is a numerical constant of order unity. The justification for (4), apart from the fact that the quantity on the right-hand side is of the right dimensions, is that for a power law, $F(k)\propto k^{-n}$, equation (4) is equivalent to the expression

$$\nu_k \sim l_k v_k \sim v_k/k,$$

derived on the picture of the eddies with wave numbers exceeding k, describing a mean free path l_k of order $1/k$ with a certain mean speed $v_k \propto k^{-\frac{1}{2}(n-1)}$.

Combining equations (1), (3) and (4) we have

$$\epsilon_k = 2\rho\left\{\nu + \kappa\int_k^\infty \frac{dk}{k^{\frac{3}{2}}}\sqrt{F(k)}\right\}\int_0^k F(k)\,k^2dk. \tag{5}$$

This is the equation in terms of which Heisenberg has discussed the spectrum of turbulence, both when the conditions are stationary and an equilibrium spectrum obtains and when the conditions are nonstationary and the turbulence is decaying.

When the equilibrium spectrum obtains

$$\epsilon_k = \text{constant}, \tag{6}$$

independent of k. On the other hand, when there is no external source of energy and the turbulence is decaying,

$$\epsilon_k = -\frac{\partial}{\partial t}\int_0^k F(k,t)\,dk. \tag{7}$$

Heisenberg has considered these two cases and derived the principal features of the spectrum. However, it appears that the mathematical problem presented by equations (5), (6) and (7) can be solved very much more completely than was attempted by Heisenberg. It is the object of this paper to present the complete solutions of the two problems discussed by Heisenberg (cf. Chandrasekhar 1949).

2. THE SPECTRUM OF STATIONARY TURBULENCE

When the conditions are stationary ϵ_k should be independent of k, and the explicit solution of equation (5) can be found in the following manner:

Differentiating equation (5) with respect to k, we obtain

$$\frac{\nu}{\kappa}+\int_k^\infty \frac{dk}{k^{\frac{3}{2}}}\sqrt{F(k)} = \frac{1}{k^2[F(k)\,k^3]^{\frac{1}{2}}}\int_0^k F(k)\,k^2\,dk. \tag{8}$$

It is now convenient to introduce the auxiliary functions

$$g = k^3F(k) \quad \text{and} \quad y = \int_0^k F(k)\,k^2\,dk. \tag{9}$$

Relations which readily follow from these definitions are

$$\frac{dk}{dy} = \frac{k}{g}, \tag{10}$$

and

$$\log k = \text{constant} + \int_0^y dy/g(y). \tag{11}$$

Using equations (9) and (10), we can rewrite equation (8) in the form

$$\frac{\nu}{\kappa}+\int_y^\infty \frac{dy}{k^2g^{\frac{1}{2}}} - \frac{y}{k^2g^{\frac{3}{2}}} = 0. \tag{12}$$

Now differentiating this equation with respect to y and making use of (10), we obtain

$$-\frac{1}{k^2g^{\frac{1}{2}}}+\frac{2y}{k^2g^{\frac{3}{2}}}-\frac{1}{k^2}\frac{d}{dy}\left(\frac{y}{g^{\frac{1}{2}}}\right) = 0. \tag{13}$$

On further reduction, this equation becomes

$$\frac{dg}{dy}-\frac{4}{y}g+4 = 0. \tag{14}$$

This equation is readily integrated, and the general solution is given by

$$g = \tfrac{4}{3}y(1-cy^3), \tag{15}$$

where c is a constant.

Inserting the solution (15) for $g(y)$ in (11), and evaluating the integral on the right-hand side we obtain

$$k = \alpha\left(\frac{y^3}{1-cy^3}\right)^{\frac{1}{4}}, \tag{16}$$

where α is a constant.

Alternative forms of the solution represented by equations (15) and (16) are

$$y^3 = \frac{k^4}{\alpha^4+ck^4} \quad \text{and} \quad g = \frac{4}{3}\left(\frac{\alpha y}{k}\right)^4. \tag{17}$$

The spectrum now follows from equations (9), (15) and (17). We have

$$F(k) = \frac{4}{3}\frac{\alpha^4}{k^{\frac{5}{3}}(\alpha^4+ck^4)^{\frac{4}{3}}}. \tag{18}$$

We can rewrite this in the form

$$F(k) = F_0\left(\frac{k_0}{k}\right)^{\frac{5}{3}} \frac{1}{[1+(k/k_s)^4]^{\frac{4}{3}}}, \tag{19}$$

where

$$k_s = \alpha/c^{\frac{1}{4}} \quad \text{and} \quad F_0 = 4/3\alpha^{\frac{4}{3}}k_0^{\frac{5}{3}}. \tag{20}$$

It remains to relate the constants α and c with the parameter ν/κ which occurs in the original equation of the problem. For this purpose we use equation (8). According to this equation (cf. equations (9) and (10))

$$\begin{aligned}\frac{\nu}{\kappa} &= \frac{y}{k^2\sqrt{g}} - \frac{\alpha^2}{2\sqrt{3}}\int_\infty^k \frac{1}{(c+\alpha^4/k^4)^{\frac{2}{3}}}\frac{d}{dk}\left(\frac{1}{k^4}\right)dk \\ &= \frac{y}{k^2\sqrt{g}} - \frac{\sqrt{3}}{2\alpha^2}\left[\left(c+\frac{\alpha^4}{k^4}\right)^{\frac{1}{3}} - c^{\frac{1}{3}}\right],\end{aligned} \tag{21}$$

or, using equations (17), we find

$$\frac{\nu}{\kappa} = \frac{\sqrt{3}}{2}\frac{c^{\frac{1}{3}}}{\alpha^2}. \tag{22}$$

This is the required relation.

Returning to the spectrum of stationary turbulence given by equation (19), we may first observe that according to equations (20) and (22)

$$k_s = \frac{1}{\sqrt{\alpha}}\left(\frac{\sqrt{3}}{2}\frac{\kappa}{\nu}\right)^{\frac{3}{4}}. \tag{23}$$

From this relation it is seen that when $\nu \to 0$ (or, equivalently, when the Reynolds number tends to infinity) $k_s \to \infty$, and the spectrum given by (19) reduces to the equilibrium Kolmogoroff spectrum. On the other hand, for any finite ν, the spectrum follows a k^{-7}-law when $k \gg k_s$; k_s is accordingly the wave number at which ϵ_k (thermal) becomes comparable to ϵ_k(mechanical) in the transaction between the eddies. These results, obtained from the explicit solution of the problem, are in agreement with Heisenberg's qualitative discussion of this same problem.

For $\nu \to 0$, the wave number k_s is related to the Reynolds number in a simple way; for, since $c \to 0$ as $\nu \to 0$, we may write in a sufficient approximation:

$$F_0 = 4/3\alpha^{\frac{4}{3}}k_0^{\frac{5}{3}} \simeq F(k_0). \tag{24}$$

Using (24) to eliminate α from (23), we find

$$k_s = k_0\left(\frac{3}{4}\frac{\kappa}{\nu}\sqrt{\frac{F(k_0)}{k_0}}\right)^{\frac{3}{4}}. \tag{25}$$

Heisenberg defines the Reynolds number R_0 of the entire motion by the equation

$$R_0 = \frac{\pi}{\nu}\sqrt{\frac{3F(k_0)}{k_0}}, \tag{26}$$

which is ν^{-1} times the product of the root-mean-square velocity of turbulent motion and the diameter of the largest eddies present. In terms of this Reynolds number the expression for k_s becomes

$$k_s = 0{\cdot}2211k_0(R_0\kappa)^{\frac{3}{4}}. \tag{27}^*$$

---

* The use of the explicit solution for the spectrum given here changes the numerical constants in Heisenberg's paper (1948*a*). The most important of these changes are that in his equations (27), (30), (31), (73) and (76) the numerical coefficients should be 0·3164, 0·2211, 4·52, 0·0756 and 0·349 instead of 0·0496, 0·16, 6·25, 0·05 and 0·42 respectively.

3. The decay of turbulence

On Heisenberg's theory, the decay of turbulence is governed by the equation (cf. equations (5) and (7))

$$-\frac{\partial}{\partial t}\int_0^k F(k,t)\,dk = 2\left\{\nu+\kappa\int_k^\infty \frac{dk}{k^{\frac{3}{2}}}\sqrt{F(k,t)}\right\}\int_0^k F(k,t)\,k^2\,dk. \tag{28}$$

If the initial spectrum $F(k,0)$ is given, the foregoing equation will determine the spectrum for all later times. A case of some importance which arises in this connexion is the following: Suppose that we have initially an equilibrium spectrum governed by equation (19) and that at a certain instant the agency maintaining the turbulence is cut off. Then in the decay of turbulence which will ensue we may distinguish three stages: an early stage during which the larger eddies ($k\sim k_0$) adjust themselves to the fact that no energy is being communicated to them; an intermediate stage during which there is a sufficient store of energy among the larger eddies to maintain an equilibrium distribution among the smaller eddies and when the Reynolds number remains approximately constant; and finally, a last stage during which the store of energy among the larger eddies is getting exhausted and the Reynolds number decreases to zero. While a unified discussion of all three stages of decay is a difficult problem, it appears that on the basis of Heisenberg's theory we can follow the second stage quite completely and in an explicit fashion. For, from the constancy of the Reynolds number which we expect during this stage, we conclude that the spectrum must be 'self-preserving' in the sense that it keeps the same form though the scale may change with time. From equation (28), the condition of self-preservation is seen to be equivalent to seeking solutions of this equation of the form

$$F(k,t) = \frac{1}{\kappa^2k_0^2t_0^2}\left(\frac{t_0}{t}\right)^{\frac{1}{2}} f\left(\frac{k}{k_0}\frac{\sqrt{t}}{\sqrt{t_0}}\right), \tag{29}$$

where k_0 and t_0 are certain constants and f is a function of the argument specified.

For $F(k,t)$ of the form (29), equation (28) becomes

$$\frac{1}{4}\int_0^x\left[f(x)-x\frac{df}{dx}\right]dx = \left\{\frac{1}{R}+\int_x^\infty\frac{dx}{x^{\frac{3}{2}}}\sqrt{f(x)}\right\}\int_0^x f(x)\,x^2\,dx, \tag{30}$$

where

$$R = 1/\nu k_0^2 t_0 \tag{31}$$

is a measure of the Reynolds number which remains constant during the stage of the decay considered.

From equation (30) it readily follows that

$$f(x)\to \text{constant}\,x \quad (x\to 0). \tag{32}$$

Heisenberg (1948*b*) has discussed in general terms the solutions of equation (30) which have the behaviour (32) at the origin and has shown that for the case of infinite Reynolds number ($\nu = 0$) the solution must have the asymptotic form

$$f(x)\to \text{constant}\,x^{-\frac{5}{3}} \quad (x\to\infty;\ \nu = 0), \tag{33}$$

while for a finite Reynolds number

$$f(x) \to \text{constant}\, x^{-7} \quad (x \to \infty;\ \nu > 0). \tag{34}$$

As Heisenberg has pointed out these behaviours at infinity are to be expected on general grounds. But it is perhaps of some interest to obtain the explicit solutions of the problem. This can be achieved in the following manner:

Differentiating equation (30) with respect to x and rearranging the terms, we obtain

$$\frac{1}{4}\left(1-\frac{x}{f}\frac{df}{dx}\right) = x^2\left\{\frac{1}{R}+\int_x^\infty \frac{dx}{x^{\frac{3}{2}}}\sqrt{f(x)}\right\} - \frac{1}{\sqrt{(fx^3)}}\int_0^x f(x)\,x^2\,dx. \tag{35}$$

It is now convenient to introduce the auxiliary functions

$$g = x^3 f(x) \quad \text{and} \quad y = \int_0^x f(x)\,x^2\,dx. \tag{36}$$

Relations which follow from these definitions are

$$\frac{dx}{dy} = \frac{x}{g}, \tag{37}$$

and

$$\frac{dg}{dy} = \left(3x^2 f + x^3\frac{df}{dx}\right)\frac{x}{g} = 3 + \frac{x}{f}\frac{df}{dx}. \tag{38}$$

Using these relations, we can rewrite equation (35) in the form

$$\frac{1}{R} - \frac{1}{x^2}\left\{\frac{1}{4}\left(4-\frac{dg}{dy}\right)+\frac{y}{\sqrt{g}}\right\} + \int_y^\infty \frac{dy}{x^2\sqrt{g}} = 0. \tag{39}$$

Now differentiating this equation with respect to y we obtain

$$\frac{2}{x^3}\frac{dx}{dy}\left\{\frac{1}{4}\left(4-\frac{dg}{dy}\right)+\frac{y}{\sqrt{g}}\right\} - \frac{1}{x^2}\frac{d}{dy}\left\{\frac{1}{4}\left(4-\frac{dg}{dy}\right)+\frac{y}{\sqrt{g}}\right\} - \frac{1}{x^2\sqrt{g}} = 0. \tag{40}$$

Inserting for dx/dy in value (37), we find that equation (40) reduces to

$$g^{\frac{3}{2}}g'' + 2y(4+g') + 2g^{\frac{1}{2}}(4-g') - 8g = 0, \tag{41}$$

where we have used primes to denote differentiation with respect to y.

Once equation (41) has been integrated, the solution can be completed by a further quadrature; for, according to equation (37),

$$\log(x/x_0) = \int^y \frac{dy}{g(y)}. \tag{42}$$

In (42), x_0 is a constant of integration. There is, however, no loss of generality in setting

$$x_0 = 1, \tag{43}$$

since this represents only a scale factor and can be absorbed in the definition of k_0 (cf. equation (29)). With this understanding, we shall adopt

$$\log x = \int^y \frac{dy}{g(y)} \tag{44}$$

as the equation relating x and y.

3·1. *The physical solutions*

As we have already stated (cf. equation (32)) the physical solutions must be such that $f(x)$ becomes proportional to x as $x \to 0$; according to equations (36) and (38) this means that we must seek solutions of equation (41) which start tangentially to the line $g = 4y$ at the origin:

$$g' = 4 \quad \text{and} \quad g = 4y \quad (y \to 0). \tag{45}$$

From equation (41) it now follows that there exists a one parametric family of solutions which have this behaviour at $y = 0$. Indeed, they arise from the continuation of the solutions represented by the following series expansion valid at $y = 0$:

$$\begin{aligned} g(y) = {} & 4y + y^{\frac{3}{2}}(a + \tfrac{4}{3}\log y) \\ & + y^2(a_2 + b_2 \log y - \tfrac{1}{3}\log^2 y) \\ & + y^{\frac{5}{2}}(a_3 + b_3 \log y + c_3 \log^2 y + \tfrac{11}{90}\log^3 y) + O(y^2 \log^4 y), \end{aligned} \tag{46}$$

where a is an arbitrary constant and

$$\left.\begin{aligned} a_2 &= -2{\cdot}861111 + 0{\cdot}958333a - 0{\cdot}1875a^2, \\ b_2 &= +1{\cdot}277777 - 0{\cdot}5a, \\ a_3 &= -2{\cdot}071525 + 1{\cdot}58889722a - 0{\cdot}383542a^2 + 0{\cdot}0515625a^3, \\ b_3 &= +2{\cdot}118629 - 1{\cdot}022777a + 0{\cdot}20625a^2, \\ c_3 &= -0{\cdot}6818519 + 0{\cdot}275a. \end{aligned}\right\} \tag{47}$$

Corresponding to this behaviour of g near the origin, the relation between x and y is (cf. equation (44))

$$\begin{aligned} \log x = {} & \tfrac{1}{4}\log y - y^{\frac{1}{2}}\left(\frac{a}{8} - \tfrac{1}{3} + \tfrac{1}{6}\log y\right) \\ & + y[(\alpha_2 - \beta_2 + 2\gamma_2) + (\beta_2 - 2\gamma_2)\log y + \gamma_2 \log^2 y] \\ & - y^{\frac{3}{2}}[(\tfrac{2}{3} - \tfrac{4}{9}\beta_3 + \tfrac{16}{27}\gamma_3 - \tfrac{32}{27}\delta_3) + (\tfrac{2}{3}\beta_3 - \tfrac{8}{9}\gamma_3 + \tfrac{16}{9}\delta_3)\log y \\ & + (\tfrac{2}{3}\gamma_3 - \tfrac{4}{3}\delta_3)\log^2 y + \tfrac{2}{3}\delta_3 \log^3 y] + O(y^2 \log^4 y), \end{aligned} \tag{48}$$

where

$$\left.\begin{aligned} \alpha_2 &= \frac{1}{4}\left(\frac{a^2}{16} - \frac{a_2}{4}\right), & \alpha_3 &= \frac{1}{4}\left(\frac{a_3}{4} - \frac{aa_2}{8} + \frac{a^3}{64}\right), \\ \beta_2 &= \frac{1}{4}\left(\frac{a}{6} - \frac{b_2}{4}\right), & \beta_3 &= \frac{1}{4}\left(\frac{b_3}{4} - \frac{a_2}{6} - \frac{ab_2}{8} + \frac{a^2}{16}\right), \\ \gamma_2 &= \tfrac{7}{144}, & \gamma_3 &= \frac{1}{4}\left(\frac{c_3}{4} - \frac{b_2}{6} + \frac{a}{8}\right), \\ \text{and} \qquad & & \delta_3 &= \tfrac{133}{4320}. \end{aligned}\right\} \tag{49}$$

The solutions which have the behaviours described by the foregoing equations have the following arrangement in the (g, y) plane (figure 1).

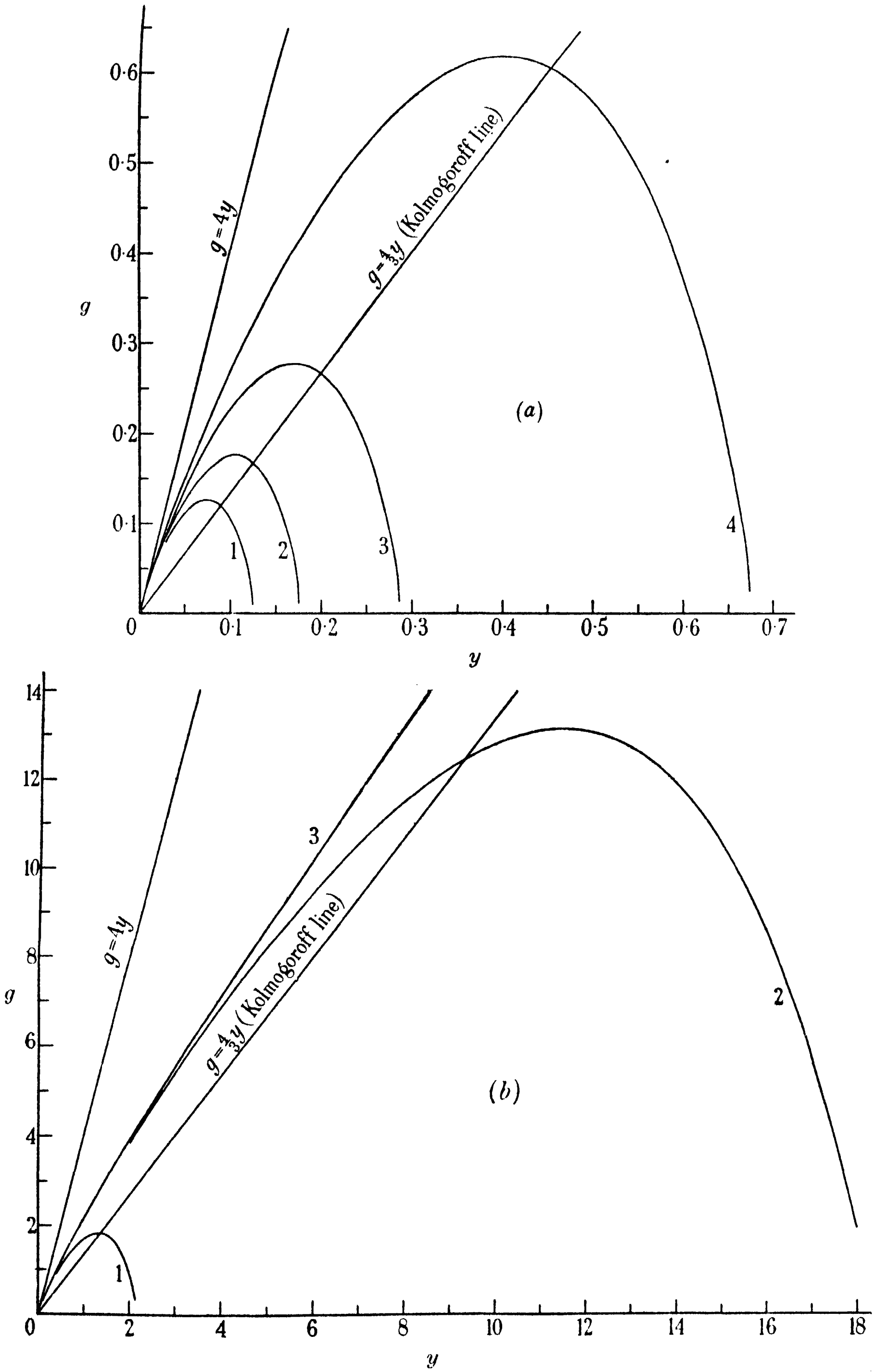

FIGURE 1. The solution curves in the (g, y)-plane. In (*a*), the curves marked 1, 2, 3 and 4 are for $a = 0$, 0·5, 1·0 and 1·5 respectively. In (*b*), the curves marked 1, 2 and 3 are for $a = 1·75$, 1·81 and 1·8104739 respectively; for $y \rightarrow \infty$, the curve 3 tends to the line $g = \frac{4}{3}y$ asymptotically.

There exists a value of $a = a^*$ ($\sim 1{\cdot}810\ldots$) such that for all $a < a^*$ the solutions are bounded and have a single maximum and reach the y-axis for a finite y ($= y_0$, say) with the behaviour

$$g(y) = 4(y_0-y)+\frac{32}{3y_0}(y_0-y)^{\frac{3}{2}}+\frac{8}{y_0}\left(\frac{16}{3y_0}-1\right)(y_0-y)^2$$
$$+O([y_0-y]^{\frac{5}{2}}) \quad (a<a^*;\ y\to y_0;\ y<y_0). \qquad (50)\dagger$$

These solutions are 'bounded' by the solution for $a = a^*$ which increases monotonically, approaching the line $g = \frac{4}{3}y$ for $y \to \infty$ with the behaviour

$$g = \tfrac{4}{3}y[1+0{\cdot}659829y^{-\frac{1}{2}}+0{\cdot}0634921y^{-1}$$
$$-0{\cdot}0674957y^{-\frac{3}{2}}-0{\cdot}0387767y^{-2}+0{\cdot}0314475y^{-\frac{5}{2}}+\ldots]. \qquad (51)$$

The solutions for $a > a^*$ have no physical meaning; they correspond to negative values for the coefficient of viscosity (see equation (57) below).

According to equation (38), the behaviours (50) and (51) correspond to

$$\frac{x}{f}\frac{df}{dx} = -7 \quad \text{and} \quad -\tfrac{5}{3} \text{ respectively.} \qquad (52)$$

Thus and

$$\left.\begin{aligned} f(x) &\propto x^{-7} \quad (x\to\infty,\ a<a^*) \\ f(x) &\propto x^{-\frac{5}{3}} \quad (x\to\infty,\ a=a^*). \end{aligned}\right\} \qquad (53)$$

The solutions for $a < a^*$ therefore correspond to finite values of the Reynolds number, while the solution for $a = a^*$ is that appropriate for zero viscosity (or infinite Reynolds number). In the former case we have the k^{-7} behaviour as $k \to \infty$, while in the latter case we have the $k^{-\frac{5}{3}}$ behaviour of the Kolmogoroff spectrum.

When $a < a^*$ but close to a^*, the solution curves in the (g, y) plane run parallel to the line $g = \frac{4}{3}y$ for a long while before turning down; this corresponds to the fact that for large Reynolds numbers there exists a portion of the spectrum in which the $k^{-\frac{5}{3}}$ law is closely followed before the k^{-7} law becomes operative.

It remains to relate the parameter a with the Reynolds number R. For this purpose we consider equation (39) for $y \to 0$. Using the relations (cf. equations (46) and (47))

$$\left.\begin{aligned} g &= 4y+y^{\frac{3}{2}}(a+\tfrac{4}{3}\log y)+O(y^2\log^2 y), \\ g' &= 4+y^{\frac{1}{2}}(\tfrac{3}{2}a+\tfrac{4}{3}+2\log y)+O(y\log^2 y), \\ x^2 &= y^{\frac{1}{2}}+O(y\log y), \end{aligned}\right\} \qquad (54)$$

valid near $y = 0$, we find that equation (39) becomes

$$y^{\frac{1}{2}}(\tfrac{1}{6}-\tfrac{3}{8}a-\tfrac{1}{2}\log y) = y^{\frac{1}{2}}\left(\frac{1}{R}+\int_y^{y_0}\frac{dy}{x^2\sqrt{g}}\right)+O(y\log^2 y). \qquad (55)$$

---

† This behaviour applies only to the *left* of y_0. Solutions intersecting the y-axis from the right have an entirely different behaviour, namely,

$$g(y) = [6y_0(y-y_0)]^{\frac{2}{3}}+b(y-y_0)+O([y-y_0]^{\frac{4}{3}}) \quad (y\to y_0;\ y>y_0),$$

where b is an arbitrary constant. In consequence of this very singular behaviour of the solutions at y_0, the series expansion (50) is very poorly convergent and does not represent the solution even when y is only very slightly different from y_0.

Now letting $y \rightarrow 0$, we obtain

$$\frac{1}{R} = \tfrac{1}{6} - \tfrac{3}{8}a - \lim_{y\rightarrow 0}\left(\int_{y}^{y_0} \frac{dy}{x^2\sqrt{g}} + \tfrac{1}{2}\log y\right). \tag{56}$$

The limit on the right-hand side exists, the logarithmic divergence of the integral as $y \rightarrow 0$ exactly cancelling the term $\frac{1}{2}\log y$. We may accordingly write

$$\frac{1}{R} = \tfrac{1}{6} - \tfrac{3}{8}a - \tfrac{1}{2}\log y_0 + \int_{0}^{y_0}\left(\frac{1}{2y} - \frac{1}{x^2\sqrt{g}}\right)dy. \tag{57}$$

This is the required relation between a and R.

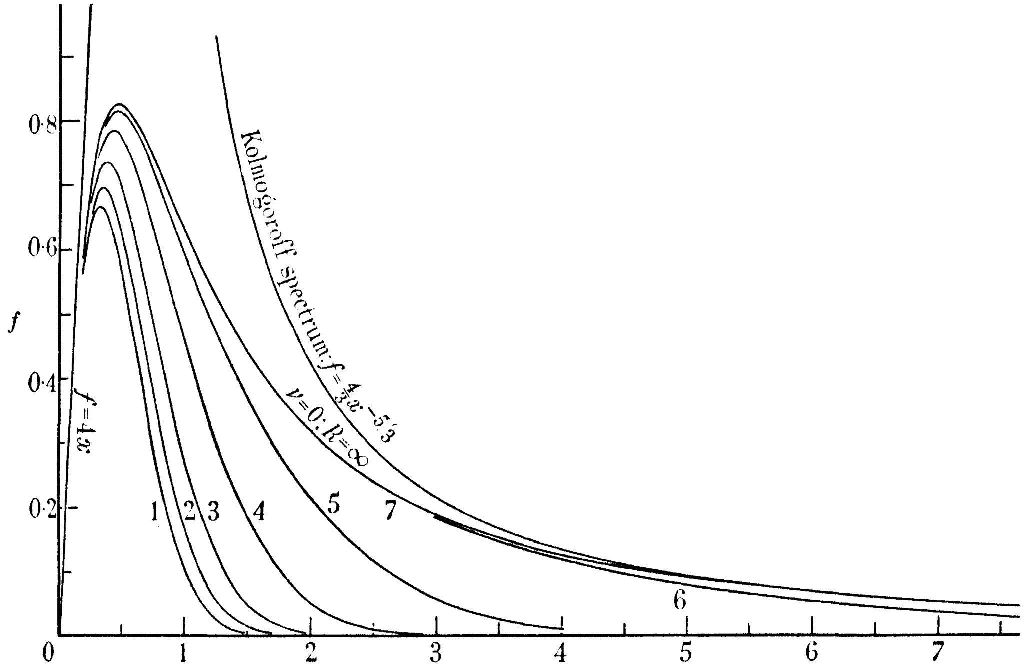

FIGURE 2. The decay spectra for various values of R. The curves marked 1, 2, 3, 4, 5, 6 and 7 are for $R^{-1} = 1\cdot65$, $1\cdot34$, $0\cdot98$, $0\cdot55$, $0\cdot22$, $\sim 10^{-3}$ and 0 respectively. The curve for $R = \infty$, is the decay spectrum for infinite Reynolds number and becomes asymptotic to the Kolmogoroff spectrum $f(x) = \frac{4}{3}r^{-\frac{5}{3}}$ for $r \rightarrow \infty$.

3·2. *Numerical form of the solutions*

To obtain the explicit form of the spectra for various Reynolds numbers, Miss Donna Elbert and the writer have integrated the differential equation (41) for various values of a. It was found that $a = 1\cdot8104\ldots$ leads to the critical solution which approaches the line $g = \frac{4}{3}y$ for $y \rightarrow \infty$.

With g determined by numerical integration, a further quadrature according to equation (44) gave the relation between x and y. The spectra $f(x)$ determined in this fashion are given in table 1 and are further illustrated in figure 2. The values of R determined according to equation (57) for the different solutions are also included in table 1.

TABLE 1. THE SPECTRUM OF TURBULENCE DURING DECAY

$a = 1{\cdot}8104739;\ R^{-1} = 0$

x	f	x	f	x	f	x	f
0·186	0·5854	0·450	0·8228	1·735	0·3755	4·365	0·1097
0·224	0·6558	0·456	0·8232	1·905	0·3369	4·460	0·1063
0·250	0·6956	0·462	0·8236	2·064	0·3058	4·554	0·1030
0·271	0·7224	0·489	0·8233	2·213	0·2803	4·647	0·1000
0·288	0·7421	0·535	0·8179	2·355	0·2589	4·739	0·0971
0·303	0·7569	0·575	0·8091	2·492	0·2406	4·830	0·0944
0·317	0·7686	0·611	0·7989	2·624	0·2247	4·921	0·0919
0·329	0·7780	0·643	0·7881	2·751	0·2109	5·010	0·0894
0·341	0·7859	0·672	0·7770	2·874	0·1987	5·099	0·0871
0·351	0·7922	0·700	0·7659	2·995	0·1878	5·187	0·0849
0·361	0·7977	0·726	0·7551	3·112	0·1781	5·274	0·0828
0·371	0·8022	0·817	0·7143	3·227	0·1693	5·361	0·0808
0·379	0·8061	0·895	0·6780	3·339	0·1614	5·446	0·0789
0·388	0·8091	0·965	0·6458	3·449	0·1541	5·532	0·0771
0·396	0·8121	1·029	0·6171	3·557	0·1475	5·616	0·0753
0·404	0·8144	1·088	0·5912	3·663	0·1415	5·700	0·0737
0·411	0·8164	1·144	0·5679	3·768	0·1359	5·825	0·0713
0·418	0·8180	1·196	0·5466	3·871	0·1307	5·989	0·0684
0·425	0·8194	1·246	0·5271	3·972	0·1259	6·151	0·0657
0·432	0·8205	1·294	0·5092	4·072	0·1214	6·311	0·0632
0·438	0·8215	1·340	0·4927	4·171	0·1172	6·469	0·0608
0·444	0·8222	1·550	0·4253	4·268	0·1134	6·625	0·0586

$a = 1{\cdot}81;\ R^{-1} \sim 10^{-8}$

x	f	x	f	x	f	x	f
0·186	0·5854	0·450	0·8227	1·738	0·3728	4·909	0·0818
0·224	0·6558	0·456	0·8230	1·908	0·3337	5·212	0·0730
0·250	0·6956	0·462	0·8234	2·068	0·3023	5·514	0·0653
0·271	0·7224	0·489	0·8231	2·218	0·2763	5·817	0·0584
0·288	0·7421	0·535	0·8176	2·362	0·2544	6·122	0·0522
0·303	0·7568	0·575	0·8088	2·501	0·2356	6·431	0·0466
0·317	0·7686	0·611	0·7986	2·634	0·2194	6·746	0·0414
0·329	0·7780	0·643	0·7876	2·764	0·2051	7·069	0·0367
0·341	0·7858	0·672	0·7766	2·890	0·1925	7·402	0·0323
0·351	0·7921	0·700	0·7655	3·013	0·1812	7·748	0·0282
0·361	0·7976	0·726	0·7546	3·133	0·1711	8·112	0·0244
0·371	0·8021	0·817	0·7136	3·251	0·1619	8·497	0·0209
0·379	0·8060	0·896	0·6771	3·367	0·1536	8·910	0·0176
0·388	0·8092	0·966	0·6448	3·481	0·1459	9·360	0·0145
0·396	0·8120	1·029	0·6159	3·593	0·1389	9·860	0·0116
0·404	0·8142	1·088	0·5900	3·704	0·1324	10·430	0·0090
0·411	0·8163	1·144	0·5666	3·813	0·1264	11·103	0·0066
0·418	0·8178	1·197	0·5452	3·922	0·1208	11·942	0·0044
0·425	0·8194	1·247	0·5256	4·029	0·1155	13·085	0·0025
0·432	0·8204	1·295	0·5076	4·135	0·1106	14·935	0·0011
0·438	0·8214	1·341	0·4909	4·293	0·1039	—	—
0·444	0·8220	1·551	0·4230	4·603	0·0920	—	—

Table 1 (*cont.*)

$a = 1{\cdot}75;\ R^{-1} = 0{\cdot}22$

x	f	x	f	x	f	x	f
0·186	0·5846	0·457	0·8142	0·924	0·6296	1·675	0·3053
0·224	0·6545	0·463	0·8143	0·946	0·6180	1·731	0·2877
0·250	0·6954	0·480	0·8136	0·967	0·6068	1·786	0·2710
0·271	0·7201	0·500	0·8116	0·988	0·5959	1·842	0·2551
0·288	0·7394	0·519	0·8086	1·008	0·5853	1·897	0·2400
0·304	0·7537	0·545	0·8029	1·028	0·5751	1·953	0·2255
0·317	0·7651	0·570	0·7963	1·048	0·5652	2·009	0·2116
0·330	0·7741	0·592	0·7891	1·067	0·5555	2·066	0·1982
0·341	0·7816	0·613	0·7816	1·086	0·5461	2·151	0·1792
0·352	0·7876	0·633	0·7739	1·104	0·5370	2·239	0·1612
0·362	0·7927	0·652	0·7662	1·129	0·5251	2·330	0·1442
0·371	0·7968	0·676	0·7558	1·152	0·5137	2·424	0·1280
0·380	0·8004	0·698	0·7454	1·193	0·4946	2·522	0·1127
0·388	0·8033	0·720	0·7352	1·226	0·4790	2·625	0·0981
0·396	0·8058	0·740	0·7250	1·259	0·4642	2·735	0·0842
0·404	0·8078	0·760	0·7152	1·292	0·4499	2·854	0·0710
0·412	0·8095	0·779	0·7056	1·323	0·4363	2·985	0·0586
0·419	0·8108	0·797	0·6961	1·354	0·4232	3·132	0·0468
0·426	0·8120	0·815	0·6868	1·385	0·4106	3·302	0·0357
0·432	0·8127	0·832	0·6778	1·445	0·3866	3·508	0·0254
0·439	0·8134	0·853	0·6668	1·504	0·3644	3·775	0·0160
0·445	0·8138	0·878	0·6539	1·562	0·3435	4·177	0·0078
0·451	0·8141	0·901	0·6415	1·619	0·3238	—	—

$a = 1{\cdot}5;\ R^{-1} = 0{\cdot}55$

x	f	x	f	x	f	x	f
0·186	0·5812	0·461	0·7797	0·897	0·5288	1·503	0·1817
0·224	0·6488	0·467	0·7788	0·925	0·5091	1·532	0·1702
0·251	0·6862	0·484	0·7750	0·952	0·4901	1·563	0·1590
0·272	0·7107	0·510	0·7690	0·979	0·4714	1·594	0·1480
0·289	0·7284	0·534	0·7586	1·005	0·4533	1·627	0·1373
0·305	0·7412	0·561	0·7472	1·031	0·4357	1·660	0·1267
0·318	0·7511	0·585	0·7352	1·057	0·4186	1·695	0·1164
0·331	0·7586	0·609	0·7228	1·083	0·4020	1·732	0·1064
0·343	0·7647	0·630	0·7104	1·108	0·3857	1·771	0·0965
0·353	0·7693	0·651	0·6980	1·133	0·3699	1·812	0·0869
0·363	0·7732	0·671	0·6856	1·158	0·3544	1·855	0·0775
0·373	0·7760	0·690	0·6733	1·184	0·3393	1·902	0·0683
0·382	0·7783	0·708	0·6612	1·209	0·3245	1·952	0·0594
0·391	0·7799	0·726	0·6492	1·234	0·3101	2·008	0·0508
0·399	0·7812	0·744	0·6373	1·260	0·2960	2·070	0·0425
0·407	0·7820	0·760	0·6257	1·286	0·2822	2·141	0·0344
0·414	0·7826	0·777	0·6143	1·311	0·2687	2·224	0·0267
0·422	0·7827	0·793	0·6030	1·337	0·2555	2·325	0·0194
0·429	0·7828	0·808	0·5918	1·364	0·2425	2·459	0·0126
0·436	0·7824	0·824	0·5810	1·391	0·2299	2·658	0·0065
0·442	0·7821	0·839	0·5702	1·418	0·2174	2·890	0·0030
0·449	0·7813	0·854	0·5596	1·446	0·2053	—	—
0·455	0·7807	0·868	0·5492	1·474	0·1933	—	—

TABLE 1 (*cont.*)

$a = 1{\cdot}0;\ R^{-1} = 0{\cdot}98$

x	f	x	f	x	f	x	f
0·186	0·5744	0·469	0·7108	0·839	0·4080	1·182	0·1606
0·225	0·6375	0·475	0·7078	0·853	0·3957	1·201	0·1514
0·252	0·6710	0·494	0·6981	0·867	0·3836	1·219	0·1423
0·273	0·6920	0·516	0·6844	0·880	0·3716	1·238	0·1334
0·291	0·7065	0·537	0·6703	0·894	0·3598	1·258	0·1246
0·307	0·7160	0·558	0·6558	0·908	0·3481	1·279	0·1159
0·321	0·7229	0·577	0·6412	0·922	0·3365	1·301	0·1073
0·334	0·7276	0·595	0·6264	0·936	0·3251	1·323	0·0989
0·346	0·7309	0·613	0·6118	0·950	0.3138	1·347	0·0906
0·357	0·7328	0·630	0·5972	0·964	0·3027	1·372	0·0825
0·367	0·7340	0·647	0·5827	0·979	0·2917	1·398	0·0745
0·377	0·7343	0·663	0·5683	0·993	0·2808	1·427	0·0666
0·386	0·7341	0·679	0·5540	1·008	0·2701	1·458	0·0589
0·395	0·7332	0·694	0·5399	1·022	0·2595	1·491	0·0514
0·404	0·7322	0·709	0·5260	1·037	0·2490	1·528	0·0441
0·412	0·7306	0·724	0·5122	1·052	0·2387	1·569	0·0370
0·420	0·7289	0·739	0·4986	1·067	0.2285	1·616	0·0300
0·428	0·7268	0·754	0·4852	1·083	0·2184	1·672	0·0234
0·435	0·7246	0·768	0·4719	1·099	0·2085	1·741	0·0170
0·442	0·7220	0·783	0·4588	1·115	0·1986	1·832	0·0110
0·449	0·7196	0·797	0·4459	1·131	0·1890	1·972	0·0055
0·456	0·7167	0·811	0·4331	1·148	0·1794	—	—
0·463	0·7139	0·825	0·4205	1·165	0·1699	—	—

$a = 0{\cdot}5;\ R^{-1} = 1{\cdot}34$

x	f	x	f	x	f
0·187	0·5677	0·504	0·6214	0·881	0·2565
0·226	0·6264	0·523	0·6058	0·896	0·2439
0·253	0·6560	0·541	0·5898	0·912	0·2316
0·275	0·6725	0·558	0·5740	0·928	0·2194
0·293	0·6832	0·574	0·5580	0·944	0·2073
0·309	0·6896	0·590	0·5422	0·960	0·1954
0·323	0·6936	0·606	0·5264	0·977	0·1838
0·337	0·6953	0·621	0·5108	0·994	0·1722
0·349	0·6959	0·636	0·4952	1·012	0·1608
0·360	0·6952	0·651	0·4798	1·031	0·1496
0·371	0·6938	0·666	0·4646	1·050	0·1386
0·381	0·6916	0·680	0·4495	1·070	0·1277
0·391	0·6890	0·695	0·4346	1·091	0·1171
0·400	0·6858	0·709	0·4200	1·113	0·1065
0·409	0·6824	0·723	0·4053	1·137	0·0963
0·418	0·6785	0·737	0·3910	1·162	0·0861
0·426	0·6746	0·751	0·3767	1·188	0·0762
0·434	0·6702	0·766	0·3628	1·217	0·0665
0·442	0·6659	0·780	0·3488	1·249	0·0570
0·450	0·6612	0·794	0·3352	1·285	0·0478
0·457	0·6567	0·808	0·3216	1·326	0·0388
0·464	0·6517	0·822	0·3083	1·374	0·0302
0·471	0·6469	0·837	0·2950	1·433	0·0219
0·478	0·6419	0·851	0·2821	1·512	0·0140
0·485	0·6368	0·866	0·2691	1·634	0·0068

TABLE 1 (*cont.*)

$a = 0$; $R^{-1} = 1{\cdot}65$

x	f	x	f	x	f
0·187	0·5608	0·509	0·5555	0·816	0·2312
0·227	0·6151	0·522	0·5414	0·829	0·2198
0·254	0·6410	0·536	0·5274	0·843	0·2086
0·276	0·6551	0·549	0·5134	0·856	0·1975
0·295	0·6625	0·562	0·4994	0·870	0·1865
0·311	0·6658	0·574	0·4855	0·885	0·1756
0·326	0·6669	0·587	0·4717	0·899	0·1650
0·339	0·6658	0·599	0·4580	0·915	0·1544
0·352	0·6637	0·611	0·4443	0·930	0·1440
0·364	0·6603	0·623	0·4307	0·947	0·1337
0·375	0·6564	0·635	0·4173	0·964	0·1236
0·385	0·6518	0·647	0·4040	0·982	0·1136
0·396	0·6468	0·659	0·3909	1·000	0·1038
0·405	0·6412	0·670	0·3778	1·020	0·0941
0·415	0·6356	0·682	0·3649	1·041	0·0846
0·424	0·6294	0·694	0·3521	1·064	0·0753
0·432	0·6233	0·706	0·3394	1·088	0·0661
0·441	0·6168	0·718	0·3268	1·115	0·0572
0·449	0·6104	0·730	0·3144	1·145	0·0484
0·457	0·6036	0·742	0·3022	1·179	0·0399
0·465	0·5970	0·754	0·2900	1·218	0·0316
0·472	0·5901	0·766	0·2780	1·265	0·0237
0·480	0·5833	0·778	0·2661	1·326	0·0160
0·487	0·5763	0·791	0·2543	1·414	0·0089
0·495	0·5695	0·803	0·2427	—	—

In conclusion, I wish to record my indebtedness to Miss Donna Elbert for valuable assistance with the various numerical integrations involved in the preparation of this paper.

REFERENCES

Chandrasekhar, S. 1949 *Phys. Rev.* **75**, 896, 1454; **76**, 158, 1949.
Heisenberg, W. 1948*a* *Z. Phys.* **124**, 628.
Heisenberg, W. 1948*b* *Proc. Roy. Soc.* A, **195**, 402.

Some theorems on perturbation theory

By E. C. Titchmarsh, F.R.S.

(*Received* 26 *July* 1949)

It is proved that the well-known formulae which give the variation in the eigenvalues and eigenfunctions arising from a differential equation $\phi''(x)+\{\lambda-q(x)\}\phi(x)=0$, when $q(x)$ is varied, are valid under certain general conditions. The analysis is extended to partial differential equations.

1. The theory of perturbations is concerned with the changes which are made in the eigenfunctions and eigenvalues associated with an eigenvalue problem

$$L\phi=\lambda\phi,$$

when the operator L is replaced by another operator $L+L'$, where L' is in some sense small. For example, the unperturbed equation may be the differential equation

$$\frac{d^2\phi}{dx^2}+\{\lambda-q(x)\}\phi=0, \tag{1·1}$$

where $q(x)$ is a given function of x, and the perturbed equation may be

$$\frac{d^2\phi}{dx^2}+\{\lambda-q(x)-\epsilon\sigma(x)\}\phi=0, \tag{1·2}$$

where $\sigma(x)$ is another given function, and ϵ is a parameter which tends to 0. Suppose that (1·1) determines eigenfunctions $\psi_n(x)$ corresponding to eigenvalues λ_n, and that (1·2) determines eigenfunctions $\Psi_n(x)$ corresponding to eigenvalues Λ_n. It is then a question of determining $\Psi_n(x)$ and Λ_n, approximately, when ϵ is small, in terms of $\psi_n(x)$ and λ_n.

The formulae which effect these approximations are to be found in the writings of many physicists; but so far as I know it is always assumed that there are formulae of the type

$$\Psi_n(x)=\psi_n(x)+\epsilon\psi_{n,1}(x)+\epsilon^2\psi_{n,2}(x)+\dots, \tag{1·3}$$

$$\Lambda_n=\lambda_n+\epsilon\lambda_{n,1}+\epsilon^2\lambda_{n,2}+\dots, \tag{1·4}$$

and that one can calculate the $\lambda_{n,1}$, etc., by substituting in (1·1) or (1·2) and equating coefficients of ϵ. So I think that physicists never contemplate the problem with which this paper is concerned, namely, to prove that in certain cases formulae of the form (1·3) and (1·4) are a consequence of the equations (1·1) and (1·2), if $q(x)$ and $\sigma(x)$ satisfy suitable conditions.

A theory of the kind which I consider here has been given by Rellich (1936*a*, *b*, 1938, 1939, 1941), for a general class of operators L. In Rellich's theory the series (1·3) and (1·4) are actually convergent infinite series, for sufficiently small values of ϵ. But the conditions which he imposes would rule out many of the cases which I consider.

In Rellich (1939, Satz 1) a condition is imposed which, in the case considered here, would be equivalent to

$$\int_0^\infty \{\sigma(x)f(x)\}^2\,dx < A\int_0^\infty \{f(x)\}^2\,dx + B\int_0^\infty \{q(x)f(x)-f''(x)\}^2\,dx,$$

for every $f(x)$ for which the right-hand side is finite. In Satz 3 the corresponding condition is

$$\left|\int_0^\infty \sigma(x)\{f(x)\}^2\,dx\right| < A\int_0^\infty \{f(x)\}^2\,dx + B\left|\int_0^\infty f(x)\{q(x)f(x)-f''(x)\}\,dx\right|.$$

Some at any rate of the theorems proved here hold in cases where these conditions are not satisfied. The theory of Friedrichs (1948) applies to the case of continuous spectra.

2. We consider primarily the case of one variable, though it will be seen that most of our arguments extend easily to the case of more variables. Consider the problem of the eigenfunction expansion arising from (1·1), with $q(x)$ continuous, the interval $(0,\infty)$, and the boundary condition

$$\phi(0)\cos\alpha+\phi'(0)\sin\alpha = 0. \tag{2·1}$$

We assume that the spectrum corresponding to this problem is discrete, its only limit-point being $+\infty$. There is, then, a set of eigenvalues λ_n of λ $(\lambda_0<\lambda_1<\lambda_2\ldots)$ for which (1·1) has solutions $\psi_n(x)$ satisfying (1·1) and (2·1), such that

$$\int_0^\infty \psi_n^2(x)\,dx \tag{2·2}$$

is convergent. The functions $\psi_n(x)$ form a normal orthogonal set. If $f(x)$ is any function of integrable square, and

$$c_n = \int_0^\infty f(x)\,\psi_n(x)\,dx, \tag{2·3}$$

then we have the 'Parseval formula'

$$\sum_{n=0}^\infty c_n^2 = \int_0^\infty \{f(x)\}^2\,dx. \tag{2·4}$$

Throughout the paper, capital letters refer to the perturbed equation, and so denote functions of ϵ. We shall suppose that $\sigma(x)$ is continuous, that the perturbed eigenfunctions also satisfy the boundary condition (2·1), and that the spectrum corresponding to the perturbed equation (1·2) is also discrete, and that $+\infty$ is its only limit-point. Then this equation has eigenvalues Λ_n, say, and eigenfunctions $\Psi_n(x)$ of integrable square; and if $f(x)$ is of integrable square, and

$$C_n = \int_0^\infty f(x)\,\Psi_n(x)\,dx, \tag{2·5}$$

then
$$\sum_{n=0}^\infty C_n^2 = \int_0^\infty \{f(x)\}^2\,dx. \tag{2·6}$$

Our main assumption is that *the integrals*

$$\int_0^\infty \{\sigma(x)\,\psi_n(x)\}^2\,dx \quad (n = 0, 1, \ldots) \tag{2·7}$$

are all convergent.

Suppose, for example, that $q(x)$ tends steadily to infinity as $x \to \infty$. Then it follows from lemma 10·3 of my book (Titchmarsh 1946) that for each n, as $x \to \infty$,

$$\psi_n(x) = O\left[\exp\left\{-\int_{x_0}^{x} \{q(t)-\lambda_n\}^{\frac{1}{2}}\,dt\right\}\right].$$

Thus

$$\psi_n(x) = O\{e^{-\chi(x)}\},$$

where $\chi(x)/x \to \infty$ as $x \to \infty$. The condition (2·7) is therefore satisfied, for example, by any function $\sigma(x)$ such that $\sigma(x) = O(e^{ax})$, where a is any positive constant.

3. *We shall also assume that*

$$\int_0^\infty \{\psi_n'(x)\}^2\,dx \tag{3·1}$$

is convergent for each n.

This is certainly the case if $q(x) \geqq 0$ for x sufficiently large. For

$$\begin{aligned}\int_0^X \{\psi_n'(x)\}^2\,dx &= [\psi_n(x)\,\psi_n'(x)]_0^X - \int_0^X \psi_n(x)\,\psi_n''(x)\,dx \\ &= \psi_n(X)\,\psi_n'(X) - \psi_n(0)\,\psi_n'(0) - \int_0^X \{q(x)-\lambda_n\}\,\psi_n^2(x)\,dx.\end{aligned}$$

Now $\psi_n(X)\,\psi_n'(X) \to 0$ as $X \to \infty$ through some sequence of values; otherwise, for $X \geqq X_0$,

$$\psi_n(X)\,\psi_n'(X) \geqq A > 0 \quad (\text{or } \leqq A < 0),$$

so that

$$A(X - X_0) \leqq \int_{X_0}^{X} \psi_n(x)\,\psi_n'(x)\,dx = \tfrac{1}{2}\{\psi_n^2(X) - \psi_n^2(X_0)\},$$

which is impossible if ψ_n is of integrable square.

Making $X \to \infty$ through such a sequence, we obtain

$$\lim \int_0^X \{\psi_n'^2(x) + q(x)\,\psi_n^2(x)\}\,dx = -\psi_n(0)\,\psi_n'(0) + \lambda_n.$$

If $q(x) \geqq 0$ for x sufficiently large, this implies the convergence of (3·1).

4. We shall now prove the following:

LEMMA. *Let*

$$A_{m,n} = \int_0^\infty \sigma(x)\,\Psi_m(x)\,\psi_n(x)\,dx, \quad D_{m,n} = \int_0^\infty \Psi_m(x)\,\psi_n(x)\,dx.$$

Then

$$(\Lambda_m - \lambda_n)\,D_{m,n} = \epsilon A_{m,n}. \tag{4·1}$$

We have

$$\Psi_m''(x) + \{\Lambda_m - q(x) - \epsilon\sigma(x)\}\,\Psi_m(x) = 0,$$

$$\psi_n''(x) + \{\lambda_n - q(x)\}\,\psi_n(x) = 0.$$

Multiplying by $\psi_n(x)$, $\Psi_m(x)$ respectively, and subtracting, we obtain

$$\frac{d}{dx}\{\Psi'_m(x)\,\psi_n(x)-\Psi_m(x)\,\psi'_n(x)\}+(\Lambda_m-\lambda_n)\,\Psi_m(x)\,\psi_n(x)-\epsilon\sigma(x)\,\Psi_m(x)\,\psi_n(x)=0. \quad (4\cdot2)$$

Integrating over $(0, X)$,

$$(\Lambda_m-\lambda_n)\int_0^X \Psi_m(x)\,\psi_n(x)\,dx=\epsilon\int_0^X \sigma(x)\,\Psi_m(x)\,\psi_n(x)\,dx \\ -\Psi'_m(X)\,\psi_n(X)+\Psi_m(X)\,\psi'_n(X),$$

the integrated term at the origin vanishing, by the boundary conditions. If the integrated term also tends to zero at infinity, the result follows.

To obtain the result without this assumption, multiply (4·2) by $1-x/X$ and integrate over $(0, X)$; then

$$(\Lambda_m-\lambda_n)\int_0^X\left(1-\frac{x}{X}\right)\Psi_m(x)\,\psi_n(x)\,dx=\epsilon\int_0^X\left(1-\frac{x}{X}\right)\sigma(x)\,\Psi_m(x)\,\psi_n(x)\,dx \\ -\int_0^X\left(1-\frac{x}{X}\right)\frac{d}{dx}\{\Psi'_m(x)\,\psi_n(x)-\Psi_m(x)\,\psi'_n(x)\}\,dx.$$

The first two terms tend to $(\Lambda_m-\lambda_n)\,D_{m,n}$ and $\epsilon A_{m,n}$ respectively, as $X\to\infty$, and it is sufficient to prove that the last term tends to zero as $X\to\infty$ through some sequence of values.

Integrating by parts, we obtain

$$\frac{1}{X}\int_0^X \{\Psi'_m(x)\,\psi_n(x)-\Psi_m(x)\,\psi'_n(x)\}\,dx,$$

the integrated terms vanishing; and, by another integration by parts, this is equal to

$$\frac{1}{X}[\Psi_m(x)\,\psi_n(x)]_0^X-\frac{2}{X}\int_0^X \Psi_m(x)\,\psi'_n(x)\,dx. \quad (4\cdot3)$$

Now
$$\left|\int_0^X \Psi_m(x)\,\psi'_n(x)\,dx\right| \leqq \left\{\int_0^X \Psi_m^2\,dx\int_0^X \psi_n'^2\,dx\right\}^{\frac12} \\ \leqq \left\{\int_0^\infty \psi_n'^2\,dx\right\}^{\frac12}$$

which is finite, by (3·1). Hence the last term in (4·3) tends to zero. Finally

$$X^{-1}\Psi_m(X)\,\psi_n(X)\to 0,$$

through some sequence of values; otherwise

$$\Psi_m(x)\,\psi_n(x)\geqq Ax \quad (\text{or} \leqq -Ax),$$

for $x\geqq X_0$; and then

$$\tfrac12 A(X^2-X_0^2)\leqq\int_{X_0}^X \Psi_m(x)\,\psi_n(x)\,dx \\ \leqq\left\{\int_{X_0}^X \Psi_m^2\,dx\int_{X_0}^X \psi_n^2\,dx\right\}^{\frac12}\leqq\left\{\int_0^\infty \Psi_m^2\,dx\int_0^\infty \psi_n^2\,dx\right\}^{\frac12}=1,$$

giving a contradiction for X large enough. This proves the lemma.

5. We next recall the known theorem that, if $q(x)$ in (1·1) is changed to $Q(x)$, where $q(x) \leqq Q(x)$ for all values of x, then $\lambda_n \leqq \Lambda_n$ for each n (see Courant & Hilbert 1931, p. 357, Satz 7). The proof may be stated briefly as follows. In the case $\sin\alpha = 0$, let

$$J(f) = \int_0^\infty \{f'^2(x) + q(x) f^2(x)\}\, dx, \quad \mathbf{J}(f) = \int_0^\infty \{f'^2(x) + Q(x) f^2(x)\}\, dx,$$

for any $f(x)$ for which the integrals exist. It is known* that

$$J(f) = \sum_{n=0}^\infty \lambda_n c_n^2, \quad \mathbf{J}(f) = \sum_{n=0}^\infty \Lambda_n C_n^2.$$

Clearly

$$J(f) \leqq \mathbf{J}(f).$$

Also $\mathbf{J}(\Psi_0) = \Lambda_0$. Hence, taking $f = \Psi_0$,

$$\Lambda_0 \geqq \sum_{n=0}^\infty \lambda_n c_n^2 \geqq \lambda_0 \sum_{n=0}^\infty c_n^2 = \lambda_0.$$

Next, let

$$f(x) = C_0 \Psi_0(x) + C_1 \Psi_1(x),$$

where

$$C_0^2 + C_1^2 = 1.$$

Then

$$\mathbf{J}(f) = \Lambda_0 C_0^2 + \Lambda_1 C_1^2 \leqq \Lambda_1 (C_0^2 + C_1^2) = \Lambda_1.$$

Also we can choose C_0/C_1 so that $c_0 = 0$. Then

$$J(f) = \sum_{n=1}^\infty \lambda_n c_n^2 \geqq \lambda_1 \sum_{n=1}^\infty c_n^2 = \lambda_1.$$

Hence $\Lambda_1 \geqq \lambda_1$; and so generally.

If $\sin\alpha \neq 0$ we argue similarly with

$$J(f) = \int_0^\infty \{f'^2(x) + q(x) f^2(x)\}\, dx - \{f(0)\}^2 \cot\alpha.$$

6. Now consider the eigenvalues λ_n and Λ_n associated with (1·1) and (1·2) respectively, and let $\epsilon \to 0$ by positive values.

THEOREM 1. *If $\sigma(x) \geqq 0$ and the integrals (2·7) converge, then $\Lambda_n \to \lambda_n$ for each n.*

It follows from § 5 that, for each n, Λ_n decreases steadily as ϵ decreases, and that $\Lambda_n \geqq \lambda_n$ for each n. Thus, for each n, Λ_n tends to a limit, say μ_n, as $\epsilon \to 0$; and $\mu_n \geqq \lambda_n$. We have to prove that actually $\mu_n = \lambda_n$.

Suppose first that $\mu_0 > \lambda_0$. Then there is a positive δ such that

$$\Lambda_m - \lambda_0 \geqq \delta$$

for every m. Hence by (4·1), with $n = 0$,

$$|D_{m,0}| \leqq \frac{\epsilon}{\delta} |A_{m,0}| \quad (m = 0, 1, \ldots).$$

Hence

$$\sum_{m=0}^\infty D_{m,0}^2 \leqq \frac{\epsilon^2}{\delta^2} \sum_{m=0}^\infty A_{m,0}^2 = \frac{\epsilon^2}{\delta^2} \int_0^\infty \{\sigma(x)\, \psi_0(x)\}^2\, dx$$

by (2·6) with $f(x) = \sigma(x)\, \psi_0(x)$. But also, by (2·6) with $f(x) = \psi_0(x)$,

$$\sum_{m=0}^\infty D_{m\,0}^2 = \int_0^\infty \psi_0^2(x)\, dx = 1.$$

This involves a contradiction if ϵ is small enough, and so $\mu_0 = \lambda_0$.

---

* Cf. Courant & Hilbert (1931, p. 397 (53)).

Next suppose that $\mu_1 > \lambda_1$. Then there is a positive δ such that

$$\Lambda_m - \lambda_1 \geqq \delta \quad (m = 1, 2, \ldots).$$

Since $\Lambda_0 \to \lambda_0 < \lambda_1$, we have also

$$\lambda_1 - \Lambda_0 \geqq \delta$$

if δ is suitably chosen and ϵ is small enough. Hence

$$|D_{m,1}| \leqq \frac{\epsilon}{\delta} |A_{m,1}| \quad (m = 0, 1, \ldots).$$

This leads to a contradiction as before (with ψ_0 replaced by ψ_1), and hence $\mu_1 = \lambda_1$. Similarly, $\mu_n = \lambda_n$ for every n.

In the above argument δ is supposed to be fixed; but a similar contradiction is obtained if $\delta = K\epsilon$ and K is large enough. Hence

$$\Lambda_n - \lambda_n = O(\epsilon) \tag{6·1}$$

for each n (not uniformly with respect to n).

7. The case where $\sigma(x) \leqq 0$ is not quite so simple as that in which $\sigma(x) \geqq 0$. For example, if $q(x) \to \infty$, then $q(x) + \epsilon\sigma(x) \to \infty$ for any positive ϵ and $\sigma(x)$, so that the perturbed spectrum is necessarily discrete. But this need not be so if $\sigma(x) \leqq 0$. Thus if $q(x) = x$, $\sigma(x) = -x^2$, then the perturbed spectrum is continuous. Such cases are interesting, but they present a problem of a different kind from that considered here.

Accordingly, if $\sigma(x) \leqq 0$, we shall suppose that $q(x) > 0$, $q(x) \to \infty$, and $|\sigma(x)| \leqq Mq(x)$, where M is a constant. Then $q(x) + \epsilon\sigma(x) \to \infty$ if ϵ is small enough, so that the perturbed spectrum is discrete.

THEOREM 2. *Under the above conditions,* $\Lambda_n \to \lambda_n$ *for each* n.

In this case each Λ_n increases steadily as ϵ decreases, and $\Lambda_n \leqq \lambda_n$.

We now argue as in § 5, but with $Q(x) = q(x) + \epsilon\sigma(x)$, so that

$$(1 - \epsilon M)\, q(x) \leqq Q(x) \leqq q(x).$$

Let $\sin\alpha = 0$. We clearly obtain

$$\Lambda_0 = \mathbf{J}(\Psi_0) \geqq (1 - \epsilon M)\, J(\Psi_0) \geqq (1 - \epsilon M)\, \lambda_0.$$

Next, let
$$f(x) = C_0\Psi_0(x) + C_1\Psi_1(x),$$

where $C_0^2 + C_1^2 = 1$ and $c_0 = 0$. Then, as in § 5,

$$\Lambda_1 \geqq \mathbf{J}(f) \geqq (1 - \epsilon M)\, J(f) \geqq (1 - \epsilon M)\, \lambda_1,$$

and so generally.

A similar argument holds in the case $\cot\alpha \leqq 0$. If $\cot\alpha > 0$ we have

$$\begin{aligned}\Lambda_0 = \mathbf{J}(\Psi_0) &\geqq (1 - \epsilon M)\int_0^\infty \{\Psi_0'^2 + q(x)\Psi_0^2\}\, dx - \Psi_0^2(0)\cot\alpha \\ &= (1 - \epsilon M)\, J(\Psi_0) - \epsilon M \Psi_0^2(0)\cot\alpha \\ &\geqq (1 - \epsilon M)\, \lambda_0 - \epsilon M \Psi_0^2(0)\cot\alpha.\end{aligned}$$

Now for any twice-differentiable $f(x)$ (see Titchmarsh 1946, § 2·14),

$$f(x)=\int_x^{x+1}(x+1-y)^2(y-x)f''(y)\,dy-\int_x^{x+1}(6y-6x-4)f(y)\,dy. \qquad (7\cdot 1)$$

Taking $f=\Psi_0$, $x=0$, we obtain

$$\Psi_0(0)=\int_0^1[(1-y)^2y\{q(y)+\epsilon\sigma(y)-\Lambda_0\}-(6y-4)]\,\Psi_0(y)\,dy.$$

Hence, by the Schwarz inequality,

$$\Psi_0^2(0)\leqq\int_0^1[(1-y)^2y\{q(y)+\epsilon\sigma(y)-\Lambda_0\}-(6y-4)]^2\,dy.$$

Since Λ_0 is bounded, it follows that $\Psi_0(0)$ is a bounded function of ϵ. Hence

$$\Lambda_0\geqq\lambda_0-O(\epsilon),$$

and similarly for $\Lambda_1, \Lambda_2, \ldots$.

8. THEOREM 3. *Let $\sigma(x)$ be not necessarily of one sign, but let* (2·7) *be convergent and $\sigma(x)\geqq -Mq(x)$. Then $\Lambda_n\to\lambda_n$ for each n.*

Let $\sigma(x)=\sigma^{(1)}(x)+\sigma^{(2)}(x)$, where $\sigma^{(1)}(x)=\sigma(x)$ if $\sigma(x)\geqq 0$, and $=0$ otherwise. Then $\sigma^{(1)}(x)\geqq 0$, $\sigma^{(2)}(x)\leqq 0$.

Let the eigenvalues for $q(x)+\epsilon\sigma^{(1)}(x)$ and $q(x)+\epsilon\sigma^{(2)}(x)$ be $\Lambda_n^{(1)}$ and $\Lambda_n^{(2)}$ respectively. Then

$$\Lambda_n^{(2)}\leqq\Lambda_n\leqq\Lambda_n^{(1)}.$$

But $\Lambda_n^{(1)}$ and $\Lambda_n^{(2)}$ both tend to λ_n. Hence so does Λ_n.

9. THEOREM 4. *Let*

$$a_{m,n}=\int_0^\infty\sigma(x)\,\psi_m(x)\,\psi_n(x)\,dx. \qquad (9\cdot 1)$$

Then, under the conditions of Theorems 1, 2 *or* 3,

$$\Lambda_n=\lambda_n+\epsilon a_{n,n}+O(\epsilon^2) \qquad (9\cdot 2)$$

(*not uniformly with respect to n*).

Let n be given, and let δ be a positive number less than the smaller of $\lambda_{n+1}-\lambda_n$ and $\lambda_n-\lambda_{n-1}$.

Consider first the case $\sigma(x)\geqq 0$. Then each Λ_m decreases steadily to the limit λ_m, and hence

$$\Lambda_m<\lambda_n-\delta \quad (m=0,1,\ldots,n-1)$$

if ϵ is small enough. Also

$$\Lambda_m\geqq\lambda_m>\lambda_n+\delta \quad (m=n+1,n+2,\ldots).$$

Hence

$$|\Lambda_m-\lambda_n|>\delta \quad (m\neq n),$$

if ϵ is small enough.

A similar argument holds if $\sigma(x)\leqq 0$, and if $\sigma(x)$ is not of one sign the same result follows by combining the two special cases.

It now follows from (4·1) that

$$\sum_{m\neq n} D^2_{m,n} = O\left(\epsilon^2 \sum_m A^2_{m,n}\right)$$

$$= O\left\{\epsilon^2 \int_0^\infty \sigma^2(x)\,\psi_n^2(x)\,dx\right\} = O(\epsilon^2).$$

But
$$\sum_{m=0}^{\infty} D^2_{m,n} = \int_0^\infty \psi_n^2(x)\,dx = 1.$$

Hence
$$D^2_{n,n} = 1 + O(\epsilon^2),$$

and so
$$D_{n,n} = \{1+O(\epsilon^2)\}^{\frac{1}{2}} = 1+O(\epsilon^2), \tag{9·3}$$

if $D_{n,n} \geqq 0$. We can always make this so, since the signs to be attached to the functions $\psi_n(x)$ and $\Psi_n(x)$ are so far arbitrary, and, once the $\psi_n(x)$ have been fixed, the $\Psi_n(x)$ can be chosen so that $D_{n,n} \geqq 0$.

Now (4·1), with $m = n$, gives

$$(\Lambda_n - \lambda_n)\,D_{n,n} = \epsilon A_{n,n}$$

$$= \epsilon a_{n,n} + \epsilon \int_0^\infty \sigma(x)\,\psi_n(x)\,\{\Psi_n(x) - \psi_n(x)\}\,dx.$$

Also
$$\left|\int_0^\infty \sigma\psi_n(\Psi_n - \psi_n)\,dx\right| \leqq \left\{\int_0^\infty \sigma^2\psi_n^2\,dx \int_0^\infty (\Psi_n - \psi_n)^2\,dx\right\}^{\frac{1}{2}},$$

and
$$\int_0^\infty (\Psi_n - \psi_n)^2\,dx = \int_0^\infty \Psi_n^2\,dx + \int_0^\infty \psi_n^2\,dx - 2\int_0^\infty \Psi_n\psi_n\,dx$$

$$= 2 - 2D_{n,n} = O(\epsilon^2). \tag{9·4}$$

Hence
$$\int_0^\infty \sigma\psi_n(\Psi_n - \psi_n)\,dx = O(\epsilon),$$

and the theorem follows.

10. THEOREM 5. *Under the same conditions*

$$\Psi_n(x) = \psi_n(x) + O(\epsilon) \tag{10·1}$$

uniformly in any finite interval.

It follows from (7·1) that

$$\psi_n(x) = \int_x^{x+1} [(x+1-y)^2\,(y-x)\,\{q(y) - \lambda_n\} - (6y - 6x - 4)]\,\psi_n(y)\,dy \tag{10·2}$$

and

$$\Psi_n(x) = \int_x^{x+1} [(x+1-y)^2\,(y-x)\,\{q(y) + \epsilon\sigma(y) - \Lambda_n\} - (6y - 6x - 4)]\,\Psi_n(y)\,dy. \tag{10·3}$$

Hence

$$\Psi_n(x) - \psi_n(x) = \int_x^{x+1} [(x+1-y)^2\,(y-x)\,\{q(y) - \lambda_n\} - (6y - 6x - 4)]\,\{\Psi_n(y) - \psi_n(y)\}\,dy$$

$$+ \int_x^{x+1} (x+1-y)^2\,(y-x)\,\{\epsilon\sigma(y) - \Lambda_n + \lambda_n\}\,\Psi_n(y)\,dy.$$

By the Schwarz inequality, the square of the first term does not exceed

$$\int_x^{x+1}[(x+1-y)^2(y-x)\{q(y)-\lambda_n\}-(6y-6x-4)]^2\,dy\int_x^{x+1}\{\Psi_n(y)-\psi_n(y)\}^2\,dy$$

$$=O\left[\int_0^\infty\{\Psi_n(y)-\psi_n(y)\}^2\,dy\right]=O(\epsilon^2)$$

by (9·4). The second term is

$$O(\epsilon)\int_x^{x+1}|\Psi_n(y)|\,dy=O(\epsilon)\left\{\int_x^{x+1}\Psi_n^2(y)\,dy\right\}^{\frac{1}{2}}$$

$$=O(\epsilon)\left\{\int_0^\infty\Psi_n^2(y)\,dy\right\}^{\frac{1}{2}}=O(\epsilon).$$

The theorem therefore follows.

11. To make further approximations to Λ_n and $\Psi_n(x)$, we appear to need greater restrictions on $\sigma(x)$.

Supposing n fixed, we have

$$\begin{aligned}(\Lambda_n-\lambda_m)D_{n,m}&=\epsilon A_{n,m}\\ &=\epsilon a_{n,m}+\epsilon\int_0^\infty\sigma(x)\,\psi_m(x)\,\{\Psi_n(x)-\psi_n(x)\}\,dx\\ &=\epsilon a_{m,n}+O(\epsilon)\left\{\int_0^\infty\sigma^2\psi_m^2\,dx\int_0^\infty(\Psi_n-\psi_n)^2\,dx\right\}^{\frac{1}{2}}\\ &=a_{m,n}+O(\epsilon^2b_m^{\frac{1}{2}}),\end{aligned}$$

where $$b_m=\int_0^\infty\sigma^2(x)\,\psi_m^2(x)\,dx.$$

Hence $$D_{n,m}=\frac{\epsilon a_{m,n}}{\Lambda_n-\lambda_m}+O\left(\frac{\epsilon^2b_m^{\frac{1}{2}}}{\lambda_m}\right)\tag{11·1}$$

(with a trivial modification if any λ_m vanishes). Now

$$\begin{aligned}(\Lambda_n-\lambda_n)D_{n,n}&=\epsilon A_{n,n}\\ &=\epsilon\int_0^\infty\sigma(x)\,\Psi_n(x)\,\psi_n(x)\,dx=\epsilon\sum_{\nu=0}^\infty D_{n,\nu}a_{n,\nu}\end{aligned}$$

(by the Parseval formula)

$$\begin{aligned}&=\epsilon D_{n,n}a_{n,n}+\epsilon\sum_{\nu\neq n}D_{n,\nu}a_{n,\nu}\\ &=\epsilon D_{n,n}a_{n,n}+\epsilon^2\sum_{\nu\neq n}\frac{a_{n,\nu}^2}{\Lambda_n-\lambda_\nu}+O\left\{\epsilon^3\sum_\nu\left|\frac{a_{n,\nu}b_\nu^{\frac{1}{2}}}{\lambda_\nu}\right|\right\}.\end{aligned}$$

Also $$\sum_{\nu\neq n}\frac{a_{n,\nu}^2}{\Lambda_n-\lambda_\nu}-\frac{a_{n,\nu}^2}{\lambda_n-\lambda_\nu}=(\lambda_n-\Lambda_n)\sum_{\nu\neq n}\frac{a_{n,\nu}^2}{(\Lambda_n-\lambda_\nu)(\lambda_n-\lambda_\nu)}$$

$$=O(\epsilon)\sum_{\nu=0}^\infty a_{n,\nu}^2=O(\epsilon)\int_0^\infty\sigma^2(x)\,\psi_n^2(x)\,dx=O(\epsilon).$$

Hence we can replace Λ_n by λ_n in the above right-hand side with error $O(\epsilon^3)$. On dividing by $D_{n,n}$, and noting that

$$\frac{1}{D_{n,n}} = \frac{1}{1+O(\epsilon^2)} = 1+O(\epsilon^2),$$

we obtain the following result:

THEOREM 6. *Under the conditions of Theorems* 1, 2 *or* 3

$$\Lambda_n = \lambda_n + \epsilon a_{n,n} + \epsilon^2 \sum_{\nu \neq n} \frac{a_{n,\nu}^2}{\lambda_n - \lambda_\nu} + O(\epsilon^3) \tag{11·2}$$

provided that the series

$$\sum_\nu \left| \frac{a_{n,\nu} b_\nu^{\frac{1}{2}}}{\lambda_\nu} \right| \tag{11·3}$$

is convergent.

Since $\sum_\nu a_{n,\nu}^2$ is convergent, it follows from the Schwarz inequality that a sufficient condition for the theorem is that

$$\sum \frac{b_\nu}{\lambda_\nu^2} \tag{11·4}$$

should be convergent.

12. We next try to improve the approximation given by Theorem 5.

The expansion of $\Psi_n(x)$ in terms of the functions $\psi_\nu(x)$ is

$$\Psi_n(x) = \sum_{\nu=0}^{\infty} D_{n,\nu} \psi_\nu(x). \tag{12·1}$$

This can be deduced from theorem 2·7 (i) of my book, the condition (2·7·2) actually being superfluous in the limit-point case. Or it can be proved as follows. Suppose x given, and let

$$\begin{aligned} \phi(y) &= (x+1-y)^2(y-x)q(x) - (6y-6x-4) && (x \leqq y \leqq x+1) \\ &= 0 && (y<x \text{ or } y>x+1), \\ \chi(y) &= (x+1-y)^2(y-x) && (x \leqq y \leqq x+1), \\ &= 0 && (y<x \text{ or } y>x+1). \end{aligned}$$

Let

$$h_\nu = \int_0^\infty \phi(y)\psi_\nu(y)\,dy, \quad k_\nu = \int_0^\infty \chi(y)\psi_\nu(y)\,dy.$$

Now (10·3) may be written

$$\Psi_n(x) = \int_0^\infty \phi(y)\Psi_n(y)\,dy - \Lambda_n \int_0^\infty \chi(y)\Psi_n(y)\,dy + \epsilon \int_0^\infty \chi(y)\sigma(y)\Psi_n(y)\,dy,$$

and hence, by the Parseval formula,

$$\Psi_n(x) = \sum_{\nu=0}^{\infty} h_\nu D_{n,\nu} - \Lambda_n \sum_{\nu=0}^{\infty} k_\nu D_{n,\nu} + \epsilon \sum_{\nu=0}^{\infty} k_\nu A_{n,\nu}.$$

Hence by (4·1)

$$\Psi_n(x) = \sum_{\nu=0}^{\infty} (h_\nu - \lambda_\nu k_\nu) D_{n,\nu},$$

and (12·1) follows from this and (10·2).

From (12·1), (9·3) and (11·1) we obtain

$$\Psi_n(x) = \psi_n(x) + \epsilon \sum_{\nu \neq n} \frac{a_{n,\nu}\psi_\nu(x)}{\Lambda_n - \lambda_\nu} + O\left\{\epsilon^2 \sum_{\nu \neq n} \left| \frac{b_\nu^{\frac{1}{2}}\psi_\nu(x)}{\lambda_\nu} \right| \right\} + O(\epsilon^2).$$

Also
$$\frac{1}{\Lambda_n - \lambda_\nu} - \frac{1}{\lambda_n - \lambda_\nu} = O\left(\frac{\Lambda_n - \lambda_n}{\lambda_\nu^2}\right) = O\left(\frac{\epsilon}{\lambda_\nu^2}\right),$$

and
$$\sum_\nu \left| \frac{a_{n,\nu}\psi_\nu(x)}{\lambda_\nu^2} \right| \leqq \left\{ \sum_\nu a_{n,\nu}^2 \sum_\nu \frac{\psi_\nu^2(x)}{\lambda_\nu^4} \right\}^{\frac{1}{2}},$$

which is convergent, since $\Sigma a_{n,\nu}^2$ and $\Sigma \lambda_\nu^{-2}\psi_\nu^2(x)$ are convergent (see § 2·13 of my book), and $\lambda_\nu \to \infty$. Hence we obtain

THEOREM 7. *The formula*

$$\Psi_n(x) = \psi_n(x) + \epsilon \sum_{\nu \neq n} \frac{a_{n,\nu}\psi_\nu(x)}{\lambda_n - \lambda_\nu} + O(\epsilon^2) \tag{12·2}$$

holds (*uniformly over any finite interval*) *provided that*

$$\Sigma \left| \frac{b_\nu^{\frac{1}{2}}\psi_\nu(x)}{\lambda_\nu} \right| \tag{12·3}$$

is (*uniformly*) *convergent.*

13. As an example, consider the case where $q(x) = x^2$ and the interval is $(-\infty, \infty)$. The above theory applies almost immediately to this case. We have $\lambda_n = 2n+1$, and $\psi_n(x) = A_n e^{-\frac{1}{2}x^2} H_n(x)$, where $H_n(x)$ is the Hermite polynomial of degree n, and A_n is a constant. The formula (9·2) is valid if

$$-Mx^2 \leqq \sigma(x) \leqq M' e^{ax^2},$$

where $a < \frac{1}{2}$.

Now it is known that

$$x\psi_\nu(x) = \sqrt{(\tfrac{1}{2}\nu)}\,\psi_{\nu-1}(x) + \sqrt{(\tfrac{1}{2}\nu + \tfrac{1}{2})}\,\psi_{\nu+1}(x).$$

By repeated application of this it follows that, if k is any positive integer, and n is given,

$$a_{n,\nu} = \int_{-\infty}^{\infty} x^k \psi_n(x)\,\psi_\nu(x)\,dx = 0,$$

except for a finite number of values of ν. Hence, if $\sigma(x) = x^k$, the series (11·3) is convergent, so that (11·2) holds.

14. *Extension to partial differential equations.* The above theory can be extended to partial differential equations of the form

$$\nabla^2\phi + (\lambda - q)\phi = 0, \tag{14·1}$$

involving two or more independent variables. As an illustration we shall consider briefly the case where there are two variables x and y, and the region is the whole (x, y) plane. The situation is similar to that described in § 2. Corresponding to (3·1), we shall assume that

$$\int_0^\infty \int_0^{2\pi} \left(\frac{\partial \psi_n}{\partial r}\right)^2 r\,dr\,d\theta \tag{14·2}$$

is convergent. This is certainly true if $q(x,y) \geqq 0$ for $r = \sqrt{(x^2+y^2)}$ sufficiently large. For consider

$$I = \int_0^R \int_0^{2\pi} \left\{ \left(\frac{\partial \psi_n}{\partial r} \right)^2 + \frac{1}{r^2} \left(\frac{\partial \psi_n}{\partial \theta} \right)^2 \right\} r\, dr\, d\theta.$$

On integrating by parts we obtain

$$I = \int_0^{2\pi} \psi_n[R,\theta] \frac{\partial \psi_n}{\partial R} R\, d\theta - \int_0^R \int_0^{2\pi} \psi_n \left(\frac{\partial^2 \psi_n}{\partial r^2} + \frac{1}{r} \frac{\partial \psi_n}{\partial r} + \frac{1}{r^2} \frac{\partial^2 \psi_n}{\partial \theta^2} \right) r\, dr\, d\theta$$

$$= \int_0^{2\pi} \psi_n[R,\theta] \frac{\partial \psi_n}{\partial R} R\, d\theta - \int_0^R \int_0^{2\pi} \psi_n^2 (q - \lambda_n)\, r\, dr\, d\theta.$$

The first term tends to zero as $R \to \infty$ through some sequence of values; otherwise

$$\int_0^{2\pi} \psi_n \frac{\partial \psi_n}{\partial r} r\, d\theta \geqq A > 0$$

(or $\leqq -A < 0$), for $r \geqq r_0$; hence

$$\int_0^{2\pi} \psi_n \frac{\partial \psi_n}{\partial r} d\theta \geqq \frac{A}{r}, \quad \int_0^{2\pi} \tfrac{1}{2} \{ \psi_n^2[r,\theta] - \psi_n^2[r_0,\theta] \} d\theta \geqq A \log \frac{r}{r_0},$$

which is impossible if $\psi[r,\theta]$ is of integrable square. Hence

$$\lim \int_0^R \int_0^{2\pi} \left\{ \left(\frac{\partial \psi_n}{\partial r} \right)^2 + \frac{1}{r^2} \left(\frac{\partial \psi_n}{\partial \theta} \right)^2 + q \psi_n^2 \right\} r\, dr\, d\theta = \lambda_n \tag{14·3}$$

as $R \to \infty$ through some sequence. If $q \geqq 0$ for r large enough, this implies the convergence of (14·2).

To extend § 4, we have, corresponding to (4·2),

$$\psi_n \nabla^2 \Psi_m - \Psi_m \nabla^2 \psi_n + (\Lambda_m - \lambda_n) \Psi_m \psi_n - \epsilon \sigma \Psi_m \psi_n = 0.$$

Multiplying by $1 - r/R$ and integrating, we obtain

$$\int_0^R \int_0^{2\pi} (\psi_n \nabla^2 \Psi_m - \Psi_m \nabla^2 \psi_n) \left(1 - \frac{r}{R} \right) r\, dr\, d\theta$$
$$+ (\Lambda_m - \lambda_n) \int_0^R \int_0^{2\pi} \left(1 - \frac{r}{R} \right) \Psi_m \psi_n r\, dr\, d\theta - \epsilon \int_0^R \int_0^{2\pi} \left(1 - \frac{r}{R} \right) \sigma \Psi_m \psi_n r\, dr\, d\theta = 0. \tag{14·4}$$

On integrating by parts, the first term reduces to

$$\frac{1}{R} \int_0^R \int_0^{2\pi} \left(\psi_n \frac{\partial \Psi_m}{\partial r} - \Psi_m \frac{\partial \psi_n}{\partial r} \right) r\, dr\, d\theta.$$

A further integration by parts gives

$$\int_0^{2\pi} \Psi_m[R,\theta] \psi_n[R,\theta]\, d\theta - \frac{1}{R} \int_0^R \int_0^{2\pi} \Psi_m \psi_n\, dr\, d\theta - \frac{2}{R} \int_0^R \int_0^{2\pi} \Psi_m \frac{\partial \psi_n}{\partial r} r\, dr\, d\theta.$$

The last two terms tend to 0 (using the convergence of (14·2)), and the first term tends to 0 through some sequence of values of R; for otherwise

$$\int_0^{2\pi} \Psi_m[R,\theta] \psi_n[R,\theta]\, d\theta \geqq A > 0$$

(or $\leqq -A < 0$) for $R \geqq R_0$, and hence

$$\int_{R_0}^{R}\int_{0}^{2\pi} \Psi_m \psi_n r\,dr\,d\theta \geqq \tfrac{1}{2}A(R^2 - R_0^2),$$

which is impossible if Ψ_m and ψ_n are of integrable square.

On making $R \to \infty$ through a suitable sequence, (14·4) therefore gives

$$(\Lambda_m - \lambda_n) D_{m,n} = \epsilon A_{m,n}, \tag{14·5}$$

with an obvious extension of the previous notation.

The rest of the theory is similar to the one-dimensional case. The main difference is that in two or more dimensions we may have 'degeneracy', i.e. more than one eigenfunction corresponding to the same eigenvalue. The modifications which have to be made in this case are well known.

As an example in two dimensions, let $q(x, y) = x^2 + y^2$. The unperturbed spectrum is discrete, the eigenfunctions being of the form

$$A_{m,n} e^{-\frac{1}{2}(x^2+y^2)} H_m(x) H_n(y),$$

corresponding to the eigenvalue $2m + 2n + 2$. Apart from the occurrence of degeneracy, the analogue of theorem 4 will hold if

$$-M(x^2 + y^2) \leqq \sigma(x, y) \leqq e^{a(x^2+y^2)},$$

where $0 < a < \frac{1}{2}$.

REFERENCES

Courant, R. & Hilbert, D. 1931 *Methoden der mathematischen Physik*, **1** (zw. Aufl.). Berlin: Springer.

Friedrichs, K. O. 1948 *Commun. Appl. Math.* **1**, 361.

Rellich, F. 1936*a* *Math. Ann.* **113**, 600.

Rellich, F. 1936*b* *Math. Ann.* **113**, 677.

Rellich, F. 1938 *Math. Ann.* **116**, 555.

Rellich, F. 1939 *Math. Ann.* **117**, 356.

Rellich, F. 1941 *Math. Ann.* **118**, 462.

Titchmarsh, E. C. 1946 *Eigenfunction expansions associated with second-order differential equations*. Oxford University Press.

Plastic deformation of silver chloride. II. Photoelastic study of the internal stresses in glide packets

By J. F. Nye, *Cavendish Laboratory, University of Cambridge*

(*Communicated by E. Orowan, F.R.S.—Received* 27 *January* 1949—
Revised 25 *July* 1949)

[Plates 1 to 4]

The pattern of birefringence caused by glide in silver chloride is most clearly resolved when the glide planes are observed edge on. It is then possible to sketch the two orthogonal sets of curves giving the directions of polarization at each point of the pattern and, by means of a compensator, to find how the magnitude of the birefringence varies from point to point. The stress distribution can be deduced from the distribution of birefringence, provided that the important influence of the relative orientation of stress axes and crystal axes is taken into account. The state of stress in each plastically deformed grain can be resolved into two parts. (1) Each glide packet is subject to pure bending about two perpendicular axes lying in the glide plane (but with a neutral plane that is not always the middle plane of the packet). This gives stresses that vary discontinuously with a period equal to the spacing of the glide zones. (2) There is also a continuously varying stress distribution which changes only slightly in distances equal to the glide zone spacing.

The curvature of the glide packets means either that all the dislocations in one glide zone have the same sign or that positive and negative dislocations are present there in unequal numbers. It is found that, throughout any one grain, the 'dislocation charge' on each zone (to use an obvious electrical analogy) has the same sign and is never more than about twice the average for the grain.

1. INTRODUCTION

If rolled sheets of silver chloride are recrystallized and then plastically deformed, some of the grains are crossed by birefringent bands. In the first paper of this series (Nye 1949), it was concluded that these bands are caused photoelastically by the internal stresses remaining in the material after deformation by pencil glide. The purpose of this paper is to examine the details of the bands and elucidate the nature of the internal stresses.

The glide direction is ⟨110⟩, but the glide surface is not, in general, crystallographic or even a plane. However, when the stress is uniformly distributed, it approximates to a plane. In studying the birefringence patterns, it is clearly best to view the glide surfaces edge on. In the polycrystalline sheets this is easily done, for it is always possible to find some grains containing glide planes set nearly perpendicular to the surfaces of the sheets; but the fact that the glide surfaces are rumpled in such a way that the only straight lines in them are those parallel to the glide direction introduces a difficulty. If we observe along the glide plane and perpendicular to the glide direction, we find a pattern made up of straight striations, but it is confused because the waviness of the glide planes causes the corresponding parts of different layers to be superposed not quite on top of one another. If, instead, we observe parallel to the glide direction, the different layers are superposed in their correct relations, but the pattern itself is very wavy (and often the glide planes branch). Most of the observations have been made by the first of these two methods of viewing. Bands produced by simple tension or simple shear (see § 5) extended through a considerable thickness of the sheet and the overlapping was serious; however, it was sometimes possible to find favourable places in which the pattern was clear. When torsion or bending was used, the bands were confined to thinner layers of the sheet, as might be expected, and the difficulty of overlapping did not arise. (Torsion was more effective than bending in this respect.) From these experiments it was evident that, apart from this observational difficulty, the pattern is essentially the same whether it is produced by simple tension, simple shear, bending or torsion or by combinations of these distortions. The description of the pattern that we now give refers to its appearance when all external forces have been removed from the specimen.

2. NOMENCLATURE AND DETAILS OF THE PATTERN

The regions, usually of submicroscopic thickness, in which the active glide planes are concentrated will be called *glide zones*. When a glide zone intersects the surface of a crystal a *glide band* (or *glide line*) is produced (to be distinguished from the *birefringent bands*). By *glide packet* we shall mean the material lying between two adjacent glide zones; it is deformed elastically but, provided there is only one set of active glide planes, not plastically.

Figure 1, plate 1, shows one of the clearest patterns so far obtained. (In the first paper the grain containing this set of bands was referred to as A in strip no. 4.) The crystal is split up into glide packets G by the glide zones p, and the distribution of birefringence in each of these glide packets is closely similar. By turning the specimen on the rotating stage of the Leitz polarizing microscope, keeping the nicols crossed and fixed in position, we could determine the two orthogonal directions of polarization at any given point, for when these directions are parallel to the vibration directions of the nicols the point appears dark. By use of a Berek compensator it was also possible to distinguish between the directions of the fast and slow rays and to measure the magnitude of the birefringence. The path differences involved were not more than a small fraction of a wave-length, and so the pattern observed between crossed nicols was not coloured. The main feature revealed by these observations was the rapid variation of birefringence in the direction perpendicular to the glide plane, as contrasted with the far smaller variations in the direction parallel to the glide plane. This latter variation is taken into account in the next section, but for the present it is neglected. With this simplification, it is possible to plot out the two orthogonal systems of curves whose directions give the two directions of polarization at any point. The result is shown schematically in figure 2.

In this figure the set of curves shown by full lines gives the directions of the fast ray and the set shown by broken lines the directions of the slow ray. For simplicity the glide zones, p, are drawn as if they were equally spaced. The following points may be noticed:

(1) The directions of polarization maintain more or less fixed directions over the greater part of the field, but turn rapidly through about 90° as they cross the planes marked q.

(2) They rotate very sharply back again as they cross the glide zones.

(3) A q plane occurs between each pair of p planes, but not necessarily midway between them.

Let us see how these assertions agree with the appearance of the bands between crossed nicols.

(a) *Nicols in maximum transmission position*

In figure 1 the vibration directions of the nicols, as shown by the cross-wires, are such that all points near the planes q extinguish; but, apart from the glide zones themselves, which show up as black lines, the other points of the pattern are approximately at the position for maximum transmission. However, the direction of the fast ray in region A (figure 2) differs from its direction in region B by nearly 90°, and the use of the Berek compensator shows this immediately. It is also shown up prettily if a gypsum plate is inserted between the analyzer and the specimen with its polarization directions at 45° to those of the nicols. The planes q are then distinguished by the sensitive purple tint, but while region A is blue region B is yellow. The line of separation between yellow and blue across plane p is often extremely sharp.

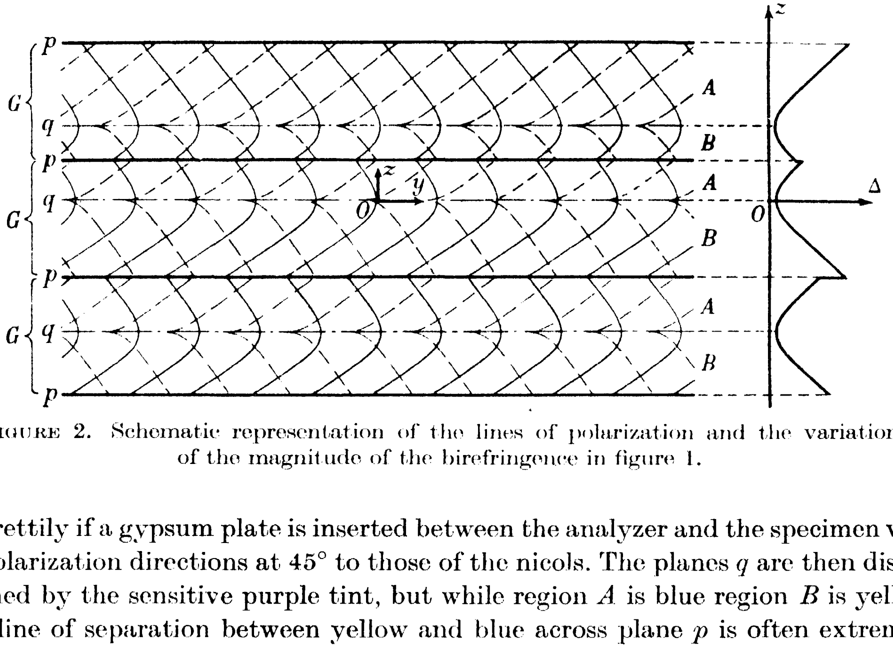

FIGURE 2. Schematic representation of the lines of polarization and the variation of the magnitude of the birefringence in figure 1.

(b) *Nicols in extinction position*

When the specimen is turned through 45°, with the nicols fixed, the pattern becomes far more uniform. According to figure 2, regions A and B are now approximately in the extinction position. However, points near plane q are equally well extinguished, although the polarization directions are at 45° to the nicols here. This is because the birefringence near q is too weak to give any marked restoration of light. The use of a circular polariscope confirms this. With the nicols in this position the planes p sometimes showed up as fine bright lines, and occasionally a fine structure could be detected within them, but this point will not be discussed further in the present paper.

We define Δ as the path difference between the slow and fast rays; it should be regarded as always positive. The precise variation of Δ is not easy to measure, and the curve shown on the right of figure 2 is qualitative only. The main point is that Δ reaches a minimum on plane q.

There is one further feature of the pattern in this figure. If we begin with the nicols set as in figure 1, and turn the specimen through a small angle, each black stripe q moves slightly to one side relative to the crystal. If the specimen is turned in the opposite direction, all the stripes move the other way. This behaviour results from the curvature of the lines of polarization shown in figure 2. This curvature also explains why extinction of the whole pattern cannot be made quite complete.

Other sets of bands give polarization lines that are more or less curved than those in figure 2; moreover, it appears that the angle between p and the predominant direction of the lines, although constant over large areas of one band system, can have quite different values in different crystals (in figure 2 it is about 35°). In other respects, however, figure 2 may be taken as representative of all band systems.

3. INTERPRETATION OF THE PATTERN IN TERMS OF STRESS

We have neglected variations of the birefringence in directions parallel to the glide plane. Acting in the same spirit, we begin by assuming that the stresses also do not vary in planes parallel to the glide plane. Taking rectangular axes Ox, Oy, Oz, with Oz normal to the glide plane and Ox as the direction of observation, we accordingly regard the stresses as functions of z only. The equations of equilibrium then reduce to

$$\frac{d\sigma_z}{dz} = 0, \quad \frac{d\tau_{yz}}{dz} = 0, \quad \frac{d\tau_{zx}}{dz} = 0.$$

In addition to satisfying the equilibrium equations, the stresses must give compatible strain components, and the simplest way of introducing this condition is to assume isotropic (non-crystalline) elasticity and to use the Beltrami equations (see, for example, Love (1944), p. 135). It then follows that σ_x, σ_y and τ_{xy} are linear functions of z. Hence we may write

$$\left.\begin{aligned} \sigma_x &= a_1 z + b_1, & \sigma_y &= a_2 z + b_2, & \tau_{xy} &= a_3 z + b_3, \\ \sigma_z &= b_4, & \tau_{yz} &= b_5, & \tau_{zx} &= b_6, \end{aligned}\right\} \tag{1}$$

where $a_1, a_2, a_3, b_1, \ldots, b_6$ are constants.

These equations represent a uniform stress, $b_1, \ldots, b_6$, superposed on a linearly varying stress distribution given by

$$\left.\begin{aligned} \sigma_x &= a_1 z, & \sigma_y &= a_2 z, & \tau_{xy} &= a_3 z, \\ \sigma_z &= 0, & \tau_{yz} &= 0, & \tau_{zx} &= 0. \end{aligned}\right\} \tag{2}$$

If we consider only this last part, (2), and change to principal stress directions in the xy plane, we have

$$P = k_1 z, \quad Q = k_2 z, \quad R = 0, \tag{3}$$

where P, Q, R are the principal stresses ($R = \sigma_z$). This is the stress system in the pure bending of a plate (that is, the glide packet) about perpendicular axes in its plane (see, for example, Timoshenko (1934), pp. 226, 227, or Timoshenko (1940), pp. 34 *et seq.*), except for the fact that the neutral plane is not necessarily the middle plane of the plate.

To see under what conditions the stresses of equations (1) give the directions of polarization shown in figure 2, it is best to proceed in two stages. We first inquire what the birefringence pattern would be if the bending stress of equations (2) were acting alone, and then see what modifications are produced by the superposition of the uniform stress $b_1, \ldots, b_6$.

Since cubic crystals are photoelastically anisotropic the directions of principal stress are not, in general, the directions of the principal axes of the indicatrix, as they would be in a truly isotropic material such as glass. In certain cases there may be large angles between these directions. The exact values of the angles will depend, in general, upon the relative directions of the crystal axes and the stress axes, and also upon the relative magnitudes of the three principal stresses. In the stress distribution given by equations (2), however, the directions of the principal stresses and the ratios of their magnitudes are the same at all points, and it may be shown that under these conditions the lines of polarization are straight (see appendix).

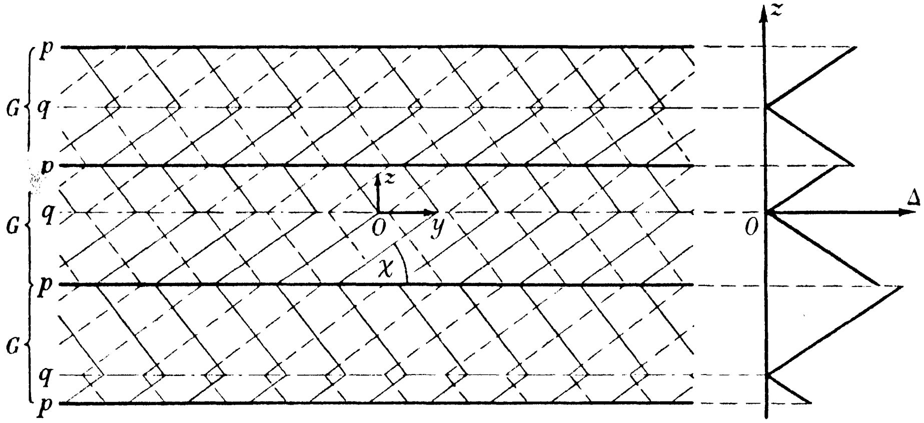

Figure 3. Polarization lines corresponding to stresses given by equations (2). The basic type of pattern.

In figure 3, which shows the pattern of polarization lines corresponding to stresses given by equations (2), the full and the broken trajectories again correspond to the fast and slow rays respectively. On the neutral planes the stress components change sign and the trajectories accordingly change direction by 90°. It is convenient to define χ as the angle between Oy and that one of the polarization directions which makes $0 \leqslant \chi \leqslant \frac{1}{4}\pi$. χ varies according to the crystal orientation and the values of a_1, a_2 and a_3. The variation of Δ across the glide packets is shown on the right-hand side of figure 3. Since the stresses are proportional to z, so also is Δ.

In a plate of photoelastically isotropic material stressed according to equations (2), χ would always be zero, but it can be shown that with silver chloride all values between 0 and $\frac{1}{4}\pi$ can be achieved. For this purpose, we may consider the following extreme case. Put $a_1 = a_2 = 0$ in equations (2). The plate is then under twisting couples about Ox and Oy, and the principal curvatures are equal and opposite (see, for example, Timoshenko (1940), p. 39). It is shown in the appendix that, in such a case, if Oy is parallel to a $\langle 110 \rangle$ direction, the glide direction, $\chi = \frac{1}{4}\pi$. If a_1 and a_2 are not zero, it is shown in the appendix that χ takes intermediate values.

(The bands in figure 1, plate 1, had very nearly this special orientation with Oy parallel to a $\langle 110\rangle$ direction; Oy was in fact 6·5° from the glide direction, and a small tilt of the sheet made the angle zero without appreciably altering the birefringence pattern.)

It is notable that, if a plate of photoelastically isotropic material were stressed with $a_1 = a_2 = 0$ and viewed along Ox, the birefringence would vanish everywhere (see appendix). The effect in the crystalline plate, *under these special conditions*, can thus be regarded as purely a consequence of its photoelastic anisotropy.

The differences between the theoretical pattern of figure 3 and the observed pattern of figure 2 are accounted for when we consider the effect of superposing the uniform stress whose components are $b_1, \ldots, b_6$. To see how this comes about suppose that, as a simple case, using the same notation as before, we have a plate of thickness c bent in plane stress about Ox, so that the only non-vanishing stress component is $\sigma_y = a_2 z$. If a stress given by $\tau_{yz} = S$ is superposed, where S is a constant, small compared with $a_2 c/2$, the stresses in the yz plane are given by

$$\sigma_y = a_2 z, \quad \sigma_z = 0, \quad \tau_{yz} = S.$$

The lines of principal stress for the three cases $S \lesseqgtr 0$ are shown in figures 4*a*, *b* and *c* (not to scale). For simplicity, only one family of curves, that showing the direction of the algebraically greater principal stress, is drawn. In figure 4*b* the trajectories are, of course, straight lines. In figure 4*a* and *c* it will be seen that on the plane q, where σ_y is zero, the principal stress directions are at 45° to Oy, but that away from this plane σ_y predominates over τ_{yz} and brings the directions parallel and perpendicular to Oy. In figure 4*a* and *c* there are no points of zero or hydrostatic stress, but the stresses are still small near the plane q.

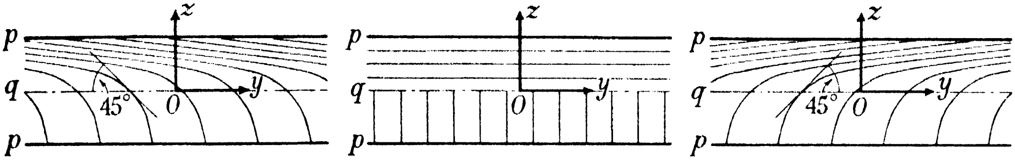

a, $S<0$ *b*, $S=0$ *c*, $S>0$

Figure 4*a*, *b* and *c*. Lines of principal stress in a uniformly bent plate with superposed shear stress.

In a similar way, when the uniform stresses $b_1, \ldots, b_6$ are superposed on the bending stresses of equations (2), the straight lines and sharp corners of the pattern of figure 3 are changed into the slightly curved lines and rounded corners of figure 2. (If $b_1 : b_2 : b_3 = a_1 : a_2 : a_3$ and $b_4 = b_5 = b_6 = 0$, an exception occurs; it corresponds only to a shift of the origin.) The linear variation of Δ with z is also altered and Δ is no longer zero on the former neutral planes. The fact that in figure 2 Δ is small on the planes q means that, in this case, the uniform stress was small compared with the bending stress.

We have assumed up to this point that there is no variation of the pattern in the y direction. Variations are observed, however, although they are small in distances equal to the glide zone spacing. An important observation is that a pattern of the type of figure 2 frequently changes gradually into a pattern of the type of figure 3 as one progresses along the glide packets. This behaviour is a result of the fact that $b_1, \ldots, b_6$ are not constant, but vary slowly from point to point of the pattern. Whenever they are zero the pattern takes the elementary form of figure 3, and we accordingly call this the basic type of pattern, the characteristic feature being that it extinguishes completely at one setting of the nicols.

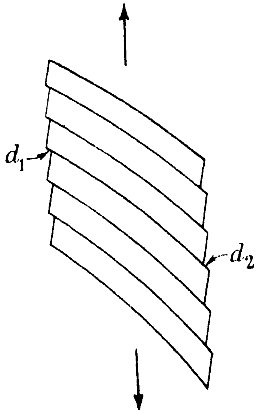

FIGURE 5. Diagrammatic representation of the curvature of the glide packets found photoelastically. Tension has been applied in the direction of the arrows. The curvature and the slip displacement are greatly exaggerated.

If one applies a gradually increasing external force (for example, tension or compression) to the specimen, the effect, as long as the elastic limit is not exceeded, is simply to modify $b_1, \ldots, b_6$. Patterns of the basic type can then be changed reversibly into the more general type of figure 2 and, conversely, it is often possible, by choosing the magnitude of the external force suitably, to change a pattern of the general type into one of the basic type. These observations are a confirmation that the stress distribution of equations (1) is correct. We do not at this stage inquire more closely into the relative values of $b_1, \ldots, b_6$, but it may be noted that when there is no external load on the specimen they are not usually as large as the bending stresses. Our observations indicate that, in common with $(b_1, \ldots, b_6)$, (a_1, a_2, a_3) vary only slowly with position, and this is to be expected; for it is necessary that a_1, a_2, a_3 should have nearly the same values in adjacent glide packets in order that successive packets may fit together without discontinuities in the z component of displacement.

To summarize the main conclusion of this section, we may refer to figure 5. A single crystal, seen in section, is split up into a series of glide packets, which in the action of slipping over one another have become curved. The plane of the section has been taken so as to include the slip direction. Since one face of each glide packet is in compression and the other face in tension, it is clear that the amounts of slip, d_1 and d_2, on the two faces of the crystal are not equal and that the difference between them is a measure of the amount of misfit between successive packets, and hence of the curvature of the packets. The figure is over-simplified in several respects; in particular the glide zones have been drawn as arcs of circles, a procedure which is equivalent to taking the a_i in equations (1) as constant for each packet and the b_i as zero.

It would be interesting to know how the directions of principal curvature in the glide packets are related to the glide direction, but we have not yet arrived at definite conclusions on this point. The main difficulty is that a knowledge of χ and the orientation of the crystal does not give these directions uniquely.

4. THE EFFECT OF A LARGE b_i STRESS

The conclusions reached in the last section may be further illustrated by an example of a set of bands, figure 6*a* to *e*, plates 1 to 3, in which the stresses $b_1, \ldots, b_6$ are exceptionally large, and in which their variation with y is easily seen. These photographs show the same set of bands at different settings of the nicols. They were found in a grain on the edge of a sheet, *A* in figure 6*a*, after the sheet had been deformed by several cycles of torsion about an axis parallel to the free edge seen at the right-hand side of the photograph. A small area of the bands is shown at higher magnification in figure 6*b* to *e*. The lines of polarization in three glide packets at the centre of this area are drawn schematically in figure 7, and for simplicity only one of the two orthogonal sets of curves is shown. In the region marked *D* the pattern is of the basic type (p. 53) with $\chi = \frac{1}{4}\pi$. To either side the lines of polarization are perturbed by the addition of another, more slowly varying, stress distribution which shows little change in the z direction but apparently changes sign across the region *D*. Hence in *C* the lines rotate clockwise with increasing z, while in *E* they rotate anticlockwise.

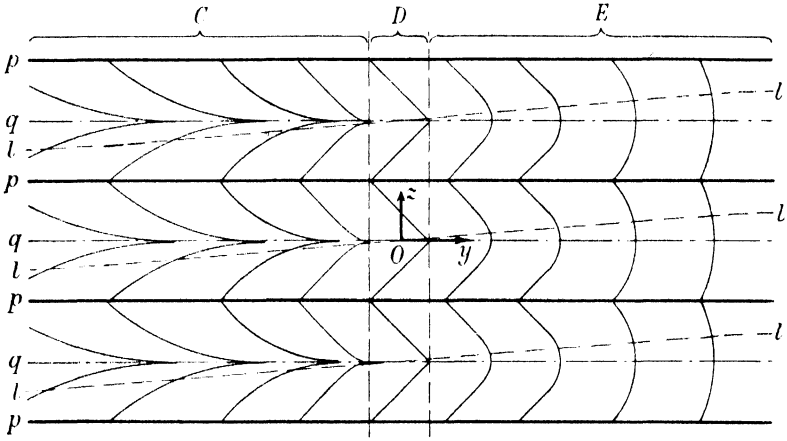

FIGURE 7. Lines of polarization for the band system of figure 6*a* to *e*, plates 1 to 3.

In figure 6*b* the nicol directions, as shown by the cross-wires, are at 45° to Oy and Oz. Region *D* is then completely extinguished, but *C* and *E* still show a periodic variation of light and shade, as they should do according to figure 7.

In figure 6*c* the nicols are parallel to Oy and Oz, and a dark stripe, seen most clearly between the glide zones lettered *p*, passes down the middle of each glide packet. In *D* this is a line of isotropic points, while in *C* and *E* it denotes that the polarization directions are parallel and perpendicular to the nicols. At this setting of the nicols, therefore, the effect of the b_i part of the stress system is not seen. (This is the reason why, in a polycrystalline sheet, the band systems which are in the right orientation with respect to the nicols to show a dark stripe down each packet do not change their general appearance when an external stress is applied. Several examples of this are seen in figure 1*a* and *b* of part I.)

In figure 6*d* the nicols are at 15° to *Oy* and *Oz*. One can see that in *C* the dark stripe has moved downwards, in *E* it has moved upwards, and in the centre of *D* it has remained stationary. The broken lines *ll* in figure 7 show this behaviour of the dark stripe. They have been constructed by plotting the loci of points whose polarization directions make 15° with *Oy* and *Oz*.

Figure 6*e* shows the result of turning the nicols so that their vibration directions make $-15°$ with *Oy* and *Oz*. The dark stripe will be seen to have moved in the opposite directions.

5. Bands produced by simple shear

A given set of bands in a polycrystalline sheet can be conveniently observed from one direction only, along the normal to the surface of the sheet. In part I a description was given of experiments in which glide was produced by simple shear of single grains. In these experiments the glide surfaces were so arranged that the same set of birefringent bands could be seen through two different surfaces. This made it possible to observe the same set of bands both at right angles to the glide direction and parallel to it. As described in § 1, the waviness of the glide surfaces complicated observations perpendicular to the glide direction. However, when observed in this direction, some places in the pattern could be seen to be of the basic type, usually with a small value of χ. Observations parallel to the glide directions showed many such places with χ sometimes, but certainly not always, zero.

6. Intersecting band systems

Figure 8*a* to *c*, plate 4, shows an example of a crystal which has deformed by glide on two different sets of planes. There were no surface glide lines following either band system, and we conclude that the $\langle 110\rangle$ glide direction lies in each case in the plane of the sheet. In view of the fact that the $\langle 110\rangle$ directions in a cubic crystal make with each other angles of either 60 or 90°, it is satisfactory to note that the angle between the bands, measured when looking down normally on the sheet, was 60·1°. The pattern can be interpreted as the superposition of two sets of bands each of the basic type and with $\chi = 45°$. In figure 8*a* the vibration directions of the nicols, as shown by the cross-wires, are at 45° to the more widely spaced set of bands. These are then almost extinguished and the closer set shows up. In figure 8*c* the nicols have been turned so as to be at 45° to the closer set of bands, and it will be seen that here the widely spaced set shows up and the close set is invisible. In figure 8*b* the nicols are in the intermediate position and both sets of bands are visible. The pattern shows up better in figure 8*c* than 8*a*, because of the corrugation of the glide surfaces forming the closely spaced set.

There are also two sets of active glide planes in the grain shown in figure 1, but here only one set is seen edge on. The surface glide lines of the second glide system could be seen crossing the grain in a vertical direction (they are clearest on the right-hand side of the photograph), but it is notable that there is no sign of a second birefringence pattern. This is a result of the stress system. Where a pattern is of the basic type (equations (2)), each plane $z = z_1$, say, is in general balanced by another plane, $z = z_2$, where the stresses are reversed in sign. As a result, the total birefringence for a wave whose normal passes through several glide packets is zero. The stress system $b_1, \ldots, b_6$ in equations (1), will, however, show up in such an oblique view.

7. MAGNITUDE OF THE BENDING STRESS

In order to calculate the magnitude of the residual stress produced by glide it is necessary to know over what thickness of the crystal the stress is acting. In the sharp band systems, where the magnitude of the birefringence can be most easily measured, it is probable that the stressed regions do not extend through the whole thickness of the sheet. If we assume that they do, however, we shall calculate a lower limit for the stress.

In grain no. 4 of strip no. 19, which was 0·58 mm. thick, the maximum relative retardation, measured in white light with a Berek compensator at a place where $b_1, \ldots, b_6$ were small, was 93 mμ. The observations were made very nearly perpendicular to the glide direction, so that if the stress system were that mentioned as a special case on p. 51 with $a_1 = a_2 = 0$, we should have had $\chi = 45°$. The measured value was 40°. If this difference of 5° is neglected, τ_{xy} is the only non-vanishing stress component. We then have $\Delta\mu = C\tau_{xy}$, where $\Delta\mu$ is the resulting difference in refractive index for the two polarized components of the light and C is a constant. A calculation, making use of the values of the photoelastic constants measured by West & Makas (1948) and the known orientation of the crystal (obtained from an X-ray back reflexion Laue photograph), gives $C = 6{\cdot}4 \times 10^{-12}$ cm.^{2}/dyne. It follows that $\tau_{xy}^{\text{max.}} \geqslant 2{\cdot}5 \times 10^7$ dynes/cm.^{2} = 25 bars. This may be compared with the following values, measured by Stepanow (1934):

Elastic limit (determined optically) of annealed single crystal in tension $\geqslant 6{\cdot}9$ bars.
Maximum yield stress of plastically deformed crystals in tension ~ 150 bars.

We may also estimate the radii of curvature, $\pm\rho$, corresponding to the calculated stress; they are given by $\rho = Gc/\tau_{xy}^{\text{max.}}$, where c is the thickness of a glide packet and G is a modulus of rigidity. In the apparent absence of any measurements of the rigidity of silver chloride, we may take 1×10^{11} dynes/cm.^{2} as a reasonable value for G. c was 0·07 mm. Hence $\rho \leqslant 28$ cm.

8. COMPARISON WITH THE RESULTS OF OBREIMOW, SCHUBNIKOFF AND BRILLIANTOW

The present experiments were suggested by previous work (Obreimow & Schubnikoff 1927; Brilliantow & Obreimow 1933) on the birefringent lamellae produced by plastic deformation in rock-salt. In comparing their results with the present ones, however, it is important to notice that the bands in rock-salt are probably produced not by glide but by kinking (Brilliantow & Obreimow 1934, 1937; Orowan 1942).

All the photographs reproduced were taken with crossed nicols with the vibration directions of the nicols parallel to the cross-wires.

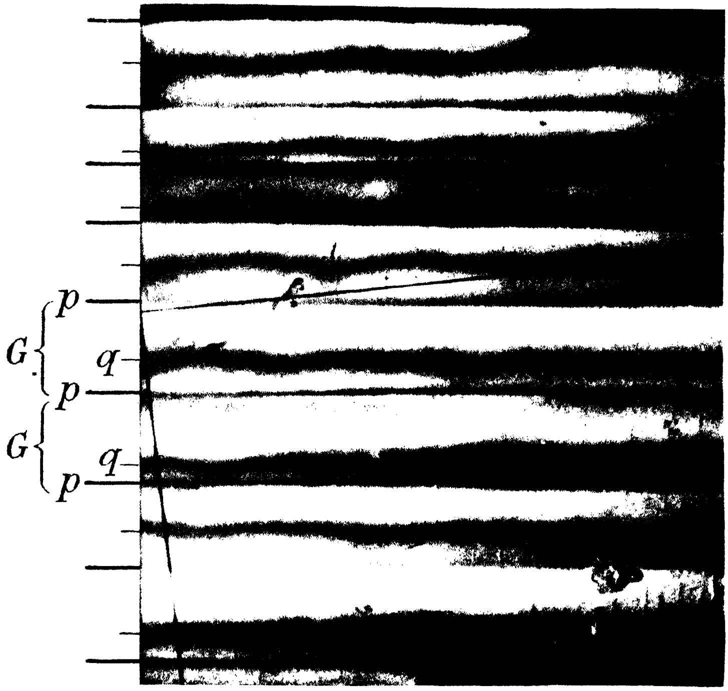

FIGURE 1. Birefringence pattern in glide packets. (Magn. × 163.)

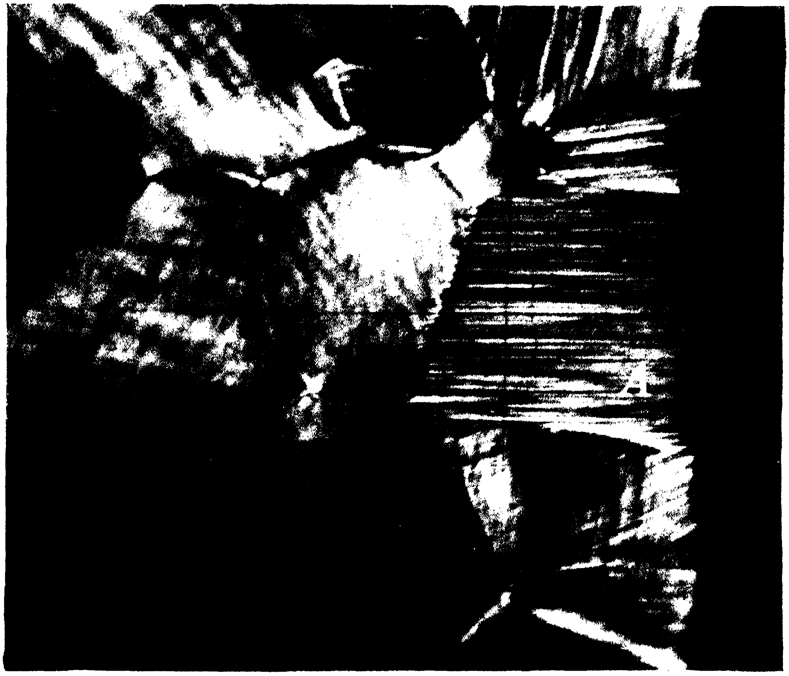

FIGURE 6*a*. Sheet of silver chloride after plastic torsion. (Magn. × 23.)

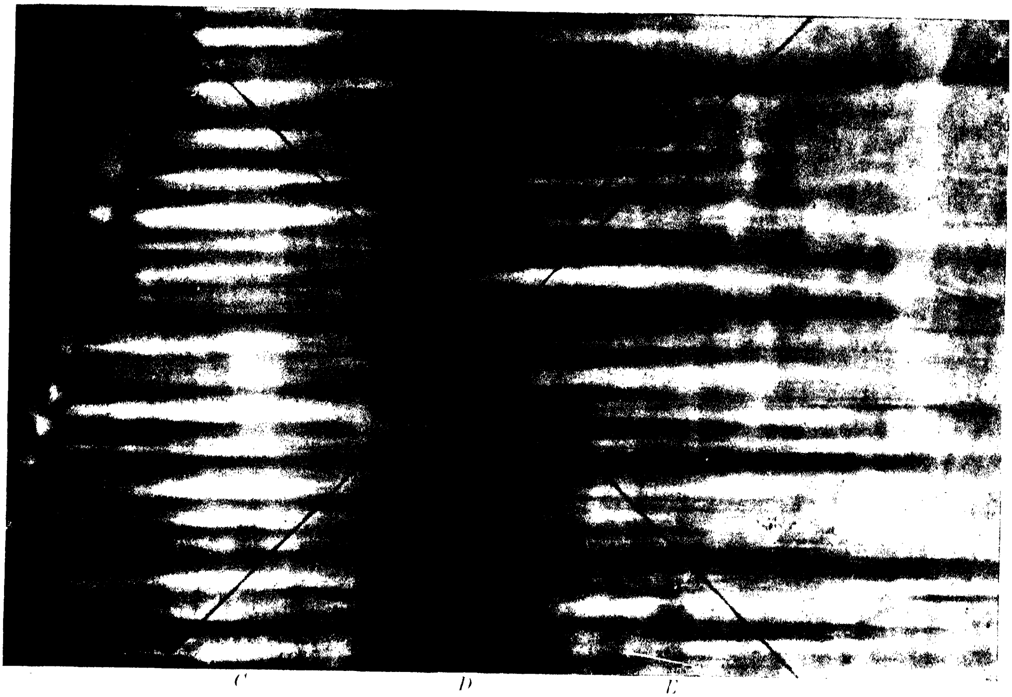

FIGURE 6*b*. Vibration directions of nicols at 45° to the bands.

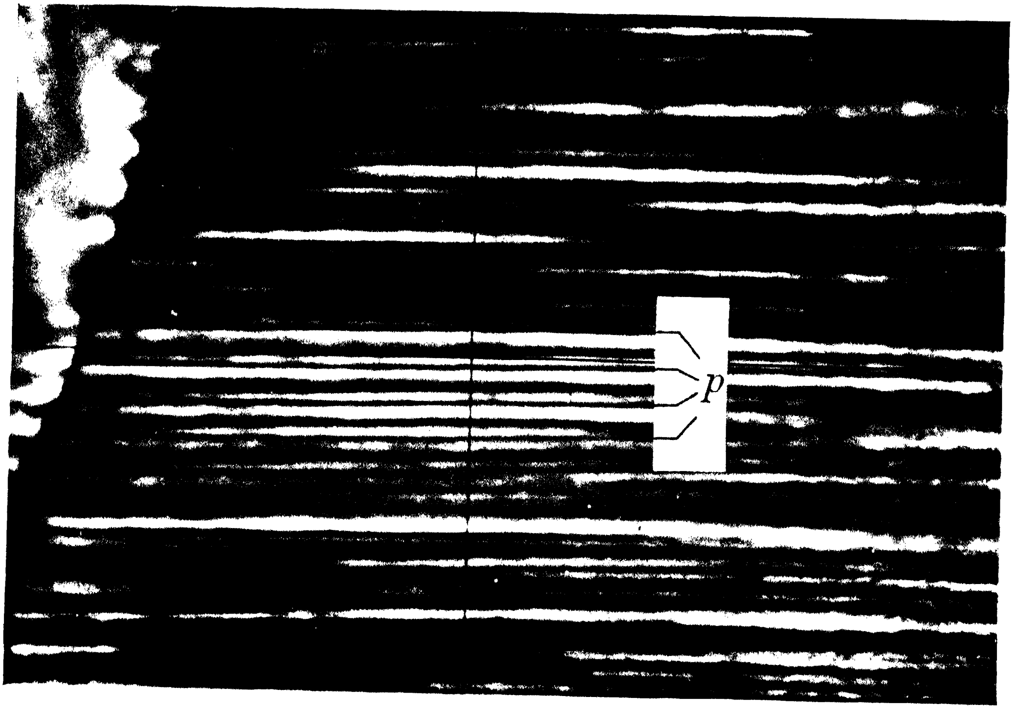

FIGURE 6*c*. Vibration directions of nicols parallel and perpendicular to the bands.

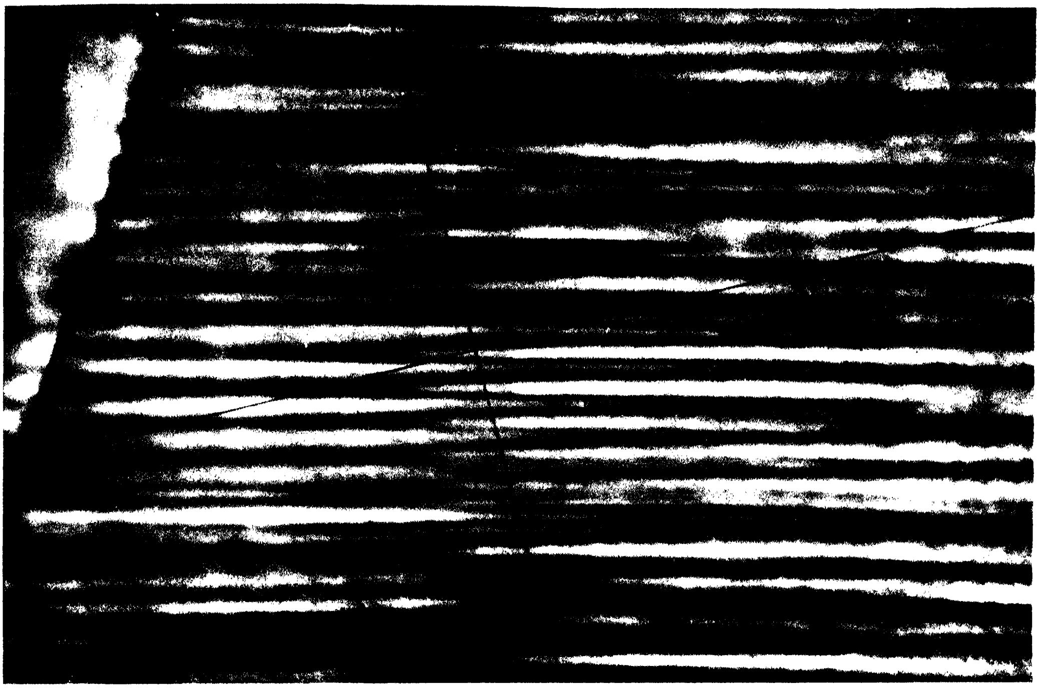

FIGURE 6*d*. Vibration directions of nicols at +15° to the bands.

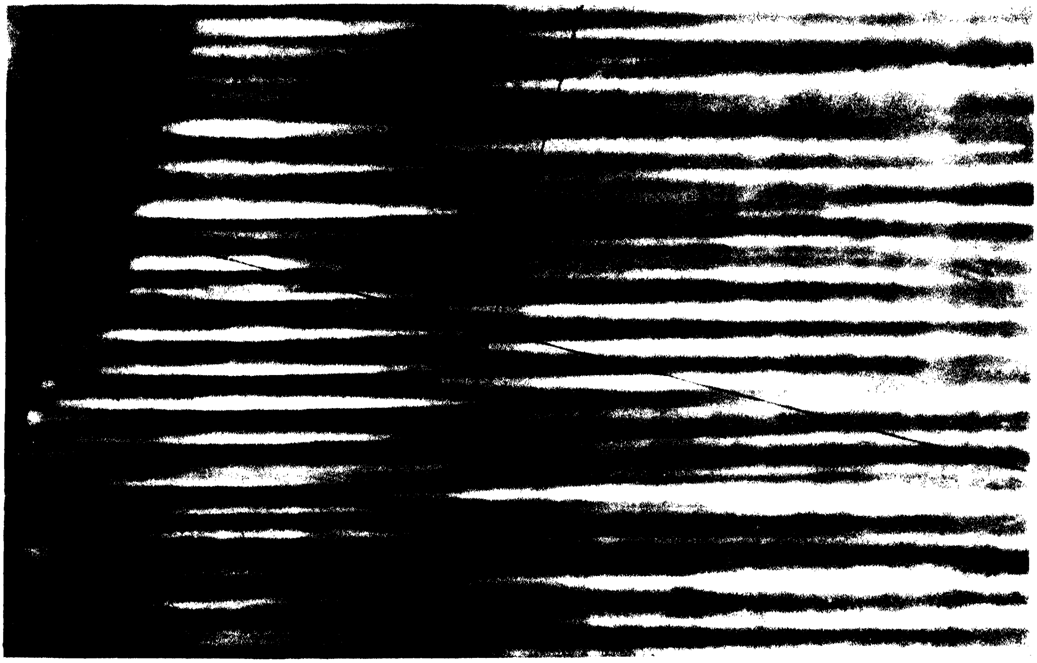

FIGURE 6*e*. Vibration directions of nicols at −15° to the bands.

FIGURE 6*b* to 6*e*. Grain on the right-hand side of figure 6*a* seen at a higher magnification. (Magn. × 109.)

Figure 8*b*. Nicols in intermediate position.

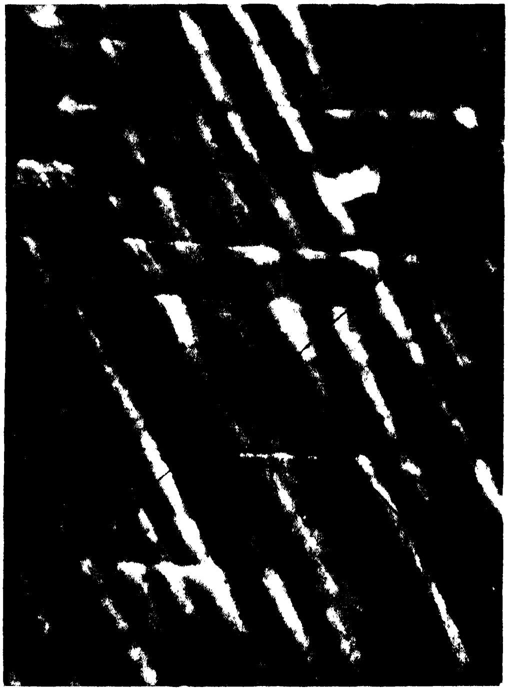

Figure 8*a*. Nicols at 45° to widely spaced set of bands.

Figure 8*c*. Nicols at 45° to closer set of bands.

Two intersecting band systems. (Magn. × 88.)

Nevertheless, it seems likely (having regard, for instance, to the marked resemblance between figure 4 of Brilliantow's & Obreimow's 1937 paper and the present figure 1) that the stresses produced by both types of deformation are much the same.

The extinction directions in the rock-salt lamellae correspond to $\chi = 0$, and the explanation of this is given in the appendix. Obreimow & Schubnikoff give a plot of the lines of principal stress between the kink planes, which is reproduced in Joffé's book *The physics of crystals*; but they assumed that the polarizing axes of the stressed material coincided with the directions of principal stress, and this is not legitimate. Their plot evidently corresponds to bent lamellae with a uniform stress superposed. Since there was no external stress acting on the crystal when the observations were made, we must conclude that there was a residual internal tension or compression acting in the region considered, and that this was balanced by equal and opposite stresses elsewhere on the kink plane.

9. PHYSICAL INTERPRETATION

We cannot explain the residual stresses in silver chloride as solely a consequence of forces exerted on the surfaces of the crystals because they occur in single crystals as well as in the grains of a polycrystalline aggregate. In the bands produced by simple shear of single crystals, for instance (§5), the zones run right across the crystals from one free surface to the other.

The stress distribution given by equations (1) involves discontinuities in σ_x, σ_y and τ_{xy} across the glide zones (regarded as infinitely thin). This is quite compatible with statical equilibrium, but such discontinuities do not usually occur in elasticity problems because they imply discontinuities of strain. To put it crudely, the material on one side of a glide zone is in tension, while that on the other side is in compression. (The discontinuity is more serious than that met in the usual theory of multiply-connected plates, for one has there discontinuities of displacement but not of strain or stress.)

Let us consider one particular crystal with free boundaries. If none of the dislocation lines whose movements we suppose to have caused the gliding remained within the crystal, there would be no residual stresses. Some dislocation lines, therefore, are retained in the glide planes. We thus picture each glide zone as a cluster of parallel planes containing dislocations of all types, and, assuming that their spacing is small compared with the thickness of the glide packets, we try to find out what stresses they would set up in the crystal.

(*a*) *Stresses due to a single glide zone*

Consider first one glide zone only and assume, as the simplest case, that the dislocation lines in it are all parallel and of the edge type (Burgers 1939, 1940). At distances large compared with their separation, the stresses due to two dislocations of opposite sign are negligible. Therefore, if we pair off positives against negatives, we shall find that at these distances the only significant stresses are due to the remaining dislocations that cannot be paired off. Suppose these are of positive sign. As a simple case, we may calculate the stress in an elastically isotropic infinite body caused by a series of positive dislocation lines extending in the x direction and equally spaced along Oy, the glide direction, at intervals t.

This is a plane problem; to avoid discontinuities in the z direction of the x component of displacement it is necessary to choose the case of plane strain (rather than, for instance, plane stress). If we consider the stresses in the yz plane, the only non-vanishing stress component, at points where $|z| \gg t$, is σ_y, which is given by

$$\sigma_y = \pm\frac{1}{2}\frac{E}{1-\nu^2}\frac{\lambda_0}{t} = \pm\frac{p}{2}, \quad \text{say,} \tag{I}$$

where the plus and minus signs correspond to $z < 0$ and $z > 0$ respectively, E = Young's modulus, ν = Poisson's ratio, and λ_0 = the amount of slip in each dislocation. This may be proved by summation and differentiation of the stress function given by Koehler (1941) for a single dislocation; but the result is perhaps evident without the complete analysis. (λ_0/t is the difference in the ϵ_{yy} component of strain above and below the slip plane. The corresponding stresses are obtained by multiplying the strain by the appropriate modulus.)

If the row of dislocations is not infinite but extends across a finite rectangular body (figure 9*a*), whose dimensions in the z direction are immaterial, we must pay attention to the boundary conditions. In order to maintain the stress distribution (I), normal surface tractions of constant amount $\pm\frac{1}{2}p$ must be applied on the bounding planes $y = \pm b$. To calculate the stresses due to the dislocations when the surfaces of the body are free from tractions, we must superpose on (I) the distribution, (II), say, set up by surface forces, equal and opposite to those shown in figure 9*a*, acting upon an identical body not containing dislocations (figure 9*b*).

A complete evaluation of (II) has not been attempted. However, the point of greatest interest for the present purpose is the behaviour of the stress component σ_y on $y = 0$. Miss E. H. Mann has kindly calculated this for the case when the body extends to infinity in the $\pm z$ directions.

The expression for σ_y is

$$\sigma_y = \frac{2p}{\pi}\int_0^\infty \frac{\sinh u + u\cosh u}{u(\sinh 2u + 2u)}\sin\frac{uz}{b}\,du.$$

σ_y has been plotted against z in figure 9*b* with the use of numerical values of the integral supplied by Miss Mann. At large distances from Oy the stresses are simply

$$\sigma_y = \pm\frac{p}{2} \quad \text{for} \quad z \gtrless 0.$$

σ_y changes sign at $z = 0$. When $|z| > 0{\cdot}91b$, $|\sigma_y|$ becomes slightly greater than $\frac{1}{2}p$. The reason for this behaviour is clear if we have regard to the symmetry of the problem and consider that the moment about Ox of the forces acting on the slab bounded by $y = 0$ and $y = b$ must be zero. $\tau_{yz} = 0$ on $y = 0$ for reasons of symmetry. Although the solution is calculated for an infinite body, it is safe to terminate it at any distance from $z = 0$ greater than about b, for beyond this the only significant stress component, σ_y, is for practical purposes constant. We then have the required distribution (II).

Superposition of (I) and (II) gives the variation of σ_y shown by the curve in figure 9*c*. For $|z| > b$, σ_y is small, and there is a discontinuity in σ_y of amount p on $z = 0$.

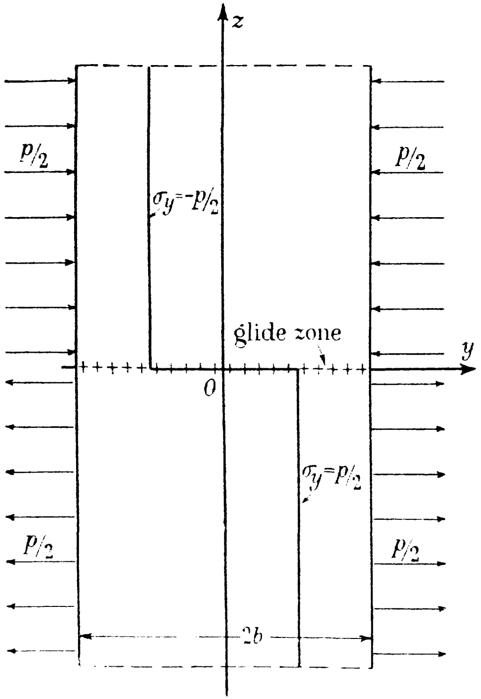

FIGURE 9*a*. Stress distribution (I) caused by single row of positive dislocations, and surface tractions.

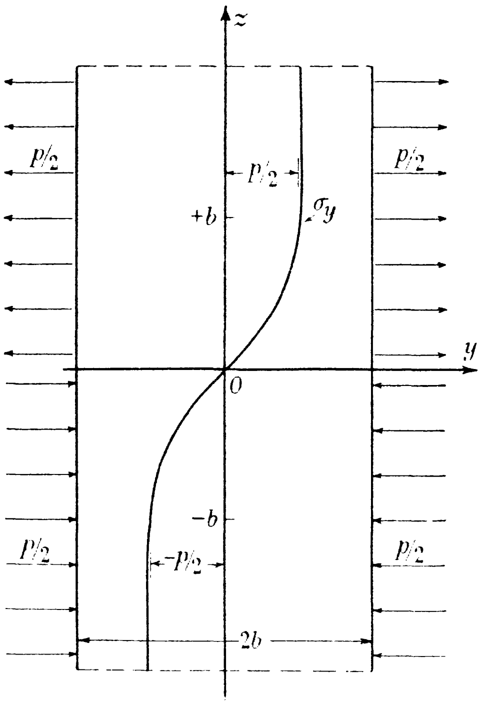

FIGURE 9*b*. Stress distribution (II) caused by the opposite surface tractions to those in figure 9*a*.

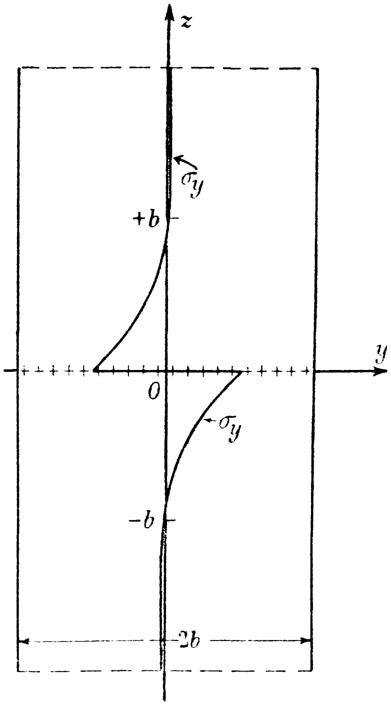

FIGURE 9*c*. Stress due to a single row of positive dislocations, obtained by superposition of (I) and (II).

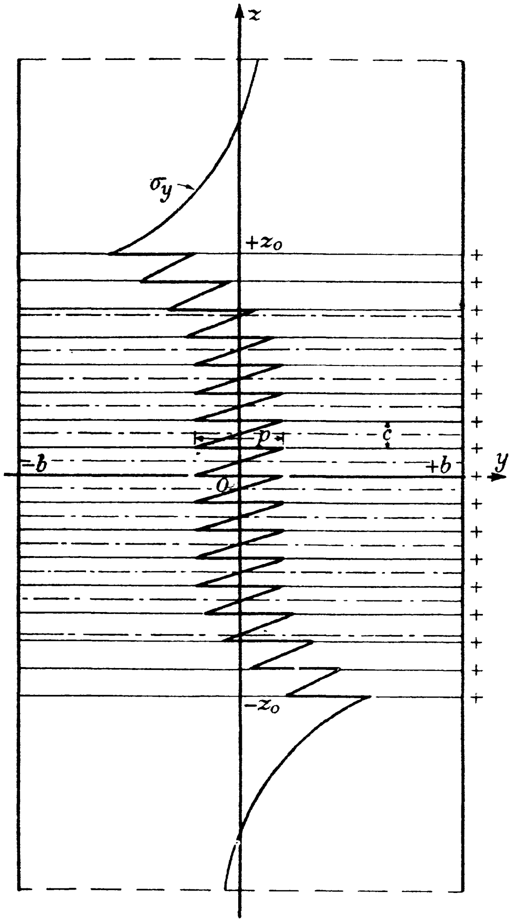

Figure 10*a*. Theoretical behaviour of σ_y component of stress when the density of unpaired dislocations is the same in each glide zone.

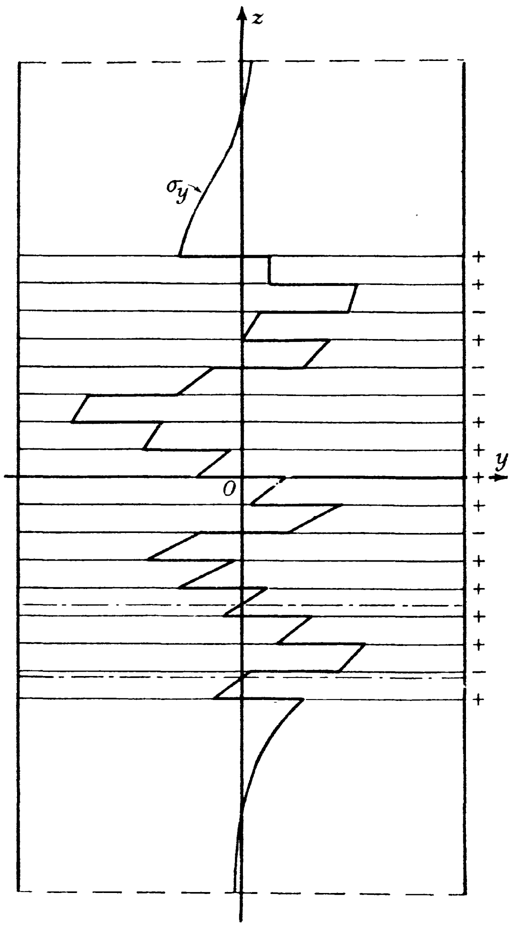

Figure 10*b*. Effect on σ_y when positive dislocations are in excess in some glide zones and negative in others.

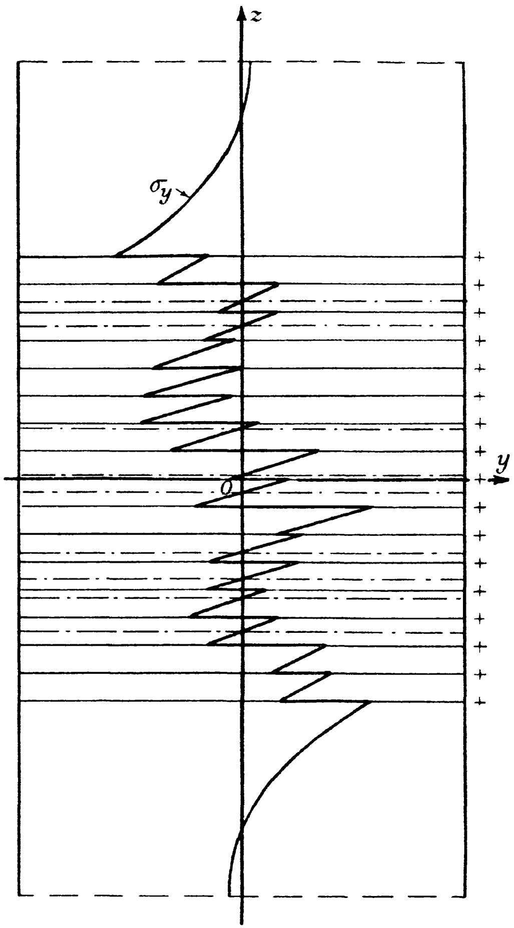

Figure 10*c*. Effect when density of unpaired dislocations is different for each zone.

(*b*) *Stresses due to N parallel glide zones*

To see, in a general way, the type of stress that would exist in a crystal crossed by N parallel glide zones, it is necessary to superpose N distributions of the type shown in figure 9*c* displaced relative to one another in the z direction. Suppose, for example, that we have N zones evenly spaced at distances c, large compared with t, that the density and sign of unpaired dislocations in each is the same, and that this sign is positive. If the zones, shown in figure 10*a* by the unbroken horizontal lines, extend from $z = -z_0$ to $z = z_0$, the variation of σ_y along Oz, for $b/c = 7{\cdot}5$ (an arbitrary value), is illustrated by the saw-tooth curve. There is a discontinuity of amount p on each glide zone, and in the central region, which is free from edge effects, it will be seen that $\partial\sigma_y/\partial z$ is practically constant and equal to p/c.

The variation of σ_y with z for $y \neq 0$ has not been calculated exactly, but it is evident that, for a single row of dislocations the form of the curve will be similar to that of figure 9*c*. The discontinuity of stress will still be p, but the height of the region over which σ_y has an appreciable value will be less than it is for $y = 0$. The result is that when we sum the effects of a series of rows we find that the curve of σ_y drawn for $y = 0$ is also approximately valid for other values of y (for at any given point in the central region the number of rows close enough to make a significant contribution to σ_y is less than it is for $y = 0$, but the individual contributions are greater). It follows that, *considering only* σ_y, each glide plane is bent in the same direction with radius of curvature $\rho = \dfrac{E}{1-\nu^2}\dfrac{c}{p}$.

Using the definition of p we then have

$$\rho = tc/\lambda_0. \tag{4}$$

If the sign of the unpaired dislocations in some zones were negative the discontinuities in stress would show differences of sign. $\partial\sigma_y/\partial z$ would not show a change of sign, however, unless the negative zones preponderated in one area of the dislocated region and the positives in another. In general, its algebraic magnitude would be reduced. Figure 10*b* illustrates this. Some of the positive rows in figure 10*a* have been replaced by negative ones. As a result, many of the neutral planes, shown by dot-dashed lines, are no longer present.

If the zones did not all contain the same density of unpaired dislocations the discontinuities in σ_y would have different values and $\partial\sigma_y/\partial z$ would change with z. In figure 10*c* each row has been allotted an arbitrary density of positive dislocations, the maximum density being six times the minimum. It will be noticed that the positions of the neutral planes vary and that some glide packets do not possess neutral planes.

10. COMPARISON WITH EXPERIMENT

In the last section we have only considered in detail the effect of edge-type dislocations. In this case the glide packets are bent in one direction only; that is, one of the principal curvatures is zero. If the glide zones contained screw dislocations (Burgers 1939, 1940) and intermediate types, the glide packets would be bent in such a way that both principal curvatures were non-vanishing.

(The conditions under which the grain of figure 6*a* to *e* was deformed would be expected to lead to a series of screw dislocations lying parallel to the free surface of the grain. A screw dislocation implies twisting about the line of the dislocation, and so the presence of such dislocations would be compatible with the twisting of the glide packets that is indicated by the photoelastic observations ($\chi = \frac{1}{4}\pi$ and hence $a_1 = a_2 = 0$).)

A significant result of the experiments is that, in general, the discontinuities in any one grain are all in the same direction, and there always seems to be a neutral plane between each pair of glide zones. This leads to the conclusion that, *throughout any one grain, the sign of the unpaired dislocations in each glide zone is the same, and their density does not rise to more than about twice the mean for the grain.*

The stress distribution $(b_1, \ldots, b_6)$ often found in the experiments superposed on the pure bending, even when there is no externally applied load, may have several causes. In a polycrystalline sheet it is no doubt partly due to the stresses caused by the reaction of the neighbouring grains (Heyn stresses). But it also occurs in single crystals, and here it is directly due to the dislocations. For at all points other than those on $y = 0$, and especially near $y = \pm b$, the distributions (II) will contribute non-vanishing components σ_z and τ_{yz} (σ_z does not vanish entirely even on $y = 0$), which will presumably have an effect, symmetrical about $y = 0$, on the final stress distribution. (These are the stresses produced by Koehler's 'image dislocations'.) A non-uniform density of unpaired dislocations in a glide zone would also cause a superposed stress. The effect would be twofold. In the neighbourhood of a place in a zone where the density was higher than the average the q planes would be shifted, for the same reason that the neutral planes in figure 10c vary in position from one glide packet to another. Secondly, the place of high density would produce components σ_z and τ_{yz} on either side. The q planes are often observed to deviate somewhat from a straight course parallel to the glide zones (see, for instance, figure 1), and this may well be due to such unevenesses in the distribution of the dislocations.

To obtain the order of magnitude of t we use equation (4) and the numerical values used already in §7. We have $t = \lambda_0 \rho / c$, where $\lambda_0 = (1/\sqrt{2}) \times 5{\cdot}54 \times 10^{-8}$, $\rho \leqslant 28$ and $c = 7 \times 10^{-3}$ cm. This gives $t \leqslant 1{\cdot}6 \times 10^{-4}$ cm. Our calculations should, therefore, be valid for points which do not lie within about 10^{-4} cm. of a glide zone, and we are justified in using them to interpret the effects in the areas about 10^{-2} cm. broad between the glide zones.

If the grain size is l, each glide zone extending across a grain must contain l/t dislocations. With $l = 1$ mm. and $t = 1{\cdot}6 \times 10^{-4}$ cm. this number is 600. On the other hand, the heights of the prominent glide steps in silver chloride sheets deformed at room temperature are about 4×10^{-4} cm. (Nye 1949), which corresponds to the passage through each glide zone of 10,000 dislocations. Referring to figure 5 then, we have that d_1 and d_2 are of the order of 10,000 λ_0, while $d_2 - d_1 \simeq 600\, \lambda_0$. In other words, for every 10,000 dislocations passing right through a crystal, 600 are trapped. Since the measurements of curvature and of glide steps are not made on the same grain, these figures should be accepted with caution. It should also be noted that, by taking our upper limit for the value of t and by assuming that the trapped dislocations all have the same sign, we may have seriously underestimated the number of trapped dislocations.

11. DISCUSSION

The distribution of residual stresses produced by pencil glide is not likely to differ essentially from that given by glide on crystallographic planes, and we think that similar stresses to those we have found probably exist in all other crystals that deform by glide, including metals.

The main question raised by the experiments is, how does the curvature of the glide packets arise? Does it represent something essential to the slip process, or is it to be regarded as accidental? It would appear that the packets bend even when the applied stress is uniformly distributed. On the other hand, very small non-uniformities can hardly be avoided in a single crystal, and in a polycrystalline specimen elastic anisotropy alone is sufficient to cause quite large non-uniformities of stress. It may be that these unavoidable irregularities play a part in initiating the curvature.

These experiments are on too large a scale to provide any experimental proof for the existence of dislocations; however, given that glide occurs by the movement of dislocations, the questions posed above become questions about dislocations. Why are positive and negative dislocations not present in equal numbers in the glide zones, and why has the 'charge' on the zones the same sign throughout any one grain? A possible explanation is that the dislocations are nucleated on one side only of each crystal.

It may also be asked why the glide packets do not straighten out, forcing the dislocations to the edges in the process. In a single crystal shear stresses in the right direction to accomplish this must be present, but they are apparently ineffective without additional help from thermal movement; in other words, the material must be annealed before straightening out under the action of these forces is possible. If the grain under consideration is imbedded in a polycrystalline aggregate, however, straightening out of the glide packets could not occur without stresses being set up in the neighbouring grains. If a completely stress-free aggregate is produced by annealing, therefore, we must imagine that the diffusion of dislocations to the grain boundaries goes hand in hand with a series of atomic rearrangements at the grain boundaries themselves, which have the effect of relieving the stresses that would otherwise be set up by the accumulated dislocations.

APPENDIX

A proof is given here of the results from the theory of stress birefringence that have been quoted on pp. 51, 52.

The indicatrix in an unstressed cubic crystal is a sphere, and its equation may be written in the form

$$a_0^2(X^2+Y^2+Z^2) = 1,$$

where OX, OY, OZ are the three cubic axes, and a_0 is the reciprocal of the refractive index.

When a stress is applied whose components, referred to these axes, at the point considered are σ_X, σ_Y, σ_Z, τ_{YZ}, τ_{ZX}, τ_{XY}, the indicatrix is distorted into the form

$$B_{11}X^2+B_{22}Y^2+B_{33}Z^2+2B_{23}YZ+2B_{31}ZX+2B_{12}XY = 1 \tag{5}$$

in such a way that the changes in the coefficients are linear functions of all the stress components (Pockels 1889, 1906). For cubic crystals of the $\bar{4}3m$, 43 and $m3m$ classes (Bhagavantam 1942) the equations for B_{11}, etc., reduce to

$$\left.\begin{aligned} B_{11} &= a_0^2+C_{12}(\sigma_X+\sigma_Y+\sigma_Z)+(C_{11}-C_{12})\sigma_X; & B_{23} &= C_{44}\tau_{YZ},\\ B_{22} &= a_0^2+C_{12}(\sigma_X+\sigma_Y+\sigma_Z)+(C_{11}-C_{12})\sigma_Y; & B_{31} &= C_{44}\tau_{ZX},\\ B_{33} &= a_0^2+C_{12}(\sigma_X+\sigma_Y+\sigma_Z)+(C_{11}-C_{12})\sigma_Z; & B_{12} &= C_{44}\tau_{XY},\end{aligned}\right\} \tag{6}$$

where C_{11}, C_{12} and C_{44} are the three stress-optical coefficients.

Using the same notation as in the main part of the paper, we consider a plate of crystal subject to stresses given by equations (2) and (3) and calculate the birefringence produced in waves whose normals are parallel to Ox. It is most convenient to work with principal stresses, so let the direction cosines of P and Q respectively be $(l, m, 0)$, $(-m, l, 0)$ referred to Ox, Oy, Oz and (L_1, L_2, L_3), (L_1', L_2', L_3') referred to OX, OY, OZ. Then the components of P referred to OX, OY, OZ are L_1^2P, L_2^2P, L_3^2P, L_2L_3P, L_3L_1P, L_1L_2P. Hence, considering only the effect of P without Q, equations (6) become

$$\left.\begin{aligned} B_{11} &= a_0^2+C_{12}P+(C_{11}-C_{12})\,L_1^2P; & B_{23} &= C_{44}L_2L_3P,\\ B_{22} &= a_0^2+C_{12}P+(C_{11}-C_{12})\,L_2^2P; & B_{31} &= C_{44}L_3L_1P,\\ B_{33} &= a_0^2+C_{12}P+(C_{11}-C_{12})\,L_3^2P; & B_{12} &= C_{44}L_1L_2P.\end{aligned}\right\} \tag{7}$$

If the coefficients of ellipsoid (5) when referred to Ox, Oy, Oz are denoted by b_{11}, b_{22}, etc., the section perpendicular to Ox is

$$b_{22}y^2+b_{33}z^2+2b_{23}yz = 1.$$

χ, the angle between the axes of this ellipse (the axes of polarization) and Oy and Oz, is given by

$$\tan 2\chi = 2b_{23}/(b_{22}-b_{33}). \tag{8}$$

To evaluate this expression, we find the values of b_{22}, b_{33} and b_{23} in terms of B_{11}, etc., by using the transformation equation

$$\begin{bmatrix} X\\ Y\\ Z\end{bmatrix} = \begin{bmatrix} l_1 & m_1 & n_1\\ l_2 & m_2 & n_2\\ l_3 & m_3 & n_3\end{bmatrix}\begin{bmatrix} x\\ y\\ z\end{bmatrix}, \tag{9}$$

and then substitute the values of B_{11}, etc., given by equations (7). Bearing in mind that the coefficients of y^2, z^2 and yz in the equation of the stress quadric referred to Ox, Oy, Oz are m^2P, 0, 0 respectively, we finally obtain

$$\left.\begin{aligned} b_{22} &= (a_0^2+C_{12}P)+(C_{11}-C_{12}-C_{44})\,(\Sigma L_i^2m_i^2)\,P+C_{44}m^2P,\\ b_{33} &= (a_0^2+C_{12}P)+(C_{11}-C_{12}-C_{44})\,(\Sigma L_i^2n_i^2)\,P,\\ b_{23} &= (C_{11}-C_{12}-C_{44})\,(\Sigma L_i^2m_in_i)\,P.\end{aligned}\right\}\quad (i = 1, 2, 3).$$

Three similar equations with Q, (L_1', L_2', L_3'), $(-m, l, 0)$ substituted for P, (L_1, L_2, L_3), $(l, m, 0)$ are obtained if we consider Q to act alone without P. To find the values of b_{22}, b_{33} and b_{23} when P and Q act together, we simply add the changes in the coefficients caused by each stress acting separately. When this is done and the values of b_{22}, etc., are substituted into equation (8), we obtain

$$\tan 2\chi = \frac{2\gamma\Sigma m_i n_i(L_i^2 P + L_i'^2 Q)}{(m^2P+l^2Q)+\gamma\Sigma(m_i^2-n_i^2)(L_i^2P+L_i'^2Q)} \quad (i = 1, 2, 3), \tag{10}$$

where $\gamma = (C_{11}-C_{12}-C_{44})/C_{44}$. γ may be regarded as a coefficient of anisotropy; it is zero for photoelastically isotropic materials and may take positive or negative values for anisotropic ones.

Special case

Since the glide direction is $\langle 110\rangle$ we may introduce the condition that [110] lies in the xy plane, viz. $n_1+n_2 = 0$. Let us, as a special case, observe the birefringence perpendicular to the glide direction. Oy is then parallel to $[1\bar{1}0]$ and the determinant of the transformation (9) becomes

$$\begin{vmatrix} l_1 & 1/\sqrt{2} & n_1 \\ -l_1 & 1/\sqrt{2} & -n_1 \\ l_3 & 0 & n_3 \end{vmatrix}. \tag{11}$$

We use this transformation to express L_1, L_2, L_3 and L_1', L_2', L_3' in terms of l and m, and then the relations between the sets of direction cosines in (11) enable us to reduce equation (10) to the form

$$\tan 2\chi = \frac{4\sqrt{2}\,\gamma l m n_1 n_3(P-Q)}{2(m^2P+l^2Q)+\gamma n_3^2\{(P+Q)-6n_1^2(l^2P+m^2Q)\}}. \tag{12}$$

This expression gives the value of χ in a plate bent according to equations (3), where $(l, m, 0)$ are the direction cosines of the principal stress P with respect to Ox, Oy, Oz and $(n_1, -n_1, n_3)$ are the direction cosines, referred to the crystal axes, of the normal to the xy plane (they are thus proportional to the Miller indices of the glide plane).

We see at once that, since P and Q are both proportional to z, χ is constant over the yz plane (p. 51). $\chi = 0$ if any one of the following conditions is satisfied:

(1) $\gamma = 0$. The material is photoelastically isotropic.

(2) $l = 0$ or $m = 0$. P and Q are parallel to Ox and Oy, as in the simple case discussed in § 9.

(3) $n_1 = 0$. The xy plane is (001).

(4) $n_3 = 0$. The xy plane is $(1\bar{1}0)$. This explains the observation of $\chi = 0$ in rock-salt crystals (§ 8), where the kink plane is $\{110\}$.

(5) $P = Q$. The plane is bent into part of a sphere.

On the other hand, if $P = -Q$ and $l^2 = m^2 = \frac{1}{2}$, $\chi = \frac{1}{4}\pi$. In this case the principal curvatures are equal and opposite, $a_1 = a_2 = 0$, and the plate is under twisting couples (p. 51).

The expression for the relative retardation of the two polarized waves after passing through a thickness t of the plate is

$$\Delta = \tfrac{1}{2}\mu^3 t\sqrt{\{(b_{22}-b_{33})^2+4b_{23}^2\}},$$

where $\mu = 1/a_0$, and it is easily shown from this that Δ is, in general, proportional to z. However, in an isotropic material ($\gamma = 0$), if $P = -Q$ and $l^2 = m^2$, it is evident that Δ vanishes everywhere (p. 52).

REFERENCES

Bhagavantam, S. 1942 *Proc. Indian Acad. Sci.* **16**, 359.
Brilliantow, N. A. & Obreimow, I. W. 1933 *Phys. Z. Sowjet.* **3**, 83 (in English).
Brilliantow, N. A. & Obreimow, I. W. 1934 *Phys. Z. Sowjet.* **6**, 587 (in English).
Brilliantow, N. A. & Obreimow, I. W. 1937 *Phys. Z. Sowjet.* **12**, 7 (in English).
Burgers, J. M. 1939 *Proc. Acad. Sci. Amst.* **42**, 293, 378 (in English).
Burgers, J. M. 1940 *Proc. Phys. Soc.* **52**, 23.
Koehler, J. S. 1941 *Phys. Rev.* **60**, 397.
Love, A. E. H. 1944 *The mathematical theory of elasticity*, 4th ed. New York: Dover.
Nye, J. F. 1949 *Proc. Roy. Soc.* A, **198**, 190.
Obreimow, I. W. & Schubnikoff, L. W. 1927 *Z. Phys.* **41**, 907.
Orowan, E. 1942 *Nature*, **149**, 643.
Pockels, F. 1889 *Ann. Phys., Lpz.*, **37**, 144.
Pockels, F. 1906 *Lehrbuch der Kristalloptik*, pp. 467 *et seq.* Leipzig: Teubner.
Stepanow, A. W. 1934 *Phys. Z. Sowjet.* **6**, 312 (in English).
Timoshenko, S. 1934 *Theory of elasticity.* New York: McGraw-Hill.
Timoshenko, S. 1940 *Theory of plates and shells.* New York: McGraw-Hill.
West, C. D. & Makas, A. S. 1948 *J. Chem. Phys.* **16**, 427.

Experiments on the superconductive transition

By D. K. C. MacDonald and K. Mendelssohn
Clarendon Laboratory, Oxford

(*Communicated by F. E. Simon, F.R.S.—Received* 24 *June*, 1949)

The change of electrical resistivity at the transition between the superconductive and the normal state in a longitudinal magnetic field has been investigated systematically. By successive elimination of a number of disturbing factors an experimental procedure has been developed which yields consistent and reproducible results. The metals lead, mercury and tin have been investigated in this manner. Contrary to the accepted view it has been found that under 'ideal' conditions the transition is *not* discontinuous. There exists a range of temperature and magnetic field in which the resistance changes gradually from normal to zero and vice versa. The extent of this transition region was found to grow rapidly with increasing absolute value of the magnetic field. Under conditions closely approximating the 'ideal' longitudinal case transitions with hysteresis were never observed. However, it could be shown that resistance hysteresis and discontinuous resistive changes are produced by deviation from the longitudinal case owing to unsuitable geometrical shape of the specimen. The general conclusion has therefore been reached that the resistance of a pure superconductor in a longitudinal field changes *continuously* in transition between the superconductive and the normal state. The significance of the results has been discussed and further experiments have been proposed.

1. INTRODUCTION

One of the most striking features of superconductivity is the *sudden* disappearance of resistivity. The phenomenon was noted by Kamerlingh Onnes in his first observations and was subsequently made the subject of more detailed investigations. In 1931 de Haas & Voogd showed that when a pure single crystal wire of tin is cooled in zero magnetic field its resistance will drop from the normal value to zero abruptly. The whole transition took place in a temperature interval of a few thousandths of a degree, and it appears that it would become truly discontinuous with vanishingly small measuring current.

Since then it has been generally assumed (cf. Shoenberg 1938) that a similar discontinuity in resistivity will exist when the transition takes place in an external magnetic field. It is, of course, necessary because of the change in magnetic induction that the wire should be investigated in a homogeneous magnetic field the direction of which is exactly parallel to that of the wire. The resistance curves observed under these conditions are not in fact discontinuous, but this broadening of the transition has usually been ascribed to strain or lack of purity. The observed transitions were, moreover, obscured in many cases by hysteresis phenomena which caused the resistance—at a given temperature—to vanish at a lower field strength than the one at which it reappeared. However, a number of experiments on lead carried out in this laboratory some years ago (Pontius 1937; Daunt 1939) yielded transition curves in which the resistance still rose at a field strength about 15 % above the field at which the resistance first appeared. In view of the great purity of the material employed it seemed difficult to account for this broadening of the transition as arising from impurities.

Such work as has been done more recently on the resistance transition (cf. Andrew 1947; Désirant & Shoenberg 1948) consists mainly of determinations of the transition curve in transverse fields which is of interest because of the correlation with the magnetic induction, but it gives no further information on the effects observed by Pontius and Daunt. It was therefore decided to carry out a systematic and detailed investigation of the longitudinal transition and to extend the work to other metals. These experiments have not only yielded the somewhat surprising result that the resistive transition is continuous but have also shown up a peculiar relation between the geometrical form of the conductor and the hysteresis phenomena. A short note on these effects has already been published (MacDonald & Mendelssohn 1948).

The object of the present paper is to give a full account of these measurements and to present in some detail the experimental material on which our conclusions are based. In view of the fact that our findings completely contradict the accepted idea of a discontinuous transition in a magnetic field it seems imperative to substantiate our conclusions by a more extensive description of the work than might otherwise have been necessary. In particular, we have found it necessary to present graphs of a considerable number of examples of transition curves, as this is the only way to show the stages in which the 'ideal' case of the longitudinal transition has been approached.

2. METHOD

The cryostat used in these experiments was that described by Daunt & Mendelssohn (1938) in which the helium is liquefied by the Simon (1936) expansion principle. The cryostat provides the facility that specimens may be removed from the liquid helium and changed during a single run. Constant temperatures below the normal boiling-point of liquid helium ($\sim 4{\cdot}2^\circ$ K) were obtained by pumping off the vapour through an automatic pressure-controlling device (Mendelssohn 1936). The absolute temperature was determined by measuring the helium vapour pressure. Each specimen was provided with current and potential leads, and the potential developed was observed on a galvanometer amplifier (MacDonald 1947). The useful sensitivity is limited by thermo-e.m.f.'s in the specimen leads and contact e.m.f.'s at the specimen in certain cases, but a sensitivity of 1 mm./10^{-8} V was quite frequently employed under continuous observation conditions.

Longitudinal magnetic fields were provided by a solenoid which furnished a field uniform to about 0·6 % over a length of 8 cm., while the longest specimen used was about 4 cm. long.

3. EXPERIMENTS ON LEAD

The first series of experiments was carried out using fine lead wires ($\sim 100\,\mu$ diam.) which had been prepared some 12 years ago by Dr R. B. Pontius using the Taylor process and then annealed for 12 hr. The source of this material was 'H.S.' brand Hilger lead (lab. no. 8334), and a purity of 99·999 % was specified. It was particularly desired in these experiments to exclude both deformation and contamination due to soldering of contacts which would themselves be superconductive. Fairly satisfactory results were obtained by using fine copper strips laid across the specimen, the whole being then held between two small ebonite blocks (figure 1*a*).

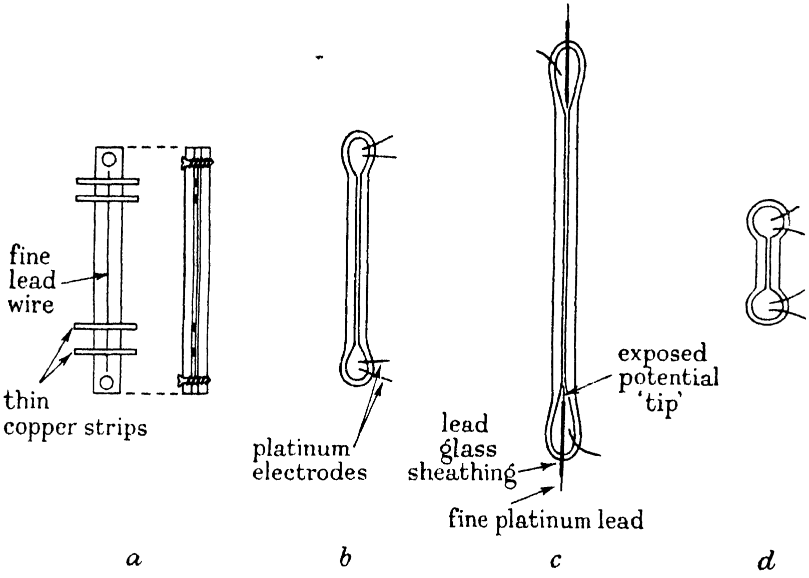

FIGURE 1. Methods of preparing specimens.

The results exhibit a certain number of salient features. In all cases extended transitions were observed in which no significant hysteresis was detected, but the curves showed a certain amount of variation in shape. Taking the critical field strength, H_c, which is well established by magnetic induction measurements (Daunt & Mendelssohn 1937; Daunt, Horseman & Mendelssohn 1939) as reference, it was observed that all curves show a variation of the resistance above H_c. While normally the first onset of resistance occurs *at* the critical field, in some cases the initial appearance lies above or below H_c.

Taking the latter case first, two types of deviation can be distinguished. The first of these is of a rather erratic nature. Spurious potentials were observed at fields well below H_c, an effect also observed occasionally by other workers. This behaviour was found to be highly current-dependent and disappeared entirely with suitable reduction of the measuring current. In one case, for instance, with a measuring current of 100 mA finite values of the resistance were observed as low as $\frac{1}{2}H_c$, while with reduction to 20 mA the transition began precisely at H_c. This fact, together with the erratic nature of the effect, seems to indicate that it is of a secondary nature and probably due to unsatisfactory contacts at which the threshold current is exceeded.

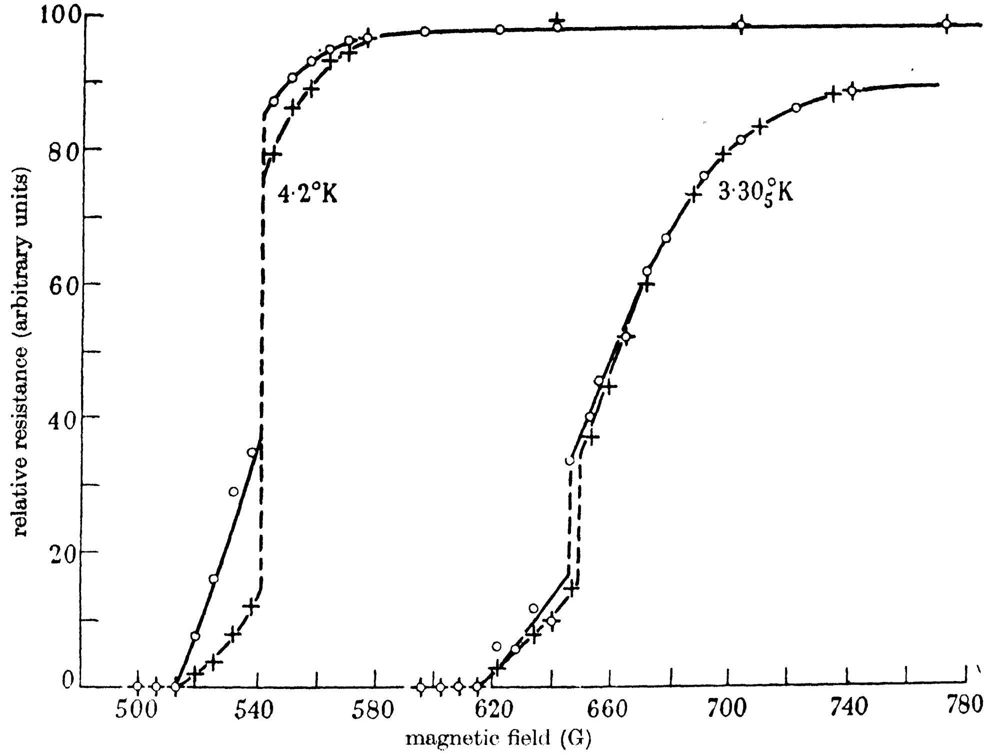

FIGURE 2. Transition curves of lead wire. ○, field increasing; +, field decreasing.

The second type of deviation of this class (figure 2) exhibits itself in a slow, reproducible, rise starting somewhat below H_c and then rising very rapidly—probably discontinuously—at the equilibrium field. The discontinuous rise, however, does not attain the normal value of resistance which is only achieved at considerably higher fields after a further gradual rise. The appearance of resistance below H_c indicates that part of the specimen was not in correct alinement with the field, and since care had been taken to have the main part of the wire parallel to the lines of force the deformations occurred probably near the contact strips. An interesting feature of such a transition lies in the discontinuity at H_c which appears to divide the whole transition into two parts, either of which is unstable with respect to the other. We draw particular attention to this connexion between imperfect alinement and instability because it appears an important consideration in the interpretation of superconductive hysteresis to be discussed below.

The curves of figure 3 relating to the same type of specimen exhibit the peculiar phenomenon already observed by Daunt (1939) that superconductivity persists to values of magnetic field well above H_c. This behaviour does not seem amenable to a simple explanation like the forementioned deviations below H_c. For instance, the fact that this late appearance of resistance is shown by some specimens only might suggest that it is brought about by the manner in which the specimen is made. On the other hand, the phenomenon appears to be confined to temperatures below ~4° K, a feature which is in general agreement with Daunt's observations, notwithstanding that he did not measure the resistance of a wire directly but rather the shielding effect of a hollow lead cylinder in an a.c. field. This makes it almost certain that the effect cannot be ascribed to the type of mounting or to the attachment of the contacts. Another indication that this delayed transition may be of a more fundamental character is provided by its strong dependency on the absolute value of the field, the delay increasing as the temperature is lowered. The curves of figure 3 show that while the percentage deviation is negligible at 4·2° K, it is more than 10 % at 1·6° K. It seems worth mentioning that these transitions are all fully reversible, the ascending and descending curves coinciding.

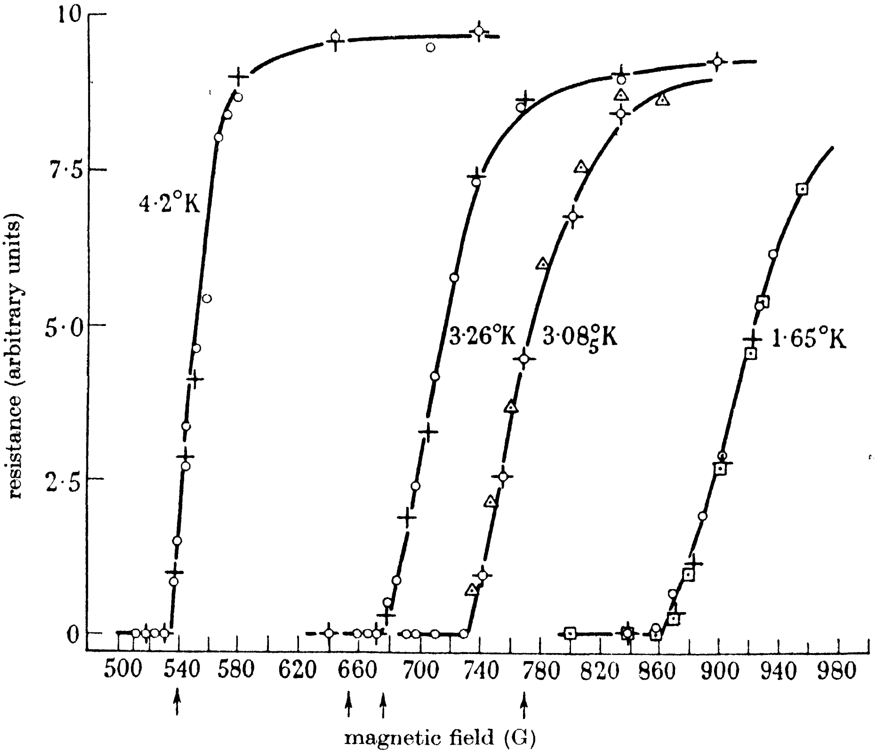

FIGURE 3. Transition curves of lead wire (~ 130 μ diam.). Measuring current, 20 mA; equilibrium transition fields shown by arrows.

Figure 4 gives transition curves of a specimen which exhibits none of these deviations. The resistance rises abruptly at the equilibrium field with a finite slope which decreases steadily until the normal resistance is attained. In this case none of the various disturbing features is present; nevertheless, the transition remains considerably extended above H_c. The possibility—though remote—that the measuring current might be responsible for the broadening had to be considered. In fact, however, a considerable reduction in measuring current (from 100 to 20 mA) merely served to emphasize the phenomenon as may be seen from figure 4. Both transitions start at the same field, the one with the smaller measuring current, however, being less steep.

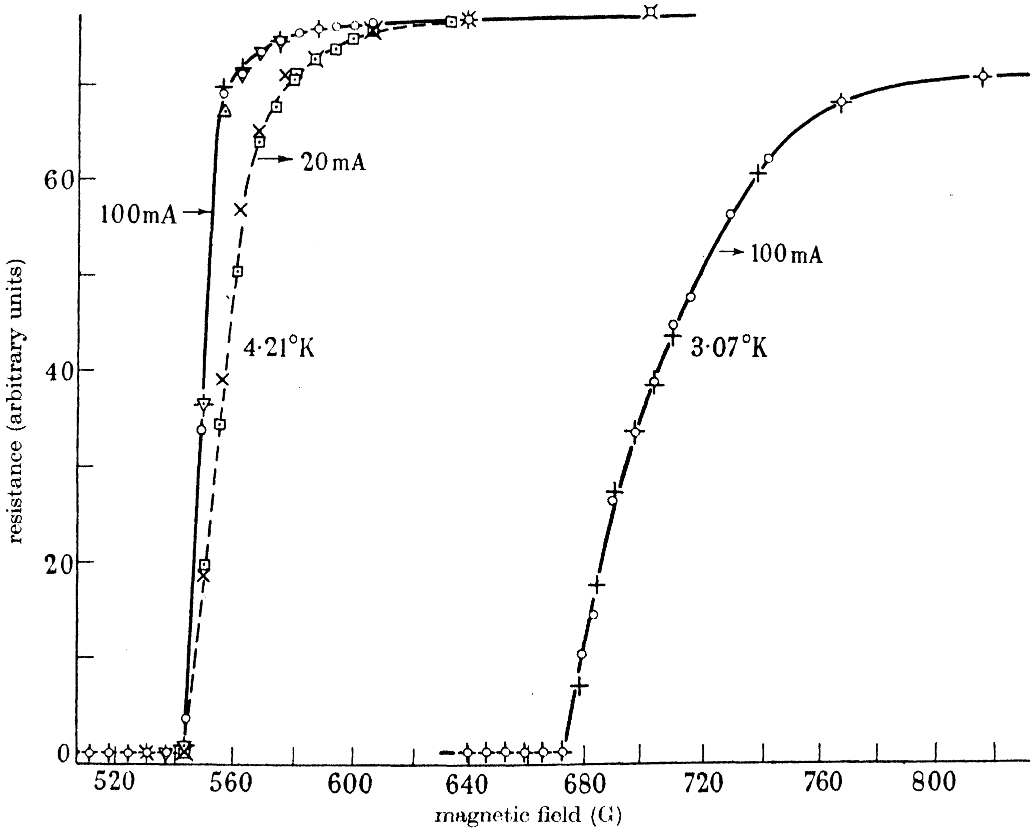

FIGURE 4. Transition curves of lead wire. □ and ○, field increasing; + and ×, field decreasing. The measuring currents are marked on the curves.

From all these experiments it appeared that variations of the transition curve result from the methods of mounting the specimen and the mode of attachment of the contacts. In order to provide a specimen whose axis would be accurately and uniformly defined and without contact difficulties, a wire was cast in a glass capillary of $\sim 100\,\mu$ diameter (see figure 1*b*). Contamination was avoided by melting the metal (Johnson, Matthey lab. no. 1932; purity better than 99·998 %) *in vacuo* and then pressing it into the capillary with pure helium gas. The capillary terminated at both ends in small bulbs into which platinum leads were sealed for current and potential measurement. The results given in figure 5 show well reproducible curves which commence exactly at H_c and show no significant hysteresis. In contradistinction, however, to the curves in figure 4 the transitions show a peculiar shape, *starting almost tangentially at H_c and rising to the normal resistance in the shape* of the letter S. This type of transition, however, clearly differs from those of figure 2, since in the latter the onset occurred below H_c and, secondly, a very careful examination of the present transitions showed no discontinuity in any part of the curve. A reduction of the measuring current (from 80 to 20 mA) produced an effect similar to that shown in figure 3. To examine whether strain on solidification of the metal might perhaps be responsible for the shape of the transition curve the specimen was annealed at 100° C for 5 hr. and the experiment repeated. The results, however, were essentially unchanged (see figure 5).

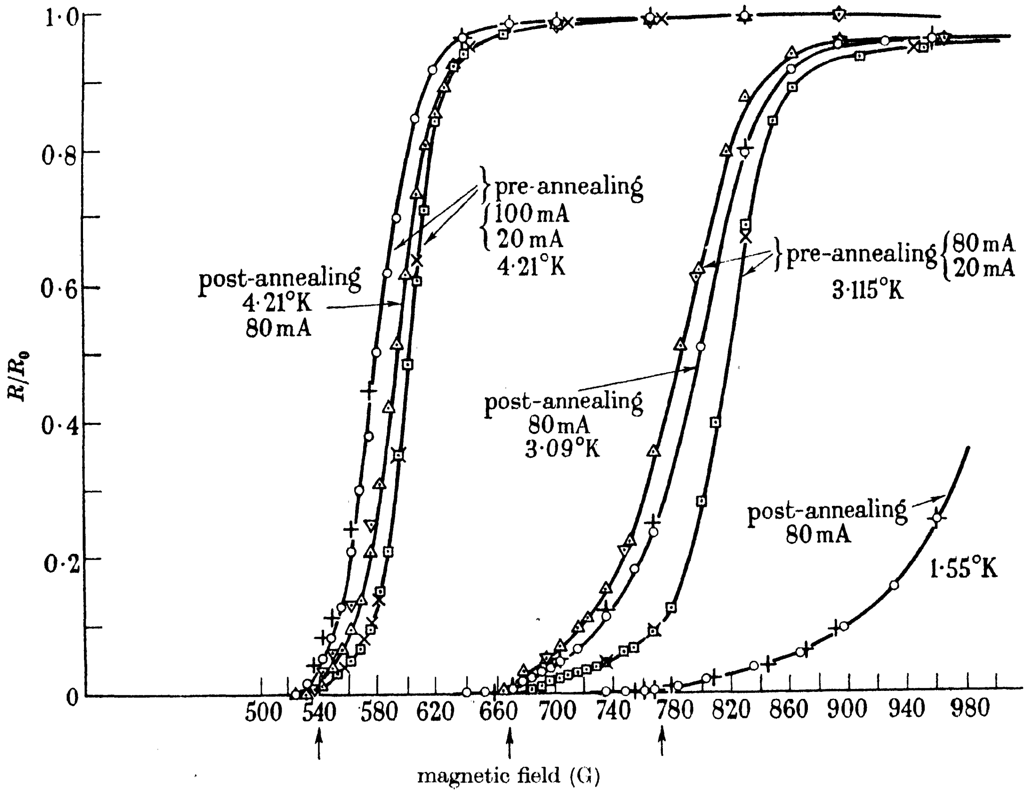

FIGURE 5. Transition curves of lead cast in capillary (see figure 1*b*). Equilibrium transition fields shown by arrows.

Since the outstanding difference between the last specimen and the mounted wires lay in the attachment and position of the contacts, it seemed important to improve these features. In particular, it appeared desirable that the potential leads should not be attached to the bulbs but rather directly to the wire itself. Accordingly, a form of glass capillary capsule was developed (figure 1*c*) in which, with careful glassblowing, the ends are very gently drawn out for some distance before the bulbs are blown to receive the electrodes. The potential electrodes are carefully inserted from the top, and the ends, made of fine platinum wire, are adjusted so as just to 'sit' at the entrance of the capillary proper. It was found during the first attempts that the liquid metal filling the capillary seriously disturbed the positioning and shape of the potential electrodes. To eliminate this the electrodes were sheathed with a layer of lead glass for strength over the greater part of their length leaving only a fine tip naked to make contact with the metal.* Even with the adoption of this technique some trouble will be found in preparing lead specimens due to the difficulty of ensuring that lead 'wets' the platinum adequately, and that the capillary wire remains continuous during solidification. If then the bulbs do cause distortion and disturbance of the magnetic field, this should not now extend appreciably beyond the 'neck', while the actual potential recorded is only that developed across the wire proper.

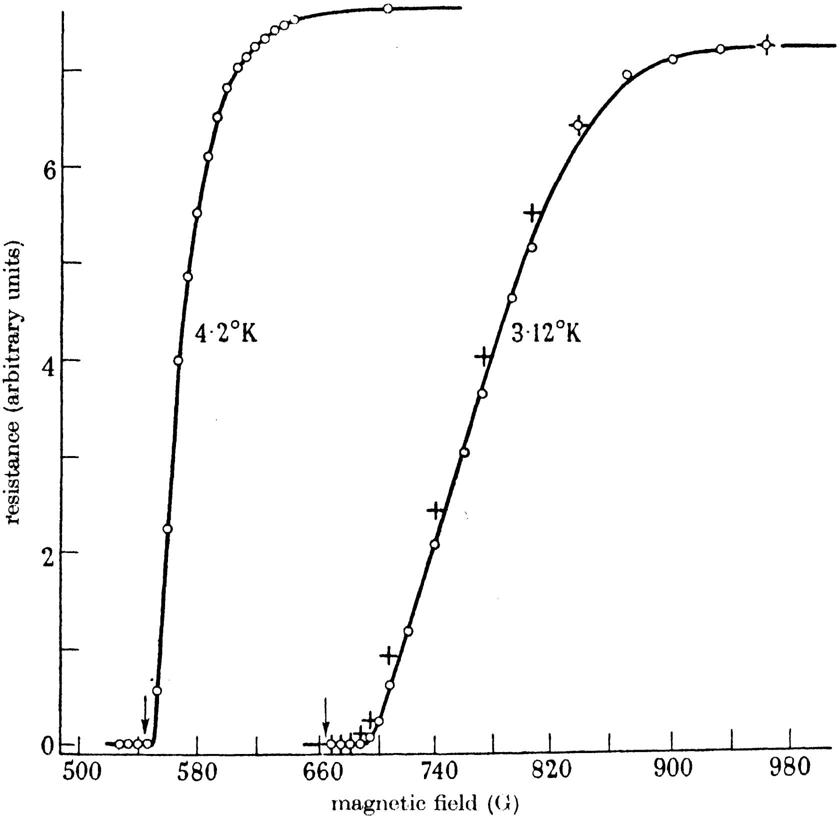

Figure 6. Transition curves of lead cast in special capillary (see figure 1c). Measuring current, 50 mA; equilibrium transition fields shown by arrows. ○, field increasing; +, field decreasing.

Figure 6 shows the type of transition curve obtained with a lead specimen made in this manner. It will be observed that the curves rise steeply at the onset of resistivity and that the transition to the normal resistance remains extended. It is, however, interesting to remark that at the lower temperature the threshold field is noticeably higher than the equilibrium value H_c. The transition curves obtained in this way resemble closely those of figure 3. In view of the information derived from experiments on the different types of specimen we conclude that the last-mentioned method of mounting and preparing the specimen is the most likely to lead to reproducible results. Since it also appears that with these specimens the essentially true character of the longitudinal transition is observed, free from secondary disturbances, the same method was adopted in the extension of the work to tin and mercury.

---

* We should like to acknowledge the skill and patience shown by Mr D. G. Saxton in making these capillaries for us.

4. EXPERIMENTS ON TIN

The metal was obtained from Messrs Johnson Matthey (lab. no. 2135; purity better than 99·995 %). The results obtained with a specimen made to the pattern of figure 1 *c* are given in figure 7. The transition curves show precisely the same characteristics as were observed in the case of lead, except that the transition is relatively much less spread out. In all cases, however, the transition was found to cover a finite range of magnetic fields, never showing any sign of discontinuity. At all temperatures the onset of resistivity coincided exactly with the measured values of H_c. The transition of this specimen was also examined in zero magnetic field so that the shape of our curve might be compared with those obtained by de Haas & Voogd (1931) when they observed the steepness of transition in mono- and poly-crystals. Our curves (see figure 8) compare favourably in fact with their data on the purest monocrystal. This provides a further check of the physical and chemical purity of our specimen. The satisfactorily low ratio of the resistance at 4·2° K to that at room temperature ($\sim 5 \times 10^{-4}$) gives additional confirmation of this.

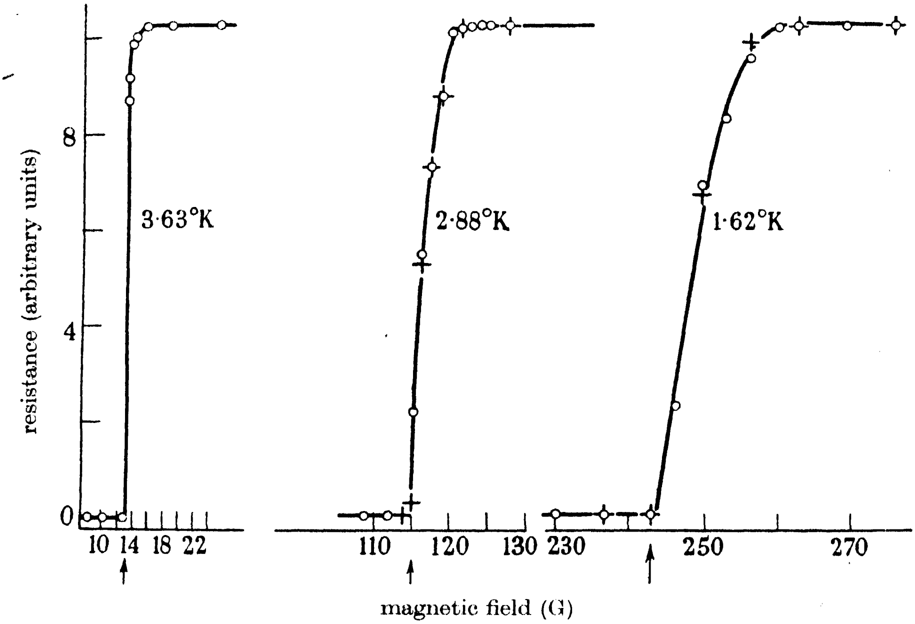

FIGURE 7. Transition curves of tin in capillary. ○, field increasing; +, field decreasing. Measuring current, 100 mA; equilibrium fields shown by arrows.

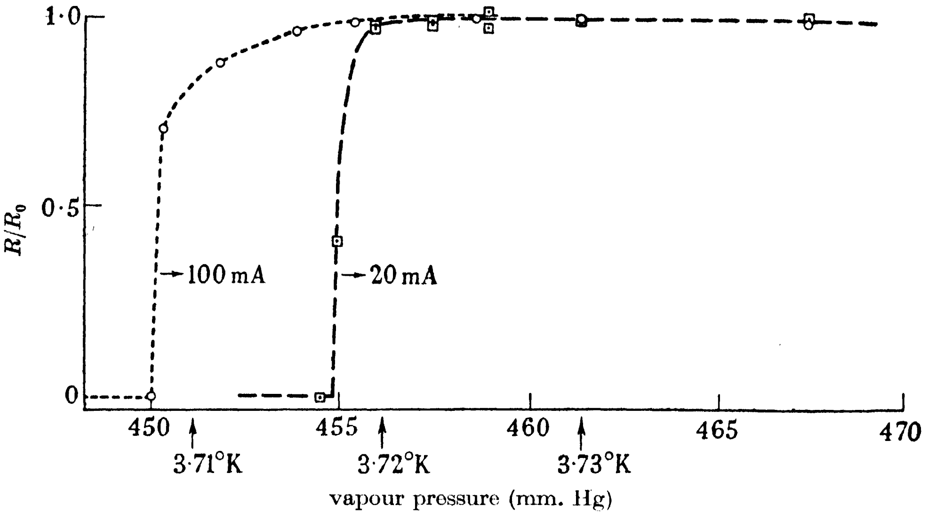

FIGURE 8. Transition curves of tin specimen in zero magnetic field.

5. EXPERIMENTS ON MERCURY

Experiments similar to those on lead and tin were also carried out on mercury. The metal was supplied by Messrs Johnson Matthey (lab. no. 3505) and was extremely pure, containing as only impurity a 'trace' of silver. The transition curves of a specimen prepared in a glass capillary with narrow neck (similar to those used with lead and tin; cf. figure 1*c*) are given in figure 9*a* and *b*. The shape of the curves is again the same as in the other metals; a sudden rise at H_c is followed by a gradual approach to the value of normal resistivity at considerably higher field strengths. The resistance ratio $R_{1.5^\circ\mathrm{K}}/R_{4.2^\circ\mathrm{K}} \approx 0{\cdot}1$ furnishes proof of the high purity of our specimen.

6. HYSTERESIS

A rather astonishing feature of our experiments thus far was the complete absence of any sign of hysteresis. This phenomenon has commonly been associated with specimens of high purity and has been found particularly in experiments with mercury (de Haas, Sizoo & Onnes 1925). De Haas (1932) has mentioned that the width of the hysteresis loop appears to be influenced by the method in which the terminals are attached to the specimen. As a result of this observation and of the magnetic effects connected with superconductivity discovered shortly afterwards (Meissner & Ochsenfeld 1933), one of us (Mendelssohn 1935) has suggested that hysteresis may in fact be caused by the geometrical shape of the specimen. Unless the demagnetization factor of the specimen is precisely zero, any change in its susceptibility will cause the value of the magnetic field in the vicinity of the specimen to differ from the actually recorded value. It is clear that in this way the mechanism of the resistive transition can be obscured by the changes in magnetic induction. Since in our experiments special care had been taken to avoid secondary magnetic effects in order to obtain undisturbed transitions, the absence of hysteresis appeared significant.

In order to test the hypothesis that resistance hysteresis is caused by the shape of the conductor a different type of mercury specimen was prepared. It consisted of a short capillary ending in large spherical bulbs into which the electrodes were sealed (figure 1*d*). While thus the shape was altered the material used and the method of preparation were identical with the mercury sample of figure 9. Measurements on this specimen show (figure 10*a*, *b*) that the character of the transition is now completely altered. At all temperatures a strong hysteresis is observed in which the ascending and the descending curves are well separated. The resistance still rises continuously at the equilibrium field, but, on decreasing the field, superconductivity is not re-established until an appreciably lower value of the magnetic field is reached. The drop then is discontinuous, occurring in one or two steps and completing a hysteresis loop similar to those observed in the Leyden experiments. It should be noted that the first drop in resistivity takes place not only below the ascending field but even below H_c. Another, and it would seem, very significant,

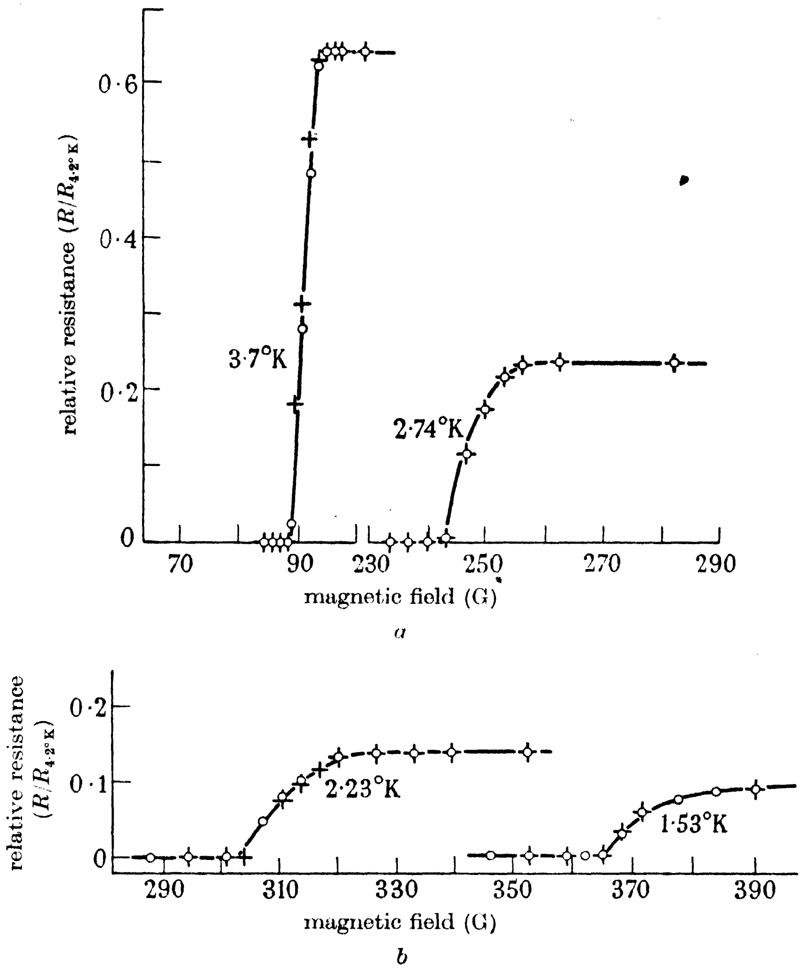

FIGURE 9. Transition curves of mercury specimen. ○, field increasing; +, field decreasing. Measuring current, 20 mA.

feature of the phenomenon is that the width of the whole transition including the hysteresis loop may now be *narrower* than the transition of figure 9. The difference is striking at the lowest temperatures.

While the result appears to demonstrate convincingly a relation between the shape of the specimen and the appearance of hysteresis, we had to keep in mind that not only the ends of the conductor had been changed but also its length. It seemed just possible, though not very likely, that the shorter length of the capillary might, by itself, have some influence on the transition. A specimen was therefore prepared which had a short capillary but whose ends were shaped so as not to distort the field, similar to those illustrated in figure 1*c*. The result shown in figure 11 proves that it is the bulbous form of the terminals and *not* the length which causes hysteresis. The transitions are again extended and reversible like those of figure 9. Only in one curve, at 3·7° K, is there a very slight indication of hysteresis. This is not really surprising because, as the specimen is shortened, the distorting effect even of the funnel-shaped ends must become noticeable. Even so the fundamental difference between the curves of figures 10 and 11 is obvious.

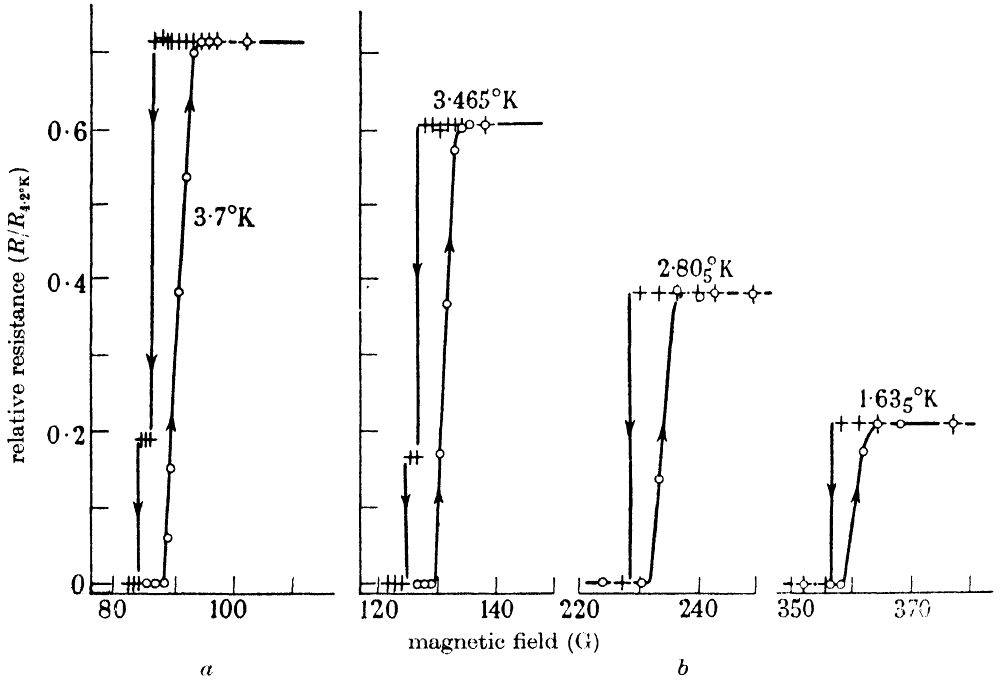

FIGURE 10. Transition curves of mercury specimen (see figure 1). ○, field increasing; +, field decreasing. Measuring current, 20 mA.

The experiments on producing hysteresis were then extended to tin and lead. A long tin specimen with terminals fitted to bulbs (figure 1*b*) which had been prepared earlier was tested and yielded transition curves which all showed hysteresis though to a much smaller extent than those of figure 10. In order to see whether under identical circumstances tin would behave similarly to mercury, a short specimen with bulbous ends was prepared. The result, shown in figure 12, is rather surprising. In none of the transitions at different temperatures was there the slightest hysteresis. On the other hand, the shape of the transition curves differed completely from those of figure 7 taken on tin of identical origin and purity. The change from normal to superconductivity and vice versa is now discontinuous. Approaching the transition from low fields there is no gradual rise of resistivity, and there is equally no indication of incipient superconductivity on lowering the field until the jump occurs. Experiments on this specimen were carried out again after it had been warmed to room temperature in the interim; the results remained the same. The remarkable difference between this and the earlier specimens is best seen by contrast with the curves of Sn 1 which have been plotted for comparison in figure 12. In fact, the transition of Sn 3 appears to be as sharp as any that have ever been observed and could be taken as an example for the current opinion that the 'ideal' transition in a magnetic field should be as discontinuous as that in zero field. However, in view of our other results and for reasons to be discussed later, we are not inclined to regard this sharp transition as characteristic of simple physical conditions representing the ideal transition in a longitudinal magnetic field.

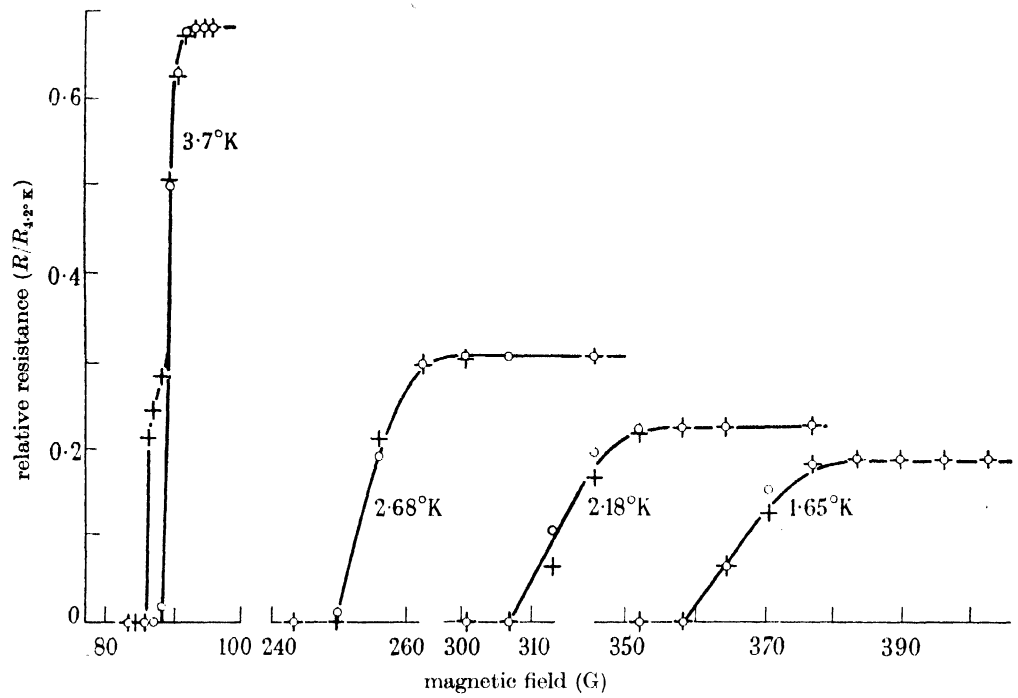

FIGURE 11. Transition curves of short mercury specimen (see text). ○, field increasing; +, field decreasing.

A short lead specimen of the type shown in figure 1*d* was also prepared and tested. This, however, showed no hysteresis, nor was the width of the transition narrowed in comparison with the other experiments on this metal. This behaviour is in agreement with all earlier work which indicates that lead does not show hysteresis.

Finally, it should be mentioned that in all experiments where this seemed interesting the possible effect of current distribution in the transition region was considered. The transition was first completed with a steady uninterrupted measuring current and was then repeated at the same values of field and temperature with the measuring current switched on and off. In no case was any difference between the two sets of values observed.

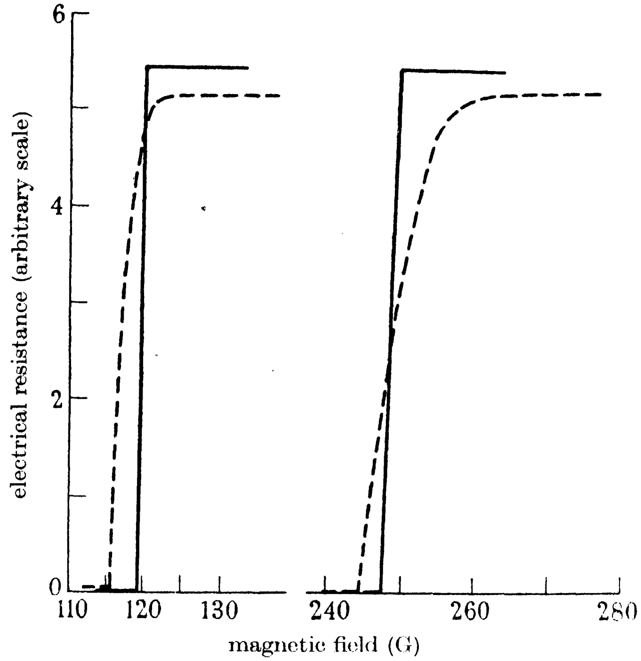

FIGURE 12. ——, transition curves for Sn 3 (short specimen with bulbous ends); – – –, transition curves for Sn 1 ('ideal' specimen). Experimental points are omitted for greater clarity.

7. DISCUSSION

When trying to interpret the results of this investigation, let us at first leave aside the observations connected with the hysteresis described in the preceding section. We are faced then with a fairly consistent picture. In all instances the change of resistivity is spread over a *finite* region of magnetic field, or, what would be the same, of temperature. In this the present work fully confirms the observations of Daunt and Pontius on lead. However, the results now obtained make it appear much more probable that the gradual nature of the transition in an external field is a general feature of all superconductors. In particular, the behaviour of the tin specimen Sn 1 strongly supports this view because in its case the transition in zero field was effectively discontinuous. It thereby fulfilled by the most sensitive test available the condition of chemical and physical purity. Nevertheless, the transitions in magnetic fields were extended.

Besides chemical and physical impurity there are evidently a number of factors, mainly connected with the shape of the specimen and the attachment of the electrodes which disturb the transition. However, the experiments of § 3 suggest that it is possible to eliminate these disturbances to a large extent and to arrive by successive steps at a method of preparation and mounting which ensures rather reproducible results. The transition curves obtained on these specimens are of the same aspect for all three metals, exhibiting the same characteristic features. Approaching the transition from low magnetic fields the resistance rises suddenly. The initial slope decreases with rising magnetic field and finally merges with the curve denoting the variation of the normal resistance with the field. Since this ordinary magneto-resistive effect is small, the effective end of the transition figure can in most cases be determined with a fair degree of accuracy. Another characteristic feature is the complete reversibility of the curves. Ascending and descending transitions coincided in all three metals perfectly. Comparing the present results with determinations of the magnetic induction it can be noted that the field strength at which the first sign of resistivity appears agrees well, in the case of mercury and tin, with the 'equilibrium field' denoting the change from normal to zero induction. The same is true for lead with lower fields.

The approach to these reproducible and evidently simple transitions was achieved by eliminating factors which on plausible grounds could be regarded as disturbing the magnetic field over that length of the wire across which the potential is measured. We thus have good reason to assume that this particular type of transition most closely approaches the ideal case of an infinitely long wire passing from the normal to the superconductive state in a longitudinal magnetic field. We must therefore conclude, that, as far as the electrical resistance is concerned, the superconductive and normal regions in the H against T diagram are not sharply divided but are connected by a transition zone in which the resistance changes *gradually* from normal to zero. This zone is very narrow at low fields but widens as the *absolute* value of the field increases. This rapid widening at high fields precludes the trivial explanation that the width may be due to faulty alinement or field inhomogeneity, since in that case the effect would be directly proportional to the field strength. An approximate sketch of the transition region in lead as deduced from our experiments is given in figure 13. The dependence on the absolute value of the field is evidently also the reason why the transition zone is less marked in tin and mercury. The smaller width of the zone in these metals cannot be simply explained by the lower transition points, since it is evident from the results that the effect is much more marked in lead for equal values of H_c/T which may be taken as a reduced parameter of state.

As to the physical state of the transition zone, not much can be said at present. According to the theories of Becker, Heller & Sauter (1933) and of London & London (1935) the magnetic threshold field should be increased when superconductors are considered whose linear dimensions become comparable with the depth λ to which the magnetic field penetrates into the metal. Experimental proof of such a deviation from the usual value of H_c was first obtained by Pontius (1937) in measurements on thin wires and has since been confirmed in a great number of investigations. The high threshold values of superconductive alloys in bulk have been interpreted by one of us (Mendelssohn 1935) as due to a spontaneous splitting up of the metal into microscopic superconductive regions, and experiments on the magnetic induction, the heat content, and the heat conductivity have amply confirmed this conception. In fact, it might appear strange that a pure metal should not split up similarly into microscopic regions under the influence of a magnetic field. The fact that in a pure metal the stable superconductive state exhibits complete expulsion of the field suggests the existence of a surface energy between the normal and superconductive phases; the total surface energy is then minimized by the overall expulsion.

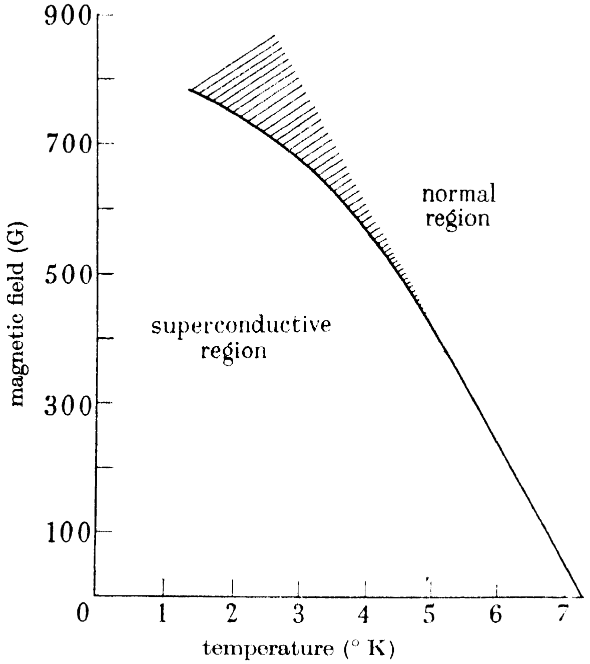

FIGURE 13. Domain diagram for lead; transition zone shown shaded.

A possible explanation then for the existence of the transition zone is that in this region the Maxwell tension is outweighing the surface tension. The possibility of such a surface energy has been envisaged by H. London (1935) in his theory of superconductive phase equilibrium. The problem has again been discussed more recently by Ginsburg (1945). It is known (e.g. Appleyard, Bristow, London & Misener 1939) when deductions of the penetration depth, λ, are made from data on the critical fields for thin films that λ varies systematically with size. This naturally disagrees with the London penetration equation $H = H_0 e^{-x/\lambda}$, where λ is a fixed parameter. Ginsburg suggests that this is due to omission of a possible difference of surface energy between the normal superconducting phases in computing the free-energy change. He finds that a very small difference of surface tension (~ 1 to ~ 0.01 %) between the phases would be sufficient to account for the discrepancy, leaving now λ as a constant parameter. Furthermore, he finds that the surface-tension difference thus deduced increases rapidly with rising magnetic field.

The observation that the width of our transition zone increases so rapidly with the value of the magnetic field seems to favour such an explanation. It is, however, by no means clear whether the transition zone in the longitudinal case should be considered as an actual mixture of small superconductive and normal domains or whether the field in the metal is homogeneous throughout. In view of the reproducible and evidently general character of the 'ideal' transition curve, it seemed worth while to try to fit a simple empirical formula. The object was to express the shape by a single parameter besides the magnetic energy. A reasonable formula is found to be

$$R = 0 \quad (H < H_c),$$

$$R = R_0\left\{1 - \exp\left(-\frac{\phi(H^2 - H_c^2)}{H_c^2}\right)\right\} \quad (H > H_c),$$

where R_0 = 'normal' resistance, and H_c = critical field at given temperature. The free parameter, ϕ, then varies quite rapidly with H_c. For example, in lead

$$\phi \approx 25 \text{ for } H_c \approx 540 \text{ G}, \quad \phi \approx 6{\cdot}3 \text{ for } H_c \approx 680 \text{ G}.$$

Whether this variation of ϕ signifies a dependence on penetration depth, λ, cannot at present be decided.

This conception of the longitudinal transition as a gradual change of the resistivity of the metal between the two states, if it is to prove satisfactory, must allow for the peculiar phenomena described in § 6. These observations seem to show that hysteresis and discontinuous transitions are closely connected. We were, in fact, only able to produce these effects by departing greatly from the ideal conditions of the longitudinal case, but we did not observe them in a single case when care had been taken to keep the field over the specimen homogeneous. There thus appears to be no doubt that the sudden changes in resistivity observed in our experiments are not a feature of the longitudinal transition itself but are due to secondary effects. This does not, of course, mean that their explanation is unconnected with characteristic features of the undisturbed transition. On the contrary, the discontinuous changes in resistivity seem to be closely linked with the existence, in the 'ideal' transition, of the transition zone. An indication of this is provided by the curves of figure 2 in which the two sides of the transition, the normal and the superconductive, are becoming unstable with respect to each other. Taking, for instance, the transition at 4·2° K it can be seen that coming from high fields the beginning of an 'ideal' curve is traced, but this curve, if it were smoothly continued, would clearly not lead to zero resistance at H_c which at this temperature is about 540 G. Such extrapolation as can be made would more likely yield a threshold value of about 510 G. The first appearance of resistivity in this specimen does in fact occur at roughly 510 G arising from imperfect alinement *in one place* causing H_c to be reached in that part of the specimen sooner than in the rest. The lower branch of the curve, however, rises slowly, and any reasonable extrapolation would lead to the attainment of normal resistivity considerably later than actually observed on the upper branch. We therefore have to consider not one but two possible transition curves, one evidently related to the main length of the wire and the other to the distorted part. These two curves differ by the value of about 30 G, and it appears that a state of affairs ensues where for the same value of field and temperature two different values of the resistance are possible. This mutual instability then leads to the *discontinuous* change in resistivity at H_c. This same peculiar instability connected with the geometrical shape in the field occurs in a much stronger manner in the mercury specimen with bulbous ends (figure 10). Any part of the specimen which does not conform to the idealized long cylinder in a longitudinal field must, as is well known, split up into a great number of superconductive needles or laminae—the so-called 'intermediate state'. This means that the specimen in transition between the superconductive and normal state has to pass through a condition involving creation of a large interface area. If, as suggested above, there exists a surface-tension difference between the two states, then this energy will oppose the formation of the intermediate state and unstable conditions akin to the supercooling of a liquid may occur. It is therefore tempting to interpret the discontinuous and hysteretic transitions observed by us on such a basis.

It has, of course, to be remembered that the bulbs will cause distortion of the external field which in turn can to some extent falsify the value of the magnetic field applied over the length of the wire. The effect of such a 'magnetic shadow' can, according to present ideas, only exist, however, at fields *below* H_c, because it is only then that the metal is strongly diamagnetic. On the other hand, it should be noted that the specimen of figure 10 could be brought through the transition zone on reducing the magnetic field without showing a drop in resistance. This is rather perplexing, as it appears difficult to account for this 'precognition' of effects to be expected only at a considerably lower field. The only straightforward explanation we can offer at present lies on the assumption of a change in magnetic susceptibility *above* H_c, which would correspond to the variation of resistivity. In this case the difference in the demagnetization factors of the 'ideal' and bulbous specimens might account for the difference in electrical conductivity. So far there is no indication of such an anomaly, but the existing experiments on the change of induction have mostly been carried out on specimens with a fairly large demagnetization factor and were, moreover, not sensitive enough to reveal a change of the order of the *normal* susceptibility. Besides accurate determinations of the magnetic induction other experiments, as, for instance, on the Hall effect and on the thermo-electric properties, may give further information on the nature of the transition zone.

Summarizing the results of this investigation we have no reason to assume that in the 'ideal' longitudinal case the transition between the normal and the superconductive states is discontinuous. Discontinuous changes with or without hysteresis only occurred when a state of instability had been produced by choosing conditions which deviate markedly from the longitudinal case.

REFERENCES

Andrew, E. R. 1947 *Phys. Soc. Camb. Conf. Rep.* (2), p. 101.

Appleyard, E. T. S., Bristow, J. R., London, H. & Misener, A. D. 1939 *Proc. Roy. Soc.* A, **172**, 540.

Becker, R., Heller, G. & Sauter, F. 1933 *Z. Phys.* **85**, 772.

Daunt, J. G. 1939 *Phil. Mag.* **28**, 24.

Daunt, J. G., Horseman, A. & Mendelssohn, K. 1939 *Phil. Mag.* **27**, 754.

Daunt, J. G. & Mendelssohn, K. 1937 *Proc. Roy. Soc.* A, **160**, 127.

Daunt, J. G. & Mendelssohn, K. 1938 *Proc. Phys. Soc.* **50**, 525.
Désirant, M. & Shoenberg, D. 1948 *Proc. Roy. Soc.* A, **194**, 63.
Ginsburg, V. 1945 *J. Phys. U.S.S.R.* **9**, 305.
de Haas, W. J. 1932 *Leipzig. Vortraege.*
de Haas, W. J., Sizoo, G. J. & Kammerlingh Onnes, H. 1925 *Commun. Phys. Lab. Univ. Leiden*, 180*d*.
de Haas, W. J. & Voogd, J. 1931 *Commun. Phys. Lab. Univ. Leiden*, 212*c*.
London, H. 1935 *Proc. Roy. Soc.* A, **152**, 650.
London, F. & London, H. 1935 *Proc. Roy. Soc.* A, **152**, 24.
MacDonald, D. K. C. 1947 *J. Sci. Instrum.* **24**, 232.
MacDonald, D. K. C. & Mendelssohn, K. 1948 *Nature*, **162**, 294.
Meissner, W. & Ochsenfeld, R. 1933 *Naturwissenschaften*, **21**, 787.
Mendelssohn, K. 1935 *Proc. Roy. Soc.* A, **152**, 34.
Mendelssohn, K. 1936 *Proc. Roy. Soc.* A, **155**, 558.
Pontius, R. B. 1937 *Phil. Mag.* **24**, 777.
Shoenberg, D. 1938 *Superconductivity*, p. 7. Cambridge University Press.
Simon, F. 1936 *Act. 7. Int. Congr. Refrig.* **1**, 367.

Correlated incompressible and compressible boundary layers

By K. Stewartson, *St Catharine's College, University of Cambridge*

(*Communicated by D. R. Hartree, F.R.S.—Received* 30 *June* 1949)

The boundary-layer equations for a compressible fluid are transformed into those for an incompressible fluid, assuming that the boundary is thermally insulating, that the viscosity is proportional to the absolute temperature, and that the Prandtl number is unity. Various results in the theory of incompressible boundary layers are then taken over into the compressible theory. In particular, the existence of 'similar' solutions is proved, and Howarth's method for retarded flows is applied to determine the point of separation for a uniformly retarded main stream velocity. A comparison with an exact solution is used to show that this method gives a closer approximation than does Pohlhausen's.

1. Introduction

This paper is concerned with a certain type of compressible boundary layer, in which it is assumed that

(*a*) the boundary is thermally insulating,
(*b*) the viscosity varies as the absolute temperature T,
(*c*) the Prandtl number (σ) of the fluid is unity.

In a previous paper on this subject by Howarth (1948) these same assumptions were discussed, and since this paper is a development of his, they will now be passed over without comment.

Accepting these three conditions, it will be found possible to transform the coordinates so that the boundary-layer equation arising from a given main stream velocity (U_1) of a compressible fluid, becomes identical with that arising from a different main-stream velocity (V_1) of an incompressible fluid. This means that any formulae or flow pattern occurring in the theory of incompressible boundary layers may be taken over into these compressible boundary layers. Having deduced the necessary transformations in § 2 the rest of this paper will be concerned with the interpretation of certain aspects of incompressible flow in terms of compressible theory. In § 3 the momentum integral of the compressible boundary layer will be obtained, and hence the differential equation of the Kármán-Pohlhausen approximation (1921). This problem has also been investigated by Howarth (1948), and the relation between his formula and this one is discussed. It is shown that the two formulae are the same, even though Howarth has introduced three functions whereas we only use two. In § 4 the 'similar' flows of the compressible boundary layer are obtained, and it is shown how the solution of problems of incompressible flow may be used to solve problems in the compressible plane. Finally, a discussion of the separation of the boundary layer under the influence of an adverse pressure gradient is given. The theory of incompressible flow furnishes two simple methods for dealing with this problem—that of Kármán-Pohlhausen, and that of Howarth (1938), which is based on the series solution of a certain separation problem. Due to the form of the main-stream velocity in the incompressible plane, corresponding to a given velocity in the compressible plane, both these methods tend to overestimate the skin friction. A critical survey of Howarth's method, however, suggests that it is a much better approximation than that of Kármán-Pohlhausen, and in a number of problems it has been shown to agree quite well with known results. Using both these methods the variation of the point of separation with Mach number, when the main-stream velocity is decreasing linearly, is investigated. The condition on γ for the point of separation to tend to the leading edge as the Mach number there tends to infinity, is found, using both methods, and compared with the exact condition which may be obtained from the differential equation of the boundary layer. This is used to determine the relative accuracy for this problem of the two approximate methods.

2. THE BOUNDARY-LAYER EQUATION

For the two-dimensional flow past a plane boundary, it is well known that, in the usual notation,

$$\rho u \frac{\partial u}{\partial x} + \rho v \frac{\partial u}{\partial y} = -\frac{\partial p}{\partial x} + \frac{\partial}{\partial y}\left(\mu \frac{\partial u}{\partial y}\right), \tag{2·1}$$

$$0 = \frac{\partial p}{\partial y}, \tag{2·2}$$

and

$$\frac{\partial}{\partial x}(\rho u) + \frac{\partial}{\partial y}(\rho v) = 0. \tag{2·3}$$

Moreover, if the Prandtl number $\sigma = 1$, and the boundary is thermally insulating, it has been shown by Crocco (1946) that the temperature T in the boundary layer is given by

$$\frac{T}{T_1} = 1 + \frac{\gamma - 1}{2a_1^2}[U_1^2 - u^2], \tag{2·4}$$

where the suffix 1 refers to conditions in the main stream and a_1 is the velocity of sound there.

The y co-ordinate will now be transformed by writing

$$Y = \frac{a_1}{a_0\sqrt{\nu_0}}\int_0^y \frac{\rho\, dy}{\rho_0}, \tag{2·5}$$

where the suffix 0 refers to some standard state, usually in the main stream when $x = 0$. Similar transformations have been used previously by Hartree and Howarth, but this one is perhaps the most convenient for these problems.

From equation (2·3) there exists a stream function ψ so that

$$\rho u = \rho_0\sqrt{\nu_0}\frac{\partial\psi}{\partial y} \quad\text{and}\quad \rho v = -\rho_0\sqrt{\nu_0}\frac{\partial\psi}{\partial x}. \tag{2·6}$$

Hence

$$u = \frac{\rho_0}{\rho}\sqrt{\nu_0}\left(\frac{\partial\psi}{\partial Y}\right)_x\left(\frac{\partial Y}{\partial y}\right)_x = \frac{a_1}{a_0}\frac{\partial\psi}{\partial Y}, \tag{2·7}$$

and

$$v = -\frac{\rho_0\sqrt{\nu_0}}{\rho}\left[\left(\frac{\partial\psi}{\partial x}\right)_Y + \left(\frac{\partial\psi}{\partial Y}\right)_x\left(\frac{\partial Y}{\partial x}\right)_y\right]. \tag{2·8}$$

Equation (2·7) is really the point at which Howarth's theory begins to diverge from this one, since the limiting value of $\partial\psi/\partial Y$ as $Y \to \infty$ is not the main-stream velocity but, effectively, the local Mach number in the main stream. Howarth chose to compare the effect of compressibility on the *same* main stream velocity. If this condition is relaxed and the main-stream velocity allowed to vary, then it will be shown below that a complete correlation between these compressible and the incompressible boundary layers may be obtained.

Continuing the transformation from x, y to x, Y

$$\left(\frac{\partial u}{\partial x}\right)_y = \frac{\partial\psi}{\partial Y}\frac{1}{a_0}\frac{da_1}{dx} + \frac{a_1}{a_0}\frac{\partial^2\psi}{\partial Y\partial x} + \frac{a_1}{a_0}\frac{\partial^2\psi}{\partial Y^2}\left(\frac{\partial Y}{\partial x}\right)_y, \tag{2·9}$$

and

$$\left(\frac{\partial u}{\partial y}\right)_x = \frac{a_1^2\rho}{a_0^2\sqrt{\nu_0}\rho_0}\frac{\partial^2\psi}{\partial Y^2}. \tag{2·10}$$

Hence

$$u\frac{\partial u}{\partial x} + v\frac{\partial u}{\partial y} = \frac{a_1^2}{a_0^2}\left[\frac{\partial\psi}{\partial Y}\frac{\partial^2\psi}{\partial x\partial Y} - \frac{\partial\psi}{\partial x}\frac{\partial^2\psi}{\partial Y^2}\right] + \frac{a_1}{a_0^2}\frac{da_1}{dx}\left(\frac{\partial\psi}{\partial Y}\right)^2. \tag{2·11}$$

Since we are assuming that the viscosity μ varies as the absolute temperature, it follows that

$$\mu\left(\frac{\partial u}{\partial y}\right)_x = \frac{\mu_0 T}{T_0}\frac{a_1^2\rho}{a_0^2\rho_0\sqrt{\nu_0}}\frac{\partial^2\psi}{\partial Y^2} = \frac{p a_1^2\mu_0}{p_0 a_0^2\sqrt{\nu_0}}\frac{\partial^2\psi}{\partial Y^2}, \tag{2·12}$$

and hence

$$\frac{\partial}{\partial y}\left(\mu\frac{\partial u}{\partial y}\right) = \mu_0\frac{p\rho a_1^3}{p_0\rho_0 a_0^3\nu_0}\frac{\partial^3\psi}{\partial Y^3} = \frac{p\rho a_1^3}{p_0 a_0^3}\frac{\partial^3\psi}{\partial Y^3}, \tag{2·13}$$

since using (2·2) the pressure p is independent of y. Also

$$\frac{1}{\rho}\frac{\partial p}{\partial x} = \frac{p_1 T}{p\rho_1 T_1}\frac{dp}{dx} = \frac{1}{\rho_1}\frac{T}{T_1}\frac{dp_1}{dx}, \tag{2·14}$$

since $p_1 = p$.

From the Eulerian equations of motion in the main stream it follows that

$$\frac{1}{\rho_1}\frac{dp_1}{dx} = -U_1\frac{dU_1}{dx} \qquad (2\cdot15)$$

and $$a_1^2+\frac{\gamma-1}{2}U_1^2 = \text{const.} = a_0^2+\frac{\gamma-1}{2}U_0^2. \qquad (2\cdot16)$$

Hence $$a_1\frac{da_1}{dx} = -\frac{\gamma-1}{2}U_1\frac{dU_1}{dx} = \frac{\gamma-1}{2}\frac{1}{\rho_1}\frac{dp_1}{dx}. \qquad (2\cdot17)$$

If now we substitute equations (2·11), (2·14) and (2·17) into (2·1) and make use of the energy integral (2·4), we get

$$\frac{a_1^2}{a_0^2}\left[\frac{\partial\psi}{\partial Y}\frac{\partial^2\psi}{\partial x\,\partial Y}-\frac{\partial\psi}{\partial x}\frac{\partial^2\psi}{\partial Y^2}\right]+\frac{\gamma-1}{2}\left(\frac{\partial\psi}{\partial Y}\right)^2\frac{1}{\rho_1 a_0^2}\frac{dp}{dx}$$
$$= \frac{p_1 a_1^3}{p_0 a_0^3}\frac{\partial^3\psi}{\partial Y^3}-\frac{1}{\rho_1}\frac{dp}{dx}\left[1+\frac{\gamma-1}{2a_1^2}\left\{U_1^2-\frac{a_1^2}{a_0^2}\left(\frac{\partial\psi}{\partial Y}\right)^2\right\}\right]. \qquad (2\cdot18)$$

It will be noticed immediately that the coefficients of $(\partial\psi/\partial Y)^2$ on both sides of (2·18) are equal, so that these terms cancel out. Moreover, in the main stream

$$p \propto \rho_1^\gamma \quad \text{and} \quad a_1^2 = \gamma p_1/\rho_1,$$

so that $$\frac{p}{p_0} = \left(\frac{a_1}{a_0}\right)^{2\gamma/(\gamma-1)}, \qquad (2\cdot19)$$

and therefore (2·18) reduces to

$$\frac{\partial^3\psi}{\partial Y^3}-\left(\frac{a_0}{a_1}\right)^{(3\gamma-1)/(\gamma-1)}\left[\frac{\partial^2\psi}{\partial x\,\partial Y}\frac{\partial\psi}{\partial Y}-\frac{\partial\psi}{\partial x}\frac{\partial^2\psi}{\partial Y^2}\right] = \frac{a_0^2+\frac{\gamma-1}{2}U_0^2}{\rho_1 a_0^2}\left(\frac{a_0}{a_1}\right)^{(7\gamma-5)/(\gamma-1)}\frac{dp}{dx}. \qquad (2\cdot20)$$

Finally, writing $$z = \int_{x_0}^{x} dx\left(\frac{a_1}{a_0}\right)^{(3\gamma-1)/(\gamma-1)}, \qquad (2\cdot21)$$

and $$V_1 = a_0 M_1 = a_0 U_1/a_1, \qquad (2\cdot22)$$

the equation of motion becomes

$$\frac{\partial^3\psi}{\partial Y^3}-\frac{\partial\psi}{\partial Y}\frac{\partial^2\psi}{\partial z\,\partial Y}+\frac{\partial\psi}{\partial z}\frac{\partial^2\psi}{\partial Y^2} = -V_1\frac{dV_1}{dz}, \qquad (2\cdot23)$$

since z is a function of x only.

The boundary conditions are that

$$u = v = 0 \quad \text{when} \quad y = 0 \quad \text{and} \quad u \to U_1 \quad \text{as} \quad y \to \infty, \qquad (2\cdot24)$$

and these, in terms of ψ, Y and z, become

$$\psi = \frac{\partial\psi}{\partial Y} = 0 \quad \text{when} \quad Y = 0 \quad \text{and} \quad \frac{\partial\psi}{\partial Y} \to V_1 \quad \text{as} \quad Y \to \infty, \qquad (2\cdot25)$$

which correspond to the boundary-layer equation for an incompressible fluid with a main stream velocity V_1.

The actual skin friction is

$$\left[\mu\frac{\partial u}{\partial y}\right]_{y=0} = \rho_0\sqrt{\nu_0}\left(\frac{a_1}{a_0}\right)^{(4\gamma-2)/(\gamma-1)}\left(\frac{\partial^2\psi}{\partial Y^2}\right)_{Y=0}. \qquad (2\cdot26)$$

If U_1 is an increasing function of x then a_1 is decreasing from (2·16) and so M_1 increases more rapidly than U_1. Similarly, if U_1 is decreasing, M_1 decreases more rapidly, and so the effect of compressibility is to emphasize any change in the velocity. (If U_1 is constant then so is M_1, and the only effect of compressibility is to change the scale of Y.) Changes in kinematic viscosity as represented by the change in ν_0 manifest themselves solely in the scale factor in the direction normal to the boundary; changes in compressibility as represented by changes in a_0, for example, enter at every stage, affecting the scale factors both along and normal to the boundary and the reference velocity distribution in the main stream. It is perhaps surprising that in a problem of this nature which is essentially viscous in origin the effects of viscosity are so much more readily separable than those of compressibility.

Clearly the relation between V_1 and U_1 is (1, 1), so that for every problem in incompressible flow there is an associated problem in compressible flow and conversely. Hence there are an infinity of 'similar' solutions of the boundary-layer equation (2·1) contrary to the conclusion of Howarth (1948).

If condition (a) in the introduction is relaxed so that the boundary condition on T is arbitrary then a relatively simple form for the fundamental equations may still be obtained. Using the method described above and writing

$$\frac{T}{T_1} = 1 + \frac{T_0}{T_1}\left(1 + \frac{\gamma - 1}{2} M_0^2\right) S + \frac{\gamma - 1}{2a_1^2}(U_1^2 - u^2), \tag{2·27}$$

where now S is the temperature function, we find after very little labour that

$$\frac{\partial^3 \psi}{\partial Y^3} - \frac{\partial \psi}{\partial Y}\frac{\partial^2 \psi}{\partial Y \partial z} + \frac{\partial \psi}{\partial z}\frac{\partial^2 \psi}{\partial Y^2} = -V_1 \frac{dV_1}{dz}[1 + S]. \tag{2·28}$$

The energy equation is

$$Jc_p\left(\rho u \frac{\partial T}{\partial x} + \rho v \frac{\partial T}{\partial y}\right) - u\frac{dp}{dx} = \frac{\partial}{\partial y}\left(Jc_p \mu \frac{\partial T}{\partial y}\right) + \mu\left(\frac{\partial u}{\partial y}\right)^2, \tag{2·29}$$

and this may also be reduced to

$$\frac{\partial \psi}{\partial Y}\frac{\partial S}{\partial z} - \frac{\partial \psi}{\partial z}\frac{\partial S}{\partial Y} = \frac{\partial^2 S}{\partial Y^2}. \tag{2·30}$$

The boundary condition on S at $Y = 0$ is arbitrary, but as $Y \to \infty$, $S \to 0$, since $T \to T_1$.

3. THE MOMENTUM INTEGRAL AND THE KÁRMÁN-POHLHAUSEN APPROXIMATION

If in the incompressible plane the thickness of the boundary layer is δ and

$$\delta_1 = \int_0^\delta \left(1 - \frac{\psi_Y}{V_1}\right) dY, \tag{3·1}$$

$$\vartheta = \int_0^\delta \left(1 - \frac{\psi_Y}{V_1}\right)\frac{\psi_Y}{V_1} dY, \tag{3·2}$$

then the momentum integral is

$$V_1^2 \frac{d\vartheta}{dz} + V_1 \frac{dV_1}{dz}(2\vartheta + \delta_1) = (\psi_{YY})_{Y=0}. \tag{3·3}$$

Using the results of the previous section this formula may be taken over immediately into the compressible plane.

Write

$$\delta_1' = \int_0^{\delta'} \left(1 - \frac{u}{U_1}\right) \frac{\rho\, dy}{\rho_1}, \tag{3·4}$$

$$\vartheta' = \int_0^{\delta'} \left(1 - \frac{u}{U_1}\right) \frac{\rho u\, dy}{\rho_1 U_1}, \tag{3·5}$$

where δ' is the thickness of the compressible boundary layer. Then

$$\sqrt{\nu_0}\,\delta_1 = \delta_1' \frac{\rho_1 a_1}{\rho_0 a_0} \tag{3·6}$$

and

$$V_1^2 \vartheta = U_1^2 \vartheta' \frac{a_0 \rho_1}{a_1 \rho_0 \sqrt{\nu_0}}. \tag{3·7}$$

Hence

$$\frac{d}{dz}(V_1^2 \vartheta) = \left(\frac{a_0}{a_1}\right)^4 \frac{1}{\sqrt{\nu_0}} \left\{ U_1^2 \frac{d\vartheta'}{dx} + \vartheta' U_1 \frac{dU_1}{dx} \left[2 + \frac{\gamma - 3}{2} M_1^2 \right] \right\} \tag{3·8}$$

and

$$\delta_1 V_1 \frac{dV_1}{dz} = \delta_1' U_1 \frac{dU_1}{dz} \left(\frac{a_0}{a_1}\right)^4 \frac{1 + \frac{\gamma - 1}{2} M_1^2}{\sqrt{\nu_0}}. \tag{3·9}$$

Hence the momentum integral becomes

$$U_1^2 \frac{d\vartheta'}{dx} + U_1 \frac{dU_1}{dx} \left\{ \vartheta' \left(2 + \frac{\gamma - 3}{2a_1^2} U_1^2 \right) + \delta_1' \left(1 + \frac{\gamma - 1}{2} M_1^2 \right) \right\} = \frac{1}{\rho_1} \left[\mu \frac{\partial u}{\partial y} \right]_{y=0}. \tag{3·10}$$

Howarth (1948) has obtained a similar result, and equation (3·10) may be shown to be identical with his, provided we adopt his definitions of δ_1' and ϑ'.

From the momentum integral (3·10) we may deduce the fundamental equation of the Kármán-Pohlhausen approximation, but this may also be obtained from the corresponding equation of incompressible flow.

If we write

$$\lambda = \delta^2 \frac{dV_1}{dz}, \tag{3·11}$$

then Kármán-Pohlhausen (1921) have shown that

$$\left(\frac{\partial^2 \psi}{\partial Y^2}\right)_{Y=0} = \frac{V_1}{\delta}(2 + \tfrac{1}{6}\lambda), \tag{3·12}$$

and

$$\frac{d\lambda}{dz} = \frac{dV_1/dz}{V_1} g(\lambda) + \frac{d^2V_1/dz^2}{dV_1/dz} (\lambda + \lambda^2 h(\lambda)), \tag{3·13}$$

where

$$g(\lambda) = \frac{15120 - 2784\lambda + 79\lambda^2 + \frac{5}{3}\lambda^3}{(12 - \lambda)(37 + \frac{25}{12}\lambda)}, \tag{3·14}$$

and

$$h(\lambda) = \frac{8 + \frac{5}{3}\lambda}{(12 - \lambda)(37 + \frac{25}{12}\lambda)}. \tag{3·15}$$

Transferring now to the compressible plane, since

$$\frac{1}{V_1}\frac{dV_1}{dx} = \frac{1}{U_1}\frac{dU_1}{dx}\left(1+\frac{\gamma-1}{2}M_1^2\right), \tag{3·16}$$

and

$$\frac{d}{dx}\left(\log\frac{dV_1}{dz}\right) = \frac{d^2U_1/dx^2}{dU_1/dx} + \frac{dU_1/dx}{U_1}(3\gamma-2)\,M_1^2, \tag{3·17}$$

the equation for λ becomes

$$\frac{d\lambda}{dx} = \frac{d^2U_1/dx^2}{dU_1/dx}(\lambda+\lambda^2h(\lambda)) + \frac{dU_1/dx}{U_1}\left[g(\lambda)\left[1+\frac{\gamma-1}{2}M_1^2\right] + (3\gamma-2)\,M_1^2(\lambda^2h(\lambda)+\lambda)\right], \tag{3·18}$$

in which

$$\lambda = \delta^2\frac{dU_1}{dx}\left[1+\frac{\gamma-1}{2}M_1^2\right]\left(\frac{a_0}{a_1}\right)^{(4\gamma-2)/(\gamma-1)}. \tag{3·19}$$

Separation still occurs when $\lambda = -12$ from (3·12).

This result (3·18) may be compared with Howarth's who obtains

$$\frac{d\lambda}{dx} = \frac{d^2U_1/dx^2}{dU_1/dx}(\lambda+\lambda^2h(\lambda)) + \frac{dU_1/dx}{U_1}\left[g(\lambda)+\gamma M_1^2\{\lambda+\lambda^2h(\lambda)\}+\frac{\gamma-1}{2}M_1^2 j(\lambda)\right], \tag{3·20}$$

where $j(\lambda)$ is a function of λ equal to

$$\frac{15120-1008\lambda+63\lambda^2}{(12-\lambda)(37+\frac{25}{12}\lambda)}. \tag{3·21}$$

However, on comparing with the corresponding formulae for $y(\lambda)$ and $h(\lambda)$ it will be seen that there is a linear relation between j, g and $\lambda^2h(\lambda)+\lambda$, namely,

$$j(\lambda) = g(\lambda)+4(\lambda^2h(\lambda)+\lambda). \tag{3·22}$$

4. PROBLEMS IN THE COMPRESSIBLE PLANE, FOR WHICH SOLUTIONS ARE KNOWN

In this section the results of § 2 will be applied to solve problems in the compressible plane, by means of known solutions in the incompressible plane.

(i) *The general 'similar' flow*

The main stream velocities in the incompressible plane are given by

$$V_1 = \beta z^m, \tag{4·1}$$

where m is a given parameter. Then if a_0 is the velocity of sound when $V_1 = 0$,

$$\beta^2z^{2m} = \frac{U_1^2a_0^2}{a_0^2-\frac{\gamma-1}{2}U_1^2}. \tag{4·2}$$

Therefore

$$U_1^2 = \frac{\beta^2a_0^2z^{2m}}{a_0^2+\frac{\gamma-1}{2}\beta^2z^{2m}}, \tag{4·3}$$

$$a_1^2 = \frac{a_0^4}{a_0^2 + \frac{\gamma-1}{2}\beta^2 z^{2m}}, \tag{4·4}$$

and
$$dx = dz\left[1 + \frac{\gamma-1}{2a_0^2}\beta^2 z^{2m}\right]^{(3\gamma-1)/[2(\gamma-1)]}. \tag{4·5}$$

If $2m = 1$, this equation may be integrated exactly to yield

$$x = \frac{4a_0^2}{5\gamma-3}\left[\left(1 + \frac{\gamma-1}{2}\frac{\beta^2 z}{a_0^2}\right)^{(5\gamma-3)/[2(\gamma-1)]} - 1\right], \tag{4·6}$$

and hence
$$U_1 = a_0\sqrt{\frac{2}{\gamma-1}}\,\frac{\left[\left(1+\frac{5\gamma-3}{4}\frac{\beta^2 x}{a_0^2}\right)^{(2\gamma-2)/(5\gamma-3)} - 1\right]^{\frac{1}{2}}}{\left(1+\frac{5\gamma-3}{4}\frac{\beta^2 x}{a_0^2}\right)^{(\gamma-1)/(5\gamma-3)}}. \tag{4·7}$$

If $\gamma = 1·4$ this reduces to

$$U_1 = a_0\sqrt{5}\left[\left(1+\frac{\beta^2 x}{a_0^2}\right)^{\frac{1}{5}} - 1\right]^{\frac{1}{2}} \Big/ \left(1+\frac{\beta^2 x}{a_0^2}\right)^{\frac{1}{10}} \tag{4·8}$$

$$= \beta\sqrt{x}\left[1 - \frac{3\beta^2 x}{10a_0^2} + \frac{7(\beta^2 x)^2}{40a_0^4} - \dots\right]. \tag{4·9}$$

For general values of m, however, such exact integration is not possible, but for given values of γ and m a graph of U_1/a_0 against $\beta x^m/a_0$ may readily be obtained by numerical integration. The first few terms of the series for U_1/a_0 as a function of $\beta x^m/a_0$ may also be readily evaluated, and we find, if $\gamma = 1·4$,

$$z = x\left[1 - \frac{4\beta^2 x^{2m}}{5a_0^2(2m+1)} + \left(\frac{16}{(2m+1)^2} - \frac{6}{4m+1}\right)\frac{\beta^4 x^{4m}}{25a_0^4} - \dots\right], \tag{4·10}$$

and
$$U_1 = \beta x^m\left[1 - \frac{\beta^2 x^{2m}(10m+1)}{10(2m+1)} + \dots\right]. \tag{4·11}$$

The skin friction may be obtained from (2·26) since $(\psi_{YY})_{Y=0}$ is proportional to $z^{\frac{1}{2}(3m-1)}$.

In this way we obtain a family of main-stream velocities which all have similar flows in the boundary layer. Graphs of these velocities for $m = -1, 0, 0·5$ and 1, together with the corresponding 'similar' velocities in the incompressible plane, are given in figure 1. If we relax the condition that the boundary is thermally insulating then it is still possible to obtain similar solutions, provided that the temperature is constant on the boundary. In this problem we shall use equations (2·28) and (2·30).

Let us suppose $V_1 = Ax^m$ and write

$$\psi = \left(\frac{2zV_1}{m+1}\right)^{\frac{1}{2}} f(\eta), \tag{4·12}$$

where
$$\eta = Y\left(\frac{(m+1)V_1}{2z}\right)^{\frac{1}{2}}. \tag{4·13}$$

Then from (2·28), f satisfies $f''' + ff'' = \beta(f'^2 - 1 - S)$, (4·14) where $\beta = 2m/m+1$, and from (2·30) S satisfies

$$S''+fS' = 0. \tag{4·15}$$

The boundary conditions are that $S = S_0, f = f' = 0$ when $\eta = 0$, and $f' \to 1$, $S \to 0$ as $\eta \to \infty$. In a similar way we may investigate the flow which corresponds to the uniformly retarded main-stream velocity, etc., and the method discussed above is adequate to deal with such problems. A question of more immediate interest is that of determining the incompressible flow corresponding to a given main-stream velocity in the compressible plane. This will be determined below for flow near a stagnation point.

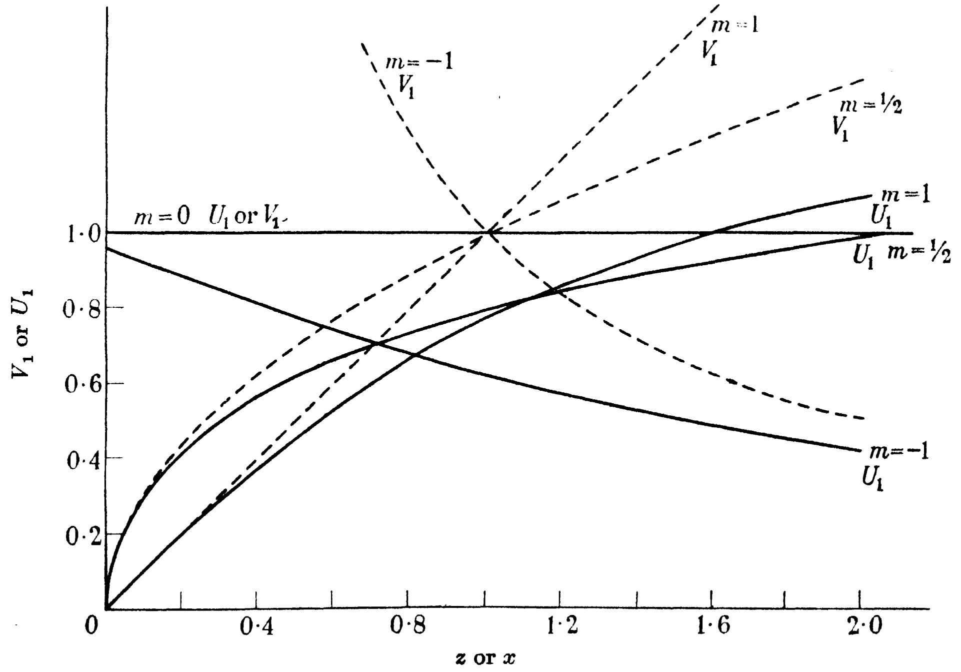

FIGURE 1. 'Similar' solutions of compressible flow. ---- Similar incompressible flow; —— corresponding compressible flow.

(2) *Flow near a stagnation point*

For this type of flow
$$U_1 = a_0\beta x, \tag{4·16}$$
and therefore taking $\gamma = 1·4$
$$a_1^2 = a_0^2[1-0·2\beta^2x^2], \tag{4·17}$$
so that
$$dz = dx[1-0·2\beta^2x^2]^4. \tag{4·18}$$
Hence
$$z = x-0·267\beta^2x^3+0·048\beta^4x^5-\dots, \tag{4·19}$$
so that
$$x = z+0·267\beta^2z^3+0·165\beta^4z^5+\dots \tag{4·20}$$
and
$$\frac{V_1}{a_0} = \frac{\beta x}{(1-0·2\beta^2x^2)^{\frac{1}{2}}} = \beta z+0·367\beta^3z^3+0·260\beta^5z^5\dots. \tag{4·21}$$

The corresponding incompressible flow is therefore of the type arising from a symmetrical obstacle. Such flows have been studied already by Howarth (1934), who obtained the first three terms of the expansion of ψ as a power series in z. The series for V_1 in (4·21) is a close approximation to V_1 provided that $\beta z < 0{\cdot}6$. This restriction is not serious in many problems, as for larger values of βz shock waves occur in the fluid. A graph of V_1 corresponding to $U_1 = a_0\beta x$ is given in figure 2. From the graph we see that $V_1 \to \infty$ as $\beta z \to 0{\cdot}909$ (precisely $\beta x \to \sqrt{5}$), so that the series expansion (4·21) will break down in the neighbourhood of $\beta z = 0{\cdot}9$. The value of the skin friction may be obtained at once from Howarth's (1934) results. He found that if the velocity in the main stream were

$$V_1 = \alpha_1 z + \alpha_3 z^3 + \alpha_5 z^5, \tag{4·22}$$

and if

$$\eta = Y(\alpha_1)^{\frac{1}{2}},$$

then

$$\psi = (\alpha_1)^{\frac{1}{2}}\left[\alpha_1 z f_1(\eta) + 4\alpha_3 z^3 g_3(\eta) + 6z^5\left(\alpha_5 g_5(\eta) + \frac{\alpha_3}{\alpha_1} h_5(\eta)\right)\right] + \dots. \tag{4·23}$$

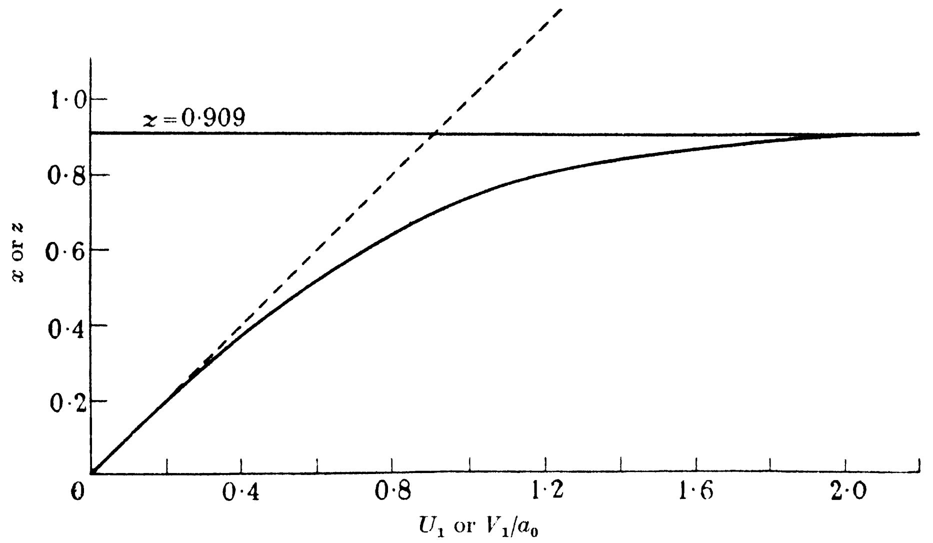

FIGURE 2. Flow near a stagnation point. ---- compressible flow $U_1 = x$; —— corresponding incompressible flow.

The functions f_1, g_3, g_5, h_5 have been tabulated, and hence we can write down the skin friction due to the velocity distribution (4·21)

$$\left(\frac{\partial^2\psi}{\partial Y^2}\right)_{Y=0} = \beta^{\frac{1}{2}}[1{\cdot}233\beta z + 1{\cdot}064(\beta z)^3 + 1{\cdot}091(\beta z)^5 + \dots]. \tag{4·24}$$

Hence

$$\left[\mu\frac{\partial u}{\partial y}\right]_{y=0} = \rho_0\left(\frac{a_1}{a_0}\right)^9 \nu_0^{\frac{1}{2}}\left[\frac{\partial^3\psi}{\partial Y^3}\right]_{Y=0}$$

$$= \sqrt{(\beta\nu_0)}\,[1{\cdot}233\beta x - 0{\cdot}374\beta^3x^3 + 0{\cdot}025\beta^5x^5 - \dots]. \tag{4·25}$$

If further terms are required it will be necessary to carry out the numerical integration of certain differential equations. Further details may be obtained from Howarth's paper (1934).

From these two flows we can see that if the velocity in the boundary layer of an incompressible fluid, arising from a general main-stream velocity distribution, is known, then we can deduce the velocity in the boundary layer of a compressible fluid for a given main-stream velocity distribution, provided that the assumptions set out in the introduction are valid. Hence only those functions used in the incompressible problem are required for the compressible one. In Howarth's paper (1948) on compressible boundary layers he introduced extra functions to specify the velocity in the boundary layer, but these functions are, in fact, related to those already known.

As an illustration, consider his discussion on flow near a stagnation point. He introduced a new function $f_3(\eta)$ (see equations (84) to (87) of his paper) satisfying

$$4f_1'f_3' - 3f_1''f_3 - f_1f_3'' = \frac{\gamma-1}{2}(1-f_1'^2) - \frac{\gamma}{2}f_1f_1''+f_3''', \tag{4·26}$$

where the dashes denote differentiation with respect to η,

$$f_1'^2 - f_1f_1'' = 1+f_1''', \tag{4·27}$$

and $$f_1(0) = f_3(0) = f_1'(0) = f_3'(0) = f_1'(\infty)-1 = f_3'(\infty) = 0. \tag{4·28}$$

Now f_1' is a complementary function of equation (4·26). Hence write

$$f_3 = \alpha g_3 + \beta f_1 + \delta\eta f_1', \tag{4·29}$$

where α, β, δ are constants and g_3 is the solution of

$$4f_1'g_3' - 3f_1''g_3 - f_1g'' = 1+g_3''', \tag{4·30}$$

such that $$g_3(0) = g_3'(0) = g_3'(\infty)-\tfrac{1}{4} = 0. \tag{4·31}$$

Substituting in equation (4·26), we find that

$$\alpha = \tfrac{2}{3}(3\gamma-2), \quad \beta = \tfrac{1}{12}, \quad \delta = \frac{1-2\gamma}{4}. \tag{4·32}$$

Now the solution of (4·30) is well known, having been worked out by Howarth (1934).

Hence $$f_3''(0) = \tfrac{2}{3}(3\gamma-2)(0{\cdot}7246)+(\tfrac{7}{12}-\gamma)(1{\cdot}2326) = 0{\cdot}0561 \quad \text{if} \quad \gamma = 1{\cdot}4, \tag{4·33}$$

in agreement with Howarth (1948). Similar formulae may be worked out for the other functions he introduced.

The use of f_1 and $\eta f_1'$ in (4·29) is not fortuitous, for f_1 corresponds to multiplying ψ by a function of x and $\eta f_1'$ corresponds to a similar transformation of Y.

The above discussion, however, brings out a difficulty inherent in the method we have developed, for the contribution to $f_3''(0)$ arising from the transformation and from the incompressible solution are both large and approximately equal. This suggests that the solution for V_1 will consist of a slowly converging series which will be difficult to handle for large Mach numbers. For certain problems, such as the flow near a stagnation point, the predominant part of this series is due to the expansion of $(p/p_0)^{\frac{1}{2}}$ (Howarth 1948), but in others, such as the flow between converging plane walls, this is not so (Stewartson 1949), and using either method so far developed the series for the skin friction is slowly convergent. The advantage of the method we have worked out in this paper is more apparent in problems where the main-stream velocity is known only in the form of an infinite series or as a graph, for then V_1 and z may easily be evaluated as a series or graphically, and the known methods for such incompressible flow problems are then directly applicable.

Finally, to complete this paper, a discussion on the application of certain approximate methods to these compressible flow problems, will be given. Since the Kármán-Pohlhausen method is usually sufficiently accurate for the accelerated flow of an incompressible fluid, it may be used, where possible, in similar compressible problems. If the flow is being retarded, however, the method is known to overestimate the drag. There is, however, another method available and we shall discuss both of them below.

5. FLOW AGAINST A PRESSURE GRADIENT

This section is concerned with the flow in the boundary layer arising from a retarded velocity in the main stream, discussing in particular the skin friction and the point of separation (x_s). Of the approximate methods developed so far to deal with this problem when the fluid is incompressible those of Kármán-Pohlhausen and Howarth (1938) are the most important. Both these methods involve a differential equation relating the velocity in the main stream with some function of the skin friction. Kármán-Pohlhausen's method has been compared with the exact solution of the problem of determining the skin friction caused by a uniformly retarded velocity in the main stream, and it has been found that the method overestimates the position of separation by about 30 %. This error is serious and is not accidental, for in other problems where separation occurs some distance after the pressure minimum there is a similar overestimation. Since the flow of a compressible fluid is equivalent to that of an incompressible one with an exaggerated pressure gradient, we can expect that there is a similar overestimation in these problems.

The method developed by Howarth is based on his series solution of the flow in the boundary layer due to a uniformly retarded main-stream velocity, and consequently, since, *a fortiori*, it gives the correct answer for this problem (in which the Kármán-Pohlhausen gives an overestimation of 30 %) we can expect that it will also be more accurate for similar problems. It has been compared with known solutions to several problems such as that of Schubauer's ellipse, and the flow with zero skin friction.

In all these problems the error is considerably less than that of any other known approximation, and so it is reasonable to expect that it will be a closer approximation in the compressible flow.

In this section both of these methods will be applied to solve the problem of flow in the boundary layer due to a uniformly retarded main stream.

(*a*) *Kármán-Pohlhausen's method*

Howarth (1948) has already carried out calculations to determine the point of separation (x_s) when the main-stream velocity is $U_1 = b_0 - b_1 x$, and so we shall content ourselves with making some comments on the behaviour of x_s at large Mach numbers, which, incidentally, will enable us to estimate the accuracy of the method. Making an affine transformation of x the main-stream velocity may be taken as $U_1 = U_0(1-x)$ and, from § 3, the equation for λ is

$$\frac{d\lambda}{dx} = \frac{1}{U_1}\frac{dU_1}{dx}\left[g(\lambda)\left\{1+\frac{\gamma-1}{2}M_1^2\right\}+(3\gamma-2)\,M_1^2\{\lambda^2h(\lambda)+\lambda\}\right]. \tag{5·1}$$

This equation may be transformed into a first-order differential equation for λ in terms of M_1 and γ only, i.e.

$$M_1\frac{d\lambda}{dM_1} = g(\lambda)+\frac{(3\gamma-2)\,M_1^2}{1+\frac{\gamma-1}{2}M_1^2}[\lambda^2h(\lambda)+\lambda], \tag{5·2}$$

with initial condition $M_1 = U_0/a_0 = M_0$ when $\lambda = 0$. Separation occurs when $\lambda = -12$. There are certain features of the equation for sufficiently high Mach number which are of interest.

If separation is to occur at all then $M_1(d\lambda/dM_1)$ must be positive when $\lambda \geqslant -12$. Since the value of λ for which the right-hand side of (5·2) is most likely to be zero is -12, we have, setting $\lambda = -12$ there,

$$198 > \frac{18(3\gamma-2)\,M_1^2}{1+\frac{\gamma-1}{2}M_1^2}, \tag{5·3}$$

or

$$22 > M_1^2(7-5\gamma). \tag{5·4}$$

Clearly separation must take place eventually, since for sufficiently large x, the main-stream velocity is reversed in direction. Hence if $\gamma < 1·4$ equation (5·4) must be regarded as an upper bound for the Mach number at separation (M_s), and hence x_s has a positive non-zero lower bound.

In fact

$$x_s > 1-\sqrt{\left[\frac{11}{(3\gamma-2)}\left(\frac{\gamma-1}{2}+\frac{1}{M_0^2}\right)\right]}, \tag{5·5}$$

and therefore letting $M_0 \to \infty$

$$x_s > 1-\sqrt{\frac{11(\gamma-1)}{2(3\gamma-2)}}. \tag{5·6}$$

If $\gamma > 1·4$, no matter how M_1 behaves between $x = 0$, and $x = x_s$, $\log M_1/M_0$ must be finite and therefore $x_s = O(1/M_0^2)$ as $M_0 \to \infty$. The critical value of γ is 1·4, and as this value is commonly assumed for practical problems, we shall discuss it in more detail. With this value of γ equation (5·2) takes on the form

$$(12-\lambda)\left(37+\frac{25\lambda}{12}\right)M_1(1+\tfrac{1}{5}M_1^2)\frac{d\lambda}{dM_1}$$
$$= 15120-2784\lambda+79\lambda^2+\tfrac{5}{3}\lambda^3+\tfrac{7}{12}M_1^2[12+\lambda]^2(36-\lambda). \tag{5·7}$$

If the coefficient of M_1^2 on the right-hand side of (5·7) did not vanish at $\lambda = -12$, there would be no difficulty in carrying out the integration and we should find that

$\log M_s/M_0$ would be $O(1)$. Due to this zero there is a new term and on integrating near $\lambda = -12$ we get

$$\log\frac{M_s}{M_0} = -\frac{\pi M_s}{10\sqrt{(77)}} + O(1), \tag{5·8}$$

and hence
$$x_s = \frac{1}{3(10\log M_0)^2}[1+o(1)] \quad \text{as} \quad M_0 \to \infty. \tag{5·9}$$

Collecting up these results the conclusions are that the point of separation x_s tends to zero as $M_0 \to \infty$ provided that $\gamma \geqslant 1{\cdot}4$, while if $\gamma < 1{\cdot}4$ this point has a non-zero lower bound, no matter how large M_0 may be.

(*b*) *Howarth's method* (1938)

Howarth began by computing the velocity field in the boundary layer due to a linear main-stream velocity $U_1^* = b_0 - b_1 x^*$, and tabulated the values of the skin friction and the momentum integral as functions of $\xi = b_1 x^*/b_0$. He then compared U_1^* with V_1, the main-stream velocity under discussion, and determined the value of ξ corresponding to z (the independent variable of the V_1 flow). The principal assumption he made was that the momentum integral was continuous and, finally, he found that

$$\frac{d\xi}{dz} = -\frac{1}{V_1}\frac{dV_1}{dz}(1-\xi) + \frac{\chi}{2d\chi/d\xi}\,\frac{d^2V_1/dz^2}{dV_1/dz}, \tag{5·10}$$

where χ was a known function of ξ and $\chi/d\chi/d\xi$ was tabulated. Moreover, a table and a graph of

$$\frac{\left(\dfrac{\partial u}{\partial y}\right)_0}{V_1\left(-\dfrac{dV_1}{dz}\right)^{\frac{1}{2}}}, \tag{5·11}$$

a dimensionless function of ξ, was given in his paper. Hence having deduced ξ in terms of x from the first-order differential equation (5·10), the skin friction may easily be deduced from (5·11). Separation occurs when $\xi = 0{\cdot}120$.

Since it is possible to reduce any problem of compressible flow, satisfying the conditions of § 1, to a problem in incompressible flow, it follows that we may reverse the process and adapt this method to the solution of appropriate compressible flow problems.

Now
$$V_1 = a_0 M_1, \tag{5·12}$$

$$\frac{dV_1}{V_1} = \frac{dU_1}{U_1}\left(1 + \frac{\gamma-1}{2}M_1^2\right), \tag{5·13}$$

and
$$d\left(\log\frac{dV_1}{dz}\right) = d\left(\log\frac{dU_1}{dx}\right) + (3\gamma-2)\,M_1^2\,d(\log U_1), \tag{5·14}$$

so that the differential equation becomes

$$\frac{d\xi}{dx} = \frac{\chi\, d\xi}{2\,d\chi}\,\frac{d^2U_1/dx^2}{dU_1/dx} - \frac{dU_1/dx}{U_1}\left[(1-\xi)\left(1+\frac{\gamma-1}{2}M_1^2\right) - \frac{(3\gamma-2)}{2}\chi\frac{d\xi}{d\chi}M_1^2\right]. \tag{5·15}$$

Hence Howarth's method is now applicable to compressible boundary layers with a retarded main stream. As an example, let us apply it to the problem of flow against a linear pressure gradient, i.e. take $U_1 = U_0(1-x)$.

Then, after a little reduction, we get

$$-M_1\frac{d\xi}{dM_1} = 1-\xi-\frac{(3\gamma-2)\chi}{2d\chi/d\xi}\frac{M_1^2}{1+\frac{\gamma-1}{2}M_1^2}, \tag{5·16}$$

and the integration of this first-order differential equation may easily be carried out. The initial condition is that $M = M_0$ when $\xi = 0$ and separation occurs when $\xi = 0·120$. Equation (5·16) is closely analogous to the corresponding differential equation obtained in Kármán-Pohlhausen's method. If the skin friction is required we know that

$$\mu\frac{\partial u}{\partial y} = \mu_0\frac{p_1 a_1^2}{p_0 a_0^2\sqrt{\nu_0}}\frac{\partial^2\psi}{\partial Y^2} \tag{5·17}$$

from (2·12), and hence

$$\frac{a_1\left(\mu\frac{\partial u}{\partial y}\right)_0}{a_0\rho_0 U_1\left[-\frac{\nu_0 p_1}{p_0}\frac{dU_1}{dx}\left(1+\frac{\gamma-1}{2}M_0^2\right)\right]^{\frac{1}{2}}} \tag{5·18}$$

is the function plotted in figure 8 of Howarth's paper (1938).

The skin friction may now be easily evaluated. In table 1 the positions of separation point for various values of M_0 are given. These may be compared with the corresponding results of the Kármán-Pohlhausen method (Howarth 1948), and it will be seen that the latter method asserts that the point of separation occurs considerably later than does Howarth's method. In fact for $M_0 = 10$ it gives separation at $x_s = 0·052$ and $M_s = 5·5$, more than twice as far from the origin as our value. Now from comparisons with known solutions it appears that Howarth's method would overestimate the skin friction if d^2U_1/dz^2 were positive. Hence since this is true here, Howarth's method should overestimate the point of separation and is therefore a closer approximation. We shall show below that this overestimation of the point of separation may be demonstrated in the limiting problem when $M_0 \to \infty$.

TABLE 1

M_0	0	1	2	3	4	6	8	10
x_s	0·120	0·110	0·096	0·077	0·062	0·044	0·032	0·024
M_s	0	0·87	1·69	2·48	3·18	4·51	5·76	6·96

To prove that as $M_0 \to \infty$ this table is more accurate than Pohlhausen's, we proceed as follows. As with the latter method we can determine the condition on γ for the point of separation to tend to the leading edge of the plate as the Mach number M_0 tends to infinity. This condition is that the right-hand side of equation (5·16) should never vanish. Again, as before, the most probable place for this to occur is when $\xi = 0·120$, and hence

$$0·880 > \frac{3\gamma-2}{2}(0·151)\frac{M_1^2}{1+\frac{\gamma-1}{2}M_1^2}, \tag{5·19}$$

or $$0{\cdot}880 > M_1^2(0{\cdot}578 - 0{\cdot}427\gamma), \tag{5·20}$$

so that if the point of separation is to be as required,

$$\gamma \geqslant 1{\cdot}35. \tag{5·21}$$

The equality sign may be dealt with as in the Pohlhausen method, and the critical value compared with 1·4 obtained there. If $\gamma < 1{\cdot}35$, Howarth's method asserts that the point of separation has a positive non-zero lower bound. If now we can show from the differential equation that the critical value of γ is less than 1·35, then we have proved the assertion made above. This may be done exactly, as follows:

(*c*) *An exact solution with* $M_0 \gg 1$

If we suppose that M_0 is very large and $t = xM_0^2$, then if t is large, but definite so that t/M_0^2 is small, then

$$a_1^2 = a_0^2(1 + (\gamma - 1)\, t), \tag{5·22}$$

and $$U_1 = a_0 M_0 + O\left(\frac{1}{M_0}\right). \tag{5·23}$$

Hence $$M_0^2 z = \int_0^t [1 + (\gamma - 1)\, t]^{(3\gamma-1)/[2(\gamma-1)]}\, dt_1, \tag{5·24}$$

so that $$z \sim [1 + (\gamma - 1)\, t]^{(5\gamma-3)/[2(\gamma-1)]}. \tag{5·25}$$

(In equation (5·25), $f \sim g$ is to be interpreted as

$$f = Ag[1 + o(1)] \quad \text{for large } t, \tag{5·26}$$

where A is a positive constant.) Hence

$$V_1 = a_0 M_1 \sim z^{-(\gamma-1)/(5\gamma-3)}. \tag{5·27}$$

Now the solution of this problem is known, having been studied by Hartree (1937). He found that if $V_1 = Az^{-m}$ then

$$(\psi_{YY})_{Y=0} = z^{-\frac{1}{2}(3m+1)}[f(m)], \tag{5·28}$$

where $f(m)$ is some function of m.

Consider the application of this result to our problem. If $(\psi_{YY})_{Y=0} > 0$ for large t, then, since V_1 is a strictly decreasing function so that $(\psi_{YY})_{Y=0}$ is also strictly decreasing. $(\psi_{YY})_{Y=0} > 0$ for all finite t, and hence separation occurs for some infinite value of t. Conversely, if $(\psi_{YY})_{Y=0} < 0$ for large t, then separation has occurred for some finite t. Actually the whole theory breaks down at the separation point and really no deduction is possible directly, but we can argue as follows. Suppose separation does not occur for some finite t and $(\psi_{YY})_{Y=0} < 0$ for large t. Then since $(\psi_{YY})_{Y=0} > 0$ when $t = 0$ there is a point at which $(\psi_{YY})_{Y=0} = 0$, i.e. a point of separation, and our hypothesis breaks down. From (5·28) the critical value of m is given by

$$f(m) = 0, \tag{5·29}$$

or $$m = 0{\cdot}0904, \tag{5·30}$$

according to Hartree (1937).

In terms of γ the critical value is

$$\gamma = 1{\cdot}33. \tag{5·31}$$

Hence if $\gamma > 1{\cdot}33$ the point of separation occurs for a finite $t = t_s$, i.e. when $x_s = t_s/M_0^2$, and approaches the origin as $M_0 \to \infty$. If $\gamma < 1{\cdot}33$ the point of separation occurs at an infinite value of t. Hence from the conclusions of (*a*) and (*b*), in terms of x it probably occurs at a non-zero distance from the leading edge.

The critical values of γ determined in the first two parts of § 5 were 1·4 and 1·35 respectively. Hence both methods discussed above overestimate the point of separation for large M_0, and in view of the discrepancy between their estimation of this point, the Kármán-Pohlhausen method must be discarded for retarded flows.

In conclusion, I should like to thank Dr L. Howarth most sincerely for his help and guidance during the writing of this paper.

REFERENCES

Crocco, L. 1946 *Monogr. Sci. Aeronaut.* no. 3.
Hartree, D. R. 1937 *Proc. Camb. Phil. Soc.* **33**, 223.
Howarth, L. 1934 *Rep. Memor. Aero. Res. Comm., Lond.*, no. 1632.
Howarth, L. 1938 *Proc. Roy. Soc.* A, **164**, 547.
Howarth, L. 1948 *Proc. Roy. Soc.* A, **194**, 16.
Pohlhausen, K. 1921 *Z. angew. Math.* **1**, 257.
Stewartson, K. 1949 *Rep. Aero. Res. Comm.* (to be published).

The sedimentation and diffusion of small particles

BY C. N. DAVIES
Member of Scientific Staff, Medical Research Council,
London School of Hygiene and Tropical Medicine

(*Communicated by H. S. W. Massey, F.R.S.—Received* 15 *July* 1949)

The concentration of particles which settle and diffuse while in suspension in a fluid is given as a function of time and position for a dilute suspension which is initially uniformly dispersed in a wide vessel. It is assumed that all particles which strike the surfaces of the container will be absorbed. Solutions are obtained for a liquid with a free surface and also for a gas or liquid which entirely fills the space between two horizontal planes. The solutions occur as eigenfunction expansions and in integral form and numerical results are given for various circumstances.

1. THE DIFFERENTIAL EQUATION

Consider a fluid containing a suspension of small particles whose sedimentation velocity is v and whose diffusion constant is Δ. These can be taken as average values for all orientations if the shape of the particles does not depart too much from the spherical (Davies 1947). Then by Einstein's relation,

$$\Delta = kT/f, \tag{1}$$

and

$$v = (m-m')g/f, \tag{2}$$

where k is Boltzmann's constant, T the absolute temperature, m the mass of the particle, m' the mass of fluid displaced and g the acceleration due to gravity or centrifuging. f represents the fluid resistance to translation at unit velocity, which is equal to $6\pi a\eta/F$ for small spheres, a being the radius, η the viscosity of the fluid and F the slip factor in gases.

Suppose A and B are two horizontal planes with co-ordinates X and $X+\delta X$, A being above B, and that the concentrations of particles at these levels are C and $C+\delta C$ respectively. In unit time vC particles fall into the zone AB across unit area of A and $v(C+\delta C)$ fall out of the zone across unit area of B. The net gain of the element δX due to sedimentation is thus $-v\dfrac{\partial C}{\partial X}\delta X$. In the same time $-\Delta\dfrac{\partial C}{\partial X}$ particles diffuse into the element across A and $-\Delta\left(\dfrac{\partial C}{\partial X}+\dfrac{\partial^2 C}{\partial X^2}\delta X\right)$ diffuse out across B. The net gain by diffusion is therefore $\Delta\dfrac{\partial^2 C}{\partial X^2}\delta X$. In the limit, the rate of increase of concentration at a point X in the suspension is given by

$$\frac{\partial C}{\partial T}=\Delta\frac{\partial^2 C}{\partial X^2}-v\frac{\partial C}{\partial X}. \tag{3}$$

If the number of particles in suspension remains constant, a steady state ensues when $\partial C/\partial T=0$, and equation (3) integrates to

$$\frac{C_1}{C_2}=\exp\{v(X_1-X_2)/\Delta\}=\exp\{(m-m')g(X_1-X_2)/kT\}. \tag{4}$$

Under these conditions equation (4) has been checked experimentally, notably by Perrin (1916).

2. THE BOUNDARY CONDITIONS

A solution of equation (3) during the transient state has been obtained by Mason & Weaver (1924), who assumed for the boundary conditions that no particles crossed the planes $X=0$ and $X=l$, these being the upper and lower surfaces of a liquid of depth l. The total number of particles in suspension was therefore constant. This assumption is reasonable in the case of many colloidal solutions in which the particles are protected by an electrical double layer and no not adhere to one another or to the surfaces of the container, nor do they adsorb at the upper surface of the liquid to an appreciable extent.

Other cases may arise, however, for example, with dust or virus particles, in which contact results in adhesion, just as Smoluchowski assumed in his theory of rapid coagulation. After a sufficient time a cloud of such particles will completely disappear from the system by elimination at the walls. This is the type of problem which is now studied.

In a liquid suspension with a free surface at the top the condition of zero adsorption at $X=0$ is retained. For a liquid which completely fills the container, or for a gas, the condition is different, since all particles diffusing to the upper surface will be adsorbed; the concentration at the upper surface, like that at the lower, is always zero. It is supposed that the side walls are too remote for diffusion towards them to matter, and the concentration of particles is taken to be small so that mutual coagulation does not occur and hydrodynamic interference is negligible. Particles striking the bottom are eliminated. Initially we will suppose the concentration uniform and equal to C for $0<X<l$. Finally, the concentration will be zero. At all times the concentration is zero at $X = l$, since the floor of the chamber or vessel is a perfect adsorber. In the liquid suspension with a free surface no particles cross the plane $X = 0$, so this condition is the same as in the problem of Mason & Weaver; the number of particles crossing any horizontal plane in the direction of X increasing is equal to $-\left(\Delta \frac{\partial C}{\partial X} - vC\right)$ in unit time; hence, at $X = 0$ this quantity is equal to zero.

We have, therefore, to solve equation (3) for the following initial, final and boundary conditions for the case of a liquid having a free surface

$$\left.\begin{aligned} C &= C_0, & T &= 0 \\ C &= 0, & T &= \infty \end{aligned}\right\} \quad (0<X<l), \tag{5}$$

$$\left.\begin{aligned} \frac{\partial C}{\partial X} &= \frac{vC}{\Delta}, & X &= 0 \\ C &= 0, & X &= l \end{aligned}\right\} \quad (T \geqslant 0). \tag{6}$$

For the gaseous suspension, or the liquid filling the whole container, we have in place of (6)

$$\left.\begin{aligned} C &= 0, & X &= 0 \\ C &= 0, & X &= l \end{aligned}\right\} \quad (T \geqslant 0). \tag{6a}$$

3. DIMENSIONLESS VARIABLES

It is convenient to reduce equation (3) to the dimensionless form by measuring the lengths, X, in units of l and the concentration C, in units equal to C_0. The times, T, are measured in units of l/v, which is the time taken by a particle to fall from the top to the bottom in the absence of diffusion.

Thus we obtain

$$X = xl, \quad T = tl/v, \quad C = cC_0, \tag{7}$$

x, t and c being pure numbers. Equation (3) transforms to

$$\frac{\partial c}{\partial t} = \alpha \frac{\partial^2 c}{\partial x^2} - \frac{\partial c}{\partial x}, \tag{8}$$

where

$$\alpha = \Delta/vl. \tag{9}$$

The solutions of (8) depend only on the dimensionless parameter α which can be evaluated from the physical constants Δ, v and l.

The initial, final and boundary conditions are now

$$\left.\begin{aligned} c &= 1, & t &= 0 \\ c &= 0, & t &= \infty \end{aligned}\right\} \quad (0<x<1), \tag{10}$$

and the boundary conditions for a liquid with a free surface

$$\left.\begin{aligned} \alpha\frac{\partial c}{\partial x} = c, \quad x = 0 \\ c = 0, \quad x = 1 \end{aligned}\right\} \quad (t \geqslant 0), \tag{11}$$

while for the gas or liquid filling the vessel

$$c = 0, \quad x = 0, \quad x = 1 \quad (t \geqslant 0). \tag{11a}$$

4. The form of the solution

If the solution of equation (8) is $c = \xi\tau$, (12)

where ξ is a function of x only and τ a function of t only, we obtain, on substitution in (8),

$$\frac{\tau'}{\tau} = \alpha\frac{\xi''}{\xi} - \frac{\xi'}{\xi}.$$

The left-hand side of this equation is a function of t and the right-hand side a function of x, so that each side must be equal to a quantity independent of x and t, say $-q$. Hence,

$$\tau' = -q\tau \quad \text{or} \quad \tau = \exp(-qt), \tag{13}$$

where q must be positive since c decreases with lapse of time. Also

$$\alpha\xi'' - \xi' + q\xi = 0,$$

which gives

$$\xi = \exp\{x/2\alpha\}\,(C_1 \sin px + C_2 \cos px), \tag{14}$$

where

$$p = \left(\frac{q}{\alpha} - \frac{1}{4\alpha^2}\right)^{\frac{1}{2}},$$

so

$$q = (1 + 4p^2\alpha^2)/4\alpha. \tag{15}$$

Substituting these results in (12) we see

$$c = \sum_p e^{-qt + x/2\alpha}(C_1 \sin px + C_2 \cos px). \tag{16}$$

5. Solution for a liquid with a free surface as an eigenfunction expansion

Applying the conditions (11) we have at $x = 0$

$$\alpha p C_1 - \tfrac{1}{2}C_2 = 0,$$

and at $x = 1$

$$C_1 \sin p + C_2 \cos p = 0,$$

so that

$$C_1/C_2 = -\cot p. \tag{17}$$

Eliminating C_1 and C_2,

$$\alpha p \cos p + \tfrac{1}{2}\sin p = 0,$$

or

$$\frac{\tan p}{p} = -2\alpha. \tag{18}$$

The solutions of equation (18) are given by the values of p at which the graph of $y = \tan p$ intersects the line $y = -2\alpha p$, other than the intersection at the origin where α is indeterminate. With increasing values of i the roots, p_i, approach gradually to the values $(2i-1)\pi/2$. They must be calculated individually for each value of α, since equation (18) cannot be solved analytically. These roots are the eigenvalues, p_i, which, when substituted in (16), yield the eigenfunction expansion for c. q is a function of p_i which is given by equation (15), and the appropriate values are to be used in each t term. Equation (17) gives the ratio of the two constants C_1 and C_2 as a function of p_i; the values of C_2 have next to be determined from the initial condition (10).

Equations (16) and (17) give

$$c\,e^{-x/2\alpha} = \sum_{i=1}^{\infty} e^{-q_i t} C_2(i)\,(\cos p_i x - \cot p_i \sin p_i x). \tag{19}$$

When $t = 0$, $c = 1$, so that

$$\begin{aligned} e^{-x/2\alpha} &= \sum_{i=1}^{\infty} C_2(i)\,(\cos p_i x - \cot p_i \sin p_i x), \\ &= \sum_{i=1}^{\infty} u_i, \quad \text{say.} \end{aligned} \tag{20}$$

Before proceeding to the calculation of the constants C_2 it is necessary to demonstrate that the functions u_i form an orthogonal set.

The functions u_j, u_k satisfy the differential equations

$$u_j'' + p_j^2 u_j = 0, \quad u_k'' + p_k^2 u_k = 0,$$

where $j, k = 1, 2, 3, \ldots$.

Multiplying the first by u_k and the second by u_j we obtain, on subtraction,

$$u_j'' u_k - u_k'' u_j = u_j u_k (p_k^2 - p_j^2).$$

Integrating over the range 0–1 gives

$$\int_0^1 (u_j'' u_k - u_k'' u_i)\,dx = (p_k^2 - p_j^2) \int_0^1 u_j u_k\,dx. \tag{21}$$

The left-hand side becomes $[u_j' u_k - u_k' u_j]_0^1$,

and the boundary conditions (11) show this to be equal to zero. Hence, supposing that j and k are different,

$$\int_0^1 u_j u_k\,dx = 0 \quad (j \neq k). \tag{22}$$

If $j = k = i$, this integral is equal to

$$\int_0^1 u_i^2\,dx.$$

Using equation (21) we see that

$$\begin{aligned} \int_0^1 u_i^2\,dx &= \{C_2(i)\}^2 \int_0^1 (\cos p_i x - \cot p_i \sin p_i x)^2\,dx \\ &= \{C_2(i)\}^2 (1 + 2\alpha + \tan^2 p_i)/2\tan^2 p_i. \end{aligned} \tag{23}$$

We now proceed to evaluate the constants $C_2(i)$. Multiplying each side of equation (20) by u_i and integrating over the range 0 to 1 gives

$$\int_0^1 \mathrm{e}^{-x/2\alpha}\, u_i\, dx = \int_0^1 u_i^2\, dx,$$

since all other terms vanish according to equation (22). Hence, using (23)

$$\begin{aligned} C_2(i) &= 2\tan^2 p_i(1+2\alpha+\tan^2 p_i)^{-1}\int_0^1 \mathrm{e}^{-x/2\alpha}\,(\cos p_i x - \cot p_i \sin p_i x)\, dx \\ &= 8\alpha^2 \sin^2 p_i(1+2\alpha+\tan^2 p_i)^{-1}\left\{\frac{1}{\alpha}+p_i\,\mathrm{e}^{-1/2\alpha}\operatorname{cosec} p_i\right\}. \qquad (24) \end{aligned}$$

We are now in a position to write down the complete solution to equation (8) by substituting the expressions for q_i (equation (15)) and for $C_2(i)$ (equation (24)) into equation (19). The result is

$$\begin{aligned} c = \sum_{i=1}^{\infty} & 8\alpha^2(1+2\alpha+\tan^2 p_i)^{-1}\exp\left[\{2x-(1+4p_i^2\alpha^2)\,t\}/4\alpha\right] \\ & \times\left(\frac{\sin p_i}{\alpha}+p_i\,\mathrm{e}^{-1/2\alpha}\right)\sin\{p_i(1-x)\}. \qquad (25) \end{aligned}$$

It is of interest to consider this solution when the sedimentation velocity, v, is negligible compared with Δ/l. Then α tends to ∞ and $\alpha t = \Delta T/l^2$. The solution now relates to very small particles which diffuse but do not settle.

When $\alpha \to \infty$, $p^{-1}\tan p \to -\infty$, so that $p_i = (2i-1)\,\pi/2$. Therefore, $\sin p_i = (-1)^{i+1}$ and $\cos p_i = \cot p_i = 0$. Hence,

$$c = \sum_{i=1}^{\infty}\frac{2}{p_i}(-1)^{i+1}\exp\{-p_i^2\Delta T/l^2\}\cos p_i x,$$

or

$$\frac{C}{C_0} = \sum_{i=1}^{\infty}\frac{4(-1)^{i+1}}{(2i-1)\,\pi}\cos\{(2i-1)\,\pi X/2l\}\exp\{-(2i-1)^2\pi^2\Delta T/4l^2\}. \qquad (26)$$

This is a well-known expression which occurs in the theory of heat conduction.

6. INTEGRAL FORM OF SOLUTION FOR A LIQUID WITH A FREE SURFACE

The general solution of equation (8) can be written as an integral instead of a sum, as was done in equation (16). This gives, instead of (16),

$$c = \int_0^{\infty}\mathrm{e}^{-qt+x/2\alpha}\,(C_1\sin px + C_2\cos px)\, dp. \qquad (27)$$

At $t = 0$, c is equal to 1 in the range $0 < x < 1$. Let us now define c for all values of x. Let $c = f(x)$. Then

$$f(x)\,\mathrm{e}^{-x/2\alpha} = \int_0^{\infty}(C_1\sin px + C_2\cos px)\, dp. \qquad (28)$$

If we substitute

$$C_1 = \frac{1}{\pi}\int_{-\infty}^{\infty} f(\gamma)\,\mathrm{e}^{-\gamma/2\alpha}\sin p\gamma\, d\gamma,$$

$$C_2 = \frac{1}{\pi}\int_{-\infty}^{\infty} f(\gamma)\,\mathrm{e}^{-\gamma/2\alpha}\cos p\gamma\, d\gamma, \qquad (29)$$

equation (28) becomes

$$f(x)\,e^{-x/2\alpha} = \frac{1}{\pi}\int_{p=0}^{\infty}\int_{\gamma=-\infty}^{\infty} f(\gamma)\,e^{-\gamma/2\alpha}\cos\{p(\gamma-x)\}\,d\gamma\,dp,$$

which is a statement of the Fourier integral theorem. Hence equation (27) satisfies the differential equation (8), and the initial condition, providing C_1 and C_2 are defined as in (29). Therefore

$$c = \frac{1}{\pi}\int_0^{\infty}\int_{-\infty}^{\infty} \exp[-\{2(\gamma-x)+(1+4p^2\alpha^2)\,t\}/4\alpha]\,f(\gamma)\cos\{p(\gamma-x)\}\,d\gamma\,dp.$$

Integration with respect to p gives

$$c = \tfrac{1}{2}(\pi\alpha t)^{-\frac{1}{2}}\int_{-\infty}^{\infty} f(\gamma)\exp\{-(\gamma-x+t)^2/4\alpha t\}\,d\gamma. \tag{30}$$

This cannot be integrated immediately because $f(\gamma)$ is only known in the range $0<\gamma<1$, where it is equal to unity. The function can be determined over a wider range by imposing the boundary conditions (11) upon c. From (30)

$$\alpha\frac{\partial c}{\partial x} = \tfrac{1}{2}\alpha(\pi\alpha t)^{-\frac{1}{2}}\int_{-\infty}^{\infty} f'(\gamma)\exp\{-(\gamma-x+t)^2/4\alpha t\}\,d\gamma,$$

which is equal to c at $x = 0$. From this we obtain

$$\int_{-\infty}^{\infty}\{f(\gamma)-\alpha f'(\gamma)\}\exp\{-(\gamma+t)^2/4\alpha t\}\,d\gamma = 0.$$

Also, at $x = 1$, $c = 0$, so that from (30),

$$\int_{-\infty}^{\infty} f(\gamma)\exp\{-(\gamma-1+t)^2/4\alpha t\}\,d\gamma = 0.$$

The last two equations can be written

$$\int_{-\infty}^{\infty}\{f(\gamma)-\alpha f'(\gamma)\}\exp\left\{-\left(\frac{\gamma}{2\alpha}+\frac{\gamma^2}{4\alpha t}\right)\right\}d\gamma = 0, \tag{31}$$

$$\int_{-\infty}^{\infty} f(\gamma)\exp\left[-\left\{\frac{(\gamma-1)}{2\alpha}+\frac{(\gamma-1)^2}{4\alpha t}\right\}\right]d\gamma = 0. \tag{32}$$

In equation (31) the term $e^{-\gamma^2/4\alpha t}$ is symmetrical about the axis $\gamma = 0$, hence for the integral to vanish it is necessary that the function

$$\Theta = \{f(\gamma)-\alpha f'(\gamma)\}\,e^{-\gamma/2\alpha} \tag{33}$$

should be skew symmetrical about the origin.

In equation (32) the term $e^{-(\gamma-1)^2/4\alpha t}$ is symmetrical about the ordinate $\gamma = 1$, hence for the integral to vanish the function

$$\Phi = f(\gamma)\,e^{-(\gamma-1)/2\alpha} \tag{34}$$

must be skew symmetrical about $\gamma = 1$. This means that

$$\Phi(\gamma) = -\Phi(2-\gamma). \tag{35}$$

From 0 to 1 we know $f(\gamma) = 1$, hence ${}_0\Phi_1 = e^{-(\gamma-1)/2\alpha}$, the value of Φ in the range $0<\gamma<1$. Using (35) we see ${}_1\Phi_2 = -e^{(\gamma-1)/2\alpha}$.

If ${}_1f_2(\gamma)$ is the value of $f(\gamma)$ between 1 and 2, this gives

$$ {}_1f_2(\gamma)\, e^{-(\gamma-1)/2\alpha} = -e^{(\gamma-1)/2\alpha} $$

or

$$ {}_1f_2(\gamma) = -e^{(\gamma-1)/\alpha}. \tag{36} $$

Now, since Θ is skew symmetrical about the origin

$$ \Theta(\gamma) = -\Theta(-\gamma). \tag{37} $$

From 0 to 1, $f(\gamma) = 1$, $f'(\gamma) = 0$. Hence ${}_0\Theta_1 = e^{-\gamma/2\alpha}$, and ${}_{-1}\Theta_0 = -e^{\gamma/2\alpha}$ by (37). Hence

$$ \{{}_{-1}f_0(\gamma) - \alpha\, {}_{-1}f_0'(\gamma)\}\, e^{-\gamma/2\alpha} = -e^{\gamma/2\alpha}, $$

or

$$ {}_{-1}f_0'(\gamma) - \frac{1}{\alpha}\, {}_{-1}f_0(\gamma) = \frac{1}{\alpha} e^{\gamma/\alpha}, $$

with $\gamma = 0$ at $f(\gamma) = 1$, giving

$$ {}_{-1}f_0(\gamma) = (1+\gamma/\alpha)\, e^{\gamma/\alpha}. \tag{38} $$

Similarly, by reflecting ${}_{-1}\Phi_0$ on to ${}_2\Phi_3$, we find

$$ {}_2f_3(\gamma) = -\{1+(2-\gamma)/\alpha\}\, e^{1/\alpha}, \tag{39} $$

and by reflecting ${}_1\Theta_2$ on to ${}_{-2}\Theta_{-1}$,

$$ {}_{-2}f_{-1}(\gamma) = (1-1/\alpha)\, e^{\gamma/\alpha}. \tag{40} $$

We have thus established $f(\gamma)$ over the range $-2<\gamma<3$, and equation (30) can now be integrated over this range. It would be possible to continue the reflexion process indefinitely and so obtain c with any desired degree of accuracy, but the expression becomes somewhat cumbersome. The terms arising from ranges of γ which are more remote are negligible for small to moderate values of t and will not be required.

Substituting in equation (30) the values of $f(\gamma)$ given by (36), (38), (39) and (40), and the value unity for the range 0 to 1, yields, after integration,

$$ 2\alpha c\, e^{-x/\alpha} = g_1(x,t) + g_2(x,t) + g_3(x,t) - g_4(x,t) - g_5(x,t), $$

where

$$ \left.\begin{aligned} g_1 &= (\alpha-1)\{\operatorname{erf}(2w+v) - \operatorname{erf}(w+v)\}, \\ g_2 &= 2(t\alpha/\pi)^{\frac{1}{2}}[\exp\{-(v+w)^2\} - \exp\{-v^2\}] + (x+t+\alpha)\{\operatorname{erf}(v+w) - \operatorname{erf} v\}, \\ g_3 &= \alpha\, e^{-x/\alpha}\{\operatorname{erf}(w-u) + \operatorname{erf} u\}, \\ g_4 &= \alpha\, e^{-1/\alpha}\{\operatorname{erf}(2w-v) - \operatorname{erf}(w-v)\}, \\ g_5 &= 2(t\alpha/\pi)^{\frac{1}{2}} e^{(1-x)/\alpha}[\exp\{-(3w-u)^2\} - \exp\{-(2w-u)^2\}] \\ &\quad + 2\, e^{(1-x)/\alpha}(2+\alpha-x+t)\{\operatorname{erf}(3w-u) - \operatorname{erf}(2w-u)\}, \\ u &= (x-t)/2\sqrt{(\alpha t)}, \quad v = (x+t)/2\sqrt{(\alpha t)}, \quad w = 1/2\sqrt{(\alpha t)}. \end{aligned}\right\} \tag{41} $$

We have here five groups of terms. The second, third and fourth are the most important and will often suffice to calculate c if t is not too large. The first group applies a small correction which is most noticeable in the region $x \to 0$, and the fifth group a similar correction which is greatest where $x \to 1$.

7. THE SERIES SOLUTION FOR A GASEOUS SUSPENSION

The boundary conditions are now

$$c = 0 \quad \text{at} \quad x = 0 \quad \text{and } 1, \quad \text{for} \quad t \geqslant 0. \tag{11a}$$

Applying these to equation (16) gives

$$C_2 = 0,$$

$$C_1 \sin p + C_2 \cos p = 0,$$

whence $p = s\pi$, $s = 0, 1, 2, 3, \ldots$, so that

$$c = \sum_{s=1}^{\infty} C_s \exp\{[2x - (1 + 4s^2\pi^2\alpha^2)\,t]/4\alpha\} \sin s\pi x.$$

Evaluating C_s at $t = 0$ in the usual way,

$$\int_0^1 e^{-x/2\alpha} \sin s\pi x\, dx = \int_0^1 C_s \sin^2 s\pi x\, dx.$$

Hence
$$C_s = \frac{2}{s\pi}\{1 - (-1)^s e^{-1/2\alpha}\}/\{1 + 1/4\alpha^2 s^2\pi^2\}. \tag{42}$$

When α is large the particles do not sediment appreciably and the solution reduces to

$$c = C/C_0 = \sum_{s=1}^{\infty} \frac{4}{(2s-1)\pi} \exp\{-(2s-1)^2\pi^2\Delta T/l^2\} \sin\{(2s-1)\pi X/l\}, \tag{43}$$

which is, again, a well-known expression in the theory of heat conduction.

8. INTEGRAL FORM OF THE SOLUTION FOR A GASEOUS SUSPENSION

Proceeding as in §6, but with the boundary conditions (11a), we now obtain from (30)

$$\left.\begin{aligned} &\int_{-\infty}^{\infty} f(\gamma) \exp -\{(2\gamma t + \gamma^2)/4\alpha t\}\, d\gamma = 0, \\ &\int_{-\infty}^{\infty} f(\gamma) \exp -[\{2(\gamma-1)\,t + (\gamma-1)^2\}/4\alpha t]\, d\gamma = 0, \end{aligned}\right\}$$

from which we see that
$$\theta = f(\gamma)\, e^{-\gamma/2\alpha} \tag{44}$$

must be skew symmetrical about the origin and

$$\phi = f(\gamma)\, e^{-(\gamma-1)/2\alpha} \tag{45}$$

must be skew symmetrical about the ordinate $\gamma = 1$. Arguing as before we obtain

$${}_1f_2(\gamma) = -e^{-(1-\gamma)/\alpha}, \qquad {}_2f_3(\gamma) = e^{1/\alpha},$$

$${}_{-1}f_0(\gamma) = -e^{\gamma/\alpha}, \qquad {}_{-2}f_{-1}(\gamma) = e^{-1/\alpha}.$$

Upon substitution in equation (30) these give

$$2C = h_1(x,t) + h_2(x,t) + h_3(x,t) + h_4(x,t) + h_5(x,t)$$

where

$$\left.\begin{aligned} h_1 &= \mathrm{e}^{-1/\alpha}\{\operatorname{erf}(2w+v) - \operatorname{erf}(w+v)\}, \\ h_2 &= -\mathrm{e}^{x/\alpha}\{\operatorname{erf}(w+v) - \operatorname{erf} v\}, \\ h_3 &= \operatorname{erf}(w-u) + \operatorname{erf} u, \\ h_4 &= -\mathrm{e}^{-(1-x)/\alpha}\{\operatorname{erf}(2w-v) - \operatorname{erf}(w-v)\}, \\ h_5 &= \mathrm{e}^{1/\alpha}\{\operatorname{erf}(3w-u) - \operatorname{erf}(2w-u)\}. \end{aligned}\right\} \tag{46}$$

and u, v, w are as in (41).

As before, the second, third and fourth groups are most important; the first and last apply corrections, unless t is too small, which are greatest at $x = 0$ and $x = 1$, respectively.

When α is very small and $t > 0$ all the terms of equation (46) vanish except those in the third and fourth groups. Under these circumstances, also, only the third and fourth groups of equation (41) remain finite and they are identical with the corresponding groups of (46). The solutions for the boundary conditions (11) and (11*a*) therefore become identical for $t > 0$ when α is small enough. This would be anticipated on physical grounds since, when the sedimentation velocity is sufficiently large, the loss of particles by diffusion to the upper surface is negligible in the latter case.

The series solutions (25) and (42) become intractable for small values of α and do not converge to a common limit.

9. COMPUTATION OF THE SOLUTIONS

Before solution (25) can be used it is necessary to compute the roots, p_i, of equation (18). There are a few tabulations of these roots available but they are not sufficiently extensive. The equation was therefore expanded by the method described by Hobson (1891) to give

$$\begin{aligned} p_i = (i-\tfrac{1}{2})\pi - \frac{1}{a} - \frac{b}{a^3} - \frac{1}{a^5}(2b^2 - \tfrac{1}{45}) - \frac{1}{a^7}(5b^3 - \tfrac{2}{15}b - \tfrac{2}{945}) \\ - \frac{1}{a^9}\left(14b^4 - \frac{28b^2}{45} - \frac{16b}{945} + \frac{1}{567}\right) - \frac{1}{a^{11}}\left(38b^5 - \frac{116b^3}{45} - \frac{2b^2}{21} + \frac{418}{14175}b + \frac{2}{4455}\right) - \dots, \end{aligned} \tag{47}$$

where $b = -(2\alpha + \tfrac{1}{3})$ and $a = -(i-\tfrac{1}{2})(2\alpha\pi)$ $(i = 1, 2, 3, \dots)$.

This formula sufficed to calculate most of the roots p_i as shown in table 1.

TABLE 1

α	roots of equation (18) calculated by formula (47)
2	p_1–p_{16}
$\frac{1}{2}$	p_2–p_{16}
$\frac{1}{3}$	p_2–p_{16}
$\frac{1}{8}$	p_3–p_{16}
$\frac{1}{30}$	p_7–p_{16}

The series did not converge for the first few roots, with the smaller values of α, so these were obtained by successive approximation guided by the tables of Carslaw & Jaeger (1947). The values of p_i are shown in table 2.

TABLE 2. VALUES OF p_i

i	$\alpha =$ 2	$\frac{1}{2}$	$\frac{1}{3}$	$\frac{1}{6}$	$\frac{1}{30}$
1	1·7155	2·0288	2·1746	2·45565	2·94756
2	4·7648	4·9132	5·0036	5·23294	5·90798
3	7·8857	7·9788	8·0385	8·20453	8·88978
4	11·018	11·086	11·130	11·2560	11·89587
5	14·155	14·2075	14·242	14·3434	14·92506
6	17·293	17·336	17·365	17·4491	17·97420
7	20·433	20·469	20·494	20·5653	21·03970
8	23·573	23·604	23·625	23·6879	24·11833
9	26·713	26·741	26·760	26·8149	27·20740
10	29·854	29·879	29·895	29·9450	30·30474
11	32·994	33·017	33·032	33·0772	33·40873
12	36·135	36·156	36·170	36·2110	36·51806
13	39·276	39·296	39·308	39·3460	39·63173
14	42·418	42·435	42·447	42·4820	42·74896
15	45·558	45·575	45·586	45·6188	45·86914
16	48·700	48·715	48·726	48·7562	48·99180

Computations based on (25) were carried out for several values of t with α equal to 2, $\frac{1}{2}$, $\frac{1}{3}$ and $\frac{1}{6}$. For α equal to $\frac{1}{30}$ the computation became very difficult with $t < 1$ since the series oscillated violently. Smaller values of α were not attempted. Equation (26) was used for $\alpha \rightarrow \infty$. Solution (41) was employed for α equal to $\frac{1}{3}$, $\frac{1}{6}$, $\frac{1}{30}$ and $\frac{1}{100}$, and agreed with (25) for the overlapping values. It was necessary to take account of the first and fifth groups of terms in the solution for the larger values of α and t; for example, at $x = 1$ the correction due to the fifth group was 0·045 when $\alpha = \frac{1}{3}$ and $t = \frac{1}{2}$. The correction seems to be negligible ($< 0{\cdot}001$), for $\alpha t < \frac{1}{60}$ within the range of values of α and t which were tried. Curves for this case, the liquid with the free surface, are shown in figures 1 to 7.

The other series, (42), was quite easy to compute for α equal to 2, $\frac{1}{2}$, $\frac{1}{3}$ and $\frac{1}{6}$. Solution (43) gave $\alpha \rightarrow \infty$. Equation (46) was used for $\alpha = \frac{1}{3}, \frac{1}{6}, \frac{1}{30}$ and $\frac{1}{100}$ and agreed with (43) when $\alpha = \frac{1}{3}$ and $\frac{1}{6}$. The first and fifth groups of equation (43) were rather more important, in general, than the corresponding ones of (41). This set of results, for a gaseous suspension or for a liquid entirely filling the container, is exhibited in figures 1*a* to 7*a*.

For $\alpha = \frac{1}{100}$ the curves for the two different conditions at the upper boundary run very close to one another, the free surface points never being more than about 0·01 unit above the others. Thus, when $\alpha < \frac{1}{100}$ the process can be regarded as independent of the upper boundary conditions except for very short times.

The lower regions of the curves are coincident, irrespective of the upper boundary condition, providing that t is small enough for part of the $x-c$ curve to touch the ordinate $c = 1$ below the point $x = 0{\cdot}5$.

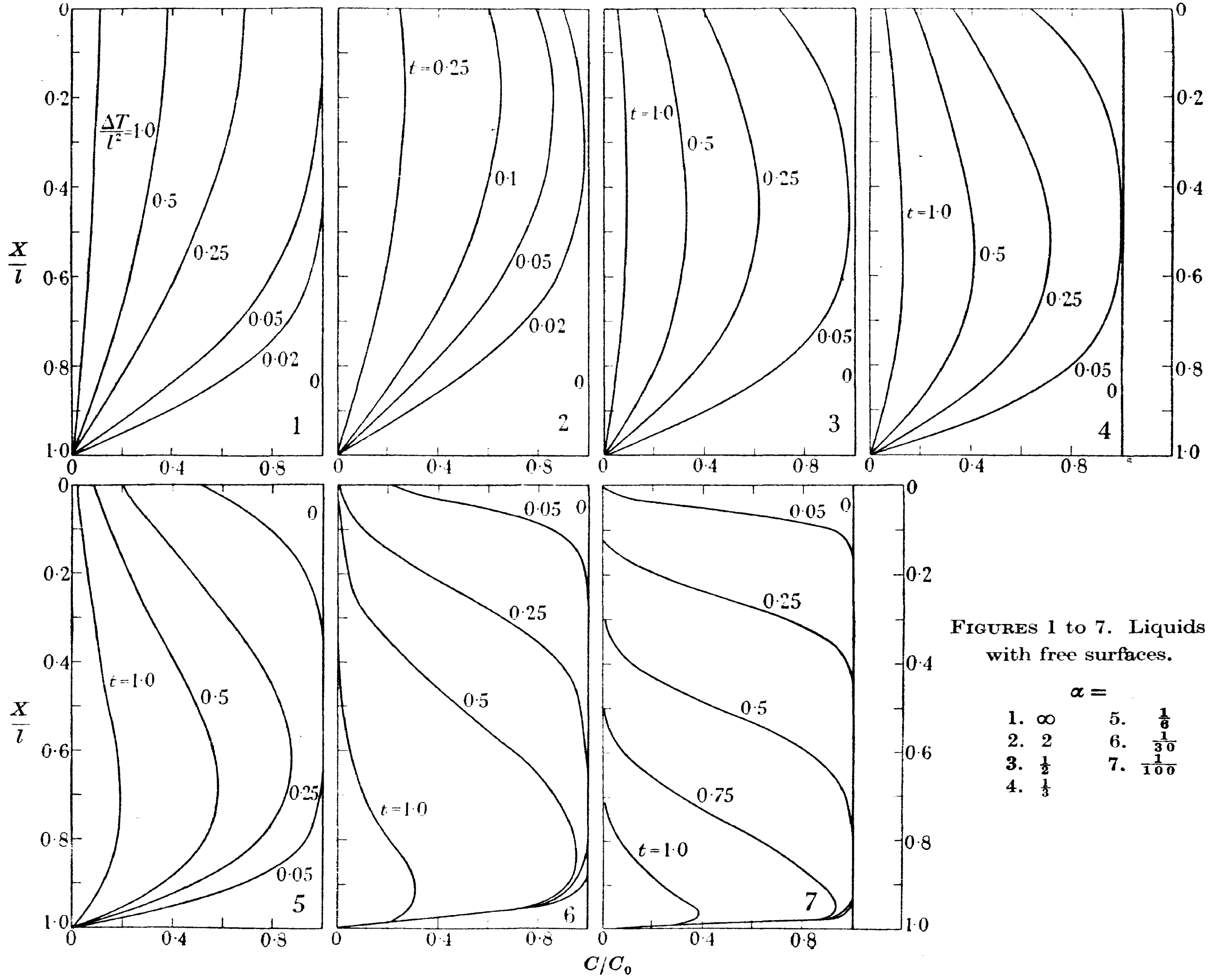

FIGURES 1 to 7. Liquids with free surfaces.

$\alpha =$

1. ∞
2. 2
3. $\frac{1}{2}$
4. $\frac{1}{3}$
5. $\frac{1}{6}$
6. $\frac{1}{30}$
7. $\frac{1}{100}$

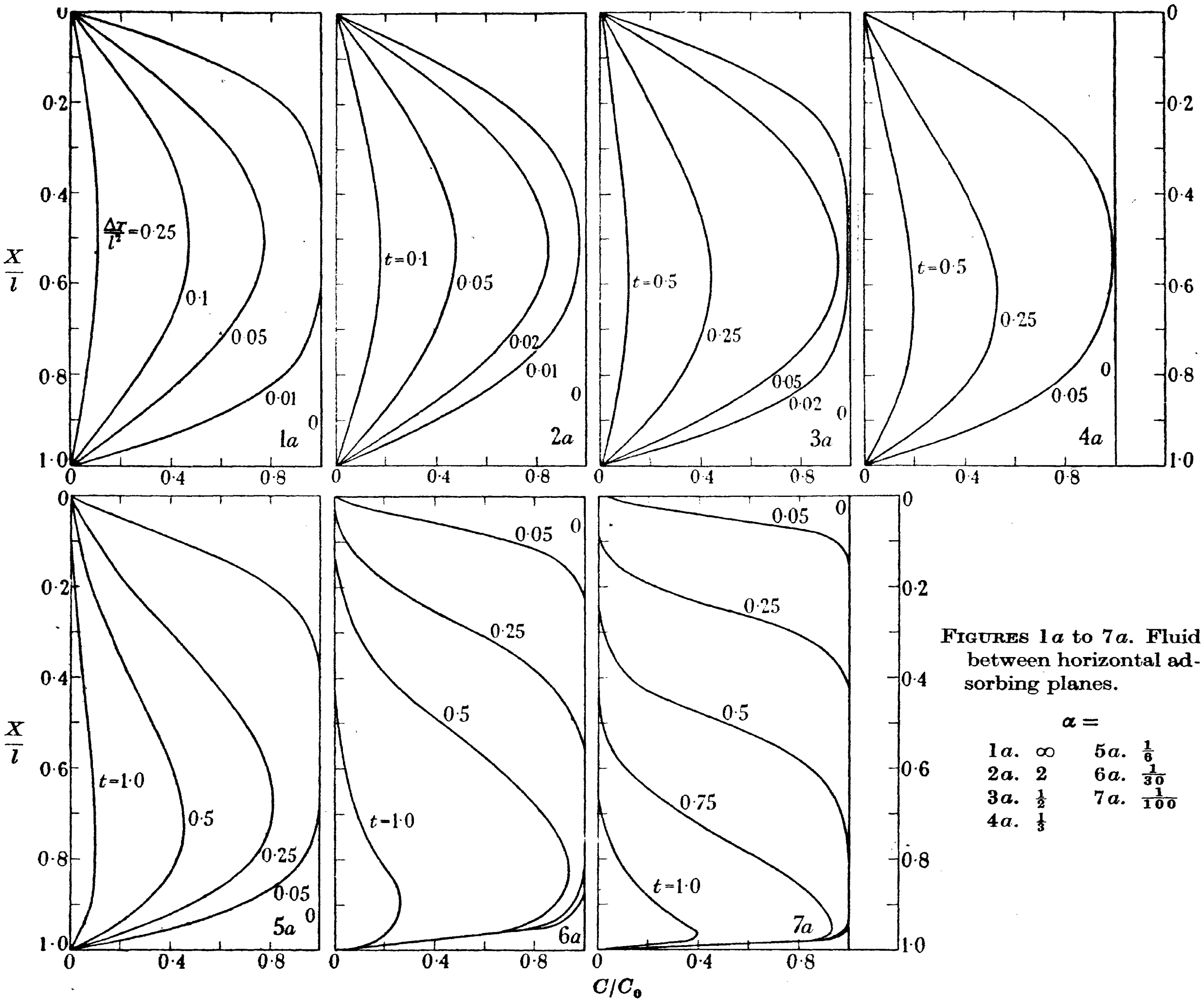

FIGURES 1*a* to 7*a*. Fluid between horizontal adsorbing planes.

$\alpha =$

1*a*.	∞	5*a*.	$\frac{1}{6}$
2*a*.	2	6*a*.	$\frac{1}{30}$
3*a*.	$\frac{1}{2}$	7*a*.	$\frac{1}{100}$
4*a*.	$\frac{1}{3}$		

10. APPLICATION OF THE RESULTS

The solutions have been obtained in dimensionless units because of the generality of such forms. Conversion into ordinary units is done by means of equations (7) and (9). The following information is given to assist in grasping the physical meaning of the general results which are plotted on the graphs.

We have from (1), (2) and (9)

$$\alpha = \frac{\Delta}{vl} = \frac{kT}{(m-m')\,gl} = \frac{1{\cdot}371\times10^{-16}\times293}{\frac{1}{6}\pi d^3(\rho-\sigma)\,981l} \tag{48}$$

for sedimentation under gravity at 20° C, where d is the particle diameter, ρ the density of the particle and σ the density of the fluid. It will be seen that α is dependent on the properties of the fluid only so far as the buoyancy effect is concerned. The fluid viscosity and, in gases, the slip factor, cancel out. The time variable, t, however, depends on the viscosity η and the slip factor F:

$$\frac{T}{t} = \frac{l}{v} = \frac{18\eta l}{d^2(\rho-\sigma)\,gF}. \tag{49}$$

Table 3 based on equations (48) and (49) can be used in interpreting the curves for sedimentation under gravity. The second column enables α to be found for a given particle; the sixth and ninth columns give quantities from which are obtainable the factors multiplying t to produce T, in seconds, for particles in water and in air. The slip factors were calculated by an equation which has been discussed elsewhere by the author (Davies 1945).

TABLE 3. SEDIMENTATION UNDER GRAVITY AT 20° C

		particles in air at 760 mm.				particles in water		
particle diameter (μ)	$\alpha(\rho-\sigma)\,l$ (c.g.s.)	$\frac{v}{\rho-\sigma}\times10^6$ (c.g.s.)	$\Delta\times10^6$ (c.g.s.)	F	$\frac{T}{t}\frac{\rho-\sigma}{l}$ (c.g.s.)	$\frac{v}{\rho-\sigma}\times10^6$ (c.g.s.)	$\Delta\times10^6$ (c.g.s.)	$\frac{T}{t}\frac{\rho-\sigma}{l}$ (c.g.s.)
0·05	0·625	37·7	23·5	5·02	26,500	0·135	0·0848	7,410,000
0·1	0·0781	86·4	6·77	2·89	11,600	0·54	0·0424	1,850,000
0·15	0·0232	149	3·45	2·21	6,710	1·215	0·0283	823,000
0·2	0·00977	225	2·20	1·88	4,440	2·16	0·0212	463,000
0·3	0·00298	422	1·22	1·57	2,370	4·86	0·0141	206,000
0·4	0·00122	679	0·832	1·42	1,470	8·64	0·0106	116,000
0·5	0·000625	993	0·623	1·33	1,010	13·5	0·0085	74,100
			$\eta = 0{\cdot}000182$				$\eta = 0{\cdot}0101$	

Most of the computations for this paper were carried out by Mary Aylward for whose care and accuracy the author is grateful. He is also indebted to Mr A. C. Stevenson for advice and criticism and to Dr T. Bedford for his sustained encouragement of fundamental research.

REFERENCES

Carslaw, H. S. & Jaeger, J. C. 1947 *Conduction of heat in solids*, p. 378. Oxford University Press.

Davies, C. N. 1945 *Proc. Phys. Soc.* **57**, 259.

Davies, C. N. 1947 *Symposium Inst. of Chem. Engineers and Soc. of Chem. Industr.* p. 12.

Hobson, E. W. 1891 *Plane trigonometry*, p. 126. Cambridge University Press.

Mason, M. & Weaver, W. 1924 *Phys. Rev.* (2), **23**, 412.

Perrin, J. 1916 *Atoms*. London: Constable.

The inflammation of alkyl nitrate vapours and the effect of inert diluents

By P. Gray and A. D. Yoffe

Research Laboratory on the Physics and Chemistry of Rubbing Solids, Department of Physical Chemistry, Cambridge

(*Communicated by F. P. Bowden, F.R.S.—Received* 16 *July* 1949)

An investigation has been made of the inflammation of methyl nitrate, ethyl nitrate and nitroglycerin vapours, and of the influence of different diluents, over the temperature range 240 to 500° C.

The explosion of methyl nitrate is facilitated by both argon and nitrogen. With oxygen as diluent, explosive conbustion occurs. The results show that the explosion is not thermal as has been suggested, but is due to chain branching. A glow region has been observed with methyl nitrate, ethyl nitrate and nitroglycerin, and this region lies below that of explosion on the pressure-temperature graph. These nitrates even when diluted from a thousand to a million times with inert gases glow on admission to a hot quartz vessel; oxygen and air are less efficient than nitrogen or argon in facilitating the glow. It is suggested that the glow is associated with the production of excited formaldehyde molecules.

Introduction

Studies of the initiation of explosion in liquids detonated by gentle impact (Bowden, Mulcahy, Vines & Yoffe 1947) led to an investigation of the vapour-phase inflammation of some alkyl nitrates and of the influence on this inflammation of different diluents. The compounds investigated were the three nitric esters, methyl nitrate, ethyl nitrate and nitroglycerin.

The explosion and thermal decomposition of methyl nitrate vapour have been examined by Appin, Chariton & Todes (1936) and by Zeldovich & Shaulov (1947), and in their account of the thermal decomposition of ethyl nitrate Bawn & Adams (1949) mention limiting conditions of pressure and temperature beyond which explosion occurs.

This paper describes experiments on the inflammation of methyl nitrate vapour, and the influence of the diluents argon and oxygen on the explosion limit. A new process in the thermal decomposition of the alkyl nitrates has been observed. At pressures too low for explosion to occur, these vapours glow on admission to a hot quartz vessel. This glow persists when the vapour is diluted even a million times with argon or nitrogen. The significance of this observation in connexion with the initiation of explosion in liquids has already been discussed (Gray & Yoffe 1949).

Experimental

The ignition limit was determined by measuring that partial pressure of explosive vapour above which inflammation occurs on admission to the vessel and below which only rapid decomposition takes place. When pressures of the order of 10 cm. Hg were necessary, the gases were admitted through a capillary tap to avoid the self-heating which occurs (White & Price 1919) if the gas is allowed to rush into the vessel. The apparatus used is illustrated in figure 1. The transparent quartz reaction vessel (volume 350 cm.^{3}, surface area 330 cm.^{2}) is maintained at a steady uniform temperature in the furnace. The state of the surface was found to be important in determining the limits of inflammation, and the first few experiments often gave erratic results. By standardizing procedure, e.g. pumping time, very reproducible results could be obtained.

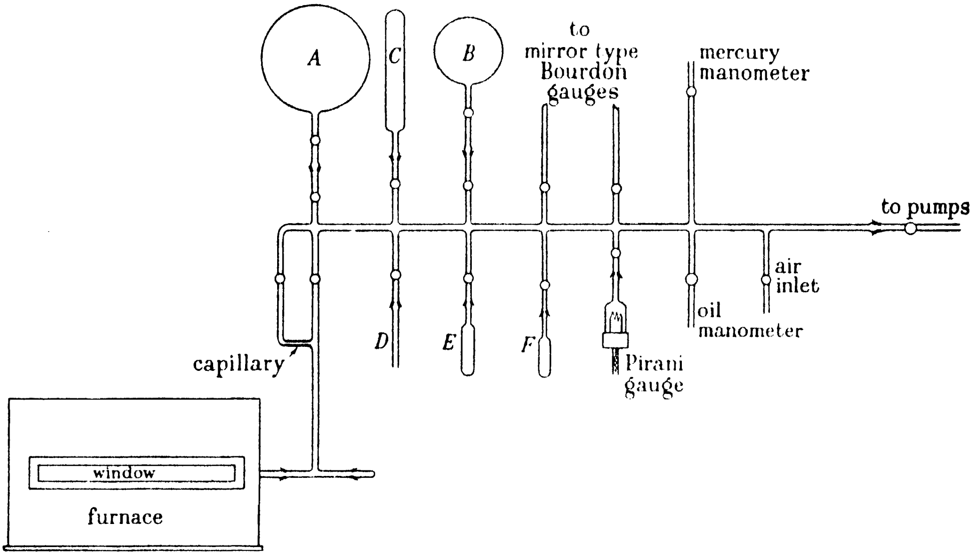

FIGURE 1. Apparatus for studying vapour-phase inflammation.

Mixtures of known composition of explosive vapours from the liquids stored in the small bulbs *D*, *E*, *F* with the gases stored in bulbs *B* and *C* can be made up in the bulb *A* by means of the sensitive mirror-type Bourdon gauge. All the taps used were lubricated with silicone grease to reduce the absorption of organic vapours. The quartz vessel and these bulbs were connected by the glass line to a liquid-air trap and a three-stage mercury diffusion pump. Between experiments the apparatus was evacuated and flushed with nitrogen; in this way any vapours adsorbed on the walls could be removed.

The furnace is built of a clear quartz tube wound with nichrome wire and mounted in a rectangular box lagged with kieselguhr. Uniformity of temperature along the tube is achieved by winding the furnace in three sections and supplying power to the middle and ends separately. In addition, the inner windings of the middle section are shunted with a variable resistance to improve the accuracy of the control. It was found possible when a metal sheath was inserted between the quartz vessel and the quartz tube to keep the temperature along the vessel uniform to within 1° at 475° C. A thermocouple is used as a probe to test for temperature uniformity. A long, coiled spiral of fine platinum wire provides a very sensitive element for an electronically operated thermostat. It forms one arm of a Wheatstone bridge; the off-balance current is amplified and made to operate a relay which shunts a fraction of the power supply. During the experiments described, this platinum spiral was used as an accurate resistance thermometer. The feeble inflammation of the explosive vapour at very low pressures and the faint pre-ignition glow were observed through a mica window in the furnace. A dark hood was used to exclude stray light. At temperatures above 475° C the background illumination from the hot furnace made accurate determination of the glow limit difficult.

Methyl nitrate and ethyl nitrate were supplied by the Explosive Research and Development Establishment, Waltham Abbey. They were distilled under reduced pressure and only the middle fractions used.

The diluents used were argon, nitrogen, air and oxygen. Both 'spectroscopically pure' argon and argon from a cylinder were available; the nitrogen was either prepared by heating dry A.R. sodium azide or taken from a cylinder; the oxygen was also taken from a cylinder. All the gases were dried thoroughly with phosphorus pentoxide or liquid air; no difference in behaviour between samples of the same gas from different sources could be detected. Nor was any influence of moisture observed, fresh and dry air behaving identically as diluents.

The explosion and glow of methyl nitrate and the influence of diluents

(1) *The explosion of pure methyl nitrate*

The critical pressure limit above which the decomposition of methyl nitrate vapour becomes explosive was measured over the temperature range 240 to 500° C (figure 2). The final pressure after explosion was about three times the initial pressure of pure methyl nitrate. A brief induction period preceded the brilliant yellow flash and audible click accompanying ignition. The higher the temperature the lower the pressure at which explosion occurred and the shorter the induction period—3 to 4 sec. at the lower temperatures and zero at the higher values. At the lower temperatures, a solid polymer of formaldehyde condensed in the apparatus. Numerical differences between these results and those of Appin *et al.* (1936), whose measurements covered a part of this temperature range, are due to differences in the geometry of the vessels and the nature of the surfaces. From their experimental results, in particular from detailed examination of measurements of induction period, Appin *et al.* concluded that the inflammation of methyl nitrate is a thermal explosion. They found that their plot of $\log \frac{p_{cr}}{T} - \frac{1}{T}$ did not give a straight line. However, our measurements, made over twice the temperature range, fit quite well a line only slightly curved (figure 3).

(2) *The explosion of methyl nitrate in the presence of diluents*

The effect on this explosion limit of added diluents has been examined. It was found that dilution of the vapour with its own volume of argon or nitrogen facilitates the explosion. These results (figure 4) suggest that the explosion develops by a branched radical-chain mechanism in which self-heating is of secondary importance. In the presence of oxygen, explosive combustion occurred at an even lower partial pressure of methyl nitrate; under these conditions the slightly unfavourable oxygen balance is redressed by the excess oxygen, and such explosions are more violent than those of the corresponding argon and nitrogen mixtures.

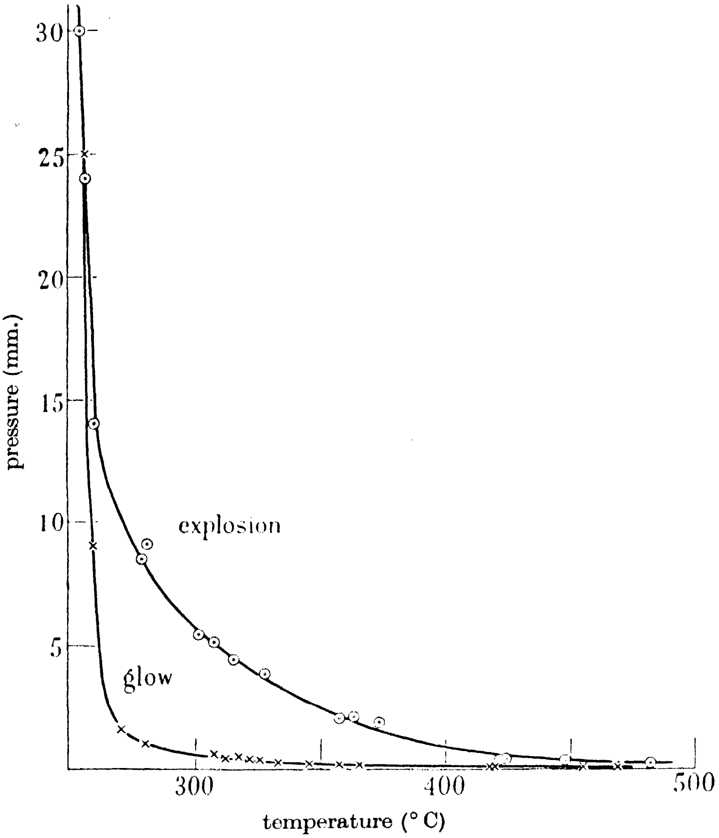

FIGURE 2. The inflammation of methyl nitrate.

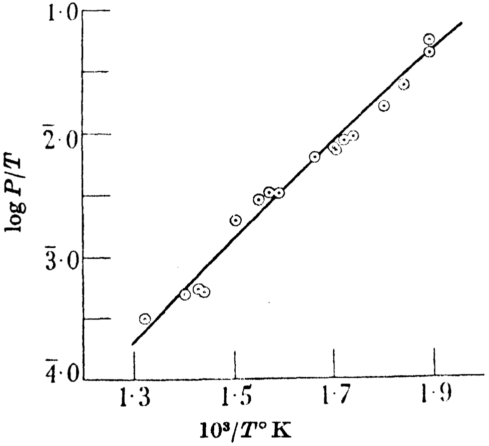

FIGURE 3

(3) *The pre-ignition glow of methyl nitrate*

Under conditions too mild for explosion, a faint, transient glow sometimes lasting several seconds could be observed when the vapour was admitted to the vessel. The pressure limit of the glow lay below that of the explosion (figure 2), though the difference between the two pressure limits for glow and explosion diminished both at low and high temperatures. When explosion occurred it was always preceded during the induction period by this glow, the faint blue illumination sometimes fading before the brilliant yellow flash of the explosion itself.

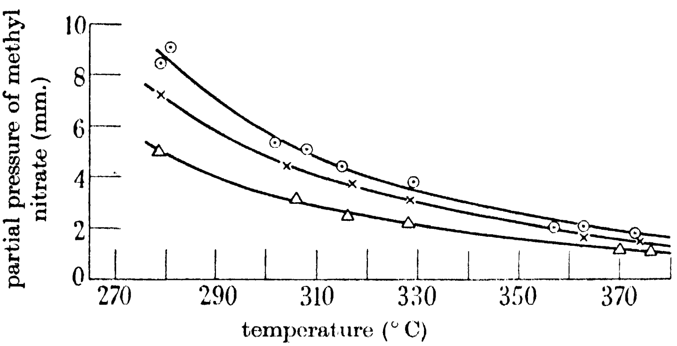

FIGURE 4. The influence of diluents on the explosion of methyl nitrate. ⊙, pure CH_3ONO_2; ×, $1.CH_3ONO_2:1.A$; Δ, $1.CH_3ONO_2:1.O_2$.

(4) *The glow of methyl nitrate in the presence of diluents*

Dilution with the inert gases argon and nitrogen facilitated the glow of methyl nitrate (figures 5, 6), especially at the higher temperatures where it was possible to observe glows even in millionfold diluted mixtures, when the partial pressure of methyl nitrate was extremely small (table 1).

TABLE 1. THE GLOW LIMIT OF METHYL NITRATE MIXED WITH DIFFERENT DILUENTS

Partial pressures required for glow (mm. Hg)

		relative concentration of methyl nitrate		
diluent	temperature	10^{-4}	10^{-5}	10^{-6}
nitrogen	425	0·0005	~0·0007	~0·00001
	460	0·0003	0·0005	—
argon	425	0·0005	0·0006	—
air	470	0·0008	—	—

Values for dilutions greater than 10^4 are not very reproducible.

Oxygen (figure 7) was less efficient than nitrogen or argon in facilitating the glow, and the differences between them became more marked at progressively higher dilutions. Thousandfold diluted mixtures with oxygen would often not glow at all at pressures up to 20 cm., and some mixtures of $100.O_2:1.CH_3ONO_2$ showed an upper pressure limit above which it was not possible to obtain the glow. Air was intermediate in behaviour between nitrogen and oxygen (figure 8).

The variation with temperature of the total pressure required for glow to occur in methyl nitrate diluted 100 times with these four gases is shown in figure 8. Argon and nitrogen behave very similarly.

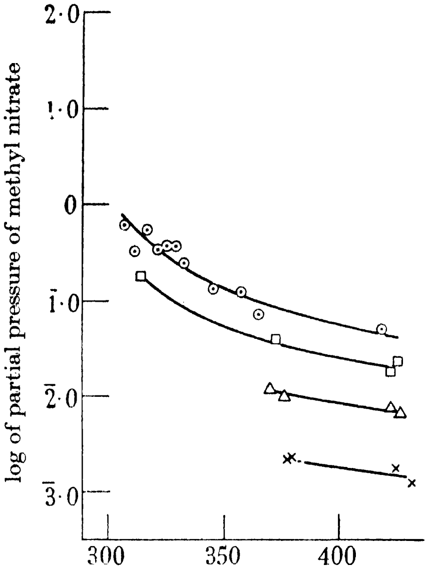

FIGURE 5. The glow limit of argon-methyl nitrate mixtures.

⊙, pure CH_3ONO_2; □, $1 . CH_3ONO_2 : 10 . A$; Δ, $1 . CH_3ONO_2 : 100 . A$; ×, $1 . CH_3ONO_2 : 1000 . A$.

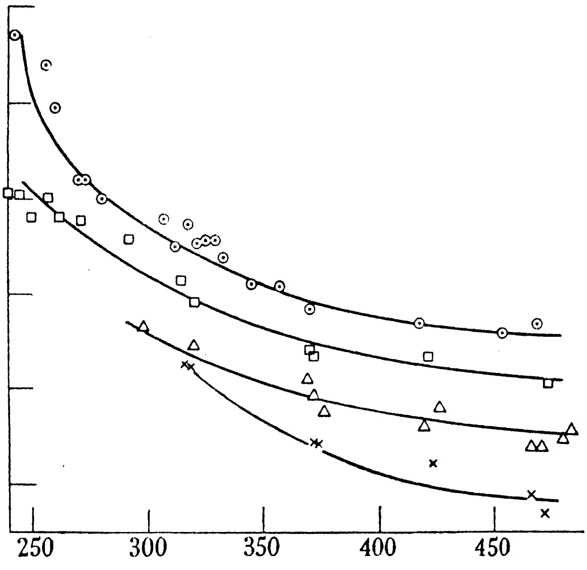

FIGURE 6. The glow limit of nitrogen-methyl nitrate mixtures.

⊙, pure CH_3ONO_2; □, $1 . CH_3ONO_2 : 10 . N_2$; Δ, $1 . CH_3ONO_2 : 100 . N_2$; ×, $1 . CH_3ONO_2 : 1000 . N_2$.

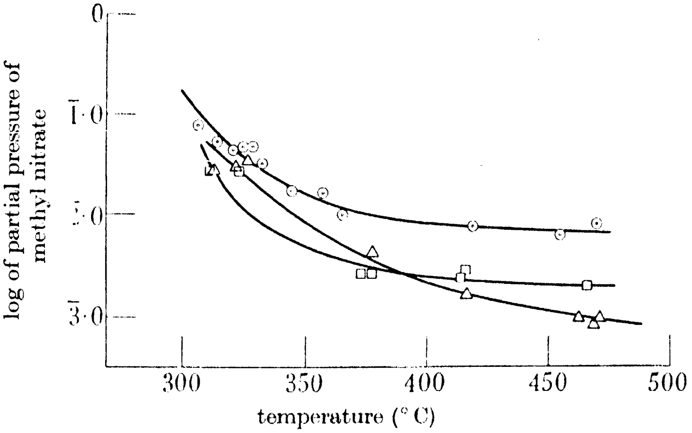

FIGURE 7. The glow limit of oxygen-methyl nitrate mixtures.

⊙, pure CH_3ONO_2; □, $1 . CH_3ONO_2 : 10 . O_2$; Δ, $1 . CH_3ONO_2 : 100 . O_2$.

The explosion and glow of ethyl nitrate and the influence of diluents

Ethyl nitrate showed the same distinct types of decomposition. The critical pressure for glow was measured over a range of temperatures and the effect of diluents on this limit examined. Both explosive decomposition of the pure vapour and the explosive combustion in the presence of oxygen were also observed.

Figure 9 shows the variation of the pressure limit of the glow from 270 to 500° C. It lies below that of methyl nitrate.

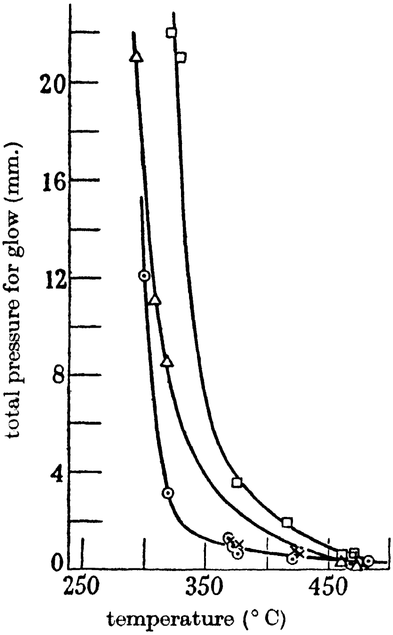

FIGURE 8. The glow limit of 1 % methyl nitrate mixtures. Comparison of argon, nitrogen, air and oxygen as diluents. □, 1. CH_3ONO_2 : 100. O_2; Δ, 1. CH_3ONO_2 : 100. air; ⊙, 1. CH_3ONO_2 : 100. N_2; ×, 1. CH_3ONO_2 : 100. A.

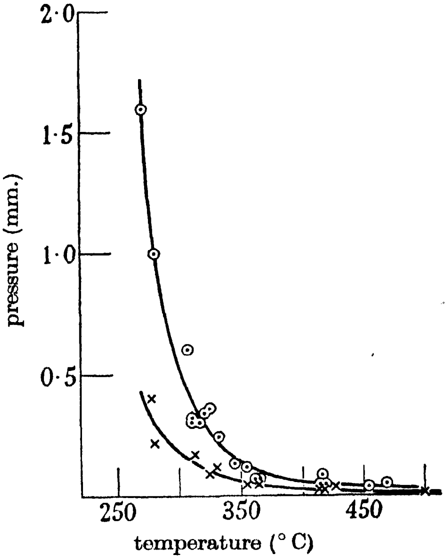

FIGURE 9. The glow limit of ethyl nitrate (×) and methyl nitrate (⊙) vapours.

The influence of dilution with argon and oxygen has been examined. Oxygen is more efficient than argon in facilitating the glow. Because the ethyl nitrate is more readily adsorbed on the walls of the apparatus, work with dilute mixtures is more difficult than with methyl nitrate, and the critical limit required for glow is less easily measured. These results are shown in figure 10.

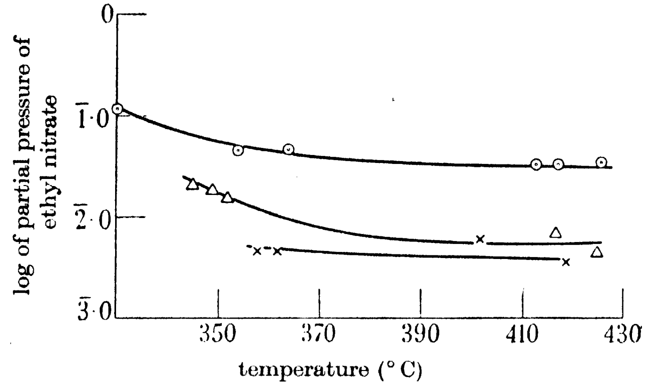

FIGURE 10. The glow limit of ethyl nitrate diluted with argon and oxygen. ⊙, pure $C_2H_5ONO_2$; Δ, $1.C_2H_5ONO_2:10.A$; ×, $1.C_2H_5ONO_2:10.O_2$.

The glow of nitroglycerin in the presence of diluents

The partial pressures required for glow of methyl and ethyl nitrates in mixtures diluted with argon and nitrogen more than a thousand times are extremely small. The vapour pressure of nitroglycerin itself (10^{-3} mm.) is such that with appreciable pressures of inert gases only very dilute mixtures can be made up. Such mixtures (total pressure about 10 cm., relative concentration 10^{-5}) have been examined and found to show the same faint, transient glow as methyl and ethyl nitrates (Gray & Yoffe 1949).

DISCUSSION

The inflammation of the alkyl nitrates is clearly a complex process, and a unique interpretation cannot be put on the results so far obtained. The behaviour of the gas-phase reaction suggests that the decomposition involves a number of intermediates of varying complexity and stability rather than a simple, monomolecular transformation accelerating itself by self heating.

(1) *The glow of the alkyl nitrates*

The pressure-temperature limits for the glow (figure 9) of ethyl and methyl nitrates show that it is possible to obtain the glow the more easily with the more complex ethyl nitrate of which the rate of thermal decomposition is greater. Appin *et al.* (1936) record a linear pressure increase during the induction period preceding explosion of methyl nitrate, viz. throughout the glow. The fact that the glow sometimes fades completely before explosion occurs suggests that the species emitting light is not itself necessary for explosion, but rather that the product which it yields builds up to a critical concentration.

Simple theory suggests that for a self-heating mechanism, or for a branching chain reaction the graph $\log \frac{p_{cr.}}{T} - \frac{1}{T}$ is a straight line. When this graph is plotted from these results a curve concave upwards is obtained so that no obvious interpretation of the chemiluminescence in terms of either of these concepts is possible.

There are marked resemblances, however, between this glow and the cool flames observed in the oxidation of many organic compounds; the very faint, blue illumination is similar to that examined by Emeléus (1926) in the oxidation of the ethers and ascribed by Fowler & Pearse (1935) to the production of formaldehyde molecules (see also Kondratiev 1930). The primary products of decomposition are NO_2, CH_2O and CH_3OH following the initial fission

$$CH_3ONO_2 \rightarrow CH_3O^{\cdot} + NO_2$$

of the methyl nitrate molecule to fragments which react further to give the final products. Harris & Siegel (1941) have recorded the readiness with which nitrogen dioxide oxidizes methyl alcohol in the cold, and Pollard & Wyatt (1949) have studied the explosion of formaldehyde-nitrogen peroxide mixtures. These reactions may well involve a step sufficiently exothermic to cause the emission of blue light, whether following the formation of an excited molecule or from the reorganization of a single radical. The inert gases, which facilitate the glow to such a remarkable extent, may serve to keep up the rate of activation (Steacie, private communication) of the methyl nitrate as its partial pressure decreases and the collisions of pairs of nitrate molecules become less frequent. They may also serve to hinder diffusion to the walls of the excited species produced from the activated methyl nitrate molecules if collisions with them in the gas phase do not deprive them of their excess energy.

The luminescence may be due to the production of excited formaldehyde molecules, and study of the emission spectrum of the glow should decide this point. Experiments made by Herzberg & Franz (1932), by showing that the fluorescence of formaldehyde was not quenched by a large excess of air, showed that excited formaldehyde molecules could survive many encounters with other species. The differences between oxygen and nitrogen, in the extent to which they facilitate the glow, may be ascribed to the possibility in the case of oxygen of removal of excited formaldehyde molecules by a reaction impossible in the cases of nitrogen or argon. Furthermore, the failure of nitromethane to show this glow may be connected with the fact that in it the nitrogen atom is joined directly to carbon and the formation of formaldehyde is made correspondingly more difficult.

(2) *The explosion of methyl nitrate*

In any exothermic reaction isothermal conditions are attained only as a limiting case when the reaction is proceeding infinitely slowly, and normally the finite speed of the change implies self-heating to a temperature above that of the surroundings and consequent acceleration of the chemical change. Loss of heat due to convection and conduction opposes this tendency. If the rate of production of heat always exceeds the rate of loss, then the self-sustaining reaction accelerates to a great speed and inflammation and explosion may occur. A simple theoretical treatment of thermal explosion was first given by van't Hoff (1884), and Christiansen (1928) discussed such energy chains further. It is clear that because of the need to attain a high temperature, dilution with inert gases will tend to quench ignition. Though simple theory does not explicitly assume any detailed mechanism for the reaction concerned, numerical values assigned, for example, to the energy of activation, give an indication of the type of process involved. Further, from the more detailed treatment of Todes (1936), Frank-Kamenetski (1939) and Rice (1940), 'a whole set of functional relationships emerges'—between induction period and temperature for example.

It is also theoretically possible for a reaction to accelerate isothermally by an autocatalytic process to explosive speeds if intermediate products are formed which provide new and easier reaction paths for converting reactants to products while being themselves regenerated. A particular case is afforded by the branched radical-chain mechanism for gaseous explosions, where more than one radical is produced from an elementary reaction involving only one reactant radical and the reaction accelerates rapidly until inflammation and explosion result. Such chains may be broken by removal of the radicals by recombination either at the walls of the vessel in pairs or in the gas phase in the presence of a third molecule. Thus two factors limit the ranges of conditions suitable for ignition; at low pressures, diffusion to the walls; at high pressures, deactivation in the gas. The addition of inert gases to a low pressure of explosive vapour impedes the former process and so facilitates explosion. The latter process can set an upper limit to the pressure leading to explosion at a given temperature in certain reactions. Theoretical distinctions may then be drawn between thermal explosions and radical-chain explosions, though Christiansen (1928) has emphasized the difficulty in practice in distinguishing between energy chains and material chains and Dainton (1942) has drawn attention to the composite, chain-thermal nature of a number of gaseous explosions. There are, however, certain practical distinctions which make it possible to decide which process predominates. From their measurements on the inflammation of pure methyl nitrate over the temperature range 210 to 350° C, and in particular from a detailed interpretation of measurements of brief induction periods, Appin *et al.* decided that the explosion of methyl nitrate is due to self heating. This view was challenged by Rice (1940), whose criticisms were answered by Frank-Kamenetski (1940).

The inference from the effect of added inert gases is clear. Explosion is aided over the whole temperature range by dilution with argon or nitrogen (figure 4), showing that self heating is of secondary importance, and that the explosion develops by a branching chain mechanism. The effect of surface/volume ratio on the explosion limit is in accord with this view if the radicals causing branching are lost principally by diffusion to the walls.

The rate of thermal decomposition of methyl nitrate is such that its half-life varies from about 5 sec. at 275° C to about 2 msec. at 425° C. That is to say, at temperatures above 300° C the whole of the methyl nitrate has decomposed during the induction period before explosion occurs, and that at these temperatures the explosion observed is probably of the complex mixture of nitrogen dioxide, methyl alcohol and formaldehyde.

We wish to express our thanks to Dr F. P. Bowden for his interest and encouragement throughout this work; to Dr G. H. N. Chamberlain and Dr A. D. Walsh for their kindness in letting us use their own apparatus for preliminary experiments on the explosion of methyl nitrate; and to Professor R. G. W. Norrish, Dr E. W. R. Steacie, Dr A. G. Gaydon and Professor C. E. H. Bawn for discussion and comments.

Our thanks are due to the Ministry of Supply (Air) for grants for equipment for the laboratory, to the Royal Society for the award to A.D.Y. of the Mackinnon Studentship; to Gonville and Caius College, Cambridge, for the award of the Dunlop Studentship and to the D.S.I.R. for a maintenance grant to P.G.

REFERENCES

Appin, A., Chariton, J. & Todes, O. 1936 *Acta Phys-chim. U.R.S.S.* **5**, 655.
Bawn, C. E. H. & Adams, R. G. 1949 *Trans. Faraday Soc.* **45**, 494.
Bowden, F. P., Mulcahy, M. F. R., Vines, R. G. & Yoffe, A. 1947 *Proc. Roy. Soc.* A, **188**, 291.
Christiansen, J. A. 1928 *Trans. Faraday Soc.* **24**, 706.
Dainton, F. S. 1942 *Trans. Faraday Soc.* **38**, 227.
Emeléus, H. J. 1926 *J. Chem. Soc.* p. 2948.
Emeléus, H. J. 1929 *J. Chem. Soc.* p. 1733.
Fowler, A. & Pearse, R. 1935 see Ubbelohde, A. R. 1935 *Proc. Roy. Soc.* A, **152**, 354.
Frank-Kamenetski, D. A. 1939 *Acta Phys-chim. U.R.S.S.* **10**, 365.
Frank-Kamenetski, D. A. 1940 *J. Chem. Phys.* **8**, 125.
Gray, P. & Yoffe, A. D. 1949 *Research*, **2**, 339.
Harris, L. & Siegel, B. M. 1941 *J. Amer. Chem. Soc.* **63**, 2520.
Herzberg, G. & Franz, K. 1932 *Z. Phys.* **76**, 720.
Kondratiev, V. 1930 *Z. Phys.* **63**, 322.
Pollard, F. H. & Wyatt, R. M. H. 1949 *Trans. Faraday Soc.* **45**, 760, 767.
Rice, O. K. 1940 *J. Chem. Phys.* **8**, 727.
Steacie, E. W. R. Private communication.
Todes, O. M. 1936 *Acta Phys.-chim. U.R.S.S.* **5**, 785.
van't Hoff, J. H. 1884 *Études de dynamique chimique.*
White, A. G. & Price, F. W. 1919 *J. Chem. Soc.* p. 1462.
Zeldovich, Y. B. & Shaulov, Y. K. 1947 *Chem. Abstr.* **41**, 2969.

One-dimensional dislocations

III. Influence of the second harmonic term in the potential representation, on the properties of the model

By F. C. Frank and J. H. van der Merwe

H. H. Wills Physical Laboratory, University of Bristol

(*Communicated by N. F. Mott, F.R.S.—Received* 21 *July* 1949)

In the previous one-dimensional dislocation model, a single sinusoidal term was taken to represent the potential energy of the deposit as a function of its position on the substrate. In this model a more general representation of the potential, containing a second harmonic term as well, is used, and it is shown that the solution in this case is also expressible in terms of elliptic integrals. The displacements corresponding to a sequence of dislocations (or a single one) are calculated. The work done in generating a single dislocation by a force on a free end is derived and the stability conditions for such a chain determined. It turns out that the properties of single dislocations, especially as concerns their application to misfitting monolayers and oriented overgrowth, remain almost uninfluenced, unless the amplitude of the second harmonic term is so large as to produce a new minimum and provided the overall amplitude of the potential energy is taken to be constant. When the amplitude of the second harmonic term is large, so that the potential curve has a second minimum, a complete dislocation splits up into two halves which are the one-dimensional analogues of Shockley's 'half-dislocations' in close-packed lattices. The equilibrium separation of the two halves, as well as the stability conditions for the existence of a single half, are determined.

1. Introduction

In the development of the theory of the one-dimensional dislocation model, the first harmonic term in a Fourier series was taken to represent the periodic potential energy V. In this model a row of identical particles (atoms), connected by identical springs (elastic constant μ), is supposed to be acted on by a substrate force which varies periodically with distance along the row. The wave-length a of the resulting periodic substrate potential energy, represented by the single harmonic term, is taken to be different from the equilibrium spacing b of the particles. It is, however, generally believed that the potential curve representing the interaction of an atom with other atoms on a crystalline plane has in reality a wider and flatter crest and a narrower trough than those given by a single harmonic term. This, incidentally, turned out to be the case for the potential energy along the straight edge of a close-packed two-dimensional lattice, as was shown by our calculations (1949) with Lennard-Jones forces. The next approximation, containing the first and second harmonic terms of the Fourier series, has the desirable properties, when the amplitude $\frac{1}{2}w$ of the second harmonic term is small compared with the amplitude $\frac{1}{2}W$ of the first harmonic term ($w/W \leqslant \frac{1}{4}$). We denote w/W by r^2; then curve a, figure 1, is a graph of V in the limiting case $r^2 = \frac{1}{4}$.

When $r^2 > \frac{1}{4}$ this potential function has a second minimum, as shown in figure 1b, and is therefore capable of carrying 'split' or 'half-dislocations' discussed previously by Heidenreich & Shockley (1948) in connexion with dislocations lying in the (111) planes of face-centred cubic crystals and the (001) planes of hexagonal close-packed crystals. Consider a monolayer on a crystal surface. Let the exposed substrate surface be the (111) face of a face-centred cubic metal. The atoms in the surface, denoted by × 's (figure 2), have a hexagonal pattern. If the monolayer is of the same substance as the substrate, its atoms, denoted by o's, will fill up a particular set of crevices on the substrate, characteristic of the face-centred cubic structure. This set of 'proper' crevices is one-half of the total number. The potential energy of an atom in these proper crevices must therefore be less than in the remaining 'improper' ones. (For the hexagonal crystal, the remaining half are the proper crevices.) The curve of the potential energy of an atom against path length, as it is moved along the surface from a proper position A, through an improper position B to a neighbouring proper position C, will therefore resemble b in figure 1, where the distance x denotes path length. A complete dislocation (displacement vector AC) when formed between the monolayer and substrate will separate into two halves, repelling each other because of their elastic energy of interaction and attracting each other, because the region between them, containing atoms in positions of higher potential energy (improper crevices), tends to contract. The treatment is only approximate, applying to the case in which the alternate deep and shallow potential troughs fall on a straight line.

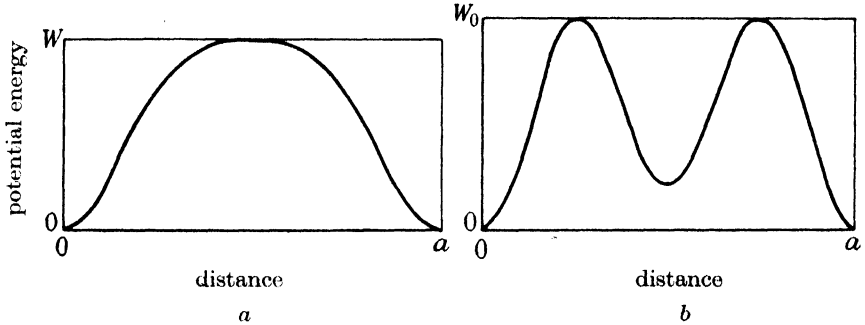

FIGURE 1. The potential energy (V) as a function of the distance x.

$$V(x) = \tfrac{1}{2}W\{1-\cos(2\pi x/a)\} + \tfrac{1}{2}w\{1-\cos(4\pi x/a)\},$$

where a is the substrate wave-length. Curve a corresponds to $w/W = \frac{1}{4}$, which is typical of the general case $w/W \leqslant \frac{1}{4}$. Curve b corresponds to $w/W = 4$, which is typical of the general case $w/W > \frac{1}{4}$.

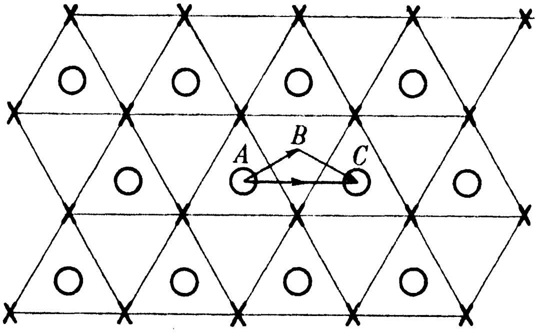

FIGURE 2. Atomic arrangement in (111) plane of face-centred cubic metal. The × 's denote atoms in one layer and the 0's denote atoms in the next monolayer above it. The potential energy of an atom is lower in the positions A, C, ..., etc. than in the positions B, D, ..., etc.

2. EQUATION OF EQUILIBRIUM AND ITS GENERAL SOLUTION

If n enumerates the troughs of the potential field and x_n is the displacement of the nth ball from the nth trough, then the total potential energy of a chain containing N atoms is given by

$$\begin{aligned} V_N &= \sum_{n=0}^{N-1} \tfrac{1}{2}\mu(x_{n+1}-x_n+a-b)^2 + \sum_{n=0}^{N-1}\left\{\tfrac{1}{2}W\left(1-\cos\frac{2\pi x_n}{a}\right)+\tfrac{1}{2}w\left(1-\cos\frac{4\pi x_n}{a}\right)\right\} \\ &= Wl_0^2\sum_{n=0}^{N-1}\left(\zeta_{n+1}-\zeta_n-\frac{1}{P_0}\right)^2+\tfrac{1}{2}W\sum_{n=0}^{N-1}\{1-\cos 2\pi\zeta_n+r^2(1-\cos 4\pi\zeta_n)\}, \qquad (1)\end{aligned}$$

where $l_0 = (\mu a^2/2W)^{\frac{1}{2}}$, $\zeta_n = x_n/a$, $1/P_0 = b/a-1$ and $r^2 = w/W$. The condition $(\partial V/\partial\zeta_n = 0)$ of equilibrium of the nth atom then gives

$$\zeta_{n+1}-2\zeta_n+\zeta_{n-1} = (\pi/2l_0^2)\{\sin 2\pi\zeta_n+2r^2\sin 4\pi\zeta_n\}.$$

If both l_0 and l_0/r are sufficiently large, we may approximate this second difference by a second derivative (by Taylor expansion, neglecting derivatives of 4th and higher orders), obtaining

$$d^2\zeta/dn^2 = (\pi/2l_0^2)\{\sin 2\pi\zeta+2r^2\sin 4\pi\zeta\}. \qquad (2)$$

Integration of (2) gives

$$d\zeta/dn = \pm\{\lambda^2-\cos 2\pi\zeta(1+2r^2\cos 2\pi\zeta)\}^{\frac{1}{2}}/2^{\frac{1}{2}}l_0, \qquad (3)$$

where the constant $\lambda^2 = 1+2r^2+2l_0^2\epsilon^2$

and $\epsilon = d\zeta/dn$ at $\zeta = 0$.

The positive sign in (3) corresponds to negative dislocations (extension of the chain with respect to the substrate) and the negative sign to positive dislocations (compression of the chain). For the sake of simplicity we shall confine our calculations to negative dislocations. The results are applicable to both cases.

Integrating (3), we obtain

$$n-n_0 = 2^{\frac{1}{2}}l_0\int\{\lambda^2-\cos 2\pi\zeta(1+2r^2\cos 2\pi\zeta)\}^{-\frac{1}{2}}d\zeta,$$

where n_0 is an integration constant.

If we put $\cos 2\pi\zeta = y \quad (0 \leqslant \zeta \leqslant 1)$,

we obtain $n-n_0 = \mp\dfrac{l_0}{2\pi r}\displaystyle\int_{-1}^{y}\{(y-\delta)(y+1)(y-1)(y-\alpha)\}^{-\frac{1}{2}}dy,$

where

$$\delta = -\{(1+8r^2\lambda^2)^{\frac{1}{2}}+1\}/4r^2 \quad (\delta \leqslant -1),$$

$$\alpha = \{(1+8r^2\lambda^2)^{\frac{1}{2}}-1\}/4r^2 \quad (\alpha \geqslant 1),$$

$$n = n_0 \text{ when } y = -1 \quad (\zeta = \tfrac{1}{2}),$$

and the $-$ sign refers to the region $0 \leqslant \zeta \leqslant \frac{1}{2}$, the $+$ sign to $\frac{1}{2} \leqslant \zeta \leqslant 1$.

This integral, which is an elliptic integral of the third kind, may be written in terms of the elliptic notation (Greenhill 1892)

$$n-n_0 = \mp l_0 F(k,\phi)/\pi r\{(1+\alpha)(1-\delta)\}^{\frac{1}{2}}, \tag{4}$$

where
$$F(k,\phi) = \int_0^{\phi} (1-k^2\sin^2\psi)^{-\frac{1}{2}}\,d\psi,$$

$$k^2 = 2(\alpha-\delta)/(1+\alpha)(1-\delta) \quad \text{and} \quad \sin^2\phi = (1-\delta)(1+\cos 2\pi\zeta)/2(\cos 2\pi\zeta-\delta).$$

There seems no point at the moment in working out this general case (representing a sequence of dislocations) in detail. We shall, however, consider the case of a single dislocation, remote from all others, corresponding to the case in which ϵ is zero, and shall show that a small second harmonic term produces only a small change in the properties of a dislocation.

3. SINGLE DISLOCATION ($\epsilon = 0$, $\lambda^2 = 1+2r^2$)

It is seen from (3) that, in this case,

$$d\zeta/dn = \sin\pi\zeta(1+4r^2\cos^2\pi\zeta)^{\frac{1}{2}}/l_0. \tag{5}$$

On integrating (5) and dividing the integrand above and below by $\cos^2\pi\zeta$, it becomes

$$n-n_0 = l_0\int\frac{\sec^2\pi\zeta\,d\zeta}{\tan\pi\zeta(1+4r^2+\tan^2\pi\zeta)^{\frac{1}{2}}},$$

where n_0 is an integration constant.

If we substitute $\tan\pi\zeta = (1+4r^2)^{\frac{1}{2}}\sinh y$ the integral is easily shown to be

$$n-n_0 = \{l_0/\pi(1+4r^2)^{\frac{1}{2}}\}\ln|\tanh\tfrac{1}{2}y|.$$

From the equality
$$\tanh\tfrac{1}{2}y = \sinh y/(1+\cosh y),$$

it is then seen that

$$n = \pm\{l_0/\pi(1+4r^2)^{\frac{1}{2}}\}\ln|\tan\pi\zeta/\{(1+4r^2)^{\frac{1}{2}}+(1+4r^2+\tan^2\pi\zeta)^{\frac{1}{2}}\}|, \tag{6}$$

when n_0 is chosen such that $n = 0$ when $\zeta = \frac{1}{2}$ and the plus and minus signs correspond to the regions in which n is less than, or greater than, zero.

The graphs of $\zeta(n)$, as given by (6), are of two distinct types depending on whether $r^2 \leqslant \frac{1}{4}$ (curves a and c, figure 3) when there is one point of maximum slope or $r^2 > \frac{1}{4}$ (curve b) when there are two such points. These points, determined by the condition $d^2\zeta/dn^2 = 0$, are given by the roots of

$$\sin 2\pi\zeta(1+4r^2\cos 2\pi\zeta) = 0. \tag{7}$$

Hence, either $\zeta = \frac{1}{2}m$, where m is an integer, or

$$\cos 2\pi\zeta = -1/4r^2. \tag{8}$$

It is seen from (5) and the graphs in figure 3 that the roots $\zeta = m$ correspond to zero slope and $\zeta = \frac{1}{2}(2m+1)$ to the slope $1/l_0$. When $r^2 < \frac{1}{4}$, (8) has no real roots, so that $1/l_0$ is the maximum slope of $\zeta(n)$ and, as in part I, l_0 defines the 'effective length' of the dislocation, measured in units of a. The graph of $\zeta(n)$ in figure 3, curve a, corresponds to the limiting value $r^2 = \frac{1}{4}$. By comparison with curve *c*, figure 3, it is seen that the effect of the second harmonic is to make the displacement tend rather more rapidly to zero on either side of the dislocation, assuming that the overall amplitude of the potential energy is taken to be constant. When, on the other hand, one takes the force exerted by the substrate on an atom in a small displacement from its stable equilibrium position to be the constant quantity, then the converse will be true.

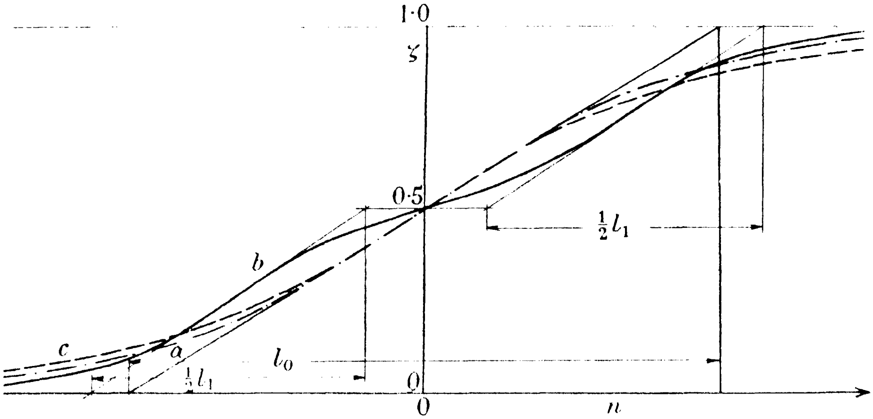

FIGURE 3. The displacement ($\zeta = x/a$) in a single dislocation as a function of the distance (n; measured in units of a) along the chain of atoms. Curves a and c correspond to the general case $w/W \leqslant \frac{1}{4}$; a for $w/W = \frac{1}{4}$ and c for $w = 0$. Curve b corresponds to $w/W = 4$, which is typical of the general case $w/W > \frac{1}{4}$. The overall amplitude of the potential energy is taken to be the same for all three curves.

4. SPLIT DISLOCATIONS ($r^2 > \frac{1}{4}$)

If, however, $r^2 > \frac{1}{4}$ the potential curve has a second minimum, in which case equation (8) also has real roots, determining the points of maximum slope of $\zeta(n)$. Substitution of (8) into (5) gives this maximum gradient

$$1/l_1 = (r + 1/4r)/l_0. \tag{8a}$$

It will be seen from figure 3 that there are two such points. When $r^2 = \frac{1}{4}$, the two roots are coincident and equal to $\zeta = \frac{1}{2}(2m+1)$, in which case $l_1 = l_0$. Since each half-dislocation represents a displacement $\frac{1}{2}a$, l_1 may be regarded as the 'effective length' of a half-dislocation, measured in units of $\frac{1}{2}a$.

Points of maximum slope in $\zeta(n)$ corresponds to maxima of the substrate potential. For equation (7) corresponds to

$$d\{\tfrac{1}{2}W(1-\cos 2\pi\zeta) + \tfrac{1}{2}w(1-\cos 4\pi\zeta)\}/d\zeta = 0$$

and hence also determines the minima and maxima of the potential energy term in (1). The maximum value W_0 of the potential energy is

$$\begin{aligned} W_0 &= W(r + 1/4r) \quad (r^2 \geqslant \tfrac{1}{4}) \\ &= W \qquad\qquad\quad (r^2 \leqslant \tfrac{1}{4}). \end{aligned}$$

In terms of W_0, l_1 becomes (see (8*a*) and the expression for l_0)

$$\begin{aligned} l_1 &= (\mu a^2/2W_0)^{\frac{1}{2}} \quad (r^2 \geqslant 0) \\ &= l_0 \qquad\qquad\quad (r^2 \leqslant \tfrac{1}{4}). \end{aligned} \qquad (8b$$

The remarkable feature of this result is that the maximum value of $d\zeta/dn$, and hence the effective length l_1 of a dislocation, depends only on the overall amplitude W_0 of the potential energy and not on the actual shape of the potential curve. It is easy to show that this result is completely general.

Let $V(\zeta)$ be the potential variation of a deposit atom with respect to the substrate, measured from one of its minima (occurring at the points $\zeta = m$) as the zero point. Let the maximum value of V be W_0. Then we have (see equations (1) and (2)) for the differential equation of equilibrium

$$d^2\zeta/dn^2 = (1/\mu a^2)\, dV/d\zeta.$$

The integration of this gives for a single dislocation (for which $d\zeta/dn = 0$ at $\zeta = m$),

$$(d\zeta/dn)^2 = 2V/\mu a^2.$$

The maximum value of $|\, d\zeta/dn \,|$ is thus seen to be

$$1/l_1 = (2W_0/\mu a^2)^{\frac{1}{2}}, \tag{8c}$$

which proves our statement.

If we now take the centres of dislocations as the points where atoms are on potential crests—these are incidentally also the points of maximum $d\zeta/dn$—then the separation L of the two halves of the dislocation, measured in units of $\frac{1}{2}a$, is given by (7) and (6).

From (7) one obtains

$$|\tan \pi\zeta_1| = (4r^2+1)^{\frac{1}{2}}/(4r^2-1)^{\frac{1}{2}}$$

and hence $$L = 4n(\zeta_1) = l_1\{(1+4r^2)^{\frac{1}{2}}/r\} \ln \{2r + (4r^2-1)^{\frac{1}{2}}\}. \tag{9}$$

5. Equilibrium of a chain with free ends

As in part I the case of a chain with free ends on a substrate which continues, is of particular interest. Dislocations can be generated in this system by displacing the atom at a free end. In equilibrium, the external force on this atom is given by the tension in the 'spring' following it. The tension in the spring between the nth and $(n+1)$th atoms is

$$t_n = \mu(x_{n+1} - x_n + a - b) = 2Wl_0^2(\zeta_{n+1} - \zeta_n - 1/P_0)/a.$$

Expanding ζ_{n+1} in a Taylor series and neglecting derivatives of order higher than the second, we obtain

$$t(\zeta) = 2Wl_0^2(d\zeta/dn - 1/P_0)/a \tag{10}$$

$$= 2Wl_0^2\{\sin \pi\zeta (1 + 4r^2 \cos^2 \pi\zeta)^{\frac{1}{2}}/l_0 - 1/P_0\}/a. \tag{10a}$$

In the case of split dislocations ($r^2 > \frac{1}{4}$) it is convenient to express this in terms of W_0 and l_1,

$$t(\zeta) = 2W_0 l_1^2\{\sin \pi\zeta (1 + 4r^2 \cos^2 \pi\zeta)^{\frac{1}{2}}/l_1(r + 1/4r) - 1/P_0\}/a. \tag{10b}$$

The graphs of $t(\zeta)$ in figure 4 correspond to the two typical cases; curve a for $r^2 \leqslant \frac{1}{4}$ and curve b for $r^2 > \frac{1}{4}$.

When the tension t_n is zero, the chain can be in equilibrium with the nth atom at a free end. If we denote the displacement of this atom by ζ_0 then ζ_0 must be a real root of the equation $t(\zeta_0) = 0$. The conditions which determine this are better understood when derived from the graphs. Referring to figure 4*a*, it is seen that this equation can only have a real solution when $0 \leqslant 1/P_0 \leqslant 1/l_0$. If the misfit exceeds the limiting value

$$1/P_0 = 1/l_0, \tag{11}$$

a pressure at the end of a chain is necessary to prevent the spontaneous formation of dislocations, while below the limiting value

$$1/P_0 = 0 \tag{11a}$$

a tension at the end of the chain is necessary to prevent a dislocation, when formed, from escaping spontaneously.

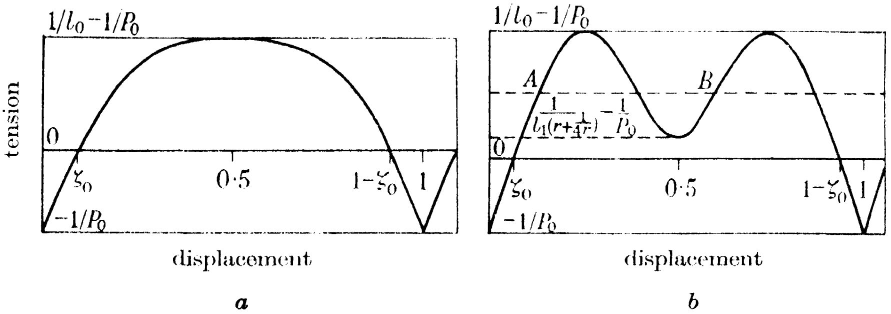

FIGURE 4. The tension (t) in a 'spring' as a function of the displacement ($\zeta = x/a$) of the 'atom' preceding it. Curve *a* is the graph of $t/(2W_0 l_1^2/a)$ for $w/W = \frac{1}{4}$, which is typical of the general case $w/W \leqslant \frac{1}{4}$. Curve *b* is the graph of $t/(2W_0 l_1^2/a)$ for $w/W = 4$, which is typical of the general case $w/W > \frac{1}{4}$.

Figure 4*b* shows that the upper limiting misfit becomes

$$1/P_0 = 1/l_1, \tag{11b}$$

when $r^2 > \frac{1}{4}$.

There may now, however, be two more real roots of the equation, namely, if

$$1/l_1(r + 1/4r) \leqslant 1/P_0 \leqslant 1/l_1,$$

where the limiting misfit

$$1/P_0 = 1/l_1 \tag{11c}$$

corresponds to the spontaneous formation of a half-dislocation and

$$1/P_0 = 1/l_1(r + 1/4r) \tag{12}$$

to its spontaneous escape. In figure 5 are graphs of these relationships.

Since equations (11*a*), (11*b*) and (11*c*) depend on the maxima of $t(\zeta)$ and hence the maxima of $d\zeta/dn$, we come, by relation (8*c*), to the interesting conclusion that also the limiting misfits for spontaneous dislocation depend only on W_0 and not on the detailed shape of the potential curve. Furthermore it turns out that the limiting misfit for the spontaneous escape of dislocations is always zero.

6. Generation of dislocations by force on free end

(i) *Complete dislocation*

The work done in forming a complete dislocation by pulling the atom at the free end of the chain reversibly from its position of stable equilibrium ζ_0 to its next position of stable equilibrium $1+\zeta_0$ (figure 4), is given by

$$W_1 = a\int_{\zeta_0}^{1+\zeta_0} t(\zeta)\,d\zeta \quad \left(= 2a\int_0^{\frac{1}{2}} t\,d\zeta\right).$$

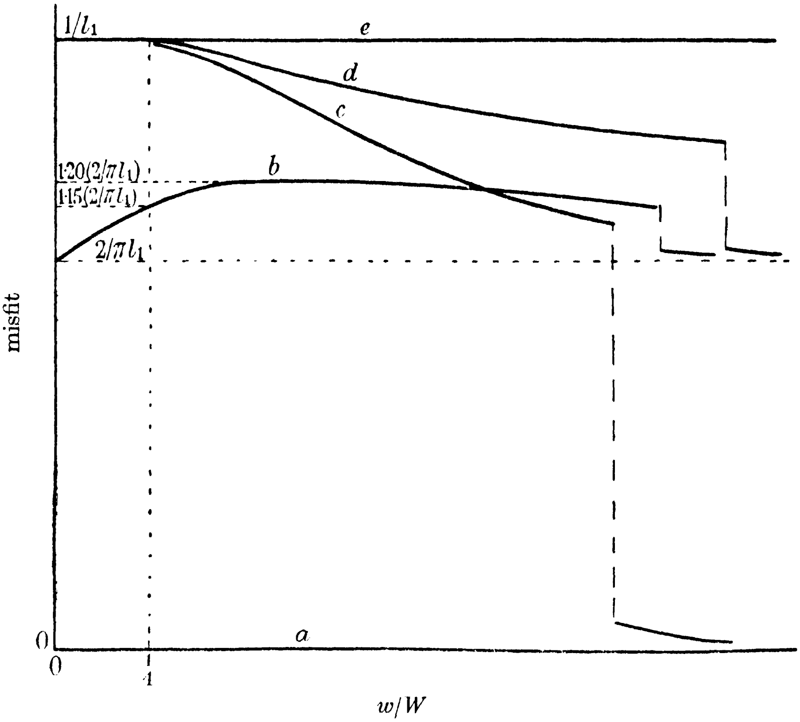

Figure 5. The limiting misfit $(1/P_0)$ as a function of the ratio w/W. Curve a, the spontaneous escape of complete dislocations; b, the lowest energy state of the system; c, the spontaneous escape of a half-dislocation; d, the state in which the energy remains stationary under the formation of a half-dislocation; and e, the spontaneous generation of complete and half-dislocations.

If we substitute for $t(\zeta)$ and make use of the integral

$$\int \sin \pi\zeta(1+4r^2\cos^2\pi\zeta)^{\frac{1}{2}}\,d\zeta = -\{\ln[2r\cos\pi\zeta + (1+4r^2\cos^2\pi\zeta)^{\frac{1}{2}}] + 2r\cos\pi\zeta(1+4r^2\cos^2\pi\zeta)^{\frac{1}{2}}\}/4\pi, \tag{13}$$

we obtain

$$W_1 = 2Wl_0^2\{[2r(1+4r^2)^{\frac{1}{2}} + \ln[2r+(1+4r^2)^{\frac{1}{2}}]]/2\pi r l_0 - 1/P_0\}. \tag{14}$$

When this work is zero (depending on the misfit) the system is in its state of lowest energy and

$$1/P_0 = \{2r(1+4r^2)^{\frac{1}{2}} + \ln[2r+(1+4r^2)^{\frac{1}{2}}]\}/2\pi r l_0. \tag{15}$$

In the case of split dislocations $(r^2 > \frac{1}{4})$ we may express (14) and (15) in terms of W_0 and l_1. A graph of (15) is shown in figure 5.

(ii) *Half-dislocation*

When the ζ-axis cuts $t(\zeta)$ (figure 4*b*) along AB (say), a single half-dislocation when formed, is in metastable equilibrium. The work done on the last atom of the chain in this process is

$$W_2 = a\int_A^B t(\zeta)\,d\zeta \quad \left(= 2a\int_{\zeta_1}^{\frac{1}{2}} t\,d\zeta\right),$$

where ζ_1 is a root of $\cos 2\pi\zeta_1 = -1/4r^2$ $(\frac{1}{4} \leqslant \zeta_1 \leqslant \frac{1}{2})$. It follows then from (13) and (10*b*) that

$$W_2 = 4W_0 l_1^2\{[\ln[(4r^2+1)^{\frac{1}{2}} + (4r^2-1)^{\frac{1}{2}}] - \tfrac{1}{2}\ln 2 + \tfrac{1}{2}(16r^4-1)^{\frac{1}{2}}]/\pi l_1(4r^2+1) - (\tfrac{1}{2}-\zeta_1)/P_0\}. \tag{16}$$

Below a certain critical misfit the energy of the system can be lowered by the formation of a single half-dislocation. This critical value, determined by $W_1 = 0$, is

$$1/P_0 = \{\ln[(4r^2+1)^{\frac{1}{2}} + (4r^2-1)^{\frac{1}{2}}] - \tfrac{1}{2}\ln 2 + \tfrac{1}{2}(16r^4-1)^{\frac{1}{2}}\}/\pi l_1(4r^2+1)(\tfrac{1}{2}-\zeta_1). \tag{17}$$

This misfit as a function of w/W $(= r^2)$ is shown in figure 5.

We may further define an activation energy for the formation of a complete dislocation as the work done on the last atom of the chain when it is displaced from its position of stable equilibrium ζ_0 to the position of unstable equilibrium $1-\zeta_0$ (figure 4). An activation energy for the formation of a half-dislocation may likewise be defined.

CONCLUSIONS

It seems at the moment that the greatest importance of the preceding calculations lies in their application to a misfitting monolayer, which is the initial stage of an oriented overgrowth (part II). Perhaps the most striking feature in this connexion is the dependence of the limiting misfit of spontaneous dislocation on the overall amplitude (W_0) of the potential energy only and not on the actual shape of the energy curve. The average value of 14 % for this misfit thus cannot be improved by a more accurate potential representation.

There is, however, a small change in the critical condition defining the lowest energy state of the system. It is seen from figure 5, curve *b*, that the maximum deviation $\Delta(1/P_0)/(1/P_0)$ is only about 20 %, which is a shift towards higher misfit. At the critical stage, $w/W = \frac{1}{4}$, this is even less, namely, 15 %. This refinement can therefore in the worst case only shift the critical misfit of 9 % to about 11 %. This incidentally reduces the gap between the critical misfit of spontaneous dislocation and the critical misfit of the state of lowest energy.

Those properties of a monolayer, which make it of importance in the theory of oriented overgrowth, depend on the possibility of the formation of a large number of dislocations and not on the existence of a single half-dislocation, say. We may therefore conclude at this stage, that the critical conditions necessary in order that a monolayer, deposited on a crystalline substrate, shall take up the same atomic spacings as the substrate, remain practically unchanged under a refinement of the potential representation, provided the overall amplitude of the analytic curve is taken to be equal to that of the actual curve.

We have, at the same time, derived some of the properties of split-dislocations that can exist in simple systems such as misfitting monolayers.

One of us (J. H. van der M.) has to thank the South African Council for Scientific and Industrial Research for a grant and special leave which rendered it possible to do this research.

REFERENCES

Frank, F. C. & van der Merwe, J. H. 1949 *Proc. Roy. Soc.* A, **198**, 205 (part I) and 216 (part II).
Greenhill, A. C. 1892 *Applications of elliptic functions*, p. 54. London: Macmillan & Co.
Heidenreich, R. D. & Shockley, W. 1948 *Report of Bristol conference on strength of solids*, p. 57. London: The Physical Society.

A discussion on the physics and chemistry of hydrocarbon gels

OPENING REMARKS BY THE LEADER OF THE DISCUSSION

E. K. RIDEAL, F.R.S., *The Royal Institution*

GELATION OF ALUMINIUM SOAPS IN HYDROCARBON

BY T. S. McROBERTS AND J. H. SCHULMAN, *Department of Colloid Science, University of Cambridge*

FACTORS WHICH AFFECT THE GELLING CHARACTERISTICS OF ALUMINIUM SOAPS

BY G. A. PARRY, J. E. ROBERTS AND A. J. TAYLOR, *Ministry of Supply*

THE SWELLING AND SOLUBILITY OF CELLULOSE ACETATE IN BENZENE/XYLENOL MIXTURES

BY A. E. ALEXANDER AND B. RABINOVITCH, *Department of Colloid Science, University of Cambridge*

ALUMINIUM SOAPS, THEIR NATURE AND GELLING PROPERTIES

BY A. E. ALEXANDER AND V. R. GRAY, *Department of Colloid Science, University of Cambridge*

SOME FLOW PROPERTIES OF CONCENTRATED HIGH-POLYMER SOLUTIONS

BY R. S. RIVLIN, *Davy Faraday Laboratory, The Royal Institution*

THE EQUILIBRIUM SWELLING OF CROSS-LINKED AMORPHOUS POLYMERS

BY L. R. G. TRELOAR, *Davy Faraday Laboratory, The Royal Institution*

RHEOLOGY OF HYDROCARBON GELS (Summary)

BY K. WEISSENBERG, *The British Rayon Research Association, Manchester*

THERMODYNAMICS AND RHEOLOGICAL BEHAVIOUR OF ELASTO-VISCOUS SYSTEMS UNDER STRESS (Summary)

BY F. H. GARNER, A. H. NISSAN AND G. F. WOOD, *Bowater Development and Research, Ltd.*

THE RHEOLOGY OF 'ELASTIC' NON-NEWTONIAN FLUIDS (Summary)

BY F. H. GARNER, A. H. NISSAN AND G. F. WOOD, *Bowater Development and Research, Ltd.*

[PLATE 5]

(*Discussion held* 24 *March* 1949.—*Complete MS. received* 10 *October* 1949)

OPENING REMARKS

BY E. K. RIDEAL, F.R.S.

The two-phase structure of gels is now generally accepted. One phase consists of a network of more or less solvated material, its interstices being filled with its saturated solution. The network may consist of relatively rigid crystals, or of elastic fibrillar macromolecules; the junction points holding the network together may be formed by mechanical interlocking, by the local action of dispersive forces, by hydrogen bonding or by true chemical links. The application of stress distorts the framework and can also stretch it. In thixotropic systems the network when broken down can reform and the rate of recovery can be varied over wide ranges. The potential energy stored in the distorted gel can be recovered as mass motion of gel. If the network material is appreciably soluble in the solution, the fibrils can grow in size, the gel becomes more rigid and syneresis occurs.

A polymer will dissolve in a hydrocarbon if the free energy of dilution ΔF is negative. A high heat of solution ΔH may counterbalance the large (for polymers) entropy of dilution. If $\Delta F = \Delta H - T\Delta S$ is positive, complete solution does not occur, but there results a gel in equilibrium with almost pure solvent. The degree of swelling of the gel phase is determined by a solvent-polymer interaction term μ. For linear polymers μ can be defined by

$$\Delta F = RT\left[\log(1-\nu)+\nu\left(1-\frac{1}{n}\right)+\mu\nu^2\right],$$

where ν is the volume fraction of the polymer and n the ratio of solute/solvent molecular weight.

To a first approximation $\mu = \mu_0 + \frac{\alpha}{RT}$ where α is related to the heat of mixing by the expression $\Delta H = \alpha\nu^2$.

To form hydrocarbon gels the network material must dissolve or be formed in the solvent, and the contacts are preferably polar in character. Changes in μ can also be made by admixture of paraffin hydrocarbons with cyclic or aromatic hydrocarbons, or their derivatives.

Aluminium soaps are effective gel-forming materials. If formed *in situ* the organic derivatives of aluminic acid $[\mathrm{Al(OH)}_6''']\mathrm{H}_3^{+++}$ can condense by the olation process of Bjerrum and undergo inner dehydration as postulated by Stiasny.

GELATION OF ALUMINIUM SOAPS IN HYDROCARBON

BY T. S. MCROBERTS AND J. H. SCHULMAN

The gelation of aluminium soaps in hydrocarbon has been studied by investigating:

(1) the degree of association of aluminium alkoxides,
(2) the effect of moisture on the viscosity of benzene solutions of aluminium soaps prepared *in situ* by the reaction of fatty acids with aluminium alkoxides,
(3) the properties of monolayers of aluminium soaps spread on water.

Results indicate that the product of reaction between an aluminium alkoxide and a fatty acid is a di-soap and that gelation only takes place when the third valency of the aluminium atom is occupied by a hydroxyl group.

The power of gelation in liquid hydrocarbon is not confined to the soaps of aluminium alone. Various workers, notably Koenig (1914), McBain & McClatchie (1932*a*) and Lawrence (1938), have found that most soaps dissolve in hot hydrocarbons and set to gels on cooling. However, aluminium soap gels are distinguished by their high viscosity, elasticity, rigidity and stability at low temperatures.

Gelation is usually caused by a reduction of solubility—for example, by cooling a hot supersaturated solution. When an aqueous sol sets to a gel there are indications that, apart from the large increase in viscosity, the physical properties do not change abruptly. For example, no change is observed in the conductance of an aqueous soap solution when it sets to a gel, and there is no change in the concentration of sodium ions or of aqueous vapour pressure (Boner 1937).

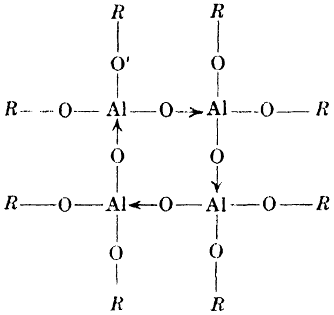

R = alkyl group

FIGURE 1. Octahedral structure of aluminium alkoxides.

There is little information available on gelation in hydrocarbons, but McBain, Mysels & Smith (1946) emphasize that there is no sharp boundary between the gel and sol, but only a continuous transformation. It would appear, therefore, that gels of soaps in hydrocarbon differ little from sols; the elastic behaviour of the gels can be attributed to the joining together, at random points, of single large molecules or aggregates of the sol.

The gelation of soaps in hydrocarbons is largely dependent on the nature of the metallic or kationic part of the molecule; Lawrence (1938) has shown that the gels of soaps in nujol fall into groups which are the ordinary chemical ones of the kations. The influence of the aluminium part of the molecule in the gelation of aluminium soaps is the purpose of the present investigation (McRoberts & Schulman 1948).

Aluminium, with stable co-ordination numbers of four and six, shows a strong tendency to accept electrons as shown by the co-ordination complexes which aluminium chloride forms with compounds such as alcohols, ethers, ketones, amines, etc. The compound $(C_2H_5)_2O \rightarrow AlCl_3$ forms colourless crystals, melting at 36° C, which can be distilled under reduced pressure.

Robinson & Peak (1935) have shown that aluminium alkoxides exist in associated complexes, each containing four units of $Al(OR)_3$. They proposed an octahedral structure which, as modified by Gray (1946), is shown in figure 1, and would account for the low melting-points of the alkoxides. In any consideration of the causes of gelation and aluminium soaps in hydrocarbon it is evident that the type of co-ordination O → Al will have to be taken into account.

Reproducible data on aluminium soaps are scarce, the chief reason being the difficulty in preparing pure soaps. The most commonly used method is the aqueous metathesis of a sodium or potassium soap with an aluminium salt. McBain and his co-workers have concluded that the normal tribasic aluminium soaps are non-existent, but claim to have isolated the mono- and di-soaps and to have characterized the latter by X-ray diffraction. However, the work of Marion & Thomas (1946) on the precipitation of aluminium hydroxide in the presence of ions indicates that soaps prepared by aqueous metathesis may contain aluminium hydroxide as an impurity. A recent paper by McBain & Mysels (1948) on the solubility of aluminium di-laurate in cyclohexane indicates that soaps prepared in this way are at least physically inhomogeneous.

Another source of discrepancy in some work is due to the large effect which traces of moisture have on the gelation of aluminium soaps. Carlile, Cawley, King & Kingman (1947) found that in some cases an increase of 1 % moisture content caused a decrease of more than 50 % in the 'ball-drop' viscosity of aluminium stearate gels. Mysels, Pomeroy & Shreve (1947) examined the sorption and desorption of water vapour by aluminium di-laurate at 50° C, and concluded that moisture is held predominantly by surface forces and capillarity. However, analysis of their 'dry' aluminium di-laurate by the Fischer method gave a 2·5 % moisture, corresponding to 0·62 mole of water per mole of soap.

The strong 'peptizing' power of water and recent work by H. M. Spurlin (private communication) on the effect of moisture on aluminium abietate suggested a quantitative estimation of its influence on gelation of aluminium soaps in general.

It is important when dealing quantitatively with the effect of moisture to ensure that the soap is initially free from water. In removing all moisture from soaps prepared by aqueous metathesis it is difficult to avoid decomposition (Mysels *et al.* 1947). For this reason the soaps were prepared by the reaction between aluminium alkoxides and fatty acids, both of which can be obtained in a highly pure and dry state. The reaction can be carried out in hydrocarbons and has the advantage that both reactants and products of reaction are soluble. On the other hand, the resulting solution will contain at least two components, one of which will be free alcohol. However, the addition of water to the 'soap' prepared in this way produced some interesting results.

It was found that these 'soaps' prepared by the reaction of alkoxide and fatty acid spread easily on fresh distilled-water surfaces to give films of reproducible properties. The results of an investigation of these films are included here, since they have some bearing on the composition stability and orientation of aluminium soap molecules.

Gray (1946) has proposed the structure for an aluminium 'di-soap' shown in figure 2. This link exists in the aluminium alkoxides, and so it is of interest to obtain some idea of its strength in compounds which can be prepared in a pure state. The association of the aluminium alkoxides has been examined.

This paper, therefore, deals with the results of the following investigations:

(*a*) The association of the aluminium alkoxides.

(*b*) The effect of water and the role of the hydroxyl group in gelation of aluminium soap.

(*c*) Some properties of monolayers of aluminium soaps on aqueous surfaces.

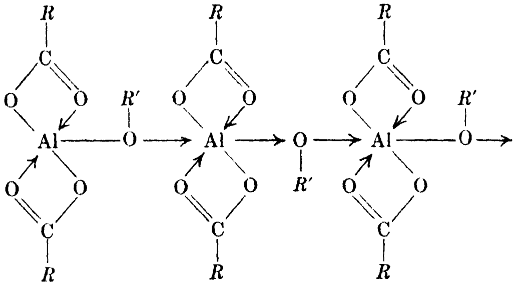

R' = H or alkyl group *R* = long chain

FIGURE 2. Suggested structure of an aluminium 'di-soap'.

The association of the aluminium alkoxides

Robinson & Peak (1935) prepared a series of aluminium alkoxides and determined their molecular weights by cryoscopic measurements in naphthalene. They concluded that all the alcoholates are polymerized fourfold, but did not examine the effect of concentration on this polymerization or association.

It is appreciated that, with solutions of such a large molecule as an aluminium alcoholate, containing polar and non-polar parts, the deviation from Raoult's law may be considerable. However, depression of freezing-point measurements should give a qualitative measure of dissociation during dilution, and extrapolation of molecular weights to zero concentration should give an approximate value of the true molecular weight, since the solute does not separate to any measurable extent during freezing-point measurements.

Experimental

The aluminium alkoxides were prepared by allowing freshly cleaned aluminium foil to react with boiling alcohol which had been dried for several days over calcium oxide. The reaction is catalyzed by mercuric chloride and carbon tetrachloride (Wilds 1944). The alkoxides were obtained dry and pure by redistilling *in vacuo* (less than 1 mm.). The lowest member of the series, aluminium methylate, could not be isolated in a pure state, since it decomposed before melting or distilling. The amylate also decomposed during distillation, but the ethylate, *n*-propylate, *iso*-propylate, *n*-butylate and *sec.*-butylate were all prepared in a pure state.

The benzene was redistilled thiophen-free and left to dry over pure sodium for at least 3 days.

The apparatus was a modified Beckmann. The thermometer was completely enclosed in a vessel which was connected to a vacuum line. Liquid could be introduced into the vessel through a valve operated by a magnet. The valve connected the vessel with a bulb reservoir which had a mercury-sealed stopper.

The apparatus was evacuated for several hours to remove all the free water vapour. Atmospheric pressure was restored by air dried over phosphorus pentoxide. Benzene or a solution of the alkoxide was then introduced from the bulb reservoir. Readings at progressive dilutions were obtained by introducing successive amounts of benzene. This method of increasing the amount of solvent was tried out with naphthalene and found to give good agreement up to three times dilution.

Molecular weights were calculated on the assumption that Raoult's law holds.

Results

The results are shown in table 1. The calculated molecular weights are those for single molecules, $Al(OR)_3$.

Table 1

	concentration (M)	molecular weight	
		found	calculated
Al ethoxide	0·0234	710	162
	0·0156	660	
	0·0117	641	
	0·0078	628	
	0·0058	634	
	0·0039	615	
Al *n*-propoxide	0·0204	740	204·2
	0·0176	746	
	0·0102	705	
	0·0068	725	
	0·0051	686	
	0·0034	703	
Al *n*-butylate	0·0188	926	246·3
	0·0126	902	
	0·0094	916	
	0·0062	970	
	0·0047	898	
	0·0031	855	
Al *sec.*-butylate	0·0200	969	246·3
	0·0133	944	
	0·0100	930	
	0·0067	907	
	0·0050	885	
	0·0033	908	

The results indicate that, within an experimental error of ± 10 %, the aluminium alkoxides show a degree of association or polymerization of 4 over the concentration ranges shown. The co-ordination link $\mathrm{Al{-}\overset{\overset{R}{|}}{O}\rightarrow Al}$ is, therefore, very stable and unlikely to be easily broken where R is an alkyl group.

An attempt was made to isolate and obtain an approximate value for the molecular weight of the soluble product of reaction between the alkoxides and fatty acids by pumping off the benzene with the free alcohol formed during reaction. It was found impossible either to isolate a soluble compound or to obtain reproducible values for its molecular weight, probably due to its extreme sensitivity to traces of moisture impossible to eliminate.

• *The effect of water and the role of the hydroxyl group in gelation of aluminium soaps*

It was found that when the reaction between alkoxide and fatty acid is carried out in anhydrous hydrocarbon liquid considerable heat is evolved, and the resultant product is not a gel but a solution of low viscosity. Addition of small quantities of water initiates gelation which passes through a maximum with the addition of more water, until finally the soap precipitates.

Although absolute viscosity measurements have little meaning from the classical point of view, a simple falling-sphere type of viscometer is a convenient method for following the effects of continued addition of water.

Experimental

The alkoxide and dry benzene were prepared as already described. The solid long-chain acids were very pure samples obtained from Albert Verley (Paris). They were dried in a vacuum desiccator over phosphorus pentoxide. The liquid acids were redistilled and dried over anhydrous calcium sulphate.

10 ml. each of the required strengths of fatty acid and alkoxide in benzene were quickly transferred into each of a series of tubes. The tubes were stoppered by corks wrapped in tin foil and thoroughly sealed by melted paraffin wax. The contents were mixed by gentle rotation and placed in a thermostat at 25° C. After an hour, when the reaction was presumed to have gone to completion, a measured volume of water was added to each tube from an 'Agla' syringe. The tubes were then sealed off and thoroughly mixed until all the water disappeared into solution. A relative measure of viscosity was obtained by observing the rate of fall of a steel sphere through the system. To avoid thixotropic effects as much as possible the first reading was taken in each case as the 'ball-drop' viscosity. Successive readings on a single sample usually resulted in a progressive decrease in viscosity.

Results

In each system the total volume approximates closely to 20 ml.; it is assumed that the change in volume on mixing the solutions of alkoxide and fatty acid is negligible. The amounts given, therefore, are the total amounts in approximately 20 ml. of each system.

The 'viscosity' recorded is the time taken for a steel sphere (0·8 mm. diam.) to fall between two marks 5 cm. apart.

Figure 3 illustrates the large changes in viscosity brought about by the addition of very small amounts of water to the 'soap' formed by reacting aluminium alkoxides with fatty acids in dry benzene. The water is calculated as moles per mole of aluminium alkoxide originally present. It can be seen that a maximum in viscosity appears at a point where approximately 1 mole of water per mole of alkoxide has been added. Owing to the great affinity of aluminium alkoxides for water it is impossible, even when working with the maximum speed and care, to prevent small traces of moisture from entering the system when transferring the reactants from one vessel to another. These would be sufficient to account for deviations in the maxima obtained.

More than the equivalent of 1 molecule of water gives a gel of decreasing viscosity, until at about the equivalent of 2 molecules of water the system becomes cloudy and soap begins to precipitate. The formation of this cloudy precipitate is a reversible process; it is always formed when water is first added to the system, but disappears on violent shaking provided less than the equivalent of 2 molecules of water are added. Once a gel has been formed, however, it is only affected very slowly by the addition of water.

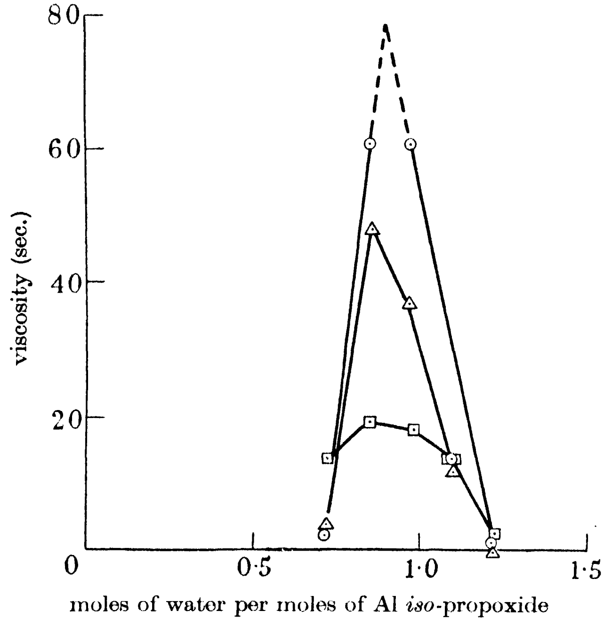

FIGURE 3. Change in viscosity on the addition of small amounts of water, $0{\cdot}216 \times 10^{-2}$ moles *iso*-propoxide; $0{\cdot}432 \times 10^{-2}$ moles lauric acid. ☐ after $1\frac{1}{2}$ hr., △ after 20 hr., ⊙ after 120 hr.

A considerable 'ageing' effect is observed in all these systems. After water has been added and the system shaken vigorously an increase in viscosity can be seen almost immediately, but the viscosity continues to increase for several days. This 'ageing' effect can be seen in the separate curves of figure 3. Increasing the temperature seemed to accelerate the process and cause a rapid increase in viscosity.

Within experimental error, the position of maximum viscosity of the systems does not appear to be influenced by the ratio of fatty acid to aluminium alkoxide molecules. The influence of this ratio on the value of the maximum viscosity is indicated in figure 4. It is difficult to determine the exact position of the maximum. To allow for the small amount of water which leaks into the systems during preparation the position of the maximum was arbitrarily fixed at 0·91 mole of water per mole of alcoholate. So although figure 4 probably does not represent the true values of the maximum viscosity at the different acid/alkoxide ratios, it does give a measure of the influence of this ratio on the degree of gelation.

The highest viscosity maxima occur between the values 1·9 and 2·1 for the fatty acid/alkoxide ratio. A higher proportion of fatty acid leads to a decrease in viscosity of the resulting gel. This is in agreement with the findings of other workers that not more than the di-soap is formed. More fatty acid than is required to form the di-soap acts as a peptizing agent to decrease the viscosity. Gels formed from a fatty acid/alkoxide ratio of less than 1·5 showed syneresis, so that it was difficult to obtain reliable viscosity readings.

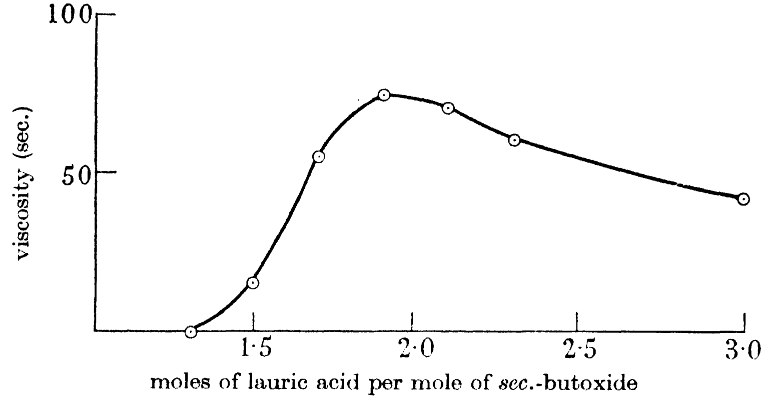

FIGURE 4. After 48 hr. 0·212 mole Al *sec.*-butoxide; 0·195 mole of water added after reaction with lauric acid.

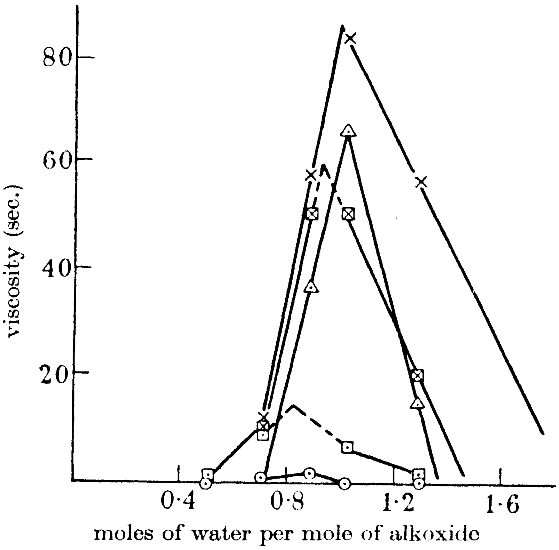

FIGURE 5. Effect on viscosity of varying chain length of fatty acid. 0·207 × 10^{-2} moles *sec.*-butoxide; 0·414 × 10^{-2} moles acid; ⊙ butyric, □ caproic, △ decanoic, ⊠ lauric, × palmitic.

Figure 5 shows the effect of varying the chain length of fatty acid on the viscosity of gels of 'soaps' prepared by the reaction of alkoxide and fatty acid. Since the amount of alkoxide is kept constant the volume fraction of 'soap' increases with increasing molecular weight of the fatty acid. This accounts for the great difference between values for butyric and palmitic acids. As expected the maximum viscosity of the gels increases steadily with increasing chain length of the fatty acid.

However, equal concentrations (by weight) of 'di-soaps' of varying chain length prepared *in situ* from the alkoxide show little variation in viscosity. The shorter chain 'soap' gels contain more molecules of 'soap' and, therefore, more molecules of free alcohol (since the soap is formed *in situ*). Free alcohol has a peptizing effect. If we assume the complete formation of 'di-soap' in these reactions the deduction is that pure di-soaps of short chain length give gels of higher viscosity than soaps of long chain length at equal weight concentrations. This would be expected if the main link in gelation is through the aluminium part of the molecule.

Some properties of monolayers of aluminium soaps on aqueous surfaces

The effect of traces of ions on the properties and reactions of monolayers on aqueous surfaces has been studied by various workers (Harkins & Myers 1937; Mitchell, Rideal & Schulman 1937). The packing of condensed films of fatty acids seems to depend on the nature of the ions. If divalent ions are present the tendency is for the chains to be close-packed at the usual area of 20·5 sq.Å per fatty-acid molecule. In the absence of such ions the curve may be that of close-packed heads approximating, if great care is taken, to 25 sq.Å per molecule.

Langmuir & Schaefer (1936) covered the surface of dilute barium and calcium hydroxide solution with films of fatty acid; the area was then reduced and the collapsed material scooped up on a platinum foil. Analysis showed, as might be expected, that it consisted of barium or calcium soap if the pH of the liquid exceeded about 11. No soap was formed at pH 3 and the film was about half soap in the neighbourhood of pH 6.

The work recorded here was an effort to determine whether a monomolecular film of an aluminium soap could be spread on an aqueous surface and, if so, what special arrangement the fatty-acid chains, attached to the aluminium, would take up.

Aluminium soaps prepared by aqueous metathesis are not easily dissolved in benzene. When such 'solutions' are spread on a clean-water surface they give unreliable and non-reproducible results. However, the product of reaction between an aluminium alkoxide and a fatty acid, provisional formula $Al(O.CO.F)_2OR$, is freely soluble in benzene. The result of hydrolyzing this compound is a soap similar to that prepared by aqueous metathesis. When a benzene solution of the compound $Al(O.CO.F)_2OR$ is placed on a clean-water surface it spreads leaving a solid, fairly stable film of reproducible properties.

Experimental

The reaction between fatty acid and alkoxide was allowed to take place in a graduated flask. Drops of the solution of the resultant 'soap', measured from an Agla syringe, were spread on a clean freshly distilled water surface of a Langmuir trough which was enclosed in a wooden box. The temperature inside the box remained fairly steady at 17 ± 1° C.

The areas are calculated in sq.Å per mole of fatty acid.

Results

The pressure-area relationships for films of 'soap' containing different ratios of palmitic acid to aluminium are shown in figure 6.

In figure 6 the ⊙ curve is for a 'soap' prepared by reacting 3 moles of palmitic acid with 1 mole of aluminium *sec.*-butoxide. Compared with the film for palmitic acid this film is more compressed and capable of standing twice as great a pressure before collapsing. However, the compression curve extrapolates to almost the same value for the cross-section of each palmitic acid molecule.

The □ and △ compression curves are for 'soaps' containing palmitic acid/alkoxide molar ratios of 2 : 1 and 1·5 : 1 respectively. Although differing in form from the ⊙ curve they show the same high compressibility and extrapolate to the same cross-sectional area.

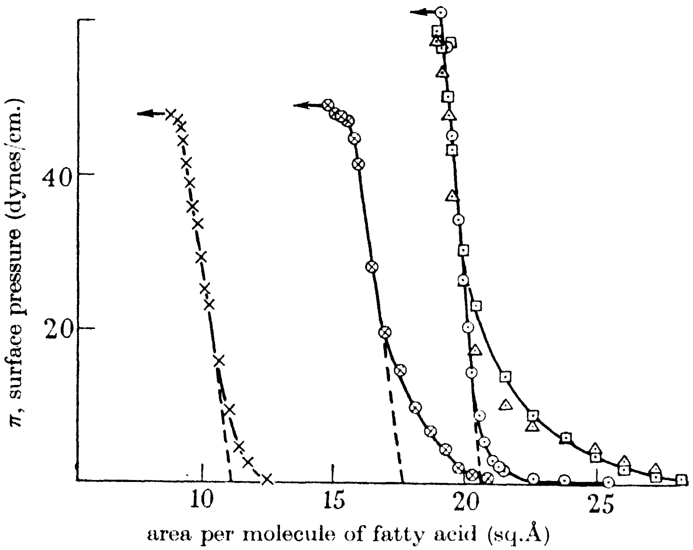

Figure 6

In the ⊗ and × curves the acid/alcoholate ratios have been still further lowered to 1·3 : 1 and 1 : 1 respectively. The result is a complete change in the properties of the films. These films, and all films of lower ratios are unstable and show a considerable progressive collapse under pressure. The small compressible portion of these films gives a π-Å relationship which extrapolates to a very low value per palmitic acid group, showing that a considerable fraction of the palmitic acid has been removed from the surface.

When any of these soaps was spread on the surface of water containing N/100, N/1000 and N/10,000-HCl the π-Å curve obtained was identical with that for palmitic acid on dilute HCl, demonstrating that most of the aluminium ions had been removed from the surface. Alkaline pH destroyed the film completely.

Palmitic acid spread on a 1 % aluminium sulphate solution was notably less stable under pressure than the 'soaps' whose π-Å curves are shown in figure 6.

An attempt was made to examine 'soaps' prepared from lauric acid whose low solution pressure gave hopes of phase separation, but the films were too weak and unstable to give consistent results.

The results show that it is possible to prepare a monolayer of aluminium soap on a freshly distilled water surface. These monolayers are fairly stable even when compressed higher than 40 dynes/cm., provided the ratio of fatty-acid groups to aluminium atoms is not less than 1·5 : 1.

The reaction between fatty acid and aluminium alkoxide can be represented as:

$$\mathrm{Al(O}R)_3 + 2\mathrm{FCOOH} \rightarrow \mathrm{Al(O.CO.F)_2O}R + 2R\mathrm{OH}, \qquad (1)$$

ROH being an alcohol.

In contact with water $\mathrm{Al(O.CO.F)_2O}R$ is immediately hydrolyzed to give the di-soap or a mixture of the mono- and di-soaps. The alcohol released is soluble in water and is removed.

Even allowing for a considerable amount of hydrolysis of the di-soap in the monolayer the results indicate that the hydrocarbon chains attached to the aluminium atom are arranged parallel to each other and not at an angle. X-ray work by McBain & Ross (1946) has shown that the same arrangement exists in the aluminium soap crystal.

Below a fatty acid/alkoxide ratio of 1·5 : 1 there is probably a certain amount of free alkoxide present in the benzene solution. In contact with water this gives a precipitate of aluminium hydroxide which may carry with it a certain amount of adsorbed soap. An alternative explanation is that the mono-soaps are unstable unless supported by di-soaps in a 1 : 1 ratio.

Discussion

It has been shown that the product of reaction between an aluminium alkoxide and a fatty acid does not gel when dispersed in benzene. The addition of water is necessary to cause gelation.

Since not more than two fatty-acid molecules react with one of aluminium alkoxide the reaction between the two can be represented empirically by equation (1) above, that is, at least one alcoholate group must still be linked to the aluminium. The compound which results from the above reaction does not give a gel in liquid hydrocarbon, even at high concentrations. The addition of water in a 1 : 1 molecular ratio is necessary to produce maximum gelation.

Now the ease with which aluminium alkoxides are hydrolyzed by water is well known. If the stopper of a bottle containing a liquid alkoxide is removed a skin of aluminium hydroxide is formed on the surface almost immediately. It is reasonable to assume, therefore, that the addition of water to the compound $\mathrm{Al(O.CO.F)_2O}R$ will result in the replacement of the alkoxide radical by hydroxyl. This replacement results in the formation of highly viscous gels. It seems, therefore, that the hydroxyl group plays a major role in the gelation of aluminium soaps in hydrocarbon.

It has also been shown that aluminium alkoxides exist as stable polymers, $[\mathrm{Al(O}R)_3]_4$, which do not show any detectable dissociation on dilution. If we assume the modified formula of Robinson & Peak (1935) for the aluminium alkoxides, (see figure 1), it is possible to explain further most of the phenomena observed.

When a fatty acid reacts with an aluminium alkoxide to replace the two most easily available alkoxide groups attached to each aluminium atom, steric hindrance may prevent further reaction. This is in agreement with the experimental observation that the tri-soap cannot be prepared by this means.

The 'stringy' nature of aluminium soap gels indicates the lateral adhesion of molecules to give unstable chain polymers. The closed-ring structure of the alkoxides must therefore be broken before gels can be formed. The replacement of alcoholate group by fatty-acid group gives a product which is a free-flowing solution in benzene. The fatty acid, therefore, either does not influence the closed-ring structure or breaks it up completely to give single molecules. In the first case the $\mathrm{Al{-}\overset{\overset{\textstyle R}{|}}{O}\rightarrow Al}$ link would be too strong to form unstable polymers and in the second case too weak. This then eliminates $\mathrm{Al{-}\overset{\overset{\textstyle R}{|}}{O}\rightarrow Al}$ as the principal linkage in gelation where R = alkyl group.

The $\mathrm{Al{-}\overset{\overset{\textstyle R}{|}}{O}\rightarrow Al}$ linkage has been shown to be strong and stable in the aluminium alcoholates, and the same is probably true in the product of reaction with a fatty acid, since R (alkyl) is a weakly electronegative group. As R decreases in chain length its electronegativity increases, increasing the electronegativity of the O and decreasing its tendency to co-ordinate. If R is replaced by the considerably more electronegative H the tendency to co-ordinate should be still further decreased. The result of hydrolysis of the last —OR group attached to the aluminium in the 'soap' molecule is a breakdown of the stable ring structure (figure 1) allowing the formation of long strings or chains by weak bonding, probably hydroxyl bonding. The gel would then have a structure somewhat like that shown in figure 7, with a random or ordered arrangement of the fatty-acid chains. Preliminary X-ray investigation indicates, contrary to the findings of Marsden, Mysels & Smith (1947) with gels from soaps prepared by aqueous metathesis, that the gels prepared as above show no ordered structure and no large X-ray scattering bands are observed up to 600 Å.

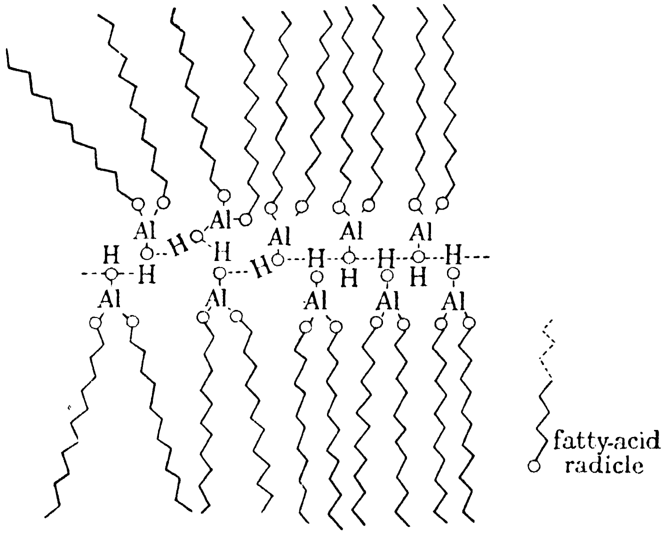

FIGURE 7

The above considerations explain why maximum gelation is obtained by adding the equivalent of one molecule of water per atom of aluminium to the 'soaps' formed by the reaction between fatty acids and alkoxides. Additional water, or peptizers such as acids, phenols, etc., which compete for hydroxyl bonds, destroy the unstable polymer chains and cause a decrease in viscosity.

It has been observed that aluminium mono-soaps give unstable gels which show syneresis to a much greater extent than the di-soaps, and give very unstable monolayers. In this case, each aluminium atom has two hydroxyl groups attached to it initially, leading one to expect, on the above theory, a greater number of links to be formed, and therefore a more stable and elastic gel. On an analogy with aluminium hydroxide, which exists chiefly as AlO(OH), an unstable mono-soap may exist not as $Al(OH)_2(O.CO.F)$ but as $AlO(O.CO.F)$, with water loosely attached. Such a soap would give gels similar to those obtained with soaps of mono- and divalent metals where some hydration seems to be necessary for gelation.

We are grateful to the Chief Scientist, Ministry of Supply, for permission to publish this communication.

FACTORS WHICH AFFECT THE GELLING CHARACTERISTICS OF ALUMINIUM SOAPS

BY G. A. PARRY, J. E. ROBERTS AND A. J. TAYLOR

Three methods of making aluminium soaps are described, and one, the metathetic reaction between a sodium soap solution and an aluminium salt solution, is discussed in detail. The effect of variations in manufacturing technique upon the gelling characteristics of the product is considered.

Recent work by various investigators on the structure of aluminium soaps is reviewed, particularly in relation to the effect of structure and peptizers upon the gelling property in hydrocarbon solvents.

Mention is made of the more important methods of moisture determination and results obtained by the use of the Karl Fischer reagent are quoted.

1. *Introduction*

The property possessed by aluminium soaps of dispersing in certain organic solvents to give more or less stable gels is widely used in industry, more particularly, for instance, in the manufacture of greases, whilst recent information has it that it is also used in the preparation of penicillin solutions for injection. It has been common experience that considerable variations exist as between batch and batch in this gelling property, and little work seems hitherto to have been done in tracking down the cause of this, or, at any rate, in developing a manufacturing technique to give a constant product.

2. *Methods available for manufacture*

There are three interesting and commercially possible methods of manufacture:

(i) *Alcoholate method*

This has been described by McRoberts & Schulman (1948) and consists in reacting an aluminium alcoholate with two equivalents of fatty acid, say lauric acid, and then adding water. The reaction between aluminium and *sec.*-butyl alcohol proceeds vigorously, to give aluminium *sec.*-butylate, which is liquid at room temperatures, and is therefore easy to handle. The other alcoholates, except the *iso*-propylate, are solid. It is best to dissolve the pure, redistilled *sec.*-butylate in *sec.*-butyl alcohol before adding the appropriate amount of fatty acid. If this mobile solution is then poured into water, the aluminium soap is precipitated, the alcohol dispersing in the water. The reaction may be expressed as follows:

$$\mathrm{Al} + 3Bu\mathrm{OH} = \mathrm{Al(O}Bu)_3 + 3\mathrm{H}, \tag{2}$$

$$\mathrm{Al(O}Bu)_3 + 2\mathrm{H}A = \mathrm{Al(O}Bu)A_2 + 2Bu\mathrm{OH}, \tag{3}$$

$$\mathrm{Al(O}Bu)A_2 + \mathrm{H_2O} = \mathrm{Al}A_2\mathrm{OH} + Bu\mathrm{OH}. \tag{4}$$

There is little in this method that can vary from one preparation to another, and it should give a constant quality of soap.

(ii) *The direct-reaction method*

This method was developed by Captain China of Burt, Boulton and Haywood Ltd., during the war, and consists in the direct reaction of free fatty acid with freshly precipitated aluminium hydroxide in accordance with equation (5):

$$\mathrm{Al(OH)_3} + 2\mathrm{H}A = \mathrm{Al(OH)}A_2 + 2\mathrm{H_2O}. \tag{5}$$

In practice, the reaction is carried out by the slow addition of ammonia to a hot aqueous solution of a soluble aluminium salt, the resulting slurry of hydrated alumina being then brought to a defined pH value. The hot, melted fatty acid is then run in slowly with vigorous agitation, when the aluminium soap is precipitated and may be filtered, washed and dried.

This reaction has been used on a commercial scale, but has not been studied as closely as has the third method, viz.

(iii) *The metathetic method*

In this method, the aluminium soap is prepared by reaction between solutions of a sodium soap and a soluble aluminium salt. Thus, the preparation of aluminium laurate proceeds as follows:

$$4\mathrm{Na}L + \mathrm{Al_2(SO_4)_3} + \mathrm{H_2O} = 2\mathrm{Al}L_2\mathrm{OH} + 2\mathrm{Na_2SO_4} + \mathrm{H_2SO_4}. \tag{6}$$

The production is normally done batchwise, but a continuous method has also been developed. In the batch method a 6·5 % sodium laurate solution is prepared at 60° C, and after adding 0·2 % of acetic acid, and 0·01 % α-naphthol, adjusted to pH 9. In another vessel, a 4 % solution of aluminium sulphate solution is prepared, also at 60° C. With violent agitation of the sodium laurate solution, the latter solution is now run in slowly, and when this has been done, the pH will be about 3·0. At this stage, a 10 % solution of sodium carbonate is run in slowly, with vigorous agitation, until the pH is 6·0; after maintaining this pH for about 15 min., the product can be filtered, washed and dried.

In order to ensure a constant product, however, there are several points of detail which demand close attention and control. In the first place it is apparent that if local variations in concentration of the reacting solutions occur, the stoichiometric relationships of the above equation will not hold, and a variable product will result.

It is important, therefore, that stirring shall be as effective as possible. This factor is all the more important the higher the concentrations employed, and in effect the feasible conditions will be a compromise between the highest possible concentration (for maximum yield), stirrer design and power, and the onset of frothing.

Another important factor that affects quality of product is the condition of acidity or alkalinity under which the reaction is carried out. In the above description, the soap is precipitated under essentially alkaline conditions. In the normal reaction between the soluble aluminium salt and the sodium soap, the product obtained contains 18 to 20 % of free fatty acid (see McGee, Mysels, Pomeroy & Smith 1948), and this can either be extracted with solvent or, as in the normal preparation described, neutralized with sodium carbonate, the resulting sodium soap then reacting with the aluminium salt. The quality of a soap is frequently dependent upon the effectiveness of this last stage, as free acid acts as a peptizer and affects gelling characteristics considerably. Some workers, however, go a step further and start off with a sodium soap solution to which 30 to 40 % excess caustic soda has been added, so that after completing the addition of aluminium sulphate, the pH is at 5 or 6, the necessity for further addition of alkali being thus avoided. Although this method is being used as standard commercial practice in America for the manufacture of Napalm, we have not been able to obtain satisfactory results with it in making the laurate. It is, again, possible to carry out the reaction under acid conditions throughout, by adding the sodium soap solution of pH 9 to the aluminium soap solution. From each of these various conditions a product of different gelling characteristics is obtained.

The temperature at which the reaction is carried out is also of importance, there being, generally, a higher and a lower limit for the reaction to proceed without undesirable side-effects.

Allied with the problems associated with pH and temperature control is that of the use of a protective colloid. If a small proportion of a protective colloid such as glue (B.P. 587,522) is added to the aluminium sulphate solution shortly before starting the reaction, the precipitate is obtained as a fine dispersion which yields the maximum surface for subsequent reaction between adsorbed free acid, and the added alkali. This also helps in preventing the occlusion of soluble aluminium and sodium salts. We have also found that a material such as hydroxy ethyl cellulose, added to the sodium soap solution, will behave similarly, and there is a limited amount of evidence that the presence of such a protective colloid enhances the stability of soap gels in hydrocarbon solvents.

In the above the observations pertain mainly to the making of the soap by a batch process. A continuous method of production is also possible, wherein the reacting solutions are fed simultaneously into a vessel, from which the mother liquor and precipitate overflow into a second vessel, the content of each vessel being, of course, stirred vigorously. The pH of the liquor in the first vessel is about 3 to 4, whilst that in the second vessel is maintained at 6 by the addition of sodium carbonate solution. This method has the merit of producing soaps under the same environmental conditions throughout, and this has a profound effect on the uniformity of the product. In the batch process, of course, the pH varies continuously throughout, and it is highly probable that the nature of the soaps obtained at the beginning differ structurally from those produced at the end of the run. A continuous method of preparation is also more flexible from the point of view of controlling the granularity of the product, which is a point of practical importance, in that a fine powder is not easy to filter and wash and tends to ball up when added to a solvent, whereas the particles of a granular material separate and solvate easily.

One of the chief causes of indifferent gelling power in commercially made aluminium soaps is thought to be inadequate washing of the product. If the water-soluble content of a soap exceeds 0·5 % a considerable reduction in its gelling power results.

Commercial supplies of natural fatty acids such as lauric may contain appreciable quantities of unsaturated acids, and the danger of spontaneous combustion during drying is considerable. This is reduced, however, by the addition of a small amount of α-naphthol, as described. Further to this, however, it has been found that iron and manganese in very small quantities (iron 0·01 %, manganese 0·001 %) exert a profoundly deleterious effect upon the quality of the product. Whether they act as oxidation catalysts, or in some other way, is not known, but it is most important to specify that all reagents used shall be free from these metals, and, moreover, that all apparatus used should be either of glass, wood, or stainless steel.

It has already been mentioned that aluminium soaps have a tendency to inflame during the process of drying. Indeed, it is most important that high temperatures should be avoided during the drying process, and if this is carried out in a tray oven, a temperature of 80° C should not be exceeded. Many interesting methods of drying have been investigated, the most promising being that in which wet material is injected into a fast current of hot air which carries the material around a duct and out through a cyclone separator. In this process, the air temperature may be as high as 200° C, but the process of drying is so rapid that the soap temperature has barely time to achieve a temperature of 80° C. Another interesting and effective method depends upon the power factor of wet and dry soaps. When the wet material is fed continuously on to a belt which moves between long flat electrodes energized with radio-frequency potential, the water throughout the bulk of the material vaporizes rapidly, leaving the dry soap which does not take up any radio-frequency energy. This process again, is rapid, and the temperature of the soap remains low. It is, however, expensive to operate.

3. *Soap structure*

An interesting problem, to which a considerable amount of attention has been directed, is the structure of the soaps, and the gel formed therefrom. Controversy has particularly centred around the probable existence of mono-, di- and tri-soaps. Lawrence (1945) maintains that tri-soaps can exist, but McBain & McClatchie (1932*b*) and his co-workers failed in their attempts to prepare the tri-palmitate, even under very dry conditions. McGee *et al.* (1948) and Coe, Mysels & Smith (1948) studied the problem in detail by the technique of extraction of pure soaps with anhydrous solvents; they conclude that in the case of aluminium stearate prepared from aqueous solutions, fatty acid unextractable by solvent, and therefore presumably molecularly combined in a compound, is present to the extent of 2 moles per atom of aluminium, so that the soap formula would be $\mathrm{Al}St_2\mathrm{OH}$. In addition to this fatty acid there is a certain amount of loosely bound, or sorbed fatty acid, as well as fatty acid completely 'free'. Any extraction of free acid in excess of that which will leave a di-soap residue is attributed to hydrolysis by moisture in the solvent. On the other hand, Gallay & Puddington (1948) produce evidence that whereas aluminium stearate, as normally prepared, is a di-soap, 1 equivalent of stearic acid can be extracted, by means of solvents, to yield the mono-soap. Their conclusion is that neither the di- nor the tri-stearate exists, but only the mono-soap. The solvents used for extraction were acetone and *iso*-octane by the former workers, and petroleum ether, ethyl alcohol and acetone by the latter.

Very recently, McGee (1949) of the McBain school, has suggested possible structures for aluminium soaps which accepts the existence of all three, i.e. mono-, di-, and tri-soaps. He adduces firm evidence for the existence of mono- and di-soaps, and makes the interesting observation that, according to his proposed structure, the tri-soap should be soluble in solvents normally used for extracting free acid. It should be found, therefore, in the filtrate, and not in the residue, where, hitherto, it has been looked for.

McGee's theory is a development of that put forward by McRoberts & Schulman (1948), who make use of the suggestion propounded by Marion & Thomas (1946), that the aluminium atom can exist as a hexa-covalent co-ordinating centre, the groups inside the complex shell in the case of soaps being water, fatty acid, fatty carboxylate groups, and hydroxy groups.

This theory would account for the batch-to-batch variations in property of the soap, as different conditions of pH, etc., might be expected to affect the composition of the complex molecule, and would also account reasonably well for the data obtained by other workers.

Interesting work on the structure of aluminium soaps has recently been published by McBain & Working (1947) and by Sheffer (1948), their measurements pertaining to molecular-weight determination by viscosity and osmotic-pressure measurements. The former workers maintain that aluminium laurate is an association colloid, whose association increases rapidly with concentration. Sheffer rejects this, however, maintaining that the soaps are, in the solid state, high polymers formed by weak bonds that break more readily the lower the concentration of the solution. He offers the possibility of hydrogen bonding between hydroxyl groups of neighbouring molecules, or between an hydroxyl group of one molecule and carboxyl oxygen of another. Again, he visualizes the possibility of co-ordination between aluminium and carboxyl oxygen, the whole being a complex system of cross-linkages. Sheffer maintains that these bonds must be formed during precipitation of the soap, and attributes variations in gelling power amongst different batches to the difficulty of reproducing conditions accurately enough to produce the same molecular weight each time. According to this theory, therefore, on adding an aluminium soap to a solvent, the viscosity should first of all increase, as the soap particles swell; this must reach a maximum, and thereafter the viscosity must either remain constant, or decrease. This behaviour is, in fact, observed with the majority of gels made, but it is not universal. The presence of polar molecules must complicate this picture, and depending on their nature they may cause increased cross-linkaging, or peptization. On the other hand, gels made by forming the aluminium soap *in situ* by the alcoholate technique increase in viscosity steadily throughout their life, and, indeed, in this case, it is difficult to visualize any mechanism for the gel formation other than by association from originally simple molecules. McRoberts & Schulman explain the action of peptizers as the result of competition by added polar molecules for hydrogen bonding, with resultant decreases in chain length, and this virtually is also the mechanism accepted by McGee. A material which acts as a strong peptizer is water, and it therefore exerts a most profound effect upon the gelling characteristics of the soaps. It is important, therefore, to be able to measure what amount is contained in any given sample of material, either molecularly bound or free.

A review of methods available for moisture determination in aluminium soaps has been carried out by D. J. Barke, who examined (i) the loss in weight after an arbitrary duration at a raised temperature, (ii) the distillation method (Dean & Stark 1948), (iii) loss in weight on vacuum desiccation at room temperatures, and (iv) a method depending upon reaction between the water removed in an air stream and calcium carbide, the resulting acetylene being absorbed in silver nitrate solution thereby releasing nitric acid which is titrated with dilute alkali. Of these methods, the first and second are entirely arbitrary, the results obtained being dependent upon the conditions chosen, such as time and method of heating or distillation, the temperature employed, and the solvent. The third method is prolonged, and like the first two, measures not only water, but, generally, matter volatile under the conditions obtaining. The fourth method is the only one that measures water, and nothing but water, but here again a complication exists in that it is not certain whether water reacts with carbide to give calcium oxide, or hydroxide:

$$H_2O + CaC_2 = CaO + C_2H_2, \tag{7}$$

$$2H_2O + CaC_2 = Ca(OH)_2 + C_2H_2. \tag{8}$$

One other method should be mentioned, namely, the Karl Fischer reagent. This most valuable method of moisture determination has been widely applied to a great diversity of materials in recent years, but no systematic work has been done with it on aluminium soaps. The only reference to it is made by Mysels *et al.* (1947), who concluded that under the intensively dry conditions of the Fischer reagent, reaction is possible between free fatty acids and basic aluminium soaps, or between aluminium soaps themselves, to give water. Thus:

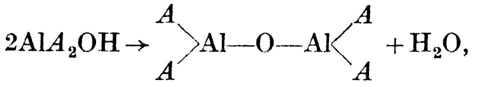

$$2AlA_2OH \rightarrow {}^{A}_{A}\!>\!Al{-}O{-}Al\!<\!{}^{A}_{A} + H_2O, \tag{9}$$

and

$$Al(OH)A_2 + HA \rightarrow AlA_3 + H_2O, \tag{10}$$

$$Al_2O(OH)_2R_2 + 2HA \rightarrow 2AlOHA_2 + H_2O. \tag{11}$$

These equations represent hypotheses only, to explain the observed results. It appeared to some of us, however, that the structure suggested by McRoberts & Schulman of a co-ordinate structure for aluminium soaps would offer a simpler explanation, especially as it is well known (see Ashby, Bryant, Mitchell & Smith

1941) that water in such a complex molecule is replaceable by methyl alcohol under the conditions of the Fischer reagent. A simple method of deciding between these two theories is presented by the alcoholate method of soap formation.

Using carefully purified materials, a quantity of aluminium *sec.*-butylate was dissolved in very dry *sec.*-butyl alcohol, and 2 equivalents of a pure, redistilled fatty acid added. The exact amount of water in accordance with equation (4) was then measured in; this was done by adding a solution of known strength in *sec.*-butyl alcohol. At this stage it is certain that free water as such is not present. If, therefore, the Fischer reagent shows the presence of water, it is apparent that reaction must have taken place in accordance with equation (9). In point of fact, water is recovered by the Fischer reagent, and obtained quantitatively, to a considerable degree of accuracy in accordance with this equation. Whilst this is satisfactory in that it allows a decision to be made as regards the relative merits of the theories put forward above, it means that a considerable correction would have to be applied to any measurements of moisture in an aluminium soap by this method, and, indeed, it would be difficult to apply any factor with confidence due to the possible interference of reactions (10) and (11).

One more factor needs mentioning as having an effect on the gelling characteristics of aluminium soaps, and that is the chain length of the fatty acid. Unpublished results by American workers showed that soaps made by the metathetic method using fatty acids from C_8 to C_{18} were progressively higher gelling as the number of carbon atoms decreased, and we have been able to confirm this by the alcoholate method, using redistilled butyric, caproic, hexoic, caprylic, capric and lauric acids. This result is not unexpected, in that on a percentage weight basis, the lower the molecular weight, the greater the number of molecules present; for the lower fatty acids, the affect of hydrogen bonding would preponderate over the van der Waals forces.

The swelling and solubility of cellulose acetate in benzene/xylenol mixtures

By A. E. Alexander and B. Rabinovitch

Mixtures of benzene/xylenol gelled by cellulose acetate were much used as incendiary materials, and the present study of these systems was undertaken to elucidate the problem of synoresis on storage.

This involved a study of the phase behaviour of the commercial cellulose acetate (heterogeneous both as regards chain length and acetyl number), in binary mixtures of xylenol (solvent) and benzene (non-solvent).

A fixed concentration (4 % by weight) of cellulose acetate in various benzene/xylenol mixtures ranging from pure benzene to 17 % xylenol (by weight) was used, and the composition of the liquid and swollen phases in equilibrium found by analysis after centrifuging. The cellulose acetate in each phase was characterized by both chain length and acetyl content. In this way it was shown that the commercial cellulose acetate contained three major fractions, which differed but little in average chain length, but to a great extent in acetyl content.

The three major fractions were then separated in sufficient quantity to enable their separate phase behaviour to be determined. It was found that the solubility of any one fraction was affected by the presence of the others, and an explanation for this has been advanced.

Introduction

The present study arose in connexion with the use of cellulose acetate as a rubber substitute in certain incendiary gels. The cellulose acetate, of acetyl number 2·80, was first dissolved in a xylenol/benzene mixture (*c.* 50 : 50 by volume), and benzol slowly mixed into the 'dough' until the final composition was reached. Difficulties concerning an adequate supply of xylenol and benzol (0·880 sp.gr.) led to attempts to reduce the xylenol content and to use benzols of lower specific gravity (and therefore containing a lower percentage of benzene). The resulting gels, although stable at the time of preparation, sometimes showed appreciable syneresis on storage, a most undesirable feature. The work described here, undertaken to elucidate the factors responsible for syneresis, deals with the phase behaviour of commercial cellulose acetate in benzene/xylenol mixtures. From such studies it was possible to say whether any given composition was thermodynamically stable or not, i.e. whether or not the gel possessed an inherent tendency to separate into two phases.

1. *Heterogeneous cellulose acetate*

Experimental

The cellulose acetate used in the present work was a commercial product of acetyl number 2·80, as determined by a method given in a private communication from Messrs Courtaulds Ltd. The exact details of its preparation were not known. Xylenol, in common with other phenols, is a good solvent for cellulose acetates of a wide range of acetyl number; the material used was also a commercial product, being a mixture of five isomers. It possessed a deep red colour, due to the presence of some associated or polymerized xylenol. The colour could readily be removed by distillation, but rapidly reformed on standing, so the xylenol was used in its original condition. Benzene is a perfect non-solvent; the material used in these experiments was again a commercial product of specific gravity 0·880.

The experimental technique was as follows: 0·2 g. of cellulose acetate was weighed out in small 10 ml. centrifuge tubes and 4·8 g. of a benzene/xylenol mixture added. The tubes were stoppered, placed in a thermostat at 25·00 ± 0·01° C and left for 10 days to reach equilibrium; the resulting two phases were then separated by centrifuging for 10 min. The two separated phases were weighed and analyzed, the swollen phase for cellulose acetate, the liquid phase for xylenol. These two data, together with the composition of the original system, were sufficient to determine completely the equilibrium system. Five systems, containing up to *c.* 17 % xylenol by weight, were analyzed in this way.

Methods of analysis

It was found impossible to remove all the liquid in the swollen phase by vacuum distillation, because, even at 100° C, a fraction of the xylenol was very strongly attached to the cellulose acetate, this fraction probably being the polymerized xylenol (coloured deep red).

The method finally employed was a viscosimetric one. A calibration curve of viscosity in an Ostwald viscometer against concentration of cellulose acetate in a benzene/xylenol mixture (2 : 1 by volume or 36·5 % by weight xylenol) was constructed. The swollen phase was dissolved in a known volume of 2 : 1 by volume mixture of benzene/xylenol, its viscosity determined in the same viscometer, and the concentration of cellulose acetate read off on the calibration curve.

For the determination of the xylenol in the liquid phase a direct chemical method was used; bromination by bromate/bromide and back-titration of the excess bromine. Known weights of xylenol were dissolved in benzene to form solutions varying in concentration from 5 to 20 % by weight, extracted with strong caustic soda solution, acidified and excess bromate/bromide added. After shaking for 10 min., during which time the xylenol becomes brominated to a greater or lesser degree according to the isomer, excess potassium iodide is added and the liberated iodine back-titrated with standard thiosulphate. In all analyses the liquid phase was diluted with benzene to a xylenol concentration of between 5 and 10 % by weight, and extracted two or three times with warm caustic soda solution. This hydrolyzes the dissolved cellulose acetate and liberates any strongly bound xylenol. The procedure is then that as described above.

Results and discussion

Table 2 shows the analysis results of the five systems used. They are plotted in figure 8 as a ternary phase diagram. Owing to the obvious heterogeneity of the cellulose acetate it is better to consider the diagram not as that of a simple ternary system, but as the superposition of two curves, the one *ANBC* following the behaviour of the swollen phase, the other *LMNOP* giving the variation in composition of the liquid phase in equilibrium with it. Point *O* is completely unknown and would in any case be very difficult to determine, while the exact position of the minimum point *B*, which corresponds to maximum swelling of the swollen phase, was determined by small-scale experiments which gave empirically the xylenol concentration for maximum swelling.

TABLE 2

% by wt. xylenol in system	percentage swollen phase			percentage liquid phase		
	cellulose acetate	benzene	xylene	cellulose acetate	benzene	xylene
0	15·0	85·0	0	1·5	98·5	0
5·1	9·9	84·3	5·8	1·7	93·8	4·5
11·1	6·1	82·3	11·6	2·3	87·5	10·2
15·0	3·3	82·9	13·8	7·1	76·4	16·5
17·4	5·2	75·1	19·7	3·7	80·3	15·9

An examination of the diagram brings out the following points:

(i) The cellulose acetate used, when in benzene alone, although swelling only to a slight degree, takes up some four to five times its *apparent* volume of benzene. This means that there must be a large number of air-spaces and capillaries in the dry cellulose acetate.

We also observe that the liquid phase contains some 1·5 % cellulose acetate at this point. Since the acetate itself is not soluble at all in benzene, it seems that either some soluble constituent of the acetate, e.g. free acetic acid, has been extracted, or a little of the most finely milled cellulose acetate has been suspended.

(ii) As the xylenol content of the system increases up to 10 % concentration, there is very little increase in the amount of cellulose acetate dissolving, while at the same time swelling increases rapidly.

(iii) Above this xylenol concentration, cellulose acetate begins to dissolve at an increasing rate while swelling goes on at a decreasing rate, reaching a maximum at point *B*, which corresponds to a xylenol concentration in the swollen phase of 17 %.

(iv) An increase in the xylenol content of the system here brings about a sudden dissolution of a large part of the swollen phase. This is manifested in figure 8 by the sudden increase in the percentage of cellulose acetate in the swollen phase, and a corresponding decrease in the liquid phase (points *C* and *P*), since, it must be remembered, the cellulose acetate is very highly swollen, and when it dissolves it takes with it into the liquid phase a far greater amount of benzene and xylenol than its own weight.

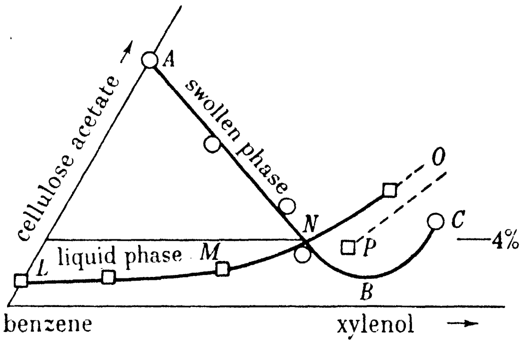

FIGURE 8

(v) After this sudden dissolution a small, but very highly swollen, phase remains behind which, with increasing xylenol concentration, swells and dissolves only slowly.

It would appear from these observations that in the present system there are three major fractions in the cellulose acetate, which vary in some factor or factors which affect their solubility in benzene/xylenol mixtures. The first fraction dissolves continuously from 0 to *c.* 17 % xylenol concentration in benzene, rather slowly up about 10 %, but at an increasing rate from there. The second dissolves very sharply at a point when the swollen phase contains 17 % xylenol, leaving behind the third fraction or residue, which dissolves only slowly. The next step, at this point, was obviously a separation of these fractions and a study of their swelling and solubility properties.

2. *Fractionated cellulose acetate*

Experimental

The fractionation was carried out by extracting the heterogeneous polymer with known xylenol/benzene mixtures under conditions approximating to those obtaining during the determination of the phase diagram. The first fraction was obtained by keeping 20 g. in contact with a 15 to 16 % xylenol in benzene mixture at 25° C for 14 days, the cellulose acetate concentration being 4 %. The two phases were then separated by centrifuging for 10 min. and decanting the liquid phase. The cellulose acetate in the liquid phase was precipitated by slowly adding, with constant stirring, petrol ether (b.p. 80 to 100° C), until no more flocculation occurred; it was then centrifuged and finally decolorized by extraction in a Soxhlet extractor with petrol ether.

The remaining swollen phase, containing the second and third fractions, was treated in a similar fashion, and after removing all petrol ether was placed in contact with an 18 to 19 % xylenol/benzene mixture to reach equilibrium. This brought into solution the second fraction which, owing to the very highly swollen state of the third fraction, was more difficult to separate than the first, even after centrifuging. The second fraction was then precipitated from the separated solution and treated as above.

The remaining swollen phase now contained only the third fraction, which again was treated precisely as above. All three fractions, before comparison, were dried in an oven at 100° C. In a number of such fractionations it was found that the first fraction, as a percentage of the heterogeneous cellulose acetate, could vary from 40 to 50 % according to whether 15 or 16 % xylenol in benzene was used. This is simply due to the fact of the large slope of NO in figure 8. Similarly, the second fraction varied from about 40 to 30 % of the total cellulose acetate, but this, it seemed, was due more to the difficulty of separating the viscous second fraction *solution* from the highly mobile third fraction *gel*. It is worthy of note here that, after extraction of the separated fractions and continuous washing with petrol ether, a deepening of colour from the first to the third was apparent, due to a retention by the cellulose acetate of the polymerized xylenol. It therefore seems that the attractive forces between the polymer chains in the third fraction are greater than those in the first fraction, which would explain its lower solubility.

Comparison of fractions

Only two properties having a bearing on the solubility of cellulose acetate were compared, namely, molecular weight and acetyl number. The first of these can be determined by a variety of methods, such as viscosity, osmotic pressure, vapour pressure lowering, etc., but for comparative purposes it is sufficient to use intrinsic viscosities $(\eta_{\text{sp.}}/c)_{c=0} = [\eta]$ without translating them into absolute molecular weights. A series of viscosity measurements was therefore made in an Ostwald viscometer of capacity about 10 ml., capillary length about 7 cm. and time of flow for water at 25° C of 12·4 sec. All measurements were done at 25° C with solutions varying in concentrations from 0·1 to 0·5 g. cellulose acetate in 100 ml. xylenol.

The determination of the acetic acid content of the fractions presented more difficulty. As Kreuger (1930) has pointed out, there are a number of methods of alkaline saponification which may vary by apparently only unimportant details, but which may give very different results. He also pointed out that for oxycellulose acetate and cellulose acetate with a large amount of bound sulphuric acid, the only reliable method is that of acid hydrolysis. Since, in general, an acid hydrolysis requires a large amount of cellulose acetate, a micro-method developed by Pregl & Soltys (1929) was tried, but had to be abandoned as no consistent results could be obtained. We were therefore confined to the use of an alkaline hydrolysis method. According to Torii who, as quoted by Kreuger (1930) has compared the data given by the various standard alkaline methods, the method given by Eberstadt (improved later by König & Knoevenagel (1922)) is the most reliable, by virtue of the fact that the result is independent of the time of hydrolysis, given a certain minimum hydrolysis time.

The method is as follows: 1 g. of cellulose acetate is refluxed with 20 ml. of a 75 % alcohol/water mixture for 30 min. at 50 to 60° C, when 50 ml. of a standard N/2-caustic soda solution is added and the whole brought to a temperature of about 50° C. The reaction mixture is allowed to stand for 24 hr. at room temperature, when phenolphthalein is added. After 10 min. excess N/2-sulphuric acid is added and the reaction vessel warmed until the regenerated cellulose is no longer coloured red. The excess sulphuric acid is then back-titrated with N/2-caustic soda solution.

Using this method, an examination of the heterogeneous cellulose acetate for acetic acid content gave the following results:

hydrolysis time (hr.)	acetic acid content (g. HA/100 g. cellulose acetate)
24	53·2
39	53·2
24	52·7

which therefore confirm the conclusion drawn by Torii concerning this method. It was clearly essential to compare this latter method with that of Courtaulds. Three different samples of cellulose acetate were saponified by the two methods and the results are compared in table 3.

As can be seen, there is an approximately constant factor between the two methods, and although the results are consistent within themselves there is no absolute criterion of their accuracy and nothing to commend the one above the other. The method of König & Knoevenagel (1922) was used in all experiments as a standard.

TABLE 3

sample of cellulose acetate	method of König & Knoevenagel (*a*)	method of Courtaulds (*b*)	*b/a*
M.B. 13	53·0	57·1	1·08
R 3803	56·4	61·5	1·09
HCL 59/60	49·0	53·9	1·10

Results and discussion

The results of the viscosity measurements were used to plot $\ln \eta_{\text{sp.}}/c$ against the concentration c, according to the Martin equation:

$$\ln \eta_{\text{sp.}}/c = \ln [\eta] + kc [\eta], \tag{12}$$

where $[\eta]$, the intrinsic viscosity, is directly proportional to the chain length. This equation, it has been found, holds very well for cellulose acetates of widely different acetyl numbers.

To an accuracy of *c.* 3 % in the determination of $\ln \eta_{sp.}/c$, one straight line satisfies all the experimental points, i.e. the weight-average molecular weight for all three fractions is identical. This seems to be in contradiction to other work on fractionation, where there is general agreement on the variation of chain length from fraction to fraction.

Table 4 gives the results of the acetic acid content determinations.

TABLE 4

fraction	acetic acid content (g. HA/100 g. cellulose acetate)			mean value	mean × b/a
1	45·1	46·2	45·65	45·6 ± 0·5	50·15
2	46·35	46·75	—	46·55 ± 0·2	51·2
3	53·6	54·1	54·6	54·1 ± 0·5	59·5

The results given are those determined by the method of König & Knoevenagel, and the last column in table 4 gives values that we might expect using the method of Courtaulds. Considering for our purpose that the amounts of the fractions present in the heterogeneous cellulose acetate are in the ratio of 2 : 2 : 1 (though this is somewhat arbitrary), a calculation from the last column gives about 52·5 as the value of the acetic acid content for the heterogeneous cellulose acetate, which is far lower than the figure of 57·1 given by Courtaulds Ltd. The reason for this is not at all clear. However, one fact emerges from the results in table 4, namely, that there is a variation of acetic acid content from fraction to fraction, and fraction three is close to the triacetate.

Solubility diagrams for fractions

In order to determine the limiting concentration of xylenol to bring about the dissolution of a fraction, and to determine a ternary phase diagram for each fraction, solubility tests were made for each fraction in benzene/xylenol mixtures at intervals of 0·5 % xylenol concentration.

First fraction. It was found here that equilibrium between the cellulose acetate and benzene gave a swollen phase containing 11·0 % cellulose acetate. On addition of xylenol to the system, swelling increased up to 13·5 % xylenol in benzene when rapid dissolution took place. This sudden dissolution was a good indication of the success of the fractionation.

Second fraction. The cellulose acetate here gave a swollen phase with benzene alone of 26·0 % cellulose acetate. Increase of xylenol concentration gave increased swelling until, at 15·5 % xylenol, sudden dissolution took place.

Third fraction. In this case, a swollen phase of 33·0 % cellulose acetate was obtained in benzene alone, but on adding xylenol to the system no fixed solution point was found. Up to 25·0 % xylenol concentration, swelling increased rather slowly, but about this point solution began to take place and continued, with increase in xylenol concentration, up to 35·0 %, by which time the whole of the third fraction had gone into solution. This, of course, is easily understood since we are not dealing with a true fraction, but with a residue left after extraction of the first and second fractions.

Figure 3 shows the phase diagrams of these three isolated fractions, and if these are compared with the phase diagram of the heterogeneous cellulose acetate (figure 2), an apparent discrepancy will be noted. According to the original phase diagram, dissolution of cellulose acetate is taking place over the range 0 to 17 % xylenol concentration, the cellulose acetate in the liquid phase constituting a first fraction. In actual fact, the first fraction was extracted at a xylenol in benzene concentration of 15·5 %, yet, on separation, we find the first fraction is completely in solution at 13·5 % xylenol.

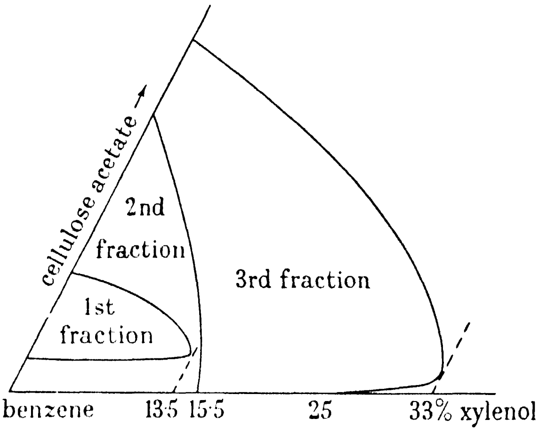

Figure 9

The same applies to the second fraction. This dissolves from the heterogeneous cellulose acetate at 17·0 % xylenol concentration. The second fraction here was actually extracted with an 18·5 % xylenol in benzene mixture, whereas after separation solution of the fraction was complete at 16·0 %.

To explain this apparent discrepancy, let us assume that a cellulose acetate I will only just dissolve in a benzene/xylenol mixture of A % xylenol. If now a cellulose acetate II is placed in a mixture containing B % xylenol ($B > A$), then xylenol will be preferentially absorbed leaving a solvent of, say A %, xylenol concentration, that is, just sufficient to bring the cellulose acetate I into solution. If, now, the two acetates are placed together on the B % xylenol mixture, cellulose acetate I will only just dissolve, and anything less than B % would be insufficient for this. But it is known that the acetate I, on separation, will dissolve in A % xylenol in benzene. In this way the above discrepancies can easily be explained. As far as the first fraction is concerned, in the presence of the second and third fractions, a concentration of 15·5 % xylenol in benzene is equivalent to 13·5 % and similarly for the second in the presence of the first and third fractions.

Conclusions

Although a given cellulose acetate may be prepared under homogeneous conditions and precipitated from solution, it seems that a small variation in acetic acid content may give rise to two or more solubility fractions for a given solvent-non-solvent system. This was clear from a study of the phase behaviour of such a ternary system.

Moreover, a study of the isolated fractions showed that this acetic acid content variation could leave a fraction which was close to being a completely acetylated product. This seemed to indicate that the cause of this heterogeneity lay either in the non-uniform acetylation of the cellulose, or the precipitation of a hydrolyzed product from solution which brings with it a proportion of the triacetate.

Determinations, by means of viscosity, of the relative molecular weights of these fractions showed that there was no variation in chain length amongst them. Summing up, then, we find, in accord with certain earlier workers, that there is a variation in acetyl number, but rather surprisingly none in average molecular weight, though no conclusions could be drawn as to the molecular-weight distributions inside the fractions.

It was shown that the solubility of any of these fractions was affected by the presence of the others, for which a reasonable explanation can be put forward.

Acknowledgement is made to the Chief Scientist, Ministry of Supply, for permission to publish this paper.

ALUMINIUM SOAPS, THEIR NATURE AND GELLING PROPERTIES

By A. E. Alexander and V. R. Gray

The chemical nature of aluminium soaps can be studied with great advantage by making use of the reaction between aluminium alkoxides and fatty acids in organic solvents. The heat of the reaction was measured as a function of fatty acid added, and this showed that not more than two fatty-acid molecules react with each $Al(OR)_3$ molecule. Even with water, not more than two molecules reacted with each $Al(OR)_3$ molecule. The resulting soaps were analyzed for aluminium and fatty acid, and this confirmed the conclusions drawn from the heat of reaction.

The product of aqueous metathesis between an alkali metal soap and an aluminium salt appears to be an adsorption complex of the fatty acid upon hydrated alumina; combination occurs during the drying process.

From the above studies a polymeric formula for aluminium soaps has been suggested, based upon sixfold co-ordination aluminium-oxygen octahedra. When these octahedra join through an apex a di-soap results, when through an edge, a mono-soap. A combination of these results in intermediate values. Some preliminary infra-red measurements of aluminium mono- and di-soaps appear to be consistent with these conclusions.

The phenomenon of peptization of aluminium soaps by organic compounds such as alcohols, phenols, amines, etc., is discussed in terms of the above formulation.

The physical nature of aluminium soaps in organic solvents has been explored by means of viscosity and streaming birefringence.

In very dilute solutions in benzene it appears that the soap units approach molecular dispersion; with increasing concentration the rapid increase in specific viscosity indicates strong intermolecular attraction and the formation of fibrillar aggregates.

With the more concentrated solutions (1 to 2 %) simultaneous streaming birefringence and viscosity measurements were made in a coaxial cylinder apparatus, and the effect of peptizers and precipitants determined. It was concluded that the soap molecules are aggregated in solution with the fatty-acid groups extended laterally with respect to the chain. Some solutions were initially birefringent, due to the influence of the walls upon the aggregation.

Introduction

The aluminium salts of the fatty acids, in the solid state and in solution, present an unusual number of problems to the chemist. Despite their widespread use in industry, e.g. the acetate in pharmacy, the oleate, stearate, etc., in paints and greases, their true chemical nature is remarkably obscure. Their solutions in organic media such as benzene resemble very closely those given by rubber; in fact, they have many properties in common with the natural and synthetic polymers.

The present paper summarizes the work carried out by us during the war years upon the physical and chemical nature of aluminium soaps, both in the solid state and in solution. The experimental details from which any conclusions drawn here are based will be found in earlier publications (Gray & Alexander 1949; Gray 1948).

The chemical nature of aluminium soaps

Aluminium soaps are made commercially by an aqueous double decomposition process, and in most academic studies some variation of this method has been used. It is clear, however, that water plays a most important part in determining the properties of the resultant material, and for that reason non-aqueous reactions, such as between an aluminium alkoxide and a fatty acid, are much preferable.

The reaction between a number of aluminium alkoxides (from *iso*-propyl alcohol, *sec.*-butyl alcohol, *m*-cresol, etc.) and several different fatty acids (acetic, lauric, oleic, stearic, etc.), in the presence and absence of solvents, was accordingly studied under a variety of conditions. In addition to analysis for aluminium, both free and uncombined fatty acid were estimated and in some cases alkoxide groups also. The effect of water was also examined. Furthermore, the heat of reaction was measured calorimetrically, and the conclusions therefrom will first be considered.

(i) *Heat of reaction between alkoxides and fatty acids*

When water was absent the heat of reaction as a function of mole ratio of added fatty acid was reproducible and independent of the nature of the fatty acid. It was also independent of the medium (except when an additional reaction was introduced), and, over a 60° C range, of temperature.

Plotting heat evolution (kcal/mole alkoxide) against moles of added fatty acid, a linear curve is found up to about 1·5 moles of acid, when it begins to curve over and beyond about 2 moles become steady at about 18 kcal per mole alkoxide. It seems, then, that under these conditions not more than 2 moles of fatty acid react per mole of aluminium alkoxide, i.e. the reaction is presumably

$$\mathrm{Al(O}R)_3 + 2\mathrm{H}L \rightarrow \mathrm{Al(O}R)L_2 + 2R\mathrm{OH}, \tag{13}$$

where R and L denote respectively the alcohol and fatty-acid radicals.

Carrying out the reaction in *sec.*-butyl alcohol, instead of in benzene or dioxane, increased the heat evolution somewhat, but the extent of reaction was not altered, showing that reaction did not terminate owing to the attainment of an equilibrium involving the reaction products.

The reaction of alkoxides with water was also examined: this, too, was complete on addition of about 2 moles of water per mole of alkoxide, suggesting

$$\mathrm{Al(O}R)_3 + 2\mathrm{H_2O} \rightarrow \mathrm{AlO(OH)} + 3R\mathrm{OH}. \tag{14}$$

It is important to point out that there is no sign whatever of any discontinuity in the heat of reaction curve at or near the composition corresponding to the mono-soap $\mathrm{Al(O}R)_2L$.

(ii) *Analysis of products from the alkoxide/fatty-acid reaction*

sec.-Butoxide in dioxane (a precipitant for aluminium soaps) reacted with a variety of fatty acids to give products containing about 1·5 to 1·7 moles of fatty acid per aluminium atom; in benzene (a solvent for aluminium soaps) the figure was somewhat higher.

The reaction utilizing *m*-cresoxide was particularly interesting, since any cresol groups present in the product could be directly estimated by bromination. Table 5 shows the results so obtained.

It will be seen that about 1·5 to 2 fatty-acid groups and about 0·4 to 1 cresol group are combined with 1 aluminium atom. In those cases easiest to handle experimentally, namely, the caprylate and acetate, the figures are close to those required for the product $Al(OR)L_2$, as in equation (13). It is quite conceivable that, under perfectly anhydrous conditions, for the complete elimination of water at all stages is extremely difficult, the other members would also approach this composition.

A number of soaps were prepared by adding less than 1 mole of fatty acid per mole of alcoholate (in dioxane), and centrifuging off the soap formed. Even under such conditions the product contained appreciably more than 1 fatty-acid group to each aluminium atom.

TABLE 5. SOAPS FROM ALUMINIUM *m*-CRESOXIDE AND FATTY ACIDS IN DIOXANE

fatty acid	molecular weight	fatty-acid group per aluminium atom	cresoxide per aluminium atom
lauric	201·2	1·51	0·36
	201·2	1·40	0·65
	201·2	1·70	0·59
oleic	284·0	1·82	0·35
	284·0	1·55	0·51
myristic	228·8	1·65	0·83
caprylic	147·5	2·0	0·81
acetic	60·0	1·78	0·90

The reaction in the absence of solvents was also studied. The observation of Lawrence that 3 moles of alcohol could be distilled off by addition of 3 moles of fatty acid to 1 mole of alkoxide was confirmed. When, however, extreme precautions against water were taken, the whole of the alcohol could be obtained only by heating to decomposition. In no case did the final product contain more than 2 fatty-acid groups per aluminium atom. This work provides further confirmation for the non-existence of the tri-soap and emphasizes once again the great importance of water in these systems.

Addition of small amounts of water to the di-soap $Al(OR)L_2$ removes the remaining alkoxide groups, giving the compound $Al(OH)L_2$ as discussed in more detail below.

(iii) *Aluminium soaps from aqueous processes*

In view of the extreme weakness of aluminium hydroxide as a base, and of the higher fatty acids as acids, it seems unlikely that true compound formation occurs to any appreciable extent in aqueous solution. The material precipitated under the usual conditions is probably an adsorption complex of fatty acid upon hydrated alumina. After drying, however, the substances possess all the properties observed for soaps prepared by the alkoxide-fatty acid reaction and which appear to be chemical compounds. It thus seems probable that combination between the adsorbed fatty acid and alumina occurs during the drying process. This would explain the value of protective colloids during the precipitation process (to hinder condensation between the hydrated aluminium oxide molecules), and why the conditions of drying so profoundly influence the properties of the final soaps.

In our view the usual products consist chiefly of the di-soap Al(OH)L_2 together with some free fatty acid and some free alumina (or hydrated alumina), for even when using a protective colloid it seems unlikely that all aggregation of the hydroxide would be prevented.

(iv) *General conclusions concerning the chemical nature of aluminium soaps*

From the work summarized here it would seem that the following conclusions regarding aluminium soaps can be drawn:

(*a*) The tri-soaps do not exist.

(*b*) The di-soaps seem to exist and to be compounds of formula Al(OR)L_2 from the anhydrous alkoxide reactions and Al(OH)L_2 from reactions in the presence of water.

(*c*) The existence of mono-soaps may be possible, but no definite evidence is forthcoming either from the heat of reaction studies or from analytical data.

These general conclusions have been strengthened by some infra-red studies. Aluminium mono- and di-stearates, prepared by an aqueous precipitation method, give essentially identical spectra in the 3 to 8 μ region. Comparison with sodium stearate (an ionic compound) and with glycerol stearates (covalent compounds) suggests that the linkages in aluminium soaps are probably covalent in nature.

Taking into account the various experimental results and the behaviour of aluminium in its better known compounds, the following structures for aluminium di-soaps and for the mono-soaps (if they exist) have been advanced:

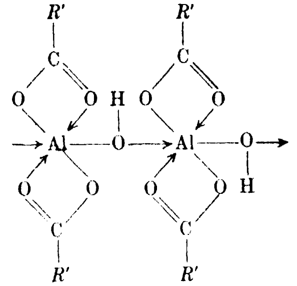

Aluminium di-soap

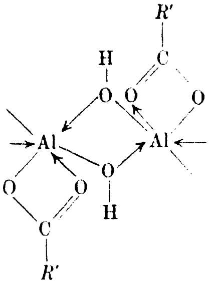

Aluminium mono-soap

The constituent molecules are believed to be linked up as shown through aluminium-oxygen tetrahedra, with the fatty-acid chains extended laterally from the main chain, and the aluminium showing sixfold co-ordination in both cases. Such physical polymerization seems essential to explain many of the results obtained with organic solutions of aluminium soaps, as discussed in a later section.

Aluminium soaps in solution

Aluminium soaps dispersed in organic liquids exist in a variety of physical states, some visibly heterogeneous, others homogeneous and apparently true solutions even though of high viscosity. Here we will consider the latter type such as given by the lower soaps in benzene or the higher members in benzene containing a little cresol or other peptizer. The nature of peptizing action is considered later.

(i) *Dilute solutions*

The viscosity of very dilute solutions was measured as a means of estimating the degree of aggregation of aluminium soaps in solution. Even members from the caproate (C_6) to myristate (C_{14}) were studied in benzene solution.

The viscosity changes rapidly with time, reaching a fairly steady value after about 20 days. This finding would indicate that on dilution the aggregated soap molecules tend to dissociate, although it is difficult to ensure the complete absence of water which would certainly have a similar effect.

The measured specific viscosities were extrapolated to zero concentration and the Staudinger equation, $(\eta_{\text{sp.}}/c)_{c=0} = KM$, utilized to estimate the molecular weight. Although K is not known for these systems a mean value from known polymers can be taken since K does not vary much with polymer type. The molecular weights of the soap units so found were in the 300 to 400 region, so that at infinite dilution the soaps would seem to approach monodispersity.

The other point of great interest was that the slope of the curve $c/\eta_{\text{sp.}}$ against c differed considerably from that for synthetic linear polymers. The viscosity increase with concentration was unusually large, indicating that the force of attraction soon suffices to convert the almost molecularly dispersed soap at high dilution into units of size comparable with those for natural and synthetic high polymers.

(ii) *More concentrated solutions*

In most solutions of interest the aluminium soap is present in concentrations of a few per cent or so. These solutions resemble those of rubber very closely, and it was thought that the study of streaming birefringence might give further information concerning the nature of the particles present. The study of birefringence in visco-elastic media is also of very general interest, for in such systems both photoelastic birefringence and orientation birefringence may occur simultaneously.

Simultaneous measurements of viscosity, extinction angle and double refraction were made using a Couette-type viscometer. The effects of concentration of the aluminium soap (1 and 2 %), of peptizer (0·5, 1 and 2 % cresol) and of a precipitant (petrol ether) were investigated.

With commercial aluminium 'laurate' all solutions were doubly refracting at rest, with extinction angle parallel to the sides of the cylinder. This would indicate orientation induced by the walls and supports the conclusions found from the 'blow-off' method for measuring wall-adjacent viscosity of oils thickened by aluminium naphthenate. The phenomenon may be termed 'surface gel formation'. On the other hand, soaps made on the laboratory scale from pure acids do not show this effect—for some reason which is not readily apparent.

The streaming birefringence and viscosity data can only be explained if the aluminium soap micelles are fibrous in character, with the metal atoms along the axis of the fibre and fatty-acid chains more or less perpendicular to it. This accords well with the formulation advanced above (p. 165). It can therefore be assumed that aluminium soap gels consist of intertwined fibrils which can be easily deformed and stretched. Upon such a basis it is possible to construct a model from which the essential features of the flow-optical properties can be derived.

Peptization phenomena

Aluminium soaps in organic liquids can exist in a number of different states, depending upon the conditions, ranging from heterogeneous systems with completely precipitated soaps (more or less swollen), through thick gels or jellies, to completely mobile solutions. The principal states may be distinguished as follows, although there is of course a complete range between the two extremes: insoluble non-swollen precipitate, paste of micro-crystals, friable gel, stringy thick solution, mobile solution.

The actual state obtained depends upon four principal factors: the chain length of the fatty acid, the presence of peptizing agents (of which water is a special case), the nature of the organic liquid used as dispersion medium, and the temperature.

Peptizers, usually compounds with pronounced co-ordination properties, such as amines, alcohols, fatty acids, etc., promote swelling and solubility of insoluble soaps, and tend to make viscous solutions more fluid. The most active peptizers are the amines and pyridine; then come the alcohols, and after that the phenols and fatty acids. This order of peptization strength appears to be the order of co-ordinating tendency in other co-ordination compounds, and also of basic strength which is a closely related property. Peptization action would thus be ascribed to a breaking of the aluminium-oxygen co-ordinate links by a preferential co-ordination with the peptizer. After addition of sufficient peptizer to bring about solution further amounts would tend to diminish the chain length of the soap aggregates and thus to diminish the viscosity, as found experimentally.

Water has a special role of its own, although it behaves to some extent like other peptizers; thus increase of moisture content in commercial soaps tends to make their solutions increasingly fluid. The special properties of water are revealed most strikingly when it is almost completely absent, as with the alkoxide decomposition method after extreme precautions to eliminate water have been taken. Under such conditions, over a wide range of variation of solvent, peptizer, alkoxide and fatty acid, the reacted system shows little change in viscosity, remaining perfectly mobile. Addition to this fluid system of very small amounts of water (*c.* 1 % calculated on the soap) generally produces a marked increase in viscosity, indicating that the formation of some type of linear aggregate has taken place. In a few cases (e.g. aluminium *sec.*-butoxide reacting with lauric acid in dry ether, or with oleic acid in benzene) a viscous solution was obtained under what were believed to be anhydrous conditions. However, in view of the difficulties of ensuring really anhydrous conditions, it would seem that water is *essential* if aluminium soaps, in low concentration, are to give viscous solutions. The action of the small amounts of water would be to remove unreacted alkoxide groups, e.g. $Al(OR)L_2 + H_2O \rightarrow Al(OH)L_2 + ROH$, the hydroxy soap thus formed then aggregating to form long chains as depicted above.

Acknowledgement is made to the Chief Scientist, Ministry of Supply, for permission to publish this paper.

SOME FLOW PROPERTIES OF CONCENTRATED HIGH-POLYMER SOLUTIONS

BY R. S. RIVLIN

A review is given of a theoretical investigation of the flow properties of fluids in which the assumptions underlying the classical hydrodynamics of viscous fluids no longer holds. For an incompressible visco-inelastic fluid—or visco-elastic fluid in steady-state laminar flow—the stress-strain-velocity relations involve two physical parameters which may or may not depend on the state of flow. One of these is the viscosity and the other the normal stress coefficient. On a simple model of a concentrated high-polymer solution, it is shown that the normal stress coefficient may have an appreciable value. Finally, the manner in which the basic assumptions of the theory may be inapplicable to real concentrated high-poylmer solutions is discussed.

1. *Introduction*

Very little systematic study of concentrated high-polymer solutions has so far been carried out. Moreover, in studying such solutions, the tendency has been to investigate just those phenomena which are of importance in the study of dilute solutions and which may be observed in exaggerated form in concentrated solutions.

It is well recognized that even at a concentration of a few per cent, the effect of interactions between the dissolved high-polymer molecules is important. It is, therefore, not surprising if concentrated high-polymer solutions exhibit phenomena which are not normally observable in dilute solutions.

Certain of the phenomena to which Weissenberg (1947) has recently drawn attention are of this type. They indicate that certain of the stress components which are zero for the steady-state laminar flow of a Newtonian fluid, such as is discussed in the classical hydrodynamics of viscous fluids, are no longer zero in the fluids with which he has experimented.

In this paper a review will be given of a theoretical study of the flow of concentrated high-polymer solutions. It has been found necessary (Rivlin 1948*a*) to re-examine the theoretical basis of the usual stress-strain-velocity relations of classical hydrodynamics and to generalize them. An attempt is made to interpret the generalized hydrodynamics so obtained by a statistical-mechanical consideration of a flowing concentrated high-polymer solution. It would be rash to assume that, in any experiment in which the anomalous effects considered are observed, they are uncomplicated by secondary effects. Accordingly, some discussion is given in § 6 of a few possible factors which may complicate the theory outlined. Unfortunately, no sufficiently detailed experimental results have been published which would enable the predictions of the theory to be compared with observation.

2. *The kinematics of flow*

If a fluid is in any state of flow, then the flow of an infinitesimal volume element may be considered to consist of the superposition of three motions: (i) a translational motion of the element as a whole, (ii) a purely rotational motion of the element as a whole, and (iii) an irrotational motion in the element in which, unlike the motions (i) and (ii), the distances between points of the element are changed.

For each element, we can choose uniquely a rectangular Cartesian co-ordinate reference system (X, Y, Z) which moves with the motions (i) and (ii) and to which the motion (iii) may be referred, so that the velocity of a point which is at (X, Y, Z) is given by (U_1X, U_2Y, U_3Z). U_1, U_2 and U_3 are called the principal irrotational velocities at the point considered. If the motion is not irrotational, the directions of the axes (X, Y, Z) vary from instant to instant due to the rotational motion (ii) and, if the motion is not homogeneous, the directions at any instant of time of the axes X, Y and Z for different points of the fluid are, in general, different.

Since the motions (i) and (ii) are of types which are possible in an ideal rigid body, no work will be expended on the element in producing them, except in so far as is necessary to change the translational or rotational kinetic energy of the element. In the motion (iii), however, forces must be applied and work will, in general, be expended in changing the relative configuration of the points of the body. These forces will depend on the physical properties of the fluid, and some physical relationship between the forces required to produce a general irrotational motion of the fluid must be derived or determined experimentally before the discussion can be taken further. The classical hydrodynamics of viscous fluids depends on the assumption, supported by experimental agreement for many fluids, of a particular relation between the forces which must be applied to the element and the principal irrotational velocities U_1, U_2 and U_3. This is not the most general relation which can be envisaged from *a priori* considerations and the derivation of a relation of considerably greater generality is discussed in the next section.

3. *Generalized stress-strain-velocity relations*

It is assumed that (i) the fluid is isotropic in its state of rest; (ii) the stress at a point of the fluid depends uniquely on the state of flow in an infinitesimal element at that point, at the instant considered, and not on the state of flow in neighbouring elements or on that in the element considered at earlier instants of time; (iii) the material is incompressible.

The validity or otherwise of assumptions (i) and (iii) for any particular system will in general be apparent or readily determinable by direct experiments. Underlying assumption (ii) is the physical picture that the microscopic structure of the material in the element depends only on the macroscopic state of flow in it at the instant considered. This assumption may well be incorrect for the materials with which we are concerned, e.g. they may be visco-elastic, in which case the stress at any point of the material will depend not only on the instantaneous state of flow in the element at that point but also on the manner in which this state of flow is changing with time. However, we shall proceed on the assumption that (ii) is valid and shall then discuss certain possible ways in which this assumption may be invalid.

Assumption (ii) is equivalent to the stress components being expressed by single-valued functions in terms of U_1, U_2 and U_3. Assumption (i) is equivalent to one that in the co-ordinate system (X, Y, Z) the tangential components of the stress vanish and the expressions for the normal components t_1, t_2 and t_3 parallel to the axes X, Y and Z respectively are given by expressions which are symmetrical with respect to U_1, U_2 and U_3. The assumption (iii) requires that the stress be indeterminate to the extent of an arbitrary hydrostatic pressure p if U_1, U_2 and U_3 are given. Expressed mathematically we have

$$t_1 = f(U_1, U_2, U_3) + p, \quad t_2 = f(U_2, U_3, U_1) + p \quad \text{and} \quad t_3 = f(U_3, U_1, U_2) + p. \tag{15}$$

By a purely mathematical argument it has been shown (Rivlin 1948*a*) that equations (15) are equivalent to

$$t_i = 2\Theta U_i + 2\Psi U_i^2 + p \quad (i = 1, 2, 3), \tag{16}$$

where Θ and Ψ are functions of K_2 and K_3, which are defined by

$$K_2 = U_1U_2 + U_2U_3 + U_3U_1 \quad \text{and} \quad K_3 = U_1U_2U_3. \tag{17}$$

The incompressibility condition may be expressed mathematically by the relation

$$K_1 = U_1 + U_2 + U_3 = 0. \tag{18}$$

The basic assumption of the classical hydrodynamics of incompressible viscous fluids is that Θ is a constant, the viscosity of the fluid, and $\Psi = 0$. It can readily be shown, from the linearity of the equations so obtained, that the fluid is isotropic as regards its flow properties not only in the state of rest but also in any state of flow. This is no longer true if Ψ is not zero.

It has been seen that the axial system (X, Y, Z) associated with an element is rotating with it. From the point of view of the solution of particular problems it is convenient to have explicit expressions for the stress components in a fixed co-ordinate system in terms of the state of flow. If we choose a fixed rectangular Cartesian co-ordinate system (x, y, z), we can describe the state of flow by the components (u, v, w) of the velocity at the point (x, y, z), parallel to the axes (x, y, z). In general u, v and w are, of course, functions of x, y, z and the time. Then the six stress components $t_{xx}, t_{yy}, \ldots, t_{xy}$ in the co-ordinate system (x, y, z) are given by

$$\left.\begin{aligned} t_{xx} &= 2\Theta a + 2\Psi A' + p, \text{ etc.,} \\ \text{and} \qquad t_{yz} &= \Theta f + \Psi F', \text{ etc.,} \end{aligned}\right\} \tag{19}$$

where

$$\left.\begin{aligned} a = \partial u/\partial x, \quad b = \partial v/\partial y, \quad c = \partial w/\partial z, \\ f = \partial v/\partial z + \partial w/\partial y, \quad g = \partial w/\partial x + \partial u/\partial z \quad \text{and} \quad h = \partial u/\partial y + \partial v/\partial x, \end{aligned}\right\} \tag{20}$$

and

$$\left.\begin{aligned} A' = a^2 + \tfrac{1}{4}(g^2 + h^2), \quad B' = b^2 + \tfrac{1}{4}(h^2 + f^2), \quad C' = c^2 + \tfrac{1}{4}(f^2 + g^2), \\ F' = \tfrac{1}{2}gh + (b + c)f, \quad G' = \tfrac{1}{2}hf + (c + a)g \quad \text{and} \quad H' = \tfrac{1}{2}fg + (a + b)h. \end{aligned}\right\} \tag{21}$$

The quantities K_2 and K_3, given by (17), may be expressed in terms of a, b, c, f, g and h by the relations

$$\left.\begin{aligned} K_2 &= ab+bc+ca-\tfrac{1}{4}f^2-\tfrac{1}{4}g^2-\tfrac{1}{4}h^2 \\ \text{and}\qquad K_3 &= abc+\tfrac{1}{4}fgh-\tfrac{1}{4}af^2-\tfrac{1}{4}bg^2-\tfrac{1}{4}ch^2. \end{aligned}\right\} \tag{22}$$

The incompressibility condition (18) may be written, as in classical hydrodynamics,

$$a+b+c = 0. \tag{23}$$

Equations (19), (22) and (23) are obtained purely by mathematical analysis from (16), (17) and (18) respectively and do not involve any further physical assumptions.

We note, from equations (19), that the flow properties of the fluid considered are to be described by two physical constants Θ, the viscosity, and Ψ, which we call the *normal stress coefficient*. Both Θ and Ψ may depend on the state of flow in the fluid.

If the forms of Θ and Ψ as functions of K_2 and K_3 are known for any particular fluid, then equations (19) can be used to determine the forces which must be exerted on a mass of the fluid to produce in it a specified state of flow. Certain simple states of flow have already been considered (Rivlin 1948*a*, 1949*a*), and some results obtained for these will be summarized in the next section. It will be seen that, in general, the non-vanishing of Ψ results in normal components, as well as tangential components, of stress being associated with states of laminar flow.

4. *Some simple states of flow*

(*a*) *Torsional motion*

We consider a circular-cylindrical mass of the fluid in which each plane of the fluid normal to the axis of the cylinder is rotating about the axis with an angular velocity Ω, which is proportional to the distance z of the plane from one end of the cylinder, so that $\Omega = \psi z$. It has been shown that such a state of motion can be produced in the fluid by the application of surface tractions to the plane ends of the cylinder. This surface traction has, at a distance r from the axis of the cylinder, an azimuthal component Θ' and a normal component Z' (taken positive when in the direction of the outward drawn normal to the surface) given by

$$\Theta' = r\psi\Theta \quad \text{and} \quad Z' = \tfrac{1}{2}\psi^2r^2\Psi+\tfrac{1}{2}\psi^2\int_a^r r\Psi\,dr, \tag{24}$$

where a is the radius of the cylinder. It should be borne in mind that Θ and Ψ are functions of K_2 and K_3, depending on the particular fluid considered. For the motion considered, K_2 and K_3 are given by

$$K_2 = -\tfrac{1}{4}\psi^2r^2 \quad \text{and} \quad K_3 = 0. \tag{25}$$

If Θ and Ψ are both constants, then the second of equations (24) yields

$$Z' = \tfrac{1}{4}\psi^2\Psi(3r^2-a^2), \tag{26}$$

so that the distribution of the normal forces, which must be applied to the plane ends of the cylindrical mass of fluid, will be that shown in figure 10. We can add to the system of forces applied a uniform hydrostatic pressure, without the state of flow being altered. Then, the normal force on the curved surface is not zero and, if it is C', the curve in figure 10 is moved parallel to the ordinate by an amount C'.

If we consider the fluid to be contained between two cylindrical cups (Weissenberg 1947), as shown in axial section in figure 11, the outer cup being rotated with respect to the inner, then between the disks AB and CD, which form the bases of the cups, the fluid will flow in the manner considered above, so that the way in which the normal surface traction on AB and CD varies should be given by (24)—and, in the particular case when Θ and Ψ are constants, by (26)—provided that the distance between the disks is small compared with their radii. The value of C' which is appropriate to the experiment will, however, be determined by the detailed flow configuration near the periphery of the disks.

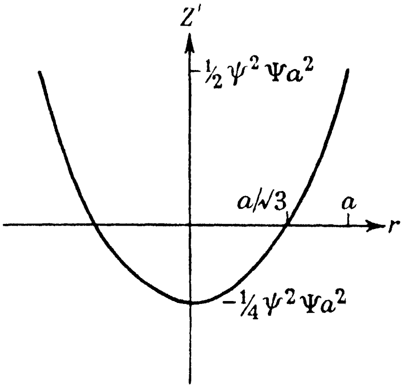

Figure 10. Radial distribution of normal surface traction Z' (Z' is positive when in direction of outward drawn normal).

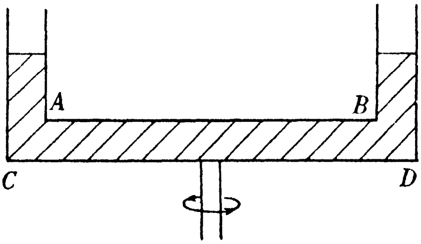

Figure 11.

(b) *Flow between rotating infinite cylinders*

We now consider the fluid to be contained between two vertical coaxial cylinders of radii a_1 and a_2 ($a_2 > a_1$) which are rotating with relative angular velocity Ω, so that each element of the fluid moves in a plane at right angles to the axis of the cylinders and in a circular orbit about it. It is found that the radial distribution of angular velocity of the fluid depends on the form of Θ and that, in general, normal surface tractions must be applied to the free surface of the fluid. In the particular case when Θ and Ψ are both constants, the magnitude of this normal surface traction Z', at a distance r from the axis of the cylinders, is given by

$$Z' = -2\Psi\Omega^2\left(\frac{a_1^2a_2^2}{a_1^2-a_2^2}\right)^2\frac{1}{r^4}+C', \tag{27}$$

where C' is an arbitrary constant which arises from the fact that, since the fluid is incompressible, an arbitrary hydrostatic pressure may be added to the system of applied forces without altering the state of flow. The normal component of the surface traction exerted on the cylindrical surfaces is C'.

If the surface forces Z' are not applied then the level of the fluid will tend to rise at the inner cylinder and fall at the outer cylinder, provided that Ψ is positive, and the state of flow near the surface will depart from that described.

5. *The significance of the normal stress coefficient*

Some calculations have been carried out (Rivlin 1948*b*, 1949*b*) with the object of finding how an appreciable value for the normal stress coefficient Ψ could arise in a concentrated high-polymer solution.

We take as our physical picture of the solution a large number of more or less flexible chain-like molecules immersed in a solvent which is idealized as a viscous continuum. Even when the solution is at rest, the high-polymer molecules are moving about as a result of their thermal energy and in doing so are subject to the viscous action of the solvent. The high-polymer molecules also interact with each other, either directly or through the medium of the viscous solvent, so that a force exerted on one molecule may be transmitted to many others. We wish to calculate the forces which will have to be exerted on such a solution in order to produce a homogeneous state of irrotational flow.

We should expect to obtain expressions for the three principal stress components t_1, t_2, t_3 in terms of the principal velocities U_1, U_2, U_3 having the form of equations (16). From the manner in which the terms $2\Psi U_1^2$, $2\Psi U_2^2$ and $2\Psi U_3^2$ arise, we can then obtain some idea of what features of the solution give rise to a large value of the normal stress coefficient Ψ. In order to carry out any calculations of this type it is necessary to idealize drastically the physical model.

The 'pearl necklace' model of a high-polymer molecule, employed by Kramers (1946) amongst others, is used. Each molecule is considered to consist of N equal massive points each of mass m connected by equal weightless rigid links of length L, which are capable of some measure of free rotation about the mass-points at their junctions. It is assumed that the solvent exerts no force on the rigid links but that a viscous drag is exerted by the solvent on each of the mass-points, which is proportional to the velocity of the mass-point relative to the solvent in its immediate neighbourhood. The coefficient of proportionality between the retarding force and the relative velocity will be denoted ζ. It is also assumed that the presence of the high-polymer molecules does not affect the flow configuration in the solvent. If we further neglect the interactions between the high-polymer molecules, as would be justified for very dilute solutions, we find that the expressions for t_1, t_2 and t_3 are in fact of the form (16). The terms $2\Psi U_1^2$, $2\Psi U_2^2$ and $2\Psi U_3^2$ arise from the fact that the individual links of the high-polymer molecules do not have random orientations in space in the flowing solution, as in the liquid at rest, but are preferentially oriented.

If the assumption is made, with Kramers, that the effect of the flowing solvent in orienting the high-polymer molecules can be considered equivalent to that of a mechanical potential field acting upon them and that the distribution of orientation is then determined by the Boltzmann law, we can obtain an estimate of both Θ and Ψ. For molecules in which the links are capable of free rotation about the mass-points at their junctions, Θ and Ψ are given by

$$\Theta = \tfrac{1}{36}\zeta L^2 N^2 \mathcal{N} \quad \text{and} \quad \Psi = \frac{1}{1620}\frac{\zeta^2 L^4 N^4 \mathcal{N}}{\boldsymbol{k}T}, \tag{28}$$

where $\mathcal{N}$ is the number of high-polymer molecules per ml. of solution, T is the absolute temperature of the solution and $\boldsymbol{k}$ is Boltzmann's constant. From equations (28) we have

$$\Psi = \frac{4}{5}\frac{\Theta^2}{\boldsymbol{k}T\mathcal{N}}. \tag{29}$$

For high-polymer molecules in which the links are capable of no rotation with respect to one another and are collinear, we obtain

$$\Theta = \tfrac{1}{72}\zeta L^2 N^3 \mathcal{N} \quad \text{and} \quad \Psi = \frac{1}{4320}\frac{\zeta^2 L^4 N^6 \mathcal{N}}{\boldsymbol{k}T}, \tag{30}$$

yielding

$$\Psi = \frac{6}{5}\frac{\Theta^2}{\boldsymbol{k}T\mathcal{N}}. \tag{31}$$

In deriving equations (28) to (31), the assumption has been made that the principal flow velocities are such that the change of potential energy of a molecule due to orientation in the mechanical potential field is small compared with $\boldsymbol{k}T$. This will, of course, only be true for sufficiently small values of the principal flow velocities. When it is not true, we find that Θ and Ψ both depend on the state of flow.

It is evident, by comparing equations (29) and (31), that provided we employ for Θ the measured contribution of the dissolved high-polymer molecules to the viscosity of the solution, the calculated value of Ψ is only very slightly dependent on whether or not the high-polymer molecules are assumed to be ideally flexible or rigid. The value of Θ per dissolved high-polymer molecule can, of course, be obtained from a measurement of the intrinsic viscosity of the solution. The value of Θ which should be employed in (29) or (31) is $\mathcal{N}$ times the contribution per molecule obtained in this way.

This value of Θ, for a concentrated high-polymer solution, is, of course, much lower than that measured experimentally. This difference is presumably due mainly to the interactions between the molecules. We might attempt to obtain an estimate of Ψ by introducing for Θ, into (29) and (31), the measured value of the viscosity of the concentrated high-polymer solution. However, we should still expect the value of Ψ so obtained to be an underestimate. For, in a concentrated high-polymer solution, the dissolved molecules interact so that a force exerted on one molecule will be transmitted to others. From the point of view of their effect on the flow properties of the solution, we might expect the $\mathcal{N}$ per ml. dissolved molecules, each containing N links, to act approximately as a smaller number $\mathcal{N}'$ of non-interacting molecules each containing a larger number of links N' given by $\mathcal{N}N = \mathcal{N}'N'$. With this model, we should obtain an estimate of Ψ from equation (29) or (31) by substituting $\mathcal{N}'$ for $\mathcal{N}$ and employing the measured value of the viscosity of the concentrated solution for Θ. An estimate of $\mathcal{N}'$ can be obtained by comparing the measured viscosity of the solution with that obtained from the intrinsic viscosity using the first of equations (28) or the first of equations (30). The value of $\mathcal{N}/\mathcal{N}'$ obtained depends on which of these two equations is used, i.e. on whether we consider the high-polymer molecules to be ideally flexible or rigid. In either case, values of Ψ are obtained for concentrated high-polymer solutions large enough to give rise to measurable effects of the types described in § 4, even for quite low velocity gradients. However, in view of the approximate nature of the calculations, it is hardly to be expected that quantitative agreement between theory and experiment would be obtained. A rough calculation has been carried out in the manner described above for a 25·7 % polystyrene-xylene solution, at 17·6° C, from the experimental data of Ferry (1942), the polystyrene having a molecular weight of about 120,000, on the assumption that the polystyrene molecules are ideally flexible. A value for Ψ of approximately 0·5 g.cm.$^{-1}$ was obtained. The value of Ψ obtained on the assumption that the molecules are rigid is approximately 0·02 g.cm.$^{-1}$.

6. *Further considerations*

We should not expect the theory so far described to give a complete account of the flow properties of concentrated high-polymer solutions. Indeed, the theory itself suggests a number of effects which may well affect the results obtained in experiments. It has been assumed, for example, that the stress at any point of the fluid depends on the state of flow in an infinitesimal element at that point at the time considered (assumption (ii) of § 3).

Now, the discussion of § 5 leads to the conclusion that the non-vanishing of Ψ may well be due to the orientation of the links of the high-polymer molecules in the flowing solution. Such an orientation would in fact give rise to the elastic properties which are observed in concentrated high-polymer solutions, and strictly assumption (ii) of § 3 would not be valid since the manner in which the principal flow velocities are changing would affect the stress.

However, these elastic properties would not be directly observable under conditions of steady-state laminar flow such as obtain in the experiments envisaged in § 4, and we shall therefore not discuss here the relationship which is suggested between the elastic properties of the solution and the non-vanishing normal stress coefficient.

Assumption (ii) of § 3 would not be valid if there were any appreciable tendency, as there may be in an inhomogeneous state of flow, for the high-polymer molecules to move from one part of the solution to another giving rise to a concentration gradient. In the case of a high-polymer solution in a steady state of inhomogeneous laminar flow between two disks, as described in § 4(*a*), the high-polymer molecules near the periphery of the disks will be subject to a higher velocity gradient and presumably to a greater degree of orientation than those near the centre. Since a state of preferred orientation is one of less probability than a randomly oriented state, a state of varying concentration, diminishing from the centre radially outwards, could conceivably be set up. It may well be, however, that this effect is negligible in practice.

Assumption (ii) of § 3 could also be invalidated if the solution showed any marked thixotropy. Material whose structure is broken down under the velocity gradients prevailing at one point of the solution might diffuse to another point at which a different velocity gradient exists. The physical state of the material at one point would then be determined not only by the state of flow at that point but also by that at other points.

It should be borne in mind, however, that although the occurrence of these possible effects would affect the detailed results of experiments on concentrated high-polymer solutions, the arguments for the basic normal stress phenomenon would still be valid for the case of homogeneous flow. Their application to the state of inhomogeneous flow would, however, have to be modified in detail.

This work forms part of a programme of fundamental research undertaken by the Board of the British Rubber Producers' Research Association.

THE EQUILIBRIUM SWELLING OF CROSS-LINKED AMORPHOUS POLYMERS

BY L. R. G. TRELOAR

The degree of swelling of an amorphous linear polymer in a low-molecular liquid is determined by the free-energy change associated with the process of mixing of polymer and liquid molecules. In the swelling of a cross-linked polymer an additional free-energy change, arising from the elastic extension of the three-dimensional molecular network, has to be taken into account. This term is dependent not only on the volume of the swollen gel, but also on its state of strain; its magnitude may be calculated from the statistical network theory.

The way in which this affects the equilibrium swelling is considered, and particular cases of swelling in the presence of external restraints are discussed. In the case of a tensile stress, both theory and experiment show that the equilibrium concentration of liquid is higher than in the unstrained polymer.

INTRODUCTION

This contribution deals with the theoretical derivation of the equilibrium absorption of liquid by a cross-linked amorphous polymer whose swelling is restricted by certain external restraints. Flory & Rehner (1943, 1944) have already considered the particular case when the polymer is stretched (or compressed) in one direction, and have shown the degree of swelling to depend on the state of strain. The purpose of this note is to cover the more general case of a homogeneous strain of any type, using a method essentially similar to that of Flory & Rehner.

Conditions for equilibrium swelling

For a swollen polymer in contact with a low-molecular liquid, in the absence of external stresses, the condition for equilibrium between the two phases is that the Helmholtz free energy A of the system shall be a minimum, i.e. that

$$A_0 = \partial A/\partial n_0 = 0, \tag{32}$$

where n_0 is the number of moles of liquid in the mixture. The quantity A_0 is the molar free energy of dilution.

In the case of a linear (i.e. not cross-linked) polymer, the free energy of dilution arises simply from the mixing of polymer and liquid molecules. Its form has been calculated by statistical methods by Huggins (1942, 1943) and by Flory (1942), and is expressed by the formula

$$A_{0m} = \boldsymbol{R}T[\ln(1-v_r)+v_r+\mu v_r^2], \tag{33}$$

where v_r is the volume fraction of polymer in the mixture, and μ is a parameter which is related to the heat of mixing of the two components. The validity of this expression for the free energy of dilution has been established experimentally for a particular system (natural rubber and benzene) from a study of vapour-pressure and osmotic-pressure data over a wide range of liquid concentration (Gee & Treloar 1942).

If the polymer is cross-linked (e.g. as in a vulcanized rubber), the expression (33) has to be modified to take account of the elastically stored free energy of the three-dimensional network of molecules. This may be obtained from the statistical theory of rubber elasticity. In the case of a pure homogeneous strain, in which a unit cube of the polymer is deformed to a rectangular block of dimensions l_1, l_2 and l_3, the expression for the free energy of deformation is (Treloar 1943)

$$A_e = \frac{\rho \boldsymbol{R}T}{2M_c}(l_1^2+l_2^2+l_3^2-3), \tag{34}$$

where ρ is the density of the polymer and M_c is the 'molecular weight' between successive points of cross-linkage. This formula has been shown to account approximately for the elastic properties of rubber in homogeneous strain (Treloar 1948). Its original derivation contained the assumption of constancy of volume during the deformation, or incompressibility of the polymer, represented by the condition

$$l_1 l_2 l_3 = 1, \tag{35}$$

but it is equally valid as an expression of that part of the free-energy change associated with the configurational entropy of the network even when this condition is not satisfied, that is, for all possible values of l_1, l_2 and l_3 corresponding to the case of a deformed *swollen* polymer. In this case we have, assuming incompressibility of both polymer and liquid,

$$l_1 l_2 l_3 = 1/v_r = 1+n_0 V_0, \tag{36}$$

where V_0 is the molar volume of the liquid, and n_0 the number of moles of liquid per unit volume of the dry polymer.

From equations (34) and (36) it is clear that A_e is a function of the four quantities l_1, l_2, l_3 and n_0, of which any three may be chosen as independent variables. Dilution of the mixture by the addition of δn_0 moles of liquid necessarily alters some or all of l_1, l_2 and l_3. Hence the free energy of dilution has a definite meaning only when the restrictions imposed on the accompanying variation of these quantities is specified.

Derivation of general equation

We shall now derive a general relation for the equilibrium swelling of a cross-linked polymer subjected to pure homogeneous strain. Consider a unit cube of polymer in contact with liquid swollen to a volume $1/v_r$ by n_0 moles of liquid, and constrained by forces applied to its faces to the form of a rectangular block having dimensions l_1, l_2 and l_3 (figure 12). Assuming the polymer to be initially isotropic, these forces will be normal to the surfaces of the block, i.e. in the direction of the principal stresses. Let t_1, t_2 and t_3 represent the principal stresses, or forces per unit area, measured in the strained state.

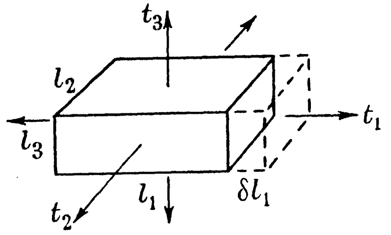

FIGURE 12

It will be assumed that the total free energy of the system is equal to the sum of the free energy of mixing A_m for a linear polymer and the free energy of network extension A_e, i.e.

$$A = A_m + A_e. \tag{37}$$

Consider now the process of absorption of a further small quantity δn_0 moles of liquid, under the condition that l_2 and l_3 are held constant, while l_1 increases by the amount δl_1. The condition for equilibrium between the swollen gel and the pure liquid is now

$$\left(\frac{\partial A}{\partial n_0}\right)_{l_2 l_3} = \delta W, \tag{38}$$

where δW is the work done by the external forces. Since l_2 and l_3 are constant, no work is done by t_2 and t_3, and therefore

$$\delta W = t_1 l_2 l_3 \delta l_1,$$

or, from (36),

$$\delta W = t_1 V_0 \delta n_0. \tag{39}$$

The condition for equilibrium is therefore

$$\left(\frac{\partial A}{\partial n_0}\right)_{l_2 l_3} = \frac{\partial A_m}{\partial n_0} + \left(\frac{\partial A_e}{\partial n_0}\right)_{l_2 l_3} = t_1 V_0. \tag{40}$$

The term $\partial A_m/\partial n_0$ or A_{0m} is given by (33), and is assumed independent of strain. It only remains to evaluate $(\partial A_e/\partial n_0)_{l_2 l_3}$.

Substituting the expression (34) for A_e, and differentiating, making use of (36), we obtain

$$\left(\frac{\partial A_e}{\partial n_0}\right)_{l_2 l_3} = \left(\frac{\partial A_e}{\partial l_1}\right)\left(\frac{\partial l_1}{\partial n_0}\right)_{l_2 l_3} = \frac{\rho R T}{M_c} l_1 \frac{V_0}{l_2 l_3} = \frac{\rho V_0 R T}{M_c} v_r l_1^2.$$

The condition for equilibrium with respect to liquid concentration is therefore

$$t_1 = \frac{A_{0m}}{V_0} + \frac{\rho R T}{M_c} v_r l_1^2, \tag{41}$$

with similar expressions for t_2 and t_3.

This equation determines the relation between the stress t_1 and the three principal extension ratios l_1, l_2 and l_3, or, alternatively, between t_1, l_1 and the concentration of polymer in the mixture, v_r, at equilibrium. It follows that if any two of t_1, l_1 and v_r are given, the third is uniquely determined. Thus the specification of l_1 and v_r automatically fixes the stress t_1, while the specification of t_1 and l_1 likewise determines v_r.

General stress-strain relations

From the three equations of the type (41) we obtain, by subtraction,

$$t_1 - t_2 = \frac{\rho \boldsymbol{R} T}{M_c} v_r (l_1^2 - l_2^2) = \frac{\rho \boldsymbol{R} T}{M_c} v_r^{\frac{1}{3}} (\lambda_1^2 - \lambda_2^2), \tag{42}$$

where λ_1 and λ_2 are the principal extension ratios referred to the *swollen unstrained* state. This general stress-strain relation, which has previously been derived from the statistical theory (Treloar 1947), describes the mechanical properties of an *incompressible* swollen rubber, *not* in contact with the swelling liquid. In such a case the principal stresses are indeterminate to the extent of an arbitrary hydrostatic pressure, hence only their differences are determined. This is a direct consequence of the incompressibility condition (36).

It is seen, therefore, that the condition for equilibrium with the swelling liquid imposes a further restriction, as a result of which the stress system becomes uniquely determined. The swollen polymer in equilibrium with pure liquid behaves, in fact, like a *compressible* material, since the superposition of a hydrostatic pressure has the effect of squeezing out liquid, or reducing the volume.

Treatment of special problems

(*a*) *Hydrostatic pressure.* In the case of a simple hydrostatic pressure p applied to the swollen polymer we have

$$t_1 = t_2 = t_3 = -p \quad \text{and} \quad l_1 = l_2 = l_3 = 1/v_r^{\frac{1}{3}}.$$

Hence, for equilibrium, equation (41) gives

$$\frac{A_{0m}}{V_0} + \frac{\rho \boldsymbol{R} T}{M_c} v_r^{\frac{1}{3}} = -p. \tag{43}$$

For the particular case of $p = 0$, corresponding to free swelling, this reduces to

$$\frac{A_{0m}}{V_0} + \frac{\rho \boldsymbol{R} T}{M_c} v_r^{\frac{1}{3}} = 0. \tag{43a}$$

The form (43*a*), with A_{0m} represented by (33), has been found by Gee (1946) to account satisfactorily for the swelling behaviour of a series of differently cross-linked natural rubbers, the values of M_c (which is related to the degree of cross-linking) being determined from the moduli of elasticity. A similar conclusion was reached by Flory (1946), who worked with a range of butyl rubbers swollen with cyclohexane.

(*b*) *Simple elongation* (*or unidirectional compression*). In the case of a tensile stress t_1 acting in the direction of l_1 we have

$$t_2 = t_3 = 0 \quad \text{and} \quad l_2^2 = l_3^2 = 1/l_1 v_r.$$

Using the expression for t_2 corresponding to equation (41), the equilibrium condition becomes

$$t_2 = \frac{A_{0m}}{V_0} + \frac{\rho RT}{M_c}\frac{1}{l_1} = 0. \tag{44}$$

This equation, originally derived by Flory & Rehner (1944), expresses the concentration of liquid in the swollen gel in terms of the length l_1 in the direction of the applied force. If l_1 is greater than $1/v_r^{\frac{1}{3}}$ this force is tensile, while if l_1 is less than $1/v_r^{\frac{1}{3}}$ it is compressive. In the particular case when $l_1 = 1/v_r^{\frac{1}{3}}$, equation (44) reduces to the condition for free swelling (equation (43*a*)).

(*c*) *Inflation*. The term 'inflation' may be used to describe a strain in which two dimensions are subjected to equal tensile stresses, while the stress in the third direction is zero. It corresponds approximately to the strain in an inflated balloon. We have, therefore,

$$t_1 = 0, \quad t_2 = t_3 \quad \text{and} \quad l_2^2 = l_3^2 = 1/l_1 v_r.$$

The strain is thus formally identical with that in a unidirectional compression; the only difference between the two systems is in the applied stress. Equation (41) now gives, for the equilibrium condition,

$$t_1 = \frac{A_{0m}}{V_0} + \frac{\rho RT}{M_c} v_r l_1^2 = 0, \tag{45a}$$

or

$$\frac{A_{0m}}{V_0} + \frac{\rho RT}{M_c}\frac{1}{v_r l_2^4} = 0. \tag{45b}$$

Since the forces are tensile, l_2 is greater than $1/v_r^{\frac{1}{3}}$. It follows that the equilibrium degree of swelling is greater than for the unstrained polymer.

It is interesting to note that this is in the opposite direction to the change in swelling ratio resulting from the application of a unidirectional compression, though the state of strain is formally the same. This illustrates again the importance of the hydrostatic pressure component of the applied stress, discussed under (*a*) above.

(*d*) *Pure shear*. Consider a unit cube of polymer swollen isotropically to the equilibrium state, corresponding to polymer concentration v_r. Let it now be subjected to pure shear in the plane perpendicular to l_1, without changing v_r, by the application of suitable stresses t_1, t_2 and t_3 at its surfaces.

For the intermediate swollen unstressed state we have

$$l_1 = l_2 = l_3 = 1/v_r^{\frac{1}{3}},$$

and the equilibrium condition is represented by equation (43*a*), i.e.

$$\frac{A_{0m}}{V_0} + \frac{\rho RT}{M_c} v_r^{\frac{1}{3}} = 0.$$

The effect of the subsequent shear (Love 1934, chapter 1) will be to change the dimensions to

$$l_1 = 1/v_r^{\frac{1}{3}}, \quad l_2 = \alpha/v_r^{\frac{1}{3}}, \quad l_3 = 1/\alpha v_r^{\frac{1}{3}},$$

and hence the stress t_1 required to maintain the state of equilibrium with respect to the liquid concentration, in accordance with equation (41), will be

$$t_1 = \frac{A_{0m}}{V_0} + \frac{\rho \boldsymbol{R} T}{M_c} v_r^{\frac{1}{3}}. \tag{46}$$

Comparing this with (43*a*) it is seen that

$$t_1 = 0. \tag{46a}$$

The other stresses are given by

$$t_2 = \frac{A_{0m}}{V_0} + \frac{\rho \boldsymbol{R} T}{M_c} v_r^{\frac{1}{3}} \alpha^2 = \frac{\rho \boldsymbol{R} T}{M_c} v_r^{\frac{1}{3}} (\alpha^2 - 1), \tag{46b}$$

$$t_3 = \frac{A_{0m}}{V_0} + \frac{\rho \boldsymbol{R} T}{M_c} \frac{v_r^{\frac{1}{3}}}{\alpha^2} = \frac{\rho \boldsymbol{R} T}{M_c} v_r^{\frac{1}{3}} \left(\frac{1}{\alpha^2} - 1\right). \tag{46c}$$

Equations (46*a*), (46*b*) and (46*c*) lead to the following significant conclusions:

(1) The application of a shear in the plane $l_2 l_3$ involves stresses in this plane only.

(2) The two principal stresses in this plane are of opposite sign, and of unequal numerical magnitude. (If $\alpha^2 - 1$ is positive $\frac{1}{\alpha^2} - 1$ is negative.) However, it can readily be shown that the total *forces* acting in the directions l_2 and l_3 respectively are of *equal* numerical magnitude, but of opposite sign, being proportional to $\alpha - \frac{1}{\alpha}$ and $\frac{1}{\alpha} - \alpha$.

(3) If the shear is small we have $\alpha^2 - 1 \simeq -\left(\frac{1}{\alpha^2} - 1\right)$, so that in this case the two principal stresses are equal and opposite. It is well known (Love 1934, chapter 2) that a stress system of this kind is equivalent to a shear stress acting on planes at an angle of 45° to the directions of the principal stresses. Since this condition no longer exists when the shear strain is large, it follows that a large shear strain cannot be maintained by a shear stress only. This result is quite generally true, as Rivlin (1948*d*) has demonstrated.

(4) It follows from (3) that the application of a *small* shear stress does not alter the equilibrium swelling of the polymer. In this respect the system is analogous to a compressible (single-phase) system, for which the application of a small shear stress produces no change of volume. This result may obviously be generalized to prove that any stress system *of small magnitude* for which the isotropic or hydrostatic component is zero (and which can therefore be represented as the sum of two shear stresses) does not affect the swelling equilibrium.

Experimental

Experimental data which have been reported on the swelling equilibrium in the presence of an external stress have been limited to the case of simple tensile stress. For this case Flory & Rehner (1944), working with butyl rubber and xylene, obtained good agreement with the theoretical relation (44), using the expression (33) for A_{0m}. More extensive data, reproduced in figure 13, have recently been reported by Gee (1946), who examined vulcanized natural rubber in the presence of a number of swelling liquids. For good swelling agents the agreement with theory is seen to be fairly good, but for poor swelling agents (not shown in figure 13) quantitative agreement was lacking. This discrepancy was shown to arise essentially from the fact that the form of A_{0m} represented by (33) is known not to hold accurately in the case of poor swelling agents.

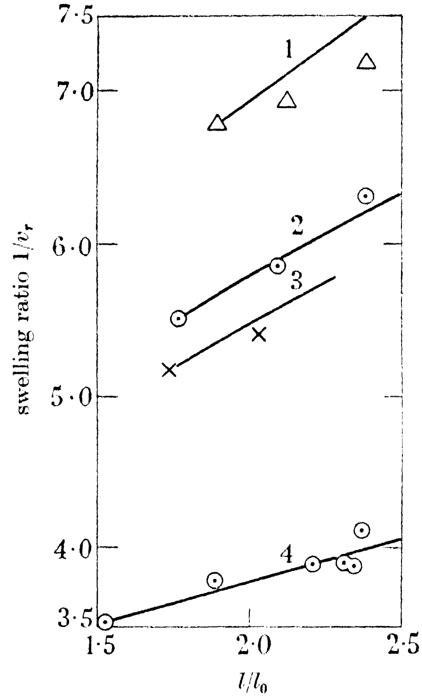

FIGURE 13. Effect of extension on swelling of vulcanized rubber (Gee 1946). Theoretical curves for: 1, chloroform; 2, benzene; 3, toluene; 4, petroleum ether.

Gee* has also made preliminary measurements of the equilibrium swelling under unidirectional compression. His data showed the expected reduction of swelling compared with the unstressed rubber, but the experiments have not yet been carried out with sufficient precision to justify quantitative comparison with the theory.

Conclusion

In the preceding theoretical treatment of homogeneous strain in cross-linked polymers it has been shown that the specification of the dimensions in the swollen state uniquely determines the principal stresses. The inverse problem, to calculate the state of strain, under equilibrium swelling conditions, when either the principal stresses, or the forces acting on the surfaces are given, is likely to prove more difficult. Indeed, even in the absence of the complications introduced by swelling, the solution of problems of this kind presents difficulties, and in certain cases a unique solution is not obtainable (Rivlin 1948*c*).

---

* Private communication.

When the state of strain in the swollen polymer is not homogeneous further difficulties arise. For, as Rivlin (private communication) has pointed out, it is necessary to satisfy not only the usual requirements of elasticity theory, but also the additional requirement relating to the equilibrium concentration of liquid at every point of the strained body. This second condition may be satisfied physically either by direct transfer of liquid between swollen gel and liquid phases, where these are in contact, or by internal diffusion of liquid where the swollen gel is not in contact with liquid.

The author desires to acknowledge his indebtedness to Dr G. Gee and Mr R. S. Rivlin for a number of helpful discussions during the preparation of this note.

RHEOLOGY OF HYDROCARBON GELS

By K. Weissenberg

[Plate 5]

(*This paper is a summary of a contribution to the discussion. A more detailed report is being prepared.*)

Hydrocarbon gels contain a number of materials, such as rubber, greases, saponified mineral oils, etc., of great interest for various engineering purposes. Specific requirements in mechanical properties have been met by producing gels in appropriately chosen patterns of constituent components of visible, colloidal, molecular and atomic sizes, ranging from coarse-grained aggregates, represented by sponges, foams, emulsions, etc., to fine-grained and apparently homogeneous ones, represented by optically clear compounds. The engineer who has to deal with the whole range of such materials will adopt a macroscopic point of view, based on an *apparent continuity* of all the material structures and of the distributions in space and time of the displacements and forces occurring under mechanical actions. It has been possible to determine these distributions in the framework of a comprehensive scheme in which the fundamental principles of the mechanics of continuous media provide the theoretical basis, and a testing instrument* of new design, termed Rheogoniometer, the means of experimental measurement (Weissenberg 1931, 1934, 1946, 1947, 1948).

The pioneer work of Cosserat (1896), Brillouin (1925) and Hencky (1929) served as a basis for a theory of elasticity and visco-elasticity in which was described how a material passes from its *virginal ground state*, where it is at rest and free from externally applied forces, to various *loaded states*, where it may be in any motion and subjected to any set of forces. The parameters characterizing the states were formed into quantities and relations which are invariant, or show simple transformation properties (co- or contra-variance) under wider and ever wider groups of changes of the kind of material, of the mechanical action applied, and of the system of reference. By this procedure laws of great generality were developed, and attention was directed in every state to the significance of the *symmetry group* which indicates for the parameters of this state the invariance against all rotations, or the lack of this invariance, by the terms *isotropic* and *anisotropic*. Explicit calculations were carried out on *isotropic materials*, i.e. materials which have isotropic symmetry in their respective ground states, with the result that any isotropic material will display in various loaded states a variety of anisotropic phenomena depending in each state on the amount of *recoverable shear strain*, i.e. on the amount of shear strain recovered from that state after a sudden release of all external forces; according as this amount is large, of medium size or infinitesimally small (or zero), the anisotropy of the phenomena in the state will be strongly pronounced, appreciable, of imperceptibly small (or zero). The theory (Weissenberg 1934) predicted the general features of the phenomena, including some new effects, such as those illustrated in figures 14, 15, 16. Experimental tests (1944)* fully confirmed the existence of the effects, as well as the general features, for a large variety of solid and liquid hydrocarbon gels over wide ranges of rheological states. Theoretical as well as experimental progress has been made since in the direction of defining

---

* Thanks are due to Messrs R. T. Russel, S. M. Freeman and J. E. Roberts for help given in the design and construction of the instrument, and to Messrs Hilger and Watts Ltd. for the production of a prototype model.

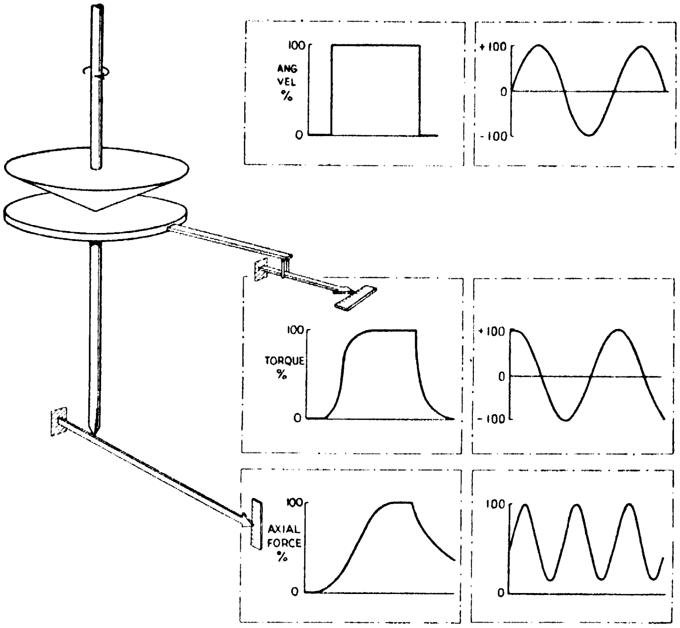

FIGURE 14

---

* Demonstrations were given in 1944 at the Imperial College, and in 1945 at the Univ. of Birmingham and at the British Rubber Producer's Association, Welwyn, where the author directed Mr Rivlin's special attention to the normal components of stress appearing in the torque of cylinders of viscoelastic liquids and of solid rubber. Mr Rivlin erroneously quoted 1947 as the year in which attention was drawn to the experiments.

the phenomena in a quantitative manner. We are, in particular, testing to what extent the experimental results can be deduced from the simple general assumption which may be formulated as follows. Let an isotropic material move from its virginal ground state to some loaded state, and consider at any point in the material any two planes of different orientation, each marked initially by a circle of unit area. We then assume that the two planes will exhibit across the marked area the same components of traction forces, provided the planes suffered throughout the movement the same changes in the normal distances from their respective parallel neighbouring planes.

We shall restrict ourselves for this lecture to the discussion of isotropic materials. The theory can be used for these to predict the presence, as well as the absence, of anisotropic phenomena within a given range of rheological states. This is done by determining in that range the amount of shear strain recovered from the various states, and classifying a material as *general* or *special* according as this amount is found to reach within the range finite values of any appreciable magnitude, or to remain throughout the range infinitesimally small or zero. Experimental tests have confirmed the theoretical expectations, as the anisotropic phenomena were clearly observed in the general class of materials but were not detected in the special class. It was found from preliminary experiments on shear strain recovery that the general class contained elastic and visco-elastic materials in the form of solid and liquid colloids, prepared from rubber, gelatine, starch, cellulose, saponified oils, etc., and the special class liquids of the Newtonian kind such as can be prepared from substances of small molecular weight (either pure or in solution), for instance water, mineral and vegetable oils, etc.

In the demonstrations* we shall use general and special materials of *liquid* and *solid* consistencies.† We start with liquids that are sensibly incompressible within the range of mechanical actions here applied. The theory here expects three distinct groups of phenomena.

The first group, illustrated in figures 15, 16, concerns stationary phenomena (Russell 1945; Weissenberg 1946, 1947).‡ In figure 15, phenomena are shown diagrammatically, whilst in figure 16, actual photographs are reproduced which correspond to the diagrams given for 'general liquids' under the heading 'high speed' in rows 3 to 7. The experimental arrangement is such that the liquid is sheared in a gap between an outer vessel and an inner member, the former rotated with an angular velocity that is kept stationary at various levels (see column subdivisions 'zero speed', 'low speed', 'high speed', 'any speed'), while the latter held against rotation, and either fixed in position, or left free to move up and down the axis.

---

* My thanks are due to Mr C. Wood for preparing and demonstrating the experiments.

† We use the term liquid for a material which cannot maintain a shearing stress, however small, without flowing, and the term solid for a material which can statically bear shearing stresses up to some limiting values.

‡ I am greatly indebted to Dr C. H. Lander and to his collaborators, Dr P. Rosin, Dr H. Fehling, Mr M. Deutsch and Mr R. J. Russel, for the generous help they gave me in these experiments, to Mr S. M. Freeman for many improvements in the experimental techniques and to Dr F. H. Garner and Dr A. H. Nissan for suggestions of a useful arrangement of pressure gauges, shown in row 6 of figure 15.

The conditions are so chosen that the combined actions of the traction forces at the boundaries, and the mass forces of gravity and inertia (centrifugal forces) in the interior, produce a stationary laminar shearing movement of the liquid. In such a movement the stress has its strength so distributed over the various directions in space as to allow the appearance of shear components, as well as of normal components, and in particular of a pull along the lines of flow.* The presence or absence of this pull distinguishes the general liquids from the special ones since

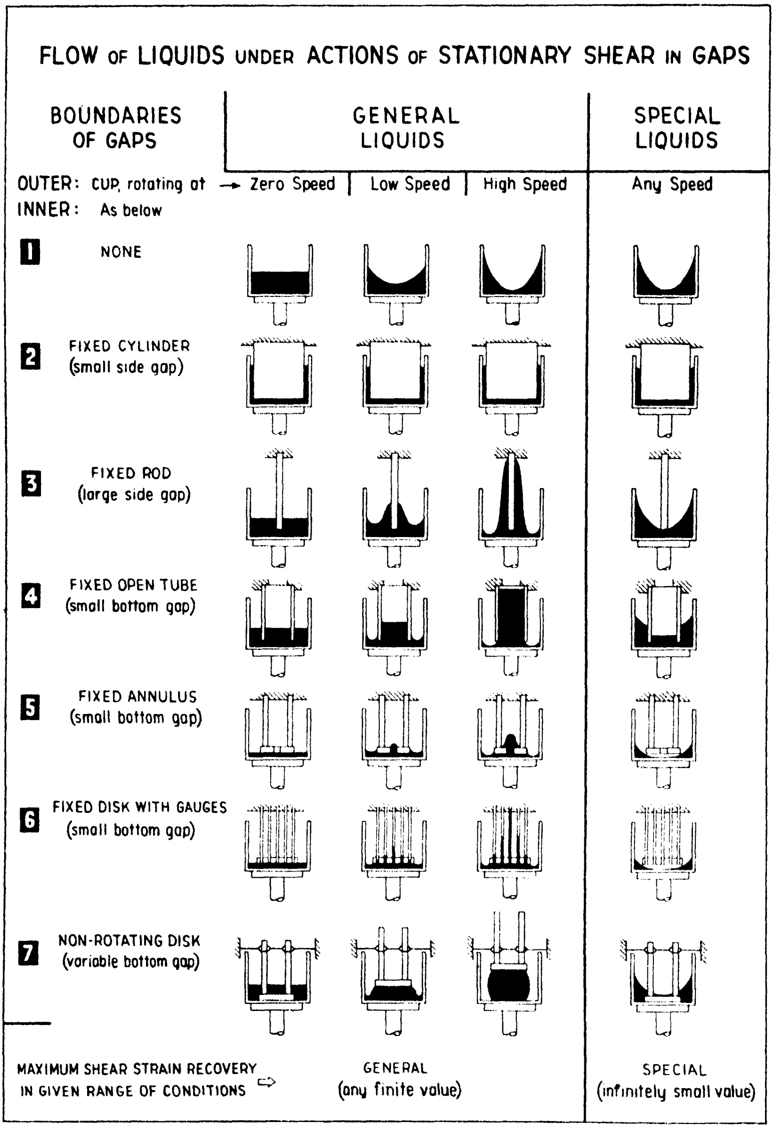
FLOW OF LIQUIDS UNDER ACTIONS OF STATIONARY SHEAR IN GAPS
BOUNDARIES OF GAPS
GENERAL LIQUIDS
SPECIAL LIQUIDS
OUTER: CUP, rotating at →
INNER: As below
Zero Speed
Low Speed
High Speed
Any Speed
1 NONE
2 FIXED CYLINDER (small side gap)
3 FIXED ROD (large side gap)
4 FIXED OPEN TUBE (small bottom gap)
5 FIXED ANNULUS (small bottom gap)
6 FIXED DISK WITH GAUGES (small bottom gap)
7 NON-ROTATING DISK (variable bottom gap)
MAXIMUM SHEAR STRAIN RECOVERY IN GIVEN RANGE OF CONDITIONS ⇨
GENERAL (any finite value)
SPECIAL (infinitely small value)

Figure 15

---

* We obtained direct experimental evidence for the presence of such a pull in a general liquid by suddenly stopping its motion, and then making cuts perpendicular to the lines of flow. The liquid used has a time of relaxation sufficiently long for the stress to persist appreciably after the stoppage and the pull component present in this stress caused the cuts to open up.

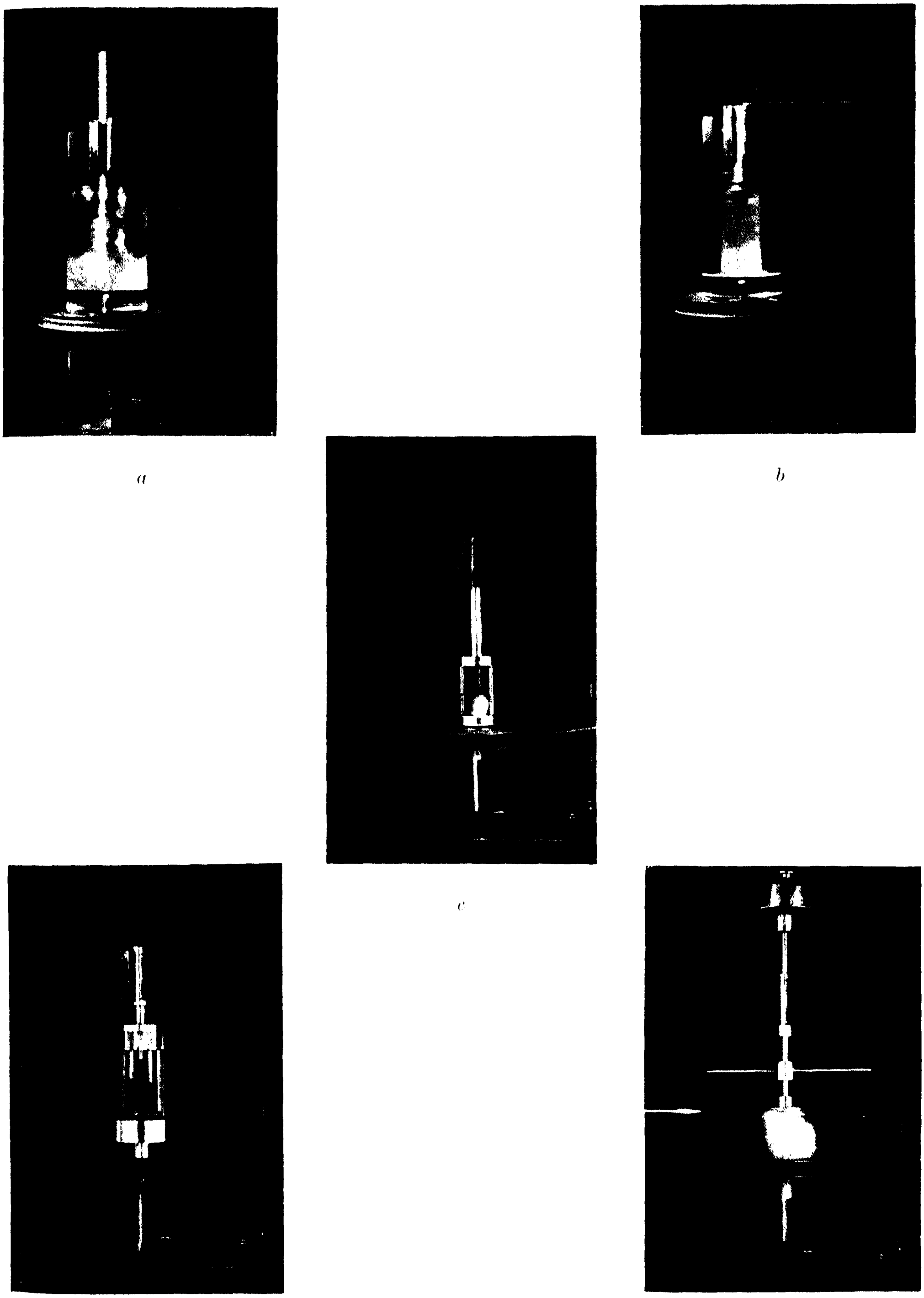

a

b

c

d

Figure 16

e

the strength of this pull is of finite magnitude, or infinitesimally small (or zero) whenever the amount of recoverable strain is finite, or infinitesimally small (or zero). In our experiments the lines of flow are closed circles, and a pull along these lines, if present, strangulates the liquid and forces it inwards against the centrifugal forces, and upwards against the forces of gravity as seen in the photographs and in the diagrams in the column 'general liquids'. In the absence of such a pull no strangulation takes place as seen in the column 'special liquids'.

The second group concerns anisotropic time effects, as illustrated in figure 14 (Freeman & Weissenberg 1948*a*, *b*; Weissenberg 1946). On the left we find the diagram of an instrument designed to apply various states of laminar shear to a material, and to measure during this application the relevant developments in time along different directions in space. Looking at the diagram we see near the middle the receptacle for the material as a wedgelike horizontal gap whose upper and lower boundaries are provided respectively by a cone, pointing with its apex downwards, and by a plane disk, both axially mounted on vertical rods, and so adjusted in height that the apex of the cone just touches the centre of the disk. The height of the gap is kept small throughout, according to a wedge angle of about 2°. (In the diagram we have shown, for greater clarity, a wider gap with a larger wedge angle and a correspondingly more pointed cone.) In all the experiments we keep the disk sensibly fixed and constrained against rotational and axial movements by two elastic cantilevers, shown at the side and the bottom of the diagram. By rotating the cone relative to the disk we force the material to execute a laminar shearing movement. The rate of shear is here, in every differential cell of the gap, the same (because of the wedgelike shape), and the changes in time are exactly proportional to the *angular velocity* of the cone (because of the small height of the gap). Thus, the kinematic conditions of the material are here fully determined by the time-graph of the angular velocity of the cone. The corresponding dynamic conditions are more complex. In a differential cell the stress may also vary in time and, in general, the variation may here be different for the components tangential and normal to the plane of the gap. As these components are transmitted to the disk, and there summed up over the disk area to a resultant *torque* (moment round the axis) and *axial force* (thrust along the axis), we can see their respective developments in time at the scales of the instrument by the deflexions of the elastic cantilevers, and detect the anisotropic time effects in the differences of these developments as recorded in the corresponding time-graphs. For ease of comparison we have plotted in these graphs every quantity as a percentage of its maximum value. The discussion of the effects will be limited here to materials belonging to the class of general liquids. In one series of experiments (see first column of graphs) we started with the liquid at rest in its ground state, then impart to it suddenly a laminar shearing motion with a rate of shear kept constant for some period of time, during which the components of stress are observed to build up gradually from zero to some stationary values. We then brought the liquid suddenly to rest, and kept it at rest for another period of time, during which the components of stress were seen to relax gradually to zero from their stationary values reached before. In a second series of experiments (see second column of graph) we proceeded as above, except that the shearing motion imparted to the liquid had a rate of shear which varied harmonically during the whole of the period, and that accordingly harmonic variations occurred in the components of stress. The two series of experiments specify for general liquids some kinematic conditions under which anisotropic time effects for various components of stress occur in a differential cell. In particular, one deduces from the graphs of the first column that the stress components tangential and normal to the plane of the gap increase at different percentage rates during the period of build up, and decrease at different percentage rates during the period of relaxation. Similarly one finds from the graphs of the second column that the two stress components have different frequencies of oscillations during a period of harmonically varying rates of shear, the frequency of the normal component being twice that of the tangential one.

The third group of experiments (Weissenberg 1931, 1934, 1946, 1948) is concerned with anisotropic effects which come under the heading of anomalous viscosity as they are revealed in a change of the apparent resistance to flow under different conditions of shear. A change of this kind must occur in all general liquids because there the tensorial quantities of stress and strain velocity show an angular derivation which depends on the conditions of shear.

Further results of the theory refer to compressible materials (Freeman & Weissenberg 1948*a*, *b*; Weissenberg 1948) for which one must expect that the anisotropic phenomena discussed above are modified and complicated by changes of volume which—according to the theory—must occur even under stresses with a mean isotropic pressure equal to zero. Even paradoxical effects must here be expected such as a contraction of volume under certain stresses with a mean isotropic pressure of negative sign, i.e. of the type of an isotropic pull. The theory has been fully confirmed by experiments which are here demonstrated on rubber sponges, foams, and various aggregates of fibres.

I am indebted to various colleagues from the Shirley Institute, and in particular to Mr G. Grundy for the diagrammatic drawings and to Mr C. Bradley and Miss Gallagher for the photographs.

THERMODYNAMICS AND RHEOLOGICAL BEHAVOUR OF ELASTO-VISCOUS SYSTEMS UNDER STRESS

BY F. H. GARNER, A. H. NISSAN AND G. F. WOOD

(*Summary of contribution*)

The systems to be discussed are obtained from dissolving aluminium and calcium soaps of fatty and naphthenic acids in hydrocarbons with the aid of peptizers like water, xylenols, alcohols, 'cellosolve' or cressols.

It was observed that when such systems were subjected to stress their free energies increased. The first series of experiments dealt with the behaviour of jets in the form of expanding conical sheets. Ordinary liquids broke up when the kinetic energy of the jet exceeded a certain function of the surface energy which tended to stabilize the sheets. With these systems the kinetic energy required to break up the conical sheets was much greater than this function calculated on the basis of the surface energy measured statically.

The second series of experiments dealt with the quantitative evaluation of the free energy on subjecting the systems to stress at different temperatures. A rod was rotated inside a stationary sleeve, the space between being full of the fluid under consideration. From the drop in the level of the fluid, it was deduced that the internal energy and the entropy were both raised by shearing the system. The increase in internal energy was greater than the rise in entropy, and hence the free energy, as a whole, increased on shearing. These facts became less noticeable as the temperature was raised.

Finally, a series of experiments were conducted on the behaviour of these systems when subjected to different states of shear between disks, cones or cylinders in each experiment, of which one member was rotated and the other held stationary. In all experiments secondary spontaneous flow from regions of high shear to regions of low shear confirmed the hypothesis that the increase in free energy on straining (or stressing) the system resulted in local instability. Surfaces of uniform shear acted as if they were semi-permeable membranes with a concentration gradient across them due to the structural units moving from regions of high to those of low shear values. Thus a species of osmotic pressure was generated which could be measured. These peculiar phenomena only occurred when there was a marked difference in the rate of shear between different points in the system; under uniform rates of shear they did not arise.

THE RHEOLOGY OF 'ELASTIC' NON-NEWTONIAN FLUIDS

BY F. H. GARNER, A. H. NISSAN AND G. F. WOOD

(*Summary of contribution*)

Characteristics of Newtonian and non-Newtonian rheological systems were summarized and the apparatus used in the present investigation described. The method consists, essentially, of forcing the fluids through pipes of various lengths and diameters and measuring the pressure losses corresponding to different rates of flow.

A detailed study of the pressure expenditure at the entry was made. It was found that, compared with entry losses of Newtonian systems, the entry losses with non-Newtonian systems were large and complex.

When the entry losses were completely accounted for, there was still the complication of a 'layer effect'. With the particular system studied, this was in the form of an apparently retarding layer at the surface, giving rise to a higher rate of shear strain obtaining in wide tubes than in narrow tubes at the same shearing stress.

Finally, the development of a rheological equation was undertaken. It was found that Eyring's equation best fitted the results. However, certain difficulties in interpreting the constants of the equation throw doubt on its validity from a physical-chemistry viewpoint.

In the conclusion, a hypothesis for the cause of the three difficulties of entry losses, retarding layer effects and the non-applicability of any known equation to the results was advanced.

REFERENCES

Ashby, E. C., Bryant, W., Mitchell, J. S. & Smith, G. H. 1941 *J. Amer. Chem. Soc.* **63**, 2924.
Boner, C. J. 1937 *Industr. Engng Chem.* **29**, 58.
Brillouin, L. 1925 *Ann. Phys., Lpz.*, **3**, 251.
Carlile, J. H. G., Cawley, C. M., King, J. G. & Kingman, F. E. T. 1947 *J. Instn Petrol. Tech.* **33**, 664.
Coe, R. H., Mysels, K. J. & Smith, G. H. 1948 *J. Colloid Sci.* **3**, 292.
Cosserat, E. & Cosserat, F. 1896 *Ann. Fac. Sci. Toulouse*, X, I, 1–I, 116.
Dean & Stark 1948 *Standard methods for testing petroleum and its products.* 9 ed., p. 555.
Ferry, J. D. 1942 *J. Amer. Chem. Soc.* **64**, 1330.
Flory, P. J. 1942 *J. Chem. Phys.* **10**, 51.
Flory, P. J. 1946 *Industr. Engng Chem.* **38**, 417.
Flory, P. J. & Rehner, J. 1943 *J. Chem. Phys.* **11**, 521.
Flory, P. J. & Rehner, J. 1944 *J. Chem. Phys.* **12**, 412.
Freeman, S. M. & Weissenberg, K. 1948*a* *Nature*, **161**, 324 and **162**, 320.
Freeman, S. M. & Weissenberg, K. 1948*b* *Proc. Int. Rheol. Congr. in Holland.*
Gallay, W., & Puddington, I. E. 1948 *Canad. J. Res.* **26**, 155.
Gee, G. 1946 *Trans. Faraday Soc.* **42** B, 33.
Gee, G. & Treloar, L. R. G. 1942 *Trans. Faraday Soc.* **38**, 147.
Gray, V. R. 1946 Ph.D. Thesis (Cambridge).
Gray, V. R. 1948 Presented at Rheological Congress, Holland.
Gray, V. R. & Alexander, A. E. 1949 *J. Phys. Colloid Chem.* **53**, 9, 23.
Harkins, W. D. & Myers, R. J. 1937 *Nature*, **139**, 367.
Hencky, H. 1929 *Ann. Phys., Lpz.*, **2**, 617.
Huggins, M. L. 1942 *Ann. N.Y. Acad. Sci.* **43**, 1.
Huggins, M. L. 1943 *Industr. Engng Chem.* **35**, 216.
Koenig, A. E. 1914 *J. Amer. Chem. Soc.* **36**, 951.
König, K. & Knoevenagel, E. 1922 *Cellulosechemie*, **3**, 113.
Kramers, H. A. 1946 *J. Chem. Phys.* **14**, 415.
Kreuger, D. 1930 *Färberztg*, **35**, 2032.
Langmuir, I. & Schaefer, V. J. 1936 *J. Amer. Chem. Soc.* **58**, 284.
Lawrence, A. S. C. 1938 *Trans. Faraday Soc.* **34**, 660.
Lawrence, A. S. C. 1945 *J. Instn Petrol. Tech.* **31**, 312.
Love, A. E. H. 1934 *Mathematical theory of elasticity.* Cambridge University Press.
Marion, S. P. & Thomas, A. W. 1946 *J. Colloid Sci.* **1**, 221.
Marsden, S. S., Mysels, K. J. & Smith, G. H. 1947 *J. Colloid Sci.* **2**, 265.
McBain, J. W. & McClatchie, W. L. 1932*a* *J. Phys. Chem.* **36**, 2567.
McBain, J. W. & McClatchie, W. L. 1932*b* *J. Amer. Chem. Soc.* **54**, 3266.
McBain, J. W. & Mysels, K. J. 1948 *J. Phys. Colloid Chem.* **52**, 1471.
McBain, J. W., Mysels, K. J. & Smith, G. H. 1946 *Trans. Faraday Soc.* **42** B, 173.
McBain, J. W. & Ross, S. 1946 *Oil & Soap*, **23**, 214.
McBain, J. W. & Working, E. B. 1947 *J. Phys. Colloid Chem.* **51**, 974.
McGee, C. G. 1949 *J. Amer. Chem. Soc.* **71**, 278.
McGee, C. G., Mysels, K. J., Pomeroy, H. H. & Smith, G. H. 1948 *J. Amer. Chem. Soc.* **70**, 1053.
McRoberts, T. S. & Schulman, J. H. 1948 *Nature*, **162**, 101.
Mitchell, J. S., Rideal, E. K. & Schulman, J. H. 1937 *Nature*, **139**, 625.
Mysels, K. J., Pomeroy, H. H. & Shreve, G. W. 1947 *J. Phys. Colloid Chem.* **51**, 963.

Pregl, F. & Soltys, A. 1929 *Mikrochemie*, **7**, 1.
Rivlin, R. S. 1948*a* *Proc. Roy. Soc.* A, **193**, 260.
Rivlin, R. S. 1948*b* *Nature*, **161**, 567.
Rivlin, R. S. 1948*c* *Phil. Trans.* A, **240**, 459.
Rivlin, R. S. 1948*d* *Phil. Trans.* A, **241**, 379.
Rivlin, R. S. 1949*a* *Proc. Camb. Phil. Soc.* **45**, 88.
Rivlin, R. S. 1949*b* *Trans. Faraday Soc.* **45**, 739.
Robinson, R. A. & Peak, D. A. 1935 *J. Phys. Chem.* **39**, 1125.
Russell, R. J. 1945 Ph.D. Thesis, Imp. Coll. London.
Sheffer, H. 1948 *Canad. J. Res.* **26**, 481.
Treloar, L. R. G. 1943 *Trans. Faraday Soc.* **39**, 241.
Treloar, L. R. G. 1947 *Trans. Faraday Soc.* **44**, 277.
Treloar, L. R. G. 1948 *Proc. Phys. Soc.* **60**, 135.
Weissenberg, K. 1931 *Abh. preuss. Akad. Wiss.* no. 2.
Weissenberg, K. 1934 *Arch. Sci. Phys. Nat.* v, **17**, 1.
Weissenberg, K. 1946 *Conference of Brit. Rheologists' Club, London.*
Weissenberg, K. 1947 *Nature*, **159**, 310.
Weissenberg, K. 1948 *Proc. Int. Rheol. Conf. in Holland.*
Wilds, A. L. 1944 *Organic reactions*, p. 198. New York: Wiley and Sons.

The tides in oceans on a rotating globe. V

By G. R. Goldsbrough, F.R.S.

(*Received* 23 *May* 1949—*Revised* 8 *September* 1949)

A method is presented of solving the dynamical equations of the tides on a rotating globe with boundaries along meridians. The method makes it possible to write down explicitly in algebraic form the terms of the double series in which the formula for the tide height is expressed.

For the case of the luni-solar tide with a restricted law of depth the coefficients are worked out and certain critical depths evaluated.

INTRODUCTION

The solution of the problem of the tides in an ocean on a rotating globe bounded by two meridians has been found in various cases by Goldsbrough (1928), Proudman (1936) and Doodson (1936, 1938, 1940).

In all these methods considerable arithmetical work is involved, and numerical parameters have to be introduced early in the process. Each method also requires the numerical solution of a set of linear algebraic equations with an infinity of unknowns, for which, of course, approximations are necessary. It is therefore of some interest to exhibit a solution which can be found in explicit literal form. The method could probably be applied to more general cases of tidal motion. But in this paper it is confined to the motion of the luni-solar tide K_2, in an ocean with a special law of depth. Under these conditions, the equations take a simpler form.

The equations are integrated by the Galerkin method in a double series of orthogonal functions each of which satisfies the boundary conditions. This process has been fully justified by Keldych (1942), who shows that the series obtained by this method converge in the mean to a solution of the equations of motion. From the relatively simple form of the work it is possible to write down the coefficient of each term of the double series in explicit algebraic form. These algebraic expressions could easily be converted into arithmetical form in any particular case. The method used is somewhat analogous to that proposed by Proudman (1916), but the introduction of the special orthogonal functions is a marked point of difference.

2. THE EQUATIONS FOR THE TIDE K_2

The Laplacian equations of the tides take a simple form if the tide-producing potential is restricted to the term K_2 for which the period is exactly half a sidereal day, and if the depth of the ocean has the form $h_0 \sin^2\theta$, h_0 being a constant and θ the co-latitude (Lamb 1932). In the usual notation these equations are

$$\left.\begin{aligned} \frac{\partial u}{\partial t} - 2\omega\cos\theta v &= -\frac{g}{a}\frac{\partial}{\partial\theta}(\zeta-\bar{\zeta}), \\ \frac{\partial v}{\partial t} + 2\omega\cos\theta u &= -\frac{g}{a\sin\theta}\frac{\partial}{\partial\phi}(\zeta-\bar{\zeta}), \\ a\frac{\partial\zeta}{\partial t} &= -\frac{1}{\sin\theta}\left\{\frac{\partial}{\partial\theta}(h\sin\theta u) + \frac{\partial}{\partial\phi}(hv)\right\}. \end{aligned}\right\} \tag{1}$$

Here ζ denotes the instantaneous displacement of the free surface of the ocean at time t at the point whose spherical co-ordinates are (θ, ϕ) on a sphere of radius a, rotating about the polar axis with angular velocity ω. At this point the depth is h $(= h_0 \sin^2\theta)$, and the current components are u, v in latitude and longitude respectively. The tide-producing potential is $g\bar{\zeta}$, which, in the case of the tide-component K_2, is the real part of $gH\sin^2\theta\, e^{(2\phi+\sigma t+\epsilon)}$, where, as stated already, $\sigma = 2\omega$.

On putting $\zeta' = \zeta - \bar{\zeta}$, $\mu = \cos\theta$, and removing the time-factor $e^{i\sigma t}$, equations (1) may be reduced to

$$u(1-\mu^2) = -\frac{g}{2\omega a}\left\{i\sqrt{(1-\mu^2)}\frac{\partial\zeta'}{\partial\mu} - \frac{\mu}{\sqrt{(1-\mu^2)}}\frac{\partial\zeta'}{\partial\phi}\right\}, \tag{2a}$$

$$v(1-\mu^2) = \frac{g}{2\omega a}\left\{\mu\sqrt{(1-\mu^2)}\frac{\partial\zeta'}{\partial\mu} + \frac{i}{\sqrt{(1-\mu^2)}}\frac{\partial\zeta'}{\partial\phi}\right\}, \tag{2b}$$

$$\zeta\frac{2\omega i a}{h_0} = \frac{\partial}{\partial\mu}\{u(1-\mu^2)^{\frac{3}{2}}\} - \sqrt{(1-\mu^2)}\frac{\partial v}{\partial\phi}. \tag{2c}$$

Finally, on writing $\beta = \dfrac{4\omega^2 a^2}{g h_0}$, and eliminating u and v, we find

$$L(\zeta') \equiv \frac{\partial}{\partial\mu}(1-\mu^2)\frac{\partial\zeta'}{\partial\mu} + \frac{1}{1-\mu^2}\frac{\partial^2\zeta'}{\partial\phi^2} + i\frac{\partial\zeta'}{\partial\phi} + \beta\zeta' = -\beta\bar{\zeta}. \tag{3}$$

These equations will be applied to determine the tide in an ocean of the assumed law of depth, and bounded by vertical cliffs extending from pole to pole along the two meridians $\phi = 0, \alpha$. We shall assume throughout that $\alpha \leqslant \pi$.

The problem may now be stated as follows: Consider a domain D on the surface of the sphere bounded by $\phi = 0, \alpha$. We then require a solution of (3) finite and continuous in D and satisfying the further conditions

(i) u, v are finite and continuous in D;
(ii) $v(\mu, 0) = v(\mu, \alpha) = 0$, for $-1 \leqslant \mu \leqslant 1$;
(iii) $hu \to 0$ as $\mu \to \pm 1$.

Also since equation (3) has singularities at $\mu = \pm 1$, the statement includes the requirement that ζ' must be finite at the poles.

We write the equation (3) in the form

$$L\{w(\mu, \phi)\} + f(\mu, \phi) = 0, \tag{4}$$

$f(\mu, \phi)$ being a given function.

The condition (ii) above is

$$\mu\sqrt{(1-\mu^2)}\frac{\partial w}{\partial \mu} + \frac{i}{\sqrt{(1-\mu^2)}}\frac{\partial w}{\partial \phi} = 0, \text{ when } \phi = 0, \alpha \text{ for all } \mu. \tag{5}$$

The method of solution to be used is that of Galerkin.

A double sequence of orthogonal functions $\{T^s_n(\mu, \phi)\}$ is chosen, each finite and continuous in D, and satisfying condition (5).

Assuming
$$w = \sum_{s, n} x^s_n T^s_n(\mu, \phi) \tag{6}$$

the x^s_n being undetermined constants, the integral

$$\iint_D [L(w) + f]\bar{T}^s_n \, dS = 0$$

gives a sequence of linear algebraic equations for the determination of the constants x^s_n.

As shown by Keldych (1942), the solution (6) obtained in this way converges in the mean to the solution of (4) with the appropriate conditions. Further, from the orthogonal property of the functions T^s_n, the resulting linear equations for x^s_n reduce to equations with one unknown in each.

3. The system of orthogonal functions

We require a system of orthogonal functions, each of which is finite and continuous in D (in particular at the singularities $\mu = \pm 1$) and each of which satisfies the boundary condition (5).

Consider the function

where
$$\left.\begin{aligned} T^{s\lambda}_n &= M^{s\lambda}_n(\mu)\,\mathrm{e}^{is\lambda\phi} + N^{s\lambda}_n(\mu)\,\mathrm{e}^{-is\lambda\phi}, \\ M^{s\lambda}_n &= \frac{1}{2s\lambda}\left\{s\lambda P^{s\lambda}_n(\mu) + \mu(1-\mu^2)\frac{dP^{s\lambda}_n(\mu)}{d\mu}\right\}, \\ N^{s\lambda}_n &= \frac{1}{2s\lambda}\left\{s\lambda P^{s\lambda}_n(\mu) - \mu(1-\mu^2)\frac{dP^{s\lambda}_n(\mu)}{d\mu}\right\}, \end{aligned}\right\} \tag{7}$$

$\lambda = \pi/\alpha$, $s\lambda$ and n are integers, and $P_n^{s\lambda}(\mu)$ is the associated Legendre function of μ.

On substituting $T_n^{s\lambda}$ for ζ' in (5), the condition is satisfied for all integers $s\lambda$, $n\,(\geqslant s\lambda)$, in the range $-1 \leqslant \mu \leqslant 1$.

In detail

$$M_n^{s\lambda} = \frac{1}{2s\lambda}\{\alpha_{n-2}^{s\lambda} P_{n-2}^{s\lambda} + (\beta_n^{s\lambda} + s\lambda) P_n^{s\lambda} - \gamma_{n+2}^{s\lambda} P_{n+2}^{s\lambda}\},$$

$$N_n^{s\lambda} = -\frac{1}{2s\lambda}\{\alpha_{n-2}^{s\lambda} P_{n-2}^{s\lambda} + (\beta_n^{s\lambda} - s\lambda) P_n^{s\lambda} - \gamma_{n+2}^{s\lambda} P_{n+2}^{s\lambda}\},$$

where
$$\alpha_{n-2}^{s\lambda} = \frac{(n+1)(n+s\lambda)(n+s\lambda-1)}{(2n-1)(2n+1)},$$

$$\beta_n^{s\lambda} = \frac{n(n+1) - 3s^2\lambda^2}{(2n-1)(2n+3)},$$

$$\gamma_{n+2}^{s\lambda} = \frac{n(n-s\lambda+1)(n-s\lambda+2)}{(2n+1)(2n+3)} \quad (n \geqslant s\lambda + 2),$$

and
$$M_{s\lambda}^{s\lambda} = \frac{1}{2s\lambda}\{(\beta_{s\lambda}^{s\lambda} + s\lambda) P_{s\lambda}^{s\lambda} - \gamma_{s\lambda+2}^{s\lambda} P_{s\lambda+2}^{s\lambda}\},$$

$$N_{s\lambda}^{s\lambda} = -\frac{1}{2s\lambda}\{(\beta_{s\lambda}^{s\lambda} - s\lambda) P_{s\lambda}^{s\lambda} - \gamma_{s\lambda+2}^{s\lambda} P_{s\lambda+2}^{s\lambda}\}.$$

Consider now a double sequence of these functions in the form $\{T_{s\lambda+6r}^{s\lambda}\}$, where r is an integer, including zero. These functions form an orthogonal set in the Hermitian sense, since if $\overline{T}_{s\lambda+6r}^{s\lambda}$ is the complex conjugate of $T_{s\lambda+6r}^{s\lambda}$,

$$\iint_D T_{s\lambda+6r}^{s\lambda} \overline{T}_{s'\lambda+6r'}^{s'\lambda}\, dS$$
$$= \int_{-1}^{1} d\mu \int_0^{\alpha} d\phi [M_{s\lambda+6r}^{s\lambda} e^{is\lambda\phi} + N_{s\lambda+6r}^{s\lambda} e^{-is\lambda\phi}] \times [M_{s'\lambda+6r'}^{s'\lambda} e^{-is'\lambda\phi} + N_{s'\lambda+6r'}^{s'\lambda} e^{is'\lambda\phi}],$$

which is seen, after ϕ-integration, to vanish if $s \neq s'$ and s, s' are both odd or both even. Also

$$\iint_D T_{s\lambda+6r}^{s\lambda} \overline{T}_{s\lambda+6r'}^{s\lambda}\, dS = \alpha \int_{-1}^{1} d\mu [M_{s\lambda+6r}^{s\lambda} M_{s\lambda+6r'}^{s\lambda} + N_{s\lambda+6r}^{s\lambda} N_{s\lambda+6r'}^{s\lambda}] = 0, \quad \text{if } r \neq r'$$
$$= \alpha \int_{-1}^{1} [(M_{s\lambda+6r}^{s\lambda})^2 + (N_{s\lambda+6r}^{s\lambda})^2]\, d\mu, \quad \text{when } r = r'.$$

There are then two independent orthogonal sequences, one corresponding to s odd, and the other to s even. It is clear that the even set includes a term independent of μ and ϕ.

On dividing each function by $R_{s\lambda+6r}^{s\lambda}$, where

$$(R_{s\lambda+6r}^{s\lambda})^2 = \alpha \int_{-1}^{1} [(M_{s\lambda+6r}^{s\lambda})^2 + (N_{s\lambda+6r}^{s\lambda})^2]\, d\mu,$$

the sequence becomes orthonormal.

For the value of this factor we have

$$
\begin{aligned}
(R_n^{s\lambda})^2 &= \frac{\alpha}{2s^2\lambda^2}\int_{-1}^{1}\Big[[(\alpha_{n-2}^{s\lambda}P_{n-2}^{s\lambda})^2 + \{(\beta_n^{s\lambda})^2 + s^2\lambda^2\}(P_n^{s\lambda})^2 + (\gamma_{n+2}^{s\lambda}P_{n+2}^{s\lambda})^2]\,d\mu \\
&= \frac{\pi}{s^2\lambda^3}\Big[(\alpha_{n-2}^{s\lambda})^2\frac{(n+s\lambda-2)!}{(n-s\lambda-2)!}\frac{1}{2n-3} + \{(\beta_n^{s\lambda})^2 + s^2\lambda^2\}\frac{(n+s\lambda)!}{(n-s\lambda)!}\frac{1}{2n+1} \\
&\qquad + (\gamma_n^{s\lambda})^2\frac{(n+s\lambda+2)!}{(n-s\lambda+2)!}\frac{1}{2n+5}\Big]. \qquad (8)
\end{aligned}
$$

Since the members of the set of functions $\{T_{s\lambda+6r}^{s\lambda}(\mu,\phi)\}$ are linear combinations of the members of the complete sequence $\{P_{s\lambda+2n}^{s\lambda}\,e^{\pm is\pi\phi/\alpha}\}$, n integral, this former sequence is also complete as a set of functions satisfying the condition (5). This result follows independently for s odd and s even.

The functions $\{T_{s\lambda+6r}^{s\lambda}(\mu,\phi)\}$ are also all even functions of μ. This is the only type required for the problem before us.

We also require the value of $(V_n^{s\lambda})^2$, or

$$
-\int_{-1}^{1} d\mu \int_0^{\alpha} d\phi\, T_n^{s\lambda}\,\Delta\overline{T}_n^{s\lambda},
$$

where
$$
\Delta \equiv \frac{\partial}{\partial\mu}(1-\mu^2)\frac{\partial}{\partial\mu} + \frac{1}{1-\mu^2}\frac{\partial^2}{\partial\phi^2}.
$$

Now
$$
\begin{aligned}
\Delta\overline{T}_n^{\lambda s} = &-\frac{1}{2s\lambda}\{(n-2)(n-1)\alpha_{n-2}^{s\lambda}P_{n-2}^{s\lambda} + n(n+1)(\beta_n^{s\lambda}+s\lambda)P_n^{s\lambda} \\
&-(n+2)(n+3)\gamma_{n+2}^{s\lambda}P_{n+2}^{s\lambda}\}\,e^{-is\lambda\phi} \\
&+\frac{1}{2s\lambda}\{(n-2)(n-1)\alpha_{n-2}^{s\lambda}P_{n-2}^{s\lambda} + n(n-1)(\beta_n^{s\lambda}-s\lambda)P_n^{s\lambda} \\
&-(n+2)(n+3)\gamma_{n+2}^{s\lambda}P_{n+2}^{s\lambda}\}\,e^{is\lambda\phi}.
\end{aligned}
$$

Hence the integral is

$$
\begin{aligned}
\frac{\pi}{s^2\lambda^3}\Big[&(\alpha_{n-2}^{s\lambda})^2\frac{(n-2)(n-1)}{2n-3}\frac{(n+s\lambda-2)!}{(n-s\lambda-2)!} + \{(\beta_n^{s\lambda})^2+s^2\lambda^2\}\frac{n(n+1)}{2n+1}\frac{(n+s\lambda)!}{(n-s\lambda)!} \\
&+ (\gamma_{n+2}^{s\lambda})^2\frac{(n+2)(n+3)}{2n+5}\frac{(n+s\lambda+2)!}{(n-s\lambda+2)!}\Big].
\end{aligned}
$$

It appears at once that

$$
\left.
\begin{aligned}
&(V_n^{s\lambda})^2 > (n-1)(n-2)(R_n^{s\lambda})^2, \quad (n \geqslant 2) \\
\text{and}\quad &(V_n^{s\lambda})^2 < (n+2)(n+3)(R_n^{s\lambda})^2.
\end{aligned}
\right\} \qquad (9)
$$

Also
$$
\begin{aligned}
\int_{-1}^{1} d\mu \int_0^{\alpha} \frac{\partial T_n^{s\lambda}}{\partial\phi}\,\overline{T}_n^{s\lambda}\,d\phi &= is\lambda\alpha\int_{-1}^{1}\{(M_n^{s\lambda})^2 - (N_n^{s\lambda})^2\}\,d\mu \\
&= \frac{2i\pi\beta_n^{s\lambda}}{\lambda(2n+1)}\frac{(n+s\lambda)!}{(n-s\lambda)!} \\
&= iA_n^{s\lambda},
\end{aligned}
$$

where
$$
A_n^{s\lambda} = \frac{2\pi\beta_n^{s\lambda}(n+s\lambda)!}{\lambda(2n+1)(n-s\lambda)!}.
$$

4. EXPANSIONS IN TERMS OF THE ORTHOGONAL FUNCTIONS

It has been shown that the functions $\{T_n^m(\mu,\phi)\}$ (where for convenience m is written for $s\lambda$ and n for $s\lambda+6r$) form two complete orthogonal sets, each term of which satisfies the boundary condition (5), and in which s is odd for one set, and s is even for the other.

Consider the complete sequence of vectors $\{\operatorname{grad} T_n^m(\mu,\phi)\}$, in which s is the sequence of odd integers.

From the properties of $T_n^m(\eta,\phi)$ it follows that

$$\iint_D \operatorname{grad} T_n^m \cdot \operatorname{grad} \bar{T}_{n'}^{m'}\, dS = -\int_{-1}^{1} d\mu \int_0^{\alpha} d\phi\, T_n^m \Delta \bar{T}_{n'}^{m'} = 0, \quad \text{if} \quad m \neq m',\ n \neq n',$$

where, as before, $$\Delta \equiv \frac{\partial}{\partial\mu}(1-\mu^2)\frac{\partial}{\partial\mu} + \frac{1}{1-\mu^2}\frac{\partial^2}{\partial\phi^2}.$$

Hence the sequence $\{\operatorname{grad} T_n^m(\mu,\ \phi)\}$ is orthogonal.

Let $F_1(\mu,\ \phi)$ be an arbitrary function, finite, continuous and differentiable in D, with the further properties:

$$\left.\begin{aligned} &\text{(i)}\ \ F_1(\mu,0) = -F_1(\mu,\alpha),\\ &\text{(ii)}\ \ \frac{\partial}{\partial\phi}F_1(\mu,0) = -\frac{\partial}{\partial\phi}F_1(\mu,\alpha),\\ \text{and}\qquad &\text{(iii)}\ \ \iint_D |\operatorname{grad} F_1|^2\, dS < \infty. \end{aligned}\right\} \tag{10}$$

Now determine a double sequence of numbers x_n^m, such that

$$x_n^m = \frac{1}{V_n^m}\iint_D \operatorname{grad} F_1 \cdot \operatorname{grad} \bar{T}_n^m\, dS, \tag{11}$$

where $$(V_n^m)^2 = \iint_D \operatorname{grad} T_n^m \cdot \operatorname{grad} \bar{T}_n^m\, dS. \tag{12}$$

It follows that $$\sum_{m,n} x_n^m \operatorname{grad} T_n^m / V_n^m$$

converges in the mean to grad F_1, with

$$\sum_{m,n} |x_n^m|^2 < \infty. \tag{13}$$

That is $$\operatorname{grad} F_1 \sim \sum_{m,n} x_n^m \operatorname{grad} T_n^m / V_n^m. \tag{14}$$

From (14) it follows that $$\frac{\partial F_1}{\partial\phi} \sim \sum_{m,n} \frac{x_n^m}{V_n^m}\frac{\partial T_n^m}{\partial\phi}. \tag{15}$$

Examination shows that the sequence $\left\{\frac{\partial}{\partial\phi}T_n^m(\mu,\phi)\right\}$ is also orthogonal in D, and therefore

$$\frac{x_n^m}{V_n^m}\iint_D \frac{\partial T_n^m}{\partial\phi}\frac{\partial \bar{T}_n^m}{\partial\phi}\, dS = \iint_D \frac{\partial F_1}{\partial\phi}\frac{\partial \bar{T}_n^m}{\partial\phi}\, dS.$$

By partial integration and use of the properties of the functions, this equality reduces to

$$\frac{(R_n^m)^2 x_n^m}{(V_n^m)^2} = \iint\limits_D F_1 \frac{\bar{T}_n^m}{V_n^m}\, dS,$$

with
$$(R_n^m)^2 = \iint\limits_D T_n^m \bar{T}_n^m\, dS,$$

as before.

Since $\dfrac{R_n^m}{V_n^m} < 1$, it follows from (13) that

$$\sum_{m,n} | R_n^m x_n^m / V_n^m |^2 < \infty.$$

Hence the series $\sum\limits_{m,n} x_n^m T_n^m / V_n^m$ converges in the mean to the function $F_1(\mu, \phi)$; or

$$F_1(\mu,\phi) \sim \sum_{m,n} x_n^m T_n^m / V_n^m. \tag{16}$$

By partial integration of (11) we also find

$$\begin{aligned} V_n^m x_n^m &= \iint\limits_D \operatorname{grad} F_1 . \operatorname{grad} \bar{T}_n^m\, dS \\ &= -\iint \Delta F_1 . \bar{T}_n^m\, dS \end{aligned} \tag{17}$$

It is thus shown that if the function $F_1(\mu,\phi)$ is such that grad F_1 can be expanded in the series (14) with a converging sum of squares of moduli of coefficients, then F_1 can be expanded as in (16) and $\partial F_1/\partial\phi$ as in (15), the convergence being in the mean in each case.

Conversely, if the series in (13) is convergent, then there exists a function $F_1(\mu,\phi)$, such that the series $\sum\limits_{m,n} x_n^m \operatorname{grad} T_n^m/V_n^m$ converges in the mean to grad F_1; the series $\sum\limits_{m,n} \dfrac{x_n^m}{V_n^m} \dfrac{\partial T_n^m}{\partial \phi}$ converges in the mean to $\partial F_1/\partial\phi$; and the series $\sum\limits_{m,n} x_n^m T_n^m/V_n^m$ converges in the mean to F_1.

Next let $F_2(\mu,\phi)$ be a similar function with the properties

$$\text{(i)} \quad F_2(\mu, 0) = F_2(\mu, \alpha),$$

$$\text{(ii)} \quad \frac{\partial}{\partial\phi} F_2(\mu, 0) = \frac{\partial}{\partial\phi} F_2(\mu, \alpha),$$

and
$$\text{(iii)} \quad \iint | \operatorname{grad} F_2 |^2 dS < \infty.$$

In the same way as before it can be shown that similar results to those obtained for F_1 are obtained for F_2 provided the series for F_2, i.e. $\Sigma x_n^m T_n^m / V_n^m$, is associated with *even* values of s.

Next consider the function $f(\mu,\phi)$ of equation (4). We shall assume for the moment that $f(\mu,0) = -f(\mu,\alpha)$. It can then be expanded in a series of the functions T_n^m/V_n^m, where $m = s\lambda$ and s is odd; i.e.

$$f(\mu,\phi) \sim \Sigma y_n^m T_n^m/V_n^m,$$

with
$$y_n^m = \frac{V_n^m}{(R_n^m)^2}\iint_D f(\mu,\phi)\,\bar{T}_n^m\,dS, \tag{18}$$

and
$$\sum_{m,n}\left|\frac{R_n^m y_n^m}{V_n^m}\right|^2 < \infty.$$

Refer now to equation (4) which may be written

$$\Delta(w) + i\frac{\partial w}{\partial\phi} + \beta w + f(\mu,\phi) = 0. \tag{19}$$

Assuming formally that $\quad \operatorname{grad} w \sim \Sigma x_n^m \operatorname{grad} T_n^m/V_n^m$

and that the series is odd in s, we may apply the results (15), (16) and (17). On multiplying (19) by $\bar{T}_n^m$ and integrating over D, we find

$$\{-(V_n^m)^2 - A_n^m + \beta(R_n^m)^2\}\,x_n^m + (R_n^m)^2\,y_n^m = 0, \tag{20}$$

and therefore
$$|x_n^m| = \frac{|y_n^m|}{|(V_n^m/R_n^m)^2 + A_n^m/(R_n^m)^2 - \beta|},$$

provided this denominator does not vanish for any pair m, n.

Since $(V_n^m/R_n^m)^2$ lies between $(n-1)(n-2)$ and $(n+2)(n+3)$, it follows that for all values of n greater than a certain value n_0,

$$|x_n^m| < |y_n^m| \quad\text{and}\quad \left|\frac{x_n^m R_n^m}{V_n^m}\right|^2 < \left|\frac{y_n^m R_n^m}{V_n^m}\right|^2 < \infty.$$

Hence the series $\sum_{m,n} x_n^m T_n^m/V_n^m$ converges in the mean to a function w which satisfies equation (19) and the boundary conditions (5). The expansions (14) and (15) also follow.

If now $f(\mu,\phi)$ be assumed to be an even function in ϕ, the same process can be repeated and a series solution of (4) determined with s even.

5. APPLICATION TO THE TIDE-COMPONENT K_2

The form of the tide-producing potential appropriate to the basin D will be taken as $g\bar{\zeta} = gH(1-\mu^2)\,e^{i(2\phi-\alpha)}$. This may be separated into two parts $\bar{\zeta}_1, \bar{\zeta}_2$ which are symmetric and asymmetric, respectively, about the central meridian $\phi = \frac{1}{2}\alpha$. These are

$$\bar{\zeta}_1 = H(1-\mu^2)\cos(2\phi-\alpha), \quad \bar{\zeta}_2 = H(1-\mu^2)\sin(2\phi-\alpha),$$

with
$$\bar{\zeta} = \bar{\zeta}_1 + i\bar{\zeta}_2.$$

Correspondingly equation (3) may be separated into the two equations

$$\Delta(\zeta_1')+i\frac{\partial\zeta_1'}{\partial\phi}+\beta\zeta_1' = -\beta\bar{\zeta}_1, \quad \Delta(\zeta_2')+i\frac{\partial\zeta_2'}{\partial\phi}+\beta\zeta_2' = -\beta\bar{\zeta}_2, \tag{21}$$

with

$$\zeta' = \zeta_1+i\zeta_2.$$

It is clear that $\bar{\zeta}_1$ may be expanded over D in a series of functions with s even, and $\bar{\zeta}_2$ in those with s odd.

Let

$$(1-\mu^2)\cos(2\phi-\alpha) = D+\sum_{s,\,r}^{s\text{ even}} {}_1D^{s\lambda}_{s\lambda+6r}T^{s\lambda}_{s\lambda+6r};$$

then

$$\begin{aligned}(R^{s\lambda}_{s\lambda+6r})^2\,{}_1D^{s\lambda}_{s\lambda+6r} &= \int_{-1}^{1}d\mu\int_{1}^{\alpha}(1-\mu^2)\cos(2\phi-\alpha)\,\bar{T}^{s\lambda}_{s\lambda+6r}\,d\phi\\ &= -2^{s\lambda-1}s\lambda\sin\alpha\,\frac{\Gamma(s\lambda+3r+\frac{1}{2})\,\Gamma(\frac{1}{2}s\lambda+3r-1)}{\Gamma(3r+1)\,\Gamma(\frac{1}{2}s\lambda+3r+\frac{5}{2})},\end{aligned}$$

and

$$D = \frac{2}{3}\frac{\sin\alpha}{\alpha}. \tag{22}$$

Also, let

$$(1-\mu^2)\sin(2\phi-\alpha) = \sum_{s,\,r}^{s\text{ odd}} {}_2D^{s\lambda}_{s\lambda+6r}T^{s\lambda}_{s\lambda+6r},$$

then

$$(R^{s\lambda}_{s\lambda+6r})^2\,{}_2D^{s\lambda}_{s\lambda+6r} = -2^{s\lambda-1}s\lambda\cos\alpha\,\frac{\Gamma(s\lambda+3r+\frac{1}{2})\,\Gamma(\frac{1}{2}s\lambda+3r-1)}{\Gamma(3r+1)\,\Gamma(\frac{1}{2}s\lambda+3r+\frac{5}{2})}. \tag{22$'$}$$

Now let

$$\zeta_1' = \sum_{s,\,r}^{s\text{ even}} {}_1C^{s\lambda}_{s\lambda+6r}T^{s\lambda}_{s\lambda+6r}, \quad \zeta_2' = \sum_{s,\,r}^{s\text{ odd}} {}_2C^{s\lambda}_{s\lambda+6r}T^{s\lambda}_{s\lambda+6r},$$

On substituting these respectively in the first and second equations (21), multiplying by $\bar{T}^{s\lambda}_{s\lambda+6r}$ and integrating over D, we have, as in (20),

$$\{(V^{s\lambda}_{s\lambda+6r})^2+A^{s\lambda}_{s\lambda+6r}-\beta(R^{s\lambda}_{s\lambda+6r})^2\}\,{}_1C^{s\lambda}_{s\lambda+6r} = (R^{s\lambda}_{s\lambda+6r})^2\beta\,{}_1D^{s\lambda}_{s\lambda+6r}, \quad (s\text{ even}),$$

$$C = -\frac{2}{3}\frac{\sin\alpha}{\alpha},$$

and

$$\{(V^{s\lambda}_{s\lambda+6r})^2+A^{s\lambda}_{s\lambda+6r}-\beta(R^{s\lambda}_{s\lambda+6r})^2\}\,{}_2C^{s\lambda}_{s\lambda+6r} = (R^{s\lambda}_{s\lambda+6r})^2\beta\,{}_2D^{s\lambda}_{s\lambda+6r}, \quad (s\text{ odd}).$$

The values of ${}_1D^{s\lambda}_{s\lambda+6r}$ and ${}_2D^{s\lambda}_{s\lambda+6r}$ are known from (22) and (22′), and the corresponding values of ${}_1C^{s\lambda}_{s\lambda+6r}$, ${}_2C^{s\lambda}_{s\lambda+6r}$ are thus completely determined in explicit algebraic form.

If this value of β is such that the coefficient of x^m_n in (20) vanishes for some values of m, n, the validity of the solution breaks down. The values of β for which this occurs are obtained by solving the equation

$$\beta(R^{s\lambda}_{s\lambda+6r})^2 = (V^{s\lambda}_{s\lambda+6r})^2+A^{s\lambda}_{s\lambda+6r}$$

for appropriate values of s, r.

These values of β determine the depths of the ocean of this type at which resonance in the luni-solar tide occurs. A simple formula for the first depth at which resonance occurs is readily obtained.

Putting $s = 1$, $r = 0$, and reducing, the equation for β becomes

$$\beta\left(1+\frac{3}{(2\lambda+3)(2\lambda+5)}\right) = \lambda(\lambda+1)-\frac{\lambda^2-\lambda-8}{(2\lambda+3)(2\lambda+5)}.$$

For an ocean of 60° width, $\lambda = 3$ and $\beta = 11{\cdot}66$, giving a mean depth of 16,600 ft.

In a former paper (Goldsbrough 1928), by a longer process, the critical mean depth for this ocean was found to be 15,500 ft.

For an ocean of 90° width, $\lambda = 2$ and $\beta = 5{\cdot}82$, giving a mean depth of 33,300 ft.

On restoring the time factor $e^{i\sigma t}$ and taking the real part of the solution just found, we have the final result

$$\begin{aligned}\zeta = H\cos\sigma t\Big[& -\frac{2}{3}\frac{\sin\alpha}{\alpha} + \sum_{s,r}^{s\,\text{even}} {}_1C^{s\lambda}_{s\lambda+6r}(M^{s\lambda}_{s\lambda+6r} + N^{s\lambda}_{s\lambda+6r})\cos s\pi\phi/\alpha \\ & - \sum_{s,r}^{s\,\text{odd}} {}_2C^{s\lambda}_{s\lambda+6r}(M^{s\lambda}_{s\lambda+6r} - N^{s\lambda}_{s\lambda+6r})\sin s\pi\phi/\alpha + (1-\mu^2)\cos(2\phi-\alpha)\Big] \\ - H\sin\sigma t\Big[& \sum_{s,r}^{s\,\text{even}} {}_1C^{s\lambda}_{s\lambda+6r}(M^{s\lambda}_{s\lambda+6r} - N^{s\lambda}_{s\lambda+6r})\sin s\pi\phi/\alpha \\ & + \sum_{s,r}^{s\,\text{odd}} {}_2C^{s\lambda}_{s\lambda+6r}(M^{s\lambda}_{s\lambda+6r} + N^{s\lambda}_{s\lambda+6r})\cos s\pi\phi/\alpha + (1-\mu^2)\sin(2\phi-\alpha)\Big].\end{aligned}$$

This expression exhibits the forms of symmetry and asymmetry as required by Proudman's theorem (1928).

A referee has drawn attention to the rather surprising fact that if the imaginary part of ζ be made zero, the boundaries will become co-tidal lines in the resulting form of solution.

It will be noticed that the special functions T^n_m are such that when $\zeta_2 = 0$ and only the even system is used, the real part of v is zero everywhere, while the imaginary part of v and the real part of u vanish on the boundary for all μ. It follows at once from equation (2c) that the imaginary part of ζ vanishes on the boundary, and hence the boundary is a co-tidal line.

REFERENCES

Doodson, A. T. 1936 *Phil. Trans.* A, **235**, 296.
Doodson, A. T. 1938 *Phil. Trans.* A, **237**, 311.
Doodson, A. T. 1940 *Phil. Trans.* A. **238**, 477.
Goldsbrough, G. R. 1928 *Proc. Roy. Soc.* A, **117**, 692.
Keldych, M. 1942 *Bull. Acad. Sci. U.S.S.R.*, Sér. Math., **6**, 309.
Lamb, H. 1932 *Hydrodynamics*, p. 332. Cambridge University Press.
Proudman, J. 1916 *Proc. Lond. Math. Soc.* **18**, 1.
Proudman, J. 1928 *Mon. Not. R. Astr. Soc., Geophys. Suppl.*, **2**, 98.
Proudman, J. 1936 *Phil. Trans.* A, **235**, 273.

A comparison of the compressibilities of some gases with that of nitrogen at pressures below one atmosphere

By G. A. Bottomley, Doreen S. Massie* and R. Whytlaw-Gray, F.R.S.

Chemistry Department, University of Leeds

(*Received* 12 *July* 1949)

A differential method for comparing the compressibilities of gases at pressures below 1 atm. has been developed in which many of the errors inherent in methods employed previously have been to a large extent eliminated, especially those due to meniscus volume changes and capillary depression.

Using pure nitrogen as a standard the low-pressure isothermals of carbon monoxide, carbon dioxide, nitrous oxide, oxygen, ethylene and propane have been determined at a temperature of 22·05° C.

The deviations of the individual points from straight lines do not in most cases exceed 2 parts in 100,000. In no case, even with propane, was any curvature in the isotherms detectable.

The contention of Moles and other recent workers that the molecular weights of liquefiable gases can be determined to a high degree of accuracy by linear extrapolation is rendered highly probable by this fresh evidence.

In the determination of the molecular weights of gases by the limiting density method it is usually assumed that the PV/P isothermals from 1 atm. downwards are strictly linear, and that Berthelot's formula $PV = P_0V_0(1-AP)$ can be used to extrapolate to zero pressure from pressures (usually above 200 mm. of mercury) where PV can be measured with accuracy. For the permanent gases this assumption is almost certainly valid far beyond the limits of error which experiments at low pressure have so far been able to reach. Further, high-pressure measurements with this group of gases when extrapolated by expansion formulae of the type $PV = A+BP+CP^2$, etc., give practically straight lines between 0 and 1 atm., the effect of the CP^2 term on P_0V_0/P_1V_1 being of the order of 1 in 10^6 at the most (see Cragoe 1941).

For compressible gases, however, it is by no means certain that the CP^2 term can be neglected. Theory predicts for gases below their critical point a slight curvature towards the pressure axis, but its magnitude at any one temperature is difficult to assess with certainty. Because of this curvature doubt has often been cast on the accuracy of the molecular weights of these gases deduced from limiting densities. Many earlier workers obtained isothermals between 760 and 200 mm. curved in the expected direction, but more modern research supports the view that departure from the linear is so slight that extrapolation can lead only to quite insignificant errors. Thus Cawood & Patterson (1936) could detect no curvatures with sulphur dioxide and dimethyl oxide over a pressure range of several metres of mercury. Moles (1938), using the density method, claimed a strict linearity between 1 and ¼ atm. for the gases ammonia, carbon dioxide, sulphur dioxide and silicon tetrafluoride. More recently the same result has been found by Casado (1943) for dimethyl oxide and by Casado, Massie & Whytlaw-Gray (1949) for propane. Keesom (1938), however, on the basis of van der Waals' equation and the law of corresponding states, has calculated the magnitude of the CP^2 term for the gases investigated by Moles as well as for other gases, and finds that it is sufficiently large to affect molecular weights by amounts varying from 4·5 parts in 10^5 in the case of carbon dioxide to 17 parts in 10^5 for ammonia. It may, however, be questioned whether any equation of state based on high-pressure data can be applied with any confidence to determine the magnitude of the deviations from linearity at low pressures. As Keesom himself points out the question of the form of the low-pressure isothermals can only be settled by fresh measurements of high accuracy, and it is with this object in view that the present investigation was undertaken.

---

* Seconded from I.C.I. Ltd., Butterwick Research Laboratories, The Frythe, Welwyn, Herts.

EXPERIMENTAL

A compressibility apparatus has been developed by means of which the compressibilities of gases can be compared directly with that of nitrogen taken as a standard.

In principle the method is identical with that used a number of years ago by Addingley & Whytlaw-Gray (1928), but the details have been considerably modified so as to obviate errors in the earlier apparatus. In the new apparatus the standard gas and the comparison gas (i.e. the gas of which the compressibility is to be measured) are contained in two spherical Pyrex glass volumeters of 600 ml. capacity, each of which is connected with its own dead space. The two dead spaces surrounding steel points are connected through mercury with each other and form the two chambers of a point manometer.

By withdrawing equal weights of mercury from the two volumeters and knowing by previous calibration the volumes of the two dead spaces and their respective connecting tubes, nearly equal and accurately known volumes of the two gases can be confined on either side of the manometer. The pressure in the two volumeters and dead spaces is then adjusted to exact equality by weighing out mercury, in small amounts, until the two points set simultaneously to the mercury surfaces. At this stage, assuming that the dead space and connecting tube volumes are known with sufficient accuracy, and that the points are strictly in the same horizontal plane, the apparatus contains known volumes of each of the gases at the same pressure. This is the starting point of a compressibility determination. Successive withdrawals of mercury from the volumeter bulbs are then made, and at each step the pressure of the gases is brought to equality. In this way a series of volume ratios is obtained at lower and lower pressures, at each of which the pressure exerted by the two gases is equalized.

Thus if P_1V_1 and P_1V_2 are the initial PV's which on expansion become P_2V_3 and P_2V_4, P_3V_5 and P_3V_6, etc., the ratios of the volumes, i.e. V_1/V_2, V_3/V_4, V_5/V_6 are the ratios of the PV's of the two gases at the pressures P_1, P_2, P_3.

Hence from a series of ratios the compressibility of the comparison gas can be computed in terms of the standard gas.

Since an accuracy of a few parts in 100,000 was aimed at, special attention had to be paid to the dead-space volumes, and some method had to be devised whereby, on the one hand, any alteration in volume of the mercury menisci in the various point settings could be measured and on the other, capillarity errors in the manometer reduced to a minimum. In the paper on the earlier apparatus of this type (Addingley & Whytlaw-Gray 1928), it was hoped to get over this difficulty by using dead spaces of wide-bore tubing (19·6 mm. diameter) which had been calibrated beforehand in terms of meniscus height. Actually the experimental correlation of dead-space volume with meniscus height proved surprisingly difficult, and it became evident that the variation of meniscus volume in the point settings constituted a serious error which was not easily corrected. Further, unless the two menisci in the manometer could always be set to the same height to within 0·1 mm., which in practice proved very difficult, small capillarity errors could not be avoided.

New apparatus

The new apparatus was designed to get over these uncertainties. The dead spaces were constructed of 30 mm. internal diameter tubing so as to reduce capillary depression to negligible proportions, and the actual volumes of the dead spaces were determined experimentally to within 1 mm.^{3} after each point setting. This was easily and conveniently done by means of two calibrated pipettes of nearly the same volume as the two dead spaces measured from the points to marks on the capillaries above. After each setting, the two limbs of the manometer were shut off from each other by closing the connecting tap, and by opening and closing appropriate stopcocks mercury was run into each dead space from its respective pipette. Variations in dead-space volume were read off on the previously calibrated capillary stems of the dead spaces. Since by this device meniscus volume changes were determined each time a point setting was made, it was not necessary to limit the diameter of the dead spaces, and tubing wide enough to eliminate capillary errors could be used without the disadvantage of increasing the dead-space uncertainty. Thus errors due to both meniscus volume variation and capillary depression could be reduced to insignificance (see Whytlaw-Gray & Teich 1948).

The manometer points and their position relatively to each other require special mention. At first, before the apparatus had been perfected, sealed-in glass points were used, but these had the disadvantage of being easily electrified on contact with mercury, and there was the possibility of a slight relative shift of the points on changing the pressure within the apparatus. Accordingly the glass points were replaced by carefully ground and sharpened steel points bent in the form of inverted hooks and screwed into a steel block. The glasswork of the dead spaces fitted into grooves cut in the block symmetrically around the points as centres and was made vacuum-tight with black Apiezon wax. The steel points were fixed originally to be as nearly as possible in the same horizontal plane as the upper face of the steel block. The latter rested on two rigid angle-iron supports fixed to the inside of the tank which served as a thermostat. The upper surface of the block carried a delicate spirit level, one division of which corresponded to 6 sec. of arc. The whole thermostat tank rested on two heavy steel screws and could be given a slight tilt so that any alteration in the reading of the spirit level during the course of an experiment could be corrected. This adjustment too allowed the points to be set initially at the same level to within 0·002 mm. at least.

This setting of the points to the same level was carried out before commencing an experiment by putting the dead spaces in connexion with the outside atmosphere, and then tilting the tank until the points touched the mercury surfaces simultaneously when the menisci were made to rise slowly by means of the fine adjustment. The mercury surfaces were illuminated by light reflected from an opal lamp placed outside and above the tank, and the points and their mirror images were observed visually with the help of a low-power magnifying glass.

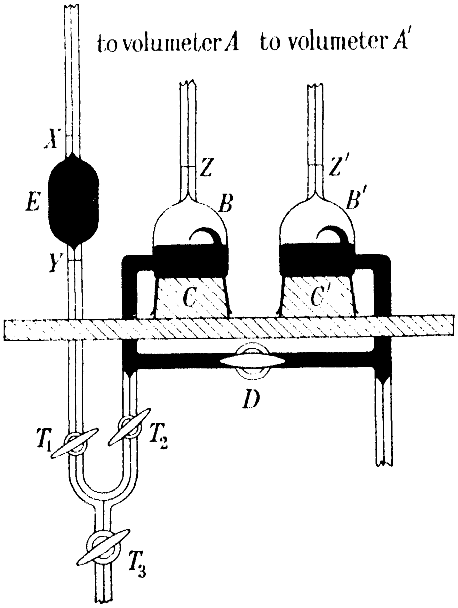

FIGURE 1

The above arrangement of the points and dead spaces worked well at first but suffered from the defect that with continued use the mercury became contaminated by its contact with the Apiezon wax and accurate settings became increasingly difficult.

The apparatus had to be partially dismantled and a new design adopted for the dead spaces. In this the inverted glass cups were fitted on to tapered and ground solid steel pillars forming gas-tight joints with the minimum of grease or wax. The pillars were screwed on to a solid steel plate. The whole arrangement is shown in figure 1, in which *B* and *B′* are the two dead spaces which fit on to solid ground steel pillars *C* and *C′* carrying the points.

The dead spaces communicate with each other through mercury and stopcock *D*, the closed barrel of which projects a small distance through the wall of the tank and is made water-tight with cement. Thus the whole manometer is inside the thermostat, and the two chambers can be isolated from each other by turning the tap *D* from the outside.

The spirit level, which is not shown in the diagram, rests on the steel plate immediately in front of the two dead spaces. A change in level of 1 division corresponded with a vertical displacement of the points relative to each other of 0·0015 mm. In figure 1 only one pipette is drawn, viz. that labelled *E* for the dead space *B*; the one for dead space *B'* is precisely similar. *E* was filled with mercury through stopcocks T_1 and T_3 before commencing a determination, using a mercury reservoir connected by pressure tubing through an air trap with the glass connexions below stopcock T_3. This mercury reservoir served also for setting the points after stopcock T_1 had been closed and T_2 and T_3 opened. For the fine adjustment of the menisci to the points a glass plunger moved by a rackwork served to raise the level of the mercury in the reservoir by small amounts and proved very effective. After the point settings had been made and no alteration after standing could be detected, stopcocks T_3 and *D*

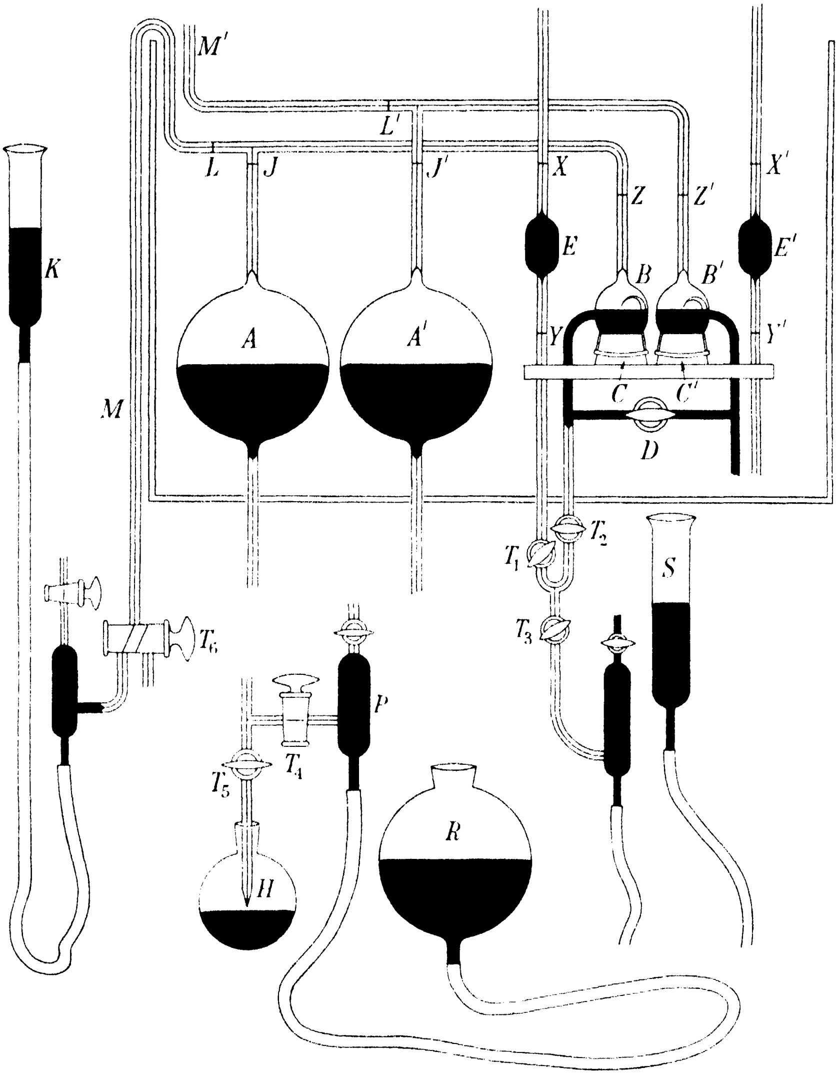

FIGURE 2

were gently closed and T_1 opened, thus allowing the mercury in the pipette E between the marks X and Y to flow into B. Usually this resulted in the mercury standing above mark Z in the dead-space capillary, for the pipette volume was adjusted to be a little greater than the average dead-space volume. When this was so it was only necessary to measure its position above Z and subtract this volume from that of the pipette. When, as sometimes happened, the dead-space volume was greater than the pipette volume, an extra quantity of mercury could be run in from the calibrated capillary until mark Z was reached; the position of the mercury below mark Y was a measure of the excess volume. The general arrangement of the apparatus is shown diagrammatically in figure 2, in which A and A' are the volumeters, B and B' the dead spaces, E and E' the pipettes, all rigidly supported inside a 35 gal. tank. The latter was carried by a strong angle-iron framework resting on a concrete floor in a thermostatically controlled room in the basement of the chemistry building.

To avoid undue complexity in the diagram the connexions outside the tank are shown for one volumeter and dead space only, viz. A, B and E; and since the apparatus was symmetrical the description of these applies equally to A', B' and E'.

A could be emptied and filled with mercury by means of reservoir R attached through the air trap P by thick-walled unvulcanized rubber tubing to the glasswork. The weighing flask H, as well as the trap, were well over 760 mm. below the bottom of the tank, and the requisite flexibility necessary when the latter was tilted was provided by a length of thin-walled glass tubing bent in zigzag form. Gas was introduced and removed from the volumeter A through the soda-glass stopcock T_6 connected by a Pyrex soda-glass seal with the Pyrex capillary tubing M outside the tank. This stopcock was sealed on to the gas train, the storage bulbs and manometer, and a high-vacuum oil pump which are not shown in the diagram. The whole of the compressibility apparatus proper with its stopcocks and connexions was of Pyrex glass. The Pyrex stopcocks were of the spring-loaded type which could be relied on to withstand an internal pressure up to 2 atm.

Before beginning an experiment the volumeters were emptied of mercury and the dead spaces and their connexions pumped down to as low a vacuum as possible, less than 0·001 mm. The apparatus was then connected through stopcocks T_6 and T_6' with a large tube filled with activated charcoal cooled in liquid air and allowed to stand overnight so as to remove traces of moisture and adsorbed gases from the glass surfaces. Mercury was then allowed to fill the volumeters to marks J and J' on the capillary stems and also the dead spaces. Gas was next admitted to the volumeters, the mercury displaced being caught in the weighing flasks H and H'. When nearly equal volumes of the two gases had been introduced the three-way taps T_6 and T_6' were reversed, and by raising the reservoirs K and K' the capillaries M and M' were filled with mercury exactly up to the marks L and L', thus confining the gases between mercury surfaces in strictly defined volumes.

Temperature control

The filling of the volumeters with mercury and the setting to the marks J and J' as well as the admission of the gases could only be carried out accurately after the temperature of the tank had been constant for a long period. At first even with a sensitive thyratron relay and vigorous stirring small fluctuations from day to day were detectable. To overcome this the temperature outside the tank in the thermostatically controlled room was set so as to be 3° lower than that of the tank itself. The room could be relied on not to vary more than 0·05° C. With this arrangement, once a steady state had been reached the tank temperature remained constant for weeks on end, and only occasionally was it possible to detect slight changes with a Beckmann thermometer. These variations rarely exceeded 0·02° C, and were probably due to fluctuations in barometric pressure affecting the volume of the toluene regulator. It was easy by a slight adjustment of the mercury contact in the regulator to restore the temperature to its original value before beginning a set of measurements.

When the stirrer was in operation no temperature difference in various parts of the tank could be detected on the Beckmann thermometer.

Calibration

The volumes of the various capillaries and connecting tubes inside the tank were determined *in situ* after the attainment of a constant temperature. To do this, capillaries and connecting tubes were filled with mercury up to the marks L and L' and J and J' by adjusting the levels of the various reservoirs.

The mercury was then run out to the marks Z and Z', giving the total volumes of the capillaries and connecting tubes. By the same procedure smaller amounts of mercury could be run out and the length of the mercury column measured and weighed so as to calibrate the various capillaries, and by a similar operation the pipette volumes were checked. In carrying out these calibrations it was found to be more convenient and accurate to run mercury out from the dead spaces rather than from the volumeters, and to do this suitable stopcocks and capillary jets, like that shown above H below volumeter A, were interposed between stopcocks T_1 and T_3 and T_1' and T_3'. These are not shown in the diagram. It was necessary during calibration to keep the pressure inside the apparatus equal to the external pressure. As was to be expected a noticeable shrinkage took place when the pressure inside the volumeters and their connexions was reduced. This was carefully measured for each side of the apparatus by noting the distance travelled by the mercury surface along one of the calibrated capillaries for a given reduction in pressure within the mercury-filled apparatus. The two sides were found to have nearly the same vacuum contraction per atmosphere, but, nevertheless, corrections were always applied when working at reduced pressures. No corrections were made for the possible change in volume of the volumeter bulbs on filling or emptying with mercury. This change would be smaller than the vacuum correction, and since it would affect both sides to very nearly the same extent it has been neglected.

As stated previously once the two sides of the apparatus had been filled with the two gases so as to occupy strictly defined and nearly equal volumes at precisely the same pressure, the measurement of the PV ratios at a series of decreasing pressures was reduced to the weighing of the mercury run out at each step. Since temperature within the tank was always constant there was no need to reduce the data to gas volumes, and the ratio of the total weights of mercury run out in order to set the manometer points gave directly the PV ratio at the particular pressure involved. In order to illustrate the manner in which the results are converted into volume ratios the details of the first two settings from a carbon dioxide, carbon monoxide experiment are given below. The data (in the two columns below) refer respectively to the two sides of the apparatus A and A'.

POINT 1

Volumeter bulbs filled with mercury and set to the marks J and J' at a pressure of 755·0 mm.

carbon dioxide in A	carbon monoxide in A'
weight of mercury run out to set the points	
1731·388 g.	1789·796 g.
position of mercury surfaces in calibrated capillaries of pipettes and dead spaces	
X set to mark	X' set to mark
Y set to mark	Y' 27·0 mm. above mark
Z 5 mm. below mark	Z' 10·8 mm. above mark

The distances between the marks and the mercury surfaces, combined with the calibrations of the capillaries, permit a determination of the small corrections to be applied to the volumes of the dead-space pipettes to obtain the true dead-space volumes. A little consideration of the way the pipettes are used will show whether a particular above or below indicates whether the dead-space volume is larger or smaller than the pipette.

dead-space volumes

	pipette B		pipette B'
	492·988 g.		507·025 g.
X	no corr.	X'	no corr.
Y	no corr.	Y'	−0·348 g.
Z	0·067 g.	Z'	−0·144 g.
dead space B	493·055 g.	dead space B'	506·533 g.

Alteration of volumes on change of internal pressure

The initial pressure of filling when the mercury in the capillaries M and M' had been brought to marks L and L' was 755·0 mm.; after the points had been set it rose to 769·9 mm., an increase of 14·9 mm. in internal pressure.

This results in the space occupied by the gas being larger than that corresponding to the quantity of mercury run out of the volumeters, and hence a slight vacuum correction must be added to the other volumes to obtain the true gas volume. The amount of the shrinkage of each volumeter and its corresponding dead space for a difference in pressure of 760 mm. had been found to be

A	A'
1·156 g. of mercury	1·308 g. of mercury

Hence for a pressure difference of 14·9 mm., since shrinkage is a linear function of pressure, the corrections are

0·022 g.	0·025 g.

The volumes of two connecting tubes and T spaces comprise the volumes between the marks L, J and Z. This space is larger than appears in the diagram, for it was found necessary to interpose between the volumeters and their respective dead spaces lengths of flexible fine-bore tubing in the form of horizontally placed zigzags in order to avoid strain on the dead spaces when the volumeters were filled with mercury. In the figure, to avoid complication, straight connexions only are shown. Summing up the various weights of mercury we have

mercury from volumeters	A = 1731·388	A' = 1789·796 g. mercury
mercury filling dead spaces	B = 493·055	B' = 506·533
connecting tubes and T space	14·317	7·489
vacuum correction	0·022	0·025
total	2238·782	2303·843 g. mercury

ratio, $R = \frac{V_{CO}(\text{in } A')}{V_{CO_2}(\text{in } A)} = \frac{2303\cdot843}{2238\cdot782} = 1\cdot029061$ at 769·9 mm. temp. 22·05° C.

POINT 2

dead-space volumes

pipette B	pipette B'
492·988	507·025
X = no corr.	X' = no corr.
Y = no corr.	Y' = 0·230
Z = 0·230	Z' = 0·104
dead space B 493·218	dead space B' 506·691

Summing up we have

mercury from volumeters (1)	1731·388	1789·796
(2)	889·585	910·953
dead spaces	493·218	506·691
connecting tubes + T space	14·317	7·489
totals	3128·508	3214·929 g. mercury

The initial pressure inside the apparatus when the menisci were set to the points and the mercury in the filling capillaries M and M' had been brought to the marks L and L' was determined from the barometric height, and the difference in levels of reservoir S and the dead spaces measured to 0·1 mm. with a cathetometer. The pressures at larger volumes were computed with sufficient accuracy from the mercury run out from the volumeter containing the standard gas (in this case CO), assuming Boyle's law and if necessary making a correction for compressibility. Thus for point 2 the approximate pressure was $769\cdot9 \times \frac{2303\cdot843}{3214\cdot576} = 550\cdot0$ mm. Hence for a pressure drop of $755 - 550 = 205$ mm. the vacuum corrections are

$$\frac{205}{760} \times 1\cdot156\text{ g. mercury} \qquad \frac{205}{760} \times 1\cdot308\text{ g. mercury}$$

$$= -0\cdot312\text{ g.} \qquad = -0\cdot353\text{ g.}$$

Final volumes 3128·196 g. and 3214·576 g.

$$\text{Ratio } R = \frac{3128\cdot196}{3214\cdot576} = 1\cdot027613 \text{ at } 550\cdot0\text{ mm.}$$

Hence for the two points the ratios are

point	R	pressure	temperature
1	1·029061	769·9	22·05° C
2	1·027613	550·0	

The weighing of the mercury was carried out on a special balance which with a load of 1 kg. was sensitive to a few milligrams and which was in the constant-temperature room. The brass weights were compared with each other and corrections to their face values applied, though as a rule these were very small. Corrections for change in buoyancy with varying barometric pressure were too small to be significant.

Errors

Volume

Usually the initial volume of gas in each volumeter and dead space varied from 100 to 150 ml., so that provided the dead-space volumes and the volumes of the connecting tubes can be determined to within 2 to 3 mm.^{3}, which with care is not difficult, the volume error at the highest pressure would not exceed 2 parts in 10^5.

At larger volumes and lower pressures the error should be correspondingly smaller.

Pressure

With care and with points carefully ground to similar shape it is possible to set a mercury meniscus to within 0·002 mm., which would give even at the low pressure of 100 mm. a maximum error of 4 parts in 10^5, so that with a sufficient number of points the slope of the PV/P graph should be fixed with the desired accuracy. If, however, the initial setting of the points to close horizontality is not made with great care a systematic error may affect the whole of a series of results, and this will be superimposed on the scatter of the points due to chance experimental errors of setting. For example, assume that initially the pressures in the two dead spaces are not exactly equal when both sides are open to the atmosphere but differ by x mm. Then the ratios obtained, i.e.

$$\frac{V_1}{V_2},\quad \frac{V_3}{V_4},\quad \frac{V_5}{V_6}$$

at pressures p_1, p_2, p_3, will all be in error by different amounts,

for V_1, V_3, V_5, become $V_1\left(1+\frac{x}{p_1}\right)$, $V_3\left(1+\frac{x}{p_2}\right)$, $V_5\left(1+\frac{x}{p_3}\right)$.

The correction factor $(1+x/p)$ increases hyperbolically as the pressure falls. If an error as large as 0·01 mm. in the initial setting of the points to horizontality is assumed the correction factor at different pressures becomes

pressure (mm.)	760	500	200	100	50
x/p	1·3	2	5	10	20×10^{-5}

so that the plot of the ratios $\frac{V_1}{V_2}$, $\frac{V_3}{V_4}$, $\frac{V_5}{V_6}$

against P will be tilted and give an erroneous slope and at very low pressures a curve. Because of the possibility of this error, and also to eliminate accidental calibration errors as well as other errors due to deformation of the apparatus when during the course of an experiment mercury is run out from the volumeters, the soundest plan is to interchange the gases in the two sides of the apparatus keeping the points in the same relative position as shown by the level. Provided there is no shift in the points and other conditions are unaltered, the mean value of the slope should give a close approximation to the true value. This procedure has, as the results show, been followed with several pairs of gases.

EXPERIMENTAL RESULTS

Determinations of the relative compressibilities of the following pairs of gases have been made:

(1) N_2 and CO, (2) CO and CO_2, (3) CO_2 and N_2O,
(4) N_2 and C_2H_4, (5) N_2 and O_2, (6) N_2 and C_3H_8.

Unfortunately in (2), (3) and (4) the gases were not interchanged, so these results are not so reliable as the others though they are valuable as evidence of the very slight deviations of the isotherms from linearity over the pressure region investigated at a temperature of 22·05° C.

All the gases used had been highly purified by low-temperature fractionation, and the N_2O, C_2H_4, C_3H_8, CO and N_2 had been used earlier for atomic weight determinations. Special care was taken to obtain N_2 and CO in the highest state of purity. The N_2 was made from the interaction of sodium azide in aqueous solution with a solution of iodine in potassium iodide, in presence of a suspension of barium thiosulphate as a catalyst. The gas evolved from this reaction is in a high state of purity and free from oxides of nitrogen and traces of hydrogen. It was, however, liquefied in a bath of liquid nitrogen through which hydrogen was passed to get a sufficiently low temperature and fractionated a number of times before collection in carefully evacuated storage bulbs. Details of the preparations as well as that of the CO are published elsewhere.

The nitrogen and carbon monoxide were the first pair of gases investigated. They were chosen because their compressibilities are so nearly alike that even at 0° C measurements made in the neighbourhood of 1 atm. have not been sufficiently accurate hitherto to distinguish definitely between their coefficients. At 22·05° C, the working temperature of the tank, the difference would be even less. Few direct determinations of $1+\lambda$ for CO at 0° C have been made. Batuecas, Maverick & Schlatter (1929) found 1·00048 and Moles obtained 1·00040. High-pressure data are not very reliable. For nitrogen the values at 0° C are more numerous and certain. $1+\lambda = 1{\cdot}000453$ accords closely with direct measurements and extrapolation from high-pressure data. It is, however, to be expected that the compressibility of carbon monoxide would even at 22° C be slightly greater than that of nitrogen. Another advantage of this pair of gases is that no adsorption error is likely, and that the isotherms below 1 atm. are linear within very small limits.

Table 1 shows the results obtained with the first apparatus.

When the experimental ratios are graphed against pressure it is evident that they lie very closely about straight lines the equations of which calculated by the least mean squares method are

$$\text{series I:}\qquad (PV)_{N_2}/(PV)_{CO} = R = 0{\cdot}9909372 + 1{\cdot}22669 \times 10^{-7}p.$$

$$\text{series II:}\qquad (PV)_{N_2}/(PV)_{CO} = R = 0{\cdot}9792040 + 2{\cdot}17540 \times 10^{-7}p.$$

It can be seen from the table that the deviations from the calculated straight lines are very small.

TABLE 1. NITROGEN AND CARBON MONOXIDE AT 22·05° C

	Series I. N_2 in A, CO in A'			*Series II.* N_2 in A', CO in A		
no.	experimental ratio $R = N_2/CO$	$\Delta \times 10^6$ (calc. − obs.)	pressure (mm.)	experimental ratio $R = N_2/CO$	$\Delta \times 10^6$ (calc. − obs.)	pressure (mm.)
1	0·991012	+7	668·0	0·979372	− 5	750·0
2	0·991003	−9	457·0	0·979330	− 8	544·0
3	0·990984	+2	398·0	0·979284	+14	434·0
4	0·990963	+4	243·0	0·979269	+ 1	305·0
5	0·990952	+8	186·0	0·979251	+ 4	235·5
6	0·990961	−5	152·0	0·979259	−14	190·0

In series I the limiting value of R when p = zero, is $R_0 = 0{\cdot}9909372$, and the value of R when $p = 760$, is $R_{760} = 0{\cdot}9910305$, so that

$$\frac{(1+\lambda)_{N_2}}{(1+\lambda)_{CO}} = \frac{R_0}{R_{760}} = 0{\cdot}999906 \quad \text{where} \quad (1+\lambda) = \frac{(PV)_0}{(PV)_{760}}.$$

From series II the corresponding value $R_0/R_{760} = 0{\cdot}999831$. These two values differ by 7·5 parts in 10^5, a divergence greater than the probable error suggested by the deviations of the experimental points from the calculated straight lines. This we attribute to apparatus error and the error in the initial setting of the points to the horizontal as already explained. In preliminary experiments with air in both volumeters a difference in the same direction of 7 parts in 10^5 in the R_0/R_{760} ratio was found.

Taking the mean of the two ratios from series I and II the final ratio is

$$\frac{R_0}{R_{760}} = \frac{(1+\lambda)_{N_2}}{(1+\lambda)_{CO}} = 0{\cdot}999869,$$

and if the compressibility of nitrogen is known that for carbon monoxide can be calculated.

Now direct measurements of the compressibility of nitrogen at pressures in the vicinity of atmospheric have only been made at 0° C, but Michels, Wouters & de Boer (1934) have made very accurate measurements at a number of temperatures and pressures varying from 19 to 52 atm. Their results extrapolated give

$$(1+\lambda)_{0^\circ\,C} = 1{\cdot}000453,$$

which is in good agreement with direct determinations made at 0° C at low pressures.

From the same data we have calculated $(1+\lambda)_{N_2}$ at 22·05° C, and find 1·000216, whence from our mean ratio

$$(1+\lambda)_{CO} = \frac{1{\cdot}000216}{0{\cdot}999869} = 1{\cdot}000347 \text{ at } 22{\cdot}05^\circ\,\text{C}.$$

Strong confirmation of the accuracy of this value is afforded by work in these laboratories carried out by Leadbeater (1945), in which the densities of identical samples of the two gases were compared at 22° C using a new microbalance method in which the difficulties inherent in measuring small pressure differences accurately on a mercury manometer were obviated. These measurements made at two different densities gave values for the molecular weight ratio N_2/CO in close agreement with international values, and assuming the above value for nitrogen, gave for

$$(1+\lambda)_{CO} = 1{\cdot}00035(8) \text{ at } 22^\circ\,\text{C},$$

which is very close to our value though obtained by an entirely different method.

A small correction has still be be made, for the pressure scale in series I and II is given in mm. of mercury at 22° C, whereas in Leadbeater's result the pressure has been corrected to 0° C.

Making this small correction our final mean value becomes

$$(1+\lambda)_{CO} = 1{\cdot}00034(8),$$

agreeing with Leadbeater's value to 1 part in 10^5.

TABLE 2. CARBON MONOXIDE AND CARBON DIOXIDE AT 22° C

	Series I. CO_2 in A, CO in A'			*Series II.* CO_2 in A, CO in A' (surfaces prepared)		
no.	experimental ratio $R = CO/CO_2$	$\Delta \times 10^6$ (calc. − obs.)	pressure (mm.)	experimental ratio $R = CO/CO_2$	$\Delta \times 10^6$ (calc. − obs.)	pressure (mm.)
1	1·029061	− 10	770·0	1·031120	+ 17	819·4
2	1·027613	+ 7	550·0	1·029583	− 12	582·5
3	1·026851	+ 15	434·2	1·028754	− 6	458·0
4	1·026002	+ 10	302·9	1·027815	+ 14	319·0
5	1·025567	− 14	232·5	1·027338	+ 2	245·0
6	1·025276	− 2	189·2	1·027037	+ 5	200·0

The equations calculated by the least mean squares method are:

series I: $R = 1{\cdot}024041 + 6{\cdot}5063 \times 10^{-6}\,p$ series II: $R = 1{\cdot}025720 + 6{\cdot}6112 \times 10^{-6}\,p$

$R_0/R_{760} = 0{\cdot}995194$ $R_0/R_{760} = 0{\cdot}995126$

In order to get an indication of adsorption different procedures were adopted in the two series. In series I the volumeter bulbs after evacuation were filled with mercury and the gas introduced in the usual way, so that after each expansion the glass surface uncovered had not been previously in contact with the gas. Hence with each successive expansion the volume of CO_2 in A would be diminished by a small increment, and at low pressure the measured ratio would be too large. In series II before beginning an experiment A was filled with CO_2 at approximately the lowest pressure that would be reached on expansion and allowed to remain for 24 hr. in contact with the gas. Mercury was then allowed to flow in slowly, compressing the gas up to about the highest working pressure and finally the gas was displaced at constant pressure. In this way it was hoped to saturate the glass with adsorbed CO_2 at pressures to which they would be exposed in the actual experiments. After the surfaces had been prepared the filling was carried out in the usual way. Of course, this procedure does not take account of adsorption on the mercury which, since the volumeter is a sphere, would be greatest when half-filled. This procedure of saturating the volumeter surfaces as described has been followed for C_2H_4 and C_3H_8. The difference in the two slopes in series I and II is in the expected direction, assuming that the points can be adequately expressed by a linear equation; further, an approximate estimation of adsorption shows it to be of the right order.

No definite indication of curvature was obtained in series II, though in series I the deviations from the mean line lie roughly about a slight curve, which may be caused by adsorption. Actually the deviations are hardly if at all greater than the experimental error. Taking the data of series II as the more reliable and

$$(1+\lambda)_{CO} = 1{\cdot}000348,$$

$$(1+\lambda)_{CO_2} = \frac{1{\cdot}000348}{0{\cdot}995126} = 1{\cdot}005213.$$

Two small corrections (*a*) for apparatus error which is assumed to be the same as in the N_2/CO ratio, i.e. $-0{\cdot}000037$, (*b*) to correct the pressure scale from 22·05° C to 0° C, i.e. $+0{\cdot}00002$ have still to be applied.

The final $(1+\lambda)_{CO_2}$ value is 1·0052(0) at 22·05° C. Not too much reliance can be placed on the accuracy of this figure because the gases were not reversed, and the same apparatus error had to be assumed as in the N_2/CO data. When work was started on the next pair of gases, CO_2 and N_2O, it was noticed that the mercury surface in dead space B was slightly fouled, and on lowering the mercury distinct indications of a grease film appeared which evidently originated in the wax used to make an air-tight seal between the glass and the grooved steel block. This defect could not be remedied without dismantling the dead spaces, and it rapidly grew worse during the next run. The menisci, too, were noticed to differ considerably in

TABLE 3. CARBON DIOXIDE AND NITROUS OXIDE AT 22·05° C

	Series I. CO_2 in A, N_2O in A'			*Series II.* N_2O in A, CO_2 in A'		
no.	experimental ratio $R = CO_2/N_2O$	$\Delta \times 10^6$ (calc. – obs.)	pressure (mm.)	experimental ratio $R = CO_2$	$\Delta \times 10^6$ (calc. – obs.)	pressure (mm.)
1	0·913146	− 7	802·0	0·974262	+ 10	818·0
2	0·912970	− 12	570·0	0·974155	− 18	596·2
3	0·912839	+ 10	440·2	0·974072	− 12	468·7
4	0·912732	+ 5	306·4	0·973945	+ 30	328·7
5	0·912677	0	235·4	0·973945	− 17	251·2

Equations by least mean squares (straight lines):

series I: $R = 0{\cdot}912479 + 8{\cdot}4089 \times 10^{-7}p$ series II: $R = 0{\cdot}973776 + 6{\cdot}0575 \times 10^{-7}p$

$R_0/R_{760} = 0{\cdot}999300$ $R_0/R_{760} = 0{\cdot}999527$

height, indicating an alteration in surface tension which may have affected capillarity. As was expected, the nitrous oxide is distinctly more compressible than carbon dioxide. The two R_0/R_{760} ratios in the two series differ from each other by nearly 23 parts in 10^5 and in the opposite direction from the N_2/CO ratios. The mean value $R_0/R_{760} = 0{\cdot}999414$. Correcting the pressure scale to 0° C we get

$$\frac{R_0}{R_{760}} = \frac{(1+\lambda)_{CO_2}}{(1+\lambda)_{N_2O}} = 0{\cdot}999412,$$

which, assuming $(1+\lambda)_{CO_2} = 1{\cdot}00520$, the previously found value, gives

$$(1+\lambda)_{N_2O} = 1{\cdot}00579,$$

which on account of the contamination of the mercury in the dead spaces is less reliable than the previous results.

At this stage the dead spaces were removed and replaced by fresh ones, the ground joints fitting on to steel cones as shown in figures 1 and 2.

TABLE 4. NITROGEN AND OXYGEN AT 22·05° C

	Series I: O_2 in A, N_2 in A'			*Series II*. N_2 in A, O_2 in A'		
no.	experimental ratio $R = N_2/O_2$	$\Delta \times 10^6$ (calc. − obs.)	pressure (mm.)	experimental ratio $R = N_2/O_2$	$\Delta \times 10^6$ (calc. − obs.)	pressure (mm.)
1	1·008620	+ 4	851·6	0·986892	− 2	848·6
2	1·008444	+ 25	591·8	0·986747	− 4	568·2
3	1·008416	− 17	467·8	0·986694	− 7	462·3
4	1·008336	− 19	322·7	0·986626	− 11	323·6
5	1·008258	+ 16	246·2	0·986547	+ 27	246·7
6	1·008250	− 3	199·0	0·986566	− 17	199·1

Equations by least mean squares (straight lines):

series I: $R = 1{\cdot}008135 + 5{\cdot}6450 \times 10^{-7}p$ series II: $R = 0{\cdot}986445 + 5{\cdot}2447 \times 10^{-7}p$

$R_0/R_{760} = 0{\cdot}999574$ $R_0/R_{760} = 0{\cdot}999585$

which gives $(1+\lambda)_{O_2} = 1{\cdot}00064(3)$, which when pressure is corrected to 0° C becomes 1·00064(5).

During the course of these experiments it was noticed that the mercury in the dead space containing oxygen showed indications on its surface of a slight film, whilst that in contact with nitrogen remained perfectly bright. This film, which did not interfere with the setting of the points, may have been due to oxide formation in which case the volume of oxygen in the gas phase would decrease during the experiment and would lead to a value of the compressibility which would be too low. To test this a careful point setting was made and the oxygen allowed to stand for some days in contact with a large surface of mercury in its volumeter. No alteration in the setting was detectable. It was hence concluded that no significant absorption of the gas had occurred. The oxygen too was completely absorbed by molten phosphorus.

TABLE 5. NITROGEN AND ETHYLENE AT 22·05° C

no.	experimental ratio $R = C_2H_4/N_2$	$\Delta \times 10^6$ (calc. – obs.)	pressure (mm.)
1	1·010574	+ 2	817·2
2	1·012111	+ 5	620·3
3	1·013129	– 3	491·1
4	1·014166	–20	360·7
5	1·014849	0	270·7
6	1·015322	+11	208·9

Equation by least mean squares (straight line):

$$R = 1{\cdot}016966 - 7{\cdot}8195 \times 10^{-6}p,$$

$$\frac{(1+\lambda)_{C_2H_4}}{(1+\lambda)_{N_2}} = \frac{R_0}{R_{760}} = 1{\cdot}005878,$$

whence $(1+\lambda)_{C_2H_4} = 1{\cdot}005878 \times 1{\cdot}000216 = 1{\cdot}006095,$

and correcting pressure to 0° C we get

$$(1+\lambda)_{C_2H_4} = 1{\cdot}006118.$$

Assuming that the setting and apparatus error was the same as in the N_2/O_2 experiments,

$$(1+\lambda)_{C_2H_4} = 1{\cdot}00611(0).$$

From the deviations from a straight line it is evident there is no marked trend which would indicate a curvature in this isothermal.

TABLE 6. NITROGEN AND PROPANE AT 22·05° C

	Series I. C_3H_8 in A, N_2 in A'			*Series II.* N_2 in A, C_3H_8 in A'		
no.	experimental ratio $R = C_3H_8/N_2$	$\Delta \times 10^6$ (calc. – obs.)	pressure (mm. mercury) at 0° C	experimental ratio $R = C_3H_8/N_2$	$\Delta \times 10^6$ (calc. – obs.)	pressure (mm.) to 0° C
1	1·005841	+25	802·94	0·983381	–27	799·16
2	1·011678	–31	544·69	0·988620	+37	557·36
3	1·014557	–26	415·83	0·992427	– 1	385·39
4	1·017274	+14	292·69	0·994332	– 2	298·55
5	1·018760	+ 2	226·86	—	—	—
6	1·019695	+11	184·70	0·996638	–19	194·15

Equations by least mean squares (straight lines):

series I: $R = 1{\cdot}023840 - 0{\cdot}00022385p$ series II: $R = 1{\cdot}000876 - 0{\cdot}000021925p,$

$$\frac{R_0}{R_{760}} \text{ for series I} = \frac{1{\cdot}023840}{1{\cdot}006827} = 1{\cdot}016898; \text{ for series II} = \frac{1{\cdot}000876}{0{\cdot}984213} = 1{\cdot}016930$$

using $(1+\lambda)_{N_2} = 1{\cdot}000216$, as before.

$$(1+\lambda)_{C_3H_8} = 1{\cdot}017117 \text{ and } 1{\cdot}017150,$$

$$\text{mean } (1+\lambda)_{C_3H_8} = 1{\cdot}01713(3).$$

This was a particularly interesting comparison on account of the high compressibility of propane, a gas which at 22° C is over 70° below its critical temperature. The gas was in a high state of purity and had been used for the determination of its molecular weight by the limiting pressure method. Notwithstanding its wide deviation from Boyle's law the results show no definite indication of curvature. The deviations from the calculated straight lines are rather larger than with the other pairs of gases studied, which may be due to a variable adsorption although the glass surfaces were saturated with gas beforehand in the way described for carbon dioxide.

It may be noted that there is a close agreement in the results obtained on interchanging the gases. With this pair of gases each individual pressure was corrected to 0° C instead of applying an overall correction to the $1+\lambda$ values. This was necessary on account of the more rapid change with pressure of the propane PV's.

The final results with the various gases are summarized in table 7.

TABLE 7. COMPRESSIBILITIES PER ATMOSPHERE AT 22·05° C

gas	pressure range (mm.)	$1+\lambda$	A	
nitrogen (standard)	—	1·000216	0·000216	calc. from results of Michels, Wouters & de Boer (1934)
carbon monoxide	750–152	1·00034(8)	0·00034(8)	Cawood & Patterson (1936) values for A at 21° C
carbon dioxide	819–200	1·00520	0·00517	0·0052(6)
nitrous oxide	802–235	1·00579	0·00576	0·0056(7)
oxygen	851–199	1·00064	0·00064	—
ethylene	817–209	1·00611	0·00607	0·0061(2)
propane	803–185	1·01713	0·01684	—

The only values in the literature directly measured at low pressure and at a comparable temperature are those of Cawood & Patterson made at 21° C with an Andrews apparatus between the pressures of 3 and 1 m. of mercury for CO_2, N_2O and C_2H_4. These are given in column 5 and show a satisfactory agreement with ours. Considering the results as a whole it is evident that the method is susceptible of a high degree of accuracy, which is due mainly to the pipette system of measuring the actual volume of the dead spaces after each point setting. The volume changes in these observed in series II of the nitrogen/oxygen measurements are appended as an example. In some cases greater variations were noticed, and it is clear that had this procedure not been followed a much lower degree of precision would have been reached. The figures below represent the corrections applied to the volumes of the dead space pipettes expressed as grams of mercury. These are positive or negative according to whether the dead space volume was larger or smaller than the volume of the pipettes.

DEAD-SPACE CORRECTIONS

series II N_2/O_2 ratio	E	E'	change in ratios if correction omitted $\times 10^6$, assuming initial volume = 100 ml.
1	0·417	0·461	40
2	0·124	0·122	negligible
3	0·137	−0·494	−260
4	0·199	0·496	80
5	−0·090	0·131	50
6	0·259	−0·071	60

Had no corrections been made the deviations of the points from a straight line would have been about ten times as great as they actually were.

The failure to detect with certainty any actual curvature with propane shows clearly that any departure from linearity of the PV/P isothermal at 22° C is very small even for so compressible a gas.

The validity of a linear extrapolation of densities claimed by Moles in his determinations of the limiting densities of gases is supported by this fresh evidence, as is also the microbalance method of limiting pressures. By taking a much larger number of points it would be possible to plot the isothermals with still greater accuracy. Then perhaps a slight curvature might be found which so far we have been unable to discover.

The method too might be applied to much lower pressures so as to obtain the isothermals of vapours. Work in this direction is now under way.

The authors wish to thank the Department of Scientific and Industrial Research, the Leverhulme Trustees and the Royal Society for financial assistance.

REFERENCES

Addingley, C. G. & Whytlaw-Gray, R. 1928 *Trans. Faraday Soc.* **24**, 378.

Batuecas, T., Maverick, G. & Schlatter, C. 1929 *J. Chim. phys.* **26**, 548.

Casado, F. L. 1943 Thesis, University of Santiago.

Casado, F. L., Massie, D. S. & Whytlaw-Gray, R. 1949 *J. Chem. Soc.* p. 1746.

Cawood, W. & Patterson, H. S. 1936 *Phil. Trans.* A, **236**, 77.

Cragoe, C. S. 1941 *Bur. Stand. J. Res., Wash.*, **26**, 495.

Keesom, W. H. 1938 *Détermination Physico-chimique des Poids Molec. et Atomique des Gaz, Collection Scientifique, Institut. Internat. Co-opération Intellectuelle*, Paris, p. 165.

Leadbeater, B. 1945 Thesis, University of Leeds.

Michels, A., Wouters, H. & de Boer, J. 1934 *Physica*, **1**, 587.

Moles, E. 1938 *Détermination Physico-chimique des Poids Molec. et Atomique des Gaz, Collection Scientifique, Institut. Internat. Co-opération Intellectuelle*, Paris, p. 189.

Whytlaw-Gray, & R. Teich, N. 1948 *Trans. Faraday Soc.* **44**, 774.

The relativity of Galilean frames

By E. A. Milne, F.R.S.

(*Received* 21 *July* 1949)

Lorentz transformations are valid only in t-time, whereas classical mechanics employs τ-time. Since classical mechanics is supposed to be valid in any Galilean frame, i.e. any frame in uniform motion relative to the substratum, it becomes important to find the transformations which should replace the Lorentz formulae when we pass from one Galilean frame to another. These are determined in the present paper, on a simple convention as to the measurement of time in a Galilean frame. They prove to differ from Lorentz formulae, but have closely allied properties. In particular, they yield Einstein's relative-velocity formulae, which are thus seen to be more general than the Lorentz formulae themselves.

1. Introduction

In previous writings by the author (partly in collaboration with G. J. Whitrow) it has been shown how two observers (particles) who part company from one another and between whom a relation of symmetry exists, can graduate their clocks so that in a well-defined sense these clocks can be said to be *congruent* to one another. They can, moreover, choose the graduations of these clocks so that each appears to the other to be receding with uniform velocity, as judged by light-signalling and the usual conventions as to the assignments of co-ordinates. This mode of clock-graduation yields what is called t-time; and in this mode of measuring time, with its associated measures of co-ordinates, the relations connecting the co-ordinates assigned by the two observers to a distant event are just the Lorentz formulae. Of the latter an independent proof has been given which shows that they are essentially epistemological in character. Moreover, the totality of observers whose clocks are congruent to one another and to those of the original two observers is precisely the aggregate of observers in uniform relative motion who have separated from one another at a common epoch, called $t = 0$. These observers, or particles, are called the fundamental observers, or fundamental particles; and when arranged in the three-dimensional private Euclidean space associated with any one of them so as to have the same density distribution whatever fundamental particle is taken as viewpoint, they constitute what is called the *substratum*.

The clocks carried by the fundamental particles or fundamental observers of the substratum may be regraduated in any arbitrary fashion, provided the same law of regraduation is applied to each, and when so regraduated the clocks remain congruent, but the description of their relative motion is changed. In particular, the substratum in uniform relative motion may be transformed by regraduation of clocks into an aggregate of relatively stationary particles. The new mode of clock-graduation is called τ-time, the reading τ of any clock being connected with its previous reading t by the relation

$$\tau = t_0 \log (t/t_0) + t_0.$$

The epoch τ of an event, unlike its epoch t, is an invariant, the same for all observers describing this event. Thus, in the relatively stationary substratum there is a world-wide simultaneity.

It is suggested that, apart from 'proper motions', the universe of the extra-galactic nebulae constitutes a substratum, the smoothed-out distribution of nebular nuclei corresponding to the fundamental particles.

When we pass from kinematics to dynamics, it has been shown that the dynamics of a free or constrained particle in t-measure is markedly non-Newtonian; but it reduces to Newtonian dynamics, locally and for not too large velocities, when we transform from t-measure to τ-measure. It therefore suggests itself that the independent time variable of Newtonian mechanics is the variable τ, not t. This is borne out by several other considerations, notably the reversibility of the Newtonian equations of motion (which occurs in τ-measure but not in t-measure), and the invariance of form of the Newtonian equations to a change of scale and a change of origin of time, which again holds good in τ-measure but not in t-measure.

But the question now arises, what is the kinematics of uniform motion, in τ-measure? If a particle-observer is in uniform motion relative to the relatively stationary particles of the substratum, what are the relations between his assignments of co-ordinates and epochs to events and the assignments made by the fundamental observers? Such uniformly moving particles will carry with them what in classical dynamics are called Galilean frames. If we return to t-measures, these frames will no longer be in uniform relative motion relatively to the now uniformly moving fundamental particles, and so the transformations from a fundamental particle to these Galilean frames cannot be of Lorentz type. This question is one of fundamental importance in theoretical physics; for in theoretical physics the use of a dynamics based on Newtonian dynamics shows that τ-time is being employed, yet the transformations connecting Galilean frames are commonly taken to be of Lorentz type.

The first question is to decide how to graduate the clock of an observer moving uniformly through the stationary substratum. Since the τ-epoch of an event is an invariant, the same for all fundamental observers, the obvious procedure is to let the moving observer 'pick up' the time τ from each fundamental particle as he passes it. In other words, let the moving observer graduate his clock so that it agrees with the clock of the fundamental observer he is instantaneously passing. This time will in fact be the absolute Newtonian time in a Newtonian *plenum*, but it has a more satisfactory ancestry than in the *Principia*, being derived from the better-founded t-time of Einstein and the Lorentz formulae.

The present paper is devoted to exploring the consequences of this procedure. It will be shown that the transformation rules for passage from a fundamental particle to a Galilean frame, or from one Galilean frame to another, are not of Lorentz type, and their form will be determined. It will be shown, however, that Einstein's relative-velocity formulae hold good without alteration. It will be shown, moreover, that the *absolute* velocity of a Galilean frame, namely, its velocity relative to the substratum, enters into the generalized Lorentz formula connecting the corresponding observer's co-ordinates with those of any other Galilean observer, and not merely the *relative* velocity of the two observers.

2. RELATION OF A UNIFORMLY MOVING OBSERVER TO THE SUBSTRATUM

Let A be a fundamental observer, and therefore at rest in the substratum. Let B be an observer who parted company with A at time $\tau = \alpha$ and subsequently moved relative to the substratum with velocity V along a geodesic in the hyperbolic space suitable for the description of the substratum. Let a light signal leave A at epoch τ_1, be reflected at B at epoch τ_2, be reflected at A at epoch τ_3, be reflected again at B at epoch τ_4 and reach A again at epoch τ_5. These epochs $\tau_1, \ldots, \tau_5$ are those assigned on the standard of time-keeping used by members of the substratum.

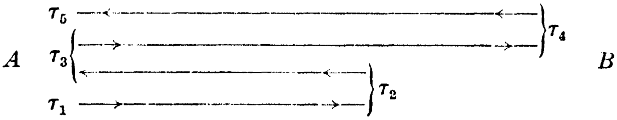

FIGURE 1

Then B's distance-epoch relation as described by A is

$$\rho_B = V(\tau_B - \alpha), \tag{1}$$

where ρ_B is the distance of B from A at epoch τ_B. We have in particular the relations, in an obvious notation,

$$\rho_2 = V(\tau_2 - \alpha), \quad \rho_4 = V(\tau_4 - \alpha). \tag{2), (3}$$

These distances ρ_2 and ρ_4 and epochs τ_2 and τ_4 are connected with the epochs of despatch of signals from A and return to A by the relations

$$\rho_2 = \tfrac{1}{2}c(\tau_3 - \tau_1), \quad \tau_2 = \tfrac{1}{2}(\tau_3 + \tau_1),$$

$$\rho_4 = \tfrac{1}{2}c(\tau_5 - \tau_3), \quad \tau_4 = \tfrac{1}{2}(\tau_5 + \tau_3),$$

where c is an arbitrary number chosen by A; c of course represents the speed of light, and relates the length- and time-scales used by members of the substratum. Solving these pairs of equations for τ_3 we have

$$\tau_3 = \tau_2 + \rho_2/c = \tau_4 - \rho_4/c, \tag{4}$$

or

$$\tau_3 = \tau_2 + (V/c)(\tau_2 - \alpha) = \tau_4 - (V/c)(\tau_4 - \alpha). \tag{5}$$

Now let B assign epochs $\tau_1', \ldots, \tau_5'$ to the same five events by his clock and the usual convention as to epochs of distant events. Since two of these occur at B, who is continually picking up the time from the fundamental particles with which he momentarily coincides, we have

$$\tau_2' = \tau_2, \tag{6}$$

$$\tau_4' = \tau_4. \tag{7}$$

Observer B assigns to A a distance ρ_A' from himself at any epoch τ_A, and so in particular

$$\rho_3' = \tfrac{1}{2}c(\tau_4' - \tau_2'), \quad \tau_3' = \tfrac{1}{2}(\tau_4' + \tau_2').$$

Hence

$$\tau_4' = \tau_3' + \rho_3'/c, \tag{8}$$

$$\tau_2' = \tau_3' - \rho_3'/c. \tag{9}$$

Our objects are to find B's description of A's apparent motion relative to himself as a function of τ' and to find the relation between τ' and τ for events not happening at B. By (6) and the first of (5)

$$\tau_2' = \frac{\tau_3 + (V/c)\alpha}{1 + V/c},$$

and hence by (9), eliminating τ_2',

$$\rho_3'/c = \tau_3' - \frac{\tau_3 + (V/c)\alpha}{1 + V/c}. \tag{10}$$

Similarly, by (7) and the second of (5),

$$\tau_4' = \frac{\tau_3 - (V/c)\alpha}{1 - V/c},$$

and hence by (8), eliminating τ_4',

$$\rho_3'/c = -\tau_3' + \frac{\tau_3 - (V/c)\alpha}{1 - V/c}. \tag{11}$$

Relations (10) and (11) give us what we want. Eliminating ρ_3'/c we have the clock-running relation in the form

$$\tau_3' - \alpha = \frac{\tau_3 - \alpha}{1 - V^2/c^2}, \tag{12}$$

and eliminating τ_3 we have the epoch-distance relation for A as seen by B in the form

$$\rho_3' = V(\tau_3' - \alpha). \tag{13}$$

These may now be rewritten for clarity in the forms

$$\tau_A' - \alpha = \frac{\tau_A - \alpha}{1 - V^2/c^2}, \tag{14}$$

$$\rho_A' = V(\tau_A' - \alpha). \tag{15}$$

It follows that A's relative motion as described by B is of the same form as B's relative motion as described by A; (1) and (15) are of the same form. On the other hand, their clock-running relations are different; (14) is to be contrasted with the relation $\tau_B = \tau_B'$.

3. CONTRACTION OF TIME-SCALE

According to (14), B will consider A's clock as running slow, by the factor $(1 - V^2/c^2)$. For if $\Delta\tau_A$ is a time interval recorded on A's clock, to B it will appear to occupy a longer time $\Delta\tau_A'$ given by

$$\Delta\tau_A' = \Delta\tau_A/(1 - V^2/c^2). \tag{16}$$

Notice the difference from the Lorentz case, where the factor in the denominator is $(1 - V^2/c^2)^{\frac{1}{2}}$ and the relation is

$$\Delta t_A' = \Delta t_A/(1 - V^2/c^2)^{\frac{1}{2}}. \tag{17}$$

4. SEMI-EQUIVALENCE

Since A's motion as described by B is of the same form as B's motion as described by A, whereas B's description of A's clock in terms of his own is not the same as A's description of B's clock, B may be described as 'semi-equivalent' to A, as contrasted with the description of the fundamental observers A as all 'equivalent' to one another. It is to be noted that

$$\frac{d\rho_B}{d\tau_B} = V, \quad \frac{d\rho'_A}{d\tau'_A} = V, \tag{18}$$

so that the relative velocity is reckoned the same by either observer.

5. ONE-DIMENSIONAL TRANSFORMATION FORMULAE FROM A TO B

Next, let A and B make observations on a distant event in line with them. Let A assign co-ordinates (ρ, τ), B co-ordinates (ρ', τ'), to the same event, by means of a light signal which leaves A at epoch τ_1 by A's clock, reaches B at epoch τ'_2 by B's clock, is reflected at the distant event and reaches B on the return journey at epoch τ'_3 by B's clock, and reaches A at epoch τ_4 by A's clock (see figure 2).

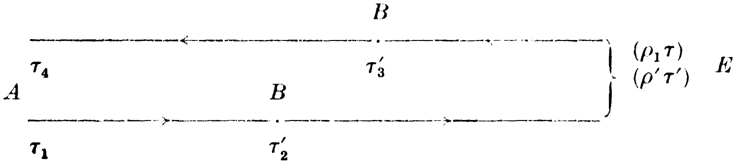

FIGURE 2

Then we have

$$\tau = \tfrac{1}{2}(\tau_4 + \tau_1), \tag{19}$$

$$\rho = \tfrac{1}{2}c(\tau_4 - \tau_1), \tag{19'}$$

$$\tau' = \tfrac{1}{2}(\tau'_3 + \tau'_2), \tag{20}$$

$$\rho' = \tfrac{1}{2}c(\tau'_3 - \tau'_2). \tag{20'}$$

But since τ'_2 and τ'_3 refer to events at B, we have

$$\tau'_2 = \tau_2, \tag{21}$$

$$\tau'_3 = \tau_3, \tag{21'}$$

where τ_2 and τ_3 are the epoch assignments by A (or by any other fundamental observer). Also since

$$\tau_2 = \tau_1 + \rho_2/c, \tag{22}$$

$$\tau_4 = \tau_3 + \rho_3/c, \tag{22'}$$

and since B is in motion relative to A with velocity V in A's measures, we have

$$\tau_2 = \tau_1 + (V/c)(\tau_2 - \alpha), \tag{23}$$

$$\tau_4 = \tau_3 + (V/c)(\tau_3 - \alpha). \tag{23'}$$

Hence, combining (20), (20′) with (21′) and (23′), and using (19), (19′),

$$\tau' + \rho'/c = \tau'_3 = \tau_3 = \frac{\tau_4 + (V/c)\alpha}{1 + V/c} = \frac{\tau + \rho/c + (V/c)\alpha}{1 + V/c},$$

and similarly

$$\tau' - \rho'/c = \tau'_2 = \tau_2 = \frac{\tau_1 - (V/c)\alpha}{1 - V/c} = \frac{\tau - \rho/c - (V/c)\alpha}{1 - V/c}.$$

Subtracting α from each side we obtain the transformation formulae in the form

$$\tau' - \alpha + \rho'/c = \frac{\tau - \alpha + \rho/c}{1 + V/c}, \tag{24}$$

$$\tau' - \alpha - \rho'/c = \frac{\tau - \alpha - \rho/c}{1 - V/c}. \tag{24'}$$

These may be called the 'modified Lorentz formulae for semi-equivalence'. They may be contrasted with the Lorentz formulae for equivalence, which are of the form

$$t' + r'/c = (t + r/c)\left(\frac{1 - V/c}{1 + V/c}\right)^{\frac{1}{2}}, \tag{25}$$

$$t' - r'/c = (t - r/c)\left(\frac{1 + V/c}{1 - V/c}\right)^{\frac{1}{2}}. \tag{25'}$$

Solving (24) and (24′) for ρ' and τ' we get

$$\rho' = \frac{\rho - V(\tau - \alpha)}{1 - V^2/c^2}, \tag{26}$$

$$\tau' - \alpha = \frac{\tau - \alpha - \rho V/c^2}{1 - V^2/c^2}, \tag{26'}$$

and solving them for ρ and τ we get

$$\rho = \rho' + V(\tau' - \alpha), \tag{27}$$

$$\tau - \alpha = \tau' - \alpha + \rho' V/c^2. \tag{27'}$$

6. CONTRACTION OF LENGTH

These formulae may be used to make deductions similar to those usually made from the standard Lorentz formulae; but of course there is no longer symmetry between A and B. If $(\Delta\rho, \Delta\tau)$, $(\Delta\rho', \Delta\tau')$ are corresponding increments in coordinates of events, by (27) and (27′) we have

$$\Delta\rho = \Delta\rho' + V\Delta\tau', \quad \Delta\tau = \Delta\tau' + (V/c^2)\,\Delta\rho'.$$

The length l assigned by A to a rod of length l' held by B in the direction of the relative motion is given by putting $\Delta\rho' = l'$, $\Delta\tau = 0$, $\Delta\rho = l$, when the equations give on elimination of $\Delta\tau'$

$$l = l'(1 - V^2/c^2),$$

so that A reckons B's rod as contracted. But the length l' assigned by B to a rod of length l held by A in the direction of motion is given by putting $\Delta\rho' = l'$, $\Delta\tau' = 0$, $\Delta\rho = l$, when we get

$$l' = l,$$

so that B sees no contraction of A's rod.

7. ONE-DIMENSIONAL VELOCITY TRANSFORMATION

By (26) and (26′),
$$\frac{d\rho'}{d\tau'} = \frac{d\rho - V\,d\tau}{d\tau - (V/c^2)\,d\rho}.$$

Putting $d\rho/d\tau = u$, $d\rho'/d\tau' = u'$, we get
$$u' = \frac{u-V}{1-uV/c^2},$$

which is Einstein's relative-velocity formula. It gives the velocity u' assigned by B to a moving particle whose velocity as assigned by A is u. Thus Einstein's relative-velocity formula holds good in spite of the co-ordinate-transformation formulae not being of Lorentz type. It follows that experimental confirmation of Einstein's velocity formula is not evidence in favour of the classical Lorentz formulae as against our 'modified Lorentz formulae' (26) and (26′).

8. TRANSFORMATION FROM B_1 TO B_2

Suppose that V_1 is the velocity of an observerB_1, in τ-measure, and V_2 the velocity of another observer B_2, collinear with A and B and moving in the same direction. Suppose B_1 to have left A at epoch $\tau = \alpha_1$, and let B_2 have left A at epoch $\tau = \alpha_2$. Let (ρ,τ), (ρ',τ'), (ρ'',τ'') be the co-ordinates assigned to a given event E (collinear with A, B_1, B_2) by A, B_1, B_2 respectively. Then by formulae (24) and (24′), we have

$$\tau-\alpha_1+\rho/c = (1+V_1/c)(\tau'-\alpha_1+\rho'/c), \tag{28}$$

$$\tau-\alpha_1-\rho/c = (1-V_1/c)(\tau'-\alpha_1-\rho'/c), \tag{28′}$$

and
$$\tau-\alpha_2+\rho/c = (1+V_2/c)(\tau''-\alpha_2+\rho''/c), \tag{29}$$

$$\tau-\alpha_2-\rho/c = (1-V_2/c)(\tau''-\alpha_2-\rho''/c). \tag{29′}$$

Eliminating τ and ρ between these four equations we are left with two relations between (ρ',τ') and (ρ'',τ'') which give the desired transformation from the Galilean frame associated with B_1 to that associated with B_2. These eliminants may be written

$$\alpha_2-\alpha_1 = (1+V_1/c)(\tau'-\alpha_1+\rho'/c)-(1+V_2/c)(\tau''-\alpha_2+\rho''/c), \tag{30}$$

$$\alpha_2-\alpha_1 = (1-V_1/c)(\tau'-\alpha_1-\rho'/c)-(1-V_2/c)(\tau''-\alpha_2-\rho''/c). \tag{30′}$$

Adding these equations we get
$$\tau'+(V_1/c^2)\rho' = \tau''+(V_2/c^2)\rho'', \tag{31}$$

and subtracting we get
$$\rho'+V_1(\tau'-\alpha_1) = \rho''+V_2(\tau''-\alpha_2). \tag{32}$$

Relations (31) and (32) allow us to pass from B_1's description of an event (ρ',τ') to B_2's description (ρ'',τ''), provided we know the 'absolute' velocities, V_1 and V_2, of B_1 and B_2 relative in each case to the standards of rest in their immediate neighbourhoods. Let us now attempt to put these in a form which involves the relative velocity of each observer as observed by the other.

9. B_1'S DESCRIPTION OF B_2'S MOTION

We obtain B_1's description of B_2's motion on putting $\rho'' = 0$ and eliminating τ''. We get

$$\rho' + V_1(\tau' - \alpha_1) = V_2[\tau' + (V_1/c^2)\rho' - \alpha_2],$$

or

$$\rho' = V'_{12}(\tau' - \alpha'_{12}) \tag{33}$$

where

$$V'_{12} = \frac{V_2 - V_1}{1 - V_1 V_2/c^2}, \tag{34}$$

$$\alpha'_{12} = \frac{V_2\alpha_2 - V_1\alpha_1}{V_2 - V_1}, \tag{35}$$

provided* $V_2 \neq V_1$.

We obtain B_2's description of B_1's motion on putting $\rho' = 0$ and eliminating τ'. We get

$$\rho'' + V_2(\tau'' - \alpha_2) = V_1[\tau'' + (V_2/c^2)\rho'' - \alpha_1],$$

or

$$\rho'' = V''_{21}(\tau'' - \alpha''_{21}), \tag{36}$$

where

$$V''_{21} = \frac{V_1 - V_2}{1 - V_1 V_2/c^2}, \tag{37}$$

$$\alpha''_{21} = \frac{V_1\alpha_1 - V_2\alpha_2}{V_1 - V_2}. \tag{38}$$

Thus

$$V'_{12} = -V''_{21}, \tag{39}$$

$$\alpha'_{12} = \alpha''_{21} \tag{40}$$

We can now put the transformation formulae from B_1 to B_2 in a more suggestive form. Between (31) and (32) we eliminate τ''. We get

$$\rho' + V_1(\tau' - \alpha_1) = \rho'' + V_2[\tau' + (V_1/c^2)\rho' - (V_2/c^2)\rho'' - \alpha_2],$$

or, using (34) and (35),

$$\rho'' = \frac{1 - V_1 V_2/c^2}{1 - V_2^2/c^2}[\rho' - V'_{12}(\tau' - \alpha'_{12})]. \tag{41}$$

Again, eliminating ρ'' between (31) and (32), we get

$$\tau' + (V_1/c^2)\rho' = \tau'' + (V_2/c^2)[\rho' + V_1(\tau' - \alpha_1) - V_2(\tau'' - \alpha_2)],$$

or

$$\tau'' - \alpha''_{21} = \frac{1 - V_1 V_2/c^2}{1 - V_2^2/c^2}[\tau' - \alpha'_{12} - V'_{12}\rho'/c^2]. \tag{42}$$

Relations (41) and (42) are the modified Lorentz transformations for passage from B_1's co-ordinates and epochs of a distant event to B_2's co-ordinates and epochs for the same event.

We now note the identity

$$\left(1 - \frac{V'^2_{12}}{c^2}\right)\left(1 - \frac{V_1 V_2}{c^2}\right)^2 = \left(1 - \frac{V_1^2}{c^2}\right)\left(1 - \frac{V_2^2}{c^2}\right). \tag{43}$$

---

* The particular case $V_2 = V_1$ is easily dealt with and is left to the reader.

Solving (41) and (42) for ρ' and τ', and using identity (43), we get

$$\rho' = \frac{1-V_1V_2/c^2}{1-V_1^2/c^2}[\rho''-V''_{21}(\tau''-\alpha''_{21})], \tag{44}$$

and

$$\tau'-\alpha'_{12} = \frac{1-V_1V_2/c^2}{1-V_1^2/c^2}[(\tau''-\alpha''_{21})-V''_{21}\rho''/c^2]. \tag{45}$$

Note that (44) and (45) are of the same form as (41) and (42), as they should be. The pair (41) and (42) may be put in the form

$$\tau''-\alpha''_{21}+\rho''/c = \frac{(1-V_1V_2/c^2)(1-V'_{12}/c)}{1-V_2^2/c^2}[\tau'-\alpha'_{12}+\rho'/c], \tag{46}$$

and

$$\tau''-\alpha''_{21}-\rho''/c = \frac{(1-V_1V_2/c^2)(1+V'_{12}/c)}{1-V_2^2/c^2}[\tau'-\alpha'_{12}-\rho'/c]. \tag{46'}$$

Now identity (43) yields the identities

$$\frac{(1-V_1V_2/c^2)(1-V'_{12}/c)}{1-V_2^2/c^2} = \frac{1-V_1^2/c^2}{(1-V_1V_2/c^2)(1+V'_{12}/c)} = \left[\frac{1-V_1^2/c^2}{1-V_2^2/c^2}\,\frac{1-V'_{12}/c}{1+V'_{12}/c}\right]^{\frac{1}{2}}, \tag{47}$$

and

$$\frac{(1-V_1V_2/c^2)(1+V'_{12}/c)}{1-V_2^2/c^2} = \frac{1-V_1^2/c^2}{(1-V_1V_2/c^2)(1-V'_{12}/c)} = \left[\frac{1-V_1^2/c^2}{1-V_2^2/c^2}\,\frac{1+V'_{12}/c}{1-V'_{12}/c}\right]^{\frac{1}{2}}. \tag{47'}$$

These identities allow (46) and (46′) to be put in the more symmetrical form

$$(\tau''-\alpha''_{21}+\rho''/c)(1-V_2^2/c^2)^{\frac{1}{2}}(1-V''_{21}/c)^{\frac{1}{2}} = (\tau'-\alpha'_{12}+\rho'/c)(1-V_1^2/c^2)^{\frac{1}{2}}(1-V'_{12}/c)^{\frac{1}{2}}, \tag{48}$$

and

$$(\tau''-\alpha''_{21}-\rho''/c)(1-V_2^2/c^2)^{\frac{1}{2}}(1+V''_{21}/c)^{\frac{1}{2}} = (\tau'-\alpha'_{12}-\rho'/c)(1-V_1^2/c^2)^{\frac{1}{2}}(1+V'_{12}/c)^{\frac{1}{2}}. \tag{48'}$$

Here, it must be remembered, V_1 and V_2 are the 'absolute' velocities of B_1 and B_2, and $V'_{12} = -V''_{21}$ is their relative velocity, in the substratum. The formulae reduce to the case of semi-equivalence on taking, for example, $V_2 = 0$.

10. SLOWING DOWN OF CLOCKS

Consider a clock moving with B_2. Then $\rho'' = 0$, and so from (41)

$$\rho' = V'_{12}(\tau'-\alpha'_{12}).$$

Hence, inserting in (42)

$$\tau''-\alpha''_{21} = \frac{1-V_1V_2/c^2}{1-V_2^2/c^2}(1-V'^2_{12}/c^2)(\tau'-\alpha'_{12}),$$

or, in virtue of the velocity identity (43),

$$\tau''-\alpha''_{21} = (\tau'-\alpha'_{12})\frac{1-V_1^2/c^2}{1-V_1V_2/c^2}.$$

Thus if $V_2 > V_1$,
$$(\tau'-\alpha'_{12}) < \tau''-\alpha''_{21},$$

So that B_1 attaches a smaller time value to a given difference of B_2's clock-readings than does B_2. Thus the reading of B_2's clock appears to run *fast* to B_1. But for a clock at rest with B_1, $\rho' = 0$, and we have by (44)

$$\rho'' = -V'_{12}(\tau''-\alpha''_{21}),$$

and so, by (45) and the velocity identity (43),

$$\tau' - \alpha'_{12} = (\tau'' - \alpha''_{21})\frac{1 - V_2^2/c^2}{1 - V_1V_2/c^2}.$$

If again $V_2 > V_1$, $$(\tau'' - \alpha''_{21}) > (\tau' - \alpha'_{12}).$$

Thus to B_2, the receding clock at B_1 appears to take more time to run through a given difference of clock-readings, and so appears to run *slow* to B_2. It appears then that there is a difference in the apparent behaviours of B_2's clock to B_1 and B_1's clock to B_2. But it must be remembered that when $V_2 \neq V_1$, B_1 and B_2 are not symmetrical. When $V_2 = V_1$, by the foregoing formulae the two clocks appear to the respective distant observers to agree.

11. ALTERATION OF LENGTHS

Consider a rod at rest relative to B_2, situated at B_2 and pointing in the direction of B_2's motion. Let its length be l'' to B_2. This means that for any two events at its two extremities, $\Delta\rho'' = l''$ whatever the value of $\Delta\tau''$. Consider in particular two such events which are simultaneous to B_1. Then, corresponding to $\Delta\rho'' = l''$, we have $\Delta\tau' = 0$, $\Delta\rho' = l'$. Hence by (41),

$$l'' = \frac{1 - V_1V_2/c^2}{1 - V_2^2/c^2}\,l'.$$

Then if $V_2 > V_1$, we have $l'' > l'$, or B_1 sees the rod at B_2 contracted as compared with its measure to B_2.

Consider next a rod at rest relative to B_1, pointing in the direction of B_1's motion and situated at B_1. Let its length be l' to B_1. This means that for any two events at its two extremities, $\Delta\rho' = l'$ whatever the value of $\Delta\tau'$. Consider in particular two such events simultaneous for B_2. Then, corresponding to $\Delta\rho' = l'$, we have $\Delta\tau'' = 0$, $\Delta\rho'' = l''$. Hence by (44)

$$l' = \frac{1 - V_1V_2/c^2}{1 - V_1^2/c^2}\,l''.$$

Thus if as before $V_2 > V_1$, we have $l' < l''$, or B_2 sees the rod at B_1 expanded as compared with its measure to B_1. This difference of apparent behaviour of rods at B_2 and B_1 again arises from the lack of symmetry between B_2 and B_1. When $V_1 = 0$, $V_2 = V$, the results reduce to those of § 6.

12. ONE-DIMENSIONAL VELOCITY TRANSFORMATION

By (41) and (42), the transformation of a velocity $u' = d\rho'/d\tau'$, as observed by B_1, into B_2's measures of the same velocity is given by

$$u'' = \frac{d\rho''}{d\tau''} = \frac{d\rho' - V'_{12}d\tau'}{d\tau' - V'_{12}d\rho'/c^2} = \frac{u' - V'_{12}}{1 - u'V'_{12}/c^2}. \tag{49}$$

As before (§ 7), where we connected B_1's velocity measures with A's, the velocity measures made by B_1 and B_2 are connected by Einstein's velocity formulae, which are thus seen to be more general than the classical Lorentz formulae from which they were originally obtained.

13. TRANSITIVENESS OF THE VELOCITY FORMULAE

The modified Lorentz formulae we have obtained lead in an obvious notation to the relations

$$(\tau''' - \alpha'''_{32} + \rho'''/c)\,(1 - V_3^2/c^2)^{\frac{1}{2}}\,(1 - V'''_{32}/c)^{\frac{1}{2}} = (\tau'' - \alpha''_{21} + \rho''/c)\,(1 - V_2^2/c^2)^{\frac{1}{2}}\,(1 - V''_{23}/c)^{\frac{1}{2}}, \tag{50}$$

and

$$(\tau''' - \alpha'''_{32} - \rho'''/c)\,(1 - V_3^2/c^2)^{\frac{1}{2}}\,(1 + V'''_{32}/c)^{\frac{1}{2}} = (\tau'' - \alpha''_{21} - \rho''/c)\,(1 - V_2^2/c^2)^{\frac{1}{2}}\,(1 + V''_{23}/c)^{\frac{1}{2}}. \tag{51}$$

Combining with (48) and (48′), we get

$$(\tau''' - \alpha'''_{32} + \rho'''/c)\,(1 - V_3^2/c^2)^{\frac{1}{2}} = (\tau' - \alpha'_{12} + \rho'/c)\,(1 - V_1^2/c^2)^{\frac{1}{2}} \left[\frac{1 - V''_{23}/c}{1 - V''_{32}/c}\right]^{\frac{1}{2}} \left[\frac{1 - V''_{21}/c}{1 - V'_{12}/c}\right]^{\frac{1}{2}}, \tag{52}$$

with a similar relation in which $-\rho'''$ and $-\rho'$ replace ρ''' and ρ' respectively, with associated changes of sign in the velocity factors. But by direct passage from B_1's measures to B_3's measures,

$$(\tau''' - \alpha'''_{32} + \rho'''/c)\,(1 - V_3^2/c^2)^{\frac{1}{2}}\,(1 - V'''_{31}/c)^{\frac{1}{2}} = (\tau' - \alpha'_{12} + \rho'/c)\,(1 - V_1^2/c^2)^{\frac{1}{2}}\,(1 - V'_{13}/c)^{\frac{1}{2}}. \tag{52′}$$

Comparing (52) with (52′), we have

$$\frac{1 - V''_{23}/c}{1 - V''_{32}/c} \cdot \frac{1 - V''_{21}/c}{1 - V''_{12}/c} = \frac{1 - V'_{13}/c}{1 - V'''_{31}/c}. \tag{53}$$

so that, omitting now the primes

$$\frac{1 - V_{23}/c}{1 + V_{23}/c} = \frac{1 - V_{31}/c}{1 + V_{31}/c} \cdot \frac{1 - V_{12}/c}{1 + V_{12}/c}. \tag{54}$$

The complementary formulae in the $-\rho$'s give the same result. These are well-known relations in the Einstein theory, and are here extended to absolute motions in the subtratum.

14. FORM OF INTERVAL

If we multiply together corresponding sides of equations (48) and (48′), we obtain

$$[(\tau'' - \alpha''_{21})^2 - \rho''^2/c^2]\,(1 - V_2^2/c^2) = [(\tau' - \alpha'_{12})^2 - \rho'^2/c^2]\,(1 - V_1^2/c^2), \tag{55}$$

and similarly by taking differentials before multiplying

$$(d\tau''^2 - d\rho''^2/c^2)\,(1 - V_2^2/c^2) = (d\tau'^2 - d\rho'^2/c^2)\,(1 - V_1^2/c^2). \tag{56}$$

These relations suggest the conjecture that if we extend our analysis to three dimensions, using a private Euclidean space for each observer, we shall get

$$[(\tau'' - \alpha''_{21})^2 - \Sigma x''^2/c^2]\,(1 - V_2^2/c^2) = [(\tau' - \alpha'_{12})^2 - \Sigma x'^2/c^2]\,(1 - V_1^2/c^2), \tag{57}$$

and

$$(d\tau''^2 - \Sigma dx''^2/c^2)\,(1 - V_2^2/c^2) = (d\tau'^2 - \Sigma dx'^2/c^2)\,(1 - V_1^2/c^2). \tag{58}$$

These would yield for the modified transverse Lorentz formulae

$$y''^2\,(1 - V_2^2/c^2) = y'^2(1 - V_1^2/c^2), \tag{59}$$

as replacing the usual $y'' = y'$ of the classical Lorentz theory.

We shall confirm this suggestion by direct investigation in a moment. In the meantime we note that the foregoing relations will enable us to define an invariant interval ds^2 by the relation

$$ds^2 = (1 - V^2/c^2)(d\tau^2 - \Sigma dx^2/c^2), \tag{60}$$

where (τ, x, y, z) are the epoch and co-ordinates used by an observer moving relative to the substratum with the absolute velocity V. This ensures that a light-wave spreading out from the moving particle observer remains a sphere both to the moving observer and to the stationary observer with whom the moving observer coincides at the instant of emission, i.e. will remain a sphere in any Galilean frame. But the magnitude of the interval depends on the absolute velocity of the observer. The upshot of this appears to be that optical phenomena will be the same on the present theory as on the classical theory.

15. THREE-DIMENSIONAL ANALYSIS

Let A be a fundamental observer, B a semi-equivalent observer in uniform motion with respect to A with velocity V in τ-measure; B carries with him a Galilean frame. Let A and B adopt private Euclidean spaces. Observer A is to locate an event E by means of signals leaving A at epoch τ_1 and returning to A at epoch τ_4, all by A's clock; E is not necessarily on the line AB. Observer B locates the same event E by means of signals departing and returning at epochs τ_2', τ_3' by B's clock, which of course agrees with the clock of the fundamental particle with which it is momentarily coincident. A and B then make the diagrams in their respective spaces: shown in figure 3. The essence of the analysis which follows is that each observer uses *one* of the 'flank' observations of the other observer to complete his location of the event. For symmetry in the algebra, *both* 'flank' observations are used, and we have then to ensure consistency.

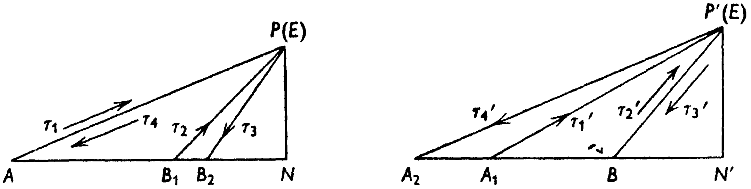

FIGURE 3

Observer A assigns an epoch τ and co-ordinates x, y to event E to satisfy

$$x^2 + y^2 = c^2(\tau - \tau_1)^2 \tag{61}$$

$$x^2 + y^2 = c^2(\tau_4 - \tau)^2, \tag{62}$$

$$[x - V(\tau_2 - \alpha)]^2 + y^2 = c^2(\tau - \tau_2)^2, \tag{63}$$

$$[x - V(\tau_3 - \alpha)]^2 + y^2 = c^2(\tau_3 - \tau)^2. \tag{64}$$

Similarly B assigns an epoch τ' and co-ordinates x', y' to E to satisfy

$$[x'+V(\tau_1'-\alpha)]^2+y'^2 = c^2(\tau'-\tau_1')^2, \tag{65}$$

$$[x'+V(\tau_4'-\alpha)]^2+y'^2 = c^2(\tau_4'-\tau')^2, \tag{66}$$

$$x'^2+y'^2 = c^2(\tau'-\tau_2')^2, \tag{67}$$

$$x'^2+y'^2 = c^2(\tau_3'-\tau')^2. \tag{68}$$

But since the suffixes 2, 3 relate to events at B, we have

$$\tau_2' = \tau_2, \tag{69}$$

$$\tau_3' = \tau_3, \tag{69}$$

and since the suffixes 1, 4 relate to events at A, we have by (14)

$$\tau_1-\alpha = (\tau_1'-\alpha)(1-V^2/c^2), \tag{70}$$

$$\tau_4-\alpha = (\tau_4'-\alpha)(1-V^2/c^2). \tag{70'}$$

We may regard the observation of τ_3' and so the introduction of τ_3 and τ_3' as redundant. Excluding relations containing τ_3 or τ_3' we have nine relations from which we may eliminate the observations τ_1, τ_4, τ_2' and the associated epochs at a distance τ_1', τ_4', τ_2. This leaves three relations determining the three relations of transformation connecting x, y, τ with x', y', τ'.

We have from (63)

$$y^2/c^2 = [(\tau-\alpha)-(\tau_2-\alpha)+x/c-(V/c)(\tau_2-\alpha)] \times [(\tau-\alpha)-(\tau_2-\alpha)-x/c+(V/c)(\tau_2-\alpha)]. \tag{71}$$

But from (69) and (67),

$$\tau_2-\alpha = \tau_2'-\alpha = (\tau'-\alpha)-(x'^2+y'^2)^{\frac{1}{2}}/c.$$

Hence from (71)

$$y^2/c^2 = [(\tau-\alpha+x/c)-(1+V/c)(\tau'-\alpha-(x'^2+y'^2)^{\frac{1}{2}}/c)] \times [(\tau-\alpha-x/c)-(1-V/c)(\tau'-\alpha-(x'^2+y'^2)^{\frac{1}{2}}/c]. \tag{72}$$

Similarly from (64)

$$y^2/c^2 = [(\tau_3-\alpha)-(\tau-\alpha)+x/c-(V/c)(\tau_3-\alpha)] \times [(\tau_3-\alpha)-(\tau-\alpha)-x/c+(V/c)(\tau_3-\alpha)]. \tag{73}$$

But from (69′) and (68),

$$\tau_3-\alpha = \tau_3'-\alpha = (\tau'-\alpha)+(x'^2+y'^2)^{\frac{1}{2}}/c.$$

Hence from (73),

$$y^2/c^2 = [(-(\tau-\alpha)+x/c)+(1-V/c)(\tau'-\alpha+(x'^2+y'^2)^{\frac{1}{2}}/c)] \times [(-(\tau-\alpha)-x/c)+(1+V/c)(\tau'-\alpha+(x'^2+y'^2)^{\frac{1}{2}}/c]. \tag{74}$$

Subtracting (72) and (74), we find on some simplification that $(x'^2+y'^2)^{\frac{1}{2}}/c$ divides out, and we are left with

$$\tau'-\alpha = \frac{\tau-\alpha-Vx/c^2}{1-V^2/c^2}. \tag{75}$$

To get a second relation involving τ, x, τ', x' is a little more troublesome. From (65) we have

$$y'^2/c^2 = [(\tau'-\alpha)-(\tau_1'-\alpha)-x'/c-(V/c)(\tau_1'-\alpha)] \\ \times[(\tau'-\alpha)-(\tau_1'-\alpha)+x'/c+(V/c)(\tau_1'-\alpha)], \qquad (76)$$

But from (70) and (61),

$$\tau_1'-\alpha = \frac{\tau_1-\alpha}{1-V^2/c^2} = \frac{\tau-\alpha-(x^2+y^2)^{\frac{1}{2}}/c}{1-V^2/c^2}.$$

Hence from (76),

$$y'^2/c^2 = \left[\tau'-\alpha-\frac{x'}{c}-\frac{(\tau-\alpha)-(x^2+y^2)^{\frac{1}{2}}/c}{1-V/c}\right]\left[\tau'-\alpha+\frac{x'}{c}-\frac{(\tau-\alpha)-(x^2+y^2)^{\frac{1}{2}}/c}{1+V/c}\right]. \qquad (77)$$

Similarly from (66)

$$y'^2/c^2 = [(\tau_4'-\alpha)-(\tau'-\alpha)+x'/c+(V/c)(\tau_4'-\alpha)] \\ \times[(\tau_4'-\alpha)-(\tau'-\alpha)-x'/c-(V/c)(\tau_4'-\alpha)]. \qquad (78)$$

But from (70) and (62)

$$\tau_4'-\alpha = \frac{\tau_4-\alpha}{1-V^2/c^2} = \frac{(\tau-\alpha)+(x^2+y^2)^{\frac{1}{2}}/c}{1-V^2/c^2}.$$

Hence from (78)

$$y'^2/c^2 = \left[-(\tau'-\alpha)+\frac{x'}{c}+\frac{(\tau-\alpha)+(x^2+y^2)^{\frac{1}{2}}}{1-V/c}\right]\left[-(\tau'-\alpha)-\frac{x'}{c}+\frac{(\tau-\alpha)+(x^2+y^2)^{\frac{1}{2}}/c}{1+V/c}\right]. \qquad (79)$$

Subtracting (79) and (77) we find on some simplication that $(x^2+y^2)^{\frac{1}{2}}/c$ divides out and we are left with

$$(\tau-\alpha) = (\tau'-\alpha)+Vx'/c^2. \qquad (80)$$

Relations (75) and (80) give the transformations from (τ, x) to (τ', x') in the three-dimensional case. Solving them for x' and $\tau'-\alpha$ in terms of x and $\tau-\alpha$ we get

$$x' = \frac{x-V(\tau-\alpha)}{1-V^2/c^2} \qquad (81)$$

and

$$\tau'-\alpha = \frac{\tau-\alpha-Vx/c^2}{1-V^2/c^2}. \qquad (81')$$

These are precisely of the form (26) and (26') with the abscissae x and x' replacing ρ and ρ'. Our modified one-dimensional Lorentz formulae (formulae for semi-equivalence) therefore persist in the three-dimensional case.

Take now any of the four relations (72), (74), (77) and (79) and use (81) and (81'), first rewriting (81) and (81') in the forms

$$\tau'-\alpha+\frac{x'}{c} = \frac{\tau-\alpha+x/c}{1+V/c}, \qquad (82)$$

$$\tau'-\alpha-\frac{x'}{c} = \frac{\tau-\alpha-x/c}{1-V/c}. \qquad (82')$$

For example, take (72). We get

$$y^2 = (1-V^2/c^2)[x'+(x'^2+y'^2)^{\frac{1}{2}}][-x+(x'^2+y'^2)^{\frac{1}{2}}] \\ = (1-V^2/c^2)y'^2. \qquad (83)$$

Relation (74) gives the same result. Or, taking, for example, (77), we get

$$y'^2 = \frac{1}{1-V^2/c^2}[-x+(x^2+y^2)^{\frac{1}{2}}][x+(x^2+y^2)^{\frac{1}{2}}]$$
$$= y^2/(1-V^2/c^2). \tag{83'}$$

Relation (79) gives the same result. Thus all our relations are self-consistent, and give

$$y = (1-V^2/c^2)^{\frac{1}{2}}y'. \tag{84}$$

Hence for two observers B_1 and B_2 we shall get

$$y = (1-V_1^2/c^2)^{\frac{1}{2}}y' = (1-V_2^2/c^2)y'', \tag{85}$$

as anticipated in § 14.

Relation (84) for the transverse co-ordinates completes the set of modified Lorentz formulae for semi-equivalence. Its derivation shows how far from obvious is the usual transverse Lorentz formula in t-measures, namely $y = y'$, which is often assumed without proof.

16. TRANSVERSE VELOCITY TRANSFORMATIONS

We have, if v, v' denote transverse velocity components of a moving particle as observed by A or B, in τ-measures,

$$v' = \frac{dy'}{d\tau'} = \frac{dy(1-V^2/c^2)^{-\frac{1}{2}}}{(d\tau - V dx/c^2)(1-V^2/c^2)^{-1}} = \frac{v(1-V^2/c^2)^{\frac{1}{2}}}{1-uV/c^2}. \tag{86}$$

Once again we have Einstein's transverse velocity transformation. Again, for transformation of a transverse velocity component from B_1's measures to B_2's measures, we get from (85), (42) and (43)

$$v'' = \frac{dy''}{d\tau''} = \frac{(1-V_1^2/c^2)^{\frac{1}{2}}}{(1-V_2^2/c^2)^{\frac{1}{2}}}\frac{dy'}{d\tau''} = \frac{(1-V_1^2/c^2)^{\frac{1}{2}}}{(1-V_2^2/c^2)^{\frac{1}{2}}}\frac{dy'}{d\tau'}\frac{1-V_2^2/c^2}{1-V_1V_2/c^2}\frac{1}{1-u'V'_{12}/c^2}$$
$$= \frac{(1-V_1^2/c^2)^{\frac{1}{2}}(1-V_2^2/c^2)^{\frac{1}{2}}}{(1-V_1V_2/c^2)(1-u'V'_{12}/c^2)}v' = \frac{(1-V'^2_{12}/c^2)^{\frac{1}{2}}}{1-u'V'_{12}/c^2}v', \tag{87}$$

which is just Einstein's velocity transformation for the transverse components, for passage from a Galilean frame B_1 to a Galilean frame B_2 moving with uniform velocity V'_{12} relative to B_1.

17. FORMULA FOR THE DOPPLER EFFECT IN τ-MEASURE

Let a beam of light-waves of frequency ν' leave a particle B (receding with velocity V) at time τ', and reach a distant observer A at time τ_2 as a beam of frequency ν_2. Let ρ be the distance of B from A as measured by A at the local epoch τ'. Then if τ is A's attribution of epoch to the event of despatch of the light-waves, we have

$$\tau' = \tau,$$

and

$$\tau_2 = \tau + \rho/c.$$

Hence $$\frac{d\tau_2}{d\tau} = 1+\frac{1}{c}\frac{d\rho}{d\tau} = 1+\frac{V}{c}.$$

But $$\nu' d\tau' = \nu_2 d\tau_2.$$

Hence the Doppler shift ratio, as observed by A, is

$$\frac{\lambda_2}{\lambda'} = \frac{\nu'}{\nu_2} = \frac{d\tau_2}{d\tau'} = \frac{d\tau_2}{d\tau} = 1+\frac{V}{c}. \tag{88}$$

This should be contrasted with the formula for the Doppler effect in t-measure, which is

$$\frac{\lambda_2}{\lambda'} = \left(\frac{1+V/c}{1-V/c}\right)^{\frac{1}{2}}. \tag{89}$$

The corresponding formula for the Doppler effect at B when B observes a beam emitted by A is obtained as follows. Let the beam leave A at epoch τ_1, and reach B at epoch τ'. If ρ is the distance of B from A at epoch τ', in A's measures, then according to A's calculations

$$\tau = \tau_1 + \rho/c.$$

Hence $$1 = \frac{d\tau_1}{d\tau}+\frac{1}{c}\frac{d\rho}{d\tau} = \frac{d\tau_1}{d\tau}+\frac{V}{c}.$$

But $$\nu' d\tau' = \nu_1 d\tau_1,$$

and $$\tau' = \tau.$$

Hence the Doppler-shift ratio as observed at B is

$$\frac{\lambda'}{\lambda_1} = \frac{\nu_1}{\nu'} = \frac{d\tau'}{d\tau_1} = \frac{d\tau}{d\tau_1} = \frac{1}{1-V/c}. \tag{90}$$

As is to be expected, since A and B are not symmetrical, (88) differs from (90), though they agree with one another and with the t-measure formula to the first order. Clearly (90) is the formula that should be used in connexion with observations within the solar system of the spectra of nuclei of extra-galactic nebulae.

18. This paper has confined itself to the *kinematics* of Galilean frames. It is hoped in a later paper to apply the results to *dynamics*.

REFERENCE

Milne, E. A. 1948 *Kinematic relativity.* Oxford: Clarendon Press. *Note.* This volume contains a bibliography of kinematic relativity, but itself summarizes all the relevant investigations.

The dynamics of the combustion products behind plane and spherical detonation fronts in explosives

By Sir Geoffrey Taylor, F.R.S.

(*Received* 16 *August* 1949)

The flow behind the detonation front of an explosive contained in a tube strong enough to confine the motion to one dimension is shown to be a progressive wave of finite amplitude of the type studied by Riemann. The wave is similar at all stages of its progress if the initiation of the explosion is instantaneous, the linear scale of the whole field of flow increasing at a uniform rate. If the products of combustion obey the law $p\rho^{-\gamma}$ = constant the distribution of gas velocity along the tube is linear. If the initiation end of the tube is closed a fixed proportion of the whole detonating column is at rest.

This last case has an analogy in three dimensions. The dynamics of spherical detonation from a point in an explosive is analyzed. As in the one-dimensional case, a fixed proportion of the whole volume of burnt gas is at rest. The radial rate of change of the variables, velocity, pressure and density become infinite at the detonation front, but it is unlikely that this result would be true in a real explosive where the time of reaction is not zero.

The results are applied in both linear and spherical cases to the detonation of T.N.T., using data given by Jones & Miller (1948).

Introduction

The existing hydrodynamical and chemical theory of detonation has been developed by supposing that the whole chemical reaction in the explosive takes place within a narrow region, the explosive being at rest before this thin detonation front reaches it. The equations of continuity, momentum and energy when applied to the two sides of the front, together with an equation of state for the products of decomposition, do not suffice to determine the five unknowns: U, u_1, p_1, ρ_1, T_1. Here U is the velocity of the detonation front, u_1, p_1, ρ_1 and T_1, are the velocity, the pressure, density and temperature of the gas close behind the front. A fifth equation is needed, and it is clear that this equation must in some way represent the reaction of the gas streaming away behind the front on the gas immediately behind it. That this must be so can be seen by imagining the case where a rigid plane moves forward behind the detonation front confining the burnt gas between it and the front. If this plane were to move fast enough it must be able to increase the value of U beyond the value found when the burnt gas can escape freely.

The Chapman-Jouget condition

To determine the fifth condition, therefore, it might be thought that it would be necessary to study the movement behind the detonation wave. The necessity for doing this, however, has been avoided by making the hypothesis that small disturbances in the gas immediately behind the detonation front travel at the same speed, U, as the front itself. The equation representing this hypothesis is

$$U = u_1 + c_1, \tag{1}$$

where c_1 is the velocity of sound in the gas immediately behind the front.

The progressive wave behind the detonation front

Though this hypothesis, which was applied in the first instance in different forms by Chapman (1899) and Jouguet (1905–6), has been confirmed indirectly by experiment, and has formed the basis of much fruitful work on explosives, no one before the late war seems to have discussed the hydrodynamics of the burnt gas and the distribution of pressure behind the detonation front. Consider the detonation of explosive contained in a tube so strong that the motion is confined to one dimension. The motion of a gas for which ρ is a function of p only has been completely analyzed by Riemann, so that if u and p are known at all points at one instant they are known at all other times. Riemann's analysis is a generalization to disturbances of finite amplitude of the simple analysis of arbitrary small disturbances in one dimension into two sound waves moving in opposite directions. When only one wave is present* the analysis is very simple and u is found to be a function of ρ only, as it is in the limiting case of a progressive sound wave, which moves in one direction only. In fact, a progressive wave of finite amplitude may be regarded as being composed of an infinite number of superposed infinitesimal progressive sound waves. Each of these sound waves changes p, ρ and u, so that

$$\delta p = \rho c \delta u = c^2 \delta \rho, \tag{2}$$

where c is the velocity of sound through the gas when its density is ρ. Since the sound waves are superposed, a change in u is always associated with the change in ρ given by (2), and since c also is a function of ρ only, u is found by integrating (2). Thus

$$u - u_1 = \int_{\rho}^{\rho_1} c \frac{d\rho}{\rho}. \tag{3}$$

Since small disturbances are propagated relative to fixed axes with velocity $u+c$ it will be seen that if p, ρ and u are known at one point P at one instant, they will have the same value at time t later at a point distant $(u+c)\,t$ from P. It will be seen therefore that a progressive wave of finite amplitude can exist behind a detonation front provided that the Chapman-Jouguet condition (1) is satisfied and the conditions behind the detonation front remain constant as the front progresses. Except for the point immediately behind the detonation front where the velocity and density are fixed by the detonation conditions, u can have any arbitrary distribution at one given instant, and the Riemann analysis will determine the motion at all subsequent times till a shock wave appears somewhere in the field. On the other hand, when the wave has progressed a distance which is large compared with the initial length in which detonation is being built up, it will tend to a definite limiting form. This may most conveniently be illustrated by plotting u against r/R or r/Ut, where r is the distance from the point of initiation. The limiting ordinates in this curve are 0 and 1, and the initial portion where the steady detonation conditions had not been attained continually shrinks into the region near $r/R = 0$ as t increases. The limiting form to which the disturbance tends as it increases is that which occurs at all times if the explosive is at rest and detonation starts instantaneously at time $t = 0$ at a point $r = 0$. This form will be discussed in two cases.

---

* This case was investigated as early as 1858 by Earnshaw (1860).

Case of gas for which $p\rho^{-\gamma}$ is constant

In this case
$$c = c_1\left(\frac{\rho}{\rho_1}\right)^{\frac{1}{2}(\gamma-1)}. \tag{4}$$

Inserting (4) in (3) and integrating
$$u = u_1 - \frac{2c_1}{\gamma-1}\left\{1-\left(\frac{\rho}{\rho_1}\right)^{\frac{1}{2}(\gamma-1)}\right\}. \tag{5}$$

It will be noticed that u and c are linearly related, so also are u and $u+c$, in fact
$$u+c = u_1+c_1-\frac{\gamma+1}{2}(u_1-u). \tag{6}$$

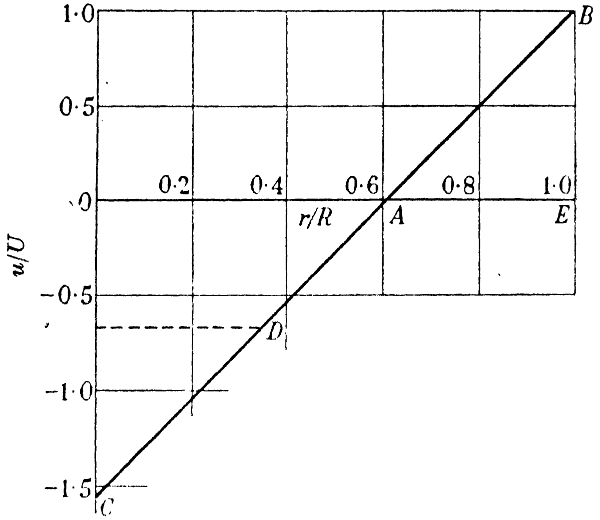

FIGURE 1. Distribution of velocity behind a plane detonation front when $p\rho^{-1\cdot 3}$ = constant.

If the distribution of u or c in space at any time is plotted against $r = (u+c)t$ a straight line will result. Figure 1 shows a particular case in which the conditions at the detonation front were such that $u_1 = \frac{1}{3}U$ and $c = \frac{2}{3}U$. If the detonation starts at one end $r = 0$ of a tube the gas velocity, u_2 at this end is found by setting $u+c = 0$ in (6), hence
$$u_2 = u_1 - \frac{2}{\gamma+1}(u_1+c_1), \tag{7}$$

and since $\gamma > 1$, u_2 must be negative, so that the gas flows backwards from the ignition point as would be expected. u_2 is represented in figure 1 by the point C. In this discussion it has been assumed that the gas can flow freely backwards through the end of the tube. It may happen that the pressure in the atmosphere outside the tube is greater than that calculated using the equation $p\rho^{-\gamma} = p_1\rho_1^{-\gamma}$. In that case a solution of the problem is found by assuming that u and p decrease with distance from the detonation front in accordance with the calculation for a Riemann progressive wave. At the point, D, in the tube where the outside atmospheric pressure is reached, the velocity becomes constant and remains constant between D and the end of the tube. A special case of some interest is when the rear end of the tube is blocked up so that $u = 0$. In that case the gas is at rest between the end and the point A, figure 1, where the line BAC cuts the axis $u = 0$. To find the ratio of the length of the portion where the gas is at rest to the whole column, i.e. OA/OE in figure 1, set $u = 0$ in (6). The ratio is

$$\frac{c}{U} = \frac{u_1+c_1}{U} - \frac{\gamma+1}{2U}u_1 = 1 - \frac{\gamma+1}{2}\left(\frac{u_1}{U}\right). \tag{8}$$

In the particular case when $u_1 = \frac{1}{4}U$ it is $1 - \frac{1}{8}(\gamma+1)$, which is 0·616 when $\gamma = 1{\cdot}3$. This is the case shown in figure 1.

It is worth noticing that when the end of the tube is open the condition $u+c = 0$ which has been applied there is the same as Reynold's condition when air at high pressures flows through a constriction in a tube. The speed at this point is equal to the speed of sound there.

Determination of detonation velocity

In the hydrodynamical theory of detonation, a detonation front is assumed to move with uniform velocity U into a stationary explosive. The equations which represent the conservation of mass, momentum and energy are

$$\rho_1(U-u_1) = \rho_0 U \qquad \text{(mass)}, \tag{9}$$

$$p_1+\rho_1(U-u_1)^2 = p_0+\rho_0 U^2 \quad \text{(momentum)}, \tag{10}$$

$$\frac{p_1}{\rho_1}+\tfrac{1}{2}(U-u_1)^2-E_1 = \frac{p_0}{\rho_0}+\tfrac{1}{2}U^2-E_0 \quad \text{(energy)}. \tag{11}$$

E_0 and E_1 are the chemical plus heat energies per unit mass, p_1, ρ_1, u_1 and p_0, ρ_0, 0, are the pressures, densities and velocities on the two sides before and after passing the shock wave.

Eliminating U and u_1 between (9), (10) and (11) the Rankine-Hugoniot equation is obtained, namely,

$$\tfrac{1}{2}(p_1+p_0)\left(\frac{1}{\rho_0}-\frac{1}{\rho_1}\right) = E_0 - E_1. \tag{12}$$

$E_1 - E_0$ may be regarded as known if p_1, ρ_1 and T_1 the temperature, are known. T_1 can be eliminated by using the equation of state, thus (12) may be regarded as a single equation between p_1 and ρ_1. If this relationship between p_1 and ρ_1 is exhibited as a curve on a diagram for which p_1 is the ordinate and $1/\rho_1$ the abscissa the curve so formed is called the Rankine-Hugoniot curve. The initial condition of the explosive is represented by the point $(p_0, 1/\rho_0)$. The Chapman-Jouguet condition is satisfied by the point on the Rankine-Hugoniot curve where the tangent from the point $(p_0, 1/\rho_0)$ touches it. Eliminating u_1 from (9) and (10) it is found that

$$U^2 = \frac{p_1-p_0}{1/\rho_0-1/\rho_1}, \tag{13}$$

and this is equal to $\tan\theta$, where θ is the angle which the tangent line described above makes with the abscissa axis. The velocity, U, which corresponds with the point on the Rankine-Hugoniot curve which satisfies the Chapman-Jouguet condition is therefore the minimum of all the velocities which are possible. The computation of the Rankine-Hugoniot curve in any particular case is complicated because the relationships between energy, temperature, pressure and density depend on the chemical composition of the constituents of the burnt gas. If these are in chemical equilibrium the composition of the mixture depends on temperature which is only known when the problem has been solved. It is therefore necessary to make a number of subsidiary calculations to find the compositions corresponding with a number of points on the Rankine-Hugoniot curve. In the case of certain mixtures (see Lewis & Friauf 1930) of oxygen and hydrogen with excess oxygen, hydrogen or nitrogen the calculations have been carried out, and the velocity of detonation found. The observed velocities agree well with those so calculated.

Application to T.N.T.

The calculations for the products of detonation of T.N.T. packed to density $\rho_0 = 1{\cdot}51$ have been performed by Jones & Miller (1948), who found $U = 6380$ m./sec., $u_1/U = 0{\cdot}2424$, $\rho_1 = 2{\cdot}00$. Jones also calculated the succession of equilibrium compositions and energies and also p and ρ as they change during an isentropic expansion after detonation. His results* are here given in the first three columns of table 1 and in columns 4, 7 and 8 of table 2. The data are therefore available for calculating the pressure distribution and gas flow in a tube sufficiently strong to withstand detonation of T.N.T.

TABLE 1. MOTION BEHIND PLANE DETONATION WAVE IN T.N.T. IN A CLOSED TUBE

$p \times 10^{-10}$ (dynes/sq.cm.)	$v\ (=1/\rho)$ (cm.^{3}/g.)	c/U	u/U	r/R
15	0·5	0·757	0·242	1·00
14	0·513	0·735	0·225	0·960
12	0·542	0·715	0·187	0·902
10	0·574	0·705	0·147	0·852
9	0·591	0·700	0·129	0·829
7	0·629	0·687	0·085	0·772
5	0·676	0·625	0·034	0·659
4	0·710	0·571	0·006	0·577
3·8	—	0·550	0	0·577
3·8	—	0·550	0	0·550

$U = 6380$ m./sec. Density of T.N.T. 1·51.

The results of using Jones's data in integrating (3) numerically to find u are given in column 4 of table 2 and the corresponding value of $c = (dp/d\rho)^{\frac{1}{2}}$ are given in column 3 of table 1. If R is the total distance through which the detonation has travelled since it was initiated, we have seen that p, ρ and u are functions at any time of $(u+c)$ only. At all times, therefore, they are functions of $\frac{u+c}{U} = \frac{(u+c)t}{R}$ or r/R only. The values of r/R are given in column 5 of table 1.

---

* The figures given in columns 4, 7 and 8 of table 2 and in columns 1 and 2 of table 1 are taken from an unpublished report by H. Jones to the Ministry of Home Security. They are not identical with the revised figures published by Jones & Miller in table 3, p. 497 of their 1948 paper but the difference was not thought to be sufficiently great to warrant the recalculation of the spherical detonation wave.

These results are plotted in figure 2. The broken curve representing the calculated values of u/U is no longer straight, as it was for a gas in which $p\rho^{-\gamma}$ is constant, but the curve has the characteristic that $u = 0$ at a value of r/R which in this case is 0·550. The calculations have not been carried beyond this point though this could easily be done. The results therefore represent those for a closed tube and they show that in such a tube the pressure is uniform from the point of detonation to $r/R = 0{\cdot}550$ and that it has a value of about $3{\cdot}8 \times 10^{10}$ dynes or 250 tons/sq.in. Beyond that point the pressure rises to that behind the detonation front, namely the value given in Jones's calculations of about 1000 tons/sq.in.

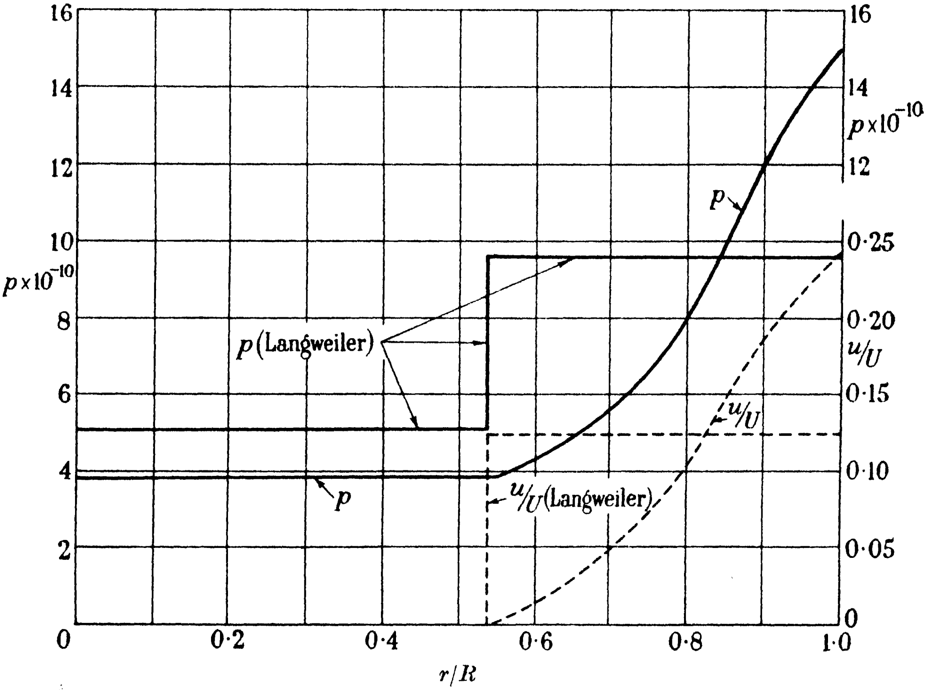

FIGURE 2. Plane detonation wave in T.N.T. (p expressed in dynes/sq.cm.).

Comparison with previous work

In his original paper (1899) Chapman recognized that when detonation occurs in a tube so that the motion is confined to one dimension the detonation wave must be followed by a region of forward-moving gas and that the length of this region must continually increase. The only attempt which has been made to calculate this length seems to be that of Langweiler (1938) who assumed that the burnt gases preserve the velocity u_1 which they acquire at the detonation front until the passage of a rarefaction shock wave reduces the velocity to zero. Langweiler's distribution of velocity is shown in figure 2 for comparison with the correct distribution. If W is the velocity of the assumed rarefaction shock wave and p_2 the pressure behind it, Langweiler uses equations which are identical with the equations (9) to (11) to determine W and p_2. He recognizes that a rarefaction shock wave cannot occur and he tries to overcome this difficulty by saying that the region of transition where the velocity is reduced from u_1 to 0 may be assumed small compared with the distances travelled by the detonation and rarefaction waves. That this assumption is untrue can be seen by inspection of figure 2, where the transition is shown extending through the whole of the forward-moving column of gas. It has been remarked by many writers that though the Rankine-Hugoniot relation appears at first sight to be applicable both to waves of condensation and to waves of rarefaction, the energy and momentum conditions being satisfied in both cases, yet the fact that there is an irreversible rise in temperature in a condensation wave precludes the possibility of reversing the motion.

Langweiler applied his calculations to T.N.T. of density 1·59. His results are shown in figure 2 for comparison with the present calculations for T.N.T. of density 1·51.

Langweiler considers also the effect of reduction in pressure at the end of the tube below p_2, the pressure which reduces the motion behind the wave to rest and therefore corresponds with a closed end. He states that the effect of this reduction would be to increase the speed of the rarefaction wave, thus reducing the thickness of the forward-moving gas which he calls the detonation head. It will be seen from figure 2 and the discussion which figure 2 illustrates that this is a mistake. Reduction of pressure behind the wave below the value p_2 leaves the forward-moving part of the detonation head unchanged but increases the total thickness of the transition layer till, when the pressure is reduced to a certain calculable value, the transition layer fills the whole tube right back to the point at which the detonation was initiated.

Spherical detonation waves

Detonation conditions in which the burnt gases are constrained to move in one dimension only can be realized experimentally in the case of a gaseous mixture which can be contained in a tube strong enough to resist the bursting pressure. It cannot be completely realized with a high explosive which exerts a pressure so high that any containing tube will burst. If spherical detonation starting from a point inside an explosive is dynamically possible it should be realizable experimentally.

If the arguments so far advanced by writers on the subject to justify the Chapman-Jouguet condition are valid, they should apply to a spherical detonation front provided the hydrodynamic flow conditions are capable of permitting a flow to exist for which $u_1 + c_1 = U$ at a sphere which is expanding with radial velocity U. Progressive spherical waves of finite amplitude analogous to progressive Riemann waves do not exist. To find out whether spherical detonation waves might be expected it is therefore necessary to find out whether it is possible to construct and solve the hydrodynamic equations for radial motion which satisfy the boundary condition $u + c = U$ at a sphere of radius $R = Ut$.

If this could be done, the Chapman-Jouguet condition would apply at the detonation front and the radial velocity U would be identical with that found using equation (12). The maximum pressure and speed of propagation would be the same as those occurring in a plane detonation, but the radial distribution of velocity and pressure would differ from those in the plane case.

The flow behind a spherical detonation wave will in general depend on the manner in which the detonation is set up, but if it could be assumed that detonation starts when the explosion has extended only a short distance from the point of initiation, then a steadily expanding regime would be set up analogous to the one-dimensional wave described in figure 1. In that case the radial velocity u and also p, ρ and c would be functions of r/t only. The equation of motion is

$$\frac{\partial u}{\partial t}+u\frac{\partial u}{\partial r}=-\frac{1}{\rho}\frac{\partial p}{\partial r}, \tag{14}$$

and the condition that u, p and ρ depend only on $x = r/t$ is

$$\left(\frac{\partial}{\partial t}+x\frac{\partial}{\partial r}\right)(u,p,\rho)=0, \tag{15}$$

so that (14) becomes

$$(u-x)\frac{du}{dx}=-\frac{1}{\rho}\frac{dp}{dx}. \tag{16}$$

The equation of continuity is

$$\frac{\partial \rho}{\partial t}+u\frac{\partial \rho}{\partial r}+\rho\left(\frac{\partial u}{\partial r}+\frac{2u}{r}\right)=0, \tag{17}$$

which in view of (15) may be written

$$\frac{u-x}{\rho}\frac{d\rho}{dx}+\frac{du}{dx}+\frac{2u}{x}=0. \tag{18}$$

Writing $c^2 = dp/d\rho$, where c is the velocity of sound, $dp/dx = c^2 d\rho/dx$ so that $d\rho/dx$ may be eliminated between (16) and (18). Hence

$$\frac{du}{dx}\left\{1-\left(\frac{x-u}{c}\right)^2\right\}=-2\frac{u}{x}. \tag{19}$$

At this stage it is of interest to compare (19) with the equivalent equation for detonation waves in one dimension. Equations (15) and (16) are identical in the two cases, the continuity equation differs only from (17) in that the term $2u/r$ is absent in the one-dimensional case. The equation equivalent to (19) is therefore

$$\frac{du}{dx}\left\{1-\left(\frac{x-u}{c}\right)^2\right\}=0. \tag{20}$$

Hence either $du/dx = 0$ or $x = u+c$. The condition $du/dx = 0$, i.e. $u =$ constant, applies over the ranges represented in figure 1 by OA. The condition $x = u+c$ is identical with Riemann's condition in a one-dimensional wave. It applies to the region represented by AB in figure 1.

The adiabatic equation of state gives c as a function of ρ or conversely ρ as a function of c^2, thus in (18) $\frac{1}{\rho}\frac{d\rho}{dx}$ may be written $\frac{1}{\rho}\frac{d\rho}{dc^2}\frac{dc^2}{dx}$, since $\frac{1}{\rho}\frac{d\rho}{dc^2}$ may be regarded as a function of c^2. Equations (18) and (19) determine u and c as functions of x when the appropriate boundary conditions are satisfied.

These equations may be expressed in non-dimensional form in several ways. One method is to write

$$\xi = u/x, \quad \eta = c^2/x^2, \quad Z = \log_e x.$$

The resulting equations are

$$\frac{d\eta}{d\xi} = \frac{2\eta}{\xi} \frac{\eta - (1-\xi)^2 + f\xi(1-\xi)}{3\eta - (1-\xi)^2}, \tag{21}$$

$$\frac{dZ}{d\xi} = -\frac{1}{\xi} \frac{\eta - (1-\xi)^2}{3\eta - (1-\xi)^2}, \tag{22}$$

where

$$f = \frac{\rho}{c^2} \frac{dc^2}{d\rho}. \tag{23}$$

This form is convenient when the burnt gases behave like a perfect gas. In that case

$$\frac{\rho}{c^2} \frac{dc^2}{d\rho^2} = \gamma - 1,$$

so that (21) determines η as a function of ξ.

Another non-dimensional form is obtained by substituting $\eta = \xi^2/\psi^2$ so that $\psi = u/c$. The equations are then

$$\frac{d\psi}{dZ} = \frac{\psi\xi}{(1-\xi)^2 - \xi^2} \{2\xi - (1-\xi)\psi^2 f\}, \tag{24}$$

$$\frac{d\xi}{dZ} = \xi \frac{3\xi^2 - (1-\xi)^2 \psi^2}{(1-\xi)^2 \psi^2 - \xi^2}. \tag{25}$$

Boundary conditions

To solve these equations in any particular case it is necessary to know the adiabatic p, ρ relationship in the burnt gases. $c^2 = dp/d\rho$ and $dc^2/d\rho$ are then calculated in terms of ρ so that f can be tabulated as a function of c.

The Chapman-Jouguet condition, together with the Rankine-Hugoniot equation, determines the detonation velocity U and also the value of $u/U = 1 - 1/\mu$ at the wave front. If R is the radius of the wave at any time $R = Ut$ and $x = r/t$ so that

$$\frac{x}{U} = \frac{r}{R}. \tag{26}$$

Since Z only enters into equations (24) and (25) as a differential its value may be taken as zero at $r = R$ so that

$$Z = \log_e (r/R), \tag{27}$$

$$u/U = \xi r/R, \tag{28}$$

$$c/U = \xi r/(\psi R). \tag{29}$$

If μ is the ratio of the density behind the detonation wave to the density of the explosive then at $r = R$

$$\xi = 1 - 1/\mu. \tag{30}$$

The Chapman-Jouguet condition, namely $u/U + c/U = 1$, gives

$$\psi = \frac{u}{c}\frac{u}{U} = \mu - 1. \tag{31}$$

As an example of the application of these equations the complete description of detonation initiated at a point in the interior of a mass of T.N.T. of density 1·51 has been worked out. The values of μ and U calculated by Dr H. Jones for T.N.T. of this density are $\mu = 1{\cdot}32$, $U = 6380$ m./sec.

The calculated adiabatic relationship between p and ρ, together with the corresponding values of f and c/U, are given in table 2* and the relationship between f and c/U is shown in figure 3.

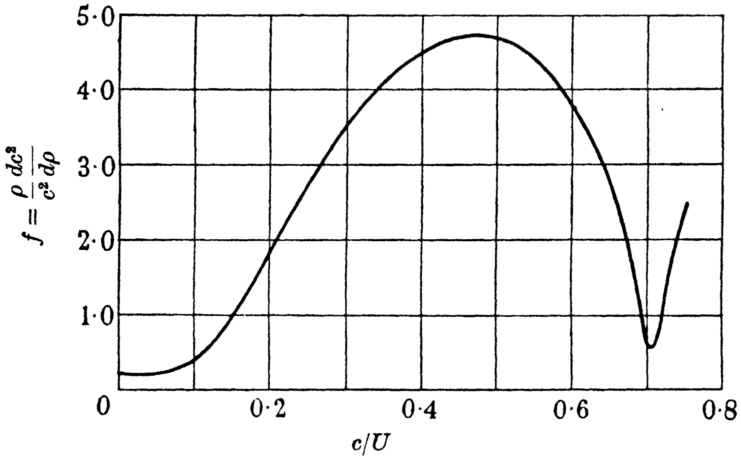

Figure 3

Equations (24) and (25) can only be integrated numerically step by step, starting from the spherical detonation surface and proceeding inwards. When the initial values $\xi = 1 - 1/\mu$, $\psi = \mu - 1$ are inserted in equations (24) and (25) it will be seen that both $d\psi/dZ$ and $d\xi/dZ$ are initially infinite because $(1-\xi)^2\psi^2 - \xi^2 = 0$. $d\psi/d\xi$ is, however, finite. The solution of (25) in the neighbourhood of $\xi = 1 - 1/\mu$ is

$$Z = -\frac{\mu^2}{\mu-1}\left(\tfrac{1}{2} + \tfrac{1}{4}f\right)\left(\frac{\mu-1}{\mu} - \xi\right)^2. \tag{32}$$

This solution may be used to find values of Z corresponding with values of ψ and ξ near the detonation surface. Using (27) to cover the region $r/R = 1{\cdot}0$ to $0{\cdot}9986$ the solution was carried step by step back to the centre by means of equations (19) and (20). At each stage the values of $d\xi/dZ$ and $d\psi/dZ$ were calculated and the increments in ξ and ψ corresponding with a small finite decrement in Z were taken, as first approximation, to be $\delta\psi_0 = (d\psi/dZ)_0\,\delta Z$, $\delta\xi_0 = (d\xi/dZ)_0\,\delta Z$, where $(d\psi/dZ)_0$, $(d\xi/dZ)_0$ represent the values calculated at the beginning of the interval δZ. The values $(d\psi/dZ)_1$, $(d\xi/dZ)_1$ at the end of the interval were then calculated using the approximate values of ξ and ψ thus found. A second approximation to ψ and ξ was then found using the formulae

---

* The range covered in table 2 is limited to values which occur in and behind the detonation wave.

$$\delta\psi = \tfrac{1}{2}\{(d\psi/dZ)_0 + (d\psi/dZ)_1\}\,\delta Z, \quad \delta\xi = \tfrac{1}{2}\{(d\xi/dZ)_0 + (d\xi/dZ)_1\}\,\delta Z.$$

The second approximations to ψ and ξ at the end of the interval were then used in equation (20) to calculate new values of $d\psi/dZ$ and $d\xi/dZ$ and these again were used to calculate a third approximation to ψ and ξ at the end of the interval. This process was repeated till the changes in ψ and ξ at the end of the interval due to proceeding to one further stage of approximation were negligible. The results of the calculations are given in table 2. The distribution of gas velocity is shown in figure 4 and for comparison the distribution in the one-dimensional case is shown in the same figure. Figure 5 shows the distribution of pressure in the spherical and the one-dimensional cases. It will be seen that the pressure and velocity drop very rapidly behind the detonation front. The pressure in fact drops to half its maximum value at a distance behind the front which is only 7½ % of its radius. In this connexion it is worth noticing that photographs taken with a rotating mirror camera of the detonation of a cylindrical charge of T.N.T. show a narrow highly luminous band behind the detonation front, while similar photographs of the detonation of gases in tubes show a much broader luminous region.

TABLE 2. SPHERICAL DETONATION WAVE IN T.N.T.

r/R	ξ	ψ	c/U	f	u/U	$p\times 10^{-10}$	ρ
1·0	0·2424	0·320	0·7575	2·60	0·2424	15·00	2·000
0·99904	0·230	0·3084	0·742	2·06	0·230	14·45	1·972
0·99632	0·220	0·2986	0·733	1·80	0·219	13·90	1·942
0·99271	0·210	0·2874	0·724	1·20	0·208	13·34	1·928
0·9885	0·20	0·2748	0·719	1·00	0·1977	12·68	1·880
0·9821	0·19	0·2612	0·714	0·70	0·1866	12·11	1·850
0·9744	0·18	0·2469	0·710	0·60	0·1754	11·09	1·797
0·9656	0·17	0·2323	0·708	0·60	0·16415	10·59	1·773
0·9557	0·16	0·2177	0·702	0·60	0·1529	9·44	1·709
0·9448	0·15	0·2028	0·700	0·62	0·14172	8·91	1·683
0·9320	0·14	0·1879	0·694	0·80	0·1305	7·94	1·639
0·9178	0·13	0·1737	0·688	1·45	0·1193	7·08	1·595
0·8997	0·12	0·1601	0·675	1·97	0·1080	6·46	1·562
0·8804	0·11	0·1468	0·659	2·52	0·09684	5·875	1·531
0·8577	0·10	0·1337	0·641	3·00	0·08577	5·43$_3$	1·506
0·8275	0·09	0·1205	0·618	3·40	0·07448	4·84	1·468
0·7960	0·08	0·1071	0·596	3·88	0·06368	4·41$_6$	1·440
0·7584	0·07	0·09350	0·568	4·22	0·05309	3·98	1·407
0·7148	0·06	0·07966	0·538	4·50	0·04289	3·56$_5$	1·372
0·6668	0·05	0·06514	0·512	4·65	0·03334	3·23$_6$	1·342
0·6166	0·04	0·05084	0·487	4·72	0·02466	2·95$_1$	1·316
0·5672	0·03	0·03673	0·461	4·74	0·01702	2·66	1·285
0·5186	0·02	0·02327	0·446	4·70	0·01037	2·48	2·265
0·4950	0·015	0·01695	0·441	4·70	0·00741	2·43	1·259
0·4723	0·010	0·01096	0·430	4·66	0·00472	2·34	1·249
0·4474	0·005	0·00527	0·425	4·64	0·00224	2·29	1·244
0·418	0	0	0·418	4·60	0	2·19	1·233

The fact that the velocity drops to zero at some point between the detonation surface and the centre shows that a spherical detonation wave can maintain itself in the particular case investigated. It is not obvious whether this is true in all cases

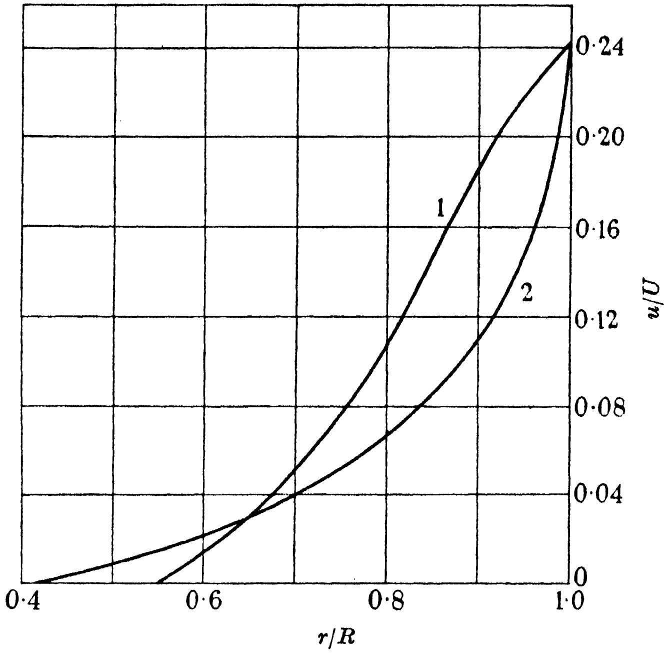

FIGURE 4. Velocity distribution (T.N.T.). Curve 1, plane detonation wave; curve 2, spherical wave.

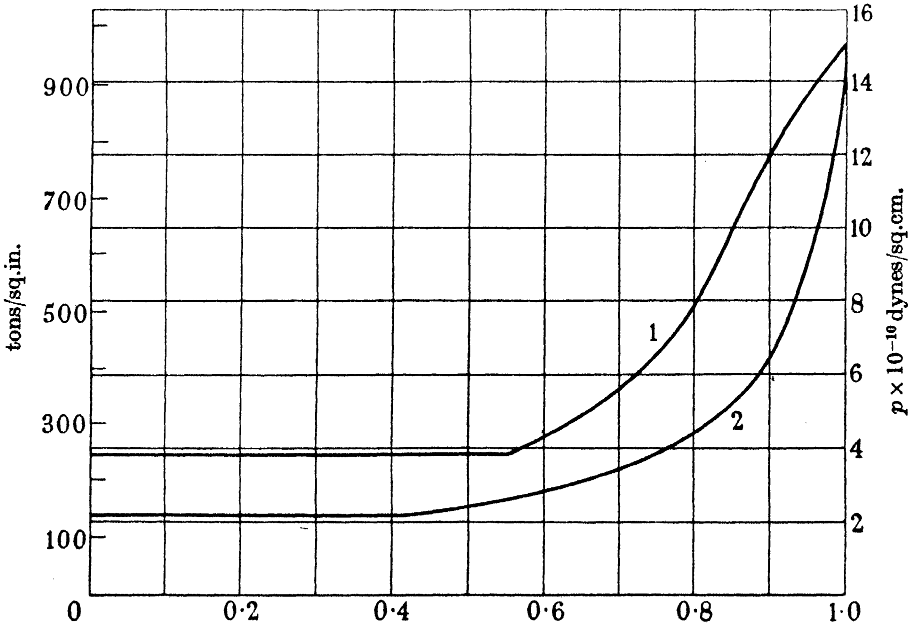

FIGURE 5. Pressure distribution (T.N.T.). Curve 1, plane; curve 2, spherical.

because the equations for the flow behind a spherical wave do not admit of a simple solution of the type obtained by Riemann for a plane wave.

Previous work on spherical detonation waves

The view here put forward is contrary to that expressed by Jouguet (1907) that spherical detonation waves moving with constant speed probably cannot exist. It seems that this view is founded partly on an expression connecting U with u_1+c_1 which shows that if the pressure and velocity decrease with distance behind the detonation front then U must be greater than u_1+c_1. Jouguet rejects all detonation waves for which $U > u_1+c_1$ as being impossible to produce. This rejection, however, is based only on an unproved 'postulate', for which I see no adequate reason. In the present analysis (19) leads to the same conclusion that $U \geqslant u_1+c_1$ for, if du/dx in (19) is positive, $1-\left(\frac{x-u}{c}\right)^2$ must be negative so that $c < x-u$, and, since at the detonation surface $x = U$, $c = c_1$, $u = u_1$, therefore $U > u_1+c_1$. Jouguet states also that his equation, which is analogous to (19), is not consistent with $U = u_1+c_1$. It will be noticed that (19) might have been interpreted in this sense if the possibility that an infinite value of du/dx may occur is rejected. It is true that infinite values of du/dx cannot actually occur in real materials, and in this sense infinitely thin shock waves are not physically possible. The effects predicted by analysis which assumes infinitely thin shock waves are in fact observed, so that it seems probable that the spherical detonation wave calculated in the present paper can be propagated if it can be started. It seems likely that the peak pressure may not be attained though the predicted detonation velocity will be realized in a spherical wave.

The only worker who has experimented with spherical detonation waves seems to be Lafitte (1925) who found that ignition by a spark at the centre of a spherical glass bulb 24 cm. diameter, containing an explosive mixture of CS_2 with $3O_2$ did not produce detonation. When the same mixture was fired by means of a detonator containing 1 g. of fulminate of mercury a spherical detonation wave was produced. This wave travelled at the same speed as that found when the same mixture was exploded in a tube.

This paper was circulated under the title 'Detonation waves' in the Ministry of Home Security in January 1941. It has now been declassified.

REFERENCES

Chapman, D. 1899 *Phil. Mag.* **47**, 90.
Earnshaw, S. 1860 On the mathematical theory of sound [1858]. *Phil. Trans.* **150**, 133.
Jones, H. & Miller, A. R. 1948 *Proc. Roy. Soc.* A, **194**, 480.
Jouguet, M. 1905–6 *J. Math.* (6) **1**, 347.
Jouguet, M. 1907 *C.R. Acad. Sci., Paris*, **144**, 633.
Lafitte, M. P. 1925 Thèses de l'Université de Paris. 'Recherches expérimentales sur l'onde explosive et l'onde de choc.'
Langweiler, H. 1938 *Z. tech. Phys.* **19**, 271.
Lewis, B. & Friauf, B. J. 1930 *J. Amer. Chem. Soc.* **52**, 3905.

The velocity of sound in general relativity, with a discussion of the problem of the fluid sphere with constant velocity of sound

By A. R. Curtis
St John's College, Cambridge

(*Communicated by H. Jeffreys, F.R.S.—Received* 31 *May* 1949)

The correct expression for the velocity of sound in general relativity is not obvious, because of ambiguity in defining the density of matter. The velocity is investigated in part I of this paper, and it is found that it never becomes greater than the velocity of light, having the value $3^{-\frac{1}{2}}$ for incompressible matter.

In part II this result is used in discussing the Schwarzchild solution for the interior of a fluid sphere. Eddington has already pointed out that this does not correspond to incompressible matter, and a solution for a sphere in which the velocity of sound is constant is sought, particular attention being paid to the special case of an incompressible fluid. No solution in closed form is found, but the equations are discussed in sufficient detail to enable the form of the solutions to be described. The limiting solution when the central pressure becomes infinite is tabulated in the incompressible case, and a number of numerical results are obtained.

Part I. The velocity of sound

Introduction

The velocity of sound in an isotropic fluid is easily calculated in classical mechanics, and is found to be $(dp/d\rho)^{\frac{1}{2}}$, where p is the pressure and ρ the density. In general relativity there is some ambiguity about applying this result, since we do not know whether ρ is the particle density T (the linear invariant of the energy tensor), the energy density T_0^0, or some combination of them.

The first part of this paper is concerned with investigating the propagation of sound in certain cosmological metrics of general relativity. We expect the velocity of sound to be a local phenomenon, depending only on the state of matter near the point considered, so that we lose no generality by restricting the investigation to a particular class of metrics.

The method used is analogous to that in classical dynamics; small perturbations are considered, so that second-order terms in the variations from undisturbed conditions may be neglected.

We can say something about the velocity of sound from general considerations. Since $T = T_\alpha^\alpha = T_0^0 + T_1^1 + T_2^2 + T_3^3 = T_0^0 - 3p$ in a locally Galilean co-ordinate system, we have

$$\frac{dT_0^0}{dp} = \frac{dT}{dp} + 3.$$

In general relativity, incompressible matter corresponds to T = constant, so that if the velocity of sound is $(dp/dT_0^0)^{\frac{1}{2}}$, it has a maximum value $3^{-\frac{1}{2}}$ (in terms of the velocity of light), which introduces no difficulty; but if it is $(dp/dT)^{\frac{1}{2}}$, it will be infinite for incompressible matter and certainly greater than unity for matter which is not quite incompressible. Such a result would be anomalous in a theory in which it is assumed that signals cannot be propagated with velocity greater than that of light, unless we assumed that it implied a definite lower limit to the compressibility of matter.

We shall find that this contingency does not arise, since the velocity of sound turns out to be $(dp/dT^0_0)^{\frac{1}{2}}$.

1. *Choice of a co-ordinate system*

We consider small perturbations of those 'cosmological metrics' of general relativity which have zero space-curvature. These metrics are given by

$$ds^2 = dt^2 - [R(t)]^2\,[dx^{1^2} + dx^{2^2} + dx^{3^2}], \tag{1·1}$$

and it is shown in the appendix, §4A, that, to the first order, we may take a perturbed metric in the form

$$ds^2 = dt^2 - [R(t)]^2\,[\delta_{ij} + \psi_{ij}]\,dx^i dx^j, \tag{1·2}$$

where the suffixes i, j run from 1 to 3. Here δ_{ij} is the Kronecker delta, while ψ_{ij} is a set of small functions of the four co-ordinates, which form the elements of a symmetrical covariant tensor for infinitesimal changes of the space co-ordinates alone. The form (1·2) is not invariant under mixed space-time transformations.

In investigating the propagation of the ψ_{ij}, we shall, of course, be taking gravitational waves into account as well as sound waves, since gravitational effects are determined by the metric.

2. *The energy tensor and the equations of propagation*

The mixed components of the energy tensor for the metric (1·2) are derived from the field equations in the appendix, §4B, and are given to first order in the perturbations by

$$\left.\begin{aligned}
8\pi T^0_0 &= -\lambda + 3\dot{R}^2/R^2 - \tfrac{1}{2}(\psi_{,kk} - \psi_{kl,kl})/R^2 + \dot{R}\dot{\psi}/R,\\
8\pi T^0_i &= -\tfrac{1}{2}(\dot{\psi}_{,i} - \dot{\psi}_{ij,j}), \quad 8\pi T^i_0 = \tfrac{1}{2}(\dot{\psi}_{,i} - \dot{\psi}_{ij,j})/R^2,\\
8\pi T^j_i &= -\lambda\delta_{ij} + (2R\ddot{R} + \dot{R}^2)\,\delta_{ij}/R^2 - \tfrac{1}{2}(\ddot{\psi}_{ij} - \ddot{\psi}\delta_{ij}) - 3\dot{R}(\dot{\psi}_{ij} - \dot{\psi}\delta_{ij})/2R\\
&\qquad - \tfrac{1}{2}(\psi_{,kk} - \psi_{kl,kl})\,\delta_{ij}/R^2 + \tfrac{1}{2}(\psi_{,ij} + \psi_{ij,kk} - \psi_{ik,jk} - \psi_{jk,ik})/R^2,
\end{aligned}\right\} \tag{2·1}$$

where a suffix following a comma denotes ordinary differentiation with respect to the corresponding co-ordinate, a dot indicates differentiation with respect to t, and $\psi = \psi_{kk}$.

Now Tolman (1934, §85) has shown that the energy tensor of an isotropic fluid can be taken in the form

$$T^{\mu\nu} = (\rho + p)\frac{dx^\mu}{ds}\frac{dx^\nu}{ds} - pg^{\mu\nu},$$

where ρ and p are the energy density and pressure in a locally Galilean co-ordinate system, while dx^μ/ds is the velocity four-vector in the actual co-ordinates. Lowering a suffix, we have

$$T^\nu_\mu = (\rho + p)\,g_{\mu\alpha}\frac{dx^\alpha}{ds}\frac{dx^\nu}{ds} - pg^\nu_\mu,$$

which yields to the first order in the perturbations

$$T^0_0 = \rho, \quad T^j_i = -p\delta_{ij},$$

since the time component of the velocity vector differs from unity by terms of the second order.

We put ρ_0, p_0 for the undisturbed values and

$$\rho = \rho_0(1+s), \quad p = p_0 + c^2\rho_0 s,$$

so that $dp/d\rho = c^2$, and we obtain the seven equations

$$\begin{aligned} 8\pi\rho_0 s &= \dot{R}\dot{\psi}/R - \tfrac{1}{2}(\psi_{,kk} - \psi_{kl,kl})/R^2, \\ 8\pi c^2\rho_0 s\delta_{ij} &= \tfrac{1}{2}(\ddot{\psi}_{ij} - \ddot{\psi}\delta_{ij}) + \tfrac{1}{2}(\psi_{,kk} - \psi_{kl,kl})\,\delta_{ij}/R^2 - \tfrac{1}{2}(\psi_{,ij} + \psi_{ij,kk} - \psi_{ik,jk} - \psi_{jk,ik})/R^2 \\ &\qquad + 3\dot{R}(\dot{\psi}_{ij} - \dot{\psi}\delta_{ij})/2R. \qquad (2{\cdot}2) \end{aligned}$$

We eliminate s from these equations, obtaining

$$\begin{aligned} 0 = {} & \tfrac{1}{2}(\ddot{\psi}_{ij} - \ddot{\psi}\delta_{ij}) + \tfrac{1}{2}(1+c^2)\,(\psi_{,kk} - \psi_{kl,kl})\,\delta_{ij}/R^2 \\ & - \tfrac{1}{2}(\psi_{,ij} + \psi_{ij,kk} - \psi_{ik,jk} - \psi_{jk,ik})/R^2 + 3\dot{R}(\dot{\psi}_{ij} - \dot{\psi}\delta_{ij})/2R - c^2\dot{R}\dot{\psi}\delta_{ij}/R. \qquad (2{\cdot}3) \end{aligned}$$

These six linear second-order partial differential equations in the six ψ_{ij} are the equations of propagation of small perturbations in the metric (1·1), and we proceed to deduce from them the velocities with which such disturbances are propagated. Once a solution of (2·3) has been found s can be calculated.

3. *Velocities of propagation*

We investigate the propagation of a wavefront over which the ψ_{ij} are discontinuous; the velocities of propagation of such a surface are the limiting velocities of propagation for small disturbances.

Let

$$\psi_{ij} = U_{ij}H(t - f(x^1, x^2, x^3)) + V_{ij}, \qquad (3{\cdot}1)$$

where f is regular, and U_{ij}, V_{ij} are regular functions of the four co-ordinates, while H is Heaviside's step function, which is zero for negative values of its argument and unity for positive values. Write f_i for $\partial f/\partial x^i$; then the velocity of propagation of the wavefront f = constant is $(f_i^2)^{-\frac{1}{2}}$, where f_i^2 stands for the sum $f_1^2 + f_2^2 + f_3^2$.

When we substitute (3·1) in (2·3), we shall get terms in H and its first and second derivatives, as well as regular terms. On the wavefront, the terms in the second derivative of H predominate, having by far the most serious infinity, and since the equations are linear these terms must vanish independently of the others.

The coefficient of this second derivative is easily seen to be, putting $U = U_{kk}$,

$$\begin{aligned} \tfrac{1}{2}[U_{ij} - U\delta_{ij} + R^{-2}(1+c^2)\,(Uf_k^2 - U_{kl}f_kf_l)\,\delta_{ij} \\ - R^{-2}(Uf_if_j + U_{ij}f_k^2 - U_{ik}f_jf_k - U_{jk}f_if_k)], \qquad (3{\cdot}2) \end{aligned}$$

and equating this to zero gives six linear homogeneous algebraic equations for the six U_{ij}, when symmetry conditions are taken into account. Then the determinant of the coefficients must vanish as a necessary condition for the existence of non-zero solutions. The equations, as well as the U_{ij}, are labelled by pairs of suffixes. Taking these pairs in the order 11, 22, 33, 23, 31, 12, and putting $R = 1$, the determinant is

$$\begin{vmatrix} c^2(f_2^2+f_3^2) & (c^2f_1^2+(1+c^2)f_3^2-1) & (c^2f_1^2+(1+c^2)f_2^2-1) & -2(1+c^2)f_2f_3 & -2c^2f_3f_1 & -2c^2f_1f_2 \\ (c^2f_2^2+(1+c^2)f_3^2-1) & c^2(f_3^2+f_1^2) & (c^2f_2^2+(1+c^2)f_1^2-1) & -2c^2f_2f_3 & -2(1+c^2)f_3f_1 & -2c^2f_1f_2 \\ (c^2f_3^2+(1+c^2)f_2^2-1) & (c^2f_3^2+(1+c^2)f_1^2-1) & c^2(f_1^2+f_2^2) & -2c^2f_2f_3 & -2c^2f_3f_1 & -2(1+c^2)f_1f_2 \\ -f_2f_3 & 0 & 0 & 1-f_1^2 & f_1f_2 & f_1f_3 \\ 0 & -f_3f_1 & 0 & f_1f_2 & 1-f_2^2 & f_2f_3 \\ 0 & 0 & -f_1f_2 & f_1f_3 & f_2f_3 & 1-f_3^2 \end{vmatrix}. \tag{3·3}$$

After evaluating it, we can restore R by noting that each f_i has to be divided by R.

The determinant has the value $-2(1-f_i^2/R^2)^2(1-c^2f_i^2/R^2)$, and since this must vanish, we have $f_i^2 = R^2$ or R^2/c^2. Then there are two velocities of propagation, R^{-1} and cR^{-1}.

The velocity R^{-1} is the fundamental velocity (velocity of light) in the metric (1·1), so we identify it in the present connexion with the velocity of gravitational waves. The other velocity is then that of sound, and is simply c times the fundamental velocity, or c in relativity units.

Remembering that $c^2 = dp/d\rho$, where ρ is the energy density, we see that the first of the alternatives discussed in the introduction is the correct one, so that the velocity of sound remains finite and less than unity even in incompressible matter.

4. *Appendix to part I*

A. The most general perturbed metric would be

$$ds^2 = (1+\phi)\,dt^2 + 2\gamma_i\,dt\,dx^i - R^2(\delta_{ij}+\psi_{ij})\,dx^i dx^j, \tag{4·1}$$

where all the functions denoted by Greek letters, except δ_{ij}, the Kronecker delta, are small, and $\psi_{ij} = \psi_{ji}$.

We wish to show that it is possible to choose co-ordinates so that the functions ϕ and γ_i are of second order in the perturbations.

Let us make the small co-ordinate change

$$t \to T = t + y^0(t, x^1, x^2, x^3), \quad x^i \to X^i = x^i + y^i(t, x^1, x^2, x^3). \tag{4·2}$$

Then writing x^0 for t, X^0 for T, and letting Greek suffixes run from 0 to 3, the changes $\Delta g_{\mu\nu}$ in the values of the $g_{\mu\nu}$ are given by

$$\begin{aligned} ds^2 &= g_{\mu\nu}dx^\mu dx^\nu = (g_{\mu\nu}+\Delta g_{\mu\nu})\,dX^\mu dX^\nu \\ &= (g_{\mu\nu}+\Delta g_{\mu\nu})\left(dx^\mu + \frac{\partial y^\mu}{\partial x^\sigma}dx^\sigma\right)\left(dx^\nu + \frac{\partial y^\nu}{\partial x^\tau}dx^\tau\right) \\ &= g_{\mu\nu}dx^\mu dx^\nu + \Delta g_{\mu\nu}dx^\mu dx^\nu + g_{\sigma\nu}\frac{\partial y^\sigma}{\partial x^\mu}dx^\mu dx^\nu + g_{\sigma\mu}\frac{\partial y^\sigma}{\partial x^\nu}dx^\mu dx^\nu, \end{aligned}$$

to first order, with a change of dummy suffixes.

Hence

$$\Delta g_{\mu\nu} = -g_{\sigma\nu}\frac{\partial y^\sigma}{\partial x^\mu} - g_{\sigma\mu}\frac{\partial y^\sigma}{\partial x^\nu}, \tag{4·3}$$

so that $$\Delta g_{00} = -2g_{00}\frac{\partial y^0}{\partial t} - 2g_{0i}\frac{\partial y^i}{\partial t} = -2\frac{\partial y^0}{\partial t} \quad \text{(to first order)}$$

and $$\Delta g_{0i} = -g_{00}\frac{\partial y^0}{\partial x^i} - g_{0i}\frac{\partial y^0}{\partial t} - g_{0j}\frac{\partial y^j}{\partial x^i} - g_{ij}\frac{\partial y^j}{\partial t} = -\frac{\partial y^0}{\partial x^i} + R^2\frac{\partial y^i}{\partial t} \quad \text{(to first order).}$$

We can now put $\Delta g_{00} = -\phi$, $\Delta g_{0i} = -\gamma_i$, and solve these equations for the y^μ, obtaining

$$y^0 = \frac{1}{2}\int \phi\, dt + \alpha(x^1, x^2, x^3), \quad y^i = \int\left[R^{-2}\left(\frac{1}{2}\int \phi_{,i}\, dt + \alpha_{,i} - \gamma_i\right)\right]dt + \beta^i(x^1, x^2, x^3), \tag{4·4}$$

where the α and β^i are small arbitrary functions of the space co-ordinates, and a suffix following a comma indicates ordinary differentiation with respect to the corresponding co-ordinate. Then, in the new system of co-ordinates, ϕ and the γ^i will vanish to first order, i.e. to the degree of approximation to which we are working, while the new ψ_{ij} will still be of first order. Clearly rotations or any infinitesimal transformations of the space co-ordinates alone will leave the metric still satisfying this condition, and ψ_{ij} will transform like a tensor.

B. Working to first order only, the non-vanishing Christoffel symbols of the second kind for the metric (1·2) are

$$\Gamma^j_{0i} = \frac{\dot{R}}{R}\delta_{ij} + \tfrac{1}{2}\dot{\psi}_{ij}, \quad \Gamma^0_{ij} = R\dot{R}(\delta_{ij} + \psi_{ij}) + \tfrac{1}{2}R^2\dot{\psi}_{ij}, \quad \Gamma^k_{ij} = \tfrac{1}{2}(\psi_{ik,j} + \psi_{jk,i} - \psi_{ij,k}), \tag{4·5}$$

while $$\frac{\partial}{\partial t}(\log\sqrt{-g}) = 3\dot{R}/R + \tfrac{1}{2}\dot{\psi}, \quad \frac{\partial}{\partial x^i}(\log\sqrt{-g}) = \tfrac{1}{2}\psi_{,i}, \tag{4·6}$$

where a suffix following a comma denotes ordinary differentiation with respect to the corresponding co-ordinate, a dot denotes differentiation with respect to t, and $\psi = \psi_{ii}$.

Then, since

$$G_{\mu\nu} = \frac{\partial^2}{\partial x^\mu \partial x^\nu}(\log\sqrt{-g}) - \frac{\partial}{\partial x^\alpha}\Gamma^\alpha_{\mu\nu} + \Gamma^\beta_{\mu\alpha}\Gamma^\alpha_{\nu\beta} - \Gamma^\alpha_{\mu\nu}\frac{\partial}{\partial x^\alpha}(\log\sqrt{-g}) \tag{4·7}$$

and $G^\nu_\mu = g^{\nu\alpha}G_{\mu\alpha}$, we find

$$\left.\begin{aligned} G^0_0 &= \tfrac{1}{2}\ddot{\psi} + (3\ddot{R} + \dot{R}\dot{\psi})/R, \\ G^i_0 &= -\tfrac{1}{2}R^{-2}(\dot{\psi}_{,i} - \dot{\psi}_{ij,j}), \quad G^0_i = \tfrac{1}{2}(\dot{\psi}_{,i} - \dot{\psi}_{ij,j}), \\ G^j_i &= \delta_{ij}(R\ddot{R} + 2\dot{R}^2)/R^2 - \tfrac{1}{2}R^{-2}[\psi_{,ij} + \psi_{ij,kk} - \psi_{ik,jk} - \psi_{jk,ik}] \\ &\quad + \tfrac{1}{2}\ddot{\psi}_{ij} + 3\dot{R}\dot{\psi}_{ij}/2R + \dot{R}\dot{\psi}\delta_{ij}/2R, \end{aligned}\right\} \tag{4·8}$$

so that $$G = G^\alpha_\alpha = 6(R\ddot{R} + \dot{R}^2)/R^2 + \ddot{\psi} - R^{-2}(\psi_{,kk} - \psi_{kl,kl}) + 4\dot{R}\dot{\psi}/R. \tag{4·9}$$

Then from the field equations

$$-8\pi T^\nu_\mu = G^\nu_\mu - \tfrac{1}{2}g^\nu_\mu(G - 2\lambda)$$

we obtain the energy tensor given in (2·1).

PART II. THE SPHERE OF FLUID WITH CONSTANT VELOCITY OF SOUND

5. *The Schwarzschild interior solution*

In 1916 Schwarzschild published a solution of the field equations of general relativity possessing spherical symmetry and giving constant energy density and isotropic fluid pressure up to a certain value of the radial co-ordinate, where the pressure vanished. At this point a Schwarzschild exterior solution, corresponding to empty space, was fitted on.

This solution was

$$\left.\begin{aligned} ds^2 &= \tfrac{1}{4}[3\surd(1-\alpha a^2)-\surd(1-\alpha r^2)]^2\,dt^2 - dr^2/(1-\alpha r^2) - r^2(d\theta^2+\sin^2\theta\,d\phi^2) \quad \text{for } 0 \leqslant r \leqslant a,\\ ds^2 &= (1-2m/r)\,dt^2 - dr^2/(1-2m/r) - r^2(d\theta^2+\sin^2\theta\,d\phi^2) \quad \text{for } r \geqslant a, \end{aligned}\right\} \tag{5·1}$$

where α, a are constants and $m = \alpha a^3/2$.

This gives an energy tensor, for $r \leqslant a$,

$$\left.\begin{aligned} T^0_0 &= \rho = 3\alpha/8\pi,\\ T^1_1 = T^2_2 = T^3_3 &= -p = -\frac{3\alpha}{8\pi}\left[\frac{\surd(1-\alpha r^2)-\surd(1-\alpha a^2)}{3\surd(1-\alpha a^2)-\surd(1-\alpha r^2)}\right], \end{aligned}\right\} \tag{5·2}$$

so that the particle density

$$T = \bar{\rho} = \frac{3\alpha}{4\pi}\left[\frac{3\surd(1-\alpha a^2)-2\surd(1-\alpha r^2)}{3\surd(1-\alpha a^2)-\surd(1-\alpha r^2)}\right],$$

the other components being zero. For $r > a$ all components of T^ν_μ are zero.

It has been pointed out by Eddington (1923, §72) that this solution does not correspond to incompressible matter, since the natural interpretation of incompressibility in general relativity is constancy of the particle density T, rather than of the energy density T^0_0. In fact, as the pressure increases in the Schwarzschild solution the particle density decreases, so that the matter has negative bulk modulus.

There are also other difficulties in having T^0_0 constant; as shown in part I of this paper, the velocity of sound is $(dp/d\rho)^{\frac{1}{2}}$, and this is infinite if T^0_0, i.e. ρ is constant. Also, since the particle density T decreases as p increases towards the centre, there is a danger of its becoming negative, and this actually happens in the Schwarzschild solution if αa^2 is too great. In his original paper Schwarzschild said that the upper limit to the radius of a sphere of given density was given by $\alpha a^2 = \frac{8}{9}$, since then the pressure becomes infinite and the velocity of light zero at the centre. But, in fact, the particle density becomes negative at the centre if $\alpha a^2 > \frac{5}{9}$, so that this must be taken as the limiting condition.

It may also be pointed out that there is no question of the limit being reached because the sphere fills the whole of space, as appears to have been tacitly assumed by Eddington (1923, §72). We can fit an exterior metric if $2m/a < 1$, i.e. if $\alpha a^2 < 1$, and this condition is satisfied whichever limit we take.

6. *The metric of the fluid sphere*

The rest of this paper will be concerned chiefly with the sphere of incompressible fluid, but as we shall discuss briefly the more general case of a fluid with constant velocity of sound, we first give the conditions to be imposed upon the metric in all such cases.

The solutions we want are static and spherically symmetrical, so we can take the metric in the form

$$ds^2 = e^{\nu}dt^2 - e^{\lambda}dr^2 - r^2(d\theta^2 + \sin^2\theta\, d\phi^2), \tag{6·1}$$

where ν and λ are functions of r only. The energy tensor of this metric is well known (Tolman 1934, §95 or Eddington 1923, §72); it is

$$\left.\begin{aligned} T^0_0 &= [\lambda'/r + (e^{\lambda}-1)/r^2]/8\pi e^{\lambda},\\ T^1_1 &= [(e^{\lambda}-1)/r^2 - \nu'/r]/8\pi e^{\lambda},\\ T^2_2 = T^3_3 &= [-\tfrac{1}{2}\nu'' - \tfrac{1}{4}\nu'(\nu'-\lambda') - (\nu'-\lambda')/2r]/8\pi e^{\lambda}, \end{aligned}\right\} \tag{6·2}$$

where a dash indicates differentiation with respect to r.

We have to impose the following conditions on this energy tensor:

(i) $T^1_1 = T^2_2 = T^3_3 = -p$, where p, the pressure, is greater than zero inside the sphere. We expect p to decrease steadily from a maximum value at $r = 0$ to zero for some value of r, say $r = a$. We shall then take this value of r as marking the surface of the sphere, and fit on a Schwarzschild exterior solution, by the condition that the metrical tensor shall be continuous at the surface. Tolman (1934, §95) has shown that we can satisfy the condition of isotropic pressure by taking

$$p' = -\tfrac{1}{2}(\rho+p)\,\nu', \tag{6·3}$$

where ρ is the energy density, and is equal to T^0_0 in the present case, since the fluid is at rest.

(ii) $T^0_0 = \rho$ is a suitable function of p for $r \leqslant a$. In the cases we are interested in this function is linear, and we write $\rho = \rho_s + kp$, where, by the result of Part I of this paper, $k = c^{-2}$, where c is the velocity of sound, and ρ_s is clearly the value of ρ at the surface. For $r > a$ we must have $\rho = 0$.

Since ρ is a linear function of p, we can integrate (6·3) obtaining

$$\nu = \text{constant} - \frac{2}{k+1}\log\left(1 + (k+1)\,P\right), \tag{6·4}$$

where $P = p/\rho_s$, so that $e^{\nu} = A(1+(k+1)\,P)^{-2/(k+1)}$.

We then eliminate p and ν between (6·3) and the first two equations of (6·2), in which we replace ρ by its value in terms of p, and we obtain an equation for λ. However, it is easier first to make certain transformations of the variables, putting

$$z = \log(2\pi\rho_s r^2) \quad \text{and} \quad \lambda = -\log(1-V).$$

We then obtain (see Appendix, §9 A)

$$4k(2\ddot{V} - \dot{V} - V)(1-V) + (2\dot{V} + (k+1)\,V - 4e^z)(2(k+1)\,\dot{V} + (k+1)\,V - 4e^z) = 0, \tag{6·5}$$

where a dot indicates differentiation with respect to z. We now discuss this equation first in the case of an incompressible fluid ($k = 3$) and then in the case of a fluid in which the velocity of sound is constant ($k \geqslant 3$). This latter case includes the other, but it is possible to give a considerably more detailed discussion when a particular value is assumed for k.

To help in interpreting the various solutions of (6·5) we have the expression for P (see §9 A)

$$1+kP = \tfrac{1}{4}e^{-z}(2\dot{V}+V). \tag{6·6}$$

7. *The sphere of incompressible fluid*

Incompressible matter corresponds to T = constant, where T is the linear invariant of the energy tensor. Since $\rho = T+3p$, this gives the value 3 for k, and the value T for ρ_s.

Then (6·5) becomes

$$3(2\ddot{V}-\dot{V}-V)(1-V)+2(\dot{V}+2V-2e^z)(2\dot{V}+V-e^z) = 0 \tag{7·1}$$

and (6·6)

$$1+3P = \tfrac{1}{4}e^{-z}(2\dot{V}+V). \tag{7·2}$$

Two types of solution of (7·1) are of physical interest (see §9 A). They can be expanded in power series in e^z, and so are regular at the centre ($z = -\infty$).

(i) A family of solutions whose power series expansion starts with the term in e^z, so that, by (7·2), the pressure at the centre is finite. If P takes the value P_c at the centre, then $V \sim 4e^z(P_c+\tfrac{1}{3})$ as $z \to -\infty$.

(ii) A solution which tends to $\tfrac{3}{7}$ as $z \to -\infty$, giving infinite central pressure. It will be shown that this solution is the limiting case of the family (i) as the central pressure tends to infinity.

First let P_c be small. Then we expect the radius of the sphere to be small, so that e^z is small throughout the sphere, and we need consider only the first two terms in the power series for V. These terms are easily seen by substitution in (7·1) to be

$$4e^z(P_c+\tfrac{1}{3})-4e^{2z}(1+4P_c)(1+6P_c)/5,$$

giving

$$P = P_c-e^z(1+4P_c)(1+6P_c)/3 = P_c-e^z/3$$

approximately, so that the boundary occurs where $e^z = 3P_c$. Then $a^2 = 3P_c/2\pi T$, and the mass m is given by $e^\lambda = (1-2m/r)^{-1}$ at the surface, i.e. by

$$m = \tfrac{1}{2}aV = 2P_c\sqrt{(3P_c/2\pi T)}.$$

These values agree with those given by the Schwarzschild solution and by classical mechanics, allowing for the difference of units.

Now let P_c be very large. It is easily shown (see §9 A) that the coefficient of e^{nz} in the power series for V is a polynomial of degree n in P_c, so we put $y = z+\log P_c$. The coefficient of e^{ny} is then a polynomial in $1/P_c$, and to a first approximation we take only the constant term of this polynomial; this means that to a first approximation P_c is merely a scale factor, not affecting the character of the solution. The transformation makes no difference to (7·1) save to change e^z into e^y/P_c, and clearly we can always take P_c sufficiently large to make this term negligible up to any fixed value of y. We therefore neglect these terms as a first approximation, obtaining an equation in which the independent variable is absent. This can be transformed (see §9 B) into a first-order equation which can be integrated approximately. The integral gives us the left-hand part of figure 1, where this first approximation to V is plotted against y, together with the corresponding curve of P/P_c. It will be seen that, to the present degree of approximation, $V \rightarrow \frac{3}{7}$ and $P \rightarrow 0$ as $y \rightarrow +\infty$. The oscillations of V about the value $\frac{3}{7}$ are quickly damped, by a factor which can be shown to be $\exp(-3y/8)$.

Since P does not vanish for any value of y which is bounded as P_c tends to infinity, we cannot say that the surface value of y tends to a limit; we must therefore take a further approximation into account.

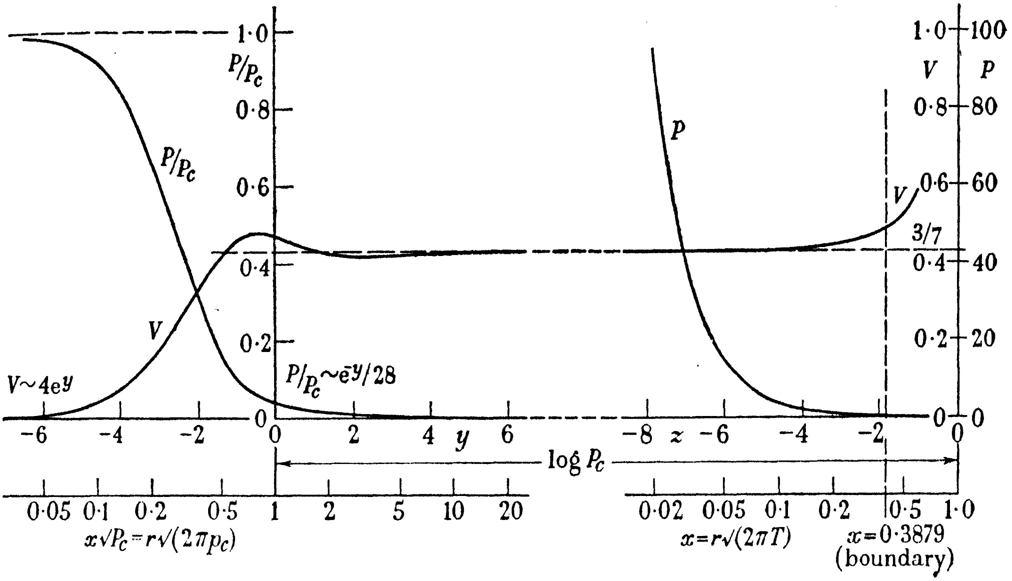

FIGURE 1

The error is clearly due to the neglect of the terms e^y/P_c in the transformed form of (7·1), for with these terms included in the equation it is easily verified that V cannot tend to any limit as y tends to infinity. We therefore assume that, calling the approximate solution already obtained V_0, $V = V_0 + V_1/P_c$. We can still suppose P_c sufficiently large for e^y/P_c to be negligible until V_0 is arbitrarily close to $\frac{3}{7}$, since this happens for a fixed value of y; then in substituting the above expression for V in the transformed equation (7·1) we can put $V_0 = \frac{3}{7}$. We shall also neglect terms in P_c^{-2}, to obtain a linear equation for V_1. By solving this equation we find (see § 9 C) that, to the next approximation in P_c^{-1},

$$V = \tfrac{3}{7} + 8e^y/21P_c = \tfrac{3}{7} + 8e^z/21.$$

The pressure is given by $84P = 3e^{-z} - 20$, so that to this degree of approximation the boundary occurs where $e^z = \frac{3}{20}$. This confirms a suspicion that z, rather than y, tends to a limit at the boundary as P_c tends to infinity; but we do not yet know whether this limit is given by $e^z = \frac{3}{20}$ to any great accuracy, since we have neglected further terms which might contribute appreciably to V and to P at a value of e^z such as this.

However, we do not need to carry on the calculation of closer and closer approximations in the way that we have been doing, as a study of figure 1 will show. This figure shows, on the left, the first approximation plotted against y, while on the right is plotted the solution, in terms of z, for which V tends to $\frac{3}{7}$ at the centre. It is clear that for large P_c this solution is the continuation we want of the approximation V_0; for the initial conditions approach $V = \frac{3}{7}$, $\dot{V} = 0$, as P_c tends to infinity, and these are just the conditions satisfied by the solution described in (ii) above.

Thus we may describe the solution for very large but finite P_c as follows: the radius of the sphere tends to the value given by the solution (ii), and in the outer region the pressure is approximately the same as in that solution; but for the central region, where the radius is of order $P_c^{-\frac{1}{2}}$, the solution deviates from the solution (ii), the pressure tending to TP_c and V to zero. V is of order $4P_c e^z$ and P of order $P_c(1-8P_c e^z)$ at the centre.

We give more exactness to this description by giving the following numerical values: the solution (ii) gives a value of V which is within 2 % of $\frac{3}{7}$ for $z < -4$, while the approximation V_0 is within 2 % of $\frac{3}{7}$ for $y > 4$. Hence if $\log P_c > 8$, i.e. if $P_c > 3000$, the solutions will match to within a few per cent. If this condition is satisfied, the values of V and P may be expected to be within some 5 % of the values for the solution (ii), which is tabulated in § 9 D, down to $y = 4$, i.e. to $r = 7{\cdot}4(2\pi p_c)^{-\frac{1}{2}}$, after which point there are considerable deviations from this solution. In fact, below this value of r, V begins to oscillate with increasing amplitude, reaching a maximum value of about 0·475 at $r = 0{\cdot}78(2\pi p_c)^{-\frac{1}{2}}$ and then decreasing steadily to zero, while the rate of increase of P falls so that P tends to P_c instead of infinity. The limiting radius of the sphere as P_c tends to infinity is $a = 0{\cdot}38791(2\pi T)^{-\frac{1}{2}}$, and the limiting value of the active gravitational mass is $m = 0{\cdot}09429(2\pi T)^{-\frac{1}{2}}$.

If we take the density equal to that of water, the limiting radius is $1{\cdot}8 \times 10^8$ km. and the active gravitational mass is $5{\cdot}9 \times 10^{40}$ g. The light-time from the centre to the boundary is 37 min.

It is worth noting that, as in the Schwarzschild solution, there is no question of the limit being reached through the sphere filling the whole of space, since $2m/r = 0{\cdot}48616$ at the boundary, i.e. $2m/r < 1$.

8. *The fluid sphere with constant velocity of sound*

The treatment of the general case of constant velocity of sound follows closely that of the incompressible case dealt with in the preceding section. We now have to use (6·5) and (6·6) instead of (7·1) and (7·2). Since these equations contain the parameter k, we require the various results, such as the limiting radius, as functions of k.

From the brief discussion of the general case given in §§ 9 A and B, it is already fairly clear that the qualitative behaviour of the solutions is the same for all relevant k; and, in fact, it needs only a brief examination of the topology of the equation corresponding to (9·5) to confirm that this is so. We may, therefore, proceed to derive some approximate numerical results, guided by those already obtained in the incompressible case.

In the solution (ii), the first two terms in the power series for V are

$$4k/(k^2+6k+1)+4e^z(k+1)/[(2k+1)(k+3)], \tag{8·1}$$

and the corresponding terms in P are

$$e^{-z}/(k^2+6k+1)-2(k+2)/[(2k+1)(k+3)], \tag{8·2}$$

so that to this degree of approximation the limiting radius is given by

$$2\pi\rho_s a^2 = e^z = \frac{(2k+1)(k+3)}{2(k+2)(k^2+6k+1)}. \tag{8·3}$$

It can be verified that the correction to this value of e^z obtained by taking the third term of the series into account is well below 1 %; it is likely, therefore, that the series converges sufficiently fast for (8·3) to be in error by 1 or 2 % at most. Substituting this value of e^z in (8·1) gives for the surface value V_s of V

$$V_s = \frac{2(2k^2+5k+1)}{(k+2)(k^2+6k+1)}. \tag{8·4}$$

The condition that the metrical tensor is continuous at the boundary gives us for the active gravitational mass $m = \frac{1}{2}aV_s$, where a is the radius of the sphere. By (8·3) and (8·4) this is

$$m = \frac{(2k^2+5k+1)}{2(k+2)(k^2+6k+1)}\left[\frac{(2k+1)(k+3)}{\pi\rho_s(k+2)(k^2+6k+1)}\right]^{\frac{1}{2}}. \tag{8·5}$$

This should be the limiting value as P_c tends to infinity with an error of at most 5 %.

These are the principal results required; but it would be interesting to obtain some estimate of the radius within which the solution (ii) ceases to be a good approximation to the solution (i) for large P_c. It is very difficult to do this in the general case, as it involves approximate integrations which are only practicable when some definite numerical value is given to k. However, by assuming that the first integral curve, corresponding to that plotted in figure 2, has a shape independent of k, it is possible to obtain the following very rough result for the region in which deviations of the order of 5 % or more may be expected:

$$2\pi p_c r^2 = e^\nu < \frac{28\exp\left[\frac{1}{4}(25k+21)/(k+3)\right]}{k^2+6k+1}. \tag{8·6}$$

The condition that the shape of the first integral curve is independent of k is only very approximately satisfied, and (8·6) may be expected to be in error by as much as a factor of 3. I should expect it to be an underestimate rather than an overestimate.

9. *Appendix to part II*

A. The first two equations of (6·2), together with (6·3) and the condition $\rho = \rho_s + kp$, give

$$\left.\begin{aligned} \rho_s(1+kP) &= [\lambda'/r+(e^\lambda-1)/r^2]/8\pi e^\lambda, \\ -p &= [-\nu'/r+(e^\lambda-1)/r^2]/8\pi e^\lambda, \\ p' &= -\tfrac{1}{2}\rho_s(1+kP)\,\nu'. \end{aligned}\right\} \tag{9·1}$$

Putting $e^z = 2\pi\rho_s r^2$, $\lambda = -\log(1-V)$ gives

$$\left.\begin{aligned} 1+kP &= \tfrac{1}{4}e^{-z}(2\dot{V}+V), \\ -P &= \tfrac{1}{4}e^{-z}(2\dot{\nu}(V-1)+V), \\ \dot{P} &= -\tfrac{1}{2}\dot{\nu}(1+kP), \end{aligned}\right\} \tag{9·2}$$

where a dot indicates differentiation with respect to z.

We eliminate P between the first two equations, obtaining

$$2k\dot{\nu} = (2\dot{V}+(k+1)V-4e^z)/(1-V), \tag{9·3}$$

and we differentiate the first with respect to z, obtaining an expression for $\dot{P}$ in terms of V. We then substitute for $\dot{\nu}$, P and $\dot{P}$ in the third equation, obtaining the second order equation (6·5) for V.

This equation has as its general solution a two-parameter family of functions. So far, I have found only the following solutions, of which, unfortunately, the most interesting do not appear to be expressible in finite terms:

(i) A one-parameter family all expansible in power series in e^z, and which tend to zero as z tends to $-\infty$, i.e. as r tends to zero. They are clearly regular functions of r at the centre, and give finite central pressure p_c. Writing then $V = \sum_{n=1}^{\infty} a_n e^{nz}$, we can obtain from the equation (6·5) a recurrence relation satisfied by the a_n for $n > 2$, which is of the form

$$a_n = f(n)\,a_{n-1} + \sum_{s=1}^{n-1} g(n,s)\,a_s a_{n-s},$$

while if P_c is the value of P at the centre, we have by the first of (9·2)

$$a_1 = 4(1+kP_c)/3,$$

whence it follows from the equation that

$$a_2 = -4k(1+(k+1)P_c)(1+(k+3)P_c)/15.$$

It then follows by induction from the recurrence relation that a_n is a polynomial of degree n in P_c.

(ii) A solution expansible in power series in e^z for which $V \to 4k/(k^2+6k+1)$ as $z \to -\infty$. By the first of equations (9·2), this gives infinite pressure at the centre. Writing this solution in the form $V = \sum_{n=0}^{\infty} a_n e^{nz}$, we obtain on substituting in (6·5) a recurrence relation of the same form as in the previous case, but with different functions f and g. This relation is again satisfied for $n > 2$, and we have in addition

$$a_1 = \frac{4(k+1)}{(2k+1)(k+3)}, \quad a_2 = \frac{4k(k-1)(k^2+6k+1)}{(2k+1)^2(k+3)(11k^2+30k+15)}.$$

For the incompressible case ($k = 3$) this solution is tabulated below up to the point where the pressure vanishes; and in this case I have proved that the series is certainly convergent for $e^z \leqslant 1$.

(iii) The one-parameter family $V = 4e^z/3(k+1) + \alpha e^{-\frac{1}{2}z}$. This gives constant negative pressure given by $P = -1/(k+1)$.

(iv) The solution $V = 4e^z/(k+3)$. This gives constant negative pressure given by $P = -1/(k+3)$.

There are undoubtedly other solutions, since the general solution is a two-parameter family, and no solution of this type has been found; but as the equation is not linear we have no way of knowing how to combine the known solutions to get the general solution, even if the latter can be obtained in this way.

B. On putting $y = z + \log P_c$ and neglecting terms in $1/P_c$, (6·5) becomes

$$4k(2\ddot{V} - \dot{V} - V)(1-V) + (k+1)(2\dot{V} + V)(2\dot{V} + (k+1)V) = 0, \tag{9·4}$$

where now the dot indicates differentiation with respect to y. The initial condition for solutions of type (i) becomes $V \sim 4k\,e^y/3$ as $y \to -\infty$.

Putting $\dot{V} = F(V)$, we get $\ddot{V} = F\,dF/dV$, and substituting these expressions in (9·4) gives a first-order equation for F which in the case $k = 3$ is

$$\frac{dF}{dV} = \frac{4F^2 + 13FV + 7V^2 - 3(F+V)}{6F(V-1)}. \tag{9·5}$$

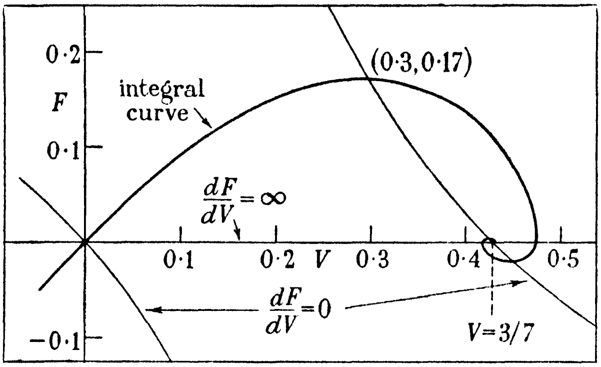

Figure 2

In the general case it has the form of (9·5), but the coefficients are functions of k. The curves dF/dV = constant in the V, F plane are always the family of conics through the four points

$$(0,0), \quad (4k/(k^2+6k+1), 0), \quad (1, -\tfrac{1}{2}) \quad \text{and} \quad (1, -\tfrac{1}{2}(k+1)),$$

the curve $dF/dV = 0$ being the member of the family whose slope is -1 at the origin; the locus $dF/dV = \infty$ is always the line-pair $F = 0, V = 1$. There are always two integrals through the origin, one being the line $F + 2V = 0$, and the other having the slope 1 at the origin. From the initial condition above for V, the latter integral is the one we require.

For any given value of k we can find this integral curve sufficiently accurately by graphical methods, and it is plotted in figure 2 for $k = 3$, the incompressible case. The result of the further integration $y = \int dV/F$, with the initial condition above taken into account, is shown at the left in figure 1.

In terms of y, we obtain, to zero order in P_c^{-1}, from (6·6)

$$kP/P_c = \tfrac{1}{4}e^{-y}(2\dot{V} + V), \tag{9·6}$$

and as $y \to \infty$,

$$V \to 4k/(k^2+6k+1) \quad \text{and} \quad P/P_c \sim e^{-y}/(k^2+6k+1).$$

C. The equation we get for V_1 is

$$8\ddot{V}_1 + 6\dot{V}_1 + 7V_1 = 8e^y. \tag{9·7}$$

The particular integral is clearly $8e^y/21$, while the complementary function consists of damped harmonic terms, the damping being due to a factor $e^{-3y/8}$. This complementary function is the oscillation already present in V_0, and is negligible at any fixed value of z if P_c is sufficiently large. For a general value of k we get a damping factor of $-(k+3)/4(k+1)$.

D. The solution (ii), together with the pressure and the value of e^ν derived from it, is given in table 1 for the incompressible case. The independent variable is

$$x = r\sqrt{(2\pi T)} = e^{\frac{1}{2}z}.$$

TABLE 1

x	V	e^λ	e^ν	P	x	V	e^λ	e^ν	P
0·00	0·42857	1·7500	0·00000	—	0·20	0·44383	1·7980	0·27039	0·6550
0·02	0·42872	1·7505	0·02722	89·05	0·22	0·44704	1·8084	0·29699	0·5000
0·04	0·42918	1·7519	0·05443	22·08	0·24	0·45055	1·8200	0·32349	0·3822
0·06	0·42994	1·7542	0·08161	9·683	0·26	0·45438	1·8328	0·34984	0·2905
0·08	0·43101	1·7575	0·10876	5·342	0·28	0·45851	1·8468	0·37606	0·2178
0·10	0·43238	1·7618	0·13587	3·333	0·30	0·46295	1·8620	0·40211	0·1592
0·12	0·43406	1·7670	0·16293	2·242	0·32	0·46770	1·8787	0·42800	0·1112
0·14	0·43604	1·7732	0·18992	1·584	0·34	0·47277	1·8987	0·45369	0·0714
0·16	0·43833	1·7804	0·21683	1·157	0·36	0·47814	1·9162	0·47918	0·0381
0·18	0·44093	1·7887	0·24366	0·8643	0·38	0·48383	1·9373	0·50449	0·0100
					0·38791	0·48616	1·9461	0·51384	0·0000

The active gravitational mass m is obtained from the condition that the metrical tensor is continuous at the boundary. For the interior solution the coefficient of dr^2 is $e^\lambda = (1-V)^{-1}$, while for the Schwarzschild exterior solution it is $(1-2m/r)^{-1}$. Hence

$$m = \tfrac{1}{2}(rV)_{bdy} = (xV)_{bdy}/2\sqrt{(2\pi T)}.$$

REFERENCES

Eddington, A. S. 1923 *Mathematical theory of relativity.* Cambridge University Press.
Schwarzschild, K. 1916 *S.B. preuss. Akad. Wiss.* p. 424.
Tolman, R. C. 1934 *Relativity, thermodynamics and cosmology.* Oxford University Press.

Thermal conductivities of organic vapours

By J. D. Lambert, E. N. Staines and S. D. Woods
Physical Chemistry Laboratory, University of Oxford

(*Communicated by Sir Cyril Hinshelwood, F.R.S.—
Received 2 August* 1949)

The variation of thermal conductivity with pressure has been investigated for a number of organic vapours at pressures between 50 and 700 mm. and at temperatures of 25, 66 and 85° C. Acetaldehyde and acetonitrile show fairly large linear increases of thermal conductivity with rise in pressure, which diminish markedly as temperature rises. This is interpreted as being due to dimerization, and a quantitative treatment is given in terms of values of K_p and ΔH for the reversible dimerization process, which are derived from previous work on the second virial coefficients of these vapours. Ethyl chloride shows similar behaviour to a much smaller degree. Methyl alcohol and acetone show fairly large non-linear increases, which diminish at higher temperatures, and which are interpreted as being due to association to polymers higher than the dimer. Benzene, cyclohexane, *n*-hexane, chloroform and diethyl ether, together with air and carbon dioxide, all show comparatively small linear increases, which become larger as temperature rises. No satisfactory quantitative explanation was found for this effect, which appears to involve factors other than simple convection. Values of the absolute thermal conductivity, corrected to zero pressure, are given for all vapours investigated.

INTRODUCTION

Recent measurements of the compressibilities of some simple organic vapours (Lambert, Roberts, Rowlinson & Wilkinson 1949) led to the view that strongly polar vapours undergo association. It was pointed out that such an association would be expected to give rise to an abnormal increase in thermal conductivity with rise of pressure. Such thermal conductivity data as were then available appeared to confirm the presence of this effect with associated vapours and its absence with non-associated vapours. Systematic investigation has now been made of the thermal conductivities of a number of vapours of both types, so that a wider range of measurements, obtained under constant conditions with different substances, might be available for comparison.

EXPERIMENTAL

Apparatus

Thermal conductivities were measured by the hot-wire method, using a long and a short wire to give compensation for end-effects. The conductivity cell, which is based on that described by Eucken (1911), is shown in figure 1. Two platinum wires both 0·05 mm. in diameter, and respectively 4 and 12 cm. long, are located centrally in circular holes 3 mm. in diameter bored lengthwise in a solid brass block. The brass block is 14 cm. long and of hexagonal cross-section 3 cm. in diameter. The ends of the 0·05 mm. wires are gold-soldered to short lengths of 1 mm. diameter platinum wire. The two upper 1 mm. wires slide loosely through Bakelite plugs, and are soldered at their top ends to small tungsten springs. These in turn are soldered to thick platinum leads which are located by holes in a Bakelite disk. The two lower 1 mm. wires are fixed in Bakelite clamps, which are fitted with brass screws making electrical contact with the wires. The 0·05 mm. wires are held under slight tension by the tungsten springs. The lower end of the hexagonal brass block is soldered to a solid brass cone and this is screwed on to a flat brass base-plate. The upper part of the cell is contained in a Pyrex tube, terminating at its lower end in a ground conical socket, which is sealed with Apiezon wax to the brass cone. The upper end of the Pyrex tube carries four capillary tubes containing the four electrical leads of copper wire, sealed in with Apiezon wax, and a central tube sealed to the vacuum and vapour supply system. The whole apparatus stands vertically in an efficiently stirred and insulated thermostat, whose temperature is regulated electrically so as to be constant to 0·02° C. Water was used as thermostat liquid for 25° C and glycerin for 60 and 80° C. Thermostat temperatures were measured by thermometers graduated to $\frac{1}{20}$° C which were checked against a standard (Physikalisch Technische Reichsanstalt).

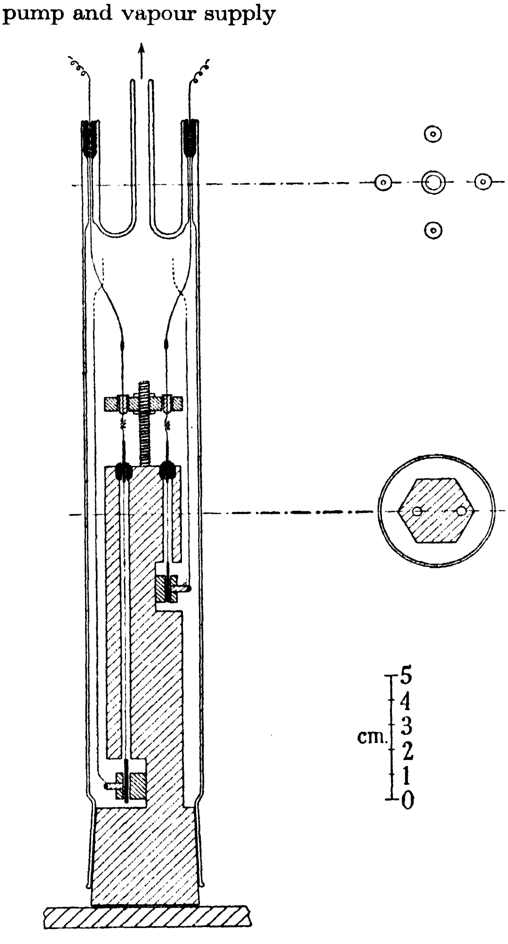

FIGURE 1

The electrical circuit connected to the cell was that described by Mann & Dickins (1932). The long and short platinum wires are inserted in the two arms of a Callendar-

Griffiths bridge, and the current flowing through the wires determined by measuring the potential drop across a standard 1 Ω resistance by means of a Tinsley potentiometer. The source of current was a 6 V accumulator, and fine adjustment was made by a mercury rheostat.

The conductivity cell was evacuated through a liquid-air trap by a mercury-vapour pump. A small discharge tube served as vacuum gauge. Vapour was admitted from a sample of liquid contained in a Pyrex bulb sealed to the apparatus through a mercury-sealed tap. Tubing and taps were wound with Nichrome wire and heated electrically to 75° C to prevent condensation of the vapours. Heated taps were lubricated with Silicone tap-grease. The pressure of the vapour in the conductivity cell was measured by a steam-jacketed mercury U-tube manometer, fitted with a gold trap to prevent mercury vapour diffusing into the cell.

Materials

Liquids were purified and introduced into the apparatus in the manner described previously (Lambert *et al.* 1949) with the exception of acetaldehyde. This was cooled in an acetone-solid carbon dioxide bath instead of being frozen in liquid air, so as to avoid low-temperature polymerization of the liquid. Air was purified by passing through Sofnolite, calcium chloride and phosphorous pentoxide. Cylinder carbon dioxide was used without purification, in order to show how a permanent gas denser than air would behave.

Experimental procedure

No attempt at absolute measurement of thermal conductivity was made; the apparatus was calibrated for each thermostat and wire temperature by measuring the conductivity of pure, dry air free from carbon dioxide. The wire temperature, T_1, was determined by using the wire as a resistance thermometer. This was calibrated by performing conductivity experiments with air at atmospheric pressure, taking several values of the current. On plotting C^2R against the resistance, a straight line was obtained, which could be extrapolated to give the resistance at zero current. Readings were taken at thermostat temperatures of 25, 40, 60 and 80° C. It was not possible to fit these measurements into the standard formulae for platinum thermometry, and the values of T_1 were therefore extrapolated from the nearest pair of measured temperature/resistance values; a procedure which involves an error not larger than $\pm 0{\cdot}3°$ C in the absolute value of T_1. This does not affect the accuracy of the conductivity measurements, which were always made by comparison with an air measurement at the *same* value of T_1. The temperature, T_2, of the brass block forming the walls of the conductivity tubes was assumed to be that of the thermostat liquid, with which its lower end was in actual contact.

At each thermostat temperature the Callendar-Griffiths bridge was first set to a reading corresponding to a suitable value of $T_1 - T_2$, and this setting remained unaltered throughout all measurements. Air was admitted to the cell, and the current adjusted by rheostats until the bridge was balanced. The value of the balancing current was then determined by means of the potentiometer. This was repeated for a number of pressures and a graph plotted showing C^2 against the pressure. The graph was linear down to a pressure of 25 cm. and showed a small increase in C^2 with rising pressure (about 0·6 % for 1 atm. rise in pressure). Extrapolation to zero pressure gave a value C_0^2 air. The apparatus was then evacuated and similar measurements made with the vapour. The conductivity of the vapour at each pressure, k_p, was then calculated from the relation

$$k_p = \frac{C_p^2\,(\text{vapour})}{C_0^2\,(\text{air})}\,k_0\,(\text{air}).$$

The values of k_0 air used were extrapolated graphically from the absolute measurements of Milverton (1934):

temperature (° C)	$10^6 k_0$ (air) (cal. cm.$^{-1}$ sec.$^{-1}$ deg. C^{-1})
31·19	63·07
65·94	69·2
84·98	72·7

The value for 84·98° C is extrapolated from experimental values obtained at temperatures within 2° C, and the extrapolation is likely to be accurate. The other two values are extrapolated over larger temperature intervals, but the variation of conductivity of air with temperature is nearly linear and the possible error in extrapolation is well within 1 %.

The net accuracy of the results given by the apparatus may be judged by comparing the experimental values of k_0 for acetaldehyde with the values of k_0 obtained by Milverton (1935) from absolute measurements. The comparison is shown in table 1. The Milverton values were all extrapolated over temperature intervals of less than 1° C from actual measurements. Agreement is within 1 % at the two lower temperatures, while, at the higher temperature, the Milverton value is 2·13 % lower than the observed value. In view of the difficulty of ensuring complete purity of acetaldehyde vapour, this seems satisfactory; it compares not unfavourably with the agreement between more recent published determinations on permanent gases.

TABLE 1

temperature $T_2 + \frac{T_1 - T_2}{2}$ (° C)	$10^6 k_0$ (acetaldehyde) (cal. cm. $^{-1}$ sec.$^{-1}$ deg. C^{-1})	
	obs.	Milverton
31·19	28·88	28·60
65·94	35·46	35·25
84·98	39·85	39·02

Very great care was necessary in pumping out the last traces of one vapour from the conductivity cell before starting on another. This sometimes required as much as twenty hours' pumping, and was hastened by flushing out several times with hydrogen. It was found that reproducible results could always be obtained if the discharge tube vacuum gauge showed a 'black' discharge ($< 10^{-3}$ mm. pressure) for at least two minutes after shutting off the pumping system.

RESULTS

The measured values of thermal conductivity are shown plotted against pressure in figures 2 and 3. The temperature conditions for the three sets of readings are given in table 2. Measurements were not normally taken in the low-pressure range where

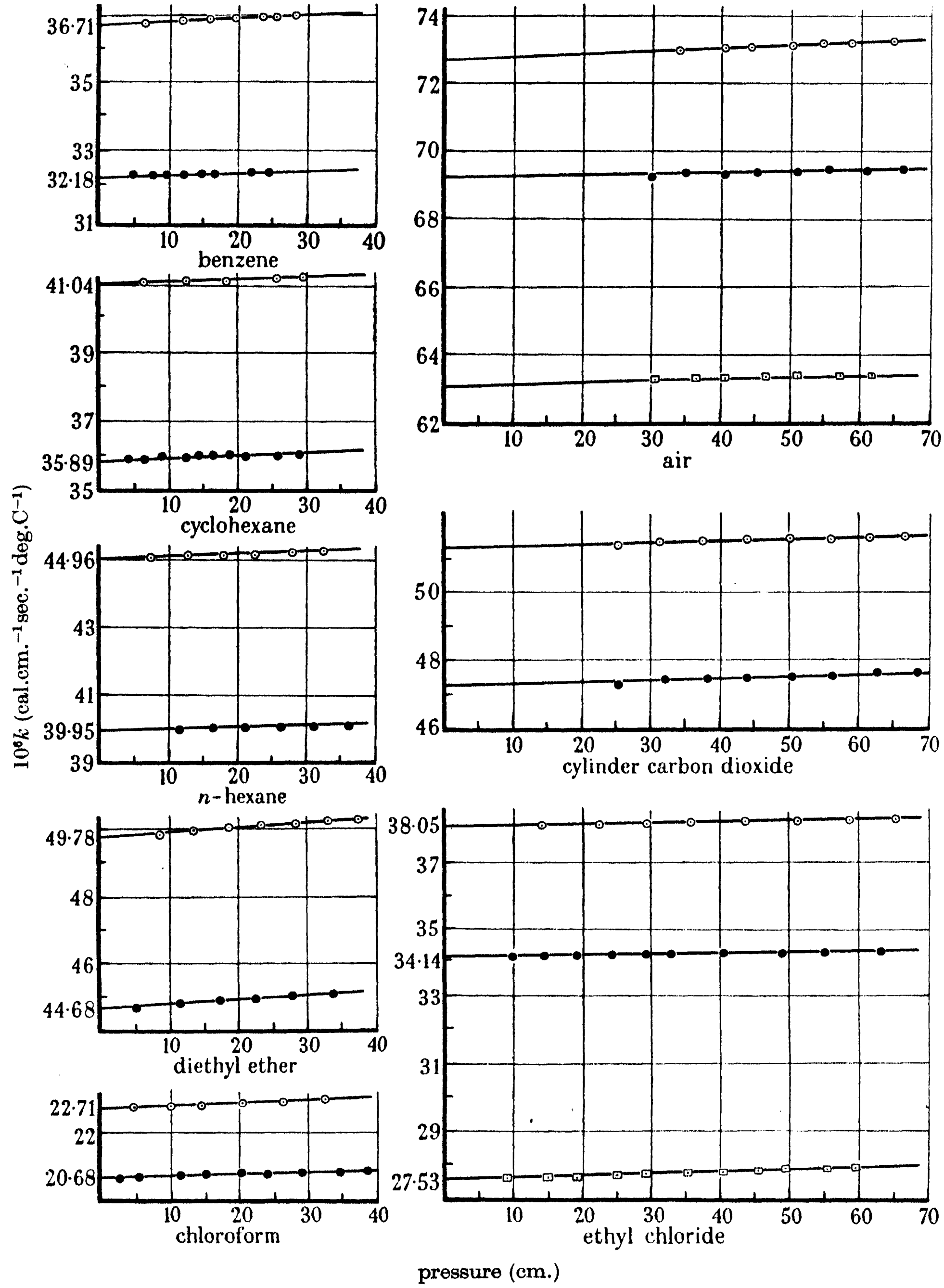

FIGURE 2. ☐ values at 31·19° C. ● values at 65·94° C. ⊙ values at 84·98° C.

falling off in conductivity occurs due to the finite ratio between mean free path and apparatus dimensions. Except in the cases of methyl alcohol and acetone, the points all fall on straight lines; these are extrapolated to zero pressure to give values of k_0, and may be fitted to an equation of the form

$$k_p = k_0(1+\delta p).$$

The percentage increases in thermal conductivity for 1 atm. rise in pressure, β ($= 100\delta$, where p is expressed in atmospheres), are shown in table 3 together with measured values of the second virial coefficient B. The substances investigated, with one exception, fall into two classes:

Class I. Substances showing a *low* value of $\beta(\leqslant 2\cdot3)$, which *increases* with rise of temperature: air, carbon dioxide, benzene, cyclohexane, *n*-hexane, chloroform, diethyl ether.

Class II. Substances showing relatively *high* values of $\beta(>2\cdot3)$ which *decrease* markedly with rise of temperature: acetaldehyde, acetonitrile, acetone, methyl alcohol.

Ethyl chloride falls in between the two classes, having a low value of β which decreases with rise of temperature.

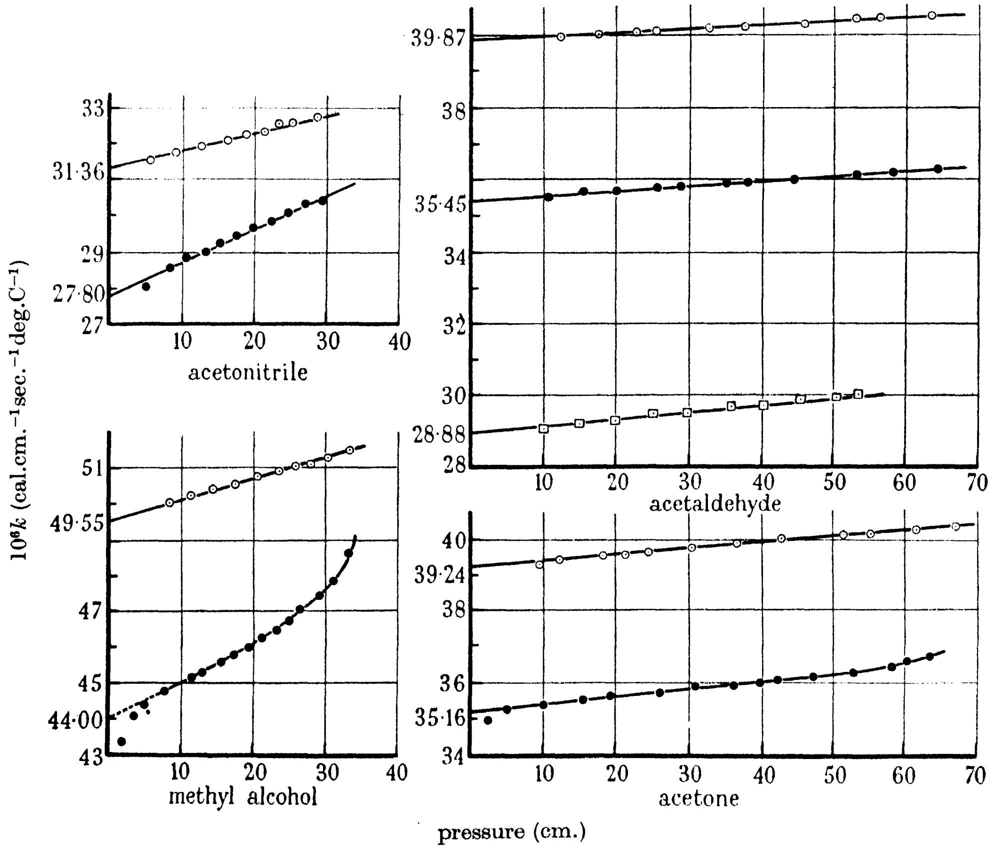

FIGURE 3. □ values at 31·19° C. ● values at 65·94° C. ⊙ values at 84·98° C.

The measured values of β are not significantly altered by changing $T_1 - T_2$ by ± 1°C, when T_2 is kept constant. The difference between the values of $T_1 - T_2$ at the different thermostat temperatures (due to an initial mistake in platinum thermometry) is therefore unimportant.

TABLE 2. TEMPERATURE CONDITIONS (° C)

thermostat T_2	wire T_1	$T_1 - T_2$	average temp. of vapour $T_2 + \frac{T_1 - T_2}{2}$
25·08	37·30	12·22	31·19
60·45	71·42	10·97	65·94
80·00	89·95	9·95	84·98

TABLE 3

	β (% atm.$^{-1}$)			$-B$ (ml./mol.)		
substance	31·19° C	65·94° C	84·98° C	31·19° C	65·94° C	84·98° C
air	0·6	0·7	0·9	7	1	−2
carbon dioxide	—	0·8	0·9	120	90	80
benzene	—	1·6	1·8	—	1050	920
cyclohexane	—	0·9	1·3	—	1190	1050
n-hexane	—	0·6	1·4	—	1220	1090
diethyl ether	—	2·0	2·1	—	760	680
chloroform	—	1·4	2·3	—	840	740
ethyl chloride	1·8	0·8	0·7	—	520	450
acetonitrile	—	25·0	11·0	—	3000	2300
acetaldehyde	5·3	2·7	2·0	1100	800	650
methyl alcohol	—	18·0*	8·0	—	1180	940
acetone	—	4·6*	3·4	—	1360	930

* Limiting values of β extrapolated to zero pressure.

DISCUSSION

It is clear from inspection of the values of β and B in table 3 that there is no functional relationship between departure from Maxwell's law and gas imperfection as measured by the second virial coefficient. This is in accordance with theoretical expectation. Modifications of the elementary formula

$$k = \tfrac{1}{3}\rho \bar{u} l C_v$$

for the case of real gases (cf. Hirschfelder, Bird & Spotz 1948, 1949) involve correction of the value of the mean free path for variation of temperature, but no dependence of k on pressure. Such a dependence would occur, if the variation of C_v with pressure for a real gas were taken into consideration, but it is likely that the factors involved have already been allowed for in the correction applied to the mean free path. The experimental results show that such an effect, if it occurs at all, must be very small.

Comparison of the results reported here with the conclusions of Lambert *et al.* (1949) shows that the four vapours here described as class II are those previously classified as showing association; while the vapours here described as class I were all previously classified as non-associated at the temperatures investigated. This suggests that the difference in behaviour between class I and class II is due to the fact that the latter are associated while the former are not. The two groups of conductivity results will therefore be discussed separately on these lines.

The most obvious explanation of the small rise in thermal conductivity with increasing pressure observed with all the vapours of class I is that it is due to convection. But it is not to be expected that convection effects should be so large in vertical tubes of 3 mm. diameter, and should increase with rise of absolute temperature. Further, the attempt to find any simple function of density, specific heat, and viscosity of the different gases and vapours which would be roughly proportional to the observed values of β proved unsuccessful. These are the only factors likely to influence a convection process under constant temperature conditions, and it seems likely that something other than convection, possibly an accommodation effect, plays a major part in the phenomenon. This might account for the fact that Milverton (1934), using a conductivity cell with wider *glass* tubes (8 mm. diameter), which would be expected to allow increased convection, found a much smaller effect of pressure on the thermal conductivity of air. The equations for an accommodation effect given by Gregory & Archer (1933) will not fit a linear increase of conductivity with pressure, and no quantitative treatment appears possible without further experiments on these vapours.

The effect of reversible dimerization on the thermal conductivity of a vapour has been theoretically treated by Schäfer & Foz Gazulla (1942), who predict a linear variation in thermal conductivity with pressure given by the equation

$$k_p = k_0\left[1 - \frac{0{\cdot}388p}{K_p} + \frac{0{\cdot}824p}{K_p}\frac{\Delta H\,\Delta U}{2RT^2C_v}\right],$$

where K_p is the mass-action equilibrium constant for the dimerization process $2A \rightleftharpoons A_2$ (i.e. $K_p = p_A^2/p_{A_2}$), ΔH the heat of dimerization at constant pressure, ΔU the heat of dimerization at constant volume, and C_v the molar specific heat of the monomer. δ the coefficient of p on the right-hand side of the equation is then given by

$$\delta = \frac{1}{K_p}\left[\frac{0{\cdot}412\,\Delta H\,\Delta U}{RT^2C_v} - 0{\cdot}388\right].$$

Values of K_p for the four vapours acetaldehyde, acetonitrile, acetone and methyl alcohol were calculated by Lambert *et al.* (1949) from the measured second virial coefficients. Plots of $\log K_p$ against T^{-1} were linear for acetaldehyde and acetonitrile, and enabled constant values of ΔH to be derived, and hence of ΔU. If these are inserted in the above equation together with the best available values of C_v, values of $\beta (= \delta \times 100)$ may be calculated. These are compared with the observed values, obtained from the thermal conductivity measurements, in table 4. C_v values for acetonitrile were taken from Thompson (1941), and for acetaldehyde from Bennewitz & Rossner (1938). Both values have been confirmed by (unpublished) sound-velocity measurements in this laboratory. In view of the fact that the observed values of β must include a small convection/accommodation effect, for which allowance has not been made, and that considerable approximations are involved in all aspects of the theoretical treatment, the agreement between observed and calculated values of β is fair, both as regards actual magnitude, and variation with temperature.

TABLE 4. COMPARISON OF β CALCULATED FROM THE SECOND VIRIAL COEFFICIENT WITH β OBSERVED FROM THE THERMAL CONDUCTIVITY

substance	temp. (° K)	K_p (atm.)	$-\Delta H$ (cal.)	C_v (cal./mol.)	β calc.	β obs.
acetonitrile	339·2	13·4	5200	11·4	25	25
	359	20·9	5200	11·84	13	11
acetaldehyde	304·2	41·2	4600	11·77	7·5	5·3
	339·2	98·2	4600	12·8	2·2	2·7
	359	132·0	4600	13·3	1·3	2·0

The other two associating vapours, acetone and methyl alcohol, both gave *curved* plots of $\log K_p$ against T^{-1}, suggesting either that ΔH varies markedly with temperature, or that in these cases association proceeds to polymers higher than the dimer, thus invalidating the calculation of K_p from the second virial coefficient. This latter view would seem to be confirmed by the fact that thermal conductivity measurements show a k_p against p curve which deviates (strongly in the case of methyl alcohol) from the linear form predicted theoretically for a dimerization, giving an unexpectedly large increase in k_p at higher pressures. Similar k_p against p curves have recently been obtained for methyl alcohol and ethyl alcohol vapours by Foz Gazulla, Colomina & Garcia (1948). This effect cannot be due merely to the vapour becoming almost saturated, as measurements on other vapours were carried closer to their saturated vapour pressures. The curvature in both cases almost vanishes at the higher temperature, as might be expected if it were due to formation of higher polymers. It is interesting that steam, whose second virial coefficient indicates that it is associated (Foz Gazulla & Vidal 1947), shows a linear k_p against p curve (Milverton 1935; Foz Gazulla *et al.* 1948), indicating simple dimerization, in contrast to methyl and ethyl alcohols.

The case of ethyl chloride was discussed in detail by Lambert *et al.* (1949), and it was then concluded that it might be a borderline case where the degree of dimerization at, or above 50° C, the lowest temperature at which the second virial coefficient was measured, is too small to have a measurable effect. The conductivity measurements, showing a small value of β, which decreases markedly between 31 and 66° C, but remains almost constant between 66 and 85° C, are in accord with the view that dimerization begins to set in to an appreciable extent only at temperatures below 50° C.

Such measurements by other observers as are available show rough quantitative agreement as far as the general behaviour of β is concerned. Foz Gazulla *et al.* (1948) obtain for methyl alcohol a limiting value (extrapolated from the lower end of the curve) of 10 for β at 79·3° C as compared with 8 (table 3 above) at 85° C, and a much lower value at 100° C. They also find a negligibly small value of β for benzene at both temperatures. Schäfer & Foz Gazulla (1942) find for ethyl chloride at 26·4° C, $\beta = 1{\cdot}7$, as compared with 1·8 (table 3) at 31·2° C, and they obtain a negligibly small value at 76·5° C. Milverton (1935) obtained β values for acetaldehyde at 31 and 85° C which are roughly double those given in table 3. There is thus general agreement that vapours which have been characterized as associated tend to have high values of β which decrease markedly with rise in temperature. The absolute value of β appears to depend to some extent on the apparatus. It may be significant that the β values reported here agree much better with those of Schäfer & Foz Gazulla (1942) and Foz Gazulla *et al.* (1948), who both used hot-wire apparatus with *brass* tubes, than with those of Milverton (1935), who used apparatus with *glass* tubes. This does not affect the validity of the measured values of k_0, as is shown by the good agreement on acetaldehyde (table 1).

The authors are grateful to Dr B. Lambert for much help and advice in the construction of the apparatus.

REFERENCES

Bennewitz, K. & Rossner, W. 1938 *Z. phys. Chem.* B, **39**, 126.
Eucken, A. 1911 *Phys. Z.* **12**, 1101.
Foz Gazulla, O. R., Colomina, M. & Garcia, J. F. 1948 *An. Soc. esp. Fis. Quim.* B, **44**, 1055, 1083.
Foz Gazulla, O. R. & Vidal, J. M. 1947 *An. Soc. esp. Fis. Quim.* B, **43**, 842.
Gregory, H. & Archer, C. T. 1933 *Phil. Mag.* **15**, 301.
Hirschfelder, J. O., Bird, R. B. & Spotz, E. L. 1948 *J. Chem. Phys.* **16**, 968.
Hirschfelder, J. O., Bird, R. B. & Spotz, E. L. 1949 *Chem. Rev.* **44**, 205.
Lambert, J. D., Roberts, G. A. H., Rowlinson, J. S. & Wilkinson, V. J. 1949 *Proc. Roy. Soc.* A, **196**, 113.
Mann, W. B. & Dickins, B. G. 1932 *Proc. Roy. Soc.* A, **134**, 77.
Milverton, S. W. 1934 *Phil. Mag.* **17**, 397.
Milverton, S. W. 1935 *Proc. Roy. Soc.* A, **150**, 287.
Schäfer, K & Foz Gazulla, O. R. 1942 *Z. phys. Chem.* B, **52**, 299.
Thompson, H. W. 1941 *Trans. Faraday Soc.* **37**, 344.

Polar structures in the theory of conjugated molecules
I. Identification of the ethylene π-electron states

By D. P. Craig

Sir William Ramsay and Ralph Forster Laboratories, University College, London

(*Communicated by C. K. Ingold, F.R.S.—Received* 21 *December* 1948)

This and two of three parts to be published subsequently are concerned mainly with the so-called valence-bond theory of conjugated and aromatic molecules. An improvement to the method is described, which consists in adding to the usual set of structures some extra ones which are 'polar' in the sense that they show two of the π-electrons on one centre, and none on another centre, making these two centres carry respectively negative and positive charges. This adds a certain flexibility to the description of molecular states which is lacking when the electrons are supposed to be distributed one to each centre throughout.

In this part a preliminary question is treated which bears on getting the new empirical parameters needed for including polar structures in the theory. This question is the assignment of the long wave-length bands in the spectrum of ethylene. The assignment is made with the help of a theoretical study of the ethylene energy levels in an approximation using antisymmetric molecular orbitals. Using this calculation as a guide, two transitions are assigned. A weak band, appearing at about 2000 Å, is taken to be ${}^1A_g$–${}^1A_g$, and a strong one, having its maximum at about 1630 Å, is taken to be ${}^1A_g$–${}^1B_{1u}$.

INTRODUCTION

There are two methods in common use for the quantitative study of the π-electron states in aromatic and conjugated molecules. They are the 'Method of valence-bond structures' (V.B.) (Hückel 1931) and the 'Method of molecular orbitals' (M.O.) (Lennard-Jones 1929; Hückel 1932; Mulliken 1932). Both were developed for dealing with molecular ground states, and in such states their agreement with one another, and the satisfactory account they give of the phenomenon of resonance stabilization, have established their correctness in essentials. However, the use of these same methods in molecular excited states is far more tentative and prescribed. Sklar (1937) used the V.B. method to establish the nature of the first excited state of benzene, and his conclusions are supported experimentally. Other calculations in aromatic molecules have since been made by the V.B. method which have gone to show excellent agreement with energy values for the low excited states, and these agreements have tended to confirm that the nature of the excited states is as described by the V.B. method. But the theory fails to give the intensities of spectral transitions; indeed, its results are that the transitions are all forbidden, and this result holds whatever formal selection rule may follow from symmetry properties.

In M.O. theory, there are special difficulties in excited states, and these have so far stood in the way of its use to any large extent. Goeppert-Mayer & Sklar (1938) used a related but much more elaborate procedure called the method of antisymmetric molecular orbitals (A.S.M.O.) to work out the low states of benzene, and the results they obtained agree qualitatively with the V.B. method, and with experiment, for the lowest excited state. Also, recently, Coulson (1948) has used the M.O. method to discuss the states of naphthalene and higher members of the 'acene series.

The failure of the V.B. calculations to give spectral intensities is closely connected with another conspicuous weakness in the method. That is the neglect of what we shall call 'polar character' in π-electron bonds. The V.B. calculation starts from 'structures' in each of which there is exactly one π-electron per carbon atom as in 1, 2 and 3 of figure 1. There are other possible structures, such as 4, in which the electrons are not uniformly distributed, and it is not physically satisfactory to suppose these to be negligible. In contrast, the M.O. method gives polar structures of all kinds great prominence, including types 5 and 6 as well as 4.

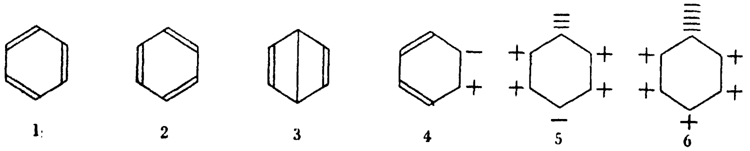
1 2 3 4 5 6

FIGURE 1

The whole question of polar structures therefore is linked with a number of important matters both in the performance of the V.B. method itself, and in its contrast with the M.O. method. Further, it is clear that without polar structures, there will be no chance of getting a V.B. theory of chemical reactivity in the many cases where reactivity is displayed towards an attacking group which carries a charge, and in conjunction with which polar structures will have to play a special part.

In this and following parts, polar structures are included in the V.B. method and some of the consequences that follow worked out in special cases. Broadly, the first two parts are given over to the details of the method, and the third to its application to benzene. Of critical importance to the whole programme is the question of the new parameters required for working with polar structures; the more of these there are the more accurate ought the treatment to be. But a limit is set by the fact that to get each new constant, a separate experimental quantity is needed, and in this work we shall use only three new parameters on this count, evaluating them from the spectrum of ethylene. In this part, therefore, the energy levels of ethylene are examined, and an assignment of the spectral bands made. From these, in part II, the parameters are obtained and the methods for including polar structures described.

$$\underset{\text{I}}{CH_2{=}CH_2} \qquad \underset{\text{II}}{CH_2^-{-}CH_2^+} \qquad \underset{\text{III}}{CH_2^+{-}CH_2^-}$$

FIGURE 2

The new parameters which have to be evaluated are the following: first, the coulomb energy of the structure II (figure 2) in excess of that of I; secondly, the interaction energy between polar and non-polar structures which settles to what extent resonance takes place between structures I and II; and thirdly, the exchange integral which comes in between pairs of polar structures such as II and III. These three parameters are found by using experimental results on three energy states of ethylene. The object of the present paper is to justify a particular interpretation of the absorption spectrum of ethylene. The central fact required is the symmetry property of the lowest excited spectral state, for it is this which enables an association to be made between calculated and experimental energy states, and which therefore enables evaluation of the parameters which appear in later computations.

PRELIMINARY DESCRIPTION OF THE π-ELECTRON STATES

The two electrons which go to the formation of the π-bond in ethylene are in orbitals which are antisymmetric to the plane of the molecule, and their interactions with the other bonding electrons can be neglected so far as exchange effects are concerned.* These two π-electrons in ethylene interact in four different ways, giving four states whose energies and symmetry properties form the subject of what follows. In the planar model of ethylene these states belong to two representations of the group D_{2h}, to which planar ethylene belongs. One of these is the A_g representation which is symmetrical to all the operations of the group, and the other is B_{1u}, which is antisymmetrical to reflexion in a plane perpendicular to the C-C direction. The naming of the axes, and a part of the character table for group D_{2h}, are given in figure 3. Capital letters will be used in symmetry symbols for molecular states, and small letters (a_g, etc.) for one-electron wave functions and for nuclear vibration wave functions.

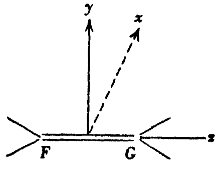

	E	C_2^x	C_2^y	C_2^z
A_g	+	+	+	+
B_{1u}	+	−	−	+
B_{2g}	+	−	+	−
B_{3u}	+	+	−	−

FIGURE 3

A simple view of the ethylene energy levels is given by the molecular orbital method, first used for this purpose by Mulliken (1932), and lately summarized by him in a review (Mulliken 1942). In terms of this method the four states of ethylene come from the four ways of assigning the two electrons (having regard for spin) to two molecular orbitals. These molecular orbitals are made up from the $2p$ orbitals ($2p_x$ orbitals with the convention of figure 3) of the carbon atoms F and G. The two orbitals, excluding overlap, are:

$$(1)\quad (\psi_F+\psi_G)\frac{1}{\sqrt{2}}\quad \text{symmetry } b_{3u}$$

$$(2)\quad (\psi_F-\psi_G)\frac{1}{\sqrt{2}}\quad \text{symmetry } b_{2g}.$$

---

* The interactions between π-electrons and the electrons in σ-bonds are interelectronic repulsions between the respective charge distributions. Arguments about wave-function symmetries say nothing about these terms, except that the π-electron distribution certainly has a node where the σ-electron distribution has its maximum, and therefore that the two are to some extent separate. There is no reason, however, for supposing these repulsive terms to be negligibly small; to justify their omission it would perhaps have to be shown that they appeared in all states with about the same magnitude.

Orbital 1 is a bonding orbital, and 2 is antibonding. When both electrons are in orbital 1 they bind the molecule to the greatest possible extent, and the state is therefore the ground state. The symmetry is $b_{3u} . b_{3u} = A_g$. When one electron is in orbital 1, and the other raised to orbital 2, the molecule is in an excited state of symmetry $b_{3u} . b_{2g} = B_{1u}$, and can be in either a singlet state (denoted by ${}^1B_{1u}$) or a triplet (${}^3B_{1u}$). When both electrons have been raised to the antibonding orbital 2 the state has the same symmetry as the ground state: $b_{2g} . b_{2g} = A_g$. Clearly the B_{1u} states of this approximation (*one* electron elevated) are lower in energy than the excited A_g state in which *both* electrons are elevated, and Mulliken has interpreted the long-wave absorption spectrum of ethylene as involving the allowed transition $A_g - {}^1B_{1u}$. The energy-level diagram obtained in this approximation is shown on the left-hand side of figure 5.

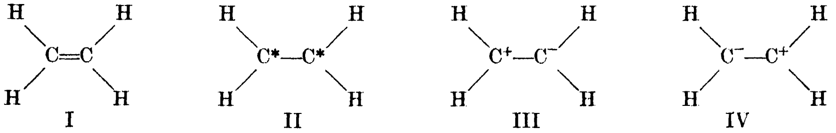

FIGURE 4

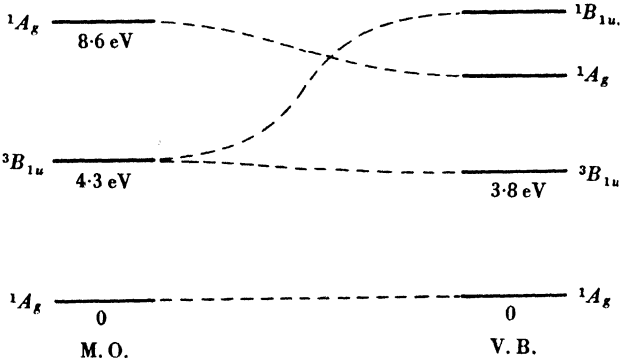

FIGURE 5

Going over to the valence-bond treatment of ethylene, we now wish to work with the augmented basis of figure 4, consisting of the ordinary non-polar structure I, the polar structures III and IV, and the triplet structure II. The triplet structure has the same symmetry properties (${}^3B_{1u}$) as were found in the molecular orbital case, and since it does not affect the singlet states no discussion is needed. The non-polar structure I has symmetry A_g; the polar structures can be combined to give A_g or B_{1u}. The former combination interacts with I to give a stabilized ground state (mostly non-polar in character) and a destabilized state (mostly polar). The B_{1u} combination cannot interact with the non-polar structure and is in full correspondence with the ${}^1B_{1u}$ state found in the M.O. method. In figure 5 the M.O. and V.B. states are set out. The M.O. values include overlap, and the value 2·0 eV has been used for the parameter β which occurs. The order of the V.B. states is settled by the sign of the exchange integral for polar structures. By analogy with the ordinary V.B. exchange integral, this is expected to be negative, and has been made so in drawing the diagram. As they stand, the two approximations are in disagreement as to the order in which the energy levels fall. In the M.O. method the unsymmetric singlet state falls lower than the symmetric one; in the V.B. method the situation is reversed. In attempting to interpret the spectrum of ethylene, therefore, it is important to find out which of these two is correct. The conclusion from the following work is, broadly, that when interelectronic repulsion is included explicitly in the calculations, the M.O. singlet and triplet states of symmetry B_{1u} (shown together in figure 5) are very strongly split up, so that the singlet component is raised to about the same energy as the excited A_g state. Starting from this a reasonable account can be given of the absorption spectra of ethylenic compounds, according to which the excited A_g state is actually slightly below the ${}^1B_{1u}$.

CALCULATION OF THE ENERGY LEVELS

We now make a calculation of the ethylene energy states by a method essentially distinct from the simple ones used in the preliminary comparison. Since there is no really satisfactory non-empirical method for getting accurate wave functions for so complex a system as ethylene, we have to adopt a method which will give, without using empirical constants, the relative magnitudes of quantities which decide the sequence of energy levels. For this limited objective we shall at first use, with slight modifications, the method of antisymmetric molecular orbitals of Goeppert-Mayer & Sklar (1938).* The required molecular orbital wave functions are the following:

$$(1)\quad {}^1A_g\,(\text{ground})\colon \frac{1}{2\sqrt{\sigma_1^2}}\{\psi_F(1)+\psi_G(1)\}\{\psi_F(2)+\psi_G(2)\}\times\frac{\alpha(1)\,\beta(2)-\alpha(2)\,\beta(1)}{\sqrt{2}},$$

$$(2)\quad {}^1A_g\,(\text{excited})\colon \frac{1}{2\sqrt{\sigma_2^2}}\{\psi_F(1)-\psi_G(1)\}\{\psi_F(2)-\psi_G(2)\}\times\frac{\alpha(1)\,\beta(2)-\alpha(2)\,\beta(1)}{\sqrt{2}}.$$

$$(3)\quad {}^1B_{1u}\colon \frac{1}{2\sqrt{(\sigma_1\sigma_2)}}\{\psi_F(1)\,\psi_F(2)-\psi_G(1)\,\psi_G(2)\}\times\frac{\alpha(1)\,\beta(2)-\alpha(2)\,\beta(1)}{\sqrt{2}},$$

$$(4)\quad {}^3B_{1u}\colon \frac{1}{2\sqrt{(\sigma_1\sigma_2)}}\{\psi_F(1)\,\psi_G(2)-\psi_F(2)\,\psi_G(1)\}\times\alpha(1)\,\alpha(2)\quad(\sigma_1=1+S;\sigma_2=1-S),$$

in which ψ_F stands for the $2p_x$ orbital of carbon atom F. One only of the triplet spin wave functions is shown. The electronic energy is now evaluated in two stages. The 'orbital' part involves calculating the energy of molecular orbitals in the field of two carbon ions, i.e. carbon atoms stripped of their $2p_x$ electrons and held, in the ground state, at 1·34 Å apart. These 'molecular orbitals' will be quite different in energies from those found in what is usually called the molecular orbital treatment. Here the orbitals are calculated for the field of two carbon ions; the Hückel molecular orbitals, on the other hand, are found for the averaged field of the two carbon ions *and one*

---

* Ethylene was first studied by Hartmann (1943) in this way, and recently by Parr & Crawford (1948), with special emphasis in the latter case on variation of the energies with twisting angle. The present discussion therefore goes into details only where the viewpoint is different, viz. in the variation of the effective nuclear charge and internuclear distance, and in the treatment of the two totally symmetric states.

electron. The energies obtained by this procedure are corrected by a term which takes care of the interelectronic repulsion. The four wave functions involve two molecular orbitals whose energies are:

$$\epsilon_1 = W_{2p} + \frac{1}{\sigma_1}(-Q - A_1 - R - B), \quad \epsilon_2 = W_{2p} + \frac{1}{\sigma_2}(-Q - A_1 + R + B),$$

in which the symbols used conform with those used by Sklar, and have the following meanings:

W_{2p} = electronic energy of a $2p_x$ carbon orbital,

$$-Q = \int \psi_G(1)\,\mathscr{H}_F\,\psi_G(1)\,d\tau_1, \qquad \mathscr{H}_F = \text{potential of neutral carbon } F,$$

$$-R = \int \psi_F(1)\,\mathscr{H}_F\,\psi_G(1)\,d\tau_1,$$

$$A_0 = \iint \psi_F^2(1)\frac{e^2}{r_{12}}\psi_F^2(2)\,d\tau_1 d\tau_2, \qquad B = \iint \psi_F^2(1)\frac{e^2}{r_{12}}\psi_F(2)\,\psi_G(2)\,d\tau_1 d\tau_2,$$

$$A_1 = \iint \psi_F^2(1)\frac{e^2}{r_{12}}\psi_G^2(2)\,d\tau_1 d\tau_2, \qquad C = \iint \psi_F(1)\,\psi_G(2)\frac{e^2}{r_{12}}\psi_F(2)\,\psi_G(1)\,d\tau_1 d\tau_2,$$

$$\sigma_1 = 1 + S, \qquad \sigma_2 = 1 - S, \qquad S = \int \psi_F(1)\,\psi_G(1)\,d\tau_1.$$

Introducing the electron repulsion, the energies of the states are:

$$E(A_g, \text{ground}) = 2\epsilon_1 + \frac{1}{4\sigma_1^2}(2A_0 + 2A_1 + 8B + 4C),$$

$$E(A_g, \text{excited}) = 2\epsilon_2 + \frac{1}{4\sigma_2^2}(2A_0 + 2A_1 - 8B + 4C),$$

$$E(^1B_{1u}) = \epsilon_1 + \epsilon_2 + \frac{1}{2\sigma_1\sigma_2}(2A_0 - 2C),$$

$$E(^3B_{1u}) = \epsilon_1 + \epsilon_2 + \frac{1}{2\sigma_1\sigma_2}(2A_1 - 2C).$$

A planar configuration is taken for all these states; the present method is not well adapted to other cases, and the fact that the absorptions of cyclic olefins differ little in frequency from that of ethylene is an assurance that the sort of information we require from this calculation will not be falsified by the assumption of planarity.

In settling on suitable values for the integrals that occur in the energy expressions, we have departed somewhat from the method of Goeppert-Mayer & Sklar. There seems to be a strong case for varying the value of the effective nuclear charge Z from the value (3·12 in the work of Coulson & Duncanson (1943)) appropriate to isolated carbon atoms, to a greater value for states where the π-electron interaction is attractive, and to a smaller value where the interaction is repulsive. Following Coulson & Duncanson, Z has been increased in the ground state by a factor of 1·1, from 3·12 to 3·432. For the other three states, Z has been reduced by a factor of 0·9, from 3·12 to 2·808. Next we need the internuclear distance $\mathscr{R}$ in excited states.

These are not available experimentally. Now double-bond formation shortens a C—C bond from 1·54 to 1·34 Å. We have supposed, therefore, that repulsive exchange interaction would stretch the C—C bond to about 1·65 to 1·7 Å. For the excited singlet states, with considerably greater repulsion at work, we have supposed the stretching to be about 0·3 Å. The nearest values to these for which the integrals are tabulated are 1·67 and 1·88 Å, and these have been used. The values are not at all critical in deciding the relative positions of the calculated states. Table 1 sets out the values of the integrals that are used. The values have been obtained from the papers by Sklar & Lyddane (1939) and Griffing (1947), and by Parr & Crawford (1948):

TABLE 1

state	$\mathscr{R}$ (Å)	Z	$Z\mathscr{R}/a_0$	S	A_0 (eV)	A_1 (eV)	B (eV)
$^1A_{1g}$	1·34	3·432	8·67	0·2395	18·272	9·501	3·230
$^3B_{1u}$	1·67	2·808	8·87	0·2265	—	7·632	2·482
$^1B_{1u}$, $^1A_{1g}$	1·88	2·808	10·00	0·164	14·950	6·913	1·719

state	C (eV)	Q (eV)	R (eV)	ϵ_1	ϵ_2
$^1A_{1g}$	0·853	0·794	1·789	$W_{2p}-12{\cdot}355$	—
$^3B_{1u}$	0·624	0·573	1·342	$W_{2p}-9{\cdot}808$	$W_{2p}-5{\cdot}664$
$^1B_{1u}$, $^1A_{1g}$	0·313	0·268	0·798	$W_{2p}-8{\cdot}43$	$W_{2p}-5{\cdot}443$

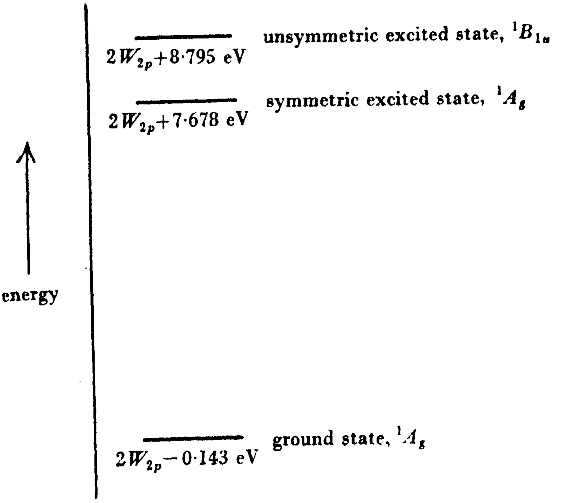

FIGURE 6

This first estimate of the energy levels enables us to gauge the different effects of electron repulsion on the two excited singlet states. Electron repulsion acts more strongly in destabilizing the $^1B_{1u}$ state than it does in the excited A_g state, and the significant result is that the two states are brought to approximate energy equality, with the same order as is expected in V.B. theory. This latter fact, however, depends on too small a margin to be significant, a point which is nicely illustrated by the reversal of order, again by a small margin, which takes place in the next approximation. The reason is that the dominating repulsive term is the one between two electrons on the same carbon atom; the $^1B_{1u}$ state is entirely polar, and consequently this repulsive term comes in with a larger coefficient than it does in the excited A_g state, which is only partly polar. It is important to note that this bringing together of the simple M.O. levels due to electron repulsion persists through a wide range of assumptions about screening constants and internuclear distances in the states. With any reasonable choice of these constants it remains true that the unsymmetric singlet state corresponding with the elevation of one electron is much more strongly destabilized by electron repulsion than the symmetric state from the elevation of two electrons.

It is a feature of the molecular orbital wave functions we have used that these introduce polar structures into the two A_g states to a fixed degree. It would be unlikely to find that this amount of participation were just that required, for example, to minimize the energy of the ground state; instead, we should expect to find that the energies of the two A_g states would be pushed further apart in a more accurate treatment. The next step therefore is to examine the effect of varying the importance of polar structures in these states. The procedure is the following. We take the wave function

$$\Psi = \frac{1}{N}[p\psi_F(1)\,\psi_F(2) + \psi_F(1)\,\psi_G(2) + \psi_F(2)\,\psi_G(1) + p\psi_G(1)\,\psi_G(2)]$$

containing a parameter p, through the variation of which the ratio of polar to non-polar components can be changed. The energy is then minimized with respect to p, giving a value for the ground state, and maximized giving a value for the excited A_g state.* The values for these states obtained in the antisymmetrical molecular orbital treatment correspond to p equal to 1 and -1 respectively. For other values of p the wave function loses its molecular orbital character, for it can no longer be split into two factors. Accordingly, the expanded form of the wave function given above has to be used for the determination of the orbital part of the energy as well as the electron repulsion part.

The value of N, the normalizing coefficient, is given by

$$N^2 = 2(p^2+1) + 8pS + 2S^2(p^2+1).$$

The energy of the electrons in the field of the carbon ions, $E(\mathrm{C})$, is

$$E(\mathrm{C}) = \frac{1}{N^2}\iint \Psi[H_F + H_G + T(1) + T(2)]\,\Psi\,d\tau_1 d\tau_2,$$

where H_F and H_G are potentials due to the carbon ions F and G, and the T's are kinetic-energy operators. H_F, for example, is the difference between the potential due to a neutral carbon atom, and the potential due to the $2p_x$ electron by which the ion differs from the neutral atom

$$H_F = \mathscr{H}_F - \int \frac{e^2}{r_{12}}\psi_F^2(1)\,d\tau_1,$$

---

* It will be recognized that if the same values of Z and $\mathscr{R}$ were used for both states this would lead to the same energy values and wave functions as come from Parr & Crawford's variation calculation between the two totally symmetric M.O. wave functions. Both calculations would give the same two stationary values of the energy and corresponding wave functions. The present procedure is useful here because it shows the roles of polar and non-polar structures explicitly, and so links up with the later discussion.

$\mathcal{H}_F$ being the potential due to a neutral carbon atom. Then

$$E(\mathrm{C}) = 2W_{2p} + \frac{1}{N^2}[4(p^2+2pS+1)(-Q-A_1)+4(p^2S+2p+S)(-R-B)],$$

in which W_{2p} is the energy of an electron in an isolated carbon $2p$ orbital. Now the electron repulsion terms, $E(\mathrm{R})$, are included:

$$E(\text{total}) = E(\mathrm{C}) + E(\mathrm{R})$$

and
$$E(\mathrm{R}) = 1/N^2(2p^2A_0 + 2A_1 + 8pB + 2p^2C + 2C).$$

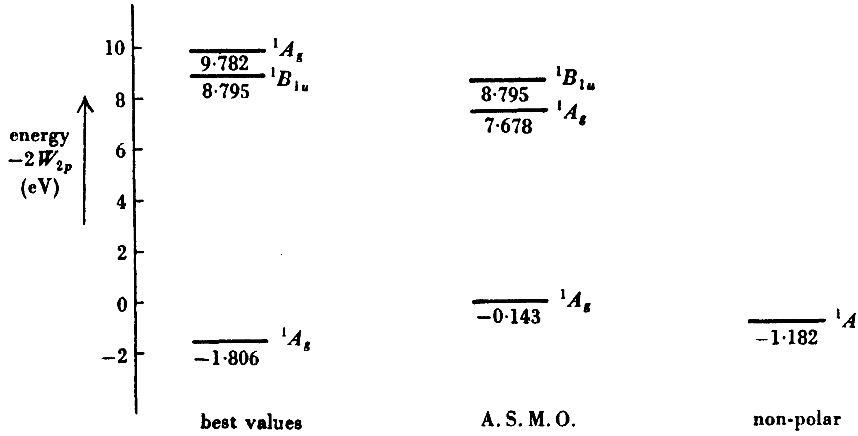

FIGURE 7

After inserting the appropriate values for the integrals, this expression has to be minimized with respect to the parameter p. For the ground state we insert the values given in table 1, and find that the energy is least for p equal to 0·264. This corresponds to an electronic energy $2W_{2p} - 12{\cdot}574$ eV, a lowering of about 1·6 eV from the A.S.M.O. ground state. For the excited A_g state the proper values of internuclear distance and screening constant are again taken from table 1, and the energy maximized with respect to p. That this energy maximum is the required approximate energy eigenvalue may be seen from the fact that it is identical with the upper root of the two-rowed secular equation arising from a variation calculation between the two M.O. totally symmetrical wave functions, both being appropriate (in values of Z and $\mathcal{R}$) to the excited configuration. The electronic energy is $2W_{2p} + 2{\cdot}10$ eV, the corresponding value of p being $-2{\cdot}17$. The energy diagram in this approximation is given in figure 7; in the same figure the information of figure 6 is given in the centre. In the right-hand column is shown the ground state energy worked out for $p = 0$; this, of course, gives a valence-bond type wave function, and it is to be noted that the ground-state energy found in this way is considerably closer to the energy minimized value than is that found by the A.S.M.O. procedure using molecular orbital wave functions. The correction for nuclear repulsion has been made in each case. It is found that in the energy minimized ground-state polar structures contribute 7 % to the wave function. The excited A_g state, on the other hand, is 82 % polar.

THE ABSORPTION SPECTRUM OF ETHYLENE

In interpreting the absorption spectrum of ethylene we start from the conclusion that follows from these calculations, namely, that electron repulsion brings the two excited singlet states to approximate energy equality. This suggests, as we shall now discuss, that what appears in the absorption spectrum of ethylene to be a very extended band is in reality two bands which overlap, involving as their final states the two excited singlet levels falling closely together according to the calculations.

The absorption spectrum of ethylene has been the object of considerable experimental study, in particular by Snow & Allsopp (1934), and by Price & Tutte (1940). Substituted ethylenes have been much studied by Carr & Stücklen (1936). Absorption in ethylene begins near 2000 Å with a very weak and diffuse band which appears to rise to a flat continuous maximum, intersected by some sharp and very narrow bands, at 1630 Å. The shorter wave-length part of this absorption has been studied in most detail by Price & Tutte (1940). They identified two transitions in this region. The sharp narrow bands start at 1750 Å and lead to a well-defined ionization limit marking the loss of one of the π-electrons. This system of bands is of no present interest. But superposed on the bands there is a diffuse region of absorption having its maximum at 1630 Å. This same region of absorption can be recognized in other olefins, and its intensity in one of them has been measured by Platt, Rusoff & Klevens (1943). They found the f value in octene-3 to be 0·25. Since absorption involving σ-electrons begins well below 1630 Å, this strong band must mark transitions between states of π-electrons. Its high intensity leaves no doubt that it is $A_g - {}^1B_{1u}$, for which Mulliken has calculated the f value to be 0·30. The diffuse and structureless character of the absorption have not been explained, but these are regular features of intense π-electron bands (e.g. the 1835 Å band in benzene) and so do not call for special discussion here.

Running to the long wave-length side of this intense absorption is an extended region of much weaker absorption which shows some structure. This absorption continues out to 2100 Å in ethylene, i.e. some 9000 cm.$^{-1}$ to the long-wave side of the intense peak. Mulliken (e.g. (1942)) has taken the view that this long-wave part is a vibrational progression of the 1630 Å band, extended with the aid of quanta of the CH_2 twisting mode of ethylene. There are, however, difficulties for this view. One would expect a sharp difference between ethylene and cyclic olefins such as cyclohexene in their twisting modes. But, as Snow & Allsopp (1934) have shown, the features of the absorption curves are very similar. Cyclohexene (Carr & Stücklen 1936) also shows a long wave-length absorption extending out from the intense band, and the long-wave part is actually rather more intense than in ethylene. Also Snow & Allsopp observed in the absorption of ethylene a vibrational progression, spaced at about 750 cm.$^{-1}$. But they found only five peaks, and then there is a gap showing no structure between the last peak and the 1630 Å maximum.

For these reasons we shall adopt an alternative explanation for the long wave-length absorption of ethylene, which is that it represents a separate transition from the 1630 Å band. This was first suggested by Snow & Allsopp (1934), and receives strong confirmation from the spectra of diallyl and, for example, cyclohexene.

Snow & Allsopp suggested that the weakness of the absorption at long wave-lengths was due to its being a singlet-triplet transition. The other possibility is that it is a symmetry forbidden A_g-A_g transition. Against the singlet-triplet view there is some evidence from the work of Lewis & Kasha (1944) who have examined the triplet states of many molecules through their phosphorescence spectra. Ethylene itself could not be studied in this way, but dichlor-, dibrom-, and di-iodo-ethylene were studied, and all three have a long-lived triplet state at 72 kg.cal./mole above the ground state. This corresponds with a singlet-triplet spectral transition at 4000 Å. Lewis & Kasha made the reasonable deduction from this and other evidence that the triplet state of the ethylenic π-electrons is what is observed in these halogen-substituted ethylenes, and therefore that its excitation from the ground state would correspond with absorption at 4000 Å. If this is correct, then the long-wave absorption at 2000 Å cannot be the singlet-triplet transition. The only other triplet state to which transitions could occur is a triplet Rydberg state. However, such Rydberg bands ought to be as sharp as those of 1750 Å are, whereas the observed bands are diffuse. Further, the band is observed in a 2 m. tube at 20 to 100 mm. pressure. This would be unusually strong for a singlet-triplet transition. For example, Lewis & Kasha had to use a 10 cm. path of almost pure *p*-dichlorobenzene to observe the singlet-triplet transition; and Sklar had to use a 20 cm. path of liquid benzene for the same purpose. On the evidence, therefore, it is unlikely that the 2000 Å band can be due to a singlet-triplet transition.

This leaves for consideration the assignment of the 2000 Å band as the symmetry-forbidden A_g–A_g transition whose energy according to the calculations we have given is near that of the A_g–B_{1u} transition at 1630 Å. The question that has to be settled is whether this transition can appear through the mixing of the excited A_g state with the B_{1u} state by nuclear vibrations. The formal symmetry requirements for such Herzberg-Teller mixing can of course be met, for there are certainly vibrations of class b_{1u}. But this is not in itself sufficient to mix the two upper states; in addition, it has to be the case that these vibrations can cause the appearance of electric dipoles in the π-electron distribution. If the π-electron distribution were determined solely by the carbon nuclear fields, then no such dipoles could appear, for there are no *carbon* vibrations of symmetries other than a_g. But provided there is some dependence of the π-electron wave function on the co-ordinates of the H atoms—and we are assured that this is the case because methyl-substituted ethylenes, for example, have different spectra from ethylene itself—then the hydrogen motions in a b_{1u} vibration will cause changes in the π-electron wave function and so make the A_g-A_g transition appear in the spectrum. The effectiveness of this sort of perturbation is rather less than that in say benzene, where carbon motions alone can cause mixing of the levels, and the ratio of stolen to total intensity is, in agreement with this, less in ethylene than in benzene.

The conclusion is that there are, apart from the Rydberg bands, two separate absorptions in the range 2100 to 1630 Å. Both are between pairs of singlet states, the weak one being symmetry forbidden and the strong one allowed. We have to settle on an 'average' energy-level diagram for a double bond, being influenced in this mainly by molecules such as cyclohexene where the environment of the double bond is like that in aromatic molecules to which later computations with polar structures are to apply. It seems best to round off the values, and this has been done, with the following result:

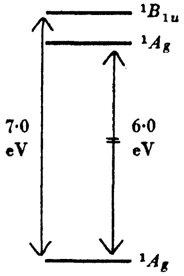

In part II these values are used for the determination of the new empirical constants for work with polar structures.

References

Carr, E. P. & Stücklen, H. 1936 *J. Chem. Phys.* **4**, 760.
Coulson, C. A. 1948 *Proc. Phys. Soc.* **60**, 257.
Coulson, C. A. & Duncanson, W. E. 1943 *Proc. Roy. Soc.* A, **181**, 378.
Goeppert-Mayer, M. & Sklar, A. L. 1938 *J. Chem. Phys.* **6**, 645.
Griffing, V. 1947 *J. Chem. Phys.* **15**, 421.
Hartmann, H. 1943 *Z. phys. Chem.* B, **53**, 96.
Herzberg, G. & Teller, E. 1933 *Z. Phys. Chem.* B, **21**, 410.
Hückel, E. 1931 *Z. Phys.* **70**, 204.
Hückel, E. 1932 *Z. Phys.* **76**, 628.
Lennard-Jones, J. E. 1929 *Trans. Faraday Soc.* **25**, 668.
Lewis, G. N. & Kasha, M. 1944 *J. Amer. Chem. Soc.* **66**, 2100.
Mulliken, R. S. 1932 *Phys. Rev.* **41**, 751.
Mulliken, R. S. 1939 *J. Chem. Phys.* **7**, 14.
Mulliken, R. S. 1942 *Rev. Mod. Phys.* **14**, 265.
Parr, R. G. & Crawford, B. L. 1948 *J. Chem. Phys.* **16**, 526.
Platt, J. R., Rusoff, I. & Klevens, H. B. 1943 *J. Chem. Phys.* **11**, 535.
Price, W. C. & Tutte, W. T. 1940 *Proc. Roy. Soc.* A, **174**, 207.
Sklar, A. L. 1937 *J. Chem. Phys.* **5**, 669.
Sklar, A. L. & Lyddane, R. A. 1939 *J. Chem. Phys.* **7**, 374.
Snow, C. P. & Allsopp, C. B. 1934 *Trans. Faraday Soc.* **30**, 93.

Flash photolysis and spectroscopy
A new method for the study of free radical reactions

By G. Porter, *Department of Physical Chemistry, University of Cambridge*

(*Communicated by R. G. W. Norrish, F.R.S.—Received* 9 *August* 1949)

(Plates 6 to 8)

Photochemistry provides us with one of the most generally useful methods of studying the reactions of free radicals and atoms, but the concentration of these intermediates in the usual photochemical systems is too low to allow the use of direct physical methods of investigation such as absorption spectroscopy.

To overcome this difficulty a new technique of flash photolysis and spectroscopy has been developed, using gas-filled flash discharge tubes of very high power. The properties of these lamps as spectroscopic and photochemical sources have been studied and details are given of their construction, spectra, duration of flash, and luminous efficiency in the photochemically useful region. An apparatus is described which produces a very great photochemical change, in some cases over 80 %, in one-thousandth of a second and in a gas at several cm. pressure contained in an absorption tube 1 m. long, and which photographs the absorption spectrum at high resolution in one twenty-thousandth of a second at short intervals afterwards.

Examples of the rapidly changing spectra of substances undergoing reaction, including the spectra of some of the intermediate radicals involved, are shown. These include the recombination of chlorine atoms, the absorption spectra of S_2 and CS obtained during the photochemical decomposition of carbon disulphide and new spectra attributed to the ClO and CH_3CO radicals.

Introduction

Investigations into the mechanism of chemical reactions have revealed that in very many cases intermediate substances are involved which, although they exist only for a very short time, determine the course and rate of the changes which take place. Much information has been obtained about these intermediates, which are usually free radicals or atoms, by induction from the kinetics of the overall change, but the indirectness of this method has so far rendered it incapable of giving the kinetic details of some of even the simplest radical reactions. We have much to learn, for example, about the combination of two methyl radicals. The mirror technique, developed by Paneth and his colleagues, is another powerful means of study, but suffers from similar limitations in so far as it depends on inference from the final products with the metal mirror, and it is also accompanied by some rather severe experimental difficulties (Norrish & Porter 1947).

The only direct methods of investigation which have been applied to the problem are spectroscopy and mass spectroscopy, and, of the two, the former is potentially the more powerful because it enables the reaction to be studied in a static system as well as giving information about the structure of the radical, and more certain identification. Furthermore, spectroscopy is ideally suited to free radical studies, as the majority of free radicals have a transition involving the ground state in the easily accessible visible or near ultra-violet regions and, as pointed out by Wieland (1947), this often forms an extremely sensitive method of detection.

Although the spectra of a large number of diatomic radicals are known from their emission bands in flames and discharge tubes, very little information about their chemical reactions can be obtained in this way because of the difficulty of estimating concentrations from emission spectra. Absorption spectroscopy, on the other hand, makes it possible to estimate concentrations and follow the reactions of the absorbing molecule without interfering with the reacting system, but unfortunately to observe a radical in absorption the concentration must be higher than is usually obtained by any method other than the electrical discharge. High equilibrium concentrations can be obtained by thermal decomposition, but it is not possible to change the temperature of the gas rapidly enough to use this method for kinetic studies. The electrical discharge method has been used very successfully by Oldenberg (1935) in a detailed study of the OH radical and also by White (1940). For the study of the chemistry of intermediate compounds, however, the method is limited to radicals which survive the violent conditions in a discharge tube, that is, virtually, to diatomic radicals, and to the pressures under which the discharge will take place. A further disadvantage is that the complexity of the reactions occurring in the discharge tube makes interpretation of the results impossible in all but the very simplest systems. Very few polyatomic radical spectra are known, and even in these cases the identity of the radical is doubtful.

Photochemical decomposition provides the best general method of preparation of free radicals as the overall reaction is relatively quite simple, the initial act and the radicals produced are better known than in any other type of reaction and nearly all radicals, both simple and complex, can be produced by photochemical means. No free radical has ever been detected in absorption in a photochemical reaction however, because the method has one great disadvantage; the concentration of radicals produced by even the most intense light sources is very low indeed. If this difficulty could be overcome, and free radicals could be followed spectroscopically in photochemical systems, an ideal combination would result. This communication describes how such a method has been developed, making use of the fact that illumination of the system for a longer time than the half-life of the radicals is not necessary so that a flash technique can be used. It is shown that a modification of a type of discharge lamp now in use as a photographic source is capable of producing a partial pressure of free radicals higher than has ever been obtained by photochemical or any other methods.

There is one other difficulty associated with kinetic absorption spectroscopy of all kinds, that of producing an image on the photographic plate in a short time, from a source of continuum. Other workers have resorted to the integration of a large number of short exposures, but this is not feasible in the apparatus described here, first, because with such a high percentage decomposition the absorption tube has to be removed and cleaned after each flash with many of the substances used, and secondly, because the high energy makes it necessary to cool the lamp between flashes, so that if several thousand flashes had to be used each spectrum would require an experiment of several days.

An attempt was made to overcome this difficulty by making use of the great sensitivity and rapid response time of photomultiplier tubes, and a rapid scanning system was built into a 10·5 ft. grating spectrograph for this purpose. If this method is to be suitable, a high resolution coupled with good signal/noise ratio is necessary. The noise, caused by statistical fluctuations in the photocurrent, can only be decreased by decreasing the band width and hence the resolution, and even with the brightest light sources available no satisfactory compromise was reached. Fortunately, investigations into the properties of flash discharge lamps as photochemical sources showed that they could be made to produce a very intense continuum over the whole spectral region, and a lamp was eventually designed which would record photographically down to 2000 Å in a large Littrow spectrograph in less than 10^{-4} sec.

The procedure adopted was to produce a high percentage decomposition of the reactant by a high intensity flash in a lamp alongside the 1 m. absorption tube and to record the absorption spectrum of the products as the reaction progressed by means of flashes from another lamp at the opposite end of the tube from the spectrograph. The requirements for these two lamps are slightly different. Both must be of very high intensity and must be capable of accurate synchronization, but whereas a maximum energy output in the region producing chemical change is the main consideration with the photolysis lamp, a continuous spectrum covering the whole ultra-violet region is required from the spectrographic source. The duration of the photolysis flash should be not greater than the half-life of the radicals which are to be studied, and the spectroflash must be shorter still if several snapshots of the changing radical spectra are to be obtained.

Of the several ways of obtaining a brief flash of light, high pressure gas-filled discharge tubes showed the best promise for this type of experiment. Very high energies can be dissipated in one flash, and by arranging the pressure to be high enough to prevent breakdown at the operating voltage until a trigger pulse is applied, accurate synchronization can be obtained without any power loss at a switch or spark gap. No previous investigation of the possibilities of this type of lamp for photochemical and spectroscopic purposes seems to have been carried out, and there follows a brief account of the properties of high-energy flash discharge lamps as emitters in the photographic ultra-violet.

FLASH DISCHARGE TUBES AS PHOTOCHEMICAL AND SPECTROSCOPIC SOURCES

The lamps used were all fundamentally very simple. They consisted of a gas-filled tube with an electrode at each end, across which the discharge condenser was connected, and some means of triggering the flash was provided near the centre of the tube, either in the form of an external coil or a third internal electrode. The main difference in design from the ordinary continuous source was in the pressure of the gas filling which must be high enough to prevent the discharge taking place until the triggering pulse is applied. Unless the lamp is to be flashed very frequently cooling is not necessary. It may be constructed in the shape and length most suitable for the particular application, and the other factors which can be varied are gas filling, gas pressure, capacity, voltage, and the material of the tube and electrodes.

Construction

Almost any ordinary continuous discharge lamp may be modified for flash work if the power per flash is not too high. Above about 100 J, however, it is necessary to use quartz tubes and large electrodes of tungsten or similar material with large current capacity seals of the type used in high-power mercury discharge lamps. Murphy & Edgerton (1941) have described the construction of lamps which were capable of dissipating 500 J per flash, and lamps of this kind are now produced commercially for photographic purposes. The maximum energy per flash used in the experiments described here was 10,000 J, and at these high values two difficulties appear. First, the discharge decomposes the material of the tube and electrodes as well as liberating any occluded gas which was not removed before filling. Although a small amount of impurity such as oxygen has very little effect on the output of the lamp, it has a very pronounced effect on the firing characteristics. The pressure of the original gas filling has to be high enough to prevent firing until the trigger pulse is applied, and after a few high-power flashes sufficient impurity may have been liberated to prevent the discharge being initiated by the application of this pulse, and evacuation of the tube and refilling is necessary. These troubles were partly overcome by intense heating of the tube during evacuation and by discharging the maximum capacity across the lamp and evacuating and refilling several times. At the highest powers used it was still necessary to refill the lamps frequently.

The other difficulties were caused by mechanical weaknesses in the seals and tubes. The high pressure developed is sometimes sufficient to explode the lamp, and the rapid heating sets up strains in the seals which may finally crack. By careful construction and the use of the latest type of tungsten-molybdenum quartz seals* these difficulties were eliminated up to powers where refilling after nearly every flash was necessary. The crazing of the tubes does not appear to weaken them unduly, and poisoning of the gas filling remains the most important energy limitation.

Duration of the flash

Edgerton found that when high capacities were used the current passed by the discharge tube tended to a maximum corresponding to a resistance of 0·2 Ω for a tube measuring 30 × 1·4 cm. That a corresponding maximum in light output is reached is shown by the oscillograph recordings in figure 1. These were taken by using a 1 P 28 photomultiplier cell which is sensitive over the whole region between 2000 and 8000 Å. The lamp was 1 m. × 1 cm. in size, was krypton filled at a pressure of 5 cm. Hg and the voltage was 4000 V. It is seen that the maximum output is reached very rapidly, and that this is followed by fairly constant emission whose duration is proportional to the capacity, and then an exponential decay. The secondary pulse is probably due to the circuit inductance.

The duration of the flash may be decreased by using shorter or wider tubes which decreases the resistance, but this reduces the power which can be dissipated per flash. For a given capacity the duration of the light pulse is proportional to the length of the tube. In figure 9 the short pulse from a 15 cm. long krypton-filled tube produced by the discharge of a 50 μF condenser charged to 4000 V is shown superposed on a 480 μF flash from the longer tube described above.

---

* These seals were supplied by Messrs Siemens and I am indebted to Dr J. N. Aldington and Mr A. J. Meadowcroft for information about the construction of photographic flash tubes.

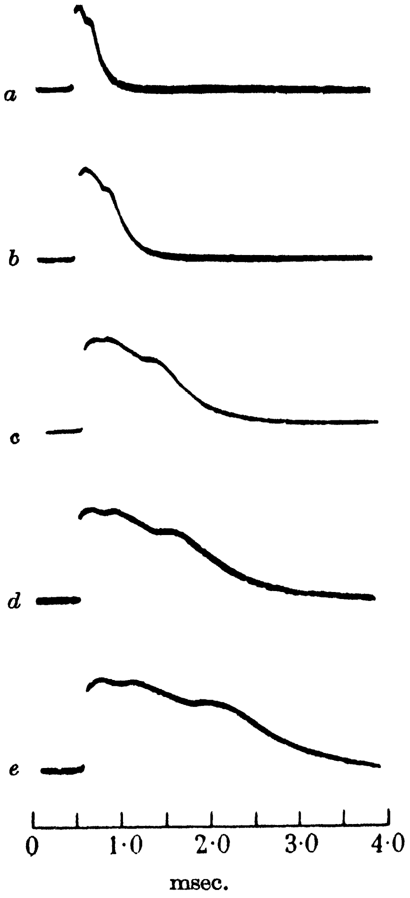

FIGURE 1. The effect of capacity on the shape and duration of the light pulse. Capacities in *a* to *e* were 48, 96, 240, 336 and 480 μF respectively.

Light output

In order to get some idea of the amount of photochemical change which could be obtained in a single flash and the efficiency of flash discharge lamps as emitters in the photochemically useful region, some experiments were carried out using a uranyl oxalate actinometer. The arrangement was exactly the same as would eventually be used in the complete apparatus. A metre-long lamp of the type described above was placed alongside a 1 m. quartz reaction vessel 2·5 cm. in diameter, both being surrounded by a cylindrical reflector coated on the inside with magnesium oxide which has a very high reflectivity in the ultra-violet. The reaction vessel was filled with 350 ml. of the oxalate solution, and the photochemical change produced by one flash was estimated by permanganate titrations using the methods recommended by Leighton & Forbes (1930). The maximum temperature rise recorded on a thermocouple placed in the solution was 0·6° C, and as the temperature coefficient is only 1·03 per 10° C this was a negligible effect.

Using a solution of 0·001 M-uranyl nitrate and 0·005 M-oxalic acid 11·6 % of the oxalate was decomposed by a single flash of 480 μF capacity which corresponds to the reaction of $2{\cdot}6 \times 10^{-4}$ g.moles in less than 2 msec. Repetition of this determination showed that the output per flash was constant to within 2 %. If we assume a quantum yield of 0·6 and that the average wave-length responsible for photochemical change is 3500 Å, the total energy necessary to produce this change is 145 J. The energy stored in the condenser is $\frac{1}{2}CV^2$ or 3840 J, so that the luminous efficiency of the whole system in the region between about 4800 and 2000 Å is 3·8 %. As the concentration of the oxalate is increased this figure also increases, and in figure 2 the efficiency, obtained as above, is plotted against the concentration of oxalate, the uranyl nitrate-oxalic acid ratio being always the same. By plotting reciprocals an extrapolation to infinite concentration corresponding to maximum absorption may be made which leads to a figure of 16·5 %. This gives a lower limit for the luminous efficiency of the flash source in the region of absorption of the uranyl ion and is a remarkably high figure, including, as it does, losses of all kinds, such as those due to incomplete discharge of the condenser and the impedance of the connexions. For an average wave-length of 3500 Å it corresponds to an output of 10^{21} quanta/flash or 5×10^{23} quanta/sec.

It is also necessary to know how the output of the lamp varies with the capacity per flash, and in figure 3 the photochemical change expressed in ml. of 0·005 N-permanganate per 25 ml. of oxalate is plotted for different capacities per flash, the total energy input into the lamp being the same in each case.

The exposures were as follows:

capacity	number of flashes	change/25 ml. (ml. 0·005 N-$KMnO_4$)
4	120	1·41
24	20	2·25
48	10	2·40
96	5	2·74
240	2	2·94
480	1	2·94

It is clear that only above a capacity of about 200 μF does the lamp reach maximum efficiency in this region, and that at higher capacities the efficiency is fairly constant.

Flash spectra

Whilst the main requirement for the spectrum of the photochemical source is that a higher percentage of the emission should be in the region to be used for the photolysis, the spectroflash must give a continuous spectrum over the whole region to be photographed with as few interfering lines as possible. Under ordinary conditions most gases give mainly a line spectrum in the discharge tube, but the continuum emitted by hydrogen is well known, and attempts were first made to produce this continuum at high intensity in a flash discharge. It was found, however, that a purer and more intense continuum could be obtained under flash conditions from the rare gases than from hydrogen. Except where otherwise stated the spectra shown were produced in a 12 mm. diameter quartz tube with tungsten electrodes in side arms 15 cm. apart, and were taken via the 1 m. absorption tube by means of a large Littrow (Hilger E 1) spectrograph using a slit width of 0·02 mm.

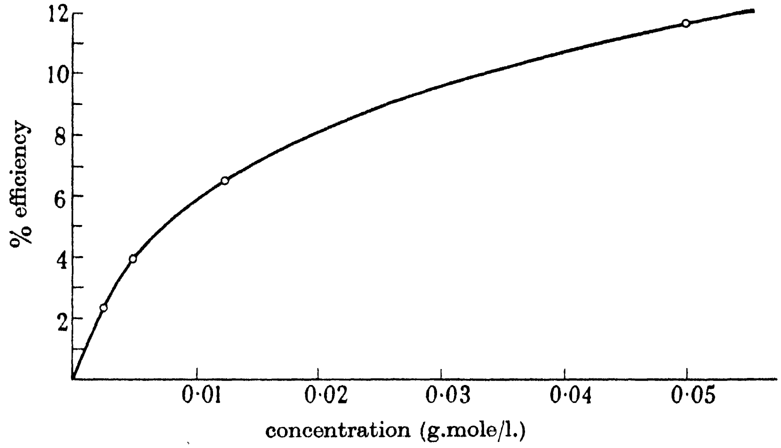

FIGURE 2. Energy efficiency of photolysis of uranyl oxalate against concentration.

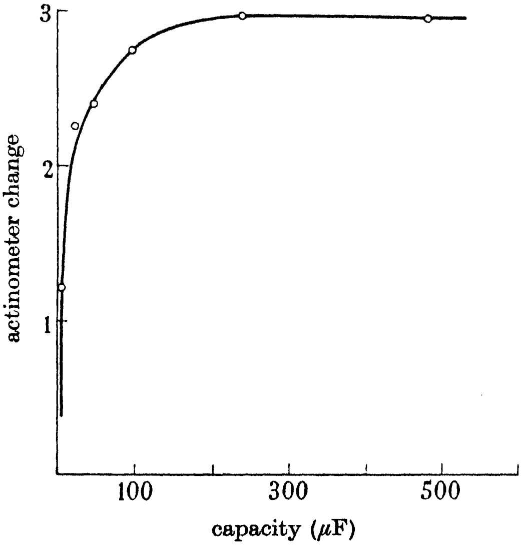

FIGURE 3. Dependence of light output on capacity per flash.

Figure 4, plate 6, shows the effect of increasing the energy per flash on hydrogen- and krypton-filled tubes. In the case of hydrogen the spectrum at low capacities is a weak continuum overlaid only by very intense Balmer lines, the secondary molecular spectrum of hydrogen being absent. The Balmer lines are broadened and partially reversed, this being especially noticeable in the Hγ line. As the capacity per flash is increased the intensity of the continuum increases, but a relatively sharp line spectrum appears covering the whole region. Wave-length measurements show that this is almost entirely the spectrum of silicon and oxygen, presumably due to the decomposition of the tube. It appears, with slight differences, in both quartz and Pyrex tubes and with tungsten or aluminium electrodes; in the latter case a few additional lines appear due to the decomposition of the electrodes. As the capacity per flash is increased the relative intensity of this line spectrum to the continuum is further increased. The spectrum in figure 4*a*, which is a single flash, is of just sufficient intensity to record down as far as 2900 Å, but any further increase of capacity renders the line spectrum too intense to be tolerated. If the lamp is run continuously at normal current densities after the flash, but without refilling, no trace of the line spectrum appears.

The krypton spectra in the same figure show that as the capacity is increased the relative intensity of the line spectrum to the continuum is decreased. In figure 4*f* the line spectrum is entirely that of krypton, and even at high capacities there are relatively very few other lines present. The krypton continuum is about six times as intense as that of hydrogen under the same conditions, and at high capacities there is less interference from the line spectrum.

Figure 5 *d*, *e* and *f*, plate 6, which are all the spectra of single flashes, show more clearly how the relative intensity of continuum to line spectrum of krypton increases with capacity, the 73 μF flash being a very good continuum of sufficient intensity to record clearly down to 2000 Å. A few lines due to silicon appear above this capacity, and if the tube is flashed continuously the group of six lines between 2506·9 and 2528·5 Å are reversed, these being the only discontinuities over the whole visible and ultra-violet region. The other spectra in figure 5 show the effect of voltage and pressure. Increasing the voltage has a similar effect to increasing the capacity, but the gas pressure has very little effect on the spectrum. These parameters cannot be varied independently over a much greater range than that shown, as the pressure is determined within these limits for a given voltage by the firing potential.

The spectra of other gas fillings are shown in figure 6, plate 7. It is seen that the only difference between the spectra of argon, krypton and xenon flashed under the same conditions is in the respective rare gas line spectrum, the intensity and distribution of the continuum being almost identical in the three cases. Figure 6*a* is the spectrum of a 1 m. lamp krypton-filled with the addition of a little liquid mercury. Although the tube was flashed cold, so that at the beginning of the flash the mercury pressure was very low, the krypton line spectrum has entirely disappeared and has been replaced by the much more intense spectrum of mercury. This has the effect of shifting the energy distribution further into the ultra-violet, and as an example of this the photochemical decomposition of acetone produced by this lamp was three times that obtained with a lamp filled with pure krypton and flashed under the same conditions.

The origin of the continuum in high-current density gaseous discharges is not known with certainty, but it seems probable that it is due to retardation and recombination radiation of the electrons in the positive column. These results show that above a certain capacity, which depends on the dimensions of the lamp, the peak light output tends to a limiting value, and this is accompanied by a rapid increase in the intensity of the continuum relative to the line spectrum of the gas and a maximum luminous efficiency in the region studied.

Triggering and synchronization

An internal electrode, sealed through the tube half-way between the main electrodes, was found to be more reliable than an external coil as a means of applying the trigger pulse. The delay between the making of the contacts in the primary of the induction coil and the firing of the lamp was constant to within a few μsec. in the apparatus described in the next section.

The above investigations are sufficient to show that this type of flash discharge lamp amply fulfils the requirements stated in the introduction for photochemical and spectroscopic purposes. In most of the experiments to be described here the photochemical source was a 1 m. quartz tube 1 cm. in diameter with 4·84 mm. ($\frac{3}{16}$ in.) tungsten electrodes through molybdenum seals and a small central trigger electrode. The filling was pure krypton at 5 cm. pressure, this being chosen because the mercury/krypton type had a rather variable output depending to some extent on the position of the mercury in the tube and its temperature. When discharged with 500 μF at 4000 V this lamp had an effective flash time of 1·5 msec.

The source of continuum chosen was a lamp of the same tube and electrode type but with the electrodes in side arms 15 cm. apart and with a flat quartz plate sealed firmly into the end. The usual filling was 10 cm. pressure of krypton which gives the purest continuum over the whole region, though argon was occasionally used for the region below 2700 Å where it is slightly better. When flashed with 70 μF at 4500 V this lamp gave a continuum of sufficient intensity to record in 50 μsec. over the whole spectrum down as far as 2200 Å. Both these lamps had a life of many hundred flashes, though refilling was necessary from time to time.

DESCRIPTION OF THE EXPERIMENTAL ARRANGEMENT

The complete apparatus is shown schematically in figure 7. The 1 m. photolysis flash lamp lies alongside the quartz reaction vessel in the reflector already described, which is constructed in two semi-cylinders to facilitate inspection and removal. The spectroflash lamp is at one end of the reaction vessel and the spectrograph slit at the other, and a small detachable mirror placed near the slit enables the iron arc or other comparison spectrum to be taken without disturbing the alinement. A current of air is blown into the centre of the reflecting cylinder and escapes at either end, and the high-voltage trigger pulse is led on to the centre electrode of the lamp via a glass insulator through this case.

The vacuum apparatus consists of the usual pumping arrangements and pressure gauges, storage bulb, purification train and gas-analysis apparatus. Provision is made for filling the lamps *in situ*, although frequent refilling is necessary unless they are heated vigorously during evacuation.

Between the reaction vessel and spectrograph is the wheel responsible for synchronization of the shutter, photolysis flash, spectroflash and oscilloscope time base. The scattered light from the photolysis flash which recorded on the plate was about one-quarter as intense as that from the spectroflash, so that for exploratory work it is possible to work without a shutter, but for intensity measurements it is necessary

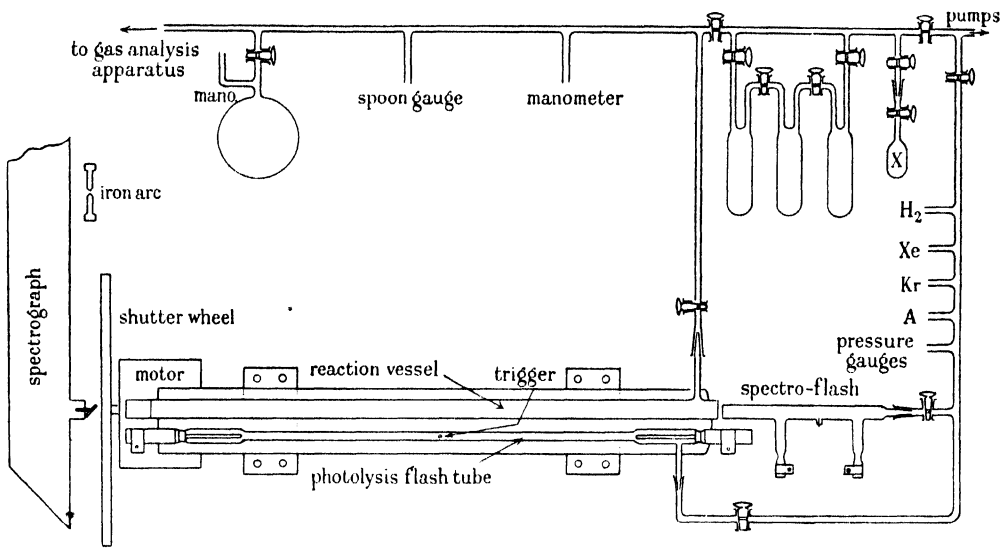

FIGURE 7. Diagram of the experimental arrangement.

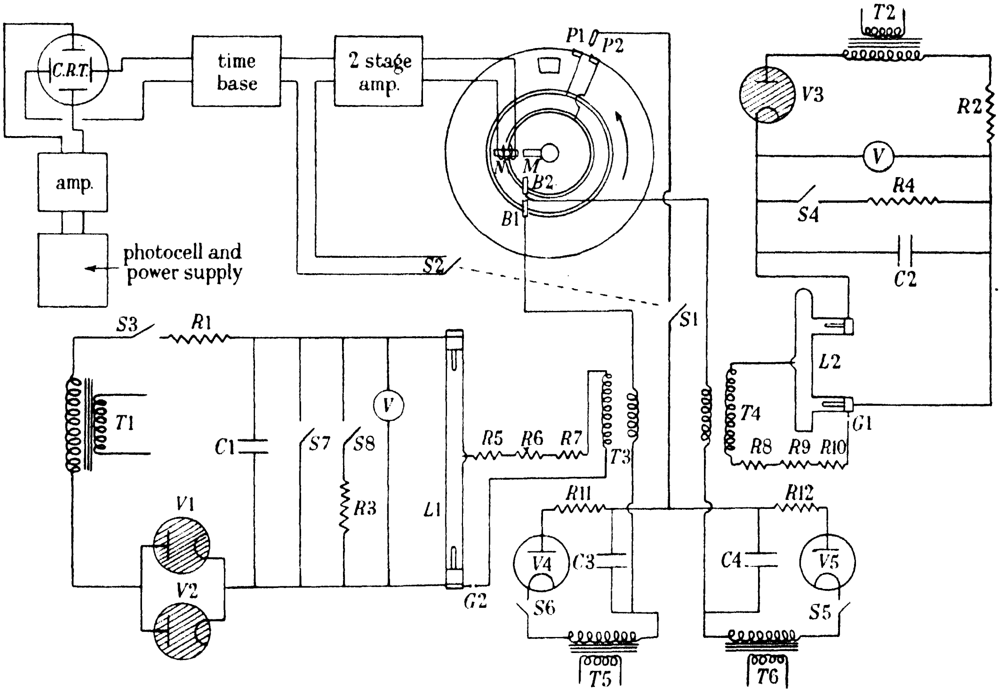

FIGURE 8. Electrical circuit diagram. Description of components: *C* 1, 1200 μF, 4000 V, in units of 1 to 4 μF; *C* 2, 125 μF, 4500 V, in units of 1 to 4 μF; *C* 3 and *C* 4, 1 μF, 1000 V; *V* 1, *V* 2 and *V* 3, mercury rectifiers, 8000 V, R.M.S. type CV 128; *V* 4 and *V* 5, rectifiers, 2000 V R.M.S.; *V*, electrostatic voltmeter, 5000 V; *T* 1, 200/3000, 4000, 5000 V, 10 A; *T* 2, 200/5000 V, 4 A; *T* 3 and *T* 4, high-ratio induction coils; *T* 5 and *T* 6, 200/1000 V, 2 A; *R* 1, 2000 Ω, 400 W; *R* 2, 40,000 Ω; 200 W; *R* 3, 30,000 Ω, 400 W; *R* 4, 4000 Ω, 400 W; *R* 5, to *R* 10, 60,000 Ω, 5 W; *R* 11 and *R* 12, 30,000 Ω, 3 W.

to eliminate it completely. A synchro-motor rotates the wheel via gears giving 8, 60, 200 and 600 r.p.m., and fine adjustment of the time interval between flashes is obtained by altering the distance apart of the two contacts on the wheel which are responsible for the trigger pulses.

The electrical arrangement is shown in figure 8. Apart from brushes, direct contacts to the wheel have been avoided so that the speed of rotation is uniform. The contacts at $P\,1$ and $P\,2$, which supply trigger pulses to the photolysis flash and spectro-flash respectively, are 0·1 mm. apart and platinum tipped, and the 1000 V primary pulse is sufficient to cross the air gap between them. $P\,1$ is fixed but $P\,2$ moves radially over the circumference of the wheel and has a scale attached enabling time intervals between 2×10^{-4} and 0·5 sec. to be selected, longer intervals being obtained by manual switching. The synchronization pulse for the cathode-ray tube time base is induced by a small permanent magnet M on the wheel shaft in a small telephone coil, N, amplified, differentiated and rectified and passed to the hard-valve time base.

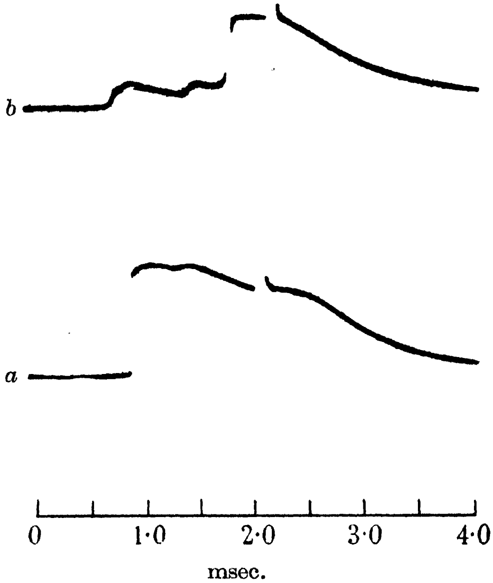

FIGURE 9. Typical oscillograph traces of the pulse and shutter timing.

A long slot, the height of the spectrograph slit, is cut in the wheel and a thin aluminium slide moves on a scale over this enabling the whole or part of the photolysis flash to be eliminated. Calibration of the time scales and regular checking was necessary as there is a considerable interval introduced between contact and the initiation of the flash. This was carried out by means of a photocell inside the spectrograph connected via an amplifier and switch $S\,2$ to the cathode-ray tube. The oscilloscope trace is photographed, and, so that only one scan shall appear, the switch $S\,2$ is ganged to the main trigger switch $S\,1$. The timing of two typical experiments is illustrated in figure 9. In 9*a* the timing between the beginning of the two flashes is 1·1 msec. and in 9*b* it is 1·5 msec. The latter also shows how the photolysis flash can be eliminated quite sharply by introducing the shutter.

The trigger pulses for the two flash tubes are obtained by discharging a 1 μF condenser charged to 1000 V through the primary of an induction coil. The condenser *C* 3 produces the trigger pulse for the photolysis flash tube when it is discharged via the primary of *T* 3, the brush *B* 1, the gap *P* 1 and the switch *S* 1. The pulse from the secondary of transformer *T* 3 discharges through the lamp *L* 1 via the gap *G* 2 and resistances *R* 6, 5 and 7. The gap avoids the necessity of a direct connexion of the lamp electrodes to the rest of the circuit, and the resistance chain is necessary to prevent the discharge short-circuiting to earth via the trigger electrode and *T* 3. The spectroflash lamp has identical trigger arrangements employing *C* 4, *T* 4, *B* 2, *P* 2, *S* 1, *G* 1 and *R* 8, 9 and 10.

C 1 is the main condenser for the photoflash which is a variable capacity having a maximum value of 1200 μF. It is made up of units of 1 to 4 μF and is housed in a separate room with remote controls. The connecting leads are of 1·27 cm. ($\frac{1}{2}$ in.) copper strip, the main leads from the whole bank are of 2·54 cm. (1 in.) diameter copper pipe in order to keep all resistances down to a minimum, and precautions were taken during construction to reduce the inductance as far as possible. *C* 2 is a similar condenser of 125 μF maximum capacity which supplies the power for the spectroflash. The master switch which fires both lamps and triggers the time base is the ganged switch *S* 1 and *S* 2.

The procedure used to photograph the spectrum a fraction of a second after photolysis is as follows. The reaction vessel is filled with the substance to be studied and the spectrograph shutter is opened. If a time check is required, the oscilloscope camera shutter is opened and the photocell, oscilloscope and trigger circuits are switched on. The shutter slide and spectroflash trigger contacts are set at the positions required to produce the desired time interval, the filament circuits of all valves are made and switches 4, 7 and 8 are opened. *S* 7 is a safety-door switch, and *S* 4 and *S* 8 are remote discharge switches. The synchromotor is started, and switches 5 and 6 made for a few seconds to charge condensers 3 and 4. Switches 3 and 4 are now made and the condenser banks charged to exactly the operating voltage. All is now ready, and switch *S* 1/2 is pressed when the following train of events occurs. The oscilloscope scan is tripped by the pulse induced in *N* and the wheel turns until *P* 1 is opposite the standing contact when *C* 3 discharges through *T* 3 and fires *L* 1. As the wheel turns farther the shutter clears the slit of the spectrograph, and when *P* 2 comes opposite the standing contact *C* 4 discharges through *T* 4 and fires *L* 2. A series of spectra at increasing time intervals is obtained by repeating this procedure for different positions of *P* 2.

Several different spectrographs have been used, but the most generally suitable is the large Littrow type as it combines high dispersion with short exposures. One flash of the type described is sufficient to record over the whole photographic region with a slit width of 0·02 mm.

RESULTS

The amount of photochemical decomposition obtained with a few typical compounds is given below. The mercury/krypton filling was used with acetone and ketene and pure krypton with the other substances; in each case the volume of gas was 500 ml. and the illumination a single flash of 4000 J:

gas	pressure (cm.)	% decomposition
NO_2	4	nearly 100
CH_3COCH_3	3	15
CH_3COBr	3	15
$CH_3COCOCH_3$	2·5	50
CH_2CO	10	40

If the lifetime of the intermediates involved in these reactions is comparable with the duration of the flash, the amount of decomposition obtained in this way makes possible the direct study of radical reactions by pressure change and the other physical methods which, hitherto, it has only been possible to apply to the overall change. The effect of high intensities on the nature of photochemical change has been mentioned in a previous note (Norrish & Porter 1949) and will be the subject of another communication.

The spectrographic technique has been applied to several photochemical reactions, and in most cases the amount of change was sufficient to be easily measurable by absorption changes. Three such systems will be mentioned here as illustrations of the potentialities of the method.

Atomic chlorine and its reactions

With a flash of 4000 J, 1 cm. of chlorine showed a Budde effect of 2·2 cm. Control experiments with inert gas showed that there was no detectable direct heating effect from the lamp. In 0·5 cm. of chlorine the absorption spectrum of the chlorine molecules almost completely disappeared, a direct demonstration of dissociation into atoms. The pressure of atoms must have been nearly 1 cm. and over 80 % of the total, a much higher concentration of atoms than has ever been obtained by photochemical or any other methods. The recombination of chlorine atoms may be studied in this way and figure 10, plate 7, shows the spectrum at increasing times after a flash of 2000 J, with a pressure of 1 cm. chlorine. The original decomposition is about 50 % in this case, and the half-life of the chlorine atom immediately after the flash, judged by visual comparison with the spectrum of the chlorine molecule at different pressures, is about 30×10^{-3} sec. Accurate estimations will have to take into account the temperature dependence of the absorption coefficient (Gibson & Baylis 1933).

When carbon monoxide was added to the system there was no permanent pressure change even after several flashes, and no phosgene or intermediate radicals were detected spectroscopically. If the mixture was illuminated in the ordinary way by a small mercury lamp, phosgene was rapidly formed, and the reaction could be taken almost to completion. On flash illumination of the mixture containing phosgene the pressure increased again and the phosgene was once more decomposed. The pressure change/flash was small at first, increased as more chlorine was formed and finally decreased when most of the phosgene had disappeared. The reaction was quite reversible and could be taken almost to completion either way by simply changing the intensity of the illumination. Two factors probably play a part in changing the mechanism of the reaction at high intensities. First, owing to the much higher concentration of atoms and radicals, interradical reactions become very frequent, so that the relative probability of the reaction

$$\mathrm{COCl} + \mathrm{Cl} = \mathrm{CO} + \mathrm{Cl_2} \tag{1}$$

to the reaction

$$\mathrm{COCl} + \mathrm{Cl_2} = \mathrm{COCl_2} + \mathrm{Cl} \tag{2}$$

will be greatly increased. Secondly, owing to the higher temperature, the reverse of reaction (2) will occur more readily.

No evidence of COCl or Cl_3 radicals was obtained in the chlorine or chlorine-carbon monoxide systems, but when phosgene was present an intense continuous absorption over the whole region studied appeared. It has not yet been decided whether this is due to an intermediate or to absorption by 'hot' phosgene molecules.

When oxygen was present a new banded spectrum appeared in the region of 2800 Å. This spectrum was also obtained with chlorine and oxygen alone, but not when nitrogen or inert gases were substituted for the oxygen. It is shown in figure 11 *a*, plate 7, and consists of a regular system of bands degraded to the red with a few weaker bands probably belonging to the $v'' = 1$ progression. The bands appear to be single headed and have a very simple rotational structure, and it seems most probable that a diatomic molecule is responsible. The most reasonable choice under these conditions is the ClO radical which has been frequently discussed as an intermediate in chlorine-sensitized oxidations. The half-life of the radical was found to be about 4×10^{-3} sec. in the presence of 1 cm. chlorine and 10 cm. oxygen. A Birge-Sponer extrapolation gives a dissociation energy to the products in the upper state of 108 kcal./g.mole. If the products of dissociation are normal chlorine atoms and ^1D oxygen atoms this would lead to a dissociation energy of the radical to atoms in the ground state of 63 kcal./g.mole.

Diacetyl

Figure 12*a*, plate 8, shows the absorption spectrum of diacetyl at 2·5 cm. pressure before photolysis, there being two distinct regions of absorption, one between 3800 and 4500 Å and the other below 3000 Å. The amount of decomposition can be judged from figure 12*e*, which is taken several minutes after a flash of 4000 J. Figure 12*b* is taken during the flash when photochemical decomposition is not complete. The reappearance of the absorption in the long wave-length region may be due to recombination of radicals, but is more probably due to a temperature effect. The increased absorption at lower wave-lengths is of too short a duration to be a temperature effect, however, the half-life being less than 1 msec., and it is difficult to find any other interpretation than that it is due to some intermediate substance of short life formed in the decomposition. The acetyl radical, which is probably formed in good yield in the reaction, might be expected to give an absorption in this region without any obvious fine structure. An analysis of the products not condensed in solid CO_2/ether gave: ethane 27 %, carbon monoxide 62 %, and methane 11 %.

Acetyl bromide on photolysis showed a similar increase of absorption in the same region, but in this case, owing to the smaller percentage decomposition, it was not possible to discriminate between this and the long-duration temperature effect on the acetyl bromide spectrum sufficiently readily to obtain a lifetime measurement.

Carbon disulphide

This substance is an example of those whose decomposition mechanism cannot easily be elucidated by analysis of the products alone. The final products of photolysis are solid sulphur and a polymer of composition $(CS)_n$, little being known with certainty about the existence of gaseous, unpolymerized CS.

The spectrum of carbon disulphide at 2 cm. pressure after illumination with a flash of 4000 J is shown in figure 13, plate 8. The decrease in the intensity of the continuum in *c* is due to clouding of the window by the solid products. The bands of the S_2 molecule are seen in *b* and continued at lower wave-lengths in *i*. The latter spectrum also shows three clear new bands with prominent heads at 2575·5, 2509·2 and 2444·5 Å, which agree closely with the wave-lengths of the 0, 0, 1, 0 and 2, 0 emission bands of carbon monosulphide measured by Jevons (1928). The 0, 0 and 0, 1 bands in absorption are shown enlarged in figure 14 *a* and *b*, plate 8, respectively. Weak bands around 2588·6 and 2523·2 Å correspond to the wave-lengths of the first two bands of the $v'' = 1$ progression, and the band head at 2504·8 Å is probably the 0, 0 band of the $^1\Sigma$–$^1\Sigma$ system observed by Crawford & Shurcliffe (1934), though its occurrence in absorption is not in agreement with their contention that a different lower state is involved in this system; as both are observed here the transition must be from the ground state in each case.

The spectra so far discussed were all taken a few msec. after the flash, and when the time interval was extended in order to measure the lifetime of the CS molecule no decrease in absorption was observable until several seconds had elapsed. The spectra in figure 13*d* to 13*h* show the decreasing absorption with time in 1 cm. of carbon disulphide, and the 0, 0 band is still faintly visible after 5 min. So persistent was this spectrum that it was observed as an impurity due to a little carbon disulphide which had dissolved in the tap grease, and it is surprising that it has not previously been observed in absorption.

The spectrum of S_2 appeared at maximum intensity immediately after the flash and disappeared much more rapidly than CS. These observations suggest the following as the most likely reaction scheme, the times given being those measured when the pressure of carbon disulphide originally present was 0·5 cm.:

	approximate time of half-reaction
$CS_2 + h\nu = CS + S$	—
$S + CS_2 = S_2 + CS$	less than $1{\cdot}5 \times 10^{-3}$ sec.
$nS_2 = S_{2n}$	10^{-1} sec.
$n\text{CS} = (CS)_n$	60 sec.

As the ground states of S and CS are triplet and singlet respectively one must be produced in the excited state from singlet carbon disulphide, and the above lifetimes indicate that it is the sulphur atom which is so liberated.

REMARKS

Only one important difficulty in the method has appeared in the course of a wide range of investigations, the fact that the adiabatic nature of the reaction produces a change in the spectra of the parent molecules themselves. It is usually possible

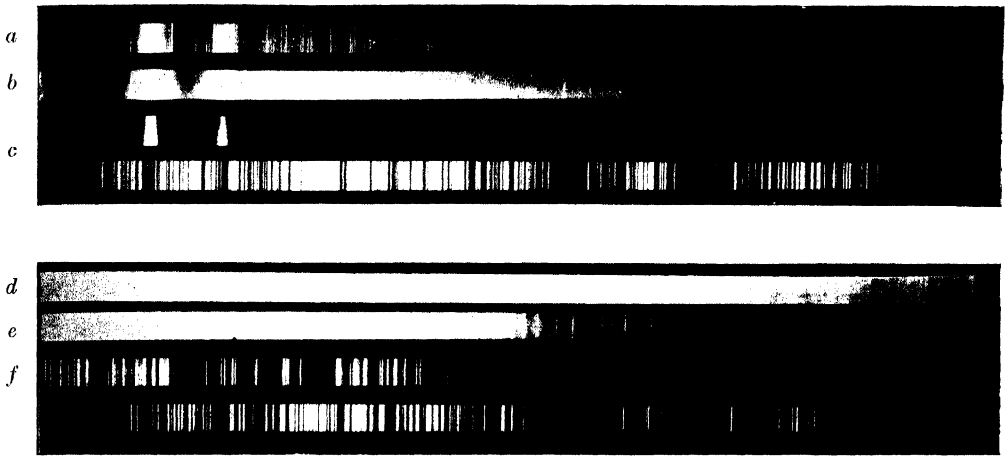

FIGURE 4

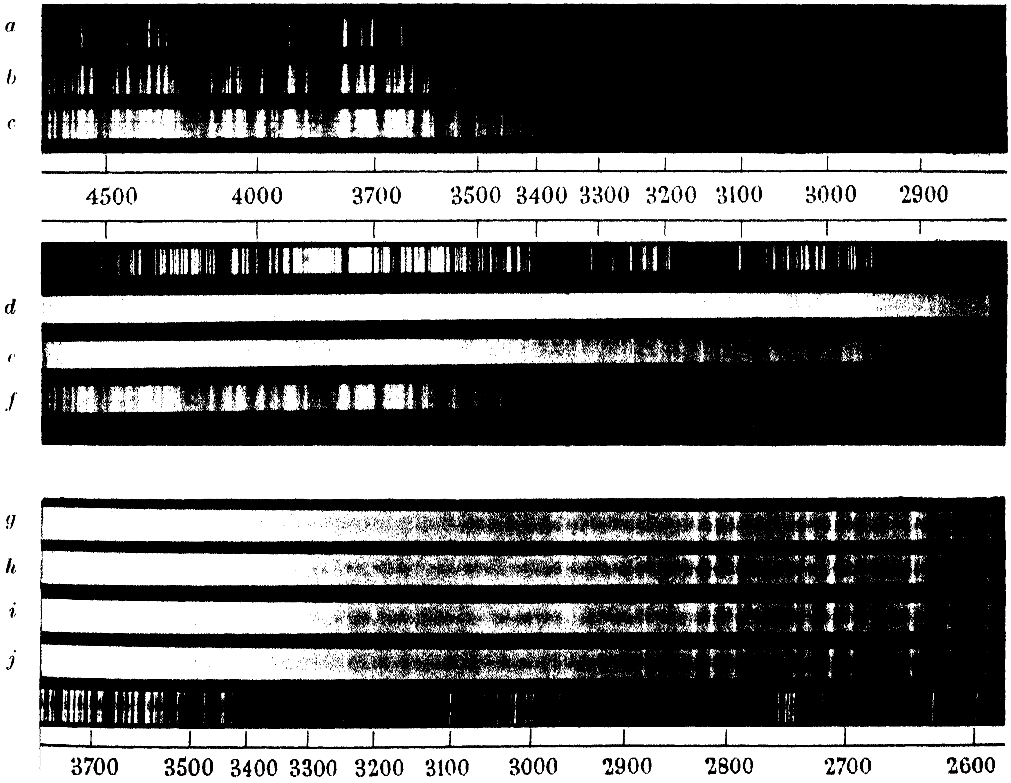

FIGURE 5

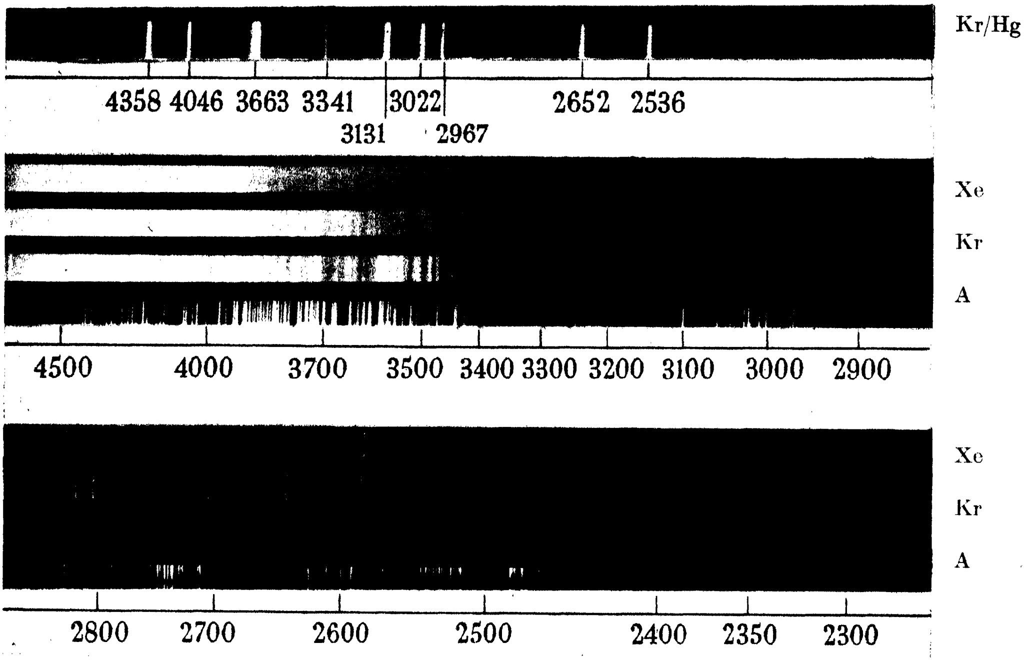

FIGURE 6

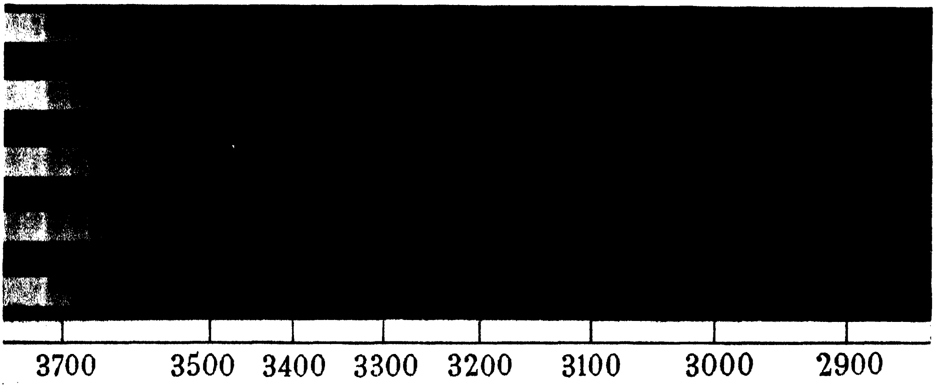

FIGURE 10

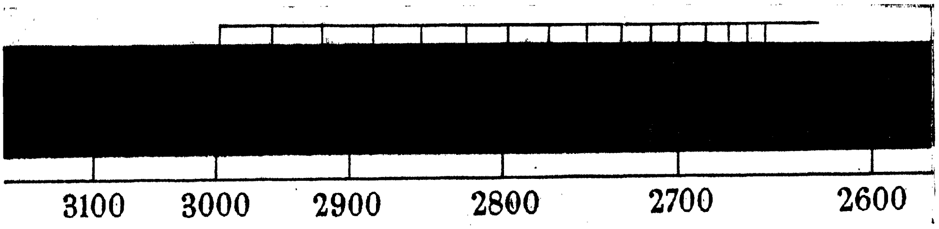

FIGURE 11

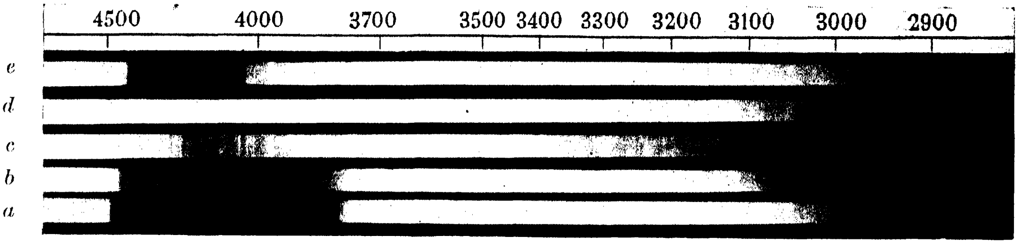

FIGURE 12

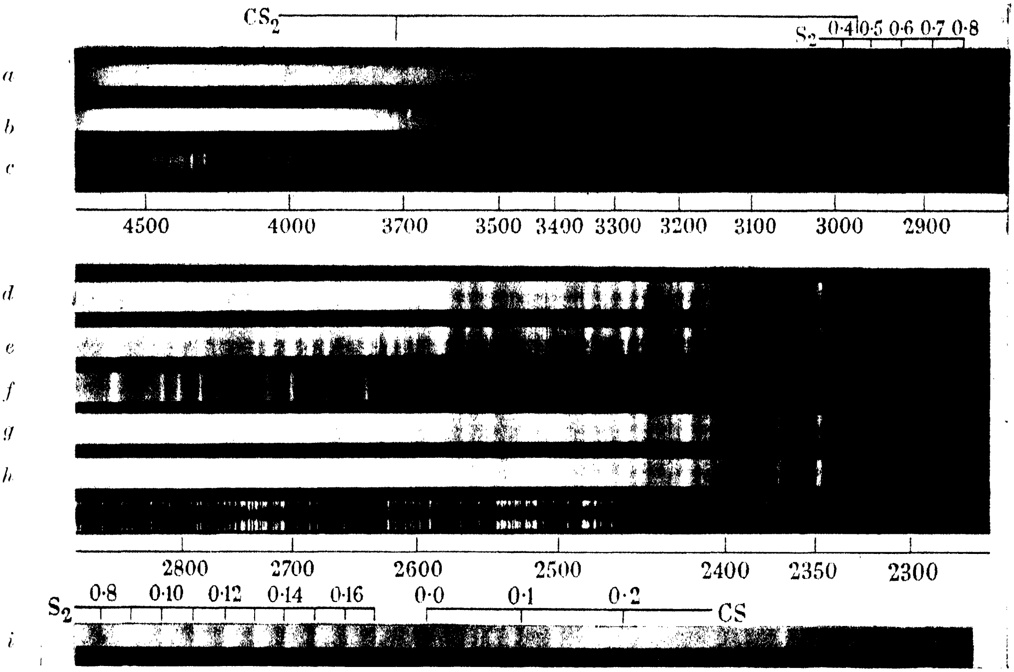

FIGURE 13

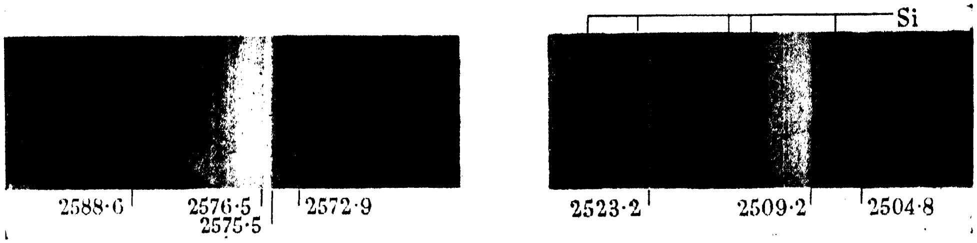

a *b*

FIGURE 14

to discriminate between the two effects by lifetime measurements as was shown in the case of diacetyl, which is a particularly difficult example, but for quantitative absorption measurements it will often be necessary to measure the temperature and make allowance for the changing absorption coefficient. On the other hand, the phenomenon suggests the possibility of thermal and kinetic measurements on radical reactions by direct pressure observations.

The results which have been described are preliminary only, and the conclusions must be verified by more detailed investigations. The main purpose here has been to illustrate the power of this method for the investigation of fast reactions, and for this reason a wide range of substances has been studied. It is believed that the results are sufficient to show that the methods of flash photochemistry and spectroscopy provide a valuable weapon for the study of the more elusive of chemical compounds.

I am extremely grateful to Professor R. G. W. Norrish, F.R.S., for his support in this work from the beginning and for much encouragement and valued advice throughout. Thanks are also due to the Anglo Iranian Oil Company for a grant for research, part of which was applied to this work.

REFERENCES

Crawford, F. H. & Shurcliffe, W. A. 1934 *Phys. Rev.* **45**, 860.
Gibson, G. E. & Baylis, N. S. 1933 *Phys. Rev.* **44**, 188.
Jevons, W. 1928 *Proc. Roy. Soc.* A, **117**, 351.
Leighton, W. G. & Forbes, G. S. 1930 *J. Amer. Chem. Soc.* **52**, 3139, 5309.
Murphy, P. M. & Edgerton, H. E. 1941 *J. Appl. Phys.* **12**, 848.
Norrish, R. G. W. & Porter, G. 1947 *Faraday Soc. Discussion. The Labile Molecule*, **2**, 142.
Norrish, R. G. W. & Porter, G. 1949 *Nature*, **164**, 658.
Oldenberg, O. 1935 *J. Chem. Phys.* **3**, 266.
White, J. U. 1940 *J. Chem. Phys.* **8**, 79.
Wieland, K. 1947 *Faraday Soc. Discussion. The Labile Molecule*, **2**, 172.

DESCRIPTION OF PLATES 6 TO 8

Plate 6

FIGURE 4. Effect of capacity on flash spectra of krypton and hydrogen. *a*, Hydrogen: 1 flash at 73 μF; *b*, 6 flashes at 16 μF; *c*, 50 flashes at 2 μF; Krypton: *d*, 1 flash at 125 μF; *e*, 2 flashes at 16 μF; *f*, 50 flashes at 2 μF.

FIGURE 5. Effect of voltage, capacity and pressure on flash spectra of krypton. All spectra are of single flashes.

	capacity (μF)	pressure (cm.)	voltage (V)		capacity (μF)	pressure (mm.)	voltage (V)
a	16	10	2000	*g*	33	3	4000
b	16	10	3000	*h*	33	6	4000
c	16	10	4000	*i*	33	9	4000
d	73	10	4000	*j*	33	15	4000
e	33	10	4000				
f	16	10	4000				

Plate 7

FIGURE 6. Effect of gas filling on flash spectra. *a*, 1 m. lamp, voltage 4000 V, capacity 1000 μF; krypton pressure 5 cm. *b* to *g*, 15 cm. lamp, voltage 4000 V, capacity 33 μF, pressure 10 cm.

FIGURE 10. Recombination of chlorine atoms. *e* was taken through 1 cm. chlorine before the flash and *d*, *c*, *b* and *a* were taken at intervals afterwards of 12, 17, 60 msec. and 60 sec. respectively.

FIGURE 11. Spectrum attributed to ClO. *b* is a comparison spectrum taken before the flash.

Plate 8

FIGURE 12. Photolysis of diacetyl. *a* was taken before and *b*, *c* and *d* 1·2, 2·0 and 3·3 msec. respectively after the beginning of the flash. *e* was taken 2 min. later.

FIGURE 13. Photolysis of carbon disulphide. *a*, *b* and *c* were taken before, during and after the flash. *h* is a comparison through a vacuum. *g*, *f*, *e* and *d* were taken before and 2 msec., 1 and 5 min. afterwards.

FIGURE 14. The 0·0 and 0·1 absorption bands of CS.

The mechanism and kinetics of the heterogeneous polymerization of vinyl monomers

I. The benzoyl peroxide catalyzed polymerization of vinyl chloride

By W. I. Bengough and R. G. W. Norrish, F.R.S.
Department of Physical Chemistry, University of Cambridge

(*Received* 18 *June* 1949)

A study has been made of the polymerization of vinyl chloride, with varying amounts of benzoyl peroxide at temperatures from 33 to 75° C. With from 0·025 to 1·0 mol. % benzoyl peroxide and over the above-mentioned temperature range, the rate of polymerization gradually accelerates over the first 30–40 % reaction. In the presence of a solvent for the polymer, such as dibutyl phthalate or tetrahydrofuran, however, the polymerization proceeds at a constant rate which decreases at later stages in the reaction. 'Dead' polyvinylchloride has been shown to act as a co-catalyst with benzoyl peroxide in the polymerization of vinyl chloride; in the absence of benzoyl peroxide, it does not catalyze the polymerization. Polyvinylchloride therefore exerts its catalytic effect when (*a*) the polymer is present in an undissolved state, and (*b*) benzoyl peroxide or another source of free radicals is also present in the reacting system. It is suggested that the co-catalytic effect of the 'dead' polymer is caused by an increase in the number of centres of polymer growth in the reacting system arising from chain transfer reactions between growing polymer chains and molecules of 'dead' polymer resulting in the accumulation of stabilized centres of polymer growth on the surface of the solid polymer; the revivified polymer grows by addition of monomer until it is finally terminated by chain transfer with monomer, with the production of a mobile free radical.

Relative values of the average molecular weight of polymer formed (*a*) at different temperatures, (*b*) at different stages in the reaction, (*c*) with different concentrations of benzoyl peroxide, and (*d*) in the presence of dibutyl phthalate, have been obtained. The results support the suggestion that chain transfer takes place to a considerable extent in the polymerization of vinyl chloride.

INTRODUCTION

The polymerization reactions of vinyl compounds such as styrene, methyl methacrylate, and vinyl acetate are now accepted as being chain processes consisting of the four steps: initiation, propagation, chain transfer and termination. The kinetics of the early stages of these polymerizations are generally explained on the assumption of the above steps, together with the additional postulate of a stationary concentration of the radicals or chain centres prevailing in the reacting system.

After about 20% polymerization, however, the rate of polymerization in the case of methyl methacrylate and vinyl acetate gradually increases to a value two or three times that of the steady initial velocity, even when the reaction is carried out under isothermal conditions. Norrish & Smith (1942) have shown that in the case of methyl methacrylate catalyzed by benzoyl peroxide, the inception of this acceleration can be advanced by the addition of a precipitant to the system, or delayed by the addition of a good solvent. Similar results have been obtained by Haward (1948) in the case of methyl *iso*-propenyl ketone, and by Trommsdorff (1944), who found that, on increasing the viscosity of methyl methacrylate monomer by the addition of cellulose tripropionate, both the rate of polymerization and the molecular weight of the polymethylmethacrylate were increased. It was suggested by Norrish & Smith (1942) that this increase in reaction rate might be consequent upon a reduction in the rate of termination, this being due to the hindrance to radical-radical reaction caused by the increase in viscosity of the system.

Prat (1945) has shown that, with vinyl chloride at 25 and at 50° C, the rate of polymerization increases over the first 40 % polymerization, remains approximately constant from 40 to 60 % polymerization, and then gradually diminishes. This acceleration, however, is quite different from that observed in methyl methacrylate or vinyl acetate polymerizations, since in the latter the polymerizing medium remains homogeneous but increases in viscosity, whilst in the case of vinyl chloride the system becomes heterogeneous almost from the beginning of the reaction owing to the precipitation of polyvinylchloride without any increase in viscosity. Prat (1945) suggested that this period of acceleration might be explained by the assumption of Gee & Rideal (1936), and Cuthbertson, Gee & Rideal (1939), that the initiation is controlled by two consecutive reactions: (*a*) the reaction between monomer and catalyst to form a complex, and (*b*) the decomposition or rearrangement of the complex, or the reaction of the complex with monomer, with the production of active initiating centres.

In early work, polymerization reactions were often characterized by periods of induction during which no trace of reaction could be observed, but it later became apparent that these induction periods were due to the presence of traces of impurities in the monomer, which react preferentially with the initiating centres and inhibit the growth.

In this paper it is shown that, in the benzoyl peroxide catalyzed polymerization of vinyl chloride, the observed period of acceleration is quite distinct from the period of induction, and is a true kinetic effect and not due to reacting impurities, but to the co-catalytic effect of the polyvinylchloride formed during the polymerization. It is concluded that the co-catalytic behaviour of the 'dead' polymer is due to chain transfer between growing polymer chains and molecules of dead polymer, which produce free valencies in the surface of the polymer, and constitute stabilized centres of polymer growth; the revivified polymer continuing to react with monomer until the process is terminated by chain transfer with monomer, with the reproduction of a mobile free radical. If steady-state conditions are postulated for the growing polymer chains, and for the revivified polymer, kinetics can be derived which explain the experimental results. Support for this mechanism is given by a study of the change in molecular weight of the polymer with variation in concentration of catalyst, the results of which indicate that chain transfer takes place to a considerable extent.

GENERAL SCHEME OF INVESTIGATION

The experimental investigation is divided into four sections:

(1) The effect of impurities on the rate of polymerizations: at various stages in the purification process, the monomer was polymerized with 0·25 mol. % benzoyl peroxide

for 2 hr., and the yield of polymer obtained was compared in each case. Kinetically pure vinyl chloride was finally obtained, and the retarding effect of additions of small amounts of acetylene to this monomer was observed.

(2) The effect of catalyst concentration and temperature: from the results over a temperature range from 33 to 75° C, an overall activation energy for the polymerization was calculated, and a relationship between the rate of polymerization and the catalyst concentration was obtained. The autocatalytic shape of the percentage polymerization versus time curve was also confirmed.

(3) The origin of the autocatalytic nature of the polymerization curve: experiments were devised to determine whether interpretations which have been put forward in the case of other 'autocatalytic' type polymerizations apply to the polymerization of vinyl chloride; the results show that a new interpretation is necessary, and a catalytic effect of the freshly formed polymer was established. This effect was estimated quantitatively. Solvents for the polymer were added to the system and their effect on the rate of polymerization was studied.

(4) The dependence of molecular weight on the kinetic parameters: relative values of the molecular weight of the polymer (*a*) at different stages of the reaction, (*b*) at different temperatures, (*c*) at different concentrations of benzoyl peroxide, and (*d*) formed in the presence of dibutyl phthalate, were obtained.

EXPERIMENTAL

Materials

Benzoyl peroxide was purified by fractional precipitation from a chloroform solution, using ethyl alcohol as precipitant.

Vinyl chloride was supplied in cylinders by the Distillers Co. Ltd., and contained as chief impurities acetylene, ethylene dichloride and other chlorinated hydrocarbons. These were removed by passing the vinyl chloride through ammoniacal cuprous chloride solution, water, dilute sulphuric acid, water, and then over soda-lime, silica gel, phosphorus pentachloride and activated carbon. The emerging gas was condensed at − 80° C, and fractionated in a 2 ft. long column packed with stainless steel Dixon gauze rings $\frac{1}{16} \times \frac{1}{16}$ in. diameter. A liquid take-off was employed, the take-off tap having a small groove cut in each end of the bore, so that the distillate could be collected at a very slow rate. The middle fraction (from about 25 to 65 % of distillate) was refractionated, the middle portion of this being retained for use. The vinyl chloride was stored in 5-l. bulbs at room temperature.

Polyvinylchloride prepared in two ways was used in experiments in which polymer was added to the system:

(*a*) 'Chalk-like' polymer was prepared by polymerizing vinyl chloride catalyzed by 0·45 mol. % benzoyl peroxide, at 47° C, to about 70 % conversion. Excess benzoyl peroxide was removed by repeatedly washing with ether and the polymer was dried at 60° C.

(*b*) Finely granulated polymer in the form of minute beads, which had been produced by emulsion polymerization, was supplied by the Distillers Co. Ltd. The material was washed free from emulsifiers and catalysts and dried at 60° C.

Dibutyl phthalate was purified by distillation in a molecular still, at a temperature of about 100° C.

Tetrahydrofuran was dried over caustic soda and fractionally distilled through an efficient column.

Procedure

The polymerizations were followed in dilatometers, or gravimetrically in small tubes, in the usual way.

The apparatus used for filling the dilatometers or reaction tubes was an all-glass high-vacuum line, using a Hyvac pump, and a three-stage mercury vapour pump with the customary liquid air traps. It consisted of two 5-l. storage bulbs, a 1-l. bulb thermostatically controlled at 25 ± 0·1° C, a mercury manometer, a McLeod gauge, and a range of stopcocks to which could be connected dilatometers or reaction tubes by ground glass joints. Apiezon L grease was used on all taps and ground-glass joints. The capillary of tubes of the dilatometers were 1·5 mm. internal diameter and 8 in. in length, and the bulbs of about 0·6 ml. capacity.

Benzoyl peroxide in chloroform solution was introduced into the dilatometer, and the chloroform removed by evacuation. The required amount of vinyl chloride was then condensed in the dilatometer which was subsequently sealed off from the apparatus. The course of the polymerization was followed by the fall of the meniscus in the capillary. The polymerizations were carried out in baths thermostatically controlled to ± 0·1° C, the whole of the dilatometer being immersed.

The percentage polymerization could be determined either by weighing the polymer formed or by measuring the monomer left by allowing it to expand to a constant volume and reading the pressure developed. Both methods gave the same results within experimental error. In experiments in which solvents were employed, the gravimetric method had to be used, the polymer being precipitated with methyl alcohol and dried at 60° C.

Degree of polymerization

Relative values of the degree of polymerization were obtained by measuring the viscosities of solutions of polyvinylchloride, the molecular weight being proportional to the intrinsic viscosity of the polymer solution. Tetrahydrofuran was used as solvent for the polymer.

The polymer was freed from benzoyl peroxide by washing with ether, and then dried. In the case of polymerization in which dibutyl phthalate was used, the gel formed was dissolved in tetrahydrofuran; the polymer was then precipitated with methyl alcohol, dried at 60° C, dissolved in the required amount of solvent and the relative viscosity of the solution measured at 33° C, in a modified Ostwald viscometer.

RESULTS

When monomer, which had not been purified, was polymerized in the presence of benzoyl peroxide, a period of complete inhibition, followed by a period of acceleration, was observed. This period of complete inhibition could be removed by the above-mentioned purification process, but not the period of acceleration. By purification, the yield of polymer in 2 hr. at 40° C from vinyl chloride catalyzed by 0·25 mol. %

benzoyl peroxide, was increased from 0·3 to 4·2 %. Further distillation gave no further increase in yield.

In some preliminary experiments, in which impure vinyl chloride was used, both the rate and the degree of polymerization in the early stages were much lower than with purified monomer.

By adding small amounts of acetylene (1 to 3 mol. %), to purified vinyl chloride catalyzed by 0·25 mol. % benzoyl peroxide, at 40° C, the yield of polymer in the first 2 hr. was halved.

In a fractional distillation of vinyl chloride, five fractions were collected, and a sample of each of these was polymerized with 0·25 mol. % benzoyl peroxide at 40° C for 2 hr. The results shown in table 1 indicate that impurities were present in both the first and last fractions. In all further polymerizations, therefore, only the middle part of the distillate (from 35 to 70 % distillate) was used.

TABLE 1. POLYMERIZATION OF FRACTIONALLY DISTILLED VINYL CHLORIDE, CATALYZED BY 0·25 MOL. % BENZOYL PEROXIDE AT 40° C

no. of fraction	% yield of polymer in 2 hr.
1	3·9
2	4·0
3	4·2
4	4·2
5	2·9

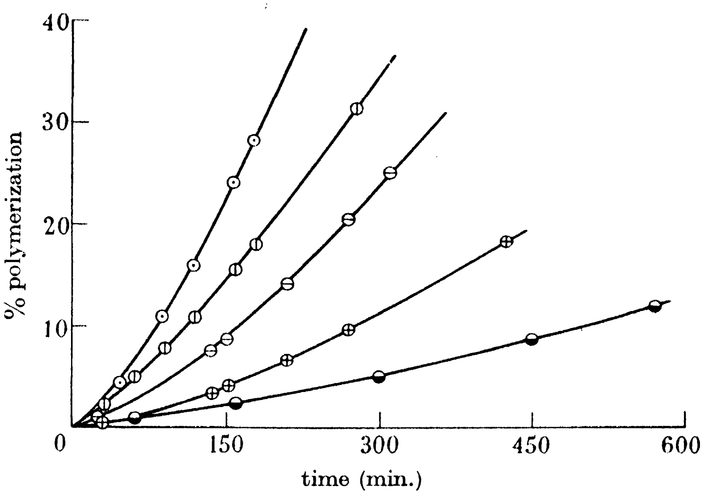

FIGURE 1. Effect of benzoyl peroxide concentration on the polymerization of vinyl chloride at 47° C. ⊙ 1·15 mol. % Bz_2O_2; ⦶ 0·533 mol. % Bz_2O_2; ⊖ 0·281 mol. % Bz_2O_2; ⊕ 0·117 mol. % Bz_2O_2; ◒ 0·0295 mol. % Bz_2O_2.

It can be seen from figure 1 that throughout the first 30 to 40 % polymerization, the rate of polymerization continually increases. This increase in rate is more marked in the early stages (e.g. from 0 to 5 % polymerization).

The rate of polymerization increases or decreases with increase or decrease in concentration of benzoyl peroxide. The general 'autocatalytic' shape of the curve, however, is not affected even when the concentration of benzoyl peroxide employed is varied from 0·025 to 1·0 mol. %.

Since the rate of polymerization increases very rapidly in the very early stages of the reaction (i.e. from 0 to 1 % polymerization), it is difficult to measure accurately the true initial rate of the reaction, but rates at higher percentages of conversion are more easily obtained, because at later stages the percentage change in rate is much smaller. In order to obtain a relationship between the rates of reaction and the catalyst concentration, other factors, such as temperature and extent of reaction, must be the same in each case. The plot of the velocities of polymerization at 5 and 20 % polymerization against the square root of the concentration of benzoyl peroxide is given in figure 2. This shows that, at equal extents of polymerization, the rate varies as the square root of the catalyst concentration.

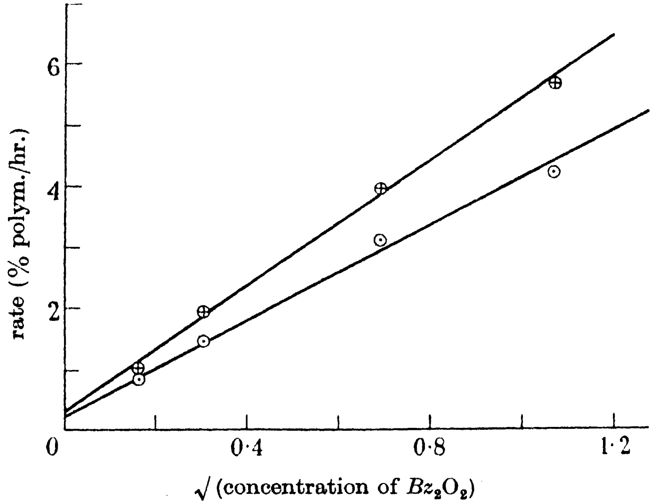

Figure 2. Polymerization of vinyl chloride at 40° C. showing relationships between rates measured at 5 % polymerization (⊙) and 20 % polymerization (⊕), and the concentration of benzoyl peroxide present.

If now the concentration of benzoyl peroxide is kept constant, and the temperature is varied, it is found that the rate increases markedly with increase in temperature. This will be apparent from figure 3, which shows the course of the polymerization of vinyl chloride catalyzed by 0·115 mol. % benzoyl peroxide at temperatures of 33, 47, 61 and 75° C. Prat (1945) has pointed out that he could detect no marked autocatalytic effect at 75° C. He stated, however, that this might have been due to experimental inaccuracies at this temperature. Our results show that even at this temperature, the rate of polymerization increases throughout the first 30 % polymerization. The polymerization thus appears to be autocatalytic over the range of catalyst concentration from 0·025 to 1·0 mol. % benzoyl peroxide, and over a range of temperature from 33 to 75°C.

When the logarithm of the average rate of polymerization over the first 10 % polymerization and from 20 to 30 % polymerization is plotted against the reciprocal of the absolute temperature for polymerizations of vinyl chloride catalyzed by

0·115 mol. % benzoyl peroxide, two straight lines are obtained which, within experimental error, are parallel. These yield an overall activation energy of 21·8 kcal./g.mol., which as far as we have been able to ascertain, has not been recorded previously. This value is very close to that of 21·6 kcal. obtained by Nozaki & Bartlett (1946) for the benzoyl peroxide catalyzed polymerization of vinyl acetate.

If *ortho*-chloro-benzoyl peroxide is employed as catalyst instead of benzoyl peroxide, the reaction again proceeds autocatalytically. This peroxide, however, has a greater catalytic effect than benzoyl peroxide and produces more rapid polymerization, for equal molar concentrations.

In order to ascertain whether the acceleration shown in figure 1 was caused by the gradual removal of inhibitors present in the vinyl chloride, two dilatometers (whose bulbs *A* and *B* were of different size), were connected to each other by a T-piece seal, as shown in figure 4. The seal, which enables either arm to be evacuated independently, could be broken by shaking the dilatometer. Benzoyl peroxide and vinyl chloride were introduced into the bulb *A* and the polymerization followed at 47° C to about 20 % polymerization. Benzoyl peroxide was then introduced into bulb *B* which was afterwards evacuated and sealed off from the apparatus; monomer was then distilled from bulb *A* into bulb *B* and the arm *B* sealed off; the course of the polymerization at 47° C. in arm *B* was then followed. The results are shown in figure 5. It is seen that the shape of the polymerization against time curve, is identical in both polymerizations, which indicates that the originally purified vinyl chloride polymerizes in the same manner as monomer which has been a part of a polymerizing mixture. That the vinyl chloride was pure, is also indicated by the results in figure 6 which show that on replacing the residual monomer after about 20 % polymerization by fresh vinyl chloride, the continued polymerization commences at the accelerated rate.

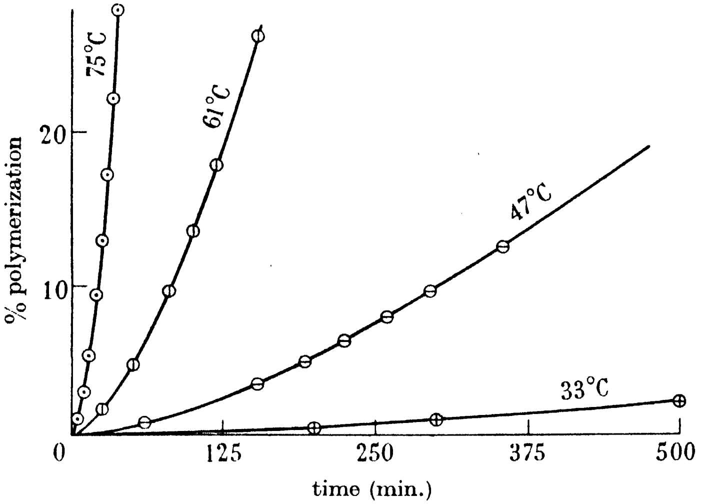

FIGURE 3. Effect of temperature on the polymerization of vinyl chloride catalyzed by 0·115 mol. % benzoyl peroxide.

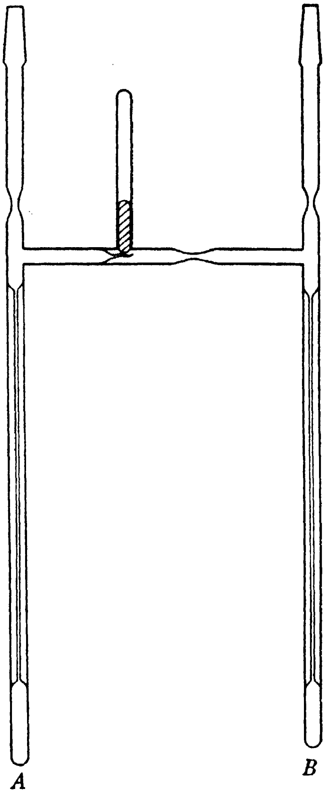

Figure 4. Twin dilatometer used for establishing purity of monomer.

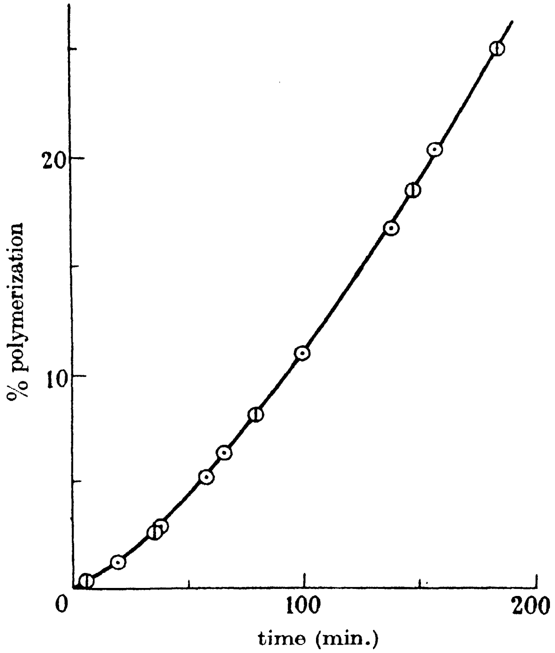

Figure 5. Comparison of the course of polymerization of vinyl chloride, catalyzed by 1·04 mol. % benzoyl peroxide at 47° C, in arms *A* and *B* of the dilatometer. ⊙ polymerization in arm *A*; ⦶ polymerization in arm *B*.

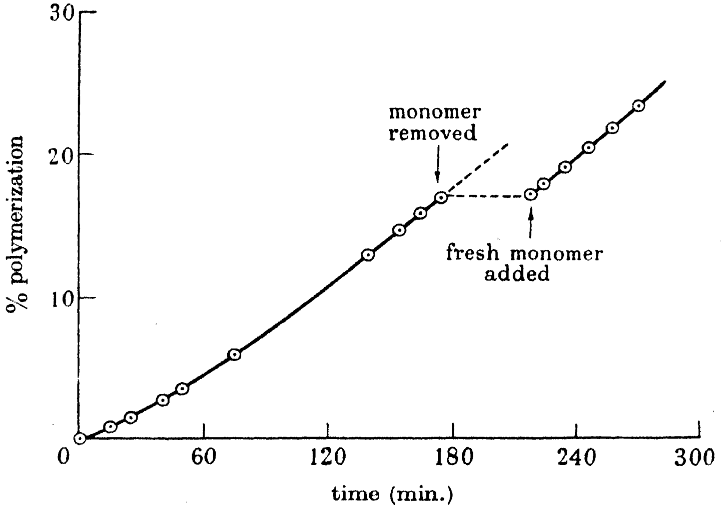

Figure 6. Effect of replacing the residual monomer by purified monomer, in the polymerization of vinyl chloride, catalyzed by 0·49 mol. % benzoyl peroxide at 47° C.

Effect of addition of 'dead' polymer

From the above results, it is apparent that the acceleration in rate of polymerization is due, in some way, to the presence of some product of the reaction. The chief product is obviously polyvinylchloride, and it is shown in figure 7 that the presence of this polymer in the system causes an increase in rate of polymerization. It can be seen that the greater the amount of polymer added, the greater is the yield of polymer in the first seventy minutes of reaction. In the case in which no benzoyl peroxide is added, there is no measurable extent of polymerization at 47° C, even after several days. Both benzoyl peroxide and 'dead' polyvinylchloride therefore appear to be necessary in order to produce this acceleration in rate.

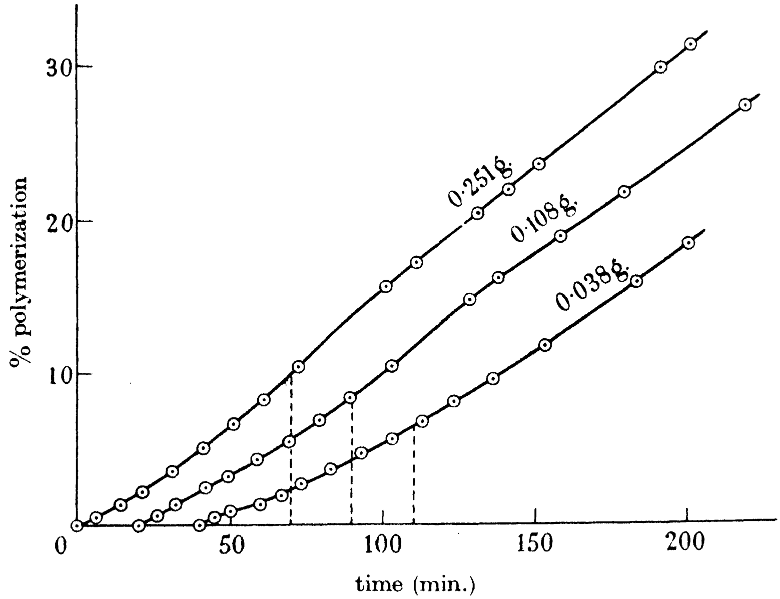

FIGURE 7. Effect of addition of chalk-like polyvinylchloride to vinyl chloride catalyzed by 0·57 mol. % benzoyl peroxide at 47° C. The origin has been moved to show more clearly the 'added polymer effect' and also the points of inflexion on the curves. The amounts of added polymer are indicated on the curves.

During the polymerization, the added chalk-like polymer was converted into a translucent glass. It is suggested that conversion of polymer into polymer-glass, might account for the points of inflexion which appear on the graphs in figure 7, since it would be accompanied by a reduction in surface area, and consequently by a reduction in rate, if the rate depends on the surface area of the added polymer.

If polyvinylchloride beads, which are of a more open texture, are used instead of the chalk-like polymer, no points of inflexion appear on the percentage polymerization against time curve, as can be seen from figure 8; it is clear that these beads of polymer also exert a co-catalytic effect, and that the greater the amount of polymer added, the greater is the rate of polymerization. The beads, after the polymerization had been stopped, were not converted into glass, but they appeared to be of a much denser texture than the untreated samples.

It is shown in figures 7 and 8 that even when large amounts of polymer are added to the system, the initial rate is rather low, and that the acceleration in rate in the first few percent polymerization is considerable. This rather unexpected result might have been caused by inhibitors which were adsorbed on the surface of the polymer prior to its introduction into the dilatometer, and which were not removed after prolonged evacuation. Support for this explanation is given by the fact that when vinyl chloride is polymerized to about 20 % conversion, the unchanged monomer

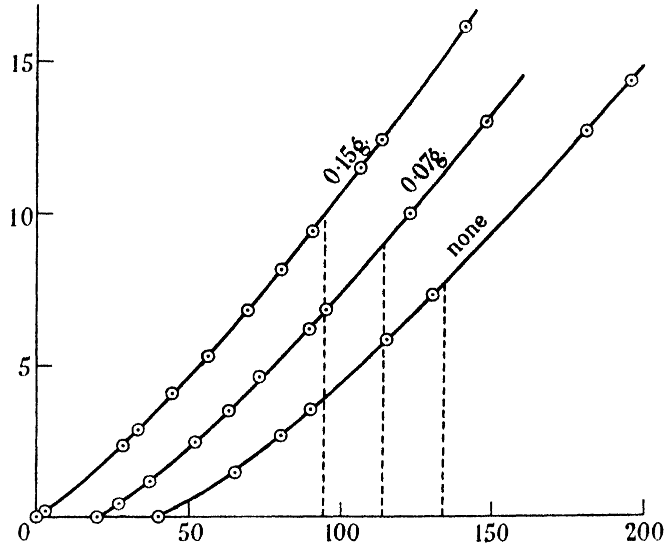

Figure 8. Effect of addition of polyvinylchloride beads on vinyl chloride polymerization, catalyzed by 0·49 mol. % benzoyl peroxide at 47° C. The origin has been displaced to show the effect more clearly. The amounts of added polymer are indicated on the curves.

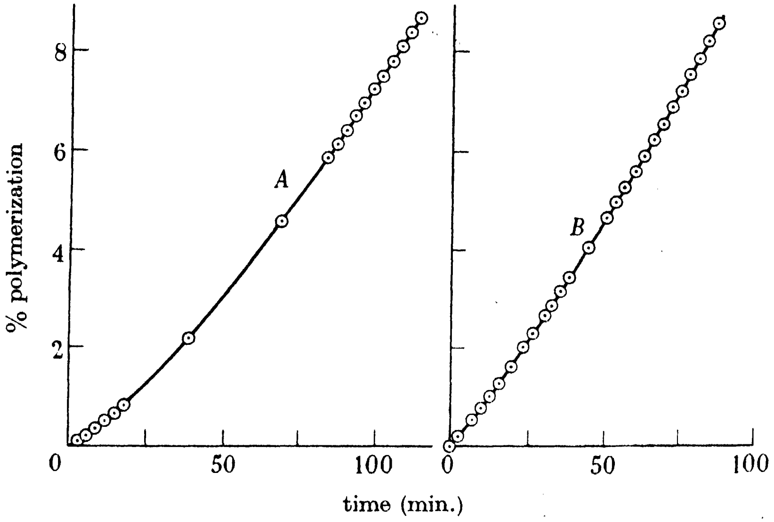

Figure 9. Polymerization of vinyl chloride at 47° C with 0·5 mol. % benzoyl peroxide. Curves *A* and *B* differ only in the amount of polymer present.

removed, and the polymer left in contact with air prior to the introduction of fresh monomer, it is found that on continuing the polymerization, there is a short period of inhibition followed by an acceleration in rate. This is in contrast with the results shown in figure 6 in which the polymer was not allowed in contact with air prior to the introduction of fresh monomer.

In figure 9, curve A shows the course of the polymerization of vinyl chloride catalyzed by 0·5 mol. % benzoyl peroxide at 47° C. The polymerization was stopped after 8·4 % polymerization had taken place, the residual monomer removed, and an amount of vinyl chloride equal to that initially used, was added; curve B shows the course of the continued polymerization. The rates at equal extents of polymerization were measured, and from a comparison of these on curves A and B, the effect of polymer on the rate of reaction was determined quantitatively. The results shown in table 2 indicate that a definite relationship exists between the rate of polymerization and the amount of polymer present in the system.

TABLE 2. VARIATION IN VALUE OF THE FUNCTION $(R_B - R_A)/(P_B^{2/3} - P_A^{2/3})$ IN THE EARLY STAGES OF POLYMERIZATION, WHERE R AND P ARE THE RATE, AND PERCENTAGE POLYMER PRESENT RESPECTIVELY, THE SUBSCRIPTS A AND B REFERRING TO THE POLYMERIZATION SHOWN IN FIGURE 9

M	P_A	P_B	$(R_B - R_A)$	$\frac{(R_B - R_A)}{P_B^{2/3} - P_A^{2/3}}$
99·40	0·60	9·00	0·0142	0·0039
98·81	1·19	9·59	0·0119	0·0035
98·21	1·79	10·19	0·0114	0·0035
97·61	2·39	10·79	0·0095	0·0031
97·02	2·98	11·38	0·0098	0·0033
96·42	3·58	11·98	0·0107	0·0037
95·82	4·18	12·58	0·0098	0·0035
95·22	4·78	13·18	0·0093	0·0034
94·63	5·37	13·77	0·0102	0·0038
94·04	5·96	14·36	0·0085	0·0032
93·43	6·57	14·97	0·0077	0·0030
92·84	7·16	15·56	0·0080	0·0032
92·24	7·76	16·16	0·0081	0·0033

From table 2 it appears that the catalytic effect of the polymer is approximately proportional to the amount of polymer to the power of two-thirds.

This catalytic effect does not occur when the polymerization is carried out in the presence of a solvent for the polymer; in the presence of dibutyl phthalate or tetrahydrofuran, the benzoyl peroxide catalyzed polymerization proceeds at a constant rate over the first 10 % reaction. If very small amounts of dibutyl phthalate (about 5 mol. %), are used, the rate remains constant up to a few per cent polymerization, and then begins to accelerate very slowly. In this case it was observed that the polymerizing mixture became a greyish white in colour, apparently due to undissolved polymer. The polyvinylchloride therefore has to be in a precipitated form in order to exhibit its co-catalytic effect on the polymerization. The course of the polymerization of vinyl chloride in the presence of these solvents is shown in figure 10 in which the fall of the meniscus in the dilatometer capillary is plotted against time.

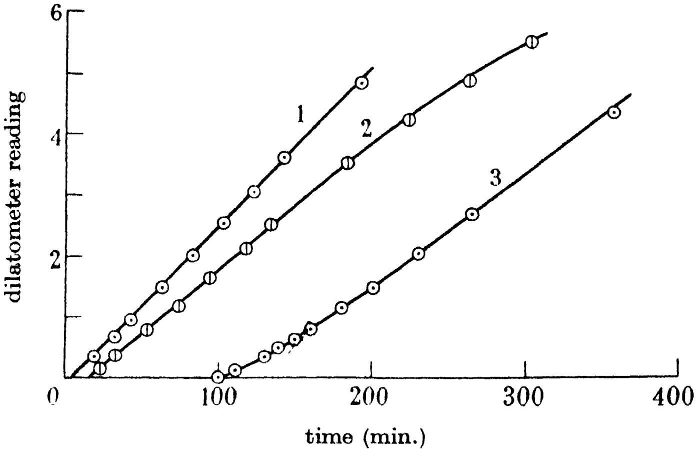

FIGURE 10. Polymerization of vinyl chloride in the presence of solvents for the polymer; curve 1, dibutyl phthalate; curve 2, tetrahydrofuran; curve 3, small amount of dibutyl phthalate. The origin of each curve has been moved to avoid superposition of the lines.

Degree of polymerization

An indication of the way in which the degree of polymerization varies with the mode and conditions of preparation of the polymer, can be obtained by determining the relative viscosities of dilute solutions of the polymer. The equivalent viscosity, λ, was defined by Mead & Fuoss (1942) as the ratio $(\ln \eta_r)/c'$, where η_r is the relative viscosity of the solution and c' the concentration of the solution in monomoles per litre. It was shown that for vinyl chloride polymers

$$\lambda = \lambda_0(1-\beta\lambda_0 c'),$$

where λ_0 is the limiting equivalent viscosity for zero concentration and β is a constant which was found to be of low value; thus for very dilute solutions we have $\lambda = \lambda_0$. Furthermore, they showed that λ_0 is proportional to the molecular weight. The value of the function $(\log \eta_r)/c$, where c is the concentration of the solution in g. of polymer per 100 ml. of solution, will therefore also be proportional to the molecular weight of the polymer. It is shown in table 3 that there is little variation in the value of this function throughout the reaction.

TABLE 3. VARIATION OF DEGREE OF POLYMERIZATION WITH PERCENTAGE POLYMERIZATION, IN THE POLYMERIZATION OF VINYL CHLORIDE, CATALYZED BY 0·625 MOL. PERCENTAGE BENZOYL PEROXIDE, AT 47° C

percentage polymerization	$(\log \eta_r)/c$
4·5	0·41
9·0	0·41
20·0	0·41
33·0	0·41
48·5	0·41
64·0	0·41
88·0	0·39

The concentration (c) of the polymer solutions, used in the above experiments, was 0·25 g. of polymer per 100 ml. of tetrahydrofuran.

Similar results are obtained if vinyl chloride is polymerized in the presence of 20 mol. % dibutyl phthalate and 0·50 mol. % benzoyl peroxide. The degree of polymerization in this case, however, is somewhat lower than when dibutyl phthalate is absent from the system. It is interesting to note that no marked increase in rate of polymerization, or in degree of polymerization was observed, although the polymerizing mixture at 30 % polymerization was a firm gel, from which the vinyl chloride escaped very slowly, even when left at room temperature; the results are shown in table 4.

TABLE 4. VARIATION OF DEGREE OF POLYMERIZATION WITH PERCENTAGE POLYMERIZATION FOR VINYL CHLORIDE CATALYZED BY 0·5 MOL. PERCENTAGE BENZOYL PEROXIDE, IN THE PRESENCE OF 20 MOL. PERCENTAGE DIBUTYL PHTHALATE AT 47° C

percentage polymerization	$(\log \eta_r)/c$
3·6	0·28
8·4	0·29
15·0	0·34
26·0	0·33
35·0	0·30
46·3	0·29
66·5	0·28
85·0	0·29

Vinyl chloride, catalyzed by 0·115 mol. % benzoyl peroxide was polymerized at various temperatures to an extent of about 10 % polymerization. Table 5 gives a comparison of the degree of polymerization at temperatures from 33 to 85° C. It is seen that at 85° C, the value of the average molecular weight is about one-third of the value obtained at 33° C.

TABLE 5. EFFECT OF TEMPERATURE ON THE DEGREE OF POLYMERIZATION

temperature (° C)	$(\log \eta_r)/c$
33	0·68
47	0·45
61	0·39
75	0·28
85	0·22

The variation of degree of polymerization with catalyst concentration was determined for polymerizations of vinyl chloride at 47° C. The concentration of benzoyl peroxide was varied from 0·008 to 2 mol. %, all polymerizations being stopped at about 10 % conversion of the monomer to the polymer.

It is seen from figure 11 that the degree of polymerization varies only slightly over a wide range of catalyst concentration. At concentrations higher than 0·5 mol. %, however, the average molecular weight becomes much more dependent on the concentration of the catalyst. At very high catalyst concentration it tends towards the familiar inverse proportionality between the average molecular weight and the concentration of the catalyst.

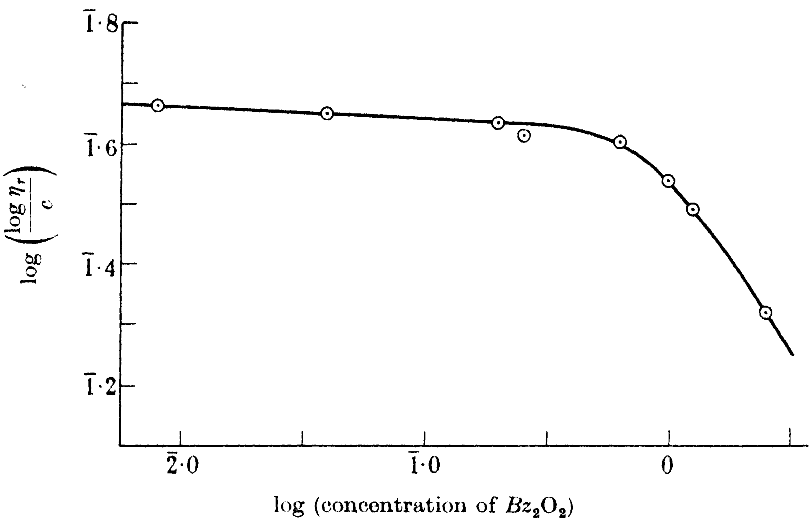

FIGURE 11. Effect of change in catalyst concentration on the average molecular weight

DISCUSSION OF RESULTS

It is evident from the above results that the polymerization of vinyl chloride differs in some respects from that of monomers such as styrene, methyl methacrylate, or vinyl acetate. The latter polymerize at a constant rate throughout the early stages of the reaction, whereas vinyl chloride polymerizes autocatalytically at temperatures from 33 to 75° C and at various catalyst concentrations. The increase in rate is not due to the removal of inhibitors as the reaction proceeds, since the reactivity of the unreacted monomer after about 20 % reaction (figure 4) is equal to that of the original monomer. Again when, after about 20 % polymerization, the unconverted monomer is replaced by fresh monomer (figure 5), the continued polymerization commences at the accelerated rate, which indicates that no inhibiting impurities are present in the purified monomer.

The view advanced by Prat (1945) that the period of acceleration might be a true period of induction (Dostal & Mark 1935), or more probably due to an initiation reaction controlled by two consecutive reactions (Cuthbertson *et al.* 1939), clearly cannot be accepted since it offers no explanation of the co-catalytic effect of 'dead' polymer. The catalytic effect of 'dead' polymer only occurs in the presence of the initiating catalyst, e.g. benzoyl peroxide, and cannot therefore be due to the formation of free radicals by fission of polymer molecules, followed by the growth of these radicals, as has been suggested by Melville (1948) for methyl methacrylate at higher temperatures. Since the catalytic effect of the 'dead' polymer, measured by the increase in reaction rate, was found to be proportional to the amount of polymer present raised to the power of $\frac{2}{3}$, we may conclude that it is in proportion to the surface area of the polymer, for to a first approximation surface area may be taken as proportional to the $\frac{2}{3}$ power of the weight, or the volume, of the polymer. Support for this conclusion is given by the following experimental observations: (*a*) when polymer is converted into a glass its catalytic effect is reduced, presumably due to a reduction in surface area, and (*b*) if the polyvinylchloride is kept in solution by the addition of a solvent such as dibutyl phthalate or tetrahydrofuran, its catalytic effect vanishes. We therefore conclude that the catalytic effect occurs only at the surface of the solid polymer separating from the polymerizing medium.

Periods of acceleration are also exhibited in the polymerization of monomers which are solvents for their polymers. This so-called 'gel effect' (Norrish & Smith 1942) does not appear until later stages of the reaction when the system has become viscous, and so differs from the period of acceleration which in the polymerization of vinyl chloride occurs from the very beginning of the reaction, and is closely associated with the separation of the solid polymer phase. Again, in the polymerization of vinyl chloride, the average molecular weight of the polymer formed during the reaction remains constant, but with monomers which give rise to the 'gel effect', it increases with increase in rate of polymerization. The 'gel effect' has been explained by Norrish & Smith (1942) as due to a reduction in the rate of the termination reaction, resulting from the great increase in viscosity of the medium, probably supplemented by the coiling of the growing polymer chains, as later suggested by Burnett & Melville (1947); this effect is not to be confused with the co-catalytic effect at present under examination.

The results can be explained on the assumption that, in addition to normal propagation in the liquid phase, the growing radical can undergo a transfer reaction with the 'dead' polymer, terminating itself with the formation of a free valence in the surface of the polymer. The active polymer then grows by addition of monomer, being eventually terminated by a transfer reaction with monomeric vinyl chloride. That chain transfer reactions play an important role in the polymerization of vinyl chloride is evident from the fact that, over a wide range of catalyst concentrations, the average molecular weight remains constant (figure 11), in agreement with the views of Nozaki (1947) who, from a consideration of the stability of radicals derived from various monomers, concluded that chain transfer with monomer was likely to predominate in vinyl chloride polymerization. Chain transfer with monomer also explains the constancy of the average molecular weight, observed by Mead & Fuoss (1942), of samples of polyvinylchloride which had been prepared by different methods.

Mechanism and kinetics

The polymerization of vinyl chloride, catalyzed by benzoyl peroxide, can be represented by the following equations, in which B, R, M, P and P^* refer to the benzoyl peroxide, mobile free radicals, monomer, dead ploymer and polymer conglomerate radicals.

For simplicity, all the mobile R radicals (i.e. phenyl, benzoate, and growing radicals) are treated as having the same reactivity; if considered separately, the general form of the kinetics will not be altered, but the picture will be more complicated.

		rate constants	
initiation	$B \rightarrow 2R$	k_i	(1)
propagation	$R+M \rightarrow R$	k_p	(2)
chain transfer with monomer	$R+M \rightarrow P+R$	k_{tr}	(3)
termination	$R+R \rightarrow P$	k_t	(4)
activation of polymer surface by transfer	$R+P \rightarrow P^*+P$	k_a	(5)
propagation on polymer surface	$P^*+M \rightarrow P^*$	k_p	(6)
termination of surface radical by transfer	$P^*+M \rightarrow P+R$	k_{tr}	(7)

At any time t, let n be the number of R radicals per mole of monomer; let M be the number of moles of monomer; let n_s be the number of surface P^* radicals per unit area; let A be the total surface area of the polymer; and let B be the total number of moles of benzoyl peroxide present in the reacting system.

The P^* radicals, which are part of the polymer conglomerates, will not be mobile like the rest of the radicals in the system, but since the polymer is bathed in liquid monomer, this immobility should not appreciably affect either the propagation rate constant or the rate constant for the chain transfer reaction with monomer. It is suggested that these immobile P^* surface radicals are terminated by chain transfer with monomer, giving rise to new mobile R radicals. The rate of formation of radicals in the system is given by the following equations:

$$M\,dn/dt = k_i B - k_t n^2 M - k_a nA + k_{tr} n_s A, \tag{a}$$

$$A\,dn_s/dt = k_a nA - k_{tr} n_s A. \tag{b}$$

Applying the conditions for a stationary state, dn/dt and dn_s/dt are each equal to zero, whence, from equation (b), we have

$$n_s = k_a n/k_{tr}, \tag{c}$$

and from equations (a) and (b)

$$n = (k_i B/k_t M)^{\frac{1}{2}}. \tag{d}$$

Now the rate of polymerization is measured by the rate of loss of monomer (i.e. $-dM/dt$), which will be proportional to the total number of radicals in the system, i.e.

$$-dM/dt = (k_p + k_{tr})(nM + n_s A). \tag{e}$$

Substituting for n_s and n in equation (e) we obtain

$$-dM/dt = (k_p + k_{tr})(M + k_a A/k_{tr})(k_i B/k_t M)^{\frac{1}{2}}. \tag{f}$$

The experimental rates have been measured as percentage of vinyl chloride polymerized per unit time, i.e. $-\frac{d}{dt}\left(\frac{100M}{M_0}\right)$, where M_0 is the value of M initially. If M_0 is taken as being equal to 100, then equation (f) gives the rate in the above-mentioned units. The expression for the rate of polymerization is therefore

$$-dM/dt = K(M + K'A)(B/M)^{\frac{1}{2}}, \tag{g}$$

where $K = (k_p + k_{tr})(k_i/k_t)^{\frac{1}{2}}$ and $K' = k_a/k_{tr}$.

Let us now assume that the effective surface area of the polymer is proportional to its weight raised to the power of $\frac{2}{3}$. The equation for the rate becomes

$$-dM/dt = K(M + K''P^{\frac{2}{3}})(B/M)^{\frac{1}{2}}, \tag{h}$$

where K and K'' are constants, which indicates that the rates at equal extents of polymerization are proportional to the square roots of the catalyst concentrations. This result has been confirmed experimentally, as can be seen from the plots in figure 2.

As polymerization proceeds, both the monomer and the catalyst are used up in the reaction. Let us assume that they are removed at a rate such that the catalyst concentration remains approximately constant during the first 30 to 40 % reaction. The two systems referred to in table 2 therefore differ only in the amount of polymer present. The results show that the difference in rates of polymerization in the two systems is approximately proportional to the difference between the weight of polymer to the power $\frac{2}{3}$, present in each system (i.e. $(R_B - R_A)$, is proportional to $(P_B^{\frac{2}{3}} - P_A^{\frac{2}{3}})$), as would be expected from the above kinetic derivation.

A value of 12·7 is obtained for K'' by substituting the experimentally determined value of the ratio of the reaction rates at 5 and 20 % polymerization (0·76), in equation (h). Using this value for K'', together with the assumption that the catalyst concentration remains constant, equation (h) can be integrated by means of the central difference formula,† and yields a relationship between the percentage polymerization and the time. Employing a suitable value for K, the theoretical percentage polymerization versus time curves for various concentrations of catalyst are plotted in figure 12, and it will be apparent that the experimental points, which are also plotted in this figure, lie very close to these curves. A comparison of the experimental and calculated extents of reaction for given periods and for various catalyst concentrations is shown in table 6.

This good agreement between experiment and theoretical calculations based upon the above-mentioned mechanism, leads us to conclude that the autocatalytic nature of the peroxide catalyzed polymerization of vinyl chloride is due to the activation and subsequent growth of dead polyvinylchloride. The mechanism which we have put forward in this paper, is also capable of explaining the results obtained from experiments on the degree of polymerization.

---

† We are indebted to Miss C. Munford for suggesting this method of integration. (See p. 260, *Mathematical physics*, by H. and B. S. Jeffreys, Cambridge University Press, 1946.) We have proceeded as follows:

$$\int_{P_0}^{P_1} f(P)\,dP = \tfrac{1}{2}(P_1 - P_0)\,[f(P_0) + f(P_1) - \tfrac{1}{12}\{\delta^2 f(P_0) + \delta^2 f(P_1)\} + \tfrac{11}{720}\{\delta^4 f(P_0) + \delta^4 f(P_1)\} + \cdots],$$

where

$$f(P) = -\frac{dt}{dM} = \frac{dt}{dP} = \frac{1}{K_1(100 - P + 12{\cdot}7P^{\frac{2}{3}})},$$

$$\delta f(P_{\frac{1}{2}}) = f(P_1) - f(P_0),$$

$$\delta^2 f(P_0) = \delta f(P_{\frac{1}{2}}) - \delta f(P_{-\frac{1}{2}}) \ldots \text{etc.},$$

and $K_1 = K(B/M)^{\frac{1}{2}}$ is assumed constant. If small intervals (P_0 to P_1) are taken then differences other than the first and second become negligibly small. The integrals were therefore calculated for unit intervals from $P = 0$ to $P = 10$ (i.e. over ranges of 0 to 1, 1 to 2, etc.), and for intervals of five units from $P = 10$ to $P = 40$, so that only the first and second differences were significant. By adding together the values of the integrals thus calculated, a relationship between the percentage polymerization and the time was obtained for the first 40 % of the reaction.

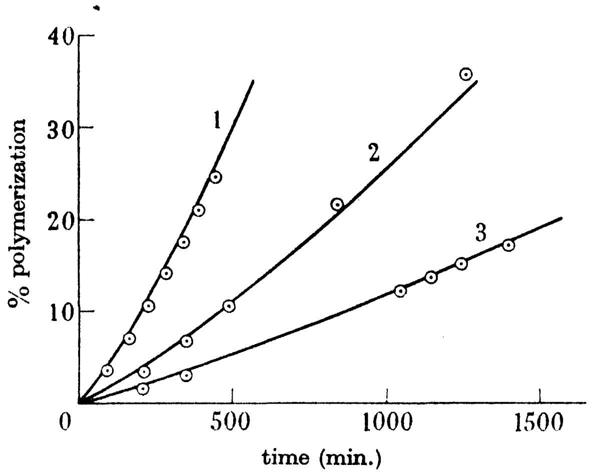

FIGURE 12. Theoretical and experimental plots of percentage polymerization against time. — theoretical; ⊙ experimental. Concentrations: curve 1, 0·48; curve 2, 0·092 and curve 3, 0·0256 mol. % Bz_2O_2.

TABLE 6. EXPERIMENTAL AND CALCULATED DATA FOR THE POLYMERIZATION OF VINYL CHLORIDE AT 40° C

benzoyl peroxide concentration (mol. %)	time (min.)	percentage polymerization	
		experimental	calculated
0·48	95	3·5	4·3
	165	7·0	8·0
	225	10·5	11·4
	283	14·1	15·0
	340	17·6	18·5
	390	21·0	21·9
	440	24·4	25·3
0·092	210	3·4	4·1
	350	6·7	7·3
	490	10·5	10·8
	840	21·6	20·4
	1260	35·6	33·7
0·0256	210	1·5	2·1
	285	3·0	2·9
	1050	12·0	12·4
	1150	13·5	13·8
	1250	15·0	15·2
	1400	16·7	17·5

Degree of polymerization

According to the mechanism which we have put forward above, an active centre once formed will grow until it is rendered inactive by transfer with monomer, or by reaction with another active centre; the polymer molecule so formed will grow no further until it undergoes a chain transfer reaction with an active centre, and the probability of this taking place will depend upon both the concentration of the active centres and the surface area of the polymer molecule. Now as the reaction proceeds, the polymer molecules coalesce with a resultant reduction in their effective surface area, and consequently a reduction in the probability of further growth; this means that if we consider one particular polymer molecule, its tendency to grow will diminish as the reaction continues and thus it will tend towards a definite molecular weight. It is shown in table 3 that the average degree of polymerization remains constant throughout the major part of the reaction, which agrees with the above mechanism provided that a polymer molecule grows for a short time only before it becomes surrounded by other molecules of polymer, and is rendered incapable of further growth. Towards the end of the reaction it might be expected that the active lifetime of a polymer molecule would be reduced, since polymerization at this stage often involves the filling up of small spaces in the chalk-like polymer. This, together with the effect of the enormous increase in catalyst concentration at very late stages in the reaction, would result in the production of lower molecular weight polymer towards the end of the reaction, as in fact was found to be the case.

It can be seen from figure 11 that, for catalyst concentrations up to about 0·5 mol. %, the average degree of polymerization remains approximately constant, but becomes dependent upon the catalyst at higher concentrations. This can be explained by postulating that at low catalyst concentrations the active centres are terminated mainly by chain transfer reactions with monomer, with the formation of polymer of constant molecular weight; at high concentrations of catalyst, the stationary concentration of centres will be much greater, and termination by mutual interaction of centres will become increasingly important since the rate of such termination reactions is proportional to the square of the number of centres, whilst chain transfer reactions depend upon the first power, and therefore the molecular weight will be dependent upon the concentration of catalyst.

The average degree of polymerization again remained constant throughout the reaction when vinyl chloride was polymerized in the presence of dibutyl phthalate, as is shown in table 4. A polymer of lower molecular weight than would have been produced in the absence of solvent was obtained as would be expected, since the augmentation of molecular weight by surface activity is now absent. The observed lowering of the degree of polymerization with increase in temperature as shown in table 5 is quite a familiar phenomenon in polymerization processes, and can be explained by the increase in value of the rate constants involved in the reaction.

Effect of acetylene impurities

The retardation of the rate of polymerization observed in the presence of acetylene impurities may be due to the formation of resonance stabilized radicals, according to the following reactions:

$$R.\mathrm{CH_2CHCl}{-} + \mathrm{CH{\equiv}CH} \rightarrow R.\mathrm{CH_2.CHCl.CH{=}CH}{-},$$

$$R.\mathrm{CH_2CHCl.CH{=}CH}{-} \xrightarrow{\text{stabilization}} R.\mathrm{CH_2}.\underset{|}{\mathrm{C}}\mathrm{Cl.CH{=}CH_2} \longleftrightarrow R.\mathrm{CH_2.CCl{=}CH.CH_2}{-}$$

Some of the free radicals formed by the reaction of growing polymer chains with acetylene might continue to grow by addition of vinyl chloride with the production of a limited amount of high polymer.

We wish to express our thanks to the Distillers Co. Ltd. for a studentship granted to one of us (W.I.B.) and for a supply of vinyl chloride and other chemicals.

REFERENCES

Burnett, G. M. & Melville, H. W. 1947 *Proc. Roy. Soc.* A, **189**, 494.
Cuthbertson, A. C., Gee, G. & Rideal, E. K. 1939 *Proc. Roy. Soc.* A, **170**, 300.
Dostal, H. & Mark, H. 1935 *Z. phys. Chem.* B, **29**, 299.
Gee, G. & Rideal, E. K. 1936 *Trans. Faraday Soc.* **32**, 656.
Haward, R. N. 1948 *J. Polymer. Sci.* **3**, 10.
Mead, K. J. & Fuoss, R. M. 1942 *J. Amer. Chem. Soc.* **o4**, 277.
Melville, H. W. 1948 *The chemistry of high polymers and surface chemistry*, pp. 19–20. Cambridge: W. Heffer and Sons.
Norrish, R. G. W. & Smith, R. R. 1942 *Nature*, **150**, 336.
Nozaki, & Bartlett, P. D. 1946 *J. Amer. Chem. Soc.* **68**, 2377.
Nozaki, K. 1947 *Disc. Faraday Soc.* **2**, 337.
Prat, J. 1945 *Mém. serv. chim. état* (Paris), **32**, 319.
Trommsdorff, E. 1944 *Colloquium on high polymers.* Freiburg. See B.I.O.S. Rep. no. 363, item no. 22.

The characters of a collineation group in five dimensions

BY J. A. TODD, F.R.S.

(*Received* 23 *August* 1949)

This paper is devoted to the calculation of the irreducible characters of a collineation group of order 6531840 in five dimensions, and of a subgroup of index 2 in this which is simple; and it is shown by examples that the employment of the table leads to the discovery of large subgroups of these two groups, which throw interesting light on the geometry of a certain configuration left invariant by them.

INTRODUCTION

The primary object of this paper is the determination of the table of characters of the primitive collineation group of order $2^8 . 3^6 . 5 . 7$ in space of five dimensions, whose existence was demonstrated by Mitchell (1914). This group is generated by 126 harmonic inversions, or *projections*, as we shall term them in the present paper, and is the least familiar of a comparatively small family of collineation groups generated by such projections. In the course of a study of this group, and a determination of the distribution of its elements in conjugate sets, Hamill (1951) was led to examine in some detail the configuration formed by the 126 points which are the centres of the generating projections. This configuration proves to have a highly complex structure and a remarkable wealth of geometrical properties, and it is quite certain that the subconfigurations described in Hamill's paper do not exhaust the features of geometrical interest in the figure. The examination of subconfigurations is obviously closely connected with the determination of subgroups of the collineation group under which the whole figure is invariant, and the subgroups which are of greatest interest in this connexion are the ones of largest order. The most systematic way of determining these subgroups is by means of a table of characters, and while it is not the purpose of the present paper to carry out such a search in detail, the last section contains a determination, by way of illustration, of the four largest subgroups of the invariant subgroup of index 2 which the collineation group is known to contain; and the fact that two of these correspond to subconfigurations of whose existence Hamill's description gives no hint illustrates the value of the table of characters, and suggests that a systematic search for large subgroups by means of the table will probably lead to further results of geometrical interest.

A secondary feature of interest in the present paper may lie in the method, described in general terms in the first section, of obtaining the characters. For the theoretical method of determining the characters of a group, as given in the standard treatises (Burnside 1911; Speiser 1937), does not lend itself to practical application except for groups of very small order, and most of the character tables in existence deal with special classes of groups, such as the symmetric groups (Littlewood 1935; Zia-ud-Din 1935, 1937), or the fractional linear groups in a modular field (Burnside 1911, 499), which present special features that can be exploited, while the table of characters of the well-known simple group of order 25920 calculated by Frame (1936) makes use of the representation of this group as a modular group. The method used here makes no use of any such special features, so that in theory it might be used for any group. But it is tentative in that the analysis to which it leads is Diophantine, and it is not possible to say whether its success is due to peculiar structural features of the group, or whether it has a really extensive field of possible application, until further applications of it have been attempted. It is also somewhat laborious, but not unreasonably so in view of the fairly high order of the group involved.

1. A TENTATIVE METHOD FOR COMPUTING THE CHARACTERS OF A GROUP

Let G be a finite group of order g, containing r classes $C_1, C_2, \ldots, C_r$ of conjugate elements, C_1 being the class consisting of the identity; and let g_ξ be the number of elements in the class C_ξ, so that $g_1 = 1$ and $g_1+g_2+\ldots+g_r = g$. If Γ is any representation of G as a group of matrices, and if ψ_ξ is the trace of the matrix corresponding to an element of G belonging to C_ξ, the set of r numbers $(\psi_1, \psi_2, \ldots, \psi_r)$—each of which is an algebraic integer—form the components of a vector ψ which is called the *character* of Γ, and the component ψ_1 is the *degree* of the character ψ.

Any representation of G is equivalent to the direct sum of a number of irreducible representations. The number of these is r, the number of classes of conjugate elements; we denote them by $\Gamma_0, \Gamma_1, \ldots, \Gamma_{r-1}$, Γ_0 being the representation in which each element of G is represented by the number 1. The characters of the irreducible representations will be denoted by $\chi^{(i)}$ $[i = 0, 1, \ldots, (r-1)]$; clearly $\chi^{(0)}_\xi = 1$ for each class C_ξ. The r characters $\chi^{(i)}$ corresponding to the irreducible representations Γ_i are the *characters* of G which it is desired to determine; the character ψ of any representation of G is a linear combination, with non-negative integral coefficients, of the r irreducible characters $\chi^{(i)}$.

The properties of these characters are developed in the standard treatises, of which Burnside (1911) is perhaps the most convenient to refer to here. They satisfy the orthogonal relations

$$\sum_{\zeta} g_{\zeta} \chi_{\zeta}^{(i)} \overline{\chi}_{\zeta}^{(j)} = g\delta_j^i, \tag{1}$$

$$g_{\zeta} \sum_{i} \chi_{\zeta}^{(i)} \overline{\chi}_{\sigma}^{(i)} = g\delta_{\sigma}^{\zeta}, \tag{2}$$

where the bar denotes the complex conjugate, and δ_j^i or δ_{σ}^{ζ} is the Kronecker delta; in view of (1) and (2) the r irreducible characters are linearly independent. Further,

$$g_{\zeta} g_{\sigma} \chi_{\zeta}^{(i)} \chi_{\sigma}^{(i)} = \chi_1^{(i)} \sum_{\tau} c_{\zeta\sigma\tau} g_{\tau} \chi_{\tau}^{(i)}, \tag{3}$$

where $c_{\zeta\sigma\tau}$ is the number of ways in which an operation of the class C_{τ} is expressible in the form $S_{\zeta}S_{\sigma}$, where S_{ζ} belongs to C_{ζ} and S_{σ} to C_{σ}.

The r irreducible representations fall into r_1 families, where $r_1 (\leqslant r)$ is the number of sets of conjugate cyclic subgroups of G. The characters of the representations which belong to any given family form a complete set of algebraic conjugates with respect to the base-field of rational numbers, and the sum of these is a compound character of G taking rational integral values for every class. These r_1 characters are linearly independent, and may be denoted for the moment by $\theta^{(j)} [j = 0, 1, \ldots, (r_1 - 1)]$, $\theta^{(0)}$ being just $\chi^{(0)}$, since Γ_0 forms a family by itself. They have the important property that any character ψ of G which takes rational values for every class is a linear combination of the characters $\theta^{(j)}$ with coefficients which are non-negative integers. The characters $\theta^{(j)}$ may be referred to as the *rationally irreducible characters* of G. When expressed in terms of the irreducible characters $\chi^{(i)}$, each rationally irreducible character $\theta^{(j)}$ is the sum of $\nu_j (\geqslant 1)$ characters $\chi^{(i)}$, which form a set of algebraic conjugates over the rational field, and each $\chi^{(i)}$ belongs to one, and only one, $\theta^{(j)}$, so that $\Sigma \nu_j = r$. In terms of the characters $\theta^{(j)}$, (1) can be rewritten in the form

$$\sum_{\zeta} g_{\zeta} \theta_{\zeta}^{(j)} \theta_{\zeta}^{(k)} = g\nu_j \delta_k^j. \tag{4}$$

If, now, ψ and ψ' be any two rational characters of G, and we put

$$\psi = \sum_{j} \lambda_j \theta^{(j)}, \quad \psi' = \sum_{j} \lambda_j' \theta^{(j)}, \tag{5}$$

we may introduce the expressions

$$[\psi, \psi'] \equiv \frac{1}{g} \sum_{\zeta} g_{\zeta} \psi_{\zeta} \psi_{\zeta}' = \sum_{j} \nu_j \lambda_j \lambda_j', \tag{6}$$

and, in particular,

$$[\psi, \psi] \equiv \frac{1}{g} \sum_{\zeta} g_{\zeta} \psi_{\zeta}^2 = \sum_{j} \nu_j \lambda_j^2. \tag{7}$$

We call $[\psi, \psi]$ the *rank* of ψ. The rank of $\theta^{(j)}$ is clearly ν_j.

Suppose, now, that H is a subgroup of G, of order h, which contains h_{ζ} elements of the class C_{ζ}. Then H determines a representation, of degree g/h, of G as a permutation group of the cosets of H in G; and the character of this representation, which may be denoted without ambiguity by the same symbol H, takes the value $h_\zeta g/g_\zeta h$ for the class C_ζ. It is certainly possible to choose r_1 subgroups

$$H^{(u)}[u = 1, 2, \dots, r_1]$$

in such a way that the corresponding characters are linearly independent, such a set, for instance, is obtained by taking one member from each of the r_1 sets of conjugate cyclic subgroups of G (though this choice would not be a convenient one in the application we contemplate). For such a set the characters satisfy relations of the form

$$H^{(u)} = \sum_j \lambda_j^{(u)} \theta^{(j)}, \tag{8}$$

where the coefficients $\lambda_j^{(u)}$ are non-negative integers, and where the determinant of these coefficients is non-zero. We then have, from (6),

$$[H^{(u)}, H^{(v)}] = \sum_j \nu_j \lambda_j^{(u)} \lambda_j^{(v)} \quad (u, v = 1, \dots, r_1), \tag{9}$$

$$r = \sum_j \nu_j. \tag{10}$$

The expressions on the left of (9) are known if the distributions of the elements of $H^{(u)}$ and $H^{(v)}$ among the conjugate sets of G are known, for, by (6),

$$[H^{(u)}, H^{(v)}] = \frac{1}{g}\sum_\zeta g_\zeta H_\zeta^{(u)} H_\zeta^{(v)} = \frac{g}{h^{(u)} h^{(v)}} \sum_\zeta \frac{h_\zeta^{(u)} h_\zeta^{(v)}}{g_\zeta}.$$

Accordingly, (9) and (10) constitute a Diophantine system of equations for the coefficients $\lambda_j^{(u)}$ and the ranks ν_j. If these equations can be solved without ambiguity, then by means of (8) we can express the characters $\theta^{(j)}$ in terms of the characters $H^{(u)}$, and hence determine the rationally irreducible characters of the group.

Now it is clear that for a given choice of subgroups $H^{(u)}$ the coefficients $\lambda_k^{(u)}$ and the ranks ν_k are determinate to within a permutation of suffixes. But it does not follow that the solution of the Diophantine system is similarly unique. It may be possible to reject a number of solutions on the ground that they fail to make the $\theta^{(j)}$ satisfy obviously necessary conditions (as, for example, that the values of $\theta_\zeta^{(j)}$ are integral, and that $\theta_1^{(j)}$ is positive and of the form $\nu_j d$, where d is a factor of g). But taking all this into account, it would appear at first sight that the project for obtaining the characters $\theta^{(j)}$ in this manner is a somewhat speculative one. Accordingly, it is a little surprising to find that the process, when applied to the particular group under discussion, goes through without any difficulty. Whether, and to what extent, this is due to particular structural features of the group is an interesting question, but one which it is pointless to attempt to answer until the method has been applied, successfully or otherwise, to a number of other groups of varying structural types.

It goes without saying that the labour involved in discussing the Diophantine system of equations may be considerably reduced by an appropriate selection of the subgroups $H^{(u)}$, and that it is desirable that most, at any rate, of the expressions $[H^{(u)}, H^{(v)}]$ should, if possible, have small numerical values. The best chance of securing this would seem to be to choose as many as possible of the subgroups $H^{(u)}$

to have comparatively large orders. This does not render nugatory the idea mentioned in the introduction of using the characters of a group to determine its larger subgroups, since if sufficient is known about a group to separate its operations into conjugate sets a certain number of large subgroups will probably be easy to determine. This, at any rate, proves to be the case in our particular example.

The separation of the rationally irreducible characters into their absolutely irreducible components presents a further problem. For this a number of resources are available, which will be understood most simply by examining their application in a special case; and accordingly we do not attempt a discussion of this problem in general terms, but explain the process in detail as applied to the particular group with which, henceforth, we shall be concerned.

2. THE GROUP G AND CERTAIN OF ITS SUBGROUPS

The particular group G whose characters will now be determined is a primitive collineation group of order $2^8.3^6.5.7$ in five dimensions, generated by 126 projections. Hamill (1951) showed that G contains 34 classes of conjugate operations, and 31 sets of conjugate cyclic subgroups, and has described in detail some of the simpler configurations formed by subsets of the 126 centres of the projections. A brief account of some of these, and explicit definitions of operations of each of the conjugate classes, has been given by the author (Todd 1950). A knowledge of the terminology of these papers will be assumed here. The sets of conjugate cyclical subgroups will be referred to by the numerals 1 to 31, the generating operations of these subgroups belonging to the types I to XXXI described in the papers just cited. Each type, with three exceptions, comprises a single set of conjugate operations, the exceptions being the generators of cyclic subgroups belonging to the sets 9, 18, 24, each of which fall into two conjugate sets. The cyclic subgroups 24 are of order 18, and if S is a generator of one of these, then S, S^7, S^{13} belong to one conjugate set, while S^5, S^{11}, S^{17} belong to the other. The two conjugate sets so obtained may be referred to as C_{24a} and C_{24b}. The squares of the operations of these sets form the two conjugate sets into which the generators of the cyclic subgroups 18 belong, and we denote these sets respectively by C_{18a}, C_{18b}; the cubes of the operations of C_{24a}, C_{24b} similarly form the sets C_{9a}, C_{9b} into which the generators of the cyclic subgroups of the set 9 divide. The notation is chosen so that, if S belongs to C_{24a}, then S^2, S^3 belong respectively to C_{18a}, C_{9a}. The remaining sets C_ζ of conjugate operations are the generators of the cyclic subgroups of the other sets ζ $(1 \leqslant \zeta \leqslant 31$, $\zeta \neq 9, 18, 24)$.

The group G contains an invariant subgroup G' of index 2, shown by Mitchell (1914) to be simply isomorphic with the linear group $HO(4, 3^2)$ (Dickson 1901). This group G' is simple. It consists of these operations of G which are expressible as the product of an even number of projections, and its operations exhaust a certain set of classes of conjugate operations of G. It will be convenient to refer to these as the *even* classes of G, and to the remaining classes as the *odd* classes.

If Γ is any representation of G, a second representation Γ^* is obtained by replacing each matrix of Γ corresponding to an operation of an odd class by its negative. Two such representations, and the characters ψ, ψ^* corresponding to them, will be said to be associated. It is evident (i) that $(\psi^*)^* = \psi$; (ii) that $\psi_\xi^* = \psi_\xi$ or $-\psi_\xi$ according as the class C_ξ is even or odd; (iii) that ψ is self-associated if, and only if, ψ_ξ is zero for every odd class; (iv) that if ψ is rational so also is ψ^*; (v) that the irreducible (or rationally irreducible) components of ψ^* are the associates of the corresponding components of ψ, and occur with the same multiplicities.

Suppose, in particular, that ψ is the character H corresponding to a representation of G as a permutation group of the cosets of a subgroup H. If H is contained in G' it is easily seen that ψ is self-associated, and conversely. In the contrary case, the intersection of H and G' is a subgroup H' of index 2 in H. The corresponding character H' is self-associated, being zero for the odd classes, and takes the value $2H_\xi$ for any even class C_ξ. Consequently, H' is the sum of the character H and its associate H^*, that is,

$$H^* = H' - H$$

is a character.

In order to obtain the rationally irreducible characters of G, our first object is to find 31 subgroups of G whose characters are linearly independent. Table 1 below[†] gives the distribution among the conjugate sets of the operations of G and 16 of its subgroups; the even classes (in the upper half of the table) being separated from the odd classes by a space. The upper half of the table alone gives 16 further subgroups, comprising G' and 15 subgroups of G' (together with the subgroup of G denoted in the table by p, which itself belongs to G'). Table 2 gives the characters of 17 corresponding permutation representations; one of these, p, is self-associated, and by changing signs in the lower half of the table we obtain 16 further characters, the associates of the 16 characters in the table other than p. Thus we have available 33 rational characters of which, it will appear, 31 are linearly independent. (The other two can be used to furnish a check on the arithmetic.) It is clear that the tentative process of § 1 can be applied to any set of rational characters, and it is more convenient to work with a pair of associates H, H^* than with a pair H, H' corresponding to a subgroup H of G and a subgroup H' of index 2 in H.

No particular point of interest arises in connexion with the construction of table 1. It will suffice here to define, in relation to the geometry of the figure, the nature of the groups which are enumerated there, the actual determination of the operations being a straightforward matter, when the discussions of the operations of G in Hamill (1951) or Todd (1950) are taken into account.

G is the whole group.

π is the subgroup, of index 126 in G, leaving fixed the centre of one of the generating projections. It is the direct product of its subgroup π' and the projection whose centre is left fixed by all the operations of π, and this subgroup π' is simply isomorphic with the known simple group of order 25920.

α_6 is the subgroup, of index 112 in G, leaving fixed an α-hexahedron. α and j_6 are subgroups of α_6, of indices 6 and 20, leaving fixed, respectively, a bounding α-prime and a plane face (and hence also the opposite plane face). These faces are j-planes. The operations of j_6 permute the six vertices of the hexahedron according to a group of order 36, the direct product of the symmetric groups of degree 3 on the sets of vertices lying in these faces, and j_6 contains a subgroup r, of index 2, which permutes the vertices in one of these faces according to the cyclic group of order 3. The subgroup r' common to r and G' is of order 729, and is a Sylow subgroup of G.

[†] The tables are printed at the end of the paper.

j_1 is a subgroup, of index 280 in G, keeping fixed a pair of polar j-planes, and j is a subgroup, of index 2 in j_1, keeping each plane of such a pair fixed. The group j_6 is a subgroup of index 4 in j.

β_6 is the subgroup, of index 567 in G, keeping fixed a β-hexahedron. β and s are subgroups of β_6, of respective indices 6 and 45. Of these, β keeps fixed a bounding β-prime of the hexahedron, while s is such that, if the vertices of the hexahedron be $B_1, B_2, \ldots, B_6$, the operations of s permute these vertices according to a group of order 16, generated by the permutations $(B_5 B_6)$, $(B_1 B_3 B_2 B_4)$, $(B_1 B_2)$. The group s, of order 256, is a Sylow subgroup of G.

π_6 is a subgroup, of index 567 in G, leaving invariant a π-hexahedron, and f is a subgroup, of index 10 in π_6, leaving invariant a pair of opposite plane faces of the hexahedron.

γ_7 is a subgroup, of index 1296 in G, leaving invariant a γ-heptahedron. It is simply isomorphic with the symmetric group of degree 7. The groups γ and p are subgroups of γ_7, γ being the symmetric subgroup of degree 6, and p the well-known simple group of order 168.

e is a subgroup, of index 2835 in G, leaving invariant an e-line.

It is now a simple matter to compute the values of the expressions $[\phi, \psi]$ defined as in (6), where each of ϕ, ψ is either one of the characters listed in table 2 or the associate of such a character. Since

$$[\phi, \psi] = [\psi, \phi] = [\phi^*, \psi^*] = [\psi^*, \phi^*]$$

and

$$[\phi, \psi^*] = [\psi^*, \phi] = [\phi^*, \psi] = [\psi, \phi^*],$$

it is sufficient to calculate, for each pair of the seventeen characters of table 2, the values of $[\phi, \psi]$ and $[\phi, \psi^*]$; so that on account of the symmetry of $[\phi, \psi]$ in the two characters only 306 values need be tabulated. The results, which appear in table 3, are to be understood as follows: if a, b is the pair of integers appearing in the table in the column corresponding to the character ϕ and in the row corresponding to the character ψ, then $[\phi, \psi] = [\phi^*, \psi^*] = a$, and $[\phi, \psi^*] = [\phi^*, \psi] = b$.

3. THE RATIONALLY IRREDUCIBLE CHARACTERS OF G

We are now in position to attempt a discussion of the Diophantine system (9) and (10), that is, to try to express the rational characters which we have at our disposal in terms of rationally irreducible ones. It will be found convenient to make two changes in the notation used in the general discussion of § 1. In the first place (as is evident from the numbers 31, 34 of rationally irreducible and absolutely irreducible independent characters), most of the rationally irreducible characters are absolutely irreducible, and to avoid a subsequent change of notation we shall use the symbol χ with a suitable affix for such a character. Secondly, it is convenient to adopt a notation which enables pairs of associated characters to be recognized, and we shall, as we have already done, use asterisks for this purpose. (This convention, incidentally, enables the size of the final character table to be almost halved). In this section, then, χ will always be used to denote an absolutely irreducible character, and θ to denote a character which is rationally, but not absolutely, irreducible.

It will be found convenient to consider the characters in turn in the order in which they occur in the rows of table 3. Evidently,

$$G = \chi^{(0)}, \quad G^* = \chi^{*(0)}. \tag{11}$$

From table 3 the character π is of rank 3, and contains $\chi^{(0)}$ but not $\chi^{*(0)}$. Hence

$$\pi = \chi^{(0)} + \psi,$$

where ψ is a rational character of rank 2. Since $[\pi, \pi^*] = 0$, ψ and ψ^* can have no common components. In the same way, we can write

$$\alpha_6 = \chi^{(0)} + \phi.$$

where ϕ is of rank 2. The relation $[\pi, \alpha_6] = 2$ now gives $[\psi, \phi] = 1$, so that ψ and ϕ have one common component, and this must be rational, since an irrational simple character belongs to one, and only one, rationally irreducible character. Accordingly, ψ and ϕ each break up into a pair of simple rational characters, one component being the same for both ψ and ϕ. So we can write

$$\pi = \chi^{(0)} + \chi^{(1)} + \chi^{(2)}, \quad \alpha_6 = \chi^{(0)} + \chi^{(1)} + \chi^{(3)}, \tag{12}$$

with similar relations connecting π^* and α^* with the associates of these characters (which are certainly distinct from $\chi^{(0)}, \ldots, \chi^{(3)}$, since

$$[\pi, \pi^*] = [\pi, \alpha_6^*] = [\alpha_6, \alpha_6^*] = 0).$$

The character j_1 is likewise of rank 3, and contains $\chi^{(0)}$ and one further character belonging to each of π and α_6, and it does not contain the associates of any of $\chi^{(0)}, \ldots, \chi^{(3)}$. Hence either $j_1 = \chi^{(0)} + \chi^{(2)} + \chi^{(3)}$, or $j_1 = \chi^{(0)} + \chi^{(1)} + \chi^{(4)}$, where $\chi^{(4)}$ is a further simple character, not self-associated since $[j_1, j_1^*] = 0$. But the former alternative, taken with (12), can be rejected, since it would lead to a negative value of $\chi_1^{(1)}$. Hence

$$j_1 = \chi^{(0)} + \chi^{(1)} + \chi^{(4)}, \tag{13}$$

and a similar relation holds for j_1^*.

It is perhaps worthy of remark that this is the only point in the whole discussion of the Diophantine system where any use is made of further conditions which the irreducible characters must satisfy. And even this can be avoided, since it is easy to see that the assumption that $j_1 = \chi^{(0)} + \chi^{(2)} + \chi^{(3)}$, together with (12), leads to an inconsistency when the character π_6 is considered.

For β_6, table 3 implies that $\beta_6 = \chi^{(0)} + \chi^{(1)} + \chi^{(3)} + \psi$, where ψ does not contain any component $\chi^{(i)}$ or $\chi^{*(i)}$ for $i \leqslant 4$, and $[\psi, \psi] = 2$, $[\psi, \psi^*] = 0$. Similarly, π_6 must have the form $\chi^{(0)} + \chi^{(1)} + \chi^{*(3)} + \phi$, where ϕ does not contain $\chi^{(i)}$ or $\chi^{*(i)}$ for $i \leqslant 4$, $[\phi, \phi] = 2$, $[\phi, \phi^*] = 0$, $[\phi, \psi] = 1$, $[\phi, \psi^*] = 0$. Hence ψ and ϕ each split up into two simple rational characters, one component being common to each. So we may write†

$$\beta_6 = \chi^{(0)} + \chi^{(1)} + \chi^{(3)} + \chi^{(5)} + \chi^{(6)}, \quad \pi_6 = \chi^{(0)} + \chi^{(1)} + \chi^{*(3)} + \chi^{(5)} + \chi^{(7)}. \tag{14}$$

---

† It is to be understood, here and henceforth, that similar relations hold for associated characters, and further, that $\chi^{(i)}$ and $\chi^{*(i)}$ are distinct. Specific attention will be drawn to any self-associated characters which arise.

As the number of characters introduced is becoming considerable, it is time to formalize our technique. We write

$$\gamma_7 = \sum_{i=0}^{7} (\lambda_i \chi^{(i)} + \lambda_i^* \chi_i^*) + \psi,$$

where ψ does not involve any of the sixteen characters already introduced. Table 3 implies that

$$\lambda_i^* = 0 \quad (i \leqslant 6), \qquad \lambda_3 + \lambda_7^* = 1,$$

and

$$\lambda_0 = 1, \quad \lambda_0 + \lambda_1 + \lambda_2 = 2, \quad \lambda_0 + \lambda_1 + \lambda_3 = 3, \quad \lambda_0 + \lambda_1 + \lambda_4 = 2,$$
$$\lambda_0 + \lambda_1 + \lambda_3 + \lambda_5 + \lambda_6 = 5, \quad \lambda_0 + \lambda_1 + \lambda_3^* + \lambda_5 + \lambda_7 = 3.$$

These equations simplify to

$$\lambda_0 = 1, \quad \lambda_1 + \lambda_2 = 1, \quad \lambda_1 + \lambda_3 = 2, \quad \lambda_1 + \lambda_4 = 1, \quad \lambda_5 + \lambda_6 = 2, \quad \lambda_1 + \lambda_5 + \lambda_7 = 2.$$

Now $\lambda_1 \leqslant \lambda_1 + \lambda_2 = 1$, $\lambda_3 \leqslant \lambda_3 + \lambda_7^* = 1$, $\lambda_1 + \lambda_3 = 2$. Hence $\lambda_1 = 1$, $\lambda_2 = 0$, $\lambda_3 = 1$, $\lambda_4 = 0$, $\lambda_7^* = 0$, and $\lambda_5 + \lambda_6 = 2$, $\lambda_5 + \lambda_7 = 1$. Hence $\lambda_5 = 0$ or 1. The former alternative would make $\lambda_6 = 2$, and $[\gamma_7, \gamma_7] > 6$. Hence $\lambda_5 = \lambda_6 = 1$, $\lambda_7 = 0$. Thus γ_7 has the form $\chi^{(0)} + \chi^{(1)} + \chi^{(3)} + \chi^{(5)} + \chi^{(6)} + \psi$, and since $[\gamma_7, \gamma_7] = 6$, $[\gamma_7, \gamma_7^*] = 0$, ψ is a simple character which is not self-associated. Hence we may write

$$\gamma_7 = \chi^{(0)} + \chi^{(1)} + \chi^{(3)} + \chi^{(5)} + \chi^{(6)} + \chi^{(8)}. \tag{15}$$

This method may be applied in succession to the characters $\alpha, j, j_6, \ldots, p$. In most cases it presents no difficulty whatever, and we shall simply list the results without comment except in a few cases where some difficulty occurs in manipulating the equations or some other new feature arises.

$$\alpha = \chi^{(0)} + \chi^{(1)} + \chi^{(2)} + \chi^{(3)} + \chi^{(6)} + \chi^{(9)}, \tag{16}$$

$$j = \chi^{(0)} + \chi^{(1)} + \chi^{(2)} + \chi^{(4)} + \chi^{(9)} + \chi^{(10)}. \tag{17}$$

In the case of j_6, the equations for λ_i and λ_i^* lead, after a little simplification, to

$$\lambda_i^* = 0 \quad (i = 0, \ldots, 6, 8, 9, 10), \qquad \lambda_3 + \lambda_7^* = 2,$$
$$\lambda_0 = 1, \quad \lambda_1 + \lambda_2 = \lambda_1 + \lambda_3 = \lambda_1 + \lambda_4 = 3, \quad \lambda_5 + \lambda_6 = 1, \quad \lambda_1 + \lambda_5 + \lambda_7 = 2,$$
$$\lambda_8 = 1, \quad \lambda_2 + \lambda_6 + \lambda_9 = \lambda_2 + \lambda_9 + \lambda_{10} = 4.$$

Since

$$\lambda_1 \leqslant \lambda_1 + \lambda_5 + \lambda_7 = 2, \quad \lambda_3 \leqslant \lambda_3 + \lambda_7^* = 2, \quad \lambda_1 + \lambda_3 = 3,$$

λ_3 must be 1 or 2. If $\lambda_3 = 2$, then

$$\lambda_1 = 1, \quad \lambda_2 = \lambda_4 = 2, \quad \lambda_6 = \lambda_7 = \lambda_{10} = 1 - \lambda_5, \quad \lambda_9 = 1 + \lambda_5, \quad \lambda_7^* = 0,$$

and

$$[j_6, j_6] \geqslant \sum_{i=0}^{10} (\lambda_i^2 + \lambda_i^{*2}) = 15 + \lambda_5^2 + 3(1 - \lambda_5)^2 + (1 + \lambda_5)^2 > 16.$$

So $\lambda_3 = 1$, and this quickly leads to

$$j_6 = \chi^{(0)} + 2\chi^{(1)} + \chi^{(2)} + \chi^{(3)} + \chi^{(4)} + \chi^{(6)} + \chi^{*(7)} + \chi^{(8)} + 2\chi^{(9)} + \chi^{(10)}. \tag{18}$$

We next get, without difficulty,

$$e = \chi^{(0)} + 2\chi^{(1)} + \chi^{(2)} + \chi^{(4)} + \chi^{(5)} + \chi^{(6)} + \chi^{(7)} + \chi^{(8)} + \chi^{*(10)} + \chi^{(11)}, \tag{19}$$

$$\beta = \chi^{(0)} + 2\chi^{(1)} + \chi^{(2)} + \chi^{(3)} + \chi^{(5)} + 3\chi^{(6)} + \chi^{(8)} + \chi^{*(10)} + \chi^{(11)} + \chi^{(12)}, \tag{20}$$

$$f = \chi^{(0)} + 2\chi^{(1)} + \chi^{*(3)} + \chi^{(4)} + 2\chi^{(5)} + \chi^{(6)} + 2\chi^{(7)} + \chi^{(8)} + \chi^{*(8)} + \chi^{(11)} + \chi^{(12)} + \chi', \tag{21}$$

where χ' is a rational simple self-associated character,

$$\gamma = \chi^{(0)} + 3\chi^{(1)} + \chi^{(2)} + 2\chi^{(3)} + 2\chi^{(5)} + 4\chi^{(6)} + \chi^{*(7)} + 3\chi^{(8)} + \chi^{(9)} + 2\chi^{(11)} + 2\chi^{(12)} + \chi' + \theta, \tag{22}$$

where θ is a character of rank 2, distinct from its associate, which is rationally irreducible. That the components of θ are not rational follows from the fact that the sum of the ranks of the 31 rationally irreducible characters is 34; if the components of θ were rational we should already have 31 independent rational *simple* characters, namely, $\chi^{(i)}$, $\chi^{*(i)}$, χ', and the components of θ and θ^*.

The character s proves rather more difficult, on account of its high rank, but with a little care the coefficients of the irreducible components can be found. The equations which involve only λ_i and λ_i^* for $i < 10$ simplify without difficulty to give

$$\lambda_0 = 1, \quad \lambda_8 = 6, \quad \lambda_0^* = \lambda_1^* = \lambda_2^* = \lambda_4^* = 0, \quad \lambda_3^* = 1, \quad \lambda_8^* = 2,$$

$$\lambda_1 + \lambda_2 = \lambda_1 + \lambda_3 = 5, \quad \lambda_1 + \lambda_4 = 6, \quad \lambda_5 + \lambda_6 = 9, \quad \lambda_1 + \lambda_5 + \lambda_7 = 12, \quad \lambda_2 + \lambda_6 + \lambda_9 = 6,$$

$$\lambda_5^* + \lambda_6^* = 1, \quad \lambda_3 + \lambda_5^* + \lambda_7^* = 3, \quad \lambda_6^* + \lambda_9^* = 1,$$

while consideration of the relations derived from $[s, j_6] - [s, j] = 17, [s, j_6^*] - [s, j^*] = 8$ yields, on simplifying by means of the relations already found, $\lambda_6 + \lambda_7^* + \lambda_9 = 6$, $\lambda_7 = 4$. From these may be deduced, in order,

$$\lambda_1 + \lambda_5 = 8, \quad \lambda_2 + \lambda_6 = 6, \quad \lambda_9 = 0, \quad \lambda_6 + \lambda_7^* = 6,$$

and so $$\lambda_3 + \lambda_5 + \lambda_5^* = (\lambda_3 + \lambda_5^* + \lambda_7^*) - (\lambda_6 + \lambda_7^*) + (\lambda_5 + \lambda_6) = 6.$$

But $\lambda_3 + \lambda_5 = (\lambda_1 + \lambda_3) + (\lambda_1 + \lambda_5) - 2\lambda_1 = 13 - 2\lambda_1$, which is odd. Hence λ_5^* is odd, and so $\lambda^* = 1$, $\lambda_6^* = 0$, and the rest is simple. We find

$$\begin{aligned} s = {} & \chi^{(0)} + 4\chi^{(1)} + \chi^{(2)} + \chi^{(3)} + \chi^{*(3)} + 2\chi^{(4)} + 4\chi^{(5)} + \chi^{*(5)} + 5\chi^{(6)} + 4\chi^{(7)} + \chi^{*(7)} \\ & + 6\chi^{(8)} + 2\chi^{*(8)} + \chi^{*(9)} + \chi^{*(10)} + 5\chi^{(11)} + 2\chi^{*(11)} + 4\chi^{(12)} + \chi^{*(12)} + 5\chi'. \end{aligned} \tag{23}$$

The part of the character r which is built up from irreducible characters already listed is easily found. The values of $[r, r]$ and $[r, r^*]$ show that the remainder consists of a character ψ of rank 4, with $[\psi, \psi^*] = 4$. The components of ψ cannot all be distinct, since otherwise there would be more than 34 independent characters; on the other hand, if they are not distinct, ψ must be of the form $2\chi''$, where χ'' is a simple character which is self-associated. So we find

$$r = \chi^{(0)} + 2\chi^{(1)} + \chi^{(2)} + \chi^{(3)} + \chi^{(4)} + \chi^{(6)} + \chi^{*(7)} + \chi^{(8)} + 2\chi^{(9)} + \chi^{(10)} + \theta + \theta^* + 2\chi''. \tag{24}$$

We have already introduced 30 rationally irreducible characters, the sum of whose ranks is 32. Thus there can remain only one further rationally irreducible character, and this must be a self-associated character θ' of rank 2. By considering the last row of table 3 it is quite easy to see that p contains θ', and that in fact

$$\begin{aligned} p = {} & \chi^{(0)} + \chi^{*(0)} + 2\chi^{(1)} + 2\chi^{*(1)} + 2\chi^{(3)} + 2\chi^{*(3)} + \chi^{(4)} + \chi^{*(4)} + 4\chi^{(5)} + 4\chi^{*(5)} \\ & + 3\chi^{(6)} + 3\chi^{*(6)} + 3\chi^{(7)} + 3\chi^{*(7)} + 6\chi^{(8)} + 6\chi^{*(8)} + 2\chi^{(9)} + 2\chi^{*(9)} \\ & + 4\chi^{(11)} + 4\chi^{*(11)} + 2\chi^{(12)} + 2\chi^{*(12)} + 8\chi' + 2\chi'' + \theta + \theta^* + 2\theta'. \end{aligned} \tag{25}$$

From (11) to (25), and the corresponding relations for the associates of the characters π, α_6, ..., s, it is a straightforward matter to express $\chi^{(i)}$, $\chi^{*(i)}$ ($i = 0, 1, \ldots, 12$), χ', χ'', θ, θ^* and θ' in terms of known characters, and hence, from table 2, to compute the rationally irreducible characters of G. The values of $\chi^{(i)}$, χ', χ'', θ, θ' are given in table 4, the remaining characters, which are the associates of $\chi^{(i)}$ and θ, are obtained by changing the signs of the values of $\chi^{(i)}$ and θ for the odd classes.

4. THE ABSOLUTELY IRREDUCIBLE CHARACTERS OF G

Of the 31 rationally irreducible characters of G, 28 are simple, while each of the remaining three, θ, θ^*, θ' is of rank 2, and must be the sum of two absolutely irreducible components. Now the rational characters have the property that their values are the same for each of the three pairs of classes ($9a$, $9b$), ($18a$, $18b$), ($24a$, $24b$). The linear independence of the characters shows that none of the components of θ, θ^* or θ' can have this property. Each of these pairs of classes, however, has the property that the inverse of an operation belonging to one class is contained in the other class of the same pair. But, in any representation of G, the values of the character for a pair of inverse operations are conjugate complex numbers. Consequently, each absolutely irreducible component of θ, θ^* or θ' takes complex values on at least one class, and the two irreducible components of each of these characters are *conjugate complex* characters. Moreover, the components of θ^* are the associates of the components of θ, while the components of θ' must be associates of each other, for the other possibility, that each is self-associated, would imply the existence of 19 independent self-associated characters of G, and this is impossible since these characters take non-zero values only for the 18 even classes. We may therefore put

$$\theta = \chi^{(13)} + \chi^{(14)}, \quad \theta^* = \chi^{*(13)} + \chi^{*(14)}, \quad \theta' = \chi^{(15)} + \chi^{*(15)}, \tag{26}$$

where asterisks, as before, indicate associated characters, and where

$$\chi^{(14)} = \bar{\chi}^{(13)}, \quad \chi^{*(14)} = \bar{\chi}^{*(13)}, \quad \chi^{*(15)} = \bar{\chi}^{(15)}. \tag{27}$$

If S is an operation belonging to one of the classes of G other than the six classes mentioned above, S^{-1} belongs to the same class as S, and so the value of every character of G for such a class is real. Hence (26) and (27) show that the values of $\chi^{(13)}$ and $\chi^{(14)}$ for any such class C_ζ are each equal to $\frac{1}{2}\theta_\zeta$, while that of $\chi^{(15)}$ is $\frac{1}{2}\theta'_\zeta$. Moreover, since $\bar{\chi}^{(15)}$ is the associate of $\chi^{(15)}$, the values of these characters are equal for each even class, so that the value of $\chi^{(15)}$ for the classes $18a$, $18b$ is half that of θ', that is, it is -1.

The characters which remain to be found may be set out in a short table as follows:

class	$\chi^{(13)}$	$\chi^{(14)}$	$\chi^{(15)}$
$18a$		$\bar{x}$	-1
$18b$	$\bar{x}$	x	-1
$9a$	y	$\bar{y}$	u
$9b$	$\bar{y}$	y	$\bar{u}$
$24a$	z	$\bar{z}$	v
$24b$	$\bar{z}$	z	$\bar{v}$

where, from (26), the known values of θ and θ' for these classes give

$$x+\bar{x} = -1, \quad y+\bar{y} = 8, \quad z+\bar{z} = -1, \quad u+\bar{u} = 0, \quad v+\bar{v} = 0. \tag{28}$$

The orthogonal relations (2) give, on simplification,

$$x\bar{x} = 7, \quad u\bar{u}+2y\bar{y} = 356, \quad v\bar{v}+2z\bar{z} = 5, \quad u\bar{v}+\bar{u}v+2(y\bar{z}+\bar{y}z) = -8. \tag{29}$$

From these it follows that x, $\bar{x}$ are the roots of the quadratic $t^2+t+7 = 0$, which are $1+3\omega$ and $1+3\omega^2$. We take

$$x = 1+3\omega, \quad \bar{x} = 1+3\omega^2, \tag{30}$$

which amounts to a definite labelling of the two conjugate complex characters $\chi^{(13)}$ and $\chi^{(14)}$.

The remaining equations are insufficient to determine y, z, u, v. Our next weapon is formula (3). While the direct calculation of all the constants $c_{\zeta\sigma\tau}$ for the group G would be formidable, it is not difficult from geometrical considerations to obtain the particular relation

$$C_2 . C_{9a} = 12C_4+9C_8+C_{13}+2C_{17}+3C_{18b}. \tag{31}$$

The argument is as follows. The operations of the class C_2 are the 126 projections. An operation S_1 of C_{9a} is the product of three projections whose centres lie in a j-plane; this j-plane contains nine of the 126 centres, and S_1 leaves a particular one, P say, of these fixed. The product of S_1 and the projection whose centre is P is an operation of C_8, the product of S_1 and the projection whose centre is one of the eight other centres in the j-plane belongs to C_4, and the products of S_1 and the projections (nine in number) whose centres lie in the polar j-plane belong to C_{13}. The remaining 108 centres of projections lie by nines in twelve S-solids through the j-plane; 36 of these centres lie in the polar prime of P, and the product of S_1 and any one of the corresponding projections belongs to C_{17}. The product of S_1 and one of the remaining 72 projections is an operation of Hamill's type XVIII. All this follows directly from the known geometry of the configuration and the definitions of the operations of various types. The only delicate point is to show that, with S_1 in C_{9a}, the operations of type XVIII which arise belong in fact to C_{18b} and not to C_{18a}, and this can be seen, for instance, by forming the matrices which give a particular operation S_1 of C_{9a} and the various operations of type XVIII which arise from it in this way, and examining the characteristic roots of these matrices. The actual work is not heavy, if use is made of the explicit definitions of these operations in Todd (1950).

By letting S_1 range over the whole class C_{9a} we obtain (31) at once, since, for instance, the 40320 operations C_4 which arise must include every one of the 3360 operations of this class 12 times. Applying (3) to $\chi^{(13)}$ we now obtain

$$126.5040.40y = 280[12.3360.10+9.560.10+1.45360.(-2)$$
$$+2.90720.1+3.120960.\bar{x}],$$

which reduces to $y = 6+4\bar{x}$. With the value of x already found, this gives

$$y = 10+12\omega^2.$$

From (28) and (29) we find that u and $\bar{u}$ are the roots of $t^2+108 = 0$, that is,

$$\pm 6i\sqrt{3} = \pm 6(\omega-\omega^2).$$

We take $$u = 6(\omega - \omega^2),$$

which amounts to a definite labelling of the characters $\chi^{(15)}$, $\chi^{*(15)}$. The relations connecting v and z then reduce to

$$v+\bar{v} = 0, \quad z+\bar{z} = -1, \quad v\bar{v}+2z\bar{z} = 5, \quad \bar{v}-v-2(\bar{z}-z) = 0,$$

of which the only solutions are $v = \omega - \omega^2$, $z = \omega$ and the conjugate $v = -\omega+\omega^2$, $z = \omega^2$.

A little consideration shows that the ambiguity here arises from the fact that no use has been made of the particular convention that associates C_{24a} with C_{9a}, C_{18a}, namely, that if S belongs to C_{24a}, S^2, S^3 belong respectively to C_{18a}, C_{9a}. [The corresponding association of C_{9a} and C_{18a} was used in obtaining (31), but this merely implies that for some operation of type XXIV, the square and cube belong respectively to C_{18a} and C_{9a}.] A further application of (3) would probably resolve the point, but the investigation of the product $C_2 . C_{24a}$ would be tiresome. An alternative method of more general application is the following.† Consider any representation of G, with character ψ, and an operation S of class $24a$. The matrix which represents S can be reduced to diagonal form, and since $S^{18} = E$, the elements of this diagonal matrix are all eighteenth roots of unity. Writing $\epsilon = \exp(2\pi i/18)$, suppose that k_r of the elements are equal to ϵ^r, for $r = 1, 2, \ldots, 18$. Then, clearly, the k's are non-negative integers, and

$$A_p \equiv \sum_{r=1}^{18} k_r \epsilon^{pr} = \psi(S^p) \quad (p = 1, 2, \ldots, 18). \tag{32}$$

We take ψ to be $\chi^{(13)}$. Since S, S^7, S^{13} belong to C_{24a}, S^5, S^{11}, S^{17} to C_{24b}, S^2, S^8, S^{14} to C_{18a}, S^4, S^{10}, S^{16} to C_{18b}, S^3 to C_{9a}, S^{15} to C_{9b}, S^6, S^{12} to C_8, S^9 to C_2 and S^{18} to C_1 we have

$$A_1 = A_7 = A_{13} = z, \quad A_5 = A_{11} = A_{17} = \bar{z}, \quad A_2 = A_8 = A_{14} = 1+3\omega,$$
$$A_4 = A_{10} = A_{16} = 1+3\omega^2, \quad A_3 = 10+12\omega^2, \quad A_{15} = 10+12\omega,$$
$$A_6 = A_{12} = 10, \quad A_9 = 40, \quad A_{18} = 280.$$

Substitution in (32) gives a set of relations between $k_1, \ldots, k_{18}$ from which, after a little manipulation, we can deduce

$$k_6+k_{15} = 32, \quad k_6-k_{15} = \tfrac{1}{3}(\omega^2 z+\omega\bar{z}+16).$$

Now z is known to be ω or ω^2, but if $z = \omega^2$ these relations do not give integral values for k_6 and k_{15}. Hence $z = \omega$, and the table of characters can be completed.

Table 4 exhibits the irreducible and rationally irreducible characters of G. To save space, only one of each pair of associated characters has been tabulated, the other can be obtained at once by changing the signs of all values for the odd classes.

Table 5 gives the irreducible characters of the simple subgroup G', which are easily deduced from those of G. For G' consists of the operations belonging to the even classes in G, and each of these classes comprises a single set of conjugate operations in G', with the exception of classes 29 and 30, each of which separates into two classes in G'. The sixteen characters $\chi^{(0)}, \dots, \chi^{(15)}$ of G which are not self-associated give rise to simple characters of G', and each of the self-associated characters χ', χ'' breaks up into a pair of conjugate complex characters of G', whose values may be determined without difficulty by the methods of the present section.

---

† Essentially the same device is used by Burnside (1911, p. 501) in the discussion of the characters of the linear fractional group.

These tables have been checked by means of the orthogonal relations. Two extra columns have been added. In column (A) we give the periods of the operations of each class. In (B), for each class for which the period is composite, we give the number of the class to which S^p belongs, for the different *prime* factors p of the period of S, arranged in ascending order.

5. SOME OBSERVATIONS ON THE CHARACTER TABLES

The existence of the character tables of G and G' opens up the possibility of further investigations into the properties of these groups. In this section attention is drawn to two problems which suggest themselves, and which seem likely to lead to results of geometrical interest.

In the first place, as has already been stated, the character tables can be used to discover subgroups of G and G', especially those of high order, which are often difficult to obtain by other methods, and which are those most likely to be of geometrical interest. The manner in which the tables can be used is explained by Littlewood (1940, chap. IX), and the underlying ideas, which are very simple, are as follows. To each subgroup H of a given group G there corresponds a rational character ψ, which must be a linear combination of the rationally irreducible characters of G. If the character ψ corresponds to a subgroup it must satisfy a number of restrictive conditions, among which are the following:

(i) ψ_1, which is the index of H in G, must be a factor of the order of g.

(ii) ψ_ξ is a non-negative integer, and $\psi_\xi g_\xi / \psi_1$ is integral, for each class C_ξ of G.

(iii) The character $\chi^{(0)}$ is a simple component of ψ.

(iv) $\psi_\xi(S^r) \geqslant \psi_\xi(S)$ for any operation S of G, for each C_ξ and all r.

These conditions are *necessary* conditions that a character ψ must satisfy in order that ψ should correspond to a representation of G as a permutation group on the cosets of a subgroup H. If a character satisfies these criteria, it is possible from the values of ψ_ξ to determine the distribution of the operations of H (if H exists) among the conjugate sets of G. To establish the effective existence of H requires, of course, further investigation in any given case, but the value of this method is that it indicates what subgroups might exist, and—more important—limits considerably the field of search.

It is hoped that later a systematic examination of the particular groups G and G' will be made along these lines. Here, in order to illustrate briefly the application of the method, and to show that it does in fact lead to results of interest, we confine ourselves to the simple problem of determining all the subgroups of G' whose index does not exceed 200, and the groups of G in which they may be contained as subgroups of index 2.

We have to consider characters ψ of G' of the form

$$\psi = \chi^{(0)} + \sum_{i=1}^{19} \lambda_i \chi^{(i)}, \tag{33}$$

with non-negative integral values of the coefficients λ_i, which satisfy the criteria (i) to (iv),[†] and which are such that $\psi_1 < 200$. Evidently we have only to consider characters $\chi^{(i)}$ ($i = 1, \ldots, 19$) for which $\chi_1^{(i)} < 200$. These are the characters $\chi^{(1)}$, $\chi^{(2)}$, $\chi^{(3)}$, $\chi^{(4)}$, $\chi^{(5)}$, $\chi^{(10)}$, whose respective degrees are 90, 35, 21, 189, 140, 35. It is not difficult to pick out those characters ψ of the form (33) such that ψ_1 is a factor of the order, $2^7 . 3^6 . 5 . 7$, of G' not exceeding 200. When these are tested by the criteria (ii) to (iv) it is found that, apart from $\chi^{(0)}$ (which clearly corresponds to G' itself), only four characters survive for consideration, namely

$$\left.\begin{aligned} \psi^{(1)} &\equiv \chi^{(0)}+\chi^{(1)}+\chi^{(3)}, & \psi_1^{(1)} &= 112;\\ \psi^{(2)} &= \chi^{(0)}+\chi^{(1)}+\chi^{(2)}, & \psi_1^{(2)} &= 126;\\ \psi^{(3)} &= \chi^{(0)}+\chi^{(1)}+\chi^{(10)}, & \psi_1^{(3)} &= 126;\\ \psi^{(4)} &= \chi^{(0)}+\chi^{(3)}+\chi^{(5)}, & \psi_1^{(4)} &= 162.\end{aligned}\right\} \qquad (34)$$

The first two characters will be recognized at once as these corresponding to the subgroups α_6' and π', the intersections of α_6 and π with G, on comparing the expressions $\psi^{(1)}$ and $\psi^{(2)}$ with those given in (12), and remembering that the irreducible characters of G which are not self-associated give rise to irreducible characters of G'. It may be pointed out, incidentally, that the table of characters of G proves quite simply that α_6 and π are the only subgroups of G whose intersection with G' is α_6' or π'. For the character corresponding to the representation of G as a permutation group on the cosets of α_6' is $\alpha_6+\alpha_6^*$, or $\chi^{(0)}+\chi^{*(0)}+\chi^{(1)}+\chi^{*(1)}+\chi^{(3)}+\chi^{*(3)}$. Any other subgroup K of G such that $(K, G') = \alpha_6'$ would correspond to a character ψ, containing $\chi^{(0)}$ as a component, and such that $\psi+\psi^* = \alpha_6+\alpha_6^*$, but the possible characters ψ of this form, other than α_6, fail to satisfy criterion (ii); for instance $\chi^{(0)}+\chi^{(1)}+\chi^{*(3)}$ takes the value -1 for the class C_{20}. A similar argument applies to π.

Consider now the character $\psi^{(3)}$. If this actually corresponds to a subgroup H' of G', this subgroup is of order 25920, and the distribution of its operations among the conjugate sets of G is the same as that of π', if the pairs of classes

$$(C_4, C_{16})\ (C_{10}, C_{17})\ (C_{18a}, C_{29a})\ (C_{18b}, C_{29b})$$

—which, in G', consist of operations of the same period—are interchanged. This information gives a hint of a possible isomorphism between H' and π'. We next consider whether H' (still tentatively assuming its existence) can be a subgroup of index 2 in a larger group H of G, and forming the common part of H and G'. The possible characters corresponding to such a group H would be

$$\chi^{(0)}+\chi^{(1)}+\chi^{(10)}, \quad \chi^{(0)}+\chi^{(1)}+\chi^{*(10)}, \quad \chi^{(0)}+\chi^{*(1)}+\chi^{(10)}, \quad \chi^{(0)}+\chi^{*(1)}+\chi^{*(10)}.$$

The last two of these give negative values for the class C_2, and the first is negative for C_{20}. But $\chi^{(0)}+\chi^{(1)}+\chi^{*(10)}$ satisfies the criteria (i) to (iv), and this justifies us in investigating the possible existence of H further. The order of H would be 51840, and the number of projections (of the class C_2) contained in it, calculated in the usual way, would be 36. These numbers, however, are highly suggestive. For 51840 is the order of the complete group of automorphisms of the 27 lines on the general cubic surface, and this group is known to admit of a representation as a collineation group in five dimensions permuting the centres of 36 generating harmonic inversions. This collineation group also belongs to the family considered by Mitchell (1914), but has also been studied by others (Room 1932; Todd 1932). In particular, in the two papers last mentioned, a set of co-ordinates of the centres of the 36 harmonic inversions is given in the form $(1, 1, 1, 1, 1, 1)$, $(1, -1, 0, 0, 0, 0)$, $(2, 2, 2, -1, -1, -1)$, where the co-ordinates may be permuted in any manner. The real form of these is at first sight discouraging, since no known set of co-ordinates of the 126 centres of projections of G has so many real points. But by a transformation of co-ordinates of the form

---

[†] Column (B) of the tables of characters will be useful in testing the criterion (iv).

$$x_i' = x_i - k(x_0 + x_1 + x_2 + x_3 + x_4 + x_5)$$

with a suitably chosen (complex) value for k, these 36 points transform into the permutations of $(1, 1, 1, 1, 1, 1)$, $(1, -1, 0, 0, 0, 0)$, $(\omega, \omega, \omega, \omega^2, \omega^2, \omega^2)$, which are a subset of the 126 centres of projections of G, the simplex of reference being an α-hexahedron. The existence of such sub-configurations among the 126 centres establishes the existence of H, and the isomorphism between H' and π', beyond question. It may be pointed out that π and H are *not* simply isomorphic, although π' and H' are; in fact π is a direct product while H is not.

Consider next the character $\psi^{(4)} = \chi^{(0)} + \chi^{(3)} + \chi^{(5)}$ of G'. If this corresponds to a subgroup, K' say, of G' then, from the values of $\psi^{(4)}$, we see that the operations of K' belong to the classes C_1, C_3, C_{11}, C_{12}, C_{14}, C_{15}, C_{30a}, C_{30b}, the number of operations in these classes being, respectively, 1, 315, 2240, 2520, 8064, 1260, 2880, 2880; and the order of K' is $20160 = \frac{1}{2} . 8!$ A moment's reflexion shows that K' is not the alternating group of degree 8 (which contains operations of period 15, while G' does not). But there is a second well-known group of order 20160 (which incidentally is simple like the alternating group of degree 8), namely the fractional linear group on three variables in the Galois field $GF(2^2)$. The operations of this group are known (Dickson 1901, p. 259) and their numbers, of various periods, agree with those suggested for K'. The temptation to identify K' with this group is strong (in spite of the probability that among the numerous unknown groups of this order there may be several others in which the operations of various periods are distributed in the same way). The search for a subconfiguration of the 126 points invariant under a group of order 20160 is complicated by the fact that, as an examination of possible characters of G makes clear, there can be no group K in G of order $2 . 20160$ such that $K' = (K . G')$, so that we cannot get a clue to the search, as we did for the group H just considered, by seeking after a particular subset of the 126 points. But in fact the existence of a subgroup of order 20160 has been recently made clear by Miss E. M. Hartley; and the very interesting geometry which lies behind it, of which it is to be hoped that an account will appear in due course, shows that this group is indeed the simple group mentioned above.

It will be observed that, of the four largest subgroups of G', two only, π' and α_6', are really obvious from the available descriptions of the configuration, and of the other two, K' was previously obtained only as the result of a fairly elaborate investigation, and H', until its existence was indicated by the table of characters, had not even been contemplated. The possibilities which a more extended investigation might reveal need no further stressing.

Another feature of interest is suggested by an examination of the tables. It will be seen that table 4 is unaltered as a whole if we interchange the pairs of classes ($9a$, $9b$), ($18a$, $18b$), ($24a$, $24b$) and at the same time interchange the pairs of characters ($\chi^{(13)}$, $\chi^{(14)}$), ($\chi^{*(13)}$, $\chi^{*(14)}$), ($\chi^{(15)}$, $\chi^{*(15)}$). This behaviour is a known feature of the table of characters of any group which possesses outer automorphisms which do not leave each class invariant.† And in fact G does possess automorphisms of this type; since the figure of the 126 points admits anticollineations which leave it invariant (for instance, in the co-ordinate system already referred to, the figure is invariant for the anticollineation $x_i' = \bar{x}_i$), and the transformation of the operations of G by such anticollineations is an outer automorphism with the required properties.

The group G' likewise possesses outer automorphisms. One, realized by the transformation of the operations of G' by one of the anticollineations just mentioned, corresponds to the invariance of table 5 under the permutations ($18a$, $18b$), ($29a$, $29b$), ($30a$, $30b$) of classes and ($\chi^{(13)}$, $\chi^{(14)}$) ($\chi^{(16)}$, $\chi^{(17)}$) ($\chi^{(18)}$, $\chi^{(19)}$) of characters; a second, realized by transforming the operations of G' by an operation of an odd class in G (and corresponding only to an inner automorphism of G), corresponds to the invariance of table 5 for the permutations ($29a$, $29b$) ($30a$, $30b$) of classes and ($\chi^{(16)}$, $\chi^{(17)}$) ($\chi^{(18)}$, $\chi^{(19)}$) of characters. But these permutations, which generate a non-cyclical group of order four, are not the only ones which leave table 5 unaltered; in fact it is not difficult to see that this table admits a group of permutations of classes and characters of order 16, generated by the two permutations just mentioned together with the permutation (4, 16) (10, 17) ($18a$, $29a$) ($18b$, $29b$) of classes and ($\chi^{(2)}$, $\chi^{(10)}$) ($\chi^{(6)}$, $\chi^{(7)}$) ($\chi^{(13)}$, $\chi^{(18)}$) ($\chi^{(14)}$, $\chi^{(19)}$) of characters. It would be very interesting to know whether a corresponding outer automorphism of G' actually exists.

I am indebted to Miss C. M. Hamill for permission to make use of the manuscript of her paper in advance of its publication.

REFERENCES

Burnside, W. 1911 *The theory of groups of finite order*, 2nd ed. Cambridge University Press.
Dickson, L. E. 1901 *Linear groups, with an exposition of the Galois field theory.* Leipzig: Teubner.
Frame, J. S. 1936 *Duke Math. J.* **2**, 477–484.
Hamill, C. M. 1951 *Proc. Lond. Math. Soc.* In the press.
Littlewood, D. E. 1935 *Proc. Lond. Math. Soc.* (2), **39**, 150–199.
Littlewood, D. E. 1940 *The theory of group characters and matrix representations of groups.* Oxford University Press.
Mitchell, H. H. 1914 *Amer. J. Math.* **36**, 1–12.
Room, T. G. 1932 *J. Lond. Math. Soc.* **7**, 147–154.
Speiser, A. 1937 *Theorie der Gruppen von endlichen Ordnung*, dritte Auflage. Berlin: Springer.
Todd, J. A. 1932 *J. Lond. Math. Soc.* **7**, 200–205.
Todd, J. A. 1950 *Proc. Camb. Phil. Soc.* **46**, 73–90.
Zia-ud-Din, M. 1935 *Proc. Lond. Math. Soc.* (2), **39**, 200–204.
Zia-ud-Din, M. 1937 *Proc. Lond. Math. Soc.* (2), **41**, 340–355.

---

† See Littlewood (1940, pp. 175, 176), where it is stated that conversely, if a table of characters presents these features then (subject to some obviously necessary restrictions) such an automorphism actually exists. This is by no means obvious, and it would be very interesting to see a proof.

TABLE 1. OPERATIONS OF G AND ITS SUBGROUPS

group class	G	π	α_6	j_1	β_6	π_6	γ_7	α	j	j_6	e	β	f	γ	s	r	p
1	1	1	1	1	1	1	1	1	1	1	1	1	1	1	1	1	1
3	2835	315	405	81	195	195	105	135	81	81	67	75	51	45	35	—	21
4	3360	480	390	120	160	—	70	210	120	66	32	80	—	40	—	66	—
8	560	80	20	74	—	—	—	20	74	20	16	—	—	—	—	20	—
10	90720	1440	810	648	480	—	210	270	648	162	224	240	—	—	—	—	—
11	40320	—	1440	144	640	640	280	360	144	144	—	—	64	40	—	144	56
12	204120	3240	7290	2916	1080	1080	630	—	—	—	216	120	216	90	56	—	42
13	45360	720	1620	810	—	—	—	540	810	324	16	—	—	—	—	—	—
14	653184	5184	11664	—	2304	2304	504	1944	—	—	—	384	—	144	—	—	—
15	34020	540	—	486	180	180	—	—	486	—	84	60	36	—	20	—	—
16	3360	240	390	120	—	160	—	30	120	66	32	—	16	—	—	66	—
17	90720	3600	810	648	—	480	—	270	648	162	224	—	48	—	—	—	—
18*a*	120960	2880	1080	432	—	—	—	540	432	108	—	—	—	—	—	108	—
18*b*	120960	2880	1080	432	—	—	—	540	432	108	—	—	—	—	—	108	—
28	272160	4320	—	972	—	—	—	—	972	—	96	—	—	—	—	—	—
29	241920	—	2160	864	—	—	—	—	864	216	—	—	—	—	—	216	—
30	933120	—	—	—	—	—	720	—	—	—	—	—	—	—	—	—	48
31	408240	—	—	2916	720	720	—	—	—	—	144	—	144	—	16	—	—
2	126	46	45	18	30	6	21	30	18	18	14	20	6	15	6	9	—
5	5670	270	405	324	150	190	105	—	—	—	102	60	46	15	30	—	—
6	60480	1920	3780	864	960	—	420	900	864	540	64	160	—	120	—	270	—
7	68040	3240	2430	—	840	360	210	810	—	—	168	320	72	90	40	—	—
9*a*	5040	400	180	234	—	—	—	120	234	72	16	—	—	—	—	36	—
9*b*	5040	400	180	234	—	—	—	120	234	72	16	—	—	—	—	36	—
19	30240	1680	270	432	—	480	—	180	432	108	160	—	48	—	—	54	—
20	544320	—	4860	—	960	—	420	1620	—	—	192	160	—	—	—	—	—
21	653184	5184	—	—	—	2304	504	—	—	—	—	—	—	—	—	—	—
22	362880	—	6480	1296	1920	640	840	—	—	—	—	—	64	120	—	—	—
23	90720	2160	4050	1296	—	160	—	—	—	—	96	—	16	—	—	—	—
24*a*	362880	2880	3240	1296	—	—	—	540	1296	324	—	—	—	—	—	162	—
24*b*	362880	2880	3240	1296	—	—	—	540	1296	324	—	—	—	—	—	162	—
25	408240	—	—	2916	720	720	—	—	—	—	144	240	144	—	16	—	—
26	34020	540	—	486	180	900	—	—	486	—	84	—	180	—	36	—	—
27	272160	4320	—	972	—	—	—	—	972	—	96	—	—	—	—	—	—
order	6531840	51840	58320	23328	11520	11520	5040	9720	11664	2916	2304	1920	1152	720	256	1458	168

TABLE 2. CHARACTERS OF PERMUTATION REPRESENTATIONS OF G

character class	G	π	α_6	j_1	β_6	π_6	γ_7	α	j	j_6	e	β	f	γ	s	r	p	g/g_ζ
1	1	126	112	280	567	567	1296	672	560	2240	2835	3402	5670	9072	25515	4480	38880	6531840
3	1	14	16	8	39	39	48	32	16	64	67	90	102	144	315	0	288	2304
4	1	18	13	10	27	0	27	42	20	44	27	81	0	108	0	88	0	1944
8	1	18	4	37	0	0	0	24	74	80	81	0	0	0	0	160	0	11664
10	1	2	1	2	3	0	3	2	4	4	7	9	0	0	0	0	0	72
11	1	0	4	1	9	9	9	6	2	8	0	0	9	9	0	16	54	162
12	1	2	4	4	3	3	4	0	0	0	3	2	6	4	7	0	8	32
13	1	2	4	5	0	0	0	8	10	16	1	0	0	0	0	0	0	144
14	1	1	2	0	2	2	1	2	0	0	0	2	0	2	0	0	0	10
15	1	2	0	4	3	3	0	0	8	0	7	6	6	0	15	0	0	192
16	1	9	13	10	0	27	0	6	20	44	27	0	27	0	0	88	0	1944
17	1	5	1	2	0	3	0	2	4	4	7	0	3	0	0	0	0	72
18*a*	1	3	1	1	0	0	0	3	2	2	0	0	0	0	0	4	0	54
18*b*	1	3	1	1	0	0	0	3	2	2	0	0	0	0	0	4	0	54
28	1	2	0	1	0	0	0	0	2	0	1	0	0	0	0	0	0	24
29	1	0	1	1	0	0	0	0	2	2	0	0	0	0	0	4	0	27
30	1	0	0	0	0	0	1	0	0	0	0	0	0	0	0	0	2	7
31	1	0	0	2	1	1	0	0	0	0	1	0	2	0	1	0	0	16
2	1	46	40	40	135	27	216	160	80	320	315	540	270	1080	1215	320	0	51840
5	1	6	8	16	15	19	24	0	0	0	51	36	46	24	135	0	0	1152
6	1	4	7	4	9	0	9	10	8	20	3	9	0	18	0	20	0	108
7	1	6	4	0	7	3	4	8	0	0	7	16	6	12	15	0	0	96
9*a*	1	10	4	13	0	0	0	16	26	32	9	0	0	0	0	32	0	1296
9*b*	1	10	4	13	0	0	0	16	26	32	9	0	0	0	0	32	0	1296
19	1	7	1	4	0	9	0	4	8	8	15	0	9	0	0	8	0	216
20	1	0	1	0	1	0	1	2	0	0	1	1	0	0	0	0	0	12
21	1	1	0	0	0	2	1	0	0	0	0	0	0	0	0	0	0	10
22	1	0	2	1	3	1	3	0	0	0	0	0	1	3	0	0	0	18
23	1	3	5	4	0	1	0	0	0	0	3	0	1	0	0	0	0	72
24*a*	1	1	1	1	0	0	0	1	2	2	0	0	0	0	0	2	0	18
24*b*	1	1	1	1	0	0	0	1	2	2	0	0	0	0	0	2	0	18
25	1	0	0	2	1	1	0	0	0	0	1	2	2	0	1	0	0	16
26	1	2	0	4	3	15	0	0	8	0	7	0	30	0	27	0	0	192
27	1	2	0	1	0	0	0	0	2	0	1	0	0	0	0	0	0	24

TABLE 3

G	1, 0																
π	1, 0	3, 0															
α_6	1, 0	2, 0	3, 0														
j_1	1, 0	2, 0	2, 0	3, 0													
β_6	1, 0	2, 0	3, 0	2, 0	5, 0												
π_6	1, 0	2, 0	2, 1	2, 0	3, 1	5, 0											
γ_7	1, 0	2, 0	3, 0	2, 0	5, 0	3, 1	6, 0										
α	1, 0	3, 0	3, 0	2, 0	4, 0	2, 1	4, 0	6, 0									
j	1, 0	3, 0	2, 0	3, 0	2, 0	2, 0	2, 0	4, 0	6, 0								
j_6	1, 0	4, 0	4, 0	4, 0	5, 0	3, 2	6, 0	8, 0	8, 0	16, 0							
e	1, 0	4, 0	3, 0	4, 0	5, 0	5, 0	6, 0	5, 0	5, 1	9, 2	13, 0						
β	1, 0	4, 0	4, 0	3, 0	8, 0	4, 1	9 ,0	8, 0	4, 1	11, 1	13, 0	21, 0					
f	1, 0	3, 0	3, 1	4, 0	6, 1	8, 0	7, 2	4, 1	4, 0	8, 4	13, 1	13, 2	21, 3				
γ	1, 0	5, 0	6, 0	4, 0	12, 0	6, 3	15, 0	12, 0	6, 0	20, 0	19, 1	31, 0	23, 8	57, 1			
s	1, 0	6, 0	6, 1	7, 0	15, 2	14, 3	21, 4	12, 2	8, 2	25, 10	37, 6	46, 7	55, 21	86, 26	196, 95		
r	1, 0	4, 0	4, 0	4, 0	5, 0	3, 2	6, 0	8, 0	8, 0	16, 0	9, 2	11, 1	8, 4	22, 2	25, 10	24, 8	
p	1, 1	3, 3	5, 5	4, 4	12, 12	12, 12	18, 18	10, 10	6, 6	24, 24	26, 26	32, 32	51, 51	76, 76	193, 193	32, 32	288, 288
	G	π	α_6	j_1	β_6	π_6	γ_7	α	j	j_6	e	β	f	γ	s	r	p

TABLE 5. THE IRREDUCIBLE AND RATIONALLY IRREDUCIBLE CHARACTERS OF G'

class	$\chi^{(0)}$	$\chi^{(1)}$	$\chi^{(2)}$	$\chi^{(3)}$	$\chi^{(4)}$	$\chi^{(5)}$	$\chi^{(6)}$	$\chi^{(7)}$	$\chi^{(8)}$	$\chi^{(9)}$	$\chi^{(10)}$	$\chi^{(11)}$	$\chi^{(12)}$	$\chi^{(13)}$	$\chi^{(14)}$	$\chi^{(15)}$	$\chi^{(16)}$	$\chi^{(17)}$	$\chi^{(18)}$	$\chi^{(19)}$	θ	ϕ'	ϕ''	(A)	(B)
1	1	90	35	21	189	140	315	315	729	210	35	896	420	280	280	560	640	640	280	280	560	1280	560	1	
3	1	10	3	5	−3	12	11	11	9	2	3	0	4	−8	−8	−16	0	0	−8	−8	−16	0	−16	2	
4	1	9	8	3	0	−4	18	−9	0	3	−1	−4	6	10	10	2	−8	−8	1	1	20	−16	2	3	
8	1	9	8	−6	27	5	−9	−9	0	21	8	32	−39	10	10	−34	−8	−8	10	10	20	−16	20	3	
10	1	1	0	−1	0	0	2	−1	0	−1	3	0	−2	−2	−2	2	0	0	1	1	−4	0	2	6	4, 3
11	1	0	−1	3	0	5	0	0	0	3	−1	−4	−3	1	1	2	1	1	1	1	2	2	2	3	
12	1	2	−1	1	1	0	−1	−1	1	−2	−1	0	0	0	0	0	0	0	0	0	0	0	0	4	3
13	1	1	0	2	3	−3	−1	−1	0	5	0	0	1	−2	−2	2	0	0	−2	−2	−4	0	−4	6	8, 3
14	1	0	0	1	−1	0	0	0	−1	0	0	1	0	0	0	0	0	0	0	0	0	0	0	5	
15	1	−2	3	1	5	4	−1	−1	−3	−2	3	0	4	0	0	0	0	0	0	0	0	0	0	4	3
16	1	9	−1	3	0	−4	−9	18	0	3	8	−4	6	1	1	2	−8	−8	10	10	2	−16	20	3	
17	1	1	3	−1	0	0	−1	2	0	−1	0	0	−2	1	1	2	0	0	−2	−2	2	0	−4	6	16, 3
18a	1	0	2	0	0	−1	0	0	0	0	−1	−1	0	$1+3\omega$	$1+3\omega^2$	−1	1	1	1	1	−1	2	2	9	8
18b	1	0	2	0	0	−1	0	0	0	0	−1	−1	0	$1+3\omega^2$	$1+3\omega$	−1	1	1	1	1	−1	2	2	9	8
28	1	1	0	−2	−1	1	−1	−1	0	1	0	0	1	0	0	0	0	0	0	0	0	0	0	12	13, 15
29a	1	0	−1	0	0	−1	0	0	0	0	2	−1	0	1	1	−1	1	1	$1+3\omega$	$1+3\omega^2$	2	2	−1	9	8
29b	1	0	−1	0	0	−1	0	0	0	0	2	−1	0	1	1	−1	1	1	$1+3\omega^2$	$1+3\omega$	2	2	−1	9	8
30a	1	−1	0	0	0	0	0	0	1	0	0	0	0	0	0	0	$\frac{1}{2}(-1+i\sqrt{7})$	$\frac{1}{2}(-1-i\sqrt{7})$	0	0	0	−1	0	7	
30b	1	−1	0	0	0	0	0	0	1	0	0	0	0	0	0	0	$\frac{1}{2}(-1-i\sqrt{7})$	$\frac{1}{2}(-1+i\sqrt{7})$	0	0	0	−1	0	7	
31	1	0	−1	−1	1	0	1	1	−1	0	−1	0	0	0	0	0	0	0	0	0	0	0	0	8	15

The irreducible characters are $\chi^{(0)}, \ldots, \chi^{(19)}$. The rationally irreducible characters are $\chi^{(0)}, \ldots, \chi^{(12)}, \chi^{(15)}, \theta, \phi', \phi''$, where

$$\theta=\chi^{(13)}+\chi^{(14)}, \quad \phi'=\chi^{(16)}+\chi^{(17)}, \quad \phi''=\chi^{(18)}+\chi^{(19)}.$$

For an explanation of columns (A) and (B) refer to the text.

TABLE 4. THE IRREDUCIBLE AND RATIONALLY IRREDUCIBLE CHARACTERS OF G

class	$\chi^{(0)}$	$\chi^{(1)}$	$\chi^{(2)}$	$\chi^{(3)}$	$\chi^{(4)}$	$\chi^{(5)}$	$\chi^{(6)}$	$\chi^{(7)}$	$\chi^{(8)}$	$\chi^{(9)}$	$\chi^{(10)}$	$\chi^{(11)}$	$\chi^{(12)}$	$\chi^{(13)}$	$\chi^{(14)}$	$\chi^{(15)}$	χ'	χ''	θ	θ'	(A)	(B)
1	1	90	35	21	189	140	315	315	729	210	35	896	420	280	280	560	1280	560	560	1120	1	
3	1	10	3	5	−3	12	11	11	9	2	3	0	4	−8	−8	−16	0	−16	−16	−32	2	
4	1	9	8	3	0	−4	18	−9	0	3	−1	−4	6	10	10	2	−16	2	20	4	3	
8	1	9	8	−6	27	5	−9	−9	0	21	8	32	−39	10	10	−34	−16	20	20	−68	3	
10	1	1	0	−1	0	0	2	−1	0	−1	3	0	−2	−2	−2	2	0	2	−4	4	6	4, 3
11	1	0	−1	3	0	5	0	0	0	3	−1	−4	−3	1	1	2	2	2	2	4	3	
12	1	2	−1	1	1	0	−1	−1	1	−2	−1	0	0	0	0	0	0	0	0	0	4	3
13	1	1	0	2	3	−3	−1	−1	0	5	0	0	1	−2	−2	2	0	−4	−4	4	6	8, 3
14	1	0	0	1	−1	0	0	0	−1	0	0	1	0	0	0	0	0	0	0	0	5	
15	1	−2	3	1	5	4	−1	−1	−3	−2	3	0	4	0	0	0	0	0	0	0	4	3
16	1	9	−1	3	0	−4	−9	18	0	3	8	−4	6	1	1	2	−16	20	2	4	3	
17	1	1	3	−1	0	0	−1	2	0	−1	0	0	−2	1	1	2	0	−4	2	4	6	16, 3
18*a*	1	0	2	0	0	−1	0	0	0	0	−1	−1	0	$1+3\omega$	$1+3\omega^2$	−1	2	2	−1	−2	9	8
18*b*	1	0	2	0	0	−1	0	0	0	0	−1	−1	0	$1+3\omega^2$	$1+3\omega$	−1	2	2	−1	−2	9	8
28	1	1	0	−2	−1	1	−1	−1	0	1	0	0	1	0	0	0	0	0	0	0	12	13, 15
29	1	0	−1	0	0	−1	0	0	0	0	2	−1	0	1	1	−1	2	−1	2	−2	9	8
30	1	−1	0	0	0	0	0	0	1	0	0	0	0	0	0	0	−1	0	0	0	7	
31	1	0	−1	−1	1	0	1	1	−1	0	−1	0	0	0	0	0	0	0	0	0	8	15
2	1	30	15	9	9	20	75	−15	81	30	−5	64	60	40	40	0	0	0	80	0	2	
5	1	6	−1	1	9	4	3	9	9	−10	−5	0	−4	−8	−8	0	0	0	−16	0	2	
6	1	3	0	3	0	2	0	−3	0	3	1	−2	0	−2	−2	0	0	0	−4	0	6	4, 2
7	1	2	3	1	−3	0	3	1	−3	−2	−1	0	0	0	0	0	0	0	0	0	4	3
9*a*	1	3	6	0	9	−7	3	3	0	3	4	−8	−3	$10+12\omega^2$	$10+12\omega$	$6(\omega-\omega^2)$	0	0	8	0	6	8, 2
9*b*	1	3	6	0	9	−7	3	3	0	3	4	−8	−3	$10+12\omega$	$10+12\omega^2$	$-6(\omega-\omega^2)$	0	0	8	0	6	8, 2
19	1	3	3	−3	0	2	−3	0	0	3	−2	4	−6	1	1	0	0	0	2	0	6	16, 2
20	1	−1	0	1	0	0	0	1	0	1	−1	0	0	0	0	0	0	0	0	0	12	10, 7
21	1	0	0	−1	−1	0	0	0	1	0	0	−1	0	0	0	0	0	0	0	0	10	14, 2
22	1	0	−1	1	0	1	0	0	0	−1	1	0	−1	1	1	0	0	0	2	0	6	11, 5
23	1	3	−1	1	0	−2	−3	0	0	−1	−2	0	2	1	1	0	0	0	2	0	6	16, 5
24*a*	1	0	0	0	0	−1	0	0	0	0	1	1	0	ω	ω^2	$(\omega-\omega^2)$	0	0	−1	0	18	18*a*, 9*a*
24*b*	1	0	0	0	0	−1	0	0	0	0	1	1	0	ω^2	ω	$-(\omega-\omega^2)$	0	0	−1	0	18	18*b*, 9*b*
25	1	0	−1	−1	1	0	1	−1	−1	0	−1	0	0	0	0	0	0	0	0	0	8	15
26	1	2	−1	−3	1	4	−1	5	−3	2	3	0	4	0	0	0	0	0	0	0	4	3
27	1	−1	2	0	1	1	−1	−1	0	−1	0	0	1	0	0	0	0	0	0	0	12	13, 26

The associates of $\chi^{(i)}$ and θ are obtained by changing signs in the lower half of the table.

The 34 irreducible characters are $\chi^{(i)}$, $\chi^{*(i)}$ ($i=0, 1, \ldots, 15$), χ', χ''. The 31 rationally irreducible characters are $\chi^{(i)}$, $\chi^{*(i)}$ ($i=0, 1, \ldots, 12$), χ', χ'', θ, θ^* and θ'. The last three of these are of rank 2 expressible in terms of absolutely irreducible components in the forms

$$\theta=\chi^{(13)}+\chi^{(14)}, \quad \theta^*=\chi^{*(13)}+\chi^{*(14)}, \quad \theta'=\chi^{(15)}+\chi^{*(15)}.$$

For the explanations of columns (A) and (B) see the last paragraph of §4.

Studies in copolymerization

I. The evaluation of the kinetic coefficients for the copolymerization of styrene and methyl methacrylate

By H. W. Melville, F.R.S. and L. Valentine
Chemistry Department, University of Birmingham

(*Received* 1 *September* 1949)

The benzoyl peroxide photosensitized copolymerization of styrene and methyl methacrylate has been studied with the object of determining all the rate coefficients. The variation of rate of copolymerization with monomer composition has been determined under standard conditions, the reaction being followed dilatometrically. The rate of initiation has also been studied as a function of monomer composition; it was found that the introduction of small quantities of styrene markedly lowered the rate of initiation. From a combination of these two studies, the absolute velocity coefficients for all the various steps have been measured. For the reaction at 30° C, it was found that the rate coefficient for the termination of two unlike radicals ($k_{tab} = 2{\cdot}06 \times 10^8$) was much greater than those for the termination of two styrene radicals ($k_{taa} = 8 \times 10^6$) or of two methyl methacrylate radicals ($k_{tbb} = 2{\cdot}7 \times 10^7$). Finally, some data are presented on the osmotic behaviour of copolymers of styrene and methyl methacrylate in benzene solution.

INTRODUCTION

In recent years knowledge of the mechanism of addition polymerization reactions has advanced considerably. Two of the fields which have attracted most attention latterly are the determination of the absolute velocity constants for the unit reactions of polymerization and the partial elucidation of the mechanism of copolymerization reactions. At present there is available a number of techniques for the evaluation of the velocity constants of polymerization reactions, and progress is such that totally different methods yield comparable values for the kinetic constants (see *inter alia*, Bamford & Dewar 1948; Burnett & Melville 1947; Melville & Valentine 1949).

Considerable progress has also been made towards an understanding of the basic principles underlying the mechanism of copolymerization reactions. From the quantitative aspect, it is now possible to predict the composition of a copolymer from the composition of monomer mixture from which it is derived, in terms of two constants which are characteristic of the monomer pair being studied. These constants, the monomer reactivity ratios, can also be utilized to provide a wealth of information as to the reactivity of one monomer for a variety of polymer-free radicals. As a result, knowledge of the correlation between chemical structure and reactivity, in a series of systems which had hitherto been inaccessible to experimental study, has been greatly advanced.

Although the study of copolymer compositions has yielded important results about the relative reactivity of radicals, the problem of the *kinetics* of the copolymerization has received very little attention. It is possible to treat the problem theoretically by the methods that have been evolved for dealing with a single monomer (Melville, Noble & Watson 1947). In this treatment there appear two factors relating to the initiation of polymerization, four coefficients relating to the attack of two kinds of radicals with two different types of monomer. If termination of polymer growth occurs by the interaction of radicals there will be two coefficients for each of the pairs of radicals and a third coefficient for the interaction of unlike radicals. The determination of the nine coefficients can, in principle, be done in the following manner. For each monomer polymerized separately, three coefficients may be determined by the now-standard techniques. The composition of the polymer yields the two pairs of ratios of growth coefficients. These, together with the monomer data, give the absolute values of the four growth coefficients. According to the theory of copolymerization, a determination of the *rate* of copolymerization will enable the calculation of the crossed termination coefficient to be made. Thus all nine coefficients can be evaluated so that for a single pair of monomers, a great variety of information about the reactivity of radicals can be obtained. The theory assumes that there are no complications, for example, in the initiation process, that transfer is absent and that any other abnormality, due to the use of two monomers, does not intrude. The object of the present work is primarily to determine all the coefficients concerned and especially to obtain information about the interaction of dissimilar radicals, since sufficient data have now been accumulated to show that polymer radical-radical interactions appear to be quite highly specific even though a very small amount of energy of activation is needed in these reactions. For example, for butyl acrylate the termination in litre mole^{-1} sec.$^{-1}$ is $1{\cdot}8 \times 10^4$, for styrene $7{\cdot}9 \times 10^6$, for methyl methacrylate $2{\cdot}7 \times 10^7$, and for vinyl acetate $5{\cdot}0 \times 10^8$. In addition, it is necessary to look for any abnormalities of the sort mentioned above, so that a reasonably sound theory of copolymerization kinetics may be established and ultimately applied to the very much more difficult conditions obtained in homogeneous systems when the reaction approaches completion, in those cases where polymerization occurs in a heterogeneous system, as in emulsions, and finally to those systems in which one of the components does not itself polymerize.

In the present paper, the experimental techniques and the actual measurements leading to the calculation of the rate coefficients are given. In part II, the validity of the treatment and a full discussion of the theoretical implications are presented, together with some calculations on other copolymer systems.

THE KINETICS OF COPOLYMERIZATION

In the kinetic analysis (Melville *et al.* 1947), various assumptions regarding the termination mechanism had to be made. In order to illustrate the kinetic treatment employed, the case of first-order initiation and mutual termination will be treated briefly, as this is the most important case practically. It is assumed that termination occurs by disproportionation and not by combination, but this does not affect the expressions for the overall rate of polymerization but only those concerned with the degree of polymerization. The general scheme of the reaction is then as follows:

Initiation

$$\left.\begin{aligned} A &\rightarrow P_1 \qquad \text{Rate} = X_a = k_a(A), \\ B &\rightarrow Q_1 \qquad \text{Rate} = X_b = k_b(B), \end{aligned}\right\} \tag{1}$$

where P_1, Q_1, represent activated monomer molecules of A and B respectively.

Propagation

$$\left.\begin{aligned} P_r + A &= P_{r+1} && \text{Rate} = k_{praa}(P_r)(A),\\ P_r + B &= Q_{r+1} && \text{Rate} = k_{prab}(P_r)(B),\\ Q_r + A &= P_{r+1} && \text{Rate} = k_{prba}(Q_r)(A),\\ Q_r + B &= Q_{r+1} && \text{Rate} = k_{prbb}(Q_r)(B).\end{aligned}\right\} \tag{2}$$

Termination

$$\left.\begin{aligned} P_r + P_s &= A_r + A_s && \text{Rate} = k_{trsaa}(P_r)(P_s),\\ P_r + Q_s &= A_r + B_s && \text{Rate} = k_{trsab}(P_r)(Q_s),\\ Q_r + Q_s &= B_r + B_s && \text{Rate} = k_{trsbb}(Q_r)(Q_s),\end{aligned}\right\} \tag{3}$$

where P_r, Q_r are radicals of chain length r and of A and B type respectively. A_r, B_r are stable ('dead') P_r and Q_r polymers respectively.

The subscripts are largely self-explanatory; e.g. k_{praa} denotes the velocity constant for the attack of a radical of chain length r and of type A (P) on a monomer molecule of type A.

In order to simplify the subsequent mathematics, certain assumptions have to be made for the termination mechanism. The simpler is to split the rate constant into two parts, as in equation (4), viz.

$$k_{trsaa} = k_{tra}\,k_{tsa}, \tag{4a}$$

$$k_{trsab} = k_{tra}\,k_{tsb}, \tag{4b}$$

$$k_{trsbb} = k_{trb}\,k_{tsb}. \tag{4c}$$

The assumptions implicit in (4*a*) and (4*b*) are similar to the normal assumptions for one-component systems (Gee & Melville 1944). Equation (4*b*), however, implies that the termination capacity depends only on the radical concerned, and is independent of the radical type with which it reacts. This can be checked only by experiment for each particular case and may well be a gross over-simplification. A more general assumption is that

$$k_{trsab} = k_{trab}\,k_{tsab}, \tag{5}$$

which is analogous to that used for a single monomer system. This leads to much more complicated expressions for the rate of polymerization. In this case, it is convenient to define a new constant:

$$\phi = \frac{k_{trab}\,k_{tsab}}{k_{tra}\,k_{tsb}}. \tag{6}$$

This gives a measure of the extent to which termination between two unlike radicals is preferred. Obviously if $\phi = 1$, then equation (6) reduces to the simple assumption of (4). A value of ϕ greater than unity indicates preferential reaction between unlike radicals, while a value of $\phi < 1$ means that most radicals will be terminated in collisions with their own kind.

Applying the usual stationary state assumptions to equations (1) to (6), and expressing concentrations in terms of mole fractions, then the values for the overall rate expressions shown in table 1 are obtained. From an inspection of these results it is obvious that if termination proceeds according to assumption (4), then the rate of copolymerization can be predicted from the rate constants for the individual monomers and the monomer reactivity ratios, σ and μ. If termination is by (6), however, then the ϕ termination constant must be determined for each system. If the reactivity ratios σ and μ, the ratios δ_a, δ_b and the rate of initiation (X_a+X_b) are all known, then the value of ϕ can be found from the rate. The most reliable procedure is to find the variation of the rates of polymerization and initiation with monomer composition, and from these curves calculate the value of ϕ; in this manner a preliminary averaging of the points is attained before ϕ is calculated. This is the procedure which was used in this investigation.

TABLE 1. EXPRESSIONS FOR THE INITIAL OVERALL RATE OF REACTION

termination	$-d((A)+(B))/dt$
mutual by (4)	$\dfrac{1}{\delta_b}\dfrac{\left\{1+\dfrac{2(1-\mu)}{\mu}(A)+\dfrac{\sigma+\mu-2}{\mu}(A)^2\right\}(X_a+X_b)^{\frac{1}{2}}}{1+\left(\dfrac{\sigma}{\mu}\delta_s-1\right)(A)}$
mutual by (5)	$\dfrac{1}{\delta_b}\dfrac{\left\{1+\dfrac{2(1-\mu)}{\mu}(A)+\dfrac{\sigma+\mu-2}{\mu}(A)^2\right\}(X_a+X_b)^{\frac{1}{2}}}{\left\{1+2\left(\phi\dfrac{\sigma}{\mu}\delta_s-1\right)(A)+\left(\dfrac{\sigma^2}{\mu^2}\delta_s^2-2\phi\dfrac{\sigma}{\mu}\delta_s+1\right)(A)^2\right\}^{\frac{1}{2}}}$

where $\sigma = \dfrac{k_{praa}}{k_{prab}}$, $\mu = \dfrac{k_{prbb}}{k_{prba}}$, $\delta_a = \dfrac{k^{\frac{1}{2}}_{trsaa}}{k_{praa}}$, $\delta_b = \dfrac{k^{\frac{1}{2}}_{trsbb}}{k_{prbb}}$, $\delta_s = \delta_a/\delta_b$.

EXPERIMENTAL

As in previous experiments, silica reaction tubes of the usual type (vol. = 3·5 cm.^{3}, diameter = 1 cm.) were employed and these were filled with the two monomers *in vacuo*. The two monomers were purified by washing and distillation as described below, and then introduced into reservoirs on the main vacuum line. The styrene was introduced directly into a graduated reservoir and then degassed, but the methyl methacrylate was first degassed and then distilled into a graduated tube which was then sealed off from the remaining monomer. These reservoirs were constructed of burette tubing, so that the volume could be read to 0·01 ml. When filling the tubes, the monomer reservoir was surrounded by a large beaker of water to maintain a constant temperature and the required amount distilled in. The other monomer was then introduced in the same manner and the volumes distilled read from the graduated tubes.

In order to convert these volumes to actual weights of monomers, the densities at the temperature of distillation have to be known accurately.

For methyl methacrylate the data of Schulz & Harborth (1947) were used, and for styrene those of the Dow Chemical Company (1946).

Previous to the filling, the calculated amount of benzoyl peroxide was introduced. This was made up in an Analar benzene solution, the requisite amount introduced from a graduated pipette and the benzene removed at low pressure. A concentration of 4·5 to 5·0 × 10^{-2} mole/l. gave satisfactory results with the experimental set-up used, so this concentration was adopted as standard. After filling, the tubes were sealed off *in vacuo* and stored over solid carbon dioxide until required.

The optical arrangement was as described previously (Melville & Valentine 1949), a silica lens being used to focus the light of a G.E.C. 'Osira' 125 W mercury vapour lamp on the reaction vessel. In order to reduce the absorption due to the monomer, various glass filters, with transmission limits at 2940 and 3150 Å, were used; the transmission of these filters is given in figure 1. The contraction of the monomer was followed with a travelling microscope reading to 0·01 mm.

Molecular weight determinations were made in a dynamic osmometer of the type described by Masson & Melville (1949). The experimental techniques of these authors were employed, as modified by Grassie & Melville (1949) for the determination of the concentration. The copolymer samples were prepared under conditions analogous to those prevailing in the rate determinations (temp. = 30° C, catalyst concentration = 5 × 10^{-2} mole/l., light of wave-length > 3150 Å).

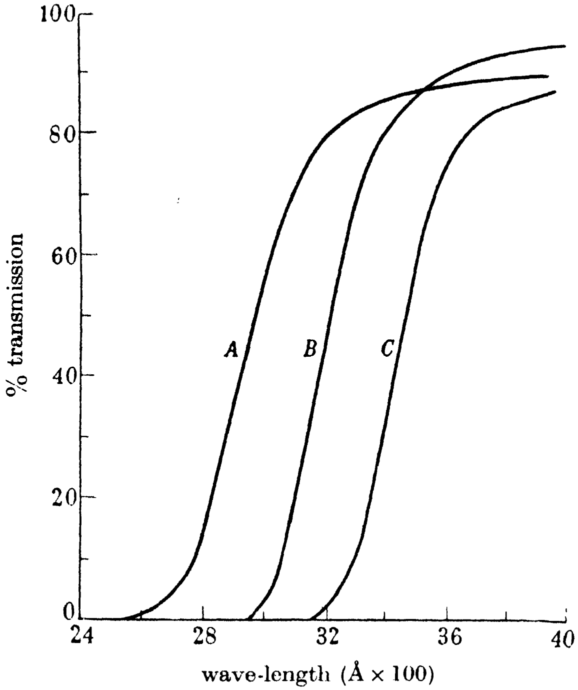

FIGURE 1. The transmission of the glass filters used. *A*, Corex D 970 (2 mm.); *B*, Pyrex glass; *C*, window glass (4 mm.).

In general, the samples were not polymerized to more than about 10 to 15 %, so that both the overall rate and the composition of the copolymer remained constant. After the desired amount of polymer had been formed, the reaction tubes were quickly opened and the contents diluted to about 15 ml. with benzene. This solution was then poured into a large excess of methanol at −10° C. This served the dual purpose of arresting the polymerization instantaneously and also converting the polymer into a form more suitable for later treatment. The polymers prepared in this way were more easily soluble than those prepared by normal methods of isolation. These samples were then filtered through a sintered glass crucible, washed with methanol and dried to constant weight in a vacuum desiccator.

Solutions of polymer in redistilled benzene were made up to a strength of about 0·7 to 1·1 g./100 g. and filtered through sintered glass before use. The osmotic pressure of these solutions was determined in the usual way, the temperature being 24·6° C, with the type of dynamic osmometer previously described, for a number of concentrations and the $\pi/c-c$ curves drawn and extrapolated. Once again a correction was made to the concentration of polymer, as not all the volatiles are removed by evaporating off the solvent. It was found that a correction factor of 4 % had to be applied to polystyrene, and one of almost 7 % for polymethylmethacrylate. It was assumed that the correction factor for the copolymer samples would be a function of their composition, an assumption which is probably correct within the experimental error.

Styrene was separated from the phenolic inhibitor by repeated washing with a 10 % NaOH solution, followed by several washings with distilled water. The monomer was then dried over calcium chloride and subjected to two distillations under a reduced pressure of carbon dioxide ($p \approx 15$ mm.). It was then stored at about − 33° C in the solid state until required. $n_D^{20} = 1{\cdot}5462$.

The inhibitor was removed from methyl methacrylate in a similar manner; the monomer was then dried over calcium chloride and stored at − 33° C. $n_D^{20} = 1{\cdot}4145$.

Benzoyl peroxide was dissolved in chloroform, separated from the aqueous layer and precipitated with excess methanol. The peroxide was then filtered, washed with methanol and stored in a vacuum desiccator in the dark.

MEASUREMENT OF THE RATE OF COPOLYMERIZATION

Dilatometry can be used to follow the progress of the polymerization, although the position is much more complicated than is the case for the polymerization of a single monomer. This arises from the fact that the percentage volume contractions for 100 % polymerization of the two monomers are not the same, and also because the composition of the copolymer is not the same as that of the initial monomer mixture. Further, the composition of the copolymer varies with the monomer mixture, so no one simple relationship exists between contraction and extent of polymerization for all monomer mixtures. If it is assumed that 1 % polymerization of a monomer A will cause the same volume contraction whether A alone or a mixture of A and B is polymerized then the following relation holds (Melville *et al.* 1947):

$$\Delta = a\Delta_a + b\Delta_b, \tag{7}$$

where Δ is the observed decrease in volume; a, b are the extents of polymerization of monomers A and B respectively (in %) and Δ_a, Δ_b are the decreases in volume for 1 % polymerization of A alone and B alone respectively.

The assumption made, that 1 % polymerization of A will cause the same contraction, no matter what the environment is, can easily be checked by calibration, and this was done here. It is unlikely on theoretical grounds that there will be any difference, since the packing of A and B units in a copolymer chain is not likely to be much different from that in a single polymer, and so the effective density of a string of A units should be the same whether it is surrounded by A or B molecules.

In order to convert an experimentally determined volume contraction into a rate of copolymerization, it is necessary to have another relationship between A and B. This is provided by the copolymer composition equation (Mayo & Lewis 1944). From this equation

$$\frac{d(A)}{d(B)} = \frac{(A)}{(B)} \cdot \frac{\sigma(A)+(B)}{(A)+\mu(B)}, \tag{8}$$

it is obvious that the ratio

$$\frac{\%\, A \text{ polymerized}}{\%\, B \text{ polymerized}} = \frac{\sigma(A)+(B)}{(A)+\mu(B)}. \tag{9}$$

Hence it is possible to construct a theoretical curve expressing the ratio on the left-hand side of equation (9) as a function of the initial monomer composition. Equations (7) and (9) then provide the two equations from which the extent of polymerization may be calculated.

It is now advisable to see what justification there is for this treatment and the degree of accuracy it may be expected to yield. This may be obtained from the data of Mayo & Lewis (1944) for the copolymerization of styrene and methyl methacrylate (table 1, experiments 4, 5 and 6 of these authors). From these data, the percentage polymerization of each monomer was calculated and the ratio

$$\frac{\%\text{ styrene polymerized}}{\%\text{ methacrylate polymerized}}$$

calculated for each experiment, giving the results shown in table 2. From these figures, it can be seen that the ratio of styrene to methacrylate entering the copolymer is fairly constant for any one monomer mixture over a wide range of polymerization. The only exception is for $S_0 = 0{\cdot}8$, where the S/M ratio increases regularly from 0·67 to 0·72 as the reaction proceeds. However, by working on the range of 5 to 10 % polymerization, the ratios S/M can be taken as constant, and equal to 0·67 for $S_0 = 0{\cdot}8$; 1·0 for $S_0 = 0{\cdot}5$; 1·5 for $S_0 = 0{\cdot}2$.

TABLE 2. THE RATIO (% STYRENE CONSUMED/% METHACRYLATE CONSUMED) AS A FUNCTION OF CONVERSION

	S/M ratio		
initial conc. (S_0)	7 to 9 % conversion	7 to 13 % conversion	20 to 26 % conversion
0·8	0·67	0·69	0·72
0·5	0·92	1·01	1·01
0·2	1·49	1·50	1·49

These figures are in exact agreement with the theoretical calculations from equation (9), putting $\sigma = \mu = 0{\cdot}50$, the values accepted as correct by Mayo & Lewis (1944) at that time. It was concluded from this that the method of computing the rate outlined above could reasonably be expected to yield accurate results within the experimental error.

The most accurate values for σ and μ for the system styrene (A)-methyl methacrylate (B) are those of Mayo, Lewis & Walling (1947), and are $\sigma = 0{\cdot}520$, $\mu = 0{\cdot}460$ at 60° C. As the work here was done at 30° C, it was necessary to recalculate these values for the lower temperature using the activation energies of Mayo *et al.* (1947). This yielded the following values at 30° C: $\sigma = 0{\cdot}485$, $\mu = 0{\cdot}422$. These figures were substituted in equation (9) and a curve constructed; the ratio of the two monomers polymerizing at any monomer mixture could then be read off this curve. The percentage volume contractions for 100 % polymerization of styrene and methyl methacrylate at 30° C were taken as 14·4 (Melville & Valentine 1949) and 23·3 (Schulz & Harborth 1947) respectively.

It has been seen that this calculation of the rate involves several assumptions, and so a direct check was desirable. This was obtained by actually weighing the amount of polymer formed and comparing this with the weight calculated by the above method. The results are shown in table 3.

TABLE 3. COMPARISON OF ACTUAL AND CALCULATED YIELDS OF COPOLYMERS

mole fraction styrene	conversion (%)	calc. weight of polymer (g.)	actual weight (g.)
0	14·9	0·48	0·403
0·031	16·4	0·53	0·47
0·131	15·7	0·48	0·46
0·338	10·3	0·326	0·296
0·622	9·8	0·286	0·247
0·888	13·5	0·434	0·434
1·0	9·7	0·339	0·299

It must be considered that the results are in satisfactory agreement, especially if the method of isolating the polymer be taken into account. The partially polymerized monomer was poured into a small amount of benzene and this was then added to a large excess of methanol at − 10° C, with rapid stirring. The reaction tubes were washed out once or twice with benzene and the washings added to the methanol. The polymer was then filtered off through a sintered glass crucible (IG 3 porosity), washed with methanol, and dried to constant weight in a vacuum desiccator. Some polymer is unavoidably left behind in the tubes, especially with the higher molecular weight samples (those with a lower styrene content), and with those samples which were polymerized to a greater extent. Since in every case the weight of the polymer was less than that calculated, probably the discrepancy is due entirely to a failure to isolate the polymer quantitatively. These values were considered sufficient justification for using the method of calculating the rate outlined above, so this was done in all future experiments.

EVIDENCE FROM KINETIC MEASUREMENTS

(a) *Preliminary experiments with radiation of wave-length greater than* 2940 Å

In order to study the kinetics in a convenient manner, it is desirable that the rate of initiation be constant over the entire range of monomer compositions, or at least vary in a regular and predictable manner. For this reason, the benzoyl peroxide photosensitized reaction was chosen for study, as it was expected that the peroxide could be decomposed at a constant rate and so provide a constant rate of initiation. In actual fact, this desirable quality was not achieved, as described below. At wave-lengths < 3000 Å, styrene, methyl methacrylate, and benzoyl peroxide all absorb strongly; these wave-lengths were, accordingly, removed by a Pyrex-glass filter (cut off at $\lambda = 2940$ Å, figure 1).

A batch of reaction tubes was filled with varying monomer compositions but with a constant catalyst concentration ($4{\cdot}57$ to $4{\cdot}94 \times 10^{-2}$ mole/l.). The rates of polymerization were followed in the usual way; all these experiments were done at 30° C. It was found that the rate was constant over an appreciable extent of the reaction, as can be seen from figure 2. This does not strictly hold at high styrene concentrations; in these cases, an effect analogous to that observed for styrene itself comes into operation. After a certain point, the rate declines and then remains constant up to about 10 % conversion. In every case the second (steady) rate was taken as being the true rate of copolymerization. All the experiments were done at low conversions, so the pronounced decrease in rate observed with pure styrene at high conversions cannot affect the issue. In calculating the percentage volume contractions, the volume occupied by the catalyst itself was again taken into account. These volume contractions were converted into overall rates of copolymerization as described above. These experiments are plotted in figure 3, where the variation of rate with the mole fraction of styrene in the initial monomer mixture is shown. In this diagram the best smooth curve was drawn through the experimental points.

From these experiments several interesting conclusions can be drawn. The addition of small amounts of styrene (about 10 %) reduces the rate of polymerization from about 12·8 %/hr. to about 3 %/hr. The addition of further quantities of styrene has relatively little effect on the rate, which remains virtually constant at about 2 %/hr. up to a styrene concentration of about 90 %. A surprising result is that the rate of copolymerization is less than that for either monomer separately over a wide range. An interpretation of these results in the light of copolymer theory showed that the simpler assumption for mutual termination could not explain the phenomena observed.

For the system styrene (A)-methyl methacrylate (B), $\delta_a = 62{\cdot}5$ (Melville & Valentine 1949), $\delta_b = 22{\cdot}5$ (Mackay & Melville 1949) and hence $\delta_s = \delta_a/\delta_b = 2{\cdot}78$. Further, defining R_a, R_b as the rates of polymerization of styrene and methyl methacrylate alone, we have

$$R_a = \delta_a^{-1}(M_a)X_a^{\frac{1}{2}}, \quad R_b = \delta_b^{-1}(M_b)X_b^{\frac{1}{2}},$$

and hence $$R_b/R_a = \delta_a/\delta_b\,(X_a/X_b)^{\frac{1}{2}} = \delta_s(X_a/X_b)^{\frac{1}{2}}.$$

The concentrations of monomers may be omitted, since we are concerned with rates expressed in moles percent per hour. X_a, X_b here refer to the rates of initiation of styrene and methyl methacrylate for the two monomers polymerizing individually. But

$$R_a = 2{\cdot}11\ \%/\text{hr.}, \quad R_b = 12{\cdot}78\ \%/\text{hr.},$$

and hence $$R_b/R_a = 6{\cdot}05, \quad X_b/X_a = 4{\cdot}74.$$

If it be assumed that there is a linear relationship between $(X_a + X_b)$ and the monomer composition, then it is possible to calculate the termination constant ϕ from the kinetic expression (table 1). Adopting this procedure, it was found that the value of ϕ lay between 30 and 50 for each experimental point, a value of $\phi = 45$ providing a very good fit between theory and experiment.

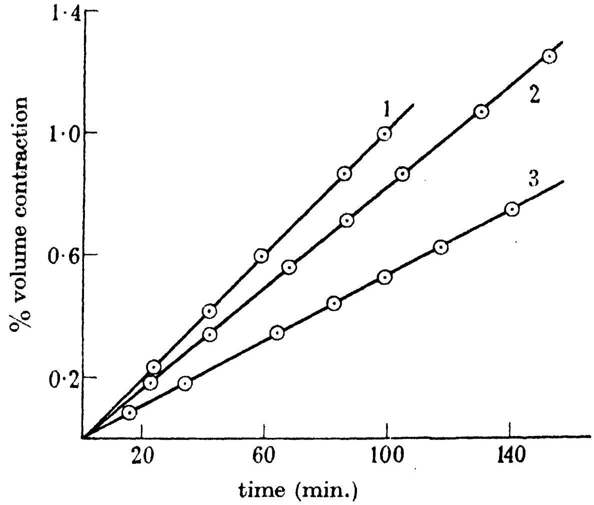

FIGURE 2. The variation of rate with time for various initial mole fractions of styrene (A_0). These values were: curve 1, 0·16; curve 2, 0·29; curve 3, 0·56.

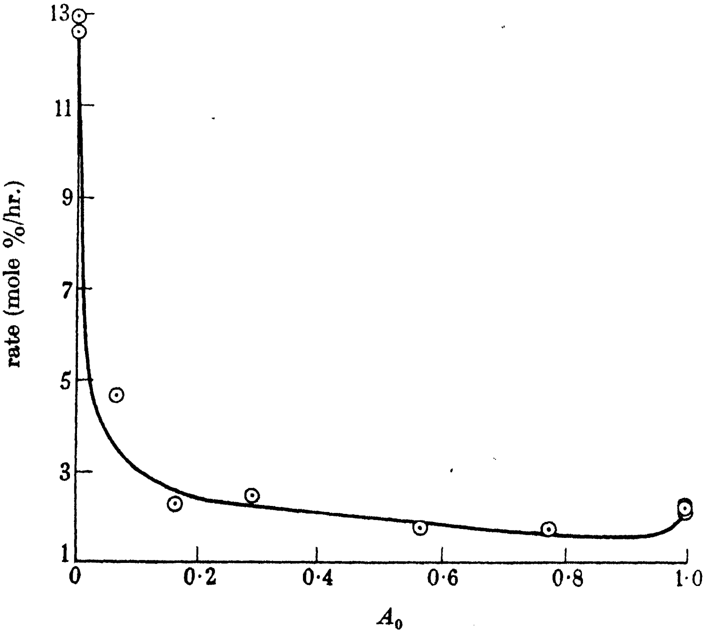

FIGURE 3. The variation of rate with monomer composition, for $\lambda > 2940$ Å, the curve being calculated with $\phi = 45$.

There are several rather unsatisfactory features about this work, however. It has been shown that the ratio $R_b/R_a = 6{\cdot}05$, i.e. methyl methacrylate polymerizes six times as fast as styrene, whereas for a constant rate of initiation it should polymerize three times as fast. Mayo & Lewis (1944) found the factor to be 5, while Norrish & Brookman (1939) reported it to be 3·5. Both these workers used the benzoyl peroxide catalysis (thermally decomposed) technique. In the light of these results, the present ratio appeared too high; this might be due to two causes. It may be that the radicals formed by the decomposition of the peroxide do not attack the two monomers at the same rate but may preferentially attack the methyl methacrylate. In this way the rate of initiation would be faster for methyl methacrylate. Another possibility is that the styrene is absorbing some of the radiation which should be absorbed by the peroxide, thus cutting down its own rate of initiation. This is a more likely explanation, especially since styrene absorbs strongly in this region (cf. next section). In order to try to prevent this possibility, it was decided to work at still longer wave-lengths of light, such that the absorption by both styrene and methyl methacrylate would be negligible. These results also showed the necessity of knowing the rate of initiation exactly, so for future work this was determined from molecular weight data. However, these preliminary experiments had shown that the simple copolymer theory was not adequate to explain the experimental results but that a large ϕ factor (indicative of preferred termination between unlike radicals) had to be introduced. Later work enabled this factor to be determined with precision.

(*b*) *Experiments with activating radiation of wave-length greater than* 3150 Å

In order to reduce absorption by the monomers to a minimum, a 4 mm. plate of window-glass with a transmission limit of 315 mμ (cf. figure 1) was used. The molar extinction coefficient, ϵ, for methyl methacrylate is only 0·01 at 3000 Å (Goodeve 1938) and was determined here to be 0·006 at 3150 Å, so that at longer wave-lengths the monomer is virtually transparent. Styrene, however, absorbs much more strongly, with $\epsilon \approx 600$ at 2950 Å (Rodebush & Feldman 1946; Arlman & Melville 1949), although the absorption drops rapidly immediately above this wave-length. At 2950 and 3200 Å, the extinction coefficients of these three substances were measured and determined to have the values given in table 4. Absorption curves for these substances will be given in part II, and the question of internal filter effects will also be thoroughly treated.

TABLE 4. THE EXTINCTION COEFFICIENTS FOR STYRENE, METHYL METHACRYLATE AND BENZOYL PEROXIDE

	ϵ	
substance	$\lambda = 3200$ Å	$\lambda = 2950$ Å
styrene	0·016	600
methyl methacrylate	0·005	0·013
benzoyl peroxide	1·36	35

However, it is obvious from these data that under the conditions of the last series of experiments, there must have been an internal filter effect, with an intense competition between the styrene and the benzoyl peroxide for the activating radiation. Even at wave-lengths greater than 3150 Å, the absorption due to the styrene is comparable with that due to the benzoyl peroxide. Although the extinction coefficient of the peroxide is 90 times greater than that of styrene, the concentration of the latter is about 170 times that of the peroxide, and so will absorb more. Unfortunately, it was not possible to work at still longer wave-lengths, since then the rate of the photosensitized reaction was reduced to such an extent that it could not be determined with certainty. Hence, in this system, it is impossible to state *a priori* the absolute rate of initiation for any given monomer mixture, since there is always the possibility of either of the monomers absorbing light.

In order to ascertain whether or not this factor would influence the rate of initiation, the two monomers were polymerized with direct photochemical initiation (i.e. no peroxide), using light of wave-lengths greater than 3150 Å, and the rates of polymerization measured. These were determined to be:

styrene rate = 0·02 %/hr.
methyl methacrylate rate = 0·23 %/hr.

This entails the surprising conclusion that although styrene absorbs much more strongly than methyl methacrylate in this region, the latter polymerizes faster. A possible explanation for this lies in the low primary quantum efficiency for styrene (Melville & Valentine 1949). However, the rates for the direct photopolymerizations are low compared with those for the sensitized reactions, the ratio being about 0·02 for styrene and 0·05 for methyl methacrylate.

In order to confirm that there were no abnormalities in the termination reaction with these mixed systems, the intensity exponent was measured at two different monomer concentrations, using the normal perforated screen technique. The following results were obtained:

styrene = 0·065 molar; $n = 0{\cdot}43$,
styrene = 0·647 molar; $n = 0{\cdot}51$.

From these figures it is obvious that the termination reaction is the normal mutual one, with the radicals interacting in pairs.

The rates of copolymerization were determined in the usual way, a catalyst concentration of 4·7 to $4{\cdot}9 \times 10^{-2}$ mole/l. being again employed. A typical set of results is shown in table 5; although the general trend is similar to that of the last series of experiments, there are some instructive points of difference.

TABLE 5. THE RATES OF COPOLYMERIZATION WITH RADIATION OF $\lambda > 3150$ Å

mole fraction styrene	rate (mole %/hr.)
0	4·60
0	4·70
0·052	1·88
0·195	1·13
0·418	0·82
0·804	0·80
1·0	1·05
1·0	1·15

The ratio of the rates of polymerization of the two monomers separately is different, being 4·23 in this case and 6·05 in the previous work. This is strong evidence in favour of the view that styrene was absorbing relatively more of the radiation at these short wave-lengths and so reducing its own rate of initiation. However, the ratio $R_b/R_a = 4{\cdot}23$ is still much greater than the theoretical value of 2·78 which holds for equal rates of initiation. It is thus still possible that the monomers are exercising some influence on the rate of initiation and causing this to deviate from the expected value. However, the general trend of the results is very similar in both cases; the addition of small amount of styrene reduces the rate very considerably. Thereafter, the rate is practically constant up to a molar fraction of styrene of 0·9, and increases again slightly for pure styrene. From the results of the preceding section it would thus appear that a large ϕ factor would need to be introduced in order to fit the experimental curve with theory. In order to measure this important factor with precision, the absolute rates of initiation for all monomer concentrations were needed. These were calculated from chain-length data, as shown below.

EVALUATION OF THE RATE OF INITIATION AND CALCULATION OF THE ϕ CONSTANT

For this system it was considered advisable to determine the rate of initiation from molecular-weight studies, since the inhibition technique would be difficult to apply. The introduction of a (probably) strongly absorbing inhibitor would almost certainly introduce an internal filter effect and so further complicate the issue. Accordingly, the molecular weights of a series of copolymers, prepared under conditions exactly analogous to those prevailing in the rate determinations, were measured in the manner described above. The full experimental results, together with a discussion of the Huggins μ-values for the copolymers, are given in appendix 1, as they are not strictly relevant to the present discussion.

It can be seen from the kinetic rate expression (table 1) that there are two unknowns, viz. the rate of initiation and the ϕ termination constant. The rate of initiation $(X_a + X_b)$ can be obtained from the molecular weight studies, since the chain-length ν ($\equiv$ degree of polymerization, $\bar{P}$, if transfer is absent) is defined by the expression

$$\nu \equiv \bar{P} = \frac{-d\{(A)+(B)\}/dt}{(X_a + X_b)}. \tag{10}$$

This is operative, of course, only if the termination reaction is a disproportionation one.

It is now necessary to see which data should be taken for the values of the velocity constants for the polymerization of the two individual monomers, as these are naturally rather critical. Although there is a wide variation in the values listed in the literature, fortunately, the absolute values do not occur in the kinetic expressions for the rate of copolymerization, as given in table 1. All that is required is the ratio of the termination and propagation coefficients, e.g. $\delta = k_t^{\frac{1}{2}}/k_p$, and the agreement is much better for this quantity. A list of the values available for this constant for styrene and methyl methacrylate at 30° C is given in table 6.

TABLE 6. VALUES OF $k_t^{\frac{1}{2}}/k_p(\delta)$ FOR STYRENE AND METHYL METHACRYLATE AT 30° C

δ		
styrene	methyl methacrylate	reference
62·5	—	Melville & Valentine (1949)
—	22·5	Mackay & Melville (1949)
77·6*, 58·6†	17·6‡	Bamford & Dewar (1947)
—	24·4	Matheson *et al.* (1949)
—	22·2	Burnett (1949)

* Calculated with α (viscosity exponent) $= 0{\cdot}65$.
† Calculated with α (viscosity exponent) $= 1{\cdot}0$.
‡ Calculated from value at 0° C, with $E = 4{\cdot}5$ kcal.

From the data in table 6, the following values were adopted:

$$\text{(styrene)} \qquad \delta_a = 62{\cdot}5,$$
$$\text{(methyl methacrylate)} \qquad \delta_b = 22{\cdot}5.$$

These values were chosen because they were both based directly on molecular weight determinations, which give the ratio $k_t^{\frac{1}{2}}/k_p$ directly, and so should be more accurate than the other values quoted.

From table 5, it can be seen that $R_b/R_a = 4{\cdot}23$, where R_b, R_a represent the rate of polymerization of methyl methacrylate and styrene respectively. Throughout this work, the subscripts a, b, are to be taken as referring to styrene and methyl methacrylate respectively. Now

$$R_b/R_a = \delta_a/\delta_b\,(X_b/X_a)^{\frac{1}{2}}.$$

Hence

$$X_b/X_a = 2{\cdot}31.$$

This means that pure methyl methacrylate is initiated 2·31 times as fast as pure styrene. If it be assumed that the rate of initiation is a linear function of the monomer composition, i.e. is proportional to the concentration of monomer, then the theoretical chain length can be calculated at various monomer compositions from equation (10) by inserting the appropriate experimental values for $-d((A)+(B))/dt$ and interpolating (X_a+X_b) from the values for X_a and X_b. These theoretical chain lengths are compared with the experimental values (cf. appendix 1) in table 7, the chain length being taken as the degree of polymerization.

TABLE 7. COMPARISON OF THEORETICAL AND ACTUAL CHAIN-LENGTHS FOR VARIOUS COPOLYMERS

A_0	$(\pi/c)_0$	mol. wt.	ν	theoret. ν
0	1·25	200,000	2,000	1,810
0·03	1·74	144,000	1,430	652
0·13	2·72	92,000	910	456
0·34	3·12	80,200	785	291
0·62	3·60	69,400	676	346
0·89	3·63	68,900	665	440
1·0	3·78	66,100	636	632

In the first place, the agreement for polystyrene and polymethylmethacrylate is quite good, that for polystyrene being well within the experimental error. The agreement for polymethylmethacrylate is not so good, but here again the discrepancy is barely outside the experimental error, which is much greater than for the lower molecular weight samples. These two samples then provide a useful check on the calculations, showing that the method should give the correct results for the copolymers also. However, the experimental and theoretical values for the chain length of the copolymers are not in agreement at all, the actual molecular weights found being about twice the expected values. This must mean that the rate of initiation does not, in fact, vary linearly with the monomer composition but is much lower than the expected value over the entire range of monomer composition. This lowering of the rate of initiation would lead to higher molecular weights, as was found to be the case.

If, now, the rate of initiation be calculated from equation (10) by inserting the experimental values for $\bar{P}$ and $-d\{(A)+(B)\}/dt$, then the results shown in table 8 are found.

The value of the rate of initiation of methyl methacrylate was calculated from a knowledge of the rate of polymerization and the velocity coefficients, since no molecular weight data were available for this substance under comparable experimental conditions.

TABLE 8. THE RATE OF INITIATION FROM MOLECULAR WEIGHT DATA

A_0	rate ($\times 10^5$) (moles/l./sec.)	$\bar{P}$	$(X_a+X_b)\times 10^8$ (moles/l./sec.)
0	—	—	11·09
0·031	7·11	1430	4·97
0·131	4·67	910	5·13
0·338	2·60	785	3·31
0·622	2·42	676	3·58
0·888	2·24	665	3·98
1·0	3·02	636	4·75

From these figures it appears that the overall rate of initiation falls very abruptly as the concentration of styrene in the system is increased. The introduction of about 10 % styrene reduces the rate of initiation from about $11{\cdot}1\times 10^{-8}$ to $5{\cdot}1\times 10^{-8}$ mole/l./sec. The rate of initiation then remains virtually constant from $A_0 = 0{\cdot}2$ to $A_0 = 0{\cdot}8$, and then increases again for pure styrene.

Since the rates of initiation and polymerization are now known, all the necessary evidence is available in order to calculate ϕ. For this copolymer system,

$$\delta_a = 62{\cdot}5,\quad \delta_b = 22{\cdot}5,\quad \delta_s = 2{\cdot}78,\quad \sigma = 0{\cdot}485\quad\text{and}\quad \mu = 0{\cdot}422.$$

Substituting these quantities in the kinetic rate expression (table 1), it is seen that

$$\frac{-d((A)+(B))}{dt} = \frac{1}{22{\cdot}5}\,\frac{(1+2{\cdot}74(A)-2{\cdot}60(A)^2)\,(X_a+X_b)^{\frac{1}{2}}}{(1+2(3{\cdot}19\phi-1)\,(A)+(11{\cdot}2-6{\cdot}38\phi)\,(A)^2)^{\frac{1}{2}}}. \tag{11}$$

This is rather an unwieldy expression to use as it stands for purposes of calculation. It is more convenient to express all rates of initiation and copolymerization as relative values, and accordingly they were all expressed relative to

$$\frac{-d((A)+(B))}{dt}_{(A)=0} = 1{\cdot}0 \quad\text{and}\quad (X_a+X_b)_{(A)=0} = 1{\cdot}0.$$

The rates of initiation and copolymerization already obtained were expressed in this manner and are plotted as functions of the mole fraction of styrene in figures 4 and 5. In figure 5, the theoretical rate of initiation, calculated on the assumption that the rate is proportional to the monomer concentration, is also shown.

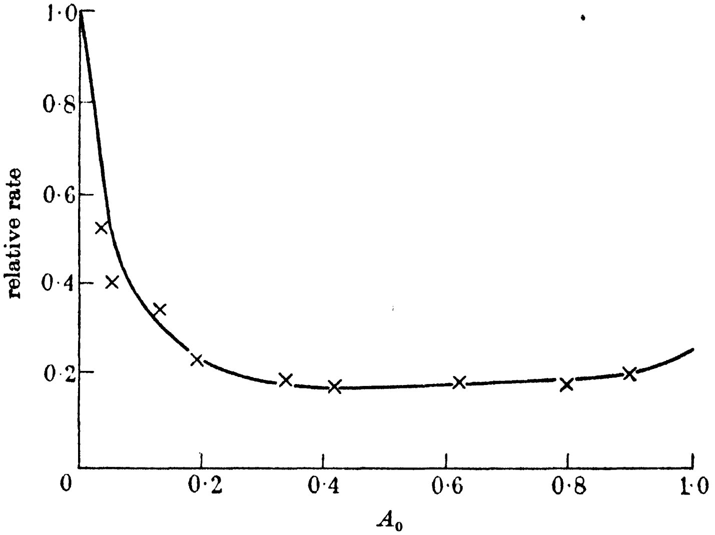

FIGURE 4. The experimental curve for the variation of rate with the mole fraction of styrene ($\lambda > 3150$ Å).

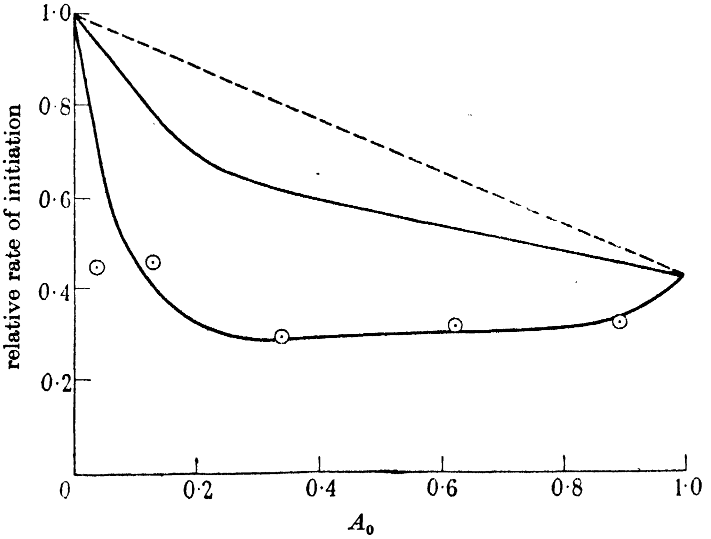

FIGURE 5. Relative rate of initiation as a function of monomer composition. - - - first order initiation; —⊙— calculated for disproportionation; ——— calculated for combination of unlike radicals.

The experimental points in figure 4 are drawn from two different sets of experiments with slightly different rates of initiation (differences in the light intensity). It can be seen that both sets lie on the one curve if the rates are expressed as relative rates.

From the data of figures 4 and 5, the value of ϕ was calculated for a number of points, e.g. $(A_0) = 0{\cdot}1$, $0{\cdot}3$, etc., by substituting for $-d\{(A)+(B)\}/dt$ and $(X_a+X_b)^{\frac{1}{2}}$ in equation (11). These calculations yielded the values of ϕ shown in table 9.

TABLE 9. VALUES OF ϕ AT VARIOUS MONOMER MIXTURES

mole fraction of styrene (A_0)	ϕ
0·1	10·6
0·3	14·7
0·5	14·4
0·7	13·6
0·9	10·2

From this table it can be seen that the value of ϕ remains constant over the entire range of monomer mixtures, in agreement with theoretical expectations. The best value of ϕ would appear to be about 14, since this is the value over the range of monomer composition from $(A_0) = 0{\cdot}3$ to $(A_0) = 0{\cdot}9$. At lower and higher concentrations, the experimental points are not so certain, since the error in determining the concentrations becomes much greater. For example, at a mole fraction of $(A_0) = 0{\cdot}05$, only about 0·15 ml. of styrene are distilled into the reaction tube, and the experimental error in determining the volume distilled is about ± 0·02 ml. This involves an error in the concentration of about ± 12 %, which is much greater than at, say, $(A_0) = 0{\cdot}5$, where it is only about 1·5 %. Taking the rate of initiation from figure 5, a theoretical curve of the rate of copolymerization with $\phi = 14$ is shown in figure 6. The theoretical curve provides a very good fit for the experimental points over the entire range, so that it may be concluded that for this system, at 30° C,

$$\phi = 14,$$

provided, of course, that all the radicals terminate in a disproportionation reaction.

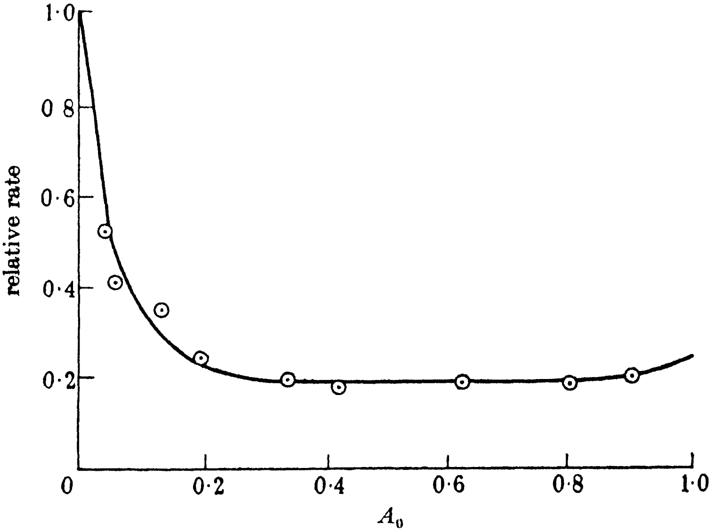

FIGURE 6. Theoretical curve of the variation of rate of copolymerization with monomer composition, drawn with $\phi = 14$ (⊙ experimental points).

It is now possible to calculate all the four propagation constants and the three termination constants for this system. The value of k_{tab} will naturally be largely dependent on those chosen for k_{taa} and k_{tbb} since, by definition, $k_{tab} = \phi\, k^{\frac{1}{2}}_{taa}\, k^{\frac{1}{2}}_{tbb}$.

In another paper (Melville & Valentine in press), an attempt was made to obtain the most probable values for the velocity constants for the polymerization of styrene and a similar scheme will be adopted here. Table 10 lists the recorded values of these constants for methyl methacrylate.

TABLE 10. VALUES OF THE VELOCITY CONSTANTS FOR METHYL METHACRYLATE AT 30° C

k_p	$k_t(\times 10^{-7})$	reference
286*	2·44*	Matheson *et al.* (1949)
380	7·3	Mackay & Melville (1949)
123†	0·39‡	Bamford & Dewar (1947)
128	0·60	Burnett & Melville (unpublished)

* Recalculated for disproportionation.
† Recalculated from the value at 0° C, with $E_p = 6$ kcal.
‡ Recalculated from the value at 0° C, with $E_t = 2$ kcal.

There is such a wide range in these results that it is desirable to take the average values. These resolve to be

$$k_p = 230\,\text{l.}\,\text{mole}^{-1}\,\text{sec.}^{-1}, \quad k_t = 2\cdot7 \times 10^7\,\text{l.}\,\text{mole}^{-1}\,\text{sec.}^{-1}.$$

These values agree well with those obtained in the present work from a limited number of lifetime and molecular weight studies for methyl methacrylate, viz. $k_p = 250$, $k_t = 2\cdot3 \times 10^7$. For styrene, at 30° C, the equivalent values are

$$k_p = 46, \quad k_t = 8\cdot0 \times 10^6.$$

The complete list of velocity coefficients for the copolymerization of styrene (A) and methyl methacrylate (B) at 30° C now reads:

l. mole^{-1} sec.^{-1}
$k_{paa} = 46$
$k_{pab} = 95$
$k_{pbb} = 230$
$k_{pba} = 545$

l. mole^{-1} sec.^{-1}
$k_{taa} = 8 \times 10^6$
$k_{tbb} = 2\cdot7 \times 10^7$
$k_{tab} = 2\cdot06 \times 10^8$

It is obvious from these figures that the 'crossed' velocity constant for termination is very much larger than those for the two individual monomers, being 8 times that for methyl methacrylate and 26 times that for styrene. The two unlike radicals e.g. radicals with styrene and methyl methacrylate type radical ends, interact much more rapidly than do two radicals of the same type. Possible explanations for this, on the basis of the electronic structures of the radicals concerned, will be given in part II. It is desirable at this stage to examine in more detail the assumptions which have been made in this derivation, in particular those referring to the rate of initiation, and see how modification of the basic assumptions would influence the value of ϕ. This is also done in part II.

Appendix 1

Molecular weight studies in copolymers

Since no previous observations have been published on the osmotic behaviour of copolymers, it may be of interest to list the experimental determinations in detail. These are given in table 11 and figure 7.

Table 11. Molecular weight data for copolymers (determined at 24·6° C)

sample	c (g./100 g.)	π cm. benzene	π/c	$(\pi/c)_0$ and mol wt.
C20	0·789	1·47	1·87	1·25
polymethylmethacrylate	0·619	1·07	1·73	200,000
	0·418	0·625	1·49	
	0·316	0·445	1·41	
	0·209	0·28	1·34	
C21	1·10	3·23	2·93	1·74
Mole fraction styrene in	0·799	2·08	2·60	144,000
polymer = 0·07	0·538	1·16	2·16	
	0·397	0·83	2·09	
	0·231	0·44	1·90	
C22	0·864	3·13	3·62	2·72
mole fraction styrene in	0·603	1·94	3·22	92,000
polymer = 0·22	0·271	0·785	2·90	
C25	0·656	2·615	3·98	3·12
Mole fraction styrene in	0·438	1·64	3·75	80,200
polymer = 0·41	0·304	1·05	3·46	
	0·198	0·64	3·22	
C26	0·562	2·56	4·56	3·60
mole fraction styrene in	0·372	1·545	4·15	69,400
polymer = 0·59	0·211	0·78	3·70	
	0·136	0·53	3·89	
C23	0·867	4·23	4·88	3·63
mole fraction styrene in	0·676	3·165	4·68	68,900
polymer = 0·82	0·472	2·08	4·40	
	0·337	1·365	4·05	
	0·254	0·98	3·85	
C24	0·637	2·85	4·48	3·78
pure polystyrene	0·432	1·83	4·24	66,100
	0·233	0·98	4·20	

These experiments furnish some interesting results on the thermodynamic properties of solutions of copolymers. For those polymers which yield a linear $\pi/c-c$ plot, the Huggins μ-constant (Huggins 1943) is given by the expression

$$\mu = 0{\cdot}50 - k.(m_1 d_2^2/RT\,d_1),$$

where m_1 = molecular weight of the solvent (benzene) = 78,
d_1 = density of solvent in g./100 ml. = 87·3,
d_2 = density of polymer in g./100 ml.,
R = 848 100 ml. cm. water/A^0,
T = 298° A,
k = slope of $\pi/c-c$ curve.

As can be seen from figure 7, in the case of these copolymers, the plot of π/c against c is not linear, but is slightly convex to the c axis. However, the deviation from linearity is never very great, and so the slopes of these lines were measured by taking the best straight line through the experimental points. This will introduce only a small error into the calculations. The density of the copolymer will naturally vary with the composition and it has been assumed here that the density will be a linear function of the composition. Adopting this procedure, the value of μ was determined for each polymer sample. Unfortunately, for those copolymers with a high styrene content (C 26, C 23, C 24), the $\pi/c-c$ curve could not be determined very exactly owing to the scatter of the points involved. The actual values of μ are listed in table 12. From these figures it is apparent that the Huggins μ-value does not vary appreciably throughout the entire range of copolymer composition. It would seem, however, that the copolymers in the middle range of composition have lower values of μ than either of the two pure polymers. As the μ-value gives a measure of the interaction between the polymer and solvent, it would thus appear that the copolymers interact with the solvent in a different manner to the pure polymers. It may be taken that the better the solvent, i.e. the more the polymer and solvent interact, then the greater the slope of the $\pi/c-c$ curves and the smaller the value of μ. From this it would seem that benzene is a better solvent for the copolymers, in a thermodynamic sense, than it is for either polymer. This must mean that owing to the change in structure in the copolymer chains, in which there will be sequences of the type -*A*-*A*-*A*-*A*-*B*-*B*-*B*-*A*-*A*- and also probably -*A*-*B*-*A*-*B*-*A*-*A*-*B*-*A*-, the attack of the monomer units by the solvent is facilitated. However, there is no pronounced change, although it does seem to be outside the experimental error. The

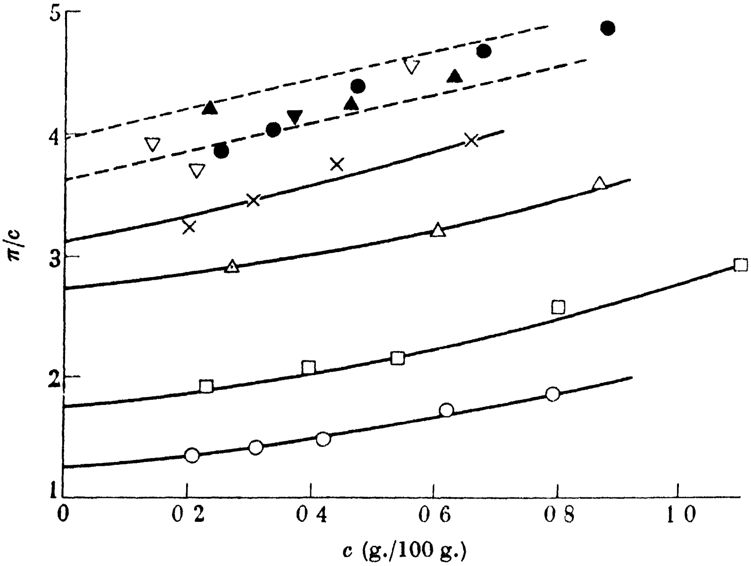

FIGURE 7. The variation of π/c with c, for various copolymers (π in cm. benzene) ⊙ polymethylmethacrylate; □ C 21, ▲ C 24, △ C 22, × C 25, ● C 23, ▽ C 26. (For explanation of symbols, see table 11.)

only other system for which accurate data are available is that of the behaviour of butyl acrylate-styrene copolymers in benzene (Arlman & Melville unpublished). In this case, again, the two polymers have μ-values of about 0·45, and the various copolymers also have μ-values which fluctuate about this figure. In this case, however, there was no definite correlation between μ-value and copolymer composition.

TABLE 12. HUGGINS μ-VALUES FOR VARIOUS COPOLYMERS

sample	mole fraction styrene in polymer	μ
polymethylmethacrylate	0	0·457
C21	0·065	0·447
C22	0·22	0·448
C25	0·41	0·428
C26	0·59	0·425
C23	0·82	0·43
polystyrene	1·0	0·45
polystyrene*	1·0	0·47

* Determined from previous results (Melville & Valentine 1949).

NOTE

Since this paper was completed, the data of C. Walling (1949, *J. Amer. Chem. Soc.* **71**, 1930) have become available. Studying the copolymerizations of styrene-methyl methacrylate and styrene-methyl acrylate with essentially the same techniques as those reported here, he finds $\phi = 13$ and $\phi = 40$ for these two systems respectively, in excellent agreement with the results of this paper. There is one interesting discrepancy between the two sets of results. Walling, using 2-azo-*bis*-*iso*butyronitrile as an initiator, claims to have a constant rate of initiation for all monomers and monomer mixtures, in contrast to the marked lowering of the rate of initiation for mixtures of styrene and methyl methacrylate described in this work. The close agreement as to the value of ϕ for styrene-methyl methacrylate would seem to indicate that termination proceeds exclusively by disproportionation, even for radicals of different chemical type.

One of us (L.V.) is indebted to the Department of Scientific and Industrial Research for the award of a maintenance grant.

REFERENCES

Arlman, E. J. & Melville, H. W. Unpublished.

Bamford, C. H. & Dewar, M. J. S. 1947 *Faraday Soc. Disc.* **2**, 310.

Bamford, C. H. & Dewar, M. J. S. 1948 *Proc. Roy. Soc.* A, **192**, 309.

Burnett, G. M. 1949 *Trans. Faraday Soc.* (in the Press).

Burnett, G. M. & Melville, H. W. 1947 *Proc. Roy. Soc.* A, **189**, 456.

Dow Chemical Co. 1946 Technical Monograph.

Gee, G. & Melville, H. W. 1944 *Trans. Faraday Soc.* **40**, 240.

Goodeve, J. W. 1938 *Trans. Faraday Soc.* **34**, 1239.

Grassie, N. & Melville, H. W. 1949 *J. Polymer Sci.* (in the Press).

Huggins, M. L. 1943 *Industr. Engng Chem.* **35**, 216, 980.

Mackay, M. H. & Melville, H. W. 1949 *Trans. Faraday Soc.* **55**, 323.
Masson, C. R. & Melville, H. W. 1949 *J. Polymer Sci.* (in the Press).
Matheson, M. S., Auer, E. E., Bevilacqua, E. B. & Hart, E. J. 1949 *J. Amer. Chem. Soc.* **71**, 497.
Mayo, F. R. & Lewis, F. M. 1944 *J. Amer. Chem. Soc.* **66**, 1594.
Mayo, F. R., Lewis, F. M. & Walling, C. 1947 *Faraday Soc. Disc.* **2**, 285.
Melville, H. W., Noble, B. & Watson, W. F. 1947 *J. Polymer Sci.* **2**, 229.
Melville, H. W. & Valentine, L. 1949 *Trans. Faraday Soc.* (in the Press).
Norrish, R. G. W. & Brookman, F. F. 1939 *Proc. Roy. Soc.* A, **171**, 147.
Rodebush, W. H. & Feldman, I. 1946 *J. Amer. Chem. Soc.* **68**, 897.
Schulz, G. V. & Harborth, G. 1947 *Angew. Chem.* **59**, 90.

Studies in copolymerization

II. A discussion of the validity of the results and some theoretical implications

By H. W. Melville, F.R.S. and L. Valentine
Chemistry Department, University of Birmingham

(*Received* 1 *September* 1949)

In this paper a critical review is made of the methods employed in part I of this series for the determination of the rate coefficients for the copolymerization of styrene and methyl methacrylate. Evidence is presented which shows that the calculations are correct, subject to the normal experimental error. Possible causes of the peculiar variation of the rate of initiation with monomer composition are suggested, based on the idea of recombination of unlike radicals. An analysis of the previous results of Norrish & Brookman, Mayo & Lewis, shows that their results can be interpreted in support of the present work. Some calculations on other copolymer systems seem to indicate that there is a high ϕ factor also for those systems, so that the phenomenon is a general one. Finally, a semi-quantitative approach to the problem of calculating, *a priori*, ϕ factors for any system is given; this theory is based on a reduction of the activation energy for the interaction of unlike radicals due to electrical charge effects.

INTRODUCTION

In the preceding paper, the steps leading up to the evaluation of all the rate constants in the copolymerization of styrene and methyl methacrylate were described. Several assumptions, some not obviously justifiable at first glance, had to be made during the derivation, and these will be discussed critically in the present paper. For example, it was assumed in the calculation of the rate of initiation that there was no chain transfer; the probable influence of this reaction is discussed here. The absorption characteristics of the three components of the reaction, viz. styrene, methyl methacrylate and benzoyl peroxide, were carefully examined in order to see whether or not there were any anomalies in the absorption process. Another possibility which was ignored in part I, namely, that the radicals combine and not disproportionate, is also examined. Although it is considered unlikely that all the radicals in a copolymerization reaction terminate by combination, quite a strong case can be argued for the combination of unlike radicals only. The effect of this on the value of the ϕ termination constant is described.

Some calculations have been made on the ϕ factors for a number of other copolymer pairs; in most cases there is an appreciable ϕ factor. As a result of this, it is suggested that most radicals prefer to terminate in a reaction with a radical of different chemical type, presumably as a result of polar interactions. It is possible to develop this theory on a semi-quantitative basis, following the procedure of Alfrey & Price (1947). This leads to the conclusion that the ϕ factor should go hand in hand with the difference in polarity of the two radicals. If this is indeed the case, then it should be possible, by carrying out a series of experiments with radicals of widely different natures, to determine the effect of substituents on the reactivity of radicals and also the factors which influence the interaction of two radicals.

THE EFFECT OF TRANSFER

It was pointed out that in the calculation of the rate of initiation from molecular weight data it had been assumed that there was no transfer. This is not strictly true, since transfer does occur to a slight extent with both styrene and methyl methacrylate and hence will also probably occur in a copolymer system. However, it can easily be shown that this will introduce only a small error, of the order of 5 %, into the calculations. This may be done by considering some molecular weight data for polystyrene (Melville & Valentine 1949, table 3).

If transfer occurs, then it can be shown that the degree of polymerization is defined by the expression

$$\frac{1}{\bar{P}} = \frac{k_f}{k_p} + \frac{k_t^{\frac{1}{2}}(I)^{\frac{1}{2}}}{k_p(M)},$$

where k_f is the transfer velocity constant and (I) the rate of initiation. In the calculations for the copolymers, the first term on the right-hand side of the equation has been omitted. The data for styrene itself can now be recalculated to obtain the rate of initiation (*a*) with transfer present and (*b*) assuming that there is no transfer, using the values obtained for k_f, k_p, k_t (Melville & Valentine). The results are shown in table 1.

TABLE 1. EFFECT OF TRANSFER ON THE CALCULATIONS OF THE RATE OF INITIATION FOR STYRENE

$1/\bar{P} \times 10^4$	$(I) \times 10^8$ (mol./l./sec.)	$(I) \times 10^8$, calculated for no transfer
12·51	2·83	2·98
16·20	4·81	5·01
17·67	5·74	5·96
21·72	8·74	9·00

It can be seen that there is very little difference between the two sets of values, and the error introduced by omitting the presence of transfer lies between 3 and 5 %. Equivalent data are not available for the case of methyl methacrylate, but the situation is very similar here. The transfer constant (k_f/k_p) for this monomer at 30° C is $2{\cdot}8 \times 10^{-5}$ (Bamford & Dewar 1947), while that for styrene is $3{\cdot}2 \times 10^{-5}$ (Melville & Valentine), so that practically identical conditions prevail for the two monomers. As a result, it may be concluded that for the copolymer system, the rates of initiation as given are possibly 5 % too high, although this is barely outside the experimental error of the molecular weight determinations. This would have the effect of lowering the value of ϕ to a slight extent, but in view of the experimental error it is not necessary to modify the value already given ($\phi = 14$).

The phenomenon of transfer certainly has nothing to do with the peculiar form of the initiation-monomer composition curve, since actually it was found that the molecular weights were considerably higher than those calculated, whereas the effect of transfer would be to lower the molecular weights below the expected values.

THE POSSIBILITY OF INTERNAL FILTER EFFECTS

In order to determine whether or not the monomers were causing an internal filter effect on the absorption of light by the peroxide, the absorption characteristics of styrene, methyl methacrylate and benzoyl peroxide were carefully examined.

The absorption of styrene and benzoyl peroxide below 3000 Å is shown in figure 1, while the absorption of all three substances above 3000 Å is depicted in figure 2. The absorption studies on styrene and methyl methacrylate above 3000 Å were made on

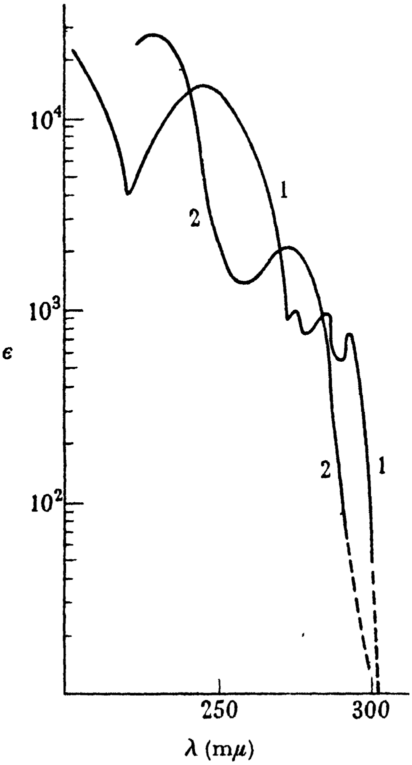

FIGURE 1. The absorption spectra of styrene (curve 1) and benzoyl peroxide curve (2) at wave-lengths below 300 mμ.

the pure monomers with a Beckmann photo-electric spectrograph, while the benzoyl peroxide was examined in cyclohexane solution. At short wave-lengths, a Hilger quartz spectrograph was used. The absorption curve for styrene at short wave-lengths is drawn from the results of Arlman. The dotted lines in these diagrams indicate the connexions between the actually measured parts and were not determined experimentally.

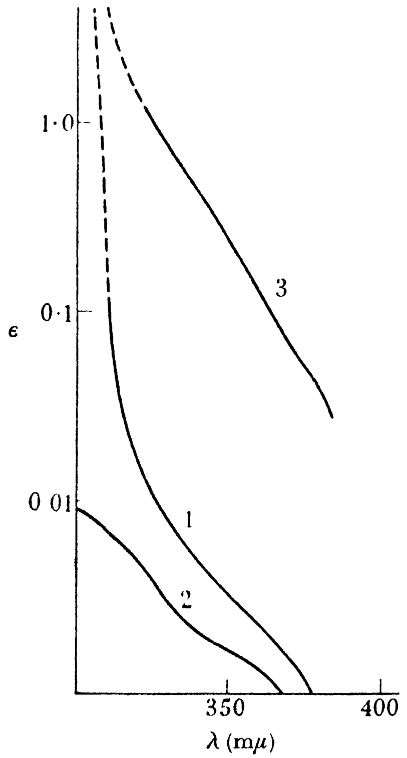

FIGURE 2. The absorption spectra of styrene (curve 1), methyl methacrylate (curve 2) and benzoyl peroxide (curve 3) at wave-lengths above 300 mμ.

From these diagrams it can be seen that the absorption of styrene and benzoyl peroxide is very intense below 3000 Å. The curve for styrene is very similar to the one reported by Rodebush & Feldman (1946), although these authors did not report the subsidiary peaks at 2750, 2860 and 2930 Å. For benzoyl peroxide,

$$\lambda^1_{\text{max.}} = 2730\,\text{Å}, \quad \epsilon^1_{\text{max.}} = 2200,$$

$$\lambda^2_{\text{max.}} = 2300\,\text{Å}, \quad \epsilon^2_{\text{max.}} = 26800,$$

in good agreement with the results of Cohen *et al.* (1948).

In order to confirm that there were no abnormalities due to the mixing of the two monomers, various mixtures of these were made up and the absorption determined in 1 cm. cells. The results of these experiments are given in table 2.

From this, it can be concluded that the presence of a mixture of monomers introduces no complications into the absorption characteristics. For example, the theoretical amount absorbed by a mixture of monomers can be calculated from a knowledge of the extinction coefficients of the two monomers. Comparing these with the experimentally determined values there is excellent agreement. At $\lambda = 330\,\text{m}\mu$, mole fraction styrene = 0·08,

TABLE 2. ABSORPTION OF VARIOUS MIXTURES OF STYRENE AND METHYL METHACRYLATE

	% transmitted mole fraction styrene				
λ (mμ)	0	0·079	0·48	0·914	1·0
310	85·0	—	—	—	9·3
320	90·1	89·3	80·5	74·8	73·2
330	93·6	92·7	87·2	84·7	84·9
340	95·2	94·5	92·0	91·0	91·0
350	96·3	95·9	—	94·5	94·3
380	98·5	97·9	97·8	98·0	98·1
410	99·0	99·2	98·5	99·4	98·8

amount absorbed (calculated) = 7·2 %,
amount absorbed (experimental) = 7·3 %.

At $\lambda = 330\,\text{m}\mu$, mole fraction styrene = 0·91,

amount absorbed (calculated) = 14·7 %,
amount absorbed (experimental) = 15·3 %.

Under the experimental conditions used, only light with a wave-length greater than 3150 Å was employed; under these conditions, it is easy to show that neither monomer should have exercised any internal filter effect on the rate of initiation, since the light is weakly absorbed by all three constituents. For example, at $\lambda = 320\,\text{m}\mu$,

$$\epsilon_{\text{St.}} = 0{\cdot}015, \quad \epsilon_{\text{Meth.}} = 0{\cdot}005, \quad \epsilon_{\text{Bp.}} = 1{\cdot}30.$$

At a mole fraction styrene = 0·9, and a concentration of benzoyl peroxide of 5×10^{-2} moles/l. (the value used experimentally in the rate determinations), then, to a first approximation,

styrene absorbs	23·7 % of the incident light,
methyl methacrylate absorbs	1·0 % of the incident light,
benzoyl peroxide absorbs	14·5 % of the incident light.

At $\lambda = 330\,\text{m}\mu$,

$$\epsilon_{\text{St.}} = 0{\cdot}008, \quad \epsilon_{\text{Meth.}} = 0{\cdot}003, \quad \epsilon_{\text{Bp.}} = 0{\cdot}75.$$

At a mole fraction styrene = 0·1, and a concentration of benzoyl peroxide of 5×10^{-2} mole/l., then

styrene absorbs	1·7 % of the incident light,
methyl methacrylate absorbs	5·6 % of the incident light,
benzoyl peroxide absorbs	8·3 % of the incident light.

From these figures it can be seen that over the entire range of monomer composition and wave-length of incident light there should be no marked influence by the monomers on the amount of light absorbed by the peroxide and hence on the rate of initiation. As a result, it appears improbable that the abnormalities of the rate of initiation can be due to any physical factors influencing the photochemical initiation process, but must be due to some inherent properties of the radical-monomer system.

THE EFFECT OF COMBINATION OF RADICALS

It was pointed out in part I that disproportionation of the radicals in the termination reaction had been assumed. As there is at present no method of directly proving this assumption, it is necessary to determine the effect of postulating combination on the calculation of ϕ. Three possibilities may be distinguished, viz. (*a*) all the radicals combine, (*b*) only unlike radicals combine, i.e. the reaction between a radical of type A and one of type B is a combination one, (*c*) the tendency towards combination is a function of chain length, being greater for radicals of very short length. Assumption (*a*) would be a rather unwarranted one, however, since the kinetic coefficients for the individual monomers were calculated on the basis of disproportionation, and this procedure seems to be largely justifiable for the case of polymerization of individual monomers (cf. e.g. Burnett & Melville 1947, Melville & Valentine 1949); (*c*) has not proved susceptible to a direct check as yet, but certainly seems quite possible. It may be that radicals are formed by the decomposition of the peroxide at a constant rate. These then add on to monomers A and B to give A- and B-type radicals respectively, of unit chain length, which then combine to form an inactive substance and so curtail the effective rate of initiation of polymeric radicals. In this case, the fraction of P_1 and Q_1 radicals which effectively initiate reaction chains is then given by an expression of the type

$$F_{\text{init.}} = \frac{M_1(P_1) + M_2(Q_1)}{M_1(P_1) + (M_2)(Q_1) + k_r(P_1)(Q_1)},$$

where $$M_1 = k_{paa}(A) + k_{pab}(B), \quad M_2 = k_{pba}(A) + k_{pbb}(B),$$

and k_r = velocity coefficient for the combination of P_1 and Q_1 radicals.

It is obvious that an expression of this type will give, qualitatively at least, the nature of the observed relationship between the rate of initiation and the monomer composition. Starting with, say, monomer A, the introduction of small amounts of monomer B will increase the term $k_r(P_1)(Q_1)$ and so decrease the effective rate of initiation. Addition of further quantities of B will reduce the rate of initiation still further, reaching a minimum at some point. In this way, the abnormal decrease in the rate of initiation for certain monomer mixtures below the rates for either pure monomer is explained. The scheme proposed above is probably an over simplification of the actual conditions, since it is most unlikely that the reactivity of the radicals would change abruptly at $n = 1$, and then remain constant from $n = 2$ to $n = \infty$. More likely, there would be a gradual decrease in reactivity with increasing chain length; it may be noted that Mayo (1948) found that the velocity constant for transfer *increased* from $n = 1$ to $n = 4$, and then remained constant. This recombination principle may be regarded as an extension of the ϕ principle, i.e. a very high 'termination' constant for radicals of very short chain length.

Unfortunately, it has not been possible to establish this hypothesis on a quantitative basis, since the (P_1) and (Q_1) terms could not be evaluated. Furthermore, the detection and isolation of the traces of very low molecular weight material which would be formed would be an extremely difficult task, so that the question must remain a matter of speculation at the present moment.

There remains for discussion only assumption (*b*). It was seen that the rate of initiation was derived from molecular weight studies on the assumption that the kinetic chain length and the degree of polymerization were equivalent. Transfer aside, this holds only if the chains are terminated by disproportionation; if combination was the terminating mechanism, then the rates of initiation would be out by a factor of two. If the chain length is ν and the degree of polymerization is $\bar{P}$, then for disproportionation $\bar{P} = \nu$, and for combination $\bar{P} = 2\nu$. As a result, for combination,

$$\frac{-d((A)+(B))/dt}{\bar{P}} = \frac{-d((A)+(B))/dt}{2\nu} = \frac{(X_a+X_b)}{2}.$$

It would, however, be a most unwarranted procedure to assume disproportionation for the polymerization of the single monomers and combination for the copolymerization reaction. There is another possibility, however. In the copolymerization there are three termination reactions, viz.

$$\text{rate of termination} = k_{taa}(P)^2 + k_{tab}(P)(Q) + k_{tbb}(Q)^2.$$

It would be quite logical, and in fact may be necessary, to assume combination in the reaction between unlike radicals P and Q, while retaining the postulate that radicals of the same chemical type react by a dismutation process. Now it has been shown that the 'crossed' termination constant k_{tab} is very much larger than either k_{taa} or k_{tbb}. It might be argued that a disproportionation reaction should not be abnormally favoured in the reaction between two unlike radicals, since the fundamental step is the transfer of a hydrogen atom between the two radicals; in this case, the chemical nature of the radicals might play no important part. It would be expected that combination reactions would be more affected by, say, polar effects and so large 'crossed' termination constants would be expected. There is no direct evidence, however, as to which mechanism is actually operating. It would be of interest, however, to see how the value of ϕ would be altered by assuming that the reaction between unlike radicals is a combination step.

In order to do this, it is necessary to evaluate each of the three terms in the above expression for the rate of termination. The fraction of combination is then given by

$$F_{\text{combination}} = \frac{k_{tab}(P)(Q)}{k_{taa}(P)^2 + k_{tab}(P)(Q) + k_{tbb}(Q)^2}.$$

An additional complication arises in these calculations, however. If it is assumed that there is a certain amount of combination, then the calculated rate of initiation will also increase. This in turn leads to a higher value of ϕ and hence k_{tab}; this automatically raises the fraction of combination and so *ad infinitum*. The experimental curve for the rate of initiation, assuming disproportionation (figure 3), gives a value of $\phi = 14$. If it be assumed that the rate of initiation varies linearly with the monomer composition, then $\phi = 45$ over the entire range of monomer composition. It seemed, then, that if combination of unlike radicals were assumed the value of ϕ would lie between 15 and 45. The value of $\phi = 30$ was chosen as a first approximation, the idea being to calculate the rate of initiation for this value of ϕ, substitute this in the kinetic expression and so obtain another value of ϕ. By a series of approximations the actual value of ϕ would be obtained.

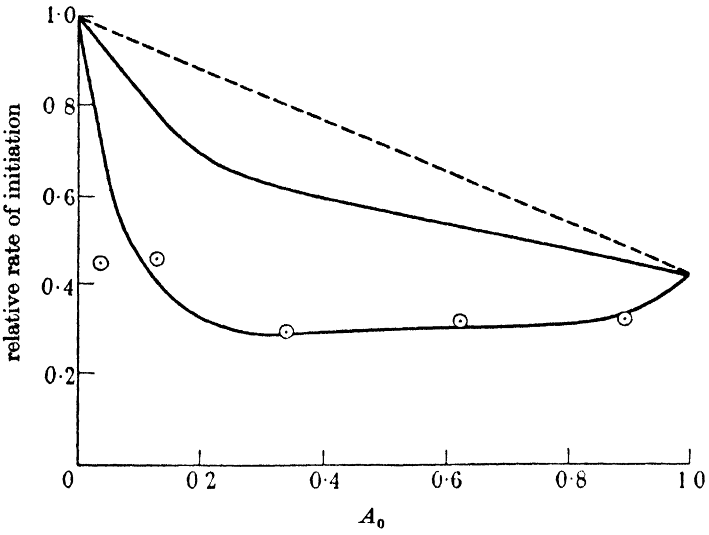

FIGURE 3. The variation of rate of initiation with monomer composition for various termination mechanisms. - - - first-order initiation; – ⊙— disproportionation; ——— combination of unlike radicals.

Now, in order to ascertain the fraction of combination the concentrations (P) and (Q) were needed. The relation between these was provided by the fact that under steady state conditions

$$k_{pab}(P)(B) = k_{pba}(Q)(A)$$

or

$$\frac{(P)}{(Q)} = \frac{k_{pba}(A)}{k_{pab}(B)} = 5{\cdot}7 \times (A)/(B).$$

The relative rate of termination could be calculated then and the amount of combination determined from the above formula; the results are listed in table 3.

TABLE 3. FRACTION OF COMBINATION CALCULATED FOR $\phi = 30$

A_0	fraction of combination
0·1	0·90
0·3	0·96
0·5	0·89
0·6	0·85
0·75	0·74
0·9	0·49

Using these figures for the amount of combination, the data of part I (table 8) were recalculated to give the new rate of initiation, which is shown in figure 3. It can be seen that the rate of initiation decreases almost linearly and is thus more in accord with theoretical expectations. From this smooth curve, the value of ϕ was recalculated by substitution in the kinetic expression for the rate of copolymerization. The following figures were obtained:

At

$$A_0 = 0{\cdot}2, \quad \phi = 26,$$
$$A_0 = 0{\cdot}5, \quad \phi = 27,$$
$$A_0 = 0{\cdot}8, \quad \phi = 27.$$

Thus this procedure is almost self-consistent. By recalculating the amount of recombination with $\phi = 27$ and proceeding as above, even better self-consistency could be attained. However, it was felt that this calculation had set a limit to the value of ϕ should there be combination between unlike radicals.

Summarizing, then, it would seem that if all the radicals disproportionate,

$$\phi = 14, \quad k_{tab} = 2{\cdot}06 \times 10^8\,\text{l. mole}^{-1}\,\text{sec.}^{-1}.$$

If unlike radicals combine, then the maximum value of ϕ can be taken as

$$\phi = 30, \quad k_{tab} = 4{\cdot}4 \times 10^8\,\text{l. mole}^{-1}\,\text{sec.}^{-1}.$$

DISCUSSION OF THE RESULTS OF NORRISH & BROOKMAN, MAYO & LEWIS

Norrish & Brookman (1939) (hereinafter referred to as N & B) studied the benzoyl peroxide (0·01 mole %) catalyzed copolymerization of styrene and methyl methacrylate at 90° C. Rates of copolymerization were determined by precipitation of the polymer, after given time intervals, and weighing of the polymer.

The experimental curve of these authors, plotting the overall rate in mole % per hour against the mole fraction of styrene, is shown in figure 4, together with the theoretical curve for $\phi = 15$. As before,

$$R_b/R_a = \delta_a/\delta_b(X_b/X_a)^{\frac{1}{2}}.$$

N & B find

$$R_b = 17{\cdot}3\,\%/\text{hr.}, \quad R_a = 4{\cdot}9\,\%/\text{hr.}, \quad \text{and hence} \quad R_b/R_a = 3{\cdot}54.$$

However, the reaction was carried out at 90° C and it is very difficult to obtain accurate values for δ_a, δ_b, at this temperature, as it involves an extrapolation of about 60° C from the recorded values. At 30° C it was seen that $\delta_s = 2{\cdot}8$, so that to a first approximation, $\delta_s \approx 3{\cdot}5$ at 90° C, assuming almost equal energies of activation for δ_a and δ_b. This then leads to the fact that the rates of initiation of the two monomers are the same, and so it may be assumed that the rate of initiation will be constant over the entire range of monomer composition. Acting on this assumption, the theoretical curve was calculated for $\phi = 15$; it can be seen from figure 4 that there is a fair measure of agreement between N & B's results and the theoretical curve. The curves are virtually superimposed from $A_0 = 0{\cdot}6$ to $A_0 = 1{\cdot}0$ and it is only at high concentrations of methyl methacrylate that the differences between the two curves become appreciable. One possible explanation for the discrepancy lies in the fact that N & B have presumably assumed that the two monomers will be consumed in equal amounts at all concentrations; this is now known definitely to be wrong, as shown by the copolymer composition equation (Mayo & Lewis 1944).

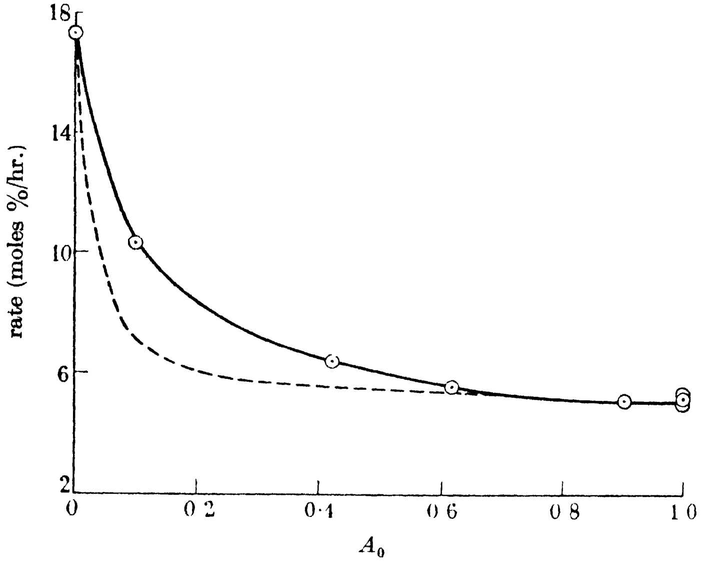

FIGURE 4. A comparison of the results of Norrish & Brookman with a theoretical curve for $\phi = 15$. - - - drawn with $\phi = 15$; —⊙— experimental points of N. & B.

Another very likely explanation for the discrepancy lies in the experimental technique used by N & B. The rate was not followed continuously throughout the reaction but was assumed constant, the rate being obtained by dividing the amount of polymer formed by the time of reaction. Now it is well known that methyl methacrylate exhibits a pronounced 'gel' effect (Trommsdorf, *BIOS Report*). As the amount of polymer formed increases, the rate of polymerization increases due to a hindering of the termination step by the increasing viscosity of the solution; such an effect was reported by N & B themselves. If the copolymer experiments were carried out at too high conversions, then the methyl methacrylate would tend to cause a gel effect and hence increased rates. As a result, the overall rates of N & B would be too high at large methyl methacrylate concentrations and so theory and experiment would be brought into better agreement. However, all things considered, the agreement can be considered reasonably good; once again, it seems likely that a value of $\phi = 15$ satisfactorily explains the nature of the behaviour found in this system.

Mayo & Lewis (1944) (hereinafter referred to as M & L) also provide some data on the rates of copolymerization of styrene and methyl methacrylate. Their reactions were carried out at 60° C, in the presence of 0·1 mol % of benzoyl peroxide. The experimental curve of M & L (determined from the data of expt. 4, table 1 of M & L), is shown in figure 5, together with the theoretical curve for $\phi = 15$.

M & L report: $R_b = 7{\cdot}85\,\%/\text{hr.}$, $R_a = 1{\cdot}60\,\%/\text{hr.}$

Hence $R_b/R_a = 4{\cdot}9.$

If δ_a and δ_b have the same activation energy, which seems quite likely, then $\delta_s = \delta_a/\delta_b$ will have the same value at all temperatures. Hence

$$(X_b/X_a)^{\frac{1}{2}} = 4{\cdot}9/2{\cdot}8 \quad \text{and} \quad X_b/X_a = 3{\cdot}10.$$

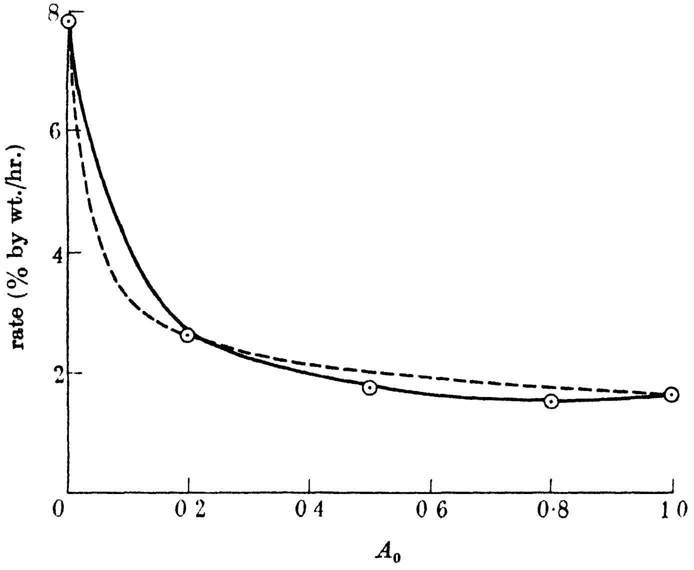

Figure 5. The results of Mayo & Lewis compared with theory. - - - calculated for $\phi = 15$; —⊙— results of Mayo & Lewis.

On the assumption that the rate of initiation varies linearly with the monomer composition, a theoretical curve was constructed with $\phi = 15$; this is plotted in figure 5. It can be seen that once again the theoretical and experimental curves are in quite good agreement. At low styrene concentrations, the theoretical curve lies slightly below the experimental one, while at higher styrene concentrations the position is reversed. Once again, then, it would seem that a value of $\phi = 15$ provides the best fit, although uncertainty as to the exact rate of initiation prevents any very accurate conclusions being drawn.

However, taking the results of N & B and M & L into conjunction with those obtained in the present work, there seems little doubt that a value of $\phi = 14$ is the most likely for this system. This involves the assumption that all types of radicals interact in termination by a disproportionation reaction, although it is not possible to state definitely whether or not combination of unlike radicals takes place to a certain extent.

Calculations on other copolymer systems

Although no accurate experiments have been made elsewhere with a view to elucidating the exact kinetics of copolymerization reactions, there are, scattered throughout the literature, various references to the rates of copolymerization. It is of some interest to consider these observations and see how they correspond with the findings for the system styrene-methyl methacrylate. Unfortunately, any conclusions from this type of examination cannot be regarded as definite, since usually the conditions were such that neither the rate of polymerization nor the rate of initiation can be obtained accurately. As a result, it is invariably necessary to make several assumptions about the rate of initiation. Since most of the systems studied were catalyzed by the thermal decomposition of benzoyl peroxide, it is usually necessary to assume that the peroxide will decompose at the same rate in both monomers and hence yield equivalent rates of initiation. This cannot be more than a first approximation, as it is well known that the rate of decomposition of benzoyl peroxide, for example, varies with the solvent. However, bearing these considerations and limitations in mind, it is possible to obtain some instructive information regarding the mechanism of these two-component systems.

One such example is provided by the data of Lewis, Mayo & Hulse (1945). In the course of an investigation into the reactivity ratios of a number of copolymer systems, they found the rates of copolymerization of equimolar mixtures of a number of monomer pairs, and also those of the pure monomers. These reactions were initiated by the thermal decomposition of benzoyl peroxide. If it is assumed that there is mutual termination, then the following relationship holds:

$$R_b/R_a = \delta_a/\delta_b \, . \, (X_b/X_a) = \delta_s \, . \, (X_b/X_a),$$

where the symbols have their usual significance.

If it now be assumed that the rate of initiation is constant for a fixed catalyst concentration, so that $X_a = X_b$, then $R_b/R_a = \delta_s$.

As a result, it is possible to calculate either the value of ϕ or the theoretical rate of copolymerization for the simple termination assumption ($k_{tab} = k_{ta}^{\frac{1}{2}} k_{tb}^{\frac{1}{2}}$). From table 1, part I, it can be seen that for the two termination possibilities, then:

$$\text{Rate} \propto \frac{1 + \dfrac{2(1-\mu)}{\mu}(A) + \dfrac{\sigma+\mu-2}{\mu}(A)^2}{1 + \left(\dfrac{\sigma}{\mu}\delta_s - 1\right)(A)} \tag{1}$$

or

$$\text{Rate} \propto \frac{1 + \dfrac{2(1-\mu)}{\mu}(A) + \dfrac{\sigma+\mu-2}{\mu}(A)^2}{\left\{1 + 2\left(\phi\dfrac{\sigma}{\mu}\delta_s - 1\right)(A) + \left(\dfrac{\sigma^2}{\mu^2}.\delta_s^2 - 2\phi\dfrac{\sigma}{\mu}\delta_s + 1\right)(A)^2\right\}^{\frac{1}{2}}}, \tag{2}$$

since $(X_a + X_b)$ is assumed constant.

Substituting the experimentally determined values of σ, μ, δ_s, and the rate of copolymerization for $(A)_0 = 0{\cdot}5$ in these expressions, the results shown in table 4 are obtained. In this table the calculated rate is that obtained from equation (1) above; the values of $1/\sigma\mu$ gives a measure of the difference in polarity between the two monomers (see below).

Since the calculated rate is higher than that found in every case, there must be some systematic error in the calculations. This error may be due to either of two causes, viz. (*a*) the rate of initiation is much lower for every monomer mixture than it is for either pure monomer, or (*b*) the ϕ factor must be greater than unity in every case. (It is, of course, possible that both factors are operating simultaneously.) Of these two alternatives, the latter seems more probable, so that a high ϕ factor would appear to be the rule rather than the exception. It is interesting to note that the value of ϕ as calculated above ($\phi = 17$) for styrene-methacrylate is in very good agreement with that reported in this work ($\phi = 14$).

TABLE 4. THE VALUE OF ϕ FOR VARIOUS MONOMER PAIRS

monomer pair *	rate (found) (%/hr.)	rate (calc.) (%/hr.)	ϕ	$1/\sigma\mu$
MM–VDC	3·9	6·0	6	1·6†
AN–VDC	4·9	13·5	45	2·9†
S–MM	1·7	3·84	17	4·2‡
MM–AN	4·7	10·0	200	5·6†
S–VDC	1·14	1·65	21	6·3§
S–AN	4·5	4·9	23	63·0†
S–BA	—	—	150	13·4‖

* S, styrene; MM, methyl methacrylate; AN, acrylonitrile; VDC, vinylidene chloride.
† Lewis *et al.* (1945).
‡ Lewis, Walling, Cummings, Briggs & Mayo (1948).
§ Mean of results of Lewis *et al.* (1945) and Doag (1948).
‖ E. J. Arlman, unpublished.

Another instructive case is the copolymerization of vinyl chloride and vinylidene chloride (Staudinger 1947). For this system, either with the benzoyl peroxide catalyzed bulk polymerization or the ammonium persulphate catalyzed emulsion polymerization, the two monomers had virtually the same rate of polymerization for any given catalyst concentration. Hence $\delta_s = \delta_a/\delta_b = (X_a/X_b)^{\frac{1}{2}}$. If $X_a = X_b$, then $\delta_s = 1{\cdot}0$; we also have that $\sigma = 0{\cdot}3$, $\mu = 3{\cdot}0$ (Mayo *et al.* 1947). Substituting the experimental results in equation (2), it was found that $\phi \approx 20$. Accordingly, theoretical curves were constructed with $\phi = 1$ and $\phi = 20$; these are compared with the experimental curves in figure 6.

The theoretical curve fits the experimental points very closely, except at the extreme minimum of the curve, where slightly higher values of ϕ would be required to bring the two curves into agreement. It may be, of course, that $X_a \neq X_b$, but it can easily be shown that this does not affect the result very much. If the controlling factor for the rate of initiation is not the absolute rate of decomposition of the peroxide but the rate of addition of the radicals to the monomer, then it might be expected that the vinylidene chloride would be initiated faster. This is because vinylidene chloride is about four more times reactive than vinyl chloride to all types of free radicals (as calculated from the reactivity ratios listed by Mayo *et al.* (1947)). We may then take

$$X_b = 4X_a, \quad \text{and hence} \quad \delta_s = 0{\cdot}5.$$

Using these values, ϕ was again calculated and it proved to have the value $\phi = 23$ (calculated for $(A) = 0{\cdot}3$).

An attempt was also made to interpret the results of Alfrey, Goldberg & Hohenstein (1946) on the copolymerization of styrene and chloroprene. There was, however, such a wide scatter in the experimental points (over 50 %) and it was impossible to draw any definite conclusions, although a value of $\phi = 1$ fitted the points quite well.

In nearly every system examined so far, a large ϕ factor has been disclosed, so that it appears that the phenomenon is a general one. Termination, then, seldom proceeds according to the simple scheme $k_{tab} = k^{\frac{1}{2}}_{taa} k^{\frac{1}{2}}_{tbb}$, but does so in a manner defined by $k_{tab} = \phi\, k^{\frac{1}{2}}_{taa} k^{\frac{1}{2}}_{tbb}$, with $\phi > 1$. This means that unlike radicals, i.e. radicals of different chemical type, interact more rapidly than do radicals of the same kind. This problem is discussed in the light of present views on radical reactivities in the next section.

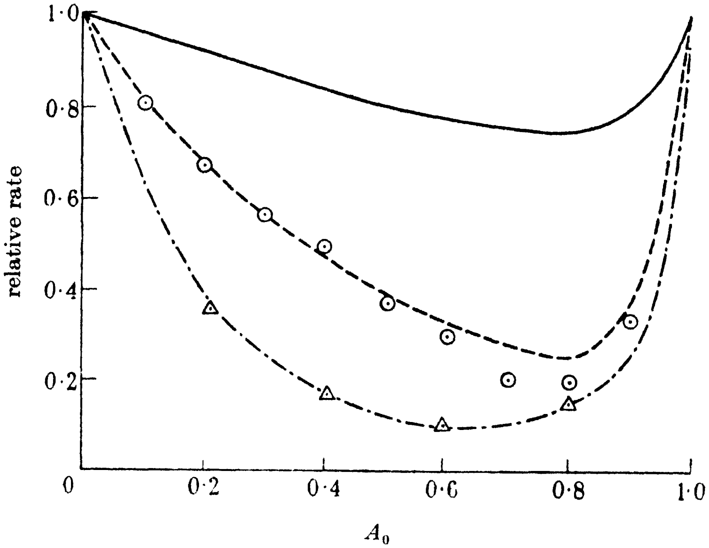

FIGURE 6. A comparison of theory and experiment for the copolymerization of vinylidene chloride and vinyl chloride. —— calculated for $\phi = 1$; ⊙ experimental points of Staudinger for benzoyl peroxide catalyzed reaction; - - - theoretical curve for $\phi = 20$; — . △ . — experimental curve of Staudinger for the ammonium persulphate catalyzed reaction.

A POSSIBLE ELECTRONIC EXPLANATION OF THE ϕ FACTOR

Arising from a study of transfer and copolymerization reactions, there has grown a considerable amount of knowledge relating to the reactivity of free radicals in polymerization reactions. As a result, it now seems that there are three main factors which determine the ease with which any given copolymerization may take place. These are (*a*) the general overall reactivities of the monomers to all types of radicals, (*b*) a tendency for monomers to alternate when entering the copolymer, and (*c*) steric effects.

The general reactivity of the monomer has usually been coupled with a resonance energy term, since it has been found that these monomers which possess the greatest amount of resonance stabilization are also the most reactive monomers towards free radicals in copolymerization. When two monomers compete for the same radical, then the monomer which forms the more stable adduct will be preferred, i.e. the monomer with the greater amount of resonance stabilization. Superimposed on this general reactivity is the tendency for monomers to alternate in entering the copolymer. In the case of complete alternation, each radical prefers to react with the other monomer, so that the monomer reactivity ratios are virtually zero and their product is zero. For the other extreme case, when there is no alternation, one reactivity ratio is the reciprocal of the other and their product is unity. The product of the reactivity ratios thus gives a measure of the tendency of the monomers to alternate.

Now, it is known that those copolymer pairs in which one monomer has an electron-repelling substituent and the other an electrophilic group copolymerize readily (Price 1946). Price has accordingly classified monomers according to whether they have a relatively positive or a relatively negative double bond, and attributes the alteration effect to the attraction between two monomers of opposing electrical charge. This theory seems to hold quite well for those monomer pairs in which one constituent is a negative monomer, e.g. styrene. There are numerous pairs of 'positive' monomers, however, which alternate strongly, e.g. acrylonitrile-vinyl chloride, vinyl acetate-vinylidene chloride. Alfrey & Price (1947) have developed these concepts on a quantitative basis with some degree of success. They assume that the controlling factor is the activation energy which is lowered by an electrical charge effect between radical and monomer. The rate constants for the addition of radical to monomer are defined by

$$k_{aa} = A_{aa}\exp(-\Delta F_{aa}/RT)$$

$$= A_{aa}\exp[-(p_a+q_a+\epsilon_a^2)]$$

and $$k_{ab} = A_{ab}\exp[-(p_a+q_b+\epsilon_a\epsilon_b)],$$

where A_{aa}, A_{ab} are probability factors, p_a is a general reactivity factor for the end-group, q_a, q_b are similar factors for the monomers and ϵ_a, ϵ_b are electrical (charge) terms. If it is assumed that $A_{aa} = A_{ab}$ and that the same charge is donated to the radical as to the monomer by any substituent, then

$$k_{aa} = P_aQ_a\exp(-\epsilon_a^2), \quad k_{ab} = P_aQ_b\exp(-\epsilon_a\epsilon_b),$$

where P_a is characteristic of radical a and Q_a, Q_b are general monomer reactivities. We thus have

$$\sigma = k_{aa}/k_{ab} = (Q_a/Q_b)\exp[-\epsilon_a(\epsilon_a-\epsilon_b)],$$

$$\mu = k_{bb}/k_{ba} = (Q_b/Q_a)\exp[-\epsilon_b(\epsilon_b-\epsilon_a)].$$

This approach has been criticised by several workers (Mayo *et al.* 1947), but it does give results of the correct order of magnitude. By an extension of this method, it is possible to derive analogous expressions for the velocity coefficients of termination reactions. For example, we may define

$$k_{taa} = A_{aa}P_a^2\exp(-\epsilon_a^2),$$

$$k_{tbb} = A_{bb}P_b^2\exp(-\epsilon_b^2),$$

$$k_{tab} = A_{ab}P_aP_b\exp(-\epsilon_a\epsilon_b),$$

where A_{aa}, A_{bb}, A_{ab} are probability factors, P_a, P_b are general reactivities of the radicals and ϵ_a, ϵ_b are again charge terms. Then

$$\phi^2 = \frac{k_{tab}^2}{k_{taa}\,k_{tbb}},$$

$$\phi^2 = \frac{A_{ab}^2}{A_{aa}A_{bb}} \exp\left(-2\epsilon_a\epsilon_b + \epsilon_a^2 + \epsilon_b^2\right)$$

$$= \frac{A_{ab}^2}{A_{aa}A_{bb}} \exp\left(\epsilon_a - \epsilon_b\right)^2$$

But $\sigma\mu = \exp - (\epsilon_a - \epsilon_b)^2$.

Therefore $$\phi^2 = \frac{A_{ab}^2}{A_{aa}A_{bb}} \frac{1}{\sigma\mu}.$$

This expression for ϕ is naturally divided into two parts, the first giving a measure of the steric effects and the second a measure of the difference in polarity between the two radicals. The value of ϕ is proportional to the square root of $1/\sigma\mu$, a factor which, as was pointed out above, gives a pointer to the degree of alternation for the two monomers. This would seem to imply that substituents have precisely the same effect on the radicals as on the parent monomers. This assumption has been widely made in such investigations, although it is rather doubtful whether it can be true. Substituents affect the distribution of electrical charge mainly by two mechanisms, viz. (*a*) a direct inductive effect, (*b*) a resonance effect (Price's 'polarizing force'). This second resonance effect can be made effective only if polarizable, labile π-electrons are present in the molecule. For example, the phenyl substituent group in styrene enters into conjugation with the olefinic double bond, and as a result the electrical charge distribution is modified appreciably. If a free radical adds on to the molecule of the styrene monomer then the conjugation is destroyed, and weak resonance interaction only is possible with the odd electron. From these considerations, it would appear that only the direct inductive effects are likely to effect any marked change in the charge distribution of the monomeric free radicals. This may not affect the question of polar interaction between two radicals, however, since in all probability it is the charge on the radical as a whole which is the determining factor, i.e. the charge developed as a result of an inductive effect.

This theory can be tested to some extent by a comparison of the ϕ values for various monomer pairs and the alternation factor, $1/\sigma\mu$ (table 4). In every case listed there, there is an appreciable ϕ factor; $1/\sigma\mu$ is also always greater than unity, indicating that the monomers tend to alternate in entering the copolymer. There is a certain degree of parallelism between ϕ and $1/\sigma\mu$, more especially if the two pairs acrylonitrile-vinylidene chloride and acrylonitrile-methyl methacrylate are omitted. Unfortunately, all these monomer pairs, with the exception of styrene-methyl methacrylate, will form insoluble copolymers, so that the termination reaction will undoubtedly be more complicated than is assumed in the theory presented above. For example, it was shown that the behaviour of the system vinyl chloride-vinylidene chloride could be adequately described in terms of a high ϕ factor ($\phi = 20$), although these two monomers copolymerize almost ideally ($\sigma = 0{\cdot}3$, $\mu = 3{\cdot}0$, $1/\sigma\mu = 1{\cdot}1$).

This is presumably to be attributed to the fact that the copolymer is precipitated out from all monomer mixtures, with consequent adsorption of the monomers and a gel effect. The termination mechanism will be much more affected by such irregularities than will the propagation step, so that the discrepancy between the behaviour of the system in the growth and cessation reactions is readily understood. In this case, no doubt, steric factors are playing the predominant role, although it is difficult to see why the frequency factor for the interaction of two different radicals should be higher than those for the two individual monomers.

For the system styrene-methyl methacrylate, the only one for which accurate data are available, there is undoubtedly a large ϕ factor. The product $\sigma\mu$ for this pair is $\sigma\mu = 0{\cdot}205$ (Lewis *et al.* 1948), and substituting the values of ϕ and $\sigma\mu$ in equation (3), we have

$$\frac{A_{ab}^2}{A_{aa}A_{bb}} = 40.$$

This would indicate that the frequency factor for the interaction of styrene and methacrylate radicals is 6 to 7 times greater than those for the interaction of two radicals of the same type. For styrene (A)-methyl methacrylate (B) we have

$$k_{tab} = 2{\cdot}06 \times 10^8, \quad k_{taa} = 8 \times 10^6, \quad \text{(part I)},$$

$$k_{tbb} = 2{\cdot}7 \times 10^7 \text{ (part I)}, \quad E_{taa} \approx E_{tbb} = 2\,\text{kcal. (Bamford \& Dewar 1947)},$$

and hence

$$A_{aa} = 2{\cdot}2 \times 10^8, \quad A_{bb} = 7{\cdot}5 \times 10^8 \quad \text{and} \quad A_{ab} = 2{\cdot}6 \times 10^9.$$

Substituting this value in the expression $k_{tab} = A_{ab} \exp(-E_{tab}/RT)$, where $k_{tab} = 2{\cdot}06 \times 10^8$, $T = 303^\circ$ K, then $E_{tab} = 1{\cdot}5$ kcal., i.e. the activation energy for termination of two unlike radicals is 500 cal. less than that for the interaction of two radicals of the same type. This must not be taken as an accurate value for the activation energy, but does give some idea of the magnitude of the quantities involved.

It will be obvious from this discussion that the problem of determining the (presumed) reduction in the energy of activation for the interradical reactions will be extremely difficult. The usual experimental error in such determinations is of the order of ± 1 kcal. so that the lowering may not be detectable, especially since the energy of activation of the termination step is the most difficult one to determine experimentally.

One of us (L.V.) is indebted to the Department of Scientific and Industrial Research for the award of a maintenance grant.

REFERENCES

Alfrey, T., Goldberg, A. I. & Hohenstein, W. P. 1946 *J. Amer. Chem. Soc.* **68**, 2464.
Alfrey, T. & Price, C. C. 1947 *J. Polymer Sci.* **2**, 101.
Arlman, E. J. Unpublished.
Bamford, C. H. & Dewar, M. J. S. 1947 *Faraday Soc. Disc.* **2**, 310.
Burnett, G. M. & Melville, H. W. 1947 *Proc. Roy. Soc.* A, **189**, 456.

Cohen, S. G., Ostberg, B. E., Sparrow, D. B. & Blout, E. R. 1948 *J. Polymer Sci.* **3**, 264.
Doag, K. W. 1948 *J. Amer. Chem. Soc.* **70**, 1525.
Lewis, F. M., Mayo, F. R. & Hulse, W. F. 1945 *J. Amer. Chem. Soc.* **67**, 1701.
Lewis, F. M., Walling, C., Cummings, W., Briggs, E. R. & Mayo, F. R. 1948 *J. Amer. Chem. Soc.* **70**, 1519.
Mayo, F. R. 1948 *J. Amer. Chem. Soc.* **70**, 3689.
Mayo, F. R. & Lewis, F. M. 1944 *J. Amer. Chem. Soc.* **66**, 1594.
Mayo, F. R., Lewis, F. M. & Walling, C. 1947 *Faraday Soc. Disc.* **2**, 285.
Melville, H. W. & Valentine, L. 1949 *Trans. Faraday Soc.* (in the Press).
Norrish, R. G. W. & Brookman, E. F. 1939 *Proc. Roy. Soc.* A, **171**, 147.
Price, C. C. 1946 *J. Polymer Sci.* **1**, 83.
Price, C. C. 1946 *Reactions at carbon-carbon double bonds.* New York: Interscience.
Rodebush, W. H. & Feldman, I. 1946 *J. Amer. Chem. Soc.* **68**, 897.
Staudinger, H. P. 1947 *Chem. & Ind.* **45**, 685.

The mechanics of large bubbles rising through extended liquids and through liquids in tubes

By R. M. Davies and Sir Geoffrey Taylor, F.R.S.

(*Received* 13 *September* 1949)

Part I describes measurements of the shape and rate of rise of air bubbles varying in volume from 1·5 to 200 cm.^{3} when they rise through nitrobenzene or water.

Measurements of photographs of bubbles formed in nitrobenzene show that the greater part of the upper surface is always spherical. A theoretical discussion, based on the assumption that the pressure over the front of the bubble is the same as that in ideal hydrodynamic flow round a sphere, shows that the velocity of rise, U, should be related to the radius of curvature, R, in the region of the vertex, by the equation $U = \frac{2}{3}\sqrt{(gR)}$; the agreement between this relationship and the experimental results is excellent.

For geometrically similar bubbles of such large diameter that the drag coefficient would be independent of Reynolds's number, it would be expected that U would be proportional to the sixth root of the volume, V; measurements of eighty-eight bubbles show considerable scatter in the values of $U/V^{\frac{1}{6}}$, although there is no systematic variation in the value of this ratio with the volume.

Part II. Though the characteristics of a large bubble are associated with the observed fact that the hydrodynamic pressure on the front of a spherical cap moving through a fluid is nearly the same as that on a complete sphere, the mechanics of a rising bubble cannot be completely understood till the observed pressure distribution on a spherical cap is understood. Failing this, the case of a large bubble running up a circular tube filled with water and emptying at the bottom is capable of being analyzed completely because the bubble is not then followed by a wake. An approximate calculation shows that the velocity U of rise is $U = 0{\cdot}46\sqrt{(ga)}$, where a is the radius of the tube. Experiments with a tube 7·9 cm. diameter gave values of U from 29·1 to 30·6 cm./sec., corresponding with values of $U/\sqrt{(ga)}$ from 0·466 to 0·490.

PART I

1. Introduction and experimental method

The rise of gas bubbles in liquids has been studied by several workers (Allen 1900; Hoefer 1913; Miyagi 1925, 1929), but in all the work so far published the bubbles have been so small that the results are not applicable to the study of the rise of large volumes of gas, such as those produced in submarine explosions. In the experiments here described, bubbles ranging in volume from 1·5 to 34 cm.^{3} were formed in nitrobenzene contained in a tank, 2 ft. × 2 ft. × 2 ft. 6 in., filled to a depth of about 2 ft. with the liquid. The bubbles were photographed by spark photography at intervals of about 10 msec. (1 msec. $= 10^{-3}$ sec.), using a revolving drum camera, and appropriate spark timing. In some further experiments, bubbles covering a range of volume from 4·5 to 200 cm.^{3} were formed in a cylindrical tank, 2 ft. 6 in. diameter, filled with water to a depth of 3 ft. 6 in., and their mean velocity of rise over a measured distance was determined. In both sets of experiments, the air volume was determined by collecting the bubble in a graduated glass cylinder.

Considerable difficulty was found in producing single, large bubbles of gas, and the method finally adopted was to pivot an inverted beaker containing air, which was then tilted so that the air was released. In general, the air is released from the beaker in a stream of bubbles of varying sizes, but by adjusting the rate of tilting, it was found possible to arrange that the air was spilled into a single bubble.

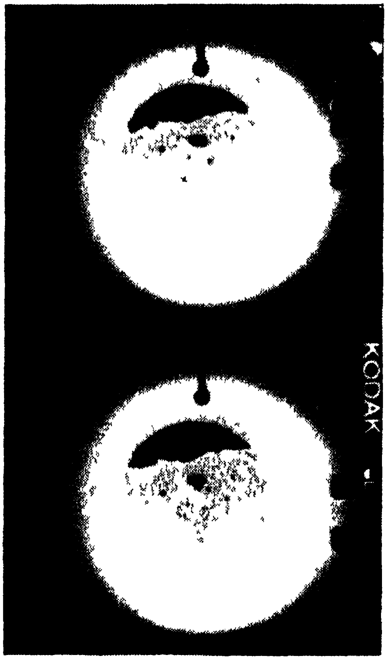

Figure 1. Successive spark photographs of an air-filled bubble rising in nitrobenzene. Time interval between photographs = 10·3 msec. Velocity of rise of bubble = 36·7 cm./sec. Diameter of steel ball in the upper part of the photographs = $\frac{1}{4}$ in.

Two successive photographs of a typical bubble formed in this way in nitrobenzene are shown in figure 1, the time interval between the two photographs being 10·3 msec. In addition to the bubble, the photographs show a steel ball, $\frac{1}{4}$ in. diameter, soldered at the lower end of a vertical rod immersed in the liquid; this arrangement was used to find the scale of the photographs and to give a reference mark from which the vertical displacement of the bubble could be measured.

The uniformity of the velocity of rise of the bubbles may be judged by figure 2, in which time, t, and the vertical displacement, X, of two bubbles are plotted as abscissae and ordinates, respectively. The actual measured values of X and t for the bubble of figure 1 are indicated by the circular dots in figure 2, and those for a second, larger bubble by crosses; the straight lines of closest fit drawn through the observed points are denoted by A and B respectively. It will be seen that the scatter of the experimental points is not excessive, and that the velocity of rise, U, of the two bubbles is reasonably constant over the interval measured.

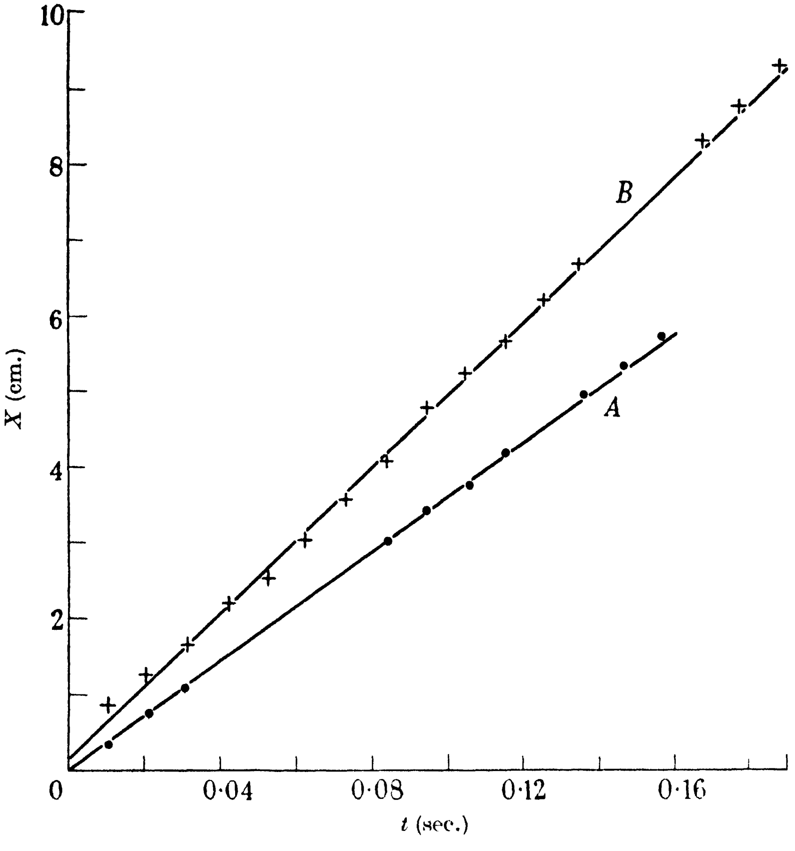

FIGURE 2. (Displacement, time) curves deduced from photographs of rising bubbles. •, + Experimental values; curve A, $U = 36{\cdot}7$ cm./sec.; curve B, $U = 48{\cdot}2$ cm./sec.

The shape of the profile of the bubbles was found by measuring the films on a travelling microscope fitted with two independent motions at right angles to one another. The results for the lower photograph of figure 1 are shown graphically in figure 3, where the circular dots represent points on the central, regular portion of the profile of the bubble, deduced from the microscope readings. In figure 3, the vertical and horizontal axes are parallel to the corresponding axes in the tank, and the origin is taken at the uppermost point on the bubble; the dimensions given refer to the actual size of the bubble. The crosses with vertical axes and with axes at 45° to the vertical in figure 3 represent points on the profile of the same bubble, obtained from measurements of photographs taken 105·7 and 132·5 msec. earlier than the lower photograph of figure 1. The agreement between the three sets of points shows that the shape of the cap of the bubble undergoes very little variation over the range of time covered by the three photographs.

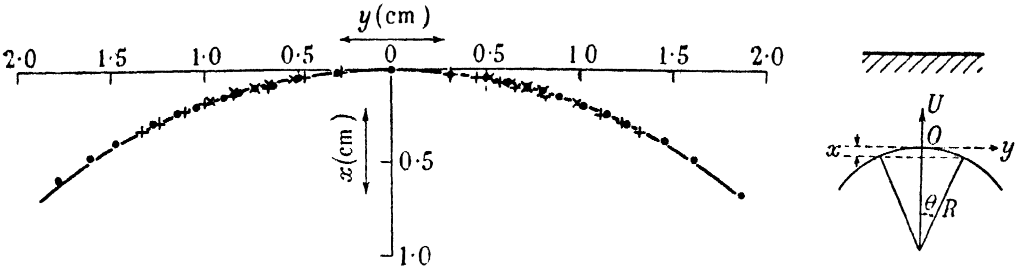

Figure 3. Shape of the profile of a bubble. • Bubble shown in the lower photograph of figure 1; + the same bubble 0·106 sec. earlier; × the same bubble 0·133 sec. earlier; —— an arc of circle of radius 3·01 cm.

The curve in figure 3 is an arc of circle of radius 3·01 cm., drawn to pass through the origin, and since the scatter of the observed points around this curve is within the limits of the errors made in measuring the film, the upper part of the bubble is a portion of a sphere within the experimental error. It is worth noticing that the angle subtended at the centre of the circle by the arc in figure 3 is about 75°, whilst the angular width of the whole bubble in figure 1 (referred to the centre) is about 90°.

2. EXPLANATION OF WHY THE TOP OF LARGE BUBBLES IS SPHERICAL

The perfection of the spherical shape of the top of the bubble led us to consider the condition which must be satisfied at its surface. The pressure there may be taken as constant, for the variations in pressure through the interior air must be so small as to be negligible. The pressure in the fluid outside the bubble is due to the dynamics of the flow round it, and to gravity. The condition that the pressure at the surface of the bubble is constant requires that these two causes shall neutralize one another. Applying Bernoulli's equation to steady flow relative to the bubble, which is assumed to be symmetrical so that the relative velocity at its highest point is zero, the surface condition is

$$q^2 = 2gx, \tag{2·1}$$

where x is the depth below the highest point, q the fluid velocity relative to the bubble and g is the acceleration of gravity.

The bubbles were observed to be spherical above and more or less flat beneath. It is not possible to calculate the flow round such a shape. Recourse was therefore had to experiment. Three models were made in brass, each had a spherical surface 1 in. radius and a flat under-surface. Small pressure holes were bored in both surfaces of each model. They were set up in a wind tunnel and the pressure distribution determined at a wind speed of 15 m./sec. The angles, θ_m, between the polar axes of the models and the radii to their rims were 75°, 55° and 30°, a range which more than covered the values observed in bubbles. The results are given in non-dimensional form in figure 4, when $(p_\theta - p_0)/\frac{1}{2}\rho U^2$ is plotted against θ, the angle which the radius from the centre of the sphere makes with the polar axis. Here p_θ is the pressure at angle θ, p_0 that at the vertex and $\frac{1}{2}\rho U^2$ the pitot pressure in the tunnel. It has long

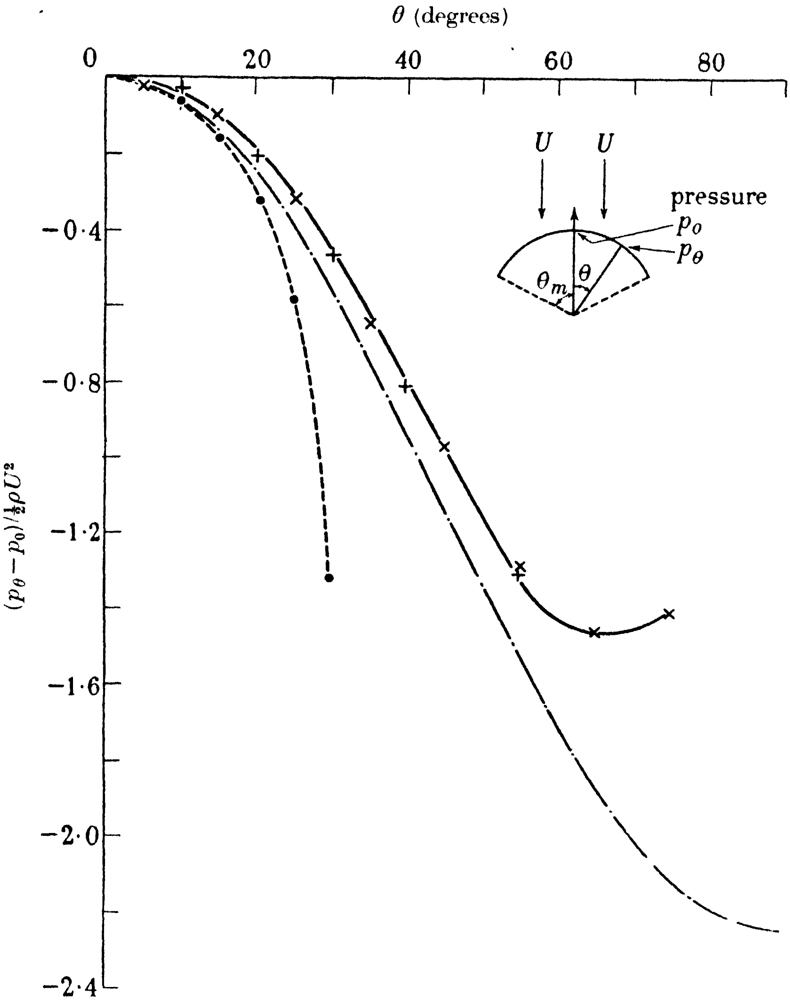

FIGURE 4. The variation of pressure over the surfaces of lenticular bodies in a wind tunnel. Experimental values: • $\theta_m = 30°$; + $\theta_m = 55°$; × $\theta_m = 75°$; ·—· · theoretical curve for a sphere, assuming ideal fluid flow.

Mean pressures p_b on the backs of the bodies:

θ_m	30	55°	75°
$(p_b - p_0)/\frac{1}{2}\rho U^2$	−1·32	−1·39	−1·41

been known that when a sphere is set up in a wind tunnel, the pressure distribution over a large part of the windward side is rather nearly the same as the theoretical distribution of pressure over a sphere obtained by classical methods using velocity potential. This is true even though the flow behind the sphere bears no relationship to the theoretical flow. For this reason the theoretical pressure distribution round a complete sphere was calculated from the well-known expression

$$\frac{q^2}{U^2} = \frac{p_0 - p_\theta}{\frac{1}{2}\rho U^2} = \tfrac{9}{4}\sin^2\theta, \tag{2·2}$$

and shown in figure 4. It will be seen that the measured distributions over all the lenticular bodies are rather close to the theoretical distribution for a sphere in the range $0 < \theta < 20^\circ$. The 55° and 75° bodies retain this property nearly out to their edges, but the drop in pressure below that at the vertex at any point is rather less than the theoretical value.

The observed values of $(p_0 - p_\theta)/\frac{1}{2}\rho U^2$, which may be equated to q^2/U^2, have been taken from the faired curve for $\theta_m = 55^\circ$ and 75° in figure 4, and their values are given in the first row of table 1. In the next row are tabulated the values of $x/R = 1 - \cos\theta$, where R is the radius of the spherical surface of the lenticular body. Below these are given the values of $q^2/U^2(1-\cos\theta) = q^2R/U^2x$. It will be seen that this ratio is nearly constant, its mean value being 3·28.

TABLE 1

θ	15°	20°	25°	30°	35°	40°	45°	50°
$\dfrac{q^2}{U^2} = \dfrac{p_0 - p_\theta}{\frac{1}{2}\rho U^2}$	0·10	0·192	0·315	0·465	0·628	0·805	0·975	1·144
$1 - \cos\theta$	0·0341	0·0603	0·0937	0·1340	0·1808	0·2340	0·2929	0·3572
$\dfrac{q^2}{U^2(1-\cos\theta)}$	2·94	3·18	3·25	3·44	3·47	3·44	3·33	3·20

Mean value of $\dfrac{q^2}{U^2(1-\cos\theta)} = 3{\cdot}28.$

The condition (2·1) that bubbles of lenticular shape may have constant pressure over their spherical surfaces is satisfied if $q^2R/U^2x = 3{\cdot}28$ is identical with $q^2 = 2gx$. Eliminating x/q^2

$$U^2 = 2gR/3{\cdot}28 = 0{\cdot}61\,gR \quad \text{or} \quad U = 0{\cdot}78\sqrt{(gR)}. \tag{2·3}$$

If the pressure had been exactly the same as the calculated pressure over a complete sphere, the condition (2·1) could be satisfied over the portion near the stagnation point only, for in that case $q^2 = \frac{9}{4}U^2\sin^2\theta$ and $x = R(1-\cos\theta)$, so that $q^2/x = 2g$ if

$$\frac{U^2}{gR} = \frac{8}{9}\left(\frac{1-\cos\theta}{\sin^2\theta}\right).$$

When θ is small, $(1-\cos\theta)/\sin^2\theta \to \frac{1}{2}$, so that the pressure condition would be satisfied near the stagnation point, i.e.

$$U^2 = \tfrac{4}{9}gR \quad \text{or} \quad U = \tfrac{2}{3}\sqrt{(gR)}. \tag{2·4}$$

3. COMPARISON WITH OBSERVATION

Fourteen bubbles, rising in nitrobenzene, were photographed. The results of the measurement of the films are summarized in table 2, where the first three columns give the volume V of the bubbles, the radius of curvature R and the velocity of rise U.

The fourth column gives the maximum transverse dimension $2A$, and the fifth column $\theta_m = \sin^{-1} A/R$. The sixth column gives the drag coefficient, C_D, of the bubble calculated from the equation

$$C_D . \pi A^2 . \tfrac{1}{2}\rho U^2 = g\rho V. \tag{3·1}$$

TABLE 2. BUBBLES IN NITROBENZENE

volume V (cm.^{3})	radius of curvature R (cm.)	velocity U (cm./sec.)	maximum transverse dimension, $2A$ (cm.)	$\theta_m = \sin^{-1}$ A/R	drag coefficient C_D	Reynolds number Re
1·48	2·41	29·2	2·86	36·4°	0·53	2780
3·50	2·09	29·6	3·14	48·6	1·02	3090
4·06	2·04	28·9	3·48	58·3	1·00	3360
4·31	2·17	28·0	3·16	46·8	1·37	2950
6·40	2·78	35·5	4·98	63·6	0·52	5900
7·30	2·65	34·2	4·40	56·1	0·80	5010
8·02	2·67	34·0	4·23	52·5	0·97	4790
—	3·01	36·7	—	—	—	—
8·80	3·17	37·2	5·26	56·1	0·58	6520
9·18	2·77	33·0	4·53	55·8	1·00	5020
18·40	3·30	37·3	5·10	50·7	1·27	6340
21·25	3·51	38·1	5·85	56·5	1·07	7440
28·1	4·16	43·0	—	—	—	—
33·8	4·27	42·1	6·19	46·5	1·25	8700
—	4·84	48·2	—	—	—	—

The last column gives the Reynolds number Re

$$Re = UA/\nu. \tag{3·2}$$

The viscosity of nitrobenzene is 0·018 poise at 14° C and the density 1·2 g./cm.^{3}, so that $\nu = 0·015$ cm.^{2}/sec.

The experimental values of U are plotted against $\sqrt{R}$ in figure 5. It will be seen that they lie closely scattered round the line $U = \frac{2}{3}\sqrt{(gR)}$ and well below the line $U = 0·78\sqrt{(gR)}$.

It is curious that the experiments agree better with the arbitrary assumption that flow over the forward part of the bubble is the same as that calculated for a sphere moving in a frictionless liquid than with calculations based on the pressure distribution measured over the surface of a solid of nearly the same shape as the bubble.

It will be noted, however, that the flow of the liquid near the front of a bubble would be expected to be more nearly a truly irrotational one than that near a solid body, because in the latter case a boundary layer would necessarily be present, whereas in the former the air in the bubble would cause no appreciable drag so that no boundary layer would be formed. The closeness with which the observed points fit the line $U = \frac{2}{3}\sqrt{(gR)}$ is remarkable. This suggests that the flow near the front of a bubble must be very close indeed to the theoretical flow near the front of a complete sphere in an inviscid fluid.

It will be noticed in figure 5 and in table 2 that C_D is much more variable than $U/\sqrt{R}$. These values of C_D are plotted as a function of θ_m in figure 6, and those found by integrating the observed pressures on the lenticular bodies in the wind tunnel are shown on the same figure.

It will be seen that there is considerable scatter, in the case of the bubbles, from the mean line representing the variation of C_D with θ_m, and that the line representing the values of C_D for the lenticular bodies is quite different from that representing the bubbles.

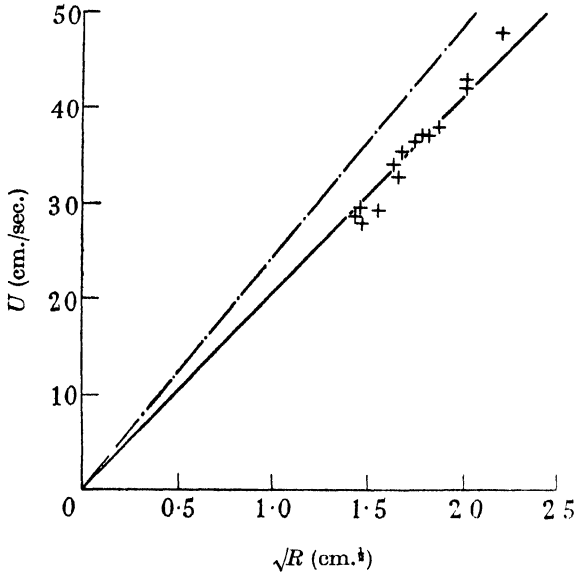

FIGURE 5. The relationship between the velocity of rise, U, of a bubble and the radius of curvature, R. + experimental values; — · — $U = 0{\cdot}78\sqrt{(gR)}$; —— $U = \frac{2}{3}\sqrt{(gR)}$.

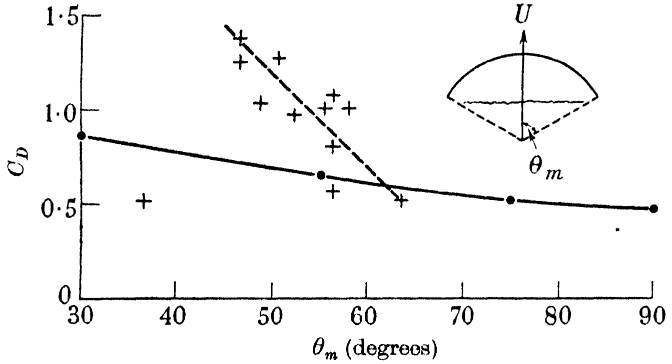

FIGURE 6. The experimental relationship between drag coefficient, C_D, and the semi-vertical angle, θ_m, subtended at the centre. + values for bubbles rising in nitrobenzene; • values for lenticular bodies in the wind tunnel.

4. THE RELATIONSHIP BETWEEN VOLUME AND RATE OF RISE OF A BUBBLE

If all the bubbles were geometrically similar the dimension A could be expressed by

$$A = \alpha V^{\frac{1}{3}}, \tag{4·1}$$

where α would then be constant. If also the drag coefficient were constant, (3·1) shows that U would be proportional to $V^{\frac{1}{6}}$; in fact, (3·1) can be expressed in the form

$$UV^{-\frac{1}{6}} = \sqrt{(2g/\pi\alpha^2 C_D)} = 25{\cdot}0/\alpha\sqrt{C_D}\,\text{cm.}^{\frac{1}{2}}\,\text{sec.}^{-1}. \tag{4·2}$$

To test how far the assumption that α and C_D and therefore $\alpha\sqrt{C_D}$ are constant, measurements were made involving thirteen bubbles rising in nitrobenzene and seventy-five in water. The results are shown in figure 7, where $UV^{-\frac{1}{6}}$ is plotted against $V^{\frac{1}{6}}$, U being expressed in cm./sec. and V in cm.^{3}. The experimental results of Miyagi and Hoefer with smaller bubbles are also shown.

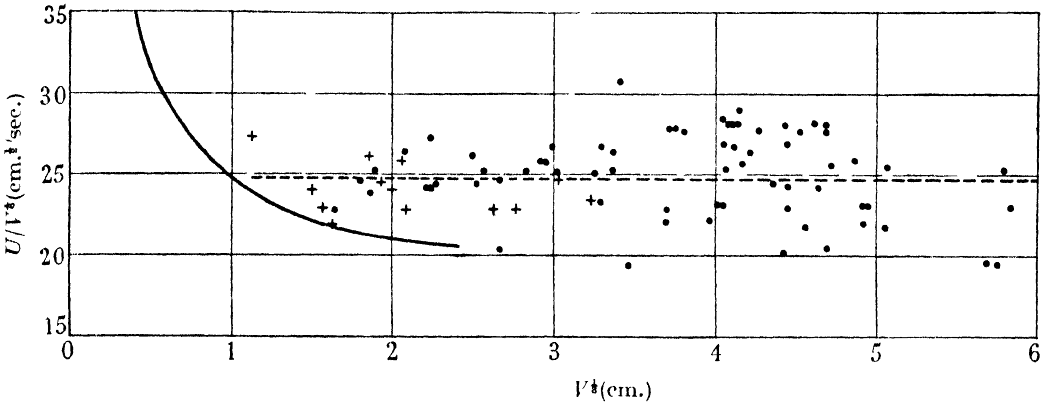

FIGURE 7. Experimental results for the velocity of rise, U, of a bubble of volume V. + bubbles in nitrobenzene; • bubbles in water; - - - $UV^{-\frac{1}{6}} = 24{\cdot}8$ (mean value); —— Miyagi and Hoefer results.

Though there is considerable scatter about the line

$$UV^{-\frac{1}{6}} = 24{\cdot}8, \tag{4·3}$$

which represents the mean value giving equal weight to all the observations, figure 7 shows that there is no systematic variation in $UV^{-\frac{1}{6}}$ with V, and that the experiments in water and nitrobenzene give the same value of $UV^{-\frac{1}{6}}$. It is of interest to compare this experimental result with (4·2). In order that bubbles may ascend with the velocity $24{\cdot}8\,V^{\frac{1}{6}}$, which represents the mean of the experimental values,

$$\alpha\sqrt{C_D} = \frac{25{\cdot}0}{24{\cdot}8} = 1{\cdot}0 \text{ approximately.} \tag{4·4}$$

It is of interest to note in table 2 that the mean value of C_D for the experiment in nitrobenzene is about 1·1. The value of α cannot be calculated unless the shape of the bottom of the bubble is known, but if the bubble were enclosed between a spherical upper surface and a flat lower one it can be shown that

$$\alpha^3 = \frac{3\sin^3\theta_m}{\pi(2-3\cos\theta_m+\cos^3\theta_m)}.$$

The values of α for a series of values of θ_m are shown in table 3.

TABLE 3

θ_m	30°	40°	50°	60°	70°	80°	90°
α	1·32	1·18	1·07	0·99	0·91	0·85	0·78

It will be seen that in range $\theta_m = 46^\circ$ to $\theta_m = 64^\circ$, which contains all the experimental values in table 2, except that found for the smallest bubble, α is within 10 % of 1·0.

Example. Application to the bubble of gas released in a submarine explosion

When an explosive detonates under water, a mass of gas which is known, at any rate approximately, is suddenly produced. The volume of this bubble oscillates violently at first, but after a short time this oscillation ceases and the bubble rises and finally reaches the surface. It is of interest to calculate how fast such a bubble would rise if it behaved like those described in the foregoing experiments. A charge of say 300 lb. of amatol might be expected to produce about $8{\cdot}8 \times 10^7$ cm.^{3} of gas at atmospheric pressure after the steam produced in the explosion had had time to condense.

The formula (4·3) gives then

$$U = 525\,\text{cm./sec.} = 17{\cdot}2\,\text{ft./sec.}$$

5. TURBULENCE IN THE WAKE BEHIND A BUBBLE

In the original photographs of bubbles in nitrobenzene, a region of turbulence is clearly shown behind the large bubble. This is due no doubt to some anisotropic optical property of nitrobenzene when subjected to viscous stresses. That such stresses exist could be inferred from the fact that, in the photograph shown in figure 1, the largest of the small bubbles in the wake of the large one is not spherical and is rapidly changing in shape. This bubble has a diameter of about 6 mm. Still smaller bubbles are less distorted, and one of diameter about 2 mm., seen to the left side of the 6 mm. bubble, is distorted so that its length to diameter ratio is about 1·1.

The rate of shear which might be expected to produce a distortion of this amount has been calculated by Taylor (1934). In the field of flow represented by the equations

$$u = Cx, \quad v = -Cy, \quad w = 0, \tag{5·1}$$

an air bubble of mean radius a would be pulled out so that

$$\frac{L-B}{L+B} = \frac{2C\mu a}{T}, \tag{5·2}$$

where L and B are the length and breadth of the bubble and μ and T the viscosity and the surface tension of the liquid. For nitrobenzene, $\mu = 0{\cdot}018$ poise, $T = 43{\cdot}9$ dynes/cm., so that for the 2 mm. bubble, $a = 0{\cdot}1$ cm., $L/B = 1{\cdot}1$ and $(L-B)/(L+B) = 0{\cdot}05$, giving

$$C = \frac{0{\cdot}05 \times 43{\cdot}9}{2 \times 0{\cdot}018 \times 0{\cdot}1} = 6{\cdot}1 \times 10^2\,\text{sec.}^{-1}.$$

The rate W of dissipation of energy per cm.^{3} in the flow represented by equation (5·1) is

$$W = \mu\left\{\left(\frac{\partial u}{\partial x}\right)^2 + \left(\frac{\partial v}{\partial y}\right)^2\right\} = 2\mu C^2 = 1{\cdot}34 \times 10^4\,\text{ergs/cm.}^3\text{/sec.}$$

If the rate of dissipation were constant through the wake, and if wake extends over the whole of the region which appears disturbed in figure 1, namely, through a diameter of 5·9 cm. and a length of 3·8 cm., the total rate of dissipation in the wake is

$$\begin{aligned}&1{\cdot}34\times10^4\times(\text{volume of wake})\\ &=1{\cdot}34\times10^4\times\tfrac{1}{4}\pi\times(5{\cdot}9)^2\times3{\cdot}8\\ &=1{\cdot}4\times10^6\,\text{ergs/sec.}\end{aligned}$$

The total rate of dissipation would be known if the drag coefficient, C_D, of the large bubble were known. Since the density ρ of nitrobenzene is 1·2 g./cm.³, whilst the velocity of rise, U, of the large bubble in this experiment was 36·7 cm./sec. and its maximum transverse dimension, $2A$, was 5·1 cm., the total rate of dissipation was

$$\begin{aligned}&C_D\,.\,\tfrac{1}{2}\rho U^2\,.\,\pi A^2\,.\,U\\ &=C_D\{\tfrac{1}{2}\times1{\cdot}20\times36{\cdot}7^3\times\pi\times(2{\cdot}55)^2\}\\ &=6{\cdot}1\times10^5\,C_D\,\text{ergs/sec.}\end{aligned}$$

Since C_D is found to be of the order of 1·0 (see table 2), it will be seen that the rate of dissipation which would distort the bubbles by the observed amount is of the same order as that deduced from the rate of rise.

For the largest of the small bubbles in the wake, viscous stresses would produce such a distortion that the formula (5·2) would not be expected to apply.

PART II. EMPTYING WATER FROM A VERTICAL TUBE

6. Theoretical discussion

It has been seen that large bubbles in water assume a form which is very nearly the lenticular volume contained between a sphere and a horizontal plane cutting it above its centre. The pressure distribution over the spherical surface is found experimentally to be approximately the same as that calculated for a complete sphere moving in an ideal fluid. This pressure, together with the hydrostatic pressure due to gravity, leads to a uniform surface pressure when the velocity of rise, U, is

$$U=\tfrac{2}{3}\sqrt{(gR)},$$

R being the radius of the upper surface of the bubble.

It has been found that when the rate of rise and radius of curvature of large bubbles have been measured simultaneously, these quantities do in fact very nearly satisfy this relationship.

This result depends on the observed fact that the pressure distribution over the forward portion of a lenticular shaped body is nearly the same as the theoretical distribution over a complete sphere. This empirical observation makes it possible to have a partial understanding of why it is that the upper surface of a large rising bubble is so nearly spherical, but it does not lead to a complete understanding because the relationship between the shape of the bubble and the pressure distribution over its surface is not understood. The main difficulty in this matter is to obtain a correct description of the currents in the wake which follows the nearly flat lower surface of the bubble.

For this reason we may consider the case where the bubble is confined inside a circular tube. In this case the fluid can run round the outside of the bubble and remain as a layer running down the surface of the tube and falling freely under gravity. In this case it is not necessary for the bubble to have a lower surface. The tube, in fact, is open to the atmosphere at its lower end. The problem thus posed is capable of being solved completely. The question to be answered is 'How fast will the air column rise in a vertical tube with a closed top when the bottom is opened?' Or, alternatively, 'How fast will a vertical tube with a closed top empty itself when the bottom is opened?'

If U is the velocity of rise of the air column in a tube of radius a, the flow can be brought to a steady motion by giving the whole system a downward velocity U. The top of the air column is now at rest, and if x is the depth below this, the condition which must be satisfied at points on the free surface of the air column is

$$q^2 = 2gx, \tag{6·1}$$

where q is the velocity of the liquid and g is the acceleration due to gravity.

The problem is, therefore, to find the shape of a body of revolution which if inserted in a circular tube will leave a space through which a perfect fluid could flow so that the velocity at its surface would be proportional to $\sqrt{x}$.

This problem could be solved by relaxation methods, but a rough approximation to the flow near the top of the air column may be obtained as follows:

The velocity potential

$$\phi = \mathrm{e}^{K_n x/a} J_0(K_n r/a) \tag{6·2}$$

represents a flow contained in a tube of radius a provided K_n is a root of the equation $J_1(z) = 0$. Here J_0 and J_1 are Bessel functions. The flow has the property that it dies away to zero, when x has large negative values.

The flow represented by

$$\phi = -Ux + \sum_n A_n \mathrm{e}^{K_n x/a} J_0(K_n r/a) \tag{6·3}$$

and by the Stokes stream function

$$\psi = -\tfrac{1}{2}Ur^2 + r\sum_n A_n \mathrm{e}^{K_n x/a} J_1(K_n r/a) \tag{6·4}$$

has the property that it has uniform velocity U for large negative values of x, and that the radial velocity is zero at $r = a$. The pressure condition which must be satisfied on the surface $\psi = 0$ is

$$\left(\frac{\partial\phi}{\partial x}\right)^2 + \left(\frac{\partial\phi}{\partial y}\right)^2 = 2gx. \tag{6·5}$$

It seems unlikely that an analytical solution of this problem could be found but a rough approximation to the flow near the top of the air column might be obtained by using only one term of the series in (6·3). The lowest root of $J_1(z) = 0$ is 3·832, so that as a first approximation (6·3) may be taken as

$$\phi = -Ux + A_1 \mathrm{e}^{3\cdot 832x/a} J_0(3\cdot 832r/a), \tag{6·6}$$

and (6·4) as

$$\psi = -\frac{Ur^2}{2} + A_1 r\, \mathrm{e}^{3\cdot 832x/a} J_1(3\cdot 832r/a). \tag{6·7}$$

The surface of the bubble is $\psi = 0$. In order that $x = 0$ may be the vertex of the air column it is necessary that the coefficient of r^2 in the expansion of ψ near the origin shall be zero. This condition is satisfied if

$$A_1 = \frac{Ua}{3{\cdot}832}. \tag{6·8}$$

It is clearly impossible to satisfy the pressure condition (6·1) at more than one point when only one term in the series expansion (6·3) is used. Assume that (6·5) is satisfied at the point $\psi = 0$ when $r = \frac{1}{2}a$. The value of x at this point is found by setting

$$A_1 = Ua/3{\cdot}832, \quad r/a = \tfrac{1}{2}, \quad \psi = 0 \text{ in (6·5).}$$

The value of $J_1[\frac{1}{2}(3{\cdot}832)]$ is 0·580, so that (6·7) gives

$$e^{3\cdot382x/a} = \frac{3{\cdot}832}{4(0{\cdot}580)} = 1{\cdot}65, \quad \text{and} \quad \frac{x}{a} = 0{\cdot}131.$$

Since $J_0[\frac{1}{2}(3{\cdot}832)] = 0{\cdot}273$, (6·5) gives

$$\frac{2ga}{U^2}(0{\cdot}131) = \{1 - (1{\cdot}65)(0{\cdot}273)\}^2 + \{(0{\cdot}580)(1{\cdot}65)\}^2,$$

hence

$$\frac{U^2}{ga} = 0{\cdot}215$$

or

$$U = 0{\cdot}464\sqrt{(ga)}. \tag{6·9}$$

This very rough approximation to the flow might be improved by using more terms in the series in (6·3). It would then be possible to satisfy the pressure condition at as many points as the number of terms taken in the series of (6·3), the values of x/a would be calculated for each assumed value of r/a, and the final equation for determining $U/\sqrt{(ga)}$ would be left. The numerical work, however, would be very heavy, and a relaxation method would probably be more satisfactory.

7. EXPERIMENTS ON EMPTYING VERTICAL TUBES

To find out whether the flow postulated in the above calculations can actually occur, a long glass tube was erected vertically over a sink in the Cavendish Laboratory. It was filled by placing the lower end in a basin of water and applying suction at the upper end through a rubber tube till the water-level reached the top. The rubber tube was then closed. To make an experiment the basin at the lower end was suddenly removed and a bubble was seen to run up the tube, the water emptying itself by running down the wall and pouring out from the bottom in the form of a tubular curtain of water. The photograph (figure 8), shows a flash-picture of the bubble running up a tube 7·94 cm. diameter. This tube was surrounded by a flat-sided glass box filled with water in order to reduce distortion by refraction.

It will be seen that the flow assumed in the analysis actually takes place. The thickness of the sheet of water that runs down the wall can be seen in the photograph, and measurements show that except close to the vertex this thickness is, as would be expected from (6·1), inversely proportional to the square root of the depth below the vertex.

Experiments were made with three tubes each about 180 cm. long and of diameters 1·23, 2·16 and 7·94 cm. The upward velocities of the tops of the bubbles were observed by timing their passage past horizontal marks with a stop-watch. The observed velocities together with the corresponding values of $U/\surd(ga)$ are given in table 4.

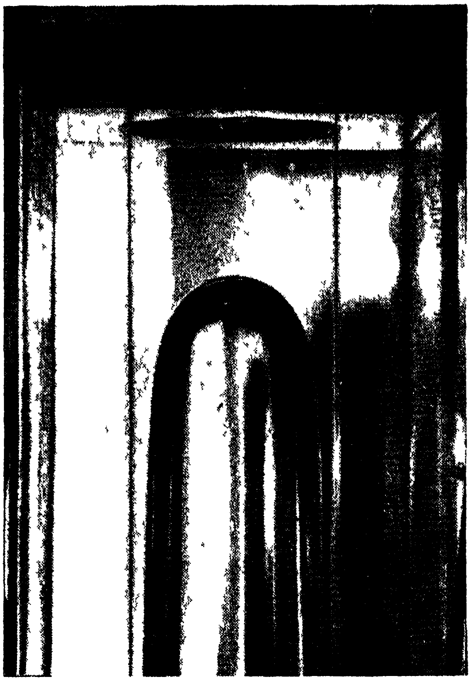

FIGURE 8. Emptying a glass tube 7 9 cm. diameter.

It will be seen that the values of $U/\surd(ga)$ are nearly constant but tend to rise slightly with diameter. This is probably an effect of viscosity. The Reynolds numbers associated with the bubbles are given in table 4. It will be seen that the Reynolds number associated with the largest tube is so great that it might be expected that the effect of viscosity would be negligible in that case.

TABLE 4

$2a$ (cm.)	1·23	2·16	7·94
U (cm./sec.)	9·8 to 10·15	14·5 to 15·2	29·1 to 30·6
$U/\surd(ga)$	0·40 to 0·41	0·447 to 0·468	0·466 to 0·490
$\dfrac{Ua}{\nu}$	600	1,600	12,000

calculated value, $U/\surd(ga) = 0{\cdot}464$.

It is remarkable that the very rough theory given above yields the value 0·464 for $U/\surd(ga)$, which is very close to the range 0·466 to 0·490 which was observed experimentally with the largest tube.

8. MEASURED PROFILE

The profile of the bubble taken from a photograph similar to figure 8 is shown in figure 9. After passing the rounded top of the bubble, the water concentrates into a sheet near the wall. At a depth of about $1{\cdot}5a$ below the vertex the horizontal component of flow becomes so small that the vertical component, U, may without appreciable error be taken as equal to q. The equation to the part of the profile below $x = 1{\cdot}5a$ is therefore approximately

$$U\pi a^2 = \pi q(a^2-r^2) = \pi(a^2-r^2)\sqrt{(2gx)},$$

or if t is written for $(a-r)$, the thickness of the layer of water running down the inside of the tube, and $U = \beta\sqrt{(ga)}$,

$$2\frac{t}{a}-\frac{t^2}{a^2} = \beta\sqrt{\frac{a}{2x}},$$

and since t is small compared with a,

$$\beta = 2\sqrt{2}\left(\frac{t}{a}\right)\sqrt{\frac{x}{a}}.$$

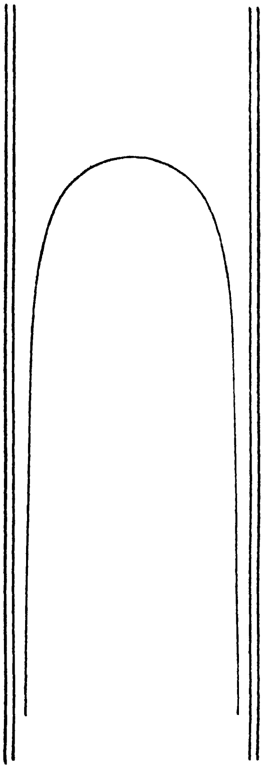

FIGURE 9. Profile of a bubble rising in a tube.

By measuring t and x in figure 9 therefore it should be possible to find β for comparison with the value deduced from velocity measurements and given in table 4. Corresponding values of t/a and x/a are given in table 5.

TABLE 5

x/a	1·71	3·43	5·14	6·17
t/a	0·171	0·123	1·103	0·093
$\beta = 2\sqrt{2}(t/a)\sqrt{(x/a)}$	0·63	0·64	0·66	0·65

It will be seen that the values of $t\sqrt{x}$ are nearly constant, but the value of β deduced from them is much larger than that found by measuring the velocity of the bubble. The difference may be due to the fact that the existence of the boundary layer at the inner wall of the tube was not considered, so that the downward flow estimated by measuring t and assuming that U is uniform through the layer gives rise to an overestimate. Another cause which gives rise to an overestimate of t is the refraction of the glass tube, an error which is not completely eliminated by surrounding it with a parallel-sided glass box, filled with water.

REFERENCES

Allen, H. S. 1900 *Phil. Mag.* **50**, 323, 519.
Hoefer, K. 1913 *Z. Ver. dtsch. Ing.* **57**, 1174.
Miyagi, O. 1925 *Phil. Mag.* **50**, 112.
Miyagi, O. 1925 *Tohoku Imp. Univ., Technol. Rep.*, **5**, 135.
Miyagi, O. 1929 *Tohoku Imp. Univ., Technol. Rep.*, **8**, 587.
Taylor, G. I. 1934 *Proc. Roy. Soc.* A, **146**, 501.

Polar structures in the theory of conjugated molecules. II. Symmetry properties and matrix elements for polar structures

By D. P. CRAIG

Sir William Ramsay and Ralph Forster Laboratories, University College, London

(*Communicated by C. K. Ingold, F.R.S.—Received* 21 *December* 1948)

The inclusion of polar structures in the valence-bond theory of π-electrons entails some additions to the usual formalism, and these are given in this part. The symmetry properties of sets of structures, both non-polar and polar, and the matrix elements that come into energy calculations, are dealt with.

Using the work of part I, and the conclusions of this part, the energy parameters for work with polar structures are evaluated.

INTRODUCTION

In part I a discussion has been given of the excited states of ethylene (Craig 1949), the object being to identify in the spectrum the energy levels whose term values can be used to give the parameters required for calculations with polar structures in the valence-bond treatment.

In this part methods are given which allow polar structures to be brought into the discussion of molecules in the same way as applies to non-polar structures in the methods developed by Hückel (1931), Pauling (1933) and Eyring & Kimball (1933). Since, in addition, molecular symmetry is of special importance when excited states are being considered, the means are given by which symmetry properties can be used to simplify the working, and also to enable the making of general statements about transition probabilities (i.e. selection rules). The results which come from the detailed section which follows are expressed finally in the form of rules for finding the symmetry properties of valence-bond structures in general, and rules for finding the new matrix elements which come in when polar structures are added to the basic set of molecular structures. The secular equation, augmented by the terms corresponding with polar structures, can then be set up for conjugated and aromatic molecules.

THE VALENCE-BOND APPROXIMATION

A description of the valence-bond approximation is given, for example, by Eyring *et al.* (1944, p. 243). The method starts from antisymmetric combinations of products of one-electron $2p_z$ wave functions. These antisymmetric combinations are called ϕ functions, or Slaterfunctions. A sample, for butadiene, is:

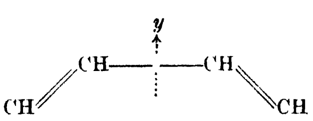

$$\phi_1 = \frac{1}{\sqrt{4!}} \begin{vmatrix} (a\alpha)_1 & (b\beta)_1 & (c\alpha)_1 & (d\beta)_1 \\ (a\alpha)_2 & (b\beta)_2 & (c\alpha)_2 & (d\beta)_2 \\ (a\alpha)_3 & (b\beta)_3 & (c\alpha)_3 & (d\beta)_3 \\ (a\alpha)_4 & (b\beta)_4 & (c\alpha)_4 & (d\beta)_4 \end{vmatrix}$$

Notation

$$\phi_1 \equiv \phi_1(\alpha\beta\alpha\beta) \quad \text{or simply} \quad \phi_1 \equiv (\alpha\beta\alpha\beta),$$

in which the symbol $(a\alpha)_1$ means occupancy by electron 1, with spin α, of the $2p_z$ orbital on carbon atom a. The other functions compatible with the same scheme of bonding are:

$$\phi_2 \equiv (\alpha\beta\beta\alpha), \quad \phi_3 \equiv (\beta\alpha\alpha\beta), \quad \phi_4 \equiv (\beta\alpha\beta\alpha),$$

obtained using the rule that the two electrons of a bond have opposed spins.

Following Eyring *et al.*, a neat procedure is to put together all the Slaterfunctions corresponding to a particular chemical bond diagram in such a way that the group of functions is antisymmetric to interchange of the spins of two bonded orbitals. Such a combination is called a 'bond eigenfunction'. It is the wave function of a chemical structure, in the sense that it enumerates with proper sign all the arrangements of spins compatible with the structure. The bond eigenfunction for the butadiene structure given above is

$$\psi = \frac{1}{\sqrt{4}}(\phi_1 - \phi_2 - \phi_3 + \phi_4).$$

To treat a particular molecule, the bond eigenfunctions are set up for an independent set of structures (Rumer 1932), and they are then used to express the wave function for the molecule as a linear combination of some or all of these structures. The energy is minimized through the varying of the coefficients with which the various structures appear in the wave function. The minimizing is done by solving the *secular equation*, and rules have been formulated (Eyring *et al.* 1944, p. 243) for setting up the secular equation simply by inspection of the (non-polar) structures which are to be included, without actually working with the ϕ functions, or the bond eigenfunctions, explicitly.

When the molecule has elements of symmetry, e.g. the axis shown as y for butadiene, the symmetry properties make the problem simpler in the following way. When the symmetry shows that certain bond eigenfunctions must occur together with the same coefficient in all wave functions, the secular equation can be reduced in degree, since allowance has not to be made for independent variations within these sets of structures. For example, since benzene is known to have hexagonal symmetry, a description of it in terms of the Kekulé structures 1 and 2 must involve these structures to the same extent, since otherwise the hexagonal symmetry would be lost. Equally, the structures 3 and 4 for naphthalene must come in with the same coefficient if the molecule is to have a plane of symmetry in the yz plane. This way of grouping structures with a common coefficient is a way of reducing the degree of the secular equation by factoring it at the start.

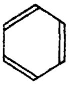
1

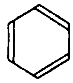
2

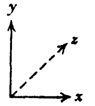

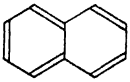
3

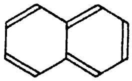
4

When more than a single energy state of a molecule is being treated, one may want to know how the states are related to each other (e.g. in the absorption of light) in terms of selection rules between the various symmetry types which the nuclear configuration admits. Then more is needed than the information that certain structures combine to transform like an irreducible representation of the symmetry group; one has to know what the symmetry properties are, and this means knowing how the several bond eigenfunctions transform under the operations of the group.*

SYMMETRY PROPERTIES OF BOND EIGENFUNCTIONS

To be definite, take the two structures for *cyclo*butadiene: The labels α, β on bonds indicate by convention which of the functions are given a positive sign in the bond eigenfunction.†

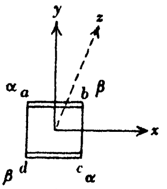

A

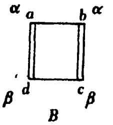

B

---

* Hückel (1931) was the first to discuss the transformation properties of ϕ functions, and it is his treatment which is here extended to bond eigenfunctions.

† In comparing the present discussion with that of Wheland (1938), it should be noted that different conventions are used for labelling bonds.

The convention is illustrated in the bond eigenfunction for structure A, the spins referring to the orbitals a, b, c, d, taken in alphabetical order:

$$\psi_A = \frac{1}{\sqrt{4}}\{\phi_1(\alpha\beta\alpha\beta) - \phi_2(\alpha\beta\beta\alpha) - \phi_3(\beta\alpha\alpha\beta) + \phi_4(\beta\alpha\beta\alpha)\}.$$

The molecular plane is a plane of symmetry. Under the operation of reflexion in this plane every atomic $2p_z$ orbital changes sign, but in the molecular wave function these atomic orbitals always occur in products of four at a time, so the bond eigenfunctions do not change sign. It is true for any aromatic or conjugated structure with an even number of π-electrons that reflexion in the molecular plane of symmetry leaves every bond eigenfunction unchanged.

In a rotation about the x axis of the diagram, the effect of the operation on a π-electron wave function is to interchange carbon atoms which make up the potential field in which the π-electrons are to be found:

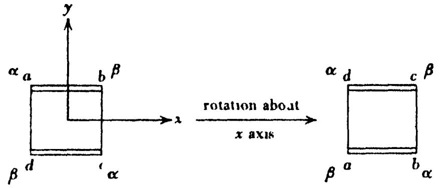

The effect on the ϕ functions is to interchange column labels:

$$\begin{vmatrix} (a\alpha)_1 & (b\beta)_1 & (c\alpha)_1 & (d\beta)_1 \\ (a\alpha)_2 & & & \\ (a\alpha)_3 & & \text{etc.} & \\ (a\alpha)_4 & & & \end{vmatrix} \xrightarrow[x \text{ axis}]{\text{rotation about}} \begin{vmatrix} (d\alpha)_1 & (c\beta)_1 & (b\alpha)_1 & (a\beta)_1 \\ (d\alpha)_2 & & & \\ (d\alpha)_3 & & \text{etc.} & \\ (d\alpha)_4 & & & \end{vmatrix}$$

$$\equiv (+) \begin{vmatrix} (a\beta)_1 & (b\alpha)_1 & (c\beta)_1 & (d\alpha)_1 \\ (a\beta)_2 & & & \\ (a\beta)_3 & & \text{etc.} & \\ (a\beta)_4 & & & \end{vmatrix}$$

that is

$$\phi_1(\alpha\beta\alpha\beta) \xrightarrow[x \text{ axis}]{\text{rotation about}} +\phi_4(\beta\alpha\beta\alpha)$$

The transformed ϕ is restored to the standard form (alphabetical order of columns by exchanging columns, going over in this case to ϕ_4 with positive sign. To find with what sign the new ϕ enters the bond eigenfunction for the transformed structure, one counts by how many *spin* interchanges the new ϕ differs from the one whose sign was conventionally fixed as positive. If an odd number of interchanges is needed the sign is negative, if an even number the sign is positive. In this case ϕ_4 differs from ϕ_1 by two interchanges, and hence appears in the bond eigenfunction with positive sign. Thus ϕ_1 transforms into ϕ_4, and since ϕ_4 appears with positive sign in the bond eigenfunction for structure A, it follows that ψ_A transforms into itself with positive sign under the operation of rotation about the x axis. The procedure is easily made general to include cases where a structure is not transformed into itself. The result may be set out in the following way:

The structures for a molecule are written down, and the signs of their eigenfunctions fixed by labelling the ends of the π-bonds with α and β. To find the sign with which a structure A is transformed into a structure B (which may or may not be the same as A) under a symmetry operation the procedure is as follows. Count the number (p) of interchanges of atoms required to obtain the transformed structure from the original; count the number of interchanges (q) required to make the new assignment of spins coincide with the standard assignment for the structure B. Then the transformation is

$$A \xrightarrow{\qquad} (-1)^{p+q} B.$$

TYPES OF POLAR STRUCTURES AND THEIR BOND EIGENFUNCTIONS

In non-polar structures, to which the usual V.B. method is adapted, there is exactly one electron in the $2p_z$ orbital of each carbon atom linked in the resonance system. In polar structures this is not true. Some carbons, marked with (+) charges, have no $2p_z$ electrons and others, marked (−), have two. More than two electrons cannot, of course, occupy a $2p_z$ orbital. The following are examples of polar structures:

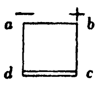

P

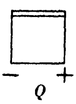

Q

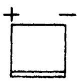

R

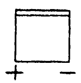

S

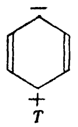

T

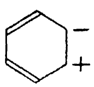

U

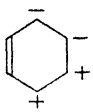

V

A first distinction marks off structure V from the others. The structures other than V differ from non-polar structures by the displacement of one electron. Structure V differs by two electrons. Now every electron displacement in this sense increases the energy of the structure for two reasons. First, the number of bonds is reduced by one for each displacement, and secondly, two electrons on the same centre have a large energy of repulsion. It follows that the more electrons there are displaced, the more energetic the structure will be. As our results will go to show, the displacement of just one electron between two adjacent centres means a large energy increase, and for a double or triple displacement it would be very much larger again, so large, indeed, that such structures may safely be ignored. The study will have to do only with structures with one pair of charged atoms, and the meaning of the term 'polar structure' will not go beyond these.

The second distinction between polar structures has to do with the separation of the charges. Except for T and V in the diagram, the charges are on adjacent carbon atoms. In T they are on remote atoms. There are two reasons for expecting structures like T to be much less important: they are more energetic by the amount of their extra electrostatic energy, and their ability to participate in resonance with a set of non-polar structures is much less. This follows because the matrix element for participation now depends on an integral involving remote, rather than adjacent, centres. We shall in the end work only with adjacent charge structures, although this limitation is not needed until actual numerical calculations come to be made. The formal steps of getting suitable bond eigenfunctions, symmetry properties, and matrix elements, apply indifferently to remote and adjacent charge structures, and it is only the difficulty of getting empirical values for the long-range integrals that influences the practical side of the problem.

Throughout the work it is useful to keep the closest parallel between polar and non-polar structures. This is assisted by establishing a correspondence between them. In the figure, structures P and R each have a 'polar bond' where A has an ordinary double bond, viz. between atoms a and b: That is, by taking the electron of atom $a(b)$ and assigning it to atom $b(a)$ we go from structure A to $R(P)$. Both T and S stand in a similar relation to L. Every polar structure has just one non-polar structure standing in this relation to it, and we shall speak of this one as the *corresponding* non-polar structure.

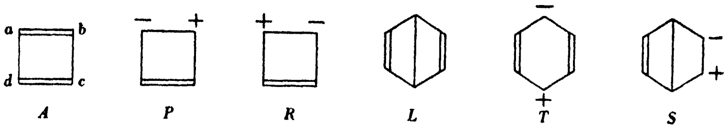

An independent set of polar structures is found from Rumer's theorem (1932) using only those atomic orbitals for which alternative assignments of spin are possible. This means omitting the doubly occupied orbital and of course the unoccupied one. An important consideration in polar structures is to have a set whose corresponding non-polar structures are, as far as possible, in the non-polar canonical set, for this simplifies the transformation properties and matrix elements, as will be plain later.

Taking structure P, the ϕ functions are

$$\phi_1 = \frac{1}{\sqrt{4!}} \left| \begin{matrix} (a\alpha)_1 & (a\beta)_1 & (c\alpha)_1 & (d\beta)_1 \\ & \text{etc.} & & \end{matrix} \right| \quad \text{and} \quad \phi_2 = \phi_2(\widehat{\alpha\beta}\beta\alpha)(a),$$

and the bond eigenfunction: $\psi_P = \frac{1}{\sqrt{2}}(\phi_1 - \phi_2)$.

In writing the short forms for the ϕ's the linked spins belong to electrons in the same $2p_z$ orbital, and the bracketed letter indicates the negatively charged atom. There is one-half as many ϕ functions for a polar structure as for the corresponding non-polar one. To go from a non-polar ϕ to that for a polar structure corresponding to it, one assigns to the atom which is to be negatively charged the electron which in the non-polar ϕ belonged to the atom which is to be positively charged. For example, the following are corresponding ϕ's:

III 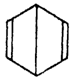 $: |(a\alpha)_1(b\beta)_1(c\alpha)_1(d\beta)_1(e\alpha)_1(f\beta)_1| = (\alpha\beta\alpha\beta\alpha\beta),$

III 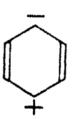 $: |(a\alpha)_1(b\beta)_1(c\alpha)_1(a\beta)_1(e\alpha)_1(f\beta)_1| = (\widehat{\alpha\beta\alpha\beta}\alpha\beta)(a).$

Determinants are here shown by their first rows. An important formal point in going from non-polar to polar ϕ's is to preserve the order of columns. For although there is the obvious relation

$$|\,(a\alpha)_1\,(b\beta)_1\,(c\alpha)_1\,(a\beta)_1\,(e\alpha)_1\,(f\beta)_1\,| \equiv |\,(a\alpha)_1\,(a\beta)_1\,(b\beta)_1\,(c\alpha)_1\,(e\alpha)_1\,(f\beta)_1\,|,$$

the first form proves a far more convenient basis for a general treatment.

TRANSFORMATION PROPERTIES OF POLAR STRUCTURES

The sign with which a polar structure transforms under a symmetry operation is the same as for the transformation of the corresponding non-polar structure. To see this, consider the transformation of a polar ϕ, (ii), and corresponding non-polar one, (i), under some operation indicated by the arrow:

$$\text{(i)}\quad |\,(a\alpha)_1\,(b\beta)_1\,(c\alpha)_1\,(d\beta)_1\,(e\alpha)_1\,(f\beta)_1 \ldots\,| \to |\,(a'\alpha)_1\,(b'\beta)_1\,(c'\alpha)_1\,(d'\beta)_1\,(e'\alpha)_1\,(f'\beta)_1 \ldots\,|,$$

$$\text{(ii)}\quad |\,(a\alpha)_1\,(b\beta)_1\,(c\alpha)_1\,(d\beta)_1\,(e\alpha)_1\,(a\beta)_1 \ldots\,| \to |\,(a'\alpha)_1\,(b'\beta)_1\,(c'\alpha)_1\,(d'\beta)_1\,(e'\alpha)_1\,(a'\beta)_1 \ldots\,|.$$

This transformation carries atom a into a', etc. As already detailed for non-polar structures, the transformed ϕ is restored to standard order of columns by a number, p say, of column interchanges. Guided by the non-polar ϕ we make the same column interchanges in the polar ϕ. The results of this are shown on the left-hand side of the following equation, the order of orbitals now being taken to be the standard order.

$$\begin{aligned}\text{(i)}\quad & |\,(d'\beta)_1\,(c'\alpha)_1\,(b'\beta)_1\,(a'\alpha)_1\,(f'\beta)_1\,(e'\alpha)_1 \ldots\,| \times (-1)^p \\ &= (-1)^{p+q}\,|\,(d'\alpha)_1\,(c'\beta)_1\,(b'\alpha)_1\,(a'\beta)_1\,(f'\alpha)_1\,(e'\beta)_1 \ldots\,|,\end{aligned}$$

$$\begin{aligned}\text{(ii)}\quad & |\,(d'\beta)_1\,(c'\alpha)_1\,(b'\beta)_1\,(a'\alpha)_1\,(a'\beta)_1\,(e'\alpha)_1 \ldots\,| \times (-1)^p \\ &= (-1)^{p+q}\,|\,(d'\alpha)_1\,(c'\beta)_1\,(b'\alpha)_1\,(a'\beta)_1\,(a'\alpha)_1\,(e'\beta)_1 \ldots\,|.\end{aligned}$$

Finally, by q interchanges of spin labels the non-polar ϕ becomes that to which a positive sign is attached by convention in the bond eigenfunction for the transformed structure. Again we make the same interchanges in the polar ϕ. Now we have the two ϕ's shown on the right-hand sides of the equations. The two are identical except that the transform of a appears in the polar ϕ where the transform of f appears in the non-polar one, and with the same spin. Evidently the transformed non-polar ϕ 'corresponds' with the transformed polar one, so that the relation of correspondence persists through the symmetry operation. It follows that any polar structure transforms with the same sign as the corresponding non-polar one.

In dealing with polar structures with remote charges it is common to find that the corresponding non-polar structures are outside the non-polar canonical set. The simplest example is the following structure for *cyclo*butadiene, shown with its non-canonical corresponding structure:

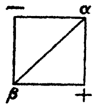

polar structure

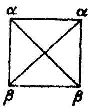

corresponding non-polar structure

The same rule for the transformation sign holds in this case as in any other, but it is important to note that a non-canonical structure cannot be given the standard spin labelling, so that polar structures of this kind have different spin labels from the others. This difference makes itself felt in the signs attached to certain matrix elements, but not otherwise.

MATRIX ELEMENTS INVOLVING POLAR STRUCTURES

When the transformation properties of the structures are known, the combinations of them transforming like the various representations can be selected and the secular equation factored. To make a calculation of energies, certain new matrix elements are required. These are the matrix elements between two polar structures, and between one polar and one non-polar structure. Again it is convenient to relate each polar structure to the corresponding non-polar one, and ultimately to give rules for the new matrix elements in terms of the rules for the corresponding non-polar elements. Only singlet states will be explicitly treated, but the extension to other states is immediate.

Taking as one example the case of *cyclo*butadiene, consider the structures

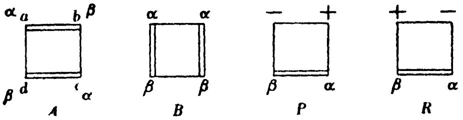

With the same notation as used in the discussion of symmetry, the normalized* bond eigenfunctions are:

$$\psi_A = \tfrac{1}{2}[(\alpha\beta\alpha\beta)-(\alpha\beta\beta\alpha)-(\beta\alpha\alpha\beta)+(\beta\alpha\beta\alpha)],$$

$$\psi_B = \tfrac{1}{2}[(\alpha\alpha\beta\beta)-(a\beta\alpha\beta)-(\beta\alpha\beta\alpha)+(\beta\beta\alpha\alpha)],$$

$$\psi_P = \frac{1}{\sqrt{2}}[(\widehat{\alpha\beta}\alpha\beta)(a)-(\widehat{\alpha\beta}\beta\alpha)(a)],$$

$$\psi_R = \frac{1}{\sqrt{2}}[(\widehat{\alpha\beta}\alpha\beta)(b)-(\widehat{\alpha\beta}\beta\alpha)(b)].$$

Any element in the energy matrix is given as a combination of terms of the type $(\phi_i H\phi_j)$ in an obvious notation. When only single exchange integrals between adjacent atoms are considered, the matrix element $(\psi_A H\psi_A)$ is

$$\begin{aligned}\frac{1}{2^2}[&(\alpha\beta\alpha\beta)H(\alpha\beta\alpha\beta)+(\alpha\beta\beta\alpha)H(\alpha\beta\beta\alpha)+(\beta\alpha\alpha\beta)H(\beta\alpha\alpha\beta)+(\beta\alpha\beta\alpha)H(\beta\alpha\beta\alpha)\\&-2(\alpha\beta\alpha\beta)H(\alpha\beta\beta\alpha)-2(\alpha\beta\alpha\beta)H(\beta\alpha\alpha\beta)-2(\alpha\beta\beta\alpha)H(\beta\alpha\beta\alpha)\\&-2(\beta\alpha\alpha\beta)H(\beta\alpha\beta\alpha)],\end{aligned}$$

---

* In this normalization, and indeed throughout, the non-orthogonality of atomic wave functions is neglected. Van Vleck (1936) has shown that the error which arises from this in problems of permutation degeneracy is small, due to a cancellation with the effects of neglected multiple exchange integrals. This is a partial justification for neglecting non-orthogonality, and it shows that nothing will be gained by including it unless multiple exchange integrals are also included, which would make for unmanageable complexity.

working from the definition of the bracketed quantities, and from the fact that spin wave functions are orthogonal, only two kinds of terms remain from this expression, of which the following are representative:

$$Q = \int (a\alpha)_1 (b\beta)_2 (c\alpha)_3 (d\beta)_4 H (a\alpha)_1 (b\beta)_2 (c\alpha)_3 (d\beta)_4 \, d\tau_1 d\tau_2 d\tau_3 d\tau_4,$$

$$\alpha = \int (a\alpha)_1 (b\beta)_2 (c\alpha)_3 (d\beta)_4 H (b\alpha)_1 (a\beta)_2 (c\alpha)_3 (d\beta)_4 \, d\tau_1 d\tau_2 d\tau_3 d\tau_4.$$

It can be verified then that

$$(\psi_A H \psi_A) = \frac{1}{2^2}[Q + Q - 2\alpha + Q - 2\alpha + Q + 2\alpha + 2\alpha + 2\alpha + 2\alpha] = Q + \alpha,$$

and similarly $(\psi_A H \psi_B) = \frac{1}{2^2}[-\alpha - Q - 6\alpha - Q - \alpha] = -\tfrac{1}{2}(Q + 4\alpha).$

To treat the polar case, again neglect all but single exchanges between adjacent atoms, and introduce the following new integrals* ξ, η, ζ, where

$$\xi = Q' - Q,$$

$$Q' = \int (a\alpha)_1 (a\beta)_2 (c\alpha)_3 (d\beta)_4 H (a\alpha)_1 (a\beta)_2 (c\alpha)_3 (d\beta)_4 \, d\tau_1 d\tau_2 d\tau_3 d\tau_4,$$

$$\eta = \int (a\alpha)_1 (a\beta)_2 (c\alpha)_3 (d\beta)_4 H (a\alpha)_1 (b\beta)_2 (c\alpha)_3 (d\beta)_4 \, d\tau_1 d\tau_2 d\tau_3 d\tau_4,$$

$$\zeta = \int (a\alpha)_1 (a\beta)_2 (c\alpha)_3 (d\beta)_4 H (b\alpha)_1 (b\beta)_2 (c\alpha)_3 (d\beta)_4 \, d\tau_1 d\tau_2 d\tau_3 d\tau_4.$$

Because of the limitation to single exchange integrals, two functions give a contribution to the energy matrix element either if they match precisely in their assignment of electrons to orbitals, or differ at most in the assignment of two electrons. This means that two polar structures can only interact if they carry charges on the same atoms. Further, in accordance with the limitation to nearest neighbour effects the only polar structures to be considered are those whose charges are on adjacent atoms.

Consider first the Coulomb type term $(\psi_P H \psi_P)$:

$$\begin{aligned}(\psi_P H \psi_P) &= \tfrac{1}{2}[(\widehat{\alpha\beta}\alpha\beta) H (\alpha\beta\alpha\beta)(aa) + (\widehat{\alpha\beta}\beta\alpha) H (\widehat{\alpha\beta}\beta\alpha)(aa) - 2(\widehat{\alpha\beta}\alpha\beta) H (\widehat{\alpha\beta}\beta\alpha)(aa)] \\ &= \tfrac{1}{2}[Q' - \zeta + Q' - \zeta + 2\alpha] = Q' - \zeta + \alpha.\end{aligned}$$

In the general case, recall first the rule for getting matrix elements between two non-polar structures for any molecule. This is given by Eyring *et al.* (1944, p. 243) in a convenient form, for which the term 'cycle' has to be defined. A cycle is a set of orbitals whose spins are all determined by the rule that bonded orbitals have opposite spin. A first spin can be assigned at will, and the rest in the cycle are then fixed. For example, consider the matrix element $(\psi_A H \psi_B)$. Atoms a and b are bonded in A, so that when the spin of a is fixed, the spin of b is determined by it. Atoms b and c are bonded in B, so the spin of c is fixed by that of b; likewise the spin of d is fixed by that of c. Thus all four atoms form part of one cycle for this matrix element. For the matrix element $(\psi_A H \psi_A)$ there are two cycles. With this meaning for the term cycle, and working with normalized bond eigenfunctions, the matrix element between any two structures is as follows:

---

* Sklar has indicated a treatment using two new integrals only. The integral ζ above is set equal to the non-polar exchange integral α in Sklar's treatment.

$(-1)^p\, 2^{-(n-x)}\{Q + 1{\cdot}5[\Sigma$(single exchange integrals between adjacent orbitals in the same cycle with opposite spin) $-\,\Sigma$(single exchange integrals between adjacent orbitals in the same cycle with the same spin)] $-\,\tfrac{1}{2}\Sigma$(all single exchange integrals between adjacent orbitals)$\}$.

Here p is the number of pairs of orbitals assigned different spins in the two structures; n is the number of pairs of orbitals, and x the number of cycles. For two polar structures having the same charge disposition, the formula can be applied directly, by supposing two π-orbitals to be made to coincide, and the exchange integral between them dropped. Then Q' is used as the coulomb integral appropriate to a polar configuration, ζ as the exchange integral when one of the orbitals belongs to the negatively charged atom, and α otherwise. The two electrons in the same orbital make a cycle for this purpose.

For the interaction between two polar structures which have reversed charges consider first the matrix element between structures P and R:

$$\psi_P = \frac{1}{\sqrt{2}}\{(\widehat{\alpha\beta}\,\alpha\beta)\,(a) - (\widehat{\alpha\beta}\,\beta\alpha)\,(a)\}, \quad \psi_R = \frac{1}{\sqrt{2}}\{(\widehat{\alpha\beta}\,\alpha\beta)\,(b) - (\widehat{\alpha\beta}\,\beta\alpha)\,(b)\},$$

$$\begin{aligned}(\psi_P H \psi_R) &= \tfrac{1}{2}[(\widehat{\alpha\beta}\,\alpha\beta)\,H(\widehat{\alpha\beta}\,\alpha\beta)\,(ab) + (\widehat{\alpha\beta}\,\beta\alpha)\,H(\widehat{\alpha\beta}\,\beta\alpha)\,(ab) \\ &\qquad - (\widehat{\alpha\beta}\,\alpha\beta)\,H(\widehat{\alpha\beta}\,\beta\alpha)\,(ab) - (\widehat{\alpha\beta}\,\beta\alpha)\,H(\widehat{\alpha\beta}\,\alpha\beta)\,(ab)] \\ &= \zeta.\end{aligned}$$

In general, since the two structures have two different orbitals doubly filled, all the ϕ's of one structure differ from all those of the other by at least the assignment of two electrons. Therefore two ϕ's contribute a term to the matrix element only if they agree in the assignment of spins to orbitals everywhere except in the orbitals belonging to the negatively charged atoms. This, in the corresponding non-polar matrix element, is the condition that determines the coefficient of Q. Therefore, while the integral that appears is ζ, as shown in the example, its coefficient is the same as the coefficient of Q in the corresponding non-polar matrix element.

As an example of the matrix element between a polar and non-polar structure, consider:

$$\begin{aligned}(\psi_A H \psi_P) &= \frac{1}{2\sqrt{2}}[(\alpha\beta\,\alpha\beta)\,H(\widehat{\alpha\beta}\,\alpha\beta)\,(a) - (\beta\alpha\,\alpha\beta)\,H(\widehat{\alpha\beta}\,\alpha\beta)\,(a) + (\alpha\beta\,\beta\alpha)\,H(\widehat{\alpha\beta}\,\beta\alpha)\,(a) \\ &\qquad - (\beta\alpha\,\beta\alpha)\,H(\widehat{\alpha\beta}\,\beta\alpha)\,(a)] \\ &= \sqrt{2}\eta, \quad \text{noting} \quad (\widehat{\alpha\beta}\,\alpha\beta)\,(a) = -(\widehat{\beta\alpha}\,\alpha\beta)\,(a),\end{aligned}$$

$$\begin{aligned}(\psi_B H \psi_R) &= \frac{1}{2\sqrt{2}}[-(\alpha\beta\,\alpha\beta)\,H(\widehat{\alpha\beta}\,\alpha\beta)\,(b) + (\beta\alpha\,\beta\alpha)\,H(\widehat{\alpha\beta}\,\beta\alpha)\,(b)] \\ &= -\tfrac{1}{2}\sqrt{2}\,\eta.\end{aligned}$$

The situation here is much as in the previous case. Every ϕ of the polar structure differs from every ϕ of the non-polar by at least one assignment, and if only single exchange integrals are counted, the assignment must match identically elsewhere. Again, therefore, only a single type of integral occurs, η, and its coefficient is $\sqrt{2}$ times that of Q in the corresponding non-polar matrix element. The multiplier $\sqrt{2}$ arises because polar bond eigenfunctions have one-half the number of ϕ's the non-polar ones have, and there is therefore a difference of a factor of $\sqrt{2}$ in the normalizing coefficients which shows up in the matrix element.

The rules for matrix elements for adjacent charge polar structures may be summarized:

(i) A polar structure has non-zero matrix elements with non-polar structures, and with other polar structures having charges on the same atoms. The sign of these matrix elements is the same as for the corresponding non-polar ones.

(ii) Between a polar structure and a non-polar one. Only η appears. Its coefficient is $\sqrt{2}$ times the coefficient of Q in the corresponding non-polar matrix element.

(iii) Two polar structures having the same charge disposition. The rule for non-polar matrix elements is used, counting the two electrons on the negative atom as a cycle. Q' appears instead of Q, and ζ replaces α for exchanges in which one orbital is on the negative atom.

(iv) Two polar structures with reversed charges. Only ζ appears, and its coefficient is the same as that of Q in the corresponding non-polar matrix element.

VALUES FOR THE INTEGRALS ξ, η, ζ

The next step is to evaluate the quantities ξ, η, ζ, using experimental results for ethylene. The three structures are:

$$\underset{A}{\mathrm{C{=}C}} \qquad \underset{B}{\mathrm{C^-{-}C^+}} \qquad \underset{C}{\mathrm{C^+{-}C^-}}$$

The unnormalized wave functions are

$$A_g:\begin{cases}\psi_{\mathrm{I}} = \psi_A,\\ \psi_{\mathrm{II}} = \psi_B+\psi_C,\end{cases}$$

$$B_{1u}:\ \psi_{\mathrm{III}} = \psi_B-\psi_C.$$

The secular equation for the A_g energy levels is

$$\begin{vmatrix} x+\alpha & 2\sqrt{2}\eta \\ 2\sqrt{2}\eta & 2x+2\xi+2\zeta \end{vmatrix} = 0, \qquad x = Q-E.$$

In part I, reasons were given for the following assignment of the experimental energy levels:

(i) Separation between the ground state and the excited A_g state, approx. 6 eV.

(ii) Separation between the ground state and the singlet B_{1u} state, approx. 7 eV.

Now since there are three constants whose values are wanted, a third empirical quantity is needed. This is the lowering of the ground state of ethylene due to the interaction between polar structures B and C and the non-polar structure A. The value taken for this is 0·2 eV, following Sklar (1937). It is the least accurate value of the three, and the inaccuracy comes out in the value obtained for the integral η.

This uncertainty appears in calculations of the lowering of non-polar states by polar structures, but not in calculations of totally polar states. With these as data, and adopting the value $-1\cdot92$ eV for the non-polar exchange integral α, the parameters take on the following values:

$$\xi = 4\cdot28\,\text{eV}, \quad \eta = -0\cdot54\,\text{eV}, \quad \zeta = -0\cdot6\,\text{eV}.$$

In the following part, this method using three extra parameters is applied to the study of benzene.

References

Craig, D. P. 1949 *Proc. Roy. Soc.* A, **200**, 272.
Eyring, H. & Kimball, G. E. 1933 *J. Chem. Phys.* **1**, 239.
Eyring, H., Walter, J. & Kimball, G. E. 1944 *Quantum chemistry*, p. 232. New York: John Wiley.
Huckel, E. 1931 *Z. Phys.* **70**, 204.
Pauling, L. 1933 *J. Chem. Phys.* **1**, 280.
Rumer, G. 1932 *Gött. Nachr*, p. 337.
Sklar, A. L. 1937 *J. Chem. Phys.* **5**, 669.
Van Vleck, J. H. 1936 *Phys. Rev.* **49**, 232.
Wheland, G. W. 1938 *Proc. Roy. Soc.* A, **164**, 397.

Polar structures in the theory of conjugated molecules

III. The energy levels of benzene

By D. P. Craig

Sir William Ramsay and Ralph Forster Laboratories, University College, London

(*Communicated by C. K. Ingold, F.R.S.—Received* 21 *December* 1948—*Revised* 20 *May* 1949)

The energy levels of benzene are calculated from a basis consisting of the five non-polar structures and twenty-four polar structures, using the method given in part II. The role of polar structures is discussed. The results include a suggested new assignment for the 2080 Å bands of A_{1g}–E_{2g}, instead of A_{1g}-B_{1u} as required by molecular orbital theory. An intense A_{1g}–E_{1u} transition is calculated at 7·9 eV instead of the observed 6·7 to 7·0 eV. The disagreement with molecular orbital theory, to be dealt with more fully in a later paper, is briefly discussed.

The basis of non-polar structures in benzene, figure 1, gives a satisfactory account (Sklar 1937) of the energy of the long wave-length absorption band but not of the intense region at 1830 Å nor of the very much weaker absorption at 2080 Å. A similar basis for naphthalene and anthracene gives the result that all spectral transitions, even when allowed, have zero transition moment, and this appears to be contrary to the experimental evidence that the long wave-length bands have considerable intensity.

These defects in the method are linked with the exclusion from it of polar structures, and in this paper we shall examine the consequences—in particular with respect to transition moments and higher excited states—of adding to the non-polar structures of figure 1 the twenty-four polar structures of figure 2. These structures have adjacent charges and 'correspond' in the sense of part II to the structures of figure 1. They fall naturally into two sets, the members of which correspond respectively to the Kekulé and Dewar non-polar structures, and together they make up a complete set of adjacent-charge structures. There is a close relation between members of the two sets; for example, *A* and *A'*, *B* and *B'*, etc., have the same charge disposition, and primed and unprimed structures combine in the same way to give representations of the symmetry group.

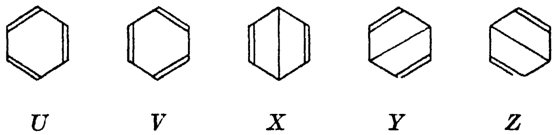

FIGURE 1

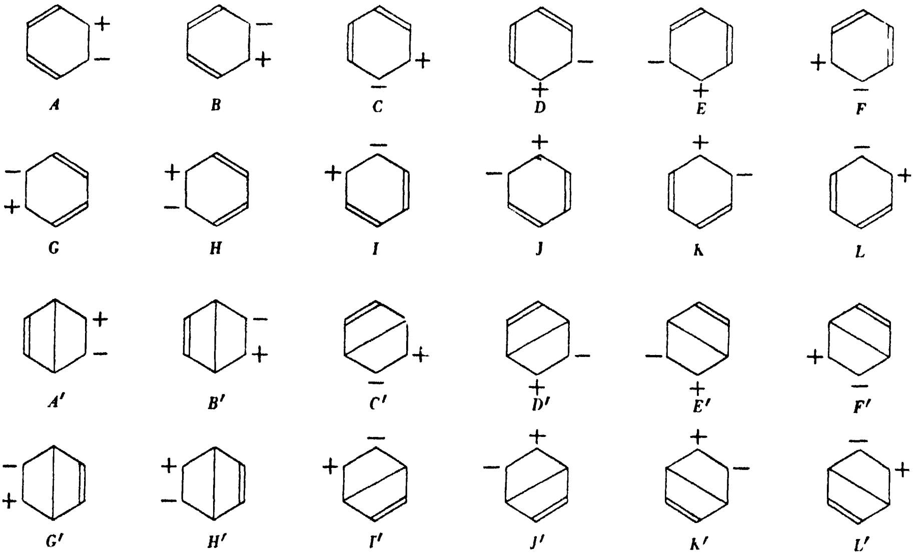

FIGURE 2

The hexagonal symmetry of benzene permits the classification of its π-electron wave functions according to the representations of the group D_{6h}. All these wave functions contain sixfold products of $2p_z$ atomic orbitals, and they are therefore symmetric to reflexion in the molecular plane. Hence the only representations which can occur are A_{1g}, A_{2g}, B_{1u}, B_{2u}, E_{2g}, and E_{1u}, in the notation of Eyring, Walter & Kimball (1944) which will be used throughout. Since the non-polar structures of figure 1 can be combined to give only A_{1g} (twice), B_{2u} and E_{2g}, the addition of polar structures may introduce totally polar states of symmetries A_{2g}, B_{1u} and E_{1u}, and states A_{1g}, B_{2u} and E_{2g} of mixed polar and non-polar character.

Combinations of polar structures may be found to transform like any of the plane-symmetric representations. This is shown by the reduction into irreducible components of Γ, the representation afforded by either of the two sets of structures:

$$\Gamma = A_{1g} + A_{2g} + B_{2u} + B_{1u} + 2E_{2g} + 2E_{1u}.$$

The proper combinations of the unprimed structures are as follows:

$$A_{1g}:\quad \Phi_1 = A+B+C+D+E+F+G+H+I+J+K+L,$$

$$A_{2g}:\quad \Phi_2 = A-B+C-D+E-F+G-H+I-J+K-L,$$

$$B_{2u}:\quad \Phi_3 = A+B-C-D+E+F-G-H+I+J-K-L,$$

$$B_{1u}:\quad \Phi_4 = A-B-C+D+E-F-G+H+I-J-K+L,$$

$$E_{2g}:\quad \begin{cases} \Phi_5 = 2A+2B-C-D-E-F+2G+2H-I-J-K-L, \\ \Phi_6 = 2A-2B-C+D-E+F+2G-2H-I+J-K+L, \end{cases}$$

$$E_{1u}:\quad \begin{cases} \Phi_7 = 2A+2B+C+D-E-F-2G-2H-I-J+K+L, \\ \Phi_8 = 2A-2B+C-D-E+F-2G+2H-I+J+K-L, \end{cases}$$

in which A, for example, stands for the bond eigenfunction for structure A of figure 2. By substituting primed for unprimed letters throughout (giving Φ_1', etc.), the proper combinations of the Dewar-like polar structures are obtained.

There are features of the work with polar structures which make it useful from the start to distinguish between states in which polar structures are combined so that pairs having opposite charge distributions (e.g. A and B of figure 2) are added, and those in which their difference is taken. Φ_5 and Φ_7 are examples of the first type, and Φ_6 and Φ_8 of the second. To mark this distinction where necessary, viz. where one symmetry type admits both sorts of states, we adopt the convention of marking states of the difference type (containing, for example, $A-B$) with a star attached to the symmetry symbol. Φ_6 then is E^*_{2g}, and Φ_8 is E^*_{1u}. The force of this distinction comes out first in considering the interaction between polar and non-polar structures. According to the rules of part II the matrix elements upon which this interaction depends can be obtained from the 'corresponding' non-polar elements. Now we notice that two structures with reversed charges, such as A and B of figure 2, both correspond to the same non-polar structure; it follows that the matrix element between structure U of figure 1 and the combination $(A+B)$ of figure 2 is the difference of two equal terms and thus vanishes. In general, provided two polar structures with reversed charges have the same coefficient, their sum, but not their difference, can interact with non-polar structures, and so appear in states of mixed polar and non-polar character. The difference combinations (containing, say, $A-B$) appear only in totally polar states.

To get the energies of the molecular states, secular equations have to be set up in the usual way for each symmetry type. The elements in these can be obtained from the rules in part II. In the A_{1g} representation all the structures of figures 1 and 2 enter the secular equation, which reduces to a quartic. The combinations of non-polar structures are $(U+V)$ and $(X+Y+Z)$, and those of the polar structures are the separate sums of primed and unprimed structures of figure 2. The secular equation is:

$$\begin{vmatrix} 2{\cdot}5x-11{\cdot}52 & 3x-17{\cdot}28 & -11{\cdot}455 & -9{\cdot}164 \\ 3x-17{\cdot}28 & 4{\cdot}5x-17{\cdot}28 & -13{\cdot}746 & -13{\cdot}746 \\ -11{\cdot}455 & -13{\cdot}746 & 12x+16{\cdot}8 & 6x-8{\cdot}88 \\ -9{\cdot}164 & -13{\cdot}746 & 6x-8{\cdot}88 & 12x+51{\cdot}36 \end{vmatrix} = 0,$$

where $x = Q-E$. To the lowest root of this equation, $E(\text{ground}) = Q-5{\cdot}7(445)\,\text{eV}$, there corresponds the ground state wave function

$$\psi(\text{ground}) = 0{\cdot}39(U+V)+0{\cdot}17(X+Y+Z)+0{\cdot}07(A+B+C+\text{etc.}) + 0{\cdot}03(A'+B'+C'+\text{etc.}).$$

If the Dewar-like polar structures are omitted, the secular equation is the cubic formed by removing the last row and column. The energy and wave function then are

$$E = Q-5{\cdot}61\,\text{eV}, \quad \psi = 0{\cdot}40(U+V)+0{\cdot}16(X+Y+Z)+0{\cdot}08(A+B+\text{etc.}).$$

And finally, if the non-polar structures alone are used, the energy is $Q-5{\cdot}0\,\text{eV}$.

Having given one detailed illustration, we may now omit further details of the calculations and proceed directly to a diagram of the results. This is given in figure 3, in which the influence of polar structures in benzene may be judged by comparing the results from (i) non-polar structures only, (ii) non-polar structures and Kekulé-like polar structures, and (iii) non-polar structures and all adjacent charge polar structures. It appears from the diagram that the influence of the Dewar-like structures is very small indeed in states which are dominantly non-polar, and quite small otherwise. The question arises as to what further effect is to be expected from the inclusion of polar structures with non-adjacent charges. On the states A_{1g} and B_{2u} which are largely non-polar the effect will evidently be very small indeed. For

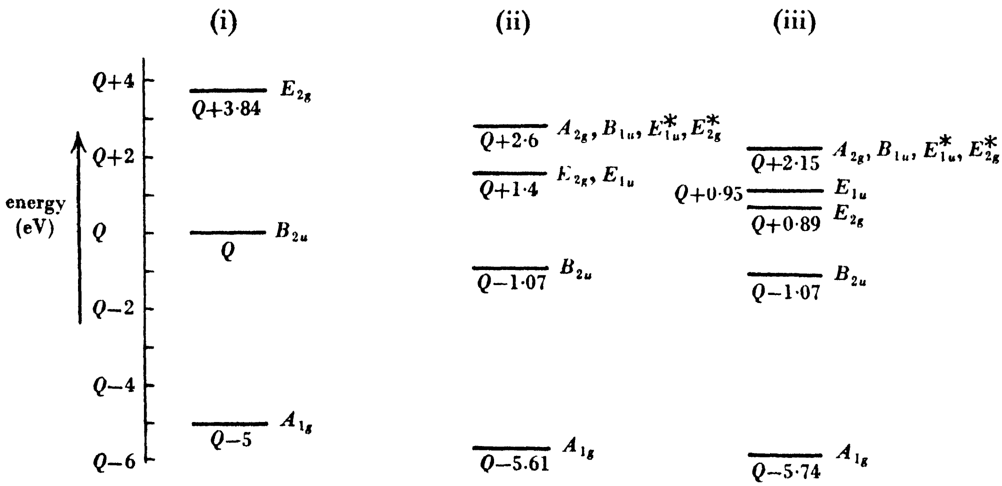

Figure 3

when this effect comes to be calculated it will depend on an integral of the same functional form as η, but involving non-adjacent, instead of adjacent, centres. η itself is already small, and will decrease rapidly with increasing separation between the charged centres. While, however, the effect on non-polar states may safely be neglected for this reason, the same is not necessarily true of polar states. These are in any case of higher energy, and the interaction terms between them and the remote charge polar structures involve integrals of unknown size. These integrals, however, are of the mixed coulomb-exchange type and they do depend on non-adjacent centres; they could hardly therefore be greater than η, and hence the influence of these additional polar structures might at most be as great as the influence of the Dewar-like structures as judged by the differences between columns (ii) and (iii) of the diagram. They might reduce the energies of the E_{2g} and E_{1u}^* states, for example, by a further 0·5 eV. Of the following types of remote-charge structures the first two types (there are six of each of them) admit combinations of symmetries A_{1g}, B_{1u}, E_{2g} and E_{1u}^*, but none of B_{2u}, A_{2g}, E_{2g}^* and E_{1u}. It follows that when the states of column (iii) of the energy-level diagram are corrected for the structures of figure 4, the E_{2g} state will be brought further below the E_{1u} state, and the E_{1u}^* and B_{1u} will be separated downward from E_{2g} and A_{2g}. The amount of these corrections, however, is unknown.

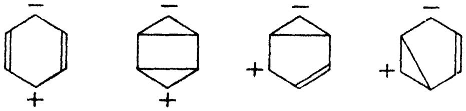

Figure 4

Before setting these results against the experimental evidence from the benzene spectrum, there is an important and general feature of the calculation of spectral intensities from wave functions made up from polar and non-polar structures. This again has to do with the two sorts of combinations of polar structures distinguished earlier in the discussion by marking one of them with a star. It was shown that where two structures with reversed charges had the same coefficient, then their sum, but not their difference, could appear in states of mixed polar and non-polar character. The difference combinations appear only in totally polar states. Now the ground state is a mixed state, and there are excited states of both kinds; what we show is that only when the excited state is totally polar is there a transition moment from the ground state, and that when both ground and excited states are mixed non-polar states with equal coefficients for oppositely charged pairs the transition moment is zero, whatever the selection rule may be. The transition moment in this case may be written

$$\int \psi(\text{ground}) \sum_i e\mathbf{r}_i \, \psi(\text{excited}) \, d\tau$$

($\mathbf{r}_i$ is the position vector of the ith π-electron) and this is the sum of a number of terms depending on the various polar and non-polar parts that compose ψ(ground) and ψ(excited). Referring to the structures of figures 1 and 2, there will occur

$$\int U \sum_i e\mathbf{r}_i V d\tau, \quad \int (K+L) \sum_i e\mathbf{r}_i (K+L)\, d\tau, \quad \int U \sum_i e\mathbf{r}_i (K+L)\, d\tau.$$

Terms of the first type, between two non-polar structures, are all zero; evidently when both structures assign exactly one electron to each centre there are no charge displacements from which a transition moment could arise. The second term, as written, expands into three parts, of which the first two cancel, and the third is zero:

$$\int K \sum_i er_i K\,d\tau + \int L \sum_i er_i L\,d\tau + 2\int K \sum_i er_i L\,d\tau.$$

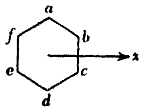

The first two give the dipole moments of structures K and L. Since K and L differ only in having reversed charges their dipole moments are equal and opposite and the sum vanishes. The third part consists of terms like

$$\begin{aligned}\int b(1)\,b(2)\,c(3)\,d(4)\,e(5)f(6) \sum_i ex_i a(1)\,a(2)\,c(3)\,d(4)\,e(5)f(6)\,d\tau \\ = eS^2(x_c + x_d + x_e + x_f) + e\int b(1)\,b(2)\,(x_1+x_2)\,a(1)\,a(2)\,d\tau \\ = eS^2x_f + eS^2(\tfrac{1}{2}x_b + \tfrac{1}{2}x_b) = 0.\end{aligned}$$

S is the overlap integral, and x_a is the x co-ordinate of nucleus a. Every term vanishes in this way, so that integrals of the second type make no contribution to the transition moment. Finally, we have to consider

$$\int U \sum_i er_i K\,d\tau + \int U \sum_i er_i L\,d\tau.$$

A representative term in the expansion of the first part is

$$\begin{aligned}\int a(1)\,b(2)\,c(3)\,d(4)\,e(5)f(6) \sum_i ex_i b(1)\,b(2)\,c(3)\,d(4)\,e(5)f(6)\,d\tau \\ = eS(x_b + x_c + x_d + x_e + x_f) + e\int a(1)\,x\,b(1)\,d\tau \\ = eSx_d + \tfrac{1}{2}eSx_b = \tfrac{1}{2}eSx_b.\end{aligned}$$

It may readily be shown that this cancels with an equal and opposite term from the second part. It follows that the transition moment between two states of the type considered must be zero, since all terms vanish or cancel upon which the transition moment depends. The same is, of course, not the case when, as for example in E^*_{1u}, the upper state involves difference combinations of polar structures. Thus in

$$\int (K+L) \sum_i er_i (K-L)\,d\tau = \int K \sum_i er_i K\,d\tau - \int L \sum_i er_i L\,d\tau,$$

the two terms on the right-hand side being dipole moments, have opposite signs and therefore do not cancel and the transition moment does not vanish.

In the absorption spectrum of benzene there are three bands in the range 2600 to 1700 Å. About the first band, at 2600 Å, there is nothing to add in the present treatment to what followed from Sklar's (1937) discussion using only non-polar structures. The first excited state is calculated to be B_{2u}, and this agrees with experiment. Of the other two bands, at 2080 and 1835 Å, the latter is very intense and obviously records an allowed transition. Now the only allowed transitions in benzene starting from a totally symmetrical ground state end at states of symmetry either A_{2u} or E_{1u}. There is no A_{2u} state of the six π-electrons, and the final state for an allowed transition must therefore be an E_{1u} state. The considerations of the last paragraph show that this state must be of the type denoted by E_{1u}^* to be strongly excited from the ground state. Hence the state E_{1u}^* shown at $Q+2{\cdot}15$ eV in figure 3 is the final state for the 1835 Å intense absorption in benzene. The calculated energy is 7·9 eV as compared with the experimental 6·7 to 7·0 eV. The calculated intensity for the transition has $f = 0{\cdot}22$, against the experimental 0·7. The discrepancies in these two comparisons, and especially the second, are both connected with the omission of structures with non-adjacent charges. It was noted earlier that the effect of the E_{1u} energy of such structures might be to reduce it by about 0·5 eV, and this would improve the energy calculations. But a far more substantial improvement would be made in the transition probability. The reason is that in calculating this the separation of charge in a polar structure enters as a square, and therefore a structure with charges on *para* atoms is four times as effective a contributor to the intensity as a structure with adjacent charges. One can understand therefore that the contribution by these structures to the wave functions may be of minor importance for an energy calculation, but of critical importance for the transition probability.

Since the E_{1u}^* state is the only final state for allowed transitions, the other transitions which show themselves in the absorption spectrum must do so by 'borrowing' some of the intensity of the allowed band. How this can happen through the disturbance caused by nuclear vibrations has been explained by Herzberg & Teller (1933). The transition which most effectively 'borrows' intensity in this way is the one at 2080 Å, for the intensity observed in it has an f value of about 0·1 electron, and this is roughly one-eighth of the whole intensity in the spectral region. This is the transition for which Goeppert-Mayer & Sklar (1938) have suggested the assignment A_{1g}–B_{1u}, based on a study of the energy levels of benzene by a refinement to the molecular orbital method of calculation. We shall discuss this assignment later in this paper. In the present calculations the excited states next above the B_{2u} are an E_{2g} and an E_{1u} state in that order, and the B_{1u} state lies well above them. Figure 3 shows that the E_{2g} state lies below the E_{1u} by a small margin, and reasons were given earlier for supposing that the inclusion of polar structure with remote charges would increase this margin, perhaps by 0·5 eV. The conclusion, therefore, is that the second excited state is E_{2g} with an E_{1u} state closely above it, and that the 2080 Å band comes from the transition A_{1g}–E_{2g} with perhaps some contribution to the intensity, starting at slightly shorter wave-lengths, by the transition A_{1g}–E_{1u}.

In considering in detail how these forbidden transitions come to appear, it is found that the transition A_{1g}–E_{2g} can appear in conjunction with a one-quantum change in any one of the vibrations b_{1u}, b_{2u} and e_{1u}, which cause perturbations of the E_{2g} state by the nearby E_{1u}^*. But a special circumstance arises in the A_{1g}–E_{1u} transition. This can appear only by the mixing of the E_{1u} state with the E_{1u}^*, and the symmetry rules suggest that this is effected by vibrations of symmetries a_{1g}, a_{2g} and e_{2g}. It is a question of the relative effectiveness of these vibrations in destroying the independence which, in the undisturbed molecule, exists between E_{1u} and E_{1u}^*. This independence is a consequence of the equal energies in pairs of structures like A and

B of figure 2, which differ only in having reversed charges, and if in a vibration of suitable symmetry this equality is destroyed then so also is the independence between E_{1u} and E^*_{1u}. It follows that no vibration such as a_{1g} or a_{2g} which preserves the regular hexagonal skeleton of the molecule can be effective. A possibly effective vibration, however, is e_{2g}, in which the carbon skeleton can be distorted to cause, for example, structures A and B to have slightly different energies, when the forces between remote nuclei and the charged atoms are taken into account. It may be taken that such a vibration may cause mixing of the E_{1u} and E^*_{1u} states and thus cause the former as well as the latter to appear in the spectrum.

To summarize this discussion, the V.B. theory makes an E_{2g} state the second excited singlet state of benzene and the one therefore which determines the long wave-length onset of the 2080 Å band through coupling with vibrations of types b_{1u}, b_{2u} and e_{1u}. Also, however, the theory finds an E_{1u} state closely above the E_{2g}, and this may contribute to the observed intensity of the band, although under more restricted perturbations by vibrations.

Comparison with the molecular orbital theory

It remains to mention the earlier assignment A_{1g}–B_{1u} for the 2080 Å band, made by Goeppert-Mayer & Sklar (1938) using the method of antisymmetrized molecular orbitals. A criticism of, and refinement to, this method appears in a later paper, but we may here mention some material points. The molecular orbitals for benzene have the symmetries a_{1u}, e_{1g}, e_{2u}, and b_{1g} in order of increasing energy. In the ground state the first of these is doubly filled, and the second (degenerate) orbital has its full complement of four electrons. Goeppert-Mayer & Sklar dealt with the excited states which arise when one electron is raised from the highest filled orbital (e_{1g}) to the lowest unfilled one (e_{2u}); there are three molecular states of this kind, B_{2u}, B_{1u} and E_{1u}. When the effect of electron repulsion is brought in, these three states are separated in energy, and the B_{2u} state is found to lie lowest, in agreement with the findings of the V.B. method. Next of the three states comes the B_{1u}, and Goeppert-Mayer & Sklar associated the 2080 Å absorption with the transition to this state. It is still conceivable, however, that in the method used by Goeppert-Mayer & Sklar, one might find that there is a lower-lying E_{2g} state. Such a state must correspond either to a two-electron jump (from the e_{1g} to the e_{2u} orbital), or to a one-electron jump between the two non-complementary orbitals (e.g. from the e_{1g} to the b_{2g} orbital). To get agreement between the two approximations it will be necessary to find that the E_{2g} state from one of these processes, or a combination of them, lies below the B_{1u} state. Such a finding would cause no surprise, for as noted in part I, the state of ethylene described in M.O. theory as having two electrons elevated is of slightly lower energy than the state (i.e. its singlet component) from the elevation of one electron. The reversal comes about because electron repulsion destabilizes the first state much less than the second, and the reduced electron repulsion more than makes up for the additional orbital energy required to elevate a second electron. It is just such a situation, with some additional complexity, which has to be anticipated in benzene.

I am very much indebted to Professor C. K. Ingold, F.R.S., Professor C. A. Coulson and Dr Allan Maccoll for discussions on these papers. The work has been carried out during the tenure of a Turner and Newall Research Fellowship in the University of London.

REFERENCES

Eyring, H., Walter, J. & Kimball, G. E. 1944 *Quantum chemistry.* New York: John Wiley.
Goeppert-Mayer, M. & Sklar, A. L. 1938 *J. Chem. Phys.* **6**, 645.
Herzberg, G. & Teller, E. 1933 *Z. phys. Chem.* **21**, 410.
Sklar, A. L. 1937 *J. Chem. Phys.* **5**, 669.

The nature of the sulphur-oxygen bond

By W. MOFFITT

British Rubber Producers' Research Association, Welwyn Garden City

(*Communicated by E. K. Rideal, F.R.S.—Received* 11 *August* 1949)

The electronic structures of certain molecules containing oxy-sulphur bonds are analyzed in some detail by means of the molecular orbital method. It is possible to make rough calculations which, despite the complexity of the systems considered, are nevertheless reasonably reliable. The physical and chemical properties of sulphur dioxide, sulphur trioxide and molecules of the types R_2SO_2 and R_2SO are discussed on the basis of these structures. In all these molecules it appears that the oxy-sulphur linkages are best described as double-bonded. A successful correlation between the molecular orbital criterion of bond strengths, namely, the bond orders, and the oxy-sulphur bond force constants may be set up. The measure of agreement attained between observed and predicted properties is quite satisfactory.

INTRODUCTION

The structure of the sulphoxides and sulphones has been a point of dissension since the earliest days of valence theory, and has more recently been revived as the chemical and physical properties of these and of the related oxides of sulphur have been more accurately determined. On increasing its valency in these compounds, does the sulphur atom form co-ordinate links with oxygen in the sense of Lewis & Sidgwick (I), or does it expand its *M* shell octet, bringing into play its 3*d* orbitals in double-bond formation (II)?

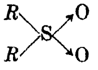
(I*a*) or

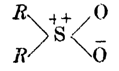
(I*b*);

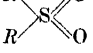
(II).

Arndt & Eistert (1941) appear, in effect, to have argued that since argon is an inert gas, the energy of promotion required to produce the requisite sulphur valence state must be exceedingly high and such as to preclude the formulation (II). Phillips, Hunter & Sutton (1945) have, however, taken the opposite viewpoint: since the dipole moments which they associate with the oxy-sulphur link is only about one-third of the value required for full-charge transference (I*b*), and because the oxy-sulphur separation is even shorter than that calculated on the basis of additivity for the S=O double bond, they infer that the best representation of the bond is given by (II). Wells (1949) is unwilling to accept these arguments and maintains that the descriptions of the conditions of bonding offered to date are all, in some way, inadequate.

The author will try in this paper to answer, on theoretical grounds, the question posed above and to obtain a more detailed picture of the various sulphur-oxygen linkages in different molecules. To this end molecular orbital theory will be used, since it appears that the pairing method, as at present applied to heteropolar systems, can only lead to a symbolic and not always very convenient restatement of their properties, when these are already known.

General considerations

As is well known, the method of molecular orbitals has been extensively developed by Mulliken and others for both inorganic and organic molecules. This method has recently been extended by the author (1949) to enable it to deal with the quantitative aspects of heteropolar systems. For the purposes of our analysis we have to elaborate the theory, since several as yet unformalized features will appear in the subsequent discussion.

To facilitate the resolution of our many-electron problem, we shall start off with a model of our systems which, at least on grounds of conventional valence theory, appears unexceptionable. We suppose that if a sulphur atom forms some sort of bonds with atoms $A, B, \ldots$, then to a first approximation the primary source of these linkages is a system of localized electron-pair bonds of unspecified polarity, represented by a system of localized molecular orbitals with approximate cylindrical symmetry about the $\mathrm{S}\text{–}A, \mathrm{S}\text{–}B, \ldots,$ axes respectively. This set of linkages will be said to constitute our σ-bond skeleton. In the next approximation, departures from localization may always be discussed, and we shall find occasion for doing this in the treatment of sulphoxides and sulphones. Each of the remaining electrons is treated as moving in the field of this framework and of the time-average field of the other remaining electrons. They may occupy non-bonding atomic, localized or non-localized molecular orbitals, the forms of which we must then decide in the different circumstances which arise. As a guide in making this assignment, the quantitative method referred to above will be used—though in this case the complexity of our molecules seems to rule out the possibility of accurate calculations.

We shall require the following lemma, that if atoms A and A' are joined to a central atom X by means of two pairs of non-localized bonding electrons $(y)^2(z)^2$—with (z) appreciably less strongly bonding than (y)—then any heteropolar character in these bonds will be taken up in (z) rather than in (y). This principle may be proved for LCAO theory except in unusual circumstances which we shall not encounter here, and is an extension of an argument used elsewhere that, in linear systems, π electrons are more readily polarized than σ electrons.

We shall also find it convenient to distinguish between two different forms of hybridization: when, as in quadrivalent carbon, the hybridization is associated with only one atomic configuration, such as sp^3, and arises in connexion with the approximation of localized molecular orbitals, we shall say that this is 'first-order hybridization'. Thus first-order hybridization enables us to construct four localized, tetrahedral bonds in methane. When, however, the hybridization is to describe the interaction of two or more different atomic configurations, each of which contains states with the same valence number as that associated with this atom in the molecule under consideration, then we speak of 'second-order hybridization'. We have had occasion to introduce second-order hybridization for the carbon atom in carbon monoxide (Moffitt 1949), where it was shown that such effects may exert a profound influence on the dipole moments of molecules.

THE SULPHUR ATOM

It is helpful to make a preliminary analysis of the atomic spectrum of sulphur, since the quantitative features of valence-state ionization processes are important for our later work. We may also discuss the relative energy levels of sulphur's various valence states. The notation and method which we use is fully described by Mulliken (1934), who carried out similar calculations for the elements of the first period and for the halogens.

In tables 1 and 2 we estimate the energies of the various valence states arising from the atomic configurations $(K)(L)(3s)^2(3p)^4$ and $(K)(L)(3s)^2(3p)^3$ of S I and S II

TABLE 1. THE ENERGIES OF STATES ARISING FROM S I, s^2p^4

state	theoretical energy (cm.$^{-1}$)	observed energy (cm.$^{-1}$)	calculated energy (cm.$^{-1}$)
^3P	$C-15G_2$	0·0	—
^1D	$C-9G_2$	8,815·6	
^1S	$C-0G_2$	18,609·0	—
$\pi^2\pi\sigma, V_2$ x^2yz, V_2	$C-13\frac{1}{2}G_2$	—	2,025
$\sigma^2\pi\pi, V_2$	$C-12G_2$	—	4,050
$\sigma^2\pi^2, V_0$	$C-9G_2$	—	8,815
$\pi^2\pi^2, V_0$ x^2y^2, V_0	$C-6G_2$		12,150

TABLE 2. THE ENERGIES OF STATES ARISING FROM S II, s^2p^3

state	theoretical energy (cm.$^{-1}$)	observed energy (cm.$^{-1}$)	calculated energy (cm.$^{-1}$)
^4S	$C-15G_2$	0·0	—
^2D	$C-6G_2$	14,867·7	—
^2P	$C-0G_2$	24,548·5	—
xyz, V_3	$C-10\frac{1}{2}G_2$	—	7,335
$\pi\pi\sigma, V_3$	$C-9G_2$	—	9,780
$\pi^2\sigma, V_1$	$C-6G_2$	—	14,670
$\sigma^2\pi, V_1$ $\pi^2\pi, V_1$ x^2y, V_1	$C-3G_2$	—	19,560

respectively. The term values of the spectroscopic states are taken from Ruedy (1933) for S I and from Bacher & Goudsmit (1933) for S II; these give us values for the Slater-Condon parameters G_2 by means of which the energies of the valence states are calculated. Since the first ionization of S I occurs at 10·31 eV, we may derive the ionization potentials given in table 3. And to complete our analysis of states arising from this normal configuration $(3s)^2(3p)^4$, we may use Glockler's (1934) extrapolated value of 2·0 eV for the electron affinity of the sulphur atom ($^3P \rightarrow {}^2P$) to obtain table 4.

TABLE 3. VALENCE-STATE IONIZATION POTENTIALS

$$\begin{tikzcd}[row sep=small] & \text{S}^+: x^2y,\ V_1 \approx 100{,}670\ \text{cm.}^{-1} \approx 12\cdot5\ \text{eV} \\ \text{S}: x^2yz,\ V_2 \arrow[ur] \arrow[dr] & \\ & \text{S}^+: xyz,\ V_3 \approx 88{,}450\ \text{cm.}^{-1} \approx 11\cdot0\ \text{eV} \end{tikzcd}$$

$$\begin{tikzcd}[row sep=small] & \text{S}^+: \pi\pi\sigma,\ V_3 \approx 90{,}890\ \text{cm.}^{-1} \approx 11\cdot3\ \text{eV} \\ \text{S}: \pi^2\pi\sigma,\ V_2 \arrow[ur] \arrow[r] \arrow[dr] & \text{S}^+: \pi^2\sigma,\ V_1 \approx 95{,}780\ \text{cm.}^{-1} \approx 11\cdot9\ \text{eV} \\ & \text{S}^+: \pi^2\pi,\ V_1 \approx 100{,}670\ \text{cm.}^{-1} \approx 12\cdot5\ \text{eV} \end{tikzcd}$$

TABLE 4. VALENCE-STATE ELECTRON AFFINITIES

$$\begin{tikzcd}[row sep=small] & \text{S}: {}^3P \approx 2\cdot0\ \text{eV} \arrow[dl] \\ \text{S}^-: {}^2P = V_1 & \left\{\begin{matrix} \text{S}: \pi^2\pi\sigma,\ V_2 \\ \text{S}: x^2yz,\ V_2 \end{matrix}\right. \approx 2\cdot3\ \text{eV} \arrow[l] \\ & \text{S}: \sigma^2\pi\pi,\ V_2 \approx 2\cdot6\ \text{eV} \arrow[ul] \end{tikzcd}$$

It is obvious that sulphur atom states of valence greater than two cannot arise from the configuration s^2p^4.

States arising from the excited configuration $(3s)^2(3p)^3(3d)$—with ionization limit $(3s)^2(3p)^3, {}^4\text{S}$ of S II—appear in the atomic spectrum of S I after about 8 eV. The number of these levels which have been identified is insufficient to determine the Slater-Condon parameters satisfactorily. There are also good reasons for supposing that the Slater rules would not, in any case, hold sufficiently well to warrant the detailed analysis of these levels, which would necessitate the rather tedious consideration of interconfigurational interactions. Accordingly, we shall content ourselves by observing that valence states from excited $(3s)^2(3p)^3(3d)$ of S I are at least 2 eV more stable than those arising from $(3s)^2(3p)^3$ of S II. Similarly and more strikingly, states from $(3s)(3p)^3(3d)^2$, S I are at least 15 eV more stable than those from $(3s)(3p)^3$, S III.

These results show that if the sulphur atom is to increase its valence number from two to three, four or more—and that it does so in the sulphoxides and sulphones seems incontrovertible—then, as regards its own valence state under such conditions, it will more readily promote its $3p$ electrons into its $3d$ levels than lose them altogether. The essential features of our problem are thus clear: We must determine where the compromise between the competing demands for a stable sulphur valence state, for strong oxy-sulphur bonds and for sulphur's electrons by electronegative oxygen atoms is attained in any particular molecule.

THE $3d$ ORBITALS OF SULPHUR

As appears from the foregoing work, we shall later be interested in sulphur's $3d$ orbitals so that it may be helpful to give a preliminary account of these before proceeding further.

It may be remarked straight away that the $3d$ orbitals are considerably more diffuse, more weakly bound to, and further removed from the sulphur nucleus than are the $3p$ orbitals: We must expect them to be quite appreciably polarized in the presence of perturbing fields $\mathscr{F}$ which remove their degeneracy. Thus whereas we may assess such splitting qualitatively by reducing the manifold spanned by the tesseral harmonics $T_l^m(\theta,\phi)$ $(l = 2; m_l = -l, \ldots, +l)$ according to the symmetry of $\mathscr{F}$ (Bethe 1929), we may no longer suppose that the angular dependence of their orbital functions may be accurately represented by linear combinations of the T_2^m. That is, the simplified atomic functions introduced by Slater (1930) will describe the symmetry properties, but not the actual forms of the orbitals which we shall find it necessary to use. This difficulty does not, of course, arise for the strongly bound $3d$ electrons of transition elements where these are the only valence electrons which the M shell contributes to bonding. Further, the covalent radii of hybrid sulphur orbitals containing $3d$ components will be greater than those of hybrid orbitals containing only $3s$ and $3p$. An inspection of the relevant spectroscopic data also shows that such hybrids will have a correspondingly lower electroaffinity (Mulliken 1934; Moffitt 1949).

A convenient set of normalized (unperturbed) $3d$ orbital functions will now be given which is appropriate for fields of symmetry C_{2v}. These may be obtained systematically by group theory or, more simply, by inspection from the set of functions $T_2^m(\theta,\phi)$, and are described by means of the symmetry symbols adopted by Herzberg (1945):

$$\begin{aligned}
\phi(3da_1) &= \frac{1}{4}\sqrt{\left(\frac{5}{\pi}\right)}.(3\cos^2\theta-1).f(r)\\
\phi(3db_1) &= \frac{1}{4}\sqrt{\left(\frac{15}{\pi}\right)}.\sin 2\theta\cos\phi.f(r)\\
\phi(3db_2) &= \frac{1}{4}\sqrt{\left(\frac{15}{\pi}\right)}.\sin 2\theta\,\sin\phi.f(r)\\
\phi(3da_2) &= \frac{1}{4}\sqrt{\left(\frac{15}{\pi}\right)}.\sin^2\theta\,\sin 2\phi.f(r)\\
\phi(3da_1)' &= \frac{1}{4}\sqrt{\left(\frac{15}{\pi}\right)}.\sin^2\theta\,\cos 2\phi.f(r),
\end{aligned}$$

where $f(r)$ is some normalized radial function. In this notation the $3p_x$, $3p_y$ and $3p_z$ orbitals of sulphur are respectively $\phi_S(3pb_1)$, $\phi_S(3pb_2)$ and $\phi_S(3pa_1)$. For sulphur trioxide, which belongs to the point group D_{3h}, we shall prefer to use the set

$$\begin{aligned}
\phi(da_1') &= \frac{1}{4}\sqrt{\left(\frac{5}{\pi}\right)}.(3\cos^2\theta-1).f(r)\\
\phi(3de''_\pm) &= \frac{1}{4}\sqrt{\left(\frac{15}{2\pi}\right)}.\sin 2\theta.e^{\pm i\phi}.f(r)\\
\phi(3de'_\pm) &= \frac{1}{4}\sqrt{\left(\frac{15}{2\pi}\right)}.\sin^2\theta.e^{\pm 2i\phi}.f(r),
\end{aligned}$$

in which case the appropriate $3p$ orbitals are

$$\phi(3pa_2'') = \phi(3p_z) \quad \text{and} \quad \phi(3pe_\pm') = \frac{1}{\sqrt{2}}\{\phi(3p_x) \pm i\phi(3p_y)\}.$$

THE STRUCTURE OF SULPHUR MONOXIDE

The simplest molecule containing an oxygen-sulphur bond is, of course, sulphur monoxide. A brief description of its electronic structure will be given here although, as will appear later, it is not well suited for purposes of comparison with other oxy-sulphur bonds. By analogy with the related molecules O_2 and S_2, it is clear that, apart from some second-order hybridization, the valence states for both oxygen and sulphur arise from atomic configurations s^2p^4. Accordingly, we have two pairs of essentially non-bonding electrons $(3s_S)^2$ and $(2s_O)^2$ and a σ-bonding pair of electrons. The remaining electrons may be represented by the molecular orbitals

$$(a\pi)^4\,(b\pi)^2,$$

where the four $(a\pi)$ electrons are bonding and the two $(b\pi)$ electrons are anti-bonding. (The symbol π here implies that the molecular orbitals to which they refer have unit components of angular momentum about the internuclear axis. To conform to current usage, this symbol will later be used in a rather different sense.)

If we express these molecular orbitals in LACO form

$$\psi(a\pi) = \gamma_S^a\phi_S(3p\pi) + \gamma_O^a\phi_O(2p\pi), \quad \psi(b\pi) = \gamma_S^b\phi_S(3p\pi) + \gamma_O^b\phi_O(2p\pi),$$

then, on setting $\gamma_S = \sin\theta$, our 'self-consistent method' gives

$$\{(I_O + E_O) - (I_S + E_S)\} = \{(I_O - E_O) + (I_S - E_S)\}\cos 2\theta - 4\beta^g_{SO}\cot 2\theta = 0,$$

where I_S, I_O and E_S, E_O are the appropriate valence-state ionization potentials and electron affinities. With $\beta^g_{SO} = -2\,\text{eV}$ (*vide infra*), it is found that the total π bond order is approximately 0·98, and that the formal charge associated with the sulphur atom is in the neighbourhood of $+0{\cdot}18$.

Essentially, therefore, it is clear that the S and O atoms are doubly bonded here. On antisymmetrizing, it is easily shown that of the three states, namely, $^1\Delta$, $^1\Sigma^+$ and $^3\Sigma^-$, which arise from this configuration, the triplet state is the most stable. The force constant, dissociation energy and internuclear separation in SO, $^3\Sigma^-$ have been determined spectroscopically as $7{\cdot}9 \times 10^5$ dynes/cm., 92 kcal./mole and 1·49 Å respectively.

THE STRUCTURE OF SULPHUR DIOXIDE

As far as the author is aware, no detailed discussion of the structure of sulphur dioxide has yet been given, although it is perhaps the simplest example of a molecule containing sulphur with a valence number greater than two. It may easily be shown that the linear form of SO_2 is energetically unstable with respect to the triangular form, so that this molecule belongs to the point group C_{2v}. (The symmetry notation is explained by Herzberg (1945); our origin of co-ordinates is taken at the sulphur nucleus, with the axes of z and y bisecting the OSO angle internally and externally respectively.) On quite general grounds the electronic structure of sulphur dioxide may now be described, qualitatively, by the molecular orbitals:

$$(ta_1)^2(tb_2)^2(ua_1)^2(wa_1)^2(wb_2)^2(xb_1)^2(va_2)^2; \tag{1}$$

we have omitted two pairs of non-bonding electrons $(2s_O)^2(2s_O)^2$ on the oxygen atoms since second-order hybridization of these is supposed to be small. The order in which the molecular orbitals are specified is, at this stage, quite arbitrary. In writing (ta_1), for example, the letter t simply serves to identify a particular orbital whose symmetry properties are represented by the species symbol a_1. The transformation properties of the various orbital functions, as irreducible representations of the point group C_{2v}, are assembled schematically in table 5. We must now attempt to assign semi-quantitative LCAO forms to these different molecular orbitals and thence to describe these oxy-sulphur bonds.

TABLE 5. SCHEMATIC REPRESENTATIONS OF THE TRANSFORMATION PROPERTIES OF THE VARIOUS MOLECULAR ORBITALS. (THE SHADED SEGMENTS REVERSE THE SIGNS OF THE CORRESPONDING UNSHADED SEGMENTS)

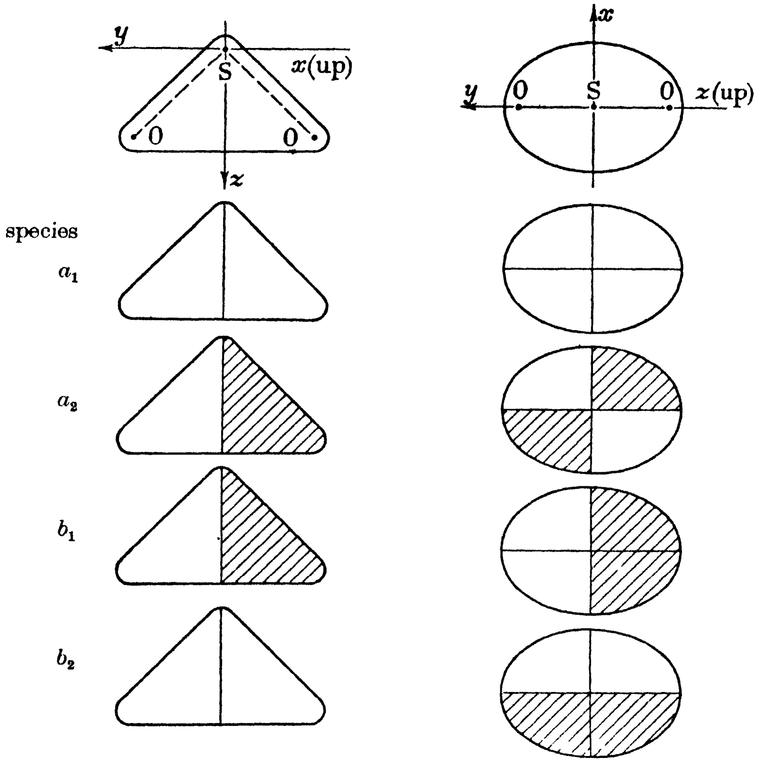

To this end we shall refer the quantization of the individual oxygen atom orbitals to local axes, one on each O atom: $2p\sigma$ denotes that $2p$ orbitals of oxygen whose component of angular momentum about the SO axis vanishes, and the nodal plane of 2π coincides with the molecular $(yz-)$ plane; $2pw$ is orthogonal to both $2p\sigma$ and

$2p\pi$. We notice that these orbitals of the two oxygen atoms O, O′ constitute a reducible representation of our symmetry group, so that we may form irreducible linear combinations from, say, $2p\sigma$ and $2p\pi$:

$$\phi_O(2pa_1) = \frac{1}{\sqrt{2}}\{\phi_O(2p\sigma)+\phi_{O'}(2p\sigma)\}, \quad \phi_O(2pb_1) = \frac{1}{\sqrt{2}}\{\phi_O(2p\pi)+\phi_{O'}(2p\pi)\},$$

$$\phi_O(2pb_2) = \frac{1}{\sqrt{2}}\{\phi_O(2p\sigma)-\phi_{O'}(2p\sigma)\}, \quad \phi_O(2pa_2) = \frac{1}{\sqrt{2}}\{\phi_O(2p\pi)-\phi_{O'}(2p\pi)\}.$$

Similarly the two $2pw$ orbitals have irreducible components $\phi_O(2pa_1)'$ and $\phi_O(2pb_2)'$, where the primes serve to distinguish these from the irreducible components of the two $2p\sigma$ orbitals.

Our model now allows us to identify two pairs of molecular orbitals of (1). For we have assumed that, in the approximation of localized molecular orbitals, we may form a σ electron pair bond between the sulphur and each of the oxygen atoms. These clearly have the form

$$\psi(q) = \gamma^q_S\phi_S(3q\sigma)+\gamma^q_O\phi_O(2p\sigma), \quad \psi(q') = \gamma^q_S\,\phi_S(3q'\sigma)+\gamma^q_S\phi_{O'}(2p\sigma),$$

where the hybrid sulphur atom orbitals $3q\sigma$, $3q'\sigma$ are directed towards O, O′ respectively. Delocalizing, we may form the molecular orbitals

$$\psi(qa_1) = \frac{1}{\sqrt{2}}\{\psi(q)+\psi(q')\}, \quad \psi(qb_2) = \frac{1}{\sqrt{2}}\{\psi(q)-\psi(q')\},$$

whose most general LCAO forms are easily shown to be

$$\psi(ta_1) = \gamma^t_S\phi_S(3ta_1)+\gamma^t_O\phi_O(2pa_1),$$

$$\psi(tb_2) = \bar{\gamma}^t_S\phi_S(3pb_2)+\bar{\gamma}^t_O\,\phi_O(2pb_2);$$

their coefficient parameters do not now satisfy $\gamma^t_i = \bar{\gamma}^t_i (i = \mathrm{S, O})$. We may therefore pick out the two pairs of σ-bonding electrons from (1).

As it seems most unlikely that (ta_1) and (tb_2) should have very much sulphur $3d$ character, $\phi_S(3ta_1)$ will be given by

$$\phi_S(3ta_1) = \cos\chi.\phi_S(3pa_1)+\sin\chi.\phi_S(3sa_1).$$

The hybridization parameter χ determines the amount of sulphur $3s$ character in the σ bonds. χ will be small and only greater than zero in order to strengthen this σ-bonding; as χ increases, so does the angle OSO (*vide infra*).

χ also determines the remaining sulphur a_1 orbital:

$$\phi_S(3ua_1) = \cos\chi.\phi_S(3sa_1)-\sin\chi.\phi_S(3pa_1).$$

Since the oxygen $\phi_O(2pa_1)'$ orbital does not overlap $\phi_S(3ua_1)$ at all strongly for any values of χ and the sulphur $3s$ electrons are only released at the expense of large atomic promotional energy, this $\phi_S(3ua_1)$ orbital of sulphur will contain two, essentially $3s$, non-bonding electrons. These are the $(ua_1)^2$ electrons of (1). As χ increases from zero, so the (ua_1) electrons are progressively directed along the negative z-axis, away from the σ-bonding region.

Further, $\phi_O(2pa_1)'$ and $\phi_O(2pb_2)'$ do not overlap any sulphur $3d$ orbitals, of favourable symmetry, sufficiently strongly to suggest that they might be bonding. For, quite apart from the energy of promotion necessary to attain the appropriate sulphur valence state, it seems unlikely that such supplementary bonding would warrant trespass into the zone of the four strongly σ-bonding electrons. It therefore seems clear that $(wa_1)^2$ and $(wb_2)^2$ of (1) must be identified with two pairs of non-bonding oxygen electrons in $\phi_O(2pa_1)'$ and $\phi_O(2pb_2)'$ respectively—and these are best regarded as localized in pairs on each of the two oxygen atoms.

By symmetry, the remaining molecular orbitals, (xb_1) and (va_2), have the LCAO forms

$$\psi(xb_1) = \gamma^x_S\phi_S(3pb_1)+\gamma^x_O\phi_O(2pb_1), \quad \psi(va_2) = \gamma^v_S\phi_S(3da_2)+\gamma^v_O\phi_O(2pa_2)$$

(the amount of $3d$ character in (xb_1) should be very small) with nodes in the molecular plane. We shall suppose that these more mobile or π electrons will take up any heteropolar character in the oxy-sulphur links. They must therefore be assigned to a framework consisting of one doubly-charged sulphur atom and two singly-charged oxygen atoms. If $\gamma^v_S = 0$ and $\gamma^x_S = \gamma^x_O$, we should have a charge distribution which may be represented by (III) with full resonance. The conditions for strict co-ordinate bonding are that $\gamma^x_S = 0 = \gamma^v_S$ when we get I; and, at the other extreme, only when $\gamma^x_S = \gamma^x_O$ and $\gamma^v_S = \gamma^v_O$ do we obtain II.

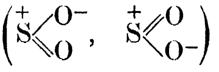
(III)

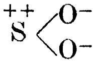
(I);

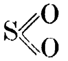
(II)

Now, according to our self-consistent LCAO theory, the γ's appear as variational parameters whose optimum values must be determined by minimizing the total zeroth-order energy with respect to these γ's. In this way we may decide which of the formulations (I), (II) and (III) most nearly represents the actual bonding conditions in sulphur dioxide. In order to follow this programme it is first necessary to have values for certain atomic terms and so-called resonance integrals. We may give adequate, if not accurate, estimates of the former by examining the spectral data on the oxygen and sulphur atoms, but we know rather less about the values which should be assigned to the latter. To avoid interrupting our argument, the resonance integrals are discussed in the following section, where our method of estimating these is adumbrated.

In a notation which was explained in an earlier paper (Moffitt 1949), we have to solve the equations

$$(\xi^x_S - \xi^x_O)+2\sqrt{2}\,.\,\beta^p_{SO}\cot 2\phi = 0,$$

$$(\xi^v_S - \xi^v_O)+2\sqrt{2}\,.\,\beta^d_{SO}\cot 2\theta = 0,$$

where we have set $\gamma^x_S = \sin\phi$ and $\gamma^v_S = \sin\theta$. The ξ^τ_i $(\tau = x, v; i = \mathrm{S}, \mathrm{O})$ represent Coulomb terms and have the form

$$\xi^\tau_i = A^\tau_i + B^\tau_i\cos 2\phi + C^\tau_i\cos 2\theta,$$

where the A_i^r, B_i^r, C_i^r are constants with the dimensions of energy which may be derived from the atomic spectra of oxygen and sulphur. We must therefore solve these equations together. It appears that, for any feasible values of the parameters, ϕ lies close to $\frac{1}{4}\pi$; we are justified in assuming that the (va_2) electrons are more polarizable than the (xb_1) electrons and may, by setting $\phi = \frac{1}{4}\pi$, attribute any heteropolar character in the oxy-sulphur bonds to the former. We infer straight away that the final charge distribution in sulphur dioxide, if it is to be represented in electron-pair symbolism, must lie between (II) and (III). The resultant positive charge on sulphur cannot exceed $+e$, where e is the numerical value of the electronic charge.

Neglecting second-order hybridization for the moment, the valence state of sulphur dioxide is therefore intermediate between

$$\mathrm{S}, V_4\colon\quad (3s)^2(3pa_1{}^*)\,(3pb_1{}^*)\,(3pb_2{}^*)\,(3da_2{}^*)$$

and

$$\mathrm{S}^+, V_3\colon\quad (3s)^2\,(3pa_1{}^*)\,(3pb_1{}^*)\,(3pb_2{}^*),$$

whereas that of each oxygen atom arises from

$$\mathrm{O}, V_2\cdot\quad (2s)^2\,(2p\sigma^*)\,(2p\pi^*)\,(2pw)^2$$

and

$$\mathrm{O}^-, V_1\colon\quad (2s)^2\,(2p\sigma^*)\,(2p\pi)^2\,(2pw)^2.$$

with the former more important than the latter. (Asterisks are used to denote valence orbitals.) Our self-consistent field method now enables us to estimate where the compromise between strong oxy-sulphur bonding and the different electro-affinities of O and S is attained.

With $\phi = \frac{1}{4}\pi$, θ and hence the form of (va_2) may be determined from the equation

$$\{(I_\mathrm{O}+3E_\mathrm{O})-2(I_\mathrm{S}^d+E_\mathrm{S}^d)\} = \{(I_\mathrm{O}-E_\mathrm{O})+2(I_\mathrm{S}^d-E_\mathrm{S}^d)\}\cos 2\theta - 8\sqrt{2}\,.\,\beta_\mathrm{SO}^d\cot 2\theta;$$

here I_S^d, E_S^d are respectively the ionization potential and electron affinity of $(3da_2{}^*)$ in our S, V_4 and I_O, E_O those of $(2p\pi^*)$ in O, V_2. The spectroscopic data are not really complete enough for us to determine I_S^d, E_S^d accurately; apparent values for I_S^d are of the order of 2 eV, but for such valence states this figure is almost certainly too low. We shall suppose that the more feasible values $I_\mathrm{S}^d = 4$ eV and $E_\mathrm{S}^d = 0$ are approximately correct when, together with $\beta_\mathrm{SO}^d = -0{\cdot}7$ eV and the known values $I_\mathrm{O} = 17$ eV, $E_\mathrm{O} = 3$ eV, we obtain $\cos 2\theta = 0{\cdot}48$. We associate the following formal charges with oxygen and sulphur respectively

$$Q_\mathrm{S} = (1-2\sin^2\theta) = +0{\cdot}48, \quad Q_\mathrm{O} = \tfrac{1}{2}(1-2\cos^2\theta) = -0{\cdot}24 = Q_{\mathrm{O}'}.$$

(We see that structure (II) and the hybrid structure (III) appear to contribute equally to the bonding—although we have no direct means of assessing the energetics of such a resonating system in the pairing approximation.)

The total π bond order for each oxy-sulphur link is then easily seen to be

$$p_\mathrm{SO}^\pi = \sqrt{2}\,.\,\gamma_\mathrm{S}^x\gamma_\mathrm{O}^x + \sqrt{2}\,.\,\gamma_\mathrm{S}^v\gamma_\mathrm{O}^v\cdot(\beta_\mathrm{SO}^d/\beta_\mathrm{SO}^p) = 0{\cdot}93,$$

with contributions 0·71 and 0·22 from the (xb_1) and (va_2) electrons respectively. The S—O bonding is therefore essentially double and very strong—as may also be seen from the relatively high dissociation energy ($\sim$ 250 kcal.) of the molecule.

We may deduce that the σ-bonding electrons are in a condition of considerable strain (Moffitt 1949) which they will tend to relieve by second-order hybridization, e.g. by increasing from zero the value of the parameter χ. In this way the covalent radius of $\phi_S(3ta_1)$ or of $\phi_S(3q\sigma)$ is decreased and the OSO angle is increased from $\frac{1}{2}\pi$. This effect, together with oxygen-oxygen repulsions, explains the large OSO angle ($\sim\frac{2}{3}\pi$) which is observed experimentally.

We might now give a rather naïve estimate of the dipole moment of SO_2 on the basis of this calculated formal charge distribution ($r_{SO} = 1{\cdot}43$ Å from experimental data):

$$\mu(SO_2) = -2r_{SO}\, e\, Q_O \cos(\tfrac{1}{3}\pi) \approx 1{\cdot}7 \text{ Debye units.}$$

But, in doing so, we have neglected such effects as arise from second-order hybridization at the sulphur and oxygen atoms, from the so-called homopolar moments, and from the polarization of $\phi_S(3da_2)$, which is almost certainly pulled towards the two oxygen atoms. The observed moment ($\sim 1{\cdot}6$ Debye units) suggests—and not unreasonably, on theoretical grounds—that these modifying factors, some of which are not small, tend to cancel out. Somewhat fortuitously, therefore, our first approximation to the dipole moment of sulphur dioxide is found to be very good.

As to its chemical reactivity, we notice that the non-bonding (ua_1) electrons of sulphur in SO_2 are in many respects similar to the non-bonding donor electrons on the carbon atom in carbon monoxide or the isonitriles and on the nitrogen atoms of amines. Its oxidation reactions to form, for example, SO_3 and SO_2Cl_2 are thus readily understood.

THE SULPHUR-OXYGEN RESONANCE INTEGRALS

In this section we shall consider the values of the mobile electron resonance integrals between sulphur and oxygen at internuclear separations r_{SO} in the neighbourhood of 1·44 Å, neglecting their variation with r_{SO}. Most generally, suppose we have a hybrid *pd* orbital $3h\pi$ of sulphur—antisymmetric with respect to reflexions in the *yz*-plane and therefore of π type—whose bonding potentialities with an oxygen $2p\pi$ orbital are to be investigated (we assume that these S and O atoms are already bound together by a σ-electron pair bond):

$$\psi(h) = \gamma_S^h \phi_S(3h\pi) + \gamma_O^h \phi_O(2p\pi).$$

$\phi_S(3h\pi)$ is of the form

$$\phi_S(3h\pi) = \cos\zeta\, \phi_S(3p\pi) + \sin\zeta\, \phi_S(3d\pi),$$

so that β_{SO}^h, the corresponding resonance integral, is given by

$$\beta_{SO}^h = \cos\zeta \,.\, \beta_{SO}^p + \sin\zeta \,.\, \beta_{SO}^d,$$

where β_{SO}^p, β_{SO}^d are the resonance integrals between $\phi_O(2p\pi)$ and $\phi_S(3p\pi)$, $\phi_S(3d\pi)$ respectively. Since both β_{SO}^p and β_{SO}^d are negative, β_{SO}^h is a minimum when $\zeta = \zeta^o$, where

$$\zeta^o = \tan^{-1}(\beta_{SO}^d/\beta_{SO}^p).$$

We see, therefore, that *ceteris paribus* the π-bonding between sulphur and oxygen is at its strongest for a hybrid and not for a pure *p*- or *d*-bonding orbital of sulphur.

But, as will appear, ζ^o and therefore also the amount of $3d$ character of the best bond is small.

Concerning the relative magnitudes of β^p_{SO} and β^d_{SO}, it is clear on grounds of overlap that $|\beta^d_{SO}| < |\beta^p_{SO}|$. The $p\pi$ orbital of sulphur has no directional preference in π-bonding; we may estimate the value of β^p_{SO} as lying somewhere near -2 eV and as remaining reasonably constant under a variety of different circumstances. The value of β^d_{SO} will, however, depend upon the particular choice of $d\pi$ (there are always two such $d\pi$ orbitals) relative to the location of the oxygen nucleus on the circle of radius 1·44 Å in the yz-plane with the sulphur nucleus as centre.

Recent unpublished work by Mulliken and his collaborators suggests that, in hydrocarbons, the value of somewhat analogous quantities are proportional to the corresponding overlap integrals S_{CC}. It would be very convenient if we could also compare the values of β^d_{SO} and β^p_{SO} on this basis, but this seems impossible: In the first place, whereas Slater functions are probably good guides for calculations of S_{CC}, or even S^p_{SO}, values of S^d_{SO} depend critically upon the screening constants assumed for the $3d$ orbitals, and these are not at all well known for sulphur. Also, as we mentioned earlier, analytical functions of the Slater type are very unlikely to give accurate representations of these polarizable orbitals. They would moreover give undue prominence to d orbital directional effects. From the results of such overlap considerations it does, however, appear that $|\beta^d_{SO}|$ increases much more rapidly with increasing electroaffinity of the sulphur atom (as caused, for example, by the effects of substituents) than does $|\beta^p_{SO}|$. We must therefore rely on what we may take to be reasonable values for the β^d_{SO} in different circumstances with no more fundamental justification for these than that which may appear on comparing our results with observed properties. We shall, depending on the environments encountered, take values for β^d_{SO} ranging from -1 to $-0{\cdot}5$ eV. Fortunately our results are not very sensitive to the particular choice adopted.

In taking π bond orders p^π_{SO} as our criteria of bond strength, more difficulties arise. Suppose, for example, that the order of a particular bond $(h\pi)^2$, formed by a hybrid $3h\pi$ orbital of sulphur and $2p\pi$ of oxygen, is p^h_{SO} according to its usual analytical definition:

$$p^h_{SO} = 2\gamma^h_S\gamma^h_O.$$

Then, in order to compare $(h\pi)^2$ with other oxy-sulphur π bonds, we shall define

$$p^\pi_{SO} = p^h_{SO}\cdot(\beta^h_{SO}/\beta^p_{SO}),$$

whereby we have tacitly assumed that β^p_{SO} remains constant for different bonds. Such a definition may evidently be extended to cover delocalized π-bonding. It should be noticed that even for a localized bond $(h\pi)^2$, p^π_{SO} will exceed unity whenever $|\beta^h_{SO}| > |\beta^p_{SO}|$ and $p^h_{SO} = 1$. (Unfortunately our obvious standard of comparison for such a scale, namely sulphur monoxide in which the π-bonding is known to be nearly pure p, is not very suitable. For the potential energy curve of such a diatomic molecule can hardly be expected to be analogous to those of S=O in polyatomic molecules.)

Now, whereas p^π_{SO} may symbolize the contribution from $(h\pi)^2$ to the total energy of bonding, it is not strictly correct to compare internuclear distances (and force constants) on such a basis. For, if $\beta^{d}_{\mathrm{SO}}/\beta^{p}_{\mathrm{SO}} = c$, we should have to assume that the ratio, of the first (and second) derivatives of β^{d}_{SO} and β^{p}_{SO} with respect to r_{SO} are equal to c also. Nevertheless, as a first approximation, we shall have to suppose that such a procedure is roughly valid and the quantities p^{π}_{SO} which we give are estimated in this way. Since the infra-red spectra of sulphoxides and sulphones have been extensively investigated recently (Barnard, Fabian & Koch 1949), we shall compare our calculated p^{π}_{SO}'s with, in particular, the observed force constants of various oxy-sulphur bonds. And it is encouraging in this respect that Coulson & Moffitt (1949) have found that the energies and force constants of other hybrid bonds appear to be comparable in a similar manner.

(The bond orders p^{π}_{SO}, which we have introduced, are particular cases of a more general definition of bond order suggested by the author (1946) in another connexion. Only in this way can the differential relationship between energy and bond order be preserved.)

THE STRUCTURE OF THE SULPHONES

The electronic structure of the sulphone group may be analyzed by means of arguments which are closely analogous to those which we have used in dealing with sulphur dioxide. Consider first a symmetric sulphone R_2SO_2, the electronegativity of whose R radicals is not very different from the electronegativity of sulphur. In accordance with our model, we may suppose that only four electrons are involved in bonding R_2 to sulphur, and that these may be represented in the approximation of localized molecular orbitals by two σ-type electron pair bonds. It may be shown that such molecules have local symmetry C_{2v}, being approximately tetrahedral, so that we may continue to use the notation introduced for SO_2. The electronic structure may be represented by the system of molecular orbitals

$$(ta_1)^2\,(tb_2)^2\,(ra_1)^2\,(rb_1)^2\,(wa_1)^2\,(wb_2)^2\,(xb_1)^2\,(va_2)^2. \tag{2}$$

The two R radicals are situated in the half of the xz-plane which corresponds to negative values of z, and are symmetrically disposed on opposite sides of the yz-plane. If the R—S bonding orbital of R is $\phi_R(r\sigma)$, we may form the linear combinations

$$\phi_R(ra_1) = \frac{1}{\sqrt{2}}\{\phi_R(r\sigma)+\phi_{R'}(r\sigma)\}, \quad \phi_R(rb_1) = \frac{1}{\sqrt{2}}\{\phi_R(r\sigma)-\phi_{R'}(r\sigma)\}.$$

As before, $(wa_1)^2$ and $(wb_2)^2$ are two pairs of non-bonding oxygen electrons and $(ta_1)^2\,(tb_2)^2$, representing the σ-bonding between S and O_2, also have the same LCAO forms as for sulphur dioxide; only whereas the parameter χ, defining $\phi_{\mathrm{S}}(3ta_1)$, represented second-order hybridization in that context, it now describes first-order hybridization in view of the greater valence number of sulphur in the sulphones. Accordingly instead of the small χ with which we were then dealing, our χ will now be in the neighbourhood of $\frac{1}{4}\pi$. $(ra_1)^2\,(rb_1)^2$ is the more general, delocalized form for the two R—S σ electron pair bonds:

$$\psi(ra_1) = \gamma^{r}_{\mathrm{S}}\phi_{\mathrm{S}}(3ra_1)+\gamma^{r}_{R}\phi_R(ra_1), \quad \psi(rb_1) = \bar{\gamma}^{r}_{\mathrm{S}}\phi_{\mathrm{S}}(3rb_1)+\bar{\gamma}^{r}_{R}\phi_R(rb_1).$$

The hybrid sulphur atom orbital $\phi_{\mathrm{S}}(3ra_1)$ has the same form as $\phi_{\mathrm{S}}(3ua_1)$ of sulphur dioxide, but is to be distinguished from this by its different value of χ:

$$\phi_{\mathrm{S}}(3ra_1) = \cos\chi\cdot\phi_{\mathrm{S}}(3sa_1)-\sin\chi\cdot\phi_{\mathrm{S}}(3pa_1).$$

$\phi_S(3rb_1)$ is also a hybrid sulphur orbital, associated with a first-order hybridization parameter ζ:

$$\phi_S(3rb_1) = \sin\zeta . \phi_S(3pb_1) - \cos\zeta . \phi_S(3db_1).$$

$(xb_1)^2$ and $(va_2)^2$ are again two pairs of π-bonding electrons between S and O_2, but whereas in sulphur dioxide the sulphur constituent of (xb_1) was almost pure $\phi_S(3pb_1)$, it is now the other hybrid defined by ζ, namely,

$$\phi_S(3xb_1) = \cos\zeta . \phi_S(3pb_1) + \sin\zeta . \phi_S(3db_1).$$

The specific value assumed by ζ for any particular sulphone will be determined by the condition of minimum energy. In the notation of the preceding section, the resonance integral representing (xb_1) bonding in these sulphones is β^h_{SO}, so that strongest oxy-sulphur bonding would result if $\zeta = \tan^{-1}(\beta^d_{SO}/\beta^p_{SO})$ ($< \frac{1}{4}\pi$, since $|\beta^d_{SO}| < |\beta^p_{SO}|$). But as the (rb_1) electrons are also strongly bonding on the other side of the sulphur atom, it is clear that these will be unwilling to surrender as much of their $3p$ character as would be required for such optimum (xb_1) bonding. For in the range of ζ considered, we may safely assume that any increase in the $3d$ character of (rb_1) corresponds to a weakening of the R—S bonds; only when (rb_1) is very weakly bonding, owing to large discrepancies between the appropriate S and R electronegatives, say, will ζ be as small as $\tan^{-1}(\beta^d_{SO}/\beta^p_{SO})$.

Let us describe the ideal case of a sulphone in which the radicals R are such that the electrons $(ra_1)^2(rb_1)^2$ represent two homopolar R—S bonds. Since $(xb_1)^2$ will, again, be considerably more strongly bonding than $(va_2)^2$, we may take it that any heteropolar nature in the oxy-sulphur links will be taken up in $(va_2)^2$, that is, that $\gamma^x_S = \frac{1}{\sqrt{2}} = \gamma^x_O$. It remains to fit the two (va_2) electrons into the skeleton formed by the two R—S and the two O—S σ bonds, the two pairs of non-bonding oxygen electrons, the two oxy-sulphur π-bonding electrons $(xb_1)^2$ and the various 'nuclei'. Such a skeleton is associated with a formal charge of $+e$ on the sulphur atom and $+\frac{1}{2}e$ on each of the oxygen atoms.

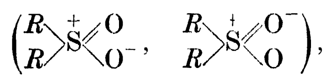
(III);

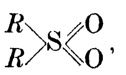
(II)

Again, before applying our modified LCAO method, we may deduce that the bonding in such a sulphone is intermediate between structure (II) and (III), and that (I) of the introduction is unimportant. Also the appropriate sulphur valence state lies between

S, V_6: $(3ta_1^*)(3tb_2^*)(3ra_1^*)(3rb_1^*)(3xb_1^*)(3da_2^*)$ of S I, sp^3d^2

and S^+, V_5: $(3ta_1^*)(3tb_2^*)(3ra_1^*)(3rb_1^*)(3xb_1^*)$ of S II, sp^3d.

In order to obtain a more detailed picture of the bonding, we find that our problem is identical with that already solved for the analogous electrons in sulphur dioxide. Accordingly, taking $\beta^d_{SO} = -0.7$ eV, the formal charges are once more

$$Q_S = +0{\cdot}48, \quad Q_O = -0{\cdot}24 = Q_{O'},$$

and the contribution from $(va_2)^2$ to the total π bond order of each oxy-sulphur link is again 0·22. The $(xb_1)^2$ bonding strength is now rather different, however, since this depends on the magnitude of β^{h}_{SO}, which is a function of ζ. In the light of our experience from SO_2, it is clear that $(xb_1)^2$ is potentially strongly bonding, as is $(rb_1)^2$. Accordingly we shall not err greatly by taking $\zeta = \frac{1}{4}\pi$; in which case the contribution to p^{π}_{SO} from $(xb_1)^2$ is approximately 0·68. (Since the $\beta^{h}_{\mathrm{SO}} - \zeta$ curve is not steep in the neighbourhood of $\frac{1}{4}\pi$, our bond orders are hardly affected by feasible departures from this value.) The total bond order in such sulphones is therefore

$$p^{\pi}_{\mathrm{SO}} = 0{\cdot}68 + 0{\cdot}22 = 0{\cdot}90.$$

Let us now see how these estimates are to be modified when we replace our idealized R radicals (chosen so as to ensure homopolar R—S bonding) by alkyl groups. The sulphur atom, with $Q_{\mathrm{S}} = +0{\cdot}48$, is easily shown to be more electronegative than the alkyl groups. As a first approximation, such an effect will not change p^{π}_{SO}, but will serve to increase the dipole moment of the molecule. Since the positive charge moves considerably farther from the negatively charged oxygen atom, we may expect these increases in moment to be quite large, probably of the order of 1 Debye unit. Further, the subsidiary factors enumerated for SO_2 will no longer cancel each other out owing to the absence of second-order hybridization moments at the sulphur atoms; these too will therefore serve to enhance the dipole moment of the alkyl sulphones. Phillips, Hunter & Sutton (1945) quote values ~4·4 Debye units for dimethyl and diethyl sulphones, which are in good agreement with these expectations.

In the next approximation, the lowering of the formal sulphur charge also serves to increase the polarities of the oxy-sulphur bonds and to lower p^{π}_{SO} slightly. This is easily shown by differentiating our equations with respect to the appropriate sulphur Coulomb terms. Our quantitative estimates should thus be revised somewhat; we shall suppose that for alkyl sulphones we have, more nearly,

$$p^{\pi}_{\mathrm{SO}} = 0{\cdot}89, \quad Q_{\mathrm{O}} = -0{\cdot}26 = Q_{\mathrm{O}'}.$$

Let us study the shapes of the alkyl sulphones more closely, discussing possible departures from a tetrahedral arrangement of oxygen atoms and alkyl groups about the central S atom. In the first place, only when $\zeta = \frac{1}{2}\pi$ and $\chi = \frac{1}{4}\pi$ will the σ bond skeleton be tetrahedral. Since, however, $\zeta \approx \frac{1}{4}\pi$ and $\chi \approx \frac{1}{4}\pi$ the sulphur $3d$ character of the R—S bonds will tend to decrease the RSR angle—though this effect is not expected to be large. Secondly, since the strong S—O bonds are short (~1·44 Å), $(ta_1)^2$ will tend to make greater demands for sulphur $3s$ character than $(ra_1)^2$, so that χ is rather greater than $\frac{1}{4}\pi$ and consequently the angles OSO and RSR are increased and decreased respectively. But steric factors favour the tetrahedral arrangements which makes it difficult to predict the magnitudes of such effects.

We may, however, expect the $3d$ character of the R—S bonds to manifest itself in other ways. For the covalent radius of $\phi_{\mathrm{S}}(3d)$ is considerably greater than that of $\phi_{\mathrm{S}}(3s)$ or $\phi_{\mathrm{S}}(3p)$. Accordingly the R—S bonds should be longer than those in the alkyl sulphides. And this is indeed observed, for Lister & Sutton (1939) find the carbon-sulphur separation in dimethyl sulphone to be 1·90 Å—which is to be compared with ~1·80 Å in the sulphides.

Finally, we consider the replacement of our idealized R groups by chlorine (sulphuryl chloride) and fluorine. These electronegative atoms will tend to form polarities in the R—S bonds whose moments oppose those in the S—O bonds. It is difficult to calculate the magnitudes of such moments, but we may discuss the effect of these on the oxy-sulphur bonds. Any heteropolar character in the sulphur-halogen bonds may be ascribed to the (rb_1) electrons, which are easily shown to be less strongly bonding than the (ra_1) electrons. Accordingly $(rb_1)^2$ will be prepared to cede some of its $3p$ character to $(xb_1)^2$, and consequently strengthen the oxy-sulphur bonding by letting ζ approach the optimum value ζ^o. At the same time the increased formal charge associated with the sulphur atom will strengthen the bonding by increasing $|\beta^d_{\mathrm{SO}}|$ (*vide supra*). In the limit, which is probably attained in F_2SO_2, we may therefore take $\beta^d_{\mathrm{SO}} \approx -1$ eV and $\zeta = \zeta^o$, when the total π bond order associated with each S—O bond becomes

$$p^d_{\mathrm{SO}} = 0{\cdot}79 + 0{\cdot}35 = 1{\cdot}14.$$

The value of p^π_{SO} for sulphuryl chloride will lie between this value and 0·90. The considerable $3d$ character of the Cl—S bonds accounts for the chlorinating properties of Cl_2SO_2.

THE STRUCTURE OF THE SULPHOXIDES

It may be shown that the sulphoxides R_2SO prefer a pyramidal (C_s) to, for example, a planar (C_{2v}) structure. On the basis of such a C_s structure, molecular orbitals may, quite generally, be assigned as follows:

$$(ta')^2\,(ra')^2\,(ra'')^2\,(xa'')^2\,(ua')^2\,(wa')^2, \tag{3}$$

and these may be analyzed in much the same way as those appropriate to the sulphones.

Co-ordinate axes, referred to the sulphur nucleus as origin, are chosen such that the axes of $-z$ and x bisect the RSR angle internally and externally respectively. Then, if second-order hybridization is neglected, we may show that the oxygen atom lies very nearly on the y axis. We therefore first consider such an idealized structure —from which the structures of actual sulphoxides may be derived later.

$(ta')^2$ represents a σ-electron pair bond between sulphur $(3pa'_y)$ and $(2p\sigma_y)$. $(ra')^2$ represents the symmetrical component of the delocalized form of the two σ-electron pair bonds which link the R radicals to sulphur $(3pa'_z)$—and $(ra'')^2$ is the corresponding antisymmetrical component bonding R_2 to sulphur $(3ra'')$. The two (wa') electrons are non-bonding $(2pw)$ on the oxygen atom, and the (ua') electrons are non-bonding $(3s)$ electrons of sulphur. $(xa'')^2$ represents what we may again call the π-bonding between sulphur and oxygen; $\psi(xa'')$, together with other a'' orbitals, is antisymmetrical with respect to reflexion in the (yz-) plane of symmetry.

$\phi_{\mathrm{S}}(3ra'')$ and $\phi_{\mathrm{S}}(3xa'')$ are pd-hybrid sulphur orbitals determined, as for the sulphones, by a first-order hybridization parameter ζ:

$$\phi_{\mathrm{S}}(3ra'') = \sin\zeta . \phi_{\mathrm{S}}(3pa'') - \cos\zeta . \phi_{\mathrm{S}}(3da''),$$

$$\phi_{\mathrm{S}}(3xa'') = \cos\zeta . \phi_{\mathrm{S}}(3pa'') + \sin\zeta . \phi_{\mathrm{S}}(3da''),$$

where $\phi_{\mathrm{S}}(3da'')$ is given by

$$\phi_{\mathrm{S}}(3da'') = \frac{1}{\sqrt{2}}\{\phi_{\mathrm{S}}(3db_1) + \phi_{\mathrm{S}}(3da_2)\}$$

in our previous notation.

If we suppose that the radicals R are such that $(ra')^2(ra'')^2$ represent homopolar R_2S bonding, the appropriate sulphur valence state lies between

$$\mathrm{S}, V_4: \quad (3s)^2(3pa_z'^*)(3pa_y'^*)(3ra''^*)(3xa''^*)$$

of S I, s^2p^3d and, essentially,

$$\mathrm{S}^+, V^3: \quad (3s)^2(3pa_z'^*)(3pa_y'^*)(3pa_x''^*).$$

The final charge distribution may be estimated in the usual way by means of the equation

$$\{(I_\mathrm{O}+E_\mathrm{O})-(I_s^h+E_s^h)\} = \{(I_\mathrm{O}-E_\mathrm{O})+(I_s^h-E_s^h)\}\cos 2\theta - 4\beta_\mathrm{SO}^h \cot 2\theta,$$

where we have put $\gamma_\mathrm{S}^\pi = \sin\theta$ and β_SO^h is a function of the parameter ζ. As a first approximation, we shall again take $\zeta = \frac{1}{4}\pi$; but since the formal sulphur charge in R_2SO is lower (*vide infra*) than that in R_2SO$_2$, we take $\beta_\mathrm{SO}^d \approx -0{\cdot}5$ eV. It then appears that

$$p_\mathrm{SO}^\pi = 0{\cdot}85 \quad \text{and} \quad Q_\mathrm{O} = -0{\cdot}29, \quad Q_\mathrm{S} = +0{\cdot}29.$$

Second-order hybridization of $(ua')^2$, which will strengthen, in particular, the oxy-sulphur bond, will tend to flatten our right-angled model. (Our p_SO^π is here more sensitive to the choice of ζ—more so than for the sulphones–and is accordingly rather less reliable.)

Factors similar to those enumerated above for the alkyl sulphones enables us to adapt our model R_2SO to the alkyl sulphoxides. We may predict dipole moments around 3·5 Debye units for these and modify our quantitative estimates as follows:

$$p_\mathrm{SO}^\pi = 0{\cdot}82, \quad Q_\mathrm{O} = -0{\cdot}32.$$

The C—S bonds here should be even weaker than those in the alkyl sulphones, since the former have hardly any sulphur $3s$ character. And, in agreement with these expectations, the C—S bonds of sulphoxides are known to be weaker chemically than those of alkyl sulphides. Sulphoxides, in addition to having a pair of donor electrons $(ua')^2$, have appreciably weaker oxy-sulphur bonds than have the sulphones. It is not surprising, therefore, that under certain conditions sulphoxides will disproportionate oxygen to form the corresponding sulphides and sulphones.

Thionyl fluoride (F$_2$SO) may again be discussed on the basis of a lower ζ value and an enhanced $|\beta_\mathrm{SO}^d|$ value, and we may predict that here

$$p_\mathrm{SO}^\pi = 1{\cdot}12.$$

The value of p_SO^π for thionyl chloride, which should (and indeed does) release chlorine more readily than Cl$_2$SO$_2$, will lie between 1·12 and 0·85.

THE STRUCTURE OF SULPHUR TRIOXIDE

Finally, before comparing the various oxy-sulphur bonds which have been described, a similar analysis of the structure of sulphur trioxide will be made. The only stable arrangement of the oxygen atoms about the S nucleus is the planar form (D_{3h}). In the symmetry notation of this point group, we may write for SO$_3$:

$$(ta_1')^2(te')^4(za_2'')^2(ve'')^4(we')^4(wa_2')^2. \tag{4}$$

The first six electrons arise from our model and represent, essentially, three sp^2 hybrid σ bonds made by sulphur with the O atoms. $(we')^4\,(wa_2')^2$ are best regarded as three pairs of non-bonding oxygen electrons whose orbital functions are symmetrical with respect to reflexion in the (xy-) plane of symmetry. (za_2''), which is antisymmetrical with respect to this operation, bonds $\phi_S(3pa_2'')$ to the (normalized) component of the three $2p\pi$ oxygen orbitals, namely $\phi_O(2pa_2'')$; we assume, as usual, that any heteropolar character in the S—O bonds is taken up in $(ve'')^4$, so that $\gamma_S^z = \gamma_O^z$. $(ve'')^4$ represents the (weaker) π-bonding between the $\phi_S(3de'')$ orbitals of sulphur and $\phi_O(2pe'')$, the remaining irreducible components of the three $2p\pi$ oxygen orbitals.

Our self-consistent LCAO method now leads us to solve

$$\{(I_O+5E_O)-3(I_S^d+E_S^d)\} = \{(I_O-E_O)+3(I_S^d-E_S^d)\}\cos 2\theta - 12\sqrt{3}\,.\,\beta_{SO}^d \cot 2\theta,$$

where $\gamma_S^\pi = \sin\theta$. Taking $\beta_{SO}^d = -1$ eV (for the formal positive charge which we shall eventually associate with the S atom here is larger than those in the sulphones and sulphoxides, for which we took $\beta_{SO}^d = -0{\cdot}7$ and $-0{\cdot}5$ eV respectively), we find

$$p_{SO}^\pi = 0{\cdot}57+0{\cdot}51 = 1{\cdot}08; \quad Q_S = +0{\cdot}90, \quad Q_O = Q_{O'} = Q_{O''} = -0{\cdot}30.$$

The final charge distribution is therefore close to that of the set of hybrid structures

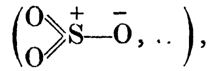

$$\left(\begin{matrix}O\\O\end{matrix}\!\!\gg\overset{+}{S}\text{—}\overset{-}{O},\ \ldots\right),$$

although this representation would mislead us in assigning bond orders. It should be noticed that the bonding from sulphur's $3d$ orbitals is quite strong, contributing $\sim 0{\cdot}51$ to the total p_{SO}^π.

A COMPARISON OF THE VARIOUS OXY-SULPHUR BONDS

Let us now compare our calculated p_{SO}^π's with the observed oxy-sulphur bond force constants. The infra-red spectra of the sulphones and sulphoxides have recently been determined by Barnard, Fabian & Koch (1949), who also showed that approximate bond-force constants k_{SO} could reasonably be assigned to the various linkages. On the basis of their data, together with those of Herzberg (1945), we may construct table 6, in which this comparison of p_{SO}^π and k_{SO} is made. (The bond orders which are quoted for Cl_2SO and Cl_2SO_2 are only rough estimates.) We plot observed values of k_{SO} against our theoretical p_{SO}^π's to obtain the graph in figure 1. The points representing R_2SO, R_2SO_2, SO_2, SO_3, F_2SO (R = alkyl) are seen to lie on a smooth curve. The force constants of Cl_2SO and Cl_2SO_2 also lie in the predicted regions. We may therefore conclude that our calculations of bond strength, based on bond orders, give a very satisfactory account of the observed force constants.

Further confirmation of our calculations may also be obtained from Koch's observations. For, on the grounds of spectral shifts due to hydrogen-bonding, he was able to show that the negative charge associated with the oxygen atoms of the sulphoxides was greater than that of the sulphones. Our calculated formal oxygen charges Q_O, which are $-0{\cdot}32$ and $-0{\cdot}26$ for R_2SO and R_2SO_2 respectively, account for this behaviour quite clearly. This point is of obvious theoretical interest, since it shows that, in a general way, an increase in the polarity of an oxy-sulphur link must be associated with a corresponding decrease in its bond strength. And this may be considered as typical double-bond behaviour.

TABLE 6. TABULATED BOND ORDERS AND BOND FORCE CONSTANTS

molecule	p_{SO}(calc.)	k_{SO}(obs.) (10^5 dyne/cm.)
dialkyl sulphoxides	0·82	6·95
thionyl chloride	~ 0·9	9·4
dialkyl sulphones	0·89	9·6
sulphur dioxide	0·93	9·97
sulphuryl chloride	~ 1·0	10·6
sulphur trioxide	1·08	10·77
thionyl fluoride	1·12	10·8
sulphuryl fluoride	1·14	—

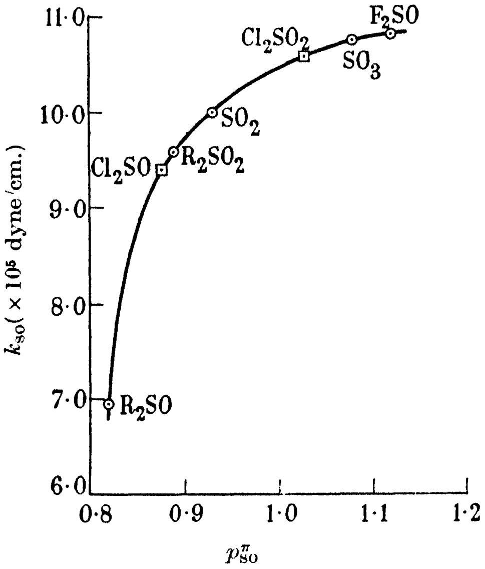

FIGURE 1. The force constant-bond order curve.

The experimentally determined bond distances r_{SO} of the molecules, which are quoted by Phillips *et al.* (1945), do not appear to differ at all significantly from 1·44 Å. This led them to consider the oxy-sulphur bond as a relatively invariant unit. From the shape of our $k_{SO} - p^{\pi}_{SO}$ curve we should have expected a definite lengthening of this bond, at least in the alkyl sulphoxides. A more recent electron diffraction study of dimethyl sulphoxide (Bastiansen & Vierroll 1948) gives $r_{SO} = 1·47$ Å, which is again in good agreement with our expectations.

On the basis of $p^{\pi}_{SO} = 0·98$, the spectroscopic values $r_{SO} = 1·49$ Å and $k_{SO} = 7·9 \times 10^5$ dynes/cm. for the sulphur monoxide molecule appear much too high and low respectively. But, as indicated above, the explanation of this is not difficult to find. For, whereas the oxy-sulphur π-bonding zones in all the other systems which we have treated each contain only two electrons, analogous regions in sulphur monoxide contain on the average three electrons. (In the polyatomic molecules, the S electrons which are not associated with the bonding in a particular S—O bond, are drawn away from that region by the valency demands of other atoms or groups.) The additional Coulomb and exchange forces, which we have neglected in our treatment, will therefore serve to weaken the S—O bonding in sulphur monoxide.

It may be shown that the success of our correlations does not depend critically on an appropriate choice of the set of parameters β^{p}_{SO}, β^{d}_{SO}. Given that β^{p}_{SO} is in the neighbourhood of -2 eV and that β^{d}_{SO} increases with the effective nuclear charge on the S atom, we have had to estimate, on grounds of plausibility, the domain of values of β^{d}_{SO}. No further assumptions, which are not inherent in our general molecular picture, have been made.

CONCLUSIONS

Using the molecular orbital method, it has been possible, on the basis of a plausible model, to analyze the electronic structures of a variety of oxy-sulphur groupings. The results may be summarized as follows:

(i) Oxy-sulphur bonds are largely double, and the sulphur 3*d* orbitals play an important role.

(ii) Variations in the physical properties of these bonds may be satisfactorily explained, as may the chemical properties of the molecules in which they occur.

More generally, it appears that our self-consistent LCAO method is capable of transcending the limits within which conventional LCAO theory seems to have been confined.

The work described in this paper forms part of the programme of fundamental research undertaken by the Board of the British Rubber Producers' Research Association. The author would like to thank Dr H. P. Koch for many stimulating criticisms during the course of this work.

REFERENCES

Arndt, F. & Eistert, B. 1941 *Ber. dtsch. chem. Ges.* **74**, 451.
Bacher, R. F. & Goudsmit, S. 1933 *Atomic energy states*. New York: McGraw-Hill.
Barnard, D., Fabian, J. M. & Koch, H. P. 1949 *J. Chem. Soc.* p. 2442.
Bastiansen, O. & Vierroll, H. 1948 *Acta chem. Scand.* **2**, 702.
Bethe, H. 1929 *Ann. Phys., Lpz.*, (5), **3**, 133.
Coulson, C. A. & Moffitt, W. 1949 *Phil. Mag.* **40**, 1.
Glockler, G. 1934 *Phys. Rev.* **46**, 111.
Herzberg, G. 1945 *Infra-red and Raman spectra*. New York: Van Nostrand.
Lister, M. W. & Sutton, L. E. 1939 *Trans. Faraday Soc.* **35**, 495.
Moffitt, W. 1946 Thesis. Oxford University.
Moffitt, W. 1949 *Proc. Roy. Soc.* A, **196**, 510, 524.
Mulliken, R. S. 1934 *J. Chem. Phys.* **2**, 782.
Phillips, G. M., Hunter, J. S. & Sutton, L. E. 1945 *J. Chem. Soc.* p. 146.
Ruedy, J. E. 1933 *Phys. Rev.* **43**, 1045; **44**, 757.
Slater, J. C. 1930 *Phys. Rev.* **36**, 56.

New terms of the $5d^8 6s^2$ and $5d^8 6s 6p$ configurations of the spectrum of Hg III

By E. W. Foster
Imperial College, London[*]

(*Communicated by Sir Owen Richardson, F.R.S.—Received* 23 *August* 1949)

The $J=0$ terms of the $5d^8\,6s^2$ configurations have been located and two others have been revised, so that all nine terms are now established. Eleven new terms of $5d^8\,6s\,6p$ are reported. The new terms and several previously reported by Johns are supported by observations of isotope shifts.

Introduction

The ground state $5d^{10}$ and the $5d^9\,6s$ and $5d^9\,6p$ terms of the spectrum of Hg III were established by McLennan, McLay & Crawford (1928) and by Mack & Fromer (1935). Johns (1937) revised Mack & Fromer's $5d^9\,6p\,|_0$ term and considerably extended the analysis to include all the terms of $5d^9\,7s$ and $7p$, several of the $5d^9\,6d$, $7d$, $5f$ and $8s$ configurations and a few unidentified members. In addition, he reported seven of the nine $5d^8\,6s^2$ terms of the 'complex' spectrum (most of which were also found by the writer about the same time, but were not published in view of Johns's much more complete analysis) and 34 of the 90 terms of $5d^8\,6s\,6p$. The present paper is mainly concerned with extending and correcting this work on the 'complex' spectrum.

The $5d^8\,6s^2$ terms are of interest because the $5d^8\,6s^2$–$5d^9\,6p$ transitions (amongst the strongest in the spectrum) involve lines with large isotope structures. In Hg III these are all of wave-length > 2480 Å, and can be studied in detail with a Fabry-Pérot interferometer or even with a large grating. According to Breit (1932) and Kopfermann (1940), the isotopic structures in heavy elements originate in the fact that each isotope of a particular element has its own characteristic nuclear field; and accordingly each isotope has its own set of term values which differ slightly from the corresponding values for the other isotopes. Since it is supposed that the nuclear fields of the isotopes depart from the Coulomb law only at small distances from and within the nucleus, the largest shifts will be shown in those lines originating in transitions which involve the greatest change in the number of deeply penetrating electrons. Thus $5d^9\,6p$–$5d^9\,6d$ transitions would normally be expected to show small or zero shifts whilst $5d^9\,6p$–$5d^8\,6s^2$ would show relatively large shifts.

To interpret these shifts and associated hyperfine structures complete knowledge of the $5d^8\,6s^2$ term structure is desirable. This interpretation will be dealt with in a later paper. In this work two of Johns's $5d^8\,6s^2$ levels have been shown to be incorrect. The proper terms have been found along with the two missing $J = 0$ levels.

Experimental

The Hg III spectrum was excited, along with the spectra of Hg I, II and IV, by means of a heavily damped electrodeless ring discharge (Thomson 1927) in continuously flowing pure Hg vapour at a pressure estimated to be between 0·01 and 0·001 mm.Hg. The temperature of the quartz or Pyrex discharge tube was 100 to 200° C so that quite sharp lines were produced. The electrodeless ring discharge is well known, and as there was nothing radically new about the technique it will not be described.

---

[*] Now with the Ministry of Supply.

The excitation conditions were controlled with care, and it was usually possible to sort out Hg III lines from the rest, from spectrograms taken with various excitation conditions, which were altered mainly by alteration of the Hg vapour pressure. Indeed, the Hg III lines themselves could often be sorted into at least three groups according to their response to changes in excitation. Those apparently of lowest excitation were classed III *a*, the next III *b*, apparently of higher excitation, and those of highest excitation III *c*. Lines which did not fall into a well-defined category apart from a general assignment to class III were often found to be blends (though they may not always be such). This sorting of the lines saved much time in the subsequent analysis. Similar, though less detailed, experiments have been carried out by Bloch & Bloch (1923) and by Déjardin (1927) and Laffay (1925), whose results were very largely confirmed during the present work. Unfortunately, the total of these previous observations was found inadequate for present purposes on account of the absence of many of the weaker lines, because of low resolution and incomplete data in the infra-red region.

The wave-length citations of these four workers were frequently inadequate (some lines only being given to the nearest angstrom), and a thorough revision was called for. Accordingly, the Hg III lines were re-sorted, from about 10,000 to about 2240 Å, and measured. Prism plates were taken over the whole range and were supplemented by grating plates from 3600 to 8600 Å. The spectrographs used were Hilger Littrow E 1 type with quartz and glass trains, and the Imperial College Eagle mounting 10 ft. Rowland concave grating with 15,000 lines per inch. Photographic plates used included Ilford: *Q* II, Monarch, H.S. Panchromatic and Astra III, Kodak: N II and I Q.

On the grating plates Fe arc standard wave-lengths were used for measurement, when possible. These were supplemented by Fe arc measures quoted by Harrison (1939). In the ultra-violet regions, after some trial and error, selected lines of Hg I, II and III, quoted respectively by Fowler (1922), Naudé (1929), Johns (1937) and Paschen (1928), were used as internal standards; their accuracy varies appreciably. It was gratifying to note the excellent agreement between Fowler's six-figure Hg I lines and the few provisional eight-figure results of the National Bureau of Standards, Washington, and the National Physical Laboratory (1948). These measurements were obtained on lines of the artificially produced isotope Hg_{198} with the special lamp devised by the National Bureau of Standards. In about half of the present measurements lines were measured on only one plate, and on two plates for most of the remainder.

In addition to the above data, use was made of wave-length lists by Déjardin (1927) below about 2200 Å, and by Bloch & Bloch (1936) from 1700 to 600 Å; many of these lines, however, particularly below 1000 Å, were not definitely assigned to any stage of ionization. The only way of making use of them in such cases was to insert them where they occurred in the predicted positions for transitions between terms otherwise fairly well established; for example, from combinations in the longer wave-length regions, where much more accurate and detailed information was available. A few vacuum lines classified by Johns have been reclassified here.

In addition, the mercury spectra were photographed through a Fabry-Pérot interferometer, with etalons ranging from 1 to 4 mm., suitable for observing the larger isotope shifts. The whole range from 10,000 to about 2240 Å was covered in this way.

RESULTS

Johns's vacuum region wave-length measurements are evidently of very high accuracy. Term differences derived from them were generally found to give very good agreement with the same term differences derived from the present observations in the longer wave-length region. The agreement is appreciably better, in fact, than is obtained from Johns's own long wave-length measurements where these are available for comparison. In order to extend the analysis, it was therefore considered advisable to recalculate a number of terms found by previous workers, by including

TABLE 1. DEEP TERMS OF Hg III BASED ON THE $5d^9$ $^2D_{\frac{5}{2}\,\frac{3}{2}}$ STATES OF Hg IV

Recalculation of previously established terms.*

configuration	term symbol even	term symbol odd	Johns's term value (cm.$^{-1}$)	revised term value (cm.$^{-1}$)
$5d^{10}$	1_0	—	0	0·0
$5d^9_{\frac{5}{2}}$ $6s$	2_3	- -	42850·0	42850·3
	3_2		46029·7	46029·5
$5d^9_{\frac{3}{2}}$ $6s$	4_1	-	58405·5	58405·8
	5_2	- -	61085·5	61085·7
$5d^9_{\frac{5}{2}}$ $6p_{\frac{1}{2}}$	—	1^0_2	103549·1	103549·4
		2^0_3	105627·5	105627·8
$5d^9_{\frac{5}{2}}$ $6p_{\frac{3}{2}}$		5^0_4	117994·4	117994·5
		3^0_2	118547·9	118548·0
$5d^9_{\frac{3}{2}}$ $6p_{\frac{1}{2}}$†	—	4^0_1	118607·6	118607·4
$5d^9_{\frac{3}{2}}$ $6p_{\frac{1}{2}}$‡	—	6^0_2	120928·1	120927·8
$5d^9_{\frac{5}{2}}$ $6p_{\frac{3}{2}}$	—	7^0_3	121601·9	121602·0
$5d^9_{\frac{5}{2}}$ $6p_{\frac{3}{2}}$§	—	8^0_1	126556·6	126556·3
$5d^9_{\frac{3}{2}}$ $6p_{\frac{3}{2}}$‖	—	9^0_0	130702·1	(130702·4)
$5d^9_{\frac{3}{2}}$ $6p_{\frac{3}{2}}$	—	10^0_3	134589·0	134588·0
		11^0_1	134998·8	134998·7
		12^0_2	136480·0	136479·0
$5d^9_{\frac{5}{2}}$ $7s$	15_3	—	178428·8	178428·2
	16_2	—	179038·9	179039·1
$5d^9_{\frac{3}{2}}$ $7s$	27_1	—	194078·7	194078·6
	28_2	—	194475·9	194476·0

* The reader is referred to Johns's paper for details of previously classified lines supporting these and certain other previously established terms not recalculated here. J values are given as subscripts.

† $5d^9_{\frac{5}{2}}$ $6p_{\frac{3}{2}}$ according to Mack & Fromer (1935).

‡ Attributed to $5d^9_{\frac{5}{2}}$ $6p_{\frac{3}{2}}$ by Johns due to misprint.

§ $5d^9_{\frac{3}{2}}$ $6p_{\frac{1}{2}}$ according to Mack & Fromer (1935).

‖ There are no new data bearing directly on this term.

TABLE 2. ALL KNOWN TERMS OF Hg III BASED ON THE $5d^8$ CONFIGURATION OF Hg V

configuration	term symbol even	term symbol odd	Johns's term value (cm.$^{-1}$)	new or revised term value (cm.$^{-1}$)	security
$5d^8_{\frac{5}{2}\frac{5}{2}}$ $6s^2$	6_4	—	97894·0	97893·8	*a*
	7_2	—	106028·2	106027·5	*a*
	8_0	—	—	122661·0	*d*
$5d_{\frac{5}{2}\frac{3}{2}}$ $6s^2$	9_3	—	112227·1	112226·0	*a*
	11_2	—	118926·7	118926·5	*a*
	10_1	—	(117055·1)	122734·9	*a*
	12_4	—	(122340·8)	126468·3	*a*
$5d_{\frac{3}{2}\frac{3}{2}}$ $6s^2$	13_2	—	133731·2	133731·5	*a*
	14_0	—	—	158909·0	*a*
$5d^8$ $6s$ $6p$	—	47^0_1	—	147142·4	*c*
	—	48^0_3	—	148426·0	*d*
	—	13^0_3	149716·9	149717·3	*d*
	—	14^0_4	150276·0	—	*e*
	—	15^0_1	150279·1	150278·7	*d*
	—	16^0_1	150857·5	150857·0	*d*
	—	17^0_1	151997·8	151997·5	*c*
	—	18^0_2	153254·6	—	*e*
	—	19^0_3	154214·0	154213·9	*d*
	—	49^0_3	—	154717·9	*d*
	—	20^0_3	155797·0	155796·1	*a*
	—	21^0_3	156580·0	156580·0	*b*
	—	50^0_2	—	157877·2	*d*
	—	22^0_2	158205·0	158204·9	*b*
	—	51^0_1	—	158835·8	*c*
	—	52^0_2	—	159861·4	*c*
	—	53^0_3	—	160015·7	*d*
	—	54^0_1	—	160170·0	*d*
	—	23^0_2	160790·5	160789·3	*d*
	—	55^0_1	—	160920·9	*c*
	—	24^0_4	161282·2	—	*e*
	—	25^0_2	161432·0	161431·4	*c*
	—	26^0_3	161462·0	161461·2	*b*
	—	27^0_4	162155·0	—	*e*
	—	28^0_2	162972·2	162972·2	*a*
	—	29^0_4	163452·7	163451·4	*d*
	—	56^0_1	—	163818·2	*c*
	—	30^0_2	164905·6	164905·3	*c*
	—	31^0_3	165004·8	—	*e*
	—	32^0_3	166180·0	166179·4	*c*
	—	33^0_2	166311·1	—	*e*
	—	34^0_3	167581·0	167580·3	*a*
	—	35^0_3	169063·0	169063·0	*c*
	—	36^0_3	169667·1	169666·8	*a*
	—	37^0_3	171366·6	171366·7	*d*
	—	57^0_3	—	171700·6	*d*
	—	38^0_2	173970·0	173968·5	*d*
	—	39^0_2	175512·5	175512·0	*a*
	—	40^0_2	177281·5	177281·0	*c*
	—	41^0_2	180247·4	180246·8	*b*
	—	42^0_3	183544·0	183544·2	*b*
	—	43^0_3	184698·7	184698·4	*b*
	—	44^0_3	187030·0	187028·5	*d*
	—	45^0_2	194904·7	194904·0	*d*
	—	46^0_2	196378·5	196377·9	*d*

the new data in the averaging of term values and making cautious allowance for the effect of known blends. Except where terms have been replaced, the differences do not exceed 1·5 cm., which amount, however, is large enough to be important in the determination of the upper terms of a spectrum of the complexity of Hg III.

The results are contained in tables 1, 2 and 3 of which explanation is given in notes at the end of each table.

DISCUSSION

It will be seen from tables 1 and 2 that a large part of the analysis as presented by Johns is confirmed, but some of the criticism by Mrozowski (1942) was justified.

Most of the strength of the newly classified lines goes into the $5d^9\,6p$–$5d^8\,6s^2$ transitions and next to transitions between the $5d^8\,6s\,6p$ terms and those of the $5d^8\,6s^2$, $5d^9\,6s$ and $5d^{10}$ configurations. A few very weak combinations between some of Johns's $5d^9\,7s$ and $5d^9\,6d$ terms and terms of the $5d^8\,6s\,6p$ configuration are included.

The distribution of the $5d^8\,6s^2$ terms reported here is consistent with such of these as are known for this configuration in the isoelectronic spectra: Pt I (Haussmann 1927; Livingood 1929) and in Au II (McLennan & McLay (1928) as revised by Mack & Fromer (1935)), but they do not appear to be in quite such good agreement with the whole of the Au II $5d^8\,6s^2$ analysis by Platt & Sawyer (1941). This may be connected with irregularities in Pt I. Moreover, the $5d^8\,6s^2$ term distribution appears to be consistent with the distribution of the corresponding terms of $3d^8\,4s^2$ in Cu II due to Shenstone (1936) and with those of $4d^8\,5s^2$ in Ag II due to Rasmussen (1940) and with the same configuration in Cd III due to Shenstone & Pittenger (1949).

In Hg III the coupling of the $5d^8\,6s^2$ levels is of an intermediate type, but it is perhaps sufficiently near to jj coupling to warrant the use of the notation. The J values, at any rate, are beyond question.

Notes to table 2

Johns's term symbol notation is used.

The letters *a*–*e* in column 6 give a cautious assessment of the security with which a term is established, based on the number and accuracy of the combinations, the available information regarding the assignment to definite spectra of the lines which determine it, and the isotope shifts and other properties observed in this investigation.

The most secure terms are labelled *a*, down to *e* for the least secure. The *e* terms are not confirmed by this investigation, though it is possible that some of them are real. They are relegated to category *e* on grounds of the small number of combinations, errors in Johns's paper, the fact that Johns's 10_1 and 12_4 $d^8\,s^2$ terms have been replaced and absence of combinations with the 8_0 and 14_0 terms where those combinations are possible. In addition, absence of expected isotope shifts and the fact that some of the combinations reported by Johns appear to belong to Hg II or IV lines almost, if not entirely, further justifies the security assessment.

The *d* terms are usually based on four or five combinations of which the properties (so far as they are known) of the supporting lines are in accordance with the transition assigned. Coincidences with lines from other ions have not ordinarily been included unless a blend has been proven or is strongly suspected. This assignment of security values seems to be the most useful way of summarizing a good deal of information obtained in this work and not presented here.

Previously reported terms are recalculated with the aid of data obtained during this work (not ordinarily presented in table 3). Reference should be made to Johns's paper for details of classified lines supporting such terms.

TABLE 3. CLASSIFIED LINES AND THEIR PROPERTIES

observer	excitation class and blend properties	isotope shift	intensity	wave-length (Å)	wave number, ν (cm.$^{-1}$)	transition	$\nu_{obs.}-\nu_{cal.}$
F	III *bl*	*S*	5, 15	8151·64	12264·1	$11^0_1-10_1$	+0·3
F	III*a*	*Sb*	50	7984·51	12520·8*	$3^0_2-\ 7_2$	+0·3
F	III	*Sb*	25	7946·75	12580·3	$4^0_1-\ 7_2$	+0·4
F	III*b*	*Sa*	7	7808·10	12803·7*	$13_2-\ 6^0_2$	0
F	III*b*	*Sa*	12	7517·46	13298·7*	$11_2-\ 2^0_3$	0
F	III*a* ? *bl*	*S*	3, ? 1	7273·85	13744·1	$12^0_3-10_1$	0
F	III	*Sb*	30	6709·29	14900·6*	$6^0_2-\ 7_2$	+0·3
F	III	*Sa*	6	6610·12	15124·1*	$13_2-\ 4^0_1$	0
F	III	*Sa*	10	6584·26	15183·5*	$13_2-\ 3^0_2$	0
F	III*b*	*Sa*	40	6501·38	15377·1*	$11_2-\ 1^0_2$	0
F	III	*Sb*	35	6418·98	15574·5*	$7^0_3-\ 7_2$	0
F	III*a*	*Sb*	25	6220·35	16071·8*	$11^0_1-11_2$	−0·4
F	III	—	1	5892·20	16966·9	$15_3-26^0_3$	−0·1
F	III	*Sb*	6	5695·71	17552·2*	$12^0_2-11_2$	−0·3
F	III*b*	*Sa*	30	5210·82	19185·5†	$10_1-\ 1^0_2$	0
F	III*a*	*Sb*	80	4973·57	20100·7*	$5^0_4-\ 6_4$	0
F	III*a*	*Sb*	10	4869·85	20528·8*	$8^0_1-\ 7_2$	0
F	III	*Sa*	50	4797·01	20840·5	$12_4-\ 2^0_3$	0
F	III*b*	*w*	1	4763·65	20986·5	$49^0_3-13_2$	+0·1
F	III*b*	*s*	12	4552·84	21958·2	$48^0_3-12_4$	+0·5
F	III*a*	*Sb*	15	4470·58	22362·2*	$10^0_3-\ 9_3$	+0·2
F	III*b*	*w*	1	4389·41	22775·7	$28_2-57^0_3$	+0·3
F	III*b*	*s*	2	4318·08	23151·9	$23_3-28^0_2$	−0·1
F	? III	—	1	4301·17	23243·0	$16_2-20^0_3$	0
F	III*b* ? *bl*	*s*	2	4299·96	23249·5	$24_2\ \ 28^0_2$	−0·1
						$13^0_3-12_4$	+0·5
F	III*a*	*Sb*	100	4216·74	23708·4*	$7^0_3-\ 6_4$	+0·2
F	III. IV	*Sa*	2, 1	4181·04	23910·8	$14_0-11^0_1$	+0·5
F	III*b*	*s*	10	4140·34	24146·0	$50^0_2-13_2$	+0·3
F	III*a*	*Sb*	70	4122·07	24252·8*	$12^0_2-\ 9_3$	−0·2
F	III*b* or *c*	*w*	1	4098·85	24390·2	$17_1-50^0_2$	−0·4
F	III*b* or *c*	—	1	4095·97	24407·4	$47^0_1-10_1$	−0·1
F	III	*w*	2	3837·33	26052·4	$24_2-54^0_1$	+0·6
F	III	*w*	15	3803·51	26284·1	$53^0_3-13_2$	−0·1
F	III	*w*	1	3792·40	26361·1	$24_2-52^0_2$	+0·7
F	III	—	2	3619·94	27616·9	? $15^0_1-\ 8_0$	−0·8
F	III	*Sa*	5	3557·24	28103·7*	$13_2-\ 2^0_3$	0
F	III ? *bl*	? *w*	? 2, 10	3543·08	28216·0	$47^0_1-11_2$	+0·1
F	III	*w*	4	3538·88	28249·5	$49^0_3-12_4$	−0·1
F	III	*Sb*	3	3500·34	28560·5*	$10^0_3-\ 7_2$	0
F	III*a*	*Sb*	5	3450·77	28970·8*	$11^0_1-\ 7_2$	−0·4
F	? III	—	1	3415·72	29268·0	$22_3-20^0_3$	−0·3
F	III	? *w*	1	3408·79	29327·5	$20^0_3-12_4$	−0·3
F	III	—	8	3389·01	29498·7	$48^0_3-11_2$	−0·8
					*	$37_3-83^0_2$	+1·0
F	III	*w*	2	3322·81	30086·4	$56^0_1-13_2$	−0·3
F	III	*Sa*	12	3312·28	30182·0*	$13_2-\ 1^0_2$	−0·1
F	III *bl*	? *w*	1	3296·2	30329	$23_3-20^0_3$	+0·9
F	III*a*	*Sb*	5	3283·02	30451·0*	$12^0_2-\ 7_2$	−0·5
F	III ? *bl*	*w*	2	3253·76	30724·8	$25_4-20^0_3$	+0·4
F	? III	—	1	3097·80	32271·6	$19_2-17^0_1$	0
F	III	*Sa*	15	3090·05	32352·6	$14_0-\ 8^0_1$	−0·1
F	? III	—	1	3015·00	33157·9	$27_1-55^0_1$	+0·2

* Previously classified.

† $87^0_1-28_2$ according to Johns, of which there is no evidence from this work.

TABLE 3 (*cont.*)

F	? III	—	? 1	2979·98	33547·5	53^0_3–12_4	+0·1
F	? III, I	*w*	2, 5	2856·93	34992·4	26^0_3–12_4	−0·5
F	III	*w*	3	2844·76	35142·0	50^0_2–10_1	−0·3
F	III	*w*	1	2818·43	35470·3	22^0_2–10_1	+0·3
F	? III	*w*	1	2786·76	35873·4	27_1–22^0_2	−0·3
F	III	*w*	6	2769·22	36100·6	51^0_1–10_1	−0·3
F	III	*Sb*	70	2724·43	36694·1*	10^0_3– 6_4	−0·1
F	III	—	2	2703·16	36982·8	29^0_4–12_4	−0·3
F	III	—	2	2692·68	37126·7	19_2–47^0_1	0
						52^0_2–10_1	+0·2
F	III	*w*	3	2670·49	37435·2	54^0_1–10_1	+0·1
F	III	*w*	2	2665·27	37508·5	54^0_1– 8_0	−0·5
F	III *bl*	*w*	4	2617·97	38186·1	55^0_1–10_1	+0·1
F	III	*w*	2	2612·92	38260·0	55^0_1– 8_0	+0·1
F	III	—	1	2583·46	38696·2	25^0_2–10_1	−0·3
F	III	—	1	2517·3	39713	32^0_3–12_4	+2
F	III	—	1	2504·91	39909·6	51^0_1–11_2	+0·3
F	III	*w*	7	2484·50	40237·4	28^0_2–10_1	+0·1
F	III	*Sa*	5	2480·56	40301·3	14_0– 4^0_1	−0·3
F	III	*w*	8	2431·65	41112·2	34^0_3–12_4	+0·2
F	III	—	2	2428·99	41156·9	56^0_1– 8_0	−0·3
F	III	? *w*	4	2380·55	41994·3	55^0_1–11_2	−0·1
F	? III	—	1	2357·8	42399	48^0_3– 7_2	0
F	III *bl*	*w*	7	2314·15	43199·1	36^0_3–12_4	+0·6
D	III	—	0	2210·19	45230·8	57^0_3–12_4	−1·5
				λ_{vac}			
J	III *D*	—	1	1894·77	52776·9	57^0_3–11_2	+2·8
					*	31^0_3– 9_3	−0·8
						39^0_2 10_1	−0·2
J	—	-	15	1759·75	56826·3	49^0_3– 6_4	+2·2
					*	15_3– 7^0_3	+0·1
J	III + *B*	–	9	1681·40	59474·2	57^0_3– 9_3	−0·4
					*	28_2–11^0_1	−3·1
B	? II		2	1161·95	86062	47^0_1– 5_2	+5
B	III +		00	1145·04	87333	48^0_3– 5_2	−7
J	III *B*		5	1068·03	93630·3	49^0_3 5_2	−1·9
						12^0_2 - 2_3	+1·6
B	*bl*		0	1033·16	96790	50^0_2– 5_2	−2
B	-		0	1010·85	98927	53^0_3– 5_2	−3
B			2	1009·29	99080	54^0_1– 5_2	−4
B	-		00	1001·70	99830	55^0_1 - 5_2	−5
B	III +	-	1	988·89	101124	47^0_1 - 3_2	+11
B			0	985 69	101452	52^0_2 - 4_1	−4
B			0	973·30	102743	56^0_1– 5_2	+10
B		—	00	894·06	111849	50^0_2– 3_2	+1
B	-	—	? 1	886·48	112806	51^0_1– 3_2	0
B	-	-	2	878·59	113819	52^0_2– 3_2	−13
B		—	00	877·30	113986	53^0_3– 3_2	0
B	III		00	876·17	114133	54^0_1– 3_2	−8
B	-	--	00	870·39	114891	55^0_1 3_2	0
B	-	—	0	854·61	117012	52^0_2- 2_3	+1
B	-	—	00	795·78	125663	57^0_3 - 3_2	−8
B		—	2	679·68	147128	47^0_1 - 1_0	−14
B	—	—	3	621·44	160917	55^0_1– 1_0	−4
B	—	—	0	610·46	163811	56^0_1– 1_0	−7

See p. 436 for ‘Notes’ to table.

Notes to table 3

Column 1 gives the initial of the observer of the excitation class and blend properties in column 2, the isotope shift of column 3, the visual intensity estimate of column 4 and the wave-length in column 5, except where otherwise indicated by the placing of an initial in the column where the exception occurs. The letters B, D, F, J refer respectively to Bloch & Bloch (1936), Déjardin (1927), Foster (this paper) and Johns (1937).

In column 2, *bl* refers to blend lines. III*a*, *b* or *c* refer to the classes of Hg III lines discussed in the experimental section of this paper.

In column 3 are given qualitative indications of the observed isotope shifts. The letter S, with or without the letters a and b, refers to a clear observation of an isotope displacement characteristic of a change of two in the number of $6s$ electrons in the two configurations involved. These displacements amount to about 0·6 cm.$^{-1}$ per two mass units per two $6s$ electrons. The shifts in all such lines are very closely similar, agreeing to about 5 %. The letters a and b refer to the direction of the shift. In the Sa lines the heavy even isotope Hg_{204} line was of highest frequency; conversely for Sb. The letter s represents a resolved isotope displacement characteristic in magnitude of a change of one in the number of $6s$ electrons in the two terms involved in the transition and w and ?w refer to unresolved s and probable s-shift lines. A $5d^9\,6d$–$5d^8\,6s\,6p$ transition should have an s shift, as also should $5d^8\,6s\,6p$–$5d^8\,6s^2$, whilst $5d^9\,6p$–$5d^8\,6s^2$ should have an S shift, a or b according as which term is uppermost. The directions of the shifts in the s and w lines were not observed for many classified lines. Several of these isotope shifts have also been observed by previous workers, especially by Johns (1937) and by Mrozowski (1942).

In some cases in the intensity column 4 two figures are quoted, these refer in order to the probable intensity of the line in question and a blend. Intensities are visual estimates, roughly on a consistent scale for F observations, but different for different observers. The F and J scales range from 1 to 100 or thereabouts; the Bloch & Déjardin scales ranging from 00 or 0 to 10.

In column 5 wave-lengths are recorded. The mean wave number of the S lines has been calculated from the wave-lengths of the individual components.

Column 6 contains wave numbers calculated using Kayser's Tables down to 2000 Å. Except in the case of J measurements the wave-number accuracy decreases slightly as the frequency increases down to the 2200 Å and thereafter more rapidly especially for the B measurements—made mostly with a 1 metre normal incidence grating above about 1000 Å and with a 1 metre grazing-incidence grating below. Many of the B lines are probably unresolved blends. Johns's vacuum lines were measured with a 3 m. grating. An asterisk denotes previous classification.

Column 7 gives the difference between the observed wave number and that calculated from the term differences and should give some measure of the accuracy of the observations.

Table 3 includes all 29 lines of the $5d^8\,6s^2$–$5d^9\,6p$ transitions. Most of these are included in Johns's paper but some new properties are listed here.

Whilst the distribution of the $5d^9\,6p$ terms in the Pt I, Au II, Hg III, Tl IV, Bi V isoelectronic sequence has been studied experimentally by Mack & Fromer (1935) and theoretically by Goble (1935) in some detail, comparatively little is known regarding the $5d^8 6s^2$ terms of the 'complex' spectra of these elements, which, as already pointed out, are of interest in connexion with isotope shifts. What has been found experimentally is contained in the sources quoted above.

The lower of the two $J = 0$ terms of $5d^8\,6s^2$ in Hg III should combine with $5d^9_{\frac{5}{2}}\,6p_{\frac{1}{2}}|_1$ to give a line in the (unobserved) for infra-red region, but probably only weakly or not at all (by analogy with Cd III and Ag II) with the $5d^9_{\frac{5}{2}}\,6p_{\frac{3}{2}}|_1$ term to give a line in the region investigated here. This lower $J = 0$ term in Hg III is the only one of the $5d^8\,6s^2$ configuration which is not firmly established by observations of the characteristic $5d^9\,6p$–$5d^8\,6s^2$ isotope shifts. However, it seems to be sufficiently well established by its combinations with four of the $J = 1$ terms of the $5d^8\,6s\,6p$ configuration to include in the term scheme.

There is no evidence of inter-configuration perturbations nor of isotope shift perturbations in that part of the Hg III spectrum so far investigated.

In conclusion some points of practical interest arise. The present work has shown that many strong lines in Naudé's list (1929) belong to Hg IV. Naudé excited mercury spectra in a hollow cathode Schüler-tube type of discharge in pure Hg vapour and in Hg-He mixtures. This type of discharge is well known for producing sharp lines with economy of the material excited. We thus have a source which excites not only the Hg I, II and III spectra (selectively in the last case) but also a part of the Hg IV spectrum. Thus as Naudé's list shows, a spectrum very rich in lines is produced, and this may be of use in devising a more efficient artificial isotope (Hg_{198}) standard wave-length source. The somewhat unexpectedly high excitation up to Hg IV and the very strong and selective excitation of Hg III in a Schüler-tube type of discharge, no doubt explains many of Mrozowski's (1942) observations.

The completion of this work has been held up for a number of reasons by circumstances beyond the author's control.

The author wishes to express his thanks to Professors Sir George Thomson, F.R.S., and H. Dingle for laboratory facilities at the Imperial College in 1936–8, when most of the experimental work was done, and to Mrs Jackson for the loan in 1938 of an excellent E 1 spectrograph which belonged to the late Dr C. V. Jackson. The author is also indebted to Sir Owen Richardson, F.R.S., and Professor R. W. B. Pearse, for facilities during a period of about three weeks in the summer of 1948 to take further spectrograms with improved photographic plates.

REFERENCES

Bloch, L. & Bloch, E. 1923 *J. Phys. Radium* (VI), **4**, 333.
Bloch, L. & Bloch, E. 1936 *Ann. Phys., Paris*, **6**, 561.
Breit, G. 1932 *Phys. Rev.* **42**, 348.
Déjardin, G. 1927 *Ann. Phys., Paris*, **8**, 424.
Fowler, A. 1922 *Report on series in line spectra.* London: The Physical Society.
Goble, A. T. 1935 *Phys. Rev.* **48**, 346.
Harrison, G. R. 1939 *M.I.T. Wavelength tables.* New York: Wiley.
Haussmann, A. C. 1927 *Astrophys. J.* **66**, 333.
Johns, M. W. 1937 *Canad. J. Res.* A, **15**, 193.
Kopfermann, H. 1940 *Kernmomente*, 73. Leipzig: Akademische Verlagsgesellschaft.
Laffay, J. 1925 *C.R. Acad. Sci., Paris*, **180**, 823.
Livingood, J. J. 1929 *Phys. Rev.* **34**, 185.
Mack, J. E. & Fromer, M. 1935 *Phys. Rev.* **48**, 357.
McLennan, J. C. & McLay, A. B. 1928 *Trans. Roy. Soc. Canad.* **22**, III, 103.
McLennan, J. C., McLay, A. B. & Crawford, M. F. 1928 *Trans. Roy. Soc. Canad.* **22**, III, 247.
Mrozowski, S. 1942 *Phys. Rev.* **61**, 605.
National Bureau of Standards, Washington and National Physical Laboratory. Results quoted in a communication by Barrell, H. and Puttock, M. J. to the 9th General Conference of Weights and Measures, Paris, 1948.
Naudé, S. M. 1929 *Ann. Phys., Lpz.*, **5**, 1.
Paschen, F. 1928 *S.B. preuss. Akad. Wiss.* **32**, 536.
Platt, J. R. & Sawyer, R. A. 1941 *Phys. Rev.* **60**, 866.
Rasmussen, E. 1940 *K. danske vidensk. Selsk. Math.-fys. Medd.* **18**, no. 5.
Shenstone, A. G. 1936 *Phil. Trans.* A, **235**, 195.
Shenstone, A. G. & Pittenger, J. T. 1949 *J. Opt. Soc. Amer.* **39**, 219.
Thomson, J. J 1927 *Phil. Mag.* (7), **4**, 1128.

A class of enumerations of importance in genetics

By R. A. Fisher, F.R.S.

(*Received* 21 *June* 1949)

(This paper has been printed in full in *Proceedings* B, **136**, 509.)

Abstract

A number of enumerations arising in genetics, e.g. of sets of isomorphic genotypes, of modes of gamete formation, of the modes of formation of ordered and unordered tetrads, etc., have been found in previous work to yield solutions expressible as the mean powers of arbitrary degree of appropriate series of bases. These are such as to yield integral values of the mean for all integral exponents.

The general combinatorial theorem governing this class of enumeration is given in § 2 Other sections illustrate the method in operation by confirming and extending the genetic formulae so far established.

In § 3·1 is a brief discussion of a partitional function which serves to enumerate the numbers of partitions of any partible number in a lattice of arbitrary dimensionality.

The utilization of carbon sources by *Bact. lactis aerogenes*

I. General survey

By A. C. Baskett and Sir Cyril Hinshelwood, F.R.S.
Physical Chemistry Laboratory, University of Oxford

(*Received* 10 *March* 1949)

(This paper has been printed in full in *Proceedings* B, **136**, 520.)

Abstract

A survey is made of the ability of various carbon compounds to support growth of *Bact. lactis aerogenes*. They are classified into those to which the cells (*a*) cannot become adapted, (*b*) become adapted by training, (*c*) are fully adapted on transfer from a glucose medium in which they are normally grown.

With class (*b*) there is usually a long initial lag on the first transfer and an initial growth rate well below the optimum.

Phenomena of 'cross-adaptation' appear, training to an earlier member of the series acetic acid, succinic acid, fumaric acid entailing adaptation to a later member but not vice versa.

With citric acid, aconitic acid and glycerol there is evidence of multiple growth mechanisms.

Additions of certain carboxylic acids shorten the lag of ageing cultures in the glucose medium.

The classes (*a*), (*b*) and (*c*) bear no relation to the number of carbon atoms or the functional groups in the molecules of the various substances. They bear, however, certain relations to the 'tricarboxylic acid cycle' which are examined in part II.

The utilization of carbon sources by *Bact. lactis aerogenes*

II. The significance of the tricarboxylic acid cycle

By A. C. Baskett and Sir Cyril Hinshelwood, F.R.S.
Physical Chemistry Laboratory, University of Oxford

(*Received* 10 *March* 1949)

(This paper has been printed in full in *Proceedings* B, **136**, 536.)

Abstract

The kinetics of a model related to the 'tricarboxylic acid cycle' are examined, and the significance of this system and of related mechanisms for the growth processes of *Bact. lactis aerogenes* is considered in the light of the experimental evidence from part I.

The utilization of potassium by *Bact. lactis aerogenes*

By A. A. Eddy and Sir Cyril Hinshelwood, F.R.S.
Physical Chemistry Laboratory, University of Oxford

With an Appendix by C. J. Danby, A. A. Eddy and
Sir Cyril Hinshelwood, F.R.S.

(*Received* 5 *April* 1949)

(This paper has been printed in full in *Proceedings* B, **136**, 544.)

Abstract

As the potassium-ion concentration of synthetic media is decreased the total population (n_s) of *Bact. lactis aerogenes* which they support tends towards zero. Added potassium gives nearly linear increases in n_s. The use of the radioactive isotope shows that the cells take up nearly all the potassium from the medium over wide ranges of concentration.

Sodium cannot replace potassium, and the use of the active isotope shows that it is probably not taken up by the cells.

Rubidium replaces potassium with about quarter efficiency, but lithium and caesium have only very small effects.

The potassium appears to play the part of an enzyme-activator and in glucose-ammonium sulphate media it is displaced by the acid formed during growth.

A quantitative treatment of the competition between K^+ and H^+ for an array of negative sites on an enzyme surface is attempted. On the assumption that a certain critical area of K^+ activated sites is necessary for growth to continue, a relationship between n_s and the $[K^+]$ is developed and shown to be in general agreement with the experimental facts.

The relation between n_s and potassium concentration varies from one medium to another. In glycerol-ammonium sulphate media, where n_s is insensitive to the initial pH, the amounts of potassium present in the ammonium or sodium salts of the buffer support considerably greater populations than they can in the glucose medium. Further increases, however, demand much greater potassium concentrations, the results being in accord with the view that other products formed in the glycerol medium can displace potassium from the relevant enzyme and limit growth.

The effect of thermal cycles on the structure of alloys: diffusion effects in two phase alloys

By R. J. Davis and W. Hume-Rothery, F.R.S.
Inorganic Chemistry Laboratory, University Museum, Oxford

(*Received* 28 *July* 1949—*Revised* 29 *September* 1949)

The effect of cyclic variation of temperature on the structure of a two-phase alloy is considered theoretically with special reference to diffusion effects. A qualitative examination is made of a simplified two-phase system consisting of a single spherical particle embedded in an isotropic matrix in which the solubility of the particle phase varies with temperature. It is shown that under continual cycles of temperature the particle will be surrounded by a 'zone of influence' in which the concentration varies with the period of the cycle, and outside which a steady state is set up where the concentration is intermediate between the equilibrium values at the two extremes of temperature. The amplitude of the concentration variation diminishes exponentially with the distance from the particle, and rapidly becomes of the same order as the statistical fluctuation in composition to be expected in a solid solution. The magnitude of the zone of influence is calculated for the case of particles of Al_2Cu embedded in an aluminium-rich solid solution and subjected to temperature cycles between 0 and 350° C, and for periods of cycle of 1 and 24 hr. The calculation is made first by assuming a diffusion constant independent of temperature, and a method is then developed to allow for the variation of the diffusion constant. More complicated periodic thermal treatments are examined qualitatively, and cases of more than one particle are described.

1. Introduction

In recent years much attention has been concentrated on the determination of equilibrium diagrams of alloy systems. The object of this work is to determine the structure and compositions of the phases existing in equilibrium at different temperatures, and this knowledge is essential for the understanding of the structure of alloys in the non-equilibrium state. Under many practical conditions alloys are repeatedly heated up and cooled down, and may then be said to undergo thermal cycles. It is of interest to examine the way in which the microstructure of an alloy is affected by thermal cycles, and in the present paper we examine theoretically some of the processes which may be expected to occur. Very little previous work of this kind appears to have been published apart from that of Boas & Honeycombe (1944–7), who showed that thermal cycles might produce marked grain growth in polycrystalline zinc and cadmium. This effect was regarded as due to the anisotropy of the hexagonal crystals whose coefficients of expansion in the direction of the hexagonal axis are much greater than those perpendicular to the axis, with the result that strains are set up in the grains of the polycrystalline specimen during heating or cooling.

2. Continuous thermal cycles

We shall assume that we are dealing with alloys in which the changes in microstructure taking place at room temperature are so slow that they may be ignored. The expression *continuous thermal cycles* may be used to describe a process in which an alloy is repeatedly heated and cooled, whilst *discontinuous thermal cycles* are those in which after heating up the specimen is maintained at the high temperature before being cooled down. A *symmetrical thermal cycle* is one in which the time taken for the temperature to increase from T_1 to T_2 during heating is the same as that taken in cooling from T_2 to T_1 over the whole range of temperature, whilst the term *uniform* may be used to describe a process in which the rate of change in temperature is constant in either heating or cooling. Thus, a uniform unsymmetrical thermal cycle would denote a cycle in which the specimen was heated up at one constant rate, and cooled down at a constant but different rate.

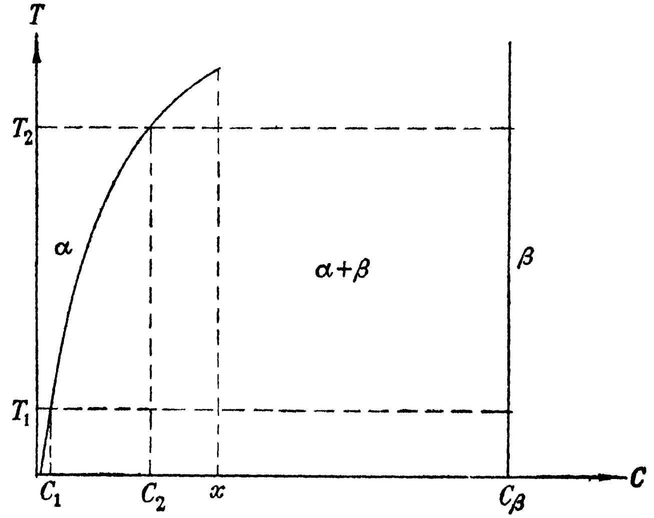

FIGURE 1. Hypothetical phase diagram of system AB, A-rich end.

Let figure 1 represent part of the equilibrium diagram of the system AB in which the solid solution of B in A, denoted α, is in equilibrium with a phase β whose composition is independent of temperature. Consider an alloy of composition x, annealed to equilibrium at T_1 at which temperature it will consist of particles of β in a ground mass of α. For simplicity let us assume first that we deal with a single crystal of α in the form of a sphere containing one crystal of β at its centre of such a size that the ratio of $\alpha:\beta$ corresponds with an alloy of composition x in equilibrium at T_1. If we then imagine a line passing through the crystal of β, the variation of the percentage of B along this line will be of the general form of the full line in figure 2 in which the sudden step up represents the α/β boundary where the percentage of B increases suddenly from the value C_1 representing the solubility limit of α at T_1 to the value representing the percentage of B in the β phase.

For simplicity we may first assume that the effects in the α and β phases are isotropic, and that the alloy is heated from T_1 to T_2 infinitely slowly so that phase equilibrium is maintained. Under these conditions the α phase will take up more B into solid solution, the β crystal will shrink in size, and at T_2 the condition may be shown by the ---·--- line in figure 2. This condition of affairs clearly requires diffusion to take place from the α/β interface throughout the whole of the α crystal.

We may now imagine that instead of being heated slowly from T_1 to T_2, the alloy is heated at a rate which permits only a limited amount of diffusion to take place. Under these conditions it seems reasonable to assume that true equilibrium is maintained at the actual α/β interface, so that when the alloy reaches T_2 the condition of affairs will be represented by a curve of the general form of the —o—o— line in figure 2. Here the percentage of B in the α phase at the α/β interface is equal to the solubility limit C_2 at T_2, whilst at large distances from the β crystal the percentage of B in the α phase is still equal to the value C_1 characteristic of equilibrium at T_1. The β crystal will have shrunk by an amount which is less than that which would have occurred under conditions of true equilibrium.

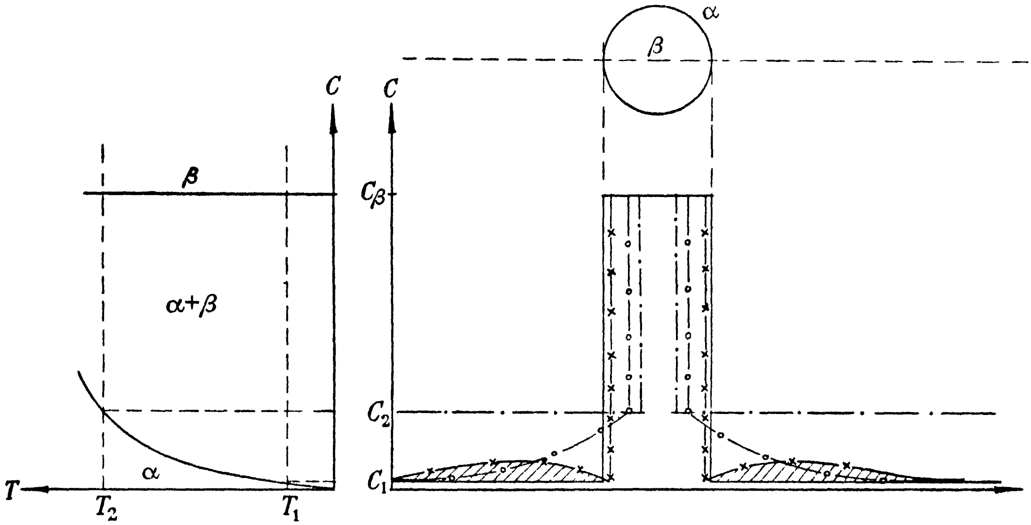

FIGURE 2. Hypothetical sketch diagram of concentration gradients about one β grain after various heat treatments. Concentrations: – ——, initially at T_1; —·—·—, after infinitely slow heating to T_2; —o—o—, after heating at a finite rate to T_2; - - × — × —, after heating to T_2 and then cooling to T_1 again at a finite rate. The phase diagram of the system is shown to the left, and the hypothetical microsection of the alloy is shown above. The shaded area represents the supersaturation in the fourth plot.

We may next imagine that after reaching the condition given by the —o—o— curve of figure 2 the alloy is cooled from T_2 to T_1 so as to give one symmetrical thermal cycle. Then at the α/β interface the concentration of B in the α phase will fall from C_2 to C_1, and the β crystal will increase in size as the result of diffusion of B towards the β crystal. Consideration of the form of —o—o— curve in figure 2 will show that in the outer parts of the α crystal B will continue to diffuse outwards away from the β crystal as the temperature falls from T_2 to T_1, and at the end of the first cycle the condition might be as shown by the — × — × — curve where the shaded region is supersaturated. It is this which constitutes the first characteristic of a thermal cycle at a rate too rapid to allow true equilibrium to be attained. The process is not a simple reversible one in which the β crystal shrinks and grows uniformly, but is rather one in which a pulse of B is sent outward and continues to travel outward during the cooling half of the cycle. The processes which follow depend on whether the supersaturation of the shaded region is relieved by the formation of new crystals of β, i.e. whether nucleation and precipitation occur. We may assume first that no nucleation takes place. In this case as the temperature first rises from the bottom of the first cycle, the β crystal may at first continue to grow in size because as long as the equilibrium composition at the interface is less than that of an adjacent region, B will continue to diffuse back to the α/β interface with a resulting growth in the β crystal. As the temperature rises the composition at the α/β interface rises and the rate of heating will determine when the β crystal begins to send out a second pulse of B, and the final effect of a second continuous thermal cycle will be to send out a second pulse of B from the β crystal which will again shrink in size. As the cycles are continued the outward pulses of B will reach the boundaries of the α crystal, after which each successive cycle will increase the resistance of the α matrix to the further absorption of B. The more detailed analysis given in § 5 shows that on the above simplifying assumptions the effect of a large number of cycles is to produce a periodic variation in the concentration of B in the whole of the α matrix surrounding the β crystal. The amplitude of these concentration fluctuations is $C_2 - C_1$ at the α/β interface, and decreases exponentially with the distance from the β crystal. Now in any random solid solution there are statistical fluctuations in composition, and it follows therefore, that on proceeding outwards from the β crystal we shall eventually reach a stage at which the concentration fluctuations resulting from thermal cycles are smaller than the deviations from the average composition to be expected statistically in a homogeneous solid solution. Beyond this limit the periodic fluctuations have no meaning, and we reach a stage of pseudo-equilibrium in which the concentration of B lies nearer to that of C_2 in figure 2 than to C_1. This condition of affairs is illustrated in figure 3, and in § 5 we

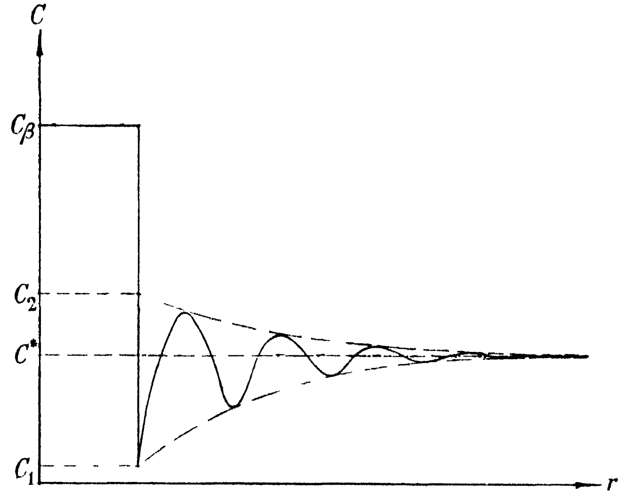

FIGURE 3. Sketch showing variation of concentration along a radius in the steady state. The full line shows the concentration at various points at the bottom of the cycle. The dash dot line indicates the mean concentration in α. The dashed line is the envelope of concentration plot at all stages of the cycle and shows the amplitude of the concentration fluctuations.

show how to estimate roughly the limit of the zone in which the periodic fluctuation in composition is greater than the mean statistical deviation; we shall call this zone the *zone of influence* of the β crystal. It is clear that the zone of influence becomes larger as the period of a cycle is increased, and the calculations show that the thickness of the zone of influence varies as the square root of the period.

In the above treatment it was assumed that the thermal cycles began with the specimen in equilibrium at the lower temperature T_1. Under these conditions it is clear that when the steady state is set up, the β crystal will have shrunk in size, and the α matrix will have been enriched in B. If we had started with the specimen in equilibrium at the higher temperature, an exactly analogous condition would have been set up, but in the steady state the β crystal would have grown in size, and the α matrix would have been impoverished in B.

3. OTHER THERMAL CYCLES

Before proceeding to more detailed calculations we may consider qualitatively the behaviour of a specimen submitted to discontinuous thermal cycles in which the temperature rises from T_1 to T_2, and then remains constant at T_2 before falling from T_2 to T_1. It can be seen that the effect of the short anneal at T_2 will be to increase the size of the pulses of B atoms in the first few cycles. We may further expect that in the steady state, the mean concentration of B in α will be nearer to C_2 than it was in the corresponding continuous thermal cycle.

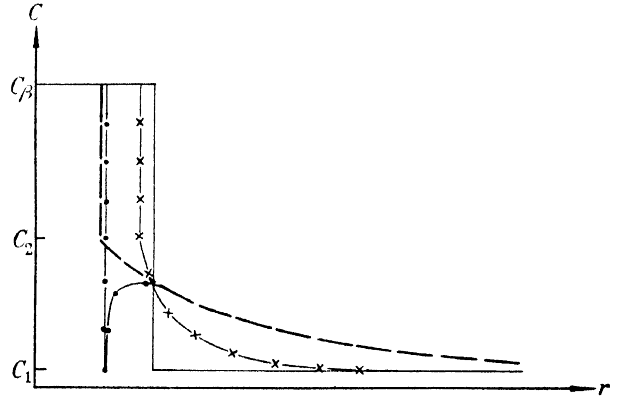

FIGURE 4. Sketch diagram of concentration variations along a radius for an asymmetrical cycle. Concentrations: – —, initial; —× –× –, after heating to T_2; — – –, after a period at T_2; —· —· – –, after rapid cooling to T_1.

Alloys are often heated under conditions in which a first rapid rise in temperature is followed by a slow approach to the highest temperature, a period at this temperature, and then by a rate of cooling which, when the source of heat is cut off, is at first rapid and then decreases as the lower temperatures are approached.† In this case the — × — × — curve of figure 4 may represent the condition when the specimen first reaches T_2, and the ——— curve the condition after the period at T_2. If then the rate of cooling through the higher temperatures be sufficiently fast, the diffusion during cooling will be small, and the condition after one unsymmetrical cycle may be as shown by the —·—·— curve of figure 4. After this stage when the second cycle begins and the temperature rises to the value at which diffusion becomes appreciable, the β crystal will at first grow as B diffuses towards it from the supersaturated α, and will then begin to redissolve at the higher temperatures. Under this kind of unsymmetrical cycle we shall therefore be able to distinguish between three zones: (1) a very narrow zone at the α/β interface in which the concentration of B fluctuates appreciably, in phase with the cycles; (2) a wider zone in which the concentration of B first diminishes and then increases during each half-cycle of heating after the first, and the fluctuations are out of phase with the cycles; (3) a region of steady state of pseudo-equilibrium.

---

† Cf. Newton's law of cooling.

The general line of argument used above can readily be applied to other combinations of heating and cooling rates.

4. THE EFFECT OF SEVERAL PARTICLES OF DISPERSE PHASE

In the preceding section we have dealt with one crystal of β in a matrix crystal of α. We may now consider the effects when a number of β crystals are present, and it is clear that two extreme cases can be recognized. If the β crystals are so few as to be outside each other's zone of influence, each crystal of β will be surrounded by a zone inside which the concentration of B fluctuates with the period of the cycle, whilst at a greater distance from the β crystals a steady state will be built up after a sufficient number of cycles. In the region of the steady state we may call the mean concentration of B in the α matrix C^*, and the corresponding temperature on the $\alpha/\alpha+\beta$ phase boundary of the equilibrium diagram may be called T^*. Under these conditions when the β crystals are few and are separated from one another by regions of concentration C^* we may compare the structural changes occurring during a number of cycles with those occurring during an anneal at a constant temperature T^*. If, on the other hand, the β crystals are sufficiently numerous to be within each other's zones of influence, then the concentration of B in the whole of the α matrix will undergo appreciable fluctuation during the cycles and the condition of affairs represents a new heat-treatment, quite distinct from an isothermal anneal.

5. CALCULATIONS OF THE DIAMETER OF THE ZONE OF INFLUENCE: FIRST APPROXIMATION

In the present section we shall attempt an approximate calculation for the size of the zone of influence and shall apply this to the particular case of particles of $CuAl_2$ embedded in an aluminium-rich solid solution matrix of an aluminium-copper alloy.

For simplicity we shall assume that the two-phase alloy is submitted to cycles in which the temperature varies sinusoidally. We shall ignore the effects of internal stresses which may arise from differential thermal expansion of the two phases, and shall treat the problem as a diffusion problem with the following simplifying assumptions:

(1) We shall assume the $\alpha/\alpha+\beta$ phase boundary of figure 1 to be linear. The approximations involved by this assumption can be removed by a method outlined in § 7.

(2) The diffusion constant D of the B atoms in the matrix will be assumed to be independent of concentration and temperature. So far as concentration is concerned it can be shown that provided the α solid solution is dilute, the error introduced by the assumption of a constant value of D is negligible. The real dependence of D upon temperature is given by an equation of the form:

$$D = D_0 \mathrm{e}^{-Q/RT},$$

and diffusion occurs much more rapidly as the temperature is raised. In § 6 we show how this temperature variation may be taken into account, and we shall use here D_m, the mean value of D over the cycle.

(3) The composition in the α phase at the α/β phase boundary is at the equilibrium value for the appropriate temperature at all stages of the cycle.

(4) The effect of the migration of the boundary as the β grain grows and shrinks during cycles is neglected.

We now consider a spherical particle of β, radius r_0, embedded in a ground mass of α, and separated by large distances from other β grains. This system is nearly spherically symmetrical about the centre of the β grain and we can apply the diffusion equation

$$\frac{\partial(cr)}{\partial t} = D_m \frac{\partial^2(cr)}{\partial r^2}, \tag{1}$$

where r is the radial co-ordinate from the centre of the β grain, and c is the concentration of B in α at distance r.

If we assume that the β grain is far away from any other β grain in the solid, we may apply to this equation the condition

$$r_0 \leqslant r \leqslant \infty. \tag{2}$$

We also have the condition, from the assumptions above,

$$c = \tfrac{1}{2}(C_2+C_1) - \tfrac{1}{2}(C_2-C_1)\cos 2\pi(t/\tau) \tag{3}$$

at the α/β interface, where τ is the period of the cycle, and C_2, C_1 are the equilibrium concentrations of B in α at T_2, T_1 respectively.

For a complete solution to the problem we should have to specify the initial condition of the alloy, for example, at equilibrium at T_1, and should then describe the process by which the steady state was reached. The simplifying assumption of an infinitely large β grain†, and of a fixed α/β interface, clearly prevent us from doing this, but we are justified in deriving that part of the solution which describes the steady state itself. This has been done for the analogous problem in heat conduction (see, for example, Carslaw & Jaeger 1947). The steady-state solution to equations (1) to (3) by the method given there is

---

† If the system started in equilibrium at T_1 with a single grain of β immersed in an infinitely large crystal of α, the β grain would dissolve completely after a sufficient number of cycles. This apparent inconsistency in the simplifications could be removed by imagining the system starting in equilibrium half-way up the cycle at $\frac{1}{2}(T_1+T_2)$. It can be shown that this produces effectively the same equation describing the steady state, only with a different zero of time, i.e. a sine term replacing the cosine term in equation (4).

$$c = \tfrac{1}{2}(C_2+C_1) - \tfrac{1}{2}(C_2-C_1)\frac{r_0'}{r}\exp\left\{-\sqrt{\left(\frac{\pi}{D_m\tau}\right)}(r-r_0')\right\}$$

$$\times\cos\left\{\frac{2\pi t}{\tau}-\sqrt{\left(\frac{\pi}{D_m\tau}\right)}(r-r_0')\right\}, \qquad (4)$$

where r_0' is the mean radius of the β grain in the steady state.

At any point in the matrix the concentration varies sinusoidally in time, with period τ. The amplitude decreases exponentially with increasing r, and is given by

$$\tfrac{1}{2}(C_2-C_1)\frac{r_0'}{r}\exp\left\{-\sqrt{\left(\frac{\pi}{D_m\tau}\right)}(r-r_0')\right\}.$$

At any instant the concentration varies periodically along a radius about a mean value $C^* = \tfrac{1}{2}(C_1+C_2)$, with constant wave-length given by

$$2\sqrt{(\pi D_m\tau)}.$$

In order to show the form of equation (4) in a graph it is convenient to measure the concentration and the radial co-ordinate on slightly different scales. Equation (4) can be rewritten in the form

$$\chi = -\frac{\rho_0}{\rho+\rho_0}\mathrm{e}^{-2\pi\rho}\cos 2\pi\left(\frac{t}{\tau}-\rho\right),$$

where $$\chi = -\frac{c-\tfrac{1}{2}(C_2+C_1)}{\tfrac{1}{2}(C_2-C_1)}, \quad \rho = \frac{r-r_0'}{2\sqrt{(\pi D_m\tau)}}, \quad \rho_0 = \frac{r_0'}{2\sqrt{(\pi D_m\tau)}}.$$

χ and ρ are thus direct measures of the concentration and the radial co-ordinate respectively, in terms of the other constants in the equation.

We have plotted χ against ρ in figure 5*a*, giving ρ_0 and t/τ the values 1 and n respectively, where n is a large integer, i.e. a plot of concentration along the radius at the bottom of a cycle in the steady state.

The geometric scale used for χ shows how the amplitude of the fluctuations (shown by the dashed curves in figure 5) falls off very rapidly as the distance from the β grain increases, but that nevertheless the fluctuations persist, although very small, far out into the grain.

The same equation is plotted on a linear scale for χ in figure 5*b* to *g* for various values of t/τ. These show the true shape of the concentration plots, and the shaded regions represent a pulse of B atoms being formed.

Consideration of figure 5 shows that the concentration plot consists of a series of troughs and crests, each smaller than the last.

A crest or trough can be regarded as a positive or negative pulse of B atoms from the grain. Each pulse is derived from a half-cycle, and once formed travels on, out into the matrix, in the form of a spherical shell of thickness $\sqrt{(\pi D_m\tau)}$, whose radii increase uniformly in time. As it travels outwards, it decays in magnitude, first because it has to spread itself over an increasing volume, secondly, because it is continuously decaying into neighbouring pulses of opposite sign. A pulse may thus be taken as a positive or negative deviation from the mean concentration in α. We will proceed to compare the magnitude of the deviation in a pulse at any point in the α with that to be expected statistically in homogeneous α at the mean concentration in the volume occupied by the spherical shell. As explained above, we define

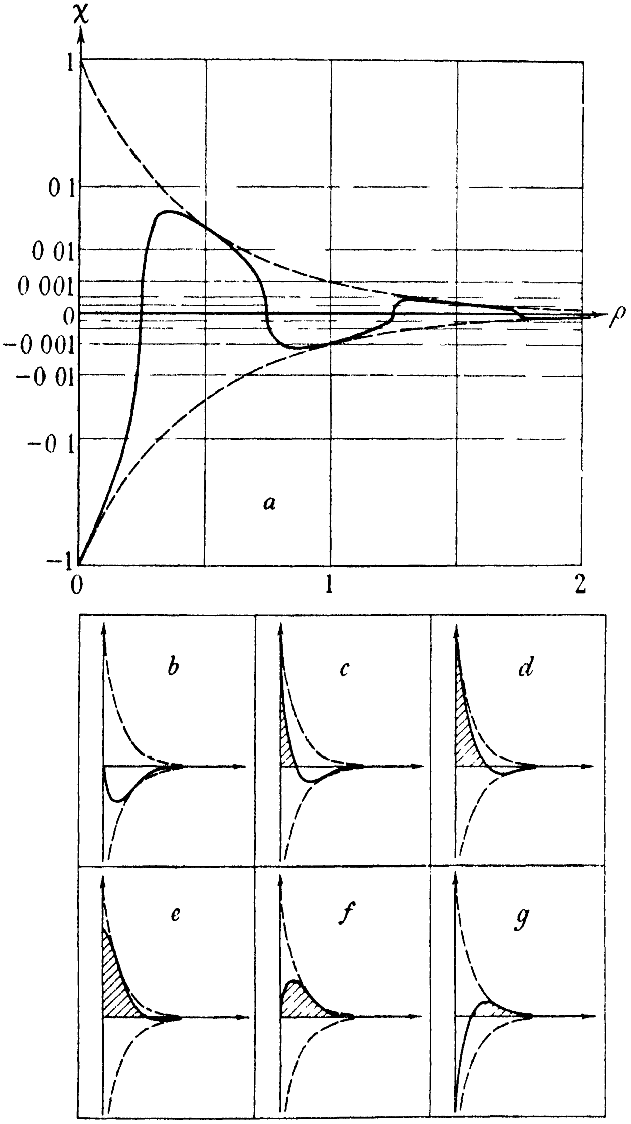

FIGURE 5. a, graph of $\chi = -\dfrac{\rho_0}{\rho+\rho_0} e^{-2\pi\rho} \cos 2\pi\left(\dfrac{t}{\tau} - \rho\right)$ against ρ on a geometric scale ($\rho = 1$, $t/\tau = n$, a large integer). The dashed curves are graphs of the amplitude term $\pm \dfrac{\rho_0}{\rho+\rho_0} e^{-2\pi\rho}$ against ρ. b to g, graphs of χ against ρ on a linear scale ($\rho_0 = 1$), showing successive stages in the formation of a positive pulse of B atoms (shaded area). Values of t/τ b, $n + \frac{1}{4}$, c, $n + \frac{3}{8}$; d, $n + \frac{1}{2}$; e, $n + \frac{5}{8}$; f, $n + \frac{3}{4}$; g, $n + \frac{7}{8}$.

the radius, r_z, of the zone of influence as that at which the magnitude of a pulse becomes equal to $\overline{\Delta c}$ that of a statistically expected concentration fluctuation.

For an approximate treatment we may use the simplest formula

$$\overline{\Delta n} = n^{\frac{1}{2}}, \tag{5}$$

where $\overline{\Delta n}$ is the most probable excess number of solute atoms to be found in concentration fluctuation over a volume containing on average n solute atoms at the mean composition. (For the derivation of equation (5) and the assumption involved see Rice (1930) and Bitter (1931).)

Whence, if V is the volume of the fluctuation, $\overline{\Delta c}$ the most probable concentration deviation, A the atomic weight of solute atoms, and N is Avogadro's number, we have

$$\overline{\Delta c} = \sqrt{\left(\frac{C^*A}{NV}\right)}. \tag{6}$$

Now in our case, V is given by

$$V = 4\pi r_s^2\sqrt{(\pi D_m\tau)},$$

where r_s is the mean radius of the spherical shell. The mean concentration deviation in the pulse is approximately $2/\pi \times$ the amplitude at r_s, i.e.

$$\Delta c = \frac{r_0'}{\pi r_s}(C_2-C_1)\exp\left\{-\sqrt{\left(\frac{\pi}{D_m\tau}\right)}(r-r_0')\right\}. \tag{7}$$

We now say that when the pulse has travelled out far enough to fulfil the conditions of equation (6), it has reached the limit of the zone of influence of the β grain, and is thenceforward indistinguishable from homogeneous solid solution. From equations (6) and (7), we may derive the radius of the zone of influence in the form

$$z = r_z - r_0'.$$

We have $$\frac{r_0'}{\pi r_z}(C_2-C_1)\exp\left\{-\sqrt{\left(\frac{\pi}{D_m\tau}\right)}(r_z-r_0')\right\} = \sqrt{\left\{\frac{C^*A}{4\pi r_z^2 N\sqrt{(\pi D_m\tau)}}\right\}},$$

i.e. $$z = r_z - r_0' = \sqrt{\left(\frac{D_m\tau}{\pi}\right)}\log_e\left\{2r_0'(C_2-C_1)\left(\frac{D_m\tau}{\pi}\right)^{\frac{1}{4}}\left(\frac{N}{C^*A}\right)^{\frac{1}{2}}\right\}. \tag{8}$$

The variation of the logarithmic term with τ is unimportant compared to the variation of the linear term, and we may write

$$z \propto \sqrt{\tau}$$

for given temperature limits and type of cycle.

We have considered, as an example, an alloy of aluminium with a little copper, sufficient to produce a few grains of θ-CuAl$_2$ phase as precipitate. For the precipitate, we have assumed an average particle radius of about $0\cdot5 \times 10^{-3}$ cm. in the steady state. This is a reasonable assumption for annealed alloys of this type.

For this alloy system, undergoing sinusoidal thermal cycles between 0 and 350° C, we shall show in § 6 how to calculate a value of $D_m = 1\cdot84 \times 10^{-13}$ cm.^{2}/sec. For cycles of period 24 hr., the wave-length of the pulses is given by

$$2\sqrt{(\pi D_m\tau)} = 0\cdot45 \times 10^{-3}\text{ cm.}$$

We shall assume for this case that r_0' is exactly one wave-length.[†]

A survey of experimental work on the solubility of copper in aluminium showed that the $\alpha/\alpha+\theta$ boundary best obeys a relation of the type

$$\frac{x}{1-x} = x_0\, e^{-E/RT}, \tag{9}$$

where x is the atomic fraction of copper in the α phase in equilibrium with θ at T° K. We find from our survey the values $x_0 = 14{\cdot}3$, $E = 10{,}300$ cal. Hence at 350° C, $x = 0{\cdot}00338$, and at 0° C, x is effectively zero.

These values are converted to weight percentage units, and thence to g./cm.^{3}, using a graph of density of equilibrium α against temperature of equilibrium from the high temperature X-ray measurements of Ellwood & Silcock (1948). This gives $C_1 = 0$, $C_2 = 0{\cdot}0210$, whence $C^* = 0{\cdot}0105$.

Using the values $N = 6{\cdot}023 \times 10^{23}$, $A = 63{\cdot}54$, we have for the 24 hr. cycle

$$\frac{z}{2\sqrt{(\pi D_m \tau)}} = 1{\cdot}90,$$

whence the zone thickness, $\quad z = 0{\cdot}85 \times 10^{-3}$ cm.

For the same system and 1 hr. sinusoidal cycles, we assume the same value of $r_0' = 0{\cdot}45 \times 10^{-3}$ cm., and obtain

$$\text{wave-length} = 2\sqrt{(\pi D_m \tau)} = 0{\cdot}091 \times 10^{-3}\ \text{cm.}$$

$$\frac{z}{2\sqrt{(\pi D_m \tau)}} = 1{\cdot}77.$$

$$\text{zone thickness} = 0{\cdot}16 \times 10^{-3}\ \text{cm.}$$

The above two values for $\dfrac{z}{2\sqrt{(\pi D_m \tau)}}$ show that a change in the period by a factor of 24 produces a change of only about 7 % in the ratio of z to $\sqrt{\tau}$.

We can conclude that for this system and cycle, the zone thickness is between 1·5 and 2·0 wave-lengths, and that this estimate is relatively insensitive to changes in period of cycle, and to inaccuracies in the estimate of particle size of precipitate.

6. A SIMPLE METHOD FOR ALLOWING FOR THE VARIATION OF THE DIFFUSION COEFFICIENT WITH TEMPERATURE[‡]

In the previous section we derived a simple formula for the thickness of the zone of influence of a precipitate grain for a simplified phase system. This was done at the expense of two main assumptions, namely, that the diffusion coefficient did not vary with the temperature, and that the $\alpha/\alpha+\beta$ boundary in the phase diagram was linear.

[†] It can be seen from equation (8), that although z depends on r_0', it is relatively insensitive to the value assumed for r_0', since the latter enters only into the logarithmic term. In the present case it can be shown that a change in r_0' by a factor of 10 produces only 20 % change in the value of z.

[‡] We are grateful to Mr F. D. Kahn for valuable discussions on this section.

These two assumptions might be justifiable in cycles over small temperature ranges, such as are found when 'hunting' takes place during annealing, but over appreciable temperature ranges the second assumption is rarely justifiable and the first never so.

The method for compensating for the variation of diffusion coefficient with temperature is best explained by a physical analogy. Suppose we set up a hypothetical time-scale in the form of a clock geared to the rate of diffusion. The clock starts from the same zero as the real time, and ticks out the same number of units of time during one complete cycle as does a real clock, but during one cycle, the hypothetical clock is made to run rapidly at the high temperature end of the cycle and very slowly at the low temperature end. With a suitable choice of hypothetical time-scale, diffusion will take place uniformly throughout the cycle, characterized by D_m, the mean diffusion coefficient during the cycle, and results obtained by solving the diffusion equation with a constant D_m are on the hypothetical time-scale. We can then obtain the corrected solution of the diffusion equation by transposing the results from hypothetical to real time, by the use of appropriate equations.

We can readily derive the conversion equation for sinusoidal temperature variations as follows, and analogous methods can be used for other temperature programmes.

In the case of a spherically symmetrical system the diffusion equation is

$$\frac{\partial(cr)}{\partial t} = D\frac{\partial^2(cr)}{\partial r^2}.$$

This can be written as $$\frac{D_m}{D}\frac{\partial(cr)}{\partial t} = D_m\frac{\partial^2(cr)}{\partial r^2},$$

and with the substitution $$\frac{\partial}{\partial\phi} = \frac{D_m}{D}\frac{\partial}{\partial t},$$

this converts to the ordinary diffusion equation, with constant coefficient D_m and ϕ, the time measured on the hypothetical time scale.

Now $$D = D_0\,e^{\;Q/RT},$$

and in our case the temperature programme is given by

$$T = \tfrac{1}{2}(T_2+T_1) - \tfrac{1}{2}(T_2-T_1)\cos 2\pi(t/\tau), \tag{10}$$

whence we have $$D = D_0\exp\left\{-\frac{\lambda}{1-\mu\cos 2\pi(t/\tau)}\right\},$$

where $$\lambda = \frac{2Q}{R(T_2+T_1)} \quad\text{and}\quad \mu = \frac{T_2-T_1}{T_2+T_1},$$

i.e. $$\frac{\partial}{\partial\phi} = \frac{D_m}{D_0}\exp\left\{\frac{\lambda}{1-\mu\cos 2\pi(t/\tau)}\right\}\frac{\partial}{\partial t}.$$

But ϕ is a function of t only. We may therefore write

$$\frac{\partial}{\partial\phi} = \frac{dt}{d\phi}\frac{\partial}{\partial t},$$

whence
$$\phi = \int_0^t \frac{D_0}{D_m} \exp\left\{-\frac{\lambda}{1-\mu\cos 2\pi(t/\tau)}\right\} dt.$$

(We may write this as a definite integral since ϕ and t start from the same zero.)

The above method has the advantage that by its use the solution to any diffusion problem solved for constant diffusion coefficient may be transposed to the solution to the corresponding problem with varying temperature during the heat treatment.

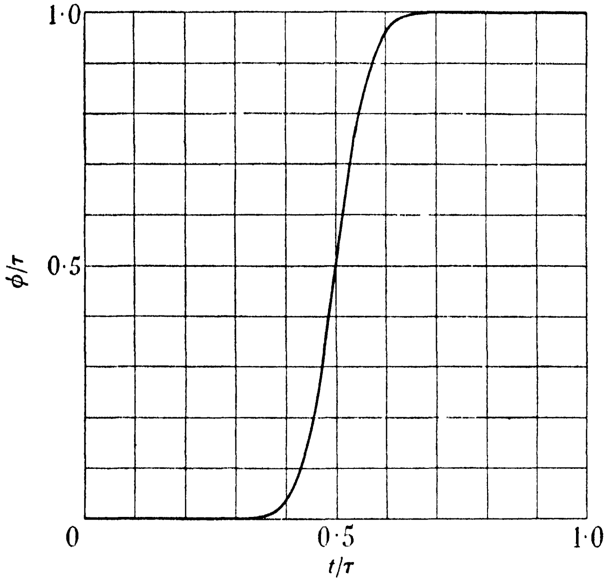

FIGURE 6. Relationship between hypothetical time and real time for sinusoidal cycles between 0 and 350° C in aluminium copper alloys.

The integral has been solved graphically,† for which purpose it was written as

$$\frac{\phi}{\tau} = \frac{D_0}{D_m}\int_0^{t/\tau} \exp\left\{-\frac{\lambda}{1-\mu\cos 2\pi\xi}\right\} d\xi. \tag{11}$$

Using the data of Brick & Phillips (1937) quoted by Barrer (1941), $D_0 = 2{\cdot}3$ cm.²/sec. $Q = 34{,}900$ cal./g.atom, we have calculated ϕ/τ as a function of t/τ for sinusoidal cycles between 0° and 350° C, for aluminium-rich aluminium-copper alloys. The curve is shown in figure 6.

† This integration can be carried out algebraically by using the parameter A, given by

$$(1-\mu\cos 2\pi\nu)\,(1-\mu\cos 2\pi\xi) = 1-\mu^2 = \gamma^2$$

and $\nu = A$ when $\xi = t/\tau$.

Putting $\lambda/\gamma^2 = \zeta$, we have

$$D_m = D_0\gamma e^{-\zeta} \sum_{n=0}^{\infty}\sum_{r=0}^{r=2n} \frac{2n\,!}{(n\,!)^2}\left(\frac{\mu}{2}\right)^{2n} \frac{\zeta^r}{r\,!},$$

$$\phi/\tau = A - \tfrac{1}{2} + \frac{\displaystyle\sum_{\substack{p=r+1\\(p+r=2t+1)}}^{\infty}\sum_{r=0}^{\infty}\sum_{s=0}^{s=p} \frac{(p-1)(p-3)\ldots(r+2)}{p(p-2)\ldots(r+3)}\,\frac{\mu^p}{r+1}\,\frac{\zeta^s}{s\,!}\sin 2\pi A\cos^r 2\pi A}{\displaystyle\sum_{n=0}^{\infty}\sum_{r=0}^{r=2n} \frac{2n\,!}{(n\,!)^2}\left(\frac{\mu}{2}\right)^{2n}\frac{\zeta^r}{r\,!}}.$$

Since these series do not normally converge at all rapidly, the graphical method of integration is less laborious.

From $t/\tau = n$ to $n+0{\cdot}3$, the imaginary clock advances very slowly. From here to $t/\tau = n+0{\cdot}5$, the clock runs increasingly rapidly until at $t/\tau = n+0{\cdot}5$ the two time-scales coincide. From here on the rapid rate is at first maintained, but decreases steadily, until at $t/\tau = n+0{\cdot}7$ the imaginary clock has again come almost to a standstill and runs very slowly to the end of the cycle ($t/\tau = n+1$).

We can imagine the concentration plots, calculated by the simple method of § 5 and shown in figure 5*b* to *g*, as being selected frames from a cinematograph film. The film calculated by this method will differ from the real film, corrected for temperature variations, only in the time intervals at which the frames occur. Corresponding frames in the two films are identical. If there are 100 frames per cycle in the film calculated by the simple method of § 5, then when the film is corrected for temperature, the first 4 frames would be shown in the first 40 % of the showing time per cycle, the next 92 frames in the next 20 % of the cycle, and the last four in the last 40 % of the cycle.

The same calculation for figure 6 gave D_m, the mean diffusion coefficient. We can compare

$$\begin{aligned} D_m &= 1{\cdot}84\times10^{-13} && \text{corresponding to } T_m = 309^\circ\text{ C},\\ D_2 &= 1{\cdot}32\times10^{-12} && \text{corresponding to } T_2 = 350^\circ\text{ C},\\ D_1 &= 2{\cdot}60\times10^{-28} && \text{corresponding to } T_1 = 0^\circ\text{ C}.\end{aligned}$$

7. SECOND APPROXIMATION TO THE DIAMETER OF THE ZONE OF INFLUENCE

To correct for temperature variation, the diffusion problem is now solved with constant D_m as in § 5, and boundary condition at the phase interface expressed as a function of ϕ rather than of t. Any $\alpha/\alpha+\beta$ phase boundary will appear in the boundary condition as a complex periodic function of ϕ, but for symmetrical thermal cycles this may be expanded by Fourier's cosine series (see, for example, Carslaw (1930)). The boundary condition takes the form

$$c = K_0 + K_1\cos 2\pi(t/\tau) + \dots + K_n\cos 2n\pi(t/\tau) + \dots, \tag{12}$$

where $$K_0 = \int_0^1 c\,d(\phi/\tau),\quad K_n = 2\int_0^1 c\cos 2n\pi(\phi/\tau)\,d(\phi/\tau)\quad (n = 1, 2, 3, \dots). \tag{13}$$

This procedure regards the boundary condition as a series of superimposed harmonic terms, which contribute separately to the solution of the diffusion problem. The solution, obtained as in Carslaw & Jaeger (1947), may be rewritten as was equation (4) in figure 5, to give

$$c = K_0 + \sum_{n=0}^{\infty} K_n \frac{\rho_0}{\rho+\rho_0}\,e^{-2\pi\sqrt{(n)}\rho}\cos 2\pi[n(\phi/\tau) - \sqrt{(n)}\,\rho]. \tag{14}$$

All terms but the first integrate to zero in real time so that $K_0 = C^*$, the mean concentration of B in the α phase.

The K_n appear as the 'weights' of successive terms in the solution. The appearance of $\sqrt{n}$ in the exponential factor means that higher harmonics decay much more rapidly as they recede from the β grain; at large distances, only the first term $n = 1$ is important.

This offers a second approximation to the radius of influence, using equation (5) of § 5, with $2K_1$ substituted for $(C_2 - C_1)$, i.e.

$$z = \sqrt{\left(\frac{D_m\tau}{\pi}\right)\log_e\left\{4K_1 r'_0\left(\frac{D_m\tau}{\pi}\right)^{\frac{1}{2}}\left(\frac{N}{K_0A}\right)^{\frac{1}{2}}\right\}}. \tag{15}$$

Second approximate values of z have been found by the above method for the examples given in § 5. The integrations in equation (13) were performed graphically from the data in equations (9) and (10), figure 6 and Ellwood & Silcock (1948). They are given in table 1 in concentration units, and in weight percentage units obtained by dividing by the density of equilibrium α at T^* corresponding to $C^* = K_0$ on the $\alpha/\alpha+\beta$ boundary.

TABLES 1 TO 4. ALUMINIUM-RICH ALUMINIUM-COPPER ALLOYS. SINUSOIDAL THERMAL CYCLES BETWEEN 0 AND 350° C

TABLE 1. FOURIER COEFFICIENTS FOR SOLUTION OF DIFFUSION PROBLEM

n	K_n (g./cm.^{3})	K_n (wt % units)
0	0·0185	0·699
1	−0·00350	−0·132
2	−0·00168	−0·063
3	−0·00108	−0·041
4	−0·00076	−0·029
5	−0·00052	−0·020

TABLE 2. RATIO OF COEFFICIENTS OF nTH COSINE TERM TO THAT OF FIRST; *I.E.* VALUES OF $K_n/K_1 \exp\{-2\pi\rho[\sqrt{(n)}-1]\}$ FOR VARIOUS VALUES OF n AND ρ

n	$\rho=0$	$\rho=0{\cdot}1$	$\rho=0{\cdot}2$	$\rho=0{\cdot}5$	$\rho=1{\cdot}0$	$\rho=1{\cdot}5$
1	1·000	1·000	1·000	1·000	1·000	1·0000
2	0·480	0·370	0·285	0·131	0·036	0·0097
3	0·309	0·195	0·123	0·031	0·003	0·0003
4	0·217	0·116	0·062	0·009	—	—
5	0·149	0·068	0·031	0·003	—	—

TABLE 3. VALUES OF THE ZONE THICKNESS, z, FOR 24 AND 1 HR. CYCLES, UNDER THE TWO APPROXIMATIONS, ASSUMING $r'_0 = 0{\cdot}45 \times 10^{-3}$ CM. THROUGHOUT

		zone thickness $= z$	
period $= \tau$ (hr.)	wave-length $= 2\sqrt{(\pi D_m\tau)}$ (cm.)	first approximation (cm.)	second approximation (cm.)
24	$0{\cdot}44_7 \times 10^{-3}$	$0{\cdot}85 \times 10^{-3}$	$0{\cdot}76 \times 10^{-3}$
1	$0{\cdot}091_2 \times 10^{-3}$	$0{\cdot}16 \times 10^{-3}$	$0{\cdot}14 \times 10^{-3}$

TABLE 4. SUMMARY OF CALCULATED TEMPERATURES, CONCENTRATIONS AND DIFFUSION COEFFICIENTS

temperature (° C)	concentration (g./cm.^{3})	concentration (wt. % units)	diffusion coefficient (cm.^{2}/sec.)
$T_1 = 0{\cdot}0$	$C_1 = 0{\cdot}5 \times 10^{-6}$	$C_1 = 1{\cdot}8 \times 10^{-5}$	$D_1 = 2{\cdot}7 \times 10^{-28}$
$T_m = 309{\cdot}5$	—	—	$D_m = 1{\cdot}84 \times 10^{-13}$
$T^* = 340{\cdot}6$	$C^* = 0{\cdot}0185$	$C^* = 0{\cdot}699$	$D^* = 8{\cdot}5 \times 10^{-13}$
$T_2 = 350{\cdot}0$	$C_2 = 0{\cdot}0210$	$C_2 = 0{\cdot}792$	$D_2 = 1{\cdot}3 \times 10^{-12}$

We can measure the relative contribution of the $(n+1)$th term in equation (15) by the ratio of the coefficient of the nth cosine term to that of the first, which is

$$\frac{K_n}{K_1}\exp\{-2\pi(\sqrt{n}-1)\rho\}.$$

Calculated values of this for various values of n and ρ are given in table 2. As ρ increases, the higher harmonic terms diminish rapidly in importance, so that whereas at 0·1 wave-length from the interface the fifth term still makes an important contribution to c, at 1·5 wave-lengths the first term only will suffice to 1 % accuracy.

In § 5 we estimated the zone thickness between 1·5 and 2·0 wave-lengths so that the second approximation is justified here. Values of K_0 and K_1 from table 1 have been substituted in equation (15), and the new estimates of z, etc., are given in tables 3 and 4.

The new values of z are less than the old, but still exceed 1·5 wave-lengths. z is therefore quite insensitive to errors in the factors in the logarithmic term, so that only D_m and τ need to be known accurately. The first approximation is clearly quite good, and the relatively small improvements in z in the second approximation indicate that further refinement is unnecessary.

8. THE EFFECT OF NUCLEATION DURING THERMAL CYCLES

In the preceding sections we have assumed that the structural changes occurring during thermal cycles are determined entirely by diffusion processes, and that the supersaturation which arises on the downward half of the cycle is not relieved by the formation of new crystals of β. We next have to consider how the structure will be affected if nucleation and precipitation occur. We may imagine that in figure 7 the

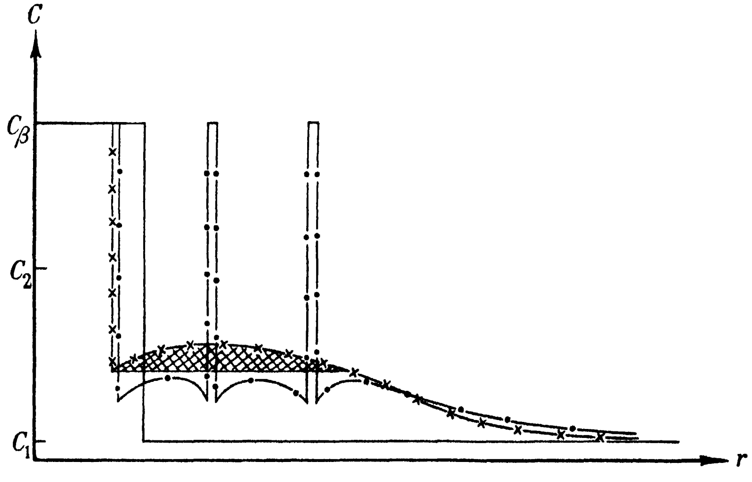

FIGURE 7. Sketch diagram of concentration variations around a β grain when nucleation occurs. Concentrations: ———, initially; —×—×—, after heating to T_2 and cooling again to an intermediate temperature just before nucleation occurs; —·—·—, just after nucleation has occurred. The shaded region represents the supersaturation in the region of nucleation.

—×—×— curve shows the state of affairs on the cooling half of the first cycle at some temperature between T_2 and T_1. The shaded region is one of supersaturation, and it seems reasonable to suppose that the rate of formation of new nuclei increases with the amount of supersaturation. It follows, therefore, that the crystal will be surrounded by a zone on which nucleation and the formation of new β crystals are relatively improbable, because the supersaturation of the α phase has been reduced by the diffusion of B towards the original β crystal. During the cooling half of the first cycle the degree of nucleation will at first increase as we proceed outward from the β crystal, and will then die away. Each time nucleation occurs and a new crystal of β is formed, the concentration of B in the α phase will fall to the equilibrium value at the α/β interface of the new crystal. If, therefore, we imagine a line passing through the original and two new β crystals, the concentration of B along the line immediately after nucleation would be of the general form shown by the —·—·— curve of figure 7. When the temperature rises at the beginning of the second cycle, the new β crystals will at first continue to grow, for reasons analogous to those given above (p. 444), and when the specimen reaches the temperature at which nucleation originally began, some of the β crystals will still remain. If nucleation occurs only at the extreme bottom of the cycle, the resulting crystals will probably dissolve when the higher temperatures are next reached, because solution will be made possible by a longer period and a higher temperature than were present during the growth of the particles. Under these conditions, repeated thermal cycles will still send out repeated pulses of B from the original β crystal, and a steady state will be set up in the outer part of the α crystal but this will differ from the state of the simplified model of p. 444 in that the overall concentration of B will sometimes result from the α phase alone, and sometimes from a mixture of α and small crystals of β which dissolve when the higher temperatures are next reached.

When the temperature falls from T_2 to T_1 it may happen that nucleation occurs in the higher part of the temperature range, and if so the resulting crystal will continue to grow as the temperature falls and will surround itself with a zone in which further nucleation is improbable (see above). The new crystal may then not redissolve during the upward half of the next cycle, and the condition of affairs will resemble that discussed on p. 446 for the case of several β crystals. It is unlikely that many new crystals will be formed which do not redissolve because at the higher temperatures the degree of supersaturation is relatively slight, and each new permanent β crystal will surround itself with a zone in which further nucleation is improbable.

A β crystal thus has a second zone of influence with respect to nucleation, which we can define by a radius of nucleation. We can again distinguish two cases: (i) where the precipitation-free zones of the original β crystals of the system overlap throughout the specimen, and no new precipitate is formed; (ii) where the β crystals are sufficiently far apart from new transient nuclei to be formed during the low temperature halves of the cycles.

A situation of the latter type can readily be observed microscopically and has been studied by the authors for aluminium-zinc alloys. It is hoped to present the results of this work later.

The authors must express their gratitude to Professor Sir Cyril Hinshelwood, F.R.S., for laboratory accommodation, and to Dr F. M. Brewer for many facilities which have greatly assisted their work. This research was started as part of a Ministry of Supply Extra-Mural Research Contract, and has been continued with support from the Department of Scientific and Industrial Research to whom one of us (R.J.D.) must acknowledge the award of a Maintenance Grant. Thanks are also due to the British Non-Ferrous Metals Association for financial support of the general research programme of which this forms a part.

REFERENCES

Barrer, R. M. 1941 *Diffusion in and through solids*, p. 275. Cambridge University Press.

Bitter, F. 1931 *Phys. Rev.* **37**, 1527.

Boas, W. & Honeycombe, R. W. K. 1944 *Nature*, **153**, 494; **154**, 338.

Boas, W. & Honeycombe, R. W. K. 1946 *Proc. Roy. Soc.* A, **186**, 57.

Boas, W. & Honeycombe, R. W. K. 1947 *Proc. Roy. Soc.* A, **188**, 427.

Boas, W. & Honeycombe, R. W. K. 1947 *J. Inst. Metals*, **73**, 433.

Brick, M. & Phillips, A. 1937 *Trans. Amer. Inst. Min. (Metall.) Engrs*, **124**, 331.

Carslaw, H. S. 1930 *Introduction to the theory of Fourier's series and line integrals*, 3rd ed. London: Macmillan.

Carslaw, H. S. & Jaeger, J. C. 1947 *Conduction of heat in solids*, pp. 46, 209. Oxford: Clarendon Press.

Ellwood, E. C. & Silcock, J. M. 1948 *J. Inst. Metals*, **74**, 457, 721.

Rice, J. 1930 *Introduction to statistical mechanics for students of physics and physical chemistry*, p. 102. London: Constable.

The kinetics of the thermal decomposition of normal paraffin hydrocarbons

I. The inhibition of chains and the nature of the residual reaction

BY F. J. STUBBS AND SIR CYRIL HINSHELWOOD, F.R.S.

(*Received* 2 *September* 1949)

The decomposition of paraffin hydrocarbons is lowered to a limiting value by additions of nitric oxide or of propylene. It has been a matter for discussion whether the residual rate corresponds to a molecular reaction or a steady state in which the chain reaction is imperfectly suppressed. Fresh evidence, including the facts that the limiting rates with the two inhibitors are identical, and that extra nitric oxide added during the reaction has no further effect, indicates that the former hypothesis is the more probable.

1. INTRODUCTION

The thermal decomposition of a normal saturated paraffin yields a paraffin of shorter chain length together with an olefine. The result of the reaction is as though a hydrogen atom is transferred from one carbon atom to an adjacent one with the simultaneous rupture of the bond between the two. This rupture may occur at various places in the carbon chain, so that a mixture of products is formed. It is usually the smaller of the two molecules produced which constitutes the saturated member. These changes are illustrated by the following equations:

$$CH_3CH_2CH_2CH_2CH_3 \longrightarrow CH_4 + CH_2 : CHCH_2CH_3, \tag{1}$$

$$CH_3CH_2CH_2CH_2CH_3 \longrightarrow C_2H_6 + CH_2 : CHCH_3. \tag{2}$$

The olefines formed in the first stage vary in stability relatively to the original hydrocarbon. Their decomposition gives two lower olefines, thus

$$CH_2 : CHCH_2CH_3 \longrightarrow CH_2 : CH_2 + CH_2 : CH_2. \tag{3}$$

According to circumstances, therefore, the observed pressure change attending the reaction could indicate either of the processes

$$\text{higher paraffin} = \text{lower paraffin} + \text{olefine}, \tag{4}$$

or

$$\text{higher paraffin} = \text{lower paraffin} + \text{two or more olefines}. \tag{5}$$

Unless the decomposition of the olefine is very rapid indeed the initial rate of the observed reaction will correspond to (4). To a limited extent the unsaturated compounds may become involved in polymerization and condensation reactions, but these are of minor importance in the initial stages.

The primary chemical processes of the type (1) and (2) are conceivable as direct molecular rearrangements. They involve only the transfer of a single hydrogen atom and the rupture of an adjacent bond, and are therefore by no means inconsistent with the general principle that chemical changes occur in stages with a high entropy of activation. On the other hand, chain mechanisms which lead quite naturally to identical products are very easily imagined. The products of (1), for example, could be formed by the chain processes

$$CH_3CH_2CH_2CH_2CH_3 \longrightarrow CH_3 + {-}CH_2CH_2CH_2CH_3,$$

$${-}CH_2CH_2CH_2CH_3 \longrightarrow CH_2 : CHCH_2CH_3 + H,$$

$$H + CH_3CH_2CH_2CH_2CH_3 \longrightarrow CH_4 + {-}CH_2CH_2CH_2CH_3.$$

Indeed, a reaction in which a methyl group captures a hydrogen atom from the rest of the molecule would be quite likely to yield the same products whether the radical became entirely free in the process or not. The molecular reaction depends upon a lower activation energy but has a rather less favourable entropy factor, since the movements of the hydrogen and of the carbon atoms have to be to some extent co-ordinated. The chain process, on the other hand, has a much higher activation energy for its initiation, but its individual steps are simpler. There is thus no theoretical reason to prefer the one or the other mechanism. The decision between them becomes a matter for experiment. The measured activation energy is little guide, since in a chain process it is a complex function of the energies of the individual steps, termination reactions contributing negative terms.

The experimental method which offers most hope of a decision is the study of the action of specific inhibitors on the rate of reaction. The most effective agents for suppressing radical chain reactions are nitric oxide, propylene and certain other olefines.

The marked inhibition of the reaction by small quantities of nitric oxide leaves no doubt about the existence of chains, but the relation between the rate and the inhibitor concentration raises fresh problems. Small amounts of nitric oxide cause a rapid fall in rate to a constant limiting value which even considerable further additions lower no more. Three views about the limiting rate are possible: that it pertains (*a*) to the primary reaction which normally starts the chain process, (*b*) to a simultaneous molecular reaction of the type which has been discussed, or (*c*) to a stationary state in which as many radicals are in some way regenerated as are removed by the inhibitor.

(*a*) is supported by Steacie & Folkins (1940) on the ground that the products formed from butane have the same composition whether the rate is controlled by nitric oxide or not. They consider it unlikely that a chain reaction and a competing molecular reaction would yield the same products. This argument, however, might be reversed. The inhibited reaction amounts to about one-fifth of the original, and if this is all primary process the point of view of Steacie & Folkins implies quite short chains. Now while, as was shown above, the initially formed radicals can easily go through cycles of reaction to give the same products as the molecular process would give, they could hardly do this if they all reacted with nitric oxide. We should prefer therefore to regard the important evidence from the work of Steacie & Folkins as support for the view that such chains as there are possess considerable length.

(*b*) has been preferred in various papers from this laboratory, on grounds of general probability, and because the limiting rate is constant over wide ranges of nitric oxide concentration, which would be difficult to explain in terms of (*c*).

(*c*), however, has been suggested by Echols & Pease (1939*b*) on the basis of observations with *n*-butane. The decomposition is strongly inhibited by nitric oxide, but as the reaction proceeds the pressure-time curve assumes a form closely parallel to that found for the system to which no nitric oxide has been added. Echols & Pease suggest that an equilibrium is set up in which, finally, as many radicals are regenerated from a combination with nitric oxide as are removed. There is also the possibility that nitric oxide might regenerate fresh radicals by entering into an oxidation reaction with the hydrocarbon itself.

In view of the various ambiguities the present work has included a further study of the mode of inhibition by nitric oxide and by propylene, and of the significance of the pressure-time curves. This will be described first. A systematic comparison of the complete series of normal paraffins from propane to decane will then be described in Part II.

2. GENERAL SURVEY OF RESULTS

The principal results and conclusions may be stated as follows.

With the lower paraffins the Δp-time curve observed in the absence of nitric oxide rises from the origin and then shows a rather pronounced curvature towards the time axis. This has now been shown by direct addition of products to be due to their inhibitory action. Since propylene and other olefines absorb free radicals this action is quite understandable (see § 6). The Δp-time curves for the reaction in the presence of nitric oxide are of a slightly sigmoid form, and for the systems with and without nitric oxide tend to become parallel as the reaction proceeds. This might give the impression that the nitric oxide inhibition is ceasing to operate. This explanation is not correct. The curves become parallel not because the nitric oxide inhibition ceases but because in the normal decomposition a product (olefine) assumes the role of inhibitor. The apparent acceleration is an inherent property of the reaction and due to the existence of a consecutive decomposition of the primary products. The sigmoid character of the pressure-time curve has been found in the present work to be much less pronounced than that shown in the diagram in the paper of Echols & Pease (1939*b*). Our results, however, agree closely with those found by Steacie & Folkins (1940).

The assumption of an equilibrium is not satisfactory and the following brief discussion of it is relevant to the general question. For butane the scheme suggested is as follows:

(*a*) $C_4H_{10} + 2R,$
(*b*) $R + C_4H_{10} = R + \text{products},$
(*c*) $2R \rightarrow X,$
(*d*) $R + NO \rightarrow S,$
(*e*) $S \rightarrow R + NO.$

If (*d*) and (*e*) come into equilibrium at once, then nitric oxide will not affect the stationary concentration of R and it will have no inhibitory effect at any stage of the reaction. This is what Echols & Pease assume for the later stages where they believe the inhibition to have disappeared. It should be equally true of the initial stages, where there is in fact inhibition. If we add a step

(*f*) $S \rightarrow$ irreversible destruction,

then it is easily shown that the form of the rate equation differs only by a constant from that obtained if (*d*) itself is irreversible. If, on the other hand, the equilibrium of (*d*) and (*e*) is assumed to be established slowly, the predictions correspond more closely but still not correctly to the facts. There would be an initial inhibition, after which the rate would rise again to a value independent of the nitric oxide pressure, provided this were fairly large. At this point the complex, S, is regenerating radicals as fast as it removes them. But the addition of fresh nitric oxide would give further inhibition, because the new equilibrium corresponding to a higher concentration of S would be established slowly. Additions of more nitric oxide half-way through the reaction do not in fact give further inhibition (see § 5), so that the hypothesis of a slow establishment of equilibrium is unsatisfactory. On the view that the inhibition remains throughout at its maximum value, provided that enough nitric oxide or olefine has been added from the start, this result is quite understandable. The solution of the equations (*a*) to (*f*) for the case of slow establishment of equilibrium is cumbrous, but the essential result is seen if (*c*) is simplified to be of the first order rather than the second with respect to R. This in no way affects the function and behaviour of the nitric oxide, but it eliminates a rather intractable quadratic form from the equations. The constants k_1 to k_5 refer to the equations (*a*) to (*e*).

For the stationary value of R we have

$$\frac{d[R]}{dt} = k_1[C_4H_{10}] - k_3[R] - k_4[R][NO] + k_5[S] = 0.$$

For $[S]$, which is not stationary,

$$\frac{d[S]}{dt} = k_4[R][\mathrm{NO}] - k_5[S].$$

Substitution of $[R]$ from the first into the second equation and solution of the latter gives

$$[S] = \frac{k_1 k_4[\mathrm{C_4H_{10}}][\mathrm{NO}]}{k_3 k_5}\left\{1 - \exp\left[-\frac{k_3 k_5 t}{k_3 + k_4[\mathrm{NO}]}\right]\right\},$$

where

$$[R] = \frac{k_1[\mathrm{C_4H_{10}}]}{k_3 + k_4[\mathrm{NO}]} + \frac{k_1 k_4[\mathrm{C_4H_{10}}][\mathrm{NO}]}{k_3(k_3 + k_4[\mathrm{NO}])}\left\{1 - \exp\left[-\frac{k_3 k_5 t}{k_3 + k_4[\mathrm{NO}]}\right]\right\}.$$

When $t = 0$ the second term is zero, so that R is completely suppressible by nitric oxide. When t becomes very large the second term ceases to depend upon it, and for large enough pressures of nitric oxide assumes the form $k_1[\mathrm{C_4H_{10}}]/k_3$. This represents a limiting rate apparently uninfluenced by the inhibitor. But if fresh nitric oxide were added, this would be equivalent to starting again from a low value of t, and the second term would fall. By this test the hypothesis of slow establishment of equilibrium fails.

A variant of the equilibrium hypothesis is that nitric oxide actually generates radicals by reaction. In this case the rate after passing through a minimum should actually rise continuously with the nitric oxide concentration, as it in fact does in the example of the acetaldehyde decomposition. There is no such effect in the hydrocarbon decomposition (§ 5).

If there is formation or regeneration of radicals in the nitric oxide system and the steady state determines the lower limit to which the reaction rate falls, then it would be a very highly improbable coincidence should two separate inhibiting agents lead to the same limit. In fact, the same limit is reached with propylene and with nitric oxide (§ 6), and the form of the curves relating rate to concentration of inhibitor is constant. These facts speak strongly in favour of the view that the residual rate is that of the molecular reaction.

In presence of nitric oxide the Δp-time curves are linear in the initial stages. Sometimes an induction period is observed lasting for a time during which about 2 mm. pressure change should have occurred. This might possibly have been interpreted as an initial complete inhibition of reaction and the gradual development of chains exempt from the action of nitric oxide. The effect was therefore studied in detail. The conclusion reached is that it is due to a secondary disturbance by a wall reaction which is attended by a pressure decrease masking the normal increase, but which is rapidly poisoned (§ 5). It is not of significance for the main reaction.

3. EXPERIMENTAL METHODS

The apparatus is shown diagrammatically in figure 1. The silica reaction vessel A (volume 300 ml.) was heated in the electric furnace B, wound in four sections so that the current in each could be independently adjusted and the temperature in the region of the reaction vessel made uniform to within less than ± 0·5° C. by an automatic control (Coates 1944), and was measured by a platinum-platinum/rhodium thermocouple.

The hydrocarbon, if liquid, was stored in the bulb *C*, and could be vaporized into the storage vessel *E* when the electrically heated bath *D* was raised. The taps *F* and *G* and the vessel *E* were immersed in an electrically heated oil thermostat to prevent condensation of hydrocarbon vapour. The pressure in *E* was read on the manometer *H*. The vapour was introduced into the reaction vessel through the tap *F*, the pressures being read on the capillary mercury manometer *I*. With knowledge of the sharing factor between *E* and the reaction vessel it was possible with a measured amount of vapour in *E* by the opening of tap *F* to introduce into the reaction vessel without appreciable delay the exact amount of hydrocarbon required.

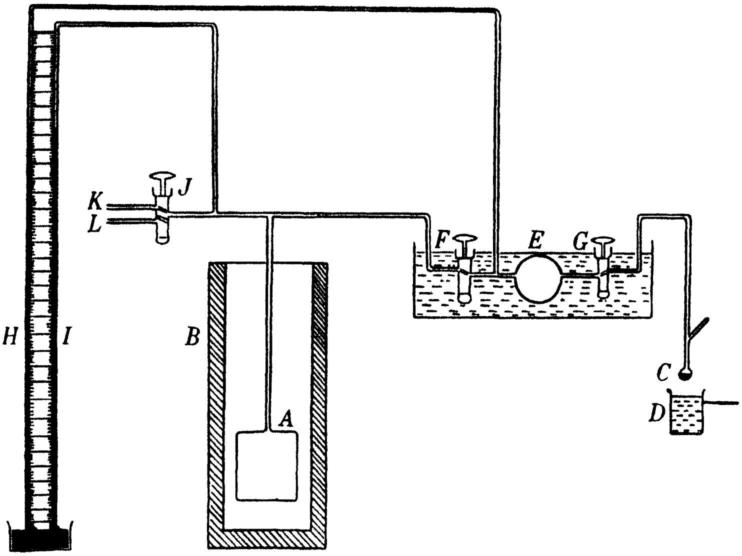

FIGURE 1. Diagram of apparatus.

The two-way tap *J* was connected at *K* to the storage bulbs containing the gaseous hydrocarbons and to the nitric oxide supply, and at *L* to a three-stage mercury diffusion pump backed by a rotary oil pump. All the connecting tubes were heated electrically to prevent condensation. Before each experiment the apparatus was evacuated to a pressure of 10^{-3} mm.

Taps *F*, *G* and *J* were lubricated with silicone grease, which proved very resistant to temperature and hydrocarbon vapour. By means of a capillary pipette, the amount of nitric oxide let into the reaction vessel could be measured to the nearest 0·1 mm.

The reaction was followed by observation of the increase of pressure (Δp), the initial rate of decomposition being obtained by the drawing of a tangent to the Δp-time curve. The results were very satisfactorily reproducible.

Pressures were measured in mm. of mercury, and rates expressed as mm./min. All experiments were made at 530° C unless otherwise stated.

The nitric oxide was prepared by the action of nitric acid upon mercury in the presence of sulphuric acid. Propane and *n*-butane, obtained from cylinders, were purified by fractional distillation, the middle fraction only being retained. All other paraffins had been specially prepared by Grignard reactions. Propylene was prepared by the dehydration of *iso*propyl alcohol with phosphorus pentoxide and fractionation of the product.

4. NORMAL DECOMPOSITION

Typical Δp-time curves for the normal decomposition in the series propane to *n*-decane are shown in figure 2 (initial hydrocarbon pressure 100 mm.).

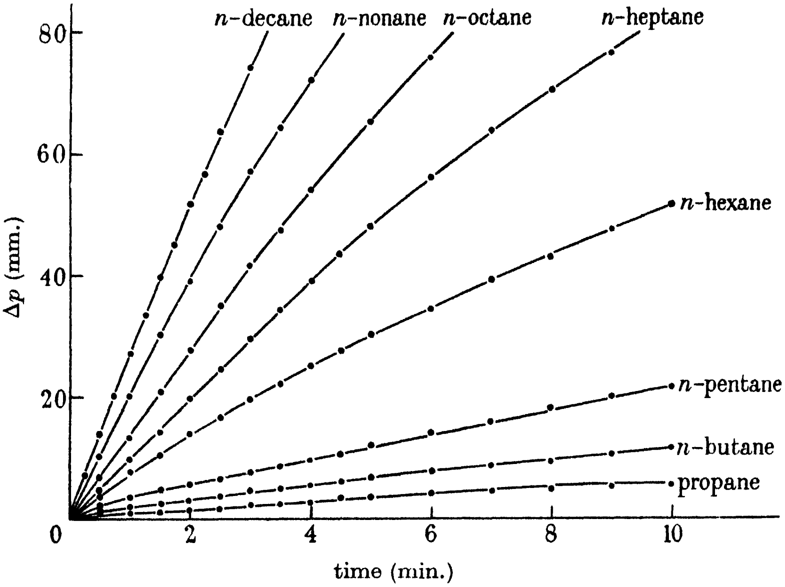

FIGURE 2. Δp-time curves for the normal decomposition at 530° C. ($p_0 = 100$ mm.)

With propane, *n*-butane and *n*-pentane the Δp-time relation near the origin shows a pronounced curvature towards the time axis. The slope of the tangent to the initial steep portion of the curve must be taken as the true initial rate of decomposition. This initial curvature is quite real and has been observed independently for *n*-butane by Steacie & Folkins (1939, 1940) and by Echols & Pease (1939*a*). The rapid initial falling off of reaction rate proved to be due to inhibition by the products of reaction. This was shown in the following way. The initial rate of decomposition for 100 mm. initial pressure of *n*-butane at 560° C was found to be 8·5 mm./min. The reaction was allowed to proceed for about 2 hr., at which time the rate had become negligible, the total pressure having risen to 200 mm. ($\Delta p = 100$ mm.). A further 100 mm. of *n*-butane was then introduced into the reaction vessel. The initial decomposition rate in the presence of the 200 mm. of reaction product was now found to be depressed to 4·0 mm./min. This establishes the inhibitory effect of the reaction products.

Rice & Polly (1938) have shown that ethylene causes no detectable inhibition, so that the effect must be due to propylene or butene-1. The major part of the 200 mm. of reaction product from butane is hydrogen, methane, ethane and ethylene, so that the effective pressure of propylene and butene-1 does not exceed about 50 mm. § 6 deals with the quantitative effect of propylene as an inhibitor, and the degree of inhibition caused by 50 mm. is in fact approximately that observed with the 200 mm. of reaction product.

Experiments with *n*-heptane showed that the initial rate of decomposition of 100 mm. at 530° C is reduced from 10 to 5 mm./min. by 100 mm. of the reaction product. The rate of the fully inhibited decomposition under these conditions is 3·6 mm./min.

Figure 2 shows that near the origin the Δp-time curves for the paraffins from hexane upwards are approximately straight lines passing through the origin. These paraffins on decomposition yield higher olefines, which probably have a very strong inhibitory effect, and it is at first sight surprising that the Δp-time relations show little sign of this. The higher olefines, however, are themselves susceptible to decomposition, and in consequence a Δp-time curve for the fully inhibited decomposition has a sigmoid character. The almost linear nature of the curves near the origin is thus very probably the resultant of two effects; the higher olefines formed subsequently tend to decompose and give an increased rate, but this is offset by their inhibitory effect.

5. Influence of nitric oxide

Small amounts of nitric oxide cause a marked reduction in the initial rate of decomposition (Staveley 1937). Partington, Stubbs & Hinshelwood (1949) found that with *n*-pentane the first small additions make the initial part of the Δp-time curve almost linear. Increasing amounts reduce the initial rate to a constant limiting value, independent, over a wide range, of the nitric oxide concentration. A plot of initial rate against nitric oxide pressure for the decomposition of 100 mm. *n*-pentane at 530° C is shown in figure 8. Steacie & Folkins (1940) found a similar effect of nitric oxide on the decomposition of *n*-butane.

Figure 3 shows the effect of increasing amounts of nitric oxide on the decomposition of *n*-heptane (100 mm. initial pressure). The initial portion of the Δp-time curve for the normal reaction is a straight line passing through the origin. The addition of nitric oxide decreases the slope of this, and after the initial straight portion the Δp-time curve shows an upward sweep, later following a course roughly parallel to that for the normal reaction. The Δp-time curves for the normal and inhibited reactions eventually converge to the same end-point. The behaviour with *n*-heptane is characteristic of that observed with all the higher paraffins.

In the presence of nitric oxide (particularly with the fully inhibited reactions) there is often a short time at the beginning of the reaction during which no increase of pressure is observed, and, in fact, occasionally a decrease occurs. The Δp-time curve cuts the axis at a finite time, as shown in figure 3. This induction period is always very short, usually of such length that if the reaction were proceeding at its steady rate the pressure would have increased not more than about 2 mm. It is most in evidence with the lower paraffins.

It is important to decide whether the induction period could represent a gradual increase of rate from zero to the final steady value, such as would occur if chains were at first completely suppressed and later only partially. The fact that an actual small pressure decrease is sometimes observed supports the view that the induction period is a secondary effect caused by the masking of the normal pressure increase.

A mercury manometer being unsuitable for the detection of very small pressure changes, a more detailed investigation of the initial stages was made by Dr C. F. Cullis with another apparatus with a differential butyl phthalate manometer protected from the hydrocarbon by a nitrogen buffer. The rate of decomposition of *n*-butane was exactly reproduced in the second apparatus. In the first experiments on the fully inhibited reaction, however, no induction period at all was observed. The initial part of the Δp-time curve was a straight line passing exactly through the origin. Experiments were next made on the fully inhibited decomposition of *n*-pentane. In the first ones the Δp-time curve passed exactly through the origin, but in subsequent experiments a definite induction period appeared, and a characteristic small initial decrease was observed. A typical example (100 mm. of *n*-pentane: 15 mm. nitric oxide) is shown in figure 4. After the induction period the pressure at first rose linearly with time, and the initial rate was identical with that observed when there had been no induction period. This showed that the method normally employed in measuring the initial rate was justified.

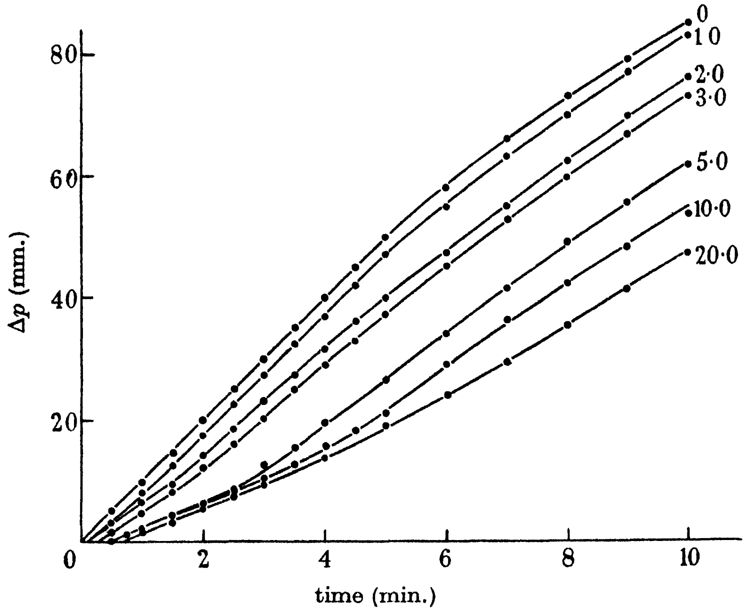

FIGURE 3. Influence of nitric oxide on the Δp-time curve for the decomposition of 100 mm. *n*-heptane at 530° C. The figures against the curves show mm. of nitric oxide.

The induction period is evidently due to a slight disturbing side reaction attended by a small decrease of pressure, which is completely eliminated once a small amount of decomposition has occurred. It is rather variable, whereas the initial rate itself is exactly reproducible, and is probably due to a transitory surface reaction which soon becomes poisoned.

The continuous curve in figure 5 refers to the fully inhibited decomposition of *n*-heptane (100 mm.) at 530° C. After the very short induction period there is a straight portion and then the curve rises, reaching a maximum slope which shows the normal decrease as the reaction comes to an end. The sigmoid nature of the curve has to be explained, and at first sight the apparent acceleration might be attributed to the removal of nitric oxide by reaction. If this occurred, then the use of greater amounts of nitric oxide would prolong the initial straight portion. Actually it is found that this is not so.

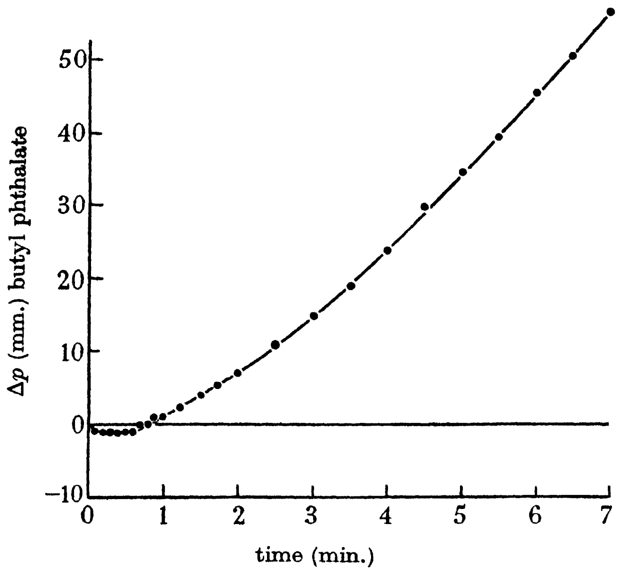

FIGURE 4. Δ*p*-time curve for the fully inhibited decomposition of 100 mm. *n*-pentane at 525° C; detail of initial disturbance.

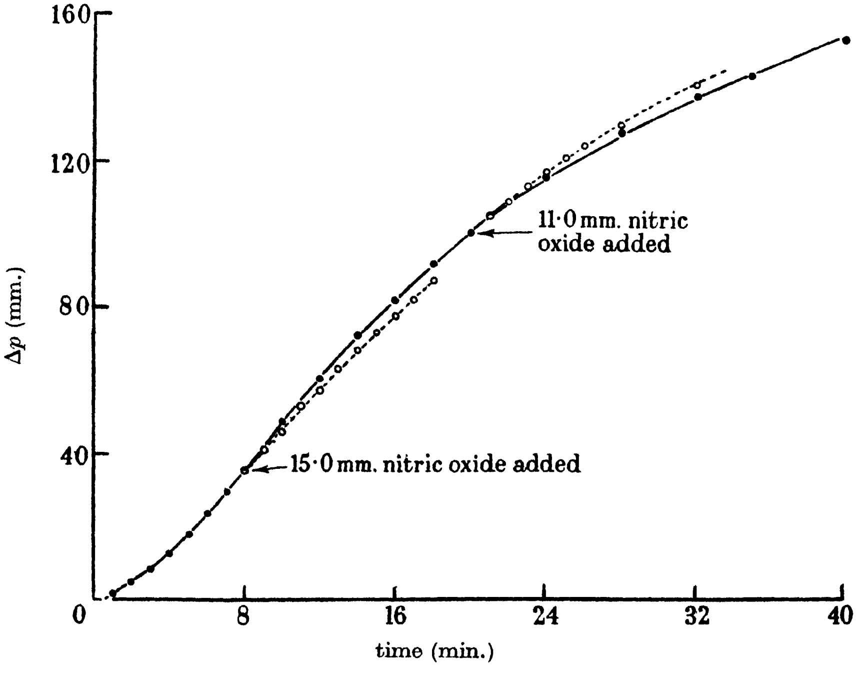

FIGURE 5. Additions of extra nitric oxide during course of decomposition (100 mm. *n*-heptane, 530° C).

Echols & Pease (1939*b*), investigating the decomposition of *n*-butane, showed by analysis that only a very small amount of the nitric oxide is used up. They concluded that the inhibitory effect is transient and that the rate of reaction in fact returns to its normal value.

To obtain more precise evidence the following experiments have now been made. The decomposition of *n*-heptane at 100 mm. initial pressure in the presence of 15 mm. of nitric oxide was allowed to proceed until the rate reached a maximum after 8 min. (Δp = 36 mm.). At this point a further 15 mm. of nitric oxide was added, the subsequent course of the Δp-time curve being indicated by the lower dotted line in figure 5. In another similar experiment a further 11 mm. of nitric oxide was added after 20 min. (Δp = 100 mm.), the new Δp-time curve being shown also in figure 5. The addition of further amounts of nitric oxide is seen to have practically no effect on the rate. This proves that the sigmoid nature of the Δp-time curve is not due to the consumption of nitric oxide.

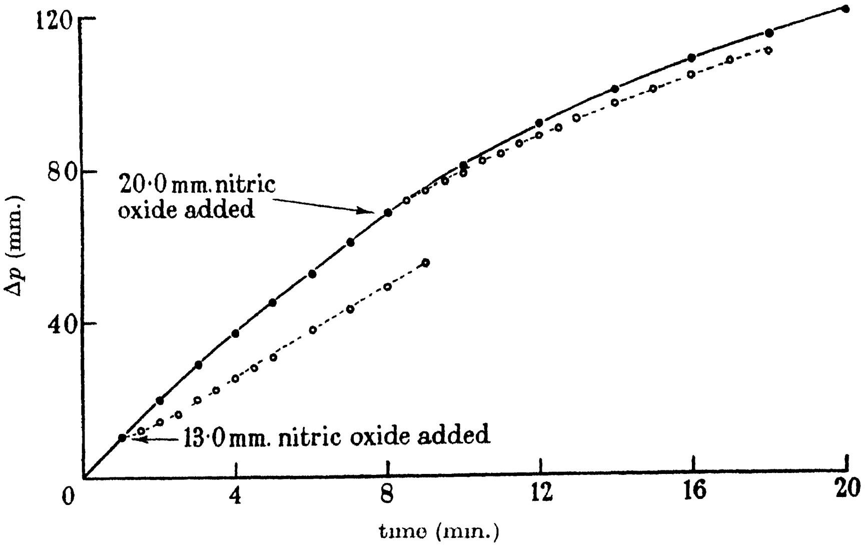

FIGURE 6. Additions of nitric oxide at different stages of reaction (100 mm. *n*-heptane, 530° C).

In view of the results on the inhibitory effect of reaction products (§ 4), it was thought interesting to determine the effect of nitric oxide added during the normal decomposition reaction. The continuous curve in figure 6 refers to the normal decomposition of *n*-heptane (100 mm.) at 530° C, the upper dotted curve to a similar experiment in which after 8 min. (Δp = 68 mm.) 20 mm. of nitric oxide was introduced. There is only a very slight depression of the rate, since at this point the chain reaction has been almost fully inhibited by the reaction products. In another experiment with 100 mm. of *n*-heptane 13 mm. of nitric oxide was added after 1 min. only. The lower dotted line in figure 6 shows that here there is a pronounced inhibition. The new rate of decomposition is identical with that observed when the nitric oxide is present initially, and, in fact, if plotted on the same axes the Δp-time curves coincide over the whole of their length. At this early stage there is no inhibition by reaction products.

The rate of decomposition increases with initial hydrocarbon pressure, and it seemed possible that the sigmoid character of the Δp-time relation might be due to a dependence of the rate on the total gas pressure. In order to test this, the decomposition of 100 mm. of *n*-heptane with 15·0 mm. of nitric oxide was followed in the presence of (*a*) 100 mm. of reaction product, (*b*) 100 mm. propane (the decomposition of this being much slower and allowed for). The initial rates were unaffected, and, in fact, the Δp-time curves coincided over the whole of their length with those observed without the addition of the effectively inert gases.

TABLE 1. THERMAL DECOMPOSITION OF *n*-PENTANE

pressure of nitric oxide (mm.)	initial rate at 530° C (mm./min.)		initial rate at 550° C (mm./min.)	
	$p_0 = 100$ mm.	$p_0 = 250$ mm.	$p_0 = 100$ mm.	$p_0 = 250$ mm.
0	4·20	13·2	9·8	29·2
1·0	1·98	7·8	6·4	23·3
2·0	1·24	6·7	4·7	20·6
3·0	0·93	5·5	4·0	18·0
4·0	—	--	3·7	—
5·0	0·73	4·4	3·1	16·0
7·0	—	—	2·6	13·7
10·0	0·58	3·3	2·3	10·7
15·0	0·58	3·3	—	- -
20·0	0·58	3·3	2·3	7·6

TABLE 2. THERMAL DECOMPOSITION OF *n*-HEXANE AT 530° C

pressure of nitric oxide (mm.)	initial rates (mm./min.)		
	$p_0 = 50$ mm.	$p_0 = 100$ mm.	$p_0 = 150$ mm.
0	3·50	8·14	13·0
1·0	2·06	5·97	11·5
2·0	1·60	4·53	10·1
3·0	—	4·01	8·5
4·0	1·34	3·61	7·6
5·0	—	—	7·1
6·0	-	3·51	6·6
8·0	—	-	6·1
10·0	1·23	3·51	5·8
20·0	1·23	3·51	5·8

The sigmoid nature of the Δp-time curve for the fully inhibited decomposition is therefore due neither to the removal of nitric oxide nor to a dependence of the rate on the total gas pressure. It is an inherent characteristic of the inhibited reaction, and due to further decomposition of the primary products.

The effect of nitric oxide on the decomposition of the different normal paraffins is shown in tables 1 to 4. In all cases it reduces the rate to a constant limiting value.

The degree of inhibition caused by a given pressure of nitric oxide can be expressed by the function $(r - r_\infty)/(r_0 - r_\infty)$, where r is the rate at the given nitric oxide pressure. r_0 the normal rate, and r_∞ the limiting rate for high pressure of nitric oxide. In figure 7 this function is plotted against nitric oxide pressure for different heptane pressures. For a given degree of inhibition, more nitric oxide is needed the higher the heptane pressure. This is true also for *n*-hexane and for *n*-pentane both at 530° and 550°. In general, the amount necessary to cause a given degree of inhibition for a constant hydrocarbon pressure increases from *n*-pentane to *n*-decane.

TABLE 3. THERMAL DECOMPOSITION OF *n*-HEPTANE AT 530° C

pressure of nitric oxide (mm.)	initial rates (mm./min.)		
	$p_0 = 50$ mm.	$p_0 = 100$ mm.	$p_0 = 150$ mm.
0	4·12	10·2	16·3
1·0	2·99	8·4	14·4
2·0	2·11	7·0	12·4
3·0	1·70	5·8	10·5
4·0	1·60	4·7	8·9
5·0	—	4·2	7·3
7·0	—	3·9	6·2
10·0	1·60	3·9	6·0
15·0	—	3·8	6·0
20·0	1·60	3·9	6·0

TABLE 4. THERMAL DECOMPOSITION AT 530° C

pressure of nitric oxide (mm.)	initial rates (mm./min.)		
	50 mm. *n*-octane	50 mm. *n*-nonane	50 mm. *n*-decane
0	5·46	8·14	11·2
1·0	2·99	5·56	6·39
2·0	2·27	4·64	4·84
4·0	1·75	3·09	4·12
6·0	1·55	—	—
10·0	1·30	2·06	3·91
20·0	1·34	2·10	2·47

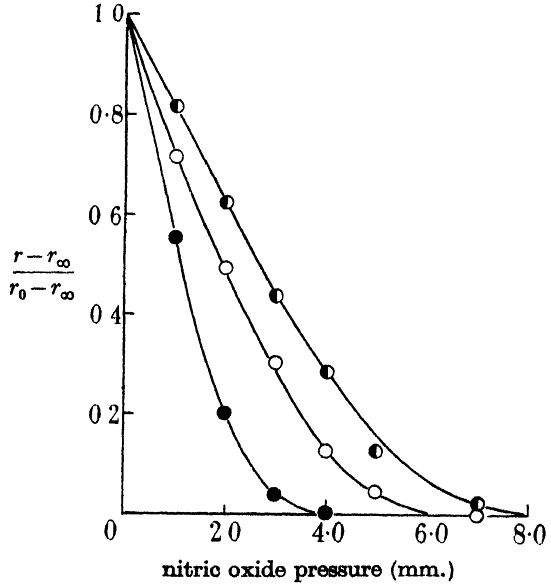

FIGURE 7. Relative inhibition by nitric oxide at different initial pressures of *n*-heptane (530° C). ◐, $p_0 = 150$ mm.; ○, $p_0 = 100$ mm.; ●, $p_0 = 50$ mm.

6. Influence of propylene

Like nitric oxide the higher olefines can act as inhibitors of free radical chain reactions (Rice & Polly 1938). Smith & Hinshelwood (1942) compared the inhibitory effects on the decomposition of propaldehyde and of diethyl ether, of nitric oxide and propylene, and found that although the latter is not such an efficient inhibitor as the former, each reduces the rate to the same limiting value.

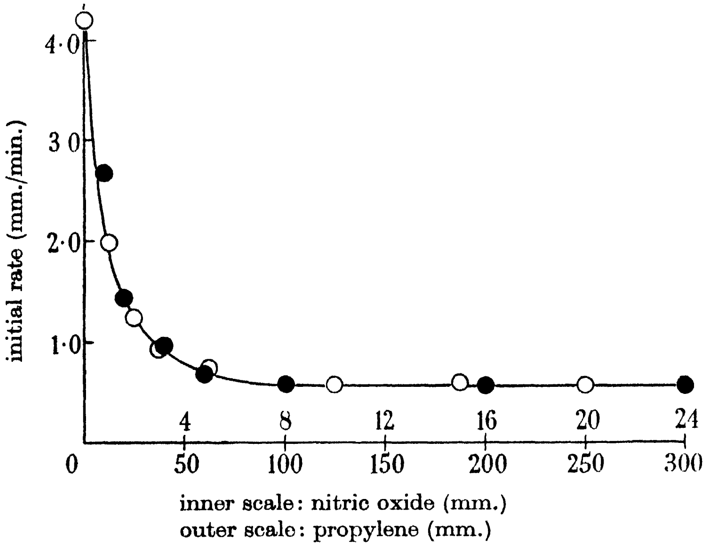

FIGURE 8. Quantitative comparison of inhibition by nitric oxide and propylene (100 mm. n-pentane, 530° C). ●, inhibition by propylene; ○, inhibition by nitric oxide.

TABLE 5. INHIBITION BY PROPYLENE OF THE DECOMPOSITION OF 100 MM. n-PENTANE AT 530° C

pressure of propylene (mm.)	initial rate (mm./min.)	pressure of propylene (mm.)	initial rate (mm./min.)
0	4·20	60	0·68
10	2·68	100	0·58
20	1·44	200	0·60
40	0·96	300	0·58

A similar comparison has now been made of the effect of the two inhibitors on the decomposition of the normal paraffins. At 530° C the decomposition of propylene alone can be neglected. Its influence on the rate of decomposition of n-pentane (100 mm.) is recorded in table 5. Figure 8 shows how increasing amounts of propylene reduce the initial rate to a well-defined limit. Results for nitric oxide are plotted on the same diagram with a simple change of the horizontal scale. Although nitric oxide is about 12 times as efficient as propylene, each reduces the rate to the same constant limiting value. This was found to be true also in experiments with 250 mm. of n-pentane.

7. Fully inhibited decomposition

Echols & Pease (1939*b*) investigated the decomposition of *n*-butane (200 mm. initial pressure) at 520° C, and according to their results, in the presence of inhibitors, the Δp-time curve shows a steady acceleration. The results of the present work with propane and butane being in disagreement with this, some of the experiments of Echols & Pease were repeated. The decomposition at 520° C of 200 mm. of *n*-butane with 15 mm. of nitric oxide was followed for 100 min., pressure readings being taken every minute. For the first 17 min. the Δp-time relation was exactly linear (there being no induction period). The curve then sloped upward very slightly but soon began to flatten once more. Steacie & Folkins (1940) show a Δp-time curve for the decomposition of 401 mm. *n*-butane at 525° C. It is exactly linear for the first 7 min., the slope then increases very slightly, but soon begins to fall off again. Quantitatively the results of Steacie & Folkins and those of the present investigation are in all respects in excellent agreement but differ greatly from those of Echols & Pease, whose rates are much lower.

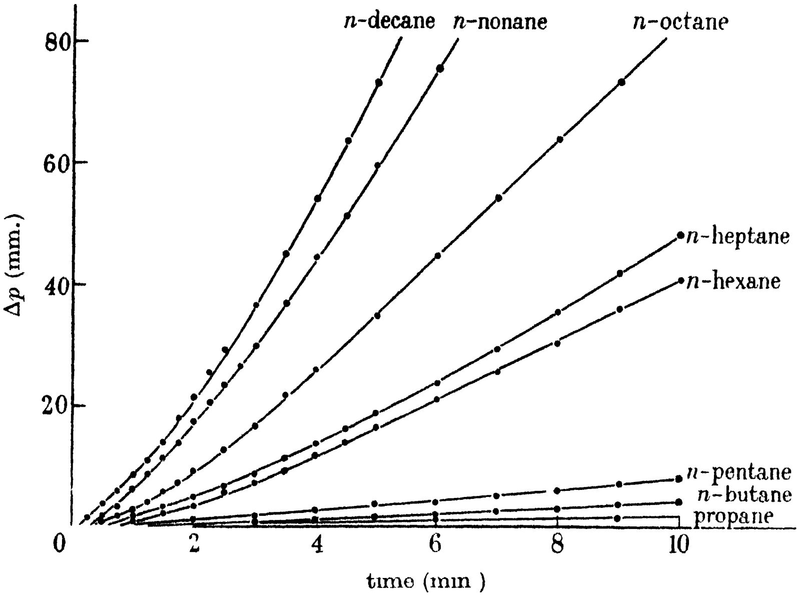

FIGURE 9. Δp-time curves for the fully inhibited decomposition at 530° C (p_0 = 100 mm).

The results of § 5 have shown that the sigmoid form of Δp-time curves is due neither to consumption of inhibitor nor to the effect of total gas pressure on the rate. It becomes more in evidence as the series is ascended, being almost imperceptible with propane and *n*-butane, but marked with *n*-decane. This is shown clearly in figure 9.

Preliminary measurements made in this laboratory have shown that the rate of decomposition of olefines increases rapidly with the number of carbon atoms, propane decomposing more rapidly than propylene, butane and butene-1 at the same rate, and hexene-1 decomposing faster than hexane. In the initial stages of the paraffin decomposition the olefine concentration is so small that its further reaction rate is negligible. As products accumulate they also decompose, and give a further increase of pressure, whence the sigmoid character of the curves. For propane and *n*-butane, the olefines formed decompose so slowly that the sigmoid form is barely perceptible.

8. GENERAL CONCLUSION

From the foregoing investigations we conclude that the reaction observable when the rate has been reduced to its lowest value by nitric oxide is that of a molecular decomposition of the hydrocarbon, which thus becomes susceptible of detailed study.

We are indebted to Imperial Chemical Industries Limited and to the Anglo-Iranian Oil Company for the gift of pure specimens of various hydrocarbons. This work is part of the programme of the Fuel Research Board of the Department of Scientific and Industrial Research and is published with the approval of the Director of Fuel Research.

REFERENCES

Coates, G. E. 1944 *J. Sci. Instrum.* **21**, 86.
Echols, L. S. & Pease, R. N. 1939*a* *J. Amer. Chem. Soc.* **61**, 208.
Echols, L. S. & Pease, R. N. 1939*b* *J. Amer. Chem. Soc.* **61**, 1024.
Partington, R. G., Stubbs, F. J. & Hinshelwood, Sir C. 1949 *J. Chem. Soc.* p. 2674.
Rice, F. O. & Polly, O. L. 1938 *J. Chem. Phys* **6**, 273.
Smith, J. R. E. & Hinshelwood, C. N. 1942 *Proc. Roy Soc.* A, **180**, 237.
Staveley, L. A. K. 1937 *Proc. Roy. Soc.* A, **162**, 557.
Steacie, E. W. R. & Folkins, H. O. 1939 *Canad. J. Res.* B, **17**, 105.
Steacie, E. W. R. & Folkins, H. O. 1940 *Canad. J. Res.* B, **18**, 1.

Configurational interaction in molecular orbital theory. A higher approximation in the non-empirical method

By D. P. Craig
Sir William Ramsay and Ralph Forster Laboratories, University College, London

(*Communicated by C. K. Ingold, F.R.S.—Received* 10 *March* 1949—
Revised 20 *May* 1949)

The disagreements between calculations of the benzene energy states by the method of antisymmetric molecular orbitals (A.S.M.O.) and by the augmented valence-bond theory given in previous papers (Craig 1950*a* to *c*) are due, at least in part, to the neglect in the former of interaction between different 'configurations'. Every scheme of assigning electrons to molecular orbitals is a configuration, and where states with different configurations have the same symmetry they interact with one another under the influence of electron repulsion and suffer energy changes. In this paper a study of these energy changes is made, using a limited set of configurations. The A.S.M.O. states are affected by amounts up to 5 eV, and this is enough to show that the A.S.M.O. theory cannot be used for the detailed understanding of molecular spectral bands. The inclusion of configurational interaction gives the next higher approximation and makes the method, in principle, as general as is compatible with the initial use of $2p$ atomic wave functions. The method ought to prove valuable for settling in a non-empirical way issues for which the correctness of the simple empirical methods is in doubt. Even in the improved theory, however, the numerical precision required to interpret spectral separations in the order of 1 eV will be difficult to attain without the use of three-centre integrals and some other refinements.

Introduction

There are considerable differences between the theories of the lower excited states of benzene according to the method of valence-bond structures (V.B.) and the method of antisymmetrized molecular orbitals (A.S.M.O.) of Goeppert-Mayer & Sklar (1938). In figure 1 the results from the two methods are set out side by side.

The theories agree in finding the first excited state to be of symmetry B_{2u}, but they disagree in the second state, and there are at present no experimental facts to settle the issue. In this paper an approach to the question is made through a critical study of the A.S.M.O. method as it applies to benzene. It is a condition of this method that a state should be adequately represented by a single 'configuration', i.e. a single scheme of assigning electrons to orbitals, and this will hold only if, within a symmetry class, the several configurations are well spaced in energy. The first part of this paper shows that this condition does not hold, for there are, relatively close together, several hitherto unrecognized A.S.M.O. states of the same symmetry type. It follows that account ought to be taken of what, in atomic theory, is called 'configuration interaction', and this is done in the second part of the paper. It represents the next approximation over the use of antisymmetric molecular orbitals. The interactions between configurations prove to be large, and their inclusion alters the whole pattern of Goeppert-Mayer & Sklar's results. The numerical performance of the method is disappointing, but so far as the order of states is concerned the results are nearer to those of the V.B. theory (Craig 1950*c*), and there are indications that a complete treatment of configuration interaction would make the agreement better still. Apart, however, from that question, one clear conclusion is that the disagreements of figure 1 are of little significance, because a more exact handling of the same antisymmetric molecular orbital wave functions considerably weakens the claim of the theory to give a satisfactory numerical account of the experimental material.

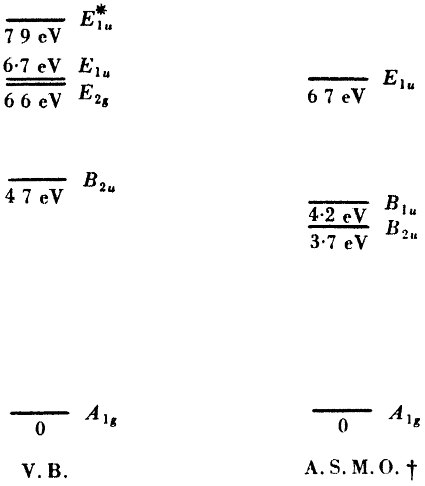

FIGURE 1

THE A.S.M.O. STATES OF BENZENE

In Goeppert-Mayer & Sklar's original paper they gave the theory of the lower benzene states, using values of integrals later published by Sklar & Lyddane (1939). These integrals were corrected at some points by Parr & Crawford (1948), and the revised values are used in this paper. Parr & Crawford, in a paper already referred to (Craig 1950*a*), worked out the simplest possible example of configuration interaction in a molecule, viz. between the two π-electron molecular orbitals in ethylene. For details of the A.S.M.O. method itself the reader is referred to the early papers; we give here only what is necessary for the development of present lines of argument.

Following Goeppert-Mayer & Sklar we write the m.o.'s for benzene in the form

$$\phi_l(\nu) = \frac{1}{(6\sigma_l)^{\frac{1}{2}}} \sum_{k=1}^{6} e^{2\pi ilk/6}\, K(\nu),$$

$$\phi_l^* = \phi_{-l}.$$

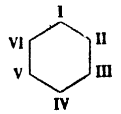

For $l = 0$, 3 the orbitals are non-degenerate, and for $l = \pm 1$, ± 2 are doubly degenerate. Under the operations of the symmetry group D_{6h} the orbitals transform according to the following scheme, in which C_n is an n-fold rotation about the principal symmetry axis, C_2' a twofold rotation about an axis in the molecular plane passing through opposite pairs of atoms, and C_2'' a twofold rotation about an axis in the molecular plane passing midway between opposite pairs of adjacent atoms:†

---

† These values were first obtained by Parr & Crawford. They were kindly communicated by the authors in advance of publication.

$$\left.\begin{aligned} C_6\phi_l &= \mathrm{e}^{\pm 2\pi il/6}\phi_l \\ C_3\phi_l &= \mathrm{e}^{\pm 4\pi il/6}\phi_l \\ C_2\phi_l &= \mathrm{e}^{\pi il/6}\phi_l \end{aligned}\right. \quad \text{Rotations about principal axis.}$$

$$C_2'\phi\begin{cases} = -\mathrm{e}^{4\pi il/6}\phi_{-l} \\ = -\mathrm{e}^{-4\pi il/6}\phi_{-l} \\ = -\phi_{-l} \end{cases} \quad \text{Twofold rotations:}$$

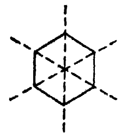

$$C_2''\phi_l\begin{cases} = -\mathrm{e}^{6\pi il/6}\phi_{-l} \\ = -\mathrm{e}^{2\pi il/6}\phi_{-l} \\ = -\mathrm{e}^{-2\pi il/6}\phi_{-l} \end{cases} \quad \text{Twofold rotations:}$$

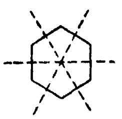

By comparing these with the character table for D_{6h} one finds the following representations for the one-electron molecular orbitals:

$$\phi_0 \subset a_{2u}, \quad \phi_{\pm 2} \subset e_{2u},$$
$$\phi_{\pm 1} \subset e_{1g}, \quad \phi_3 \subset b_{2g}.$$

In the ground state ϕ_0 and $\phi_{\pm 1}$ are fully occupied. Goeppert-Mayer & Sklar examined the excited states which differ in configuration from the ground state by having one electron lifted into $\phi_{\pm 2}$, leaving a hole in $\phi_{\pm 1}$. The symmetries of these states are B_{2u}, B_{1u} and E_{1u}, and their energies based on the integrals of Parr & Crawford (1948) are shown on the right-hand side of figure 1. Corresponding to other configurations of occupied orbitals and holes there are further molecular states. Of these we shall deal only with states which differ in configuration by the elevation of either one or two electrons from the orbitals occupied in the ground state. We shall call these one- and two-electron states respectively, and shall show that the energies of several of the two-electron states are comparable to those of the one-electron states considered by Goeppert-Mayer & Sklar. The symmetries to which these states belong are set out in table 1. Configurations are shown relative to the ground state which has ϕ_0 and $\phi_{\pm 1}$ fully occupied. For example, the configuration indicated in table 1 as $1 \rightarrow 2$ has a hole in $\phi_{\pm 1}$ and one electron in $\phi_{\pm 2}$.

The antisymmetric wave functions for these states are most conveniently written in determinantal form. For example, the ground-state wave function is written

$$\psi^{\mathrm{I}}(A_{1g}) = 1/\sqrt{6!}\begin{vmatrix} \phi_0\alpha(1) & \phi_0\beta(1) & \phi_1\alpha(1) & \phi_1\beta(1) & \phi_{-1}\alpha(1) & \phi_{-1}\beta(1) \\ \phi_0\alpha(2) & \phi_0\beta(2) & \phi_1\alpha(2) & \phi_1\beta(2) & \phi_{-1}\alpha(2) & \phi_{-1}\beta(2) \\ \phi_0\alpha(3) & \phi_0\beta(3) & \phi_1\alpha(3) & \phi_1\beta(3) & \phi_{-1}\alpha(3) & \phi_{-1}\beta(3) \\ \phi_0\alpha(4) & \phi_0\beta(4) & \phi_1\alpha(4) & \phi_1\beta(4) & \phi_{-1}\alpha(4) & \phi_{-1}\beta(4) \\ \phi_0\alpha(5) & \phi_0\beta(5) & \phi_1\alpha(5) & \phi_1\beta(5) & \phi_{-1}\alpha(5) & \phi_{-1}\beta(5) \\ \phi_0\alpha(6) & \phi_0\beta(6) & \phi_1\alpha(6) & \phi_1\beta(6) & \phi_{-1}\alpha(6) & \phi_{-1}\beta(6) \end{vmatrix}$$
$$= (|\phi_0\bar{\phi}_0\phi_1\bar{\phi}_1\phi_{-1}\bar{\phi}_{-1}|).$$

---

† The symmetry notation throughout is that of Eyring, Walter & Kimball (1944), *Quantum Chemistry*, New York: John Wiley.

A suitable notation for determinants of this type is provided by the bracketed expression, in which the occupied molecular orbitals are written in the order of columns. Orbitals with spin β are marked with a bar, and the normalizing coefficient, which is in every case $1/\sqrt{6!}$, is dropped.

TABLE 1

ground state	one-electron states
A_{1g}	$1 \to 2$: B_{2u}, B_{1u}, E_{1u}
	$1 \to 3$: E_{2g}
	$0 \to 2$: E_{2g}
	$0 \to 3$: B_{1u}

two-electron states

	$1 \to 2$	$1 \to 3$	$0 \to 2$	$0 \to 3$
$1 \to 2$	A_{1g} A_{2g} E_{2g}	B_{1u} B_{2u} E_{1u}	B_{1u} B_{2u} E_{1u}	A_{1g} A_{2g} E_{2g}
$1 \to 3$	—	A_{1g} A_{2g} E_{2g}	A_{1g} A_{2g} E_{2g}	E_{1u}
$0 \to 2$	—	—	A_{1g} A_{2g} E_{2g}	E_{1u}
$0 \to 3$	—	—	—	A_{1g}

All the wave functions have to transform properly under the symmetry operations, and this leads to some complexity when there are half-filled orbitals. For example, an A_{1g} two-electron wave function having two electrons in $\phi_{\pm 2}$ is:

$$\psi^{\mathrm{II}}(A_{1g}) = \tfrac{1}{2}(|\phi_0\bar{\phi}_0\phi_1\bar{\phi}_{-1}\phi_2\bar{\phi}_{-2}| - |\phi_0\bar{\phi}_0\bar{\phi}_1\phi_{-1}\phi_2\bar{\phi}_{-2}| - |\phi_0\bar{\phi}_0\phi_1\bar{\phi}_{-1}\bar{\phi}_2\phi_{-2}| + |\phi_0\bar{\phi}_0\bar{\phi}_1\phi_{-1}\bar{\phi}_2\phi_{-2}|)$$

Energy values

The method for evaluating the energies of these states was the special contribution of Goeppert-Mayer & Sklar's theory (1938). The energy is separated into two parts. One is the energy of the electrons each moving independently of the rest in the field of six carbon 'ions', meaning carbon atoms stripped of their $2p_z$ electrons. This 'orbital' energy is then corrected by adding the other part, which is interelectronic repulsion, treated as a perturbation over the molecular orbital wave function. Thus if ϵ_l stands for the energy of ϕ_l, the energy of $\psi^{\mathrm{I}}(\mathrm{A}_{1g})$ is

$$W^{\mathrm{I}}(A_{1g}) = 2\epsilon_0 + 4\epsilon_1 + \iint \psi^{*\mathrm{I}}(A_{1g}) \sum_{u<v} \frac{e^2}{r_{\mu\nu}} \psi^{\mathrm{I}}(A_{1g})\, d\tau_\mu d\tau_\nu.$$

Evidently the integral in this expression will break up into integrals taken over M.O.'s. These will each have one of the following forms:

$$\gamma_{ll'} = \iint \phi_l^*(\mu)\phi_l(\mu)\frac{e^2}{r_{\mu\nu}}\phi_{l'}^*(\nu)\phi_{l'}(\nu)\, d\tau_\mu d\tau_\nu \quad \text{(Coulomb type),}$$

$$\delta_{ll'} = \iint \phi_l^*(\mu)\phi_{l'}(\mu)\frac{e^2}{r_{\mu\nu}}\phi_{l'}^*(\nu)\phi_l(\nu)\, d\tau_\mu d\tau_\nu \quad \text{(exchange type)}$$

$$\xi = \iint \phi_1^2(\mu)\frac{e^2}{r_{\mu\nu}}\phi_2^2(\nu)\, d\tau_\mu d\tau_\nu,$$

$$\eta = \iint \phi_1(\mu)\phi_2(\mu)\frac{e^2}{r_{\mu\nu}}\phi_1(\nu)\phi_2(\nu)\, d\tau_\mu d\tau_\nu.$$

We require the values of these integrals, and of the orbital energy differences $\epsilon_l - \epsilon_{l'}$. Both can be expressed in terms of integrals over atomic orbitals. The results are summarized in table 2. The values of integrals over atomic orbitals are from Parr & Crawford's paper (1948). They apply to a C-C distance of 1·40 Å, and to an effective nuclear charge $Z = 3{\cdot}18$. The energy operator in the last two integrals is the attractive potential of a carbon atom.

TABLE 2. INTEGRALS OVER ATOMIC ORBITALS

$$A_0 = \iint \mathrm{I}^2(1)\frac{e^2}{r_{12}}\mathrm{I}^2(2)\,d\tau_1 d\tau_2 = 16{\cdot}9310\ \mathrm{eV}$$

$$A_1 = \iint \mathrm{I}^2(1)\frac{e^2}{r_{12}}\mathrm{II}^2(2)\,d\tau_1 d\tau_2 = 9{\cdot}0225\ \mathrm{eV}$$

$$A_2 = \iint \mathrm{I}^2(1)\frac{e^2}{r_{12}}\mathrm{III}^2(2)\,d\tau_1 d\tau_2 = 5{\cdot}6668\ \mathrm{eV}$$

$$A_3 = \iint \mathrm{I}^2(1)\frac{e^2}{r_{12}}\mathrm{IV}^2(2)\,d\tau_1 d\tau_2 = 4{\cdot}9744\ \mathrm{eV}$$

$$B_{12} = \iint \mathrm{I}^2(1)\frac{e^2}{r_{12}}\mathrm{I}(2)\,\mathrm{II}(2)\,d\tau_1 d\tau_2 = 3{\cdot}3136\ \mathrm{eV}$$

$$C_{12} = \iint \mathrm{I}(1)\,\mathrm{II}(1)\frac{e^2}{r_{12}}\mathrm{I}(2)\,\mathrm{II}(2)\,d\tau_1 d\tau_2 = 0{\cdot}9522\ \mathrm{eV}$$

$$Q = -\int \mathrm{I}(1)\,\mathscr{H}_{\mathrm{II}}\,\mathrm{I}(1)\,d\tau_1 = 0{\cdot}8542\ \mathrm{eV}$$

$$R = -\int \mathrm{II}(1)\,\mathscr{H}_{\mathrm{II}}\,\mathrm{I}(1)\,d\tau_1 = 1{\cdot}8880\ \mathrm{eV}$$

TABLE 3

energies of M.O.'s

$\epsilon_2 - \epsilon_1 = -\ 8{\cdot}6404$ eV
$\epsilon_2 - \epsilon_0 = -14{\cdot}1704$
$\epsilon_3 - \epsilon_1 = -13{\cdot}2173$
$\epsilon_3 - \epsilon_0 = -18{\cdot}7473$

repulsion integrals over M.O.'s

$\gamma_{00} = 5{\cdot}2107$ eV
$\gamma_{01} = 6{\cdot}2640$
$\gamma_{02} = 8{\cdot}0378$
$\gamma_{11} = 7{\cdot}5379$
$\gamma_{12} = 9{\cdot}6979$
$\gamma_{22} = 12{\cdot}5737$
$\xi = 0{\cdot}6565$

$\delta_{01} = 3{\cdot}2620$ eV
$\delta_{02} = 2{\cdot}1234$
$\delta_{12} = 2{\cdot}9504$
$\delta_{1-2} = 1{\cdot}5610$
$\delta_{1-1} = 2{\cdot}7945$
$\delta_{2-2} = -0{\cdot}7191$
$\eta = 0{\cdot}4602$

At this point it is necessary to consider the limitation which is implied in using only the integrals in table 2 to evaluate those in table 3. To these ought to be added, in an exact treatment, a number of integrals of the type

$$\iint \mathrm{I}^2(1)\frac{e^2}{r_{12}}\mathrm{II}(2)\,\mathrm{III}(2)\,d\tau_1 d\tau_2,$$

in which there appear wave functions at three different centres. These integrals have never been computed analytically as have those of table 2, but would have to be given values which are at best rather rough estimates. This uncertainty makes it doubtful whether the small corrections these integrals represent ought to be applied at all, although in principle they are essential to the highest accuracy. In the work of London (1945), where these integrals were included in the four A.S.M.O. states shown in figure 1, they had the effect of depressing the ground state relative to the others without affecting much the remaining intervals. On balance of these considerations it has seemed best to use only those integrals whose values have been accurately computed and to examine the consequences of the theory in that form. No claim to high numerical accuracy will be possible, but on the other hand the main themes of this paper can be followed out on this basis without weakening the force of the conclusions.

Using the integrals of table 2 the energy of any A.S.M.O. state may readily be found. For example, in the lowest configuration,

$$\begin{aligned} W^{\mathrm{I}}(A_{1g}) &= 2\epsilon_0 + 4\epsilon_1 + \gamma_{00} + 8\gamma_{01} + 6\gamma_{11} - 4\delta_{01} - 2\delta_{1-1} \\ &= 2\epsilon_0 + 4\epsilon_1 + 81{\cdot}9131\,\mathrm{eV} \\ &= W_0 + 81{\cdot}9131\,\mathrm{eV}, \quad \text{where} \quad W_0 = 2\epsilon_0 + 4\epsilon_1. \end{aligned}$$

In table 4 the energy expressions, and numerical values, are summarized for the states lying within a range of 10 eV of the ground state. Within this range there are thirteen states amongst which all the symmetry types are represented. There are, for example, five E_{2g} states and four A_{1g} states. Figure 2, which shows these results plotted on the energy scale, contains the information of figure 1 with the addition of those states which arise from configurations not dealt with by Goeppert-Mayer & Sklar.

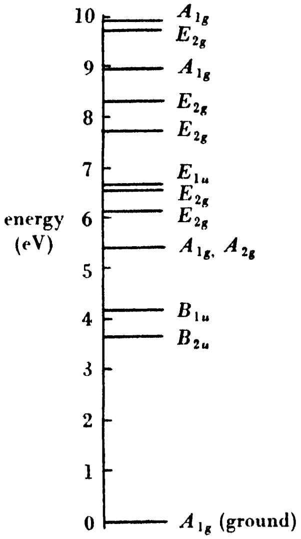

FIGURE 2

INTERACTIONS BETWEEN A.S.M.O. STATES

In figure 2 the order in which the A.S.M.O. states fall in the energy scale does not follow the order of the orbital part of their energies. Thus it is not the case that states obtained by elevating two electrons lie higher than all states obtained by elevating one electron. There are in fact three two-electron states (E_{2g}, A_{1g}, A_{2g}) lying below the E_{1u} one-electron state. It appears therefore that electron repulsion terms in this method do not enter simply as a small correction to a pattern of energy levels settled by the orbital energies, but themselves play the dominating part. This is also clear from table 4, which shows that the electron repulsion perturbations are about 20 times larger than the energy intervals that are at issue. To this fact has to be added that in figure 2 there lie very close together several A.S.M.O. states of the same symmetry type between which resonance might be expected to take place. One comes therefore to question the assumption which allows perturbation theory, as opposed to a variation treatment, to be used in this way for the effect of electron repulsion on molecular orbital states. The assumption is that interaction energies between different states are small compared with the perturbation energy of any one state. Evidently this would be quite satisfactory if it were not for the fact that interest here centres on *differences* between perturbation energies, and that these differences are themselves small fractions of the whole. The question therefore is whether or not the interactions between states of the same symmetry satisfy the much more stringent test of being, say, an order of magnitude smaller than the separations between the states.

To indicate the magnitudes concerned, consider the interaction term between two of the A_{1g} wave functions. For example

$$\iint \psi^{*\mathrm{I}}(A_{1g}) \sum \frac{e^2}{r_{\mu\nu}} \psi^{\mathrm{II}b}(A_{1g})\, d\tau_\mu d\tau_\nu = -\delta_{12} - \delta_{1-2} = -4{\cdot}5114\,\mathrm{eV}.$$

Since these states are only 8·9 eV apart, it is clear that a matrix component between them of 4·5 eV cannot be ignored. The effect of this interaction term alone is to reduce the energy of the ground state by 1·8 eV. Evidently energy changes of this size may alter considerably the energy level diagram of figure 2.

It follows that a better technique will be a variation treatment carried out to get the best *combination* of A.S.M.O. states of a given symmetry type falling within a selected energy interval. This will introduce the interaction terms between states and if all the A.S.M O. wave functions were used, would give the best energies and wave functions compatible with the initial use of $2p_z$ atomic orbitals.

We denote by $\psi^{\mathrm{I}}, \psi^{\mathrm{II}}, \psi^{\mathrm{III}}, \ldots$, the A.S.M.O. wave functions of any one symmetry type in order of increasing energy. To get the energy eigenvalues W and corresponding composite wave functions we shall have to solve secular equations of the type

$$\begin{vmatrix} W^{\mathrm{I}} - W & \left(\psi^{\mathrm{I}} \sum \frac{e^2}{r_{\mu\nu}} \psi^{\mathrm{II}}\right) & \left(\psi^{\mathrm{I}} \sum \frac{e^2}{r_{\mu\nu}} \psi^{\mathrm{III}}\right) \ldots \\ \left(\psi^{\mathrm{II}} \sum \frac{e^2}{r_{\mu\nu}} \psi^{\mathrm{I}}\right) & W^{\mathrm{II}} - W & \\ \text{etc.} & & \end{vmatrix} = 0,$$

where
$$\left(\psi^{\mathrm{I}} \sum \frac{e^2}{r_{\mu\nu}} \psi^{\mathrm{II}}\right) = \iint \psi^{*\mathrm{I}} \sum_{\mu<\nu} \frac{e^2}{r_{\mu\nu}} \psi^{\mathrm{II}}\, d\tau_\mu d\tau_\nu.$$

The diagonal elements of this determinant contain the A.S.M.O. perturbation energies of table 4. As a practical matter a limit has to be placed on the number of

TABLE 4

state	orbital energies				coefficients of repulsion integrals														repulsion energy (eV)	total energy (eV)
	ϵ_0	ϵ_1	ϵ_2	ϵ_3	γ_{00}	γ_{01}	γ_{02}	γ_{11}	γ_{12}	γ_{22}	δ_{01}	δ_{02}	δ_{1-1}	δ_{12}	δ_{1-2}	δ_{2-2}	ξ	η		
$\psi^{I}\ (A_{1g})$	2	4	-	-	1	8	-	6	-	-	−4	-	−2	-	-	-	-	-	81·9131	$W_0+81{\cdot}9131$
$\psi^{IIa}\ (A_{1g})$	2	2	2	-	1	4	4	1	4	1	−2	−2	-	−2	-	-	-	-	104·6496	$W_0+87{\cdot}3688$
$\psi^{IIb}\ (A_{1g})$	2	2	2	-	1	4	4	1	4	1	−2	−2	1	−1	−1	1	-	-	108·1144	$W_0+90{\cdot}8336$
$\psi^{III}\ (A_{1g})$	-	4	2	-	-	-	-	6	8	1	-	-	−2	−2	−2	1	-	-	120·0534	$W_0+91{\cdot}7126$
$\psi^{I}\ (B_{2u})$	2	3	1	-	1	6	2	3	3	-	−3	−1	−1	−1	1	-	1	−2	94·2205	$W_0+85{\cdot}5801$
$\psi^{I}\ (B_{1u})$	2	3	1	-	1	6	2	3	3	-	−3	−1	−1	−1	1	-	−1	2	94·7483	$W_0+86{\cdot}1079$
$\psi^{I}\ (E_{2g})$	1	4	1	-	-	4	1	6	4	-	−2	1	−2	−1	−1	-	-	-	102·6118	$W_0+88{\cdot}4414$
							γ_{03}		γ_{13}			δ_{03}								
$\psi^{II}\ (E_{2g})$	2	3	-	1	1	6	2	3	3	-	−3	−1	−1	-	-	-	-	-	102·8540	$W_0+89{\cdot}6367$
$\psi^{III}\ (E_{2g})$	2	2	2	-	1	4	4	1	4	1	−2	−2	-	-	−2	-	-	-	107·4284	$W_0+90{\cdot}1476$
$\psi^{IV}\ (E_{2g})$	2	2	2	-	1	4	4	1	4	1	−2	−2	-	−1	−1	1	-	-	105·3199	$W_0+88{\cdot}0391$
$\psi^{V}\ (E_{2g})$	2	2	2	-	1	4	4	1	4	1	−2	−2	1	−1	−1	-	-	-	108·8335	$W_0+91{\cdot}5527$
$\psi^{I}\ (A_{2g})$	2	2	2		As for $\psi^{II}\ (A_{1g})$														104·6496	$W_0+87{\cdot}3688$
$\psi^{I}\ (E_{1u})$	2	3	1	-	1	6	2	3	3	-	−3	−1	−1	1	−1	-	-	-	97·2632	$W_0+88{\cdot}6228$

wave functions included in the variation function, and we shall here take only those belonging to one- and two-electron states whose energies fall within 10 eV of the lowest of the symmetry type under consideration. The taking of a limited number of wave functions in the basis will mean that we shall be able to deal with any accuracy only with the lowest 'hybrid' state of each symmetry type.

The matrix components appearing in the secular equations require a number of new integrals over molecular orbitals, which we denote as follows:

$$\zeta_{pq}^{mn} = \iint \phi_m(\mu)\,\phi_n(\mu)\,\frac{e^2}{r_{\mu\nu}}\,\phi_p(\nu)\,\phi_q(\nu)\,d\tau_\mu\,d\tau_\nu.$$

The super- and subscripts refer to integrals cleared of complex conjugates by using the relation $\phi_l^* = \phi_{-l}$.

The integrands have to be totally symmetrical under the operations of D_{6h}. They have, for example, to be symmetrical to sixfold rotation which has the effect of multiplying each ϕ_l by $e^{2\pi i l/6}$. The implied condition on the quantities m, n, p, and q is that

$$e^{(2\pi i/6)(m+n+p+q)} = 1, \quad \text{i.e.} \quad m+n+p+q = 0, \quad \pm 6, \quad \pm 12, \quad \ldots.$$

The expression for the integrals in terms of the elementary ones in table 2 is

$$\begin{aligned}\zeta_{pq}^{mn} = \frac{1}{6(\sigma_m\sigma_n\sigma_p\sigma_q)^{\frac{1}{2}}}\Bigg[A_0 &+ A_1\left\{2\cos\frac{2\pi(m+n)}{6}\right\} \\ &+ A_2\left\{2\cos\frac{4\pi(m+n)}{6}\right\} + A_3\{\cos\pi(m+n)\} \\ &+ 2B_{12}\left\{\cos\frac{2\pi q}{6}+\cos\frac{2\pi p}{6}+\cos\frac{2\pi n}{6}+\cos\frac{2\pi m}{6}\right\} \\ &+ 2C_{12}\left\{\cos\frac{2\pi(n+q)}{6}+\cos\frac{2\pi(m+q)}{6}\right\}\Bigg].\end{aligned}$$

This is a general formula for the integrals of table 3 as well as the following ones in table 5.

TABLE 5

$\zeta_{1-2}^{10} = 3{\cdot}2456$ eV

$\zeta_{23}^{10} = 2{\cdot}3896$

$\zeta_{13}^{20} = 1{\cdot}2017$

$\zeta_{22}^{20} = 0{\cdot}4299$

$\xi_{11}^{-20} = 2{\cdot}4498$

$\zeta_{21}^{30} = 1{\cdot}0062$

$\zeta_{13}^{11} = 1{\cdot}4819$

$\zeta_{23}^{2-1} = 1{\cdot}5449$ eV

$\zeta_{22}^{-18} = -0{\cdot}2359$

$\gamma_{03} = 9{\cdot}0683$

$\gamma_{13} = 10{\cdot}9638$

$\gamma_{23} = 14{\cdot}2987$

$\delta_{03} = 1{\cdot}0019$

$\delta_{13} = 0{\cdot}3952$

$\delta_{23} = -0{\cdot}7352$

The A_{1g} states: calculation of the ground state

According to figure 2, there are four A_{1g} states, including the A.S.M.O. ground state, in the first 10 eV range. One of these, $\psi^{\text{II}a}$ in table 4, interacts only very weakly with the lowest A_{1g} state, and we therefore omit it, leaving the following A.S.M.O. A_{1g} functions to enter the secular equation for the ground state:

$$\psi^{\mathrm{I}}(A_{1g}) = (|\phi_0\overline{\phi_0}\phi_1\overline{\phi_1}\phi_{-1}\overline{\phi_{-1}}|) \qquad W^{\mathrm{I}} = W_0+81\cdot9131\,\mathrm{eV}$$

$$\begin{aligned}\psi^{\mathrm{II}b}(A_{1g}) = \tfrac{1}{2}(&|\phi_0\overline{\phi_0}\phi_1\overline{\phi_{-1}}\phi_2\overline{\phi_{-2}}| \\ &-|\phi_0\overline{\phi_0}\overline{\phi_1}\phi_{-1}\phi_2\overline{\phi_{-2}}|-|\phi_0\overline{\phi_0}\phi_1\overline{\phi_{-1}}\overline{\phi_2}\phi_{-2}| \\ &+|\phi_0\overline{\phi_0}\overline{\phi_1}\phi_{-1}\overline{\phi_2}\phi_{-2}|)\end{aligned} \qquad W^{\mathrm{II}b} = W_0+90\cdot8336\,\mathrm{eV}$$

$$\begin{aligned}\psi^{\mathrm{III}}(A_{1g}) = \frac{1}{\sqrt{2}}(&|\phi_1\overline{\phi_1}\phi_{-1}\overline{\phi_{-1}}\phi_2\overline{\phi_{-2}}| \\ &-|\phi_1\overline{\phi_1}\phi_{-1}\overline{\phi_{-1}}\overline{\phi_2}\phi_{-2}|)\end{aligned} \qquad W^{\mathrm{III}} = W_0+91\cdot7126\,\mathrm{eV}$$

The off-diagonal matrix elements are

$$\left(\psi^{\mathrm{I}}\sum\frac{e^2}{r_{\mu\nu}}\psi^{\mathrm{II}b}\right) = -\delta_{12}-\delta_{1\ 2} = -4\cdot5114\,\mathrm{eV},$$

$$\left(\psi^{\mathrm{I}}\sum\frac{e^2}{r_{\mu\nu}}\psi^{\mathrm{III}}\right) = \sqrt{2}\delta_{02} = 3\cdot0029\,\mathrm{eV},$$

$$\left(\psi^{\mathrm{II}b}\sum\frac{e^2}{r_{\mu\nu}}\psi^{\mathrm{III}}\right) = -\sqrt{2}\delta_{01} = -4\cdot6132\,\mathrm{eV}.$$

Leading to the following secular equation, which has to be solved for the energy eigenvalues W

$$\begin{vmatrix} x & -4\cdot5114 & 3\cdot0029 \\ -4\cdot5114 & x+8\cdot9205 & -4\cdot6132 \\ 3\cdot0029 & -4\cdot6132 & x+9\cdot7995 \end{vmatrix} = 0 \qquad x = W_0+81\cdot9131-W$$

The lowest root of this equation is $x = 1\cdot9877\,\mathrm{eV}$, which shows that interactions amongst this set of A_{1g} states depresses the lowest of them by about 2 eV. The ground state energy in this approximation is

$$W(A_{1g};\ \text{ground}) = W_0+79\cdot9(254)\,\mathrm{eV}$$

States of other symmetries

Having given this example of the calculation of configurational interaction, the results in the other symmetries are summarized in table 6. It is to be noted that our programme of calculating interactions between states over a 10 eV range requires more A.S.M.O. states than are given in table 4. The additional ones however can be dealt with in exactly the same way.

TABLE 6

representation	number of configurations	depression relative to lowest A.S.M.O. state (eV)	energy
A_{1g}	3	1·9877	$W_0+79\cdot9$ (254)
B_{2u}	3	4·5204	$W_0+81\cdot0$ (597)
B_{1u}	4	2·8676	$W_0+83\cdot2$ (403)
E_{2g}	6	5·1463	$W_0+82\cdot8$ (928)
A_{2g}	1	—	$W_0+87\cdot3$ (688)
E_{1u}	5	3·79	$W_0+84\cdot8$ (3)

A comment is required about the E_{1u} calculation in table 6. According to table 1 there are five configurations admitting E_{1u} symmetry. From these there arise 9 states, of which 8 fall within a 10 eV range. Closely outside the 10 eV limit however there lies a series of two- and three-electron states which have large matrix components with the lower states, and these will certainly have some influence on the lowest E_{1u} state. We have not therefore thought it worth while to solve the eighth degree equation that the 10 eV range suggests, but have simply selected from the eight functions five which seem to interact most strongly (including of course the lowest) and have used them to get an estimate of the E_{1u} interaction. In considering this estimate it has to be reckoned that there might be a further lowering of 0·5 eV if additional configurations were brought in.

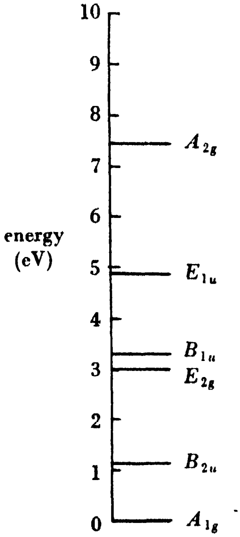

FIGURE 3

DISCUSSION

Acceptance of the A.S.M.O. method as giving an account of spectral states depended on the close agreement there appeared to be between the calculated and experimental intervals A_{1g}-B_{2u} in benzene, and on that basis the disagreements of figure 1 between the augmented V.B. and A.S.M.O. theories had to be taken seriously. It is now clear that the agreement with experiment was accidental, for errors have been identified in the A.S.M.O. energies of as much as 5 eV. It follows that, whatever errors may attach to the V.B. results, the disagreements of figure 1 cannot reveal them. Equally, since the A.S.M.O. method is subject to errors comparable with spectral transition energies, it follows that it will not be useful for the detailed understanding of absorption spectra.

To assess the performance of the next higher approximation, which is to include configuration interaction, we have the results of figure 3. These results represent an approach, and probably a very close approach, to a full solution of the problem within the framework of nearest neighbour exchanges. The discrepancies between those results and exact values are probably due, in order of seriousness, to neglect of interactions between non-neighbours, neglect of higher configurations and, jointly, to neglect of in-plane electrons and to the assumed form of the core potential. It is however material to this discussion to recognize that even if the obvious defects in the non-empirical configuration interaction theory were put right, numerical exactness could not be expected. The energy intervals on which attention centres in understanding molecular absorption spectra occur in the theory as differences between the solutions of a variation problem, each solution having the character of a perturbation energy of about 100 eV over a combination of M.O. wave functions. Thus to get an accuracy of 1 eV in the final energy intervals, we require to know the individual energies to better than 1 %. Such would be a good performance even in a calculation of atomic energy states, and one not likely within the present framework.

This leads to the question whether the method of configuration interaction is likely to be useful as a general method for the study of π-electron states. It is the next higher approximation to the A.S.M.O. theory and its wave functions are as general as any that can be made up from $2p$ atomic orbitals. Thus in principle it provides a non-empirical general method, having exactly the same degree of flexibility in its description of states as a method based on a complete set of valence-bond structures including all possible polar and non-polar ones. It does, however, appear to lack one feature essential to a method of wide applicability. In every case except the very simplest molecules it would be practicable only to work with a small proportion of the full set of configurations;† what the method lacks is a means of selecting, without prior calculation, this small number of configurations to be the ones which are of dominant physical importance. The point is illustrated by contrast with the V.B. theory, in which the basis of structures divides naturally into sets consisting of all non-polar, all singly polar, all doubly polar structures, etc., and by selecting from these just the non-polar, or the non-polar and singly polar structures we get a good set of approximate wave functions and energies for certain of the states. This natural way of selecting, for example, 5 non-polar structures out of a total of 175 structures of all types makes the method relatively simple to handle. It is just such a simple division of configurations into sets of different physical prominence that is at present lacking in the method of configuration interaction. For this reason, and for those given earlier in the discussion, the method is unlikely to be valuable generally, though it should be useful for the solution of relatively special problems where a non-empirical method is indicated to settle particular points. In other problems, especially where large molecules are concerned, empirical

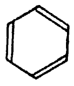

non-polar structure

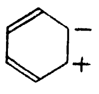

singly polar structure

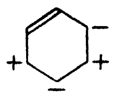

doubly polar structure

---

† In naphthalene there are 8953 configurations and 19404 independent singlet wave functions.

methods will have to continue in use, and it is here that the augmented V.B. method of (Craig 1950*a* to *c*) may be useful until better non-empirical techniques come to be worked out.

This work has been carried out during the tenure of a Turner and Newall Research Fellowship in the University of London.

REFERENCES

Craig, D. P. 1950*a* *Proc. Roy. Soc.* A, **200**, 272.
Craig, D. P. 1950*b* *Proc. Roy. Soc.* A, **200**, 390.
Craig, D. P. 1950*c* *Proc. Roy. Soc.* A, **200**, 401.
Goeppert-Mayer, M. & Sklar, A. L. 1938 *J. Chem. Phys.* **6**, 645.
London, A. 1945 *J. Chem. Phys.* **13**, 396.
Parr, R. G. & Crawford, B. L. 1948 *J. Chem. Phys.* **16**, 1049.
Sklar, A. L. & Lyddane, R. H. 1939 *J. Chem. Phys.* **7**, 374.

Ionospheric cross-modulation at oblique incidence

BY L. G. H. HUXLEY*, *The Department of Physics, The University of Adelaide*

(*Communicated by M. L. Oliphant, F.R.S.—Received* 24 *June* 1949)

This paper is an account of an extensive series of investigations on ionospheric cross-modulation (wave interaction) in special tests arranged in collaboration with the British Broadcasting Corporation. Special attention is paid to seasonal and nocturnal changes in the cross-modulation and to the theoretical interpretation of the experimental results. It is shown how a variety of evidence is consistent with the assumption that the cross-modulation is highly localized in the E-region at one or two regions near the lower of the surfaces of reflexion of the wanted and disturbing waves. An estimate is made of the gradients of electronic concentration and collisional frequency at a height of about 86 km.

Certain theoretical formulae used in the paper are derived in the appendix.

1. INTRODUCTION

During the last three years, systematic experimental studies of ionospheric cross-modulation (radio-wave interaction) have been carried out by teams of observers at Cambridge and at Birmingham in collaboration with the Engineering Research Department of the British Broadcasting Corporation. Some of the results of these investigations have already been published (Huxley, Foster & Newton 1947; Ratcliffe & Shaw 1948; Huxley *et al.* 1948; Huxley & Ratcliffe 1949; Huxley 1949), but they are not sufficiently extensive to permit general conclusions to be drawn concerning nocturnal and seasonal changes in the cross-modulation. In what follows, these and other matters are discussed in relation to extensive observations made at Birmingham during the period July 1946 to December 1948. Because the work of early investigators has been fully treated in the papers mentioned above, it is not discussed in this paper.

---

* Formerly of the Department of Electrical Engineering, The University of Birmingham.

2. TERMINOLOGY AND SYMBOLS*

In order to investigate ionospheric cross-modulation by experiment, it is necessary to radiate from two transmitters simultaneously. The one transmitter, the *disturbing transmitter*, radiates a carrier wave, amplitude-modulated by an audible tone, whereas the radiation of the second transmitter, the *wanted* transmitter, is unmodulated. The respective waves are called the *disturbing wave* and the *wanted wave.*

It is found that cross-modulation of the wanted wave by the disturbing wave can take place if the electromagnetic fields of the waves overlap appropriately in the lower E-region.

The *modulation transferred* at audio-frequency f (or angular frequency $\omega = 2\pi f$) is denoted by T_f (or T_ω) and that at a low frequency $f \rightarrow 0$ by T_0.

The *electric field of the disturbing wave*, where the cross-modulation takes place, is denoted by

$$E_D = {}_0E_D[1+M\cos\omega t]\cos p_D t,$$

and that of the wanted wave when it has acquired its full transferred modulation by

$$E_W = {}_0E_W[1+T_\omega\cos(\omega t-\phi_\omega-\pi)+T_{2\omega}\cos(2\omega t-\phi_{2\omega}-\pi)+\text{etc.}]\cos p_W t.$$

Thus, $T_\omega, T_{2\omega}$, etc., are the *coefficients of transferred modulation* at modulation frequencies $\omega/2\pi$, $2\omega/2\pi$, etc., and $\phi_\omega, \phi_{2\omega}$, etc., are the corresponding phase constants of the modulation relative to the modulation of E_D.

Power communicated to a free electron in the ionosphere by the field of the disturbing wave. If the unmodulated carrier $E_D = {}_0E_D\cos p_D t$ communicates mean power w_0 to a free electron then the modulated carrier

$$E_D = {}_0E_D[1+M\cos\omega t]\cos p_D t$$

communicates power

$$w(t) = w_0[1+M\cos\omega t]^2 = \overline{w}+2w_0[M\cos\omega t+\tfrac{1}{4}M^2\cos 2\omega t],$$

where $\overline{w} = w_0(1+\frac{1}{2}M^2)$ is the average value of $w(t)$ over many cycles of $M\cos\omega t$.

The kinetic energy of agitation of a free electron. When $w(t) = 0$ $[E_D = 0]$, the mean energy of an electron is the same as the thermal energy of agitation of the gas molecules. This energy is denoted by Q_0.

When $w(t)$ is not zero, the mean energy of agitation of an electron becomes time-dependent and is denoted by $Q(t)$.

When $w(t)$ fluctuates about its mean value $\overline{w}$, as shown above, then $Q(t)$ fluctuates about the value $\overline{Q}$ that is maintained by $\overline{w}$ alone.

The collisional frequencies of electrons with gas molecules, that correspond to Q_0, $Q(t)$ and $\overline{Q}$, are ν_0, $\nu(t)$ and $\overline{\nu}$.

The parameter G enters as follows: the theory of ionospheric cross-modulation proposed by Bailey & Martyn embodies the hypothesis that in collisions between electrons with energies Q and gas molecules with energies Q_0, the mean loss of energy ΔQ in a collision (that is the mean of the excess of losses over gains) is proportional to the energy difference $(Q-Q_0)$. Thus

$$\Delta Q = G(Q-Q_0).$$

---

* Based on a symbolism agreed in discussion with Mr J. A. Ratcliffe.

Laboratory measurements (Huxley & Zaazou 1949) have given the provisional value $G = 1{\cdot}3 \times 10^{-8}$ for electrons in dry air free from carbon dioxide. Because of the importance of this parameter further measurements of it with an improved apparatus are in progress.

The absorption of a radio wave. The absorption in nepers of a radio wave along a path ds is written $d\rho = \kappa ds$. Thus for the disturbing and wanted waves, $d\rho_D = \kappa_D ds$, $d\rho_W = \kappa_W ds$.

3. THEORETICAL FORMULAE FOR T_ω AND ϕ_ω—EARLY TESTS

Consider an element of path ds within the region of cross-modulation (figure 1) along which the wanted wave is attenuated by $d\rho_W = \kappa_W ds$ nepers. Let $\bar{\nu}$ be the mean collisional frequency along ds, then, as shown in the appendix, the coefficient of transferred modulation acquired by the wanted wave along ds at a frequency of modulation $\omega/2\pi$, is given by

$$dT_\omega = dT_0 \Big/ \left[1 + \left(\frac{\omega}{G\bar{\nu}}\right)^2\right]^{\frac{1}{2}}, \tag{1}$$

where dT_0 is the value of dT_ω as ω approaches zero. According to the theory, dT_0 is given by the following formula (Appendix).

$$dT_0 = \left(\frac{d\kappa_W}{d\bar{\nu}}\right) \frac{Mw_0}{\bar{Q}G} ds, \tag{2}$$

in which the various symbols are defined in §2.

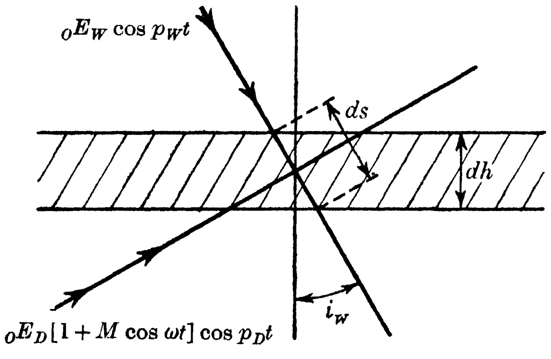

FIGURE 1. Elementary section of region of cross-modulation.

The quantity dT_ω is the amplitude of the transferred modulation acquired along ds. The phase of this modulation relative to that of the modulation of the disturbing field at the element of path ds is $-(\phi_\omega + \pi)$, where

$$\phi_\omega = \tan^{-1}\left(\frac{\omega}{G\bar{\nu}}\right). \tag{3}$$

The corresponding amplitude and phase of the modulation transferred at the octave frequency are

$$dT_{2\omega} = dT_0 M \Big/ \left\{4\left[1 + \left(\frac{2\omega}{G\bar{\nu}}\right)^2\right]^{\frac{1}{2}}\right\}, \tag{4}$$

and

$$\phi_{2\omega} = \tan^{-1}\left(\frac{2\omega}{G\bar{\nu}}\right). \tag{5}$$

The total modulation T_0 transferred to a wanted wave at a low frequency $\omega/2\pi$ such that $\omega/G\bar{\nu}$ is everywhere small ($\phi_\omega \rightarrow 0$) along the path length s is

$$T_0 = \int\left(\frac{dT_0}{ds}\right)ds, \tag{6}$$

in which the integration is made along the whole path of the wanted wave in the ionosphere.

Since the quantity (dT_0/ds) is not known initially as a function of s, it is not possible, without special assumptions, to predict the dependence of the total transferred modulation T_ω and its phase constant ϕ_ω upon ω and $G\bar{\nu}$. As a first step it is convenient to adopt the simplifying assumption that the distance s along which the modulation is transferred to the wanted wave is relatively short, so that along it dT_0/ds and $\bar{\nu}$ are effectively constant, and this is what has been done consciously or unconsciously in most previous work. Since dT_ω is then the same as T_ω it follows from equations (1) to (6) that the field* of the wanted wave on emergence from the region of cross-modulation is

$$E_W = {}_0E_W[1 + T_\omega\cos(\omega t - \phi_\omega - \pi) + T_{2\omega}\cos(2\omega t - \phi_{2\omega} - \pi)]\cos p_\omega t, \tag{7}$$

where

$$T_\omega = T_0\Big/\left[1 + \left(\frac{\omega}{G\bar{\nu}}\right)^2\right]^{\frac{1}{2}}, \tag{8}$$

$$T_{2\omega} = MT_0\Big/\left\{4\left[1 + \left(\frac{2\omega}{G\bar{\nu}}\right)^2\right]^{\frac{1}{2}}\right\}, \tag{9}$$

$$\omega/G\bar{\nu} = \tan\phi_\omega = \tfrac{1}{2}\tan\phi_{2\omega}, \tag{10}$$

$$T_0 = \left(\frac{d\kappa_W}{d\bar{\nu}}\right)\frac{Mw_0}{G\bar{Q}}s. \tag{11}$$

It follows, therefore, that if the region of cross-modulation is effectively localized within the ionosphere then the transferred modulation observed at the ground is the simple function of $\omega/G\bar{\nu}$ shown in (8). Further, the second harmonic in the observed modulation should be given by (9). These features were tested systematically in the first tests (July and November 1946) provided by the B.B.C. in which Droitwich (200 kc./sec., 170 kW) and Stagshaw (1050 kc./sec., 120 kW, $M = 0{\cdot}8$) served as wanted and disturbing transmitters respectively, with Dundee as the point of observation (figure 2). The transferred modulation T was measured as a function of ω when the Stagshaw transmission was modulated to a depth of 80 % in a sequence of pure tones $\omega/2\pi$. In order to discover the degree of concordance between the measured values of T_ω and those predicted from formula (7), this formula was transformed as follows:

$$\omega^2 = (T_0)^2(G\bar{\nu})^2/T_\omega^2 - (G\bar{\nu})^2. \tag{12}$$

When the experimental values of $1/T_\omega^2$ were plotted as abscissae against the corresponding values of ω^2 as ordinates, it was found that the points fell near a straight line as required by equation (12). According to this equation the line intercepts the ω^2-axis at a distance $(G\bar{\nu})^2$ below the origin and thus provides the value of $(G\bar{\nu})$. T_0 is found from the interception with the $1/T_\omega^2$-axis which occurs at the distance $1/T_0^2$ from the origin. The values of $G\bar{\nu}$ found in this way were $G\bar{\nu} = 950$ with the frequency of the disturbing wave equal to 1050 kc./sec. (Huxley *et al.* 1947).

---

* It is assumed that one component only of the sky wave emerges from the ionosphere, the other being totally absorbed.

The values of T_0 were comparatively large, being of the order of 8 %. Whether this is truly an example of gyro-resonance is difficult to decide in the absence of a knowledge of the vertical polar diagram of the aerial of the disturbing transmitter, but is certainly greater than the values of T_0 obtained in other transmissions with the disturbing transmitter operating on a frequency of 200 kc./sec. under comparable conditions.

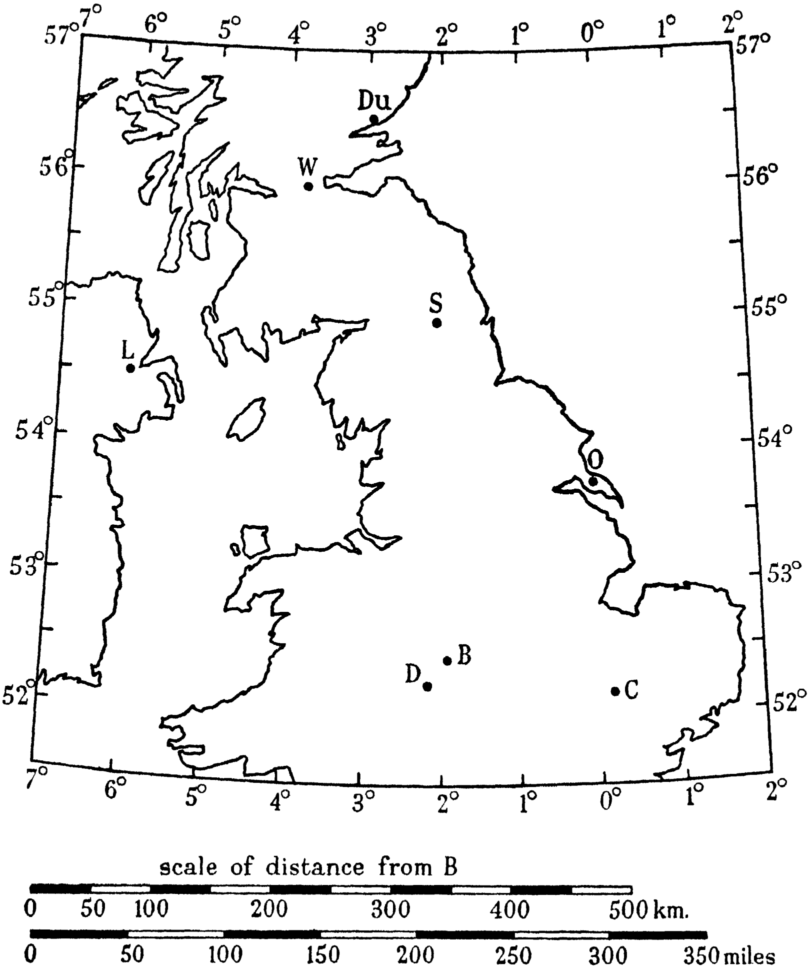

FIGURE 2. Map showing positions of the points of observation and of the transmitters. Gnomonic projection centred on B. B, Birmingham; C, Cambridge; D, Droitwich; Du, Dundee; L, Lisnagarvey; O, Ottringham; S, Stagshaw; W, Westerglen.

According to (11), T_0 is proportional to M and also to w_0, which is itself proportional to the power radiated by the disturbing transmitter. The proportionality of T_0 to M was roughly confirmed, but tests to check the proportionality of T_0 to w_0 were marred by interference from a foreign station.

It could therefore be concluded from these tests that the Bailey-Martyn theory was in essential agreement with experiment, and that the simplifying assumption concerning the localization of the region of interaction was at least a first approximation to the truth. This matter will be considered again in what follows.

Figure 2 is a gnomonic map showing the positions of the various transmitters used throughout the work. Their positions are marked by the appropriate initial letter.

4. OBSERVATIONS IN THE PERIOD JANUARY TO AUGUST 1947

In this period a number of test transmissions were arranged by Mr J. A. Ratcliffe of the Cavendish Laboratory and by the Engineering Research Department of the B.B.C., systematic observations of which were also made at Birmingham within the period May to August, with improved techniques.

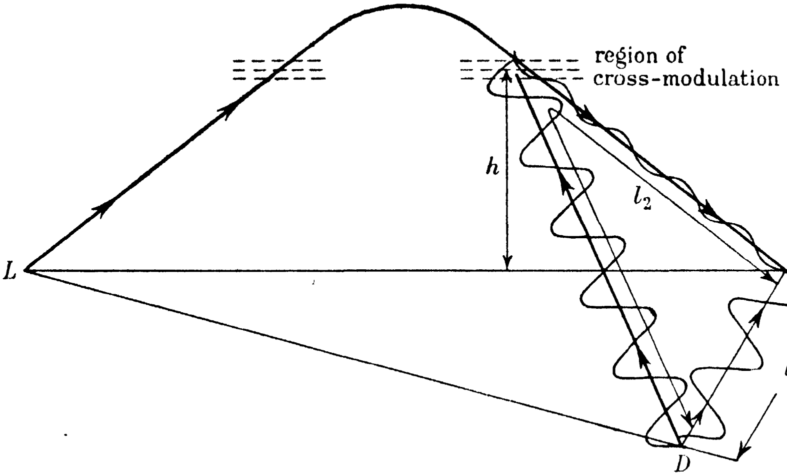

FIGURE 3. Transference of modulation at a centre and the associated geometrical configuration.

The pair of stations chiefly used in these transmissions comprised Lisnagarvey (near Lismore, Northern Ireland, 1050 kc./sec., 60 kW)—wanted transmitter—and Droitwich (200 kc./sec., 170 kW)—disturbing transmitter (figure 2). The geometry of this system is that indicated in figure 3. A few observations were also made with Ottringham (167 kc./sec., 170 kW) as disturbing transmitter, and Westerglen (near Falkirk, 1050 kc./sec., 60 kW) and Lisnagarvey as alternative wanted transmitters.

These investigations, which have already been described (Ratcliffe & Shaw 1948 Huxley *et al.* 1948) showed that $(G\bar{\nu})$ ranged in value from about 10^3 to 3×10^3.

A rough method of height measurement (Ratcliffe & Shaw 1948) gave a mean height of about 85 km. for the region of cross-modulation.

The value of T_0 observed at Birmingham in tests using Lisnagarvey and Droitwich was about 2 % when $M = 0{\cdot}8$.

5. The value of the collisional frequency

In order to obtain the collisional frequency $\bar{\nu}$ from $G\bar{\nu}$ it is necessary to know the value of G which is a property of the gas. If it is assumed that the gas at the seat of cross-modulation is ordinary air, then we may use the value of G determined in the laboratory. Recent measurements of G for air (Huxley & Zaazou 1949) give $G = 1{\cdot}3\times10^{-3}$. These laboratory measurements also give the collisional cross-section A of the air molecules in collisions with electrons as a function of the mean velocity $\bar{U}$ of the electrons, use of which is made in § 6.

Since $G\bar{\nu}$ is of the order $1{\cdot}6\times10^{3}$ and $G = 1{\cdot}3\times10^{-3}$, it follows that the collisional frequency $\bar{\nu}$ is approximately $1{\cdot}2\times10^{6}\,\text{sec.}^{-1}$. This locates the phenomenon in the lower E-region.

6. Measurement of the height of the region of cross-modulation

J. A. Ratcliffe has proposed a method (Ratcliffe & Shaw 1948) of locating the seat of the cross-modulation from measurements of the phase of the transferred modulation received at the ground.

Reference to figure 3 shows that modulation on the tone $\omega/2\pi$ may be received at B not only as transferred modulation (1050 kc./sec. carrier) via the path l_2 (D → region of cross-modulation → B), but also on the ground wave (200 kc./sec. carrier) from the disturbing transmitter via the direct path $\text{DB} = l_1$.

Thus, if the phase of the modulation received at B along the path DB be taken as the zero for comparison, the phase retardation ψ of the transferred modulation received at B via the path l_2, on reference to equations (4) and (10), is seen to be

$$\psi = 360f(l_2-l_1)/v+\tan^{-1}(2\pi f/G\bar{\nu})+180^\circ, \tag{13}$$

where v is the velocity of light.

As $f=\omega/2\pi$ is increased, $\tan(2\pi f/G\bar{\nu})$ approaches 90°, consequently the slope of the ψ-f curve tends to the constant value $d\psi/df = 360(l_2-l_1)/v$, and the curve approaches asymptotically to the straight line with this slope which intercepts the ψ-axis at $\psi = 270^\circ$. Thus if the series of tones is continued to a frequency f which makes the ψ-f curve approximate to its asymptote, the quantity $(l_2-l_1)/v$ may be deduced from the slope of the asymptote. Since l_1 in kilometres is known and $v = 3\times10^5$, l_2 is also known.

In order, however, to find the height of the region of cross-modulation from l_2 with the given geometry, it is necessary also to assume a value for the angle of descent of the sky-wave. The method thus leads, even with the simplifying assumption of transference at a single centre, to approximate estimates only of the height.

Because of the uncertainty of this method it seemed worth while to attempt an estimate of the height by an alternative method.

Such a method is briefly the following (Huxley 1949a, b): from $G\bar{\nu} = 1{\cdot}6\times10^3$ and $G = 1{\cdot}3\times10^{-3}$, we find $\bar{\nu} = 1{\cdot}2\times10^6$. Since the laboratory experiments give the collisional cross-section A of air molecules as a function of electron velocity $\bar{U}$, it follows that if the temperature of the air be assumed then the collisional cross-section is known. The mean free path l is $1/nA$, where n is the molecular density, and the collisional frequency $\bar{\nu}$ is $\bar{U}/l = nA\bar{U}$. Let the pressure of the air be p and its temperature θ, then $p = n\mathbf{k}\theta$, where $\mathbf{k}$ is Boltzmann's constant. Thus

$$p = 7{\cdot}6\times 10^{-4}\bar{\nu}\mathbf{k}\theta/(A\bar{U})\,\text{mm.Hg}. \tag{14}$$

Thus if θ be assumed, then A and $\bar{U}$ are known and p may be estimated from the value of $\bar{\nu}$. Thus with $\theta = 210°\,\text{K}$ and $\bar{\nu} = 1{\cdot}2\times 10^6$, the laboratory value of $A = 5{\cdot}8\times 10^{-16}\,\text{cm.}^{-2}$ and $\bar{U} = 9\times 10^6\,\text{cm.sec.}^{-1}$, whence $p = 5\times 10^{-3}\,\text{mm.Hg}$, which according to rocket soundings in America (Best, Havens & La Gow 1947) corresponds to a height of 85 km.

If the temperature could be reliably determined this method would in principle give the height with fair accuracy.

For instance, with $G\bar{\nu} = 2000$, $\bar{\nu} = 1{\cdot}5\times 10^6$, $p = 6{\cdot}3\times 10^{-3}\,\text{mm.Hg}$, $h = 83\,\text{km.}$; and with $G\bar{\nu} = 1000$, $h = 87\,\text{km}$. That is, wide variations in $G\bar{\nu}$ correspond to relatively small changes in height. It may be remarked that since in (14) A increases with θ the quantity $\theta/(A\bar{U})$ varies slowly with θ, consequently p is not sensitive to the particular value chosen for θ within wide limits.

7. Observations in the period September 1947 to December 1948

The test transmissions within this period were planned jointly by the Cambridge and Birmingham teams and the Engineering Research Department of the B.B.C. The majority of tests were made with the pair of transmitters Westerglen (767 kc./sec., 60 kW)—wanted transmitter—and Ottringham (167 kc./sec., 170 kW, $M = 80\,\%$)—disturbing transmitter—but other transmitters were used on occasion to examine particular matters of theoretical interest (figure 2).

The systematic observation of cross-modulation throughout a complete year, together with progressive improvement in techniques of observation and in observational skill, have led to a more detailed and deeper appreciation of the phenomenon than was possible on the basis of the earlier tests, although the conclusions drawn from the earlier tests concerning the magnitude of T_0 and of $G\bar{\nu}$ have been confirmed.

It is now possible to make general statements about the behaviour of T_0 and $G\bar{\nu}$ throughout the year, from night to night and during a single night. These and other matters are discussed below under separate headings, since the mass of observations is so great that it is impossible to summarize them in a single section.

The various techniques employed throughout the work will be described elsewhere. The more precise observations of this period have also revealed certain 'anomalies'. For instance, the dependence of T_ω upon ω does not usually conform precisely to the simple formula (8).

8. Theoretical considerations bearing on the location and vertical extent of the region of cross-modulation

It was explained in § 3 that the simplifying assumption of a single centre of cross-modulation localized in height led to theoretical formulae which were not strikingly at variance with the experimental facts. This assumption may therefore be regarded as a first approximation to the truth. A considerable theoretical advance can, however, be achieved by considering the features of the propagation of the disturbing and wanted waves. Consider the case, comprising the great majority of the actual test transmissions, in which the disturbing transmitter operates on a relatively low frequency (about 200 kc./sec.) with the wanted transmitter on a frequency of the order of 1 Mc./sec. It follows that in general the sky-wave from the wanted transmitter is reflected in the ionosphere at a level which is nowhere reached by the radiation from the disturbing transmitter.

Since modulation can only be transferred to the wanted wave in that region of the ionosphere where the fields of the two waves coexist, it follows that this region possesses a well-defined upper boundary formed by the surface at which the strongly absorbed component of the disturbing wave is reflected. This boundary covers the disturbing transmitter like a canopy, being most elevated near the transmitter and falling with distance to a surface of roughly constant height. It follows that the sky-wave received at the point of observation has acquired its transferred modulation along two distinct sections of its path, the one on its upward journey through the region of cross-modulation and the other on its downward journey. Before it can be asserted that these distinct sections may be regarded as localized in height, it is necessary to consider the effective extent in depth below its bounding surface of the whole region of cross-modulation.

The modulation transferred to the wanted wave along an element of path ds when ω is very small is given by equation (2), which may be written

$$\frac{dT_0}{ds} = \left(\frac{d\kappa_W}{d\bar{\nu}}\right)\frac{Mw_0}{\bar{Q}G}. \tag{15}$$

When, as in the case under consideration, the wanted wave is reflected at a height appreciably above the reflexion surface of the disturbing wave, we may suppose it to be undeviated in the region of cross-modulation, and the angle i_W between the path element ds and the vertical to be the same for all such elements of the path within the region. It follows, therefore, that

$$\frac{dT_0}{dh} = \left(\frac{d\kappa_W}{d\bar{\nu}}\right)Mw_0/(\bar{Q}G\cos i_W).$$

The total modulation transferred at 'zero frequency' to the wanted wave on a single passage across the region of cross-modulation is

$$T_0 = \left(\frac{M}{\bar{Q}G\cos i_W}\right)\int_0^\infty \left(\frac{d\kappa_W}{d\bar{\nu}}\right) w_0\,dh, \tag{16}$$

in which the agitational energy $\bar{Q}$ has been assumed, for simplicity, to be independent of height, and the integral extends downwards from the point where the wanted ray crosses the reflexion surface of the disturbing wave ($h = 0$).

If it can be shown that the value of the integral is essentially unchanged by replacing infinity, the upper limit of integration, by a comparatively short distance h_1 over which $\bar{\nu}$ does not change by a large factor, then it is legitimate to treat the region of cross-modulation as a relatively thin layer.

Consider in turn the factors $(d\kappa_W/d\bar{\nu})$ and w_0 in the integrand, and for simplicity neglect the presence of the earth's magnetic field in the ionosphere:

The term $(d\kappa_W/d\bar{\nu})$

Since the frequency $(p_W/2\pi)$ of the wanted wave is about 10^6 c./sec. and the collisional frequency $\bar{\nu}$ is of the same order of magnitude, then $p_W^2 \gg \bar{\nu}^2$. In this case the absorption coefficient κ_W may be written

$$\kappa_W = 8\pi Ne^2\bar{\nu}/(3mcp_W^2), \tag{17}$$

whence
$$\left(\frac{d\kappa_W}{d\bar{\nu}}\right) = 8\pi Ne^2/(3mcp_W^2), \tag{18}$$

in which e is the electronic charge in e.s.u., $c = 3 \times 10^{10}$, and m is the mass of the electron in grams. N is the number of electrons per cubic centimetre.

Thus the term $(d\kappa_W/d\bar{\nu})$ is independent of $\bar{\nu}$ and depends on height only through N.

The term w_0 (power supplied to an electron by the unmodulated disturbing wave).

This may be shown to be

$$w_0 = {}_OE_D^2e^2\left(\frac{x}{1+x^2}\right)\bigg/(3mp_D), \tag{19}$$

in which $x = \bar{\nu}/p_D$.

In a more precise formula the factor $\left(\frac{x}{1+x^2}\right)$ is replaced by $\left(\frac{x}{1+x^2}\right)\left(1+\frac{x}{1+x^2}\right)$ (Huxley 1949*a*).

Since it has been supposed that $(p_D/2\pi)$ is about 2×10^5 and $\bar{\nu}$ about 10^6, it follows that x lies between unity and 3. Since $x/(1+x^2)$ assumes its maximum value of $\frac{1}{2}$ at $x = 1$, and is equal to $\frac{1}{3}$ at $x = 3$, it follows that w_0 changes but little within a range of height of the order of the scale height of, say, 7 km. It may be concluded, therefore, that the height dependence of the integrand is to be sought chiefly in the factor ${}_OE_D^2N$.

The distribution of the amplitude of the electric field below the reflexion level is that of an E-type wave formed by the superposition of the incident and reflected waves. To a first approximation the components of this wave may be considered to be distributed sinusoidally in height.

Little information exists concerning the distribution of N in height. It is known that at night N attains its maximum value in the E-region at about a height of 105 km., where it possesses a value of the order of 10^4 electrons/cm.^{3}

It is also known that N diminishes rapidly at first and later more slowly with vertical distance downwards below the reflexion level and reaches a small value, of say 1 electron/cm.^{3}, at a height of 70 km. Since the reflexion of the disturbing wave in fact occurs where dN/dh is still large, the integrand diminishes rapidly as h is increased below $h = 0$.

We conclude therefore that when the reflexion surface of the wanted wave in the ionosphere lies above that of the disturbing wave, then the modulation is transferred to the wanted wave within the two relatively localized regions of its path where it penetrates the reflexion level of the disturbing wave, on its upward and downward trajectories respectively.

The transferred modulation received at the ground may therefore be regarded as originating in a pair of distinct centres, differing in general, in strength, $G\bar{v}$ and phase. It is not to be anticipated therefore that, in general, the dependence of T_ω and ϕ_ω upon ω will conform precisely to the simple relationships (8) and (10), namely,

$$T_\omega = T_0 \Big/ \left[1 + \left(\frac{\omega}{G\bar{v}}\right)^2\right]^{\frac{1}{2}}, \quad \phi_\omega = \tan^{-1}(\omega/G\bar{v}). \tag{20}$$

To predict the form of those relationships when the strengths, $G\bar{v}$ values, and phases of the sources are all permitted to range in value would be a formidable investigation, and in what follows reference is made to simple cases only.

It is convenient to consider next the results of observation on the test transmissions. This is done in a series of separate sections each concerned with some particular feature of the phenomenon.

9. MEASURED T_ω-ω RELATIONSHIPS

It was found in practice that in many instances the observed values of T_ω agreed closely with formula (20) over a fairly wide range of frequencies $\omega/2\pi$. Since $G\bar{v}$ is obtained from the ratio of any two values T_{ω_1} and T_{ω_2} corresponding to modulation frequencies $\omega_1/2\pi$ and $\omega_2/2\pi$, it was found convenient to transform equation (20) into a form which permitted the construction of a nomogram for finding $G\bar{v}$ and T_0 directly from the ratio $T_{\omega_1}/T_{\omega_2}$. Thus, from (20),

$$[(T_{\omega_1}/T_{\omega_2})^2 - 1] = [(f_2/f_1)^2 - 1]/[(G\bar{v}/2\pi f_1)^2 + 1],$$

which is of the form $F_1(X_1) = F_2(X_2)/F_3(X_3)$, which can be represented by a simple N-nomogram.

This nomogram greatly lightened the labour of analyzing the large volume of observational data.

Figure 4 is an example of plot of a set of experimental observations which conforms closely to equation (20) when $200 < f < 800$ c./sec. The values of $G\bar{v}$ derived from the ratios $T_{\omega_1}/T_{\omega_2}$ of various pairs of ordinates are indicated on the figure. It is evident that since the same value of $G\bar{v}$ is obtained in all cases, the corresponding portion of the curve is consistent with (20). The modulation depths T_ω refer to transmissions from Westerglen (767 kc./sec.—wanted transmitter) and Ottringham (167 kc./sec., 170 kW—disturbing transmitter) as observed at Birmingham on 8 August 1948, at 00.05 G.M.T. The value $T_0 = 3\,\%$ is typical of this combination to transmissions as observed at Birmingham [$M = 0{\cdot}8$].

Not all sets of observations of T_ω versus ω conform strictly to relation (20); in particular, as was first pointed out by the Cambridge observers, T_ω diminishes more rapidly at large values of ω than would be anticipated from the prototype formula (20). In such cases the values of $G\bar{v}$ differ somewhat according to the pairs of ordinates chosen, although fairly consistent values are obtained provided the portion of the curve beyond about $\omega/2\pi = 600$ c./sec. is ignored.

To explain this phenomenon consider figure 5*a* which, although based on the relative locations of Birmingham O, the Droitwich transmitter D (disturbing) and

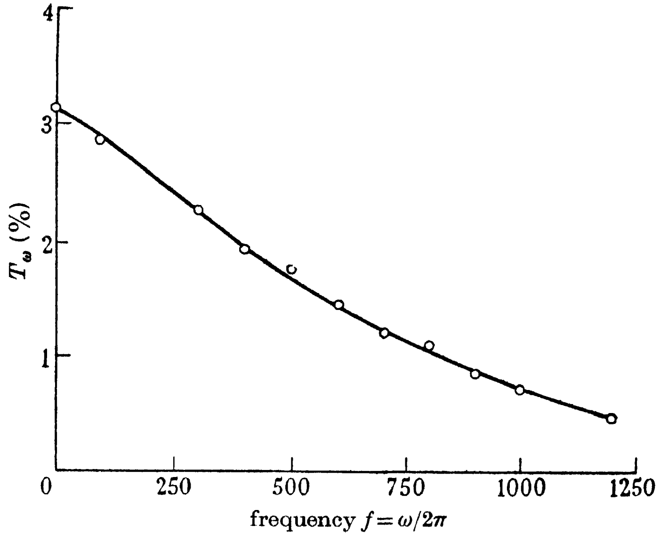

FIGURE 4. Experimental T_ω-ω curve and values of $G\bar{\nu}$ derived from pairs of ordinates. Westerglen (wanted) 767 kc./sec., 60 kW, and Ottringham (disturbing) 167 kc./sec., 170 kW, $M = 0{\cdot}8$; 8 August 1948.

T_{f_1}/T_{f_2}	T_{100}/T_{200}	T_{100}/T_{300}	T_{200}/T_{400}	T_{200}/T_{600}	T_{100}/T_{700}
$G\bar{\nu}$	2100	2200	2230	2120	1900

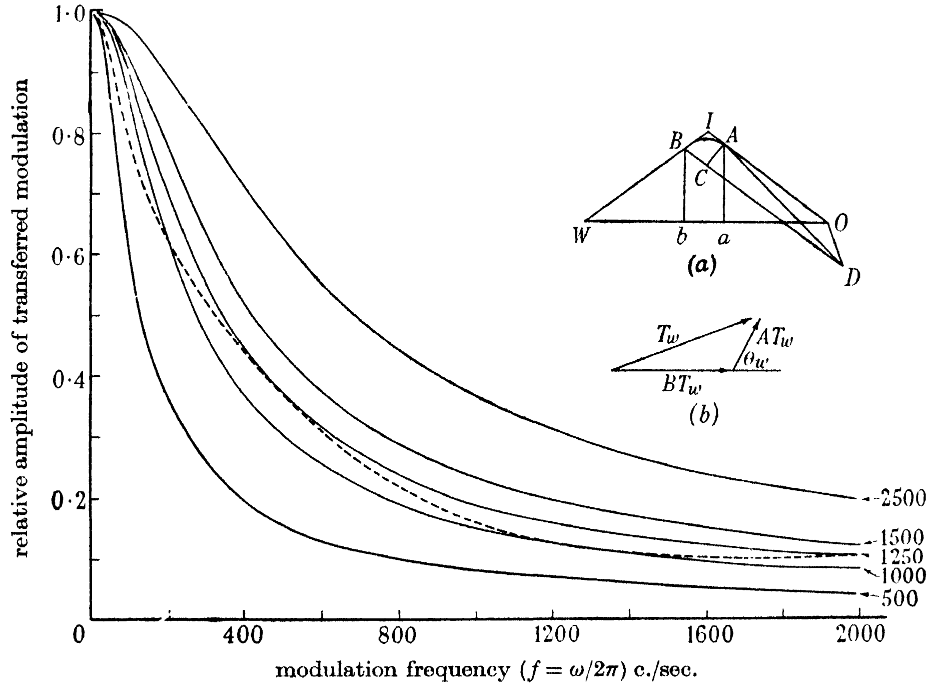

FIGURE 5. Illustration of T_ω-ω relationship for a pair of centres. The numbers against the curves give values of $G\bar{\nu}$. ----, pair of centres A and B.

Westerglen W (wanted), may be considered to be a typical situation. Let the wanted wave from W cross the reflexion surface of the disturbing wave from D, at B and A which, in view of the discussion in § 8 represent the localized centres at which the modulation is transferred to the wanted wave. Since the angle of incidence of the ray DA exceeds that of DB, the height of the centre A exceeds that of B. Suppose, for example, that their heights are 90 and 81 km. and let the corresponding values of $G\bar{v}$ be 500 and 2500. Let the equivalent reflexion point I of the wanted wave be at a height of 100 km. Put $WO = 408$ km., $OD = 25$ km., $Oa = 180$ km. and $Ob = 230$ km. Assume, for simplicity, that the modulations ${}_AT_0$ and ${}_BT_0$ transferred at A and B are equal each being T_0, that is the centres A and B have equal strengths.

The modulation ${}_BT_\omega = T_0\Big/\Big[1+\Big(\dfrac{\omega}{G\bar{v}_B}\Big)^2\Big]^{\frac{1}{2}}$ transferred at B is added vectorially to the modulation ${}_AT_\omega = T_0\Big/\Big[1+\Big(\dfrac{\omega}{G\bar{v}_A}\Big)^2\Big]^{\frac{1}{2}}$ transferred at A, the phase retardation of ${}_BT_\omega$ with respect to ${}_AT_\omega$ being

$$\theta_\omega = \left\{\frac{\omega L}{v} + \tan^{-1}\left(\frac{\omega}{G\bar{v}_B}\right)\right\} - \tan^{-1}\left(\frac{\omega}{G\bar{v}_A}\right), \tag{21}$$

in which L is the 'optical path' CBA (figure 5a). (Thus, from figure 5b,

$$T_\omega = [{}_AT_\omega^2 + {}_BT_\omega^2 + 2\,{}_AT_\omega\,{}_BT_\omega \cos\theta_\omega]^{\frac{1}{2}}, \tag{22}$$

from which T_ω may be calculated for any value of ω when $G\bar{v}_A$, $G\bar{v}_B$ and L are specified.)

Suppose, for instance, $L = 120$ km., $G\bar{v}_A = 1000$ and $G\bar{v}_B = 2000$. In this way the T_ω-ω relationship corresponding to this hypothetical case can be calculated. It is represented graphically in figure 5 by the curve for a 'pair of centres'. The curves designated $G\bar{v} = 2500$, 1500, 1250, 1000 and 500 represent respectively the T_ω-ω relationships for single centres with strengths $2T_0$ with these $G\bar{v}$ values respectively.

A striking feature of the composite curve for a pair of centres is the pronounced flattening of the curve when f is large. The curve, in fact, shows that T_ω passes through a minimum value near $f = 1600$ c./sec., corresponding to $\theta_\omega = \pi$ in equation (22). This flattening of the (T_ω-ω) curve is a characteristic feature of the majority of the experimental curves, although the minimum is not attained in practice at a frequency less than 2000 c./sec.

This fact suggests that the disparity in values of $G\bar{v}$, viz. 2500 and 500, and therefore of heights, assumed in constructing the theoretical curves is greater than actually occurs in practice. A similar synthetic curve for heights 87·5 and 82·5 km. and $G\bar{v}$ values, 2000 and 1000, corresponds closely to the curve for a single centre of strength $2T_0$, with $G\bar{v} = 1400$ over a frequency range 200 to 800 c./sec. Thus, it appears that the values of $G\bar{v}$ calculated from the experimental curves within this range of frequencies correspond approximately to the mean of the $G\bar{v}$ values of the separate centres. The procedure adopted in estimating $G\bar{v}$ from the experimental curves was to employ only that portion of a curve falling within the frequency range 200 to 600 c./sec.

It is clear from figure 5b that the phase of the resultant modulation is intermediate between that of ${}_BT_\omega$ and ${}_AT_\omega$.

With increasing ω the vector ${}_AT_\omega$ shortens more rapidly than ${}_BT_\omega$ and the phase centre of the pair of sources remains near B. When $\theta_\omega = \pi$ the phase centre in fact coincides with B.

Consider the particular case in which the disturbing transmitter D lies on the perpendicular bisector of the line WO joining the observer and the wanted transmitter. The heights, strengths and $G\bar{\nu}$ values of the centres A and B are now roughly the same for each, and the phase centre lies midway between the centres at top of the trajectory of the wanted wave.

The resultant modulation becomes $T_\omega = 2{}_AT_\omega \cos\left(\frac{\omega L}{2v}\right)$, and since L is now the ray path BA the angle $(\omega L/2v)$ is small for frequencies less than 800 c./sec. Thus $T_\omega \doteqdot 2{}_AT_\omega$ and the T_ω-ω curves resemble those for a single centre when f is less than 800 c./sec.

These conditions obtained when Ottringham was the disturbing transmitter, Westerglen the wanted transmitter and Birmingham the point of observation.

The more consistent $G\bar{\nu}$ values were in fact obtained in tests with these transmitters.

In the general case it has been supposed that the inequality of the $G\bar{\nu}$ values arises from the difference of height of the reflexion level of the disturbing wave at the centres A and B arising from difference in angle of incidence. Another cause of disparity could be difference in the electronic concentration of the ionosphere in the vicinity of A and B with an associated difference in height of reflexion of the wanted wave. In any case the measurements of T_ω as a function of ω are consistent with the hypothesis that in general two localized centres of cross-modulation are concerned, and that these lie near the reflexion level of the wanted wave.

It has been supposed in this discussion that one component only of the wanted wave is received.

This point was checked in practice by pulse transmissions distributed throughout the night. In those transmissions where the ground component of the wanted wave was present, it was eliminated by using a frame aerial to receive the sky-wave with its plane normal to the ground ray.

It may be remarked that if the geometry and carrier frequencies are such that the wanted wave is reflected below the reflecting level of the disturbing wave, then a single centre of cross-modulation is obtained. It is then to be expected that the T_ω-ω relationships should conform closely to the simple formulae (20).

10. NOCTURNAL AND SEASONAL BEHAVIOUR OF $G\bar{\nu}$ AND T_0

10·1. *Undisturbed ionosphere. Behaviour of $G\bar{\nu}$*

It was found that on nights when 'disturbed' conditions prevailed in the ionosphere, the behaviour of the transferred modulation was also irregular. However, under normal conditions with a single sky-wave relatively free from large fluctuations of amplitude it was found that both T_0 and $G\bar{\nu}$ exhibit regularities in their behaviour. Consider figure 6, which shows the typical dependence of $G\bar{\nu}$ on time during a night near midsummer (15 June) and nights in August, October and December.

It will be remarked that in June 1948 (figure 6*a*) $G\bar{\nu}$ decreases steadily from a large value exceeding 3×10^3 at about 00.45 G.M.T. to about 2×10^3 at dawn, after which it again increases. It is reasonable to attribute this behaviour to a progressive diminution of the electron concentration N in the E-region during the night and a concomitant rise in the surface at which the disturbing wave is reflected.

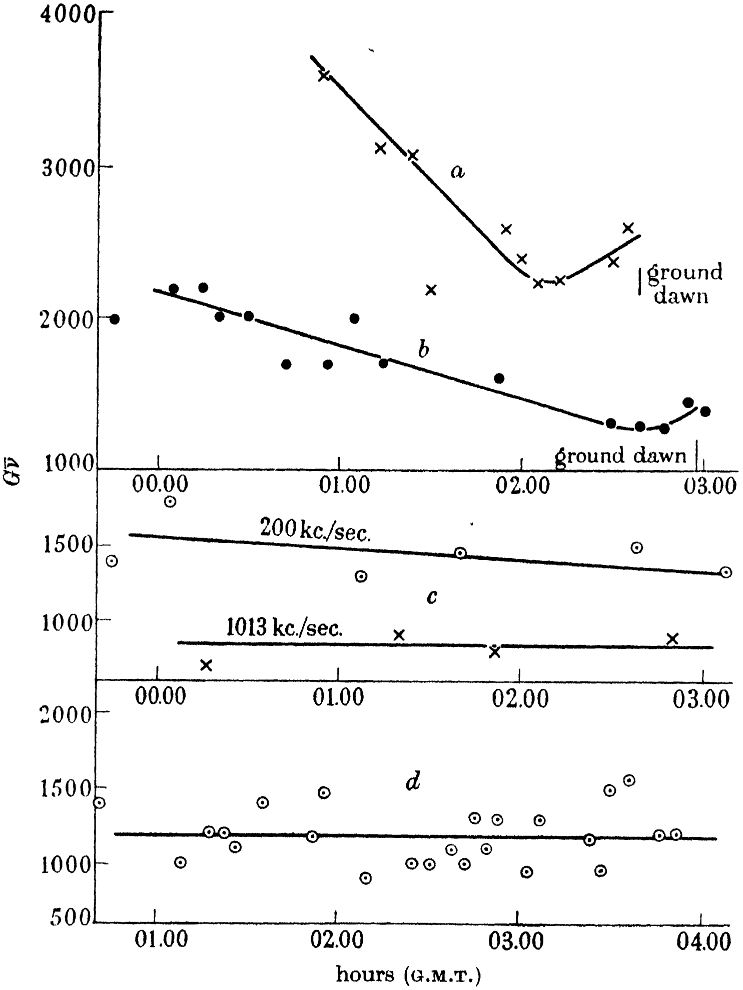

FIGURE 6. Nocturnal and seasonal behaviour of $G\bar{\nu}$ on undisturbed nights. *a*, 15 June 1948: Lisnagarvey (1050 kc./sec.)—wanted; Droitwich (200 kc./sec., 170 kW)—disturbing. *b*, 8 August 1948: Westerglen (767 kc./sec.)—wanted; Ottringham (167 kc./sec., 170 kW)—disturbing. *c*, 31 October 1948: Westerglen (767 kc./sec.)—wanted; Droitwich (200 kc./sec., 170 kW; 1013 kc./sec., 60 kW)—disturbing. *d*, 17 December 1948: Westerglen (767 kc./sec.)—wanted; Ottringham (167 kc./sec., 170 kW)—disturbing. $M = 0{\cdot}8$.

During the longer night of 8 August 1948 (figure 6*b*), $G\bar{\nu}$ decreased relatively slowly except for sporadic departures from the mean trend.

On 31 October and 17 December 1948 (figure 6*c* and *d*) there was no distinguishable diminution in the mean level of $G\bar{\nu}$ in the course of 4 hr., with either of the two disturbing transmitters used.

We conclude therefore:

(*a*) The mean value of $G\bar{\nu}$ is notably greater on a summer night than in the latter half of a winter night, and that presumably the electronic concentration N is greater during the former.

(*b*) $G\bar{\nu}$ diminishes notably during a summer night but is virtually constant during an undisturbed winter night. It is to be inferred that N diminishes at first but attains a distribution independent of time after a period of some 5 or 6 hr. after sunset.

Behaviour of T_0

The modulation T_0 does not exhibit a regular change between midnight and dawn, comparable with that of $G\bar{\nu}$. This is evident from the curves in figure 7 which refer to nights on which the ionosphere was undisturbed.

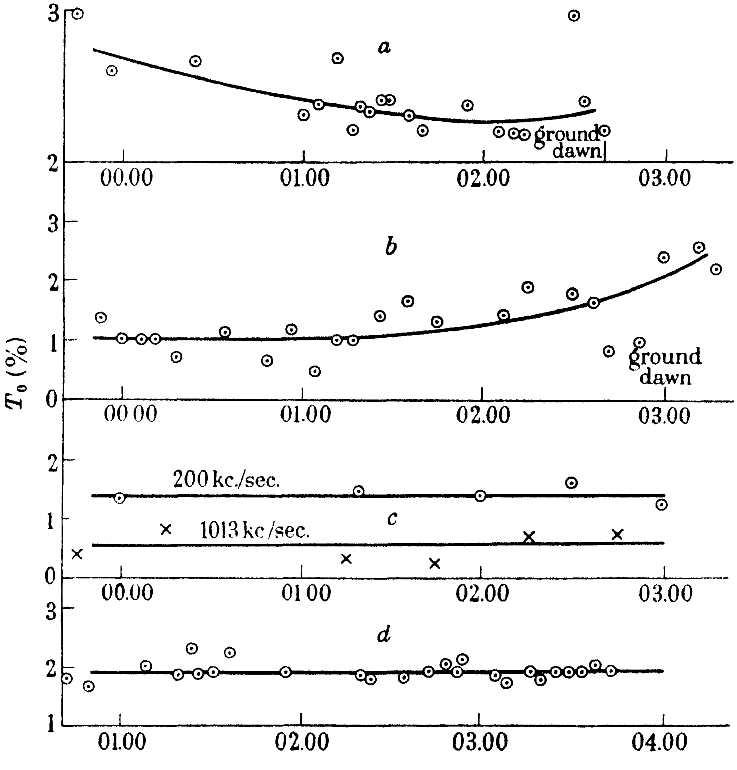

FIGURE 7. Nocturnal and seasonal behaviour of T_0—undisturbed nights. Transmitters as in figure 6*a* to *d*.

At dawn, however, it was generally found that although the carrier level of the wanted wave was usually evanescent, yet the coefficients of transferred modulation T_ω persisted or somewhat increased (figure 7*b*). Further observations at dawn are required before the typical behaviour of the modulation can be specified.

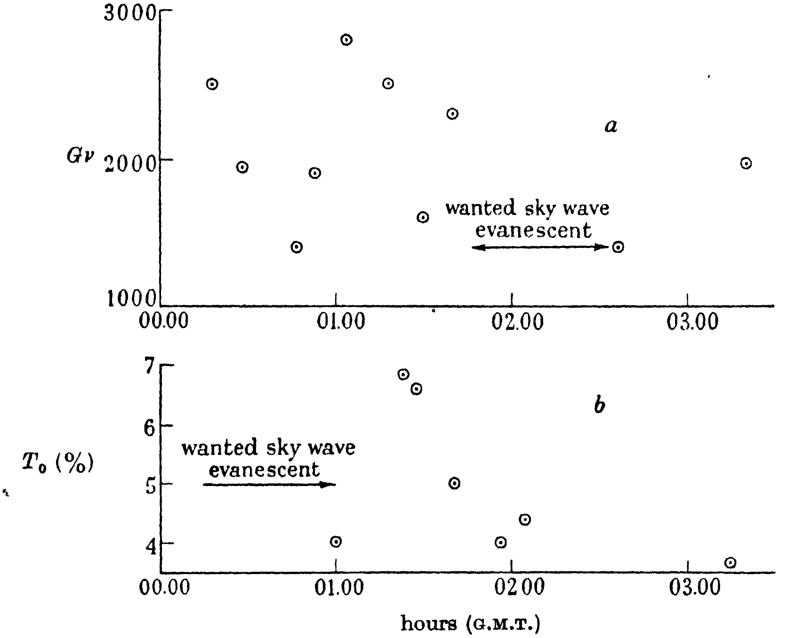

a, 10 August 1948; *b*, 9 August 1948.

FIGURE 8.

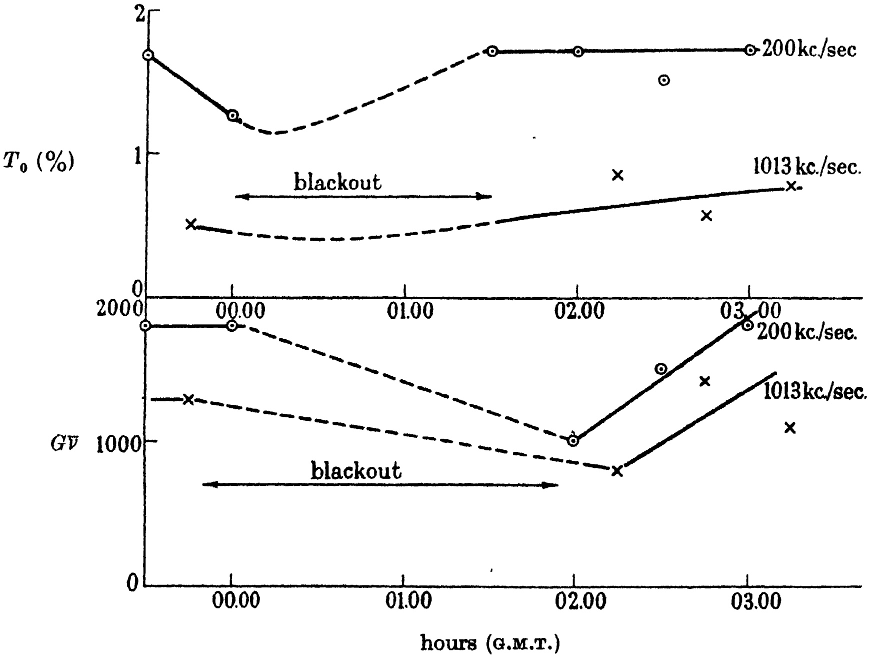

FIGURE 9. Behaviour of $G\bar{v}$ and T_0 on nights of ionospheric disturbance. Westerglen (767 kc./sec.)—wanted; Droitwich (200 kc./sec., 170 kW, 1013 kc./sec., 60 kW)—disturbing; 30 October 1948.

10·2. *Disturbed nights*

On nights when the ionosphere is disturbed both $G\bar{\nu}$ and T_0 exhibit wide and irregular fluctuations about their mean values. Figure 8 refers to nights of considerable ionospheric disturbance.

Another type of irregular behaviour observed on a number of occasions is illustrated by the curves in figure 9. It is not unusual, during an otherwise undisturbed night, for the carrier amplitude of the wanted wave to fall to a small value, which it may retain for a period of any length from 15 min. to more than an hour when it is impossible to measure the transferred modulation. It is found that $G\bar{\nu}$ immediately before and immediately after the 'black-out' period has notably different values and that T_0 behaves in a similar manner.

The three types of behaviour associated respectively with undisturbed nights, disturbed nights and nights of black-out are consistent with the following picture: On undisturbed nights the E-region possesses a stable distribution of N, the concentration being constant or virtually so, at each height. On nights of black-out it would appear that large clouds of ions and electrons, with concentrations above or below the average, drift through the E-region, and on disturbed nights these drifting clouds are of smaller extent, the ionosphere being flocculated.

11. DEPENDENCE OF $G\bar{\nu}$ ON THE FREQUENCY OF THE DISTURBING WAVE

In order directly to test the hypothesis that when the disturbing wave is reflected below the wanted wave, then the modulation is transferred near the lower reflexion surface, it suffices to note whether or not the value of $G\bar{\nu}$ is diminished when the frequency of the disturbing wave is increased, other factors remaining unchanged. This follows from the fact that the greater the frequency of a wave, the higher is its reflexion surface, and consequently the smaller the collisional frequency $\bar{\nu}$ over this surface.

A test of this nature was made on 30 and 31 October 1948, in a series of transmissions using Westerglen (767 kc./sec.) as wanted transmitter and two transmitters at Droitwich, whose frequencies were 200 kc./sec. (170 kW) and 1013 kc./sec. (60 kW). The results of these tests, which are shown in figures 7 and 10, provide immediate support for the basic hypothesis adopted in §§ 8 and 9. For instance, in figure 7, $G\bar{\nu} = 1500$ and 1050 respectively at the frequencies 200 and 1013 kc./sec. of the disturbing wave.

The waves from the disturbing transmitters travelled to the centres of cross-modulation very nearly in the vertical plane containing the magnetic meridian with their electric vectors almost parallel to the earth's magnetic field.

The influence of the earth's field on the propagation of the disturbing wave may therefore be neglected.

12. DEPENDENCE OF $G\bar{\nu}$ ON THE FREQUENCY OF THE WANTED WAVE

It follows from the theory given in §§ 8 and 9 that the mean value obtained for $G\bar{\nu}$ should be independent of the frequency of the wanted wave provided that wave is reflected at a greater height than the disturbing wave. This prediction was subjected to a test in a series of transmissions on 26 July 1948, in which wanted waves with the frequencies in kc./sec. of 767, 668 and 167 were radiated from Ottringham and were observed at Birmingham, with Droitwich (200 kc./sec, 170 kW, $M = 80\,\%$) acting as disturbing transmitter.

The measured $G\bar{\nu}$ values at the respective frequencies are shown in figure 10. Although it is not possible to distinguish the curves relating to 767 and 668 kc./sec., that for 167 kc./sec. lies distinctly above them. The test was repeated on the following night with the same result.

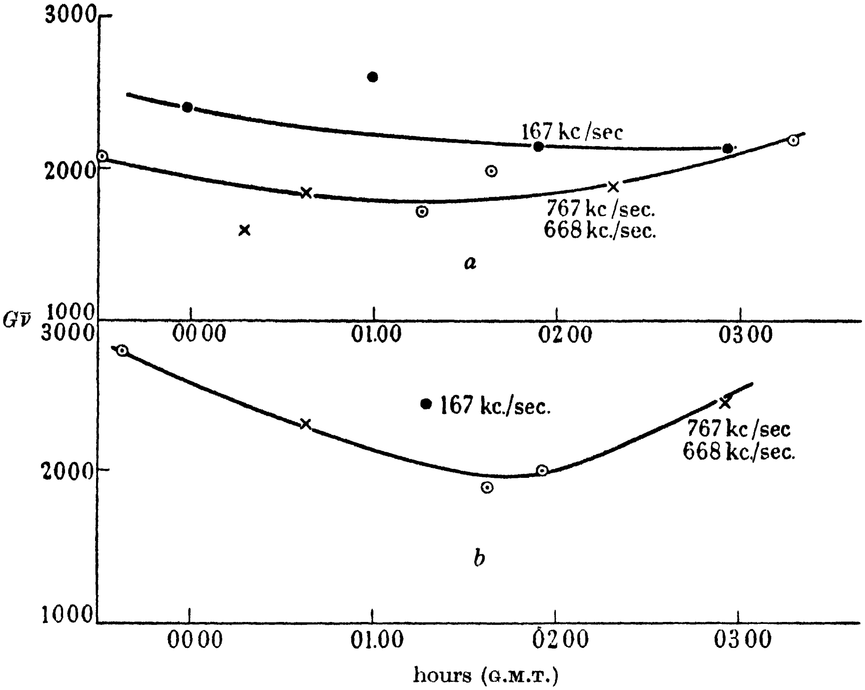

FIGURE 10. Dependence of $G\bar{\nu}$ on carrier frequency of wanted wave. *a*, 26 July 1948: wanted transmitters—Ottringham, 167, 668 and 767 kc./sec. 26 July 1948: disturbing transmitter —Droitwich, 200 kc./sec., 170 kW., $M = 0{\cdot}8$. *b*, 27 July 1948: transmitters as in *a*.

13. COMPARISON OF THE GRADIENTS OF ELECTRON CONCENTRATION AND OF COLLISIONAL FREQUENCY

From the results of the tests described in § 11, which are shown in figure 7, it is possible to estimate the ratio $(dN/dh)/(d\bar{\nu}/dh)$ at a height of about 86 km.

The values of the quantity $G\bar{\nu}$ corresponding to the two frequencies 200 and 1013 kc./sec. of the disturbing wave were found to be respectively 1500 and 1050. The mean collisional frequencies at the pairs of centres of cross-modulation are therefore in the ratio

$$\bar{\nu}_{200}/\bar{\nu}_{1013} = (G\bar{\nu})_{200}/(G\bar{\nu})_{1013} \doteqdot 1{\cdot}5.$$

If the scale height for $\bar{\nu}$ be taken as 6·5 km., this ratio corresponds to an increment in height of 2·6 km.

With $G = 1{\cdot}3 \times 10^{-3}$, $\nu_{200} = 1{\cdot}15 \times 10^{6}$ and $\nu_{1013} = 8{\cdot}1 \times 10^{5}$.

To estimate the mean electron concentration N at each pair of centres, the following formula for the value of N at the reflexion level of the disturbing waves is used, i_D being the angle of incidence:

$$N = 4{\cdot}73 \times 10^{-10} p_D^2 \cos^2 i_D / \psi(x_D)\,\text{cm.}^{-3}, \tag{23}$$

in which

$$x_D = \bar{\nu}/p_D, \quad \psi(x_D) = [1/(1+x_D^2)]\,[\tfrac{1}{2} + 1/(1+x_D^2)]. \tag{24}$$

Put

$$f_D = p_D/2\pi = 2 \times 10^5, \quad \bar{\nu}_{200} = 1{\cdot}15 \times 10^6.$$

Then

$$x_D = 0{\cdot}91 \quad \text{and} \quad \psi(x_D) = 0{\cdot}56.$$

Whence

$$N_{200} = 1{\cdot}34 \times 10^3 \cos^2 i_D. \tag{25}$$

Similarly,

$$N_{1013} = 1{\cdot}30 \times 10^4 \cos^2 i_D. \tag{26}$$

The geometry of the situation (§11) with a reflexion height of 86 to 88 km. gives $\cos^2 i_D \doteqdot 0{\cdot}19$ in both (25) and (26), whence $N_{200} = 190$ and $N_{1013} = 1820$.

Thus, in the same increment of height, 2·6 km., whereas $\bar{\nu}$ diminishes by a factor of 1·5, N increases by a factor of about 9. Cogent experimental evidence is thus provided for the existence of a sharp gradient in the distribution of N with height in the vicinity of 90 km.

This evidence at the same time supports the theory presented in §8 according to which the cross-modulation occurs at a pair of localized centres, or at a single centre according as the wanted wave is reflected above or below the disturbing wave.

14. ATTEMPTS TO DEMONSTRATE GYRO CROSS-MODULATION

Sets of transmissions were made during the periods 00.00 to 04.30 G.M.T. on the days 6 to 9 February 1948, to seek evidence of the existence of resonance or gyro cross-modulation by examining the value of the transferred modulation when the frequency of the disturbing wave was given different values in the vicinity of the gyro-frequency, 1·3 Mc./sec. Westerglen (767 kc./sec.) was used as wanted transmitter and Ottringham as disturbing transmitter, operating in turn on the frequencies 1122, 1312 and 1474 kc./sec. The transferred modulation in each instance was small, and on no occasion did T_0 exceed 0·5 % at Birmingham. On the other hand, the typical value of $T_0 = 3{\cdot}3$ % was obtained with Ottringham operating on a frequency of 167 kc./sec. (170 kW).

Thus, there was no clear evidence in these tests of exceptionally pronounced cross-modulation near the gyro-frequency. [It should be noted, however, that according to Bailey's theory of gyro-interaction somewhat stringent geometrical requirements must be satisfied if the effect is to be appreciable.]

Investigations of gyro cross-modulation have recently been made in Italy by Cutolo and colleagues (Cutolo 1948).

15. ABNORMALLY LARGE TRANSFERRED MODULATION

During the test transmissions described in §14, observations were also made at Birmingham when Ottringham 167 kc./sec. was wanted transmitter, with Ottringham (60 kW, M = 80 %) 1122, 1312 and 1474 kc./sec. in turn acting as disturbing transmitters. A frame aerial was used to balance out the ground wave of the wanted wave (167 kc./sec.).

The modulation transferred to the wanted wave when the frequencies of the disturbing wave were 1122 and 1312 kc./sec. was small with T_0 about 0·5 %. A most surprising effect was observed when the frequency of the disturbing transmitter was changed to 1474 kc./sec. An abnormally large percentage of transferred modulation was observed, with a T_ω-ω dependence which was normal, giving $T_0 = 40\ \%$ and $G\bar{\nu} = 2000$ (9 February, 01.00 G.M.T.).

The values of $T_0 = 3{\cdot}25\ \%$ and $G\bar{\nu} = 2000$ were found with Westerglen (767 kc./sec.—wanted wave) and Ottringham (167 kc./sec., 170 kW—disturbing wave) at 00.00 G.M.T. on the same evening, and $T_0 = 3{\cdot}3\ \%$ and $G\bar{\nu} = 1950$ at 04.00 G.M.T. This result suggests that the abnormal modulation was transferred at the reflexion level of Ottringham 167 kc./sec.

On the previous night also abnormal cross-modulation was observed between Ottringham 167 kc./sec. (wanted wave) and Ottringham 1474 kc./sec. (disturbing wave), with $T_0 = 18\ \%$.

It is not thought that these abnormal cross-modulations represent a gyro-resonance cross-modulation, and it is suggested that they may be associated with a coincidence of the reflexion levels of the disturbing and wanted waves. Further investigation of this effect is required before a convincing explanation can be offered.

16. DEPENDENCE OF TRANSFERRED MODULATION ON THE RADIATED POWER DISTURBING TRANSMITTER

According to equation (2) the modulation transferred along a path element ds is

$$dT_0 = \left(\frac{d\kappa_W}{d\bar{\nu}}\right)\frac{Mw_0}{\bar{Q}G}\,ds. \tag{27}$$

The mean energy of agitation $\bar{Q}$ of an electron to which mean power $\bar{w}$ is supplied by the disturbing wave is given by

$$G\bar{\nu}(\bar{Q}-Q_0) = \bar{w} = w_0(1+\tfrac{1}{2}M^2), \tag{28}$$

in which the term on the left represents the rate of dissipation of the power $\bar{w}$, in collisions of the electrons with gas molecules, and M is the modulation depth of the disturbing wave.

It follows from (27) that dT_0 is proportional to w_0 provided the change in $\bar{Q}$ with increasing w_0 can be neglected. According to (28) the proportionate rise in the electron temperature is $(\bar{Q}-Q_0)/Q_0 = \bar{w}/(Q_0 G\bar{\nu})$, and this is small when

$$\bar{w}/(Q_0 G\bar{\nu}) \ll 1.$$

When this condition obtains throughout the centres where the modulation is transferred then the total transferred modulation T_ω is proportional to w_0, which is itself proportional to the carrier power of the disturbing transmitter.

The total transferred modulation T_0 is therefore, according to (27), at first proportional to the radiated carrier power but ceases to be so when the power is increased to a value at which $\bar{w}/Q_0 G\bar{\nu}) \doteqdot 1$.

A test of the proportionality of T_0 to radiated power was made on 22 and 23 March 1948. The transferred modulation T_0 was observed on Westerglen 767 kc./sec. as wanted wave with Ottringham 167 kc./sec. as disturbing transmitter. Ottringham radiated in turn at a maximum power of 520 kW and at two-thirds and one-third of this value, and was modulated at 60 c./sec. with $M = 60\,\%$.

T_0 appeared to be proportional to the radiated carrier power up to the maximum of 520 kW. For instance, the following results were obtained:

21 and 22 March 1948

G.M.T.	Ottringham power	T_{60} c./sec.
23.40	$\frac{1}{3}$	2·1
23.45	$\frac{2}{3}$	4·4
23.50	full	6·4
00.15	full	6·8
00.20	$\frac{2}{3}$	4·25
00.25	$\frac{1}{3}$	2·3

Similar results were obtained on the following night.

It would appear, therefore, that with modulation depths T_0 of a few per cent the term $\bar{w}/(Q_0 G\bar{\nu}) \ll 1$.

17. ANOMALOUS T_ω-ω DEPENDENCE WHEN ω IS SMALL—DOUBLE-TONE TECHNIQUE

In addition to the departure, at large values of ω, of the (T_ω, ω) curve from that for a single centre of cross-modulation, the observations also reveal the existence occasionally of an anomaly at the smallest modulation frequencies (less than 200 c./sec.).

This anomalous behaviour when ω is small was first reported by Mr Hunt of the B.B.C., and was very marked in some observations made at Birmingham in the period 24 to 27 July, when a new double-tone technique was employed. In this technique the disturbing transmission is modulated with a pair of tones simultaneously, and the transferred modulation is measured on each tone by means of a pair of wave analyzers. In the course of these transmissions, which have already been described in § 12, Droitwich was modulated in turn by the pairs of simultaneous tones, 60 c./sec. at 30 % and 200 c./sec. at 50 %, and then by 60 c./sec. at 30 % and 400 c./sec. at 50 %.

Thus, in order to obtain $(G\bar{\nu})$ from the formula $T_\omega = T_0/[1+(\omega/G\bar{\nu})^2]^{\frac{1}{2}}$ it was necessary first to reduce the measured modulations to a common standard by comparing $5 \times T_{60}$, $3 \times T_{200}$ and $3 \times T_{400}$. In many instances it was found that $5 \times T_{60}$ and $3 \times T_{200}$ were roughly equal, and that it was not possible to find a value for $G\bar{\nu}$ from them, the wanted wave frequency being 767 or 668 kc./sec. On the other hand, a comparison of T_{200} and T_{400} gave normal values of the order of 2000 for $G\bar{\nu}$. These observations showed very clearly the existence of the low-frequency anomaly.

The double-tone technique is a valuable method for measuring $G\bar{\nu}$, since it eliminates the effect of fluctuations in the intensity of the wanted wave.

18. General comments

It has been shown that a variety of experimental evidence is consistent with the hypothesis that the modulation is transferred to the wanted wave within a narrow range of height bounded above by the reflexion surface of the disturbing wave when that wave is reflected below the wanted wave. This feature of ionospheric cross-modulation is significant for the understanding of the absorption of waves of medium wave-length reflected within the E-region. Since the absorption coefficients depend upon $w_0 N$, it follows that most of the absorption of a medium wave occurs near the reflexion surface. The calculation of absorption requires a knowledge of the distribution in height of both collisional frequency $\bar{\nu}$ and electron concentration N. By means of a systematic use of the method described in § 13, it should be possible to determine these functions experimentally. The chief difficulty lies in the determination of the height at which the modulation is transferred. The presence of a pair of centres and the lack of precise knowledge of the angle of descent of the wanted wave make height measurement from phase an uncertain procedure with oblique incidence (§ 6). To obtain a single centre, it is suggested that the measurements of phase be carried out with the wanted wave reflected below the disturbing wave. Since this single centre would lie directly above the mid-point of the line joining the wanted transmitter and the observer, the geometrical problem is soluble.

For instance, in tests using the combination Westerglen (wanted)—Ottringham on 10 August 1948, careful measurements of phase were made. On the assumption of a pair of identical centres of cross-modulation the mean phase centre lies over the point midway between Westerglen and Birmingham. On this assumption the height of the phase centre was found to be 83·5 km. with $G\bar{\nu} = 2300$. Since the mean phase centre lies somewhat above the actual pair of centres, the height corresponding to $G\bar{\nu} = 2300$ is somewhat less, say 82 km., and $\bar{\nu}$ at this height is $1{\cdot}8 \times 10^6$. The pressure is $p = 7 \times 10^{-3}$ mm.Hg.

The alternative is to estimate the pressure of the gas from $G\bar{\nu}$, using G and the collisional cross-section A of the molecules, and to obtain the height from the pressure-height relationships obtained in experiments with rockets, as already described (§ 6).

Experimental work of the character described in this paper is essentially the product of the co-operative effort of many people. It is a pleasure to express appreciation of the indispensable assistance afforded by the Engineering Research Department of the B.B.C., in particular to Mr H. L. Kirke, Mr R. A. Rowden, the observers at Tatsfield and Caversham and to the engineers at the transmitters. The author has also derived considerable benefit from discussions with the Cambridge team under the direction of Mr J. A. Ratcliffe of the Cavendish Laboratory.

He is also greatly indebted to Professor A. Tustin for much encouragement.

Finally, the author records his indebtedness to Messrs C. C. Newton, F. J. Hyde and H. G. Foster of the Birmingham team, without whose assistance in observation, in construction of equipment and in the reduction of data it would have been impossible for him to proceed.

APPENDIX

Theory of ionospheric cross-modulation

The disturbing wave is absorbed as it traverses the E-region and therefore communicates power to the electrons. The power w_0 communicated by the field $E_D = {}_OE_D \cos p_D t$ to an electron in the ionosphere is proportional to ${}_OE_D^2$. When E_D is modulated it becomes $E_D = {}_OE_D(1+M\cos\omega t)\cos p_D t$, and the power $w(t)$ communicated to an electron becomes a function of the time.

It follows that

$$w(t)/w_0 = (1+M\cos\omega t)^2,$$

i.e.

$$\begin{aligned} w(t) &= w_0(1+\tfrac{1}{2}M^2+2M\cos\omega t+\tfrac{1}{2}M^2\cos 2\omega t) \\ &= \overline{w}+w_0(2M\cos\omega t+\tfrac{1}{2}M^2\cos\omega t), \end{aligned} \tag{29}$$

where $\overline{w} = w_0(1+\tfrac{1}{2}M^2)$ is the mean power supplied by the modulated wave to an electron.

With no wave, the mean energy of agitation Q_0 of an electron is the same as that of the mean energy of thermal agitation of the gas molecules, but when power $\overline{w}$ is supplied the energy of the electrons is increased to a value $\bar{Q}$ at which energy is lost by an electron in collisions with gas molecules at the same rate $\overline{w}$ as it is supplied by the wave.

In order to estimate $\bar{Q}$ it was assumed by Bailey that the mean loss of energy per collision by an electron in its collisions with molecules of the gas is proportional to its energy excess $(\bar{Q}-Q_0)$. It follows that in the state of dynamical equilibrium

$$G\bar{\nu}(\bar{Q}-Q_0) = \overline{w} = w_0(1+\tfrac{1}{2}M^2), \tag{30}$$

where G is a constant of proportionality and $\bar{\nu}$ is the collisional frequency appropriate to $\bar{Q}$.

When, however, as in (29), $w(t)$ fluctuates about its mean value $\overline{w}$, the average energy Q of the electrons in a group also becomes a function of the time. The energy Q satisfies the following equation:

$$\frac{dQ}{dt}+G\nu(Q-Q_0) = w(t). \tag{31}$$

To solve equation (31) approximately, neglect the fluctuation of ν about its mean value $\bar{\nu}$ in the second term on the left and replace it by $\bar{\nu}$ which is constant. Next subtract (30) from (31) and use (29) to obtain

$$\frac{d}{dt}(Q-\bar{Q})+G\bar{\nu}(Q-\bar{Q}) = w_0(2M\cos\omega t+\tfrac{1}{2}M^2\cos 2\omega t), \tag{32}$$

in which dQ/dt has been replaced by $d(Q-\bar{Q})/dt$, which is equal to it. The particular solution of (32) is

$$Q = \bar{Q}[1+2m_\omega\cos(\omega t-\phi_\omega)+2m_{2\omega}\cos(2\omega t-\phi_{2\omega})], \tag{33}$$

where

$$\left.\begin{aligned} m_\omega &= Mw_0/[\bar{Q}G\bar{\nu}\{1+(\omega/G\bar{\nu})^2\}^{\frac{1}{2}}], \\ m_{2\omega} &= M^2w_0/[4\bar{Q}G\bar{\nu}\{1+(2\omega/G\bar{\nu})^2\}^{\frac{1}{2}}], \\ \tan\phi_\omega &= \tfrac{1}{2}\tan\phi_{2\omega} = \omega/G\bar{\nu}. \end{aligned}\right\} \tag{34}$$

The collisional frequency ν is proportional to the velocity of agitation and the energy Q to the square of this velocity, consequently

$$\nu/\bar{\nu} = (Q/\bar{Q})^{\frac{1}{2}} = 1 + m_{\omega}\cos(\omega t - \phi_{\omega}) + m_{2\omega}\cos(2\omega t - \phi_{2\omega}) + \cdots. \tag{35}$$

In practice m_{ω} and $m_{2\omega}$ are small compared with unity, so that terms involving their squares and higher powers may be neglected.

Along an element of path ds of the wanted wave through the ionosphere where ν is being modulated as in (35), the absorption coefficient κ_W, which depends on ν is also a function of the time and may be written

$$\kappa_W = \bar{\kappa}_W + \left(\frac{d\kappa_W}{d\bar{\nu}}\right)(\nu - \bar{\nu}) = \bar{\kappa}_W + \left(\frac{d\kappa_W}{d\bar{\nu}}\right)\bar{\nu}[m_{\omega}\cos(\omega t - \phi_{\omega}) + m_{2\omega}\cos(2\omega t - \phi_{2\omega})]. \tag{36}$$

If the amplitude of E_W, the field of the wanted wave, is ${}_0E_W$ at one end of ds and ${}_0E_W\exp(-\kappa_W ds)$ at the other, this latter amplitude may be written

$$\begin{aligned}{}_0E_W\exp(-\bar{\kappa}_W ds)\exp\left[\frac{d\kappa_W}{d\bar{\nu}}(\nu - \bar{\nu})\,ds\right] &\doteqdot [{}_0E_W\exp(-\bar{\kappa}_W ds)]\left[1 - \left(\frac{d\kappa_W}{d\nu}\right)(\nu - \bar{\nu})\,ds\right] \\ &= {}_0E_W\exp(-\bar{\kappa}_W ds)\{1 + dT_{\omega}\cos(\omega t - \phi_{\omega} - \pi) + dT_{2\omega}\cos(2\omega t - \phi_{2\omega} - \pi)\},\end{aligned} \tag{37}$$

in which, from (36) and (34),

$$dT_{\omega} = \left(\frac{d\kappa_W}{d\bar{\nu}}\right)\bar{\nu}m_{\omega}\,ds,$$

i.e.

$$\left.\begin{aligned}(dT_{\omega}/ds) &= (dT_0/ds)/[1 + (\omega/G\bar{\nu})^2]^{\frac{1}{2}}, \\ (dT_{2\omega}/ds) &= M(dT_0/ds)/4[1 + (2\omega/G\bar{\nu})^2]^{\frac{1}{2}}, \\ \tan\phi_{\omega} &= \tfrac{1}{2}\tan\phi_{2\omega} = \omega/G\bar{\nu},\end{aligned}\right\} \tag{38}$$

and

$$dT_0/ds = \left(\frac{d\kappa_W}{d\bar{\nu}}\right)Mw_0/\bar{Q}G. \tag{39}$$

The total modulation transferred to the wanted wave when $\omega/G\bar{\nu}$ is everywhere small, and $\phi_{\omega} \doteqdot 0$, is

$$T_0 = \int (dT_0/ds)\,ds. \tag{40}$$

When the region of transference is localized, as discussed in the text, then

$$T_{\omega} = T_0/[1 + (\omega/G\bar{\nu})^2]^{\frac{1}{2}},$$

and

$$T_0 = (M/\bar{Q}G)\int (d\kappa_W/d\bar{\nu})\,w_0\,ds \doteqdot M\left(\frac{d\kappa_W}{d\bar{\nu}}\right)w_0 s/\bar{Q}G.$$

It is of interest to remark that the general solution of (31) is

$$(Q - Q_0) = \left[\exp\left(-\int_0^t G\nu\,dt\right)\right]\int_0^t w(t)\left[\exp\left(\int_0^t G\nu\,dt\right)\right]dt + a\exp\left(-\int_0^t G\nu\,dt\right),$$

where a is a constant of integration. Equation (33) is obtained from this by putting $\nu \doteqdot \bar{\nu} =$ constant, $a = 0$, and by using (29) and (30).

REFERENCES

Best, N., Havens, R. & La Gow, H. 1947 *Phys. Rev.* **71**, 915.
Cutolo, M. 1948 *Nuovo Cimento*, **5**, 475.
Cutolo, M. & Ferrero, R. 1948 *Nuovo Cimento*, **5**, 518.
Huxley, L. G. H. 1940 *Phil. Mag.* (7), **29**, 313.
Huxley, L. G. H. 1948 *J. Inst. Elect. Engrs*, **95**, III, 37, 328.
Huxley, L. G. H. 1949 *Proc. Roy. Soc.* A, **196**, 427.
Huxley, L. G. H., Foster, H. G. & Newton, C. C. 1947 *Nature*, **159**, 300.
Huxley, L. G. H., Foster, H. G. & Newton, C. C. 1948 *Proc. Phys. Soc.* **61**, 134.
Huxley, L. G. H. & Ratcliffe, J. A. 1949 *J. Inst. Elect. Engrs*, **96**, III, 43, 433.
Huxley, L. G. H. & Zaazou, A. A. 1949 *Proc. Roy. Soc.* A, **196**, 402.
Ratcliffe, J. A. & Shaw, I. J. 1948 *Proc. Roy. Soc.* A, **193**, 311.

The supersonic flow of compressible fluid through axially symmetric tubes of uniform and varying section

BY R. K. TEMPEST, *Department of Applied Mathematics, University of Liverpool*

(*Communicated by L. Rosenhead, F.R.S.—Received* 25 *July—*
Revised 24 *October* 1949)

The paper considers potentials representing the supersonic flow of a compressible, inviscid fluid in axially symmetric tubes or diffusers. General formulae are given to determine the linearized flows completely when the inlet distributions of velocity are known, in cases where the slope of the nozzle wall is continuous, and where there are no discontinuities in the velocity field or in the rates of change of velocity. Particular reference is made to the flows resulting from velocity distributions which are initially parabolic.

Formulae are given to enable the computer to tabulate a very wide class of axisymmetric flows, mention being made of the propagation of other profiles which are non-parabolic. A further method is given for extending the field by use of power series approximation.

A discussion of rotational flows in divergent diffusers will be given in a later paper.

1. INTRODUCTION

In recent years, the literature associated with solutions of the linearized equation of motion of a compressible fluid has increased fairly rapidly. The method of approach originated in a paper by Karman & Moore (1932) is essentially one in which approximations are made to the exact equations of motion of a compressible fluid by the method of small perturbations. The assumptions made are that: (*a*) the viscosity of the fluid can be neglected, (*b*) the pressure is a known function of the density, (*c*) the flow is irrotational and (*d*) the velocity of the flow nowhere departs considerably from the velocity of the main stream. The significance of (*a*) is that a non-zero velocity of slip over bounding surfaces is possible and of (*d*) that this velocity of slip must not differ very considerably from the velocity of the main stream.

A major problem in gas dynamics is the estimation of velocity and Mach number in the axially symmetric flow through a tube or diffuser. Contributions to this problem have been made by various authors. Ward (1945) applied linearized solutions to estimate the flow in a uniform tube, whilst Tupper (1945) constructed a flow in a slightly convergent tube by consideration of the propagation of disturbances along characteristics. Squire (1947) measured the distribution of velocity across various sections of a divergent diffuser, which effectively illustrated the propagation of an inlet velocity distribution which decreased from a maximum value on the axis of the tube to some value at the diffuser wall. It should be noted, however, that in the experiments of Squire, the entry-velocity distribution consisted of a uniform subsonic core, with only a thin boundary layer falling-off of velocity near the wall; the diffusers were conical, thus giving a discontinuity in the slope of the boundary profile at the point where the cone was attached to the end of a parallel section. Green & Southwell (1944) applied relaxation methods to examine particular subsonic flows in convergent-divergent diffusers in which regions of high velocity appear near the wall at the narrowest part of the tube. In the present paper the velocity potentials of various flows are expressed as series of Bessel functions; a further section is devoted to the possibilities of building up power series representations.

Emphasis is laid on the propagation of profiles with maximum velocity on the axis in diffusers which are concave to the axis. Green & Southwell's work related to high subsonic flows in divergent tubes convex to the axis. Were it possible to obtain an inlet velocity distribution with a minimum value on the axis in a totally supersonic flow, the results given below could be used to describe the irrotational propagation of this profile in such divergent tubes. This could be effected merely by reversing the sign of the curvature of the profile in the formulae quoted.

2. STATEMENT OF THE PROBLEM

A compressible fluid flows under high pressure through a tube which has axial symmetry with reference to the z co-ordinate. The section $z = 0$ corresponds to the inlet, and for convenience, it is supposed that the unit of length is chosen to be the radius of the tube at $z = 0$. In cylindrical co-ordinates, the contour of the tube may thus be expressed as

$$r = 1 + F(z), \tag{2·1}$$

where $F(0) = 0$. We may assume the inlet distribution of velocity to consist of an axial component $f(r)$ and a radial component $g(r)$. Under the restrictions imposed by the linearized theory, $(f^2+g^2)^{\frac{1}{2}} - U$ must be small, where U is some constant velocity which may be taken to be $f(0)$.

We shall investigate the possibility of constructing irrotational flows in diffusers of general shapes, and in the cases where this is possible we shall investigate potentials which satisfy the linearized equation of motion

$$\frac{\partial^2\phi}{\partial r^2} + \frac{1}{r}\frac{\partial\phi}{\partial r} = \beta^2\frac{\partial^2\phi}{\partial z^2}, \tag{2·2}$$

where $\beta^2 = M^2 - 1$, M being the Mach number of the flow. In the supersonic case β^2 is positive.

It may be noted in the following work that approach to the problem by linearized methods is not capable of detecting the various mathematical singularities which may occur in the exact solutions for the velocity field.

3. General discussion of rotational and irrotational motions

It is necessary to establish the fact that a velocity potential exists before we try to represent a particular flow by such a potential. The method of approach for finding such a potential varies according to the simplifying approximations applied to the fundamental equations of motion.

In supersonic potential flow the only curves or surfaces along which distinct solutions of the potential equation can be joined together are characteristic curves or surfaces. (This is the 'patching' property of characteristics; see, for instance, Murnaghan and others 1945 or Hadamard 1903.) It follows that, in any supersonic diffuser, the region of flow which is influenced by the diffuser begins along a characteristic. In the case of an axisymmetric supersonic diffuser the flow is only influenced by the diffuser in the region in front of the forward characteristic surface through the boundary of the diffuser inlet. Behind this characteristic surface the flow must be completely specified independently of the diffuser. It follows then that the natural boundary from which to start studying a supersonic flow in a diffuser is the forward characteristic surface through its inlet rim, and that if a start is made on any other surface care must be taken to ensure that the conditions specified are complete and compatible.

As an example, let us consider the flow in a divergent nozzle of the type indicated in figure 1 in which the inlet profile is wholly axial and of the form indicated in figure 2. The slope of the nozzle is zero at the inlet and is everywhere continuous. The linearized theory so far developed does not allow any discontinuities in the potential or of its derivatives which might result in the formation of shock waves, and hence vorticity. A unique solution for the potential representing the linearized flow bounded by the nozzle may be found when the shape of the nozzle, the inlet velocity profile and the Mach number at some point are specified. It does not seem likely that the 'linearized' approach can be used successfully to represent flows with discontinuities such as those that are dealt with by the method of characteristics. It is proposed to return to a more detailed study of this question at a later time.

To return to the particular continuous flow that we are considering, let us suppose that the flow is governed by a potential ϕ. The boundary condition is expressed by the equation

$$\frac{dF}{dz} = \left(\frac{\partial\phi}{\partial r}\bigg/\frac{\partial\phi}{\partial z}\right)_{r=1+F} = \frac{h(z)}{k(z)}, \quad \text{say.} \tag{3·1}$$

Then

$$\frac{d^2F}{dz^2} = \frac{1}{k}\frac{dh}{dz} - \frac{h}{k^2}\frac{dk}{dz}. \tag{3·2}$$

At $z = 0$, h, which is the radial velocity at the inlet wall, is zero, and hence

$$\left(\frac{d^2F}{dz^2}\right)_{z=0} = \left(\frac{1}{k}\frac{dh}{dz}\right)_{z=0}. \tag{3·3}$$

At $z = 0$, k is the value of the axial velocity at the inlet wall, which is positive, whilst, if a velocity potential exists, $(dh/dz)_{z=0}$ is equal to $(\partial^2\phi/\partial z\,\partial r)_{z=0,\,r=1}$, or $(\partial^2\phi/\partial r\,\partial z)_{z=0,\,r=1}$, which is the r-variation of the inlet profile at the wall. This is essentially negative, and we arrive at the conflicting result that $(d^2F/dz^2)_{z=0}$ is negative, implying that the nozzle wall is concave towards its axis, whereas the nozzle was assumed to be convex towards the axis. It will readily be seen that the only assumption leading to this result is the condition of integrability, which is equivalent to the assumption that the flow is irrotational. In simpler form: if the flow be irrotational, the variation of radial velocity along the tube at $r = 1$ is equal to the variation of axial velocity across the section $z = 0$ at $r = 1$. The latter is negative, for we have assumed the inlet profile to have a maximum velocity on the axis of the tube and to decrease as we pass towards the wall of the tube. Hence the streamlines in an irrotational flow with an inlet profile similar to the one depicted in figure 2 must be deflected towards the axis of the tube, which cannot therefore be of the form shown in figure 1. A divergent flow with streamlines convex to the axis is therefore rotational in character. It is obvious that the vorticity is not confined to a region near the bounding surface, as the above argument applies at any point of the inlet section and hence throughout the whole body of the fluid. This is because the rate of change of radial velocity with z must equal the rate of change of axial velocity with r, which is negative across the whole of the inlet.

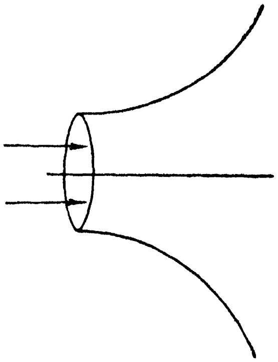

FIGURE 1

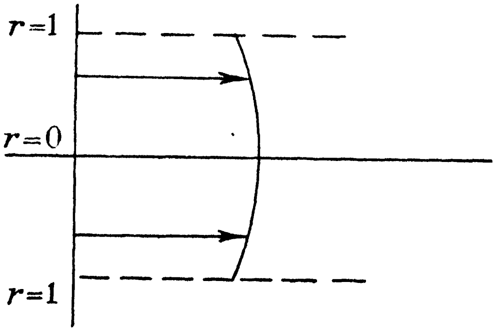

FIGURE 2

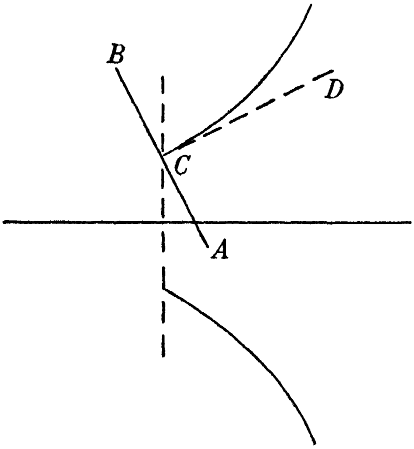

FIGURE 3

Let us now consider the propagation of a velocity profile with axial distribution $f(r)$ and radial distribution $g(r)$ in the nozzle of shape $r = 1+F(z)$ (see figure 3).

We note that: (*a*) linearized potentials would be confined to those flows in which f is approximately constant and g/f small, (*b*) the boundary condition implies that $(dF/dz)_{z=0} = g(1)/f(1)$, and (*c*) in order to describe the type of flow under consideration it must be assumed that f is a decreasing function of r.

At any point on the line AB, at right angles to the inlet wall, the component of velocity parallel to the tangent to the wall is approximately

$$\frac{f(1)}{[\{f(1)\}^2+\{g(1)\}^2]^{\frac{1}{2}}}\left\{f+\left(\frac{dF}{dz}\right)_{z=0}g\right\},$$

which to the first order of small quantities is f, which decreases. If the motion were irrotational, the rate of change of $\overrightarrow{AB}$ velocity along CD would equal the rate of change of $\overrightarrow{CD}$ velocity along AB. It is clear that this can only be the case if the streamlines and the bounding surface curve towards the axis. Thus no irrotational flow of this type exists in a trumpet-shaped divergent diffuser which is a solution of the linearized equation of motion of a compressible fluid. Our study of irrotational flows, and particularly linearized flows, is thus confined to flows whose streamlines are concave towards the diffuser axis.

4. POTENTIALS EXPRESSIBLE AS SERIES OF BESSEL FUNCTIONS

In our study of irrotational flows in tubes, we are led to consider solutions of equation (2·2), subject to the condition that ϕ and its derivatives remain finite on the axis, $r = 0$. Such a potential is

$$\phi = A_0 z+\sum_{n=1}^{\infty} A_n \sin\frac{\lambda_n z}{\beta} J_0(\lambda_n r)+\sum_{n=1}^{\infty} B_n \cos\frac{\mu_n z}{\beta} J_0(\mu_n r). \tag{4·1}$$

The inlet distributions of axial and radial velocity are given by

$$\left.\begin{aligned} \left(\frac{\partial\phi}{\partial z}\right)_{z=0} &= A_0+\sum_{n=1}^{\infty} A_n\frac{\lambda_n}{\beta} J_0(\lambda_n r),\\ \text{and}\qquad \left(\frac{\partial\phi}{\partial r}\right)_{z=0} &= -\sum_{n=1}^{\infty} B_n\mu_n J_1(\mu_n r). \end{aligned}\right\} \tag{4·2}$$

We may express prescribed distributions $f(r)$ and $g(r)$ as series such as those of (4·2) giving the coefficients A_0, A_n, B_n, and hence the potential ϕ. This may be effected provided that the λ's satisfy an equation

$$\lambda J_1(\lambda)+\nu J_0(\lambda) = 0, \tag{4·3}$$

and that the μ's satisfy an equation

$$\mu J_0(\mu)+\epsilon J_1(\mu) = 0, \tag{4·4}$$

where ν and ϵ are two arbitrary constants. Thus the expansions of f and g in Bessel series are not unique. We may assign values of ν and ϵ to obtain a certain sequence of λ's from (4·3) and a certain sequence of μ's from (4·4). With these sequences and appropriate coefficients we ultimately obtain a potential which represents the propagation of the f and g profiles in a certain diffuser. A different choice of ν and ϵ would ultimately produce the propagation of the f and g profiles in another diffuser.

From different expansions of f and g we obtain flows in diffusers of different shapes, all with the same inlet distributions. The boundary condition may be expressed in the form

$$\frac{dF}{dz}=\frac{-\sum_{n=1}^{\infty}A_n\lambda_n\sin\frac{\lambda_n z}{\beta}J_1(\lambda_n+\lambda_n F)-\sum_{n=1}^{\infty}B_n\mu_n\cos\frac{\mu_n z}{\beta}J_1(\mu_n+\mu_n F)}{A_0+\sum_{n=1}^{\infty}A_n\frac{\lambda_n}{\beta}\cos\frac{\lambda_n z}{\beta}J_0(\lambda_n+\lambda_n F)-\sum_{n=1}^{\infty}B_n\frac{\mu_n}{\beta}\sin\frac{\mu_n z}{\beta}J_0(\mu_n+\mu_n F)}, \tag{4·5}$$

and the shape of the diffuser is given by

$$= 1+F(z) = 1-\int_0^z dz\frac{\sum_{n=1}^{\infty}A_n\lambda_n\sin\frac{\lambda_n z}{\beta}J_1(\lambda_n+\lambda_n F)+\sum_{n=1}^{\infty}B_n\mu_n\cos\frac{\mu_n z}{\beta}J_1(\mu_n+\mu_n F)}{A_0+\sum_{n=1}^{\infty}A_n\frac{\lambda_n}{\beta}\cos\frac{\lambda_n z}{\beta}J_0(\lambda_n+\lambda_n F)-\sum_{n=1}^{\infty}B_n\frac{\mu_n}{\beta}\sin\frac{\mu_n z}{\beta}J_0(\mu_n+\mu_n F)}, \tag{4·6}$$

which, if F is small, is approximately

$$r = 1-\int_0^z dz\frac{\sum_{n=1}^{\infty}A_n\lambda_n\sin\frac{\lambda_n z}{\beta}J_1(\lambda_n)+\sum_{n=1}^{\infty}B_n\mu_n\cos\frac{\mu_n z}{\beta}J_1(\mu_n)}{A_0+\sum_{n=1}^{\infty}A_n\frac{\lambda_n}{\beta}\cos\frac{\lambda_n z}{\beta}J_0(\lambda_n)-\sum_{n=1}^{\infty}B_n\frac{\mu_n}{\beta}\sin\frac{\mu_n z}{\beta}J_0(\mu_n)}. \tag{4·7}$$

The procedure of this paper is, essentially, to expand a given distribution of axial and radial velocity in as many ways as possible, and thus in each case to determine the bounding surfaces containing the flows. For example, if the λ eigenvalues are chosen to be the zeroes of $J_1(\lambda)$ (i.e. if $\nu = 0$), and if, in addition, $B_n = 0$, it immediately follows from (4·7) that the bounding surface is a tube of constant cross-section. On the other hand, if the λ eigenvalues are the zeroes of $J_0(\lambda)$ (i.e. if $\nu = \infty$), and $B_n = 0$, we should obtain the bounding surface in the form

$$r = 1+\frac{\beta}{A_0}\sum_{n=1}^{\infty}A_nJ_1(\lambda_n)\left(\cos\frac{\lambda_n z}{\beta}-1\right), \tag{4·8}$$

which is the appropriate integral of (4·7). The two flows would have the same inlet distribution of axial velocity with no initial radial velocity; the two different potentials would represent respectively the propagation of that profile in a tube of uniform section and a tube of varying section given by equation (4·8).

In order to calculate the coefficients A_n and B_n we must use certain orthogonality relations. If we assume that the functions $\Theta(r)$ and $\chi(r)$ are expressible as

$$\sum_{n=1}^{\infty}H_nJ_0(\lambda_n r) \quad\text{and}\quad \sum_{n=1}^{\infty}G_nJ_1(\mu_n r),$$

the terms of the series are mutually orthogonal with respect to the weight r in the interval $0 \leqslant r \leqslant 1$, provided that the relations (4·3) and (4·4) hold. We finally obtain

$$H_n = \frac{2}{[\{J_0(\lambda_n)\}^2+\{J_1(\lambda_n)\}^2]}\int_0^1 r\Theta(r)\,J_0(\lambda_n r)\,dr = \frac{2}{\{J_1(\lambda_n)\}^2\left(1+\frac{\lambda_n^2}{\nu^2}\right)}\int_0^1 r\Theta(r)\,J_0(\lambda_n r)\,dr \tag{4·9}$$

and

$$G_n = \frac{2}{\{J_1(\mu_n)\}^2\left(1+\frac{\epsilon^2}{\mu_n^2}+\frac{2\epsilon}{\mu_n^2}\right)}\int_0^1 r\chi(r)\,J_1(\mu_n r)\,dr. \tag{4·10}$$

As example, the radial distribution $g(r) = \nu r$ is expressible as $-\sum_{n=1}^{\infty} B_n \mu_n J_1(\mu_n r)$ in $0 \leqslant r \leqslant 1$, and finally

$$\nu r = \nu(2+\epsilon)\sum_{n=1}^{\infty} \frac{1}{(\epsilon+\frac{1}{2}\epsilon^2+\mu_n^2)}\,\frac{J_1(\mu_n r)}{J_1(\mu_n)}. \tag{4·11}$$

These series are valid only if $r \leqslant 1$. The eigenvalues are not uniformly spaced but for large n tend to the roots of $J_1(\lambda) = 0$ provided that $\nu^{-1} \neq 0$. As ν varies continuously from zero to infinity, the roots of equation (4·3) vary continuously from the zeroes of $J_1(\lambda)$ to the zeroes of $J_0(\lambda)$. The distribution of eigenvalues may be estimated from figure 4. If y is equal to $\lambda J_1(\lambda) + \nu J_0(\lambda)$, it is seen that y is alternately positive and negative at the zeroes of $J_0(\lambda)$, and has the sign of $(-)^n \nu$ at the nth zero of $J_1(\lambda)$, 3·8317 corresponding to $n = 1$. If ν is positive, the roots of (4·3) are interlaced between the zeroes of J_0 and J_1, the first root lying between 2·4048 and 3·8317. If ν is negative the roots again interlace but the first lies between 0 and 2·4048.

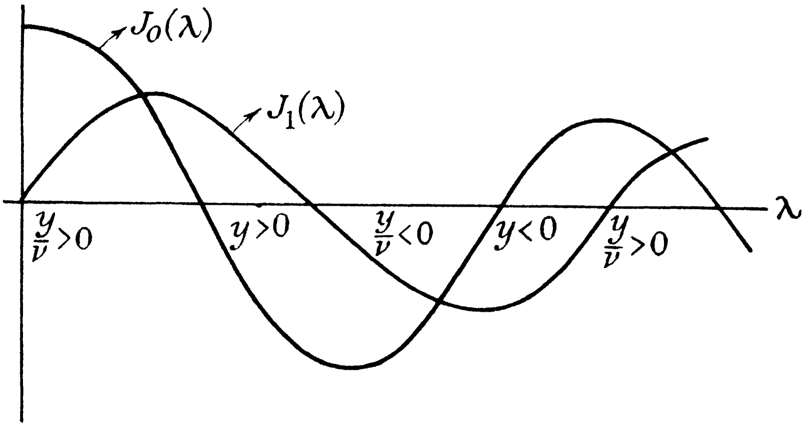

FIGURE 4. Graphs of $J_0(\lambda)$ and $J_1(\lambda)$. $y = \lambda J_1(\lambda) + \nu J_0(\lambda)$.

Other Bessel series exist, one such example being that given by Schlomilch (Whittaker & Watson 1920), in which the eigenvalues are equally spaced; the coefficients are obtained by analogous integral formulae.

5. FLOW THROUGH A UNIFORM TUBE WITH INITIAL PARABOLIC DISTRIBUTION OF AXIAL VELOCITY

In this section $\nu = 0$ and the λ's are the zeroes of $J_1(\lambda)$. This is to ensure that the radial velocity at $r = 1$ is always zero. We shall suppose that the initial axial profile is $U - vr^2$, whilst there is no initial radial velocity. The linearized theory will apply for some distance down the tube, provided that the perturbation velocity, depending on v, is small. If the linearized equation were exact throughout the flow, v would not have to be small, as the mathematical analysis does not depend on this point. The potential representing the motion is

$$\phi = A_0 + \sum_{n=1}^{\infty} A_n \sin\frac{\lambda_n z}{\beta} J_0(\lambda_n r), \tag{5·1}$$

where $$f(r) = U - vr^2 = A_0 + \sum_{n=1}^{\infty} A_n \frac{\lambda_n}{\beta} J_0(\lambda_n r). \tag{5·2}$$

The equations determining the coefficients are

$$\left. \begin{aligned} A_n &= \frac{2\beta}{\lambda_n \{J_0(\lambda_n)\}^2} \int_0^1 r f(r)\, J_0(\lambda_n r)\, dr, \\ A_0 &= 2\int_0^1 r f(r)\, dr, \end{aligned} \right\} \tag{5·3}$$

which reduce to $$A_n = -\frac{4\beta v}{\lambda_n^3 J_0(\lambda_n)}, \quad A_0 = U - \tfrac{1}{2}v. \tag{5·4}$$

Finally, the potential and velocities at any point in the fluid are obtained. It is apparent from simple computations that small radial components of velocity appear and persist, whilst the central axial velocity decreases and the profile tends to become more uniform.

An interesting numerical check on the above formulae is given by the evaluation of the slip velocity at the wall, $r = 1$, $z = 0$. This predicts that $\sum_{n=1}^{\infty} \frac{1}{\lambda_n^2} = \frac{1}{8}$, which is easily verified.

6. FLOW THROUGH THE GENERAL DIFFUSER WITH INITIAL $U - vr^2$ PROFILE

In § 5, the propagation of the wholly axial parabolic profile was discussed using as eigenvalues the zeroes of $J_1(\lambda)$. This corresponds to a value $\nu = 0$ in equation (4·3). In this section we shall use an arbitrary value of ν to discuss the propagation of that profile in a tube of non-uniform section. We now obtain

$$U - vr^2 = A_0 + \sum_{n=1}^{\infty} A_n \frac{\lambda_n}{\beta} J_0(\lambda_n r), \tag{6·1}$$

where $$\lambda_n J_1(\lambda_n) + \nu J_0(\lambda_n) = 0. \tag{6·2}$$

By multiplying equation (6·1) by $rJ_0(\lambda_n r)$ and integrating from 0 to 1 we obtain

$$A_0 + A_n \frac{\lambda_n^2}{2\beta}\left(1 + \frac{\lambda_n^2}{\nu^2}\right) J_1(\lambda_n) = U - v + \frac{4v}{\lambda_n^2} + \frac{2v}{\nu}. \tag{6·3}$$

In addition, the velocity at $\left.\begin{matrix} r = 1 \\ z = 0 \end{matrix}\right\}$ is $U - v$; thus

$$U - v = A_0 + \sum_{n=1}^{\infty} A_n \frac{\lambda_n}{\beta} J_0(\lambda_n). \tag{6·4}$$

The solution of the equations (6·3) and (6·4) is obtained by elimination of the A_n's to give

$$A_0 = U - v + \frac{2}{\nu} \frac{\sum_{n=1}^{\infty}\left(U - v + \frac{4v}{\lambda_n^2} + \frac{2v}{\nu}\right) \Big/ \left(1 + \frac{\lambda_n^2}{\nu^2}\right)}{1 + \frac{2}{\nu}\sum_{n=1}^{\infty}\left(\frac{1}{1 + \lambda_n^2/\nu^2}\right)}. \tag{6·5}$$

Hence when ν is assigned, A_0 and hence A_n may be calculated, and the shape of the nozzle containing the flow is obtained. As a check, if $\nu = 0$, the A_0 of equation (6·5) should reduce to $U - \frac{1}{2}v$. As $\nu \to 0$ in (6·5), A_0 tends to $U - v + 4v \sum_{n=1}^{\infty} \frac{1}{\lambda_n^2}$, which is

$U-\frac{1}{2}v$. At the other extreme, we have $\nu=\infty$, $J_0(\lambda_n)=0$ and $A_0=U-v$. There is continuity in the variable ν throughout, and hence the general flow is intermediary between the flow in a uniform tube and the flow characterized by the value $\nu=\infty$.

If v be replaced by $-v$, we obtain formulae relating to the propagation of a profile with a minimum velocity on the axis in a divergent diffuser.

As a numerical example, the shape of the tubes corresponding to $\nu=0$, 1, and ∞ have been calculated, with an initial velocity profile $U(1-\frac{1}{5}r^2)$. The variation of the cross-sections may be estimated from figure 5, which is drawn to scale.

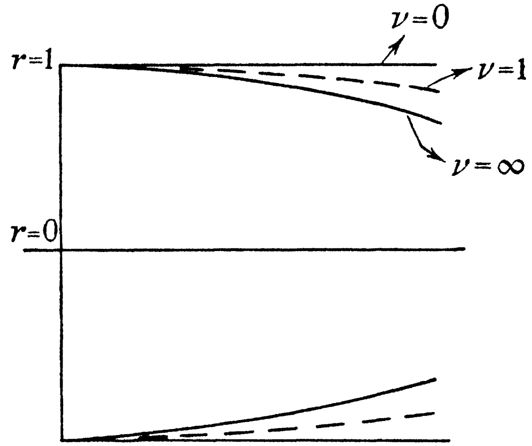

FIGURE 5. Initial $U\left(1-\dfrac{r^2}{5}\right)$ profile propagated in tubes defined by $\nu=0$, 1, ∞.

A few points emerge from the numerical investigation. When v is small (say of the order of 2 or 5% of U), it is almost impossible to detect any departure from constant area of cross-section. The change of velocity along the axis of the tube is quite large however, and reaches a value v in approximately 0·6 of the radius measured along the axis. In the cases quoted above, when $v=\frac{1}{5}U$, the velocity on the axis at $z=0{\cdot}6$ is $0{\cdot}76\,U$, $0{\cdot}78\,U$, and $0{\cdot}8\,U$ when $\nu=0$, 1 and ∞ respectively.

The question arises as to the length of tube in which the solution is valid. Ideally, the linearized solutions are true in the limiting case given by $v=0$, but this presents no problem and is trivial. As v is increased, or as the shape of the tube departs more and more from the uniform, the velocity changes at some distance down the tube will become greater and the theory increasingly inaccurate. The discrepancy can be measured only by comparison with actual measurements or by comparison with results afforded by exact theory, neither of which are at the moment forthcoming.

7. PROPAGATION OF THE $U-vr^m$ PROFILE

If we allow the initially axial profile to assume the form $U-vr^m$, by increasing m we make the profile more uniform in the centre and more sharply decreasing at the wall. The corresponding equation relating the Bessel series is

$$U-vr^m=A_0+\sum_{n=1}^{\infty}A_n\frac{\lambda_n}{\beta}J_0(\lambda_n r), \tag{7·1}$$

which gives, on integrating,

$$U\frac{J_1(\lambda_n)}{\lambda_n} - v\int_0^1 r^{m+1}J_0(\lambda_n r)\,dr = A_0\frac{J_1(\lambda_n)}{\lambda_n} + \frac{A_n\lambda_n}{2\beta}[\{J_0(\lambda_n)\}^2 + \{J_1(\lambda_n)\}^2]. \qquad (7\cdot 2)$$

The integral contained in (7·2) may be estimated from the reduction formula

$$\int_0^1 r^{m+1}J_0(\lambda_n r)\,dr = \frac{J_1(\lambda_n)}{\lambda_n} + \frac{m}{\lambda_n^2}J_0(\lambda_n) - \frac{m^2}{\lambda_n^2}\int_0^1 r^{m-1}J_0(\lambda_n r)\,dr, \qquad (7\cdot 3)$$

and finally, if m is even,

$$\begin{aligned}\int_0^1 r^{m+1}J_0(\lambda_n r)\,dr = {} & \frac{J_1(\lambda_n)}{\lambda_n}\left\{1 - \frac{m^2}{\lambda_n^2} + \frac{m^2(m-2)^2}{\lambda_n^4} - \ldots(-)^{\frac{1}{2}m}\frac{m^2(m-2)^2\ldots2^2}{\lambda_n^m}\right\} \\ & + J_0(\lambda_n)\left\{\frac{m}{\lambda_n^2} - \frac{m^2(m-2)}{\lambda_n^4} + \frac{m^2(m-2)^2(m-4)}{\lambda_n^6}\ldots(-)^{\frac{1}{2}m+1}\frac{m^2(m-2)^2\ldots4^2.2}{\lambda_n^m}\right\}\end{aligned} \qquad (7\cdot 4$$

The coefficients may now be calculated as in § 6 and the potential describing the flow obtained. It will be noted that in all of these formulae obtained in §§ 5, 6 and 7, if $v = 0$, we recover the potential $\phi = Uz$ for uniform flow in a uniform tube, confirming the previous observations that a linearized flow in a non-uniform tube with initially uniform conditions is a rotational flow and cannot be described by a potential.

8. POWER SERIES APPROXIMATIONS FOR FLOWS IN UNIFORM TUBES

The investigation of flows in tubes of uniform section may be carried out in a different way, by use of power series approximations to Bessel functions.

Let us consider a solution of equation (2·2) which is a series of Bessel functions of purely imaginary arguments:

$$\phi = C_0 z + \sum_{n=1}^{p} C_n\left\{z - \frac{\beta I_0(\lambda_n r)}{\lambda_n I_0(\lambda_n)}\sinh\frac{\lambda_n z}{\beta}\right\}. \qquad (8\cdot 1)$$

The advantage of this type of solution is that each term of the series itself represents the propagation of a profile which would be reasonable from the physical point of view. The significance of C_0 is that this is the velocity of slip at $z = 0, r = 1$. The profile at $z = 0$ is

$$\left(\frac{\partial\phi}{\partial z}\right)_{z=0} = C_0 + \sum_{n=1}^{p} C_n\left\{1 - \frac{I_0(\lambda_n r)}{I_0(\lambda_n)}\right\} = C_0 + \sum_{n=1}^{p} C_n\,\omega_n. \qquad (8\cdot 2)$$

The form of the functions ω_n is shown in figure 6. The axial profile at the inlet is thus a linear combination of these functions.

The boundary condition is that the wall is a streamline and therefore

$$\left(\frac{\partial\phi}{\partial r}\right)_{r=1} = 0. \qquad (8\cdot 3)$$

This implies that

$$\sum_{n=1}^{p} C_n \sinh\frac{\lambda_n z}{\beta}\frac{I_1(\lambda_n)}{I_0(\lambda_n)} = 0 \qquad (8\cdot 4)$$

for all positive z. Equation (8·4) cannot be satisfied identically, but values for the C_n's may be chosen to satisfy this approximately. Since

$$\sinh\frac{\lambda z}{\beta} = \sum_{k=1}^{\infty}\left(\frac{\lambda z}{\beta}\right)^{2k-1}\Big/(2k-1)!,$$

we approximate to equation (8·4) by finding C_n's to satisfy the equations

$$\sum_{n=1}^{p} C_n\lambda_n\frac{I_1(\lambda_n)}{I_0(\lambda_n)} = \sum_{n=1}^{p} C_n\lambda_n^3\frac{I_1(\lambda_n)}{I_0(\lambda_n)} = \dots = \sum_{n=1}^{p} C_n\lambda_n^{2p-3}\frac{I_1(\lambda_n)}{I_0(\lambda_n)}. \tag{8·5}$$

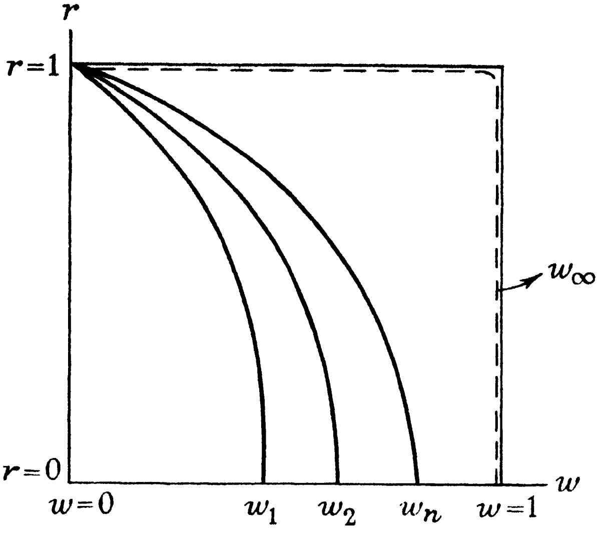

FIGURE 6

The solution of this set of equations is

$$\frac{C_q}{C_1} = (-)^{q+1}\frac{\lambda_1}{\lambda_q}\frac{I_1(\lambda_1)\,I_0(\lambda_q)}{I_0(\lambda_1)\,I_1(\lambda_q)}\frac{\prod_{r=2}^{p}(\lambda_r^2-\lambda_1^2)}{\prod_{r=1}^{q-1}(\lambda_q^2-\lambda_r^2)\prod_{r=q+1}^{p}(\lambda_r^2-\lambda_q^2)}. \tag{8·6}$$

As in § 4, different sequences of λ's represent different flows, but all these flows are confined to the tube of uniform section. A numerical example follows in which, in order to effect considerable reduction in computation, the nth eigenvalue is taken to be $n\pi$. This introduces an analogy with the series of Schlomilch mentioned in § 4.

In this case

$$\frac{C_q}{C_1} = (-)^{q+1}\frac{q(p-1)!\,(p+1)!}{(p-q)!\,(p+q)!}\frac{I_0(q\pi)\,I_1(\pi)}{I_1(q\pi)\,I_0(\pi)} = (-)^{q+1}f_{q,p}\frac{I_0(q\pi)\,I_1(\pi)}{I_1(q\pi)\,I_0(\pi)}. \tag{8·7}$$

Since the axial velocity at $\left.\begin{matrix} z=0 \\ r=0 \end{matrix}\right\}$ is U we may finally calculate the C's explicitly:

$$C_1 = (U-C_0)\frac{I_1(\pi)}{I_0(\pi)}\left\{\sum_{q=1}^{p}(-)^{q+1}f_{q,p}\frac{I_0(q\pi)}{I_1(q\pi)}\left(1-\frac{1}{I_0(q\pi)}\right)^{-1}\right\}. \tag{8·8}$$

The solution is finally obtained in terms of C_0, which remains to be specified. If $p = 10$, table 1 results.

TABLE 1

q	1	2	3	4	5
$\left(\dfrac{C_q}{U-C_0}\right)$	5·5361	−7·4294	6·6482	−4·3668	2·1652
q	6	7	8	9	10
$\left(\dfrac{C_q}{U-C_0}\right)$	−0·8075	0·2206	−0·0418	0·0050	−0·0005

and the velocity profile at $z = 0$ is given by

$$\left(\frac{\partial\phi}{\partial z}\right)_{z=0} = C_0 + (U - C_0)\{5{\cdot}5361\,\omega_1 - 7{\cdot}4294\,\omega_2 + \ldots\}. \tag{8·9}$$

We have thus derived a non-trivial potential which (*a*) satisfies the appropriate differential equation, (*b*) contains coefficients chosen from table 1 to give no radial velocity at $r = 1$, within the limits of approximation and (*c*) represents a flow which is plausible from the practical view-point.

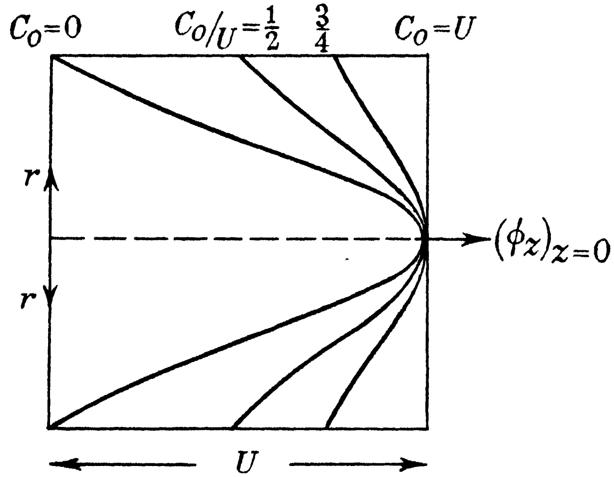

FIGURE 7

Figure 7 gives an indication of the form of the profile which the above numerical example suggests.

It again appears from computation that in the propagation of this profile (which is very similar to the parabolic one discussed previously) the axial velocity rapidly becomes constant over sections at right angles to the axis, while small radial components of velocity appear. These results were anticipated in § 5 by very different methods of approach.

The author would like to express his thanks to Professor L. Rosenhead for valuable advice and criticism throughout the work, and to Dr C. W. Jones for reading and commenting on the paper. He is also very grateful to the Royal Society referee for very valuable comments given whilst reviewing the paper. During the investigation the author was in receipt of a grant from the Department of Scientific and Industrial Research.

REFERENCES

Green, J. R. & Southwell, R. V. 1944 *Phil. Trans.* A, **239**, 367.
Hadamard, J. 1903 *Leçons sur la propagation des ondes*, p. 158. Paris: Hermann.
Karman, T. & Moore, N. B. 1932 *Trans. Amer. Soc. Mech. Engrs*, 54, A.P.M. 27.
Murnaghan, F. D. and others. 1945 *Bumblebee Report*, no. 26. Johns Hopkins University, U.S.A.
Squire, H. B. 1947 *Rep. Roy. Air. Est., Farnborough*, no. 2216.
Tupper, S. J. 1945 *Rep. Brit. Aero. Res. Coun., Lond.*, no. 8576.
Ward, G. N. 1945 *Rep. Brit. Aero. Res. Coun., Lond.*, no. 9205.
Whittaker, E. T. & Watson, G. N. 1920 *Modern analysis*, p. 377. Cambridge: University Press.

On the formulation of rheological equations of state

BY J. G. OLDROYD, *Courtaulds Limited, Research Laboratory, Maidenhead, Berks.*

(*Communicated by A. H. Wilson, F.R.S.—Received* 26 *July* 1949—
Revised 4 *November* 1949)

The invariant forms of rheological equations of state for a homogeneous continuum, suitable for application to all conditions of motion and stress, are discussed. The right invariance properties can most readily be recognized if the frame of reference is a co-ordinate system convected with the material, but it is necessary to transform to a fixed frame of reference in order to solve the equations of state simultaneously with the equations of continuity and of motion. An illustration is given of the process of formulating equations of state suitable for universal application, based on non-invariant equations obtained from a simple experiment or structural theory. Anisotropic materials, and materials whose properties depend on previous rheological history, are included within the scope of the paper.

1. INTRODUCTION

In the present paper some aspects of the theory of deformation and flow of a homogeneous continuous material are treated generally. It is assumed that the properties of a material element may depend upon the previous rheological states through which that element has passed, but not in any way on the states of neighbouring elements and not on the motion of the element as a whole in space. A theory of rheological phenomena can then be built up in two stages. First, it is necessary to specify the rheological properties of an arbitrary element of the material by means of a set of *rheological equations of state*. The second stage is the prediction of the behaviour of the material in bulk, when subjected to different initial and boundary conditions, body forces, etc., by making use of the equations of state, the stress equations of motion, and the equation of continuity; if the temperature is unknown, equations of heat transfer are also involved. All the equations other than the equations of state can be written in forms which do not depend on the rheological properties of the particular material considered. Thus, the familiar equations of motion and continuity,

$$p^{ki}{}_{,k} + \rho F^i = \rho \dot{v}^i, \qquad (1)^*$$

and

$$\dot{\rho} + \rho v^i{}_{,i} = 0, \qquad (2)$$

relating the tensor components of stress p^{ki}, body force F^i, velocity v^i and density ρ, apply to all materials.

Idealized materials whose rheological properties have been discussed in detail, notably the Hookean elastic solid and the incompressible viscous liquid of constant viscosity μ, are characterized by equations of state of a simple form. For example, the Newtonian liquid is specified by

$$e^{(1)i}_{i} = 0, \quad p_{ik} - \tfrac{1}{3}p^m_m g_{ik} = 2\mu e^{(1)}_{ik}, \qquad (3)$$

where g_{ik} is the metric tensor and

$$e^{(1)}_{ik} \equiv \tfrac{1}{2}(v_{k,i} + v_{i,k}) \qquad (4)$$

is the rate-of-strain tensor. But, in general, simple relationships connecting the familiar stress, strain and rate-of-strain tensors of the classical theories of elasticity and hydrodynamics will not suffice to describe the rheological properties of a material completely. In the most general case contemplated, the equations of state defining the properties of an element at any instant may involve all the kinematic and dynamic quantities which define the states of the same element during its previous history. On the other hand, experiments designed to measure the rheological properties of particular materials must, for easy interpretation, relate to simple types of motion, and the resulting simple equations of state will require generalization before they can be applied to more complicated types of motion. There may be many ways of generalizing the results of a single experiment, and the method of generalization so as to give a universally valid form of the equations of state is by no means obvious. The form of the completely general equations must be restricted by the requirement that the equations describe properties independent of the frame of reference. It is the object of the present paper to investigate the possible types of functional relation between kinematic and dynamic quantities associated with the material which could define the properties of a homogeneous continuum completely.

Equations of state must be considered as equations defining the properties of an arbitrary material element, *moving as part of a continuum*. The quantities which may be involved in the equations are then quantities associated with that particular element over a period of time during which the element has moved and has been deformed continuously in an arbitrary manner. Since they necessarily represent physical concepts with a significance independent of any particular co-ordinate system, they may be regarded as three-dimensional tensors. *Moreover, only those tensor quantities need be considered which have a significance for the material element independent of its motion as a whole in space.* In order to specify these quantities in the general case, it is not at first convenient to use a frame of reference fixed in space, but a convected co-ordinate system of the type first envisaged by Hencky (1925). The co-ordinate surfaces ξ^i = constant are chosen as surfaces drawn in the material and deforming continuously with it, and the ξ^i's and the time t are taken as the independent variables. In the formal expression of rheological properties, it will in general be necessary to add quantities associated with the same material at different times, i.e. quantities associated with different points in space. *The device of representing all tensor quantities associated with the material by their convected-components (i.e. the components referred to a convected system of reference) allows similar quantities associated with the same material at different times to be added, component by component, to give a similar tensor quantity as the sum.*

---

* Covariant suffixes are written below, contravariant suffixes above, and the usual convention of summation over the values 1, 2, 3 applies to repeated small Latin suffixes. A suffix i following a comma indicates covariant differentiation with respect to a space co-ordinate x^i, and the Newtonian dot denotes intrinsic differentiation with respect to the time t.

For the purpose of discussing the flow of material in bulk, it will be necessary to express the equations of state finally in terms of the same kinematic and dynamic variables as are used to express the equations of motion and continuity and the boundary conditions, so that all the associated equations can be solved simultaneously. The question of changing the dependent variables and recasting the equations of state in terms of the fixed-components of tensor fields associated with the material (i.e. the components referred to a co-ordinate system fixed in space) must therefore be discussed, when it has been established what form these equations can take. This aspect of the problem is treated in § 3.

2. EQUATIONS OF STATE REFERRED TO A CONVECTED CO-ORDINATE SYSTEM

The equations* $\xi'^i = \xi'^i(\xi)$ relating two sets of convected co-ordinates ξ^i and ξ'^i do not involve the time explicitly. Therefore the general transformation law for tensor components is independent of the time, so long as all co-ordinates are understood to be convected co-ordinates in relation to a given continuum. Hence the convected-components of tensors associated with the same point *of the material* can be manipulated in the same way as the fixed-components of tensors at a point fixed in space, and the usual rules of tensor calculus apply with the exception of those which are affected by the metric tensor being a function of the time explicitly. This means simply that the operations of differentiation and integration with respect to time do not commute with the operation of raising or lowering a suffix, or with the operation of covariant or contravariant differentiation with respect to a space co-ordinate, although they do commute with that of contracting a pair of suffixes and that of partial differentiation with respect to a space co-ordinate. In order to avoid confusion of notation later, the symbol D/Dt will always be used to denote a partial differentiation with respect to time holding convected co-ordinates constant.

It is now possible to enumerate the quantities which may be involved in the equations of state for the material at ξ^i at any instant t. Excluding as irrelevant all quantities which refer to absolute motion in space, the only kinematic quantities involved are those which define the relative distances and the relative motion of the parts of the arbitrary element at ξ^i. A knowledge of the distance ds between an arbitrary pair of neighbouring particles at ξ^i and $\xi^i + d\xi^i$ at every instant $t' \leqslant t$ constitutes complete information about the internal kinematics of the element during its previous history, and the metric tensor γ_{jl} gives all the required information, since

---

* ξ is used as an abbreviation for ξ^1, ξ^2 ξ^3.

$$[ds(t')]^2 = \gamma_{jl}(\xi, t')\,d\xi^j d\xi^l. \tag{5}$$

Therefore all kinematic quantities in the equations of state must be derivable from the tensor function $\gamma_{jl}(\xi, t')$ $(t' \leqslant t)$.

The dynamic quantities involved are those which measure surface forces on an arbitrary element at ξ^j, since body forces on an infinitesimal element are of a smaller order of magnitude. Although there are several ways of representing the forces across an arbitrary surface element as the components of a tensor (Brillouin 1925), all forms of stress tensor are derivable from each other by simple operations defined in terms of the metric tensor and universally constant tensors. The symmetric second-order covariant absolute tensor π_{jl}, which is completely determined by the equality of its orthogonal-Cartesian components with those of the usual Cartesian stress tensor (Jeffreys 1931), will usually be referred to as the stress tensor, and all other forms considered as derived tensors. All dynamic quantities associated with the arbitrary element at ξ^j are therefore expressible in terms of the functions $\pi_{jl}(\xi, t')$ and $\gamma_{jl}(\xi, t')$ $(t' \leqslant t)$.

It follows that the equations of state are essentially relationships between the six independent functions of the time $\gamma_{jl}(\xi, t')$ and the six independent functions $\pi_{jl}(\xi, t')$. If the stresses on an element at all times are given, the equations must be sufficient in number to determine the deformation of the element at all times; six independent equations of state are therefore needed. They will involve, incidentally, physical constants associated with the material, and possibly also the time-lag $t - t'$ explicitly (cf. equations (54) to (56)). Since rheological properties will in general depend on the temperature, it is necessary to introduce explicitly, as a variable in the equations of state, the temperature $T(\xi, t')$ of the material during its history, in order to reserve the term physical constant for strictly constant tensors

$$\kappa_{N\cdot j\cdot\cdot\cdot}^{\cdot\cdot l\cdot\cdot\cdot}(\xi) \quad (N = 1, 2, 3, \ldots)$$

associated with the material at ξ^j, i.e. certain quantities satisfying

$$D\kappa_{N\cdot j\cdot\cdot\cdot}^{\cdot\cdot l\cdot\cdot\cdot}/Dt' = 0. \tag{6}$$

The operations of differentiation (D/Dt') and integration with respect to time may occur in the equations of state, because these operations introduce no dependence on any (fixed or convected) co-ordinate system. But no space derivatives may occur, since these would introduce implicitly a dependence on the states of neighbouring elements of the material.

Hence, in their general form, the equations of state for a homogeneous continuum can be written as an invariant set of integro-differential equations (cf. Volterra 1909), *of which six are independent, relating the following functions of the time:*

$$\gamma_{jl}(\xi, t'), \quad \pi_{jl}(\xi, t'), \quad T(\xi, t'), \quad \kappa_{N\cdot j\cdot\cdot\cdot}^{\cdot\cdot l\cdot\cdot\cdot}(\xi) \quad (N = 1, 2, 3, \ldots;\ t' \leqslant t); \tag{7}$$

the ξ^j's occur as three independent parameters in the equations. In simple cases, the equations can be reduced to differential equations by the processes of rearrangement and differentiation. For example, the equations

$$D\gamma/Dt = 0, \quad \pi_{jl} - \tfrac{1}{3}\pi^n_n\gamma_{jl} = \mu D\gamma_{jl}/Dt, \tag{8}$$

where γ is the determinant of the metric tensor, are ten differential equations relating $\gamma_{jl}(\xi, t)$ and $\pi_{jl}(\xi, t)$, of which six are independent; they are the equations of state for an incompressible viscous liquid of constant viscosity μ.

The above general result has been derived without making full use of the postulate of homogeneity, and without distinguishing between elastic solids, plastic solids and fluid materials. Homogeneity implies that the relations between physical constants at different points of the material are known. If the material is inherently anisotropic,* i.e. not all physical constants are combinations of scalar constants and universally constant tensors, it suffices to know the values of the anisotropic constants at some particular instant t_0. The constants at all other times can then be obtained from (6). If it may be assumed that at a time t_0 all elements of the material are similarly oriented in space so far as their physical properties are concerned, the physical constants satisfy

$$\kappa_{N}{}^{\cdot}{}_{\cdot}{}^{\cdot}{}_{j}{}^{l\cdots}{}_{\cdots, n} = 0 \quad (t = t_0). \tag{9}$$

If the convected co-ordinate system is chosen to be Cartesian at such a time t_0 we can write

$$\partial \kappa_{N}{}^{\cdot}{}_{\cdot}{}^{\cdot}{}_{j}{}^{l\cdots}{}_{\cdots} / \partial \xi^n = 0 \quad (t = t_0). \tag{10}$$

Then, from (6), the individual components $\kappa_{N}{}^{\cdot}{}_{\cdot}{}_{j}{}^{l\cdots}{}_{\cdots}$ are, by the special choice of the co-ordinate system, made simple constants for the whole material.

The basic form of the equations of state will vary with different classes of material, according to the degree to which an initial configuration may be supposed to have a lasting significance during any subsequent motion. For example, in an elastic solid,† the whole configuration at an initial instant t_0 may be supposed to have a permanent significance for the material, namely that it will eventually be regained if the initial temperatures and stresses are restored (and subsequently maintained) at any later time. In such a material, the initial-metric tensor $\gamma_{jl}(\xi, t_0)$, the initial-stress tensor $\pi_{jl}(\xi, t_0)$ and the initial temperature $T(\xi, t_0)$ can occur explicitly in the equations of state. If, as in many materials, there is only an equilibrium volume with a permanent significance, which may be taken as an initial volume at some instant t_0, only the determinant $\gamma(\xi, t_0)$ of the initial-metric tensor can occur explicitly. In the equations of state for any material, the only times which can occur explicitly when all integrations have been performed are the current time t and, in so far as the configuration at some such time may be supposed to have a permanent significance, a special reference time t_0. In the case of an elastic solid it will not be necessary to consider the history previous to t_0, and t_0 will be the lower limit in any integrations which occur.

It is useful for easy reference to name some of the kinematic tensors which must occur frequently in equations of state. When the configuration at a time t_0 has a permanent significance, the tensor whose components are

$$\eta_{jl}(\xi, t, t_0) \equiv \tfrac{1}{2}[\gamma_{jl}(\xi, t) - \gamma_{jl}(\xi, t_0)] \tag{11}$$

---

* An isotropic material may behave anisotropically in a deformed or flowing state, but such behaviour must be predictable from the equations of state without introducing anisotropic physical constants.

† This term is used in its widest sense, including solids which show a delayed response to applied stresses.

is the *strain tensor* at time t. In any material, the tensor defined by (11), where t_0 is an arbitrarily chosen fixed time, can be called the *relative-strain tensor* at time t. The *rate-of-strain tensor* at time t has components

$$\eta^{(1)}_{jl}(\xi, t) \equiv D\eta_{jl}(\xi, t, t_0)/Dt \equiv \tfrac{1}{2}D\gamma_{jl}(\xi, t)/Dt, \tag{12}$$

and, generalizing,

$$\eta^{(N)}_{jl} \equiv D^N\eta_{jl}/Dt^N \equiv \tfrac{1}{2}D^N\gamma_{jl}/Dt^N \quad (N = 1, 2, 3, \ldots) \tag{13}$$

defines the *Nth rate-of-strain tensor*. The immediate physical significance of these tensors is apparent from (5), which implies that

$$[ds(t)]^2 - [ds(t_0)]^2 = 2\eta_{jl}\,d\xi^j\,d\xi^l, \quad \frac{d^N[ds(t)]^2}{dt^N} = 2\eta^{(N)}_{jl}\,d\xi^j\,d\xi^l. \tag{14}$$

The (*relative-*) *dilatation* Δ in relation to the configuration at a fixed time t_0 can be defined by

$$\Delta(\xi, t, t_0) \equiv \tfrac{1}{2}\log\,[\gamma(\xi, t)/\gamma(\xi, t_0)], \tag{15}$$

and it is noted that

$$\frac{D\gamma}{Dt} = 2\gamma\eta^{(1)j}_{j}, \quad \frac{D\Delta}{Dt} = \eta^{(1)j}_{j}. \tag{16}$$

3. TRANSFORMATION TO A FIXED CO-ORDINATE SYSTEM

In any specific flow problem, the equations of state are to be solved simultaneously with the equations of motion and continuity for certain kinematic and dynamic quantities which are to be determined as functions of position and time. It is easy to express all the unknown dynamic variables in these equations in terms of the components of a varying stress tensor field $\pi_{jl}(\xi, t')$; these components are independent except for the symmetry relations $\pi_{jl} = \pi_{lj}$. But the convected-components of the metric tensor field $\gamma_{jl}(\xi, t')$ are unsuitable as the dependent kinematic variables. First, they are not mutually independent, since the associated Riemann-Christoffel tensor must vanish identically. Secondly, the kinematic quantities associated with motion of the material as a whole in space, which necessarily occur in the equations of motion and in the boundary conditions, cannot be expressed in terms of the metric tensor alone. It is therefore necessary to express all kinematic variables in the equations in terms of some kind of displacement function, and to regard three components of displacement—or, in special cases when the displacement itself is not required, the derived components of velocity—as the dependent kinematic variables. Further, because of the references to position in space which are usually introduced in expressing boundary conditions, it is desirable at this stage to express all the equations in terms of tensor quantities referred to an arbitrarily chosen fixed co-ordinate system x^i.

In general, the convected- and fixed-components of the same tensor will be denoted by corresponding Greek and Latin letters; but it is unnecessary to introduce two notations for absolute scalars such as T and Δ. Fixed-components are regarded as functions of fixed co-ordinates x^i and the time t as independent variables, and partial differentiation with respect to time, holding fixed co-ordinates constant, is denoted by $\partial/\partial t$. Tensors associated with a single instant t may be transformed from a convected to a fixed system of reference by the usual transformation law:

$$\beta_{\cdot j \cdots}^{\cdot\, l \cdots}(\xi, t) = \left\| \frac{\partial x}{\partial \xi} \right\|^{W} \Pi\left(\frac{\partial x^i}{\partial \xi^j}\right) \Pi'\left(\frac{\partial \xi^l}{\partial x^k}\right) b_{\cdot i \cdots}^{\cdot\, k \cdots}(x, t), \tag{17}$$

where Π (Π') denotes a product of all similar terms, one for each covariant (contravariant) suffix, W is the weight of the tensor and $\| \partial x/\partial \xi \|$ denotes the Jacobian determinant of the co-ordinate transformation. The fixed-components of the metric tensor are, of course, known functions of position $g_{ik}(x)$. The fixed-components of the varying stress tensor field $p_{ik}(x, t)$ are taken as the dependent dynamic variables.

Displacement functions suitable for use as the dependent kinematic variables can be defined in the following way. If at any time t the material whose convected coordinates are ξ^j has fixed-components x^i, the functional relationships

$$x^i = x^i(\xi, t), \quad \text{or} \quad \xi^j = \xi^j(x, t), \tag{18}$$

give complete information about the kinematics of the whole continuum. The material which is at x^i at time t is therefore at a position $x'^i = x^i(\xi, t')$, where $\xi^j = \xi^j(x, t)$, at any other time t'. Hence we can write

$$x'^i = x'^i(x, t, t'), \tag{19}$$

and these three functions of the x^i's, t and t' serve the purpose of displacement functions. The velocity vector is defined by

$$v^i(x, t) \equiv Dx^i/Dt, \tag{20}$$

and can be expressed explicitly in terms of the displacement functions by solving the three equations

$$0 = \frac{Dx'^i}{Dt} = \frac{\partial x'^i}{\partial t} + \frac{\partial x'^i}{\partial x^k} v^k, \tag{21}$$

in which t' takes any constant value. The intrinsic derivatives

$$\dot{\rho} = \partial\rho/\partial t + v^i \rho_{,i}, \quad \dot{v}^i = \partial v^i/\partial t + v^k v^i_{\ ,k}, \tag{22}$$

which occur in equations (1) and (2) are therefore also expressible in terms of the displacement functions.

If the equations of state were algebraic relations connecting functions of a single instant t, they could be transformed to a fixed reference system simply by replacing all convected-components at ξ^j by fixed-components of the same tensor at $x^i(\xi, t)$. But the operations of differentiation with respect to time, addition of quantities associated with different times, and integration with respect to time, require the introduction of new transformation rules. These rules, which are discussed separately below, involve the displacement functions. In general, therefore, the transformed equations of state will take the form of functional relationships, involving differentiations and integrations, between the stress tensor components $p_{ik}(x, t)$, the temperature $T(x, t)$, physical constants $k_{N\cdot i \cdots}^{\ \ \cdot\, m \cdots}$ and the displacement functions (19). The equations of state, the equations of motion and the equation of continuity are then ten simultaneous equations for the functions $p_{ik}(x,t)$, $x'^i(x,t,t')$ and $\rho(x,t)$, the temperature distribution being here regarded as known. Because of the form of equations (1) and (2), a considerable simplification will result if the equations of state can be expressed in terms of the velocity vector field, without involving the displacement functions explicitly.

(a) *Convected differentiation with respect to time*

Differential equations of state, in which all quantities are associated with the current time t, are transformable to a fixed co-ordinate system if the law of transformation for the time derivative $D\beta^{\cdot\, l \cdots}_{\cdot j \cdots}(\xi,t)/Dt$ of any tensor $\beta^{\cdot\, l \cdots}_{\cdot j \cdots}(\xi,t)$ is known. This is provided by the following theorem. *The tensor whose convected-components are* $D\beta^{\cdot\, l \cdots}_{\cdot j \cdots}/Dt$ *has fixed-components*

$$\frac{\mathfrak{d} b^{\cdot\, k \cdots}_{\cdot i \cdots}}{\mathfrak{d} t} \equiv \frac{\partial b^{\cdot\, k \cdots}_{\cdot i \cdots}}{\partial t} + v^m \frac{\partial b^{\cdot\, k \cdots}_{\cdot i \cdots}}{\partial x^m} + \Sigma \frac{\partial v^m}{\partial x^i} b^{\cdot\, k \cdots}_{\cdot m \cdots} - \Sigma' \frac{\partial v^k}{\partial x^m} b^{\cdot\, m \cdots}_{\cdot i \cdots} + W \frac{\partial v^m}{\partial x^m} b^{\cdot\, k \cdots}_{\cdot i \cdots}, \tag{23}$$

or, what is equivalent,

$$\frac{\mathfrak{d} b^{\cdot\, k \cdots}_{\cdot i \cdots}}{\mathfrak{d} t} \equiv \frac{\partial b^{\cdot\, k \cdots}_{\cdot i \cdots}}{\partial t} + v^m b^{\cdot\, k \cdots}_{\cdot i \cdots, m} + \Sigma v^m_{,i} b^{\cdot\, k \cdots}_{\cdot m \cdots} - \Sigma' v^k_{,m} b^{\cdot\, m \cdots}_{\cdot i \cdots} + W v^m_{,m} b^{\cdot\, k \cdots}_{\cdot i \cdots}, \tag{24}$$

where Σ (Σ') *denotes a sum of all similar terms, one for each covariant (contravariant) suffix.*

The proof is as follows. The transformation law (17) is first written in the form

$$\Pi'\left(\frac{\partial x^k}{\partial \xi^l}\right) \beta^{\cdot\, l \cdots}_{\cdot j \cdots} = \left\| \frac{\partial x}{\partial \xi} \right\|^W \Pi\left(\frac{\partial x^i}{\partial \xi^j}\right) b^{\cdot\, k \cdots}_{\cdot i \cdots}. \tag{25}$$

In operating on both sides of (25) with D/Dt, we put

$$\frac{D}{Dt}\frac{\partial x^i}{\partial \xi^j} = \frac{\partial}{\partial \xi^j}\frac{Dx^i}{Dt} = \frac{\partial v^i}{\partial \xi^j}, \tag{26}$$

and hence also

$$\frac{D}{Dt}\left\| \frac{\partial x}{\partial \xi} \right\| = \left\| \frac{\partial x}{\partial \xi} \right\| \frac{\partial v^i}{\partial x^i}. \tag{27}$$

The differentiated equation then reduces to

$$\begin{aligned} \Pi'\left(\frac{\partial x^k}{\partial \xi^l}\right) \frac{D\beta^{\cdot\, l \cdot q \cdots}_{\cdot j \cdot n \cdots}}{Dt} &+ \Sigma' \frac{\partial v^k}{\partial \xi^l} \cdots \frac{\partial x^p}{\partial \xi^q} \cdots \beta^{\cdot\, l \cdot q \cdot}_{\cdot j \cdot n \cdots} \\ &= \left\| \frac{\partial x}{\partial \xi} \right\|^W \left\{ \Pi\left(\frac{\partial x^i}{\partial \xi^j}\right) \left[\frac{\partial b^{\cdot\, k \cdot p \cdots}_{\cdot i \cdot m \cdots}}{\partial t} + v^r \frac{\partial b^{\cdot\, k \cdot p \cdots}_{\cdot i \cdot m \cdots}}{\partial x^r} \right] \right. \\ &\qquad \left. + \Sigma \frac{\partial v^i}{\partial \xi^j} \cdots \frac{\partial x^m}{\partial \xi^n} \cdots b^{\cdot\, k \cdot p \cdots}_{\cdot i \cdot m \cdots} + W \frac{\partial v^r}{\partial x^r} \Pi\left(\frac{\partial x^i}{\partial \xi^j}\right) b^{\cdot\, k \cdot p \cdots}_{\cdot i \cdot m \cdots} \right\}. \end{aligned} \tag{28}$$

This equation holds whatever system of convected co-ordinates ξ^j may have been chosen, and a special choice of convected system is now made, namely that for which the co-ordinate surfaces ξ^j = constant coincide with the surfaces x^i = constant (so that $\xi^j = x^j$ everywhere) at the instant t under consideration. We may then write

$$\frac{\partial x^i}{\partial \xi^j} = \delta^i_j, \quad \beta^{\cdot\,l\cdots}_{\cdot j\cdots} = b^{\cdot\,l\cdots}_{\cdot j\cdots}, \quad \frac{D\beta^{\cdot\,l\cdots}_{\cdot j\cdots}}{Dt} = \frac{\mathfrak{d}b^{\cdot\,l\cdots}_{\cdot j\cdots}}{\mathfrak{d}t}, \tag{29*}$$

after differentiation at the instant t, using the same suffixes in fixed and convected co-ordinate systems, and equation (28) simplifies to give the general formula (23). The tensor nature of $\mathfrak{d}b^{\cdot\,k\cdots}_{\cdot i\cdots}/\mathfrak{d}t$ is not immediately apparent from (23), but becomes so when this is written in terms of the covariant space derivatives defined by

$$b^{\cdot\,k\cdots}_{\cdot i\cdots,m} \equiv \frac{\partial b^{\cdot\,k\cdots}_{\cdot i\cdots}}{\partial x^m} - \Sigma\left\{{p \atop im}\right\} b^{\cdot\,k\cdots}_{\cdot p\cdots} + \Sigma'\left\{{k \atop pm}\right\} b^{\cdot\,p\cdots}_{\cdot i\cdots} - W\left\{{p \atop pm}\right\} b^{\cdot\,k\cdots}_{\cdot i\cdots}, \tag{30}$$

and

$$v^k_{;m} \equiv \frac{\partial v^k}{\partial x^m} + \left\{{k \atop pm}\right\} v^p. \tag{31}$$

(The Christoffel three-index symbols of the second kind $\left\{{i \atop km}\right\}$ are defined in terms of the metric tensor $g_{ik}(x)$ in the usual way.) When the partial space derivatives are eliminated between equations (23), (30) and (31), the terms involving Christoffel symbols vanish identically. We are left with the formula (24) in which every term is manifestly a tensor of the same kind as $b^{\cdot\,k\cdots}_{\cdot i\cdots}$.

It is the operator of convected differentiation $\mathfrak{d}/\mathfrak{d}t$, *defined by* (23) *or* (24), *which must everywhere replace* D/Dt *when equations of state are transformed from a convected to a fixed system of reference.* The physical significance of the operation of convected differentiation with respect to time, applied to a tensor intrinsically associated with the material of a moving continuum, is that it is a kind of total differentiation following a material element which introduces no dependence on a fixed frame of reference or on the way the material is moving in space. The convected derivative of an absolute scalar is seen to be identical with the intrinsic derivative.

Applying (24) repeatedly to the metric tensor, we find the following formulae for the fixed-components of the rate-of-strain tensors $e^{(N)}_{ik}(x,t) \equiv \frac{1}{2}\mathfrak{d}^N g_{ik}(x)/\mathfrak{d}t^N$:

$$e^{(1)}_{ik} = \tfrac{1}{2}(v^m_{,i}\, g_{mk} + v^m_{,k}\, g_{im}) = \tfrac{1}{2}(v_{k,i} + v_{i,k}), \tag{32}$$

$$e^{(2)}_{ik} = \frac{1}{2}\left(\frac{\partial v_{k,i}}{\partial t} + \frac{\partial v_{i,k}}{\partial t} + v^m v_{k,im} + v^m v_{i,km} + v^m_{,i}\, v_{k,m} + 2v^m_{,i}\, v_{m,k} + v_{i,m}\, v^m_{,k}\right), \tag{33}$$

and so on. It is worthy of note that (32) is the usual formula for the (first) rate-of-strain tensor components in terms of the velocity distribution. The physical significance of the $e^{(N)}_{ik}$'s is made apparent by rewriting the second equation (14) as

$$d^N(ds)^2/dt^N = 2e^{(N)}_{ik}\, dx^i\, dx^k, \tag{34}$$

where ds is now the distance between the two particles which are at x^i and $x^i + dx^i$ at the instant t. We require the formulae

$$\frac{1}{2g}\frac{\mathfrak{d}g}{\mathfrak{d}t} = \frac{\mathfrak{d}\Delta}{\mathfrak{d}t} = e^{(1)i}_{i} = v^i_{,i} \tag{35}$$

(obtained by transforming (16)) and

$$\mathfrak{d}g^{ik}/\mathfrak{d}t = -2e^{(1)ik} \tag{36}$$

---

* δ^i_j denotes a Kronecker delta, a component of the substitution tensor.

(obtained by applying (24) to the contravariant metric tensor directly). The following commutation relations can then be deduced by applying the usual rule for differentiating a product:

$$\frac{\mathfrak{d}b^{\cdot\cdot\cdots}_{\cdot im\cdots}}{\mathfrak{d}t}-g_{km}\frac{\mathfrak{d}b^{\cdot\cdot k\cdots}_{\cdot i\cdots}}{\mathfrak{d}t} = 2e^{(1)}_{km}b^{\cdot\cdot k\cdots}_{\cdot i\cdots}, \tag{37}$$

$$\frac{\mathfrak{d}b^{\cdot mk\cdots}_{\cdots}}{\mathfrak{d}t}-g^{im}\frac{\mathfrak{d}b^{\cdot\cdot k\cdots}_{\cdot i\cdots}}{\mathfrak{d}t} = -2e^{(1)im}b^{\cdot\cdot k\cdots}_{\cdot i\cdots}, \tag{38}$$

$$\frac{\mathfrak{d}(g^{M}b^{\cdot\cdot k\cdots}_{\cdot i\cdots})}{\mathfrak{d}t}-g^{M}\frac{\mathfrak{d}b^{\cdot\cdot k\cdots}_{\cdot i\cdots}}{\mathfrak{d}t} = 2Mg^{M}e^{(1)m}_{m}b^{\cdot\cdot k\cdots}_{\cdot i\cdots}. \tag{39}$$

As an illustration, it is observed that the differential equations of state (8) for a Newtonian liquid transform by the above rules to give the familiar equations (3). When these equations of state are taken in conjunction with equations (1) and (2), it is seen that no explicit reference to a displacement function occurs, so that the three components of velocity, the six independent components of stress and the density can be used as the ten dependent variables. This very simple example shows how a transformation of the equations of state to a fixed reference system makes their form much more suitable for applications, but may to some extent mask the obvious invariance properties of the original form.

(*b*) *The addition of quantities associated with different times*

The equations which express the properties of the material at ξ^j (i.e. at x^i) at a certain instant t will usually involve quantities which are primarily associated with the same material at an earlier time t', when its fixed co-ordinates would be $x'^i(x,t,t')$. But tensors associated with different points in space x'^i and x''^i cannot ordinarily be added, fixed-component by fixed-component, because the sum of such components is not the component of a tensor. Therefore, in order to preserve the tensor form of the transformed equations of state for the material at x^i at time t, it is necessary to regard every quantity associated with the material during its history as measured by a tensor *at the single point of space* x^i. This can be achieved in the following way.

We suppose that $b^{\cdot\cdot k\cdots}_{\cdot i\cdots}(x,t)$ is any tensor associated with the material at x^i at time t (defined for all x^i and t). The components $b^{\cdot\cdot k\cdots}_{\cdot i\cdots}(x',t')$ are therefore the fixed-components of a tensor which may be involved in the equations of state for the material at x^i at time t, being primarily associated with the same material at the instant t'. The convected-components of this tensor are, by the usual rule,

$$\beta^{\cdot\cdot l\cdots}_{\cdot j\cdots}(\xi,t') = \left\|\frac{\partial x'}{\partial \xi}\right\|^{W}\Pi\left(\frac{\partial x'^m}{\partial \xi^j}\right)\Pi'\left(\frac{\partial \xi^l}{\partial x'^p}\right)b^{\cdot\cdot p\cdots}_{\cdot m\cdots}(x',t'), \tag{40}$$

where ξ^j's denote arbitrary convected co-ordinates, which will have the property $\xi^j(x,t) = \xi^j(x',t')$. This tensor quantity, associated with the point ξ^j in the convected frame of reference, can now be regarded as associated with the point x^i at time t, and has at that point the fixed-components

$$B^{\cdot\cdot k\cdots}_{\cdot i\cdots}(x,t,t') = \left\|\frac{\partial \xi}{\partial x}\right\|^{W}\Pi\left(\frac{\partial \xi^j}{\partial x^i}\right)\Pi'\left(\frac{\partial x^k}{\partial \xi^l}\right)\beta^{\cdot\cdot l\cdots}_{\cdot j\cdots}(\xi,t'); \tag{41}$$

on substitution from (40), this simplifies to give

$$B^{\cdot\,k\cdots}_{\cdot\,i\cdots}(x,t,t') = \left\| \frac{\partial x'}{\partial x} \right\|^{W} \Pi\left(\frac{\partial x'^m}{\partial x^i}\right) \Pi'\left(\frac{\partial x^k}{\partial x'^p}\right) b^{\cdot\cdot\,p\cdots}_{\cdot\,m\cdots}(x',t'). \tag{42}$$

It is observed that the formula (42) is independent of the particular set of convected co-ordinates chosen as intermediary, being now expressed in terms of the displacement functions $x'^i(x,t,t')$. It is convenient to give a special name to the components $B^{\cdot\,k\cdots}_{\cdot\,i\cdots}(x,t,t')$; we shall call them the *Eulerian components* of the tensor $b^{\cdot\,k\cdots}_{\cdot\,i\cdots}(x',t')$ at x^i. The name is chosen because, although it is not possible to express all quantities associated with the past history of the material at x^i at time t as functions of x^i and t alone as the conventional Eulerian point of view would suggest (the additional variable t' being also involved), one can regard the consistent use of the fixed coordinate system at x^i for representing all tensor quantities associated with this material as the nearest approach to the Eulerian system of reference which it is possible to adopt in the general case.

In transforming the equations of state to a fixed system of reference, it is sufficient to replace the convected-components of all tensors by their Eulerian fixed-components. Where a time derivative $D\beta^{\cdot\,l\cdots}_{\cdot\,j\cdots}(\xi,t')/Dt'$ occurs, it is replaced by the Eulerian components of $\mathfrak{d}b^{\cdot\,k\cdots}_{\cdot\,i\cdots}(x',t')/\mathfrak{d}t'$, namely

$$\frac{\partial B^{\cdot\,k\cdots}_{\cdot\,i\cdots}(x,t,t')}{\partial t'} = \left\| \frac{\partial x'}{\partial x} \right\|^{W} \Pi\left(\frac{\partial x'^m}{\partial x^i}\right) \Pi'\left(\frac{\partial x^k}{\partial x'^p}\right) \frac{\mathfrak{d}b^{\cdot\cdot\,p\cdots}_{\cdot\,m\cdots}(x',t')}{\mathfrak{d}t'}.$$

We require the two general properties of Eulerian components expressed by

$$B^{\cdot\,k\cdots}_{\cdot\,i\cdots}(x,t,t) = b^{\cdot\,k\cdots}_{\cdot\,i\cdots}(x,t) \tag{43}$$

and

$$\mathfrak{d}B^{\cdot\,k\cdots}_{\cdot\,i\cdots}(x,t,t')/\mathfrak{d}t = 0. \tag{44}$$

The last equation is simply equivalent to $D\beta^{\cdot\,l\cdots}_{\cdot\,j\cdots}(\xi,t')/Dt = 0$.

The metric tensor $\gamma_{jl}(\xi,t')$ has Eulerian components

$$G_{ik}(x,t,t') = \frac{\partial x'^m}{\partial x^i}\frac{\partial x'^p}{\partial x^k} g_{mp}(x'), \tag{45}$$

and hence the (relative-) strain tensor at x^i at time t, defined in terms of t_0 as a reference time, has Eulerian components

$$e_{ik}(x,t,t_0) \equiv \tfrac{1}{2}[g_{ik}(x) - G_{ik}(x,t,t_0)] \tag{46}$$

(cf. equation (11)). Allowing for the difference in notation, these are identical with the components of the strain tensor as usually defined (e.g. by Murnaghan 1937), when an Eulerian point of view is adopted in finite-strain elasticity theory. The immediate physical significance of the Eulerian components of strain is apparent when we write the first equation (14) as

$$[ds(t)]^2 - [ds(t_0)]^2 = 2e_{ik}(x,t,t_0)\,dx^i dx^k. \tag{47}$$

By convected differentiation of equation (46), and using the property (44), we obtain the simple equation

$$e^{(1)}_{ik}(x,t) = \mathfrak{d}e_{ik}(x,t,t_0)/\mathfrak{d}t \tag{48}$$

relating the strain and first rate-of-strain tensors, whatever reference time t_0 is chosen in defining a strain tensor.*

A remark is necessary concerning physical constants. It may happen in an anisotropic material that a physical constant is known as a function of position in space, only at some special reference time t_0, e.g. at a time at which it may be supposed that all elements of the material are similarly oriented in space so far as directional properties are concerned. In that case the fixed-components $k_{N\cdot i\cdots}^{\cdot h\cdots}(x_0, t_0)$ of the physical constant associated with the material at x_0^i at time t_0 are known. Since the convected-components $\kappa_{N\cdot j\cdots}^{\cdot l\cdots}(\xi)$ are independent of the time, the Eulerian components $K_{N\cdot i\cdots}^{\cdot h\cdots}(x, t, t')$ are independent of t'. In particular, from the property (43), they are equal to the fixed-components of the physical constant primarily associated with the instant t itself, and we can therefore express these components in terms of known constants and the displacement functions as

$$k_{N\cdot i\cdots}^{\cdot h\cdots}(x,t) = K_{N\cdot i\cdots}^{\cdot h\cdots}(x,t,t_0) = \left\| \frac{\partial x_0}{\partial x} \right\|^W \Pi\left(\frac{\partial x_0^m}{\partial x^i}\right) \Pi'\left(\frac{\partial x^h}{\partial x_0^p}\right) k_{N\cdot m\cdots}^{\cdot p\cdots}(x_0, t_0); \tag{49}$$

here, $x_0^i = x'^i(x, t, t_0)$ is the position of the material (x^i, t) at time t_0, and W is the weight of the tensor concerned.

(c) *Convected integration with respect to time*

An integration is to be regarded as a special case of the addition of quantities associated with the material at different times, and no new principle is involved in transforming to a fixed system of reference. When an integrand is transformed to Eulerian components, the integrands at different times t' are summable, component by component, to give the fixed-component of a tensor at x^i as the integral. Any integral $\int_{t_0}^{t} \beta_{\cdot j\cdots}^{\cdot l\cdots}(\xi, t')\, dt'$ transforms into $\int_{t_0}^{t} B_{\cdot i\cdots}^{\cdot k\cdots}(x, t, t')\, dt'$, i.e.

$$\int_{t_0}^{t} \left\| \frac{\partial x'}{\partial x} \right\|^W \Pi\left(\frac{\partial x'^m}{\partial x^i}\right) \Pi'\left(\frac{\partial x^k}{\partial x'^p}\right) b_{\cdot m\cdots}^{\cdot p\cdots}(x', t')\, dt',$$

when referred to fixed co-ordinates. This is the fixed-component of a tensor which may be called the *convected integral* of the tensor $b_{\cdot i\cdots}^{\cdot k\cdots}(x, t)$ in relation to the moving continuum. It is noted that, from their definitions in terms of a convected co-ordinate system, the operations of convected integration and convected differentiation are reciprocal operations. The identities which this statement implies, when written in full in terms of the fixed-components of tensors, are

$$\frac{\mathfrak{d}}{\mathfrak{d}t} \int_{t_0}^{t} \left\| \frac{\partial x'}{\partial x} \right\|^W \Pi\left(\frac{\partial x'^m}{\partial x^i}\right) \Pi'\left(\frac{\partial x^k}{\partial x'^p}\right) b_{\cdot m\cdots}^{\cdot p\cdots}(x', t')\, dt' = b_{\cdot i\cdots}^{\cdot k\cdots}(x, t) \tag{50}$$

and

$$\int_{t_0}^{t} \left\| \frac{\partial x'}{\partial x} \right\|^W \Pi\left(\frac{\partial x'^m}{\partial x^i}\right) \Pi'\left(\frac{\partial x^k}{\partial x'^p}\right) \frac{\mathfrak{d} b_{\cdot m\cdots}^{\cdot p\cdots}(x', t')}{\mathfrak{d}t'}\, dt'$$
$$= b_{\cdot i\cdots}^{\cdot k\cdots}(x, t) - \left\| \frac{\partial x_0}{\partial x} \right\|^W \Pi\left(\frac{\partial x_0^m}{\partial x^i}\right) \Pi'\left(\frac{\partial x^k}{\partial x_0^p}\right) b_{\cdot m\cdots}^{\cdot p\cdots}(x_0, t_0). \tag{51}$$

---

* The concept of the convected derivative clearly introduces a great simplification of notation; the relationship between finite-strain and rate-of-strain tensors could not without it be regarded as a simple one.

It will be observed that, if a set of equations of state for a material (in their original invariant form referred to a convected system of reference) involve integrations which cannot be eliminated by processes of rearrangement and differentiation, the new equations obtained by transformating to a fixed system of reference will generally involve the displacement functions $x'^i(x, t, t')$ in a somewhat complicated manner. The simultaneous solution of the transformed equations of state and the equations of motion and continuity is a matter in which each material must be discussed on its own merits.

4. ILLUSTRATION OF THE PROCESS OF FORMULATING INVARIANT EQUATIONS OF STATE

The procedure to be adopted in developing a comprehensive theory of deformation and flow for a new (idealized) type of continuous material is now established in principle. Equations of state—based on experiment or on a structural theory for the material—must be written in a form which is readily recognizable by the rules of § 2 as having the right invariance properties; the frame of reference generally required for this purpose is a convected system of co-ordinates. For the purpose of proceeding to the second stage in the development of a theory of flow, that is, the solution of boundary-value problems, the equations of state are recast in terms of the fixed-components of a stress tensor field and the displacement functions as the dependent variables in accordance with the principles established in § 3.

Examples of this process of formulating equations of state will now be given, in order to demonstrate some of the difficulties which can arise in particular cases. For simplicity, we shall consider liquids which may be supposed incompressible, i.e. which resist any change in volume with an indefinitely great bulk modulus of elasticity. Mathematically, it is convenient to regard the stresses at any point in such a material as the superposition of two independent stress systems, one represented by a tensor p'_{ik} related to the distortion (deformation at constant volume) and the other an isotropic tensor $p''_{ik} = -p''g_{ik}$, where p'' is an absolute scalar related to the dilatation. With the further assumption that no measurable dilatation occurs however p'' varies (so that an arbitrary isotropic pressure can be superposed on any stress system without affecting the kinematics of a material element), the equations of state take the form

$$p_{ik} = p'_{ik} - p''g_{ik}, \tag{52}$$

with

$$e^{(1)i}_{i} = 0 \quad (\text{all } p'') \tag{53}$$

as the limiting form for the equation for p'', and a set of six equations relating* p'_{ik} and $e^{(1)}_{ik}$. The equations of state (3) for a Newtonian liquid can clearly be written in this form with $p'_{ik} = 2\mu e^{(1)}_{ik}$ as the last six equations. In this especially simple case it follows that p'_{ik} is a deviatoric tensor (i.e. $p'^i_i = 0$). But it must be emphasized that p'_{ik} will not be a deviator in the general case, when the only restriction on the p'_{ik}, $e^{(1)}_{ik}$

---

* An incompressible liquid is not a material for which a special reference time t_0 may be supposed to exist, such that the configuration at time t_0 has a permanent significance in any subsequent motion. We deduce that the equations of state can be written in a form which does not involve a strain tensor e_{ik} explicitly.

relationship is that it must be transformable into an invariant relation connecting the quantities (7) (with a primed stress tensor).

In order to indicate the kind of integro-differential equations of state which could arise in practice, we consider very briefly a hypothetical set of equations of state which cannot be reduced by simple processes of rearrangement and differentiation to a set of differential equations. We suppose that an incompressible material exists for which it is established experimentally that the equations of state referred to a convected co-ordinate system take the invariant form*

$$\pi_{jl} = \pi'_{jl} - \pi''\gamma_{jl}, \tag{54}$$

$$D\Delta/Dt = 0 \quad (\text{all } \pi''), \tag{55}$$

$$\pi'_{jl}(\xi,t) + \lambda\frac{D\pi'_{jl}(\xi,t)}{Dt} - \int_{-\infty}^{t}\psi(t-t')\,\pi'_{jl}(\xi,t')\,dt' = \mu\left\{\frac{D\gamma_{jl}(\xi,t)}{Dt} - \int_{-\infty}^{t}\psi(t-t')\frac{D\gamma_{jl}(\xi,t')}{Dt'}dt'\right\}. \tag{56}$$

In these equations, μ and λ are absolute scalar constants with the dimensions of viscosity and time respectively. The function $\psi(\omega)$ is an absolute scalar associated with the material, i.e. a function all the coefficients of which are absolute scalar physical constants of the material; this function can be regarded as a measure of the effect, on rheological properties at time t, of the rheological state at any previous instant $t-\omega$. The material whose properties are specified by equations (54) to (56) is clearly isotropic. When ψ does not vanish identically, equation (56) is not reducible to a differential equation by simple processes of rearrangement and differentiation.

On transforming the equations of state to a fixed system of reference, we obtain equations (52), (53) and

$$p'_{ik}(x,t) + \lambda\frac{\mathfrak{d}p'_{ik}(x,t)}{\mathfrak{d}t} - \int_{-\infty}^{t}\psi(t-t')\,p'_{mr}(x',t')\frac{\partial x'^m}{\partial x^i}\frac{\partial x'^r}{\partial x^k}dt' = 2\mu\left\{e^{(1)}_{ik}(x,t) - \int_{-\infty}^{t}\psi(t-t')\,e^{(1)}_{mr}(x',t')\frac{\partial x'^m}{\partial x^i}\frac{\partial x'^r}{\partial x^k}dt'\right\}, \tag{57}$$

where it is noted that $e^{(1)}_{ik}(x',t') = \frac{1}{2}[v_{k,i}(x',t') + v_{i,k}(x',t')]$ occurs in an integrand. The equations therefore involve the velocity vector near the previous position x'^i of the material under consideration, the displacement functions $x'^i(x,t,t')$ explicitly and also, through the process of covariant differentiation, the metric tensor near x'^i. (If it is possible to use an orthogonal Cartesian system of co-ordinates there will be some simplification; for example, the covariant derivatives become ordinary partial derivatives.) Associated with the equations of state we have the equation of continuity, which reduces to ρ = constant for a homogeneous incompressible material, and the three equations of motion (1); these must, of course, be regarded as identities which hold at all positions and times. We have therefore arrived at a system of integro-differential equations for the stress tensor components and the functions $x'^i(x,t,t')$, which, it may be anticipated, will not be easy to solve even with the simplest possible choice of boundary conditions.

---

* This form seems theoretically feasible. Such a material would have properties in a shearing motion represented symbolically by a rheological model with an elastic and a viscous element in series (see, for example, Burgers (1935)), in which the elastic element is now considered to have the elastic after-effect properties formulated mathematically by Boltzmann (1876). The material is in fact an elastico-viscous liquid with rather complicated elastic properties.

In order to demonstrate more fully the whole process of formulating equations of state, beginning with a structural model and ending with the solution of a boundary-value problem, we shall examine a type of material with more tractable, ***differential*** equations of state. We consider the incompressible elastico-viscous liquid for which Fröhlich & Sack (1946) have derived equations of state which are equivalent, in our notation, to equations (52) and (53), together with

$$\left(1+\lambda\frac{\partial}{\partial t}\right)p'_{ik} = 2\mu\left(1+\tau\frac{\partial}{\partial t}\right)e^{(1)}_{ik}. \tag{58}$$

These equations are based on a structural model for a colloidal suspension, in which Hookean elastic spherical particles are supposed distributed in a Newtonian viscous liquid. Three scalar constants, the viscosity μ and two constants λ and τ with the dimensions of time, occur in equation (58). The material is essentially a liquid, and the physical model is such that $\lambda > \tau$ and such that, as λ and τ tend to equality, the material must become more and more exactly a Newtonian liquid of viscosity μ. An examination of the original paper shows that equation (58) was derived by considering what must be regarded as a single stationary macroscopic element of material, and that an assumption was made which effectively restricts the stresses and rates of strain to be small. Also the co-ordinates were orthogonal and Cartesian. Equation (58) is not as it stands suitable for general use, and the immediate problem is that of generalizing the equation so that the equations of state can be applied to material in general motion, in which the rates of strain will not necessarily be small. We seek to formulate invariant equations which reduce to (58) under the specially simple conditions of the original derivation, and we must also decide whether this can be done without ambiguity. The problem is of a kind which will frequently arise in practice, as soon as an attempt is made to express the findings of experiment or structural theory in a single set of equations.

One obvious possible generalization of equation (58) is

$$\left(1+\lambda\frac{\mathfrak{d}}{\mathfrak{d}t}\right)p'_{ik} = 2\mu\left(1+\tau\frac{\mathfrak{d}}{\mathfrak{d}t}\right)e^{(1)}_{ik}, \tag{59}$$

an equation which is immediately recognized as invariant in form* provided that, as the notation implies, p'_{ik} and $e^{(1)}_{ik}$ are covariant absolute tensors and λ, μ, τ are absolute scalars. When the convected derivatives are written in full, (59) becomes

$$\begin{aligned} p'_{ik} + \lambda(\partial p'_{ik}/\partial t + v^m p'_{ik,m} + v^m_{,i}p'_{mk} + v^m_{,k}p'_{im}) \\ = 2\mu e^{(1)}_{ik} + 2\mu\tau(\partial e^{(1)}_{ik}/\partial t + v^m e^{(1)}_{ik,m} + v^m_{,i}e^{(1)}_{mk} + v^m_{,k}e^{(1)}_{im}), \end{aligned} \tag{60}$$

involving product terms which do not occur in (58), but which would be negligibly small under the conditions of small rates of strain in a stationary material element—

---

* The equation when referred to a convected system of co-ordinates need not be written down in a simple case such as this.

the conditions which were assumed in the initial derivation of (58). But it is easy to see that (59) is not the only possible generalization of (58). For, in orthogonal Cartesian co-ordinates, the components of the covariant tensor p'_{ik} are indistinguishable from those of the contravariant or mixed tensors p'^{ik}, p'^{k}_{i}, or those of any relative tensor formed by multiplying one of these by a power of the determinant of the metric tensor, such as the covariant tensor-density $P'_{ik} \equiv g^{\frac{1}{2}} p'_{ik}$. Similarly, associated tensors can be substituted for the covariant rate-of-strain tensor. So we could choose to write the originally proposed equation of state (58) as, for example,

$$g_{km}\left(1+\lambda\frac{\partial}{\partial t}\right)p'^{m}_{i} = 2\mu\left(1+\tau\frac{\partial}{\partial t}\right)e^{(1)}_{ik} \tag{61}$$

or

$$g^{-\frac{1}{2}}\left(1+\lambda\frac{\partial}{\partial t}\right)P'_{ik} = 2\mu\left(1+\tau\frac{\partial}{\partial t}\right)e^{(1)}_{ik}, \tag{62}$$

and to generalize it as, for example,

$$g_{km}\left(1+\lambda\frac{\mathfrak{d}}{\mathfrak{d}t}\right)p'^{m}_{i} = 2\mu\left(1+\tau\frac{\mathfrak{d}}{\mathfrak{d}t}\right)e^{(1)}_{ik} \tag{63}$$

or

$$g^{-\frac{1}{2}}\left(1+\lambda\frac{\mathfrak{d}}{\mathfrak{d}t}\right)P'_{ik} = 2\mu\left(1+\tau\frac{\mathfrak{d}}{\mathfrak{d}t}\right)e^{(1)}_{ik}. \tag{64}$$

It follows from the rules (37) to (39) that, when they are written in full, equations (63), (64), etc., are the same as (60), except for additional terms such as $-2\lambda e^{(1)}_{km}p'^{m}_{i}$ or $\lambda e^{(1)m}_{m}p'_{ik}$ on the left side of the equation, or terms such as $-2\mu\tau e^{(1)}_{km}e^{(1)m}_{i}$ on the right, all of which would be negligible under the conditions of the initial derivative of (58).

We therefore arrive at an infinite number of possible sets of invariant* equations of state, all based on a single proposed non-invariant set of equations valid for a restricted type of motion. Only a further examination of the structural model, or further experiments on particular materials which it is desired to study, will distinguish between the possible alternatives. Such experimental work, possibly involving more complicated types of motion or more refined measurements, must be continued on any particular material until invariant equations of state are established without ambiguity. We shall conclude by giving the solution to a particular problem, thereby demonstrating how an apparently trivial change in the form of a set of equations of state might lead to very different properties of the material in bulk, flowing under conditions not contemplated in the initial derivation of non-invariant equations.

Two hypothetical types of incompressible elastico-viscous liquid will be compared, with equations of state (52) and (53) together with equation (59) in case (A) and

$$\left(1+\lambda\frac{\mathfrak{d}}{\mathfrak{d}t}\right)p'^{ik} = 2\mu\left(1+\tau\frac{\mathfrak{d}}{\mathfrak{d}t}\right)e^{(1)ik} \tag{65}$$

in case (B). At first sight these might appear to be trivially different generalizations of (58). We note that the Newtonian liquid (in which $p'_{ik} = 2\mu e^{(1)}_{ik}$ and, equally, $p'^{ik} = 2\mu e^{(1)ik}$) is included as a limiting case of either A or B when λ and τ tend to equality. If $\lambda > \tau$, however, the materials A and B can exhibit very different bulk properties. We consider two-dimensional steady flow between two upright coaxial cylinders rotating about their axis with different angular velocities. It is convenient to work in orthogonal Cartesian co-ordinates $x^i = x, y, z$, the z axis being along the axis of the cylinders, but to quote the final results in terms of the physical components of tensors in cylindrical polar co-ordinates r, ϕ, z ($r\cos\phi = x$, $r\sin\phi = y$), i.e. the Cartesian components in directions coinciding with the polar co-ordinate directions locally at any particular point under consideration. The 'stress tensor components' usually denoted by $\widehat{rr}$, $\widehat{\phi\phi}$, $\widehat{zr}$, etc., in elasticity theory are simply the physical components of the stress tensor in polar co-ordinates, and it is useful to retain this notation here. The velocity vector has, from symmetry, Cartesian components of the form

---

* There is no difficulty in expressing any of these equations in terms of the convected-components of tensors, and so recognizing at a glance that they have the right kind of invariance for universally valid equations of state.

$$v_i = v^i = [-y\omega(r), x\omega(r), 0],$$

and the rate-of-strain and stress tensors have Cartesian components

$$e^{(1)}_{ik} = e^{(1)ik} = \frac{1}{2}\left(\frac{\partial v_k}{\partial x^i} + \frac{\partial v_i}{\partial x^k}\right) = \begin{pmatrix} -\dfrac{xy}{r}\dfrac{d\omega}{dr} & \dfrac{x^2-y^2}{2r}\dfrac{d\omega}{dr} & 0 \\ \dfrac{x^2-y^2}{2r}\dfrac{d\omega}{dr} & \dfrac{xy}{r}\dfrac{d\omega}{dr} & 0 \\ 0 & 0 & 0 \end{pmatrix}$$

and

$$p'_{ik} = p'^{ik} = \begin{pmatrix} \dfrac{x^2\widehat{rr}' + y^2\widehat{\phi\phi}' - 2xy\widehat{r\phi}'}{r^2} & \dfrac{xy(\widehat{rr}' - \widehat{\phi\phi}') + (x^2-y^2)\,\widehat{r\phi}'}{r^2} & 0 \\ \dfrac{xy(\widehat{rr}' - \widehat{\phi\phi}') + (x^2-y^2)\,\widehat{r\phi}'}{r^2} & \dfrac{y^2\widehat{rr}' + x^2\widehat{\phi\phi}' + 2xy\widehat{r\phi}'}{r^2} & 0 \\ 0 & 0 & \widehat{zz}' \end{pmatrix},$$

where $\widehat{rr}'$, $\widehat{\phi\phi}'$, $\widehat{zz}'$ and $\widehat{r\phi}'$ may be supposed functions of r only. From these expressions and the formula (23), the Cartesian components of $\mathfrak{d}p'_{ik}/\mathfrak{d}t$, $\mathfrak{d}p'^{ik}/\mathfrak{d}t$, $\mathfrak{d}e^{(1)}_{ik}/\mathfrak{d}t$ and $\mathfrak{d}e^{(1)ik}/\mathfrak{d}t$ are readily found; the algebra is omitted in the interests of conciseness. Finally, the physical components of these quantities in polar co-ordinates are obtained by considering the Cartesian axes rotated, with the results:

$$e^{(1)}_{ik} = e^{(1)ik} = \begin{pmatrix} 0 & \dfrac{r}{2}\dfrac{d\omega}{dr} & 0 \\ \dfrac{r}{2}\dfrac{d\omega}{dr} & 0 & 0 \\ 0 & 0 & 0 \end{pmatrix}, \quad p'_{ik} = p'^{ik} = \begin{pmatrix} \widehat{rr}' & \widehat{r\phi}' & 0 \\ \widehat{r\phi}' & \widehat{\phi\phi}' & 0 \\ 0 & 0 & \widehat{zz}' \end{pmatrix}, \tag{66}$$

$$\frac{\mathfrak{d}e^{(1)}_{ik}}{\mathfrak{d}t} = \begin{pmatrix} r^2\left(\dfrac{d\omega}{dr}\right)^2 & 0 & 0 \\ 0 & 0 & 0 \\ 0 & 0 & 0 \end{pmatrix}, \quad \frac{\mathfrak{d}p'_{ik}}{\mathfrak{d}t} = \begin{pmatrix} 2r\dfrac{d\omega}{dr}\widehat{r\phi}' & r\dfrac{d\omega}{dr}\widehat{\phi\phi}' & 0 \\ r\dfrac{d\omega}{dr}\widehat{\phi\phi}' & 0 & 0 \\ 0 & 0 & 0 \end{pmatrix}, \tag{67}$$

$$\frac{\mathfrak{d}e^{(1)ik}}{\mathfrak{d}t} = \begin{pmatrix} 0 & 0 & 0 \\ 0 & -r^2\left(\dfrac{d\omega}{dr}\right)^2 & 0 \\ 0 & 0 & 0 \end{pmatrix}, \quad \frac{\mathfrak{d}p'^{ik}}{\mathfrak{d}t} = \begin{pmatrix} 0 & -r\dfrac{d\omega}{dr}\widehat{rr}' & 0 \\ -r\dfrac{d\omega}{dr}\widehat{rr}' & -2r\dfrac{d\omega}{dr}\widehat{r\phi}' & 0 \\ 0 & 0 & 0 \end{pmatrix}. \tag{68}$$

Equations (59) and (65) therefore imply, respectively,

$$(A)\quad \left\{\begin{aligned} &\widehat{rr}' + 2\lambda r\frac{d\omega}{dr}\widehat{r\phi}' = 2\mu\tau r^2\left(\frac{d\omega}{dr}\right)^2, \\ &\widehat{r\phi}' + \lambda r\frac{d\omega}{dr}\widehat{\phi\phi}' = \mu r\frac{d\omega}{dr}, \\ &\widehat{\phi\phi}' = \widehat{zz}' = 0, \end{aligned}\right\} \tag{69}$$

and

$$(B)\quad \left\{\begin{aligned} &\widehat{\phi\phi}' - 2\lambda r\frac{d\omega}{dr}\widehat{r\phi}' = -2\mu\tau r^2\left(\frac{d\omega}{dr}\right)^2, \\ &\widehat{r\phi}' - \lambda r\frac{d\omega}{dr}\widehat{rr}' = \mu r\frac{d\omega}{dr}, \\ &\widehat{rr}' = \widehat{zz}' = 0. \end{aligned}\right\} \tag{70}$$

The equation (53) is automatically satisfied by the form of velocity distribution assumed above, and the equation of continuity requires ρ to be a constant. The equations of steady motion are, for our present purpose, most conveniently taken in the form

$$\frac{\partial\widehat{rr}'}{\partial r} + \frac{\widehat{rr}' - \widehat{\phi\phi}'}{r} = \frac{\partial p''}{\partial r} - \rho r\omega^2, \quad \frac{\partial\widehat{r\phi}'}{\partial r} + \frac{2\widehat{r\phi}'}{r} = 0, \quad \frac{\partial\widehat{zz}'}{\partial z} = \frac{\partial p''}{\partial z} + \rho\bar{g}, \tag{71}$$

in which account has been taken of equation (52); $\bar{g}$ denotes the gravitational acceleration, z being measured vertically upwards. It is possible to solve the seven equations (71) and (69)—or (70)—for six functions of r, namely $\widehat{rr}'$, $\widehat{\phi\phi}'$, $\widehat{zz}'$, $\widehat{r\phi}'$, ω and p'', the boundary conditions being that ω takes given constant values on the two bounding cylinders. It is easy to verify that the equations require velocity and stress distributions defined by

$$(A)\quad \left\{\begin{gathered} \widehat{rr}' = -8\mu(\lambda-\tau)\,b^2r^{-4}, \quad \widehat{\phi\phi}' = 0, \quad \widehat{zz}' = 0, \\ \widehat{r\phi}' = 2\mu br^{-2}, \quad \omega = a - br^{-2}, \\ p'' = \rho(\tfrac{1}{2}a^2r^2 - 2ab\log r - \tfrac{1}{2}b^2r^{-2}) - 6\mu(\lambda-\tau)\,b^2r^{-4} - \bar{g}\rho z + c, \end{gathered}\right\} \tag{72}$$

and

$$(B)\quad \left\{\begin{gathered} \widehat{rr}' = 0, \quad \widehat{\phi\phi}' = 8\mu(\lambda-\tau)\,b^2r^{-4}, \quad \widehat{zz}' = 0, \\ \widehat{r\phi}' = 2\mu br^{-2}, \quad \omega = a - br^{-2}, \\ p'' = \rho(\tfrac{1}{2}a^2r^2 - 2ab\log r - \tfrac{1}{2}b^2r^{-2}) + 2\mu(\lambda-\tau)\,b^2r^{-4} - \bar{g}\rho z + c, \end{gathered}\right\} \tag{73}$$

where a, b and c are constants in each case; b is defined in terms of the relative angular velocity $\omega_2 - \omega_1$ of the cylinders and their radii $r_1, r_2(>r_1)$ by $b = r_1^2r_2^2(\omega_2-\omega_1)/(r_2^2-r_1^2)$ and does not vanish. To fix ideas we consider the case in which ω_2 vanishes. If the material is sufficiently viscous, and $\lambda > \tau$, more precisely if $\mu(\lambda-\tau)$ is sufficiently large compared with ρr_2^4, the terms in the expressions for p'' arising from the centripetal acceleration can be neglected compared with those involving the viscosity. The forces across a horizontal plane required to maintain steady two-dimensional motion are then normal pressures

$$-\widehat{zz} = -\widehat{zz}' + p'' = -6\mu(\lambda - \tau)\, b^2 r^{-4} + \text{a constant} \tag{74}$$

in material A, and

$$-\widehat{zz} = 2\mu(\lambda - \tau)\, b^2 r^{-4} + \text{a constant} \tag{75}$$

in material B; in the first case the constraining pressure increases with r and in the second case decreases as r increases. Hence, if the liquid, initially in steady motion constrained to be two-dimensional, were suddenly given a free horizontal surface, the free surface of material A would begin to rise near the outer cylinder and fall near the inner cylinder, but the material B would show the opposite effect, tending to 'climb up' the inner cylinder.*

A difference of this kind in the predicted behaviour of material in bulk, arising from a difference in form of the equations of state, can be used to distinguish experimentally between various possible generalized equations of state for a particular material. For example, if it were already known that either (59) or (65) applied to a certain incompressible elastico-viscous liquid, a simple experiment in a Couette viscometer would decide which of the two alternatives was correct.

REFERENCES

Boltzmann, L. 1876 *Ann. Phys. Chem.* (*Poggendorff*), Ergänzungsband **7**, 624.

Brillouin, L. 1925 *Ann. Phys., Paris*, **3**, 251.

Burgers, J. M. 1935 *First report on viscosity and plasticity*, chap. I. Royal Netherlands Academy of Sciences.

Fröhlich, H. & Sack, R. 1946 *Proc. Roy. Soc.* A, **185**, 415.

Hencky, H. 1925 *Z. angew. Math. Mech.* **5**, 144.

Jeffreys, H. 1931 *Cartesian tensors*, chap. VIII. Cambridge University Press.

Murnaghan, F. D. 1937 *Amer. J. Math.* **59**, 235.

Reiner, M. 1948 *Amer. J. Math.* **70**, 433.

Reiner, M. 1949 *Deformation and flow*, pp. 321–325. London: Lewis.

Rivlin, R. S. 1948 *Proc. Roy. Soc.* A, **193**, 260.

Volterra, V. 1909 *R.C. Accad. Lincei*, (5), **18**, 295, 577.

Weissenberg, K. 1947 *Nature*, **159**, 310.

Weissenberg, K. 1948 *Proc. Int. Rheological Congr., Holland*, **1**, 29.

---

* Such an effect has been demonstrated experimentally by Weissenberg (1947, 1948), using various liquids, and has been attributed by him to a combination of viscous and elastic properties, giving rise to a tensile stress in the direction of the streamlines ($\widehat{\phi\phi'} > 0$, as in material B).

[*Note added* 29 *October* 1949.] Reiner (1948, 1949) regards the effect observed by Weissenberg as a manifestation of *cross-elasticity*, a term used of materials in which a single applied shear stress gives rise to elastic strains in all directions. On the other hand, Rivlin (1948) has shown in detail how the same phenomenon could arise in a non-Newtonian viscous liquid exhibiting no elasticity, but is mistaken in suggesting that elastic properties could not be a contributory cause. (His argument is that the 'time derivatives of the stress components' which occur in the equations of state of an elastic liquid vanish in a steady state of flow, so that the equations of state are then indistinguishable from those of an inelastic liquid. In fact, the simplest equations of state representing elastico-viscous behaviour must be expressible as equations relating the rate-of-strain tensor, the stress tensor and the convected derivative of the stress tensor. In a steady state, partial time derivatives in an Eulerian system of reference vanish, but the convected derivative of the stress tensor does not vanish and does not reduce to an algebraic combination of the stress and rate-of-strain tensors. Therefore, an elastico-viscous liquid will in general behave differently from any inelastic viscous liquid, even in steady-state experiments.)

Electronic wave functions

I. A general method of calculation for the stationary states of any molecular system

By S. F. Boys, *Theoretical Chemistry Department, University of Cambridge*[*]

(*Communicated by Sir Alfred Egerton, F.R.S.—Received* 31 *August* 1949)

This communication deals with the general theory of obtaining numerical electronic wave functions for the stationary states of atoms and molecules. It is shown that by taking Gaussian functions, and functions derived from these by differentiation with respect to the parameters, complete systems of functions can be constructed appropriate to any molecular problem, and that all the necessary integrals can be explicitly evaluated. These can be used in connexion with the molecular orbital method, or localized bond method, or the general method of treating linear combinations of many Slater determinants by the variational procedure. This general method of obtaining a sequence of solutions converging to the accurate solution is examined. It is shown that the only obstacle to the evaluation of wave functions of any required degree of accuracy is the labour of computation. A modification of the general method applicable to atoms is discussed and considered to be extremely practicable.

1. INTRODUCTION

In this communication is described the first of a series of investigations undertaken with the general aim of developing better methods of evaluating electronic wave functions and of using these to obtain new and more accurate data on atomic and molecular structure. It is well known that if the electronic stationary state wave functions can be evaluated for the various configurations of a system of atomic nuclei, then most of the spectral, chemical and physical properties of the corresponding system of atoms can be calculated. This is true when the atoms form a stable molecule, or when the system consists of a single atom, or when the system corresponds to an unstable configuration of atoms such as occur in the intermediate stages of a chemical reaction. Hence this general problem includes in principle a large number of the problems of theoretical chemistry, and a converging method of solution would effectively solve these problems.

The first purpose of this communication is to describe such a method of successive approximation by which this stationary state electronic wave function for any configuration of atoms can be calculated to any desired degree of accuracy by inclusion of sufficient terms. This method does not depend on any numerical integration processes. Such a method has not been previously reported. The new mathematical analysis which has been carried out to make this possible consists essentially of the evaluation of the Schrödinger integrals between Gaussian probability functions. The most complicated integral which is required is that of the electronic interaction between one product of two Gaussians on different centres with another product of two other Gaussians. These integrals and the simpler ones required are all evaluated explicitly. These integrals also provide the bases for the evaluation of all integrals derived from these by first multiplying the Gaussians by any polynomials.

---

[*] Formerly I.C.I. Research Fellow, Imperial College, London.

The actual procedure in which it is proposed that the Gaussian functions should be used consists of the construction of many Slater determinants from these and the use of these determinants in the Ritz variational method. The type of procedure considered most promising has been called the variational selection procedure. It corresponds in some degree to previous calculations, but it has not been formulated or discussed previously. Since this method is applicable to other sets of functions if the integrals for these can be evaluated, the general discussion of this may be regarded as a second purpose of this communication.

A third topic which it is convenient to discuss here is the fact that it is possible to use the variational selection method applied to Slater determinants constructed from simple exponential functions for atoms, and that this appears the most promising method for calculating the wave functions of complex atoms with converging accuracy. Several applications of this will be reported in subsequent papers.

Finally, the mathematical analysis on Gaussian functions may be regarded as fulfilling another purpose. Several approximate and non-converging methods of evaluating wave functions of molecules have been widely used for making deductions on the general nature of molecules. The best known of these are the molecular orbital and the localized bond methods. It has, however, never been possible to make *a priori* predictions by such procedures in cases other than the very simplest, since the requisite integrals could not be evaluated and had to be estimated empirically. However, if the orbitals used in any of these cases were taken to be linear combinations of functions derived from Gaussian functions all the required integrals could be evaluated explicitly. The analysis derived here does, therefore, provide for the first time a method of applying quantitatively, and in a fundamental way, the approximate methods of the molecular orbital and localized bond types.

The previous state of affairs in the calculation of atomic and molecular energies and wave functions is that converging methods without numerical integrations have been developed for two-electron problems such as He (Hylleraas 1929) and H_2 (James & Coolidge 1933), but no converging methods are available for more general molecules. The only method which is converging in principle for general atoms is the 'superposition of configurations' method (Hartree, Hartree & Swirles 1939), but this does not appear practicable for use with more than two or three terms, and depends on laborious numerical integrations.

With regard to the practical application of the methods described here it is not intended to apply the most general procedure immediately. It is intended first to gain experience in the variational selection procedure with Slater determinants using exponentials for atoms instead of Gaussian functions for molecules. This will provide useful data for atoms, and it will also provide an opportunity to find simplifications of the numerical techniques. The direct computation for molecules of interest would be very laborious, and it is hoped that either the numerical techniques can be considerably shortened or that the present scheme might lead to a more powerful method.

In work of this kind Slater determinants built up from orthogonal normalized single-particle functions occur so frequently that it appears worth while to suggest a short synthetic name for these. It is proposed that the word 'detor' be used to describe the Slater determinant of the general type

$$(1/n!)\sum_u \sigma_u P_u f_1(\mathbf{r}_1)\,\mu_1(v_1) f_2(\mathbf{r}_2)\,\mu_2(v_2)\ldots f_n(\mathbf{r}_n)\,\mu_n(v_n), \tag{1}$$

where

$$\int f_i^*(\mathbf{r}) f_j(\mathbf{r})\,d\mathbf{r} = \delta_{ij},$$

where v_i represent the spin variables which can only take the values $\frac{1}{2}$ and $-\frac{1}{2}$, where the μ_i can each be either the α or β function defined by

$$\left.\begin{array}{ll}\alpha(\frac{1}{2}) = 1, & \alpha(-\frac{1}{2}) = 0,\\ \beta(\frac{1}{2}) = 0, & \beta(-\frac{1}{2}) = 1,\end{array}\right\} \tag{2}$$

where the operators P_u represent all the possible permutations of the different sets of four variables $\mathbf{r}_i$, v_i, and where σ_u is $+1$ or -1 according as the permutation is even or odd. The author proposes using such extensions as poly-detor to denote linear combinations of detors where all the original functions are orthonormal. The convenience of these definitions is that these are just the types of function for which the integrals required in the variational problem can be reduced to a very simple form. Also, as is well known and simple to prove, the detors made from an orthonormal set are themselves orthonormal.

The term 'a complete system of functions' will be used in its usual sense to mean an ordered system $\{f_r\}$ for which m and the coefficients X_r can always be chosen for any given function F of the domain under consideration, so that

$$S\left(F - \sum_r^m X_r f_r\right)^*\left(F - \sum_r^m X_r f_r\right) d\tau < \epsilon, \tag{3}$$

where ϵ is any small positive number. The term 'a complete class of functions' will be used to mean a class of functions out of which it is possible to choose at least one complete system.

We shall be concerned with the many-electron Schrödinger equation for stationary states. We shall express it in atomic units and denote it as

$$H\psi \equiv \left\{\sum_i K_i - \sum_{I,i} Z_I V_{Ii} + \tfrac{1}{2}\sum_{i,j} M_{ij}\right\}\psi = E\psi, \tag{4}$$

where

$$\left.\begin{aligned} K_i &\equiv -\frac{1}{2}\left\{\frac{\partial^2}{\partial x_i^2} + \frac{\partial^2}{\partial y_i^2} + \frac{\partial^2}{\partial z_i^2}\right\},\\ V_{Ii} &\equiv 1/\sqrt{[(x_i - P_{Ix})^2 + (y_i - P_{Iy})^2 + (z_i - P_{Iz})^2]},\\ M_{ij} &\equiv 1/\sqrt{[(x_i - x_j)^2 + (y_i - y_j)^2 + (z_i - z_j)^2]}\end{aligned}\right\} \tag{5}$$

where x_i, y_i, z_i, v_i are the space and spin variables corresponding to the total number of electrons, where P_{Ix}, P_{Iy}, P_{Iz} are the positions of the nuclei, which are to be regarded as fixed and with integral charges Z_I. ψ is a function anti-symmetric with respect to the different sets of variables (x_i, y_i, z_i, v_i).

The notation $(\,|\,|\,)$ will be used to denote integration over all the space co-ordinates and summation over all the spin variables of the contained functions, the complex conjugate of the first function being taken. The same notation will be used for many- and single-electron functions, and for functions dependent on space and spin variables or only on either space or spin variables. The integrals are independent of the variables of integration and these will generally be omitted, thus

$$(f_r|V_I|f_s) \equiv \int d\mathbf{r}\{f_r^*(\mathbf{r})\,(1/r_I)f_s(\mathbf{r})\}. \tag{6}$$

It is also convenient to define

$$[f_rf_s|M|f_tf_u] \equiv \int\!\!\int d\mathbf{r}_1 d\mathbf{r}_2\{f_r^*(\mathbf{r}_1)f_s(\mathbf{r}_1)\,(1/r_{12})f_t^*(\mathbf{r}_2)f_u(\mathbf{r}_2)\}. \tag{7}$$

In § 2 we evaluate all the Schrödinger integrals between Gaussian functions which are required to establish the general scheme. § 3 deals with the convergent method of calculating energies and wave functions in terms of linear combinations of increasing numbers of detors. In § 4 are discussed other modifications of the general method and particularly the calculations for atoms, and in § 5 the general aspects of the methods are reviewed.

2. THE EVALUATION OF ALL THE SCHRODINGER INTEGRALS FOR DETORS CONSTRUCTED FROM THE COMPLETE CLASS OF GAUSSIAN FUNCTIONS

We define the complete class of Gaussian functions to consist of all functions, and of all linear combinations of functions, of the type $x^l\, y^m\, z^n \exp(-ar_A^2)$, where l, m, n, have any integral values, where a has any positive value, where we have used the general notation

$$x_A = x - A_x, \text{ etc.,} \quad r_A^2 = x_A^2 + y_A^2 + z_A^2, \tag{8}$$

and where A_x, A_y, A_z have any real values. The fact that this class is complete in the sense defined above follows immediately, since it contains the well-known complete system of Hermitian functions around any point. It actually contains an infinite number of complete systems. If any orthonormal set of these are taken and detors constructed from them after multiplication by the α and β spin functions, we wish to show that all Schrödinger integrals among these can be evaluated by quite simple formulae. The only step of any difficulty is that of evaluating integrals of the types

$$(g_r\,|\,g_s),\quad (g_r\,|\,K\,|\,g_s),\quad (g_r\,|\,V_I\,|\,g_s),\quad [g_rg_s\,|\,M\,|\,g_tg_u], \tag{9}$$

when g_r, g_s, g_t, g_u are members of the complete class. If, however, we evaluate these integrals when g_r, g_s, g_t, g_u are restricted to belong to the subclass of functions of the type $\exp(-ar_A^2)$ we can easily derive the formulae for the general class by differentiation with respect to the parameters in the integral formulae, followed by taking the appropriate linear combinations; since we can obtain any function of the whole class from the functions of the subclass by this procedure. We shall, therefore, limit our examination to deriving all the integrals for the subclass.

The values of the first of these integrals are obtained by simple direct integration; we get

$$(aA \mid bB) = \left(\frac{\pi}{a+b}\right)^{\frac{3}{2}} \exp\left(-\frac{AB^2ab}{a+b}\right), \tag{10}$$

$$(aA \mid K \mid bB) = \left(\frac{3ab}{a+b} - \frac{2AB^2a^2b^2}{(a+b)^2}\right)\left(\frac{\pi}{a+b}\right)^{\frac{3}{2}} \exp\left(-\frac{AB^2ab}{a+b}\right), \tag{11}$$

where

$$aA \equiv \exp(-ar_A^2) \quad \text{and} \quad AB^2 = \sum_{x,y,z} (A_x - B_x)^2. \tag{12}$$

To evaluate the remaining integrals we have

$$\begin{aligned}\int (1/r_{12}) \exp(-ar_{2A}^2)\, d\mathbf{r}_2 &= (4\pi/r_{1A}) \int_0^{r_{1A}} r_{2A}^2 \exp(-ar_{2A}^2)\, dr_2 + 4\pi \int_{r_{1A}}^{\infty} r_{2A} \exp(-ar_{2A}^2)\, dr_2 \\ &= (2\pi/ar_{1A}) \int_0^{r_{1A}} \exp(-ar_{2A}^2)\, dr_2,\end{aligned} \tag{13}$$

by the well-known transformation of the Coulomb potential of a spherical charge distribution. The integrals $(aA \mid V_c \mid bB)$, corresponding to a nucleus at C, can be reduced to an integral of the above type, since putting

$$P_x = \frac{aA_x + bB_x}{a+b}, \text{ etc.,} \tag{14}$$

we have

$$\begin{aligned}(aA \mid V_c \mid bB) &= \int (1/r_c) \exp\left[-\sum_{x,y,z} \{a(x-A_x)^2 + b(x-B_x)^2\}\right] d\mathbf{r} \\ &= \exp\left(-\frac{AB^2ab}{a+b}\right) \int (1/r_c) \exp\left[-\sum_{x,y,z} (a+b)(x-P_x)^2\right] d\mathbf{r}.\end{aligned} \tag{15}$$

If we define

$$F(z) = z^{-\frac{1}{2}} \int_0^{\sqrt{z}} e^{-u^2}\, du \tag{16}$$

and

$$CP^2 = \sum_{x,y,z} (C_x - P_x)^2,$$

we have

$$(aA \mid V_c \mid bB) = \frac{2\pi}{(a+b)} \exp\left(-\frac{AB^2ab}{a+b}\right) F\{CP^2(a+b)\}. \tag{17}$$

To evaluate the remaining type of integral it is convenient first to evaluate

$$\begin{aligned}I &\equiv \iint (1/r_{12}) \exp\left\{-u \sum_{x,y,z} (x_1 - P_x)^2\right\} - v \sum_{x,y,z} (x_2 - Q_x)\, d\mathbf{r}_1\, d\mathbf{r}_2 \\ &= \frac{2\pi}{v} \int d\mathbf{r}_1 \exp\left\{-u \sum_{x,y,z} (x_1 - P_x)^2\right\} (1/r_{1Q}) \int_0^{r_{1Q}} \exp(-va^2)\, da.\end{aligned} \tag{18}$$

This transformation is obtained by integrating with respect to $d\mathbf{r}_2$ using relation (13). Now if we use the two centre variables r_P, r_Q, ϕ in place of x_1, y_1, z_1 with

$$dr_1 = (r_P r_Q/PQ)\, dr_P\, dr_Q\, d\phi,$$

we obtain
$$I = \frac{2\pi}{vPQ}\left(\int_0^{PQ} dr_Q \int_{PQ-r_Q}^{PQ+r_Q} dr_P + \int_{PQ}^{\infty} dr_Q \int_{r_Q-PQ}^{r_Q+PQ} dr_P\right)\int_0^{2\pi} d\phi$$
$$\times r_P \exp(-ur_P^2)\int_0^{r_Q}\exp(-va^2)\,da$$
$$= \frac{2\pi^2}{uvPQ}\int_{-\infty}^{\infty} dr_Q \exp\{-u(PQ-r_Q)^2\int_0^{r_Q}\exp(-va^2)\,da. \tag{19}$$

Hence we require to evaluate an integral of the type
$$J \equiv \int_{-\infty}^{\infty} dx \exp\{-\alpha(x-R)^2\}\int_0^{x}\exp\{-\beta y^2\}\,dy \tag{20}$$
when $\alpha > 0$ and $\beta > 0$. We have
$$\frac{dJ}{dR} = -2\alpha\int_{-\infty}^{\infty} dx(R-x)\exp\{-\alpha(x-R)^2\}\int_0^{x}\exp\{-\beta y^2\}\,dy$$
$$= \sqrt{\left(\frac{\pi}{\alpha+\beta}\right)}\exp\left(-\frac{\alpha\beta R^2}{\alpha+\beta}\right), \tag{21}$$
and since $J = 0$ when $R = 0$ we obtain
$$J = \sqrt{\left(\frac{\pi}{\alpha+\beta}\right)}\int_0^{R}\exp\left(-\frac{\alpha\beta R^2}{\alpha+\beta}\right)dR. \tag{22}$$

Substituting this back in (19) we get
$$I = \frac{2\pi^{\frac{5}{2}}}{uv\sqrt{(u+v)}}F\left(\frac{PQ^2uv}{u+v}\right). \tag{23}$$

The actual integral which we require to evaluate is
$$[aAbB \mid M \mid cCdD] = \iint (1/r_{12})\exp\{-(ar_{1A}^2 + br_{1B}^2 + cr_{2C}^2 + dr_{2D}^2)\}\,d\mathbf{r}_1 d\mathbf{r}_2$$
$$= \exp\left\{-\frac{AB^2ab}{a+b} - \frac{CD^2cd}{c+d}\right\}\iint (1/r_{12})\exp\{-(a+b)\,r_{1P}^2 - (c+d)\,r_{2Q}^2\}\,d\mathbf{r}_1 d\mathbf{r}_2, \tag{24}$$
where $\quad P_x = (aA_x + bB_x)/(a+b)\quad$ and $\quad Q_x = (cC_x + dD_x)/(c+d)$, etc. (25)

The integral is just of the form of I so that
$$[aAbB \mid M \mid cCdD]$$
$$= \frac{2\pi^{\frac{5}{2}}}{(a+b)(c+d)\sqrt{(a+b+c+d)}}\exp\left\{-\frac{AB^2ab}{a+b} - \frac{CD^2cd}{c+d}\right\}F\left(\frac{PQ^2(a+b)(c+d)}{a+b+c+d}\right). \tag{26}$$

In view of the fact that the formulae for all functions of the complete Gaussian class can be derived from the above formulae by differentiation we have shown that all Schrödinger integrals can be evaluated for this class, and it only remains to show that the integrals between the derived detors reduce to these integrals. This is apparent by simple examination. The detors are merely finite linear combinations of the form
$$g_1(\mathbf{r}_1)\,\mu_1(v_1)\,g_2(\mathbf{r}_2)\,\mu_2(v_2)\ldots g_n(\mathbf{r}_n)\,\mu_n(v_n), \tag{27}$$

where g_i are members of the complete Gaussian class and each μ_i represents either α or β. Hence if we expand $(S_g \mid H \mid S'_g)$, where S_g and S'_g are detors of this type, we obtain only a finite number of terms of the types

$$\left.\begin{aligned}&(g_1 \mid g'_1)\,(\mu_1 \mid \mu'_1)\,(g_2 \mid g'_2) \ldots (g_i \mid V_{iI} \mid g'_i) \ldots (g_n \mid g'_n)\,(\mu_n \mid \mu'_n),\\ &(g_1 \mid g'_1)\,(\mu_1 \mid \mu'_1) \ldots (g_i \mid K_i \mid g'_1) \ldots (g_n \mid g'_n)\,(\mu_n \mid \mu'_n),\\ &(g_1 \mid g'_1)\,(\mu_1 \mid \mu'_1) \ldots [g_i g'_i \mid M_{ij} \mid g_j g_j] \ldots (g_n \mid g'_n)\,(\mu_n \mid \mu'_n).\end{aligned}\right\} \tag{28}$$

The factors $(\mu_i \mid \mu'_i)$ are all 0 or 1 by the definition of the μ_i, and the other factors are all integrals of the general types which we have shown can be evaluated. In actual practice powerful techniques are available to obtain the integrals between detors without explicit expansion, but these do not affect the final form of the answer. Hence we see that all matrix elements of the form $(S_g \mid H \mid S'_g)$, where H is the Schrödinger-Hamiltonian and S_g and S'_g are detors formed from functions of the complete Gaussian class can be expressed in terms of tabulated functions.

3. THE VARIATIONAL SELECTION METHOD USING DETORS FROM A COMPLETE CLASS OF FUNCTIONS

In this section what is regarded as the most promising converging method of obtaining electronic wave functions for atoms and molecules will be explained and justified. It will not be possible to prove rigorously the theorems which are required, but we shall give what justification we can. Difficulties of rigorous justification are well known in this field, in which theorems are required, appropriate to many dimensions, concerning the solutions of equations with singularities in spaces which are not bounded. The requisite theorems may not be true for any mathematical function but are very probably true for the functions permissible for wave functions. It is probably the difficulties of knowing and introducing such conditions for permissible functions which have prevented rigorous proofs of various desirable theorems up to the present.

We shall first assume the convergence of the Ritz variational procedure for eigenvalues and eigenfunctions. It is convenient to summarize as a theorem all the assumptions that are made in applying this procedure. This theorem has not been proved rigorously, but if various plausible assumptions (such as the convergence of $\sum_s(\phi_r \mid H \mid \phi_s)\phi_s$ when the ϕ_r form a complete system of functions) are made, it can be proved except for the convergence of the higher eigenfunctions ψ_2, $\psi_3 \ldots$ (see Kemble 1937). The assumption of the convergence of these is, however, generally made in practical numerical calculations.

THEOREM 1. If ψ_k and E_k are the (k)th eigenfunction and eigenvalue of

$$(H - E_k)\,\psi_k = 0, \tag{29}$$

these being labelled in order of ascending E_k, if Φ_r represents a normalized orthogonal system of functions, if $\psi^p_k = \sum_r^p X_r^{kp}\Phi_r$ and E^p_k satisfy

$$\sum_s^p(\Phi_r \mid H \mid \Phi_s)\,X_s^{kp} - E^p_k X_r^{kp} = 0, \tag{30}$$

the E_k^p being labelled in ascending order, then we have

$$E_k^p > E_k^{p+1} > E_k.$$

If Φ_r is a complete system of functions then E_k^p converge monotonically downwards to E_k, and ψ_k^p converge in the mean square sense to ψ_k.

It has been considered simplest to ignore the possibility of degenerate eigenvalues in this formulation. A considerably longer statement would be necessary to include this possibility, but this could be done without any essential difference of content.

A variational method will now be considered which is not the final method the author will advocate, but which forms an introduction and a justification of the final method. This method will be referred to as the single-system detor method, and the final method as the variational selection method. In the single-system method we commence with $\{\phi_r\}$, a single complete system of orthonormal functions of the variables x, y, z. If we are solving an n electron problem we form an ordered system of (n)th order detors constructed from the $\{\phi_r\}$ in accordance with the general procedure of placing all possible detors which contain ϕ_m but not ϕ_p for $p > m$ before all detors which contain any of ϕ_p. This system is then to be used as a complete system of functions for the variational procedure as stated in theorem 1. The E_k^M and $\psi_k^M = \sum_r^M X_r^{kM} \Phi_r$ will converge according to the theorem if $\{\Phi_r\}$ is a complete orthonormal system of functions. The orthonormality follows from the definition of the detors as mentioned above, but to show the completeness of the system a theorem is required which has not been established for general functions for the infinite ranges of integration for which it is required, although it can be proved for finite ranges of integration. The proof for finite ranges is given by Courant & Hilbert (1931, p. 47), but its general validity will be assumed for infinite ranges for the types of functions which will be used in these calculations.

THEOREM 2. If $\{\phi_r\}$ denotes a complete system of functions for the space x, y, z, then the system

$$\phi_{s1}(\mathbf{r}_1)\,\phi_{s2}(\mathbf{r}_2)\,\phi_{s3}(\mathbf{r}_3)\cdots\phi_{sn}(\mathbf{r}_n), \tag{31}$$

where each pair $s1$, $s2$, etc., denotes a single suffix of the r type, and where the products are ordered so that all products containing ϕ_m but no ϕ_p $(p > m)$ are placed before all products containing any of the ϕ_p, is a complete system for the space $(\mathbf{r}_1, \mathbf{r}_2, \ldots, \mathbf{r}_n)$.

It follows from this theorem that the products

$$\phi_{s1}(\mathbf{r}_1)\,\mu_{k1}(v_1)\,\phi_{s2}(\mathbf{r}_2)\,\mu_{k2}(v_2)\cdots\phi_{sn}(\mathbf{r}_n)\,\mu_{kn}, \tag{32}$$

where μ_{ki} have the possible values $\mu_{\frac{1}{2}} = \alpha$ and $\mu_{-\frac{1}{2}} = \beta$, is a complete system of functions for the space $(\mathbf{r}_1, v_1, \mathbf{r}_2, v_2, \ldots, \mathbf{r}_n, v_n)$, since the system would be complete for each of the combinations of the μ_{ki} functions.

If we consider an anti-symmetric function F, then by definition

$$\sigma_u P_u F = F, \tag{33}$$

and if F is expanded in terms of the complete system of products with coefficients $A(si, ki)$ we can operate on both sides of the equation and obtain

$$(1/n!)\sum_u \sigma_u P_u F = F = (1/n!)\sum_u \sigma_u P_u \sum_{si,\,ki} A(si, ki)\,\phi_{s1}\,\mu_{k1}\,\phi_{s2}\,\mu_{k2}\cdots\phi_{sn}\,\mu_{kn}, \tag{34}$$

thus expressing F as a sum of detors.

Hence for anti-symmetric functions the detor system is a complete system, and the use of the single-system detor method for obtaining converging anti-symmetric solutions of Schrödinger's equation is in accordance with theorem 1.

The variational selection method can now be stated. This is a general procedure with considerable liberty of choice, which can be applied to a complete class of functions. When approximating to a particular E_k and ψ_k we take the M(th) approximation to be given by the use in the variational method of M detors formed from any m orthonormal ϕ_r^M out of the complete class. We do not specify the choice of the ϕ_r^M or of Φ_r^M the M detors, which need not be all the detors that can be formed from the ϕ_r^M, beyond one condition. We specify that the E_k^M obtained from this choice must be less than $E_k'^M$ where this is the value given by the (M)th approximation in the single-system detor method when using some complete system of $\{\phi_r'\}$ chosen out of the complete class. This definition of the variational selection method makes it include a large variety of particular processes. For a given value of M we could take considerable pains to minimize E_k^M with respect to the various parameters which designate the members of the complete class, or we could perform many schemes of less exhaustive tests. In actual fact the postulated comparison with some single-system method will be only nominal, because in minimizing at all we shall generally have implicitly compared with the use of a single complete system of the functions. Single complete systems, such as those based on

$$\exp(-\alpha r^2),\ \exp(-2\alpha r^2),\ \text{etc.},$$

and the spherical harmonics, would be so simple to work with that no other choice would be made, unless the energy could be considerably lowered by doing so.

The significance of the procedure is probably shown most clearly by summarizing the basic assumptions as a conjectured theorem.

THEOREM 3. If ψ_k and E_k are the (k)th eigenfunction and eigenvalue of

$$(H-E_k)\,\psi_k = 0,$$

these being labelled in order of ascending E_k, if $\{\phi_r\}$ denotes a complete class of functions x, y, z, if (ϕ_r') denotes a complete system of functions occurring in $\{\phi_r\}$ and $\{\Phi_r'\}$ the complete system of detors formed from these, if $E_k'^M$ denotes the (k)th eigenvalue in the variational approximation using the first M of these detors, if Φ_r^M denotes a set of M detors made from any set of orthogonal functions out of $\{\phi_r\}$ such that these give a value $E_k^M < E'^M_k$ for the (k)th eigenvalue when used in the variational procedure, then E_k^M converge monotically to E_k and ψ_k^M, the corresponding eigenfunction, converges in the mean square sense to ψ_k.

This theorem cannot be proved rigorously, but it is justified to a degree corresponding to assumptions of the ordinary variational method. The convergence of E_k^M follows from the variational theory when we assume the completeness of the detors formed from a complete system. The convergence of ψ_1^M follows from the convergence of E_1^M just as given by Kemble (1937) for the ordinary variational procedure. The convergence of $E_k^M (k>1)$ has not been proved. However, all practical experience has justified the assumption of the variational theorem (1), and it appears practically certain that theorem (3) will be similarly justified.

The only quantities which we require to carry out the process numerically for particular molecules are the values of the Schrödinger integrals between the detors used to approximate to the wave function. But it has been shown that, if we work with the complete class of Gaussian functions, all these can be expressed very simply in terms of tabulated functions. Since this complete class contains all Gaussian and Hermitian functions situated at all points of space, it is particularly appropriate for molecules and systems of atoms where the nuclei and concentrations of electrons occur at large distances. We can facilitate the rate of convergence by using linear combinations of functions centred round the different centres of electronic concentration. The early terms can correspond to complete systems of functions on the several centres concerned. The essential virtue of the complete Gaussian class is that it is the only complete class in which there occur complete systems of functions situated round all points and for which all the integrals involved in the variational selection method of detors can be evaluated.

It has thus been established that the only difficulty which exists in the evaluation of the energy and wave function of any molecule, or other system of atomic nuclei and electrons, when the complete Gaussian class is used with the variational selection method, is the amount of computing necessary. This computing consists only of ordinary arithmetical processes and of reading from existing function tables and does not involve any numerical integrations. Whether this method will be finally used or whether a modification or a separate method may be developed, cannot at present be foreseen, but this represents a definite step forward, since it is the first time it has been possible to state such a scheme.

4. The application of the variational selection method for non-Gaussian functions, and the application to atoms

It will have been noted that the practical application of the variational selection method to detors constructed from complete classes of functions $\{f_r\}$ other than the Gaussian class would be quite possible if the integrals

$$(f_r\,|\,f_s),\quad (f_r\,|\,V_I\,|\,f_s),\quad (f_r\,|\,K\,|\,f_s),\quad [f_rf_s\,|\,M\,|\,f_tf_u] \tag{35}$$

could be evaluated. It is, however, very desirable that the complete class of functions used contains complete systems of functions which can be placed round all the different atomic nuclei in the system. No other class satisfying these requirements is known, unless we are prepared to consider the possibility of straightforward numerical integration of the necessary integrals. This is not feasible because, even allowing for considerable simplification, a numerical integration over six dimensions with infinite ranges is completely prohibitive. Hence, unless new methods of the requisite integral evaluation are developed, the use of the Gaussian class constitutes the only method for general molecules.

If the necessary integrals could be evaluated the functions which would be generally considered to be most useful and rapidly convergent would be the class composed of the functions $x^ly^mz^n\exp(-\alpha r_A)$, together with all linear combinations of these. Reasonable accuracy would be expected with small numbers of terms in this case. This follows since, if the electrons did not interact and were only subject to the field of one nucleus at a time, perfectly accurate solutions of this form could be written down. Even when electronic interaction is allowed for, such functions have given surprisingly good results for approximations to atomic wave functions using only very few terms. However, it is well known that the evaluation of the general integrals in such cases has proved to be a singularly intractable problem, and the use of these functions cannot be considered unless some definite progress is made in the evaluation of these integrals.

The situation for atoms is much simpler. In this case the class of all linear combinations of functions $x^l y^m z^n \exp(-\alpha r)$ situated about the single nucleus is likely to give rapidly convergent approximations and all the necessary integrals can be evaluated. A first result using this method for beryllium is reported in a subsequent paper. Actually it is convenient to write the functions in the form

$$S^{lm}(\theta, \phi)\, r^{l+p} \exp(-\alpha r),$$

where S^{lm} is a spherical harmonic. The methods of evaluation of the necessary integrals are well known and the manipulation is particularly simple. The class can be easily shown to contain complete systems of functions since a system

$$\exp(-nkr), \ (n = 1, 2, \ldots)$$

is complete with respect to the radial variation, while the spherical harmonics are complete with respect to the angular variation. By considering different values of k we have infinite numbers of complete systems in our general class. The use of such functions for approximate wave functions consisting only of single detors has been made several times, the most systematic calculations being those of Morse, Young & Haurwitz (1935). However, the systematic use as a converging method by means of increasing numbers of detors has not previously been attempted.

The method which has been most extensively used for atoms is the Hartree-Fock method. The relation of this to our present considerations can be stated by saying that numerical functions of the type $f(r)\, S^{lm}(\theta, \phi)$ are used. In the ordinary case only a single detor has been used, and there is no attempt to obtain ultimate convergence. In the modification which is called 'superposition of configurations' more detors have been used, but actually, since all the integrals have to be evaluated numerically, it does not appear to be feasible to use more than two or three such terms. However, in principle this method can be regarded as a particular case of the procedure we have called variational selection, although in practice it is very dissimilar from the use of explicit functions.

In conclusion, the author wishes to state that, in his opinion, we shall ultimately be driven to the general method of variational selection of detors from one or other complete class of functions for more accurate data on the structure of atoms and molecules. Since the method using Gaussian class of functions for molecules would be laborious although possibly necessary, it appears best to develop and systematize the common aspect, the variation selection method. This can be done by some calculations for atoms while at the same time obtaining useful results. Numerical and theoretical results along these lines will be reported in the subsequent parts of this series of papers.

5. Discussion

The value of the present treatment lies not so much in the fresh mathematical analysis, which is relatively elementary, but in the fact that it provides for the first time a systematic scheme by which the wave functions of the stationary states of the electrons in the field of any arrangement of nuclei can be evaluated. In general, the necessary computation would be laborious, but there are cases where such calculations provide the only hope of obtaining data otherwise almost inaccessible, and where long calculations might be worth while. On the other hand, it may be possible to improve the scheme either by modifications of the mathematical method, or by developments purely in the numerical procedure. For atoms the use of the variational selection method for detors from exponentials instead of Gaussian functions appears as if it will provide a powerful method without further modification.

An interesting aspect of the general method is that it has a certain heuristic value. By slightly specializing the most general method one is able to give an extremely compact statement of a procedure to which quantum mechanics reduces the general problem of predicting the energy and structure of any system of atoms and molecules. 'Consider Gaussian polynomial products situated around each nucleus of the system. Take orthogonal linear combinations of these and form the detors after combining these functions with the spin functions. Calculate the energy of a linear combination of these detors with adjustable coefficients. Choose these coefficients and the original parameters of the orthogonal functions to minimize the energy. As the number of functions considered is increased this energy will converge to the ground state. Alternatively, by minimizing a higher eigenvalue of the variational equation, we can converge to the energy of an excited state. All the necessary integrals can be evaluated by simple formulae.' The only errors which are not decreased indefinitely by taking larger numbers of detors are of the nature of relativistic corrections. It is the author's opinion that it is simpler to explain this general method than to explain many of the more approximate and restricted methods.

The relation of the present analysis to approximate theories, such as molecular orbitals, localized bonds, and modifications of these, is twofold. In the first place the integrals evaluated provide for the first time a possibility of applying these methods in a quantitative *a priori* manner for a general molecule without the necessity of the prohibitive numerical integrations over six dimensions. Previously, if calculations were attempted for any system more complicated than the simplest diatomic molecule, the only practical procedure was to derive the energy in terms of unknown integrals and then estimate these by comparison with experimental energies (Coulson 1947). In the second place an examination of the numbers of integrals which would be required for these approximate non-converging methods and for the variational selection of detors when using the same set of initial functions shows that the computation would not be very much greater in the general method. Hence it appears that in *a priori* calculations it will be most worth while to use the many detor procedure.

CONCLUSIONS

The methods developed above give for the first time a quantitative method of evaluating the stationary state wave functions and energy levels of all atoms and molecules to any required degree of accuracy. Direct application to complicated cases would involve very heavy computing but may be worth while in special cases. On the other hand, it may be possible to derive shorter modifications of the method. A related method, applicable only to atoms, appears to be of great practical value.

REFERENCES

Coulson, C. A. 1947 *Chem. Soc. Quart. Rev.* **1**, 144.
Courant, R. & Hilbert, D. 1931 *Methoden der Mathematischen Physik.* Berlin: J. Springer.
Hartree, D. R., Hartree, W. & Swirles, B. 1939 *Phil. Trans.* A, **238**, 229.
Hylleraas, E. A. 1929 *Z. Phys.* **54**, 347.
James, H. L. & Coolidge, A. S. 1933 *J. Chem. Phys.* **1**, 825.
Kemble, E. C. 1937 *Fundamental principles of quantum mechanics.* New York: McGraw. Hill Book, Co.
Morse, P. M., Young, L. A. & Haurwitz, E. S. 1935 *Phys. Rev.* **48**, 948.

The diffraction of blast. II.

BY M. J. LIGHTHILL, *Department of Mathematics, University of Manchester*

(*Communicated by S. Goldstein, F.R.S.—Received* 12 *August* 1949)

The head-on encounter of a plane shock, of any strength, with a solid corner of angle $\pi-\delta$ is investigated mathematically, when δ is small, by a method similar to that of part I. The incident shock is found to be reflected from each face as a straight segment, the two segments being joined by a shorter curved portion. Behind each straight segment is a region of uniform flow, the two regions being joined by one of non-uniform flow, bounded by arcs of a circle with centre at the corner, which expands at the local speed of sound, and by the shock, which is curved only where intersected by the said circle. The pressure is approximately equal in the two regions of uniform flow, but is less in the region of non-uniform flow between them; and it is found that if the deficiency of pressure therein, divided by the angle δ and by the excess of pressure behind the reflected shock, over that of the atmosphere, be plotted at points along the solid surface, after the incident shock has travelled a given perpendicular distance beyond the corner, then the curve is independent of δ and of the precise angle of incidence of the shock, and changes remarkably little in the whole range of incident shock strengths from 0 to ∞ (see figures 5 to 8). It is suggested that some of the above qualitative conclusions may be true even if δ is not small.

The case $\delta<0$, when the corner is concave to the atmosphere, is also considered. Shock patterns are found in cases when the incident shock has already been reflected from one, or both, walls before reaching the corner (figures 9 to 11).

1. INTRODUCTION

Let a plane shock, travelling horizontally into still air, encounter the corner of a building, which is assumed to extend indefinitely upwards and downwards for the purposes of the following analysis. Let the two faces of the building make angles δ_1 and δ_2 with the shock, so that the angle of the corner is $\pi-(\delta_1+\delta_2)=\pi-\delta$. Choose

(X, Y) co-ordinates with the corner as origin, and the direction of motion of the shock as the negative X-direction (figure 1). Then, as in the problem of part I (Lighthill 1949), the only physical constants (besides the angles) which define the state of affairs are U, the incident shock velocity, and p_0, ρ_0, the pressure and density in still air; hence no fundamental length or time scale exists, and, measuring the time t from the initial encounter with the corner, the pressure and velocity fields depend only on X/t and Y/t. By methods similar to those of part I, these are found below when δ is small.

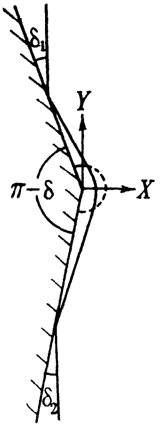

FIGURE 1

In § 2 the theory of the reflexion of a shock by an infinite plane wall is recalled. It seems plausible that in the present problem, even with δ not small, there will be regions behind the reflected shock where the flow is uniform, and bounded by a straight portion of the shock (whose position can be deduced from the simple reflexion theory of § 2); these will be those regions at a distance greater than roughly at from the corner (where a is a mean velocity of sound in the region behind the reflected shock). The fact that a mathematical solution, on this hypothesis, is discovered below when δ is small (when the region of non-uniform flow is partly bounded by a circle, since variations therein of the velocity of sound are then negligible) gives strong support to it also for larger values of δ. The curved portion of the reflected shock (where it is inside the circle) is found to be weaker than the rest, and may be regarded as the product of reflexion followed by diffraction.

The boundary value problem in the region of non-uniform flow is formulated (neglecting δ^2) in § 3, and solved by use of a Busemann transformation and a conformal transformation (as in part I) in § 4. The shape of the shock pattern, and the pressure distribution along the wall, are discussed in §§ 5 and 6 and illustrated for various incident shock strengths in figures 5 to 8. The change in shock pattern, due to taking δ_1 (or δ_2, or both) negative, is also noted in § 5. It is hoped that, in later parts, a more general account of shock diffraction will be given, involving extrapolation from the work of part I and this paper on shocks of arbitrary strength and small angles δ, and from the acoustic theory, where the shocks are weak but δ may be arbitrary.

2. Reflexion at an infinite plane wall

As in part I, let suffix unity denote the values of the pressure p, the density ρ, the velocity q or the local velocity of sound a, behind the undisturbed incident shock, and let suffix 2 denote those behind the reflected shock, when reflexion takes place at an infinite plane wall, so that p_2, ρ_2, q_2, a_2 are constants. (Suffix zero is reserved for the values of quantities in still air.) Let the velocity and angle of incidence of the shock be U, δ, let the velocity and angle of reflexion be V, δ' (see figure 2, where the directions of the airflow in the two disturbed regions are also shown). Since the shocks always meet at the wall, $V \operatorname{cosec} \delta' = U \operatorname{cosec} \delta$. Using equations (I, 2)* on the reflected shock, replacing U therein by the velocity $V + q_1 \cos(\delta + \delta')$ (relative to the air ahead of it) of the shock normal to itself, q_1 by the change $q_1 \cos(\delta+\delta') + q_2 \sin\delta'$ in normal velocity at the shock, and $p_1, \rho_1, p_0, \rho_0, a_0$ by $p_2, \rho_2, p_1, \rho_1, a_1$, and expressing also the condition of continuous tangential velocity, the equations

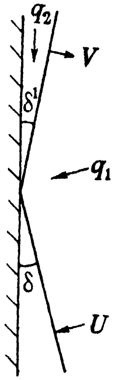

Figure 2

$$\left.\begin{aligned}
q_1 \cos(\delta+\delta') + q_2 \sin\delta' &= \frac{5}{6}\left[V + q_1\cos(\delta+\delta') - \frac{a_1^2}{V + q_1\cos(\delta+\delta')}\right],\\
p_2 &= \tfrac{5}{6}\rho_1[(V+q_1\cos(\delta+\delta'))^2 - \tfrac{1}{7}a_1^2],\\
\rho_2 &= 6\rho_1\left[1 + \frac{5a_1^2}{(V+q_1\cos(\delta+\delta'))^2}\right]^{-1}, \quad q_1\sin(\delta+\delta') = q_2\cos\delta',
\end{aligned}\right\} \tag{1}$$

result. Neglecting the squares of δ and δ', the cosines may be replaced by 1, and $q_2 \sin\delta'$ ignored compared with q_1. This gives simplified equations, which are easily solved. Using (I, 2) the answers may be put in the form

$$\left.\begin{aligned}
&V = \tfrac{1}{3}U(1+2M^{-2}), \quad \delta' = \tfrac{1}{3}\delta(1+2M^{-2}), \quad q_2 = q_1\delta(\tfrac{4}{3}+\tfrac{2}{3}M^{-2}),\\
&p_2 = \frac{5(7M^2-1)(4M^2-1)}{21M^2(M^2+5)}\rho_0 U^2, \quad \rho_2 = \frac{3M^2(7M^2-1)}{(M^2+5)(M^2+2)}\rho_0,\\
&a_2 = \left(\frac{7p_2}{5\rho_2}\right)^{\frac{1}{2}} = \tfrac{1}{3}U(4M^2-1)^{\frac{1}{2}}(M^2+2)^{\frac{1}{2}}M^{-2},
\end{aligned}\right\} \tag{2}$$

---

* This notation signifies 'equation (2) of part I (Lighthill 1949)'.

where $M = U/a_0$ is the Mach number of the incident shock. It should be noticed that p_2, ρ_2 and a_2 are independent of δ if δ^2 be neglected.*

3. CONDITIONS IN THE REGION OF NON-UNIFORM FLOW

If $\mathbf{q}_3$, p_3, ρ_3 denote velocity, pressure and density in the region of non-uniform flow, then where this adjoins the regions of uniform flow behind the reflected shocks, namely, on two circular arcs, the work of § 2 shows that $p_3 = p_2$, $\rho_3 = \rho_2$ on both, and that $\mathbf{q}_3$ is $(0, q_1\delta_1(\frac{4}{3}+\frac{2}{3}M^{-2}))$ on the one and $(0, -q_1\delta_2(\frac{4}{3}+\frac{2}{3}M^{-2}))$ on the other, if δ_1^2 and δ_2^2 be neglected. This indicates that a solution should be sought with $\mathbf{q}_3$, p_3-p_2, and $\rho_3-\rho_2$ small throughout the field. On this assumption the equations of motion, namely (I, 4), with suffix 3 replacing 2, become approximately

$$\frac{\partial \rho_3}{\partial t}+\rho_2 \operatorname{div} \mathbf{q}_3 = 0, \quad \frac{\partial \mathbf{q}_3}{\partial t}+\frac{1}{\rho_2}\nabla p_3 = 0, \quad \frac{\partial s_3}{\partial t} = 0. \tag{3}$$

Replacing $\partial\rho_3/\partial t$ by $a_2^{-2}\partial p_3/\partial t$ by virtue of the last equation, and putting

$$\frac{X}{a_2 t} = x, \quad \frac{Y}{a_2 t} = y, \quad \mathbf{q}_3 = (u, v), \quad \frac{p_3-p_2}{a_2\rho_2} = p, \tag{4}$$

the first two equations of (3) become the fundamental three equations (I, 8) in u, v, p in terms of x, y.

The region of non-uniform flow in the (x, y) plane is the part of the unit circle between the wall and the shock. (This represents a circle in the (X, Y) plane expanding with velocity a_2.) On both wall and shock change in x is slow compared with change in y; hence both may be approximated by straight segments, in the case of the wall clearly $x = 0$. The approximate value of X on the shock, where it is curved (figure 1), is the distance Ut/δ_1 so far travelled along the upper face by the original shock, multiplied by the angle of reflexion δ_1' at the upper face; this gives

$$x = \frac{U\delta_1'}{a_2\delta_1} = \frac{3M^2}{(4M^2-2)^{\frac{1}{2}}(M^2+2)^{\frac{1}{2}}}\tfrac{1}{3}(1+2M^{-2}) = \left(\frac{M^2+2}{4M^2-1}\right)^{\frac{1}{2}} = k_0 < 1. \tag{5}$$

Thus the region of non-uniform flow in the (x, y) plane is approximately $0 < x < k_0$, $x^2+y^2 < 1$ (figure 3). The approximate shock position $x = k_0$ replaces the $x = k$ of part I.

The boundary condition at the wall is that $u/v = -\delta_1$, δ_2 on the two faces; but v is small, and therefore these may be replaced by $u = 0$ on $x = 0$. On the circular arc boundary with $y > 0$, $p = u = 0$ and $v = q_1\delta_1(\frac{4}{3}+\frac{2}{3}M^{-2})$; on that with $y < 0$, $p = u = 0$ and $v = -q_1\delta_2(\frac{4}{3}+\frac{2}{3}M^{-2})$.

To get the boundary condition on $x = k_0$, let the shock (inside the circle) be, to a higher approximation, $x = k_0+f(y)$, where $f(y)$ is small: then it expands (as does the whole field) with velocity $(X/t, Y/t) = a_2(k_0+f, y)$. The shock conditions are (I, 2), with U replaced by the velocity $q_1+a_2(k_0+f)-a_2yf'$ (relative to the air ahead of it) of the shock normal to itself, and q_1 replaced by the change q_1+u in normal velocity at the shock, and with p_1, ρ_0, a_0 replaced by p_3, ρ_1, a_1. With the condition of continuous tangential velocity, these are

---

* The arguments in § 2 would have to be reworded if δ were zero. The same will be true in what follows if δ_1 or δ_2 were zero, but it is easily seen that the conclusions hold without modification and no further special mention of this case will be made.

$$\left.\begin{aligned} q_1+u &= \frac{5}{6}\left[q_1+a_2(k_0+f-yf')-\frac{a_1^2}{q_1+a_2(k_0+f-yf')}\right], \\ p_2+a_2\rho_2 p &= \tfrac{5}{6}\rho_1[(q_1+a_2(k_0+f-yf'))^2-\tfrac{1}{7}a_1^2], \quad v = -q_1 f'. \end{aligned}\right\} \tag{6}$$

Continuing to neglect squares of small quantities, one obtains from (6)

$$p = \frac{5(M^2+2)}{9M^2}U(f-yf'), \quad u = \frac{5(4M^2+2)(4M^2-1)^{\frac{1}{2}}(M^2+2)^{\frac{1}{2}}}{9M^2(7M^2-1)}U(f-yf'),$$
$$v = -\frac{5(M^2-1)}{6M^2}Uf', \tag{7}$$

from which f can be eliminated, as in (I, 14), to give

$$u = A_0 p, \quad y\partial v/\partial y = B_0\,\partial p/\partial y \quad \text{on} \quad x = k_0, \tag{8}$$

where
$$A_0 = \frac{4M^2+2}{7M^2-1}\left(\frac{4M^2-1}{M^2+2}\right)^{\frac{1}{2}}, \quad B_0 = \frac{3(M^2-1)}{M^2+2}. \tag{9}$$

This completes the account of the boundary value problem in the region $x^2+y^2<1$, $0<x<k_0$.

4. Solution of the boundary value problem

As in part I, the problem is solved by first eliminating u and v, and then applying Busemann's transformation. In terms of p alone, which satisfies the second-order linear partial differential equation (I, 16), the boundary condition at the wall is $\partial p/\partial x = 0$ (since by (I, 8) this gives $\partial u/\partial y = 0$ on $x = 0$). On the curved portions of the boundary $p = 0$. At $x = k_0$, where condition (8) exactly reproduces condition (I, 14), but with the constants changed (as the zero suffix indicates), the condition on p must be (I, 19) with A, B, k replaced by A_0, B_0, k_0. There will also be the condition that the change in v along the shock from bottom to top be

$$\int \frac{\partial v}{\partial y}dy = \int \frac{B_0}{y}dp = q_1\delta(\tfrac{4}{3}+\tfrac{2}{3}M^{-2}). \tag{10}$$

When the problem has been solved for p under these conditions, the last two equations of (I, 8) will give the radial derivatives of u and v; hence u and v can be evaluated, by integration along radii, from their values on the circular portions of the boundary and on $x = k_0$. The latter are given in terms of p by equations in § 3, which will be consistent provided that (10) holds. (No logarithmic infinity for u or v at the origin, such as occurred in part I, will result from the last two equations of (I, 8), since it will be found that in the present problem $\partial p/\partial x = \partial p/\partial y = 0$ at $x = y = 0$.) Hence the boundary value problem just formulated, in terms of p alone, is equivalent to that previously formulated in terms of u, v and p.

When Busemann's transformation to a (ρ, θ) plane is made, where

$$x = 2\rho\cos\theta/(1+\rho^2), \quad y = 2\rho\sin\theta/(1+\rho^2), \tag{11}$$

the equation for p, as in (I, 22), becomes Laplace's equation in (ρ, θ) as plane polar co-ordinates. The boundary conditions are as follows. On the wall $\theta = \pm\frac{1}{2}\pi$,

$\partial p/\partial n = 0$. On the two arcs of the circle $\rho = 1, p = 0$. On $x = k_0$, which becomes that arc of the circle $2\rho\cos\theta = k_0(1+\rho^2)$ which is inside $\rho = 1$ (which it cuts orthogonally),

$$\frac{\partial p/\partial n}{\partial p/\partial s} = \frac{A_0k_0\tan\theta - B_0\cot\theta}{(1-k_0^2\sec^2\theta)^{\frac{1}{2}}}, \tag{12}$$

exactly as in (I, 28). Here ∂n is along the outward normal, and ∂s in the positive tangential direction.

Now put $\zeta = \rho e^{i\theta}$ and make the following conformal transformation:

$$z_1 = \log\left(\frac{1+\zeta}{1-\zeta}\right) + \tfrac{1}{2}\pi i. \tag{13}$$

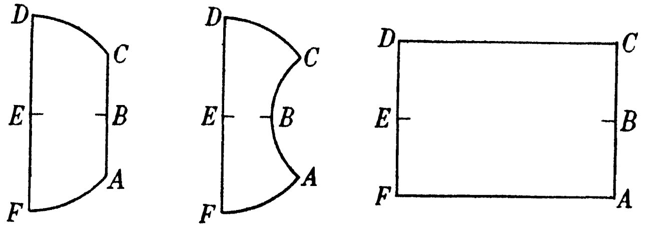

(x, y) plane. ζ plane. z_1 plane.

FIGURE 3.

Then (figure 3) the diameter DEF becomes the segment $x_1 = 0$, $0 < y_1 < \pi$ (where $z_1 = x_1 + iy_1$); the circular arcs DC and FA become parts of $y_1 = \pi$ and $y_1 = 0$ respectively; while on ABC

$$\begin{aligned} z_1 &= \tfrac{1}{2}\log\frac{1+2\rho\cos\theta+\rho^2}{1-2\rho\cos\theta+\rho^2} + i\left(\tfrac{1}{2}\pi + \tan^{-1}\frac{\rho\sin\theta}{1+\rho\cos\theta} + \tan^{-1}\frac{\rho\sin\theta}{1-\rho\cos\theta}\right) \\ &= \tfrac{1}{2}\log\frac{1+k_0}{1-k_0} + i\left(\tfrac{1}{2}\pi + \tan^{-1}\frac{2\rho\sin\theta}{1-\rho^2}\right) = \lambda + iy_1, \end{aligned} \tag{14}$$

where λ is the constant shown, and

$$\tan(y_1 - \tfrac{1}{2}\pi) = k_0\tan\theta(1-k_0^2\sec^2\theta)^{-\frac{1}{2}},$$

so that the relationship between y and y_1 on ABC is

$$y = k_0\tan\theta = -(1-k_0^2)^{\frac{1}{2}}\cos y_1 = -k_0'\cos y_1. \tag{15}$$

Thus the z_1 plane is a rectangle $0 < x_1 < \lambda$, $0 < y_1 < \pi$. On DC and FA $p = 0$; on DEF $\partial p/\partial n = 0$, i.e. $\partial p/\partial x_1 = 0$. On ABC, by (12) and (15), and since in a conformal transformation the local deformation of plane elements is a pure dilatation,

$$\frac{\partial p/\partial n}{\partial p/\partial s} = \frac{-A_0k_0'\cos y_1 + B_0k_0k_0'^{-1}\sec y_1}{k_0'\sin y_1}, \tag{16}$$

or

$$-\frac{\partial p}{\partial x_1}\sin y_1\cos y_1 = \frac{\partial p}{\partial y_1}\left(A_0\cos^2 y_1 - \frac{B_0k_0}{k_0'^2}\right) \text{ on } x_1 = \lambda. \tag{17}$$

By symmetry of the boundary conditions p is an even function of y, so that its derivative normal to EB vanishes; hence also on EB ($y_1 = \frac{1}{2}\pi$) in the new plane,

$\partial p/\partial y_1 = 0$. Hence $w(z_1) = \partial p/\partial x_1 - i\partial p/\partial y_1$, a regular function of z_1 which is purely imaginary on DEF, DC and FA, vanishes at E. On ABC

$$\arg w(z_1) = \tan^{-1}\left(\frac{\tan y_1}{A_0 - B_0 k_0 k_0'^{-2}\sec^2 y_1}\right) = \tan^{-1}(\alpha \tan y_1) + \tan^{-1}(\beta \tan y_1), \quad (18)$$

where
$$\frac{1}{\alpha+\beta} = A_0 - \frac{B_0 k_0}{k_0'^2}, \quad \frac{\alpha\beta}{\alpha+\beta} = \frac{B_0 k_0}{k_0'^2}, \quad (19)$$

so that by (9) α, β are the two positive numbers

$$\frac{(7M^2-1)(M^2+2)^{\frac{1}{2}} \pm (M^2-1)(21M^2-3)^{\frac{1}{2}}}{(M^2+5)(4M^2-1)^{\frac{1}{2}}}. \quad (20)$$

As $y_1 \to 0$ or π, expression (18) tends to 0 or 2π respectively. But on $y_1 = 0$ and $y_1 = \pi$, $w(z_1)$ is purely imaginary. Hence $\arg w(z_1)$ is discontinuous at $(\lambda, 0)$ and (λ, π), so that $w(z_1)$ has a zero or a pole at each of these points. In what follows a solution will be found with $w(z_1)$ regular inside and on the boundary, and *therefore* with zeroes at E, C and A, but with no other zeroes and with these all simple ones. It must be the only solution regular inside and on the boundary, because if there were another, say $w_1(z_1)$, then $w_1(z_1)/w(z_1)$ would also be regular inside and on the boundary, but by the boundary conditions would be purely real on the boundary. Hence it would be a mere constant, which can have only one determination by condition (10).

The assumption as to zeroes at E, C, A means that since $\arg w(z_1)$ varies from 0 to 2π along ABC, it is $\frac{3}{2}\pi$ on EDC and $\frac{1}{2}\pi$ on EFA. Now expression (18), if the constant π be subtracted from it, has the Fourier sine series

$$-\sum_{n=1}^{\infty} (2 - a^n - b^n)\, n^{-1} \sin 2ny_1, \quad (21)$$

where $a = (\alpha-1)/(\alpha+1)$, $b = (\beta-1)/(\beta+1)$. Hence the function

$$W(z_1) = \exp\left\{-\sum_{n=1}^{\infty} (2 - a^n - b^n)\, n^{-1} \operatorname{cosech} 2n\lambda \cosh 2nz_1\right\}, \quad (22)$$

the imaginary part of whose logarithm is (21) on $x_1 = \lambda$, and is zero on $y_1 = 0, \pi$ and on $x_1 = 0$, satisfies the boundary condition on ABC, but has zero argument on EDC and EFA.

To get $w(z_1)$, $W(z_1)$ must be multiplied by a function whose argument is π on ABC, $\frac{3}{2}\pi$ on EDC and $\frac{1}{2}\pi$ on EFA. Such a function is clearly doubly-periodic, by repeated application of Schwarz's reflexion principle; and on reference to (say) Whittaker & Watson (1935) one finds that (in their notation)

$$i\frac{\vartheta_2(-iz_1, q)}{\vartheta_4(-iz_1, q)}, \quad \text{where} \quad q = e^{-2\lambda} = \frac{1-k_0}{1+k_0}, \quad (23)$$

satisfies the said conditions. Since by (5) $0 < q < \frac{1}{3}$ in $1 < M < \infty$, these theta functions are given by extremely rapidly convergent series.

Putting then

$$w(z_1) = Ki\frac{\vartheta_2(-iz_1)}{\vartheta_4(-iz_1)} W(z_1), \quad (24)$$

the constant K must be determined by condition (10). This requires the value of $\partial p/\partial y_1$ on $x_1 = \lambda$, which is

$$\left(\frac{\partial p}{\partial y_1}\right)_{x_1=\lambda} = -K\frac{\vartheta_3(y_1)}{\vartheta_1(y_1)}\,|\,W(\lambda+iy_1)\,|\,\sin\left[\tan^{-1}(\alpha\tan y_1)+\tan^{-1}(\beta\tan y_1)\right], \qquad (25)$$

using (18) and the formulae for changing the argument of the theta functions by a half-period. Here

$$|\,W(\lambda+iy_1)\,| = \exp\left\{-\sum_{n=1}^{\infty}(2-a^n-b^n)\,n^{-1}\coth 2n\lambda\cos 2ny_1\right\}, \qquad (26)$$

and since $\coth 2n\lambda = (1+q^{2n})/(1-q^{2n}) = 1+2q^{2n}+2q^{4n}+\ldots$, and since

$$-\sum_{n=1}^{\infty} r^n n^{-1}\cos 2ny_1 = \tfrac{1}{2}\log(1-2r\cos 2y_1+r^2),$$

(26) can be rewritten as the rapidly convergent infinite product

$$|\,W(\lambda+iy_1)\,| = \prod_{m=0}^{\infty}{}'\left[\frac{(1-2q^{2m}\cos 2y_1+q^{4m})^2}{(1-2aq^{2m}\cos 2y_1+a^2q^{4m})\,(1-2bq^{2m}\cos 2y_1+b^2q^{4m})}\right], \qquad (27)$$

where Π' signifies that in the case of the term $m = 0$ only the square root should be taken. Expression (25) can now be computed, and condition (10), which by (15) takes the form

$$\int_0^{\pi}\left(\frac{\partial p}{\partial y_1}\right)_{x_1=\lambda}\sec y_1\,dy_1 = -\frac{q_1\delta k'_0}{B_0}\left(\tfrac{4}{3}+\tfrac{2}{3}M^{-2}\right), \qquad (28)$$

then gives K by numerical integration (see table 1). By (25) and (28) $K>0$; if an odd multiple of π had been added to (18) (as would have been permissible at that stage), so that values of $\arg w(z_1)$ different by this amount would have appeared all round the boundary, the final value of K would have been negative, contradicting that assumption and leading back to the solution deduced above.

TABLE 1

p_1/p_0	2	3	∞
$K/q_1\delta$	0·420	0·331	0·158

The expression (25) is also used to obtain the shape of the shock (§ 5). To get the wall-pressure distribution (§ 6),

$$\left(\frac{\partial p}{\partial y_1}\right)_{x_1=0} = -K\frac{\vartheta_2(y_1)}{\vartheta_4(y_1)}\,W(iy_1) \qquad (29)$$

is required. Here

$$\begin{aligned} W(iy_1) &= \exp\left\{-\sum_{n=1}^{\infty}(2-a^n-b^n)\,n^{-1}\operatorname{cosech} 2n\lambda\cos 2ny_1\right\} \\ &= \prod_{m=0}^{\infty}\left[\frac{(1-2q^{2m+1}\cos 2y_1+q^{4m+2})^2}{(1-2aq^{2m+1}\cos 2y_1+a^2q^{4m+2})\,(1-2bq^{2m+1}\cos 2y_1+b^2q^{4m+2})}\right]. \qquad (30)\end{aligned}$$

In computing (25) and (29) the equivalence of the series and product forms for the theta functions has been freely used.

As the strength of the incident shock tends to zero, i.e. $M \to 1$, $K/q_1\delta$ actually tends slowly to infinity. However, a limiting form of the pressure distribution can still be found, as in § 9 of part I, and checked satisfactorily with the limiting form of the acoustic theory as $\delta \to 0$. This work is omitted; it is actually easier than in part I, as there is no non-uniformity in the equivalence of the two methods. The wall-pressure distribution is found to be given by

$$p = -\frac{2}{\pi} q_1 \delta (1-y^2)^{\frac{1}{2}}. \tag{31}$$

The shock shape, in the small portion where it is curved, is a circular arc. These facts will be used, for comparison with the theory for strong shocks, in what follows.

5. The shock pattern

One finds that a reasonably clear indication of the variation of shock pattern, and of wall-pressure distribution, with the strength of the incident shock, is given by evaluating these when the pressure ratio across the incident shock is successively 1, 2, 3 and ∞ (the first and last being of course limiting cases). The variation is considerably smoother than in the problem of part I.

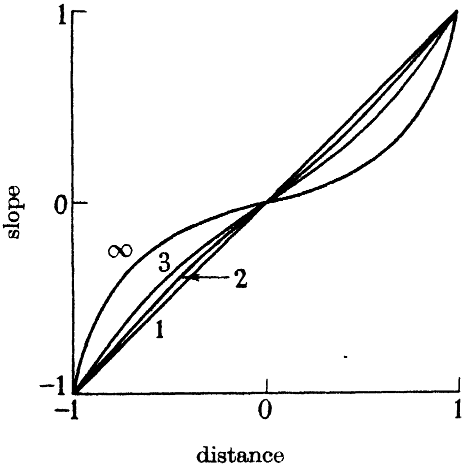

Figure 4. Slope of curved portion of shock, against distance along it, each altered in scale so as to run from − 1 to + 1. The numbers on the curves are the values of p_1/p_0.

The slope of the curved portion of the reflected shock is

$$\begin{aligned}\frac{dx}{dy} = f'(y) = -\frac{v}{q_1} &= \delta_2(\tfrac{4}{3}+\tfrac{2}{3}M^{-2}) - \frac{1}{q_1}\int_{-k'_0}^{y} \frac{B_0}{y}\,dp \\ &= \delta_2(\tfrac{4}{3}+\tfrac{2}{3}M^{-2}) - \frac{B_0}{q_1 k'_0}\int_0^{y_1} \left(\frac{\partial p}{\partial y_1}\right)_{x_1=\lambda} \sec y_1\, dy_1. \end{aligned} \tag{32}$$

Its distribution along the length of the said curved portion is shown in figure 4, where

$$\left[-\frac{dx}{dy} + \tfrac{1}{2}(\delta_2 - \delta_1)\,(\tfrac{4}{3}+\tfrac{2}{3}M^{-2})\right] \Big/ [\tfrac{1}{2}(\delta_2+\delta_1)\,(\tfrac{4}{3}+\tfrac{2}{3}M^{-2})] \tag{33}$$

is tabulated against y/k'_0—in other words, the scales of slope, and of distance along the curved portion of the shock, are altered (differently for each incident shock strength) so that each runs from − 1 to + 1. This brings out the fact that, for the stronger shocks, there is a considerably flatter portion in the centre of the diffracted reflected shock.

The slope has been integrated to enable the shape to be plotted in figures 5 to 8, where the wall-pressure distribution, to be discussed in § 6, is also shown. In these figures, to ease comparison of the effect of varying p_1/p_0, the same values of δ_1, δ_2 have been taken throughout, namely, $\delta_1 = \delta_2 = \frac{1}{4}$ radian $= 19°$. If the shape is required for any other values of δ_1, δ_2 with the *same* sum δ, it is obtained by drawing the reflected shocks in their new positions, and joining them by a curve congruent to the one shown in the figure (for the appropriate value of p_1/p_0). If the sum δ is different, by a given factor, then the curve required to join the two shocks must be expanded, normally but not tangentially, by that factor. Each of figures 5 to 8 represents the shock pattern after the incident shock has travelled unit perpendicular distance beyond the corner. Using this scale, the circle of non-uniform flow contracts (like a_2/U) as p_1/p_0 increases; the angle of reflexion also decreases (like $\frac{1}{3}+\frac{2}{3}M^{-2}$).

There is no subsidiary shock on (or near) the circular arc boundaries of the region of non-uniform flow, at least according to the test proposed in part I, that a positive pressure gradient radially inwards (i.e. one which $\rightarrow +\infty$ as the boundary is approached) represents a shock. For this condition can be written $\partial p/\partial n < 0$, if ∂n is along the outward normal in the ζ plane, and this implies that, in the z_1 plane, $\partial p/\partial y_1 < 0$ on EDC and $\partial p/\partial y_1 > 0$ on EFA. Since it was found in § 5 that the converse of both these conditions in fact holds, the conclusion is that at the circular arc boundaries there is not a shock but a rapid expansion; they are accordingly shown dotted in figures 5 to 8.

However, if $\delta = \delta_1 + \delta_2$ were negative, so that the corner were concave to the atmosphere, then p would everywhere change its sign, and there would be shocks approximately along these circular arcs. This case is illustrated in figure 9, where the incident shock is shown approaching the corner (with its two reflected shocks) and then shown after reflexion is complete, with the subsidiary weak circular shocks; here p_1/p_0 was taken as 3. Again figures 10 and 11 show two cases when δ_1 and δ_2 have opposite signs, also giving the initial and final patterns for $p_1/p_0 = 3$. It is hoped the reader will agree that these figures give considerable information about shock reflexion, especially if it is assumed that the behaviour discovered is qualitatively correct even when the angles δ_1, δ_2 are considerably larger in magnitude.

6. WALL-PRESSURE DISTRIBUTION

The distribution of pressure deficiency along the wall, obtained by integrating (29), is shown, divided by an appropriate factor, in figures 5 to 8. In choosing this factor to make the results as instructive as possible, an essential requirement was that the curves should remain finite and non-zero even in the limiting cases $p_1/p_0 \rightarrow 1$ and $p_1/p_0 \rightarrow \infty$. For the one finally selected, $\delta(p_2 - p_0)$, the curves (besides being independent of δ_1 and δ_2, which makes it unnecessary to draw further curves in figures 9 to 11) vary in scale remarkably little over the whole range $1 < p_1/p_0 < \infty$.

Perhaps the most important quantitative conclusion is this, that, in a given problem, the distribution of $(p_2 - p_3)/(p_2 - p_0)$ after the incident shock has travelled a given distance beyond the corner is (to within about 25 %) independent of shock

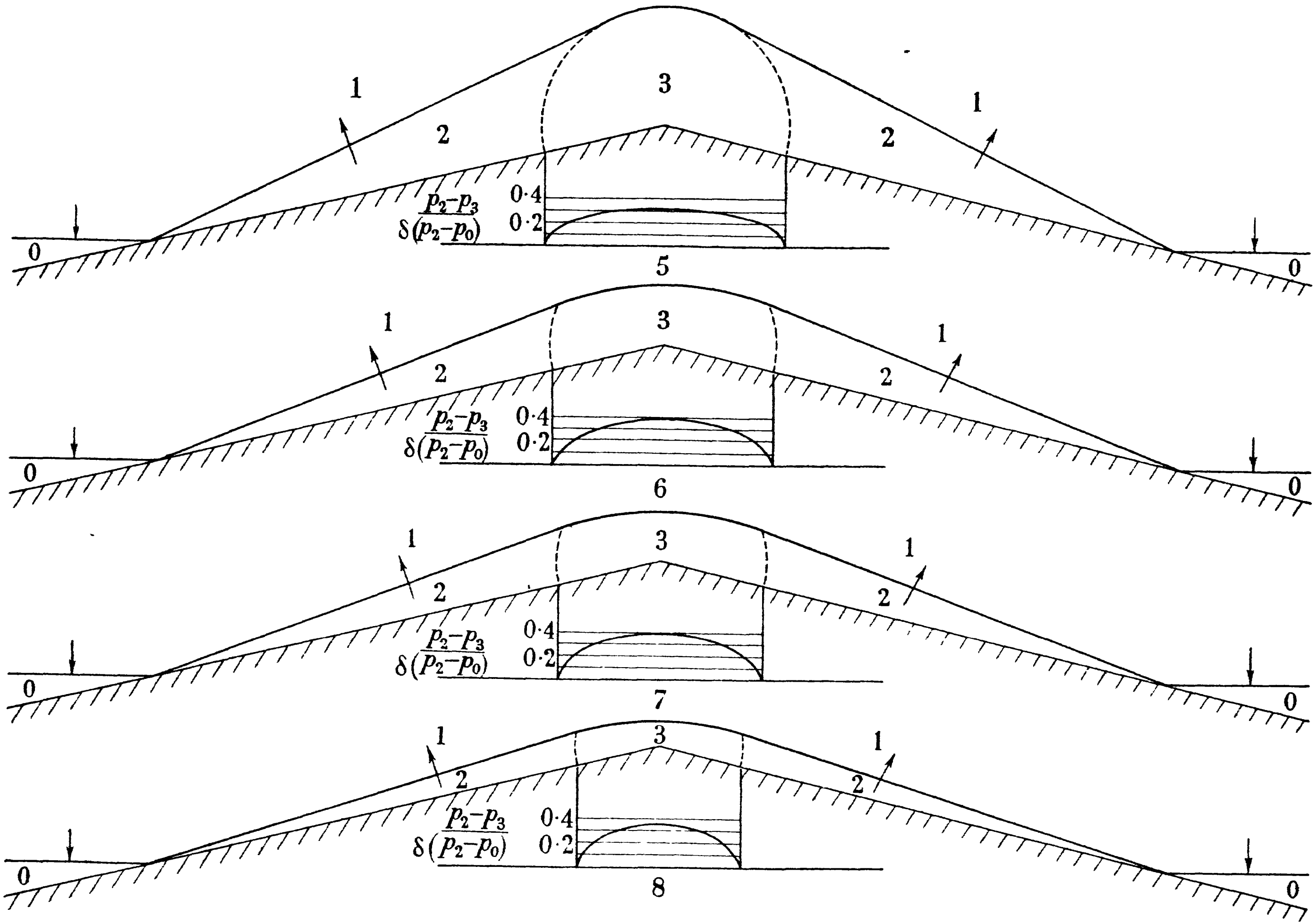

Figures 5 to 8. Shock pattern and wall-pressure distribution after reflexion ($\delta_1 = \delta_2 = \frac{1}{4}$, $\delta = \frac{1}{2}$). Suffixes on the pressure p refer to values in the regions so numbered in the figures. Values for p_1/p_0 are 1, 2, 3 and ∞ in figures 5, 6, 7 and 8 respectively.

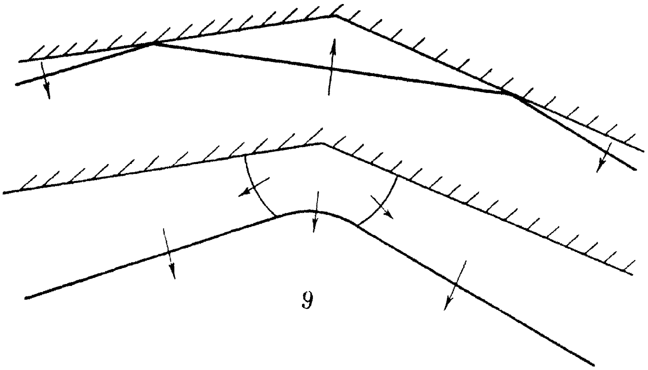

9

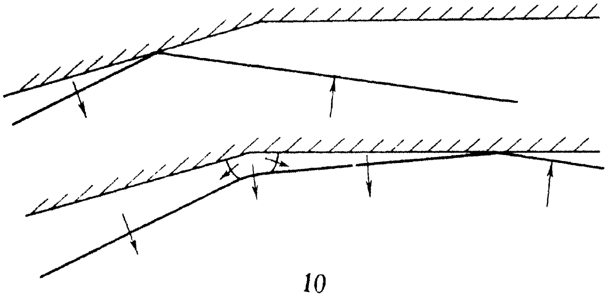

10

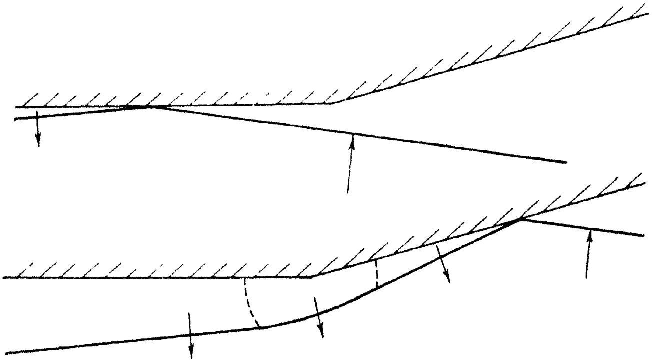

11

FIGURES 9 to 11. Incident and reflected shock systems. 9: $\delta_1 = \delta_2 = -\frac{1}{4}$, $p_1/p_0 = 3$; 10: $\delta_1 = \frac{1}{8}$, $\delta_2 = -\frac{3}{8}$, $p_1/p_0 = 3$; 11: $\delta_1 = \frac{3}{8}$, $\delta_2 = -\frac{1}{8}$, $p_1/p_0 = 3$.

strength. If it could be assumed that this was still true even when δ is large, then since the solution is known, for weak shocks, with δ arbitrary, an estimate of wall pressure could be given for all cases of shock reflexion from a corner.

REFERENCES

Lighthill, M. J. 1949 *Proc. Roy. Soc.* A, **198**, 454–470.
Whittaker, E. T. & Watson, G. N. 1935 *Modern analysis*, pp. 462–487. Cambridge University Press.

The dimerization of ammonia and amines

By J. D. Lambert and E. D. T. Strong

Physical Chemistry Laboratory, University of Oxford

(*Communicated by Sir Cyril Hinshelwood, F.R.S.—Received* 23 *September* 1949)

The second virial coefficients of ammonia and the vapours of the primary, secondary and tertiary methylamines and ethylamines have been measured at temperatures between 20 and 130° C. The results are interpreted as showing that dimerization occurs with ammonia and with the primary and secondary amines, but not with the tertiary amines. The dimerization is attributed to hydrogen bonding, and the energy of the N—H···N bond is discussed.

INTRODUCTION

Measurements of the compressibilities of organic vapours (Lambert, Roberts, Rowlinson & Wilkinson 1949) have shown that, under certain conditions, the second virial coefficient may be used as a quantitative criterion of the degree of dimerization of the vapour. Appreciable dimerization was found to occur only with strongly polar substances, where the energy of attraction between molecules, due to dipole interaction or to hydrogen bonding, exceeds kT. Measurements have now been made on ammonia and the primary, secondary and tertiary methylamines and ethylamines, in order to investigate whether dimerization occurs, and how the interaction between molecules is influenced by the progressive replacement of hydrogen atoms by alkyl groups.

EXPERIMENTAL

Measurements were made by the method previously described. Materials were purified as follows:

(*a*) *Gaseous*

Ammonia. Synthetic ammonia gas from a cylinder was dried by passing up a tower filled with freshly ignited quicklime and condensed in a bulb cooled in solid carbon dioxide and acetone. Air was removed by pumping off after freezing in liquid air, and the ammonia was then fractionally distilled *in vacuo*, and stored in a 4 l. bulb connected to the main apparatus through a mercury sealed tap.

Methylamine. Gaseous methylamine was prepared by dropping a 33 % solution of methylamine in water on to solid potassium hydroxide. The gas was dried by passing through towers filled with potassium hydroxide pellets and with freshly ignited quicklime, and was condensed in a bulb cooled in solid carbon dioxide and acetone. Removal of air and fractionation proceeded as with ammonia.

Ethylamine was prepared in the same way as methylamine.

Dimethylamine was prepared in the same way as methylamine. The sample prepared in this way gave consistent results with a different sample prepared from the anhydrous liquid and used as liquid (see below).

(*b*) *Liquid*

All liquids were introduced into the apparatus and stored in the way described previously. Preliminary purification was carried out as follows:

Dimethylamine was dried by standing over potassium hydroxide pellets and then introduced into the main apparatus and fractionally distilled *in vacuo.* Owing to the low boiling-point (7·4° C) no other procedure was practicable. Consistent results were obtained from different liquid samples and from a gaseous sample (see above).

Diethylamine was dried by standing over solid potassium hydroxide and distilled with a fractionating column. The fraction boiling at 55·5° C was introduced into the main apparatus and distilled *in vacuo.*

Trimethylamine was prepared in the same way as dimethylamine.

Triethylamine was prepared in the same way as diethylamine. The fraction used boiled at 89·5° C.

RESULTS

The measured values of the second virial coefficient, B, are shown plotted against temperature in figure 1. The results for ammonia are plotted together with values calculated by Stockmayer (1941) and Hirschfelder, McClure & Weeks (1942) from measurements by Meyers & Jessup (1925). Values of B calculated from the critical data by the Berthelot equation are shown on all the graphs as a full line. Critical data were obtained from Landolt & Bornstein *Tables*, and B calculated from the equation

$$B = \frac{9}{128}\frac{RT_c}{P_c}\left(1 - \frac{6T_c^2}{T^2}\right).$$

The values used for the various substances were as follows:

	T_c (° C)	P_c (atm.)	B
ammonia	132·5	112·3	$20{\cdot}8 - 2{\cdot}05 \times 10^7 T^{-2}$
methylamine	156·9	73·6	$33{\cdot}7 - 3{\cdot}73 \times 10^7 T^{-2}$
dimethylamine	164·5	52·35	$48{\cdot}2 - 5{\cdot}54 \times 10^7 T^{-2}$
trimethylamine	160·5	41·0	$61{\cdot}05 - 6{\cdot}88 \times 10^7 T^{-2}$
ethylamine	183·4	55·54	$47{\cdot}4 - 5{\cdot}93 \times 10^7 T^{-2}$
diethylamine	223·3	36·58	$78{\cdot}4 - 11{\cdot}58 \times 10^7 T^{-2}$
triethylamine	259·0	30·0	$102{\cdot}3 - 17{\cdot}38 \times 10^7 T^{-2}$

It will be seen from figure 1 that the measured values of B for trimethylamine and triethylamine fall on the Berthelot curve within the limits of experimental error. The measured values for ammonia and the primary and secondary amines all rise consistently above the Berthelot values at lower temperatures.

DISCUSSION

It was shown by Lambert *et al.* (1949) that the second virial coefficients of vapours which do not undergo association may be calculated from the critical data by the Berthelot equation for temperatures between $0{\cdot}5T_c$ and $1{\cdot}2T_c$. Vapours which associate give values of the second virial coefficient higher than those calculated by the Berthelot equation; if a reversible dimerization, $2A \rightleftharpoons A_2$, is assumed, the equilibrium constant, $K_p(=p_A^2/p_{A_2})$, may be calculated from the relation

$$K_p = \frac{-RT}{B-B_0},$$

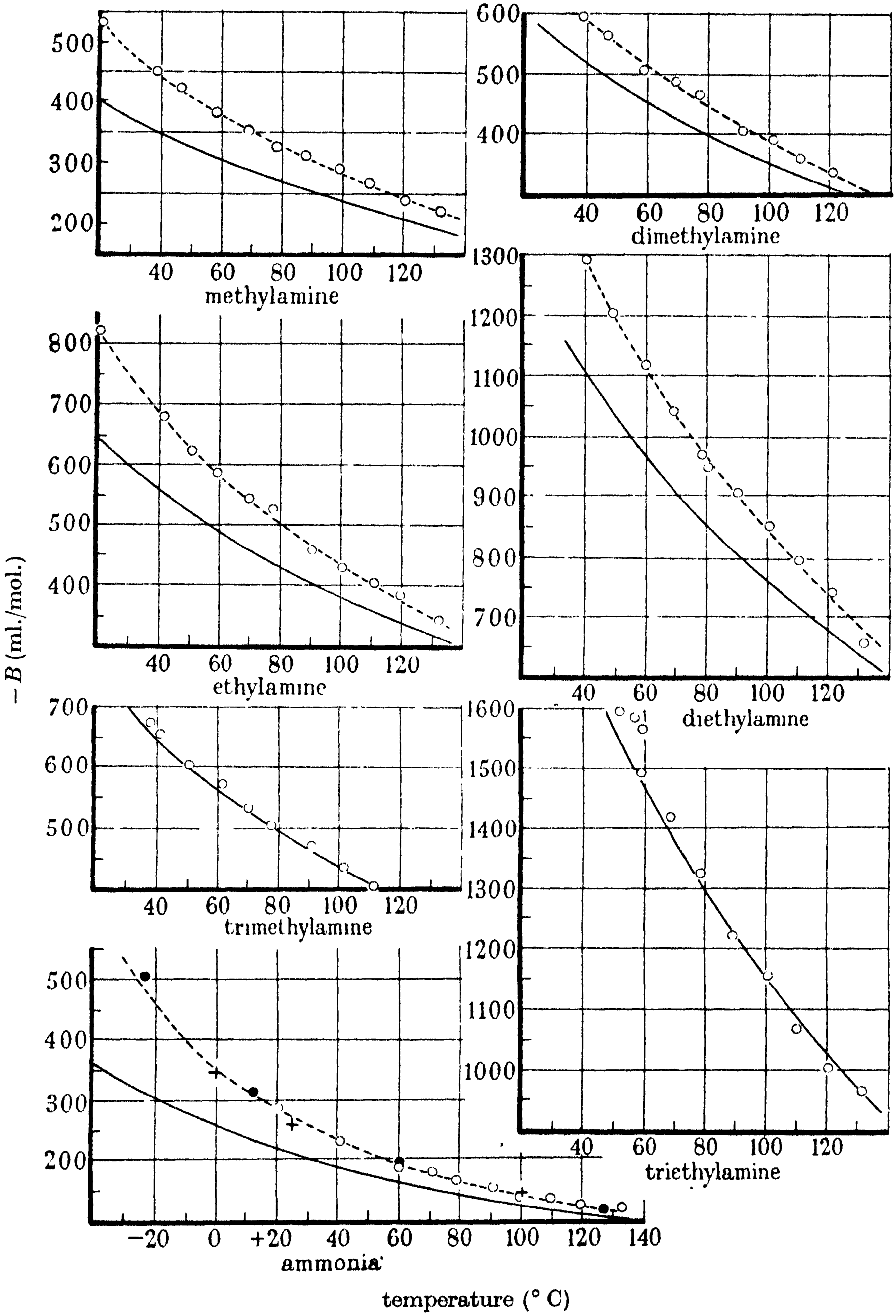

FIGURE 1. ○, observed values; ●, Stockmayer; +, Hirschfelder; ——, Berthelot curve.

where B is the observed value of the second virial coefficient, and B_0 the value calculated by the Berthelot equation. The measurements described here were all made in the temperature range from $0{\cdot}56T_c$ to $1{\cdot}0T_c$. Trimethylamine and triethylamine may

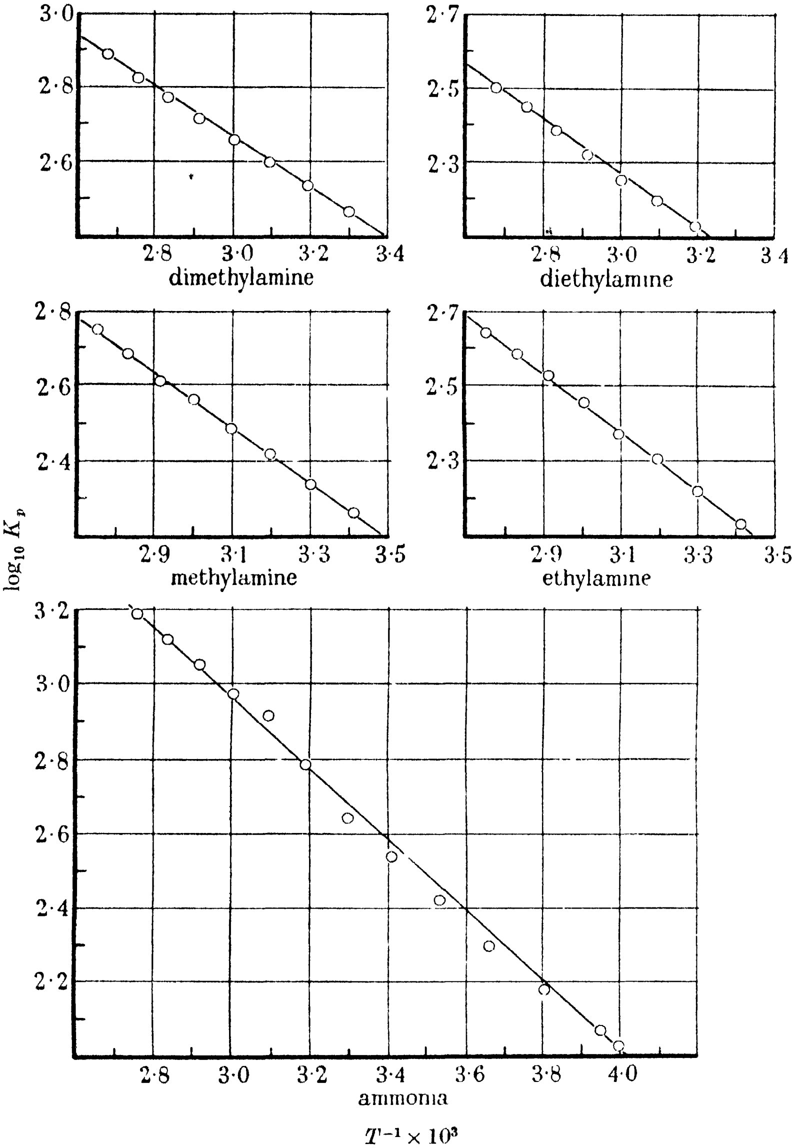

FIGURE 2

therefore be regarded as non-associated, while ammonia and the primary and secondary amines are associated. Values of K_p may be calculated for the latter substances from the data in figure 1 (assuming the association to be a dimerization), and $\log K_p$ is shown plotted against T^{-1} in figure 2. The points for all five substances fall on straight lines from whose slopes the values for the heats of dimerization given in table 1 are calculated. The fact that linear plots of log K_p against T^{-1} are obtained confirms that the process involved is essentially a dimerization in all cases (cf. Lambert, Staines & Woods 1950), and that higher polymers are not formed to any appreciable extent.

TABLE 1

substance	$-\Delta H$ (cal./mol.)	$-\Delta U_{298}$ (cal./mol.)
ammonia	4400	3800
ethylamine	3600	3000
methylamine	3400	2800
diethylamine	3300	2700
dimethylamine	3100	2500

The occurrence of dimerization with the five substances containing an $>$N—H group, and its absence with the two tertiary amines, which do not contain this group, suggests that hydrogen bonding is responsible. If this is so, the energy of the N—H····N bond for ammonia, 3800 cal./mol., is almost exactly three times the value 1300 cal./mol. given by Pauling (1940) for the hydrogen bond in solid ammonia. This latter value is calculated from the heat of sublimation of the ammonia crystal, in which each nitrogen atom has six neighbours at 3·38 Å, on the assumption that each nitrogen atom is linked by a hydrogen bond to *six* other nitrogen atoms. The discrepancy cannot be accounted for merely on the grounds that the heat of sublimation is lower than expected owing to the vapour phase being partially dimerized. The vapour pressure of solid ammonia at its melting-point (191·8° K) is 4·6 cm., and the value of $K_p \doteqdot 7$ atm., so that the saturated vapour is less than 3 % dimerized. If, however, it is assumed that each ammonia molecule in the crystal is only capable of forming two hydrogen bonds

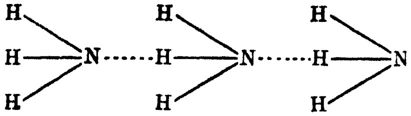

so that each nitrogen atom in the crystal lattice is only hydrogen bonded to *two* of its neighbours, a value of 3900 cal./mol. would be obtained for the energy of the N—H····N bond, which is in fair agreement with the value obtained above for gaseous ammonia. An alternative explanation would be to assume that, if the one unshared electron pair on the nitrogen atom of the ammonia molecule has to serve *three* hydrogen bonds in the ammonia crystal,

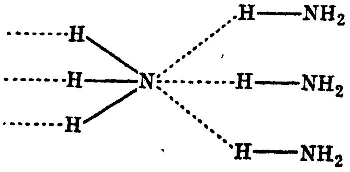

the resulting energy of each hydrogen bond is about one-third of that in the gaseous ammonia dimer, where the unshared electron pair only serves *one* hydrogen bond.

This may be contrasted with the case of water, where two unshared electron pairs are available on the oxygen atom for hydrogen bond formation. Each oxygen atom in the ice crystal is hydrogen bonded to four other oxygen atoms, so that the two unshared electron pairs on the oxygen atom serve only one hydrogen bond each. Values of hydrogen bond energy calculated from the latent heat of sublimation of ice, 4500 cal./mol. (Pauling 1940) and 6400 cal./mol. (Searcy 1949), lie reasonably close to the energy of dimerization of steam, 5000 cal./mol., calculated from the second virial coefficient by Rowlinson (1949) suggesting that the water molecule is capable of forming four hydrogen bonds of full strength.

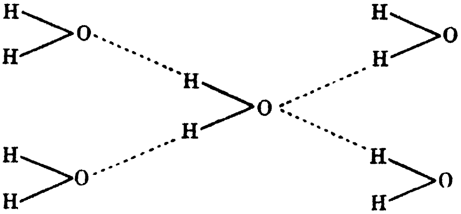

The hydrogen bond energies for the amines are less than for ammonia, and diminish in the same order as the dipole moments (see table 2), as would be expected.

TABLE 2

substance	$\mu \times 10^{18}$ (e.s.u.)	r (Å)	$-\Delta U$ calc. (cal./mol.)	$-\Delta U$ obs. (cal./mol.)	$-\Delta U$ calc. / RT (298° K)
ammonia	1·46 (*a*)	3·0	2290	3800	3·8
ethylamine	1·37 (*b*)	3·0	2020	3000	3·4
methylamine	1·32 (*c*)	3·0	1880	2800	3·2
diethylamine	1·10 (*d*)	3·0	1300	2700	2·2
dimethylamine	1·02 (*c*)	3·0	1120	2500	1·9
triethylamine	0·74 (*d*)	3·0	590	—	0·99
trimethylamine	0·65 (*c*)	3·0	450	—	0·76

(*a*) Watson (1928); (*b*) Trunel (1939); (*c*) Groves & Sugden (1937); (*d*) Higashi (1937).

It is also possible that the mechanism of dimerization of ammonia and the amines should be simple interaction between dipoles. Examination of solid models of the molecules concerned shows that, if the molecules are regarded as made up of combinations of rigid bond lengths and van der Waals radii, the nearest approach of two dipoles is in the end to end position to a distance equal to twice the van der Waals radius of the nitrogen atom (slightly greater for the tertiary amines, if regarded as rigid). Values of ΔU for dipole interaction can be calculated from the approximate formula $\Delta U = 2\mu^2/r^3$, where μ is the dipole moment, and r the distance apart of the centres of the dipoles. Values of ΔU calculated in this way are compared with the observed values in table 2. It will be seen that this mechanism would explain the absence of observed dimerization with the two tertiary amines, since, for both, $\Delta U/RT < 1$ at all temperatures where measurements were made. On the other hand, all the values of ΔU calculated on the basis of dipole interaction are much lower than the observed values. It seems, on the whole, that hydrogen bonding is the more satisfactory explanation; particularly in view of the fact that for ammonia evidence from the crystal structure is in favour of hydrogen bonding (Pauling 1940), while for methylamine there is evidence from the Raman spectrum that hydrogen bonding occurs in the liquid (Kirby-Smith & Bonner 1939).

REFERENCES

Groves, L. G. & Sugden, S. 1937 *J. Chem. Soc.* p. 1779.
Higashi, K. 1937 *Sci. Pap. Inst. Phys. Chem. Res. Tokyo*, **31**, 311.
Hirschfelder, J. O., McClure, F. T. & Weeks, I. F. 1942 *J. Chem. Phys.* **10**, 201.
Kirby-Smith, J. S. & Bonner, L. G. 1939 *J. Chem. Phys.* **7**, 880.
Lambert, J. D., Roberts, G. A. H., Rowlinson, J. S. & Wilkinson, V. J. 1949 *Proc. Roy. Soc.* A, **196**, 113.
Lambert, J. D., Staines, E. N. & Woods, S. D. 1950 *Proc. Roy. Soc.* A, **200**, 262.
Meyers, C. H. & Jessup, R. S. 1925 *Refrig. Engng*, **11**, 345.
Pauling, L. 1940 *Nature of the chemical bond*, 2nd ed. Cornell University Press.
Rowlinson, J. S. 1949 *Trans. Faraday Soc.* **45**, 974.
Searcy, A. W. 1949 *J. Chem. Phys.* **17**, 210.
Stockmayer, W. H. 1941 *J. Chem. Phys.* **9**, 398.
Trunel, P. 1939 *Ann. Chim. (Phys.)*, **12**, 93.
Watson, H. E. 1928 *Proc. Roy. Soc.* A, **117**, 43.

On the asymptotic distribution of eigenvalues

BY J. S. DE WET, *Balliol College, University of Oxford*
AND F. MANDL, *Lincoln College, University of Oxford*

(*Communicated by E. C. Titchmarsh, F.R.S.—Received* 5 *October* 1949)

It is well known that the asymptotic distribution of the eigenvalues of the one-dimensional Schrödinger equation is provided by the so-called W.K.B. formula. Most proofs of this depend on the approximate solution of the equation in two regions and the joining up of these solutions at the boundaries of the regions in a certain way. These methods are not easily generalized to the Schrodinger equation for dimensions greater than one. In the present paper the methods of Courant & Hilbert are applied to this problem and they lead very simply to a proof of the known result in one dimension and to analogous formulae for the eigenvalue distribution of the Schrodinger equation in two and three dimensions.

INTRODUCTION

It is well known (Kemble 1937, chapter III; Titchmarsh 1946, chapter VIII) that the nth eigenvalue E_n of the one-dimensional Schrödinger equation is given asymptotically by the so-called W.K.B. formula

$$n+\tfrac{1}{2}=\frac{2}{h}\sqrt{(2m)}\int_{x_1}^{x_2}\sqrt{(E_n-V)}\,dx,$$

where $V(x)$ is the potential function and x_1, x_2 the two values of x $(x_1<x_2)$ for which $V(x)=E_n$ (it being assumed that the potential is such that the equation has only two

roots). This formula is known to be accurate down to $n = 1$ for the harmonic oscillator. In a recent paper Langer (1949) has established the approximate validity of the formula down to low values of n for a fairly wide range of potentials, while Titchmarsh (1946, p. 130) has proved a similar result for a rather restricted kind of potential. One would expect analogous formulae for the asymptotic distribution of the eigenvalues of the Schrödinger equation for higher dimensions. Fowler (1936, p. 19) has verified that the expected result is true for certain potentials in the case of the two- and three-dimensional Schrödinger equation and clearly believed the result to hold generally (this is the content of what Fowler calls the limiting principle), but as far as we know no proof of this has been given. Certainly the methods usually used in the treatment of the one-dimensional case are not easily generalized to the case of higher dimensions.

In the present paper the methods of Courant & Hilbert (1931, chapter VI) are applied to the determination of the eigenvalue distribution of the Schrödinger equation. They lead very simply to a proof that the W.K.B. formula gives the asymptotic distribution in the one-dimensional case. Precisely the same argument leads to analogous formulae for the case of two and three dimensions. In § 1 we quote a few of the relevant results of Courant & Hilbert (1931). In § 2 we discuss the application of these to the one-dimensional case, and finally in §§ 3 and 4 we deal with the case of two and three dimensions.

1. SOME RESULTS OF COURANT & HILBERT

Consider the following eigenvalue problem: λ is an eigenvalue of a linear self-adjoint differential operator L for a given domain D and given boundary conditions if the differential equation $L[\psi]+\lambda\psi = 0$ has a solution, not everywhere zero, in D, and satisfies the boundary condition on the boundary of D. Courant & Hilbert (1931) have shown that if the eigenvalues form an increasing infinite sequence $\lambda_0, \lambda_1, \lambda_2, \ldots$, then these eigenvalues are determined by a certain maximum-minimum property of a quadratic functional associated with the operator L. Using this maximum-minimum property the following two theorems follow quite simply:

THEOREM I. *If $D^1, D^2, \ldots, D^n$ are a finite number of subdomains of the domain D which do not overlap and $A(\lambda)$ is the number of eigenvalues of the operator L less than λ for the domain D and boundary condition $\psi = 0$, while $A^r(\lambda)$ has a similar meaning for the domain D^r and the same boundary condition, then*

$$A(\lambda) \geqslant \sum_{r=1}^{n} A^r(\lambda).$$

THEOREM II. *If the domain D is subdivided into a finite number of subdomains $D^1, D^2, \ldots, D^n$, no pair of which overlap, and $B(\lambda)$ is the number of eigenvalues less than λ of the operator L for the domain D and boundary condition $\partial\psi/\partial n = 0$ ($\partial\psi/\partial n$ is the derivative normal to the boundary), while $B^r(\lambda)$ has the same meaning for the domain D^r and the same boundary condition, then*

$$B(\lambda) \leqslant \sum_{r=1}^{n} B^r(\lambda).$$

It also follows very simply that $B(\lambda) \geqslant A(\lambda)$, so that combining the results of the two theorems

$$\sum_{r=1}^{n} B^r(\lambda) \geqslant B(\lambda) \geqslant A(\lambda) \geqslant \sum_{r=1}^{n} A^r(\lambda).$$

The operators we will be concerned with will be of the form $M-q$, where M is one of the operators d^2/dx^2, $\partial^2/\partial x^2+\partial^2/\partial y^2$, $\partial^2/\partial x^2+\partial^2/\partial y^2+\partial^2/\partial z^2$, while q is a function of the appropriate variables. Then one can easily prove that for a domain D and boundary condition $\partial\psi/\partial n = 0$, if $B(\lambda, \text{max.})$ and $B(\lambda, \text{min.})$ are the number of eigenvalues less than λ of the operators $M-q_{\text{max.}}$ and $M-q_{\text{min.}}$, while $B(\lambda)$ has the same meaning for the operator $M-q$, then

$$B(\lambda, \text{min.}) \geqslant B(\lambda) \geqslant B(\lambda, \text{max.}),$$

$q_{\text{min.}}$ and $q_{\text{max.}}$ being the maximum and minimum of q in the domain D. A similar result holds for the eigenvalue distribution with the boundary condition $\psi = 0$, namely,

$$A(\lambda, \text{min.}) \geqslant A(\lambda) \geqslant A(\lambda, \text{max.}).$$

Combining these two results with the previous one we have

$$\sum_{r=1}^{n} B^r(\lambda, \text{min.}) \geqslant B(\lambda) \geqslant A(\lambda) \geqslant \sum_{r=1}^{n} A^r(\lambda, \text{max.}), \tag{1·1}$$

where $A^r(\lambda, \text{max.})$ and $B^r(\lambda, \text{min.})$ have the same meaning as the corresponding expressions above but for D^r instead of D.

Courant & Hilbert (1931) have used the above results extensively to determine the asymptotic distribution of eigenvalues for the case of finite domains. We now apply these results to the Schrödinger equation for infinite domains. The applicability of these methods to the Schrödinger equation for infinite domains is assured, for all the types of potential we will consider, by the work of Friedrichs (1934).

2. THE ONE-DIMENSIONAL SCHRÖDINGER EQUATION

The one-dimensional Schrödinger equation is the following:

$$\frac{d^2\psi}{dx^2} + \frac{8\pi^2 m}{h^2}[E - V(x)]\psi = 0, \tag{2·1}$$

which can be written as

$$\frac{d^2\psi}{dx^2} + \{\lambda - q(x)\}\psi = 0, \tag{2·2}$$

where $\lambda = 8\pi^2 mE/h^2$ and $q(x) = 8\pi^2 mV(x)/h^2$.

We consider in this section the eigenvalue distribution of the equation (2·2) for the domain $(-\infty, +\infty)$ with the boundary condition that ψ should be integrable square over the whole domain and therefore tend to 0 rapidly enough as $|x|$ tends to infinity. We restrict ourselves, for convenience, to potentials $q(x)$ with the following properties: (i) $q(x)$ has a strict minimum at the origin $x = 0$ and increases steadily to the right and left of the origin; (ii) $q(x)$ tends to $+\infty$ as $|x|$ tends to infinity or $q(x)$ tends to K as $|x|$ tends to ∞. For such potentials we prove the following result:

If $A(\lambda)$ be the number of eigenvalues of (2·2) less than λ while $I(\lambda)$ is defined by

$$I(\lambda) = \frac{1}{\pi}\int_{x_1(\lambda)}^{x_2(\lambda)} (\lambda - q(x))^{\frac{1}{2}}\, dx, \tag{2·3}$$

$x_1(\lambda)$ and $x_2(\lambda)$ $(x_1 < x_2)$ being the two roots of $\lambda - q(x) = 0$, then

$$|\,A(\lambda) - I(\lambda)\,| \leqslant R(\lambda), \tag{2·4}$$

where
$$R(\lambda) = 2\sqrt{(2/\pi)}\,(\lambda - q_0)^{\frac{1}{4}}\,(x_2 - x_1)^{\frac{1}{2}}, \tag{2·5}$$

q_0 being the minimum value of q, $q(0)$.

By means of this result one can show for wide classes of potentials that

$$\lim_{n\to\infty} \frac{R(\lambda_n)}{I(\lambda_n)} = 0, \tag{2·6}$$

λ_n being the nth eigenvalue of (2·2). For such potentials $I(\lambda)$ gives the asymptotic distribution of eigenvalues. We shall see, however, that there are potentials for which (2·6) does not hold. For such potentials our approximation to $A(\lambda)$ is not good enough to establish the desired result. The eigenvalue distribution of (2·1) of course follows from that of (2·2), the relevant result being

$$|\,A(E) - \alpha I(\lambda)\,| \leqslant \alpha R(\lambda), \tag{2·7}$$

where $A(E)$ is the number of eigenvalues of (2·1) less than E and $\alpha^2 = 8\pi^2 m/h^2$.

In order to prove (2·4) let us subdivide the domain $(-\infty, +\infty)$ into the following subdomains:

$$(-\infty, x_1),\quad (x_1, z_1),\quad (z_1, z_2),\quad \ldots,\quad (z_{2n-1}, x_2),\quad (x_2, +\infty),$$

where $z_1 < z_2 < \ldots < z_{2n-1}$ are $(2n-1)$ points between x_1 and x_2, for the moment arbitrarily chosen. Denote these subdomains by $D^0, D^1, \ldots, D^{2n+1}$. In D^0 and D^{2n+1}, $q(x) > \lambda$ and consequently

$$B^0(\lambda) = A^0(\lambda) = B^{2n+1}(\lambda) = A^{2n+1}(\lambda) = 0.$$

Consequently, using (1·1),

$$\sum_{r=1}^{2n} B^r(\lambda, \text{min.}) \geqslant A(\lambda) \geqslant \sum_{r=1}^{2n} A_r(\lambda, \text{max.}). \tag{2·8}$$

Now for any subdomain D^r of length δ_r we have

$$\left.\begin{aligned} A^r(\lambda, \text{max.}) &= \left[\frac{\delta_r}{\pi}(\lambda - q_{\text{max.}})^{\frac{1}{2}}\right] \geqslant \frac{\delta_r}{\pi}(\lambda - q_{\text{max.}})^{\frac{1}{2}} - 1,\\ B^r(\lambda, \text{min.}) &= \left[\frac{\delta_r}{\pi}(\lambda - q_{\text{min.}})^{\frac{1}{2}}\right] + 1 \leqslant \frac{\delta_r}{\pi}(\lambda - q_{\text{min.}})^{\frac{1}{2}} + 1, \end{aligned}\right\} \tag{2·9}$$

the square brackets in (2·9) meaning the integral part of the bracketed quantity. Hence from (2·8) and (2·9)

$$\sum_{r=1}^{2n} \frac{\delta_r}{\pi}(\lambda - q_{\text{min.}})^{\frac{1}{2}} + 2n \geqslant A(\lambda) \geqslant \sum_{r=1}^{2n} \frac{\delta_r}{\pi}(\lambda - q_{\text{max.}})^{\frac{1}{2}} - 2n. \tag{2·10}$$

Choose the points of subdivision z_i $(i = 1, 2, \ldots, 2n-1)$ in such a way that $z_n = 0$ and such that the oscillation of $\sqrt{(\lambda - q)}$ in each subinterval is equal to $\sqrt{(\lambda - q_0)}/n$. Then we have

$$I(\lambda) + \frac{(\lambda-q_0)^{\frac{1}{2}}}{n}\frac{(x_2-x_1)}{\pi} \geqslant \sum_{r=1}^{2n}\frac{\delta_r}{\pi}(\lambda - q_{\text{min.}})^{\frac{1}{2}} \geqslant \sum_{r=1}^{2n}\frac{\delta_r}{\pi}(\lambda - q_{\text{max.}})^{\frac{1}{2}}$$
$$\geqslant I(\lambda) - \frac{(\lambda-q_0)^{\frac{1}{2}}}{n}\frac{(x_2-x_1)}{\pi}. \tag{2·11}$$

Combining (2·11) and (2·10) we get

$$|A(\lambda) - I(\lambda)| \leqslant \frac{(\lambda-q_0)^{\frac{1}{2}}}{n}\frac{(x_2-x_1)}{\pi} + 2n. \tag{2·12}$$

Choosing n so as to minimize the right-hand side of (2·12) this becomes

$$|A(\lambda) - I(\lambda)| \leqslant 2\sqrt{(2/\pi)}\,(\lambda-q_0)^{\frac{1}{4}}\,(x_2-x_1)^{\frac{1}{2}}, \tag{2·13}$$

which is the result we wished to establish.

Let us consider the form the inequality (2·13) takes for some general types of potential:

(i) $q(x) \rightarrow +\infty$ as $|x| \rightarrow \infty$ and $q''(x) > 0$ for all x.

For this potential one easily shows that $I(\lambda) > (x_2 - x_1)\sqrt{(\frac{1}{2}\lambda)}/2\pi$, and therefore $R(\lambda) < 8\sqrt{I(\lambda)}$. In this case (2·13) becomes

$$\left|\frac{A(\lambda)}{I(\lambda)} - 1\right| < \frac{8}{\sqrt{I(\lambda)}}, \tag{2·14}$$

and the right-hand side tends to 0 as $\lambda \rightarrow \infty$, showing that for large λ, $I(\lambda)$ gives the number of eigenvalues less than λ.

(ii) $q(x) = a\,|x|^{\alpha}$ $(\alpha > 0,\ a > 0)$.

For this potential (2·13) is of the same form as (2·14).

(iii) $q(x) = K(1 - 1/|x|^{\alpha})$ for $|x| > 1$ $(0 < \alpha < 1)$,
$q(x) = |x| - 1$ for $|x| \leqslant 1$.

For this potential $\lambda_n \rightarrow K$ as $n \rightarrow \infty$ and (2·13) becomes

$$\left|\frac{A(\lambda)}{I(\lambda)} - 1\right| < C\{I(\lambda)\}^{(\alpha-1)/(2-\alpha)}. \tag{2·15}$$

Since $0 < \alpha < 1$ and $I(\lambda) \rightarrow \infty$ as $\lambda \rightarrow K$,

$$\lim_{\lambda \rightarrow K}\left|\frac{A(\lambda)}{I(\lambda)} - 1\right| = 0.$$

Thus for $\lambda < K$ but nearly equal to K, $I(\lambda)$ gives very nearly the number of eigenvalues less than λ.

As an example of a potential for which the approximation (2·13) is not good enough to show that $A(\lambda_n)/I(\lambda_n) \rightarrow 1$, consider the potential (iii) above with $\alpha = 1$. For this one easily sees that $\lim_{\lambda \rightarrow K} R(\lambda)/I(\lambda) =$ non-zero constant. We have thus established an approximation (2·13) to the number of eigenvalues of (2·2) and shown that for some general classes of potential function the eigenvalue distribution is given asymptotically by $I(\lambda)$, which is equivalent to the result that the eigenvalue distribution of the Schrödinger equation is given asymptotically by the W.K.B. formula.

3. THE TWO-DIMENSIONAL SCHRÖDINGER EQUATION

We now apply the methods of the previous sections to the problem of estimating the eigenvalue distribution of the equation

$$\frac{\partial^2\psi}{\partial x^2}+\frac{\partial^2\psi}{\partial y^2}+\{\lambda-q(x,y)\}\psi=0, \tag{3·1}$$

the domain being the whole plane and the boundary condition as before that ψ be integrable square over the whole domain and therefore tends to zero rapidly enough as the distance from the origin tends to infinity. From this the distribution of eigenvalues of the corresponding Schrödinger equation follows immediately.

The position is rather more complicated than in the one-dimensional case because, subdividing the whole domain in the same way as we did there, one gets subdomains bounded by curves $q(x,y)=$ constant, and in order to apply the method one needs to have an estimate of the eigenvalue distribution for such domains and *constant* potential. In the one-dimensional case the corresponding results are the simple formulae (2·9). Courant & Hilbert (1931, p. 385) have considered the eigenvalue distribution of (3·1) for a domain bounded by an arbitrary curve with continuously turning tangent (for the case $q=0$) and have proved the following result:

If D is a domain bounded by a simple closed curve with continuously turning tangent and F is the area of the domain, then $A(\lambda)$ for the equation (3·1) with $q=0$ for the domain D satisfies the following inequality:

$$\left|A(\lambda)-\frac{\lambda F}{4\pi}\right|<C\sqrt{\lambda}\log\lambda, \tag{3·2}$$

where C is a constant. An argument similar to that used to establish this result leads fairly easily to the rather more general result we need which provides an estimate of $A(\lambda)$ and $B(\lambda)$ for all domains D bounded by one or two members of the family of curves $q(x,y)=$ constant, provided this family of curves satisfies certain restrictive conditions. This result, the proof of which will not be given here, is the following:

If $\Gamma(\mu)$ is a one-parameter family of simple closed curves with continuously turning tangents satisfying the following conditions: (*a*) $\Gamma(\mu_1)$ contains $\Gamma(\mu_2)$ if $\mu_1>\mu_2$, (*b*) there are positive numbers A and B (independent of μ) such that for every curve of the family the number of points on the curve with the magnitude of the slope equal to A is less than B, (*c*) for every $\epsilon>0$ there is a $\delta(\epsilon)>0$ (independent of μ) such that on any curve of the family the tangent turns through an angle less than ϵ in any segment of the curve of length less than δ, then the eigenvalue distributions $A(\lambda)$ and $B(\lambda)$ of (3·1) for constant potential q and any domain D bounded by one or two members of the family $\Gamma(\mu)$ satisfy the following inequality:

$$\frac{F(\lambda-q)}{4\pi}-R(\lambda,q)<A(\lambda)\leqslant B(\lambda)<\frac{F(\lambda-q)}{4\pi}+R(\lambda,q), \tag{3·3}$$

where

$$\left.\begin{aligned} R(\lambda,q) &= (C_1L+C_2)(\lambda-q)^{\frac{1}{2}}\log(\lambda-q)+C_3F(\lambda-q)^{\frac{1}{2}} \quad \text{if} \quad \lambda-q>\alpha>0,\\ R(\lambda,q) &= (C_1L+C_2)\,\alpha^{\frac{1}{2}}\log\alpha+C_3F\alpha^{\frac{1}{2}} \quad \text{if} \quad 0\leqslant\lambda-q\leqslant\alpha, \end{aligned}\right\} \qquad (3{\cdot}3a)$$

F being the area of the domain, L the total length of the bounding curve (or curves), and C_1, C_2, C_3 and α constants depending on the family of curves but not the domain.

Using the above result it is now an easy matter to arrive at a formula like (2·4) for the eigenvalue distribution of (3·1) with a potential function $q(x,y)$ satisfying the following restrictions: (i) $q(x,y)$ has a strict minimum at the origin, and for convenience we choose the potential zero so that $q(0,0)=0$; (ii) if $q[r,\theta]$ be the potential function in polars, $q[r,\theta]$ is a strictly increasing function of r for each θ and $q[r,\theta]$ tends to infinity as r tends to infinity for each value of θ; (iii) the curves $q(x,y)=\lambda$, which we will denote by $\Gamma(\lambda)$, have continuously turning tangents for $\lambda\geqslant\mu>0$; (iv) the curves $\Gamma(\lambda)$ $(\lambda\geqslant\mu)$ satisfy the conditions (b) and (c) for the validity of (3·3) (they also satisfy (a) because of (ii) above).

For a potential function $q(x,y)$ subject to the above restrictions we now prove the following result:

For $\lambda>\lambda_0$

$$|\,I(\lambda)-A(\lambda)\,| < K_1\lambda^{\frac{3}{4}}\{F(\lambda)\,L(\lambda)\}^{\frac{1}{2}}\sqrt{(\log\lambda)}+K_2F(\lambda)\,\lambda^{\frac{1}{2}}, \qquad (3{\cdot}4)$$

where $A(\lambda)$ *has the usual meaning,* $F(\lambda)$ *is the area inside the curve* $\Gamma(\lambda)$, $L(\lambda)$ *is the maximum length of one of the curves* $\Gamma(\sigma)$ $(\sigma\leqslant\lambda)$, K_1, K_2 *and* λ_0 *are constants which can be explicitly determined for the given potential* $q(x,y)$, *while* $I(\lambda)$ *is given by*

$$I(\lambda)=\frac{1}{4\pi}\iint\limits_{D(\lambda)}\{\lambda-q(x,y)\}\,dx\,dy, \qquad (3{\cdot}5)$$

$D(\lambda)$ *being the domain inside* $\Gamma(\lambda)$.

In order to prove this result, let us subdivide the plane into $(N+2)$ subdomains $D^0, D^1, \dots, D^{N+1}$ as follows: D^0 is the domain inside $\Gamma(\mu)$, $D^i (i=1,2,\dots,N)$ is the annular domain between $\Gamma[\mu+(i-1)(\lambda-\mu)/N]$ and $\Gamma[\mu+i(\lambda-\mu)/N]$, while D^{N+1} is the domain outside $\Gamma(\lambda)$, λ being assumed greater than μ. We now apply (1·1) to this subdivision of the plane, noting that $A^{N+1}(\lambda)=B^{N+1}(\lambda)=0$, since in D^{N+1} $q(x,y)\geqslant\lambda$. Using (3·3) this gives

$$\begin{aligned} &\sum_{i=0}^{N}\frac{F_i[\lambda-q_i(\text{min.})]}{4\pi}+\sum_{i=0}^{N}R(\lambda,q_i(\text{min.}))>A(\lambda)\\ &\qquad\qquad >\sum_{i=0}^{N}\frac{F_i[\lambda-q_i(\text{max.})]}{4\pi}-\sum_{i=0}^{N}R(\lambda,q_i(\text{max.})), \end{aligned} \qquad (3{\cdot}6)$$

where F_i is the area of D^i and $q_i(\text{max.})$ and $q_i(\text{min.})$ are the maximum and minimum of $q(x,y)$ in D^i. Now, for $\lambda\geqslant q\geqslant 0$, $R(\lambda,q)\leqslant R(\lambda,0)$. Therefore, from (3·3$a$) for $\lambda>\alpha$ (3·6) becomes

$$\begin{aligned} &\sum_{i=0}^{N}\frac{F_i[\lambda-q_i(\text{min.})]}{4\pi}+\sum_{i=0}^{N}(C_1L_i+C_2)\,\lambda^{\frac{1}{2}}\log\lambda+C_3\sum_{i=0}^{N}F_i\lambda^{\frac{1}{2}}>A(\lambda)\\ &\qquad >\sum_{i=0}^{N}\frac{F_i[\lambda-q_i(\text{max.})]}{4\pi}-\sum_{i=0}^{N}(C_1L_i+C_2)\,\lambda^{\frac{1}{2}}\log\lambda-C_3\sum_{i=0}^{N}F_i\lambda^{\frac{1}{2}}, \end{aligned} \qquad (3{\cdot}6a)$$

where L_i is the total length of the boundary of D^i. From the way the domains have been chosen it follows that

$$I(\lambda)-\frac{F_0\mu}{4\pi}-\frac{F(\lambda)\,\lambda}{4\pi N}<I(\lambda)-\frac{F_0\mu}{4\pi}-[F(\lambda)-F_0]\frac{(\lambda-\mu)}{4\pi N}\leqslant\sum_{i=0}^{N}\frac{F_i[\lambda-q_i(\text{max.})]}{4\pi}$$
$$<\sum_{i=0}^{N}\frac{F_i[\lambda-q_i(\text{min.})]}{4\pi}<I(\lambda)+\frac{F_0\mu}{4\pi}+[F(\lambda)-F_0]\frac{(\lambda-\mu)}{4\pi N}<I(\lambda)+\frac{F_0\mu}{4\pi}+\frac{F(\lambda)\,\lambda}{4\pi N}, \tag{3·7}$$

where $I(\lambda)$ is given by (3·5). From the definition of $L(\lambda)$ we have $L_i\leqslant 2L(\lambda)$. Using this and combining (3·6a) and (3·7) we have, for $\lambda>\alpha$,

$$|\,I(\lambda)-A(\lambda)\,|<\frac{F_0\mu}{4\pi}+(C_1L_0+C_2)\,\lambda^{\frac{1}{2}}\log\lambda+C_3F(\lambda)\,\lambda^{\frac{1}{2}}$$
$$+\frac{F(\lambda)\lambda}{4\pi N}+N\lambda^{\frac{1}{2}}\log\lambda[2C_1L(\lambda)+C_2]. \tag{3·8}$$

Choosing N to minimize the right-hand side of (3·8) we get (for $\lambda>\alpha$)

$$|\,I(\lambda)-A(\lambda)\,|<\frac{F_0\mu}{4\pi}+(C_1L_0+C_2)\,\lambda^{\frac{1}{2}}\log\lambda+C_3F(\lambda)\,\lambda^{\frac{1}{2}}$$
$$+\left[\frac{F(\lambda)}{\pi}\{2C_1L(\lambda)+C_2\}\right]^{\frac{1}{2}}\lambda^{\frac{3}{4}}\surd(\log\lambda). \tag{3·9}$$

From this follows that for suitably chosen constants K_1, K_2 and λ_0

$$|\,I(\lambda)-A(\lambda)\,|<K_1\lambda^{\frac{3}{4}}\{F(\lambda)\,L(\lambda)\}^{\frac{1}{2}}\surd(\log\lambda)+K_2F(\lambda)\,\lambda^{\frac{1}{2}} \tag{3·10}$$

for $\lambda>\lambda_0$. We have thus proved that for potential functions $q(x,y)$ satisfying the conditions preceding equation (3·4) above, the eigenvalue distribution $A(\lambda)$ of (3·1) satisfies the inequality (3·10).

It is instructive to apply the formula (3·4) for a potential for which the eigenvalues are known and to see to what extent it deviates from the actual result. For the Schrödinger equation of the two-dimensional harmonic oscillator

$$\frac{\partial^2\psi}{\partial x^2}+\frac{\partial^2\psi}{\partial y^2}+\frac{8\pi^2m}{h^2}[E-2\pi^2\nu^2m(x^2+y^2)]\,\psi=0,$$

the number of eigenvalues $A(nh\nu)$ less than $nh\nu$ is $\frac{1}{2}n(n+1)$, while the corresponding number $I(nh\nu)=\frac{1}{2}n^2$. The potential clearly satisfies the conditions for the validity of (3·4) and this becomes

$$|\,A(\lambda)-I(\lambda)\,|=|\,\tfrac{1}{2}n(n+1)-\tfrac{1}{2}n^2\,|=\tfrac{1}{2}n<K_1n^{\frac{3}{2}}\log n+K_2n^{\frac{3}{2}},$$

which shows that (3·4) is rather a poor approximation. None the less it suffices to show that the eigenvalue distribution is given asymptotically by $I(\lambda)$ for a wide range of potential functions. Consider, for instance, a potential which is such that (in addition to satisfying the other conditions) $\partial^2q/\partial r^2>0$ for all r and θ and such that $L(\lambda)\leqslant F(\lambda)$. For such a potential (3·4) gives the following result:

$$\left|\frac{A(\lambda)}{I(\lambda)}-1\right|<C\lambda^{-\frac{1}{4}}\surd(\log\lambda), \tag{3·11}$$

and the right-hand side of (3·11) tends to zero as $\lambda\to\infty$. Similar results follow for other general types of potential.

4. THE THREE-DIMENSIONAL SCHRÖDINGER EQUATION

Clearly the method used above can be applied equally well to the determination of the eigenvalue distribution of the equation

$$\frac{\partial^2\psi}{\partial x^2}+\frac{\partial^2\psi}{\partial y^2}+\frac{\partial^2\psi}{\partial z^2}+\{\lambda-q(x,y,z)\}\psi=0. \tag{4·1}$$

All one needs for this purpose is a formula like (3·3) for the eigenvalue distributions $A(\lambda)$ and $B(\lambda)$ of (4·1) for a constant potential and domains bounded by one or two members of a suitable one-parameter family of surfaces. With restrictions on the family of surfaces like the conditions (*a*), (*b*) and (*c*) for the curves in the case of (3·3) one can prove in this case that for $\lambda>\alpha$

$$\begin{aligned}\frac{V(\lambda-q)^{\frac{3}{2}}}{6\pi^2}-(C_1F+C_2L)(\lambda-q)\log(\lambda-q)-C_3V(\lambda-q)<A(\lambda)\\ \leqslant B(\lambda)<\frac{V(\lambda-q)^{\frac{3}{2}}}{6\pi^2}+(C_1F+C_2L)(\lambda-q)\log(\lambda-q)+C_3V(\lambda-q),\end{aligned} \tag{4·2}$$

where V is the volume of the domain, F the area of the bounding surface or surfaces, L the side of the smallest cube with sides parallel to the axes and containing the domain, and C_1, C_2 and C_3 are constants depending on the particular family of surfaces but independent of the domain.

With the help of this result one can prove that *if the potential satisfies conditions like* (*i*) *and* (*ii*) *of* (3·4) *and in addition is such that the family of surfaces* $q(x,y,z)=\lambda$ $(\lambda\geqslant\mu)$, *satisfies the conditions for the validity of* (4·2), *then for* $\lambda>\lambda_0$ *the eigenvalue distribution* $A(\lambda)$ *of* (4·1) *satisfies the following inequality:*

$$|I(\lambda)-A(\lambda)|<\{K_1F(\lambda)+K_2L(\lambda)\}^{\frac{1}{2}}\{V(\lambda)\}^{\frac{1}{2}}\lambda^{\frac{5}{4}}\sqrt{(\log\lambda)}+K_3V(\lambda)\lambda, \tag{4·3}$$

where $V(\lambda)$ *is the volume inside* $S(\lambda)$ (*the surface* $q(x,y,z)=\lambda$), $F(\lambda)$ *is the maximum area of one of the family of surfaces* $S(\sigma)$ $(\sigma\leqslant\lambda)$, $L(\lambda)$ *is the side of the smallest cube with sides parallel to the axes containing* $S(\lambda)$, *and* K_1, K_2, K_3 *and* λ_0 *are constants determined by the given potential, while* $I(\lambda)$ *is given by*

$$I(\lambda)=\frac{1}{6\pi^2}\iiint\limits_{D(\lambda)}\{\lambda-q(x,y,z)\}^{\frac{3}{2}}\,dx\,dy\,dz, \tag{4·4}$$

$D(\lambda)$ *being the domain inside* $q(x,y,z)=\lambda$.

One of us (F.M.) is indebted to the Department of Scientific and Industrial Research for a maintenance grant. We are indebted to Professor E. C. Titchmarsh for helpful criticism.

REFERENCES

Courant, R. & Hilbert, D. 1931 *Methoden der Mathematischen Physik*, vol. **1**, 2nd ed. Berlin: Julius Springer.

Fowler, R. H. 1936 *Statistical mechanics*, 2nd ed. Cambridge University Press.

Friedrichs, K. 1934 *Math. Ann.* **109**, 685.

Kemble, E. C. 1937 *The fundamental principles of quantum mechanics*. New York: McGraw Hill Book Co.

Langer, R. E. 1949 *Phys. Rev.* **75**, 1573.

Titchmarsh, E. C. 1946 *Eigenfunction expansions associated with second-order differential equations.* Oxford: Clarendon Press.

INDEX TO VOLUME 200 (A)

Alexander, A. E. & Gray, V. R. Aluminium soaps, their nature and gelling properties, 162.
Alexander, A. E. & Rabinovitch, B. The swelling and solubility of celluslose acetate in benzene/xylenol mixtures, 154.
Alkyl nitrite vapours, inflammation (Gray & Yoffe), 114.
Allene, vibration-rotation bands (Miller & Thompson), 1.
Alloys, structure (Davis & Hume-Rothery), 441.
Aluminium soaps, their nature and gelling properties (Alexander & Gray), 162.
Ammonia and amines, dimerization (Lambert & Strong), 566
Asymptotic distribution of eigenvalues (De Wet & Mandl), 572.

Baskett, A. C. & Hinshelwood, Sir Cyril. The utilization of carbon sources by *Bact. lactis aerogenes*. I. General survey (Abstract), 438.
Baskett, A. C. & Hinshelwood, Sir Cyril. The utilization of carbon sources by *Bact. lactis aerogenes*. II. The significance of the tricarboxylic acid cycle (Abstract), 439.
Bengough, W. I. & Norrish, R. G. W. The mechanism and kinetics of the heterogeneous polymerization of vinyl monomers. I. The benzoyl peroxide catalyzed polymerization of vinyl chloride, 301.
Bottomley, G. A., Massie, Doreen S. & Whytlaw-Gray, R. A comparison of the compressibilities of some gases with that of nitrogen at pressures below one atmosphere, 201.
Boundary layers (Stewartson), 84.
Boys, S. F. Electronic wave functions. I. A general method of calculation for the stationary states of any molecular system, 542.
Bubbles, mechanics of (Davies & Taylor), 375.

Chandrasekhar, S. On Heisenberg's elementary theory of turbulence, 20.
Characters of a collineation group in five dimensions (Todd), 320.
Class of enumerations of importance in genetics (Abstract) (Fisher), 438.
Cole, A. R. H. & Thompson, H. W. Vibration-rotation bands of some polyatomic molecules, 10.
Combustion products of explosives, dynamics (Taylor), 235.
Comparison of the compressibilities of some gases with that of nitrogen at pressures below one atmosphere (Bottomley, Massie & Whytlaw-Gray), 201.
Compressibilities of gases (Bottomley, Massie & Whytlaw-Gray), 201.
Configurational interaction in molecular orbital theory. A higher approximation in the non-empirical method (Craig), 474.
Copolymerization studies (Melville & Valentine), 358.
Correlated incompressible and compressible boundary layers (Stewartson), 84.
Craig, D. P. Configurational interaction in molecular orbital theory. A higher approximation in the non-empirical method, 474.
Craig, D. P. Polar structures in the theory of conjugated molecules. I. Identification of the ethylene π-electron states, 272.
Craig, D. P. Polar structures in the theory of conjugated molecules. II. Symmetry properties and matrix elements for polar structures, 390.
Craig, D. P. Polar structures in the theory of conjugated molecules. III. The energy levels of benzene, 401.
Curtis, A. R. The velocity of sound in general relativity, with a discussion of the problem of the fluid sphere with constant velocity of sound, 248.

Davies, C. N. The sedimentation and diffusion of small particles, 100.
Davies, R. M. & Taylor, Sir Geoffrey. The mechanics of large bubbles rising through extended liquids and through liquids in tubes, 375.
Davis, R. J. & Hume-Rothery, W. The effect of thermal cycles on the structure of alloys: diffusion effects in two phase alloys, 441.
De Wet, J. S. & Mandl, F. On the asymptotic distribution of eigenvalues, 572.

Diffraction of blast. II. (Lighthill), 554.
Dimerization of ammonia and amines (Lambert & Strong), 566.
Discussion on the physics and chemistry of hydrocarbon gels (Rideal and others), 135.
Dynamics of the combustion products behind plane and spherical detonation fronts in explosives (Taylor), 235.

Eddy, A. A. & Hinshelwood, Sir Cyril. The utilization of potassium by *Bact. lactis aerogenes* (Abstract), 439.
Effect of thermal cycles on the structure of alloys: diffusion effects in two phase alloys (Davis & Hume-Rothery), 441.
Electronic wave functions. I. A general method of calculation for the stationary states of any molecular system (Boys), 542.
Equilibrium swelling of cross-linked amorphous polymers (Treloar), 176.
Experiments on the superconductive transition (Macdonald & Mendelssohn), 66.

Factors which affect the gelling characteristics of aluminium soaps (Parry, Roberts & Taylor), 148.
Fisher, R. A. A class of enumerations of importance in genetics (Abstract), 438.
Flash photolysis and spectroscopy. A new method for the study of free radical reactions (Porter), 284.
Formulation of rheological equations of state (Oldroyd), 523.
Foster, E. W. New terms of the $5d^86s^2$ and $5d^86s6p$ configurations of the spectrum of Hg III, 429.
Frank, F. C. & Merwe, J. H. van der. One-dimensional dislocations. III. Influence of the second harmonic term in the potential representation, on the properties of the model, 125.

Garner, F. H., Nissan, A. H. & Wood, G. F. The rheology of 'elastic' non-Newtonian fluids (summary), 189.
Garner, F. H., Nissan, A. H. & Wood, G. F. Thermodynamics and rheological behaviour of elasto-viscous systems under stress (summary), 188.
Gelation of aluminium soaps in hydrocarbon (McRoberts & Schulman), 136.
Goldsbrough, G. R. The tides in oceans on a rotating globe. V, 191.
Gray, P. & Yoffe, A. D. The inflammation of alkyl nitrate vapours and the effect of inert diluents, 114.
Gray, V. R. *See* Alexander & Gray.

Heisenberg's elementary theory of turbulence (Chandrasekhar), 20.
Hinshelwood, Sir Cyril. *See* Baskett & Hinshelwood; also Eddy & Hinshelwood; also Stubbs & Hinshelwood.
Hume-Rothery, W. *See* Davis & Hume-Rothery.
Huxley, L. G. H. Ionospheric cross-modulation at oblique incidence, 486.
Hydrocarbon gels (Discussion) (Rideal and others), 135.

Inflammation of alkyl nitrate vapours and the effect of inert diluents (Gray & Yoffe), 114.
Ionospheric cross-modulation at oblique incidence (Huxley), 486.

Kinetics of the thermal decomposition of normal paraffin hydrocarbons. I. The inhibition of chains and the nature of the residual reaction (Stubbs & Hinshelwood), 458.

Lambert, J. D., Staines, E. N. & Woods, S. D. Thermal conductivities of organic vapours, 262.
Lambert, J. D. & Strong, E. D. T. The dimerization of ammonia and amines, 566.
Lighthill, M. J. The diffraction of blast. II, 554.

Macdonald, D. K. C. & Mendelssohn, K. Experiments on the superconductive transition, 66.
Mandl, F. *See* De Wet & Mandl.

Massie, Doreen S. *See* Bottomley, Massie & Whytlaw-Gray.
McRoberts, T. S. & Schulman, J. H. Gelation of aluminium soaps in hydrocarbon, 136.
Mechanics of large bubbles rising through extended liquids and through liquids in tubes (Davies & Taylor), 375.
Mechanism and kinetics of the heterogeneous polymerization of vinyl monomers. I. The benzoyl peroxide catalyzed polymerization of vinyl chloride (Bengough & Norrish), 301.
Melville, H. W. & Valentine, L. Studies in copolymerization. I. The evaluation of the kinetic coefficients for the copolymerization of styrene and ethyl methacrylate, 337.
Melville, H. W. & Valentine, L. Studies in copolymerization. II. A discussion of the validity of the results and some theoretical implications, 358.
Mendelssohn, K. *See* MacDonald & Mendelssohn.
Merwe, J. H. van der. *See* Frank & van der Merwe.
Miller, C. H. & Thompson, H. W. Vibration-rotation bands of allene, 1.
Milne, E. A. The relativity of Galilean frames, 219.
Moffit, W. The nature of the sulphur-oxygen bond, 409.

Nature of the sulphur-oxygen bond (Moffit), 409.
New terms of the $5d^86s^2$ and $5d^86s6p$ configurations of the spectrum of Hg III (Foster), 429.
Nissan, A. H. *See* Garner, Nissan & Wood.
Norrish, R. G. W. *See* Bengough & Norrish.
Nye, J. F. Plastic deformation of silver chloride. II. Photoelastic study of the internal stresses in glide packets, 47.

Oldroyd, J. G. On the formulation of rheological equations of state, 523.
One-dimensional dislocations. III. Influence of the second harmonic term in the potential representation, on the properties of the model (Frank and van der Merwe), 125.
Organic vapours, thermal conductivities (Lambert, Staines & Woods), 262.

Paraffin hydrocarbons, decomposition (Stubbs & Hinshelwood), 458.
Parry, G. A., Roberts, J. E. & Taylor, A. J. Factors which affect the gelling characteristics of aluminium soaps, 148.
Perturbation theory (Titchmarsh), 34.
Plastic deformation of silver chloride. II. Photoelastic study of the internal stresses in glide packets (Nye), 47.
Polar structures in the theory of conjugated molecules (Craig), I. Identification of the ethylene π-electron states, 272.
Polar structures in the theory of conjugated molecules (Craig), II. Symmetry properties and matrix elements for polar structures, 390.
Polar structures in the theory of conjugated molecules (Craig), III. The energy levels of benzene, 401.
Polymerization of vinyl monomers (Bengough & Norrish), 301.
Porter, G. Flash photolysis and spectroscopy. A new method for the study of free radical reactions, 284.

Rabinovitch, B. *See* Alexander & Rabinovitch.
Relativity of Galilean frames (Milne), 219.
Rheological equations of state (Oldroyd), 523.
Rheology of 'elastic' non-Newtonian fluids (summary) (Garner, Nissan & Wood), 189.
Rheology of hydrocarbon gels (summary) (Weissenberg), 183.
Rideal, E. K. (and others). A discussion on the physics and chemistry of hydrocarbon gels (opening remarks), 136.
Rivlin, R. S. Some flow properties of concentrated high-polymer solutions, 168.
Roberts, J. E. *See* Parry, Roberts & Taylor.

Schulman, J. S. *See* McRoberts & Schulman.
Sedimentation and diffusion of small particles (Davies), 100.
Silver chloride, plastic deformation (Nye), 47.
Some flow properties of concentrated high-polymer solutions (Rivlin), 168.
Some theorems on perturbation theory (Titchmarsh), 34.
Staines, E. N. *See* Lambert, Staines & Woods.
Stewartson, K. Correlated incompressible and compressible boundary layers, 84.
Strong, E. D. T. *See* Lambert & Strong.
Stubbs, F. J. & Hinshelwood, Sir Cyril. The kinetics of the thermal decomposition of normal paraffin hydrocarbons. I. The inhibition of chains and the nature of the residual reaction, 458.
Studies in copolymerization (Melville & Valentine), I. The evaluation of the kinetic coefficients for the copolymerization of styrene and methyl methacrylate, 337.
Studies in copolymerization (Melville & Valentine), II. A discussion of the validity of the results and some theoretical implications, 358.
Sulphur-oxygen bond (Moffitt), 409.
Superconductive transition (MacDonald & Mendelssohn), 66.
Supersonic flow of compressible fluid through axially symmetric tubes of uniform and varying section (Tempest), 511.
Swelling and solubility of cellulose acetate in benzene/xylenol mixtures (Alexander & Rabinovitch), 154.

Taylor, A. J. *See* Parry, Roberts & Taylor.
Taylor, Sir Geoffrey. *See* Davies & Taylor.
Taylor, Sir Geoffrey. The dynamics of the combustion products behind plane and spherical detonation fronts in explosives, 235.
Tempest, R. K. The supersonic flow of compressible fluid through axially symmetric tubes of uniform and varying section, 511.
Thermal conductivities of organic vapours (Lambert, Staines & Woods), 262.
Thermodynamics and rheological behaviour of elasto-viscous systems under stress (summary) (Garner, Nissan & Wood), 188.
Thompson, H. W. *See* Miller & Thompson, also Cole & Thompson.
Tides in oceans on a rotating globe. V (Goldsbrough), 191.
Titchmarsh, E. C. Some theorems on perturbation theory, 34.
Todd, J. A. The characters of a collineation group in five dimensions, 320.
Treloar, L. R. G. The equilibrium swelling of cross-linked amorphous polymers, 176.

Utilization of carbon sources by *Bact. lactis aerogenes* (Abstract) (Baskett & Hinshelwood). I. General survey, 438.
Utilization of carbon sources by *Bact. lactis aerogenes* (Abstract) (Baskett & Hinshelwood). II. The significance of the tricarboxylic acid cycle, 439.
Utilization of potassium by *Bact. lactis aerogenes* (Abstract) (Eddy & Hinshelwood), 439.

Valentine, L. *See* Melville & Valentine.
Velocity of sound in general relativity, with a discussion of the problem of the fluid sphere with constant velocity of sound (Curtis), 248.
Vibration-rotation bands of allene (Miller & Thompson), 1.
Vibration-rotation bands of some polyatomic molecules (Cole & Thompson), 10.

Weissenberg, K. Rheology of hydrocarbon gels (summary), 183.
Whytlaw-Gray, R. *See* Bottomley, Massie & Whytlaw-Gray.
Wood, G. F. *See* Garner, Nissan & Wood.
Woods, S. D. *See* Lambert, Staines & Woods.

Yoffe, A. D. *See* Gray & Yoffe.

END OF THE TWO HUNDREDTH VOLUME (SERIES A)

I.A.R.I. 75

INDIAN AGRICULTURAL RESEARCH
INSTITUTE LIBRARY, NEW DELHI

Date of Issue	Date of Issue	Date of Issue

GIPNLK—H-40 I.A.R.I.—29-4- 5—15,000